Published Scientific Papers by

Prof. Dr. *Gomaa M. Dawod*

v.1 (87 papers between 1992 – 2025)

شكر و تقدير

لكل أساتذتي و زملائي الذين اشتركت معهم في إعداد هذه البحوث

م	الاسم (بالترتيب الأبجدي)
1	إبراهيم عسكورة
2	أحمد الشوني
3	أحمد أمين
4	أحمد شاكر
5	أشرف عبد الله
6	بهاء شاهين
7	جمال الفقي
8	خالد الغامدي
9	دلال النجار (رحمها الله)
10	رمزي الزهراني
11	شيرين إسماعيل
12	طارق عجاج
13	عبد الله سعد
14	عصام الكرارجي
15	غادة حجاج
16	مجدي حسني
17	محمد البارودي
18	محمد القليش
19	محمد دوما
20	محمد مرزا
21	مسعد مندور
22	مصطفي السماني
23	معراج مرزا
24	مني القاضي (رحمها الله)
25	نبيل كوشك
26	وسام الدين محمد
27	هالة عبيد
28	هدي فيصل محمد

Table of Contents

No.	Title	Page
1	Dawod, G., **1992**, A method for detecting no-check observations in GPS networks, Water Science Magazine, No. 12, October, pp.10-12.	13
2	Dawod, G., **1992**, On the use of pseudo-Kinematic GPS satellite positioning technology in surveying reclaimed lands in Egypt, Proceedings of the First National Conference on Land Reclamation and Development in Egypt, Al-Minia University, Al-Minia, November 2-5, pp.237-246.	19
3	Dawod, G. and El-Kady, M, **1993**, Recovering Orthometric Height Differences from GPS Data and Geopotential Models, Proceedings of the 6th International Technical Meeting of the Satellite Division of The Institute of Navigation (ION GPS 1993), September 22 – 24, 1993, Salt Palace Convention Center, Salt Lake City, UT, USA.	26
4	Alnaggar, D., and Dawod, G., **1995**, Increasing the reliability of GPS geodetic networks, Proceedings of the First International Conference on Satellite Positioning Systems, Alexandria, December 12-13.	27
5	Alnaggar, D., and Dawod, G., **1995**, Potential of GPS observations in the Egyptian National Gravity Standardization Network (ENGSN97) for geoid determination and associated comparisons, Proceedings of Al-Azhar Engineering Fourth International Conference, Cairo, December 16-19, Volume 4, pp. 341-353.	39
6	Alnaggar, D., and Dawod, G., **1997**, The use of high-precision gravity data for detecting groundwater resources in the southern valley, Egypt, Presented in the International Water Resources Association (IWRA) Conference, Montreal, Canada, Sept. 1-6.	40

7	Dawod, G., and Alnaggar, D., **1997**, Performance of relative gravity meters and processing software over the new absolute gravity stations in Egypt, Proceedings of Al-Azhar Engineering Fifth International Conference, Cairo, December 19-22, Volume 5, pp. 113-125.	41
8	Dawod, G., and El-Sammany, M., **2003**, Efficiency of new solutions for surveying and mapping problems in integrated water resources management, Proceedings of the First International Conference on Civil Engineering, Assiut University, Volume 2, pp. 238-245, October 7-8.	42
9	Dawod, G., and Abdel-Aziz, T., **2003**, Establishment of precise geodetic control networks for updating the River Nile maps, Proceedings of Al-Azhar Engineering Seventh International Conference (CD No. 3), Al-Azhar University, Cairo, April 7-10.	51
10	Dawod, G., **2003**, Productive GPS topographic mapping for national development projects in Egypt, Proceedings of the First International Conference on Civil Engineering, Assiut University, Volume 2, pp. 246-253, October 7-8.	61
11	Dawod, G., **2003**, Modernization plan of GPS in 21st century and its impacts on surveying applications, Proceedings of Al-Azhar Seventh International Engineering Conference (CD No. 3), Al-Azhar University, Cairo, April 7-10.	70
12	Dawod, G., **2003**, Proposed standards and specifications for GPS geodetic surveys in Egypt, Water Science Magazine, No. 33, April. Pp. 33-39.	80
13	Saad, A., and Dawod, G., **2001**, A Precise Integrated GPS/Gravity Geoid Model for Egypt, Civil Engineering Research Magazine (CERM), Al-Azhar University, V.24, No. 1, Jun, pp.391-405.	91
14	Alnaggar, D., Saad, A., and Dawod, G., **2002**, Establishment of Egyptian national gravity standardization network, FIG XXII International Congress Washington, D.C. USA, April 19-26 2002.	105

15	داود، جمعة (٢٠٠٢) استخدام أحدث تقنيات الرصد علي الأقمار الصناعية لتحديد حجم المنخفضات لمشروعات إدارة الموارد المائية، مجلة علوم المياه، العدد ٣٢، ص ٢٣-٣١	106
16	Dawod, G., and Mohamed, H., **2002**, The Establishment of the First Modern Sea Level Monitoring System in Egypt, Proceedings of the Twelfth International Conference on Environmental Protection, Ain Shams University, Alexandria, May 14-16, pp. 12-23.	117
17	Shaker, A., Alnaggar, D., Dawod, G., and Saad, A., **2001**, Analysis of the Established Egyptian National Gravity Standardization Network of 1997 (ENGSN97), Civil Engineering Research Magazine (CERM), Al-Azhar University, V. 23, No. 3, July, pp. 999-1021.	129
18	Dawod, G., **2001**, The magnitude and significance of long-term sea level rise in Egypt from a geodetic perspective, Proceedings of the Eleventh International Conference on Environmental Protection, Alexandria University, Alexandria, May 8-10, pp. 207-215.	152
19	Dawod, G., and Alnaggar, D., **2000**, Optimum geodetic datum transformation techniques for GPS surveys in Egypt, Proceedings of Al-Azhar Engineering Sixth International Engineering Conference, Al-Azhar University, September 1-4, Volume 4, pp. 709-718.	161
20	Dawod, G., and Alnaggar, D., **2000**, Quality control measures for the Egyptian National Gravity Standardization Network, Proceedings of The Second International Conference on Civil Engineering, Helwan University, Cairo, April 1-3, pp. 578-587.	171
21	Alnaggar, D., and Dawod, G., **1999**, Efficiency of GPS techniques in national applications, Proceedings of the International Conference on Integrated Management of Water Resources in the 21st Century, Cairo, November 21-25, Volume II, pp. 741-752.	183
22	Ismail, S. and Dawod, G., **2005**, Effect of high floods on Naga Hammadi barrage scour hole, Proceedings of the ninth international water technology Conference, Sharm Al-Sheikh, Egypt, March 17-20, Volume 3, pp. 1041-1050.	195

23	Dawod, G., **2005**, Developing a precise geoid model for hydrographic surveying of the River Nile, Al-Azhar University Engineering Journal (AUEJ), V. 8, No. 1, January, pp. 96 – 107.	205
24	Dawod, G., Meligy, M., and Mohamed, H., **2005**, Assessment and modelling of sea level rise and metrological changes in Egypt, Ain-Shams First International Conference on Environmental Engineering (ASCEE-1), Cairo, Egypt, April 11-12, pp. 573-582.	217
25	داود، جمعة (٢٠٠٥) دراسة الفروق بين مناسيب رخامات الري و مناسيب روبيرات المساحة لمحطات قياس مناسيب المياه علي نهر النيل، مجلة علوم المياه، مجلد ٣٨، ص. ٩-١٦	227
26	Dawod, G., and Ismail, S., **2005**, Enhancing the integrity of the national geodetic data base in Egypt, Proceedings of the FIG working week and GSDI-8 International Conference, Cairo, Egypt, April 16-21.	237
27	Dawod, G., **2007**, New strategies in the utilization of GPS technology for mapping and GIS activities in Egypt, Civil Engineering Research Magazine (CERM), V. 29, No. 1 (Jan.), pp. 292-310.	247
28	Ismail, S., Mohamed, H., and Dawod, G., **2007**, Evaluation of River Nile high flood effects by Geographic Information System, Proceedings of the second national GIS symposium in Saudi Arabia (on CD), Al-Khobar City, Saudi Arabia, April 23-25.	262
29	Mohamed, H., Dawod, G., and Ismail, S., **2007**, Assessment of a cost-effective GPS data processing alternative in Egypt utilizing international on-line processing services, Journal of Al-Azhar University Engineering Sector (JAUES), V. 2, No. 12 (April), pp. 364-375.	274
30	Dawod, G., and Mohamed, H., **2008**, Fitting gravimetric local and global quasi-geoids to GPS/levelling data: The role of geoid/quasi-geoid variations in Egypt, CERM, V. 30, No. 1 (January), pp. 233-244	286
31	Dawod, G. and Mohamed, H., **2008**, Estimation of Sea Level Rise Hazardous Impacts in Egypt within a GIS Environment, Proceedings of the Third National GIS	299

	Symposium in Saudi Arabia (on CD), Al-Khobar City, Saudi Arabia April 7 – 9.	
32	Dawod, G., **2008**, Towards the redefinition of the Egyptian geoid: Performance analysis of recent global geoid models and digital terrain models, Journal of Spatial Science, V. 53, No. 1, pp. 31-42.	313
33	Dawod, G., Mohamed, H., and Ismail, S., **2010**, Evaluation and Adaptation of the EGM2008 Geopotential Model along the Northern Nile Valley, Egypt: Case Study, ASCE Journal of Surveying Engineering, V. 136, No. 1, pp. 36-40, Feb. 2010.	325
34	Dawod, G., and Mohamed, W., **2009**, Data management of different height systems within GPS/GIS integrated spatial technology, Middle East Spatial Technology Conference (MEST2009), December 7-9, Kingdom of Bahrain.	331
35	Dawod, G., Mirza, M., and Al-Ghamdi, K., **2011**, Simple precise coordinates transformations for geomatics applications in Makkah metropolitan area, Saudi Arabia, FIG Working Week 2010, Marrakech, Morocco, May 18-22.	345
36	Mirza, M., Dawod, G., and Al-Ghamdi, K., **2011**, Accuracy and relevance of digital elevation models for geomatics applications – A case study of Makkah municipality, Saudi Arabia, International Journal of Geomatics and Geosciences, V. 1, No. 4, pp. 803-812.	355
37	Mirza, M., Dawod, G., and Al-Ghamdi, K., **2011**, Assessment of global and national digital elevation models for geodetic and geomorphologic applications in Makkah metropolitan area, Saudi Arabia, The XXV IUGG General Assembly, 28 June – 7 July, Melbourne, Australia.	365
38	Dawod, G., Mirza, M., and Al-Ghamdi, K., **2011**, Assessment of several flood estimation methodologies in Makkah metropolitan area, Saudi Arabia, Arabian Journal of Geosciences, DOI 10.1007/s12517-011-0405-5	373
39	Dawod, G., and Koshak, N., **2011**, Developing GIS-	381

	Based Unit Hydrographs for Flood Management in Makkah Metropolitan Area, Saudi Arabia, Journal of Geographic Information System, V. 3, No. 2, pp. 153-159.	
40	Dawod, G., Mirza, M., and Al-Ghamdi, **2011**, GIS-based spatial mapping of flash flood hazards in Makkah city, Saudi Arabia, Journal of Geographic Information System, V. 3, No. 3, pp. 217-223.	389
41	Mirza, M., Dawod, G., and Al-Ghamdi, K., **2011**, Developing a GIS for flood estimation in Makkah city and shrines (in Arabic), The Eleventh Scientific Conference on Hajj Researches, Umm Al-Qura University, Makkah, Saudi Arabia, June 12-14	395
42	Koshak, N. and Dawod, G., **2011**, A GIS morphometric analysis of hydrological basins for flood management within Makkah Metropolitan Area, International Journal of Geomatics and Geosciences, V. 2, No. 2, pp. 544-554.	415
43	Al-Ghamdi, K. Mirza, M. Elzahrany, R. and Dawod , G., **2011**, Impacts of Urban Growth on Flood Hazards in Makkah City, Saudi Arabia, International Journal of Water Resources and Environmental Engineering, V 4, No. 2, pp. 23-34.	427
44	Dawod, G., Mirza, M., and Al-Ghamdi, **2012**, GIS-based estimation of flood hazard impacts on road network in Makkah city, Saudi Arabia, Journal of Environmental Earth Science. V. 67, No. 8, pp. 2205-2215.	439
45	Al-Ghamdi, K., Mirza, M., Elzahrany, R., and Dawod, G., **2012**, GIS evaluation of urban growth and flood hazards: A case study of Makkah city, Saudi Arabia, , FIG Working Week 2012, Rome, Italy, May 6-10.	450
46	Dawod, G., Mirza, M., Al-Ghamdi, K., and Elzahrany, R., **2013**, Projected impacts of land use and road network changes on increasing flood hazards using a 4D GIS: A case study in Makkah metropolitan area, Saudi Arabia, Arabian Journal of Geosciences, DOI 10.1007/s12517-013-0876-7, Published online January 14.	474
47	Mirza, M., Dawod, G., Elzahrany, R., and Al-Ghamdi, K.,	493

	2013, Utilizing GIS for the assessment of relationship between urban growth and flood hazard increase in Makkah city, Saudi Arabia, for the period 1990-2030, Presented in the flood hazard workshop of the Saudi Geographic Association, Prince Sultan University, Al-Kharj, Saudi Arabia, Feb. 26-28.	
48	البارودي/ محمد، مرزا، معراج، داود، جمعة (**٢٠١٢**) استخدام نظم المعلومات الجغرافية في تقدير أحجام السيول و مدي خطورتها عند المجري الأدنى لوادي نعمان جنوب مدينة مكة المكرمة من خلال تطبيق نموذج سنايدر و اعتماد نموذج الارتفاعات الرقمية ASTER، المؤتمر الجغرافي الدولي، جامعة طيبة، المدينة المنورة، ١-٤ أبريل.	494
49	Al-Ghamdi, K., and Dawod, G. (**2014**) Accuracy assessment of global geopotential models for GIS and geomatics applications in Makkah metropolitan area, The ninth national GIS symposium in Saudi Arabia, April 28-30, 2014.	570
50	Dawod, G., Mirza, M., Elzahrany, R., and Al-Ghamdi, K. (**2013**) GIS-based public services analysis based on election areas: A case study of Makkah city, Saudi Arabia, Journal of Geographic Information System, (5)4:378-395, doi: 10.4236/jgis.2013.54036.	581
51	Dawod, G. (**2013**) Suitability analysis for tourist infrastructures utilizing multi-criteria GIS: A case study in Al-Hada city, Saudi Arabia, International Journal of Geomatics and Geosciences, V. 4, No. 2, pp. 313-24.	599
52	Al-Krargy, E., Doma, M. and Dawod, G. (**2014**) Towards an accurate definition of the local geoid model in Egypt using GPS/levelling data: A case study at Rosetta zone. International Journal of Innovative Science and Modern Engineering, V. 2, No. 11, pp. 10-15.	611
53	Al-Krargy, E., Hosny, M. and Dawod, G. (**2015**) Investigating the precision of recent global geoid models and global digital elevation models for geoid modelling in Egypt, Regional Conference on Surveying and Development, Sharm El-Sheikh, Egypt, Oct. 3-6.	617
54	Mohamed, H., Shaheen, B., Hosney, M., and Dawod, G.	629

	(**2015**) High-precision GPS monitoring of the land subsidence in the Nile Delta: Status and preliminary results, Regional Conference on Surveying and Development, Sharm El-Sheikh, Egypt, Oct. 3-6.	
55	Mirza, M. Dawod, G., Elzahrany, R., and Mirza, M. (**2015**) Building a historical GIS for the city of Makkah, Saudi Arabia, Regional Conference on Surveying and Development, Sharm El-Sheikh, Egypt, Oct. 3-6.	640
56	Dawod, G. (**2015**) The new Cairo capital mega development project from geodetic and environmental perspectives, Regional Conference on Surveying and Development, Sharm El-Sheikh, Egypt, Oct. 3-6.	654
57	Dawod, G., and Mandoer, M. (**2016**) Optimum sites for solar energy harvesting in Egypt based on multi-criteria GIS, The first Future University international conference on new energy and environmental engineering, April 11-14, Cairo, Egypt, pp. 450-456.	663
58	Al-Krargy, E., Mohamed, H., Hosny, M. and Dawod, G. (**2016**) A high-precision geoid for water resources management: A case study in Menofia governorate, Egypt, The International Conference on Research and Technology Development for Sustainable Water Resources Management (REDWARM), December 4-6, 2016, Cairo, Egypt	671
59	داود، ج، الغامدي، خالد، مندور، مسعد (٢٠١٧) تحديد أفضل المواقع لتجميع الطاقة الشمسية في منطقة مكة المكرمة الإدارية باستخدام نظم المعلومات الجغرافية متعددة المعايير، المؤتمر الحادي عشر لتطبيقات نظم المعلومات الجغرافية في المملكة العربية السعودية، جامعة الإمام عبد الرحمن بن فيصل، الدمام، ١١-١٣ أبريل.	684
60	Dawod, G. and Hosny, M. (**2017**) Toward a centimeter-geoid model for engineering surveying in Egypt: Status and undergoing activities, Journal of Scientific and Engineering Research, V. 4, No. 10, pp. 312-319.	696
61	Dawod, G. and Al-Ghamdi. K. (**2017**) Reliability of recent global digital elevation models for geomatics applications in Egypt and Saudi Arabia, Journal of Geographic Information System, V. 9, No. 6, pp. 685-698, Doi.org/10.4236/jgis.2017.96043	704
62	El Shouny, A., Al-Krargy, E., Mohamed, H. and Dawod,	718

	G. (**2018**) GIS-based accuracy assessment of global geopotential models: a case study of Egypt, American Journal of Geographic Information System, V.7, No. 4, pp.118-124. DOI: 10.5923/j.ajgis.20180704.03	
63	El-Quilish, M., El-Ashquer, M., Dawod, G., and El Fiky, G. (**2018**) Development and accuracy assessment of high-resolution digital elevation model using GIS approaches for the Nile delta region, Egypt, American Journal of Geographic Information System, V.7, No. 4, pp.107-117. DOI: 10.5923/j.ajgis.20180704.02	724
64	Dawod, G., Mohamed, H. and Al-Krargy, E. (**2019**) Accuracy Assessment of the PGM17 Global Geopotential Model: A Case Study of Egypt and Northeast Africa, Arabian Journal of Geosciences, V. 12, No. 7, DOI: https://doi.org/10.1007/s12517-019-4418-9.	736
65	Dawod, G., Mohamed, H. and Haggag, G. (**2019**) Relative and absolute sea level rise based on recent heterogeneous geospatial data: A case study in the Nile delta, Egypt, Journal of Scientific And Engineering Research, V. 6, No. 6 (July), pp. 55-64.	751
66	Dawod, G. and Abdel-Aziz, T. (**2019**) Utilization of geographically weighted regression in geoid modelling: A Cases Study of Egypt, Applied Geodesy, Published Online: Oct., 10, DOI: 10.1515/jag-2019-0009.	761
67	Abdel-Aziz, T., Dawod, G., and Ebaid, H., (**2020**) DEMs and reliable sea level rise risk monitoring in Nile Delta, Egypt, Discover Sustainability, V. 1, No. 1, DOI: 10.1007/s43621-020-00006-7	773
68	Al-Krargy, E. and Dawod, G. (**2021**) Optimum combinations of GGM and DEM models for precise national geoid development, Proceedings of Engineering and Technology Innovation, V. 18, pp. 15-24, DOI: https://doi.org/10.46604/peti.2021.6452	784
69	Dawod, G. and Ascoura, I. (**2021**) The Validity of open-source elevations for different topographic map scales and geomatics applications, Journal of Geographic Information System, V. 13, No. 2, pp.	793

	148-165	
69 B	Dawod, G. and Ascoura, I. (**2021**) La Validité des Élévations Open-Source pour Différentes Échelles de Cartes Topographiques et Applications Géomatiques, Bul. Soc. Geog. D'Egypte (BSGE), V. 94, No. 1, pp. 1-23.	812
70	Dawod, G. and Mohamed, H. (**2021**) Assessing ITRF Conversion Models for Kinematic GNSS Topographic Mapping in Coastal Areas: A Case Study in Egypt, Presented in the FIG e-Working Week 2021, June 21-25, The Netherlands.	835
71	Dawod, G., Ebaid, H., Haggag, G. and Al-Krargy, E. (**2021**) An integrated geomatics approach for projecting sea level variations and risks: A case study in the Nile Delta, Egypt, Journal of Architecture and Civil Engineering, V. 6, No. 8, pp. 24-38.	847
72	Abdallah, A., Agag, T., and Dawod, G. (**2021**) ITRF-Based Tectonic Coordinates Changes using GNSS-CORS Networks: A Case Study of Egypt, Surveying and Land Information Science, vol. 80, No. 2, pp. 69-78.	861
73	Dawod, G., Al-Krargy, E., and Amer, H. (**2022**), Accuracy assessment of horizontal and vertical datum transformations in small-areas GNSS surveys in Egypt, Journal of Research in Environmental and Earth Sciences, V. 8, No. 1, pp. 19-28.	872
74	Dawod, G. and Mohamed, H. (**2022**) GIS-based estimation of land subsidence impacts on water resources infrastructures: a case study in the Nile Delta, Egypt, Journal of Scientific and Engineering Research, V. 9, No. 3, pp. 83-90.	882
75	Dawod, G. and Amin, A. (**2022**) Enhancing vertical accuracy of global digital elevation models for coastal and environmental applications: A case study in Egypt, American Journal of Geographic Information System, V. 11, No. 1, pp. 1-8, doi:10.5923/j.ajgis.20221101.01	890
76	Dawod, G. and Mohamed, H. (**2022**) GIS-based geoid refinement by GNSS/Levelling data: A case study of	898

	Egypt, International Journal of Engineering Science Invention, V. 11, No. 2, pp. 25-32.	
77	Dawod, G., Amin, A. and Mohamed, H. (**2022**) Accuracy and applicability of GNSS PPP for GNSS surveys: A case study in the Nile Delta, Egypt, American Journal of Engineering Research, V. 11, No. 5, pp. 10-18.	906
78	Mohamed, H. and Dawod, G. (**2022**) Recent GNSS-based estimates of vertical land movements in the Nile Delta, Egypt over 2012-2019, Journal of Scientific and Engineering Research, V. 9, No. 4, pp. 7-16.	915
79	Dawod, G., Mohamed, H. and Haggag, G. (**2022**) Mean sea level and tides variations at Alexandria, Egypt over 1906-2020, Journal of Engineering Sciences, V. 50, No. 4, pp: 175-188, DOI: 10.21608/JESAUN.2022.114295.1105.	925
80	Dawod, G., Amin, A. and Haggag, G. (**2022**) Variations of sea levels and atmospheric elements along the Egyptian coasts over 2008-2020, Journal of Scientific and Engineering Sciences, V. 9, No. 5, pp: 85-100.	938
81	El-Quilish, M., El-Ashquer, M., Dawod, G., and El Fiky, G. (**2023**) Development of an Inundation Model for the Northern Coastal Zone of the Nile Delta Region, Egypt Using High-Resolution DEM, Arabian Journal for Science and Engineering, 48:601–614, DOI: 10.1007/s13369-022-07013-y	955
82	Dawod, G. and Ascoura, I (**2023**) The Validity of open-source elevations for different topographic map scales and geomatics applications in Egypt and Saudi Arabia, In: Turkman, M. [Ed.] Novel Perspectives of Geography, Environment and Earth Sciences Vol. 2, pp. 1-19, https://doi.org/10.9734/bpi/npgees/v2/17786D	969
83	Dawod, G., Al-Krargy, E., and Haggag, G. (**2023**) The Role of Geodetic Data Infrastructures (GDI: A case study in the Nile Delta, Egypt, International Research Journal of Earth Sciences, V. 11`, No. 1, pp. 1-6.	988
84	Dawod, G. and Al-Krargy, E. (2023) Recent high-order global geopotential models for geoid modelling in	994

	Egypt, Geophysica, V. 58 , No. 1, pp. 33–45.	
85	Dawod, G., Mohamed, H. and Amin, A. (**2023**) Monitoring vertical land movements in the Nile delta, Egypt By GNSS datasets over 2012-2023,Journnal of Scientific and Engineering Research, V .10, No.11, pp. 63-71.	1007
86	Dawod, G. and Haggag, G. (**2025**) Factors affecting the fitting of a global geopotential model to local geodetic datasets over local areas in Egypt using multiple linear regression approach, Journal of Applied Geodesy, https://doi.org/10.1515/jag-2024-0102	1016
87	Dawod, G. and Al-Krargy, E. (**2025**) Recent estimates of crustal deformation and land subsidence in the Nile delta, Egypt using GNSS-PPP datasets over 2012-2024, Applied Geodesy, https://doi.org/10.1515/jag-2025-0026	1025

Water Science Magazine, National Water Research Center,
No. 12, October 1992, pp. 10-12

A METHOD FOR DETECTING NO-CHECK OBSERVATIONS IN GPS NETWORKS

By

Eng. Gomaa M. Dawod*

ABSTRACT

The harmful impact of no-check observations in GPS networks is discussed. The concept of redundancy number as an indication of no-check observations is examined. A new method is proposed to detect these observation defects. The suggested algorithm is based on analyzing the least-squares adjustment results and, therefore, it could be easily included in any least-squares adjustment procedure without additional computations.

1. INTRODUCTION

With the high precision of GPS relative positions, effects of no-check observations are critical and must be considered. A no-check observation is that observation which is not checked by other observations in the network. An example of no-check observations is a sideshot observed only once. No-check observations can be thought of as observation defects in an observation campaign, i.e. the number and geometry of the observations are inadequate to estimate uniquely the network parameters.

* Survey Research Institute, National Water Research Center,
308 Al-Ahram street, Talbia, Giza 12111,Egypt

The hazard of this type of observation defects lies in two features: (1) a blunder detection algorithm will fail to detect any gross error in a no-check observation; (2) the uncertainties of the distant point of a no-check observation (the point that is not connected to the network) cannot be judged correctly even though this point might have small standard deviations. Moreover, gross errors in no-check observations will adversely affect the estimated coordinates of the network stations. Consequently, this type of observation defect must be detected and proper actions should be taken to overcome the danger effects of no-check observations. Such a procedure becomes a must in high precision GPS networks as far as the network quality is concerned.

2. IMPLEMENTATION OF REDUNDANCY NUMBERS

The quality of an observation is described by two measures. One is precision (the standard deviation is set up as a measure of precision), and the other is reliability. A redundancy number is used to judge the reliability of the adjustment of individual observations. To define the redundancy number mathematically, the cofactor matrix of the residual, Q_v, can be written as:

$$Q_v = Q_Y - Q_{AY} \qquad (1)$$

where Q_Y and Q_{AY} are the cofactor matrices of the observations and the adjusted observations respectively.

Equation (1) could be rewritten as:

$$Q_v = P^{-1} - A(A^T PA)^{-1} A^T \qquad (2)$$

where A is the design matrix, and P is the weight matrix.

Multiplying Q_v by P yields the so-called redundancy matrix:

$$R = Q_v P = I - A(A^T PA)^{-1} A^T P \qquad (3)$$

The matrix $[A(A^TPA)^{-1} A^T P]$ is an idempotent matrix (Pope 1976) i.e.,

$$[A(A^TPA)^{-1} A^TP] [A(A^TPA)^{-1} A^TP] = [A(A^TPA)^{-1} A^TP] \quad (4)$$

This implies that the redundancy matrix, R, is also idempotent. It is known (Koch 1988) that the trace of an idempotent matrix equals its rank. Therefore, the sum of the diagonal elements of the redundancy matrix can be written as:

$$\Sigma_{i=1}^{n} (r_i) = \text{trace}(R) = \text{rank}(R) = n-m \quad (5)$$

where n is the number of observations, m is the number of estimable parameters, and r_i is the i-th diagonal element of the redundancy matrix, i.e., r_i is the **redundancy number**. Since (n-m) is the degree of freedom, the redundancy number r_i reflects the contribution of the i-th observation to the total redundancy in the network (Milbert 1985).

It can be shown that (Leick 1990)

$$0 \leq r_i \leq 1 \quad (6)$$

Many investigators (e.g. Caspary 1987) find that the redundancy number of a no-check observation equals zero. Therefore, any gross error in this uncontrolled observation will be directly transferred to the estimated parameters. However, a more efficient algorithm for detecting no-check observations can be developed if we include some additional information about possible errors that might be present in the observations.

3. THE SUGGESTED METHOD FOR DETECTING NO-CHECK OBSERVATION

Concerning possible setup errors (those errors associated with setting up antennas relative to ground marks), a no-check observation will not reveal these errors in the residuals. This concept is the key for the proposed algorithm.

The residuals vector, V, can be written as:

$$V = [\ I - A(A^T PA)^{-1}\ A^T\ P\ ]\ Y \qquad (7)$$

Instead of using the usual observation equations model

$$Y = A\ X + \varepsilon \qquad (8)$$

we will use the model which is often used in hypothesis testing for outliers (Kok 1984):

$$Y = A\ X + B\ \tau + \varepsilon \qquad (9)$$

where τ is a vector containing the setup errors assumed to be present in the observations, B is a matrix of derivatives of the observations with respect to the assumed errors such that rank $[A\ B] \leq n$, and ε is the vector of random observational errors.

Substituting equation (9) in equation (7) and differentiating w.r.t the setup errors vector, τ, yields:

$$[\delta V/\delta\tau^T] = [\ I - A\ (A^T PA)^{-1}\ A^T\ P\ ]\ B \qquad (10)$$

With the concept that a no-check observation is characterized by "uncontrollable" setup errors, we can conclude that the submatrix of $[\delta V/\delta\tau^T]$ corresponding to a no-check observation will be zero.

After detecting no-check observations in a GPS networks, it is recommended that additional baselines are observed to provide some independent checks in this weak part of the network.

4. MERITS OF THE PROPOSED METHOD

The test for detecting no-check observations is carried out based on the computed matrix $[\delta V/\delta\tau^T]$, which is the product of two matrices: the redundancy matrix, R; and the matrix B. This fact gives the algorithm three advantages over the redundancy number concept. First, the test includes some other information, throughout the matrix B, about any possible setup error that might be present in the observations. The second advantage is that the matrix $[\delta V/\delta\tau^T]$ may contain some zero elements even if one of the two matrices (R and B) has non-zero elements on the diagonal. The third advantage of the new method is that $[\delta V/\delta\tau^T]$ reveals the influence of the off-diagonal elements of the redundancy matrix, R. Consequently, the suggested algorithm identifies no-check observations more efficiently.

5. SOME PRACTICAL CONSIDERATIONS

The matrix B, as appeared in equation 10, has 'n by d' size, where n is the number of observations, and d is the number of total possible setup errors which is three times the number of total stations occupations in the GPS campaign. It would not be appropriate to construct B with this relatively huge size. However, the test could be performed with some modifications considering the idea that the presence of setup errors in a GPS station will affect only those baselines that pass by this station and are observed in the same session. Therefore, the test may be carried out session by session and baseline by baseline. For each point in a baseline, n becomes the number of baselines connected to this point in the current session, and the number of possible setup errors, d, is always 3. This procedure reduces the size of the required matrices involved in the test (equation 10) and, hence, facilitate the test from a practical point of view.

6. CONCLUSIONS

No-check observations are due to lack of observations in a GPS observation campaign. This type of observation defects must be detected since no-check observations can dramatically decrease the quality of the results. Based on analyzing the least-squares adjustment results, a new

algorithm is developed to detect no-check observations. The method has some advantages over the redundancy number concept as far as the detection of no-check observations is concerned. The main advantage of the proposed algorithm is its simplicity which enables it to be easily integrated in any least-squares adjustment procedures without additional computations. Detecting observation defects could be thought of as an indicator for reliable GPS networks.

REFERENCES

Caspary, W., 1987, *Concepts of networks and deformation analysis,* Monograph No. 11, School of Surveying, University of New South Wales, Australia.

Koch, K-R., 1988, *Parameters estimation and hypothesis testing in linear models,* Springer-Verlag, New York.

Kok, J., 1984, *On data snooping and multiple outlier testing,* NOAA Technical Report NOS NGS 30, U.S. Department of Commerce.

Leick, A., 1990, *GPS Satellite Surveying*, John Wiley & Sons, Inc., New York.

Milbert, D., 1985, A note on observation decorrelation, variance of residuals, and redundancy numbers, *Bulletin Geodesique*, 59, pp. 71-80.

Pope, A., 1976, *The statistics of residuals and the detection of outliers,* NOAA Technical Report NOS 65 NGS 1, U.S. Department of Commerce.

Proceedings of the First National Conference on Land Reclamation and Development in Egypt, Minia University, Minia, Nov. 2-5, 1992, pp. 237-246

ON THE USE OF PSEUDO-KINEMATIC GPS SATELLITE POSITIONING TECHNOLOGY IN SURVEYING RECLAIMED LANDS IN EGYPT

GOMAA MOHAMED DAWOD

WATER RESEARCH CENTER
SURVEY RESEARCH INSTITUTE
308 AL_AHRAM St.
GIZA

Abstract

Planning, developing, and policy making of land reclamation require economical and accurate source of collecting spatial data to produce different types of maps. Advances in satellite positioning in the last years have focused attention on the use of the satellite-based GPS system for a wide range of applications. GPS techniques have been used world wide to acquire very precise positioning data in an economically suitable way. Of the various GPS observation methods, the pseudo-kinematic approach is considered to be more sensible in open areas. Due to specific characteristics of this GPS mode, it would be more productive and easy-to-use in surveying reclaimed lands. It is demonstrated that the precision of pseudo-kinematic GPS surveying could achieve the first order geodetic network specifications. An overview of the satellite-based GPS positioning is presented along with the advantages of the pseudo-kinematic GPS observation method. Based on results of surveying projects, it is proposed to use this advanced technology in mapping large areas of reclaimed lands in Egypt with high level of precision and with reduced costs.

1. Introduction

One of the most exciting aspects after any research and development stage is the actual implementation of the newly developed technology in novel ways where mankind can make potentially extensive use of it. It is a common belief world wide that the application of surveying with the satellite-based Global Positioning System (GPS) has reached this level. With the extensive use of GPS data all over the world, with Egypt being no exception, the increased productivity and superior precision that

had not been economically available prior to GPS have been demonstrated. Increases in productivity of a factor of six over conventional terrestrial surveying techniques have been shown (Goad 1989).

The NAVSTAR (Navigation Satellite Time And Ranging) Global Positioning System (GPS) is a satellite-based positioning system currently under development by the U.S Department of Defense (DoD). In its final constellation (by the end 1993), the GPS may consist of 21 operational satellites plus 3 in-orbit spares. Once fully operational, GPS will provide 24-hour all-weather navigation and positioning capabilities any part of the world. There are more than six different observation techniques to collect and process GPS data (Kleusberg 1990). The classic GPS observation approach is the static mode in which more then one receiver are kept fixed over ground stations and record satellite signals for more then one hour of observations. of the different GPS observation techniques, the Pseudo-Kinematic (or semi-kinematic) mode is now within grasp. The idea is to have one GPS receiver moving from one station to another while another receiver is not moving and therefore providing a reference to location determination. Because of some observation difficulties (details in section 3), the pseudo-kinematic GPS surveying technique becomes more practical, easy-to-use, and economically suitable system in open areas. In agricultural and reclaimed lands, this mode of the GPS technology gains more popularity. Studies show that accuracy of 1 part per million (i-e., 1 mm error in a 1-Km distance length) could be achieved in a production environment (Remondi 1985).

This paper demonstrates the applications of the GPS surveying technology especially for the agricultural and reclamation community. The paper proposes the use of the pseudo-kinematic GPS technique in surveying the new reclaimed lands citing the advantages of this mode in gaining high precision positioning and mapping data in a matter of few hours rather than few weeks as in the traditional surveying techniques. An overview of the GPS system is provided in section two. Section three gives a simple idea about the technical problems in using the pseudo-kinematic approach in urban areas and why it would be more applicable in open lands. Results of previous studies are shown in section four with some numerical tables about the expected accuracies of the pseudo-kinematic GPS technique. Section five concludes the paper and provides some recommendations about the use of this satellite-based advanced technology in the agricultural and reclamation environment in Egypt.

2. Global Positioning System (GPS)

Since the early 1980s, many geodetic networks have been established using GPS measurements to provide baseline vector components at or better than 1 part per million (ppm) level of precision (Goad 1985, Remondi 1985). With this high precision, accurate maps could be produced and used in many development stages

and policy making process. Each of the 21 GPS satellites continuously transmits at two frequencies: L1=1575.42 MHz; and L2=1227.060 MHz modulated with two types of code and with a navigation message. The L1 signal is modulated with a precise (P) code, and a Coarse Acquisition (C/A) code, which is known as the Standard Positioning Service (SPS); the L2 signal is modulated with only the P code, which is known as the Precise Positioning Services (PPS). The P code is 10 times more precise than the C/A code (Spilker 1978). For national security purposes, the U.S DoD may restrict access of the PPS only for military users. The 50 Hz navigation message contains, among other data, the broadcast satellites coordinates parameters so that the ground receivers consider the satellites as " fixed targets " in the sky. With this description in mind, the GPS can be thought of as a "space-triangulation " techniques which revolutionizes the surveying concepts. No visibility between ground stations is required, no atmospheric-dependant restrictions are included, and no personal interface is needed. Observing these advantages, the GPS has been used all over the world for a wide range of civil applications (Fig. 1).

Cadastral Surveying Geodetic Network identification High precision aircraft positioning Photogrammetry without ground control Monitoring deformation Hydrographic Surveys	World Wide GPS	Navigation on land Navigation on seas Navigation in rivers Resources management GIS/LIS Kinematic Surveys

Figure 1: Some Civil GPS Applications

There are two types of GPS observations: pseudo ranges and carrier phases. The pseudo range is a measure of the distance between the satellite and the receiver at the epochs of transmission and reception of the signals. In high-precision surveying the carrier phase observations are used. The phase observable is complicated and involves advanced techniques in electronics. However, we have to understand the basic concepts in using the phase mathematical model in order to infer the potential advantages of the pseudo-kinematic mode which will be presented in section 3. In a simplified expression (neglecting satellite clock errors, receiver clock errors, and tropospheric and ionospheric effects) the phase equation can be written as (Leick 1990):

$$\phi^p_k = \phi^p(t) - \phi_k(t) + N^p_k + \text{noise} \qquad (1)$$

where ϕ^p_k is the phase observables in units of cycles for satellite p and receiver k, $\phi^p(t)$ is the received phase of satellite p as measured at the receiver k, and $\phi_k(t)$ denotes the receiver oscillator phase. The constant term indicates N^p_k an integer ambiguity unknown parameter of the first epoch of measurements. The four

unknowns in a typical GPS adjustment process are the three station coordinates (X, Y, and Z) and the receiver clock correction. Consequently, at least four GPS satellites must be tracked simultaneously. But, more than four satellites are desired to increase the redundancy and reliability of the estimation process.

3. Pseudo-Kinematic GPS Technique

The surveying techniques used to collect GPS observations can be divided, in general, into three categories: static; kinematic; and pseudo-kinematic (Dawod 1991). In this paper, the pseudo-kinematic mode is given more emphasis. Pseudo- (or Semi-) kinematic surveying is tracked back to the pioneering work of Remondi (1985 and 1988), where one receiver is kept fixed over a known station while another receiver moves to survey other stations for few minutes of observations at each site. The two main sources of troubles in GPS phase observations are the phase ambiguity and the cycle slip. The phase ambiguity unknowns (one per each satellite) are the constant term N^p_k that appears in equation 1. Some mathematical procedures are used to estimate these unknowns, with the result that unambiguous rang measurements are processed in order to increase the precision of the station position determination (for more details, the interested reader can refer to, for example, Goad and Mueller 1988 and Schaffrin and Bock 1988). The second observation-dependant problem is the so-called "cycle-slip". In simple words this critical situation occurs when the satellite signals are blocked by some obstructions, for example trees or buildings, and when the receivers re-record the signals, the phase ambiguity takes on a new unknown value. Cycle slips can be considered as the main restriction for using pseudo-kinematic GPS technique in urban areas due to the huge number of expected obstructions.

With the current constellation of the GPS satellites, four satellites can be observed in Egypt for eighteen hours while a five-satellite window is available for about 5 hours each day (Fig. 2). Concerning the cycle slip restriction, it is clear that this is not a problem at all in open areas such as agricultural and newly-reclaimed lands. That is the main advantage of using the pseudo-kinematic approach in obtaining high-precision geodetic positioning information about large open areas. The output of GPS surveying could be:

Cartesian coordinates of ground marks (X, Y, and Z)
Geographic coordinates (latitude, longitude, and height)
which could be used to produce :

Topographic maps
Contour maps
Digital data bases
Base maps for a Land Information System (LIS)
Reference frame for a Geographic Information System (GIS)

Figure 2: Approximate GPS satellites Window in Egypt for January 1992

4. Results of Pseudo-Kinematic Surveys

The pseudo-kinematic GPS technique has been used in many production projects in the last few years. Because of the specific characteristics of this mode of satellite positioning, most of the surveys have been carried out in open areas with no obstructions. e.g. airports and dams. Many studies show that the precision of first order geodetic networks could be achieved, in lees time and reduced costs, with the pseudo- kinematic GPS technology.

Goad (1989) concludes that the results of a comparison between the static and pseudo-kinematic GPS approaches are better than 1 ppm over relatively short base lines. Table 1 shows that the largest difference in repeatability was 10 mm, with 5 mm or less being more typical.

Table 1: Comparison between static and pseudo-kinematic GPS surveys

Base Line	dx (m)	dy (m)	dz (m)	Distance (m)
A-B	355.079 355.074	126.428 126.426	-305.280 -305.286	485.037 485.037
B-C	365.674 365.684	56.560 56.562	-305.761 -305.754	479.986 479.982
C-D	458.894 458.884	70.984 70.979	-308.012 -308.015	600.026 600.020

Another study over relatively long base lines was reported by Minkel (1989). Table 2 summarizes the differences between the vector components as derived from pseudo-kinematic and static GPS solutions over long base lines along with their root mean square error (rms).

Table 2: Results of Long Base Lines pseudo-kinematic GPS survey: Component Differences in meters

Base line	Distance (Km)	DDX	DDY	DDZ	RMS
A-B	54.4	0.012	-0.027	0.029	0.041
A-C	46.8	0.016	-0.027	0.064	0.076

Both surveys' results have verified that the pseudo-kinematic could achieve centimeter level accuracy over traversing chains up to few tens of kilometers.

5. Conclusions

One of the main factor in the future of land reclamation and development is the accuracy and costs of providing maps and spatial information. Satellite-based GPS positioning technology has been used in Egypt for an extensive amount of surveying, mapping, and natural resources applications. The pseudo-kinematic GPS technique is an easy-to-use, automatic, time-saving, cost-reducing, and accurate surveying method. When fully operation, GPS will provide 24-hour, all-weather positioning technology that will be a very helpful tool in developed areas. The pseudo-kinematic mode of GPS surveying has been used to obtain high precision spatial information and accurate maps especially in open areas such as reclaimed lands. Within few hours of observation, geodetic positions in a large piece of land could be determined accurately and with a great deal of cost reduction than the traditional surveying methods. Having accurate and complete set of spatial data about the lands, the policy making and planning processes could be benefit a lot.

References

Dawod, G., 1991, Some considerations in the adjustment of GPS-derived base lines in the network mode, MSc Thesis, Geodetic Science and Surveying department, The Ohio State University, Columbus, Ohio, USA.

Goad, C., 1985, Precise relative positioning with the GPS, Proceedings of the First International Symposium on Precise Positioning with the Global Positioning System, Volume II, April 15-19, 1985, Rockville, Maryland, USA, pp.347-356.

Goad, C. Mueller, A., 1989, An automated procedure for generating an optimum set of independent double difference observables using Global Positioning System carrier phase measurements, Manuscripta Geodaetica, 13, pp. 365-369.

Goad, C., 1989, Kinematic survey of Clinton Lake dam, ASCE Journal of Surveying Engineering, 115, No. 1, pp.67-77.

Kleusberg, A., 1990, A review of kinematic and static surveying procedures, Proceedings of the Second International Symposium on Precise Positioning with the Global Positioning System, September 3-7, 1990, Ottawa, Canada, pp. 1102-1113.

Leick, A., 1990, GPS satellite surveying, John Wiley & Sons, Inc., New York.

Minkel, D., 1989, Demonstration and discussion of the pseudo-kinematic method, Proceedings of the Fifth International Geodetic Symposium on Satellite Positioning, March 13-17, 1989, New Mexico, USA, pp. 577-588.

Remondi, B., 1985, Performing centimeter accuracy relative surveys in seconds with GPS carrier phase, Proceedings of the First International Symposium on Precise Positioning with the Global Positioning System, Volume II, April 15-19, 1985, Rockville, Maryland, USA, pp.789-797.

Remondi, B., 1988, Kinematic and pseudo-kinematic GPS, Paper presented at the ION GPS-88 in Colorado Springs, Colorado, USA.

Schaffrin, B., Bock, Y., 1988, A unified scheme for processing GPS dual-band phase observations, Bull. Geod., 62, pp. 142-160.

Spilker, J., 1978, GPS signal structure and performance characteristics, in GPS papers in navigation, reprinted by the U.S. Institute of Navigation, Volume I, 1980, pp.29-54.

https://www.ion.org/publications/abstract.cfm?articleID=4346

Title:	Recovering Orthometric Height Differences from GPS Data and Geopotential Models
Author(s):	Gomaa Dawod and Mona El-Kady
Published in:	Proceedings of the 6th International Technical Meeting of the Satellite Division of The Institute of Navigation (ION GPS 1993) September 22 - 24, 1993 Salt Palace Convention Center Salt Lake City, UT
Pages:	1089 - 1089
Cite this article:	Dawod, Gomaa, El-Kady, Mona, "Recovering Orthometric Height Differences from GPS Data and Geopotential Models," *Proceedings of the 6th International Technical Meeting of the Satellite Division of The Institute of Navigation (ION GPS 1993)*, Salt Lake City, UT, September 1993, pp. 1089-1089.
Full Paper:	ION Members/Non-Members: 1 Download Credit Sign In
Abstract:	Determining orthometric heights is required for most engineering projects. In order to convert the ellipsoidal heights obtained from GPS observations to orthometric heights, some knowledge of the geoidal undulations is needed. The use of the spherical harmonic geopotential models can be a time saving and cost-effective tool to perform this task. Using the OSU9 1 A geopotential model, a strategy is presented to transform the GPS-derived geodetic height differences to orthometric height differences. The method is used to perform a regression analysis to fit the computed undulation differences (of points having both geodetic and orthometric heights) over the area of interest, in order to obtain a mathematical model that is a function of geographic coordinates. The predicted undulation differences are then added to the GPS height differences to compute orthometric height differences. A data set in Egypt is used to test the proposed technique. The obtained results show an average error value of 8 cm for orthometric height differences. This error magnitude may be suitable for densification purposes, particularly for resource management in such areas where sufficient precise leveling is unavailable.

© 2013 The Institute of Navigation

Proceedings of the first international conference on satellite positioning systems, Alexandria, December 12-13, 1995.

INCREASING THE RELIABILITY OF GPS GEODETIC NETWORKS

By

Dr. Dalal S. Alnaggar [1] Eng. Gomaa M. Dawod [2]

ABSTRACT

The use of outlier detection is an important step in the statistical analysis of precise GPS surveys. A special GPS adjustment program was developed with a built-in automatic outlier detector which utilizes the τ (TAU) statistical test. Using a 20-station GPS network, the developed program was examined and the quality of outlier detection was investigated. Significant improvements were obtained after identifying and removing erroneous observations. Standard deviations of the station coordinates were in the range of millimeters.

1. INTRODUCTION

Precise measurements, such as the Global Positioning System (GPS) satellite positioning data, require a careful screening of the field data to detect and identify those observations that may have been affected by gross errors. Including these erroneous observations in the computation process may significantly affect the final results and may give misleading interpretations. Also, it is a matter of fact that gross errors are not avoidable in measurements. Consequently, detecting outliers in high-precision GPS surveys becomes a must.

A great deal of research has been carried out in past years on the development of statistical and numerical techniques to detect outliers in precise engineering measurements. Barada (1968) and Pope (1976) are examples of such researches in geodesy. El-Hakim (1981) provides applications in photogrammetry. However, not much research has focused

---

١ Director of the Survey Research Institute, National Center for Water Researches, 308 Al-Ahram St., Giza 12111, Egypt.

٢ Assistant Researcher, the Survey Research Institute.

on the applications of outliers identification in GPS data which posses special characteristics.

The main objective of this study was to design an efficient computer program that adjusts GPS networks and, during each iteration, checks for the presence of outliers and identifies them. The wide use of GPS data within the Survey Research Institute (SRI) activities has made this task very important in order to obtain reliable results.

Section Two of this paper presents an overview of the statistical theory behind outliers identification. The developed computer program is described in section Three. Section Four demonstrates the obtained results and the improvements in a small GPS network that was carried out by SRI. Concluding remarks are given in section Five.

2. STATISTICAL TESTS FOR OUTLIERS DETECTION

Gross errors may be defined as the results of a malfunctioning of either the instrument, or the surveyor. It is naturally expected that outliers are caused by gross errors. But, what is an outlier?. Caspary (1987) defines an outlier as " a residual which, according to some test rule, is in contradiction to assumptions on the stochastic properties of the residuals". Therefore, the detection of outliers depends on the selected risk level, the assumed distribution, and the test procedure.

Generally, the methods used in identifying outliers may be grouped according to two basic concepts of modeling the outliers (Chen et al. 1987):

(i) outliers have a mean shift model with the distribution of $N(\mu+\delta,\sigma^2)$ instead of $N(\mu,\sigma^2)$ where μ is the expectation, σ^2 is the variance, and δ is the mean shift value.

(ii) outliers come from a variance inflation model with the distribution $N(\mu,a^2\sigma^2)$ where $a^2>1$.

Barada (1968) follows the first concept and develops the so-called data-snooping method under the assumption that the a priori standard error of unit weight (σ_o) is known. Pope (1976) presents another test strategy considering σo to be unknown in practice, but its a posterior estimate ($\sigma\wedge_o$) is available. Krarup et al (1980) prefer the second concept and develop a strategy based on the idea that large residuals indicate less accurate observations and they use an iterative method for reweighting the observations. Pope's method was used in this study in detecting outliers in GPS data.

In the least squares adjustment of full rank observation equations

$$A\ X + L = \varepsilon \tag{1}$$

where,

$$L \sim N\ (\ AX\ ,\ \sigma^2_o\ \Sigma\ ) \tag{2}$$

$$\varepsilon \sim N\ (\ 0\ ,\ \sigma^2_o\ \Sigma\ ) \tag{3}$$

the nx1 vector L represents the observations, the nxn matrix A is the design matrix, X is the mx1 vector of unknowns, $\Sigma = \sigma^2_o\ P^{-1}$ is the nxn covariance matrix of the observations, P is the nxn weight matrix, ε is the nx1 vector of observation errors, n is the number of observations, and m is the number of unknown parameters.

After the adjustment, the residuals and their estimated covariance matrix are:

$$V = [\ I - A\ (A^T\ P\ A\ )^{-1}\ A^T\ P\ ]\ L \tag{4}$$

$$\Sigma^{\wedge}_V = [\ P^{-1} - A\ (A^T\ P\ A)^{-1}\ A^T\ ]\ \sigma^{\wedge 2}_o \tag{5}$$

Instead of the residual (V), another quantity

V' = normalized (or standardized) residual = $|V| / \sigma_v$

is used in the test statistics of the i-th observation:

$$T_i = \frac{|V|}{\sigma_v} \sim \tau(f) \tag{6}$$

using the τ (tau) distribution with f degrees of freedom.

Pope (1976) provides an algorithm which computes the critical τ value. Tables of the τ distribution are also given. Although the τ-distribution is used in geodetic applications, it is not found in some statistical literature. However, it should be stated that the τ distribution can be transformed from the known Student's t-distribution.

Some characteristics of the τ distribution are (Patterson 1985):

1- The population mean is zero.
2- The variance is unity for all degrees of freedom.
3- The τ distribution coverages is distribution to N(0,1).
4- The τ distribution has finite limits.
5- For high degrees of freedom the τ distribution is greatly resemble the normal distribution.
6- Due to property 4, the τ distribution differs markedly from the normal distribution for low degrees of freedom.

The null hypothesis of the τ-test assumes that all observations are normally distributed with E(L) = AX, so that the expectation of the residuals is zero:

$$Ho : E(V_i) = 0 \quad (7)$$

The alternative hypothesis is:

$$Ha : E(V_i) \neq 0 \text{ for one residual.} \quad (8)$$

Ho is rejected for a residual V_j, if

$$Tj = \frac{|V_j|}{\sigma_{Vj}} > \tau_{\alpha,f} \quad (9)$$

for a certain type I error percentile (α).
From the above methodology, it can be said that the use of normalized residuals is much more meaningful than the use of the residuals themselves. If a residual (even with small magnitude) is much larger than its standard deviation, then it is likely that the corresponding observation is an outlier.

3. THE DEVELOPED ADJUSTMENT PROGRAM

One of the most important characteristic of assessing adjustment programs is how the program deals with possible numerical problems that sometimes may arise from the algorithm used to reduce, solve, and invert the system of normal equations. In this regard, the developed adjustment program (NADO: Network Adjustment and Detecting Outliers) possesses several properties that make it an efficient program.

The program utilizes the inner constraint technique, known also as free

network adjustment, in order to detect the internal precision and consistency of the field observations. For GPS networks, it is essential to define only an origin for the (WGS-84) datum since the orientation and scale are implicitly known from the phase observables because the coordinates of the GPS satellites are assumed to be known. Consequently, to overcome the (three) expected datum defects, one station is held fiducial to its coordinates deduced from the observations (i.e., in the WGS84 coordinate system). By this method, problems due to errors in the coordinates of fixed stations are avoided.

When solving the normal equations system, NADO implements the concept of observation equations with weighted parameters which can be found in details in several adjustment texts (e.g. Uotila 1986, pp. 104). Dawod (1991, pp. 32) demonstrates that this method is just a simplified least-squares adjustment in the Gauss-Markoff model with pseudo observations (i.e., the prior information about the coordinates of the fiducial station).

Inverting the normal equation matrix (N=ATPA) requires a rigorously stable algorithm to remove numerical problems. The Cholesky factorization algorithm is employed in the developed program and hence makes the solution three times faster than any other similar inversion procedure (Press et al. 1989). The normal equation matrix, N, is decomposed to the product of a lower triangular matrix, S, and its transpose:

$$N = S\,S^{T} \tag{10}$$

The inverse of N could be written as

$$N^{-1} = (S\,S^{T})^{-1} = (S^{T})^{-1}\,S^{-1} = (S^{-1})^{T}\,S^{-1} \tag{11}$$

To invert the lower triangular matrix, S, less execution time is required when compared to the inversion of the full matrix N.

Another advantage of the Cholesky factorization algorithm is that it reveals the defects in the normal equation matrix. The number of generated zeros on the diagonal represents the number of defects. This property is important in detecting outliers and removing observations because the removed observations might create observational defects in the network. This case happened in one of the iterations explained in section Four. In such situations, NADO informs the user about the locations of the new defects in the normal equation matrix. Therefore, singularities are properly handled by not solving for the unknowns causing those singularities.

Considering the covariance matrix of the observations, Σ, is a diagonal matrix, both the (A^TPA) matrix and the (A^TPL) vector can be formed by summing or accumulating the contribution of the observations one by one. Therefore, there is no need to store the full A(nxm), Σ(nxn), or L(nx1) in the computer memory. This concept is used in the developed program in order to reduce the required computer memory and, hence, adjust larger GPS networks in a PC environment.

NADO also converts the estimated parameters, i.e., the Cartesian coordinates of the network stations, to a geodetic coordinate system (latitude, longitude, and height) along with their covariance matrices.

For detecting outliers, the program uses equation 6. Normalized residuals are computed for each GPS vector component. Each base line therefore has 3 normalized residuals, one for each of its 3 components. The largest value is compared against the computed critical τ value using a risk level of 5%. Equation 9 is then used to flag outlying observations. The structure of the program is depicted in Figure 1.

4. RESULTS AND ANALYSIS

A small GPS network was examined from the point of view of detecting outliers in GPS networks, where coordinate differences from individual base line processing are used as observables in a network configuration. The project is a 20-station GPS network designed and observed by SRI in 1992 (Fig. 2). The main purpose of the project was to establish a control GPS network in Aswan area and around lake Nasser for crustal movement monitoring. The network covers an area extending approximately 50 Km in the north-south direction and a width ranging from 2 to 10 Km. The network was observed with 5 Trimble GPS receivers, two of them are dual-frequency receivers.

After processing the raw GPS phase observations, 55 fixed solutions were obtained and used as observables for the developed adjustment program. Therefore, the number of observations in the first adjustment was 165 with 108 degrees of freedom. The relatively large estimated standard deviation of unit weight may be thought of as a global indicator that the observations may be contaminated by gross errors. Applying the built-in subroutine for detecting outliers shows that 11 base lines are flagged as candidate outliers. In the subroutine, 5% type I error was used. Results of the initial adjustment are shown in table 1.

Table 1
Results of the First Adjustment

Number of base lines	55
Number of observations	165
Number of stations	20
Number of unknowns	60
Degrees of freedom	108
Estimated $\hat{\sigma}^2_o$	19.2
Critical τ value	3.52
Flagged outliers	11

Based on these results, it was decided to delete only the base line that had the largest normalized residual. Most of the literature dealing with outlier detection stressed that any algorithm should not be used as a black box which automatically cleans the observations. This warning may be explained when we remember the original assumptions behind the τ -test for outlier detection: (1) all observations are normally distributed; and more important (2) only one outlier is assumed to be present in the data set. Consequently, the whole theory breaks down if the observations include two or more gross errors.

The following rational approach is followed in order to obtain as much correct results as possible:

* Initial adjustment is carried out using all observations.
* If more than one normalized residual exceed the critical τ value, only the base line with the largest normalized residual is deleted.
* The adjustment is repeated again with n-3 observations leading to new residuals and new $\hat{\sigma}^2_o$
* This process is repeated until all outliers are flagged.

Applying this methodology, 13 different adjustments were carried out. Results of the last two adjustment are shown in table 2.

Table 2
Results of the Last Two Adjustments

	Adjustment 12	Adjustment 13
No. of Observations	102	99
No. of Base Lines	34	33
Degrees of Freedom	45	42
Estimated $\hat{\sigma}^2_o$	1.299	0.483
No. of Outliers	4	1

Although four outliers were flagged in the iteration 12, it was decided to accept its results as the optimum. Two reasons may legitimize that acceptance: (1) the estimated standard deviation of unit weight of iteration 13 goes below one; and (2) the last GPS base line deleted in iteration 13 creates a new observation defect because it was the only remaining base line connecting station 18 to the rest of the network. NADO is capable of detecting any new observation defects after fixing the datum. This is done by observing singularities (i.e., zeros on the diagonal) when inverting the lower triangular matrix, S, of the Cholesky factorization algorithm. This property is very important and should be applied in any adjustment program. NADO displays on screen the locations of the newly created defects in an interactive mode with the user. Therefore, the results of adjustment 12 were accepted as final for the GPS network stations to avoid additional observations.

In order to investigate the improvements in the estimated parameters, a comparison is carried out between the results of the first and the twelfth adjustments. Some results are given in table 3. Significant improvements in terms of the estimated standard deviations of the station coordinates are clearly visible after removing outliers. Standard deviations of the stations coordinates are in the range of millimeters.

Table 3
Improvements After Detection Outliers

Adj.	St.	X	Y	Z
1 12	2	4896330.813±0.091 30.822±0.008	3167453.249±0.096 53.231±0.009	2575259.755±0.101 59.752±0.009
1 12	3	4900749.351±0.080 49.353±0.008	3165047.939±0.107 47.921±0.011	2569831.582±0.125 31.549±0.013
1 12	4	4899907.405±0.123 07.358±0.024	3164614.389±0.089 14.384±0.017	2571940.935±0.085 40.925±0.016
1 12	5	4899546.297±0.078 46.303±0.010	3166777.201±0.103 77.204±0.013	2569984.087±0.125 84.204±0.016

5. CONCLUSIONS

Significant consideration has been given to the detection of outliers in the field of precise surveys. The τ-test, among other statistical tests, offers statistical tools used to identify those erroneous observations that may be contaminated by gross errors. Using the τ criteria, a special GPS adjustment program with a built-in subroutine for outlier detection was developed. A GPS network that was carried out by SRI in 1992 was used to examine the new program. The program shows efficiency in solving the system of normal equations and identifying suspected observations.

The τ test is based on the assumption that only one outlier is present in the data set. A difficulty with this procedure is encountered when two or more observations are flagged as outliers. The approach used in this study was to delete the observation that has the largest normalized residual in each iteration. Then, the adjustment is repeated with n-3 observations leading to new residuals. Because of the assumption behind the τ test, it is emphasized that only one observation is deleted every time the adjustment is repeated. It is also stressed that any outlier detection algorithm should be used in an interactive way with the user and not in an automatic mode of cleaning the observations.

In the GPS network used in this study, 13 different adjustments were

carried out. Even having four remaining outliers, iteration 12 was accepted as the final step because deleting any new outlier will create observation defects and cause some stations to be disabled from the network. It was accepted to avoid having to obtain new observations. A comparison between the first and last adjustments shows significant improvements in the estimated parameters after detecting and removing outliers. Millimeter level standard deviations of the stations coordinates were obtained after identifying outlying observations. It is recommended that outlier detection procedures should be implemented in the adjustment of precise GPS surveys in order to obtain reliable results and proper interpretations.

LIST OF REFERENCES

Barada, W., 1968, A testing procedure for use in geodetic networks, Publications on Geodesy, New Series, Netherlands Geodetic Commission, V. 2, N. 5, Delft, The Netherlands.

Caspary, W., 1987, Concepts of networks and deformation analysis, Monograph No. 11, School of Surveying, University of New South Wales, Australia.

Chen, Y., Kavouras, M., Chrzanowski, A., 1987, A strategy for detection of outlying observations in measurements of high precision, The Canadian Surveyor, V. 41, N. 4, pp. 529-540.

Dawod, G., 1991, Some considerations in the adjustment of GPS-derived base lines in the network mode, MSC thesis, Department of Geodetic Science and Surveying, The Ohio State University, Ohio, USA.

El-Hakim, S., 1981, A practical study of gross-error detection in bundle adjustment, The Canadian Surveyor, V. 35, N. 4, pp. 373-386.

Krarup, T., Kubik, T., Juhl, J., 1980, Gotterdammerung over least squares adjustment, International Archives of Photogrammetry, V. XXIII, Part B3, Commission III, ISP, Hamburg, pp. 369-378.

Patterson, R., 1985, Outlier detection: Some distribution theory, Australian Journal of Geodesy, Photogrammetry, and Surveying, N. 43, pp. 1-30.

Pope, A, 1976, The statistics of residuals and the detection of outliers, NOAA Technical Report NOS 65 NGS 1, U.S. Department of Commerce, Washington, D.C., USA.

Press, W., Flannery, B., Teukolsky, S., Vetterling, W., 1989, Numerical recipes: The art of scientific computing, Cambridge University Press.

Uotila, U., 1986, Notes on adjustment computations: Part I, Lecture notes, Department of Geodetic Science and Surveying, The Ohio State University, Ohio, USA.

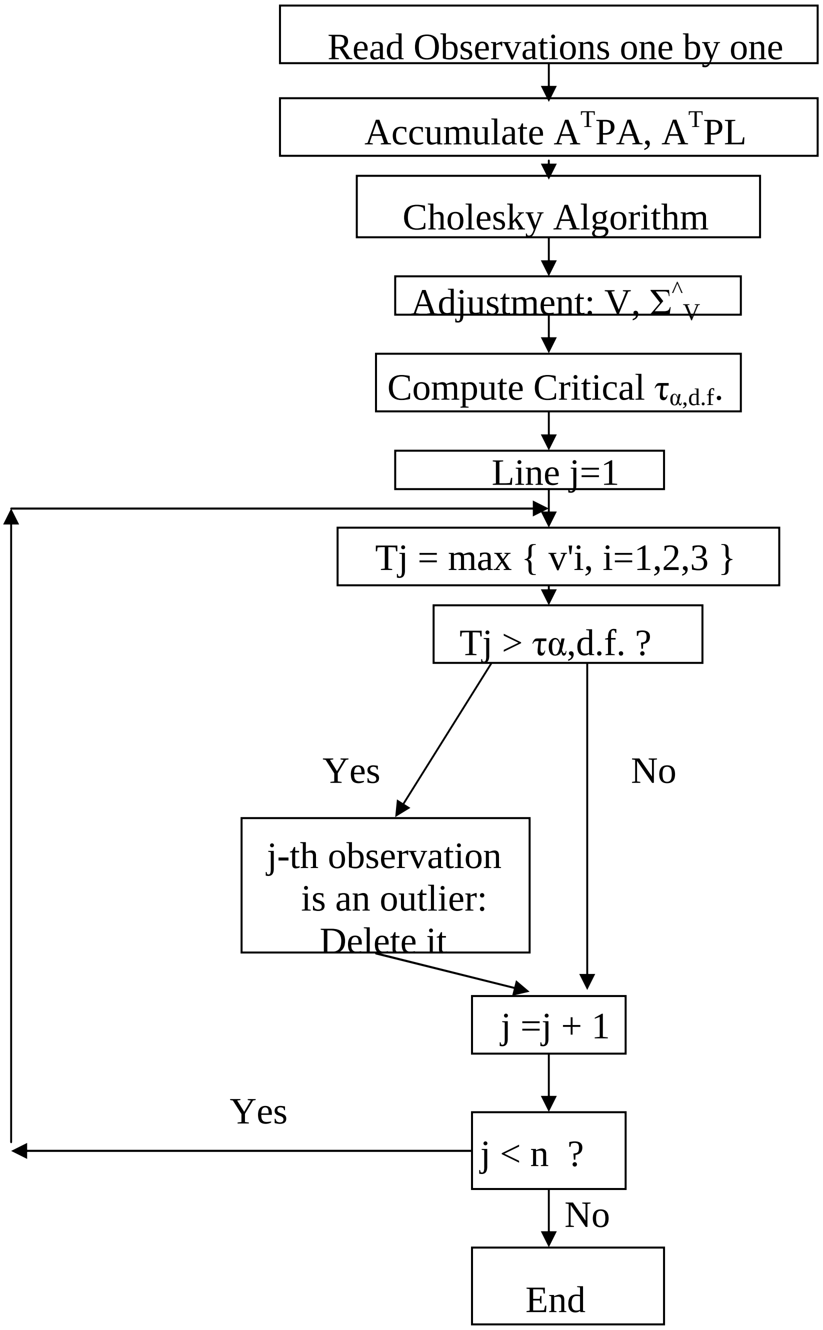

Fig. 1
Structure of the Developed Program

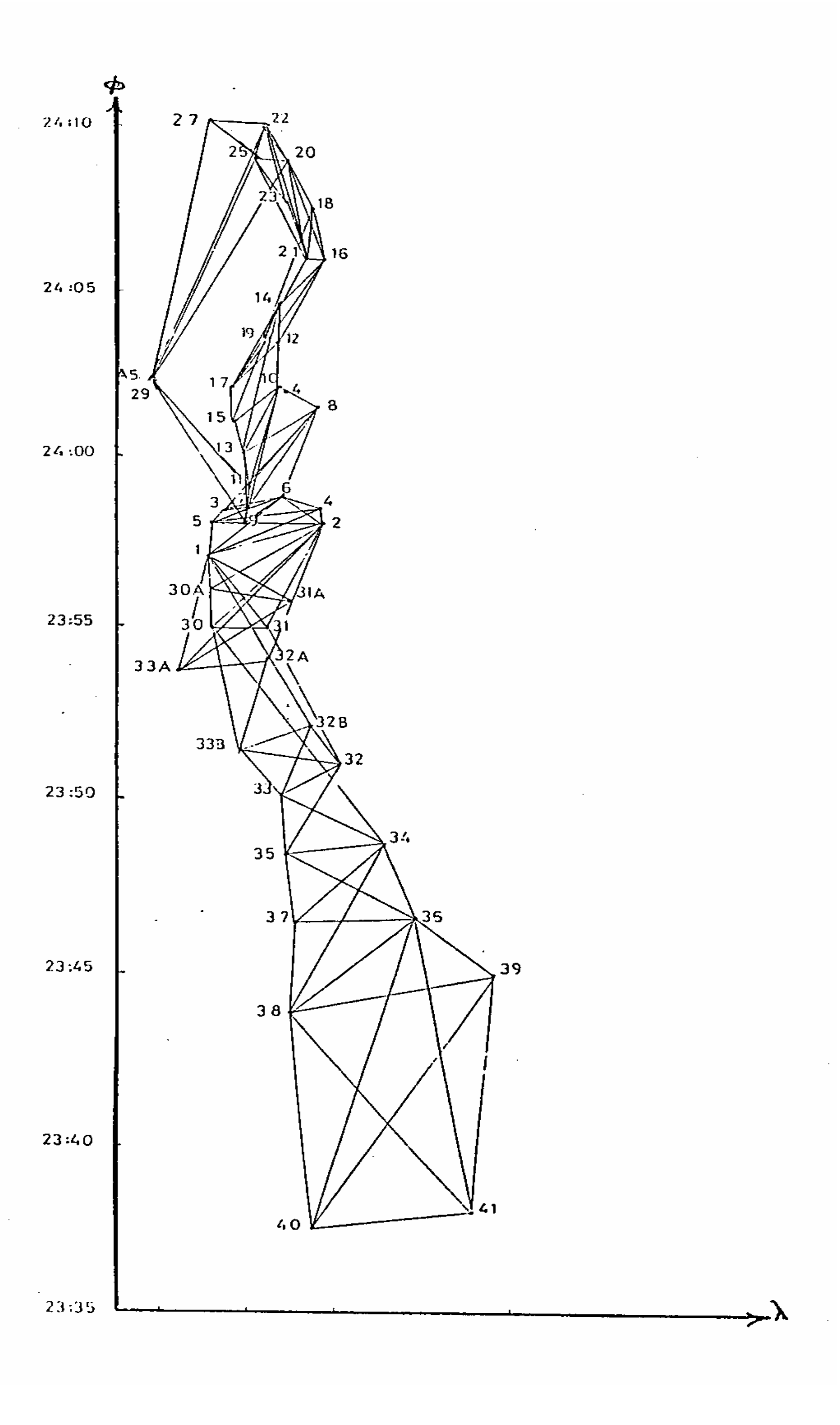

Fig 2
The GPS Network

No. 5

Alnaggar, D., and Dawod, G., **1995**, Potential of GPS observations in the Egyptian National Gravity Standardization Network (ENGSN97) for geoid determination and associated comparisons, Proceedings of Al-Azhar Engineering Fourth International Conference, Cairo, December 16-19, Volume 4, pp. 341-353.

Unfortunately, this article's source is missing right now !!

No. 6

Alnaggar, D., and Dawod, G., **1997**, The use of high-precision gravity data for detecting groundwater resources in the southern valley, Egypt, Presented in the International Water Resources Association (IWRA) Conference, Montreal, Canada, Sept. 1-6.

Unfortunately, this article's source is missing right now !!

No. 7

Dawod, G., and Alnaggar, D., **1997**, Performance of relative gravity meters and processing software over the new absolute gravity stations in Egypt, Proceedings of Al-Azhar Engineering Fifth International Conference, Cairo, December 19-22, Volume 5, pp. 113-125.

Unfortunately, this article's source is missing right now !!

1st International Conference of Civil Engineering Science, ICCES1, Assiut University , Volume 2, pp. 238-245, October 7-8, 2003

EFFICIENCY OF NEW SOLUTIONS FOR SURVEYING AND MAPPING PROBLEMS IN INTEGRATED WATER RESOURCES MANAGEMENT

Gomaa M. Dawod[1], and Moustafa S. El-Sammany[2]

[1] Survey Research Institute, National Water Research Center, Cairo, Egypt.
[2] Nile Research Institute, National Water Research Center, Cairo, Egypt.

ABSTRACT

Maps play a vital role in the overall framework of the undergoing integrated water resources management in Egypt. Satellite-based technologies, especially GPS, have been utilized exclusively in the last two decades as positional data collection tools for a wide variety of water resources national applications. Neglecting the complicated geodetic datum transformation computational process, the collected positions will be biased by approximately 150 meters horizontally.

Instead of the mathematically complicated conventional approach, a new simple technique is derived. Two regression formulas and two conversion surfaces have been developed to convert GPS coordinates. The efficiency of this model is investigated for hydrographic surveying, as a candidate of water resources management applications. Control networks cover 203 Km, over the second reach of the river Nile, has been used to examine the new scheme. It has been found that this method produces improvements in positional accuracy by approximately 22 %. Simplicity and ease-of-use, even in the field, are the main merits of the developed system. Such a technique solves one of the main difficulties in surveying and mapping applications in an economical manner.

1. INTRODUCTION

Acquisition of accurate and up-to-date topographic and hydrographic maps is a key element in the context of water resources management. It is a matter of reality that the Egyptian mapping system, as established by the Egyptian Survey Authority (ESA), has been built based on a specific geodetic datum. This national datum, called the Old Egyptian Datum (OED), has been designed related to the Helmert 1906 ellipsoid. That ellipsoid was the best mathematical surface representing the figure of the Earth in the beginning of the twentieth century. Each country has its own mapping system referenced to a specific ellipsoid. Although many other ellipsoid have been defined worldwide over that long time, the process of changing the entire mapping system is too expensive and time consuming to be carried out.

The Satellite-based Global Positioning System (GPS) is the current most precise and widely used positioning technology worldwide. As a positional data collection tool, GPS has been utilized in water resources management applications [e.g. 1 and 3]. However, the GPS-derived coordinates are referenced to a global geodetic datum called World Geodetic Datum 1984 (WGS84). Hence, GPS data have to be transformed from that global datum to the national Egyptian one. Neglecting this datum transformation computational process, the collected positions will be biased by approximately 150 meters horizontally. With the rapid growth of GPS utilization, the issue of datum transformation becomes a great concern of the surveying and mapping community [e.g. 6]. Several conventional models for datum transformation have been proposed and utilized since 1960's. Most of these traditional approaches are complicated, in a mathematical sense, and require a lot of field and data processing steps. A new simple approach based on multiple regression or conversion surfaces has been proposed lately [2]. This paper aims to develop and investigate the utilization of a similar technique to solve the datum transformation issue in water resources mapping projects.

2. TRADITIONAL DATUM TRANSFORMATION MODELS

Traditionally, the similarity datum transformation models have been introduced and utilized in geodetic applications since the sixties. This type of datum transformation has gained a great focus since it has a geometrical interpretation of the determined parameters. A similarity transformation model is based on 7 parameters: three translation parameters (dX, dY, and dZ), three rotation parameters ($\omega_{x,}$ $\omega_{y,}$ and ω_z); and a parameter (s) for the scale difference between the two coordinate systems. There are many similarity transformation models, e.g. Bursa-Wolf model, Molodensky-

Badekas model, Veis model, and Vanicek and Wells model. It is not an objective of the current paper to present the complicated mathematical formulation that defines each model. Details concerning these models are found in various literatures [e.g. 4].

3. UNCONVENTIONAL DATUM TRANSFORMATION APPROACH

Dawod and Alnaggar [2] have utilized the stepwise multiple regression technique for datum transformation determination for two basic reasons: the need for better accuracy than could be achieved through the similarity datum transformation formulas; and the need for a technique more manageable for field use. This technique is based on modeling the differences ($\Delta\phi$ and $\Delta\lambda$) between the geodetic coordinates of two systems by two polynomials in order to spatially represent the differences over the network, to a given degree of accuracy. They have found that, over the Egyptian territories, the differences in latitude range from 0.2104“ to 0.8654” with an average of 0.4678”, while the differences in longitude range from 5.8129“ to 6.0897”. Similar methods have been proposed and applied worldwide in several surveying applications [e.g. 7].

The same principle has been utilized in this research study with slight modifications for seek of simplicity. The developed conversion formulas, for transforming coordinates from the WGS84 to the OED systems are:

$$\Delta\phi'' = a_o - a_1\,\phi_{84} + a_2\,\lambda_{84} \qquad (1)$$

$$\Delta\lambda'' = b_o + b_1\,\phi_{84} + b_2\,\lambda_{84} \qquad (2)$$

where:

$\Delta\phi$ and $\Delta\lambda$ are obtained in arc of seconds,
a_o , a_1 , a_2 , b_o , b_1 , and b_2 are the unknown parameters to be estimated,
ϕ_{84} and λ_{84} are the WGS84 latitude and longitude coordinates in degrees.

Therefore, the transformed coordinates on the OED coordinate system are given by:

$$\phi_{OED} = \phi_{84} + \Delta\phi \qquad (3)$$

$$\lambda_{OED} = \lambda_{84} + \Delta\lambda \qquad (4)$$

4. AVAILABLE DATA

The utilized data consists of a geodetic control network established by NRI in 1995. The objective of this network was to support hydrographic and land surveying activities in the Esna – Nag Hammadi reach (Figure 1). That network consisted of 82 horizontal control points covering the distance between upstream Esna barrage by approximately 10 Km to Nag Hammadi barrage, with a total distance of 203 Km (Figure 2). Another two stations, A4 and B4 from the national horizontal control networks, have been observed too in order to tie the network to the national mapping system of Egypt. The network covered both banks of the Nile with a distance separation of almost 5 Km apart. GPS geodetic high-precision receivers have been utilized to observe the network in a static (network) mode. Each field observation session contained four points, and continued for at least one hour. In some cases, the session time was extended to three hours for quality control purposes over large sections of the entire network [NRI, 1996].

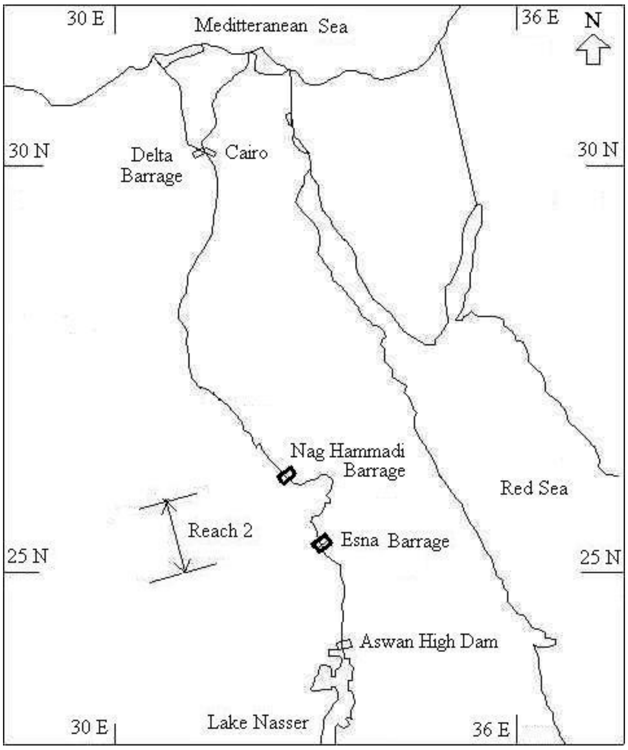

Figure 1: The study area

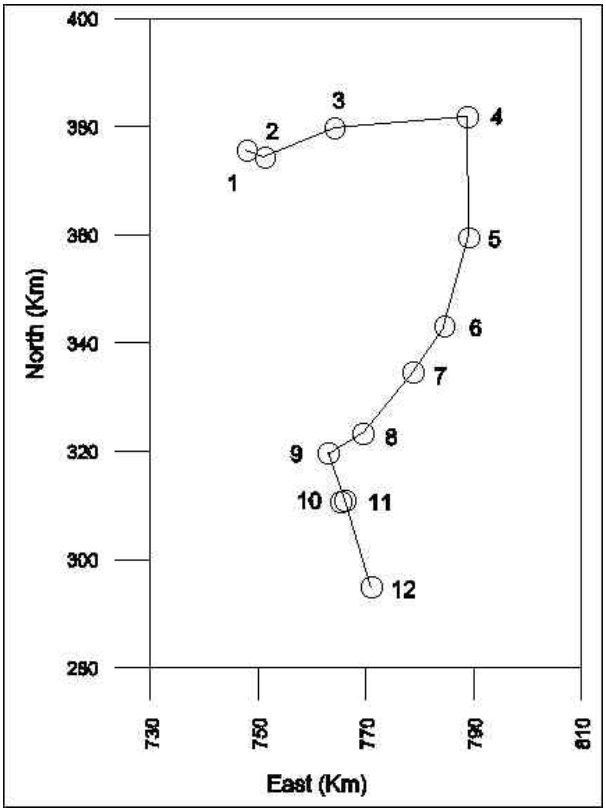

Figure 2: The utilized GPS Network

5. OBTAINED RESULTS

The available control network has been utilized in testing and comparing the two approaches of geodetic transformation. The following sub-sections document the obtained results.

5.1 Results of traditional geodetic transformation approach

Based on field reconnaissance, it has been found that twelve stations of that network belong to the Kenting control network established over the Nile in the period from 1978 to 1982. Those stations have been found in good and trustable conditions. They have known coordinates on the Old Egyptian Datum of 1906, simply known as OED. Based on the collected static GPS observations, coordinates on the WGS84 global geodetic datum are computed for these stations. Having known coordinates of these stations on both geodetic datums, traditional geodetic datum transformation parameters have been determined using the Molodensky-Badekas model. Four control stations (No. 1, 4, 6, and 12) have been utilized to come up with the transformation parameters presented in Table 1 [5]. In order to check the accuracy of the transformation set, OED coordinates have been computed, using equations 3 and 4, and compared against the known (true) values for the remaining eight points. In order to visualize the error estimates in a

simple view, they have been computed on the two-dimensional mapping coordinate system (Easting and Northing coordinates). Table 2 gives the error values of this approach over the check points. From this table it can be seen that the errors in the east direction range from -1.4 m to 0.98 m, while the errors in the north direction vary from -0.58 m to 0.76 m. Additionally, these error figures have been translated to the corresponding linear (distance) error for each station. Linear errors rang from 0.44 m to 1.59 m, with an average value of 0.83 m.

Table 1: Results of traditional datum transformation method

Parameter		Value
Shift dX	(m)	136.669
Shift dY	(m)	-118.399
Shift dZ	(m)	37.546
Rotation about X axis	(“)	41.871628
Rotation about Y axis	(“)	1.446345
Rotation about Z axis	(“)	31.253743
Scale factor	(part per million: ppm)	169.902065

Table 2: Errors of traditional datum transformation method (m)

Error in Easting	Error in Northing	Linear Error
0.98	0.74	1.23
-0.50	-0.58	0.76
-0.38	-0.37	0.53
-0.39	-0.56	0.68
0.24	-0.48	0.54
-0.87	0.23	0.90
-0.08	0.43	0.44
-1.40	0.76	1.59

5.2 Results of new geodetic transformation approach

The same four control stations have been used to solve the regression formulas 1 and 2, and estimate the unknown parameters. The final obtained regression equations are:

$$\Delta\phi'' = -0.1394996 - 0.0376027\ \phi_{84} + 0.0432308\ \lambda_{84} \quad (5)$$

$$\Delta\lambda'' = -3.8239521 - 0.0519775\ \phi_{84} - 0.0324810\ \lambda_{84} \quad (6)$$

In order to judge the accuracy of the model, errors have been computed for the remaining eight stations. Table 3 presents the values of these errors. From this table it can be seen that the errors in the east direction range from -1.12 m to 0.78 m, while the errors in the north direction vary from -0.57 m to 0.74 m. Additionally, these error figures have been translated to the corresponding linear (distance) error for each station. Linear errors rang from 0.38 m to 1.32 m, with an average of 0.69 m.

The differences in latitude, between the WGS84 and the OED datums, have a minimum of 0.278” and a maximum of 0.315”, with a mean value of 0.298”. The corresponding differences in longitude vary from -6.245”to -6.198”, with an average equals -6.221”. Figures 3 and 4 depict contour maps for these differences, which can be considered as conversion surfaces between both geodetic datums.

Table 3: Errors of new datum transformation method (m)

Error in Easting	Error in Northing	Linear Error
0.78	0.74	1.08
-0.05	-0.57	0.58
-0.33	-0.26	0.42
-0.51	-0.26	0.57
0.21	-0.37	0.43
-0.71	0.23	0.75
-0.08	0.37	0.38
-1.23	0.70	1.32

5.3 A comparison of results

Comparing the obtained results from both datum transformation approaches, it can be seen that the second one is optimum. In terms of accuracy, the conversion surface method produces improvements in positional accuracy that is approximately 21.7 %. However, the second technique is trouble-free and can be used quickly even by means of a calculator. There is no need to utilize a sophisticated computer programs to convert GPS positions to the national mapping system. Moreover, the achieved conversion surfaces, figures 3 and 4, can also be used to interpolate the differences between both datums in an effortless manner. Hence, this approach is appropriate for almost all applications in water resources management.

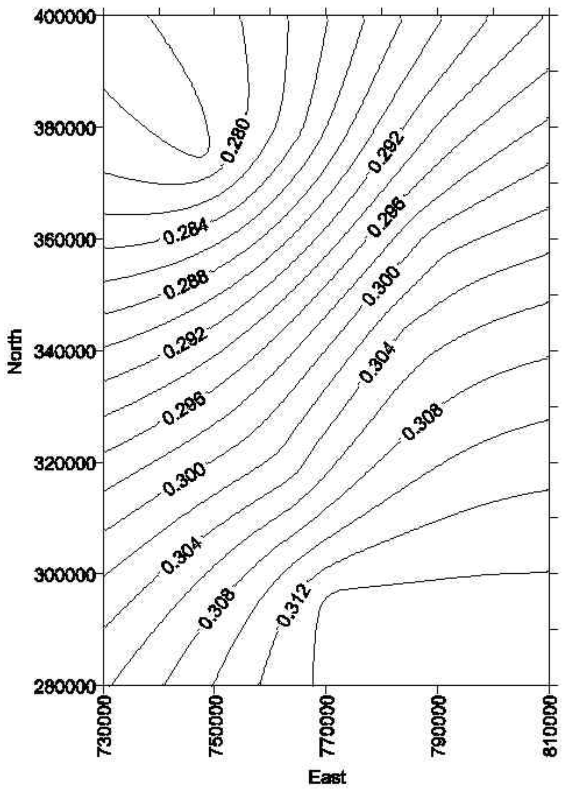

Figure 3 : Latitude conversion surface

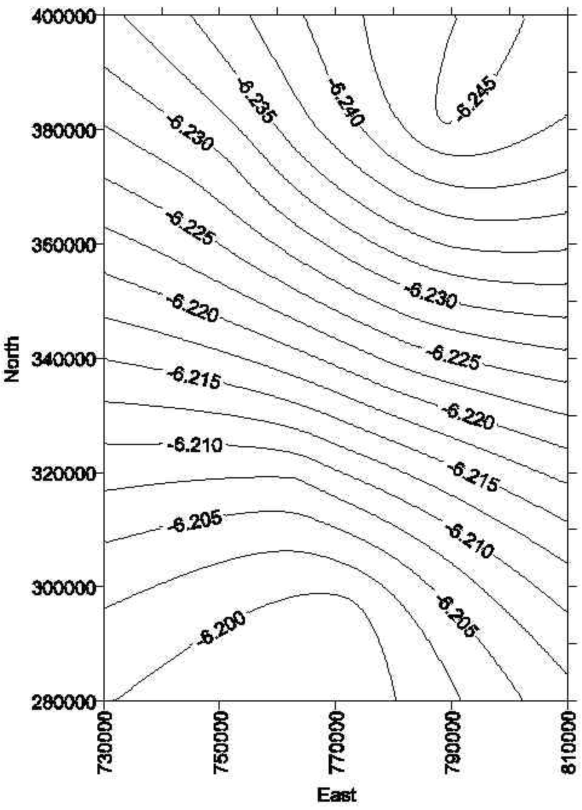

Figure 4: Longitude conversion surface

6. CONCLUSIONS

Recently, the GPS satellite technology has been employed widely in integrated water resources management projects as a positional data collection tool. Hence, the issue of converting GPS data to the Egyptian national mapping system becomes a fundamental significance. Instead of the mathematically complicated similarity transformation approach, a new simple technique is derived and investigated. Two regression formulas and two conversion surfaces have been developed for the second reach of the Nile, extending 203 Km, to convert GPS coordinates. It has been found that this method produces improvements in positional accuracy by approximately 22 %. Moreover, it is an effortless procedure, that can be used quickly even by means of a calculator. Additionally, the achieved conversion surfaces can also be used to interpolate the differences between both datums in a straightforward manner. So, the developed scheme is proper for mapping applications in the integrated water resources management process in Egypt. It is recommended that the same procedure is employed for the other reaches of the Nile and its two branches.

REFERENCES

[1] Dawod, G., 2002, Utilization of recent GPS techniques in estimation of depression volumes for water resources applications, Water Science Magazine, National Water Research Center, October.

[2] Dawod, G., and Alnaggar, D., 2000, Optimum geodetic datum transformation techniques for GPS surveys in Egypt, Proceedings of Al-Azhar Engineering Sixth International Engineering Conference, Cairo, September 1-4, Volume 4, pp. 709-718.

[3] Gibbs, P., 2001, Surveying for water resources, Water International, V. 26, No. 4, pp. 547-557.

[4] Nassar, M. (1984), Geodetic position computations in two and three dimensions: Part II, Lecture notes, Faculty of Engineering, Ain-Shams University, Cairo, Egypt.

[5] NRI (Nile Research Institute), 1996, Report on establishing the horizontal control DGPS network for Esna – Nag Hammadi reach, NRI Technical Report No. A505040203-9603-01-FR.

[6] Reit, B. (1998), The 7-parameter transformation to a horizontal geodetic datum, Survey Review, V. 34, No. 268, pp. 400-404.

[7] Smith, D. and Milbert, D., 1997, Evaluation of preliminary models of the geopotential in the United States, Int. Geoid Service Bulletin No. 6, pp. 7-32.

Proceedings of Al-Azhar Engineering 7th International Conference,
Cairo, April 7-10, 2003.

ESTABLISHEMENT OF A PRECISE GEODETIC CONTROL NETWORK FOR UPDATING THE RIVER NILE MAPS

Gomaa M. Dawod [1] and Tarek M. Abdel-Aziz [2]

[1] Survey Research Institute, National Water Research Center, Egypt
[2] Nile Research Institute, National Water Research Center, Egypt

ABSTRACT

Geodetic control networks play the most crucial role in the attainable accuracy and reliability of surveying and mapping applications. Since the mid 1980's, several geodetic control networks have been established for a wide range of mapping projects utilizing the Global Positioning System (GPS) technology. On the other hand, there are no official documented specifications and standards for GPS-based geodetic control networks in Egypt.

The Nile Research Institute (NRI) of the National Water Research Center (NWRC) has initiated a national project to create modern digital topographic and hydrographic maps of the River Nile and its two branches. The main core of this pioneer project is a multi-fold precise geodetic control network utilizing the state-of-the-art GPS instrumentation and techniques. The network consists of approximately 600 control stations spacing 5 km apart on both banks of the Nile, which is almost 1435 km long. Orthometric heights of all control stations will also be determined, which enables the creation of a precise geoid model of the Nile valley. This paper presents the characteristics and the designed unique standards and specifications of the geodetic control network. It is anticipated that this network will improve the reliability, availability, and integrity of the national geodetic networks, and have a great economical impact on surveying and mapping activities in Egypt, particularly for water resources management.

KEY WORDS
Geodetic Networks, River Nile Maps, GPS; Specifications.

[1] dawod_gomaa@hotmail.com

1. Introduction

Geodetic control networks are mandatory for a wide variety of disciplines such as mapping, urban management, engineering projects, hydrography, aerial photography, astronomy, geophysics, and deformation monitoring. The GPS technology has been considerably employed in Egypt to establish geodetic control networks since 1985. Only one GPS network achieves high degree of accuracy, reliability, and integrity. A main reason behind this fact is the lack of official documented series of GPS standards and specifications to be fulfilled in Egypt.

Currently, a new GPS network is established over the river Nile and its two branches. Previous GPS networks in Egypt have been thoroughly studied to conquer their limitations and defects. Moreover, recent international GPS specifications have been collected and thoroughly analyzed prior to designing the new network. The developed characteristics of this network, in terms of hardware, data capture, data processing and adjustment, have been worked out to ensure acquiring a high-precision GPS network. This research study presents the derived set of standards and specifications being implemented to establish the new national GPS control network.

2. Status of GPS geodetic control networks in Egypt

GPS has been extensively utilized in Egypt to establish geodetic control networks for a wide range of surveying and mapping applications. However, most of these networks are limited in coverage and availability. The most important GPS network in Egypt is the so-called High Accuracy Reference Network (HARN). The HARN network has been established by the Egyptian Survey Authority (ESA) in the mid 1990s, with the cooperation of some American partners. The HARN network is divided into two sub-networks: HARN order-A, and HARN order-B. The HARN order-A network, Figure 1, consists of 30 stations covering the Egyptian territory with an average spacing of approximately 200 km. Its relative accuracy estimate is 1:10,000,000 or 10 part per million (ppm). This network has been tied to some International Geodynamic Service (IGS) global precise GPS stations in order to obtain such a high accuracy estimate. Few stations from the old Egyptian first-order triangulation network have been utilized as GPS stations in this network. The HARN order-B network, also called the National Agricultural Cadastral Network (NACN), consists of 140 stations. The NACN covers the Nile valley and delta with a spacing of approximately 50 km. The relative accuracy estimate of this network is 1:1,000,000 or 1 ppm.

Rather than the HARN network, the remaining GPS networks in Egypt are limited in coverage. The following are few examples of GPS networks in Egypt (Figure 2):

* A network established in 1980s by ESA and Finnmap Inc. for producing 1:50,000 topographic maps for the Eastern desert. It consists of 31 first-order stations with a mean baseline length equals 112.5 km [Finnmap, 1988].
* A network established by the Survey Research Institute (SRI) in 1980s for producing 1:50,000 topographic maps for Sinai. It consists of 70 stations with average spacing of 25 km covering north and central Sinai [Mohamed, 1992].
* A network established by SRI in 1996 for developing the navigational route of Rosetta branch of the Nile. It consists of 44 stations with average spacing of 5 km on both banks of the branch [SRI, 1996].
* A network established by the Nile Research Institute (NRI) in 1995 to support hydrographic and land surveying activities in the Esna – Nag Hammadi reach. It consists of 82 stations, covering a total distance of 203 Km, with average spacing of 5 km on both banks of the Nile [NRI, 1996].
* A network established by SRI in 2000 for developing the navigational route of Dammitta branch of the Nile. It consists of 48 stations with average spacing of 5 km on both banks of the branch [SRI, 2000a].
* A network established by SRI in 2000 for several management activities of the Nile. In its first stage, the network consists of 146 stations with average spacing of 2 km on both banks of the Nile from Delta barrage to Bani-Swaif city [SRI, 2000b].

A crucial issue, regarding GPS control networks, is that there are no official documented sets of standards and specifications. Although a recent study has proposed a preliminary series, it requires extensive revision and modifications to be officially accepted [Dawod 2002]. Therefore, the integrity and reliability characteristics of control networks in Egypt vary seriously from one network to another. Moreover, many of these networks have not tied to a high-precision GPS datum that can be used to unify them. Usually, the coordinates of at least one station are determined by point positioning for a relatively long session, and then kept fixed for the entire network. Hence, the obtained network coordinates are completely dependant on such station’s coordinates, which are implicitly biased by satellites and receiver errors. The same conclusions have been drawn by other investigators [e.g. Saad, 1998].

3. River Nile mapping

Hydrographic and topographic maps play a crucial role in the management of water resources in Egypt. Since the Nile constitutes the main source of fresh water in Egypt, its precise maps are a key element in the context of integrated water resources management policy. The existing complete hydrographic maps of the Nile have been produced by Kenting Earth Science Ltd Co. in 1982. That project has been executed from 1978 to 1982 by NRI, through Canadian funds, resulted in 380 topographic maps of scale 1:10,000. These maps were originally derived from aerial photographs taken in 1978. They cover 2 km beyond either sides of the Nile. Contour lines are also obtained on these maps with a contour interval of 1 m, enhanced with 0.5 m interpolated contours in areas of little relief. Moreover, 249 hydrographic maps with scale 1:5000 have been derived for the Nile and its two branches. They represent the relief of the river bed with the same contour intervals.

Geodetic control networks have been established with a station separation of 5 km on both banks of the Nile and its two branches. Traditional terrestrial surveying techniques have been utilized to determine the coordinates of the networks' stations on the Old Egyptian Datum of 1906. Orthometric heights have been also determined for most stations. Therefore, these geodetic networks have considered the core of the produced Nile maps.

In order to study the recent morphological and hydrological changes of the Nile, NRI has initiated a four-year national project to produce precise digital hydrographic and topographic maps covering the river and its two branches. The project consists of the following components:

- Conducting 1:15,000 aerial photography for the area of study, that is approximately 4,000 square kilometers.
- Production of 1:5,000 digital topographic maps, covering 1 km from each bank of the Nile. The maps show contours with a 0.5 m interval, which implicitly require dense terrestrial levelling measurements.
- Performing precise hydrographic surveys to represent the river relief with the same contour interval.

The main core of this pioneer project is a multi-fold precise geodetic control network utilizing the state-of-the-art GPS instrumentation and techniques. The network consists of approximately 600 control stations spacing 5 km apart on both banks of the Nile, which is almost 1435 km long. Orthometric heights of all control stations will also be determined,

which enables the creation of a precise geoid model of the Nile valley. It should be stated, herein, that the hydrographic surveys do not necessarily require the usage of a first-order control network [CHS, 1994]. However, it is decided, in the current project, to establish a high-precision GPS network that can be utilized in various national surveying and mapping applications and remarkably enhances the geodetic data bases in Egypt. In order to fulfill these objectives, a series of standards and specifications has been planned for the current project. The first fundamental step was to collect and thoroughly analyze recent international GPS specifications [e.g. FGCC 1991, GSD 1992, GSD 1996, ICSM 1997, and ICSM 2000].

4. Specifications of the new national GPS network

Classifications of geodetic networks depend on the geometric distance accuracy. It is defined as the ratio of the relative positional error of a pair of control points to the separation of these points. Minimum distance accuracy is assigned to each order of geodetic networks. With the development of GPS survey observation systems, a modification to the geometric distance accuracy criterion was proposed by the U.S. Federal Geodetic Control Committee (FGCC) [FGCC, 1989]. This revision reflects the performance of systems include a base error, so that the accuracy standard, in the 95% confidence level, is divided into a base error, e.g. a receiver setup error, and a length-dependant part. Based on this scheme, the standards of national GPS networks are shown in table 1. It has been decided that the GPS network, established for the current project, should fulfill the standards of order B, or better. Based on this criterion, other specifications have been designed as discussed in the next sub-sections.

Table 1: Standards of GPS Geodetic Networks

Category	Order	Base Error (cm)	Length-Dependant Error	
			ppm	1:a
Primary National Geodetic Network	A	0.5	0.1	1:10,000,000
Secondary National Geodetic Network	B	0.8	1	1:1,000,000

4.1 Station monumentation

Unfortunately, many geodetic control stations are quickly damaged and lost due to the way it was constructed. For example, considerable percentage of the HARN-order B' stations have been constructed in urban

areas by just fixing a steel nail on the floor of a bridge or on the top of a building. Such a monumentation style can be easily broken. Hence, the monumentation of the current GPS stations is rigid enough to survive rough circumstances. Each mark consists of a 50x60x100 cm concrete box with half of its height burned under the ground. A 100-cm steel cylinder is fixed in the middle of the concrete box, with an aluminum cover on its top. The project name and the station serial number are engraved on that cover. The location of each station is chosen to be at least 50 meters away from any artificial structures in order to minimize the harmful multipath effects. Site accessibility should also be considered in the reconnaissance stage.

4.2 GPS hardware

There are several characteristics to choose 'good GPS receivers' from the available wide market. It is a fact of reality that dual-frequency GPS receivers meet the accuracy specifications for precise geodetic networks with no constraints, while the single-frequency receivers may not fulfill these specifications with the presence of significant ionospheric disturbances. The advantage of having dual-frequency data is the capability to develop the so-called ionospheric-free observables's combination that results in a more precise solution. Moreover, multi-channel receivers are more reliable and have better signal-to-noise ratio, which means they can receive even weaker signals. Additionally, GPS measurements can be significantly corrupted by GPS signals that reflecting off surfaces near (within some 30 meters) the antenna. The sensitivity of multipath corruption depends on the reflectivity of the surfaces in the antenna environment, and on the antenna gain (sensitivity) in the direction of these reflectors. The placement of the antenna and the use of absorption material can significantly reduce the multipath effects.

4.3 GPS field work

The most affecting error sources in GPS fieldwork are the antenna setup errors. These errors contain the centering error and the error in measuring the antenna height. Consequently, the following field procedures are considered to minimize antenna setup errors:

- Measure and record antenna height before and after each station occupation.
- GPS operators, if more than one, should verify all measurements.
- Check collimation and levelling of the antenna before and after each station occupation.

- Log antenna serial number as a part of the station record in order to verify, later, that the correct phase center correction is applied.
- Redundant station occupation should be performed as much as possible.

The designed guidelines to be fulfilled regarding the GPS data capture include:

- Number of utilized receivers in a session is more than 4.
- Minimum number of healthy satellites to be tracked by all receivers is 4.
- The session interval is 60 minutes or more.
- The sample rate of observations is 15 seconds.
- Minimum cut-off angle above the horizon is 15^o.
- GDOP value does not exceed 6.
- At least two points are observed commonly between two successive sessions.
- Minimum number of points having redundant occupations is 30%.

Considering tying the Nile GPS network to the HARN network, the following procedures must be satisfied:

- Whenever possible, the new GPS net should be tied to the HARN order-A network. Otherwise, HARN order-B is used to reference the new network.
- The tying observation process should be carried out every 50 km of the longitudinal direction of the net.
- In each tie, a minimum of two HARN stations (one from each side of the Nile) should be utilized.
- The minimum occupation time in the tying is two hours, but it should be proportional to the baselines' length.

4.4 GPS data processing

Based on the international GPS specifications of high-precision networks, the following procedures are designed:

<u>(A) For a base line:</u>

- Root Mean Square error (RMS) should fill in the range from 0.01 to 0.2 cycles.
- The ratio test should be greater than 3.
- The iono-free L1/L2 fixed solution must be obtained for the Nile network.
- Ionospheric and tropospheric models should be implemented.
- Percentage of rejected measurements should be less than 10%.

- Maximum standard deviation of a base line is 2 cm.
- Tolerance of base line processing should be better than 2 cm horizontally and 4 cm vertically.
- Precise ephemeredes are preferable to be utilized rather the broadcasted values.

(B) For a session:

- All combination of baselines in a session should be processed.
- Maximum loop closure in vector components is 25 cm.
- Loop closure does not exceed 12.5 ppm.

4.5 GPS adjustment

For any GPS network, it is necessary to describe how to position and orient the network on the earth's surface (i.e., datum definition). This can be done, in general, in several ways:

- Holding one point fixed (fixed-point approach).
- Holding one point properly weighted (fiducial-point approach).
- Holding no point fixed (free-net approach).
- Holding several points fixed (over-determined approach).
- Holding several points properly weighted.

The first three approaches use the minimum necessary number of positional constraints, and therefore known as minimally constrained adjustment. It is known that a GPS network has three (out of seven) datum defects since the orientation and scale are implicitly known from the phase observations because the coordinates of the satellites are assumed to be known. A method for overcoming this problem is to use inner constraints to allow the adjustment to proceed by using the centroid of the unadjusted coordinates to control coordinates translation. The last two approaches belong to the so-called over-constrained adjustment. The process of GPS network adjustment is recommended to be performed in the following sequence of procedures to come up with optimum results:

A. Analyze the loops' closure to verify that the closure errors are within the accuracy Specifications required.
B. Perform a free net adjustment (i.e., fix a single, often arbitrary, point) to analyze the internal consistency of the survey data.
C. Use the statistical information of the free net adjustment to detect blunders and residual outliers. Detecting and removing erroneous observations is a must in geodetic networks to improve the network reliability.

D. Perform a final constrained adjustment (minimal or over-constrained) to fit the GPS survey to existing geodetic frameworks.

The precision of the adjusted control points in a GPS geodetic network is expressed as a ratio by converting its standard errors into a linear distance and dividing this distance by the distance to the nearest control point. These precision ratios of all the network points should meet the geodetic network proposed specifications (shown in table 1).

5. GPS/Levelling measurements

Another important requirement of the current project is to relate the collected height information to the Mean Sea Level (MSL) datum of Egypt. Hence, orthometric heights of all control stations will also be determined by, at least 2nd order, levelling techniques. This procedure enables the creation of a precise geoid model of the Nile valley, which can be further utilized to transform GPS ellipsoidal heights to orthometric values for any other surveying applications.

6. Conclusions

The Nile Research Institute has initiated a project to produce topographic and hydrographic digital maps of the Nile and its two branches. Within the multi-purpose activities of this pioneer national project, a GPS geodetic control network is established with a station separation of 5 km. The network consists of approximately 600 stations to cover both sides of the river in an area extends 1435 km. A set of standards and specifications has been designed and currently being implemented in order to achieve a high-precision national GPS network. This network, along with the HARN GPS network, will furnish a precise national GPS datum in Egypt. It is recommended that the geodetic community in Egypt should collect unify all available geodetic control networks in a unique complete data base for improved management of surveying and mapping activities. Additionally, it is highly recommended that the surveying and mapping community should carry out maximum efforts to formulate a national official series of GPS standards and specifications in Egypt. A preliminary step has been proposed recently, but it requires extensive revision and modifications to be officially accepted.

References:

CHS (Canadian Hydrographic Service), 1994, Standards for hydrographic surveys, Ottawa, Canada.

Dawod, G., 2002, Proposed standards and specifications for GPS geodetic networks in Egypt, Water Science Magazine, October.

Finnmap, 1988, Final report of the Eastern desert 1:50,000 topographic mapping project, The Egyptian Survey Authority, Cairo, Egypt.

FGCC (U.S. Federal Geodetic Control Committee), 1989, geometric geodetic accuracy standards and specifications for using GPS relative positioning technique, Version 5, August, Rockville, Maryland, USA.

FGCC, 1991, Standards and specifications for geodetic networks, Rockville, Maryland, USA.

GSD (Canadian Geodetic Survey Division, Geomatics Canada), 1992, Guidelines and specifications for GPS surveys, Release 2.1, Ottawa, Canada.

GSD, 1996, Accuracy standards for positioning, Version 1.0, Ottawa, Canada.

ICSM (Australian Inter-Governmental Advisory Committee on Surveying and Mapping), 1997, Best practice guidelines use of GPS for surveying applications, ICSM technical report.

ICSM, 2000, Standards and practice for control survey, ICSM Publication No. 1.

Mohamed, H.F., 1992, Consistency of GPS surveys using different geodetic receivers and processing software, MSc thesis, Faculty of Engineering, Cairo University, Cairo, Egypt.

NRI (Nile Research Institute), 1996, Report on establishing the horizontal control DGPS network for Esna – Nag Hammadi reach, NRI Technical Report No. A505040203-9603-01-FR.

Saad, A., 1998, Unification of the GPS work in Egypt, CERM, V. 20, No. 4, pp. 462-470.

SRI (Survey Research Institute), 1996, Establishment of GPS control networks for Rosetta branch of the River Nile, SRI Technical Report.

SRI, 2000a, Establishment of GPS control networks for Dammitta branch of the River Nile, SRI Technical Report.

SRI, 2000b, Establishment of GPS control networks for the Nile River Development Project, Part 1: From El-Kanater to Bani Swaif, SRI Technical Report.

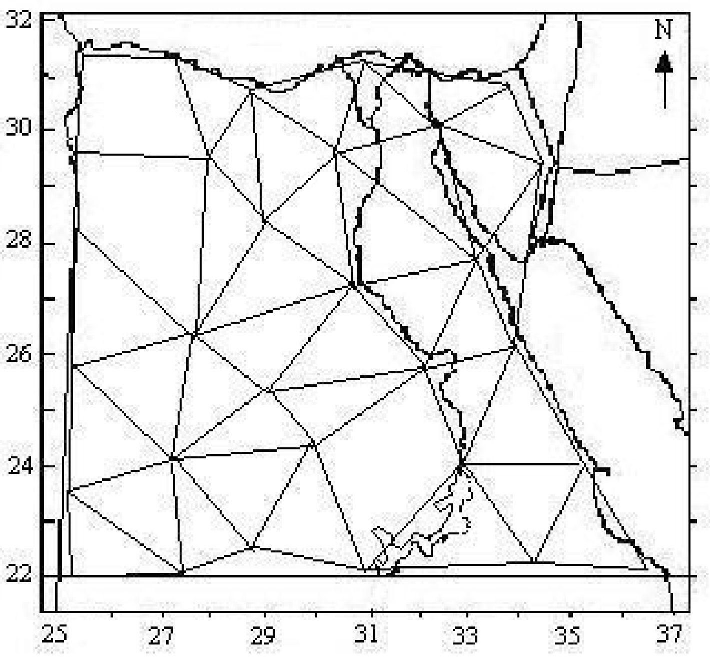

Figure 1
The High Accuracy GPS Reference Network (Order A)

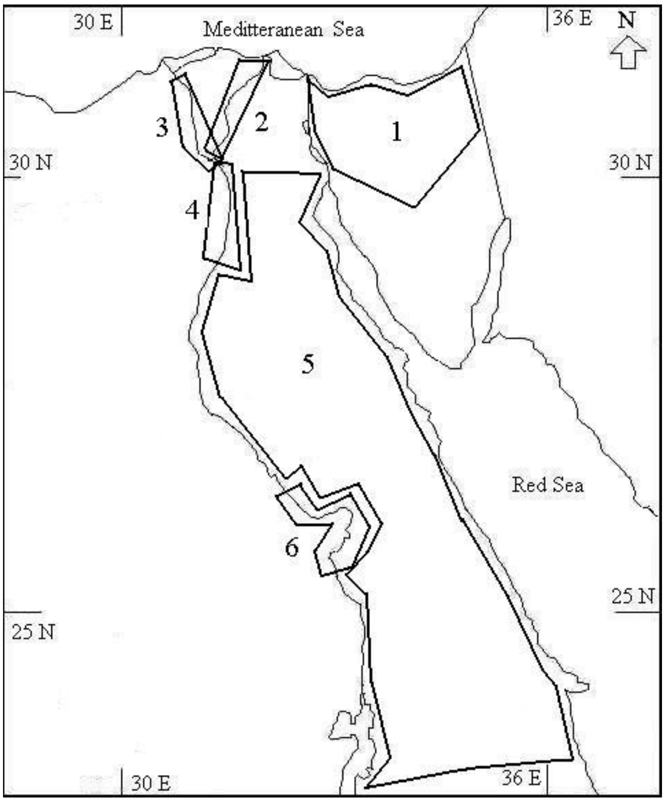

1- SRI: 70 stations. 2- SRI: 44 stations. 3- SRI: 48 stations.
4- SRI: 146 stations. 5- Finnmap: 31 stations. 6- NRI: 82 stations.

Figure 2
Examples of GPS Networks in Egypt

Proceedings of the First International Conference on Civil Engineering, Assiut University, Volume 2, pp. 246-253, October 7-8.

PRODUCTIVE GPS TOPOGRAPHIC MAPPING FOR NATIONAL DEVELOPMENT PROJECTS IN EGYPT

By

Gomaa M. Dawod

Survey Research Institute, National Water Research Center, Cairo, Egypt.

ABSTRACT

The employment of the traditional terrestrial surveying tools for the production of topographic maps is limited in time. The impact of the Global Positioning System (GPS) is undeniable in surveying, mapping, and even navigation environments. Recent GPS surveying methodologies have been adapted in Egypt to produces topographic maps with significant factors of cost and time savings [2]. However, one of the leading problems in such applications in the conversion of GPS heights, which have no physical interpretation, to the usual orthometric heights commonly utilized in engineering applications.

This research study presents a new simple approach for height transformation to benefit from the GPS-resulted heights in engineering environments. The obtained results yield transformed orthometric heights that have error estimates ranging from 4 mm/km to 8 mm/km. These accuracy levels are suitable for topographic mapping, digital terrain modeling, mapping from remote sensing images, and Geographic Information System (GIS). Hence, this paper proposes an efficient technical scheme for productive topographic mapping to be utilized in national development projects.

1. INTRODUCTION

GPS provides three-dimensional coordinates with respect to the defined global World Geodetic System 1984 (WGS84). Concerning heights, GPS yields ellipsoidal heights (h) that are unlikely be used for practical surveying or engineering applications, as they have no physical meaning. For instance, when using this type of heights there is the possibility that water will appear to flow up-hill because the physical force of gravity is not considered. On the other hand, orthometric heights (H), which are used in practice, are related to the geoid surface. The geoid is the equipotential or level surface that is closely associated with the Mean Sea Level (MSL) on a global basis. Thus, a transformation is required to convert ellipsoidal heights into orthometric ones. This transformation implicitly describes the relationship between WGS84 and the geoid (Figure 1). On a global scale, the geoid departs from the WGS84 ellipsoid by approximately 100 meters, ranging from about –30 meters to about +70 meters [5].

It has been demonstrated that GPS kinematic techniques reduces the time and costs of topographic map production by considerable factors [2, and 3] However, this production process encounter the problem of height transformation. There are mainly two approaches in converting the ellipsoidal height into the orthometric one. These include the utilization of a global or national geoid model, and interpolation between geometrically-derived geoid undulations where both h and H have been measured. The second approach is the main aim of this research study, since the first one has several limitations in Egypt as will be discussed in the following section.

2. THE STATUS OF THE GEOID MODELING IN EGYPT

The determination of the geoid has become a main objective for the geodetic community in Egypt for several decades. Several local and nation-wide geoid models have been developed in Egypt. The first countrywide geoid solution for Egypt, relative to WGS72 geocentric geodetic datum, using heterogeneous geodetic data has been developed in 1986 [1]. In this pioneer geoid, several sources of geodetic data have been combined, such as terrestrial gravity measurements, Doppler observations; and astronomical observations. Shaker et al [10] have developed a combined GPS/Gravity geoid model for the Eastern Desert region. Dawod [4] has developed two national geoid models relative to WGS84: a gravimetric model (SRI-GEOID98A) based on the OSU91A global geopotential model of the Earth, and an integrated GPS/Gravity geoid solution (SRI-GEOID98B). The most recent and accurate geodetic measurements have been utilized in the development of these models, especially the data of the

Egyptian National Gravity Standardization Network (ENGSN97) and the GPS High-Accuracy Reference Network (HARN95). The SRI-GEOID98B model gives geoid undulation (N) varying from 7.22 meters at Abu-Simbol to 22.55 meters at Balteem, with the mean of 15.31 meters.

Recently, two high resolution national geoid models for Egypt (32^{o} <latitude> 22^{o}, 37^{o} <longitude> 25^{o}) have been developed based on the utilization of the Earth Geopotential Model (EGM96) as the most recent long-wavelength representation of the Earth geopotential, incorporated with the recent precise geodetic data base available in Egypt [7]. Both EGM96 and OSU91A were used to compute the geoid undulations over 195 known GPS/Levelling stations. The obtained results show that the mean and RMS values of EGM96 undulations exhibit a better consistency with the measured undulations than the OSU91A corresponding values. The first 5'x5' geoid solution, called SRI2001A, is a gravimetric geoid model utilizing 240 first-order gravity stations, a local Digital Elevation Model (DEM); and the EGM96 in a remove-compute-restore Fast Fourier Transform (FFT) processing methodology. The most recent national combined geoid model for Egypt is the second 5'x5' geoid model, called SRI2001B. It has been developed based on integrating the gravimetric SRI2001A geoid model to an undulation datum defined by GPS/Levelling observed undulations on a national scale. SRI2001B has a minimum undulation value of 9.44 m and a maximum value of 21.39 m with an average of 13.62 m [ibid].

It worth mentioning that the present amount and distribution of geodetic data sets in Egypt is not reliable enough to produce a detailed national geoid model. For instance, the average station separation for the ENGSN97 gravity network is approximately 66 km, while the average baseline length of the GPS HARN95 network is about 200 km. Furthermore, in some regions over the Egyptian territory there exist a good distribution of geodetic data but with less accuracy level, such as in the Eastern desert [4]. Hence, the interpolation approach may be useful in small areas.

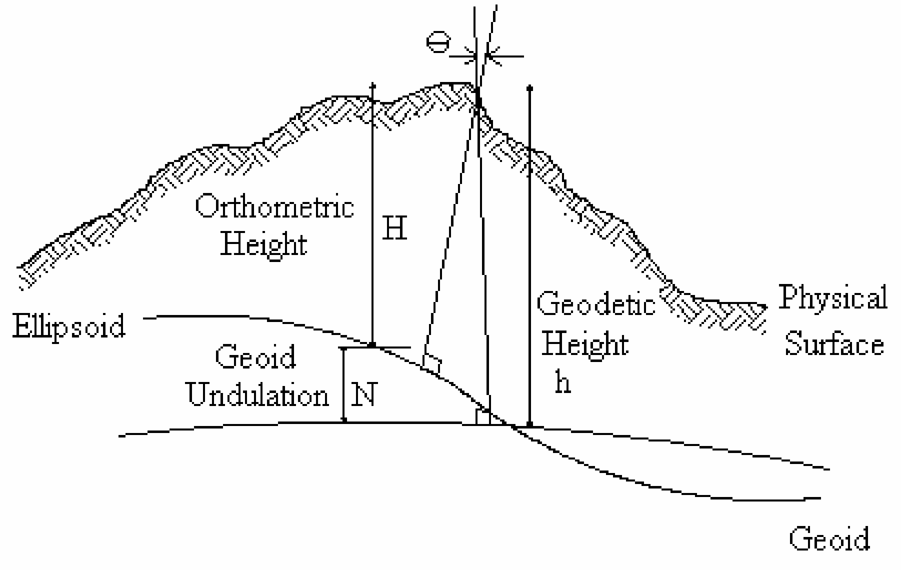

Figure 1: Height Systems

3. INTERPOLATION TECHNIQUES TO OBTAIN ORTHOMETRIC HEIGHTS

Several strategies have been suggested for the interpolation of geoid heights or undulation differences. Smith and Roman [11] have developed a conversion surface that comprises the differences between both height datums for the United States. Saad [8] has suggested several formulas to convert ellipsoidal to orthometric heights. Other research studies [e.g., 6] proposed the usage of a lower-order polynomial surface to model the errors of geoid models in local areas. The least-square collocation technique is also proposed to model geoid errors in relatively small areas [9] As mentioned earlier, the density and accuracy of geoid models in Egypt are not appropriate to attain reasonable accuracy in small areas. Even more, the current study aims to develop a simple scheme that is easy to be applied on a small scale, and helpful in increasing the productivity of contour mapping. Hence, the following technique is suggested and being investigated. A comparable scheme has been presented in a similar research to interpolate geoid undulations [5].

The basic relationship between the three quantities in hand is:

$$H = h - N \qquad (1)$$

which in a differential sense becomes:

$$H_1 - H_2 = h_1 - h_2 - (N_1 - N_2)$$

i.e.,

$$\Delta H = \Delta h - \Delta N \tag{2}$$

For a very small area, it can be assumed that the geoid may be approximated by a flat surface. In this case, linear interpolation can be utilized to estimate geoid undulation differences. For medium profiles (longer than a few kilometers), another more efficient interpolation technique may be suggested as:

$$N = N_o + N_1\, e + N_2\, n \tag{3}$$

Where the coefficient N_o represents a bias, N_1 and N_2 represent tilts of the geoid plane with respect to the WGS84 ellipsoid, e is the easting and n is the northing on a plane coordinate system.

In order to solve equation (3) and estimate the three unknown parameters N_o, N_1, and N_2, GPS observations should be made at a minimum of three benchmarks that surround the survey area. Hence, three formulas of equation (3) are formed for the GPS/Levelling stations A, B, and C, which in a matrix notation can be written as:

$$\begin{bmatrix} N_0 \\ N_1 \\ N_2 \end{bmatrix} = \begin{bmatrix} 1 & e_A & n_A \\ 1 & e_B & n_B \\ 1 & e_C & n_C \end{bmatrix}^{-1} \begin{bmatrix} N_A \\ N_B \\ N_C \end{bmatrix} \tag{4}$$

If more than three GPS/Levelling stations are used, equation (4) becomes over-determined and the least-squares adjustment technique is performed to come up with unique un-biased estimates of the three parameters.

4. DATA AND RESULTS

Twenty six GPS/Levelling stations are established in a profile, where the average station separation is about 4.3 km. Three different scenarios have been investigated to validate the accuracy of interpolating geoid heights using the presented approach. The obtained results are summarized in Table 1.

In the first case, only thirteen points (a point out of every two successive points) have been utilized to solve equation (4). The average distance between these points became about 8 km. The remaining points have been reserved for checking and validation purposes. The estimated parameters are:

$N_o = 13.825$ m, $N_1 = 0.00003105$, and $N_2 = 0.00000297$

The obtained results have been used to interpolate geoid heights, and consequently compute orthometric heights, for the check points. Errors between known and interpolated orthometric heights are computed. These errors have an average value of 2.9 cm. In the second scenario, only seven points (a point out of every three successive points) are used in the least-square estimation process. The average station separation has changed to approximately 12 km. The obtained errors over the check points have a mean of 7.2 cm. The estimated values of the unknowns are:

$N_o = 15.852$ m, $N_1 = 0.00001669$, and $N_2 = 0.00000898$

In the third investigated case, only five points (a point out of every four successive points) are utilized in the solution of equation (4). The average station separation has changed to approximately 16 km. The obtained errors over the check points have a mean of 12.6 cm. The estimated values of the unknowns are:

$N_o = 16.799$ m, $N_1 = 0.00002398$, and $N_2 = 0.00003232$

Table 1: Results of Geoid Undulation Interpolation

Case	No. of Stations	Average Distance (km)	Estimated Parameters			Average Error (cm)
			N_o	N_1	N_2	
1	13	8	13.825	3105 $x10^{-8}$	297$x10^{-8}$	2.9
2	7	12	15.852	1669 $x10^{-8}$	898 $x10^{-8}$	7.2
3	5	16	16.799	2398 $x10^{-8}$	323 $x10^{-8}$	12.6

In order to realize these results in a more convenient way, the accuracy may be evaluated in the relative form of mm/km. The above mentioned three cases give estimates equal to 4 mm/km, 6 mm/km, and 8 mm/km respectively. There are several engineering applications that do not require high accuracy of orthometric heights, and hence could be benefit from the presented approach to convert GPS heights to orthometric heights. Some of these applications are: mapping for preliminary planning, digital terrain modeling, mapping from remote sensing images, and Geographic Information System (GIS).

5. PRODUCTIVE TOPOGRAPHIC MAPPING SCHEME

It worth mentioning that recent modified GPS techniques (especially the on-the-fly method) increase the productivity and decrease the costs and

time needed for topographic mapping of large areas, as in the South Valley (Toshka) development project [2]. In that study, topographic maps for an area of 75,000 feddans (approximately 315 million squared meters) have been developed. This comprised the production of 50 topographic maps of scale 1:5,000 with a contour interval of 1 meter. Each map covers a 3x2 km piece of land whose area is 1500 feddans. A modern productive technique was suggested and implanted, in which the field data campaigns consists of three types of geodetic observations, namely static GPS, OTF relative kinematic GPS; and levelling. An integrated processing strategy has been, also, developed. The current developed simple height transformation scheme can be utilized within that productive strategy in order to obtain orthometric heights needed for contour mapping. In order to convert GPS heights to the corresponding orthometric values, the total area is divided into 3x3 km blocks. At least 3 GPS/Levelling stations should be established in each block. Static, or even Rapid Static, GPS modes are utilized to get accurate GPS positions for these stations. Spirit differential levelling is performed to obtain their orthometric heights. Hence, the presented approach is utilized to estimate the bias and tilts unknown parameters. The computed unknowns are, then, used to convert the ellipsoidal heights of other GPS epochs to orthometric heights, and the contour map is generated.

6. CONCLUSIONS

Recent techniques of the GPS satellite technology have increased the production level of topographic mapping, especially in national development projects in Egypt. GPS provides ellipsoidal heights relative to the WGS84 global ellipsoid. This type of heights does not have the physical meaning we need in geodetic applications. Orthometric heights, relative to the Mean Sea Level, are the most common height type used in the Ministry of Water Resources & Irrigation and in all other engineering applications. An approach of converting GPS heights to orthometric heights has been developed. The obtained results show that the accuracy estimate of this technique is enough for several applications as: topographic mapping, digital terrain modeling, mapping from remote sensing images, and Geographic Information System (GIS). The integration of recent GPS observation methods (as the on-the-fly method) and the approved height conversion approach used for the production of topographic maps in national projects in Egypt.

REFERENCES

[1] Alnaggar, D., 1986, Determination of the geoid in Egypt using heterogeneous geodetic data, Ph.D. dissertation, Faculty of Engineering, Cairo University, Cairo, Egypt.

[2] Alnaggar, D., and Dawod, G., 1999, Efficiency of GPS techniques in national applications, Proceedings of the International Conference on Integrated Management of Water Resources in the 21st Century, Cairo, November 21-25, Volume II, pp. 741-752.
[3] Dawod, G., 2002, Utilization of modern GPS techniques to estimate depressions volumes for water resources management, Water Science Magazine, October.
[4] Dawod, G., 1998, A national gravity standardization network for Egypt, Ph.D. Dissertation, Shoubra Faculty of Engineering, Zagazig University, Cairo, Egypt.
[5] Featherstone, W., Dentith, M., and Kirby, J., 1998, Strategies for the accurate determination of orthometric heights from GPS, Survey Review, No. 267, pp. 278-296.
[6] Martensson, S., 2002, Height determination by GPS: Accuracy with respect to different geoid models in Sweden, FIG XXII International conference, Washington, D.C., USA, April 19-26.
[7] Saad, A., and Dawod, G., 2002, A Precise Integrated GPS/Gravity Geoid Model for Egypt, Civil Engineering Research Magazine (CERM), Al-Azhar University, V.24, No. 1, pp..
[8] Saad, A., 1998, Productivity analysis for obtaining orthometric heights without levelling in Egypt, CERM V. 20, No. 3, pp.430-440.
[9] Seker, D., and Yildirim, A., 2002, Orthometric height derivation from GPS observations, FIG XXII International conference, Washington, D.C., USA, April 19-26.
[10] Shaker, A., Saad, A., and El Sagheer, A., 1997, Enhancement of the Egyptian gravimetric geoid 1995 using GPS observations, Proceedings of the International Symposium on GIS/GPS, Istanbul, Turkey, Sept. 15-19.
[11] Smith, D., and Roman, D., 2001, GEOID99 and GS99SSS: 1-arc-minute geoid models for the United States, Journal of Geodesy, V. 75, No.9, pp. 469-490.

Proceedings of Al-Azhar Engineering 7th International Conference
Cairo, April 7-10, 2003.

MODERNIZATION PLAN OF GPS IN 21st CENTURY AND ITS IMPACTS ON SURVEYING APPLICATIONS

G. M. Dawod

Survey Research Institute, National Water Research Center, Egypt

ABSTRACT

The Global Positioning System (GPS) has been developed in 1970's as a military, and partially a civilian, navigation system. Over the last three decades, GPS has become the primary tool in surveying and mapping applications worldwide with Egypt be no exception.

A new modernization plan is currently underway by the U.S. Department of Defense in order to make GPS cope with the requirements of advanced technologies in the 21st century. The first step in this strategy, carried out in May 2000, was turning off the Selective Availability (SA) accuracy degradation. Additionally, a new civil signal (called L2C) will be transmitted by modernized Block IIR (IIR-M) and all subsequent satellite starting from 2003. For military purposes, a new military code (called L2M) will be added to the L2 frequency. Furthermore, another completely new civil signal (called L5) will be transmitted on a frequency of 1176.45 MHZ as early as 2005 by the Block IIF satellites. Also, the modernization plan includes several improvements to enhance the performance of the GPS control segment. This paper presents the characteristics of each component of the GPS revolutionizing plan, and investigates its anticipated influences on surveying and mapping applications in terms of system integrity and availability, attainable positioning accuracy and reliability.

KEYWORDS
Surveying, GPS, Satellites; Signals and codes

[1] dawod_gomaa@hotmail.com

1. Introduction

Since the mid-1980s, the Global Positioning System (GPS) has been extensively utilized in a wide range of civil and military applications worldwide. Today, GPS is used almost exclusively employed by the geodesy and surveying community for a large variety of mapping projects. The GPS technology is entering a new era in the 21st century through the undergoing execution of a fifteen-year revolutionizing modernization plan. This program focuses on improving position and timing accuracy, availability, integrity monitoring support capability and enhancement to the control system. This paper aims to present the characteristics of the components of the GPS modernization strategy, and to investigate its anticipated influences on surveying applications.

2. The need for GPS Modernization

The development of GPS technology has started in the early 1970s by the U.S. Department of Defense (DoD). The first generation of GPS satellites (Block I) has been launched in space starting February 23, 1978. GPS has been officially declared "fully operational" as of April 27, 1995. However, the basic structural characteristics of GPS, i.e., satellites, transmitted signals, and even the control segment, have not been changed significantly in the last quarter of the twentieth century. This is a relatively a long time on the technology development time scale. Several reasons and motivations were behind the development of a fifteen-year modernization plan to make GPS cope with the requirements of technologies in the 21st century.

Starting in 1997, special technical meetings have been carried out by the Interagency GPS Executive Board (IGEB) to develop a new modernization strategy. Several procedures have been suggested to meet the civilian and military requirements of GPS services. The main civilian goal was to enhance the performance of the GPS Standard Positioning Service (SPS). SPS refers to the signal-in-space provided free of direct user charges for peaceful, commercial, and scientific use on a continuous, worldwide basis. It is known that only one fully accessible signal (The Course-Acquisition C/A coded signal at L1 frequency) is available for civilian applications. Moreover, the Selective Availability (SA) was implemented starting July 4, 1991 to degrade the full real-times GPS accuracy for civilian users. On a military basis, the modernization plan aims to provide another Precise Positioning Service (PPS) for U.S. military and other authorized users, and to develop measures to prevent the hostile use of GPS. Today, only the Y (encrypted precise P) code is modulated on the L2 frequency for military applications.

Some of the overall objectives of the modernization program, as described in the FRP official U.S. document, are [1]:
- Worldwide coverage.
- User-passivity.
- Resistance to interference and jamming.
- Resistance to natural disturbance and hostile attacks.
- Resistance to radio frequency (RF) interference.
- Effectiveness of real-time response.
- Existence in appropriate radionavigation bands.
- High positional accuracy.
- Continuous availability of information.
- Continuously reliable for navigation.
- Cost effectiveness.

3. Components of the modernization plan

GPS Modernization is a multi-phase effort to be executed over the next 15+ years by DoD. In order to achieve the previously mentioned objective, the modernization strategy consists of several elements. On a civilian basis, the first real step toward modernizing GPS took place on May 1, 2000 by turning off the SA error source. This step afforded GPS civil users at least a five-fold improvement in accuracy. In absence of SA, accuracy estimates would be 22 meters horizontal and 33 meters vertical (95% of the time) [2]. Another civilian component of GPS modernization is providing additional coded civil signals (L2C on the L2 frequency and a completely new signal called L5). For military applications, a new military code (known as M code) will be transmitted on both L1 and L2 frequencies. The GPS satellites will also be an important part in the innovation strategy. The IGEB has accepted a DoD recommendation to develop a new generation of satellites (Block III) that meet the military and civilian requirements through 2030. The last module of the modernization plan is upgrading the GPS operational control segment and its facilities. Each element of this revolutionizing plan will be discussed in more details in the following sections.

3.1 New GPS civilian signals

Two new codes are planned to be transmitted by GPS satellites for civilian applications. The first civilian signal, called L2C, was announced by a white house press release on March 30, 1989. L2C is a modified C/A code transmitted on the L2 frequency by the modernized block IIR (IIR-M) and all subsequent satellites. The first IIR-M satellite is scheduled to be launched in 2003. The designed structural characteristics of the L2C code, as will be discussed, prove that it will become the most widely used GPS signal of all since. The second

civilian signal, called L5, has features that depart significantly from the other GPS frequencies, making it much more robust and more resistant to interference. The code transmitted on L5 has special design characteristics, and is not a replica of the other codes on the new L5 frequency.

The main key feature of L2C is that it better matches to 21st century capabilities and requirements The actual technical development of L2C has been carried out in January 2001. Two primary requirements drove the design of L2C. The first objective is to eliminate need for the semi-codeless tracking techniques now used to acquire the L2 measurements. L2C enhances tracking performance by having no data on one of its codes, and provides full-wavelength carrier phase measurements without having to resolve the phase ambiguity inherent in signals with bi-phase data modulation. The L2C signal structure consists of: (1) The CM, which is a moderate-length code contains 10,230 chips, repeats every 20 milliseconds, and is modulated with message data; and (2) The CL, which is a long-length code contains 767,250 chips, repeats every 1.5 seconds, and has no data modulation [4 and 5]. The second key objective was to let L2 lower the data modulation threshold, making it possible to read the message when barely tracking the signal. In order to achieve this goal, L2C has cross-correlation performance of 45 dB, compared to the unacceptable 21 dB cross-correlation of the L1 C/A code [6].

The second civil signal, called L5, will be transmitted on a frequency of 1176.45 MHZ by Block IIF satellites as early as 2005 [7]. The L5 band is set aside by the International Telecommunication Union for the aeronautical radionavigation service in order to satisfy the safety-of-life requirements for aircraft navigation. However, L5 also will serve as a robust third civilian signal for all users and applications. There are a lot of factors drove the design of the L5 signal based on manufactures and users' points of view. An important user requirement, affected the L5 signal design, is the request for data-free carrier component. This is a crucial demand for users perform real-time kinematic (RTK) carrier tracking operations. A data-free component provides users with a capability to track whole carrier cycles and enhances tracking the carrier at significantly lower signal-to-noise rations. A carrier component that carries the navigation data is also required, so that the L5 signal is independent of the other civil GPS signals.
The L5 signal structure was developed by the RTCA special committee SC159 working group 1 in 1999. In order to make L5 more powerful than the existing L1 and L2 signals, significant signal structural changes have been performed in terms of bandwidth, signal power, code structure, chipping rate, data structure; and data modulation. L5 is designed with a center frequency of 1176.45 MHZ, a minimum bandwidth of 20 MHZ, and a signal power four times stronger than the L1 C/A [7]. Moreover, the L5 offers two components: one with and one without a superimposed navigation data messages. Each component is

modulated with a different, but synchronized, L5 code. Different PRN codes (known as I5 and Q5) are used in the two components to prevent tracking biases by making each component completely independent of the other, except for the carrier phase. A more efficient data message structure is employed in L5 providing navigation data with integrity in a more timely manner [8].

3.2 New signal availability

It is known that since the 1974 when the first Block I satellite was launched, there have been only three navigation signals: C/A on L1, P/Y on L1; and P/Y on L2. The modernization plan will double the total number of signals by 2003. Launching the first Block IIF satellite in 2005, the number of signals will be seven. This dramatic change is illustrated in table 1. Figures 1 and 2 depict expected time line of new signals availability based on the estimated satellites launching scheme. The first Block IIR-M satellite are expected to be launched in 2003, while Block IIF satellites are anticipated to be launched starting 2005. As shown in these two figures, it is probable that by 2011 there will be 28 satellites transmit L2C signals and 18 satellites transmit L5 signal. The initial operation capability (IOC) of L2C service, i.e., 18 satellites on orbit, is planned for 2008, while the full operational capability (FOC), i.e., 24 satellites on orbit, is planned for 2010. For the L5 service, the IOC is planned for 2005, while the FOC is planned for 2014 [1].

Table 1
GPS Navigation Signals

Signals \ Year	Now: Block IIR satellites	2003: Block IIR-M satellites	2005: Block IIF satellites
C/A on L1	X	X	X
P/Y on L1	X	X	X
M on L1		X	X
L2C on L2		X	X
P/Y on L2	X	X	X
M on L2		X	X
Civil L5			X

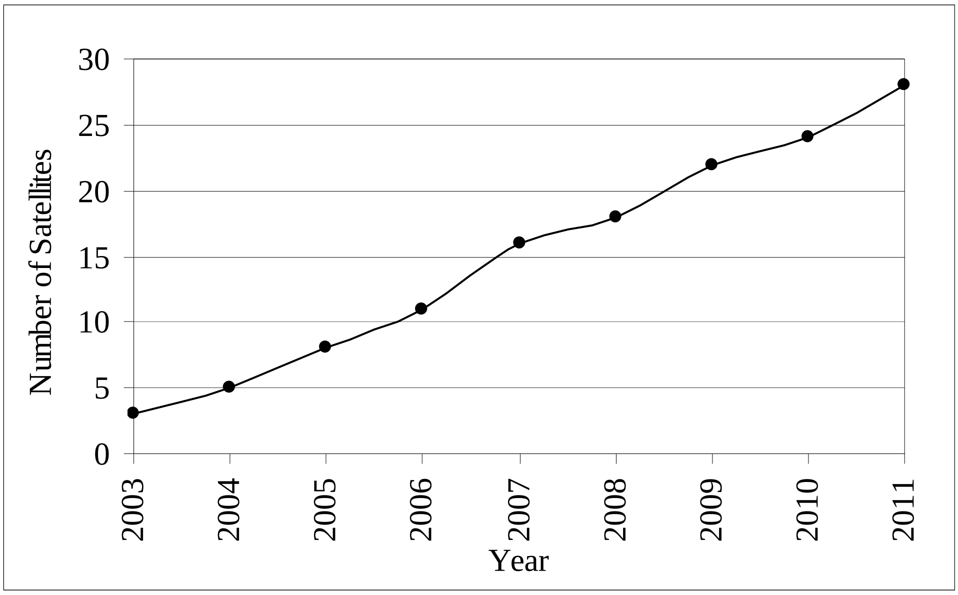

Figure 1
Planned L2C Availability Schedule

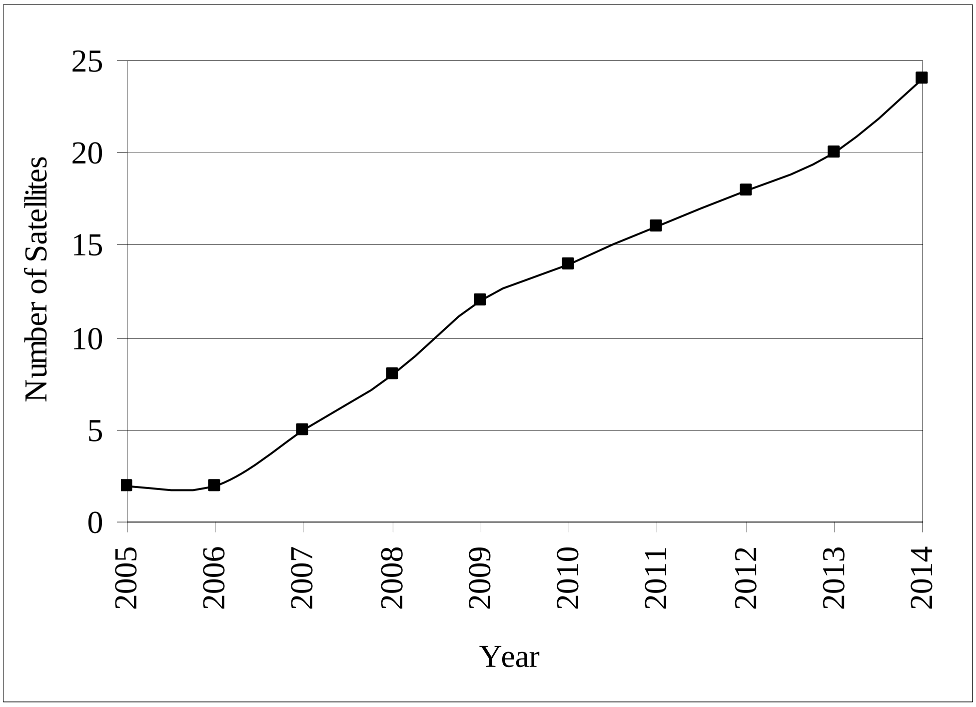

Figure 2
Estimated L5 Availability Schedule

3.3 Improvements of GPS satellites

The current GPS operation plan carries the constellation through approximately the year 2010, considering the use of 12 Block IIF satellites. To fulfill military and civilian requirements, the IGEB recommends the development of a new generation of satellites that is called Block III. In 2000, the U.S. DoD initiated a study that examines candidate acquisition and architectural concepts satisfying system requirements [8]. A crucial element of Block III satellites, from a military perspective, is the need for a higher power M code to improve resistance to intentional and unintentional signal interference. Optimized costs, high performance, risk, and technology insertion are the main elements of the undergoing development plan of Block III satellites [1].

3.4 Improvements of GPS control segment

Updating the control segment is another essential element in the GPS modernization program. Several improvements are currently being carried out to enhance the capabilities of satellite monitoring and to increase the positioning accuracy of both military and civilian services. Some of the improvement procedures are [8]:

- Upgrading the monitoring stations and ground facilities.
- Replacing existing mainframe computers with high-technology ones.
- Establishing an alternate master control station.
- Implementing new more-robust mathematical techniques for computing satellites' orbits and clock errors.
- Incorporating data from other monitor stations operated by the National Imagery and Mapping Agency, known as NIMA, to increase the accuracy of computed orbits and clock parameters.

4. Overall merits of the modernization program

The overall plan of GPS modernization intends to enhance the system performance to meet the technology requirements in 21st century. Military and civil GPS users will attain a lot of advantages. Turning off the selective availability (SA) in 2000 afforded GPS civil users accuracy of 22 meters (compared with accuracy of 100 meters under SA). With the absence of SA, the next largest error source is the signal delay caused by the Earth's atmosphere. Having a second and a third civilian code (L2C and L5) will enable the GPS civilian users to correct the ionospheric error by forming a linear combination of pseudorange measurements. This will be reflected in more accuracy in real time situation such as aircraft approaching and landing. The L2C signal will achieve more reliable and accurate positioning and navigation even in wooded areas.

The new structural design of L5 offers more robust carrier phase tracking and provides grater accuracy even in the presence of noise and multipath. The underway modernization of the control segment is expected to reduce ephemeris and clock error by approximately 50% [8]. Additionally, the new Block III satellites will improve the resistance of signal interference. The GPS modernization components will increase the horizontal accuracy estimate to be 6 meters or better for standalone GPS receivers. The modernization program will make GPS an even more powerful utility, serving the needs of civilian users well into 21st century.

5. Impacts of GPS modernization on surveying and mapping

With the GPS modernization program, the surveying and mapping applications will enter a new era. Several GPS-based 'traditional' problems and situations that faced the surveying community in the last quarter of the twentieth century will no longer exist. Even more, GPS will be efficiently utilized in new applications. The 6-meter accuracy level for non-differential (standalone) mode will make Geographic Information System (GIS) data collection less expensive and more reliable by only using hand-held cheap code receivers. The same is true for image rectification process of remote-sensing images with pixels size of five meters or larger. For static survey applications, centimeter-level accuracies will be achievable more quickly and cost effectively than is possible today. This is obtained through the existence of three frequency wide lanes (L1-L5, L1-L2, and L2-L5) to resolve integer ambiguities and making precise carrier phase measurements. Since the position accuracy is the most-crucial demand from the geodetic and mapping community, it was an objective of the modernization strategy to afford high-level of accuracy for this sector of users. Table 2 presents some estimates of the anticipated accuracy for survey applications [3]. Current civil GPS users will be able to operate at the same, or better, levels of performance that they enjoy today. It should be mentioned that in order to benefit from the advantages of the GPS modernization plan, the user have to pay non-direct use costs. Updating current hardware (receivers and software), or even purchasing new ones, will be a must to cope with the modernized components of GPS technology in 21st century.

Table 2
Anticipated achievable accuracy for survey applications
(centimeters)

Task	Absolute Accuracy		Relative Accuracy		
	Horizontal	Vertical	Horizontal	Vertical	Remarks
Static Survey	30	50	1.0	2.0	0-25 Km 30 min
Geodetic Survey	10	20	1.0	2.0	0-6000 Km 4 hours
Rapid Survey	30	50	2.0	5.0	0-20 Km 5 min
On-The-Fly Kinematic Survey	30	50	2.0	5.0	0-20 Km Real Time

6. Conclusions

Since the development of GPS technology in the early 1970s, its basic structural characteristics have not been changed significantly. A fifteen-year modernization plan is currently underway to make GPS cope with the requirements of technologies in the 21st century. In 2000, the SA error source was turned off affording standalone position accuracy of 22 meters horizontal and 33 meters vertical. The modernization program includes transmitting two new civil codes: L2C and L5. L2C is a modified C/A code transmitted on the L2 frequency by the modernized block IIR satellites starting 2003. L5 will be transmitted on a new frequency of 1176.45 MHZ by Block IIF satellites as early as 2005. Additionally, a modern generation of GPS satellites, called Block III, is currently under development. Updating the control segment is another essential element in the GPS modernization program.

Through the GPS modernization program, the surveying and mapping applications will enter a new era. The expected 6-meter accuracy level for non-differential mode will make GIS and remote sensing data collection more cost-effective and more reliable. For static survey applications, centimeter-level accuracies will be achievable more quickly and cost effectively than is possible today. Even though current geodetic and surveying GPS users will be able to operate at the same, or better, levels of performance, they have to pay non-direct use costs in order to benefit from the advantages of the GPS modernization plan. Updating existing hardware (receivers and software), or even purchasing new ones, will be a must to cope with the modernized components of GPS technology in 21st century.

References

[1] Department of Defense, 2001a, The Federal Radionavigation Plan: FRP2001, 64 pp.

[2] Department of Defense, 2001b, The Global Positioning System Standard Positioning Service Performance Standard, 66 pp.

[3] Department of Defense, 1999, The Federal Radionavigation Plan: FRP1999, 169 pp.

[4] Dierendonck, A., 2000, The new L5 civil GPS signal, *GPS World*, September.

[5] Fontana, R., Cheung, W., and Stansell, T., 2001, The modernized L2 civil signal, *GPS World*, September.

[6] Navstar GPS Joint Program Office, 2001, ICD-GPS-200C document for L2 civil (L2C) signal, Distributed by ARINC Inc., El Segundo, California, USA, 43 pp.

[7] Navstar GPS Joint Program Office, 2002, ICD-GPS-705 document for Navstar GPS space segment / user segment L5 interfaces, Distributed by ARINC Inc., El Segundo, California, USA, 100 pp.

[8] Shaw, M., Sandhoo, K., and Tuner, D., 2000, Modernization of the Global Positioning System, *GPS World*, October.

Published in: Water Science Magazine, No. 33, 2003, April. pp. 33-39.

PROPOSED STANDARDS AND SPECIFICATIONS FOR GPS GEODETIC SURVEYS IN EGYPT

By

Gomaa M. Dawod
Researcher, Survey Research Institute

ABSTRACT

High-precision positioning with the Global Positioning System (GPS) with a precision of a few parts per million has become a routine task worldwide, with Egypt be no exception. Since the mid 1980's, GPS bas been utilized in Egypt for a wide range of applications on a national scale, especially the extensive geodetic employment of this revolutionizing satellite technology in the huge national south valley development project. However, there is no set of Egyptian standards and specifications for applying GPS in geodetic surveys in order to be able to unify different GPS projects and results towards the establishment of nation-wide geodetic data banks.

A series of standards and specifications is designed for Egypt for the first time. This set includes specifications for equipment and software to be used, GPS network design, site selection and monumentation, field procedures, data processing, network adjustment; and GPS final output documentation. This set is just a starting required step. Hence, it is highly recommended that the geodetic community in Egypt should make extended efforts to come up with a final form of specifications for the manipulation of GPS geodetic surveys in Egypt.

1. Introduction

> "Sometimes one hears the opinion that every thing in geodesy can now be done by GPS, and GPS receivers can be operated by technicians without university education, so that geodesists are no longer needed."

The above statement by the sole father of geodesy 'Helmut Moritz', [17], is just an example of how GPS has been spread in the surveying community worldwide. The performance of GPS for precise relative positioning has lead the geodetic community to believe that base lines of a few tens of kilometers in length could be determined in a routine fashion to a relative precision level of a few parts per million. Moreover, some global GPS networks have produced excellent results of one part per billion (i.e., an error of 0.001 mm in a base line of one-kilometer length) for base line lengths up to 4000 kilometers [4].

The rapidly growing use of GPS for geodetic surveys in Egypt, in the last decade, makes it critical to develop a set of acceptable accuracy standards. Specifications reflect the measurement systems, and therefore will be developed and refined as improvements to measurement systems are demonstrated. Standards, on the other hand, must provide the user with a stable, understandable and usable identification scheme for control points. This research study proposes an Egyptian series of standards and specifications that include most of the practical issues in: pre-planning, network design, field procedures, data processing, network adjustment; and presentation of the final results. The current study is restricted, for the time being, to only the first and second order geodetic networks.

2. Specifications of geodetic networks

Classifications of geodetic networks depend on several approaches such as the geometric distance accuracy in USA [13] and the semi-major axis of error ellipse in Canada [8]. It is inferred that the first approach was implemented when the first-order Egyptian geodetic networks were established [5]. The geometric distance accuracy is the ratio of the relative positional error of a pair of control points to the separation of these points. Minimum distance accuracy is assigned to each order of geodetic networks. For the first-order conventional geodetic network in Egypt, the distance accuracy was 1:100,000 where the average side length ranges from 40 to 50 km [ibid.].

With the development of GPS survey observation systems, a modification to the geometric distance accuracy criterion was proposed by the U.S. Federal Geodetic Control Committee (FGCC) [10]. This revision reflects the performance of systems include a base error, so that the accuracy standard, in the 95% confidence level, is divided into a base error, e.g. a receiver setup error, and a length-dependant part. Based on this recent approach, a proposed classification of GPS geodetic networks in Egypt is shown in table 1.

Table 1: Standards of GPS Geodetic Networks

Category	Order	Base Error (cm)	Length-Dependant Error ppm	1:a
Primary National Geodetic Network	A	0.5	0.1	1:10,000,000
Secondary National Geodetic Network	B	0.8	1	1:1,000,000

3. Specifications for GPS network design and pre-planning

Prior to starting a GPS field campaign, some stereotyped items must be settled for the network design, the selection of GPS hardware to be used, the campaign pre-planning; and the site selection and monumentation for geodetic GPS stations. Each item is further investigated in the next sub-sections.

3.1 GPS network design

Generally, the quality of a geodetic network is characterized by three factors: economy, productions; and reliability. Economy expresses the costs of monumentation, observations, transportation,.. etc. Precision, as expressed by the standard deviation, is the measure of the network's characteristics in propagating random errors. Reliability describes the ability of the network to check model errors. Although the accuracy of GPS techniques is less sensitive than terrestrial techniques to network design geometry, the accuracy can be improved by taken some considerations into account in the network design process. For a GPS network to fulfill its primary role as a strong and reliable reference framework, it must maintain the following basis:

- Homogenous coverage.
- Reasonable redundancies.
- Well-shaped closed individual figures (loops).
- Stations should be as evenly spaced as possible.
- The ratio of the longest to the shortest baseline should never be greater than five and usually be much less.

3.2 Selection of GPS hardware

The GPS hardware market has a wide variety of GPS receivers, which could be classified based on several factors as shown in figure 1. Testing several single and dual-frequency GPS receivers shows that dual-frequency ones meet the accuracy specifications for precise geodetic networks with no constraints, while the single-frequency receivers may not fulfill these specifications with the presence of significant ionospheric disturbances [11 and 12]. At a frequency of 1.575 GHZ, ionospheric refraction can delay the transmission of information modulated onto the carrier wave by up to 300 nanoseconds from its free space velocity, which corresponds to a range error of 100 meters [14]. The advantage of having dual-frequency data is the capability to develop the so-called ionospheric-free observables's combination that results in a more precise solution. Code GPS receivers, on the contrary to codeless type, can access the information contained in the transmitted navigation message of satellites. Multi-channel receivers are more reliable

and have better signal-to-noise ration, which means they can receive even weaker signals. Hence, the specifications of GPS receivers to be used in establishing first and second-order geodetic networks are summarized in table 2.

Table 2: Specifications of Geodetic GPS Receivers

- Static - Differential positioning - Dual-frequency - Code - Multi-channel with at least 8 independent channels - Built-in or external memory for at least 6 hours of data collection. - Internal power sources enough for at least 6 hours of observations.

GPS measurements can be significantly corrupted by GPS signals that reflecting off surfaces near (within some 30 meters) the antenna. The sensitivity of multipath corruption depends on the reflectivity of the surfaces in the antenna environment, and on the antenna gain (sensitivity) in the direction of these reflectors. Signal multipath interference could be 4 meters numerical standard deviation [9]. The placement of the antenna and the use of absorption material can significantly reduce the multipath effects. Therefore, a geodetic GPS receiver's antenna should have the characteristics shown in table 3.

Table 3: Characteristics of Geodetic GPS Antennas

- Resistance to multipath effects - Phase-center determination accuracy - High sensitivity - Ease of antenna centering

3.3 Pre-planning

Prior to conducting a GPS project, a certain amount of office planning is essential. The following factors should be carefully checked so that the GPS survey meets the accuracy standards required:
- Maximum number of control points available.
- Maximum and minimum station spacing.
- Location of control points.
- Number of receivers observing simultaneously.
- Session interval.
- Subset of tracked satellites that give good Position Dilution Of Precision (PDOP).
- Independent occupations per stations.
- Repeated baseline measurements.

One of the most important factors in the pre-planning step to be taken into consideration is the PDOP value, which is a measure of the accuracy of pseudorange measurements in three-dimensional positioning. PDOP values in the range 3-5 m/m are considered very good, while values greater than 10 m/m are considered poor [2].

A simulation computer program should be used to estimate several PDOP values to select beforehand the subset of satellites, which should be tracked to give the best station-satellite geometry.

3.4 Selection of GPS stations and monumentation

Selecting sites for GPS stations must fulfill the following criteria:

- Monuments set on stable solid rock.
- Visible sites (placed in areas with clear sky above 15^{o} elevation).
- No multipath targets nearby.
- Easily accessible.
- Apt to remain intact for a long time.
- Convenient for use.

The proposed Specifications for design GPS geodetic networks are summarized in table 4.

Table 4: GPS Network Design Specifications

Items	1st order net	2nd order net
Maximum station spacing (km)	100	50
Minimum control points	3	3
Bench marks included	minimum 4	optional
Maximum number of lines in a loop	10	10
Maximum loop overall length (km)	100	100
Maximum percentage of stations with 2 or more occupations	50 %	30 %
Minimum degree of freedom	12	9

4. Specifications for GPS field work

The most affecting error sources in GPS fieldwork are the antenna setup errors. These errors contain the centering error and the error in measuring the antenna height. The phase measurements made by GPS receivers referee to the antenna phase center, while the station positions and baseline vectors should be referenced to the ground survey marks. Therefore, a correction is needed to tack into account the height difference between the antenna center and survey marks. Some GPS receivers are equipped with a means to measure this vertical height difference directly. Other receivers have a way to measure the diagonal distance between the circular antenna edge and the survey mark, and hence, another correction is required to compute the vertical height difference knowing the radius of the antenna plate. For example, using the non-corrected antenna diagonal heights (0.84 and 1.39) instead of the corrected vertical heights (0.81 and 1.37) results in an error of about 1 cm in each component of a baseline vector of 60,060 meter length, which is a significant error in precise geodetic networks. Consequently, suggested field procedures to minimize antenna setup errors include:

1- Measure and record antenna height, in both meters and inches, before and after each station occupation.
2- GPS operators, if more than one, should verify all measurements.
3- Check collimation and levelling of the antenna before and after each station occupation.

4- Log antenna serial number as a part of the station record in order to verify, later, that the correct phase center correction is applied.
5- Redundant station occupation should be performed as much as possible.
6- Photographs of every station mark are required to allow verification that the mark occupied was in fact the correct one.

Proposed Specifications for GPS field procedures for geodetic surveys are given in table 5.

Table 5: GPS Field Procedures Specifications

Items	1^{st} order net	2^{nd} order net
L1/L2 observations	Yes	optional
Minimum number of receivers	3	3
Minimum number of satellites	4	4
Session interval (minutes)	90-120	45-90
Sample rate of observations (seconds)	15-30	15-30
Minimum mask angle above horizon	15^o	15^o
Minimum antenna height measurements	2	2
Maximum difference in antenna height measurements (cm)	2	2
Photograph required	yes	yes

5. Specifications for GPS data processing

Data processing is the most crucial stage in any GPS project. Computer software are used to process the raw satellite signals, apply required corrections, and solve the normal equation system in a least-square sense to come up with the precise vector components and related results. The data processing criteria to be considered are [18]:

- How the antenna offsets are applied.
- The cut-off angle.
- Ephemeredes source and age.
- Measured data quality.
- Measurements rejection criteria.
- Maximum residuals.
- Baseline or session adjustment specifications.

Important measures for judging the quality of the data are: RDOP, RMS, ratio test; and the solution for phase ambiguities. Relative Dilution Of Precision (RDOP) is a quantity describes the geometry of the satellites and its impact on the precision of the recovery of carrier phase measurements. RDOP values around 0.1 m/cycle are considered acceptable [15]. Root Mean Square (RMS) is a measurement, in unite of cycles, of the quality of the observed data collected during a point of time. Factor ratio is the ration of sum-of-squares of two solutions using different sets of phase ambiguity integers. RMS is considered good in the range from 0.01 to 0.2 cycles, while the ratio test should be greater than 3 to obtain fixed solutions. Careful screening of these quality measures is desired to decide which base line solution to be finally accepted and included in the network adjustment. It worth mentioning that some adjustment software has an “automatic selection” option to figure which

solution is the "best". However, some recommendations in this issue are shown in table 6. Still, the substantial question is "which post-processing software to be used?". Table 7 gives some proposed Specifications for GPS processing software for precise geodetic applications, while table 8 presents some Specifications for performing GPS data processing and judging the obtained solutions.

Table 6: Recommended Procedures in GPS Data Processing

RMS	Factor Ratio	Distance	Integer Solution	Recommendations
Small	Large	< 20 km	Yes	Use fixed solution
High	Large	> 20 km	Yes	More inspection, use fixed solution
High	Large	< 20 km	Yes	Re-process fixed solution or repeat measurement
Small	Large	20-65 km	No	Use float solution
High	Large	> 65 km	No	Use triple solution or repeat measurement

Table 7: Specifications for GPS Data Processing Software

- Process pseudoranges and carrier phase observations.
- Support point, baseline; and network modes of positioning.
- Automatically detect and resolve cycle slips.
- Endure single, double; and triple processing modes.
- Accept up to 10 base line, or more, in a single session.
- Provide fixed, float; and triple solutions.
- Output statistical information along with each solution.
- Support several values of processing parameters (e.g. sample rate, tropospheric models, meteorological data, mask angles, … etc.).
- Interactive with users when changes are needed.
- Hold up different antenna types.
- Provide pre-analysis modules (e.g. compute PDOP in advance).
- Accept different sources of satellite ephemeredes (broadcast or precise).
- Support both single and dual-frequency data.
- Sustain manual, interactive; and automatic batch modes.
- Preferable: menu-driven, easy-to-use; and friendly software.

Table 8: Proposed GPS Data Processing Specifications

Items	1st order net	2nd order net
Precise ephemeredes	Recommende	Optional
Maximum loop closure in vector components (cm)	d	30
Maximum loop closure (ppm)	25	25
Maximum percentage of rejected measurements	12.5	10 %
Standard deviation of base line solution (cm)	10 %	1 to 4
	0.1 to 2	

6. Specifications for GPS adjustment

For any GPS network, it is necessary to describe how to position and orient the network on the earth's surface (i.e., datum definition). This can be done, in general, in several ways [18]:

- Holding one point fixed (fixed-point approach).
- Holding one point properly weighted (fiducial-point approach).
- Holding no point fixed (free-net approach).
- Holding several points fixed (over-determined approach).
- Holding several points properly weighted.

The first three approaches use the minimum necessary number of positional constraints, and therefore known as minimally constrained adjustment. It is known that a GPS network has three (out of seven) datum defects since the orientation and scale are implicitly known from the phase observations because the coordinates of the satellites are assumed to be known [6]. A method for overcoming this problem is to use inner constraints to allow the adjustment to proceed by using the centroid of the unadjusted coordinates to control coordinates translation. The last two approaches belong to the so-called over-constrained adjustment. The factors that may be considered as proposed Specifications for GPS adjustment software are shown in table 9.

Table 9: Specifications for GPS Adjustment Software

Support processed solutions from several GPS manufactures.
Sustain minimally and fully constrained adjustments.
Support datum definition and transformations.
Maintain several map projections.
Support pre-analysis modules (e.g. loop misclousure).
Allow data editing by the user.
Provide statistical information (e.g. RMS, chi-squares, ppm, …etc).
Preferable: menu-driven, easy-to-use, friendly, handles big networks, fast; and provides plotting capability.

The process of GPS network adjustment is recommended to be performed in the following sequence of procedures to come up with optimum results:

A. Analyze the loops' closure to verify that the closure errors are within the accuracy Specifications required (refer to table 7).
B. Perform a free net adjustment (i.e., fix a single, often arbitrary, point) to analyze the internal consistency of the survey data.
C. Use the statistical information of the free net adjustment to detect blunders and residual outliers. Detecting and removing erroneous observations is a must in geodetic networks to improve the network reliability [3].
D. Perform a final constrained adjustment (minimal or over-constrained) to fit the GPS survey to existing geodetic frameworks.

The precision of the adjusted control points in a GPS geodetic network is expressed as a ratio by converting its standard errors into a linear distance and dividing this distance by the distance to the nearest control point. These precision ratios of all the network points should meet the geodetic network proposed specifications (shown in table 1).

7. Specifications for GPS final results documentation

Presenting and documenting the final results of a GPS project is an important step to summarize all the procedures of design, fieldwork, data processing; and network adjustment. Unless there are certain Specifications for such a step, the unification of GPS networks in Egypt for the sake of developing geodetic data banks, will not be easily established. Table 10 presents a form of the final documentation of a GPS project.

Table 10: A Form for Final Documentation of GPS Projects

- The project name, location; and objectives.
- Design criteria:
  - Objective and classification of the GPS network.
  - Network design Specifications (table 4).
- Field work procedures:
  - Types and number of receivers and antennas used.
  - Session interval.
  - Redundant station occupations.
  - Meteorological data (if measured).
  - PDOP, RDOP.
  - Field data records of all stations.
- Processing procedures: sample rate, cutoff angles, …etc.
- Types and versions of software used for data processing and adjustment.
- Adjustment Specifications:
  - Adjustment model (minimally or over constrained).
  - Number and names of fixed points.
  - Source and values of fixed points coordinates.
  - Datum on which the adjustment was performed.
  - Statistical information: ppm, RMS, Tau values, ..etc.
- Plots: Network plot, error ellipses; and histogram of residuals.
- Final results:
  - Cartesian and geographic coordinates of all stations along with the corresponding standard deviations.
  - Distances and their relative precision (ppm).

8. Conclusions

The GPS positioning technology has been used for several geodetic projects in Egypt since the mid 1980’s. However, there is no set of specifications and standards available. Primary specifications and standards are proposed in this research study for first and second-order geodetic GPS networks in Egypt. The suggested set includes specifications for network design, selection of equipment and software, pre-analysis, station monumentation, field procedures, data processing, network adjustment; and final results documentation. This set provides GPS users in Egypt with standard, understandable; and usable procedures for precise geodetic surveys. The geodetic community in Egypt should make extensive efforts to come up with national final specifications for the use of GPS advanced positioning technology in Egypt.

References

[1] Acharya, B., and Rapp, R., 1991, Project planning for a GPS static geodetic control network, Proceedings of ACSM-ASPRS fall convention, Atlanta, USA, Oct. 28 – Nov. 1, pp. A65-74.

[2] ACE (U.S. Army Corps of Engineering), 1991, NAVSTAR GPS Surveying, Manual No. EM1110-1-1003, Washington D.C., USA.

[3] Alnaggar, D., and Dawod, G., 1995, Increasing the reliability of GPS geodetic networks, Proceedings of the first international conference on satellite positioning, Dec. 12-13, Alexandria, Egypt.

[4] Anderson, P., Hauge, S., and Kridtiansen, O., 1993, GPS relative positioning at a precision level of one part per billion, Bulletin Geodesique, V. 67, No. 2, pp. 91-106.

[5] Cole, J., 1944, Geodesy in Egypt, Egyptian Survey Authority, Government Press, Cairo, Egypt.

[6] Dawod, G., 1991, Some considerations in the adjustment of GPS-derived baselines in the network mode, MSc thesis, Ohio State University, Columbus, Ohio, USA.

[7] DMA (U.S. Defense Mapping Agency), 1987, Supplement of Department of Defense WGS 1984 Technical Report Part II: Parameters, formulas; and graphics for the practical applications of WGS84, DMA No. TR8350.2-B, Washington D.C., USA.

[8] EM&R (Canadian Energy, Mines; and Resources), 1978, Specifications and recommendations for control surveys and survey networks, Ottawa, Canada.

[9] Evans, A., and Carr, J., 1989, Effect of signal multipath errors at DMA GPS satellite tracking sites on orbit accuracy, Manuscripta Geodaetica, V. 14, No. 3, pp.143-148.

[10] FGCC (U.S. Federal Geodetic Control Committee), 1989, geometric geodetic accuracy standards and specifications for using GPS relative positioning technique, Version 5, August, Rockville, Maryland, USA.

[11] FGCC, 1990a, Test and demonstration of GPS satellite survey systems, Report No. IS-90-1, Rockville, Maryland, USA.

[12] FGCC, 1990b, Test and demonstration of three dual-frequency (L1/L2) GPS satellite survey systems, Report No. IS-90-2, Rockville, Maryland, USA.

[13] FGCC, 1991, Standards and specifications for geodetic networks (originally in 1984, re-printed Feb. 1991), Rockville, Maryland, USA.

[14] Finn, A., and Matthenwman, J., 1989, A single frequency ionospheric refraction algorithm for Transit and GPS, Proceedings of the fifth international geodetic symposium on satellite positioning, New Mexico, March 13-17, pp. 737-756.

[15] Goad, C.C., 1989, On the move with GPS, P.O.B., April, pp. 18-22.

[16] Mohamed, H.F., 1992, Consistency of GPS surveys using different geodetic receivers and processing software, MSc thesis, Faculty of Engineering, Cairo University, Cairo, Egypt.

[17] Moritz, H., 1992, Geodesy after GPS, Proceedings of the sixth international geodetic symposium on satellite positioning, Columbus, Ohio, USA, March 17-20, pp. 3-12.

[18] Wells, D. (ed.), 1987, Guide to GPS positioning, Canadian GPS Associates, Ottawa, Canada.

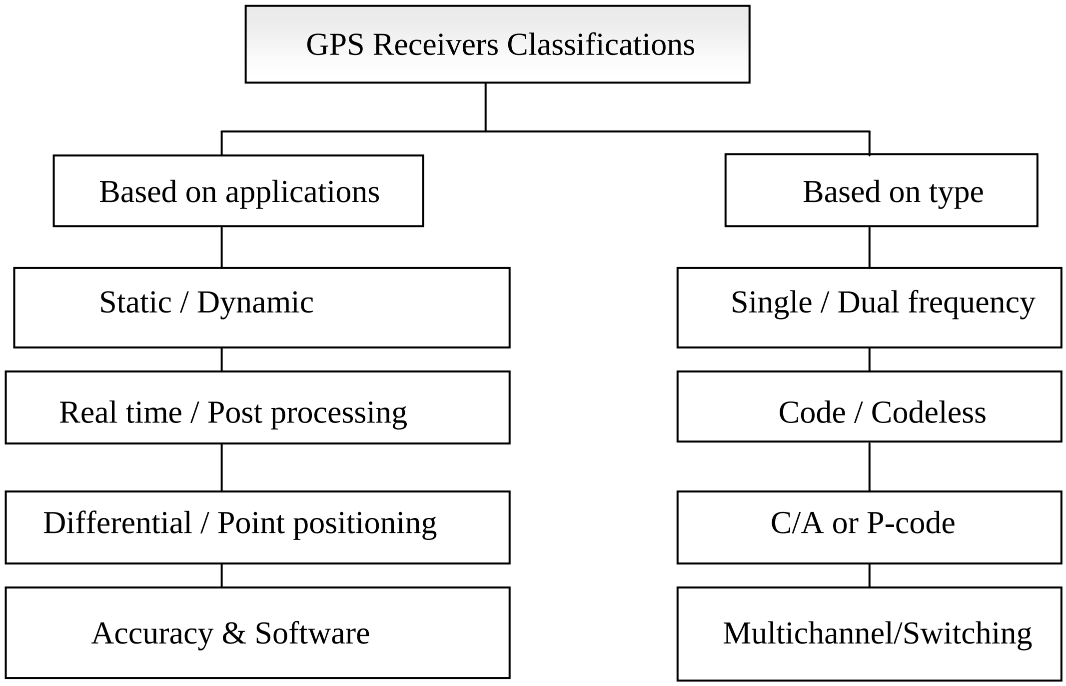

Figure 1: GPS Receivers Classifications

Published in: Civil Engineering Research Magazine (CERM), Al-Azhar University, V.24, 2001, No. 1, pp.391-405

A Precise Integrated GPS/Gravity Geoid Model for Egypt

BY

Ass. Prof. Abd-Allah. A. Saad
Shoubra Faculty of Engineering
Zagazig University-Benha Branch

Dr. Gomaa M. Dawod
Survey Research institute
National Water Research Center

Abstract

A precise geoid is a crucial demand in many scientific and practical fields of applications as: determination of the size and shape of the Earth, the geoid is the datum for a height system, the geoid undulations are used in geodynamics monitoring applications. The rapid growth of the Global Positioning System (GPS) applications in Egypt has resulted in an increasing need for precise geoid models in order to transform the GPS-based ellipsoidal heights to orthometric heights needed for engineering applications.

Two high resolution geoid models for Egypt (32^{o} <latitude> 22^{o}, 37^{o} <longitude> 25^{o}) have been developed based on the utilization of the Earth Geopotential Model (EGM96) as the most recent long-wavelength representation of the Earth geopotential, incorporated with the recent precise geodetic data base available in Egypt. Both EGM96 and OSU91A were used to compute the geoid undulations over 195 known GPS/Levelling stations. The obtained results show that the mean and RMS values of EGM96 undulations exhibit a better consistency with the measured undulations than the OSU91A corresponding values. A 5'x5' geoid solution, called SRI2001A, is a gravimetric geoid model utilizing 240 first-order gravity stations, a local Digital Elevation Model (DEM); and the EGM96 in a remove-compute-restore Fast Fourier Transform (FFT) processing methodology. Then, another 5'x5' geoid model, named SRI2001B, is developed based on integrating the SRI2001A model to an undulation datum defined by GPS/Levelling observed undulations. SRI2001B has a minimum undulation value of 9.44 m and a maximum value of 21.39 m with an average of 13.62 m. The values of the estimated undulations from the SRI2001B model have been compared against the pure GPS undulation of some independent GPS/Levelling stations. The differences range from –0.01m to –0.28 m with an average of –0.10 m. Consequently, it can be concluded that SRI2001B is the most precise geoid model in Egypt based on the current available data.

1. Introduction

The geoid is the equpotiential surface of the Earth's gravity field approximating mean sea level in an optimum way, and extended under the continents. A precise geoid is a crucial demand in many scientific and practical fields of applications as: determination of the size and shape of the Earth, the geoid is the datum for height systems, the geoid undulations are used in geodynamics monitoring applications. Recently, the rapid growth of the Global Positioning System (GPS) applications in Egypt has resulted in an increasing need for precise

geoid models in order to transform the GPS-based ellipsoidal heights to orthometric heights needed for engineering applications [Alnaggar and Dawod, 1999].

In September 1998, the Egyptian National Gravity Standardization Network (ENGSN97) has been established, by the Survey Research Institute (SRI), as the accurate gravity datum for Egypt. ENGSN97 consists of 5 absolute gravity stations and 145 high-precision relative gravity stations, which GPS 3-D coordinates besides orthometric heights are measured. Moreover, a new first-order High Accuracy Reference GPS Network (HARN) has also established, by the Egyptian Survey Authority (ESA), to furnish the New Egyptian Datum (NED95). Both networks constitute the most recent and accurate geodetic database in Egypt. The global Earth Geopotential Model (EGM96) is considered as the most precise spherical harmonic model representing the potential of the Earth.

The main objectives of this research study are: to investigate the performance of EGM96 geopotential model in Egypt, to use this recent global model in developing a new precise gravimetric geoid solution for Egypt based on utilizing the available Egyptian precise gravity data bas; and to integrate all available geodetic measurements to develop a high-precision combined GPS/Gravity geoid model for Egypt. Therefore, a brief description of ENGSN97 network in given in section two, followed by a summary of the three basic methods of geoid determination methodologies, namely: gravimetric, geometric satellite; and spherical harmonic expansion. Section four sums up the characteristics of both OSU91A and EGM96 geopotential models, while section five presents the available data and the procedures of developing the two gravimetric and GPS/Gravity geoid solutions for Egypt. The summary and obtained conclusions are given in section six.

2. The Egyptian National Gravity Standardization Net of 1997 (ENGSN97)

The establishment and re-calibration of the Egyptian National Gravity Standardization Net (ENGSN97) is a project executed by the Survey Research Institute during 1994-1998, and has aimed to: the establishment of a fundamental national gravity network for Egypt, the updating of the gravity-anomalies maps of Egypt; and accurate definition of the figure of the earth, the geoid, in Egypt. According to the ENGSN97 project’s goals, the field observation campaigns include the collection of three types of measurements: relative gravity, GPS coordinates, and precise levels. This is, of course, beside the necessary absolute gravity measurements at some selected stations.

Five absolute gravity stations have been established and observed to serve as an absolute gravity framework for the ENGSN97 network. The locations of these sites are: Giza, Helwan, Marsa Matrouh, Aswan, and El-Kharga (Figure 1). The measurements have been carried out using the FG5 absolute gravity meter. The FG5 instrument has a higher level of robustness, reliability and an instrumental uncertainty estimate of 0.0011 mGal. The ENGSN97 gravity network contains 145 relative gravity stations. Seven LaCoste and Romberge (LCR) gravimeters have been used in measuring the relative gravity values of the ENGSN97. The main observation schemes that have been applied in ENGSN97 are the step method and the profile method. Both techniques are useful in controlling the gravimeters’ drift. A number of dual-frequency GPS receivers have been used to obtain accurate coordinates of the ENGSN97 stations. In each gravity loop in the ENGSN97 project, the orthometric height of each station is determined by the precise levelling technique. Wild N3 precise levels, with a precision of 0.1 mm, and Invar rods are used in levelling routes, each starts from a first-order bench mark [Dawod, 1998].

The final solution of the ENGSN97 contains 1045 observations for the 150 gravity stations, after removing 44 outlier observations. A number of 133 virtual gravimeters was used in terms of estimating the orientation and the drift unknowns for each virtual gravimeter. Hence, there were 408 unknowns to be estimated, and 632 degrees of freedom. The most essential information of the final adopted solution of the ENGSN97 network is summarized in table 1. Concerning the estimated gravity values at the network 150 stations, the obtained results indicate that the minimum adjusted gravity value was 978679.776 mGal at Abu-Sombol station while the maximum adjusted gravity value was 979504.981 mGal at Balteem station. Therefore, the gravity range over Egypt is 825.205 mGal with an average gravity value of 979126.005 mGal. As an indication of the precision of the ENGSN97, the standard deviations of the adjusted gravity values range from 0.002 mGal to 0.048 mGal [Shaker et al, 2001].

Table 1: Essential Information for the Final Adjustment of the ENGSN97 Network

Number of stations	150	
Number of observations	1045	
Number of loops	51	
Number of relative gravimeters	7	
Average station separation	66	Km
Number of unknowns	408	
Number of degrees of freedom	637	
Minimum standard deviation of gravity values	0.002	mGal
Maximum standard deviation of gravity values	0.048	mGal
Minimum adjusted gravity value	978679.776	mGal
Maximum adjusted gravity value	979405.981	mGal

3. Geoid Determination

The geoid is the equpotiential surface of the Earth's gravity field approximating mean sea level in an optimum way, and extended under the continents. The determination of the geoid is an old problem of physical geodesy and a numerous number of geoid evaluations have been carried out world wide, and in Egypt [e.g., Nassar et al, 1993; and Shaker et al, 1997]. The geoid is determined using several techniques based on a wide variety of using one or more of the different data sources such as: Gravimetric method using surface gravity data, Satellite positioning based on measuring both ellipsoidal heights for stations with known orthometric heights, Geopotential models using spherical harmonics coefficients determined from the analysis of satellite orbits, Satellite altimetry using satellite-borne altimetric measurements over the oceans, Astrogeodetic method using stations with measured astronomical and geodetic coordinates; and Oceanographic levelling methods used mainly by the oceanographers to map the geopotential elevation of the mean surface of the ocean relative to a standard level surface. Only the first three methods are used in this research study, while the other methods are found in several literatures [e.g. Nassar, 1986].

Stockes' boundary value problem (BVP) is the gravimetric determination of the geoid. BVP deals with the determination of a potential field, harmonic outside the masses, from gravity anomalies given everywhere on the geoidal surface. A lot of reference materials are available for this subject [e.g. Heskanien and Moritz, 1967]. The final formula of the geoid undulations, N, is given as [Sideris, 1994]:

$$N = (R/4\Pi\gamma) \times \iint_{\sigma} (\Delta g + \delta\Delta g + \delta A) \times S(\Psi)\ d\sigma + (1/\gamma)\delta T \tag{1}$$

where R is the mean radius of the Earth, Δg is the free-air gravity anomaly, γ is the normal gravity, $\delta\Delta g$ is the indirect effect on gravity, δA is the attraction change, δT is the indirect effect on the potential, σ denotes the Earth's surface, $d\sigma$ is the infinitesimal surface element; and $S(\Psi)$ is the Stokes' function. There are several processing techniques for geoid determination, such as the Fast Fourier Transformation (FFT) and the Least-Squares Collocation (LSC). The adopted mathematical processing technique, in the current research study, is taken as the FFT technique. The effect of a global geopotential model, as assumed to represent coarse-scale smoother geoid, is removed from the observed gravity measurements. The contributions of the topography are also removed since they are implicitly included in the Stokes' equation to be evaluated. The residual gravity anomalies are used as input to the FFT routine to obtain fine-scale geoid. The final geoid height model is the sum of the coarse-scale and fine-scale models along with the indirect effect or the terrain contribution. This is called "the remove-compute-restore" processing strategy.

The idea of geoid computations, from geometric satellite geodetic results, is to make benefit from the derived satellite ellipsoidal height h, to compute the geoid undulation N at the same point. This necessitates that, the orthometric height H of the same point of interest to be known, since the relationship among those three quantities, is given as:

$$N = h - H \tag{2}$$

Of course, for precise determination of N, using this technique, in the order of the same precision of the satellite vertical component positioning, which can nowadays reach few tenth of a centimeter, the orthometric height H must be determined with at least the same precision. The best accurate method for determining H will be the use of the precise levelling technique.

The geoid undulations may be computed using the following spherical harmonic expansion [Heskanien and Moritz, 1967]:

$$N = (GM/r\gamma) \times \sum_{n=2}^{360} (a/r)^n - \sum_{m=0}^{n} ((\bar{C}_{nm} \times \cos m\lambda) + (\bar{S}_{nm} \times \sin m\lambda)) \times \bar{P}_{nm}(\sin\phi) \tag{3}$$

where: n is the maximum degree of the model, m is the maximum order of the model, γ is the normal gravity of the reference ellipsoid, r is the geocentric radial distance of the computation point projected on the ellipsoid, G is the Newtonian gravitational constant, M is the mass of the Earth, a is the semi-major axis, ϕ is the geocentric latitude, λ is the geocentric longitude, $\bar{C}_{nm}$ and $\bar{S}_{nm}$ are the fully normalized harmonic coefficients, and P_{nm} is the fully normalized associated Legendre polynomial.

4. EGM96 and OSU91A Global Geopotential Models

The Earth Geopotential Model (EGM96) and the Ohio State University (OSU91A) are examples of the recent global geopotential models representing the Earth gravitational potential as spherical harmonic coefficients. Both models are complete to degree and order 360. Therefore, the shortest wavelength of these models is one degree, and their resolution is one-half degree (about 50 km). The geoid undulations of OSU91A and EGM96 models over Egypt are represented as contour maps in figures 2 and 3, respectively.

Smith and Milbert [1997a] stated that there is an error in the order of one meter in geoid undulation determination using OSU91A model and Geodetic Reference System (GRS80) as the chosen reference field. This effect is due to the difference between the normal potential of GRS80 and the potential of the geoid, and in the case of OSU91A model, it is due to the fact that its implemented value for the gravitation-mass constant does not equal the corresponding value of the GRS80. In the case of EGM96-based geoid undulations computed by NIMA, a constant bias of 0.41 m was taken into account [Smith and Milbert, 1997b]. This result was also evident when comparing two sets of EGM96 undulations: the first set is computed using spherical harmonic processing software, and the second set contains the corresponding values interpolated from the global undulation grid distributed by the U.S. NIMA. Over 5'x5' grid covers Egypt, the differences between the two sets of EGM96 undulations have an average value of 0.46 m. This is an important note when dealing with EGM96 in geoid determination. As a primarily comparison, both EGM96 and OSU91A were used to compute the geoid undulations over 195known GPS/Levelling stations. The obtained results are tabulated in table 2. From this table, it can be noticed that, for EGM96 model, the undulation differences range from –0.11 m to 1.89 m with an average of –0.43 m and RMS of 0.78 m. The corresponding undulation differences values of the OSU91A model have a minimum of –0.53 m, a maximum of –1.97 m, an average of –1.53 m; and RMS of 1.86 m. In addition, it can be noticed that the mean and RMS values of EGM96 undulations exhibit a better consistency with the measured undulations than the OSU91A corresponding values. Hence, it may be concluded that, although both global geopotential models do not represent the short wavelength of the potential over Egypt, the EGM96 is more precise than OSU91A in the sense of geoid determination.

Table 2: Statistics of Geoid Undulations from GPS/Levelling, OSU91A, and EGM96

Item	Minimum	Maximum	Average	RMS
N (GPS/Levelling)	9.42	17.66	14.44	2.15
N (EGM96)	9.43	18.40	14.87	2.04
N (OSU91A)	9.95	18.51	15.96	2.42
N (GPS/Levelling) –N (EGM96)	-0.11	1.89	-0.43	0.78
N (GPS/Levelling) –N (OSU91A)	-0.53	-1.97	-1.53	1.86

5. Data Used and Obtained Results

The available data include gravity, GPS; and precise levelling measurements. A total of 240 gravity stations have been used in generating this geoid solution (Figure 4). The data used consists of the 150 ENGSN97 stations, 67 stations of the National Gravity Standard Base Network of 1977 (NGSBN77); and some gravity stations observed by the Survey Research Institute. These gravity values used are considered as first-order stations. Less-accurate available gravity measurements were not considered in this study in order to develop a precise geoid. All point gravity measurements have been corrected first to the terrain effect before generating the 5'x5' free-air gravity anomaly grid. A total of 195precise GPS stations, with known orthometric heights, have been collected (Figure 5). They include the Egyptian National High Accuracy Reference Network (HARN) observed by the Egyptian Survey Authority to form the New Egyptian Datum 1995 (NED-95). These data sets have been used to develop two geoid models for Egypt.

5.1 Developing a Gravimetric Geoid Model (SRI2001A)

The FFT technique is utilized in developing a gravimetric geoid (called SRI2001A) for Egypt, i.e., from 22^o to 32^oN in latitude, and from 25^o to 37^o E in longitude. The available 240 gravity stations have been used to generate a 5'x5' grid of free-air gravity anomalies. Table 3 presents the statistics of the obtained free-air gravity anomalies. From this table, it can be seen that the obtained free-air gravity anomalies range from a minimum of –122.42 mGal to a maximum of 128.65 mGal with a mean value of –2.93 mGal and Root Mean Square (RMS) error of 29.51 mGal. The EGM96 geopotential model was used as the reference global model in the FFT processing of the SRI2001A geoid. The corresponding free-air gravity anomalies of EGM96 have a minimum of –130.36 mGal, a maximum of 152.99 mGal, an average of 6.19 mGal; and an RMS equals 24.59 mGal. The differences between the two sets of free-air gravity anomalies range from –129.91 mGal to 254.84 mGal with a mean value of 9.17 mGal and RMS of 40.16 mGal.

Table 3: Statistics of used anomalies from both gravity measurements and EGM96 global model

Item	Minimum	Maximum	Average	RMS
Free-Air Gravity Anomalies from Terrestrial Gravity Data	-122.42	128.65	-2.93	29.51
Free-Air Gravity Anomalies from EGM96	-130.36	152.99	6.19	24.59
Differences in Free-Air Gravity Anomalies	-129.91	254.84	9.17	40.16

The obtained results of the developed gravimetric geoid are three 5'x5' grids of the geoid undulations and the two components of the deflection of the vertical. Table 4 summarizes the obtained results, and figures 6, 7, and 8 present the findings in three contour maps. It can be noticed from these figures and table, that the computed geoid undulations range from 5.42 m to 22.40 m with a mean value of 14.54 m and RMS equals 2.96 m. The obtained values of the deflection of the vertical in the meridian component have a minimum of –20.53", a maximum of 21.88", an average of –0.92"; and RMS of 4.26". The deflection of the vertical in the prim vertical direction ranges from –24.93" to 25.48" with a mean value of 1.11" and RMS equals 3.98".

Several comparisons have been carried out between the obtained gravimetric geoid model, SRI2001A, and the global geopotential models OSU91A and EGM96. Table 5 presents the results of these comparisons. From this table, it can be seen that the SRI-GEOID98 undulations range from 7.22 m to 22.55 m with an average of 15.31 m and RMS equals 3.10 m. The corresponding minimum, maximum, average, and RMS values of the EGM96 undulations are 5.90, 21.52, 14.16, and 2.92 m respectively. The OSU91A model gives undulations range from 6.77 m to 23.12 m with a mean value of 14.81 m and RMS equals 3.29 m. The developed geoid model differs from the EGM96 model by a mean value equals to 0.38 m with RMS equals 2.75 m, while it differs from OSU91A model by an average of –0.27 m and RMS of 3.03 m. A similar comparison shows that the undulation differences between the EGM96 and a gravimetric geoid of the USA range from –1.86 m to 3.34 m [Smith and Milbert, 1997b].

Table 4: Statistics of the SRI2001A gravimetric Geoid

Item	Minimum	Maximum	Average	RMS
Geoid Undulations (m)	5.42	22.40	14.54	2.96
Deflection of the vertical in the meridian direction (“)	-20.53	21.88	-0.92	4.26
Deflection of the vertical in the prime vertical direction (“)	-24.93	25.48	1.11	3.98

Table 5: Statistics of Comparisons of the SRI2001A and Two Global Geoid Models

Item	Minimum	Maximum	Average	RMS
SRI2001A	5.42	22.40	14.54	2.96
EGM96	5.90	21.52	14.16	2.92
OSU91A	6.77	23.12	14.81	3.29
SRI2001A – EGM96	-10.13	7.54	0.38	2.75
SRI2001A – OSU91A	-10.62	9.30	-0.27	3.03

5.2 Developing a Combined GPS/Gravity Geoid (SRI2001B)

The issue of combining gravity and GPS data in developing high-precision geoid models gains a lot of attention in the last few years. Several research studies have handled this point and investigated different fitting polynomials (e.g. Shaker et al, 1997, Smith and Milbert, 1997b, Veronneau, 1997; and Denker, et al, 1996). Forty five common stations, between gravity and GPS available data sets, have been used, to relate the obtained gravimetric geoid model to a precise geoid undulation datum as obtained from GPS measurements on precise levelling known stations. The developed combined geoid model, depicted in figure 9, has a minimum undulation value of 9.437 m and a maximum value of 21.39 m with an average of 13.623 m and RMS of 2.62 m.

Several comparisons have been made in order to investigate the reliability of the developed GPS/Gravity geoid. The first comparison has been made between the developed geoid and a previously determined GPS/Gravimetric geoid, SRI-GEOID98, based on OSU91A geopotential model [Dawod, 1998]. The differences between the two geoids range from –5.40 m to 5.71 m with a mean of –0.57 m and RMS equals 1.88 m. In order to investigate the accuracy of SRI2001B, fifteen independent GPS/Levelling stations have been used. The values of the estimated undulations from the SRI-GEOID98 model have been compared against the pure GPS undulation of these stations. These results are summarized in table 6. From this table, it can be seen that the differences range from –0.01m to –0.28 m with an average of –0.10 m and RMS of 0.49 m. The corresponding differences of the previous SRI-GEOID98 model have a minimum of –1.69 m, a maximum of –0.05 m, a mean of 0.41 m; and RMS of 0.79 m. Consequently, it can be concluded that SRI2001B is more precise than SRI-GEOID98, which indicates that the EGM96 global geopotential model represents the most precise geopotential model to be used for geoid determination in Egypt.

Table 6: Statistics of Comparisons of the SRI2001B and SRI-GEOID98 Geoid Models

Item	Minimum	Maximum	Average	RMS
SRI2001B	9.44	21.39	13.62	2.62
SRI-GEOID98	7.22	22.55	15.31	3.10
(SRI2001B) – (SRI-GEOID98)	-5.40	5.71	-0.57	1.88
N (SRI-GEOID98) – N(pure GPS)	-1.69	-0.05	-0.41	0.79
N (SRI2001B) – N(pure GPS)	-0.28	-0.01	-0.10	0.49

6. Summary and Conclusions

The EGM96 is the most recent and precise spherical harmonic model representing the potential field of the Earth. New terrestrial gravity and satellite altimetric data have been used in the development of EGM96 and lead to significant improvements in the precision of geoid determination using this model. Compared to the OSU91A geopotential model, EGM96 proves to be more precise and reduces the uncertainties (in terms of RMS) in geoid undulations over Egypt from 1.86 to 0.78 m, when compared with GPS/Levelling undulations. Two precise geoid models have been developed for the entire Egyptian territory. The first geoid, called SRI2001A, is a gravimetric geoid model utilizing the most recent and accurate first-order gravity measurements, and is based on the GRS80 reference datum. The EGM96 global geopotential spherical harmonic model is used to provide the long wavelength of the Earth gravitational field, along with a local DEM in the remove-compute-restore FFT processing technique. The obtained geoid undulations range from 5.42 m to 22.40 m with a mean value of 14.54 m and RMS equals 2.96 m. A GPS/Levelling data set of 195precise stations have been used to generate a geometric-satellite geoid model. A second-order polynomial as a function of the distance from the network origin is found to be the best fitting function to integrate gravimetric undulations and GPS/Levelling undulations. Therefore, a combined GPS/Gravity geoid for Egypt, SRI2001B, has been generated. It has a minimum undulation value of 9.437 m and a maximum value of 21.39 m with an average of 13.623 m and RMS of 2.62 m. The SRI2001B geoid model is compared to a previously determined GPS/Gravimetric geoid, SRI-GEOID98, based on OSU91A geopotential model. The differences between the two geoids range from –5.40 m to 5.71 m with a mean of –0.57 m and RMS equals 1.88 m. The values of the estimated undulations from the SRI-GEOID98 model have been compared against the pure GPS undulation of some independent GPS/Levelling stations. The differences range from –0.01m to –0.28 m, with an average of –0.10m, and RMS of 0.49 m. The corresponding differences of the previous SRI-GEOID98 model have a minimum of –1.69 m, a maximum of –0.05 m, a mean of 0.41 m; and RMS of 0.79 m.

From the obtained results, it can be concluded that:

* The EGM96 global geopotential model represents the most precise geopotential model to be used for geoid determination in Egypt.
* The developed gravimetric geoid SRI2001A is more precise than previously determined gravimetric geoid solutions in Egypt, mainly because of the utilization of the precise ENGSN97 gravity values. Moreover, it gives smaller RMS compared with the gravimetric geoid SRI-GEOID98 that was developed based on OSU91A model.
* The developed combined GPS/Gravity SRI2001B geoid model is the most precise geoid model for Egypt based on the available data.

Based on the previous conclusions, some recommendations may be suggested:

* It is highly recommended that the ENGSN97 gravity network being incorporated into any new global geopotential models in order to increase the accuracy of those models in representing at least the medium wavelength of the gravity field over Egypt.
* The accuracy of the geoid determination in Egypt can be significantly improved by making additional geodetic measurements in void areas, especially the south-west part of the western desert.
* The established ENGSN97 gravity network should be used in the process of redefinition of the Egyptian geodetic datum and the associated reduction and computations of geodetic quantities needed for surveying and mapping activities.

References

Alnaggar, D., and Dawod, G., 1999, **Efficiency of GPS techniques in national applications**, Proceedings of the International Conference on Integrated Management of Water Resources in the 21st Century, Cairo, November 21-25, Volume II, pp. 741-752.

Dawod, G., 1998, **A National Gravity Standardization Network for Egypt**, Ph.D. thesis, Shoubra Faculty of Engineering, Zagazig University, Cairo, Egypt.

Denker, H., Behrend, D., and Torge, W., 1996, **The European gravimetric quasigeoid EGG96**, Proceedings of the IAG International Symposium No. 117, Tokyo, Japan, Sept. 30 - Oct. 5, 1996, pp. 532-539.

Heiskanen, W., and Moritz, H., 1976, **Physical geodesy**, Freeman And Company, San Francisco.

Nassar, M., 1986, **Comparative study of different mathematical models for geoid determination – with special emphasis on the Egyptian situation**, The Scientific Bulletin of the Faculty of Engineering, Ain Shams University, No. 19, Cairo.

Nassar, M., Hanafy, M., and El-Tokhey, M., 1993, **The 1993 Ain Shams university (ASU93) geoid solutions for Egypt**, Proceedings of Al-Azhar Third International Engineering Conference, Cairo, Sept. 18-21, V. 4, pp. 395-407.

Sideris, G., 1994, **Geoid determination by FFT techniques**, Lecture Notes, The International school for the determination and use of the geoid, Milan.

Shaker, A., Saad, A., and El Sagheer, A., 1997, **Enhancement of the Egyptian gravimetric geoid 1995 using GPS observations**, Proceedings of the International Symposium on GIS/GPS, Istanbul, Turkey, Sept. 15-19.

Shaker, A., Alnaggar, D., Dawod, G., and Saad, A., 2001, **Analysis of the established Egyptian National Gravity Network of 1997**, Al-Azhar Engineering Magazine, No.

Smith, D. and Milbert, D., 1997a, **Evaluation of preliminary models of the geopotential in the United States**, Int. Geoid Service Bulletin No. 6, pp. 7-32.

Smith, D. and Milbert, D., 1997b, **Evaluation of EGM96 model of the geopotential in the United States**, International Geoid Service Bulletin No. 6, pp. 33-47.

Veronneau, M., 1997, **Evaluation of the NASA/NIMA Earth Geopotential Model (EGM96) over Canada**, International Geoid Service Bulletin No. 6, pp. 47-69.

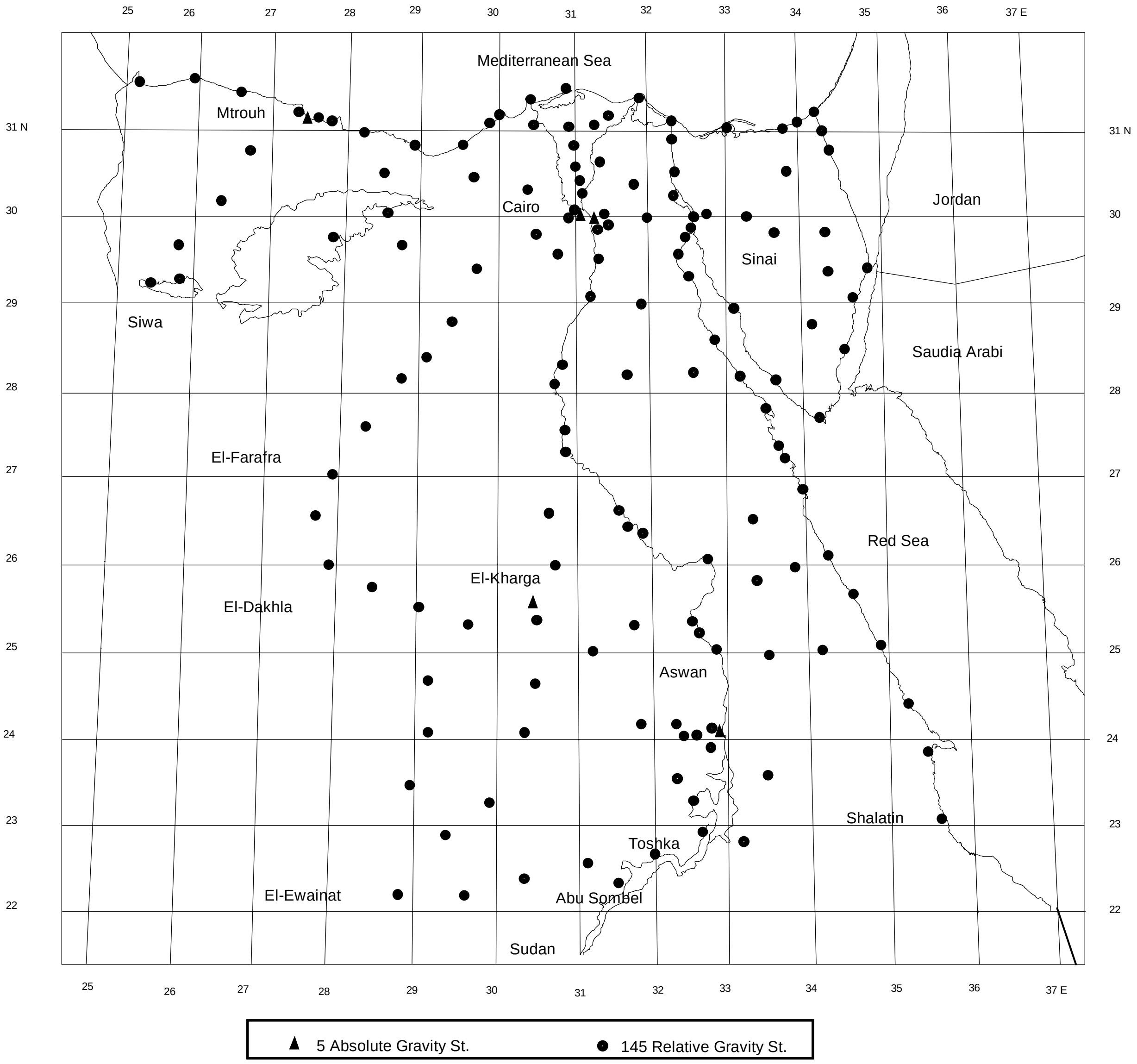

Figure 1: The Egyptian National Gravity Standardization Network of 1997 (ENGSN97)

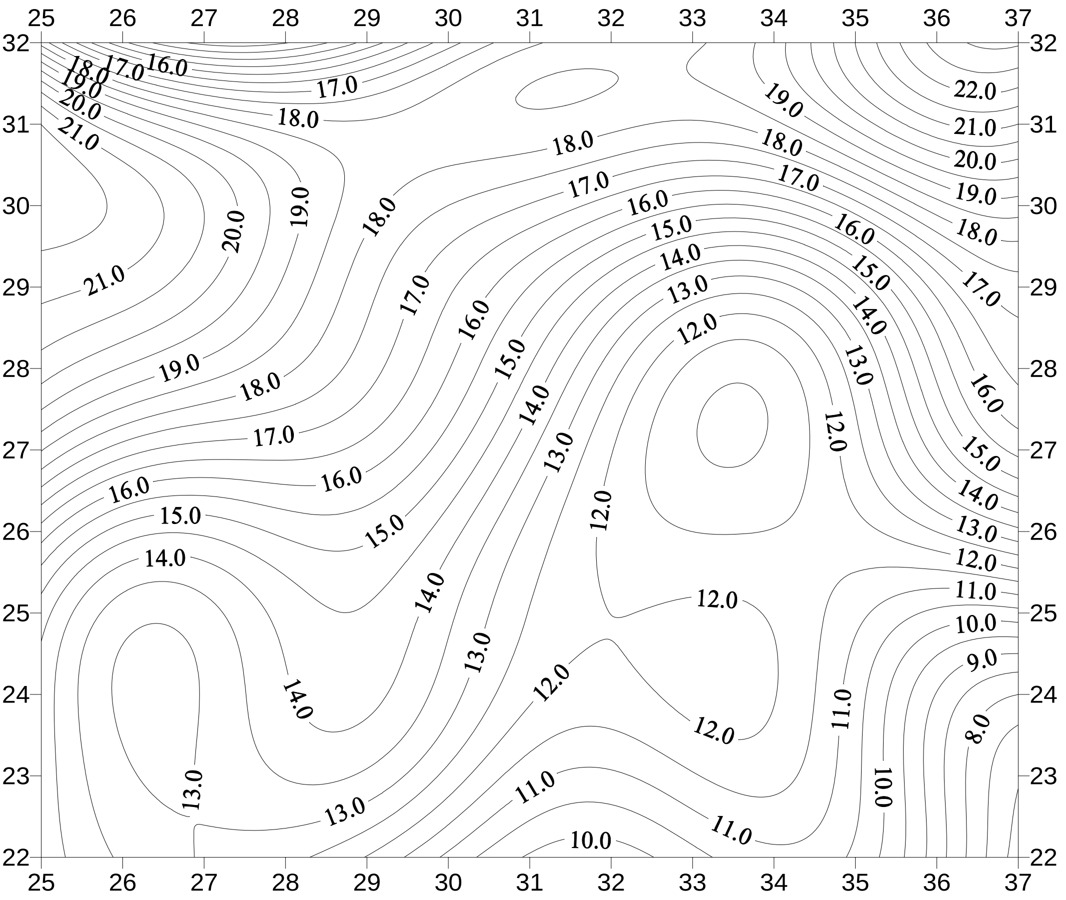

Figure 2: The Geoid Undulations of the OSU91A Global Model

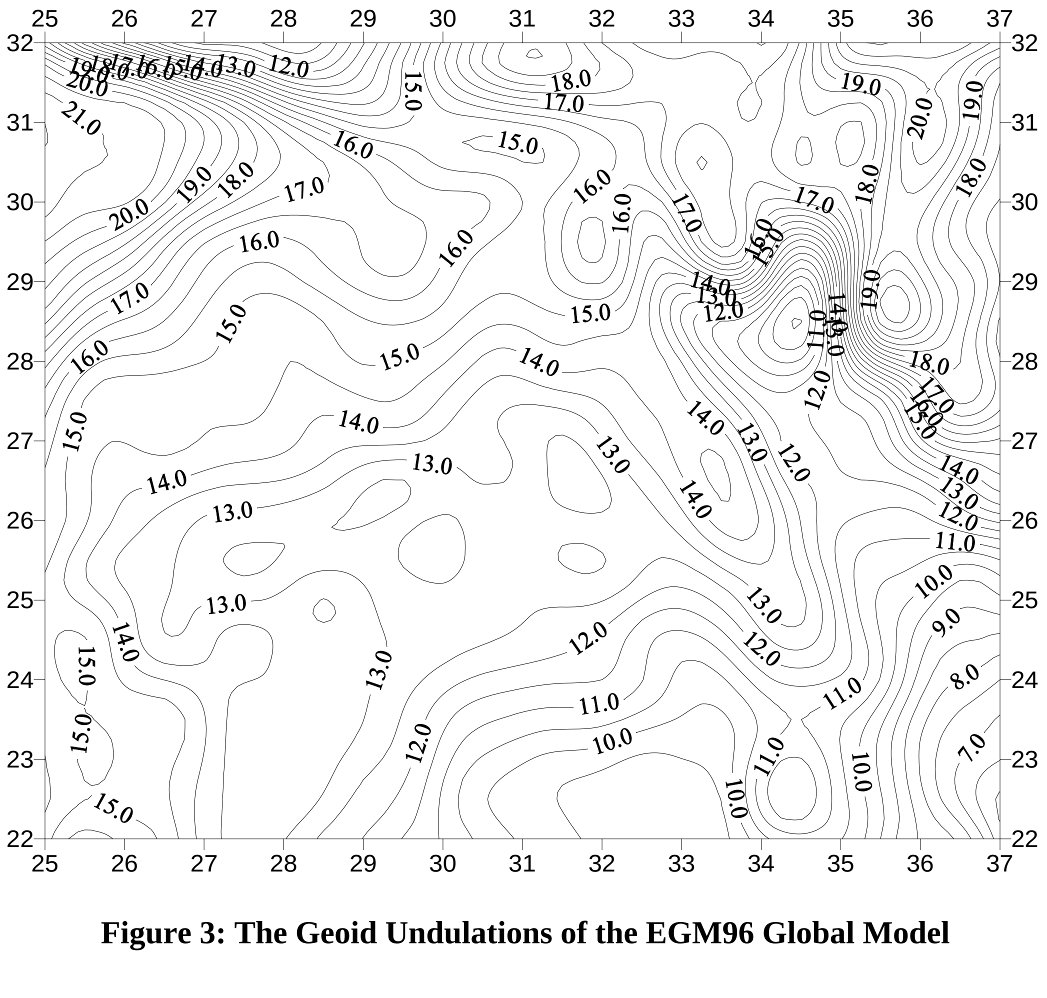

Figure 3: The Geoid Undulations of the EGM96 Global Model

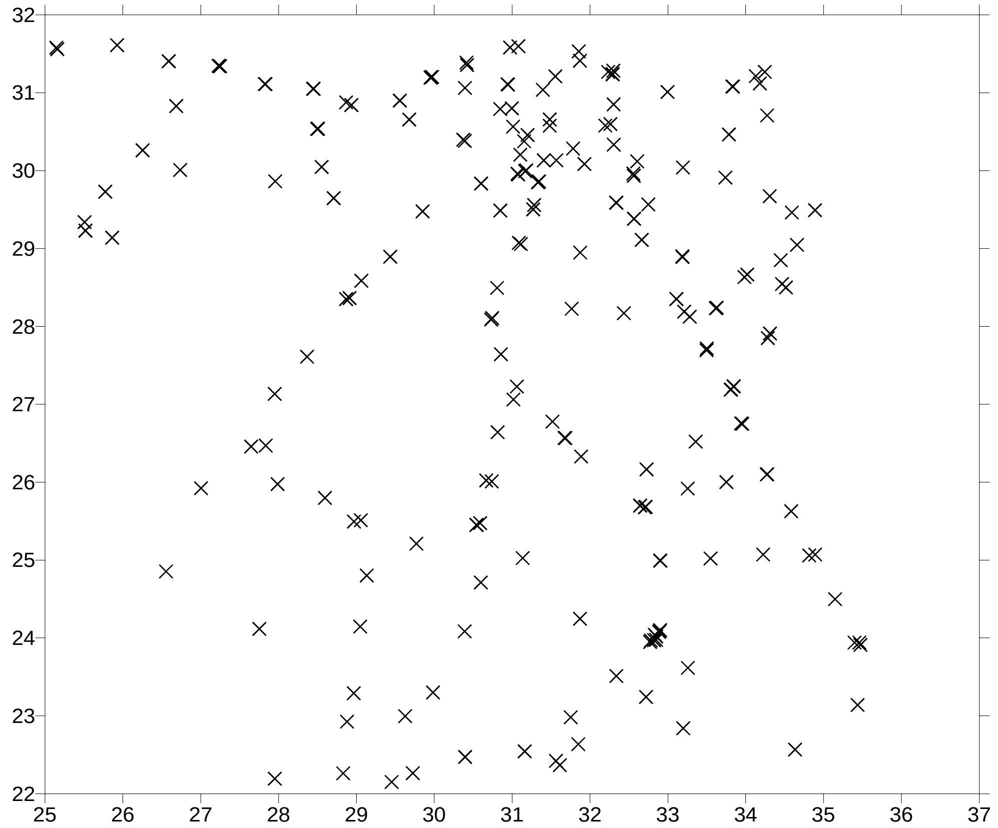

Figure 4: The Available Gravity Stations

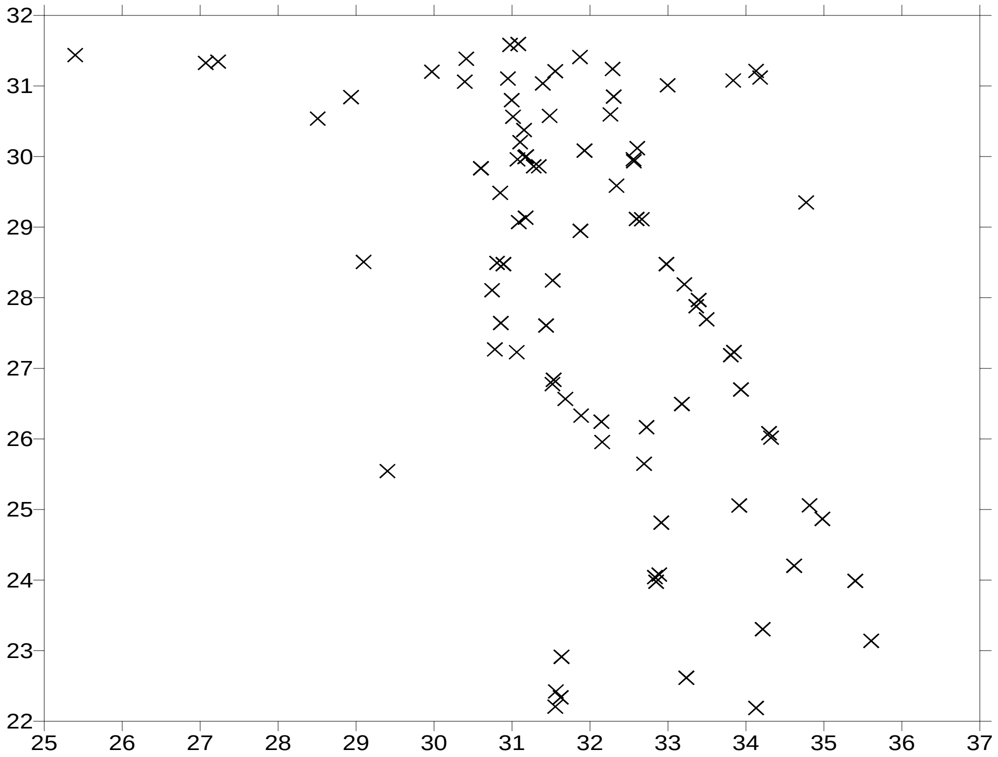

Figure 5: The Available GPS Stations

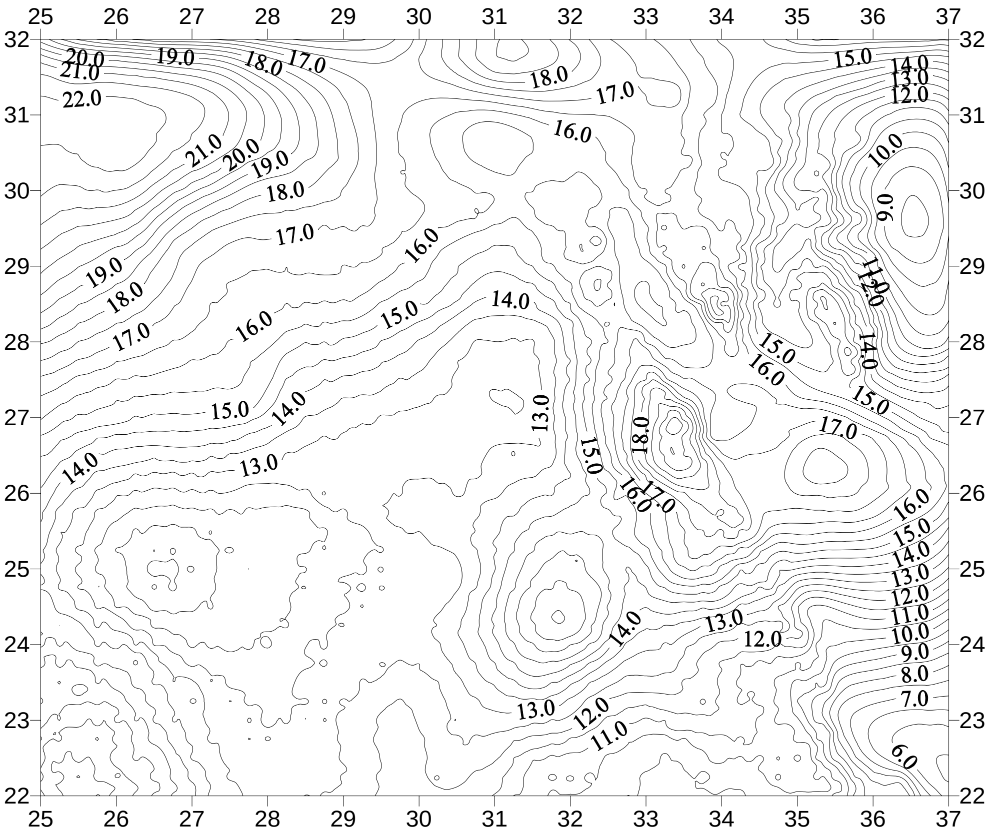

Figure 6: The Geoid Undulations of SRI2001A Gravimetric Geoid Model

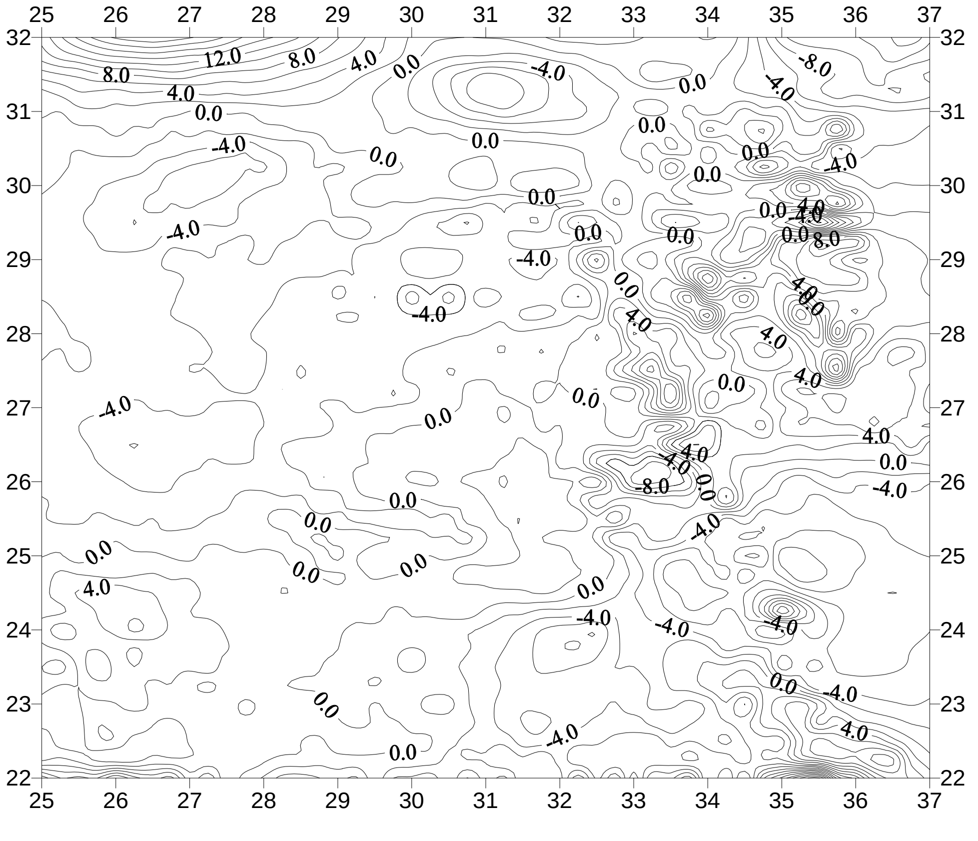

Figure 7: The SRI2001ADeflection of the Vertical in the Meridian Plane

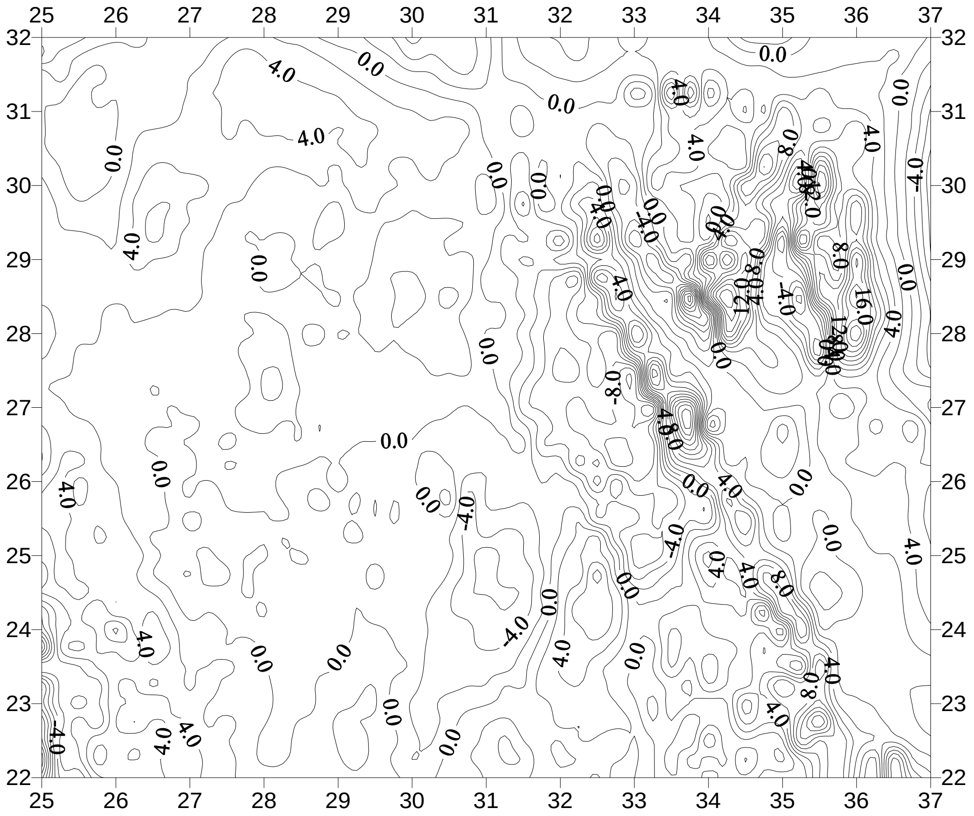

Figure 8: The SRI2001A Deflection of the Vertical in the Prime Vertical Plan

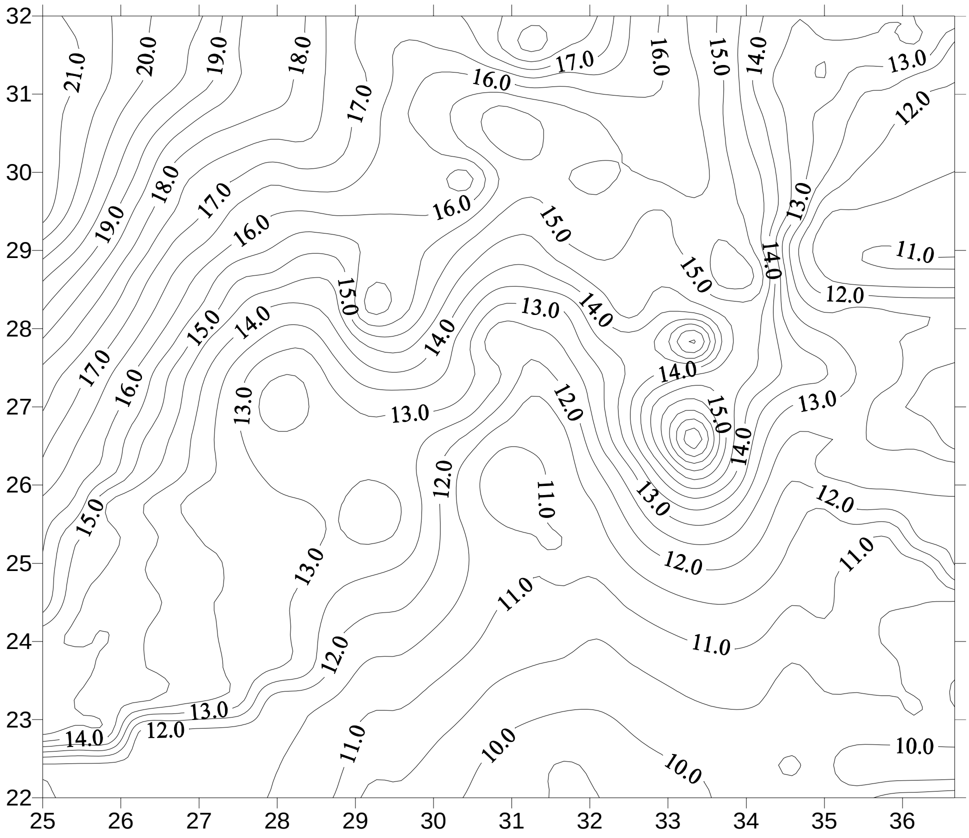

Figure 9: The Geoid Undulations of SRI2001B Combined Geoid Model

Establishment of Egyptian National Gravity Standardization Network

Dr. Dalal S. ALNAGGAR, Dr. A. A. SAAD and Dr. G. M. DAWOOD, Egypt

Key words:

ABSTRACT

Local gravity field representations are required for establishing geodetic control networks in geodetic and engineering surveys. With the rapid growth of the use of the satellite-based Global Positioning System (GPS), high resolution gravity field data are needed to transform the ellipsoidal heights into orthometric heights. In geophysics, gravity data are used in a wide range of applications such as exploration of mineral and underground water resources, monitoring crustal movements, and the study of the orbits of natural and artificial celestial bodies.

Gravity control networks are essential to support several applications on a national and international scales. The Potsdam gravity system provides an example of an international gravity datum from 1909 to 1971. In Egypt, the National Gravity Standard Base Net (NGSBN-77) afforded the gravity framework in the second half of the twentieth century. In addition, the Egyptian Survey Authority (ESA) usually is carrying out gravity measurements, for some specific applications, especially for correcting precise levelling observations. However, all such gravity measurements, can not satisfy the modern precise applications in Egypt. Consequently, the establishment of a precise new national gravity base network becomes an essential and urgent task for the geodetic community in Egypt, and this is actually the main point of our interest in the current investigation. The Egyptian National Gravity Standardization Network of 1997 (ENGSN97) serves as the precise national gravity datum for Egypt. So, the ENGSN97 will be documented in details in this research.

CONTACT

Prof. Dr. Eng. Dalal S. Alnaggar
Director of Regional Training Center
EGYPT
E-mail: Dalnagar@training-center.com

Ass. Prof. Dr. Eng. A. A. Saad
Surveying Dept.
Shoubra Faculty of Engineering Institute
Zagazig university-Benha Branch
EGYPT

Dr. Eng. G. M. Dawood
Surveying Research
Ministry of Water Researches and Irrigation

مجلة علوم المياه – القاهرة – العدد ٣٢ – أبريل ٢٠٠٢ - صفحة ٢٣-٣١

استخدام أحدث تقنيات الرصد على الأقمار الصناعية لتحديد حجم المنخفضات لمشروعات إدارة الموارد المائية

د. جمعة محمد داود *

ملخص:

تقوم وزارة الموارد المائية و الري في بداية القرن الحادي والعشرين بتنفيذ العديد من المشروعات القومية المتعددة الأغراض والتي تهدف إلى خلق مجتمعات عمرانية جديدة خارج الوادي الضيق. ومن أهم هذه المشروعات المشروع القومي الرائد لتنمية شمال سيناء والذي يعتمد في المقام الأول على شق ترعة الشيخ جابر الصباح لإقامة مجتمع متكامل حديث في سيناء.

قام معهد بحوث المساحة باستخدام أحدث التقنيات المساحية العالمية بالرصد على الأقمار الصناعية (On-The-Fly Kinematic GPS Technique) لتمثيل طبوغرافية الأرض بدقة وإنشاء خريطة طبوغرافية رقمية وذلك في إطار دراسة – قام بها معهد بحوث إدارة المياه وطرق الري- لإنشاء مفيض عند الكيلو ٥ر٨٦ من ترعة الشيخ جابر . وبدراسة الخريطة المستنتجة باستخدام برامج الحاسب الآلي المتخصصة تم تحديد خمسة منخفضات على جانبي الترعة. وأشارت النتائج أن أكبر هذه المنخفضات يقع على بعد ٥٠ متر شمال كوبري الكيلومتر رقم ٤٥٠ر٨٥ على ترعة الشيخ جابر الصباح وتبلغ مساحته السطحية (عند منسوب ١٢ متر) ٦٠٠١٥٢ مترا مربعا بينما تبلغ سعته الاستيعابية (حتى نفس المنسوب) ١٦٩٢٣٠٨ مترا مكعبا. وقد اشتملت خطوات الدراسة على استنباط نموذج تطبيقي (في كلا من الأعمال الحقلية والمكتبية) بهدف الدمج بين أرصاد الأقمار الصناعية وأرصاد الطرق المساحية التقليدية وخاصة الميزانيات. ويهدف هذا النموذج التكاملي إلى دمج مميزات تكنولوجيا الرصد على الأقمار الصناعية مع متطلبات إنشاء الخرائط طبقا للمرجع المساحي المصري. وعلى الجانب الاقتصادي - بمقارنة هذه التقنية الحديثة بالطرق المساحية التقليدية - فقد أثبتت النتائج الحصول على وفر في الوقت اللازم لإنجاز الأعمال الحقلي يصل إلى ٧٠% بالإضافة إلى تقليل التكلفة الاقتصادية للمشروع بنسبة ٥٠%. وبناء على هذه النتائج يوصى البحث بتطبيق هذا الأسلوب التكاملي الدقيق في كافة مشروعات إنتاج الخرائط الطبوغرافية في مصر.

* باحث بقسم الجيوديسيا الطبيعية
معهد بحوث المساحة – المركز القومي لبحوث المياه – مصر
بريد إلكتروني: Dawod_gomaa@yahoo.com

١- مقدمة

في إطار مشروع تنمية شمال سيناء تم تنفيذ دراسة لإنشاء مفيض عند الكيلو ٨٦٫٥ من ترعة الشيخ جابر الصباح شرق مدينة بئر العبد. وتطلبت هذه الدراسة إنشاء خريطة مساحية دقيقة ورقمية لمنطقة الدراسة (مساحتها حوالي ١٥٠٠ فدان) لتمثيل طبوغرافية الأرض بأسلوب عالي التقنية وكذلك التحديد الدقيق لحجوم المنخفضات الموجودة بالمنطقة لبيان كمية المياه الممكن استيعابها. تتكون منطقة الدراسة من جزأين على جانبي ترعة الشيخ جابر الصباح كالآتي: المنطقة الأولى من الكيلو ٨٣٫٠ إلى الكيلو ٨٦٫٥ وبعرض ١ كم شمال مسار الترعة بينما المنطقة الثانية تقع بدايتها على بعد ٠٫٥ كم جنوب الكيلو ٨٦٫٥ وتمتد ٠٫٥ كم جنوبا و ١ كم شرقا (شكل ١) .

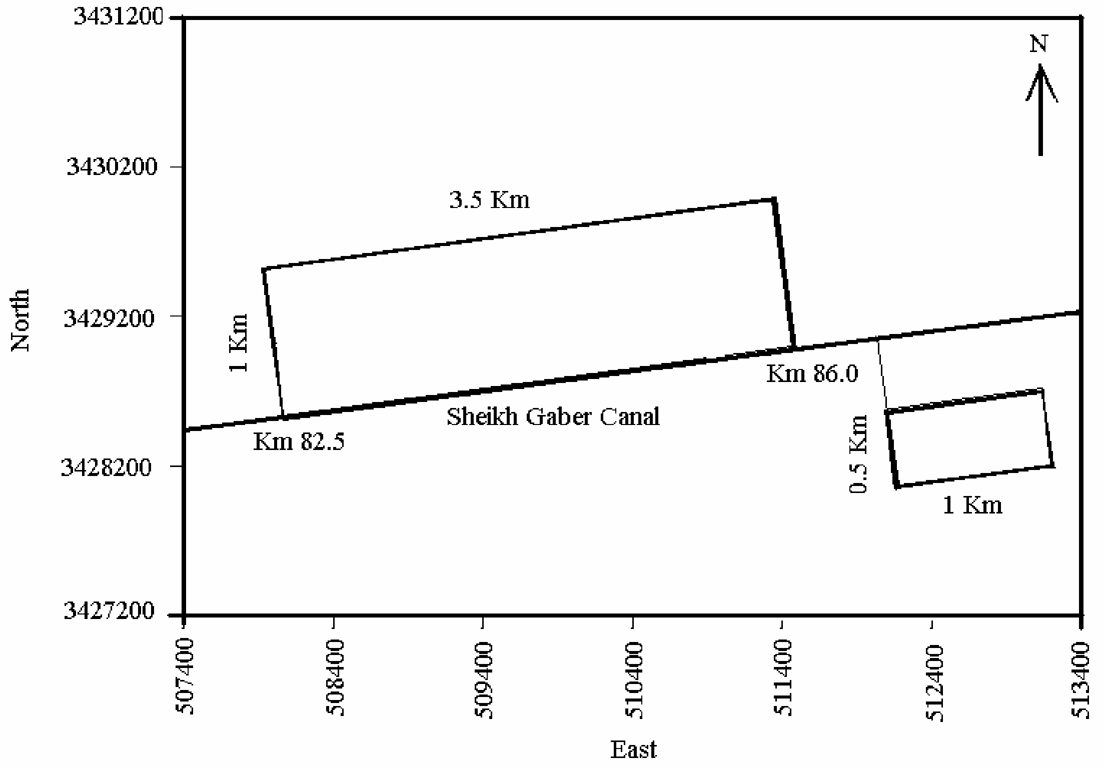

شكل ١
منطقة الدراسة

٢- أحدث تقنيات الرصد على الأقمار الصناعية

أحدثت تكنولوجيا الرصد على الأقمار الصناعية ثورة هائلة في مجال علوم المساحة والخرائط منذ بدء تطبيقها في السبعينيات من القرن العشرين ، إلا أن النظام العالمي لتحديد الموقع (GPS) كان له بالغ الأثر في زيادة الدقة وخفض تكلفة تنفيذ الأعمال المساحية. وقد كان لمعهد بحوث المساحة السبق في اقتناء أول أجهزة هذا النظام في مصر في عام ١٩٨٦ . ويتكون هذا النظام من ٢٤ قمرا صناعيا (٢١ قمر عامل بالإضافة إلى ٣ أقمار احتياطية) يدورا حول الأرض على ارتفاع حوالي ٢٠ر٠٠٠ كيلومتر. وبذلك فأنه يمكن رصد ٤ أقمار صناعية من أي مكان على سطح الأرض في أي وقت من اليوم.

يتمتع نظام GPS بالعديد من المميزات التي أهلته ليحتل المرتبة الأولى في نظم الرصد على الأقمار الصناعية على المستوى العالمي. ومن هذه المميزات:

- الدقة العالية: تبلغ دقة الإحداثيات الناتجة من استخدام هذا النظام (على الأقل) عشرة أضعاف الدقة التي يمكن الحصول عليها باستخدام طرق الرصد الأرضية التقليدية.
- الإتاحة: يمكن استقبال إشارات الأقمار الصناعية طوال الأربع والعشرون ساعة يوميا.
- العالمية: أرصاد النظام متاحة في أي مكان على سطح الكرة الأرضية.
- عدم التأثر بالظروف المناخية: العوامل المناخية (الأمطار والثلوج والحرارة والرياح) لا تؤثر على الإشارات المرسلة من الأقمار الصناعية.
- تلاشى الأخطاء البشرية: أجهزة GPS لها طبيعة شبه آلية ولا تحتاج لتدخل الراصد ولا تعتمد على التوجيه البصري مما يقلل بنسبة كبيرة من حدوث الأخطاء البشرية.
- سهولة الاستخدام: تتميز أجهزة GPS بسهولة الاستخدام مقارنة بأجهزة المساحة الأرضية التي تتطلب خبرة كبيرة من الراصد.
- العائد الاقتصادي: أثبتت الدراسات في مصر والعالم أن استخدام نظام GPS يوفر حوالي ٥٠ % من الوقت والتكلفة مقارنة بالطرق المساحية التقليدية.

وتوجد العديد من أساليب الرصد عند استخدام نظام GPS وأهمها [١]:

- الرصد الثابت (Static Positioning) وفيه يتم احتلال نقطتين على الأقل لمدة لا تقل عن ٤٥ دقيقة للوصول إلى دقة عالية مناسبة للتطبيقات الجيوديسية.
- الرصد المتحرك (Kinematic Positioning) حيث يثبت جهاز الاستقبال على جسم متحرك مثل الطائرات والسفن مما لا يتطلب دقة عالية في تحديد المواقع.

- مجموعة من طرق الرصد التي تحاول الجمع بين مميزات كلا الأسلوبين الثابت والمتحرك لزيادة الدقة وخفض الزمن اللازم للرصد ، ومنها أساليب:
Stop and Go, Semi-Kinematic, Pseudo-Kinematic, On-The-Fly

ويعتبر أسلوب (On-The-Fly (OTF من أحدث الأساليب التي تتيح دقة عالية مع وفر في الزمن اللازم للرصد الحقلي. ويشمل الملحق رقم ١ التفاصيل الرياضية المستخدمة في هذا الأسلوب الحديث للرصد على الأقمار الصناعية .

٣- الرصد الحقلي وتجميع البيانات

بعد إجراء الدراسات الأولية للأعمال المطلوب تنفيذها تم اختيار مجموعة من أحدث وأدق الأجهزة لإجراء أعمال الرصد الحقلي والحسابات المكتبية وطبع الخرائط. ويجدر الذكر أن أجهزة GPS الجيوديسية المستخدمة تتمتع بأعلى مستوى من التقنية الحديثة والمواصفات الدقيقة اللازمة لتنفيذ الأعمال المساحية عالية الدقة حيث أن مواصفاتها كالتالي:

- Dual-Frequency GPS Receivers (use both L1 and L2 frequencies)
- Capable of receiving both C/A and P codes
- Use 24 independent channels for receiving satellite signals
- Track up to 12 GPS satellites simultaneously
- Record received signals on a built-in memory enough for up to 12 continuous hours
- Use a high-precision geodetic antenna with minimum multipath effect
- Capable of performing both static and kinematic observation techniques
- Perform On-The-Fly (OTF) initialization technique
- The normal accuracy of the obtained baseline length, in a static mode, is 5 mm ± 1 ppm (part per million). In other words, this means that for a baseline of 10 km, the expected mean square error is 15 mm.

تكونت الأعمال الحقلية من عدة مهام لتنفيذ أهداف المشروع وشملت ما يلى:

- الاستكشاف:

تم استخدام أجهزة GPS المحمولة لعمل استكشاف عام لمنطقة الدراسة والتغير في طبوغرافيتها تمهيدا لتصميم أمثل أسلوب لتجميع البيانات الحقلية التي تؤدى الغرض المطلوب ودقة الخريطة الطبوغرافية المرجوة. هذا بالإضافة إلى استكشاف أقرب نقط الشبكة الجيوديسية القومية لاستخدامها في أعمال الربط المساحي للحصول على إحداثيات دقيقة.

- إنشاء شبكة ثوابت أرضية:

تم إنشاء شبكة مكونة من ستة نقاط جيوديسية لتكون الهيكل الجيوديسى الأساسي لمنطقة المشروع. وتوجد أربعة محطات من هذه الشبكة على الضفة الشمالية للترعة - عند علامات كيلومترية ثابتة من التدريج المستخدم في أعمال المشروع - حتى يمكن استخدام هذه العلامات في أية تطبيقات هندسية في إطار المشروع. وقد تم رصد الإحداثيات الجغرافية لنقاط هذه الشبكة باستخدام أسلوب الرصد الثابت مع ربطها على نقطة Y23 إحدى نقاط الشبكة الجيوديسية القومية لأرصاد GPS في جمهورية مصر العربية والتي أقامتها الهيئة المصرية العامة للمساحة بغرض إيجاد مرجع جيوديسى واحد للجمهورية.

- أعمال الميزانيات الأرضية:

من المعلوم أن الارتفاع الناتج من أرصاد GPS يكون مقاسا إلى سطح المجسم العالمي الممثل للكرة الأرضية والمعروف باسم World Geodetic System 1984 (WGS84) مما يدل على أن هذه الارتفاعات تكون من النوع الجيوديسى Ellipsoidal Heights (h). ألا أن المشروعات الهندسية تعتمد على استخدام المناسيب وهى الارتفاعات المقاسة إلى متوسط منسوب سطح البحر Mean Sea Level وبذلك تندرج تحت نوع الارتفاعات الارثومترية (H) Orthometric Heights . ويمثل شكل ٢ رسما توضيحيا للعلاقة بين كلا نوعى الارتفاعات. وتوجد العديد من الطرق الجيوديسية للتحويل بين كلا نوعى الارتفاعات [٥] إلا أن أدقها هي طريقة استنباط علاقة رياضية بين كلا نوعى الارتفاعين عند مجموعة نقاط في منطقة محددة وهذا ما يسمى بأسلوب استنباط الجيويد المحلى. ولذلك فقد تم رصد ٦ خطوط ميزانية أرضية للحصول على مناسيب نقاط الشبكة الجيوديسية لاستخدامها في تحويل الارتفاعات الجيوديسية لكل أرصاد GPS إلى مناسيب.

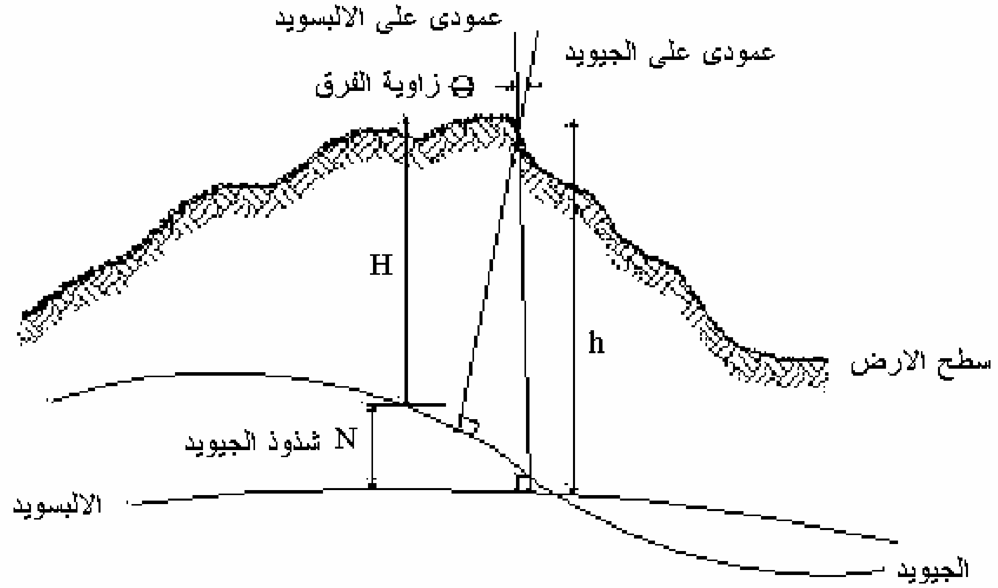

شكل ٢
أنواع الارتفاعات

- أعمال الرفع الطبوغرافى :

تم استخدام أجهزة GPS الجيوديسية لتنفيذ الرفع الطبوغرافى لمنطقة الدراسة باستخدام أسلوب OTF للحصول على دقة مناسبة مع خفض التكلفة الاقتصادية. وفى هذا الأسلوب كان يتم احتلال بعض نقط الشبكة الجيوديسية التي تم إنشاؤها في وضع الرصد الثابت بينما يتم وضع جهاز آخر على سيارة مجهزة تتحرك في خطوط مستقيمة متوازية لتجميع الأرصاد بصفة آلية مستمرة. وبهذا الأسلوب تم رفع حوالي ١٥٫٠٠٠ نقطة تغطى منطقة الدراسة . وبعد ذلك أمكن حساب الإحداثيات ثلاثية الأبعاد لهذه النقاط لاستخدامها في إنشاء الخريطة الكنتورية.

٤- الحسابات وإنشاء الخريطة الطبوغرافية

تكونت الأعمال المكتبية من العديد من الخطوات وباستخدام أحدث برامج الحاسب الآلي المتخصصة. وشملت هذه الأعمال مايلى:

* حسابات الشبكة الجيوديسية التي تم إنشاؤها بالموقع مع ربط هذه الشبكة على الشبكة الجيوديسية القومية لجمهورية مصر العربية والحصول على إحداثيات ثلاثية الأبعاد (خط الطول - خط العرض - الارتفاع الجيوديسى) دقيقة لجميع النقاط على المجسم العالمي WGS84. وتم تطبيق جميع الاختبارات الإحصائية لبيان جودة ودقة النتائج والتي أدت إلى الحصول على دقة ± ٥ مللي للإحداثيات الأفقية ، ودقة ± ٩ مللي للإحداثيات الرأسية.
* حسابات خطوط الميزانيات لإيجاد مناسيب جميع نقط الشبكة.
* حسابات الرفع الطبوغرافى للمنطقة للحصول على إحداثيات حوالي ١٥ ٠٠٠ نقطة على المجسم العالمي WGS84 بدقة ± ٣ سم للإحداثيات الأفقية ، ودقة ± ٥ سم للإحداثيات الرأسية.
* استنباط الجيويد المحلى لتحويل الارتفاعات الجيوديسية إلى مناسيب لجميع النقط .
* حسابات إسقاط الخرائط لتحويل الإحداثيات ثلاثية الأبعاد إلى إحداثيات ثنائية الأبعاد لتوقيع الخريطة الكنتورية.
* إنشاء وتوقيع الخريطة الكنتورية بفترة كنتورية ٠٫٥ متر.
* تحديد المنخفضات الموجودة في المنطقة التي تم رفعها.
* حسابات مساحة وحجم كل منخفض وتمثيلها في جداول وأشكال بيانية.

٥- المميزات الاقتصادية لاستخدام التقنية الحديثة

من أهم عيوب الطرق المساحية التقليدية لإنشاء الخرائط الطبوغرافية (باستخدام أجهزة المحطات الشاملة أو الموازيين) طول الوقت المستخدم في تجميع القياسات الحقلية ومن ثم ارتفاع التكلفة الاقتصادية للمشروع. وعلى الجانب الآخر فان التقنيات المساحية الحديثة بصفة عامة - ونظم الرصد على الأقمار الصناعية بصفة خاصة – تقدم مميزات أهمها الدقة العالية وإنجاز العمل الحقلي في أقل وقت ممكن مما يؤدى إلى خفض التكلفة الاقتصادية. ولذلك فان النظام الذي تم تطبيقه في هذه الدراسة والذي يعتمد على دمج كلا النظامين الحديث والتقليدي يقدم أنسب الطرق العملية لإنشاء الخرائط الطبوغرافية. وبإجراء مقارنة اقتصادية بين تكلفة إنجاز هذه الدراسة باستخدام النظم المساحية التقليدية والنظام التكاملي الذي تم تطبيقه تبين أن النظام التكاملي الجديد قلل من زمن تجميع القياسات الحقلية بنسبة ٧٥% وأدى إلى خفض تكلفة المشروع بنسبة ٥٠% كما هو موضح بالجدول رقم ١ .

جدول رقم ١
مقارنة اقتصادية بين الطرق المساحية التقليدية والنظام التكاملي الجديد

البند	الطرق التقليدية	النظام التكاملي
عدد الأفراد	٢٠	٥
الوقت المستهلك للأعمال الحقلية	٤ أسابيع	١ أسبوع
تكلفة الفدان	١٦ جنيه	٨ جنيه
الوفر في الوقت اللازم	-	٧٥%
نسبة خفض تكلفة المشروع	-	٥٠%

٦- حسابات حجوم المنخفضات

من أهم أهداف المشروع دراسة اختيار منخفض في المنطقة المحددة لاستخدامه كمفيض لتخزين مياه ترعة الشيخ جابر. وبتحليل الخريطة الكنتورية وجد أن هناك ٤ منخفضات مغلقة عند منسوب ١٤ متر ومنخفض آخر مغلق عند منسوب ١٢ متر (مازال مفتوحا عند منسوب ١٤ متر). وتم اعتبار هذه المنخفضات الخمسة لإجراء الحسابات التفصيلية لمساحاتها وحجومها.

تم حساب المساحة السطحية والحجم لكل منخفض على حدي عند مناسيب متعددة تبدأ من منسوب ١٤ متر (١٢ متر للمنخفض رقم ١) وحتى أقل منسوب في أرض المنخفض وعلى فترات ٥ر٠ متر. وكذلك فقد تم استنباط علاقتين بيانيتين لكل منخفض كالآتي: العلاقة بين المنسوب والمساحة السطحية للمنخفض ، العلاقة بين المنسوب وحجم المنخفض. يمثل الجدول رقم ٢ ملخصا لما تم الحصول عليه من نتائج للمنخفضات الخمسة. بينما يوضح شكلي ٣ ، ٤ العلاقات البيانية التي تم استنتاجها للمنخفض الأول . وتخلص الحسابات إلى أن أكبر هذه المنخفضات هو المنخفض رقم ١ والذي يقع على بعد ٥٠ متر شمال كوبري الكيلومتر رقم ٤٥٠ر٨٥ على ترعة الشيخ جابر الصباح وتبلغ مساحته السطحية (عند منسوب ١٢ متر) ٦٠٠١٥٢ مترا مربعا ، كما تبلغ سعته الاستيعابية (حتى نفس المنسوب) ١٦٩٢٣٠٨ مترا مكعبا.

جدول رقم ٢
مساحات وأحجام المنخفضات

المنخفض	المنسوب (متر)	الحجم (متر مكعب)	المساحة السطحية (متر مربع)
١	١٢	١٦٩٢٣٠٨	٦٠٠١٥٢
٢	١٤	٧٥٤٣٠١	٢٦٨٩٥٥
٣	١٤	١٩٥٤٦٢	٥٨٣٠٣
٤	١٤	٣١١٧٥	٢٦٠٥٨
٥	١٤	٣٢٣٤٧	٣٤٤٧٩

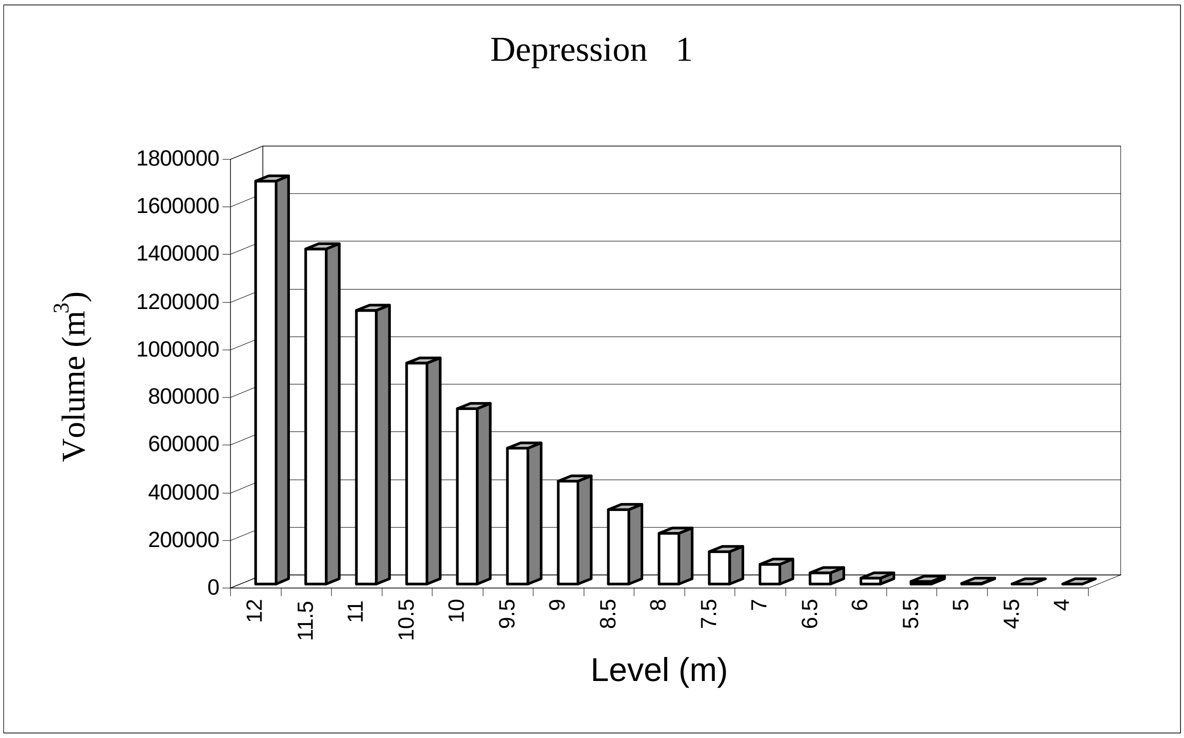

شكل رقم ٣
تقديرات حجم المنخفض رقم ١

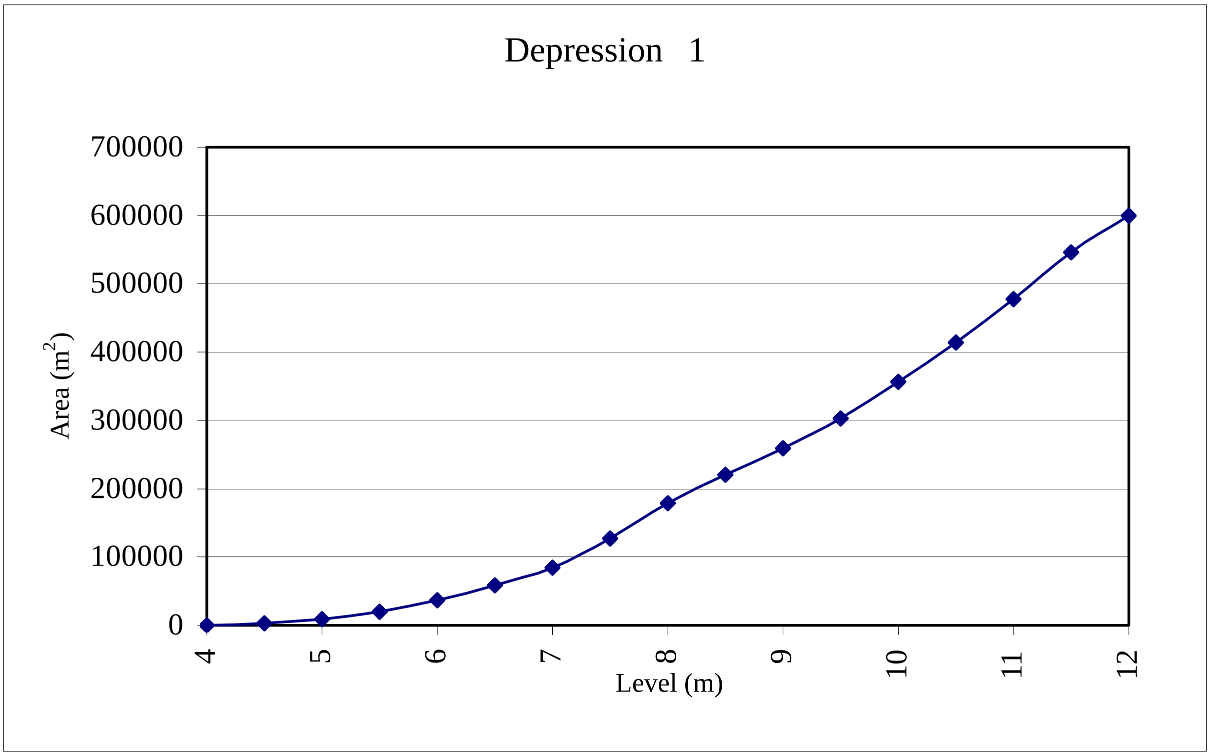

شكل رقم ٤
تقديرات المساحة السطحية للمنخفض رقم ١

٧- الخلاصة والتوصيات

لتمثيل طبوغرافية الأرض و المنخفضات الموجودة بها بغرض اختيار أفضل مفيض على ترعة الشيخ جابر الصباح بشمال سيناء فقد تم استخدام أحدث التقنيات المساحية للرصد على الأقمار الصناعية مع دمجها ببعض الأرصاد المساحية التقليدية لإنشاء خريطة طبوغرافية رقمية لمساحة ١٥٠٠ فدان. وبمقارنة هذا الأسلوب التكاملي الحديث بالطرق المساحية التقليدية فقد أثبتت النتائج الحصول على وفر في الوقت اللازم لإنجاز الأعمال الحقلي يصل إلى ٧٥% بالإضافة إلى خفض العمالة اللازمة إلى أكثر من النصف بالإضافة إلى التقليل من الأخطاء البشرية الممكن حدوثها حيث أن الأجهزة المستخدمة تعمل بطريقة شبه آلية. كما أثبتت هذه المقارنة أن التقنية الجديدة قد قللت من التكلفة الاقتصادية للمشروع بنسبة ٥٠%. وبناء على هذه النتائج يوصى البحث بتطبيق هذا الأسلوب التكاملي في كافة مشروعات إنتاج الخرائط الطبوغرافية في مصر.

References:

[1] Chen, X, Liu, J., and Li, D., 1999, OTF method for GPS aided photogrammetry, Proceedings of the IUGG XXII General Assembly, Birmingham, U.K, July 18-30.

[2] Dawod, G., 1992, On the use of pseudo-kinematic GPS satellite positioning technology in surveying reclaimed lands in Egypt, Proceedings of the first national conference on reclamation and development in Egypt, El-Minia University, November 2-5, pp. 237-246.

[3] Mervart, L., Beutler, G., Rothacher, M., and Wild, U., 1994, Ambiguity resolution strategies using the results of the International GPS Geodynamics Services (IGS), Bulletin Geodesique, V. 68, No. 1, pp. 29-38.

[4] Sickle, J., 1996, GPS for land surveyors, Ann Arbor Press, Inc., Michigan, USA.

[5] Tscherning, C., Radwan, A., Tealeb, A., Mahmoud, S., Abd El-Monum, M., Hassan, R., El-Sayed, I., and Saker, K., 2001, Local geoid determination combining gravity disturbances and GPS/levelling: A case study in the Lake Nasser area, Aswan, Egypt., Journal of Geodesy, V. 75, No. 7, pp. 343-348.

Appendix 1: OTF Kinematic GPS Technique

GPS is the most advanced satellite positioning system currently in use for a wide range of civilian and military applications. The classic GPS observation approach is the static mode in which more than one receiver is kept fixed over ground stations and record satellite signals for more than thirty minutes of observation. Positioning of moving platforms with GPS (the kinematic mode) is the last frontier in GPS surveying. Kinematic positioning can be classified into two main groups: absolute kinematic and relative kinematic. The absolute kinematic deals with positioning of a moving antenna with respect to an implied coordinate system. On the other hand, relative kinematic positioning is performed relative to one or more receivers at known stations. There are several modes of relative kinematic GPS surveying based on the way of the receivers capabilities, data processing; and field observation procedures. Some of these modes are: pseudo-kinematic, rapid static, stop and go, antenna swap; and On-The-Fly (OTF). Details concerning those kinematic techniques are found in a lot of surveying literature [e.g. 4].

One of the main aspects of data processing in GPS positioning is the so-called ambiguity resolution. It is known that GPS receivers measure the accumulating phase over time, but do not have knowledge about the integer number of full cycles of phase that occur from the first moment of the lock on a satellite. The number of full cycles of phase, which does not change unless that lock is lost, is known as the integer ambiguity or phase ambiguity and could be solved for easily in the static GPS positioning, since the receivers collect data from the same satellites for a period of time. On The Fly (OTF) relative kinematic approach is the most advanced technique for resolving the phase ambiguity while the receiver is actually in motion. This implies that unlike all other relative kinematic GPS techniques, the initialization process tack place with no delay. The mathematical model behind OTF technique is called wide-lane observable, which is based on the linear combination of the measured phases from both GPS frequencies, L1 and L2. The strategy starts by solving for the phase ambiguity on the fictional wide-lane observable, which is then used to resolve the phase unknowns on both L1 and L2 frequencies, as follows [3]:

$L^i_{1k} = \rho^i_k - I^i_k * (f^2_2 / (f^2_1 - f^2_2)) + \lambda_1 b^i_{1k}$
(1)
$L^i_{2k} = \rho^i_k - I^i_k * (f^2_1 / (f^2_1 - f^2_2)) + \lambda_2 b^i_{2k} - \Delta\rho^i_k$ (2)
$L^i_{3k} = (1/(f_1 - f_2)) * (f_1 L^i_{1k} - f_2 L^i_{2k})$ (3)
$= \rho^i_k + I^i_k * (f_1 f_2 / (f^2_1 - f^2_2)) + \Delta\rho^i_k (f_2 / (f_1 - f_2)) + \lambda_3 b^i_{5k}$ (4)
$b^i_{1k} = N^i_{1k} + \delta\Phi_{1k} - \delta\Phi^i_1$ (5)
$b^i_{2k} = N^i_{2k} + \delta\Phi_{2k} - \delta\Phi^i_2$ (6)
$b^i_{3k} = b^i_{1k} - b^i_{2k}$ (7)
$\lambda_3 = c / (f_1 - f_2)$ (8)

where: k is the receiver index, i is the satellite index, L^i_{1k} , L^i_{2k} are the carrier-phase pseudoranges, ρ^i_k is the non-dispersive delay, lumping together the effects of geometric delay, ionospheric delay, tropospheric delay, clock signatures, and any other delays which affect the observables, $\Delta\rho^i_k$ is the differential delay between the L1 and L2 antenna phase centers, I^i_k is the difference in ionospheric delay between the L1 and L2 carriers, f_1 , f_2 are the frequencies of the L1 and L2 carriers, which equal1575.42 MHz and 1227.60 MHz respectively, λ_1 , λ_1 are the wavelengths of the L1 and L2 carriers, which equal 19.0 and 24.4 cm respectively, λ_3 is the wavelength of the wide-lane observable, which equals 86.2 cm, b^i_{1k} , b^i_{2k} are the phase biases on the L1 and L2 carriers, b^i_{3k} is the wide-lane phase ambiguity to be estimated, N^i_{1k} , N^i_{2k} are the initial phase ambiguities, $\delta\Phi_{1k}$, $\delta\Phi_{2k}$ are un-calibrated components of phase delay originating from the receivers (assumed to be common for all satellite channels), and $\delta\Phi^i_1$, $\delta\Phi^i_2$ are un-calibrated components of phase delay originating from the satellites (assumed to be common for all receivers).

Proceedings of the Twelfth International Conference on Environmental Protection, Ain Shams University, Alexandria, May 14-16, 2002, pp. 12-23.

ESTABLISHMENT OF THE FIRST MODERN SEA LEVEL MONITORING SYSTEM IN EGYPT

Gomaa M. Dawod [(1)] and Hoda F. Mohamed [(2)]

ABSTRACT

Even though, the current sea level rise is consisted of oscillations of small amplitude, yet it is still essential to be monitored due to the anticipated harmful effects from environmental and development points of view. Results of changes of sea level in Egypt over the last century, based on analysis of collected data of old tide gauges, verify that the Mediterranean sea level is rising by a rate of 1.7 mm/year at Alexandria, and 2.4 mm/year at Port Said.

The Survey Research Institute (SRI) has started a pioneer research project to precisely monitor the rise of the sea level in Egypt. Within this study, a state-of-the-art sea level monitoring system has been established and operated in Alexandria. This advanced system consists of three accurate devices in a unified scheme: a tide gauge, a meteorological unit; and a satellite-based geodetic GPS receiver. This paper describes the present high-technology system in terms of design, accuracy, and suitability. The new multi-purpose observing system has several merits especially in terms of accuracy and compatibility. It is recommended that several monitoring stations of this structure should be established over the Egyptian coasts in order to obtain more precise and reliable frames describing the sea level rise phenomena in Egypt. The precise estimates and results of such systems must be taken into consideration in the development planes of the coastal areas in Egypt.

[(1)] Researcher, Survey Research Institute, National Water Research Center
308 Al-Ahram St., Giza, Egypt. E-mail: p_geod@sri-eg.org
[(2)] Assistant Researcher, Survey Research Institute

1- INTRODUCTION

Mean Sea Level (MSL) is defined as the average level of the sea, usually based on hourly values taken over a period of at least a year. The major effective cause for long-periodic sea level oscillations is the glacial melt and the yield of the earth to the melt load. Some estimates of this effect vary between 6 and 10 cm per century. Recent long-period sea level measurements at several stations show that there is a general increase of MSL of about 0.10-0.20 meter per century (IOC, 1985).

Sea level observing systems, or traditional tide gauges, have been employed since the nineteenth century when most devices were simply graduated markings inscribed on rocks, or on masonry or boards at the entrances of harbors, with measurements of sea level made visually. Only in 1830's did the first mechanical gauges appear which were equipped with clocks and charts recorders and with a stilling well.

The Survey Research Institute (SRI) has designed, acquired, and implemented a precise sea level observing system in Alexandria. It can be considered as the first, out of many, observing system to be employed for precisely monitoring changes of sea level in Egypt. Section Two of this paper presents a brief of tide gauge types. Section Three discusses the need and objectives of the current sea-level observing project executing by SRI. Section Four focuses on the design and structure criteria of the up-to-date system admitted in Egypt. Section Five illustrates results of recent data analysis studies for estimating sea-level changes in Egypt. Drawn conclusions and some future recommendations are contributed in Section Six.

2- TYPES OF TIDE GAUGES

Mainly, there are four categories of tide gauge equipment available now, which are of significant differences in terms of accuracy and costs. These groups are floating, pressure, acoustic, and radar systems. Each category is summarized in the following sub-sections.

2.1 Floating gauges

The traditional type of tide gauge is the analogue floating type. The main reasons to use a float gauge are its low technology and, hence, low price. Recently, other types of tide gauge are available that are more precise and convenient to use. For example, there are floating tide gauges that uses punched tape recorders instead of the paper sheets for data recording. This type of gauges does not give a continuous record of the tidal level but records spot heights at pre-determined time intervals. These instruments contain a coding unit driven from the float mechanism that is designed to transfer a height reading into a recording tape at each recording period. The height is punched out in a binary code form. An automatic reader is usually used to translate the information on the tape into a more usable form. Another improvement that can be added to a working float gauge is attaching an encoder device in order to be able to store recorded data on a local data logger in electronic form. Most types of floating tide gauges suffer from several problems such as the long-term drift, possibly due to ‘tidal hystresis’, and jumps when float and counterweight collide if disturbed [IOC, 2000].

2.2 Pressure gauges

The more convenient, cost-effective, and practical recent tide gauges are those instruments depend on measuring the hydrostatic pressure of the water column above a fixed pressure point and converting this pressure to a sea level equivalent. There are two main categories of pressure tide gauges, namely the pneumatic bubbler system and the direct reading, or transducer, system, as discussed below.

2.2.1 Transducer gauges

The second category of pressure tide gauges measure the sea level by fixing a waterproof pressure transducer below the lowest expected tide level with the power/signal cable connected to an on-shore data logging unit or built-in memory. Transducer pressure gauges are basically described by the following mathematical relationship [ibid]:

$$h = (p - p_a) / (\rho g) \qquad (1)$$

where

- h is the sea level above the pressure point
- p is the total pressure due to both the sea level and the atmospheric measured at the pressure point
- p_a is the atmospheric pressure at the sea surface
- ρ is the average water density in the water column above the sensor
- g is the local gravity acceleration

An important factor in this family of tide gauge is whether the instrument measure absolute or differential pressure. Based on this element, there are two sub-categories of transducer systems. In an absolute pressure transducer, the sensor provides a measurement of the total pressure ‘p’, and consequently, a separate barometer is required in order to provide a separate measurement of p_a. Obviously, both measurements should be recorded using the same clock so they can be readily subtracted to yield the sea level. In a differential pressure transducer, there is a vented power/signal cable in which the reference side of the transducer is vented to atmosphere providing continuous correction for changes in atmospheric pressure.

The majority of these pressure sensors use strain gauge or ceramic technology. Changes in water pressure causes changes in resistance or capacitance in the pressure element. The signal is amplified, displayed, and stored in shore-based data logging equipment. The datum of a transducer mounted underwater is the sensor diaphragm or pressure cell. Pressure transducers are sensitive to temperature variations, and hence, the expected range of temperature to be experienced at the site should not produce an error greater than 0.01% of the full working range. Otherwise, it is recommended that the transducer temperature is monitored for later correction of the recorded data or the transducer is housed in a constant-temperature enclosure. It worth mentioning that pressure transducer tide gauges comprise a major subset of those utilized in the international Global Sea Level Observing System (GLOSS) network [IOC, 1994].

2.2.2 Bubbler pressure gauges

In a pneumatic bubbler tide gauge, the air is passed at a metered rate through a small bore to a pressure point fixed below the lowest expected tide level. Provided that the air-flow rate is low and the air supply tube is not too long, the pressure of the air in the system will equal the hydrostatic pressure plus atmospheric pressure. A pressure recording instrument connected to the air supply tube will record changes in water level as changes in pressure. Most pneumatic instruments using the bubbler principle operate in the differential mode, sensors being so constructed that the system pressure is opposed by atmospheric pressure within the instrument. Therefore, the resultant pressure experienced by the sensor becomes the difference in pressure and hence, making height directly proportional to the pressure [IOC, 1985].

2.3 Acoustic gauges

Another category of tide gauges is known as acoustic tide gauges. These instruments depend on measuring the travel time of acoustic pulses reflected vertically from the air/sea interface [IOC, 2000]. To ensure continuous and reliable operation, the acoustic pulses are generally contained within a vertical tube or well which can provide some degree of surface stilling. Averaging a number of measurements will also have a stilling effect and give improved accuracy.

2.4 Radar gauges

One of the most recent technologies of tide gauges is that system uses the time of flight of a pulse of radar, rather than sound, to measure water level. A radar gauge produces a radar source down onto the water from a sensor in the open air. The sensor transmits the pulse and receives the return pulse, hence determining the time of flight and range. Other radar sensors use pairs of cables or rods, between which the radar pulse is transmitted as a wave guide, and therefore could be deployed in a stilling well [ibid].

3- THE NEED AND OBJECTIVES OF A SEA-LEVEL OBSERVING SYSTEM

Although there are several agencies in Egypt operate measuring equipment for determining sea level changes, most of them suffer from several disadvantages in terms of structure, accuracy, and compatibility. For example, the installed out-of-date floating devices are not accurate enough to produce reliable results or estimates for the sea level rise rate. Additionally, there is no distinguishing between the relative and the absolute sea-level rise in these projects. Moreover, most of these activities are designed for a specific goal serving a specific area, with no national interest in mind.

The Survey Research Institute (SRI) has designed, purchased, and implemented a precise sea level observing system in Alexandria. It can be considered as the first, out of many, observing system to be employed for precisely monitoring changes of sea level in Egypt. The research project has several objectives to fulfill both geodetic and environmental goals including:

* Precise monitoring the sea-level rise in Egypt.
* Accurate definition of the vertical geodetic datum in Egypt.
* Study the vertical movement of the Egyptian coasts with respect to the MSL.

* Study of the meteorological effects and the observations methods on the sea-level data quality.
* Development of computer strategy and models to re-define the vertical datum.
* Definition of topography of both Mediterranean and Red seas using terrestrial and altimetric satellite data.
* Analysis of levelling networks in Egypt and study the different methods to enhance these networks and detect any errors.
* Analysis and adjustment of precise levelling networks in the Nile valley area and development of specifications and standards.
* The optimum accurate models for meteorological effects on the levelling measurements in Egypt.
* The use of GPS and a precise geoid of Egypt to obtain accurate orthometric height differences compared with the terrestrial levelling techniques in new developed areas.
* Developing data bases for levelling networks in the Nile valley.

4- THE DESIGN AND STRUCTURE OF A SEA-LEVEL OBSERVING SYSTEM

Instantaneous measurements of sea level in a series may be considered as the sum of three components: mean sea level, tide, and meteorological residuals. Consequently, in order to obtain mean sea level, both tide and meteorological residuals should be estimated and removed out from the observed sea level data [IOC, 1985].

Although the acoustic and the radar gauges produce sea-level measurements of one-millimeter accuracy, their price and operational costs are considerably high. On the other hand, the floating gauges are relatively cheap, but their accuracy may not be suitable for recent sea level monitoring applications. If accuracy and costs are to be balanced, the pressure tide gauge has proven to be the optimum choice in modern sea level observing systems.

Atmospheric conditions should be monitored and recorded in order to study their effects on the recorded sea level data. For example, changes in atmospheric pressure produce changes in the pressure acting vertically on the sea surface. One-millibar increase of atmospheric pressure decreases sea level by one centimeter. Additionally, the drag of the wind on the sea surface increases as the square of the wind speed, to a first approximation (IOC, 1994). Consequently, a precise sea level observing system should include a device for monitoring meteorological factors.

Recent geodetic and oceanographic MSL studies have shown that neither the sea levels nor the land are permanent with respect to time variations. The data analysis of tide gauges produces "relative" sea level changes. For the purpose of monitoring and understanding long term variations in sea level, the contribution of land motion should be precisely determined. That means that in order to monitor "absolute" changes in sea level, the rates of any vertical land movements at a tide gauge must be determined [e.g. Bingley et al, 2000]. Consequently, a geodetic monitoring technique is required to perform this task at tide gauge sites. The Global Positioning System (GPS) is the most recent and precise geodetic tool used, among a wide range of applications, to monitor crustal movements. The GPS is a global military and civilian navigation system operated by the U.S. Department of Defense for. It consists of 21 satellites (and 3 spares) orbiting the Earth at an altitude of about 20,000 km. Interested readers may obtain detailed information concerning the GPS technology in a variety of publications [e.g. Leick, 1998, and Mohamed and Alnaggar, 1999]. GPS has been utilized in several modern sea level observing projects worldwide [e.g. Zibini et al, 2000, and Bingley et al,

2000]. Another crucial merit of utilizing GPS at tide gauges is the unification of global network of tide gauges in a unique coordinates system, which permits the analysis of sea-level measurements on a global scale. Absolute gravimetry may also be adopted as an alternative procedure to monitor vertical crustal movements at a tide gauge site.

Beside the three mentioned elements of a sea level observing system, the site in which the gauge is installed should fulfill the following criteria (IOC, 2000):

- When completed, the installation must be capable of withstanding the worst storm conditions.
- The ground on which the installation is to be built must be stable.
- The water depth must extend at least two meters beneath the lowest astronomical tide.
- River estuaries should, if possible, be avoided.
- Areas where impounding (becoming cut-off from the sea) can occur at extreme low level should be avoided
- Sharp headlands and sounds should be avoided since theses are places where high currents occur.
- Proximity to outfalls can result in turbulence, currents, dilution and deposits, and should be avoided.
- Electrical power source must be available to operate instruments.
- Accessibility of the site should be easy.

The new installed state-of-the-art system consists of three devices integrated together in a unified scheme: a tide gauge, a meteorological unit; and a satellite-based GPS geodetic receiver (Figure 1). The three components will be presented in details in the following sub-sections.

4.1 Utilized Tide Gauge Instrument

The utilized tide gauge is a high-accuracy temperature-compensated self-contained instrument for measuring and recording tide and wave data. The employed technology in this state-of-the-art device is based on the Silicon-On-Sapphire semi-conductor strain gauge pressure type.

The instrument, which is called Wave and Tide Gauge WTG904 Series 3, measures instantaneously the water column pressure, and converts it to height of water with respect to a specific user-defined location (Figure 2). The pressure sensor output is digitized at a 2 Hz sampling rate via a 14-bit A/D converter controlled by a 32-bit CMOS microprocessor. The tide is calculated continuously and recorded automatically every 10 minutes. The measuring depth range of the gauge is from 0 to 35 meters, with a precision of ± 0.15 % of the measuring range, and a resolution of 0.006 % of the measuring range. Knowing that the depth of the water in the steeling well in Alexandria is approximately 1.5 meters, it can be expected that the accuracy of the measurements is 0.2 cm. The apparatus has a built-in battery-backed 64KB RAM memory that can record measurements up to 90 days. A communication interface (RS485 or RS232C) is used to download the recorded data to an attached computer. There are two ASCII output files, for both tide and wave recorded data, which could be used for further analysis and plotting procedures. The device works in operating temperature from -5 ^{o}C to 35 ^{o}C. The equipment uses internal alkaline batteries that can provide the required power up to 90 days in normal conditions [InterOcean, 1999].

4.2 Utilized meteorological device

The utilized device, WMS-14 from Omega Inc., is a state-of-the-art microprocessor-based weather station (Figure 3). Measurements of wind speed, wind direction, temperature, humidity, and precipitation are collected and processed by the control module of this station. The device consists of five sensors connected to a control unite. Build-in memory can store measured data up to 32 days for later retrieval. The time interval between recordings is user-defined ranging from one to sixty minutes. The device is powered by an external 12V source from a standard 220V outlet. A 12V battery can be plugged into the auxiliary power jack to provide emergency backup power in the event of a loss of main power. A fully charged battery will run the device for five days.

The WMS-14 instrument has five accurate and reliable sensors for collecting different types of meteorological data. A wind speed sensor combines a three-cup anemometer and a wind vane on a single axis. This sensor measures, computes, and stores wind speed and wind direction. Barometric pressure is sensed using a piezoresistive sensing element, which responds to changes in pressure with a corresponding change in resistance. The resistance is converted to a voltage form, which the microprocessor calculates the pressure at the elevation at which the barometer is located. Temperature is sensed using a thermistor element whose resistance changes in response to temperature fluctuations. Relative humidity is sensed by changes in capacitance of a thin polymer film as it absorbs moisture, or sheds it to, the surrounding air. The rain gauge used with the WMS-14 is a traditional tipping bucket design. The accuracy measures of the five sensors are [Omega, 1999]:

For barometric pressure:	± 5 mb
For Wind Speed:	± 3 mph
For Wind Direction:	± 2^o
For Rain precipitation:	± 1 %
For Temperature:	± 2^o F
For Relative Humidity:	± 3%

4.3 Utilized satellite-based GPS receiver

Lieca GPS system 500 comprises GPS receiver, terminal and post-processing software (Figure 4). The SR520 dual-frequency GPS receiver has 12 L1 and 12 L2 continuous data tracking channels that track both codes and carrier phases of the transmitted satellite signals. It tracks up to 12 simultaneously satellites. The collected data is stored on a standard PCMCAI cards that has storage capacity up to 85MB (i.e., up to three months of measurements). An alphanumeric TR500 terminal is connected to the receiver, either via a connection cable or directly to a certain port, in order to configure and control the receiver options. A high-precision AT504 choke-ringe type antenna is utilized in the GPS project configuration.

The normal accuracy of the obtained baseline length, in a static mode, is 5 mm ± 1 ppm (part per million) [Lieca 1999]. In other words, this means that for a baseline of 10 km, the expected mean square error is 15 mm. It worth mentioning that this accuracy limits could be improved using several items, e.g. using precise satellite orbits instead of the normal ones broadcasted in real-time from the GPS satellites.

5- RESULTS OF ESTIMATING SEA LEVEL RISE IN EGYPT

Tide observations, from different sources, have been collected for two tide gauges at Alexandria, and one tide gauge at Port Said [Dawod, 2001]. The available measurements span from 1944 to 1999 for Alexandria, and from 1926 to 1987 for Port Said. The MSL defined in 1906 as the national Egyptian vertical datum has been used to unify all measurements. The annual averages of sea level at Alexandria and Port Said have been analyzed using the available data sets. The results are summarized in Table 1. The annual change of sea level at Alexandria varies from –11.7 cm to 11.5 cm, while it ranges from –7 cm to 12 cm at Port Said. Considering the zero-value for MSL defined in 1906 as a datum, it has been found that the MSL at Alexandria varies from 1.6 cm (in 1947) to 23.5 cm (in 1987) above that datum, with a mean value of 11.1 cm. At Port Said, MSL changes between –1.7 cm (in 1929) to 24.0 cm (in 1980), with an average of 9.0 cm. Figures 5 and 6 depict the MSL annual changes for Alexandria and Port Said respectively, while figures 7 and 8 present the MSL values, above the selected datum, for both tide gauges.

Regression analysis has been performed to compute the rising rates of sea level at Alexandria and Port Said over the last decades. The least-squares estimation technique has been utilized to solve the linear over-determined equations since there exist degrees of freedom. The obtained results are:

For Alexandria:

$$H = 6.09 + 0.1718 * YN_1 \tag{2}$$

For Port Said:

$$H = 2.29 + 0.2390 * YN_2 \tag{3}$$

where,

H is the height of the sea level, in cm, above the chosen datum.
YN_1 = Year – 1943, i.e., the number of years from the start of the data series at Alexandria.
YN_2 = Year – 1925, i.e., the number of years from the start of the data series at Port Said.

Table 1
Long-Term MSL Rise

	Alexandria	Port Said
Data Span	1944-1999	1926-1987
Minimum Annual Change	-11.7	-7.0
Maximum Annual Change	11.5	12.0
Minimum MSL Value	1.6	-1.7
Maximum MSL Value	23.5	24.0
Average MSL Value	11.1	9.0

Based on these findings, it can be concluded that the Mediterranean sea level is rising by a rate of 1.7 mm/year at Alexandria, and 2.4 mm/year at Port Said. These estimates are close to results of similar previous studies [e.g. Alam El-Din, 1993, and Frihy, 1992]. However, it worth mentioning that the data utilized in the present study cover longer time span, and hence could be considered more reliable for long-term MSL rise determination.

6- CONCLUSIONS

The sea level rise is one of the main factors that cause shoreline retreat, coastal erosion, lowlands overflow, and increase the salinity of lakes and aquifers. Consequently, there exists a critical demand to explore, on geodetic and environmental basis, the consequences of sea level changes in Egypt. It has been found that the annual change of sea level at Alexandria varies from –11.7 cm to 11.5 cm, while it ranges from –7 cm to 12 cm at Port Said. Considering the zero-value for MSL defined in 1906 as a datum, it has been found that the MSL at Alexandria varies from 1.6 cm (in 1947) to 23.5 cm (in 1987) above that datum, with a mean value of 11.1 cm. At Port Said, MSL changes between –1.7 cm (in 1929) to 24.0 cm (in 1980), with an average of 9.0 cm. Moreover, it has been concluded that the Mediterranean sea level is rising by a rate of 1.7 mm/year at Alexandria, and 2.4 mm/year at Port Said.

The installed state-of-the-art multi-purpose sea level observing system satisfies the recent recommendations and standards of the international respective organizations. It is the first outstanding monitoring system in Egypt that fulfils several geodetic and environmental goals. It is recommended that several such systems must be installed on the Egyptian coastlines in order to obtain more precise and reliable frames describing the sea level rise phenomena in Egypt. The precise estimates and results of such systems must be taken into consideration in the development planes of the coastal areas in Egypt.

REFERENCE

Alam El-Din, K., 1993, Sea level fluctuations along the Suez Canal, MSC Thesis, Faculty of Science, Alexandria University, Egypt.

Bingley, R., Dodson, A., Penna, N., and Booth, S., 2000, Using a combination of continuous and episodic GPS data to separate crustal movements and sea level changes at tide gauges in the UK., Proceedings of the tenth general assembly of the WEGENER project, San Fernando, Spain, Sept. 18-20.

Dawod, G., 2001, The magnitude and significance of long-term sea level rise in Egypt from a geodetic perspective, Proceedings of the Eleventh International Conference on Environmental Protection, Alexandria University, Alexandria, May 8-10, pp. 207-215.

Frihy, O., 1992, Sea level rise and shoreline retreat of the Nile Delta promontories, Egypt, Natural Hazards, No. 5, pp. 65-81.

InterOcean Systems, Inc., 1999, User manual of model WTG904 Series 3 wave and tide gauge, Revision E., California, USA.

IOC (Intergovernmental Oceanographic Commission), 1985, Manual on sea level measurement and interpretation, Volume 1: Basic procedures, UNESCO.

IOC, 1994, Manual on sea level measurement and interpretation, Volume 2: Emerging technologies, UNESCO.

IOC, 2000, Manual on sea level measurement and interpretation, Volume 3: Reappraisals and recommendations as of the year 2000, UNESCO.

Lieck, A., 1998, GPS satellite surveying, John Wiley & Sons, New York.

Lieca Inc., 1999, GPS System 500 User Manual, Heerbrugg, Switzerland.

Mohamed, H., and Alnaggar, D., 1999, Consistency of GPS surveys using different geodetic receivers and processing software, the IUGG conference, Birmingham, UK, July 19-24.

Omega, Inc., 1999, WMS-14 Weather station Operator's Manual, Stamford, CT, USA.

Zibini, S., Negusini, M., Romagnoli, C., Domenichini, F., Richter, B., and Simon, D., 2000, Separating sea-level variations from crustal movements, Proceedings of the tenth general assembly of the WEGENER project, San Fernando, Spain, Sept. 18-20.

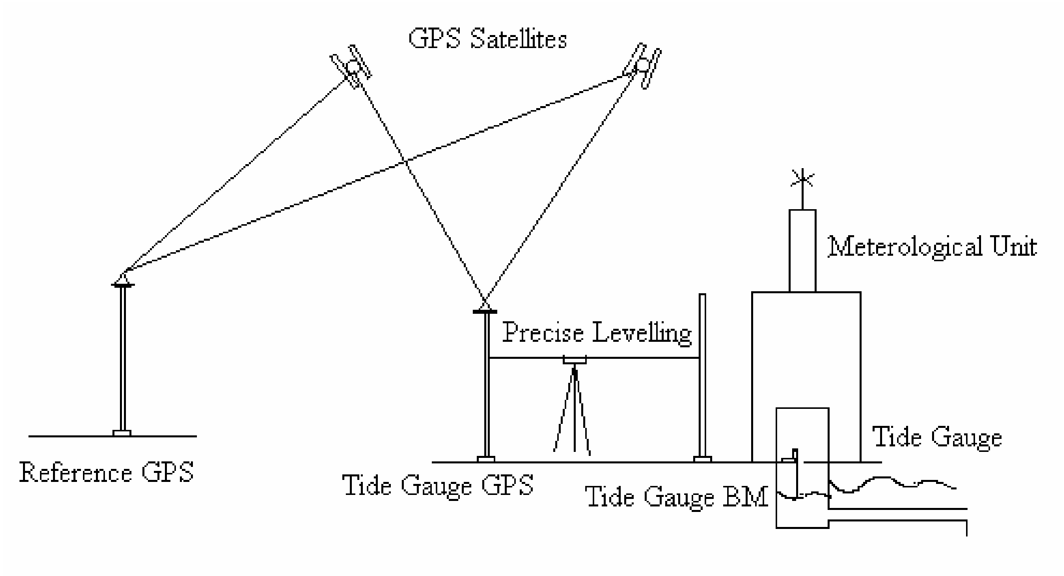

FIGURE 1
MODERN SEA-LEVEL MONITORING SYSTEM

FIGURE 2
WTG904 TIDE GAUGES

FIGURE 3
WMS-14 METEOROLOGICAL STATION

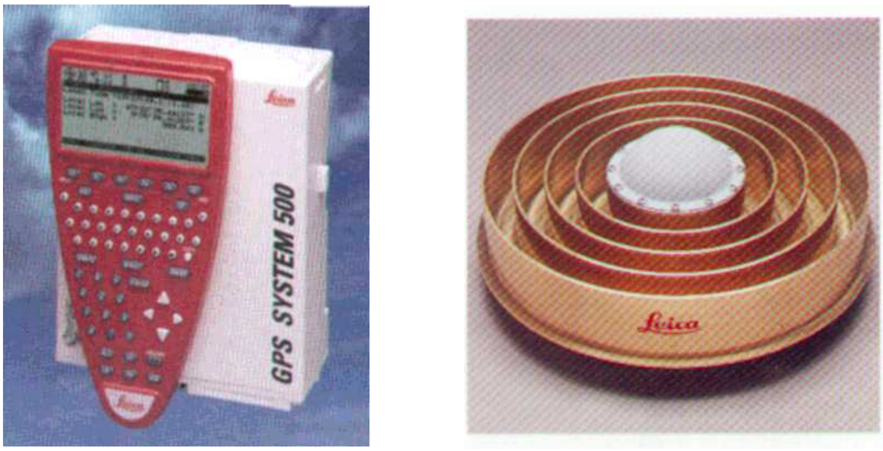

FIGURE 4

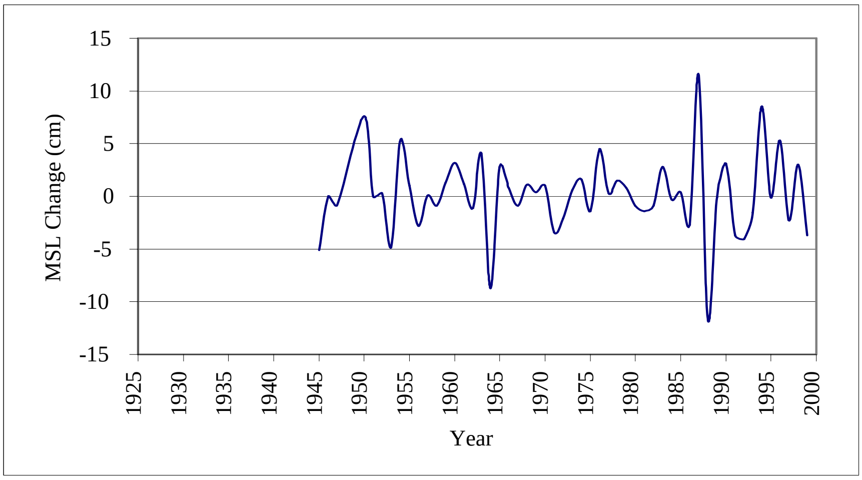

LIECA SYSTEM 500 GPS RECEIVER

FIGURE 5

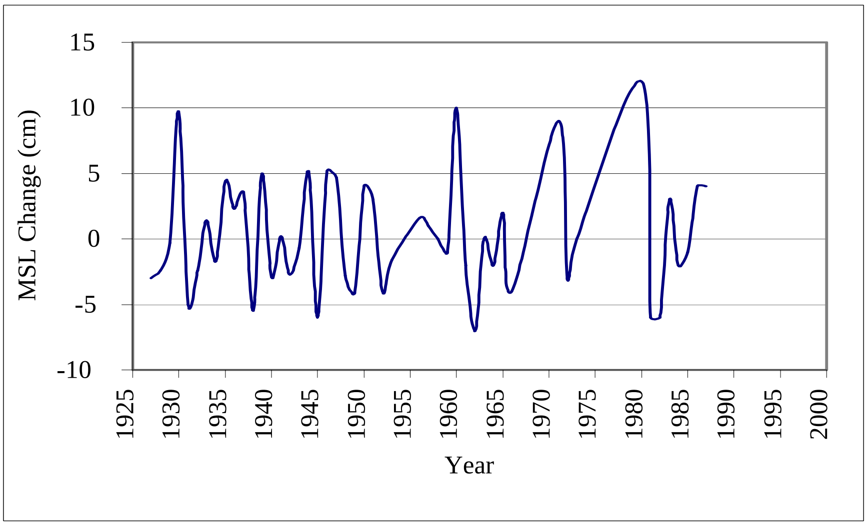

ANNUAL VARIATIONS OF SEA LEVEL AT ALEXANDRIA

FIGURE 6

ANNUAL VARIATIONS OF SEA LEVEL AT PORT SAID

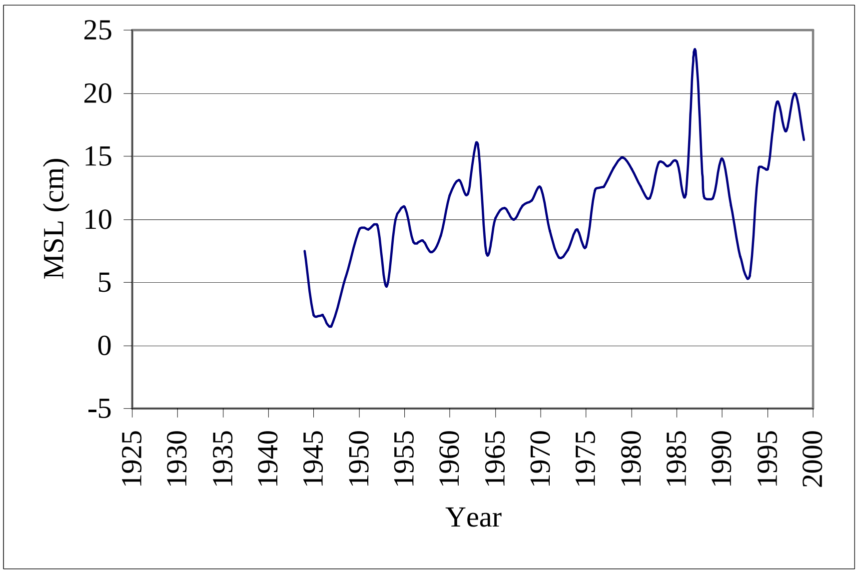

FIGURE 7
LONG-TERM CHANGES OF MSL VALUES AT ALEXANDRIA
(RELATIVE TO THE 1906 NATIONAL DATUM)

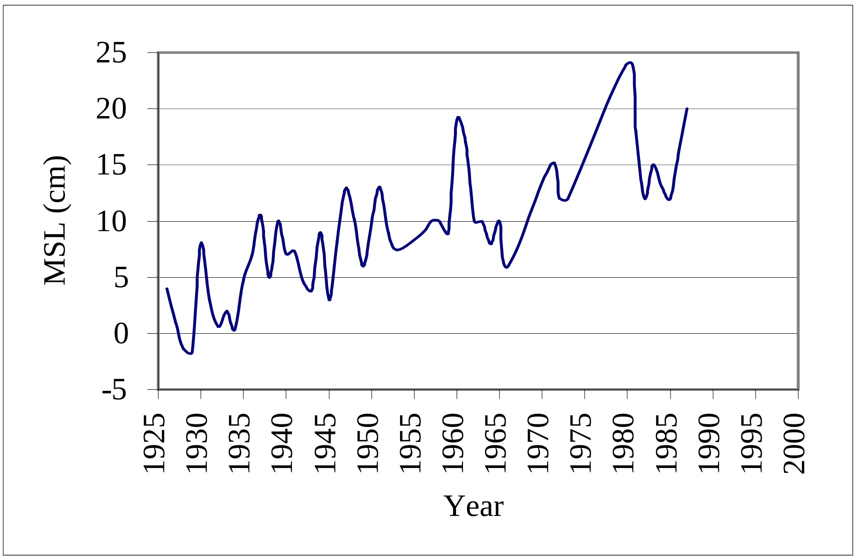

FIGURE 8
LONG-TERM CHANGES OF MSL VALUES AT PORT SAID
(RELATIVE TO THE 1906 NATIONAL DATUM)

Analysis of the Established Egyptian National Gravity Standardization Network of 1997 (ENGSN97)

BY

Prof. Dr. Eng. A. A. Shaker
Shoubra Faculty of Engineering
Zagazig University-Benha Branch

Prof. Dr. Eng. D. S. Alnagar
Ministry of Water Resources and Irrigation
Central Administration for Training

Dr. Eng. G. Dawood
Surveying Research Institute

Ass. Prof. Dr. Eng. A. A. Saad
Shoubra Faculty of Engineering

تلعب قيم واتجاهات الجاذبية الأرضية دورا مهما فى مجال علوم الأرض وخاصة الجيوديسيا والجيوديسيا الطبيعية وفيزياء الأرض. من أهم أهداف علم الجيوديسيا تحديد شكل الأرض وكذلك مجال الجاذبية لها. لذا يهتم العلماء بوضع نموذج رياضى لمجال الجاذبية حتى يتسنى لهم استنتاج قيمه المختلفة من الارصاد المأخوذة . مع النمو السريع فى استخدام اجهزة ال GPS فى الاعمال الجيوديسية والمساحية وتحديد الارتفاعات الجيوديسية بدقة عالية بهذه الاجهزة فقد تطلب ذلك معرفة نماذج دقيقة امجال الجاذبية (الجيويد) وذلك لتحويل الارتفاعات الجيوديسية الغير مطلوبة عمليا الى ارتفاعات ارثومترية (منسوبة للجيويد) مطلوبة عمليا.

ولشبكات الجاذبية اهمية كبيرة فى تطبيقات قومية وعالمية عديدة . شبكة الجاذبية المسماه بنظام بوتسدام مثال للشبكات الدولية من عام ١٩٠٩ الى عام ١٩٧١ . كانت الشبكة القومية للجاذبية (NGSBN-77) الهيكل الاساسى فى النصف الثانى من القرن العشرين فى مصر لهيئة المساحة المصرية ايضا مجهوداتها فى قياسات الجاذبية وذلك لتصحيح ارصاد الميزانيات الخاصة بها لكن كل هذه الارصاد للجاذبية لاتكفى لمتطلبات اليوم وذلك من وجهة نظر الدقة والكثافة وكذلك لفقد معظم هذه النقاط. لذا فمن الضرورى جدا انشاء شبكة جديدة تستجيب لمتطلبات اليو م والتطبيقات الحديثة . هذا البحث يشرح عملية انشاء هذه الشبكة الحديدة وبيان ارصادها وشرح لخطوات معالجتها وضبطها.

Abstract

Gravity data find multiple demands basically in two major fields of geosciences: geodesy and geophysics. The principle task of geodesy is the determination of the figure of the earth, that is extended to the determination of the exterior gravity field. The gravity field has to be modeled in order to derive geometrically defined quantities from the observations. Local gravity field representations are required for establishing geodetic control networks in geodetic and engineering surveys. With the rapid growth of

CERM Vol. (23) No. (2) July 2001 Page. 999-1021

the use of the satellite-based Global Positioning System (GPS), high resolution gravity field data are needed to transform the ellipsoidal heights into orthometric heights. In geophysics, gravity data are used in a wide range of applications, such as exploration of mineral and underground water resources, monitoring crustal movements, and the study of the orbits of natural and artificial celestial bodies.

Gravity control networks are essential to support several applications, on a national and international scales. The Potsdam gravity system provides an example of an international gravity datum, from 1909 to 1971. In Egypt, the National Gravity Standard Base Net (NGSBN-77) afforded the gravity framework in the second half of the twentieth century. In addition, the Egyptian Survey Authority (ESA) usually is carrying out gravity measurements, for some specific applications, especially for correcting precise levelling observations. However, all such gravity measurements, can not satisfy the modern precise applications in Egypt. Consequently, the establishment of a precise new national gravity base network becomes an essential and urgent task for the geodetic community in Egypt, and this is actually the main point of our interest in the current investigation.

A project for re-calibration and updating the old gravity networks, and initiating a new Egyptian national gravity network was carried out. Such network will be named as the Egyptian National Gravity Standardization Network of 1997 (ENGSN97). The ENGSN97 network serves as the precise national gravity datum for Egypt. So, the ENGSN97 will be documented in details in this research.

1- Introduction

The earliest absolute gravity observations in Egypt have been carried out in 1908 at Helwan observatory. This station was considered as the fundamental gravity station in Egypt with a gravity value of 979.295 Gal [Cole, 1944]. Other seven gravity stations in Egypt and Sudan have been observed in that year. These stations have been tied to Kew, London. The Egyptian Survey Authority, formally the Survey of Egypt, has started its first gravity survey in 1927 using a pendulum apparatus [ibid].

Starting from 1922, some foreign oil companies have carried out gravimetric survey as a geophysical exploration tool, mainly in the Gulf of Suez. From 1922 to 1938, more absolute gravity measurements have been carried out at Ras Gharib, Helwan, Suez, Shadwan, Rahmi, Wadi El-Natrun, and Amria. From 1938 to 1950, more precise gravimeters have been used in gravimetric surveys. Within an international gravity program, twenty-one stations have been established in Egypt in 1950-1951 and tied to the Potsdam gravity reference system [Kamel and Nakhla, 1985].

In August 1971, the International Gravity Standardization Net (IGSN-71) was introduced as the new global gravity reference system. The network contains 473 primary stations (eight of them are absolute stations). The standard errors for the net's gravity values are less than 0.1 mGal [Morelli et al., 1974]. As a part of the IGSN-71 activities, eleven gravity stations have been measured in Egypt with standard deviations range from 0.024 to 0.035 mGal.

A ten-year project (1974-1984) for compilation of gravity maps of Egypt has resulted in the National Gravity Standard Base Net (NGSBN-77). The NGSBN-77 consists of 66 stations, and has been tied to IGSN-71 stations located at Cairo International airport, Helwan observatory, Luxor, Aswan, and Port Said. The mean square errors for the observations range between 0.04 - 0.47 mGal [Kamel and Nakhla, 1985].

ESA has carried out some gravimetric surveys along first order leveling lines. concentrated in the Northern part of Egypt. ESA is usually conducting several gravity missions, needed to compute the required corrections for the first-order levelling routes, see [Nassar, 1976] and [Nassar, 1977]. Several other authorities in Egypt conduct gravity missions for special purposes. The National Research Institute of Astronomy and Geophysics, for example, has observed several small gravity nets, as a part of multi-observables geodetic networks, serving for the detection of crustal deformation. Most of these loops are concentrated in the active crustal movement zone of Aswan lake [Groten and Tealeb, 1995].

According to the ENGSN97 project's goals, the field observation campaigns include the collection of three types of measurements: relative gravity, GPS coordinates, and precise levels. This is, of course, beside the necessary absolute gravity measurements at some selected stations. Consequently, each ENGSN97 station has known precise values of:

gravity acceleration (g), geodetic latitude (ϕ), geodetic longitude (λ),
geodetic height (h), and orthometric (H) height.

Regarding the above conditions, a design of the ENGSN97 has been optimized as depicted in Figure (1). Prior to starting the field campaigns, a reconnaissance survey has run and showed that, unfortunately, almost all of the NGSBN-77 stations have been lost, except about five stations only. Therefore, it was decided to re-establish the NGSBN-77 stations at the same locations as long as the station selection conditions are satisfied. In areas where new infrastructures have been built, new locations are selected as close as possible to the old locations. In addition, the reconnaissance showed also that most of the IGSN-71 stations have been lost except two stations at Helwan Observatory. Consequently, the establishment of a precise new national gravity base network becomes an essential and urgent task for the geodetic community in Egypt, and this is actually the main point of our interest in the current investigation.

2- Description and field measurements of ENGSN97 gravity network

The gravity network consists of 145 relative gravity stations and 5 new absolute gravity stations established in Egypt in 1997, Figure (1). The network has been observed through 51 loops, Figure (2). The minimum, maximum, and average distance spacing between stations are 0.136, 128.144, and 65.988Km respectively. Seven LaCoste and Romberge relative gravimeters have been utilized in the observation campaigns of ENGSN97 network. Table (1) presents a summary of the ENGSN97 input statistics.

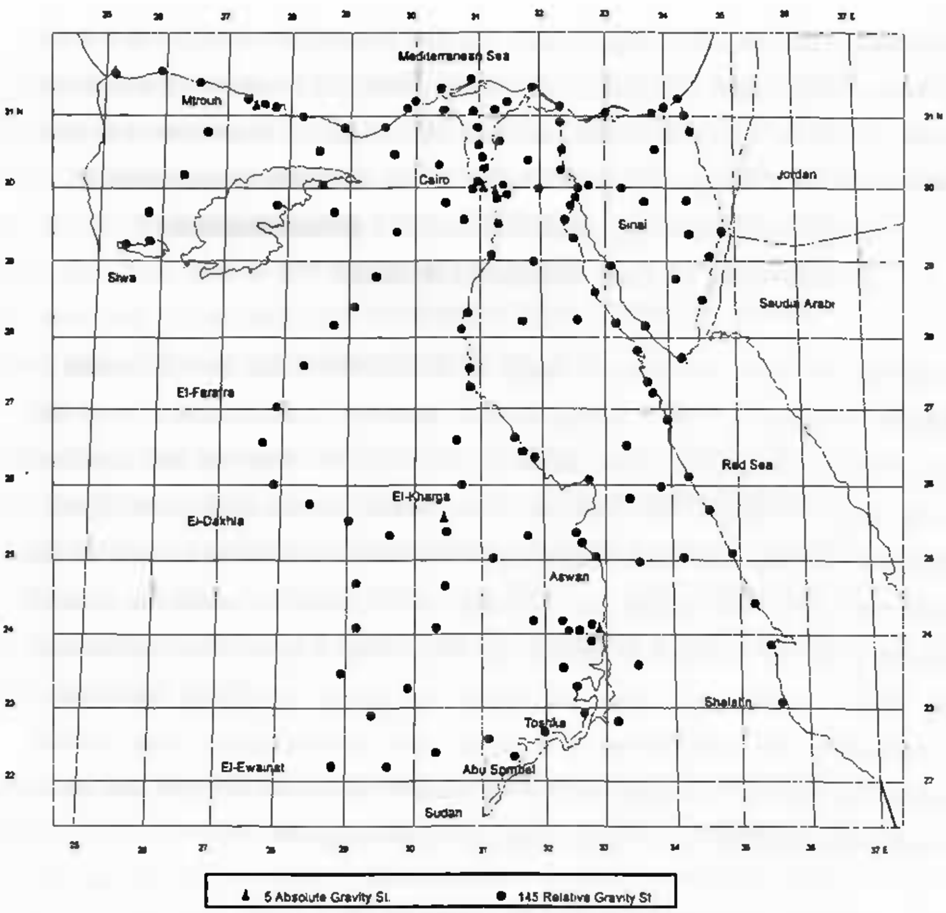

Figure 1

The Egyptian National Gravity Standardization Network " ENGSN97"

The gravimeter reading is converted to corresponding milligal values by using the calibration table of each gravimeter provided by the manufacture. It is worth mentioning that there were no trustable absolute gravity stations still existing in Egypt before 1997 to perform field calibration of the gravimeters. The solar-plus-linear tide correction, subtracted from the observations, are computed based on the formula of Longman except that the values are increased by 16% to compensate for the finite deformation or compliance of the Earth [LaCoste and Romberge, 1989b]. The GRAVPAC software was used to perform these two steps and to produce the so-called metered-gravity values which become the basic observables, to be input to the developed processing programs.

Two different observation scenarios are applied in the field campaigns in this network: the step method; and the profile method. Both of them give precise results regarding the drift control. However, the step method is economically expensive since it requires three stops over every station while in the profile method only two stops per stations are needed. The original scenario of the profile observation scheme is observing the station sequence as 1-2-3-4-4-3-2-1. Tacking the time break after the first observation over station 4 will divide the loop into two parts: 1-2-3-4 and 4-3-2-1. Both of the new data series do not have any repeated observations, which makes the drift estimation is impractical. Two alternatives are proposed:

(1) If the loop observation time is relatively short, there is no need for the break and the observation scenario should be modified to be: 1-2-3-4-5-4-3-2-1, where station 5 is any arbitrary station, not of interest. This station is observed just to separate the two consecutive observations over the network station 4 and to avoid having gravimeter dial remain fixed.

(2) In case of a long observation time of the loop, the observation scenario should be: 1-2-3-4-4-break-4-4-3-2-1.

GPS observations are taken to obtain accurate geodetic coordinates at all the network stations. The stations are tied to first order stations of ESA. In the same time, levelling observations are made to obtain the orthometric heights of the network stations. The network stations are connected to the nearest Bench Marks of ESA in every case.

3- Assessment of the developed program GNPA

A comparison has been carried out between the results of the developed GNPA program and the GRCOMP program, for the purpose of checking and assessment of the performance of the former one. GRCOMP is a program developed by the U.S. Defense Mapping Agency (DMA) for processing field gravity data. Although GRCOMP can use gravity observations from different gravimeters in a loop, it processes the data from each instrument separately [Stizza, 1997]. GRCOMP starts with the dial readings of the gravimeters, applies the Earth tide correction, and estimate the instrument drift correction. GRCOMP is an easy-to-use program in an interactive way with the user. On the other hand, A disadvantage of GRCOMP is that it is designed to process the data

from the global-range model G gravimeters only. An advantage of GRCOMP is the utilization of the least-squares adjustment to provide standard deviations of the station gravity values as a tool for judgment the executed gravity loops in the field.

Both programs have been used to process the same loop, that includes the new absolute gravity station in Helwan (named SRI5), the triangulation station O1, and the IGSN-71 gravity station in Helwan (Cairo-B). Seven LaCoste and Romberge relative gravimeters have been used to conduct this loop. The loop consists of 63 total observations, 9 observations per gravimeter. The results show agreement, in the point gravity value between GRCOMP and GNPA programs within 0.005 mGal, after performing the least-squares adjustment [Dawod and Alnaggar, 1997].

4- Methodology of gravity data analysis and network adjustment

This part is devoted to the data processing of the ENGSN97 network, including the highlight of the developed computer programs, needed for all involved computations, as well as performing different solutions, for investigating all effecting factors on the final results, one at a time. The efficient newly-developed processing models have been utilized. Several LF90-language computer programs have been developed to process, adjust, and analyze gravity networks in several stages as follows:

4.1 Primary analysis for each loop using one gravimeter at a time

The first program processes data of one loop conducted by one gravimeter utilizing the equation:

$$r_j = g_j - O + \Delta t_{ij} \cdot d \qquad (1)$$

where,

Δt_{ij} is the difference in time between the running station j and the initial fixed station i,

d is the drift of the used gravity meter (assuming linear function).

This is the basic equation describing the mathematical relationship between the gravimeter readings as observables, and the gravity values of the observed stations, taking the systematic drift error of the gravity meter, as well as the unknown gravity

orientation parameter (O) at the fixed station i, into considerations. Every gravimeter reading on any station in the observed gravity loop gives one equation of that form.

Note that, in the above observation equation, the only observed quantity is the gravimeter reading, r_j, whereas the unknown parameters will be three quantities, g_j , O, and d. In other words, for " n " observed gravity stations, there will be " n " observation equations, and the number of unknowns will be two plus the number of unknown gravity stations. Therefore, if "n" equals the number of unknowns, there will be one solution only for the system of observation equations. However, this is not the case in practice, where there should be as many redundant observations as possible. In such a case, one will be faced with an over-determined mathematical model, whose solution becomes possible on the basis of least-squares principle, see [Nassar, 1981].

The objective of this program is to analyze each gravimeter's observation separately to investigate the quality and the performance of each gravimeter in a loop. The data input of this developed program include:

* the gravimeter dial readings (in mGal units),
* the corresponding time of observations (in hours),
* the apriori variance factor to be used in the measurement weighting process,
* the absolute gravity value of at least one station to be held fixed in the adjustment,
* an alphabetic stations names and gravimeters numbers to be tabulated in the output.

The program output contains:

* the estimated gravity value for each gravity station along with its estimated standard deviation,
* the estimated apostoriori variance factor,
* the estimated gravimeter drift coefficient with its estimated standard deviation,
* the estimated gravity orientation parameter with its estimated standard deviation.

4.2 Analysis of each loop using different gravimeters combined together

The second developed program handles the gravity data of all gravimeters used in observing a loop. Therefore, the unknowns to be estimated are the gravity values of all stations beside a gravity orientation and a drift unknowns for each virtual gravimeter. This program has a built-in outlier detection subroutine used to flag the erroneous observations based on the results of the τ statistical test. The corresponding observation equation model is read as follows:

$$r_{jk} = g_j - O_k + \Delta t_{i,j,k} \cdot d_k \qquad (2)$$

where,

k is the gravity meter number,

r_{jk} is the reading of the k^{th} gravity meter on station j,

$\Delta t_{i,j,k}$ is the difference in time between the running station j and the initial fixed station i, using the k^{th} gravity meter,

d_k is the drift of the k^{th} gravity meter, and the remaining symbols are the same as defined before.

In this case, there will be " n" observation equations of that type, where the number of unknown parameters will be equal to the number of unknown gravity stations " j ", and twice the number of the used gravity meters "k". The data input of this developed program includes:

* the virtual gravimeter dial readings (in mGal units), i.e., a change in the gravimeter number means either an occurred drift or a new gravimeter data will be followed,
* the corresponding time of observations (in hours),
* the apriori variance factor to be used in the measurement weighting process,
* the absolute gravity value of at least one station to be held fixed in the adjustment, and
* an alphabetic stations names and virtual gravimeters numbers to be tabulated in the output.

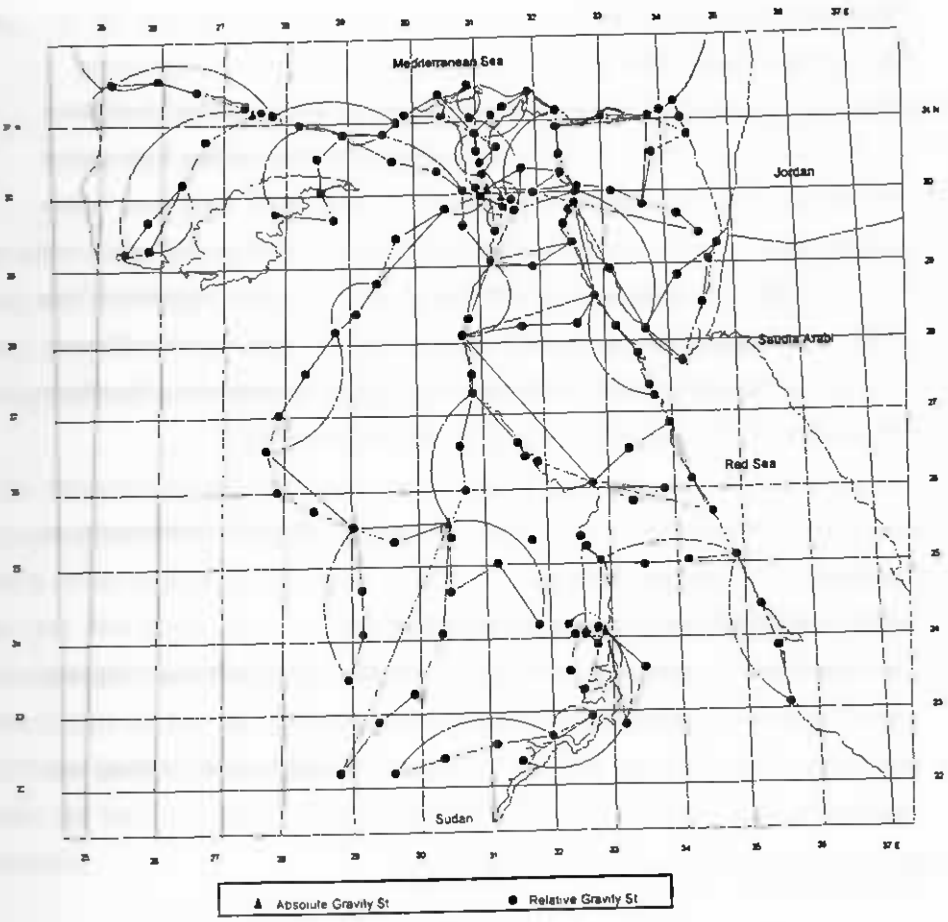

Figure 2

ENGSN97 Used Gravity Loops

The program output contains:

* the estimated gravity value for each gravity station along with its estimated standard deviation,
* the estimated apostoriori variance factor,
* the estimated drift coefficient for each virtual gravimeter with its estimated standard deviation,
* the estimated gravity orientation parameter for each virtual data series with its estimated standard deviation,
* the estimated residuals with their estimated standard deviation.
* the critical tau value corresponding to the computed degrees of freedom,

* the normalized residuals, and
* A list of the flagged outliers.

When dealing with gross-error detection, it was decided to delete only the observation that had the largest normalized residual. Most of the literature dealing with outlier detection stressed that any algorithm should not be used as a black box which automatically cleans the observations. This warning may be explained when we remember the original two assumptions behind the Tau-test for outlier detection [Chen et al, 1987]: (1) all observations are normally distributed; and more important (2) only one outlier is assumed to be present in the data set, at a time. Consequently, the whole theory breaks down if the observations include two or more gross errors.

The following rational approach is followed in order to obtain as much correct results as possible [Alnaggar and Dawod, 1995a]:

* Initial adjustment is carried out using all observations.
* If more than one normalized residual exceed the critical τ value, only the observation with the largest normalized residual is deleted.
* Adjustment is repeated again with n-1 observations leading to new residuals and new σ_0^2
* This process is repeated until all outliers are flagged.

4.3 The processing of the entire ENGSN97 gravity network

The third developed computer program, GNPA: Gravity Network Processing and Adjustment, is the main computational tool used in this research study. It processes and adjusts a gravity network that consists of several field loops observed by several gravimeters using the newly-developed model where the observation equations model will be:

$$r_{j,k,l} = g_j - O_{k,l} + Z_{j,l,k} \cdot e_{k,l} + \Delta t_{l,j,k,l} \cdot d_{k,l} \qquad (3)$$

where,

$Z_{j,k,l}$ is the original dial reading (in counter units) of this observation j in the l^{th} data series using the k^{th} gravimeter, and

$e_{k,l}$ is the unknown error in the used linear calibration coefficient for the k^{th} gravimeter, that was used in transforming the dial reading in counter units into the equivalent mGal units, as estimated from the gravimeter readings on gravity stations with known absolute values.

In addition, the symbol "l" in the equation represents either the data set number before and after each break in the same loop, or indicates the data set number for each added new observed loop. By this way, one can expect more accurate estimation for all the unknown parameters, especially the gravity values at the unknown gravity stations.

The unknowns contain the gravity values of observed stations and two unknowns (orientation and drift) for each " virtual instrument ". If a loop contains a break, its data set is further divided into two virtual data series and two unknowns have to be estimated to each data series. This situation resembles the case as if two different " virtual instruments " have been used in this loop. Regarding the gravimeter drift estimation, this implies the fact that during the break time a zero static drift is assigned and two different dynamic drift coefficients are to be estimated for the two data series. The data input and the output results of this developed program are the same as in the previous program.

5- Performed different solutions to obtain the best optimum results for the ENGSN97 network

In this section, the developed program GNPA has been run to adjust the entire ENGSN97 gravity network. Six solutions are made as follows:

5.1 First solution: Introducing one absolute gravity station as completely fixed in the adjustment of the network

The purpose of this solution is to investigate the consistency between the relative gravity measurements, taken by both G and D models of LCR gravimeters, and those absolute gravity measurements, taken at five stations only by the FG5 absolute free-fail device. In this case, one absolute gravity station only is held fixed, which is taken in our case here

as the SRI5 station at Helwan, as the nearest absolute station to the center of gravity of the entire ENGSN97 network. In other words, the remaining four absolute stations will be retained aside, as if they were not absolutely measured at all. Following the same computational approach, of assigning very large weights for absolute station to be held fixed, the corresponding diagonal element of the normal-equation matrix pertaining to SRI5, will be assigned a very large value. In this case, an estimate of the gravity value at each of the four absolute stations will be obtained after the least-squares adjustment process, which gives one a chance to be compared against the already-known absolute value at the same station. The analysis of the difference between the two sets of gravity values, for those four absolute stations, will indicate a good idea about the consistency between the relative and absolute gravity measurements performed in our network here. Of course, such an adjustment follows the ordinary known minimal-constrained approach of the least-squares adjustment.

The differences between the known absolute gravity values, and the corresponding estimated values from the above adjustment, for the four absolute stations mentioned above are computed. Recall that, the assigned precision, in terms of standard deviations, for all relative gravity measurements were taken as 0.030 mGal. The above mentioned differences are almost in the same order of the precision of the relative gravity measurements, which indicates the existing consistency between both types of gravity measurements, namely the absolute and relative measurements.

5.2 Second solution: Introducing appropriate weights for the absolute gravity stations

Following the same approach of treating the absolute gravity stations, as quasi-observables or weighted parameters, with their appropriate estimated standard deviations, as obtained from the absolute measurement technique, the residual equation for each one of the five absolute stations will be:

$$V_i(abs) = g_i\,(\text{to be estimated}) - g_i(\text{ absolute}), \qquad i = 1,2,3,4, \text{ and } 5$$

This means that each value of the absolute gravity station will receive a certain correction or residual $V_i(abs)$, after the adjustment. Of course, all those five pseudo-

observations or residual equations, will be added to the ordinary system of observation equations for relative gravity measurements, while the whole system is combined together and will be solved simultaneously

The differences between those estimated values, from the combined adjustment, and the corresponding known absolute values, as obtained from direct absolute measurements are computed. The differences between the estimated gravity values and the known absolute values are almost zero value. This means that, the treatment of the absolute gravity stations as quasi-observables, gives almost the same results as if they were treated as fixed quantities.

5.3 Third solution: Investigating non-linear drift against linear drift functions

In this solution, the validity of taking the drift function of the used relative gravimeters as non-linear instead of the usual linear function, will be investigated, whether it could improves the quality of the network or not. A non-linear drift model has been tried for all loops. Therefore, the term on the right-hand side of the gravimeter reading observation equation, say in the general model given by equation (3), becomes ($d_1 \Delta t + d_2 \Delta t^2$) in which two unknown coefficients d_1 and d_2 are needed to be estimated, instead of only one coefficient in case of linear drift function.

The entire ENGSN97 network was adjusted, again, using the second solution above, after introducing the non-linear drift function. After the least-squares adjustment, an estimated value for the second drift coefficient d_2 was obtained, along with its estimated standard deviation, as one new unknown parameter. In addition, the estimated value for gravity station and their covariance matrix, are obtained as the main output results. The obtained results show the following three remarks:

- The value of the second term $d_2 \Delta t^2$, of the non-linear drift function contribution, is relatively very small compared to the first part $d_1 \Delta t$, which in most of the cases does not exceed the 5% level.

* The estimated standard deviation for the drift coefficient d_2 exceed, in most of the cases, the value of the coefficient itself, which means that the drift coefficient d_2 is statistically insignificant, that is it can not be distinguish from the zero value, from the statistical point of view.
* The adjusted point gravity values of the network attain relatively large values for their standard deviations, at a number of stations, when compared to the corresponding good estimate obtained from the second solution above.

Based on the above obtained results and remarks, it can be concluded that the second part of the non-linear drift function is statistically insignificant, and should be neglected, particularly since it deteriorates the overall quality of the entire gravity network by about 18% in our network here. In other words, the linear drift function for LCR gravimeters will be the best to be used instead of any suggested non-linear functions.

5.4 Forth solution: Introducing different weights for different gravimeters

Several gravity surveys show that the precision of the D model of LCR gravimeters is better than that of the G model gravimeters [Torge, 1989a]. In the previous solutions, all relative observations were assigned a standard deviation of 0.03 mGal, that is equal weights for both G and D LCR gravimeter models. In the present solution, the entire ENGSN97 network was adjusted, again, using a better precision (standard deviation of 0.02 mGal) for the observations carried out by the D model of the relative gravimeters. This data series contains 248 observations in 37 virtual loops. The rest of the observations were assigned a standard deviation of 0.03 mGal, for the G model gravimeters.

The obtained results, in terms of the estimated standard deviations of the point gravity values of the entire ENGSN97 network stations, indicated that there is a slight improvement in the precision (in the order of approximately 13%), as compared to those obtained from the second solution above, when equal weights were used. This may be due the fact that the number of the observations of the D-model gravimeters is slightly

small compared with the total observations (23% approximately). Such slight improvement has occurred especially for the stations observed by the d model gravimeters in addition to the original G gravimeters.

5.5 Fifth solution: Introducing different weights for loops according to their observation times

Although a gravity loop must not exceed seventy two hours as observation time, it is the author's experience from the field campaigns that the longer the time span of a loop, the more problems encountered in the field regarding the observation circumstances. Tare (unexpected jump) is an example of these sudden problems that are quite difficult to be modeled. In order to avoid these uncertainties, a worse precision (standard deviation of 0.050 mGal) was assigned to all observations taking along the loops, which their observation have been continued for more than one-day. These observations are found to be 228 in 12 virtual loops. The remaining observations of the rest of the loops, observed over a time span less than one day, were assigned the pre-specified standard deviation of 0.030 mGal, which amounted to 857 observations over 39 virtual loops.

The obtained results of the estimated gravity values, indicated that there is slight improvements in their precision compared to the corresponding values from the standard adjustment of the second solution, in the order of approximately 18%.

5.6 Sixth solution: After satisfying all significant-affecting criteria

Based on the obtained results from the above discussed five solutions, it can be concluded that the best appropriate way of adjusting the entire ENGSN97 gravity network, will be performed with the following items taken into consideration:

- The five absolute gravity stations should not be treated as purely fixed, but taken as quasi-observables with appropriate large weights.
- Each used gravimeter should be assigned different weight for all observations taken by it, depending upon the reported precision of the manufacturer and by previous

investigators, where a linear drift function should be used for all LCR gravimeter models.

* For all loops observed over span times exceeding the one-day limit, should be assigned less weights for their encountered observations, as opposed to those loops completed in a period less than one day.

After satisfying all the significantly influence factors, another adjustment of the network has been performed, which is named as solution number six. However, such adjustment included all the 1085 gravimeter readings taken over the 51 virtual loops, as collected by using five actual G-model gravimeters and two D-model gravimeters of the LCR type. Of course, one should assume a hypothesis of possible outlier observations, existing for some of those collected gravimeter readings. In order to have meaningful-final results, based on good-quality observations, all such erroneous readings must be filtered out from the system, and a best solution is obtained using all the remaining cleaned observations, as will be given in the next sub-section.

5.7 Final solution: After filtering out all outlier observations

Filtering out the observations from existing outliers can be simply performed, using the appropriate tau test for detecting outliers, which is based on testing the normalized residuals against a critical tau value, instead of testing the pure residuals themselves.

Each estimated residual V_i of a gravimeter reading r_i, should be normalized first by dividing its value by its corresponding standard deviation. The critical value of the tau statistic is then computed, based on the degree of freedom and the probability level using the student t-distribution function. If the normalized residual T_i exceeds the computed critical limit, the corresponding observation is suspected to contain some sort of gross errors, and hence, should be rejected from the system. The least-squares adjustment is repeated again using the remaining observations, after rejecting the outliers, and a new set of estimated residuals can be obtained, and the tau test is performed again, and repeating the process until all measurements are cleaned out.

For the ENGSN97 gravity network, in our hands here, eight consecutive solutions were repeated, for the purpose of detecting and rejecting outliers, until no more outliers are flagged. A total of 44 observations out of the original 1085 observations have been flagged and removed. These observations constitute only about 4 % of the total number of the measurements, which is another indication of the goodness of the ENGSN97 network. The solution of adjusting the network, as performed free from all the rejected 44 outliers, represents the final best-optimized solution for our ENGSN97 network.

Comparing the estimated standard deviations of the final solution, with the corresponding values as obtained from the sixth solution, one can notice significant improvement in the overall precision of the finally adjusted network. In other words, the removal of all existing outliers from the set of gravimeter readings, will certainly improve the overall quality of the final solution of the network. Such improvement amounts to approximately 37%.

6- Essential characteristics of the final solution of the ENGSN97 network

The most essential information of the final adopted solution of the ENGSN97 network are summarized in Table (1).

It may be interesting to investigate the distribution of the residuals, of the 1045 cleaned gravimeter readings, as estimated from the final solution of the network, which are depicted in Figure 3. The general trend of such a distribution, approximately follows the ordinary Gussian normal distribution curve. This indicates that the remaining residuals of the cleaned gravimeter readings, are representing random errors only, with their mean value approaching the statistical mean value of zero. In other words, such cleaned used gravimeter readings are not affected by any sort of systematic errors or biases, associated with the used instruments, and used observational techniques and computations.

It is worth to mention here that, after finishing the data processing and the final adjustment solution of the ENGSN97 network, the obtained results are checked out at the Technical University in Graz (TU-Graz). Austria. The data of ENGSN97 have been re-processed and re-adjusted again on the university mainframe computer using the classified computer programs available in the physical geodesy department of TU-Graz.

The results show an agreement in the order of few microGals between the final solution and that solution of TU-Graz [Sünkel, 1998]. It means that, this check proves that all processing and adjustment stages carried out, for ENGSN97 are of high quality and reliability and emphasis that ENGSN97 has a high-level of precision as a gravity datum for Egypt. This has been supported by the performed re-adjustment of the network at TU-Graz, using different independent computer packages.

Table 1

Essential Information For The Final Adjustment Of The ENGSN97 Network

Number of stations	150
Number of observations	1045
Number of loops	51
Minimum station separation	0.136 Km
Maximum station separation	128.144 Km
Average station separation	65.988 Km
Number of actual gravimeters	7
Number of virtual gravimeters	133
Number of unknowns	408
Number of degrees of freedom	637
Minimum standard deviation of gravity values	0.002 mGal
Maximum standard deviation of gravity values	0.048 mGal
Minimum adjusted gravity value	978679.776 mGal
Maximum adjusted gravity value	979405.981 mGal
Gravity range over Egypt	825.205 mGal

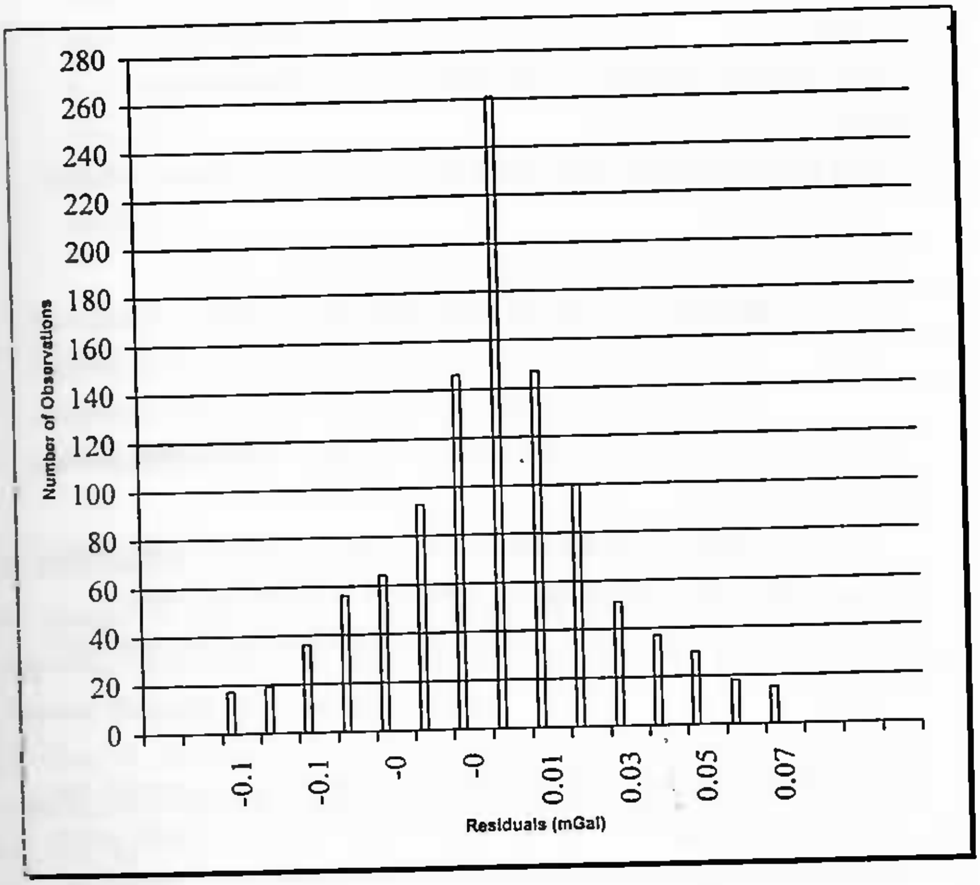

Figure 3
Frequency Distribution of the Residuals of the Gravimeter Readings Over the ENGSN97 Network

7- Conclusions

Based on the above-mentioned processing and adjustment trials in this study, The final solution of the ENGSN97 has been processed according to the following processing specifications:

- Using weighted parameter approach in least-squares adjustment for the five absolute gravity stations,
- Using 0.02 mGal standard deviation for the D-gravimeter relative gravity observations,

- Using 0.03 mGal standard deviation for the G-gravimeter relative gravity observations,
-Using standard deviation of 0.05 mGal for long gravity loops completed over one day period,
- Using standard deviation of 0.03 mGal for loops completed within a period of less than one day,
- Using linear-drift model for LCR relative gravimeters, and
-Applying outlier detection routine for cleaning the data from gross errors.

The obtained results from the final solution and adjustment of ENGSN97 gravity network indicated that:

- the gravity field over the Egyptian territory, expressed in terms of the gravity acceleration value g ranges between 978679.776 and 979405.981 mGal
- the Standard Deviation of the gravity values ranges between 0.002 and 0.048 mGal

Consequently it can be concluded that the present Egyptian gravity network can be categorized as first order gravity network, with about 150 gravity points evenly distributed across the Egyptian territory. Such present gravity network can be considered to be more reliable, more gravity stations, and strengthened with addition precise positional information, namely horizontal position in terms of Latitude and Longitude, as well as orthometric height, as compared to the previous national gravity network (NGSBN-77)

In the context of establishing and adjusting the new National Gravity Standardization Net (ENGSN-97), the following information can be considered as great achievement and wealth information that can be added to the Egyptian geodetic data bank, which includes:

- Five absolute gravity stations

- 145 relative gravity stations with almost the same accuracy of the absolute ones, and they are well distributed in the country
- at all 150 stations, the geodetic coordinates are determined precisely using GPS
- at all 150 stations, the orthometric heights are determined using precise levelling

Such geodetic data will be essentially needed for future updating of the Egyptian geoid, which will be in turn used for related geodetic network computation and adjustment, as well as associated mapping and other geodetic applications.

8- References

1) Alnaggar, D., and Dawod, G., 1995, **Increasing the reliability of GPS geodetic networks**, Proceedings of the First International Conference on Satellite Positioning Systems, December 12-13, Alexandria, Egypt.

2) Chen, Y., Kavouras, M., Chrzanowski, A., 1987, **A strategy for detection of outlying observations in measurements of high precision**, The Canadian Surveyor, V. 41, N. 4, pp. 529-540.

3) Cole, J., 1944, **Geodesy in Egypt**, Government Press, Cairo, Egypt.

4) Dawod, G. and Alnaggar, D., 1997, **Performance of relative gravimeters and processing software over the new absolute gravity stations in Egypt**, Proceedings of Al-Azhar Fifth International Engineering Conference, December 19-22, Volume 5, pp. 113-125, Cairo, Egypt.

5) Groten, E., and Tealeb, A., 1995, **The first part of repeated relative gravimetry in the active zone of Aswan lake, Egypt**, Bulletin of National Research Institute of Astronomy and Geophysics, Volume XI, pp. 255-264.

6) Kamel, H., and Nakhla, A., 1985, **Gravity map of Egypt**, The Egyptian Academy of Scientific Research and Technology, Cairo, Egypt.

7) LaCoste and Romberge, 1989a, **GRAVAC, GMODEL, TERRAIN: MS-DOS programs for the reduction and interpolation of gravity survey data**, LaCoste and Romberge Gravity Meters, Inc., Texas, USA.

8) LaCoste and Romberge, 1989b, **Instruction manual for model G & D gravity meter**, LaCoste and Romberge Gravity Meters. Inc., Texas, USA.

9) Morelli, C. et al., 1974, **The International Gravity Standardization Net 1971 (IGSN71)**, IUGG - IAG, Publication Special No. 4, Paris, France.

11) Sünkel, H. (**Technical University Graz, Austria**), 1998, Personal Communications.

12) Stizza, D., (U.S. Defense Mapping Agency), 1997, Personal communications.

13) Torge, W., 1989, **Gravimetry**, Walter de Gruyter, New York.

14)Nassar, M. M., 1981, **Matrix treatment of adjustment computations in surveying**, Lecture Notes No. 4, Department of Public Works, Faculty of Engineering, Ain Shams University, Cairo, Egypt.

15)Nassar, M. M., 1977, **Gravity field and leveled heights in Canada**, Department of Surveying Engineering, University of New Brunswick, U.N.B. Report No. 41, N.B., Canada.

16)Nassar, M. M., 1976, **The Earth gravity field**, Lecture notes, In the course of Physical Geodesy laboratory assignments, given at the Department of Surveying Engineering, University of New Brunswick, N.B., Canada.

Proceedings of the Eleventh International Conference on Environmental Protection, Alexandria University, Alexandria, May 8-10, 2001, pp. 207-215.

THE MAGNITUDE AND SIGNIFICANCE OF LONG-TERM SEA LEVEL RISE IN EGYPT FROM A GEODETIC PERSPECTIVE

By

Dr. Gomaa M. Dawod*

ABSTRACT

On a global scale, the sea level exhibits a relatively rapid rise from 20,000 years ago until present levels were reached some 4,000 years ago. Since that time, the changes have consisted of oscillations of small amplitude. From a geodetic point of view, the significance of sea level is based on the reality that the Mean Sea Level (MSL) is conventionally taken as the vertical datum of the precise levelling (heights) network.

This research study aims to evaluate the variations occurred in MSL over the twentieth century. Long-term tide observations have been collected for two tide gauges at Alexandria, and one tide gauge at Port Said. The obtained results show that the MSL at Alexandria varies from 1.6 cm to 23.5 cm above the current national vertical geodetic datum, with a mean value of 11.1 cm. At Port Said, MSL changes between –1.7 cm to 24.0 cm, with an average of 9.0 cm. Furthermore, it has been concluded that the sea level is rising by a rate of 1.7 mm/year at Alexandria, and 2.4 mm/year at Port Said, which indicates the existence of sea level slop as well.

The sea level rise is one of the main factors that cause shoreline retreat, coastal erosion, lowlands overflow, and increase the salinity of lakes and aquifers. Consequently, there exists a critical demand to explore, on geodetic and environmental basis, the consequences of sea level changes in Egypt. Moreover, an accurate multi-purpose monitoring system has to be established, over the Egyptian shores, to measure precisely the sea level rise.

* Researcher, Survey Research Institute, National Water Research Center.
308 Al-Ahram Street, Talbia, Giza 12111, Egypt.
E-mail: dawod_gomaa@yahoo.com

1. Introduction

Mean Sea Level (MSL) is the average level of the sea, usually based on hourly values taken over a period of at least a year. Long-term changes of measured sea level are called secular changes, where the global changes are called eustatic changes. The combination of sea level changes measured by several techniques shows a relatively rapid rise of sea level from 20,000 years ago, gradually slowing down 8,000 years ago when levels were some 15 meters below those of today. The increase then proceeded more gradually until present levels were reached some 4,000 years ago [8]. Since that time, the changes have consisted of oscillations of small amplitude. The major effective causes for long-periodic sea level oscillations are [11]:

- Changes due to atmospheric pressure that may, under special conditions, reach up to several decimeters.
- Changes due to wind stress, that are much smaller over long periods, but could reach a few decimeters in some places.
- Thermohaline (thermal and solution) structure of sea water is among the most important causes of long periodic changes in sea level. However, it is generally stable with superimposed seasonal variations of thermal origin in the uppermost layers.
- The time variations of sea current are little known and could be treated among the higher-order factors that could not be modeled.
- River discharge fluctuations can contribute significantly to long-term variations depending on location.
- Glacial melt and the yield of the earth to the melt load are the main constitutes of the secular water rise. Some estimates of this effect vary between 6 and 10 cm per century.
- The magnitude of long-periodic tidal contstituents is so small as to be of little practical consequence. There are two cycles of lunar motion, namely the lunar perigee every 8.85 years and the lunar node every 18.6 years. It was originally thought that it is necessary to have at least 18.6 years of sea level data available to eliminate the influence of the nodal cycle. Recently, it appears that this assumption is no longer justified since recent investigations show that both lunar cycles produce variations of the order of 1 cm only.
- Vertical crustal movements of a local and regional nature affect the tide gauge readings. Their effect should be eliminated if at all possible.

Recent long-period sea level measurements at several stations show that there is a general increase of MSL of about 0.10-0.20 meter per century [8]. However, there are considerable variations from this average value. Table 1 presents estimates of sea level rise at some tide gauges with long records of measured data. The annual rates of sea level rise vary from –2.5 mm/year to 3.8 mm/year [4]. Moreover, analysis of MSL data for several stations in the United States has revealed MSL rise ranging from –2.4 mm/year to 7.9 mm/year in the period from 1930 to 1993 [7].

Table 1
Estimates of Sea Level Change at Some Global Sites

Site		Data Span	MSL Rate (mm/year)
Alaska	(57^o 03’ N)	1939 – 1979	-2.5
Newlyn	(50^o 06’ N)	1916 – 1980	1.7
Brest	(48^o 23’ N)	1807 – 1981	0.9
Halifax	(44^o 40’ N)	1897 – 1980	3.7
San Francisco	(37^o 48’ N)	1854 – 1979	3.8
Honolulu	(21^o 19’ N)	1905 – 1980	1.6
Bombay	(18^o 55’ N)	1878 – 1978	1.0
Sydney	(33^o 51’ S)	1897 – 1981	0.7
CBBT	(37^o 00’ N)	1930 – 1993	6.7
Cambridge	(38^o 34’ N)	1930 – 1993	7.9

2. Sea Level Rise in Egypt

The vertical datum of the precise levelling network Egypt has been set as the Mean Sea Level (MSL) at Alexandria harbor. It was taken as the mean between the daily readings of high and low water level during the years 1898 to 1906. These were the only available recorded observations when the survey department undertook the levelling in 1906 [3]. It has been found that this imaginary surface is 33.8 cm above the zero of the installed tide gauge.

In the late sixty, an investigation has been carried out to study the variation of MSL at Alexandria in relation to the meteorological elements, namely wind speed and pressure. That study used real data of monthly average water level from 1962 to 1966. From these results, it can be concluded that the new MSL, as calculated from this five-year data set, is 45.0 cm above the gauge zero. Consequently, an increase of 11.2 cm was detected in the definition of the vertical datum of Egypt [10]. A recent study has utilized hourly-recorded data of water level from 1995 to 1998 for the tide station installed in the Western (military) Harbor of Alexandria [9]. The obtained results show that the new MSL, as calculated from this four-year data set, is 51.5 cm above the Egyptian defined zero value. Hence, an increase of 17.7 cm was detected in the definition of the vertical datum of Egypt.

3. Sea Level Slop in Egypt

Many investigations have revealed that in addition to the MSL rise, there is slop in the sea level. For example, In the western coast of the United States, an apparent northward slope of 26 cm was reported [12]. Similar studies in the United Kingdom, based on an analysis of monthly MSL between 1960 and 1975, show that there exist a latitudinal slope of MSL of 5.3 ± 0.4 cm per degree of latitude [2].

In Egypt, the Suez Canal Company (SCC) had established two Mareographs at both Port Said and Suez in 1925. The recorded observations in the period 1923-1937 concluded that the MSL of the Mediterranean Sea at Port Said is 3.9 cm below the MSL at Alexandria, and the MSL of the Red Sea at Suez is 22.2 cm above the MSL of the Mediterranean Sea at Port Said [3]. Nassar et al [6] has concluded that the MSL at Port Said is 5.4 cm below that at Alexandria.

Alam El-Din [1] has analyzed daily records of MSL data at Port Said and Suez in the period 1980-1986. He has found that the rate of increase of the Mediterranean MSL at Port Said is 2.78 mm/year, while it is 0.61 mm/year for the Red Sea at Suez. Hence, the MSL of the Red Sea is 11.9 higher than that of the Mediterranean. Also, he has concluded based on results of several investigations that this difference decreases with time.

4. Available Data

Tide observations, from different sources, have been collected for two tide gauges at Alexandria, and one tide gauge at Port Said. The available measurements span from 1944 to 1999 for Alexandria, and from 1926 to 1987 for Port Said. The first step was to reference all data sets to a common datum. The MSL defined in 1906 as the national Egyptian vertical datum has been used to unify all measurements. Monthly averages of measured tide are applied in the analysis herein. These average values have been computed from hourly tide observations, and then utilized to compute annual MSL for the specific time periods.

5. Results and Analysis

The obtained data sets are utilized to investigate the characteristics of the MSL of the Mediterranean in terms of behaving patterns, magnitude of rising, and the rate of its change in the last century. Environmental and geodetic impacts of MSL rise are discussed in view of the obtained results.

5.1 Pattern of the Seasonal Mediterranean Sea Level

The average monthly tide measurements depict the seasonal variations of the sea level. The data of the last five years, from 1994 to 1999, have been averaged for Alexandria and presented in Table 2, and depicted in Figure 1. From these figure and table, it is obviously seen that the tide has small variation and is semi-diurnal in nature. The tide range over these five years varies from 18.6 cm to 22.9 cm, with a mean of 20.5 cm. Figure 1 shows that the maximum tide value occurs in August, while the minimum exists in April. Also, it can be noticed that the sea level in the winter (February to April) is lower compared with its values in the summer (July to September). This may be due to the differences in the barometric pressure and temperature between the summer and winter seasons.

5.2 Long-Term Rise of Mediterranean Sea Level

The annual averages of sea level at Alexandria and Port Said have been analyzed using the available data sets. The results are summarized in Table 3. The annual change of sea level at Alexandria varies from –11.7 cm to 11.5 cm, while it ranges from –7 cm to 12 cm at Port Said. Considering the zero-value for MSL defined in 1906 as a datum, it has been found that the MSL at Alexandria varies from 1.6 cm (in 1947) to 23.5 cm (in 1987) above that datum, with a mean value of 11.1 cm. At Port Said, MSL changes between –1.7 cm (in 1929) to 24.0 cm (in 1980), with an average of 9.0 cm. Figures 2 and 3 depict the MSL annual changes for Alexandria and Port Said respectively, while figures 4 and 5 present the MSL values, above the selected datum, for both tide gauges.

Table 2
Average Monthly Sea Level at Alexandria (1995-1999)

Month	Ave. Sea Level (cm)
January	49.9
February	43.7
March	43.4
April	41.8
May	45.6
June	50.8
July	57.1
August	59.6
September	55.3
October	55.8
November	55.6
December	55.2

Regression analysis has been performed to compute the rising rates of sea level at Alexandria and Port Said over the last decades. The least-squares estimation technique has been utilized to solve the linear over-determined equations since there exist degrees of freedom. The obtained results are:

For Alexandria:

$$H = 6.09 + 0.1718 * YN_1 \quad (1)$$

For Port Said:

$$H = 2.29 + 0.2390 * YN_2 \quad (2)$$

where,

H is the height of the sea level, in cm, above the chosen datum.
YN_1 = Year – 1943, i.e., the number of years from the start of the data series at Alexandria.
YN_2 = Year – 1925, i.e., the number of years from the start of the data series at Port Said.

Table 3
Long-Term MSL Rise

	Alexandria	Port Said
Data Span	1944-1999	1926-1987
Minimum Annual Change	-11.7	-7.0
Maximum Annual Change	11.5	12.0
Minimum MSL Value	1.6	-1.7
Maximum MSL Value	23.5	24.0
Average MSL Value	11.1	9.0

Based on these findings, it can be concluded that the Mediterranean sea level is rising by a rate of 1.7 mm/year at Alexandria, and 2.4 mm/year at Port Said. These estimates are close to results of similar previous studies [e.g. 1 and 5]. However, it worth mentioning that the data utilized in the present study cover longer time span, and hence could be considered more reliable for long-term MSL rise determination.

6. Conclusions

On a global scale, recent long-period sea level measurements at several stations show that there is a general increase of MSL of about 0.10-0.20 meter per century. Data of tide gauges have been utilized, in this research, to study the behavior of the Mediterranean Sea rise. The utilized data sets span the period 1944-1999 for Alexandria, and the period 1926-1987 for Port Said. It has been found that the annual change of sea level at Alexandria varies from –11.7 cm to 11.5 cm, while it ranges from –7 cm to 12 cm at Port Said. Considering the zero-value for MSL defined in 1906 as a datum, it has been concluded that the MSL at Alexandria varies from 1.6 cm to 23.5 cm above that datum, with a mean value of 11.1 cm. At Port Said, MSL changes between –1.7 cm to 24.0 cm, with an average of 9.0 cm. Furthermore, the obtained results prove that the sea level is rising by a rate of 1.7 mm/year at Alexandria, and 2.4 mm/year at Port Said.

The sea level rise is one of the main factors that cause shoreline retreat. Additionally, the sea level rise, combined with other factors, could accelerate coastal erosion, overflow lowlands, and increase the salinity of lakes and aquifers. Consequently, sea level behavior should be taken into consideration in the development planning for the coastal areas in Egypt. From a geodetic point of view, the concept of time-varying geoid definition should be studied in details and its consequent results on vertical datum, levelling networks, and mapping activities should be considered. Moreover, an accurate multi-purpose monitoring system has to be established, over the Egyptian shores, to measure precisely the sea level rise.

References

[1] Alam El-Din, K., 1993, *Sea level fluctuations along the Suez Canal*, MSC Thesis, Faculty of Science, Alexandria University, Egypt.

[2] Ashkenazi, V., Basker, G., Davison, M., Dodson, A., Hipkin, R., Stewart, M., and Baker, T., 1990, *The determination of mean sea level by GPS*, Proceedings of the IAG symposium on Determination of the geoid: Present and future, Italy, June 11-13, pp. 139-147.

[3] Cole, J., 1939, *Revision of first order levelling lower Egypt*, Survey Department Paper No. 44, Egyptian Survey Authority, Giza, Egypt.

[4] Intergovernmental Oceanographic Commission (IOC), 1985, *Manual on sea level measurements and interpretation*, Volume I: Basic procedures, IOC, Merseyside, U.K.

[5] Frihy, O., 1992, *Sea level rise and shoreline retreat of the Nile Delta promontories, Egypt*, Natural Hazards, No. 5, pp. 65-81.

[6] Nassar, M., Baraka, M., and El-Shazly, A., 1998, *Modeling local sea surface topography in Egypt based on zero frequency response analysis*, Scientific Bulletin of Faculty of Engineering, Ain Shams University, V. 33, No. 1.

[7] Nerem, R., vanDam, T., and Schenewerk, M., 1997, *A GPS network for monitoring sea level in the Chesapeake Bay: BAYONET*, Proceedings of the IGS-PSMSL workshop on: Methods for monitoring sea level, March 17-18, Pasadena, USA, pp. 107-115.

[8] Permanent Service of Mean Sea Level (PSMSL), 1989, *Data holdings of the Permanent Service for Mean Sea Level*, Bidston Observatory, United Kingdom.

[9] Shalaby, M., 2000, *Waves and surge forecasting along the Egyptian coast of the Mediterranean sea*, MSC Thesis, Arab Academy of Science and Technology and Maritime Transport, Alexandria, Egypt.

[10] Sharaf El-Din, S., and Rifat, E., 1968, *Variation of sea level at Alexandria*, The International Hydrographic Review, V. XLV, No. 2, July.

[11] Vanicek, P., and Krakiwsky, E., 1986, *Geodesy The Concepts*, Elsevier Science Publishers, The Netherlands.

[12] Zilkoski, D., and Kumar, M., 1988, *Geodetic leveling and sea slope along the southern California coast: An update*, Marine Geodesy, V. 12, pp. 315-325.

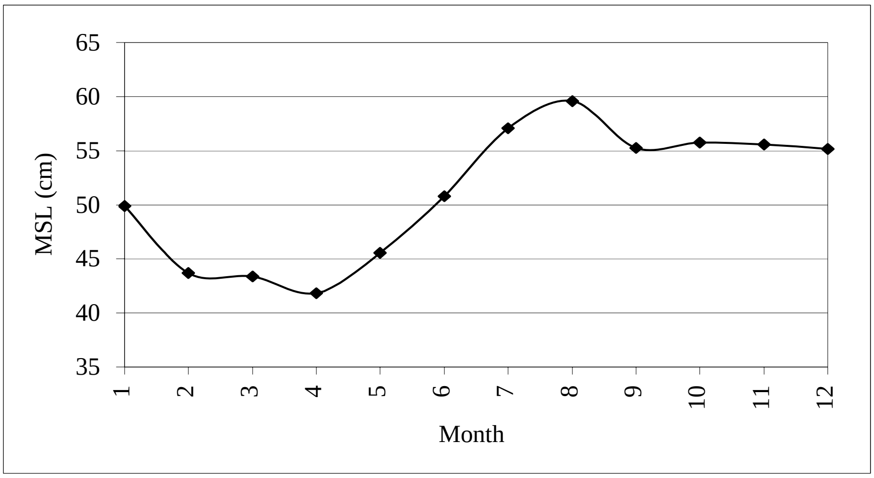

Figure 1: Seasonal Variations of Sea Level at Alexandria (1995-1999)

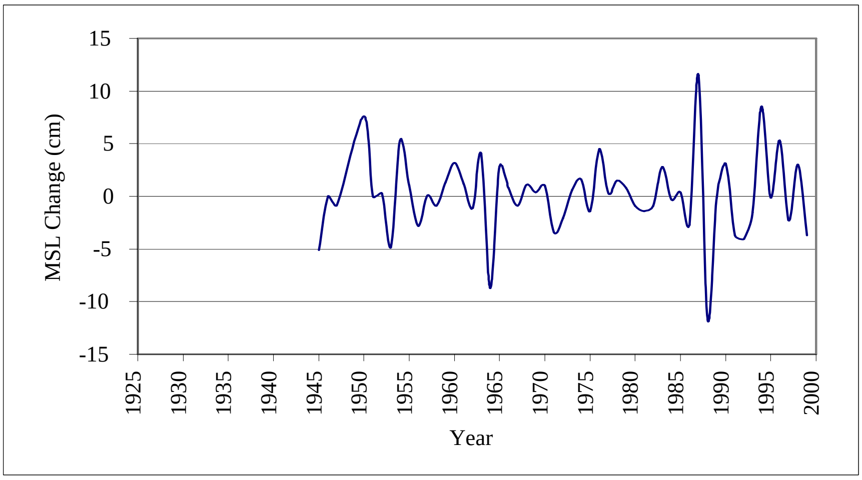

Figure 2: Annual Variations of Sea Level at Alexandria

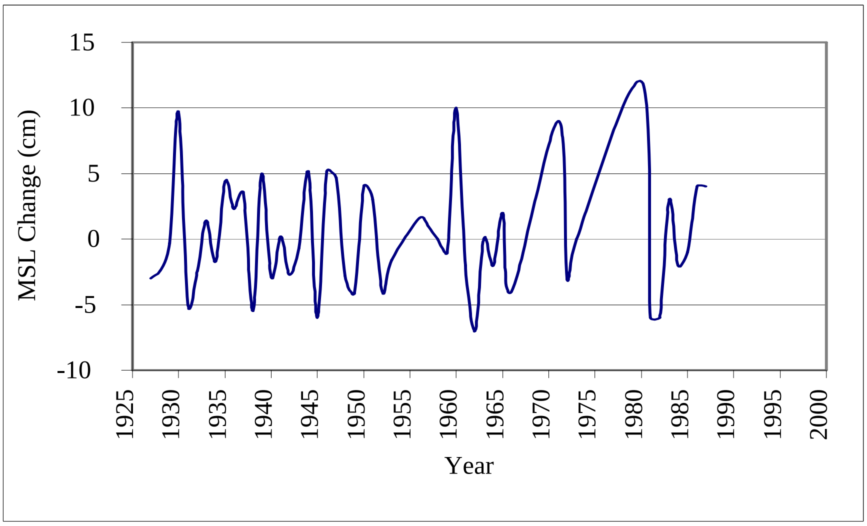

Figure 3: Annual Variations of Sea Level at Port Said

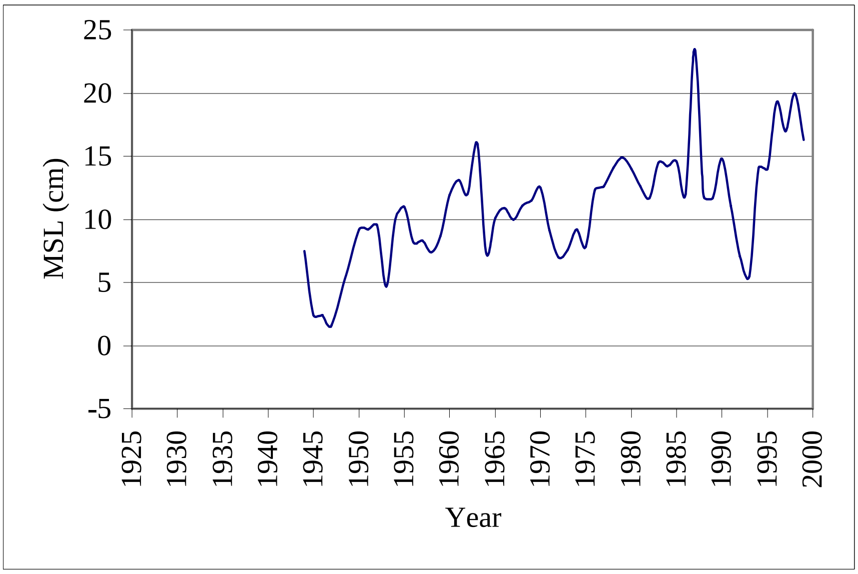

Figure 4: Long-Term Changes of MSL Values at Alexandria
(Relative to the 1906 national datum)

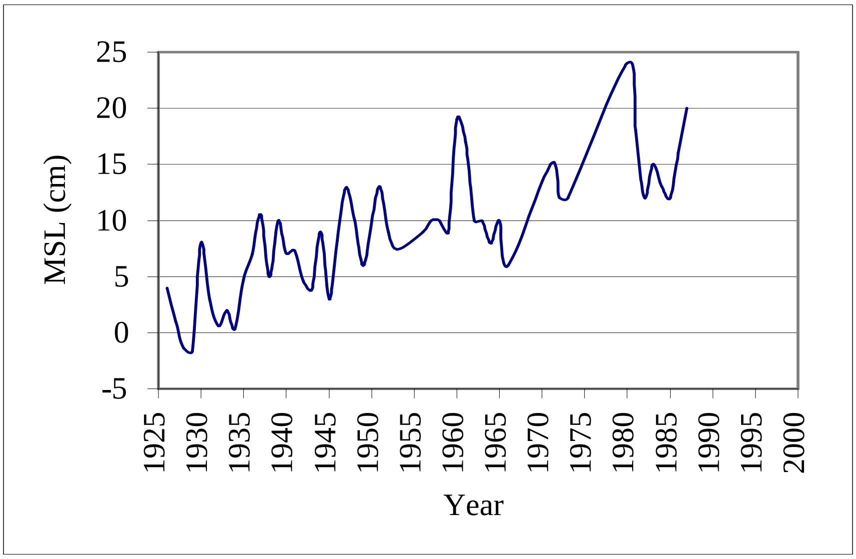

Figure 5: Long-Term Changes of MSL Values at Port Said
(Relative to the 1906 national datum)

Proceedings of Al-Azhar Engineering Sixth International Conference, Sept. 1-4, 2000, Cairo, Egypt, Volume 4, pp. 709-718.

OPTIMUM GEODETIC DATUM TRANSFORMATION TECHNIQUES FOR GPS SURVEYS IN EGYPT

By

Dr. Gomaa M. Dawod
Researcher, Survey Research Institute

Prof. Dalal S. Alnaggar
Director, Survey Research Institute

ABSTRACT

The issue of datum transformation of GPS output coordinates from the global geocentric WGS84 datum to the local national Egyptian non-geocentric coordinate system is a crucial dilemma in Egypt. Although the traditional similarity datum transformation models have been used for several decades, recent research studies show that this approach may not be the optimum technique to describe the mathematical relationship between geodetic datums.

In this paper, the available recent and accurate geodetic databases in Egypt are used to investigate the accuracy of traditional and unconventional approaches of datum transformations. Moreover, the famous models of the traditional similarity datum transformation technique have been examined in several scenarios with different number of unknown parameters. New regression formulas have been developed to transform the GPS coordinates from the global datum to the local one. The obtained results show that the overall accuracy of the traditional transformation technique is in the order of approximately 3 meters, while it is almost 0.5 m for the developed regression approach.

KEYWORDS
Geodetic Datums, GPS; Transformation Techniques

INTRODUCTION

Geodetic datum transformation is the determination of a mathematical relationship to be used in transforming a set of coordinates from one geodetic datum to another. In transforming coordinates from one datum to another, two items should be taken into consideration. The first item is the location of the geometric centers of each reference ellipsoid with respect to the center of gravity of the earth, or with respect to each other. The second point to be concerned is the differences is size and shape between the two ellipsoid.

There are several practical reasons necessitate the geodetic datum transformation. The most recent practical application of the geodetic datum transformation has been raised with the advent of satellite positioning techniques in the fifties. With the rapid growth of utilizing these space systems all over the world, the datum transformation determination has become a

major practice in order to transform the coordinates from the global geodetic datum to several local datums for different countries [e.g. Moore and Smith 1998; Reit 1998]. In Egypt, the Global Positioning System (GPS) technique has been used since 1985 in establishing more precise geodetic control networks and for other surveying and mapping applications. Hence, the establishment of a precise mathematical relationship between the GPS-based global geodetic datum, known as the World Geodetic System (WGS84), and the Old Egyptian Datum (OED) becomes a crucial task for the Egyptian geodetic community. This problem has been investigated by several researchers [e.g. Alnaggar 1990; Rashwan 1993; Abd-Elmotaal and El-Tokhy 1997; and Finnmap 1988]. However, the data sets used did not posses a national coverage of the country and their satellite-coordinates were not of a high quality, especially the GPS data of the Finnmap project [Saad 1998, Dawod 1998]. More accurate GPS data are utilized in this research study to define several models of transformation between the WGS84 and OED geodetic datums.

DATUM TRANSFORMATION TECHNIQUES

Traditionally, the similarity datum transformation models have been introduced and utilized in geodetic applications since the sixties. This type of datum transformation has gained a great focus since it has a geometrical interpretation of the determined parameters. However, other mathematical models could be used to describe the relationship between different geodetic datums in a simpler manner that is easier in practice.

Traditional Similarity Transformation Models

A similarity transformation model is based on 7 parameters: three translation parameters (dx, dy, and dz), three rotation parameters (ω_x, ω_y, and ω_z); and a parameter (s) for the scale difference between the two coordinate systems. There are many similarity transformation models. Bursa-Wolf transformation model was introduced by Bursa and Wolf in 1963. Molodensky-Badekas model was introduced in 1962 by Molodensky and the more common interpretation of the model's differential transformation equations was given by Badekas in 1969. Hence, the model is commonly refereed as Molodensky-Badekas. Although these two models are the most famous transformation models used in geodetic applications, there are several other developed similarity transformation models. Veis proposed his transformation model in 1960. Vanicek and Wells developed another transformation model in 1974. Details concerning these models are found in various literatures [e.g. Rapp 1989; Nassar 1984; Lieck and van Gelder 1975].

Unconventional Transformation Techniques

The traditional similarity datum transformation models assume that the relationship between two coordinate systems could be modeled by a selected number of parameters, which is usually seven. However, in reality the actual parameterization is not as simple as implied in those models. For example, the old geodetic datum, that has been built up over a period of time, does not have a uniform accuracy. Also, there exist distortions in the old datums as new precise data are fitted into these geodetic frames. Hence, the development of more precise relationships between geodetic datums should be considered.

The stepwise multiple regression technique is recently utilized for datum transformation determination for two basic reasons: the need for better accuracy than could be achieved through the similarity datum transformation formulas; and the need for a technique more

manageable for field use. This technique is based on modeling the differences ($\Delta\phi$, and $\Delta\lambda$, and ΔH) between the geodetic coordinates of two systems by three polynomials of sufficient terms in order to represent the differences over the network, to a given degree of accuracy. The stepwise multiple regression process starts by fitting a linear function, that is a constant and a variable. The procedure then sequentially adds one variable at a time to the equation, and its significance is tested in order to decide whether this variable is kept or removed from the model. This stepwise addition or removal of variables ensures that only significant variables are retained in the final equation. The procedure continues until the precision desired for the equation is obtained. This unconventional datum transformation technique has been used to describe the relationships between the WGS84 and 83 local geodetic datums all over the world [DMA 1987]. A similar approach has been used in Egypt based on the concept of modeling variable datum shifts (ΔX, ΔY, and ΔZ) at available stations not just one set of datum shifts for the entire region [Rashwan 1993]. However, a limited number of common points between WGS84 and OED systems (concentrated only in the Eastern Dessert) has been used, which enforces the polynomial degree not exceed 2.

The number of unknowns in the stepwise multiple regression equations is determined based on several factors: the available coordinates number and distribution; and the use of statistical measures to determine the significance of the models. Of the different available statistical measures, two indicators are of great importance: the standard error of estimation; and the coefficient of determination. The standard error estimation is an indicator of the precision of the developed regression equation, and is computed by (for $\Delta\phi$ as an example):

$$\sigma\,(\delta\Delta\phi) = \sqrt{\left(\sum_{i=1}^{n} [\,(\Delta\phi_i \text{ known}) - (\Delta\phi_i \text{ computed})\,]^2 / n\right)} \quad (1)$$

The coefficient of determination is the indicator of how much of the variability in the dependant variable is explained by the independent variables used in the regression formula. For example, the coefficient of determination for the latitude differences can be computed by:

$$r^2\,(\delta\Delta\phi) = \sum_{i=1}^{n} [\,(\Delta\phi_i \text{ computed}) - (\Delta\phi_{mean})\,]^2 \Big/ \sum_{i=1}^{n} [\,(\Delta\phi_i \text{ known}) - (\Delta\phi mean)\,]^2 \quad (2)$$

DATA USED AND DEVELOPED FORMULAS

Precise geodetic coordinates of 19 first-order geodetic stations known in both the WGS84 and OED geodetic datums has been used in this investigation (Figure 1). These GPS coordinates are the most accurate database available in Egypt. The coordinates come basically from two sources: the High Accuracy Reference Network (HARN95) established by the Egyptian Survey Authority and tied to some International Geodetic Stations (IGS); and the remaining stations have been observed by the Survey Research Institute as part of the Egyptian National Standardization Gravity Network (ENGSN97). Regarding the development of the stepwise multiple regression, a set of formulas has been tried out for each of the latitude differences and the longitude differences. The first formula is the linear equation, and then one variable is sequentially being added at a time to the equation. The following formulas are used:

For $\Delta\phi$:

$$\Delta\phi = c_o + c_1\,\phi \quad (3)$$

$$\Delta\phi = c_o + c_1\,\phi + c_2\,\lambda \quad (4)$$

$$\Delta\phi = c_o + c_1 \phi + c_2 \lambda + c_3 \phi^2 \quad (5)$$

$$\Delta\phi = c_o + c_1 \phi + c_2 \lambda + c_3 \phi^2 + c_4 \phi^3 \quad (6)$$

$$\Delta\phi = c_o + c_1 \phi + c_2 \lambda + c_3 \phi^2 + c_4 \phi^3 + c_5 \lambda^2 \quad (7)$$

$$\Delta\phi = c_o + c_1 \phi + c_2 \lambda + c_3 \phi^2 + c_4 \phi^3 + c_5 \lambda^2 + c_6 \lambda^3 \quad (8)$$

$$\Delta\phi = c_o + c_1 \phi + c_2 \lambda + c_3 \phi^2 + c_4 \phi^3 + c_5 \lambda^2 + c_6 \lambda^3 + c_7 \phi^4 \quad (9)$$

$$\Delta\phi = c_o + c_1 \phi + c_2 \lambda + c_3 \phi^2 + c_4 \phi^3 + c_5 \lambda^2 + c_6 \lambda^3 + c_7 \phi^4 + c_8 \lambda^4 \quad (10)$$

For $\Delta\lambda$:

$$\Delta\lambda = d_o + d_1 \lambda \quad (11)$$

$$\Delta\lambda = d_o + d_1 \lambda + d_2 \lambda^2 \quad (12)$$

$$\Delta\lambda = d_o + d_1 \lambda + d_2 \lambda^2 + d_3 \phi \quad (13)$$

$$\Delta\lambda = d_o + d_1 \lambda + d_2 \lambda^2 + d_3 \phi + d_4 \lambda^3 \quad (14)$$

$$\Delta\lambda = d_o + d_1 \lambda + d_2 \lambda^2 + d_3 \phi + d_4 \lambda^3 + d_5 \lambda^4 \quad (15)$$

$$\Delta\lambda = d_o + d_1 \lambda + d_2 \lambda^2 + d_3 \phi + d_4 \lambda^3 + d_5 \lambda^4 + d_6 \phi^2 \quad (16)$$

$$\Delta\lambda = d_o + d_1 \lambda + d_2 \lambda^2 + d_3 \phi + d_4 \lambda^3 + d_5 \lambda^4 + d_6 \phi^2 + d_7 \phi^3 \quad (17)$$

$$\Delta\lambda = d_o + d_1 \lambda + d_2 \lambda^2 + d_3 \phi + d_4 \lambda^3 + d_5 \lambda^4 + d_6 \phi^2 + d_7 \lambda^5 \quad (18)$$

$$\Delta\lambda = d_o + d_1 \lambda + d_2 \lambda^2 + d_3 \phi + d_4 \lambda^3 + d_5 \lambda^4 + d_6 \phi^2 + d_7 \lambda^5 + d_8 \lambda^6 \quad (19)$$

where $\Delta\phi$ and $\Delta\lambda$ are in arc of seconds, while ϕ and λ are WGS84 coordinates in degrees. It has been found that the differences in latitude range from 0.2104“ to 0.8654” with an average of 0.4678” and a standard deviation equal 0.2042”. The differences in longitude range from 5.8129“ to 6.0897” with an average of 5.9450” and a standard deviation equal 0.0873”. Figures 2 and 3 depict contour maps for these differences.

RESULTS AND ANALYSIS

The available data sets have been utilized to determine mathematical relationships between the WGS84 and OED coordinate systems. In order to test the obtained results, four stations have been considered as check points that have not been used in the processing stage. Another criterion has been chosen in order to increase the creditability of the results, which is the use of statistical tests to identify any outlier in the data. Coordinates of three stations have been flagged as erroneous observations, and hence, were removed. Identifying and removing outliers in precise geodetic networks increase the reliability of the obtained results [Alnaggar and Dawod 1995]. Both traditional similarity and unconventional multiple regression techniques have been evaluated.

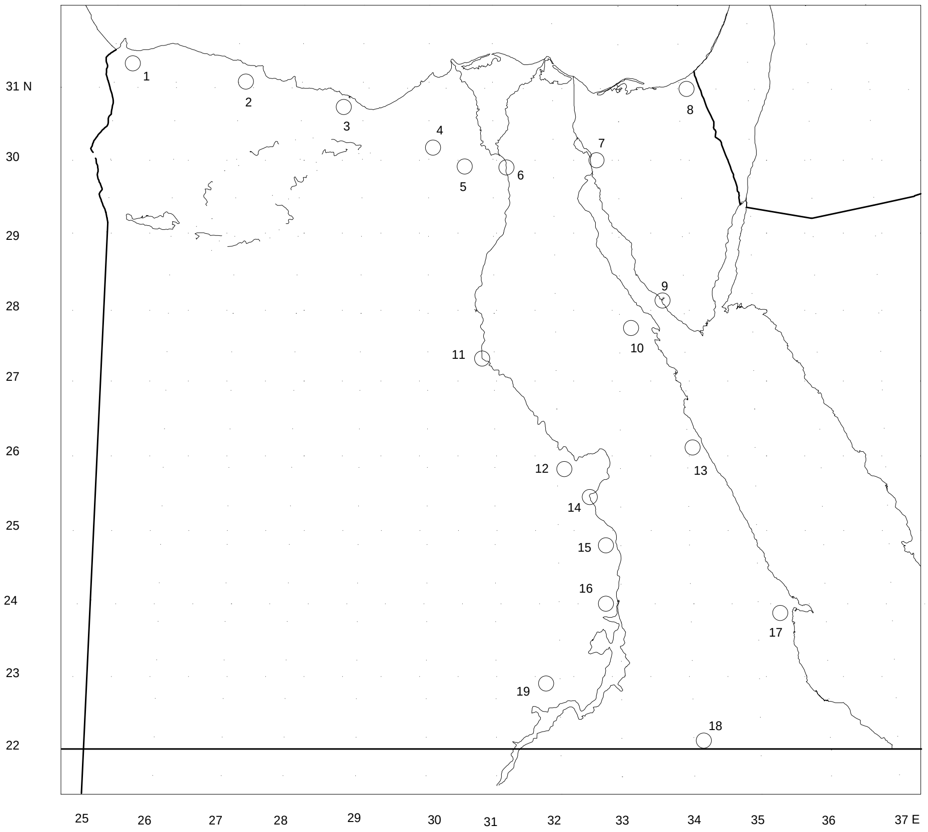

Figure 1: Available Geodetic Stations

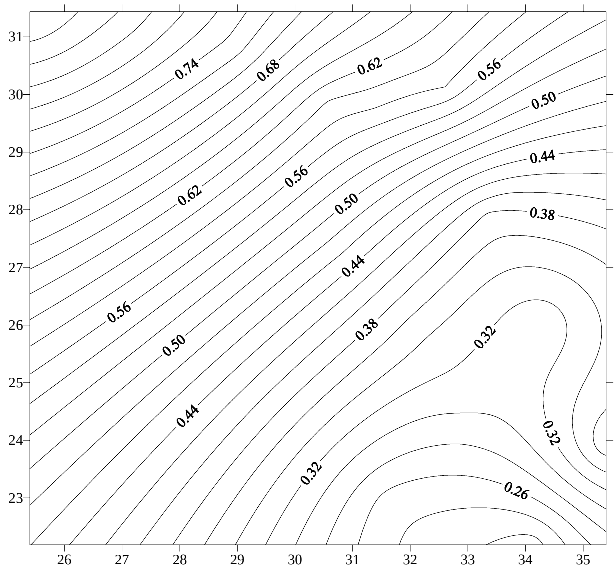

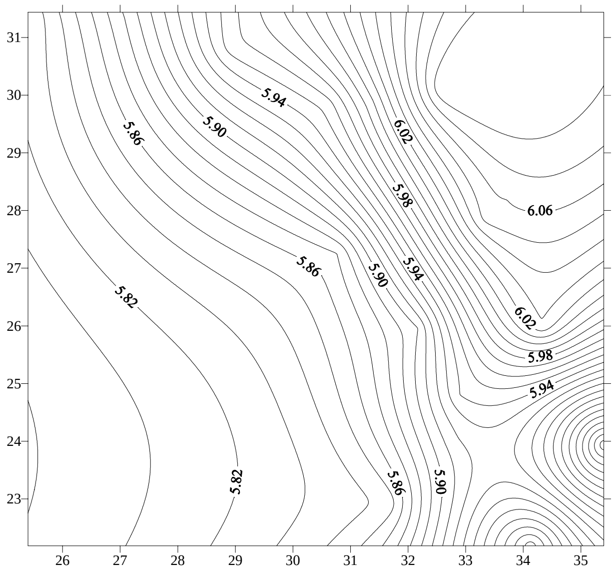

Figure 2
A Contour Map of Latitude Differences
(WGS84 – OED in seconds)

Figure 3
A Contour Map of Longitude Differences
(WGS84 – OED in seconds)

Results of similarity datum transformation

Transformation parameters using both Bursa-Wolf and Molodensky-Badekas datum transformation models have been determined. For each model, three, four, and seven-parameter cases are developed. The obtained results are summarized in Table 1. Carefully analyzing this table, the following concluding remarks may be drawn:

* Both models give identical results and precision estimates for the three-parameter case.
* When solving for the translations and scale parameters, the Molodensky-Badekas give more precise results regarding the three translation unknowns, although the value and precision of the scale factor is the same in both models.
* The Molodensky-Badekas model results in identical values for the translation parameters in the three cases, even though their precision estimates are different. That is because this model solves for mean datum shift parameters.
* Comparing the seven-parameter case for both models, it is clear that the Molodensky-Badekas model is superior to the Bursa-Wolf model.
* The Molodensky-Badekas seven-parameter model is proved to be the most precise similarity transformation model.

Results of multiple regression datum transformation

The second stage in the processing is the investigation of the stepwise multiple regression technique for geodetic datum transformation. The differences in both latitude and longitude between the WGS84 and OED systems have been computed and used as the independent variables in the regression equations. Formula (3) through (19) have been used to determine the unknown coefficients. The obtained results are presented in tables 2 and 3.

Table 1: Traditional Similarity Transformation Parameters (WGS84 to OED)

Model	B-W	M-B	B-W	M-B	B-W	M-B
ΔX (m)	123.842	123.842	143.587	123.842	70.281	123.842
$\sigma_{\Delta X}$	± 0.96	± 0.96	± 10.83	± 0.96	± 16.48	± 0.96
ΔY (m)	-114.878	-114.878	-102.540	-114.878	5.836	-114.878
$\sigma_{\Delta Y}$	± 0.96	± 0.96	± 6.74	± 0.96	± 15.12	± 0.96
ΔZ (m)	9.590	9.590	22.003	9.590	34.008	9.590
$\sigma_{\Delta Z}$	± 0.96	± 0.96	± 6.57	± 0.96	± 13.91	± 0.96
R_X (“)	---	---	---	---	-1.35314	-1.35314
σ_{RX}					± 0.17	± 0.17
R_Y (“)	---	---	---	---	-1.67408	-1.67408
σ_{RY}					± 0.35	± 0.35
R_Z (“)	---	---	---	---	5.24269	5.24269
σ_{RZ}					± 0.30	± 0.30
S (ppm)	---	---	-5.466	-5.466	-5.466	-5.466
σ_S			± 0.78	± 0.78	± 0.78	± 0.78

Table 2: Stepwise Multiple Regression for Differences in Latitude (WGS84 to OED)

Formula	No. of Coefficients	Degree of Freedom	Standard Error of Estimation $\sigma(\delta\Delta\phi)$	Coefficient of Determination $r^2(\delta\Delta\phi)$
3	2	10	0.0879	0.83
4	3	9	0.0645	0.91
5	4	8	0.0565	0.93
6	5	7	0.0468	0.95
7	6	6	0.0477	0.95
8	7	5	0.0403	0.96
9	**7**	**5**	**0.0360**	**0.97**
10	8	4	0.0469	0.95

Table 3: Stepwise Multiple Regression for Differences in Longitude (WGS84 to OED)

Formula	No. of Coefficients	Degree of Freedom	Standard Error of Estimation $\sigma(\delta\Delta\lambda)$	Coefficient of Determination $r^2(\delta\Delta\lambda)$
11	2	10	0.0974	0.19
12	3	9	0.0915	0.05
13	4	8	0.0720	0.41
14	5	7	0.0611	0.58
15	6	6	0.0386	0.83
16	7	5	0.0316	0.88
17	8	4	0.0258	0.92
18	**8**	**4**	**0.0110**	**0.98**
19	9	3	0.0227	0.95

From tables 2 and 3, it can be seen that the regression formula (9) and (18) are the most precise equations to represent the differences in latitude and longitude between the WGS84 and OED systems respectively. The values of the coefficients of determinations prove that these two formulas almost describe these differences perfectly. The corresponding standard errors of estimation prove that this technique is of a reasonable level of precision for GPS surveys. The final multiple regression formulas, for transforming coordinates from the WGS84 to the OED systems, recommended to be used in GPS surveys in Egypt are:

$$\Delta\phi'' = -320.474 + 30.6751\,\phi_{84} + 3.0402\,\lambda_{84} - 1.7380\,\phi^2_{84} + 0.0436\,\phi^3_{84} - 0.0004\,\phi^4_{84} - 0.1056\,\lambda^2_{84} + 0.0012\,\lambda^3_{84} \tag{20}$$

$$\Delta\lambda'' = 4357.7294 - 734.6377\,\lambda_{84} + 49.4639\,\lambda^2_{84} - 0.1705\,\phi_{84} - 1.6600\,\lambda^3_{84} + 0.0278\,\lambda^4_{84} + 0.0037\,\phi^2_{84} - 0.0002\,\lambda^5_{84} \tag{21}$$

where: $\Delta\phi$ and $\Delta\lambda$ are obtained in arc of seconds, while ϕ_{84} and λ_{84} are the WGS84 coordinates in degrees.

Therefore, the transformed coordinates on the OED coordinate system are given by:

$$\phi_{OED} = \phi_{84} + \Delta\phi \tag{22}$$

$\lambda_{OED} = \lambda_{84} + \Delta\lambda$ (23)

Comparison of both techniques

In order to compare the validity of results obtained from both transformation techniques, four check points have been utilized. The coordinates of those stations have been computed through the final precise model for each technique that are the Molodensky-Badekas seven-parameter model as long as equations 9 and 18 for the multiple regression approach. Then, the transformed coordinates are compared with the corresponding known coordinates. The obtained results are given in table 4 and 5.

Table 4: Accuracy of similarity transformation over check points

St.	φ" (obs)	φ" (comp)	Δφ " (obs-comp)	λ" (obs)	λ " (comp)	Δλ " (obs-comp)
1	48.292	48.25155	0.04045	36.3080	36.34625	-0.03825
2	31.8621	31.89153	- 0.02943	01.1468	01.05376	0.0934
3	48.8467	48.80847	0.03933	45.0296	45.12296	-0.09336
4	33.1216	33.14792	- 0.02632	31.2929	31.21780	0.0751
Mean			**0.00601"**			**0.00913 "**

Table 5: Accuracy of regression transformation over check points

St.	φ" (obs)	φ" (comp)	Δφ " (obs-comp)	λ" (obs)	λ " (comp)	Δλ " (obs-comp)
1	48.2920	48.26612	0.02588 "	36.3080	36.32019	-0.01219
2	31.8621	31.85634	0.00576 "	01.1468	01.12932	0.01748
3	48.8467	48.86464	-0.01794 "	45.0296	45.03211	-0.00251
4	33.1216	33.13322	-0.01162 "	31.2929	31.29999	-0.00709
Mean			**0.00052 "**			**-0.00051 "**

From tables 4 and 5, it can be seen that the overall accuracy of the traditional transformation technique is in the order of approximately 3 meters, while it is almost 0.5 m for the utilized regression approach. Hence, it may be concluded that the developed multiple regression datum transformation is one order more accurate than the traditional similarity datum transformation technique. The reason for that is the disability of the similarity transformation models to represent the distortions existing in the old local geodetic networks. The same situation happens for several national and regional coordinate systems all over the world [DMA 1987].

CONCLUSIONS

The issue of datum transformation of GPS coordinates from the WGS84 to the OED coordinate systems is an important dilemma in Egypt. The famous models of the traditional similarity datum transformation technique (namely Bursa-Wolf and Molodensky-Badekas models) have been investigated. It has been found that both models give identical results and precision estimates for the three-parameter case. When solving for the translations and scale parameters, the Molodensky-Badekas give more precise results regarding the three translation unknowns. Additionally, it has been concluded that the Molodensky-Badekas model results in

identical values for the translation parameters in the three cases. Moreover, the comparison of the seven-parameter case for both models reveals that the Molodensky-Badekas model is superior to the Bursa-Wolf model. Hence, it is concluded that this model is the most precise similarity transformation pattern. On the other hand, the traditional similarity datum transformation approach seems not to be the best technique to describe the mathematical relationship between the global and national datums. Consequently, the development of more precise relationships between WGS84 and OED geodetic datums has been considered. The stepwise multiple regression technique has been utilized for datum transformation determination. New regression formulas have been developed to transform the GPS coordinates from the global WGS84 datum to the local national Egyptian coordinate system. The obtained results show that the overall accuracy of the traditional transformation technique is in the order of approximately 3 meters, while it is almost 0.5 m for the utilized regression approach. Hence, it may be concluded that the developed multiple regression datum transformation approach is one order more accurate than the traditional similarity datum transformation technique. This approach is proved to be more simple, manageable, practical; and accurate for different types of GPS surveys in Egypt. Consequently, it is recommended to be applied using all available geodetic stations, with a national coverage, to come up with an accurate set of regression equations to transform GPS coordinates into the Egyptian national coordinates system.

ACKNOWLEDGMENT

The authors would like to acknowledge Prof. Dr. Ahmed A. Shaker, Vice Dean, Shobra Faculty of Engineering, Zagazig University, for providing some data sets and for his constructive criticism and stimulating discussion.

REFERENCES

Abd-Elmotaal, H., and El-Tokhy, M. (1997), The role of geoid in the coordinate transformation, Survey Review, V. 34, No. 263, pp. 31-40.

Alnaggar, D. (1990), Estimation of the transformation parameters between local and geocentric datums of Egypt, Proceedings of the IAG third international symposium on recent crustal movements in Africa, Aswan, Egypt.

Alnaggar, D., and Dawod, G. (1995), Increasing the reliability of GPS geodetic networks, Proceedings of the first international conference on GPS positioning, Alexandria, Egypt.

Dawod, G. (1998), A national gravity standardization network for Egypt, Ph.D. Dissertation, Shoubra Faculty of Engineering, Zagazig University, Egypt.

DMA: The U.S. Defense Mapping Agency (1987), The Geodetic System 1984 (WGS84): Its definition and relationship with local geodetic systems, DMA Technical Report 8350.2.

Finnmap (1988), Final report of the Eastern desert 1:50,000 topographic mapping project, The Egyptian Survey Authority, Cairo, Egypt.

Leick, A., and van Gelder, B. (1975), On similarity transformations and geodetic networks distortions based on Doppler satellite observation, Ohio State University Report No. 235.

Moore, T., and Smith, M. (1998), Geodetic transformations, Survey Review, No. 270, pp. 509-516.

Nassar, M. (1984), Geodetic position computations in two and three dimensions: Part II, Lecture notes, Faculty of Engineering, Ain-Shams University, Cairo, Egypt.

Rapp, R. (1989), Geometric Geodesy: Part II, Lecture notes, Ohio State University, USA.

Rashwan, A. (1993), Evaluation of the current Egyptian geodetic surveying and mapping framework towards the establishment of national unified specifications, MS.c., Ain Shams University, Cairo, Egypt.

Reit, B. (1998), The 7-parameter transformation to a horizontal geodetic datum, Survey Review, V. 34, No. 268, pp. 400-404.

Saad, A. (1998), Unification of the GPS work in Egypt, Civil Engineering Research Magazine, Al-Azhar University, V. 20, No. 4, pp. 462-470.

Proceedings of The Second International Conference on Civil Engineering, Helwan University, Cairo, April 1-3, 2000, pp. 578-587.

QUALITY CONTROL MEASURES FOR THE EGYPTIAN NATIONAL GRAVITY STANDARDIZATION NETWORK (ENGSN97)

Gomaa M. Dawod*   and   Dalal S. Alnaggar**

ABSTRACT

A precise national gravity datum for Egypt has been established through the Egyptian National Gravity Standardization Network (ENGSN97). The ENGSN97 net consists of 5 absolute gravity stations and 145 relative gravity stations covering the Egyptian territory [1]. A rational approach has been developed and applied for processing and adjusting absolute and relative gravity measurement in a unique package with the utilization of statistical tools to filter the data from outliers. Several processing and adjustment solutions have been developed for the ENGSN97 network taking into considerations the different factors affecting relative and absolute gravity measurements.

In order to judge the accuracy of obtained solutions, various control measures have been determined and analyzed. Those statistics include the distribution of the residuals, the internal reliability of the network; and the external reliability measures. It has been found that the residuals of the final optimum solution range between ±0.07 mgal, with a distribution peak over the interval between zero and 0.005 mgal [1]. Furthermore, the obtained standard deviations of the estimated gravity values range from 0.002 mgal to 0.048 mgal. Additionally, the final adjustment solution of the ENGSN97 network produces an external reliability measure of 0.022 mgal. All these quality control items emphasis that the ENGSN97 network meet the international standards for accurate gravity networks.

KEYWORDS: Gravity Networks; Adjustment; Quality Control

* Researcher, Survey Research Institute, National Water Research Center,
308 Al-Ahram St., Giza 12111, Egypt. E-Mail: sriidnet@brainy1.ie-eg.com
** Professor of Surveying, Director of the Survey Research Institute.

1. INTRODUCTION

The Egyptian National Gravity Standardization Network (ENGSN97) has been established, by the Survey Research Institute (SRI), as the new accurate gravity framework for Egypt. The ENGSN97 consists of 5 absolute gravity stations and 145 high-precision relative gravity stations. For all field campaigns in this project, the GPS satellite positioning technology has been utilized to obtain accurate three-dimensional coordinates of all stations (with a precision of 1 part per million), whose orthometric heights have been determined by precise levelling. However, this research study focuses on the data processing criteria and the quality control measures of the gravity measurements.

2. THE EGYPTIAN NATIONAL GRAVITY STANDARDIZATION NETWORK

The ENGSN97 has been established by SRI and partially financed by the Egyptian academy of sciences and technology from 1994 to 1998. The project aimed to: establishment of a fundamental national gravity network for Egypt, updating the gravity anomaly maps; and the recent accurate definition of the geoid in Egypt. In order to achieve these objectives, the field observation campaigns include the collection of three types of measurements: relative gravity, GPS positioning; and precise levelling. This is, of course, beside the necessary absolute gravity measurements at some selected stations.

Five absolute gravity stations have been established and observed as an absolute gravity framework for the ENGSN97 network. The measurements have been done with collaboration of the U.S. National Imagery and Mapping Agency (NIMA, formally DMA). The locations of these sites have been selected to cover the largest portion of the Egyptian territory at Giza, Helwan, Marsa Matrouh, Aswan; and El-Kharga (Figure 1). The measurements have been carried out using the Micro-g FG5 absolute gravimeter that has an instrumental uncertainty estimate of 0.0011 mgal [4]. Up to seven LaCoste and Romberge (LCR) relative gravimeters (models G and D) have been used in relative gravity measurements of the ENGSN97 network. The main observation schemes applied in this network are the step and the profile methods, which control the gravimeter drift systematic error. The step method is suitable for a central-point loop such as in the Delta area, while the profile method is suited for a loop extends in one direction such as in Upper Egypt.

3. DATA PROCESSING AND ADJUSTMENT FOR THE ENGSN97 NETWORK

A modified gravity processing approach has been developed and utilized in the final stage of the ENGSN97 network. This approach is mainly based on the results of analyzing several processing models used in national, regional; and international gravity networks [1]. The main characteristics of this approach are:

- The model serves two functions: processing gravimetric measurements, and perform least square adjustment to come up with the best linear un-biased estimates of the required quantities.
  - The basic observables of the model are just the original dial readings of the gravimeters after converting them to milligal unites and being corrected to tide effects.
  - The model is general enough to accept introducing some systematic errors in the estimation process, to be treated as nuisance unknown parameters.
  - The model is capable of dealing with absolute gravity measurements as long as the relative gravity measurements.
  - The model is compatible with some methods of detecting outliers so that this step being applied as a built-in routine to scan the data and flag any erroneous observations in order to increase the reliability of the estimated parameters.

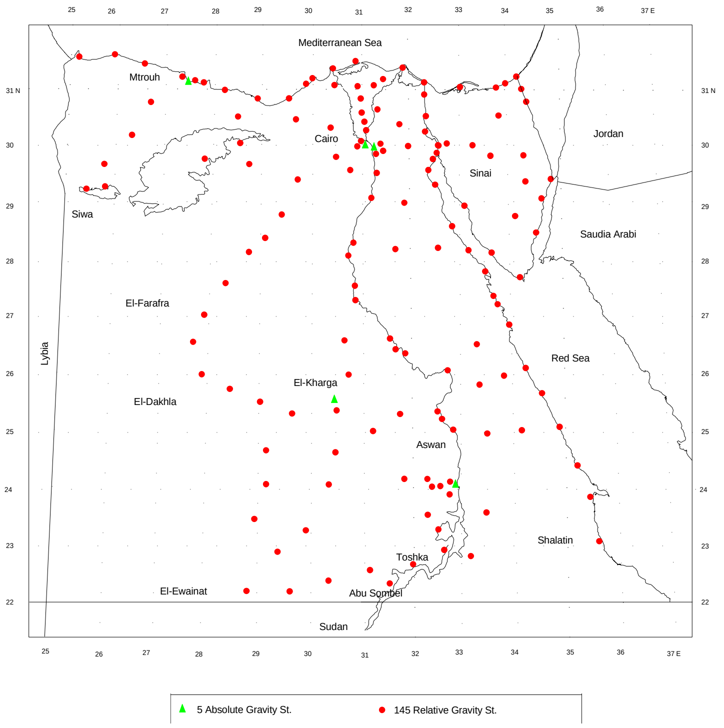

Figure 1: The Egyptian National Gravity Standardization Network (ENGSN97)

The observation equation for relative gravity measurements is given as [1]:

$$r_{ijkl} = g_j - O_{kl} + Z_{jlk} \,.\, e_{kl} + \Delta t_{ijkl} \,.\, d_{kl} \qquad (1)$$

where: r_{ijkl} is the $i^{\underline{th}}$ gravimeter reading, in milligal units corrected to the tidal effect, on station j using the gravimeter k in the data series l, g_j is the unknown gravity value, in milligal, of station j, O_{kl} is an unknown quantity describing the orientation of the gravimeter k in the $l^{\underline{th}}$ data series, Z_{jlk} is the original dial reading, in gravimeter counter units, of observation i on station j in the $l^{\underline{th}}$ data series using the $k^{\underline{th}}$ gravimeter, e_{kl} is the unknown error in the used linear calibration coefficient for the $k^{\underline{th}}$ gravimeter, that was used in transforming the dial reading in counter units into the equivalent milligal units, as estimated from the gravimeter reading on gravity stations with known absolute gravity values, Δt_{ijkl} is the difference in time between the running station j and the initial fixed station i in the $l^{\underline{th}}$ data series using the $k^{\underline{th}}$ gravimeter; and d_{kl} is the unknown drift coefficient of the $k^{\underline{th}}$ gravimeter in the $l^{\underline{th}}$ data series.

Observation equations for absolute gravity measurements at some stations of the network are incorporated into the model to process and adjust the entire network within the absolute gravity reference system. The corresponding observation equation model takes the following form [1]:

$$r_{j,k,l}\,(abs) = g_j\,(abs) - O_{k,l} + Z_{j,l,k} \,.\, e_{k,l} + \Delta t_{i,j,k,l} \,.\, d_{k,l} \qquad (2)$$

where: $r_{j,k,l}\,(abs)$ is the reading of the $k^{\underline{th}}$ gravity meter on the absolute gravity station j in the $l^{\underline{th}}$ data series, and $g_j\,(abs)$ is the known absolute gravity value of station j. The construction of the normal equation system and its solution based on the least-square theory could be found in several adjustment literature [e.g. 3 and 7].

A great deal of research has been carried out in past years on the development of statistical and numerical techniques to detect outliers in precise engineering measurements. The detection of outliers depends on the selected risk level, the assumed distribution, and the test procedure. Instead of using the residual (v_i) for each observation, another quantity, T_i ,which is the normalized or standardized value of v_i can be used, that is defined as:

$$T_i = |V| \,/\, \sigma_V \sim \tau(f) \qquad (3)$$

is used as the test statistics of the $i^{\underline{th}}$ observation using the τ (tau) distribution with f degrees of freedom. An algorithm that computes the critical τ value with

the corresponding tables of the τ distribution is presented in [5]. If some of the gravimeter readings are flagged as candidate outliers, the least-squares solution procedure, taking into considerations the remaining readings after the rejection process into account only, must be repeated, and the Tau test is applied again, until all the data is filtered out.

4. INVESTIGATED SOLUTIONS OF THE ENGSN97 NETWORK

A developed computer program for Gravity Network Processing and Adjustment (GNPA) has been utilized to process and adjust the ENGSN97 gravity network [1]. Of course, there are several items or criteria, associated with the adjustment of such entire network. These items depend upon the way of treating the gravimeter drift function,; the way of treating the five absolute gravity stations included in the network,; the way of treating the gravimeter reading observations for the two different LCR used G and D models; and the way of treating the different involved observation loops in the network according to the length and the time span of observations for each loop. Consequently, several solutions have been obtained as presented in the following sub-sections.

4.1 Solution 1: Adjustment with one fixed absolute gravity station

The purpose of this solution is to investigate the consistency between the relative gravity measurements and those absolute gravity measurements. In this case, one absolute gravity station only is held fixed, which is taken in our case here as the SRI5 station at Helwan (Figure 1), as the nearest absolute station to the center of gravity of the entire ENGSN97 network. It has been found that the differences between the known absolute gravity values, and the corresponding estimated values from the above adjustment, for the four absolute stations, range between –0.032 and 0.049 mgal, with a mean value of 0.007 mgal, and RMS of 0.029 mgal. Recall that, the assigned precision, in terms of standard deviations, for all relative gravity measurements were taken as 0.030 mgal. This means that the above mentioned differences are almost in the same order of the precision of the relative gravity measurements, which indicates the existing consistency between both types of gravity measurements, namely the absolute and relative measurements.

4.2 Solution 2: Adjustment with appropriate weights for absolute gravity stations

The appropriate way of treating the available absolute stations is to make benefit of such important information at all of them, by considering them as

quasi-observables with their estimated weights from the absolute measurement technique. One requirement here is to assign some appropriate weights for those five pseudo-observations, which is taken as the reciprocal of their variances, as estimated from the absolute measurement technique used, for which the actual standard deviations range between 0.002 mgal and 0.005 mgal. Accordingly, the second solution is carried out on the basis of this concept. It has been found that the differences between the obtained and known gravity values range between –0.018 mgal and 0.001 mgal, with a mean of –0.004 mgal and RMS of 0.009 mgal. This means that, the treatment of the absolute gravity stations as quasi-observables, gives almost the same results as if they were treated as fixed quantities, however, the former approach is the best one from the theoretical point of view.

4.3 Solution 3: Investigating a non-linear gravimeter drift function

In this solution, a non-linear drift model of relative gravimeters has been tried for all loops. The entire ENGSN97 network was adjusted, again, using the second solution above, after introducing the non-linear drift function. After the least-squares adjustment, an estimated value for the second drift coefficient was obtained, along with its estimated standard deviation, as one new unknown parameter. In addition, the estimated value for gravity station and their covariance matrix, are obtained as the main output results. The obtained results show the following three remarks:

* The value of the second term of the non-linear drift function contribution, is relatively very small compared to the first part, which in most of the cases does not exceed the 5% level.
* The estimated standard deviation for the second drift coefficient exceed, in most of the cases, the value of the coefficient itself, which means that this drift coefficient is statistically insignificant, that is it can not be distinguish from the zero value, from the statistical point of view.
* The adjusted point gravity values of the network attain relatively large values for their standard deviations, at a number of stations, when compared to the corresponding good estimate obtained from the second solution above.

Based on the above results and remarks, it can be concluded that the second part of the non-linear drift function is statistically insignificant, and should be neglected.

4.4 Solution 4: Validity of using different weights for different gravimeters

Several gravity surveys showed that the precision of the D model of LCR gravimeters is better than that of the G model gravimeters [6]. In the present solution, the entire ENGSN97 network was adjusted, again, using a better precision (standard deviation of 0.02 mgal) for the observations carried out by the D model of the relative gravimeters. This data series contains 248 observations in 37 virtual loops. The rest of the observations were assigned a standard deviation of 0.03 mgal, for the G model gravimeters. The obtained results indicated that there is a slight improvement in the precision as compared to those obtained from the second solution above, where equal weights were used. This may be due the fact that the number of the observations of the D-model gravimeters is slightly small compared with the total observations (23 % approximately). Such slight improvement, has occurred especially for the stations observed by the D model gravimeters in addition to the original G gravimeters.

4.5 Solution 5: Changing weights for observation loops

It is known that the longer the time span of a loop, the more problems encountered in the field regarding the observation circumstances. Tare (unexpected jump) is an example of these sudden problems that are quite difficult to be modeled. In order to avoid these uncertainties, a worse precision (standard deviation of 0.05 mgal) was assigned to all observations taking along the loops, which their observation have been continued for more than one-day. The obtained results of the estimated gravity values, indicated that there is slight improvements in their precision compared to the corresponding values from the standard adjustment of the second solution.

4.6 Solution 6: After satisfying all significant affecting criteria

Based on the obtained results from the above five solutions, it can be concluded that the best appropriate way of adjusting the entire ENGSN97 gravity network, will be performed taking the following items into consideration:

* The five absolute gravity stations should not treated as purely fixed, but taken as quasi-observables with appropriate large weights.
* Each used gravimeter should be assigned different weight for all observations taken by it, depending upon the reported precision of the manufacturer and by previous investigators, where a linear drift function should be used for all LCR gravimeter models.

* For all loops observed over span times exceeding one-day limit, should be assigned less weights for their encountered observations, as opposed to those loops completed in a period less than one day.

After satisfying all the significantly influence factors, one the adjustment of the entire ENGSN97 gravity network, another adjustment of the network has been performed. In order to have meaningful final results, based on good-quality observations, all erroneous readings must be filtered out from the system, and a best solution is obtained using all the remaining cleaned observations. Filtering out the observations from existing outliers can be simply performed, using the appropriate Tau statistical test for detecting outliers, as explained in section 5, which is based on testing the normalized residuals against a critical Tau value, instead of testing the pure residuals themselves. In other words, each estimated residual V_i of a gravimeter reading r_i, should be normalized first by dividing its value by its corresponding standard deviation. The critical value of the Tau statistic is then computed, based on the degree of freedom and the probability level using the student t-distribution function. If the normalized residual T_i exceeds the computed critical limit, the corresponding observation is suspected to contain some sort of gross errors, and hence, should be rejected from the system. The least-squares adjustment is repeated again using the remaining observations, after rejecting the outliers, and a new set of estimated residuals can be obtained, and the Tau test is performed again, and repeating the process until all measurements are cleaned out. The usual way, from the theoretical point of view, is to reject only one observation at a time, whose normalized residual is the largest in each solution. For the ENGSN97 gravity network, eight consecutive solutions were repeated, for the purpose of detecting and rejecting outliers, until no more outliers are flagged. A total of 44 observations out of the original 1085 observations have been flagged and removed. The solution of adjusting the network, as performed free from all the rejected 44 outliers, represents the final optimized solution for the ENGSN97 network.

5. QUALITY CONTROL MEASURES OF THE ENGSN97 NETWORK

For any precise geodetic network, the accuracy and specification of the network should also be determined and presented to the users. Economy, precision, and reliability usually describe the specifications of geodetic networks. Conceptually, the network precision describes how the precision of the observations affects the results through network geometry. The precision is a measure of the network's characteristics in propagating random errors, presuming the absence of gross errors in the observations. On the other hand, network reliability describes how the network reacts to small biases in the observations, which means the ability of the network to resist undetectable

gross errors in the observation data. Various measures for precision and reliability have been proposed for geodetic network analysis. Those measures include, for example, eigenvalues of the covariance matrix, the confidence hyper-ellipsoid, confidence regions, error curve, error ellipses, internal and external reliability, and standard deviations [2].

Of the available quality control measures, the following items have been studied: number of outliers detected, distribution of residuals, internal reliability; and external reliability of the network. As stated in the previous section, only 44 observations have been flagged as outliers. These observations constitute only about 4 % of the total number of the measurements, which is a first indication of the strength of the ENGSN97 network. Another quality control measure is to investigate the distribution of the residuals of the observations as estimated from the final solution of the network, which are depicted in Figure 2. From this figure, it can be noticed that, those residuals range between ±0.07 mgal, with a distribution peak over the interval between zero and 0.005 mgal. The general trend of such a distribution, approximately follows the ordinary Gussian normal distribution curve. This indicates that the remaining residuals of the cleaned gravimeter readings, are representing random errors only, with their mean value approaching the statistical mean value of zero. In other words, such cleaned used gravimeter readings are not affected by any sort of systematic errors or biases, associated with the used instruments, and used observational techniques and computations. The third statistical measure is the internal reliability (or precision) of the network as represented by the obtained standard deviations of the final adjusted gravity values. The final results show that the minimum standard deviation is 0.002 mgal while the maximum standard deviation is 0.048 mgal (Figure 3).

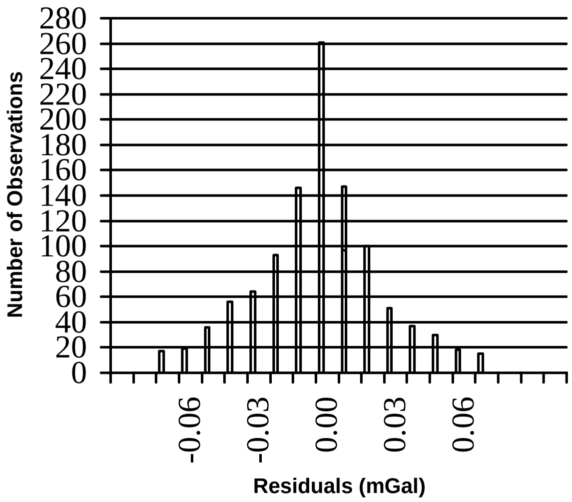

Figure 2: Frequency distribution of the residuals

An external measure of the overall reliability of each adjustment solution of the ENGSN97 was evaluated as [7]:

$$ER_s = \sqrt{(\sum^{n}_{i=1} \sigma^2_i)} / n \qquad (4)$$

where:
ER_s is the external reliability measure of the adjustment solution S,
σ_i is the standard deviation of the estimated gravity value of station i, and
n is the number of network stations (n=150 for ENGSN97)

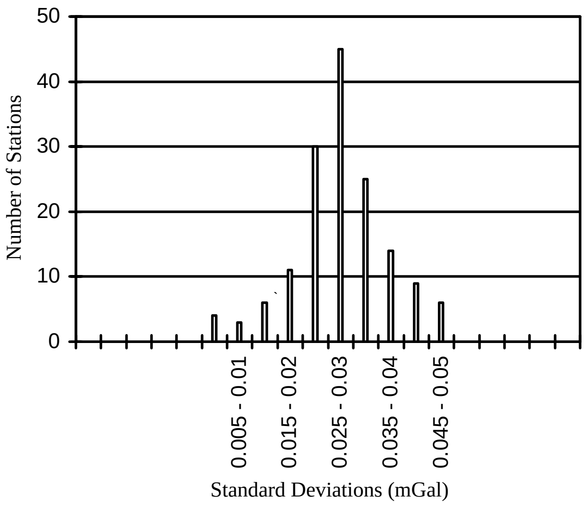

Figure 3: Distribution of the standard deviations

The obtained results of all solutions are tabulated in table 1. Additionally, the percentage of improvement is computed comparing each individual solution to the second solution, which was taken as the basis of the comparison. From this table, it can be seen that the external reliability measures for the developed solutions are 0.040, 0.035, 0.042, 0.031, 0.029; and 0.022 mgal respectively. The percentage of improvement of the five solutions are found to be 11, -18, 13, 18; and 37 % respectively. The first remark is that the third solution does not improve the final results of the network at all, since it gives a negative percentage of improvement and the largest external reliability measure. Hence, it can concluded again that the non-linear drift function of the LCR relative gravimeters is not the optimum function describing the nature of the systematic drift of this modern instruments. From the listed values of the external reliability measures and the percentages of improvement, it can be concluded that the six solution is the most reliable one among all other adjustments carried out for the ENGSN97 network. The final results show that the external reliability of the ENGSN97 network equals 0.022 mgal, which emphasis that

this national gravity network of Egypt is within the international specifications for precise gravity networks.

Table 1
Quality control measures of the ENGSN97 network

Item (all values in mgal)	**Results of Adjustment Solutions**					
	1	2	3	4	5	6
Minimum standard deviation	0.010	0.002	0.002	0.002	0.002	0.002
Maximum standard deviation	0.070	0.070	0.077	0.065	0.063	0.048
External reliability measure	0.040	0.035	0.042	0.031	0.029	0.022
Percentage of improvement	11	--	-18	13	18	37

6. SUMMARY AND CONCLUSIONS

Several processing and adjustment solutions have been developed for the ENGSN97 network taking into considerations the different factors affecting relative and absolute gravity measurements. In order to judge the results of the obtained solutions, various quality control measures have been determined and analyzed. Those statistical tools include the distribution of the residuals, the internal reliability of the network as expressed by the standard deviations of the adjusted quantities; and the external reliability measures. It has been found that the residuals of this final solution range between ±0.07 mgal, with a distribution peak over the interval between zero and 0.005 mgal. The general trend of such a distribution, approximately follows the ordinary Gussian normal distribution curve. This indicates that the remaining residuals of the cleaned gravimeter readings, are representing random errors only, with their mean value approaching the statistical mean value of zero. In other words, such filtered used gravimeter readings are not affected by any sort of systematic errors or biases, associated with the used instruments, and used observational techniques and computations.. Furthermore, the obtained standard deviations of the estimated gravity values (the measures of the network precision) range from 0.002 mgal to 0.048 mgal. Additionally, the final adjustment solution of the ENGSN97 network produces an external reliability measure of 0.022 mgal. All these quality control items emphasis that the ENGSN97 network meet the standards for quite examples with references to other international experiences in the same field. Therefore, it is recommended to use these quality control measures in the analysis of the adjustment results of geodetic networks in order to insure the goodness and effectiveness of the obtained results.

REFERENCES

[1] Dawod, G., 1998, A national gravity standardization network for Egypt, Ph.D. Dissertation, Shoubra Faculty of Engineering, Zagazig University, Cairo, Egypt.

[2] Kuange, S., 1996, Geodetic network analysis and optimal design: Concepts and applications, Ann Arbor Press Inc., Michigan, USA.

[3] Nassar, M., 1987, Matrix treatment of adjustment computations in surveying, Lecture notes, Department of Public Works, Faculty of Engineering, Ain Shams University, Cairo, Egypt.

[4] Niebauer, T., Sasagawa, G., Faller, J., Hilt, R., and Klopping, F., 1995, A new generation of absolute gravimeters, Metrologia No. 32, pp. 159-180.

[5] Pope, A., 1976, The statistics of residuals and the detection of outliers, NOAA Technical Report NOS 65 NGS 1, U.S. Department of Commerce, Washington D.C., USA.

[6] Torge, W., 1989, Gravimetry, Walter de Gruyter, New York, USA.

[7] Uotila, U., 1986, Notes on adjustment computations, Part I, Lecture notes, Department of Geodetic Science and Surveying, The Ohio State University, Columbus, Ohio, USA.

Proceedings of the International Conference on Integrated Management of Water Resources in the 21st Century, Cairo, Egypt, November 21-25, 1999, Volume II, pp. 741-752.

EFFECIENCY OF GPS TECHNIQUES IN NATIONAL APPLICATIONS

By

Prof. Dr. Dalal S. Alnaggar* **Dr. Gomaa M. Dawod****

ABSTRACT

The horizontal expansion and land reclamation has been the dream of Egypt's successive generations. The new delta project south of Egypt is a way for recomposing the demographic map by establishing a national integrated development project, which has agricultural, industrial, environmental, and social points of view. The availability of accurate topographic maps is one of the crucial elements in the decision making stage in large engineering projects.

The use of the traditional terrestrial surveying tools for the production of topographic maps is limited in time. On the other hand, maps created from romte-sensing satellite techniques do not fulfill the accuracy requirements for the project detailed planning. The ideal solution inherently combines a new challenge of employing integrated Global Positioning System (GPS) with conventional terrestrial techniques. New GPS surveying methodologies have been applied, for the first time in Egypt at a large scale, to produces topographic maps for an area of 75,000 feddans (315 millions squared meters approximately). This paper describes the formulation and practical application of the new approach of combining GPS and terrestrial surveying observations in a unique framework, including steps for data acquisition, transformation, and map production. It has been found that those techniques result in 50% cost saving and 75% time saving, yet satisfying the national standards and specifications for topographic maps.

* Director, Survey Research Institute, National Water Research Center, Egypt
** Researcher, Survey Research Institute.

1. Introduction

Precise topographic maps are one of the crucial elements for planning and decision making in large engineering projects. Traditional surveying techniques for the production of topographic maps are limited in productivity since they are time and cost consuming. On the other hand, the Global Positioning System (GPS) has been applied in Egypt since 1985, but only in static mode for establishing geodetic control points. Advances in GPS positioning technologies and instrumentation have led to new surveying approaches that are efficient and productive for topographic mapping. For example, pseudo-kinematic methods, have been exercised worldwide and proposed to be applied in Egypt for huge surveying projects [Dawod, 1992]. However, no attempt has been made to apply these new GPS techniques at a national production level.

The integration of advanced GPS techniques with terrestrial surveying measurements is the optimum approach for topographic mapping in open areas. This study presents the development and application of this modern methodology for surveying an area of 75,000 feddans in the south valley development project (Toshka). Section two presents a brief description of this national development project in Egypt. Basics of kinematic GPS positioning modes are offered in section three, with specific emphasis on the On-The-Fly (OTF) observation mode. Section four introduces the collected field data including the static GPS, kinematic GPS; and levelling measurements. The computational procedures and results of the integration of all data types, coordinates transformation; and map projection are given in section five. The economical aspects and the comparison between the traditional and the new approaches are provided in section six. The conclusions and obtained recommendations are given in section seven.

2. The south valley development project

The south valley development project, known also as Toshka project, is a strategic ambitious national program that embraces a number of development fields covering activities the areas of agriculture, industry, transport, communication and roads, as well as social and environmental aspects. The overall objectives of the projects are:

* Addition of new areas of agricultural land of some two million feddans.
* Establishment of agricultural and industrial communities south of Egypt.
* Recomposing the demographic map of Egypt by establishment of new communities that gradually alleviating the problem of overpopulation in the old Delta.
* Establishment of a network of main and side roads.
* Promotion of touristic activities in these regions rich in ancient monuments.

The project area extends from latitude 22.5^{o}N to 23.5^{o}N, and from longitude 30.5^{o}E to 33^{o}E (Figure 1). The project starts with a giant major pumping station to be set on the left bank of lake Nasser 8 km north of Toshka. The station is designed to have a maximum static lifting of about 52.5 meters to guarantee its operation when the water level in lake Nasser reaches its lowest level of storage, namely 147.5 meters, and the main canal water level is 200 meters. Since the average of the water level in the lake throughout the years is 165 meters, the quantity of the average lifting

reaches about 35 meters. Twenty four pumps, each with a discharge of 16.7 m^3/sec, will be housed inside the pumping station. The irrigation system of canals in the project is characterized by a main canal (Shiekh Zaied canal) of a length of 70 km, and four branch canals with a total area served in the first stage of 540,000 feddans of first-degree agriculture lands. The cross section of the main canal was designed to be lined to prevent any water leakage with a bed of 30 meters width and water depth of 6 meters.

The implementation plan of the project anticipates the construction of the main canal to be accomplished by December 2001, while the development of the four branch canals is planned to be finished by December 2000. A primary project budget, including the civil and social structures, starting from fiscal year 1996/1997 to fiscal year 2003/2004 is estimated to equal 6807 million Egyptian pounds [NWRC, 1998].

3. Kinematic GPS techniques

GPS is the most advanced satellite positioning system currently in use for a wide range of civilian and military applications. Compared with traditional terrestrial surveying systems, several advantages of GPS surveying have been accomplished. For example, there are no intervisibility requirements and practically no limit to distance between receivers. Additionally, the obtained coordinates are three dimensional, in a unique coordinate system, with a superior level of accuracy.

The classic GPS observation approach is the static mode in which more than one receiver are kept fixed over ground stations and record satellite signals for more than thirty minutes of observation. Positioning of moving platforms with GPS (the kinematic mode) is the last frontier in GPS surveying. The kinematic applications include surveying on land, aerial photogrammetry without control points, airborne gravimetry; and altimeter profiling on land and sea. Kinematic positioning can be classified into two main groups: absolute kinematic and relative kinematic [Nassar, 1994]. The absolute kinematic deals with positioning of a moving antenna with respect to an implied coordinate system. On the other hand, relative kinematic positioning is performed relative to one or more receivers at known stations. Relative kinematic GPS surveying starts with two receivers being located initially at two stations of known relative position. One of the stations is called the fixed (or base) site, where the antenna remains stationary at this point. The antenna of the other station, called the roving antenna, moves to points whose positions to be located. There are several modes of relative kinematic GPS surveying based on the way of the receivers capabilities, data processing; and field observation procedures. Some of these modes are: pseudo-kinematic, rapid static, stop and go, antenna swap; and On-The-Fly (OTF). Details concerning those kinematic techniques are found in a lot of surveying literature [e.g. Sickle, 1996].

One of the main aspects of data processing in GPS positioning is the so-called ambiguity resolution. It is known that GPS receivers measure the accumulating phase over time, but do not have knowledge about the integer number of full cycles of phase that occur from the first moment of the lock on a satellite. The number of full cycles of phase, which does not change unless that lock is lost, is known as the integer ambiguity or phase ambiguity and could be solved for easily in the static GPS positioning, since the receivers collect data from the same satellites for a period of

time. However, this requires specific field procedures in the relative kinematic positioning modes. Actually, the resolution of the integer ambiguity is the main point leaded to the development of several relative kinematic positioning techniques. Relative kinematic observation modes try to resolve the phase ambiguity before the survey starts, in a process called initialization that requires some sort of static positioning for a specific period of time.

On The Fly (OTF) relative kinematic approach is the most advanced technique for resolving the phase ambiguity while the receiver is actually in motion. This implies that unlike all other relative kinematic GPS techniques, the initialization process tack place with no delay. OTF has been used recently in various applications for precise GPS coordinates determination [e.g. Chen et al, 1999]. The mathematical model behind OTF technique is called wide-lane observable, which is based on the linear combination of the measured phases from both GPS frequencies, L1 and L2. The strategy starts by solving for the phase ambiguity on the fictional wide-lane observable, which is then used to resolve the phase unknowns on both L1 and L2 frequencies, as follows [Mervart et al, 1994]:

$$L^i_{1k} = \rho^i_k - I^i_k * (f^2_2 / (f^2_1 - f^2_2)) + \lambda_1 b^i_{1k} \quad (1)$$
$$L^i_{2k} = \rho^i_k - I^i_k * (f^2_1 / (f^2_1 - f^2_2)) + \lambda_2 b^i_{2k} - \Delta\rho^i_k \quad (2)$$
$$L^i_{3k} = (1/(f_1 - f_2)) * (f_1 L^i_{1k} - f_2 L^i_{2k}) \quad (3)$$
$$= \rho^i_k + I^i_k * (f_1 f_2 / (f^2_1 - f^2_2)) + \Delta\rho^i_k (f_2 / (f_1 - f_2)) + \lambda_3 b^i_{5k} \quad (4)$$
$$b^i_{1k} = N^i_{1k} + \delta\Phi_{1k} - \delta\Phi^i_1 \quad (5)$$
$$b^i_{2k} = N^i_{2k} + \delta\Phi_{2k} - \delta\Phi^i_2 \quad (6)$$
$$b^i_{3k} = b^i_{1k} - b^i_{2k} \quad (7)$$
$$\lambda_3 = c / (f_1 - f_2) \quad (8)$$

where:

k	is the receiver index,
i	is the satellite index,
L^i_{1k} , L^i_{2k}	are the carrier-phase pseudoranges,
ρ^i_k	is the non-dispersive delay, lumping together the effects of geometric delay, ionospheric delay, tropospheric delay, clock signatures, and any other delays which affect the observables,
$\Delta\rho^i_k$	is the differential delay between the L1 and L2 antenna phase centers,
I^i_k	is the difference in ionospheric delay between the L1 and L2 carriers,
f_1 , f_2	are the frequencies of the L1 and L2 carriers, which equal1575.42 MHz and 1227.60 MHz respectively,
λ_1 , λ_1	are the wavelengths of the L1 and L2 carriers, which equal 19.0 and 24.4 cm respectively,
λ_3	is the wavelength of the wide-lane observable, which equals 86.2 cm.
b^i_{1k} , b^i_{2k}	are the phase biases on the L1 and L2 carriers,
b^i_{3k}	is the wide-lane phase ambiguity to be estimated,
N^i_{1k} , N^i_{2k}	are the initial phase ambiguities,
$\delta\Phi_{1k}$, $\delta\Phi_{2k}$	are un-calibrated components of phase delay originating from the receivers (assumed to be common for all satellite channels),
$\delta\Phi^i_1$, $\delta\Phi^i_2$	are un-calibrated components of phase delay originating from the satellites (assumed to be common for all receivers),

4. Data and practical field procedures

The objective of the mission carried out by the Survey Research Institute (SRI) was the development of topographic maps for an area of 75,000 feddans (approximately 315 million squared meters) in the south valley development project. This comprises the production of 50 topographic maps of scale 1:5,000 with a contour interval of 1 meter. Each map covers a 3x2 km piece of land whose area is 1500 feddans. The required maps are required to be referenced to the Helmert 1906 ellipsoid and projected using the Transverse Merecator map projection in order to fit the Egyptian national horizontal mapping system, and the heights must be referred to the Mean Sea Level (MSL). Therefore, 75 GPS stations have been established as the corners of the individual areas (Figure 2). The field data campaigns consists of three types of geodetic observations, namely static GPS, OTF relative kinematic GPS; and levelling.

4.1 Static GPS observations

Six dual-frequency geodetic GPS receivers have been used to obtain accurate coordinates for the 75 established control stations. These receivers contain two Trimble 4000SST, two Trimble 4000SSI; and two Leica 300 receivers. Ten observation sessions have been performed whose time period varied from 1 to 3 hours of observations based on the baseline length. Eight local GPS control points established by the Egyptian Survey Authority (ESA) have been included in order to work in the same unique coordinate framework of the Toshka project. Both Trimble GPSURVEY and Leica SKI processing software have been employed to process the GPS data separately so that the results comes from two independent sources. Of course, the Receiver INdependent EXchange (RINEX) data format have been used to transfer the collected observations between both software. The GEOLAB software is utilized in the GPS adjustment process because of its flexibility and richness of statistical tools that are useful in increasing the reliability of the final adjusted coordinates. Table 1 summarizes the results of the final adjusted coordinates of static GPS networks.

Table 1
Summary of Static GPS Networks

No of stations	89
No. of baselines	164
No. of observations	492
No. of unknowns	243
Degrees of freedom	249
Minimum residual	0.02 m
Maximum residual	0.13 m
Minimum standard deviation	0.01 m
Maximum standard deviation	0.09 m

4.2 OTF relative kinematic GPS observations

Four of the available GPS receivers are equipped with the OTF option, namely the Trimble 4000SSI and Leica 300 brands. The remaining two receivers, the Trimble 4000SST models, are reserved to occupy two stationary base stations in each session. As mentioned previously, no static initialization is required since the OTF technique is utilized (Figure 3). In order to achieve a high accuracy level, a set of configuration have been predetermined for the surveys. It includes:

* A minimum of 5 tracked satellites is a must from the first epoch forward.
* A sample observation rate of 5 seconds is unified in all receivers' configurations.
* The raw observations are recorded in the compact format.
* No loss of lock on satellites in the first 200 epochs.
* Good satellite-receiver geometry (low GDOP).
* Vehicles speed do not exceed 30 km/h.
* Distance between two adjacent car trajectory is in the order of 100 m.
* Two stationary base receivers are used for obtaining more robustness in the OTF solution.

4.3 Levelling observations

GPS positioning produces three-dimensional coordinates (latitude φ, longitude λ; and ellipsoidal height h) relative to a global geocentric ellipsoid called the World Geodetic System 1984 (WGS84). However, topographic maps are usually based on orthometric heights (H) relative to the geoid that coincides with the Mean Sea Level. The difference between ellipsoidal and orthometric heights is known as geoid undulation or geoidal height (N):

$$N = h - H \tag{9}$$

Orthometric heights of 20 established GPS control stations have been determined by running levelling routes from the available bench marks in the region (Figure 2). The determined orthometric heights are utilized to model the local geoid surface in the area.

5. Data processing and results of the new integrated approach

There are several data processing aspects of integrating OTF kinematic GPS and terrestrial measurements, for topographic map production, to be taken into account. They include: geoid determination, geodetic datum transformation; and map projection.

5.1 Geoid determination

Geoid undulations are required to convert the GPS ellipsoidal heights to orthometric heights to produce meaningful topographic maps. There are several terrestrial and satellite measurements utilized for geoid determination, such as gravimetric, astronomical, altimetric data types. A combination of gravity, GPS, and levelling data is one of the most precise geoid determination techniques used world-wide and in Egypt. Although global geoid models exist and usually integrated in

commercial GPS software(e.g. OSU91A and EGM96 models), their accuracy is in the order of few meters [Dawod, 1998]. An optimum solution is the integration of global geoid models with terrestrial local measurements.

Geoid undulations from the OSU91A geoid model have been interpolated for the twenty established control points whose orthometric heights are determined. The differences between the model geoid undulations and the computed corresponding values have been determined:

$$\Delta N = N_{OSU91A} - N_{(h-H)} \qquad (10)$$

The obtained geoid undulation differences range from 1.8 to 2.9 meters. These differences have been modeled over the area under study. Consequently, refined geoid undulations (N') are determined for all static and kinematic GPS measured points, and their orthometric heights are determined:

$$H = h - N' \qquad (11)$$

5.2 Datum transformation

The issue of datum transformation determination has been one of the crucial elements of GPS applications in Egypt in the last decade [Alnaggar, 1990]. The Egyptian geodetic coordinate system is based on the Helmert 1906 ellipsoid as the figure of the Earth. However, GPS produces coordinates relative to the global WGS84 ellipsoid. Therefore, a datum transformation procedure is a must in any precise GPS surveys in Egypt. This step basically utilizes known values for seven parameters that describe the mathematical relationship between the two ellipsoids. These parameters include three translation unknowns (ΔX, ΔY, and ΔZ), which describe the 3D shift of the origin of one ellipsoid relative to the origin of the second ellipsoid), three rotation parameters (ω_x, ω_y, and ω_z) that describe the angular relationship between the axes of both system in the Euclidean space; and a scale factor (s) describes the size differences between both ellipsoids. The Bursa-Wolf datum transformation model is given by:

$$\begin{bmatrix} X_{Helmert1906} \\ Y_{Helmert1906} \\ Z_{Helmert1906} \end{bmatrix} = \begin{bmatrix} \Delta X \\ \Delta Y \\ \Delta Z \end{bmatrix} + s \begin{bmatrix} 1 & \omega_z & -\omega_y \\ -\omega_z & 1 & \omega_x \\ \omega_y & -\omega_x & 1 \end{bmatrix} \begin{bmatrix} X_{WGS84} \\ Y_{WGS84} \\ Z_{WGS84} \end{bmatrix} \qquad (12)$$

In order to cup with the same coordinate system for the south valley development project, the transformation parameters determined by ESA are applied to transform the 3D Cartesian coordinates from the WGS84 to the Helmert 1906 ellipsoid. Table 2 gives the values of these parameters.

Table 2
Transformation Parameter From WGS84 to Helmert 1906 Ellipsoids

Translation Unknowns	ΔX (m) ΔY (m) ΔZ (m)	121.8 -98.1 10.7
Rotation Unknowns	ω_x (seconds) ω_y (seconds) ω_z (seconds)	0.0 0.0 -0.02
Scale Factor	S (part per million: ppm)	0.226

5.3 Map projection

For the production of maps, the cartesian three-dimensional coordinates are projected into a two-dimensional coordinate system. The Egyptian mapping system is based on the Transverse Merecator map projection model, which uses a projection cylinder whose axes is imagined to be parallel to the earth's equator and perpendicular to its axes of rotation. In order to minimize the projection distortions, the local mapping system is divided into three belts or zones. The area under study is located in the Red Belt, whose defining parameters are given in table 3. It worth mentioning that the false northing value has been set as 1,000,000 m in order to ensure positive northing coordinates for the so-called negative strip close to the Egyptian-Sudan borders, neglecting the originally defined false northing value of 816,000 m.

Table 3
Parameters of the Red Belt Zone of the Egyptian Mapping System

Latitude Origin Central Meridian Zone Width	30^{o} 31^{o} 4^{o}
False Easting False Northing	615,000 m 1,000,000 m
Scale Factor	1.0

Those parameters have been applied to obtain the horizontal easting and northing coordinates of all measured points, whose orthometric heights are computed. Then, a contouring software was utilized to create 50 topographic maps of scale 1:5,000 with a contour interval of 1 meter. A final topographic map for the entire area has been developed with a scale 1:50,000 (Figure 4). Table 4 summarizes the essential information about the surveyed area. From these figure and table, it can be seen that the orthometric heights of the area range from 186 m to 254 m, with an average of 222 m.

Table 4
Essential Data of The Surveyed Area

Item	Minimum	Maximum	Average
Latitude φ (degree) Longitude λ (degree)	22.923 31.495	23.213 31.761	23.068 31.628
Northing (m) Easting (m)	27992 665823	58194 692832	43093 679328
Orthometric Height (m)	**186**	**254**	**222**

6. Economical aspects of the new integrated approach

A comparison is performed between the traditional surveying system, using total stations and levels, with the newly practiced approach of integrating kinematic GPS and terrestrial measurements. The only disadvantage of the new technique, from the authors' point of view, is its requirement of advanced theoretical background of modern geodesy. A detail understanding of the concepts underlying the satellite positioning techniques, coordinate systems; and the role of geoid is a must in order to be able to precisely integrate satellite and terrestrial measurements. On the other hand, the integrated approach has many benefits over the traditional methods. The ease of use of GPS instrumentation, the capability of collecting data over 24 hours under any weather conditions; and the achieved high accuracy level are some examples of these merits.

The cost-benefit comparison between the new and conventional surveying approaches is shown in table 5. Regarding the traditional terrestrial surveying methods, it has been found that field and office stages of this job is expected to be done by means of 40~60 persons in 36~48 weeks, so that the cost estimate would be 12 L.E. per feddan approximately. Applying the new integrated approach, the job has been completed by 10~15 persons in 9~12 weeks resulting in actual cost of 6 L.E. per feddan approximately. Therefore, the new integrated approach wins time shortcut of 75% and cost-effectiveness of 50%.

Table 5
An Economical Comparison Between
Traditional and New Approaches

	Traditional Surveying	Integrated Surveying
Time needed (weeks) Persons Needed	36 ~ 48 40 ~ 60	9 ~ 12 10 ~ 15
Cost per feddan	≈ 12 L.E.	≈ 6 L.E.
Time saving Cost saving	- -	75 % 50 %

7. Conclusion

For the first time in Egypt, an integrated approach of combining GPS positioning and terrestrial surveying techniques has been developed and utilized for the production of topographic maps at a large scale. The new approach has several merits over other traditional surveying methods in terms of accuracy, productivity, time and cost savings. This advanced approach has been utilized for the production of topographic maps cover an area of 75,000 feddan (approximately 315 million square meters) in the south valley (Toshka) development project. Results have shown that this advanced technique reduces the needed time by 75% and results in 50% saving of the costs of applying traditional surveying methods. Furthermore, the new approach yet satisfies the national standards and specifications for topographic maps. Hence, it is recommended to utilize this modern methodology for the production of topographic maps at the national scale in Egypt.

References

Alnaggar, D., 1990, Estimation of the transformation parameters between local and geocentric datums of Egypt, Proceedings of the IAG third international symposium on recent crustal movements in Africa, Aswan, Egypt.

Chen, X, Liu, J., and Li, D., 1999, OTF method for GPS aided photogrammetry, Proceedings of the IUGG XXII General Assembly, Birmingham, U.K, July 18-30.

Dawod, G., 1992, On the use of pseudo-kinematic GPS satellite positioning technology in surveying reclaimed lands in Egypt, Proceedings of the first national conference on reclamation and development in Egypt, El-Minia University, November 2-5, pp. 237-246.

Dawod, G., 1998, A national gravity standardization network for Egypt, Ph.D. Dissertation, Shoubra Faculty of Engineering, Zagazig University, Cairo, Egypt.

Mervart, L., Beutler, G., Rothacher, M., and Wild, U., 1994, Ambiguity resolution strategies using the results of the International GPS Geodynamics Services (IGS), Bulletin Geodesique, V. 68, No. 1, pp. 29-38.

Nassar, M., 1994, Advanced geometric geodesy, Lecture notes, Faculty of Engineering, Ain Shams University, Cairo, Egypt.

NWRC (The National Water Research Center), 1998, Southern Egypt Development Project, Unpublished Report, Cairo, Egypt.

Sickle, J., 1996, GPS for land surveyors, Ann Arbor Press, Inc., Michigan, USA.

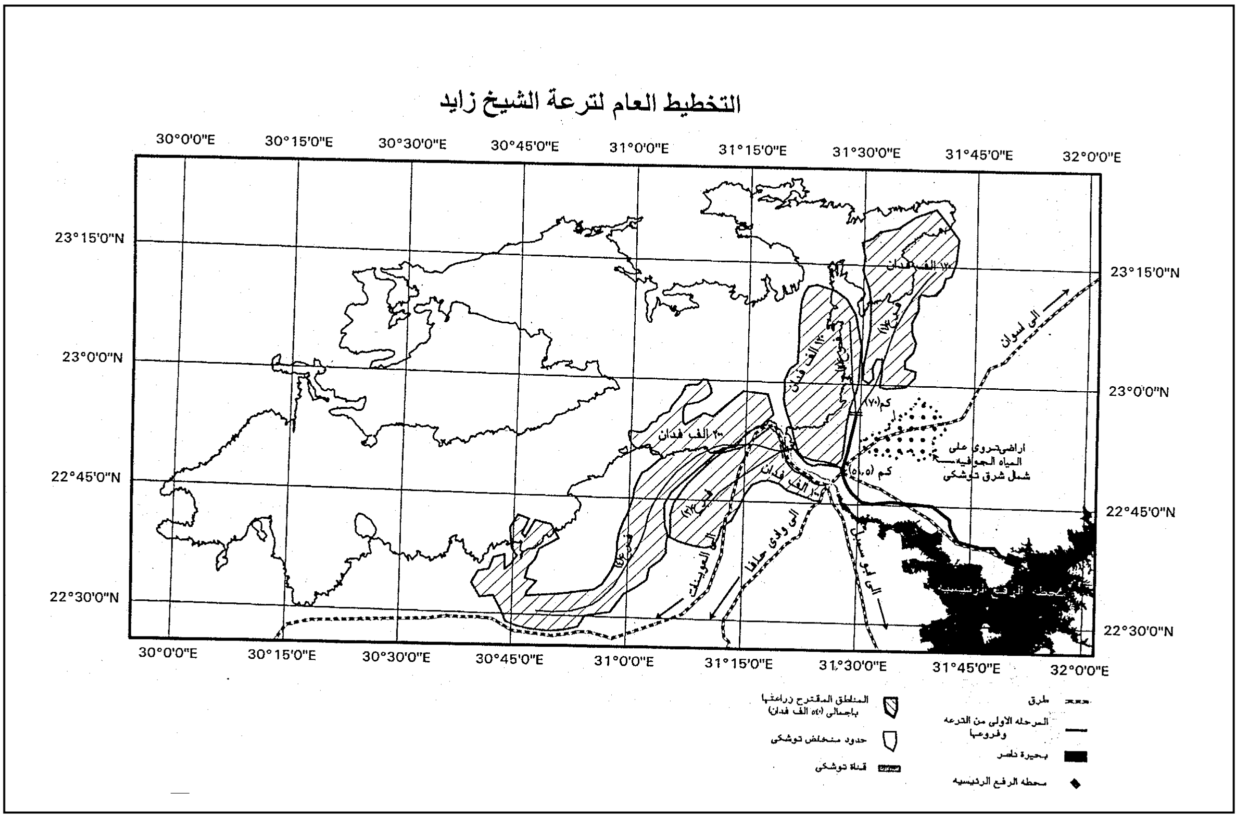

Figure 1
The South Valley (Toshka) Development Project Layout

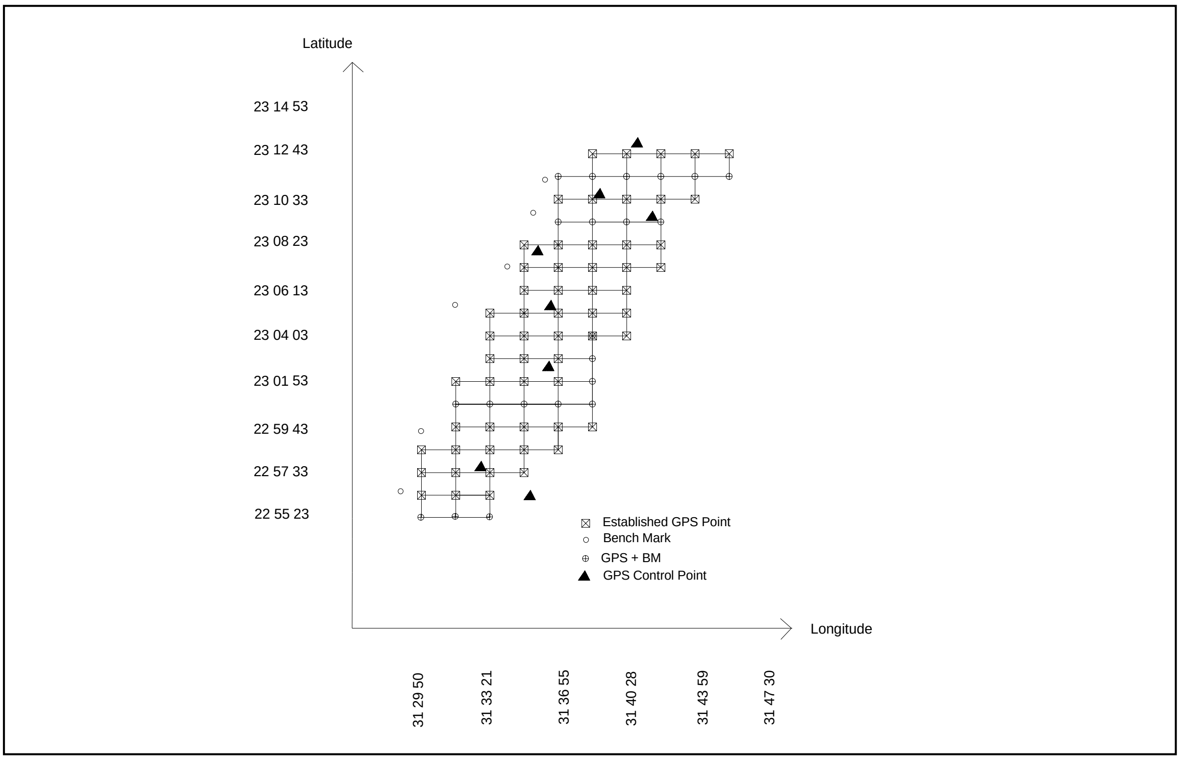

Figure 2
The Established GPS Control Network

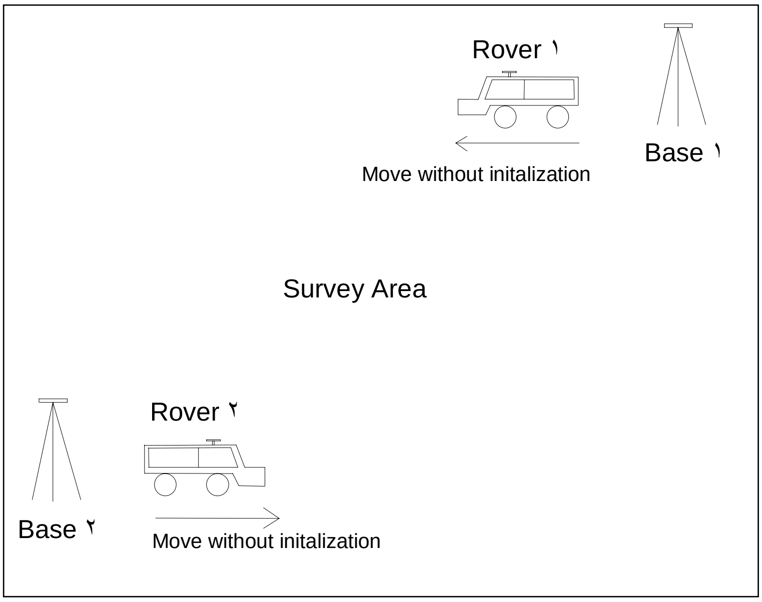

Figure 3
The OTF Relative Kinematic GPS Technique

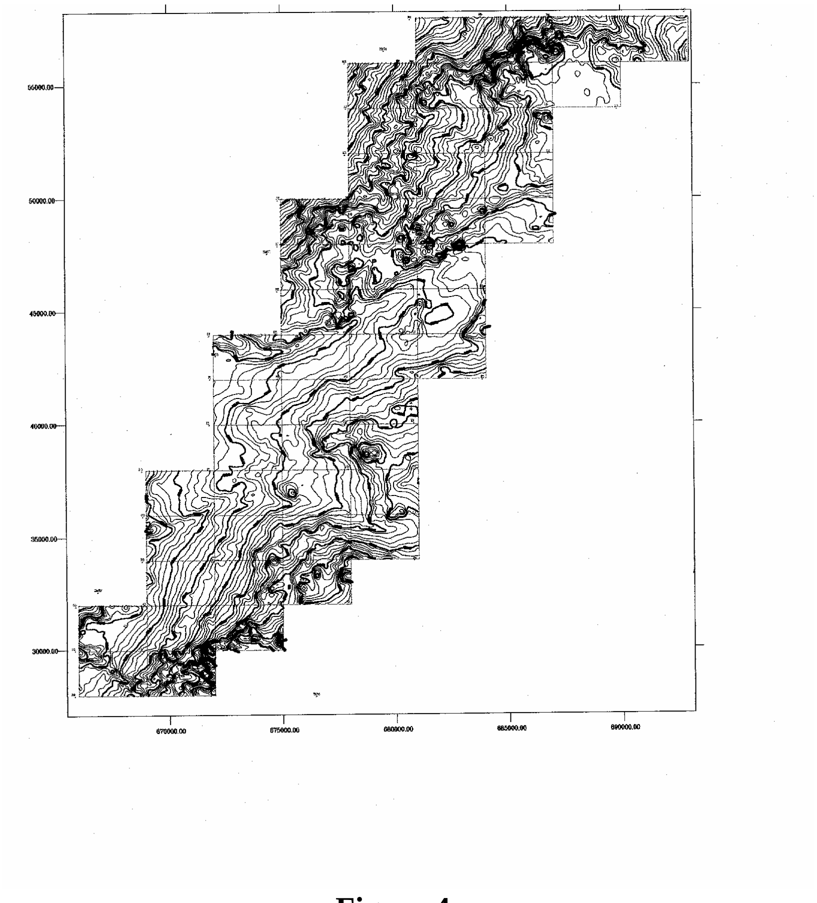

Figure 4
The Developed Topographic Map

EFFECT OF HIGH FLOODS ON NAGA HAMMADI BARRAGES SCOUR HOLE

Sherine S. Ismail * and Gomaa M. Dawod **

* Researcher, Nile Research Institute, NWRC, Egypt
Email: sherine_shawky@hotmail.com
** Associate Professor, Deputy Director, Survey Research Institute SRI, NWRC, Egypt

ABSTRACT

Local scour is a threat for hydraulic structures, and the removal of material downstream these structures, around piers, abutments, spurs, embankments and in curves affects their safety. Many factors affect local scour downstream barrages, such as the head difference between upstream and downstream, flow conditions, gates' operation, suspended sediment concentration, downstream concrete length, filter length if any and soil characteristics. Scour depth and location differ from one barrage to another according to operating conditions, local soil and geometric conditions. This local scour has a negative effect on the overall stability of the structures.

The purpose of this paper is to study the effect of high floods on Naga Hammadi Barrage scour hole. A mathematical model was used for scour analysis which is based on stream tubes concept to simulate the two-dimensional and three-dimensional effects. It is also used to simulate the response of the scour hole for different high floods with different duration. The calibration results showed close relationship between the measured and the predicted values. Different sediment approaches were used for the calibration analysis and they were compared to show the best approach for this study. Floods of 300, 350, 400, 500, and 600 million cubic meters per day were considered for this analysis and the flood duration ranged from one week up to four months. The average eroded thickness for the scour hole was computed for each case.

INTRODUCTION

Local scour involves removal of material downstream hydraulic structures, around piers, abutments, spurs, embankments and in curves. There are two mechanisms that are causing local scour downstream barrages;

- Local scour resulting from the flowing water due to the flow conditions and deficit of sediment which makes water tend to erode soil particles downstream the concrete flooring. In this case, the fluid characteristics can be described by Reynolds number and Froude number and sediment properties for non cohesive sediments which can be characterized by critical tractive force and the standard deviation. While for cohesive soils, a term of critical scouring velocity should be considered in addition (ASCE, 1975).

- Local scour due to the seepage downstream the barrage which enables seeping water under the flooring to carry soil particles and erode them downstream the flooring. The seepage analysis should be studied to determine the critical conditions for exit gradient to avoid piping and removing of soil particles. The factor of safety against piping is described by the ratio of the actual hydraulic exit gradient and the critical exit gradient at which the soil particles downstream the flooring start to move. There are many factors affecting the seepage forces under the flooring such as the head differences, flooring lengths, filter lengths, soil conditions and layers descriptions. Many studies are performed to measure, analyze the local scour downstream barrages in Egypt by the Nile Research Institute specially downstream Esna Barrage, Naga Hammadi Barrage and Assiut Barrage. An example of these studies is the analysis performed for Naga Hammadi Barrage, which describes and monitor the lowest point movements downstream the barrage and their effect on the barrage for the period from 1979 to 1996 (Aziz, Samuel, and Abdelbary, 1998) and a brief summary is given in this paper.

NAGA HAMMADI BARRAGE

Naga Hammadi Barrage was built during the period 1927-1930 about 359 km downstream Aswan Dam. It consists of 100 openings separated by 99 piers with a total length of 818 meters between abutments. These openings are 6 m wide and are numbered from 1 (at the west) to 100. It has a navigation lock on the western side of a length of 80 m and width of 16 m. The proposed new Naga Hammadi Barrage will have 7 openings each 17.0 m wide. Figure (1) shows the cross section of Naga Hammadi Barrage. The scour measurements are referenced to barrage center line in the horizontal direction. Scour downstream Naga Hammadi Barrage has been a continuing problem. Stones were dumped in the scour holes during the period from 1939 to 1978 and then a monitoring program was established on a regular basis. NRI (1990) concluded that the scour hole was becoming deeper and was not shifting nearer to the barrage. It also concluded that there was not overall shift towards or away from the barrage from 1979 to 1989. A description of Naga Hammadi scour hole is given in Table 1. This table shows the lowest levels for the scour hole during 1979, 1989, and 1996 surveys (Aziz, Samuel, and Abdelbary, 1998).

Table 1 Naga Hammadi Barrage scour hole

Year	Lowest Level (m)	Distance from C.L. of Barrage (m)
1979	49.0	123.93
1989	44.35	129.0
1996	46.5	131.5

THE EFFECT OF HIGH FLOODS ON NAGA HAMMADI BARRAGE

To study the effects of high floods on Naga Hammadi Barrage, flood conditions and scour hole responses have to be simulated using a suitable mathematical or physical model. In this study, the required analysis was simulated by using a mathematical model to overcome scale ratio difference problems such as sediment grain sizes and their motion according to different approaches. The mathematical simulation represents the actual dimensions of the study area and the bed materials.

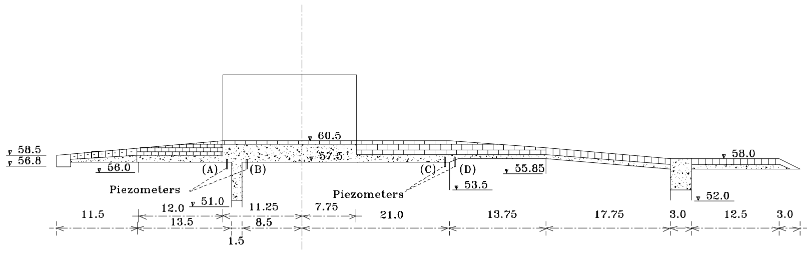

Figure (1) Naga Hammadi Barrage longitudinal section.

THE USED MODEL

In this study, the model GSTARS 2.000, which was developed by U.S. Bureau of Reclamation, 1998, was used for the analysis. The assumptions for this model and its capabilities are shown in the literature review. Flow pipes were used to simulate the three dimensional flow conditions to be able to study the changes in both the transverse and the longitudinal directions without facing the actual three-dimensional calibration difficulties. Figure (2) shows a brief description for the model. Different sediment motion approaches have been used for the model calibration such as:

- Meyer-Peter and Muller's method.
- Laursen's method.
- Toffaleti's method.
- Engelund and Hansen's method.
- Ackers and White's 1973 method.
- Yang's 1973 sand and 1984 gravel formulas.
- Yang's 1979 sand and 1984 gravel formulas.
- Parker's method
- Yang's 1996 modified method.
- Ackers and White’s method with the revised 1990 coefficients.

NAGA HAMMADI SCOUR HOLE MODEL CALIBRATION

The scour hole data for the period 1986 to 1989 were used to calibrate the mathematical modeling analysis. The 1989 data were predicted from 1986 data using the model according to:

- The actual flow discharges and water levels during this period,
- The geometry of the scour hole during 1986,
- The grain size distribution of the bed materials,
- Different sediment computing approaches, and
- The different roughness coefficients.

The predicted data were compared with the actual measured data to determine which sediment approach to be used and how close is the simulation using the model. The comparison of the different methods for the simulation showed that Yang's 1996 modified method is more suitable for the scour hole mathematical simulation. This method was used for the calibration and the prediction. Figure (3) shows an example of the comparison of some of these different approaches to predict one of the cross section in 1989 from 1986 data. Figures (4), (5) and 6 show the comparison of the scour hole cross sections in 1986, 1989, and the predicted 1989 using Yang’s approach. These cross sections are located at 99.00m, 139.00m, and 149.00m from barrage center line (the cross section locations are selected to represent the critical scour hole configuration). It is very complicated to predict the actual changes of the scour hole bed configuration because of many local factors, barrage operation rules, and local flow conditions. For this study, the different comparisons show close relationships between the actual parameters and the predicted parameters using the mathematical model.

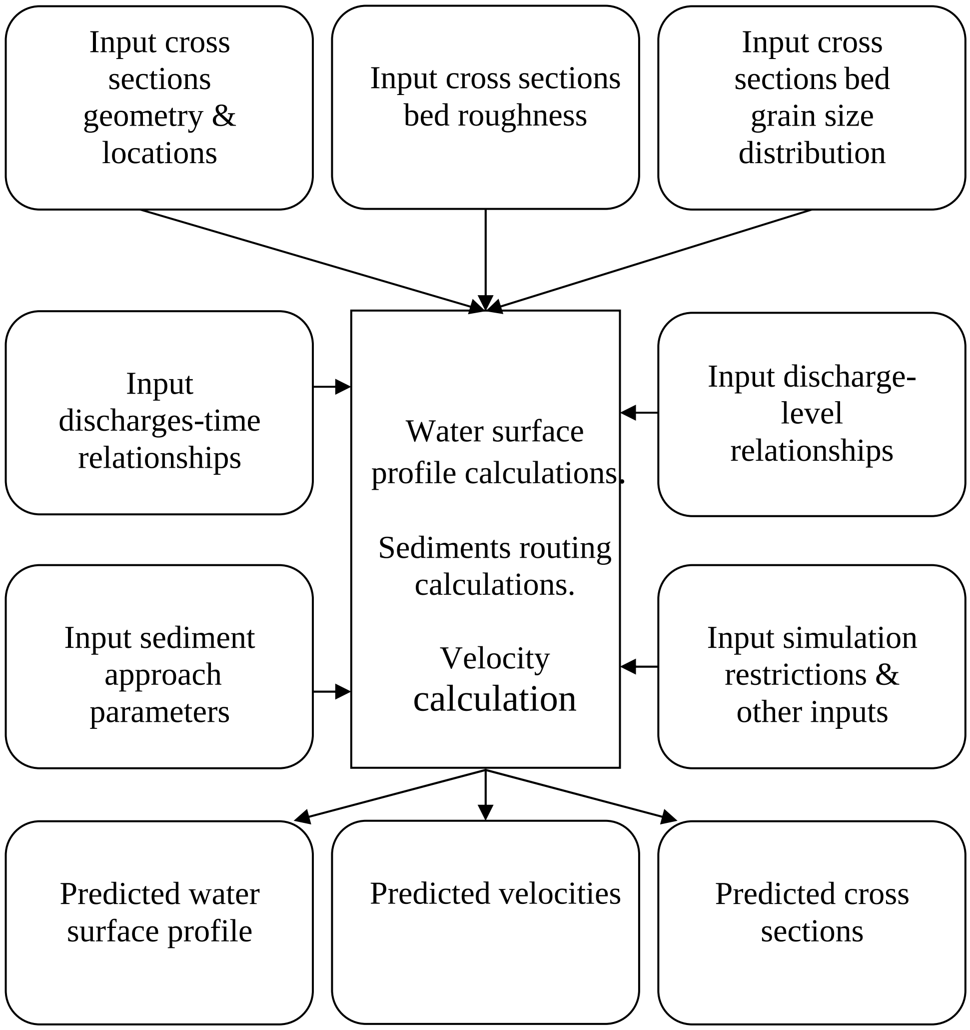

Figure (2) GSTARS 2.000 model brief description

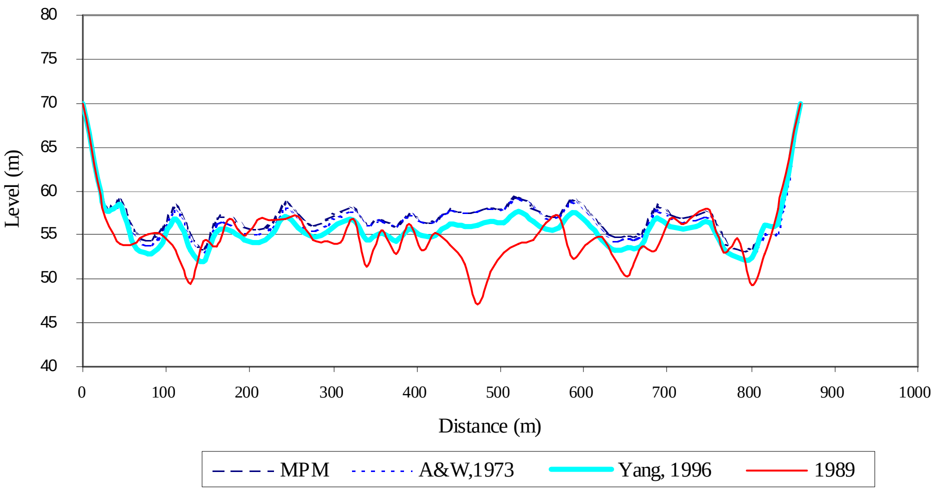

Figure (3) Some of sediment calibration approaches for cross section at distance 109.0 m from Naga Hammadi Barrage

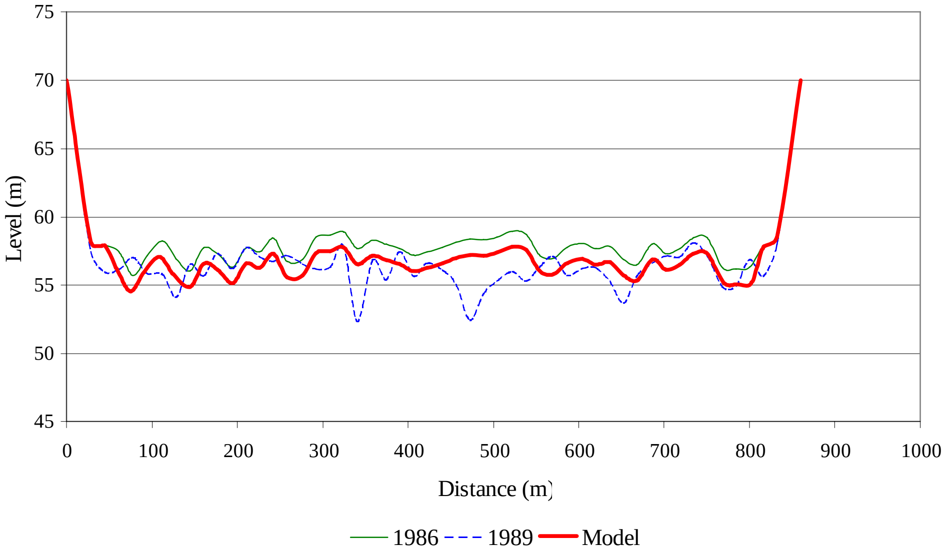

Figure (4) Model calibration for cross section at distance 99.0 m from Naga Hammadi Barrage center line.

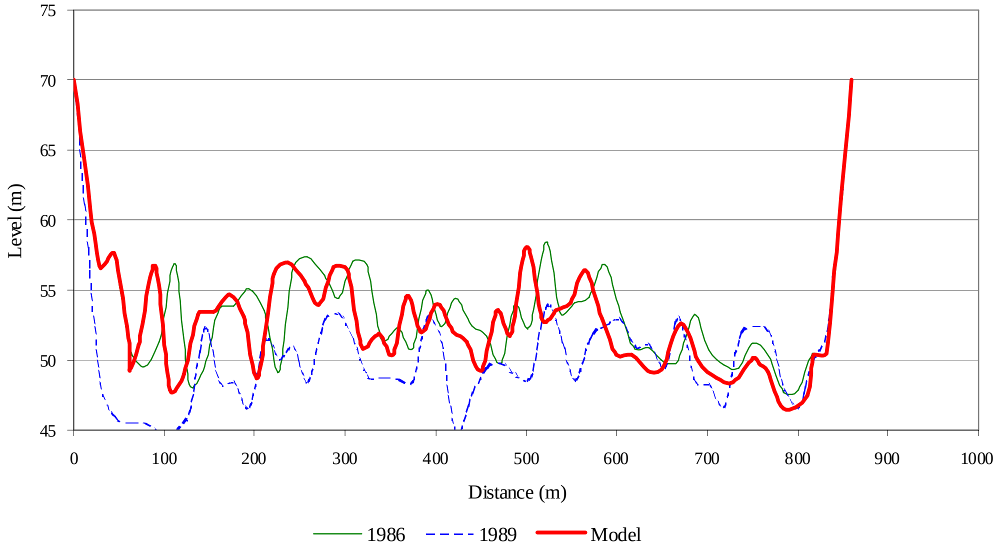

Figure (5) Model calibration for cross section at distance 139.0 m from Naga Hammadi Barrage center line.

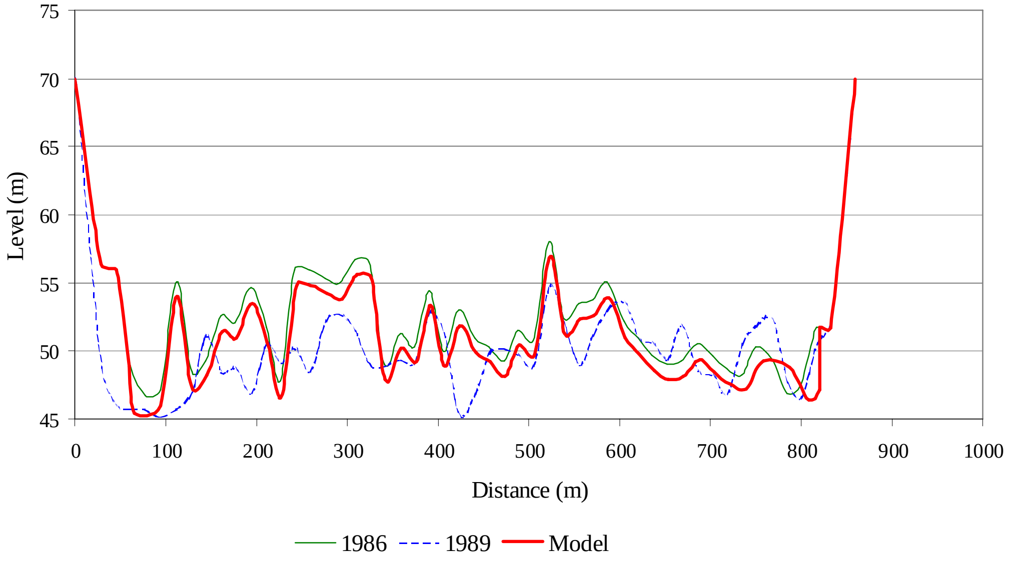

Figure (6) Model calibration for cross section at distance 149.0 m from Naga Hammadi Barrage center line.

NAGA HAMMADI BARRAGE FLOOD ANALYSIS

For the flood analysis, five different high floods were considered for this analysis:

- 300 million cubic meters per day,
- 350 million cubic meters per day,
- 400 million cubic meters per day,
- 500 million cubic meters per day, and
- 600 million cubic meters per day.

These different floods were simulated using the model, and their effect on the scour hole, were analyzed. The duration period for each flood was taken into consideration. For this study different flood duration periods were considered and simulated from one week and up to four months. The results of this analysis are shown on Figure (7) and Table 2. The figure and the table show the average eroded thickness for the scour hole for each flood during the simulation period. The average eroded thickness was selected for this research instead of the lowest point changes because of the following reasons:

- To reduce modeling errors for computation at certain point and increase the accuracy by computation for all points and using their average.
- The effect of the average depth drop on the stability of the barrage may cause more damages than the effect of only one point local scour. From Figure (7) and Table 2 it can be shown that the average eroded thickness is decreasing with the increasing of the flood duration, reaching stability conditions for the same flood and boundary conditions (Ismail, 2001).

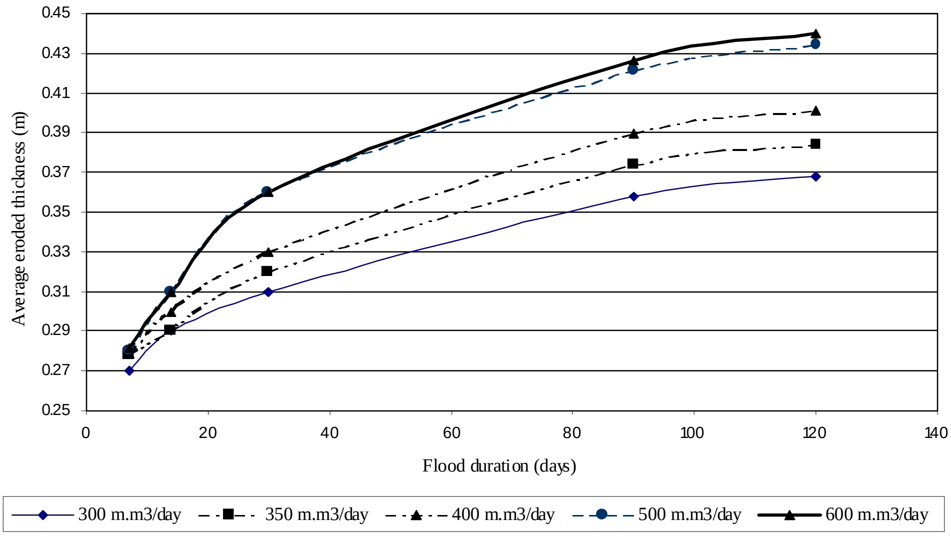

Figure (7) Average erosion prediction downstream Naga Hammadi Barrage for different floods and duration (Ismail, 2001).

Table 2 Average eroded thickness for Naga-Hammadi Barrage flood analysis

Flood Duration (Days)	300 (m.m^3/day)	350 (m.m^3/day)	400 (m.m^3/day)	500 (m.m^3/day)	600 (m.m^3/day)
7	0.27	0.28	0.28	0.28	0.28
14	0.29	0.29	0.30	0.31	0.31
30	0.31	0.32	0.33	0.36	0.36
90	0.36	0.37	0.39	0.42	0.43
120	0.37	0.38	0.40	0.43	0.44

CONCLUSIONS

Most of Egyptian Barrages are suffering from downstream local scour. To study the effect of high floods on Egyptian Barrages, these flood conditions and scour hole responses were simulated using the model GSTARS 2.000, which was developed by U.S. Bureau of Reclamation (1998). For this study, the different comparisons show close relationships between the actual and the predicted parameters using the mathematical model for Naga Hammadi Barrage. The results of the analysis of the average eroded thickness for Naga Hammadi Barrage show the following:

a) 300 million cubic meters per day flood:

The results range from 0.27 m for one-week flood period to 0.37 m for four-month flood period.

b) 350 million cubic meters per day flood:

The results range from 0.28 m for one-week flood period to 0.38 m for four-month flood period.

c) 400 million cubic meters per day flood:

The results range from 0.28 m for one-week flood period to 0.40 m for four-month flood period.

d) 500 million cubic meters per day flood:

The results range from 0.28 m for one-week flood period to 0.43 m for four-month flood period.

e) 600 million cubic meters per day flood:

The results range from 0.28 m for one-week flood period to 0.44 m for four-month flood period.

RECOMMENDATIONS

The recommendations for future studies can be summarized as follows:

- The collection of more calibration data are required in three dimensional models for local scour. This includes different velocity values in different directions and the most recent data about the bed grain size distribution.

- The continuous monitoring and design of suitable solutions for scour hole downstream hydraulic structures are very important to avoid critical conditions.

REFERENCES

1. ASCE, Sedimentation Engineering. ASCE Manuals and Reports on Engineering Practice-No. 54. pp. 745, 1975.
2. Aziz, M., M. Samuel, and M. Abdel Bary. Effect of Scour Holes on the Stability of Hydraulic Structures. pp. 1.7-1 1.7-7, Proceeding of Conference on Coping with Water Scarcity, Hurghada, August, Egypt, 1998.
3. NRI, Pre-feasibility Study of Development for Naga Hammadi Barrage, Nile Research Institute, National Water Research Center. El-Qanater, Egypt, pp. 130, 1990.
4. U.S. Bureau of Reclamation, “Gstars 2.000 Model Manual”, U.S. Bureau of Reclamation, Denver, Colorado. pp. 532, 1998.

مؤتمر الأزهر الهندسي الدولي الثامن

AL-AZHAR ENGINEERING
EIGHTH INTERNATIONAL CONFERENCE
December 24 - 27, 2004

Code: C43

DEVELOPING A PRECISE GEOID MODEL FOR HYDROGRAPHIC SURVEYING OF THE RIVER NILE

Gomaa Mohamed Dawod

Nile Research Institute National Water Research Center, Egypt

ABSTRACT

A national project is currently undergoing to update the hydrographic and topographic maps of the River Nile and its two branches. The utilization of GPS technology in hydrographic surveying has resulted in an increasing demand for precise geoid models in order to transform the GPS-based ellipsoidal heights to orthometric heights needed for mapping. Geoid undulations of 130 GPS/Levelling stations have been computed covering the fourth reach of the Nile from Assiut barrage to Delta barrage. Some recent global harmonic geopotential models, namely the PGM2000A and UCPH2002, have been analyzed, and it is found that the EGM96 model produce smaller undulation differences at the control stations. Consequently, a conversion surface has been constructed to model the short-wavelength uncertainties of EGM96. These irregularities range from -1.22 m to -0.49 m with an average value of -0.76 m over the study area. Hence, rectified geoidal undulations have been obtained for 482 GPS stations. Finally, a precise 50x50 m geoid model, named NILE2004, has been developed over the 408-km reach. The achieved results show that the external accuracy of the attained model over 30 check points, with known undulations, has a mean value of 0.02 m and a standard deviation equals 0.04 m. It can be concluded that the acquired model is the most precise one available in Egypt. Accordingly, it is recommended to apply the new geoid model in hydrographic surveying of the River Nile and all other mapping activities of the integrated water resources applications.

© 2004 Faculty of Engineering, Al-Azhar University, Cairo, Egypt. All rights reserved.

1. INTRODUCTION

Accurate and up-to-date hydrographic maps play a valuable role in the overall context of water resources management in Egypt. With the wide spread of GPS technology in surveying and mapping applications, the development of efficient geoid models becomes an essential demand. A precise geoid model converts the obtained GPS-based ellipsoidal heights to the orthometric height type utilized in civil engineering applications. Recently, few new global geoid models have been released and become available worldwide. Latest national geoid models are also reviewed and assessed. Detailed analysis of the performance of these models has been performed in order to obtain reliable measures of their accuracy estimates over Egypt. Based on new precise geodetic data sets, a new high-precision geoid model has been developed for the fourth reach of the Nile. Description of the utilized GPS/Levelling networks and the performed processing procedures are presented.

2. RECENT GLOBAL SPHERICAL HARMONIC GEOPOTENTIAL MODELS

Several global geopotential models have been developed and released in the last few years as a result of new satellite missions. Careful analysis of the data and objectives of these models reveals important information that should be kept in mind about their characteristics. Two models are briefed, and their performance over Egypt is given in the following sub-sections.

2.1 THE UCPH2002 MODEL

On July 2000, the German CHAPM (CHAllending Ministellite Payload) satellite was launched. It is in a near polar orbit about 450 km over the surface of the Earth. The satellite's scientific objectives include the mapping of the Earth's gravity field. Hence, the satellite carries an accelerometer which measures the non-conservative forces acting on it. The EGM96 to degree 24 was utilized, and the fast spherical collocation technique was used to estimate the spherical harmonic coefficients up to degree and order 90. The result is the UCPH2002 geopotential spherical harmonic model. The differences between EGM96 and UCPH2002 models exist in areas where it is known that for the determination of EGM96 very little data were used [6].

2.2 THE PGM2000A MODEL

The two years (1993-1994) mean Dynamic Ocean Topography (DOT) field was used to develop normal equations for DOT in a spherical harmonic representation. These normal equations were combined with normal equations from satellite tracking data, surface gravity data, and altimeter data from TOPEX/Posedon, and ERS-1. Several least-squares combination solutions were developed and the optimal solution designated as PGM2000A. The PGM2000A, up to degree and order 360, was developed mainly as a marine geoid to improve the marine geoid modeling of the EGM96 model [8].

2.3 PERFORMANCE OF GLOBAL GEOPOTENTIAL MODELS IN EGYPT

Several version of the UCPH2002 model have been modified. The UCPH2002_02_05 spherical harmonic coefficients have been obtained (http://www.gfy.ku.dk/~stenseng/sagrda/). The PGM2000A spherical harmonic coefficients have been obtained (http://bowie.gsfc.nasa.gov/926/pgm2000a/). The well-known Rapp's F477 computer program is used to compute gravitational quantities, mainly the geoid undulation, the gravity anomaly, and the two components of the deflection of the vertical, based on a specific set of spherical harmonic coefficients. Grids of geoid undulations of 5' x 5' spacing have been developed for both UCPH2002 and PGM2000A models, as depicted in figures 1 and 2 respectively. The grids cover the Egyptian territory as: $32^{o} <$ latitude $< 22^{o}$ and $37^{o} <$ longitude $< 25^{o}$. The statistical information of both models is tabulated in table 1. From these figures and tables, it can be seen that the UCPH2002-based undulations range from 7.38 m to 21.10 m with a mean of 14.84 m and

a standard deviation equals 2.80 m. For the PGM2000A model, the undulations range from 6.02 m to 21.95 m with a mean of 14.67 m and a standard deviation equals 2.99 m. A comparison has been performed for both models against the EGM96 model. The results of the undulation difference over Egypt are depicted in figures 3 and 4 and tabulated in table 2. From these figures and tables, it can be seen that the NUCPH2002-EGM96 undulation differences range from -5.23 m to 6.30 m with a mean of 0.21 m and a standard deviation equals 1.38 m. For the PGM2000A-EGM96, the undulation differences range from -0.09 m to -0.12 m with a mean of -0.11 m and a standard deviation equals 0.01 m. Also, the figures show that the differences mainly concentrated along the coastal regions and the western desert. Again, it should be kept into considerations that both models are primary modifications of the EGM96 one to improve its marine geoid capabilities. It is a matter of reality that almost all global geopotential models do not include surface gravity data in Egypt, and therefore, they do not depict the short wavelength of the national gravity field. Another comparison is performed to justify the performance of the global geoid models in the study area as presented in the following sections.

Table 1. Statistics of global geopotential models undulations over Egypt.

	N_{EGM96}	$N_{UCPH2002}$	$N_{PGM2000A}$
Minimum (m)	6.14	7.38	6.02
Maximum (m)	22.03	21.10	21.95
Mean (m)	14.63	14.84	14.67
Standard Deviation (m)	2.98	2.80	2.99

Table 2. Statistics of global geopotential models undulations differences over Egypt.

	$N_{UCPH2002} - N_{EGM96}$	$N_{EGM96} - N_{PGM2000A}$
Minimum (m)	-5.23	-0.09
Maximum (m)	6.30	-0.12
Range (m)	11.51	0.03
Standard Deviation (m)	1.38	0.01

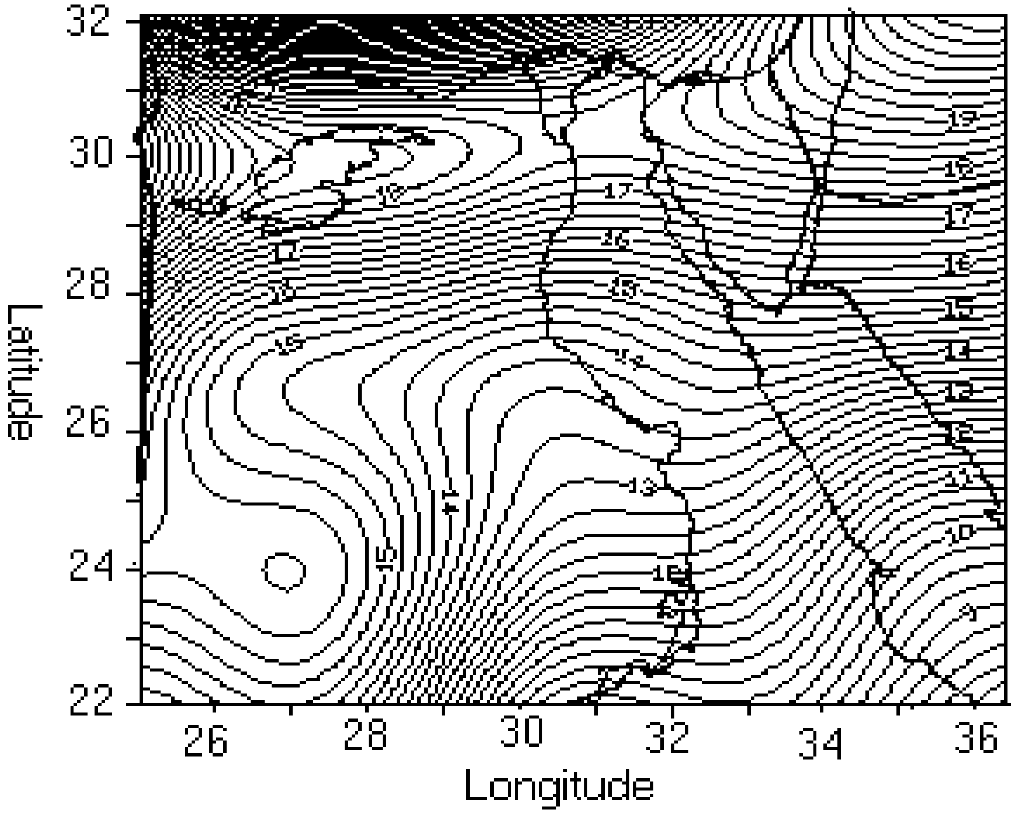

Fig. 1. The UCPH2002 Global Geoid Model .

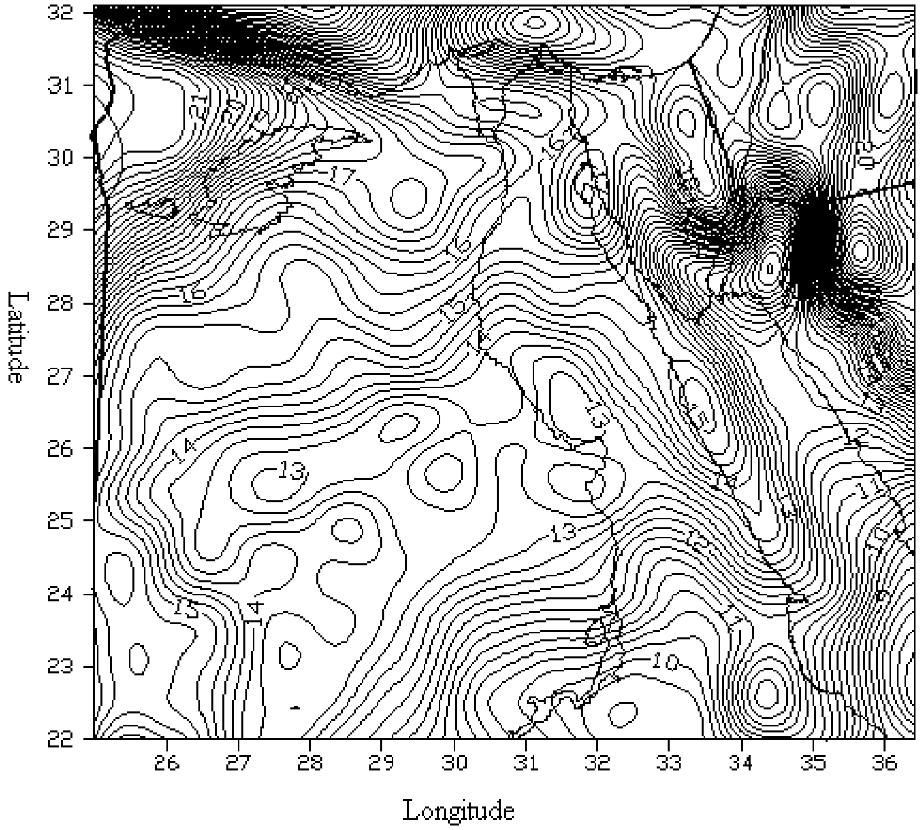

Fig. 2. The PGM2000A Global Geoid Model.

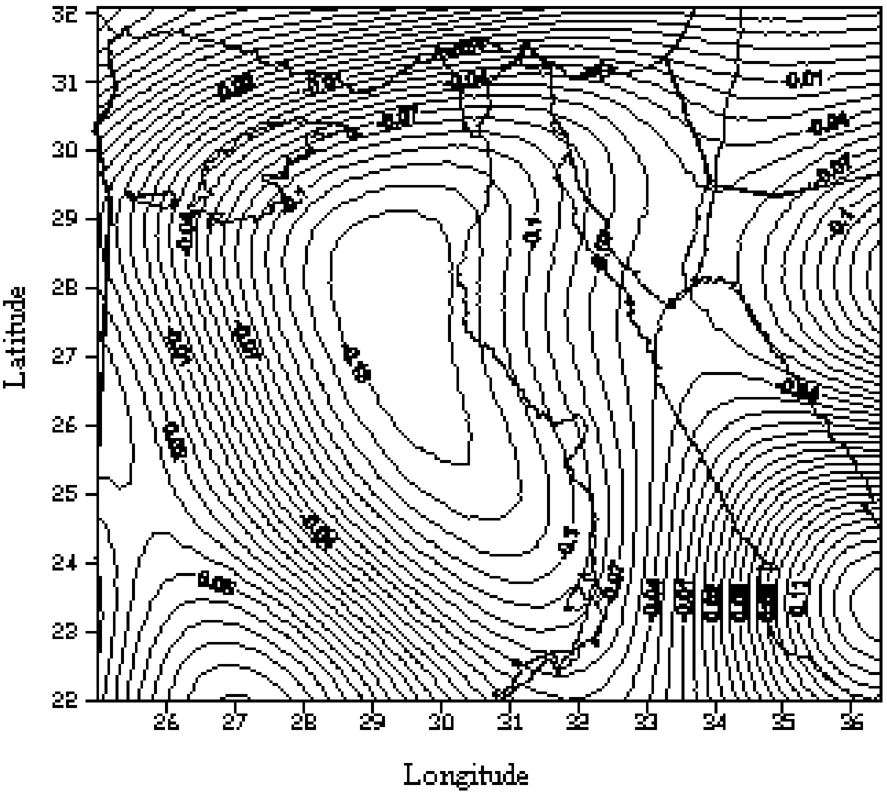

Fig. 3. Undulation differences PGM2000A – EGN96 .

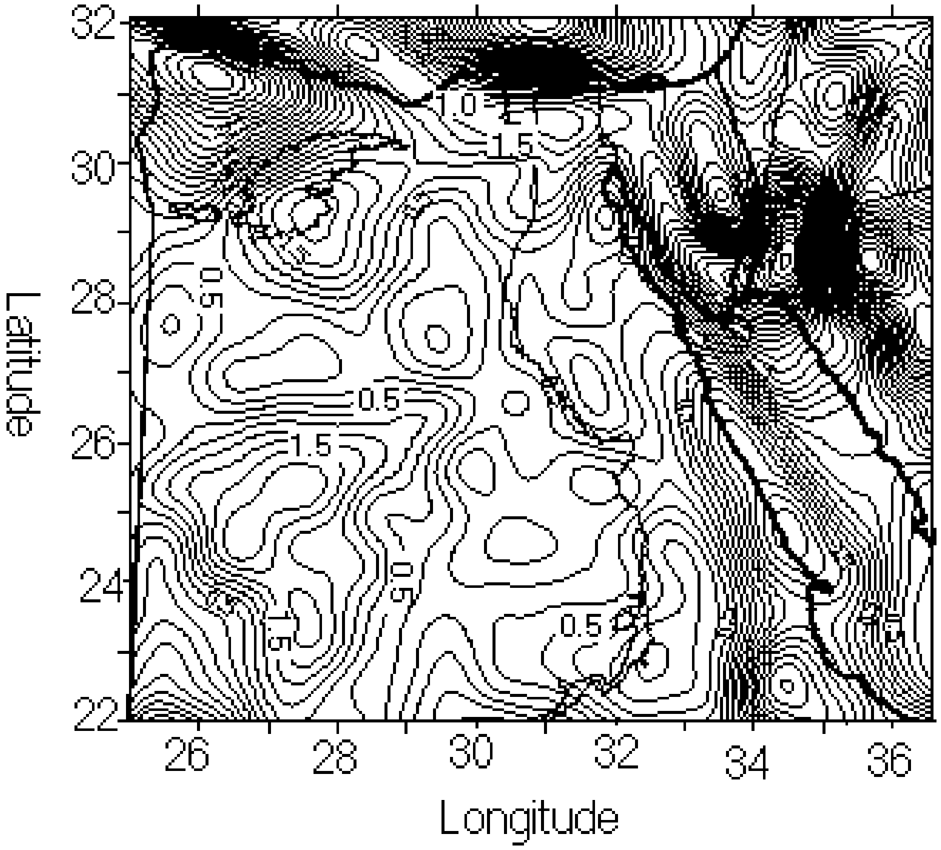

Fig. 4. Undulation differences EGM96 - UCPH2002.

3. RECENT NATIONAL GEOID MODELS IN EGYPT

Saad and Dawod [9] developed two precise geoid models for the entire Egyptian territory. The first geoid, called SRI2001A, is a gravimetric geoid model utilizing the most recent and accurate first-order gravity measurements, and is based on the GRS80 reference datum. The EGM96 global geopotential spherical harmonic model is used to provide the long wavelength of the Earth gravitational field, along with a local DEM in the remove-compute-restore FFT processing technique. The obtained geoid undulations range from 5.42 m to 22.40 m with a mean value of 14.54 m and RMS equals 2.96 m. A GPS/Levelling data set of 195 precise stations has been used to generate a geometric-satellite geoid model. A second-order polynomial as a function of the distance from the network origin is found to be the best fitting function to integrate gravimetric undulations and GPS/Levelling undulations. Therefore, a combined GPS/Gravity geoid for Egypt, SRI2001B, has been generated. This geoid model, depicted in Figure 5, has a minimum undulation value of 9.437 m and a maximum value of 21.39 m with an average of 13.623 m and RMS of 2.62 m. The values of the estimated undulations from the SRI2001B model have been compared against the pure GPS undulation of some independent GPS/Levelling stations. The differences range between –0.01 m and –0.28 m, with an average equals –0.10 m, and RMS of 0.49 m.

Abdel-Motaal [1] developed a gravimetric geoid for Egypt using 1D-FFT technique and the EGM96 geopotential model. Moreover, this geoid was fitted to GPS-derived geoid through removing a Krigging (collocation) trend function. The undulation difference at a single GPS check point was estimated as 9.2 cm. However, it has been noticed that the GPS stations utilized in the fitting are those of the High Accuracy Reference Network (HARN) established by the Egyptian Survey Authority (ESA). Even though the HARN network is the most precise GPS framework in Egypt, almost half of its stations, especially those located in the Western desert, do not have observed orthometric heights. Hence those stations can not be an optimum set of geodetic data to be used in geoid modeling.

Hassouna [5] developed a 2'x2' national geoid model for Egypt utilizing heterogeneous geodetic data and a developed 30"x30" digital elevation model. The EGM96 global geopotential model was first tailored to the local data, and a new version was developed up to degree and order 650 in order to account for the local topographic signals. Over several GPS check points, this gravimetric geoid produced undulation differences ranging from -2.76 m to 3.23 m, with a mean value of -0.28 m and a standard deviation equals 1.25 m. Furthermore, this geoid solution was fitted to a GPS-based geoid model. The obtained national combined geoid gave geoid undulations range from 5.46 m to 22.70 m with a mean value of 14.34 m. Over check points, the undulation differences range from -0.39 m to 0.93 m, with a mean value of 0.07 m and a standard deviation of 0.27 m.

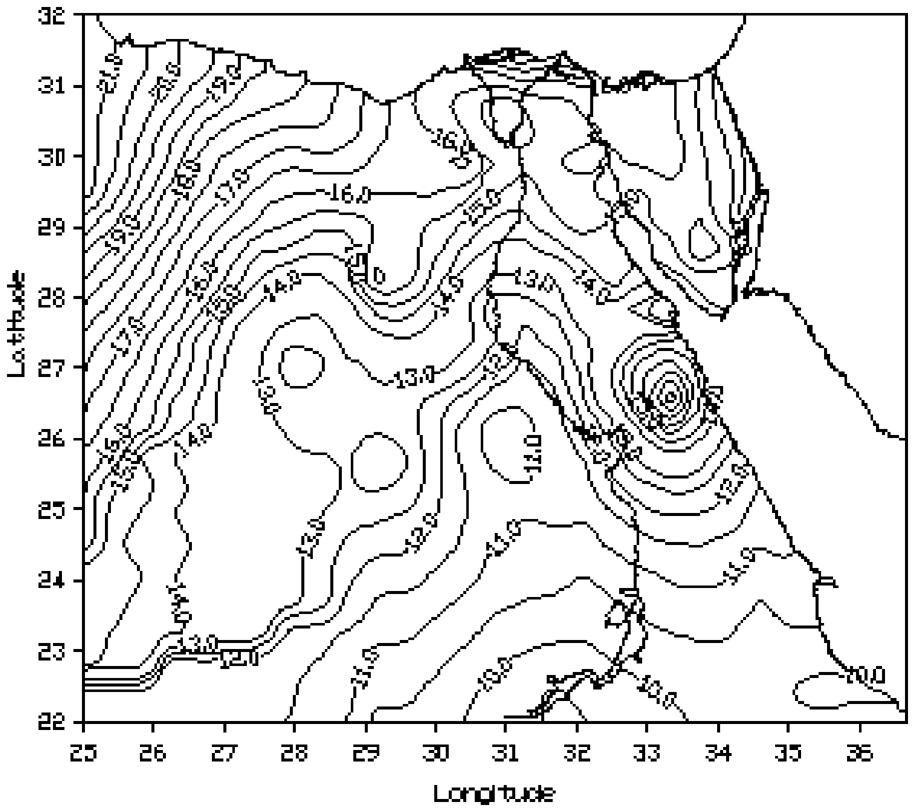

Fig. 5. The SRI2001B National Geoid Model.

4. HYDROGRAPHIC SURVEYING OF THE NILE

Hydrographic and topographic maps play a crucial role in the management of water resources. Since the Nile constitutes the main source of fresh water in Egypt, its precise maps are a key element in the context of integrated water resources management policy. The existing hydrographic maps of the Nile have been produced by Kenting Earth Science Ltd Co. in 1982. In order to study the recent morphological and hydrological changes of the Nile, the Nile Research Institute (NRI) has initiated a four-year national project to produce precise digital hydrographic and topographic maps covering the river and its two branches. The project consists of the following components:

- Conducting 1:15,000 aerial photography for the area of study, that is approximately 4,000 square kilometers.
- Production of 1:5,000 digital topographic maps, covering 1 km from each bank of the Nile. The maps show contours with a 0.5 m interval, which implicitly require dense terrestrial levelling measurements.
- Performing hydrographic surveys to represent the river relief with the same contour interval.

The main core of this pioneer project is a multi-fold precise geodetic control network utilizing the state-of-the-art GPS instrumentation and techniques. The network consists of approximately 600 control stations spacing 5 km apart on both banks of the Nile, which is almost 1435 km long. Orthometric heights of all control stations will also be determined. Unique national standards and specifications of GPS geodetic control networks have been developed and applied in this project [3]. It is anticipated that this network will improve the reliability, availability, and integrity of the national geodetic networks, and have a great economical impact on surveying and mapping activities in Egypt, particularly for water resources management.

5. AVAILABLE DATA

Two GPS control network have been established on both banks along the forth reach of the Nile, that is from Delta barrage to Assiut barrage extending about 408 km. The main network, depicted in Figure 6, constitutes the overall geodetic framework in the study area, and consists of 168 control points. Among this network, 130 stations have observed orthometric heights, which station separation ranges from 0.2 km to 9.2 km with an average equals 5.7 km. The network has been observed and processed in the optimum way to insure the quality and reliability of precise geodetic control networks. It has been tied to the HARN national network through 16 tie stations. Precise ephemeredes have been utilized in the baselines' processing stage among other designed standards [ibid]. The secondary network consists of 482 stations, which their orthometric heights are needed. The station separation ranges from 0.2 km to 7.3 km with an average equals 2.4 km. The networks' statistics are summarized in Table 3.

To continue the judgment of the recent global geopotential models and their performance in Egypt (as discussed in previous section), the GPS/Levelling stations have been employed. Geoidal undulations values of the EGM96, PGM2000A, and UCPH2002 models have been computed for the 130 stations. The obtained results are tabulated in table 4. From this table, it can be seen that the observed undulations range from 12.68 m to 15.52 m with a mean value of 14.27 m and a standard deviation equals 0.90 m. The EGM96 model produces undulation estimates ranging from 13.23 m to 16.05 m, with an average equals 15.04 m and a standard deviation of 0.97 m. Moreover, the PGM2000A model gives undulations range from 13.33 m to 16.14 m with a mean value of 15.15 m and a standard deviation equals 0.96 m. Additionally, the UCPH2002 model produces undulation estimates ranging from 14.07 m to 17.64 m, with an average equals 15.94 m and a standard deviation of 1.26 m.

Furthermore, the computed undulations have been compared against the known values over the GPS/Levelling stations. The obtained results are tabulated in table 5. From this table, it can be seen that the EGM96 model produces undulation differences ranging from -1.22 m to -0.49 m, with an average equals -0.76 m and a standard deviation of 0.22 m. On the other hand, the PGM2000A model gives undulation differences range from -1.33 m to -0.59 m with a mean value of -0.86 m and a standard deviation equals 0.22 m. Additionally, the UCPH2002 model produces undulation differences ranging from -2.91 m to -1.09 m, with an average equals -1.66 m and a standard deviation of 0.47 m.

Table 3. Statistics of available geodetic data.

	GPS Control Networks		GPS/Levelling Stations
	Primary	Secondary	
No. of stations	168	482	130
Minimum distance (km)	0.2		0.2
Maximum distance (km)	7.3		9.2
Mean distance (km)	2.4		5.7

Table 4. Statistics of geoidal undulations at GPS/Levelling stations.

	N_{obs}	N_{EGM96}	$N_{UCPH2002}$	$N_{PGM2000A}$
Minimum (m)	12.68	13.23	14.07	13.33
Maximum (m)	15.52	16.05	17.64	16.14
Mean (m)	14.28	15.04	15.94	15.15
Standard Deviation (m)	0.90	0.97	1.26	0.96

Table 5. Statistics of geoidal undulation differences over GPS/Levelling stations.

	$N_{obs} - N_{EGM96}$	$N_{obs} - N_{UCPH2002}$	$N_{obs} - N_{PGM2000A}$
Minimum (m)	-1.22	-2.91	-1.33
Maximum (m)	-0.49	-1.09	-0.59
Mean (m)	-0.76	-1.66	-0.86
Standard Deviation (m)	0.22	0.47	0.22

From both tables, it can be concluded that all these global harmonic geopotential models do not represent the actual gravity field in the study area. This is due to the fact that most global models do not include much of the Egyptian terrestrial geodetic measurements. However, on a comparative basis, it can be noticed that the EGM96 produced less undulation differences in the study area, and then it can be concluded that it is still the "best" global geoid model. Similar results have been obtained by other researchers using other geodetic data sets [e.g. 5]. However, it worth mentioning that the estimated accuracy of the EGM96 model is of the order of 0.50 m [7], and it should not be considered as an alternative geoid model for surveying activities in Egypt.

6. DEVELOPMENT OF A GEOID MODEL OF THE RIVER NILE

As stated in the previous section, it has been realized that the EGM96 is still the best global geoid model to represent the long wavelength of the gravitational field in Egypt. Therefore, it has been decided to model the irregularities between its geoid undulations and the observed estimates at GPS/Levelling stations in the study area. Firstly, a simple linear function (in terms of a bias and two tilt parameters) has been performed. The coefficient of determination, as a statistical tool, is the indicator of how much of the variability in the dependant variable is explained by the independent variables used in the regression formula. The planner coordinates (Easting X and Northing Y) have been computed for all stations based on the Modified Transverse Merecator (MTM) national map projection as defined by the Egyptian Survey Authority (ESA). It has been found that the coefficient of determination of such a linear function equals 45%. Consequently, it can be concluded that a simple polynomial is not able to fit the irregular structure of the undulation differences.

The second procedure is to use the kriging (collocation) technique to model the undulation differences and develop a correction surface. Kriging is a geostatistical gridding method that has proven useful and popular in many fields, especially in producing maps from irregularly spaced data. Kriging attempts to express trends suggested in a specific data set by utilizing the spatial and temporal correlation properties of the underlying phenomenon and incorporating the measures of the error and uncertainties when determining the estimates. The mathematical principle underlines kriging is the variogram, which is a measure of how quickly things change on the average. The primary hypothesis is that, on the average, two observations closer together are more similar than two observations farther apart. Because the underlying processes of the data often have preferred orientations, values may change more quickly in one direction than another. As such, the variogram is a function of direction. Details of kriging and variogram modeling can be found in several literatures [e.g. 2]. The linear variogram, for example, takes the form [ibid]:

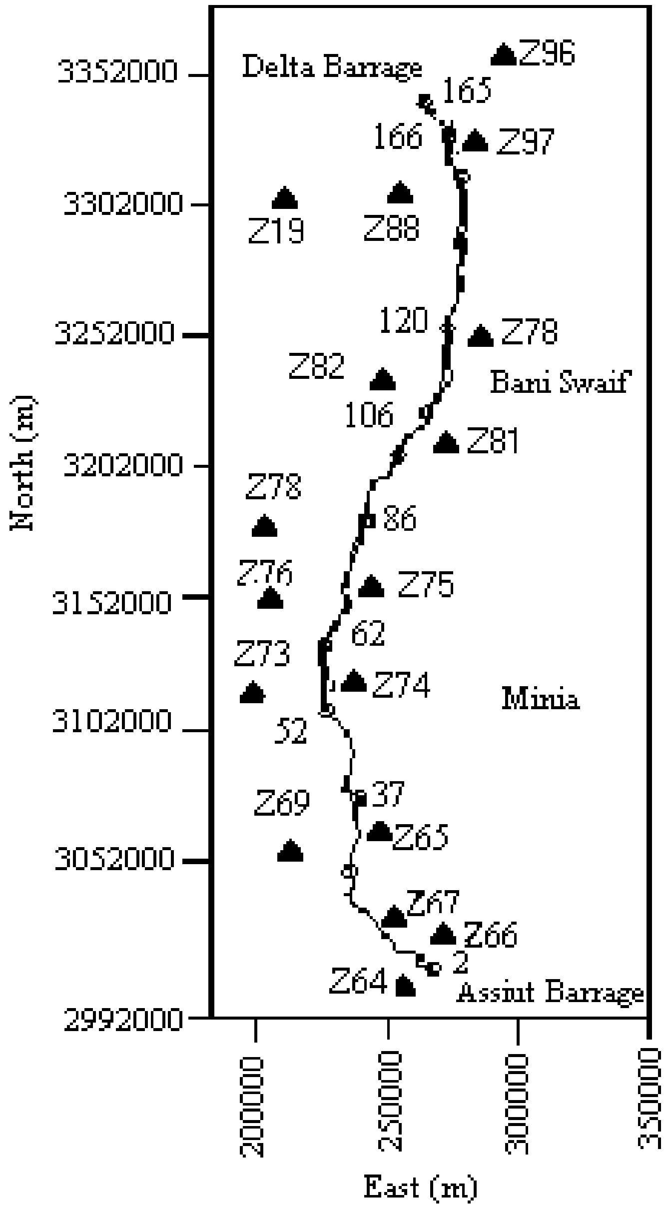

Fig. 6. The main GPS network.

$$g(h) = C_o + S\,h \quad (1)$$

Where C_o is the unknown nugget effect and S is the unknown slope. We need two defining equations to solve for these two unknown parameters. According to theory, the expected value of the sample variance is the average value of the variogram between all possible pairs of sample locations; this yields one equation. The second equation is generated by equating the experimental sample variogram for nearest neighbors to the modeled variogram. Thus, it can be written:

$$Var = C_o + S\,D_{avg} \quad (2)$$

$$G_{nn} = C_o + S\,D_{nn} \quad (3)$$

where,

D_{nn} is the average distance to the nearest neighbor
D_{avg} is the average inter-sample separation distance
G_{nn} is one half of the averaged squared differences between nearest neighbors
Var is the sample variance

By solving equations (2) and (3) for the two unknown parameters, the final formulas are:

$$S = \max ([(Var - G_{nn})/(D_{ave} - D_{nn})] , 0) \quad (4)$$

$$C_o = \max ([(G_{nn} * D_{avg} - Var * D_{nn})/(D_{ave} - D_{nn})] , 0) \quad (5)$$

The kriging approach has been recently utilized in similar geodetic situations [e.g. 1, 4, and 10]. Its principal advantage is the usage of more complicated mathematical models, rather than a linear function, to achieve the optimum fitting of irregular scatter quantities over the area of interest. Accordingly, a correction or conversion surface has been developed to fit the undulation differences on a 50 x 50 meter grid. This surface has a minimum value of -1.22 m and a maximum value of -0.49 m with an average of -0.75 m and a standard deviation of 0.19 m. In order to judge the external quality of the correction surface, the interpolated undulation differences have been compared against the known values at the 30 check points. The obtained results, as tabulated in Table 6, range from -0.04 m to 0.11 m with a mean of 0.02 m and a standard deviation of 0.04 m.

Table 6. Statistics of the correction surface.

	Minimum	Maximum	Mean	Standard Deviation
The correction surface undulation differences (m)	-1.22	-0.49	-0.75	0.19
Undulation errors of the correction surface at check points (m)	-0.04	0.11	0.02	0.04

Hence, a final correction surface has been produced utilizing all available data at the 130 GPS/Levelling stations. The accuracy of this surface may be considered better than 0.04 m. The final step is to interpolate undulation differences from the obtained correction surface at the secondary GPS network in order to rectify their EGM96-based geoidal heights. Hence, a precise geoid model, named NILE2004, is obtained covering the fourth reach of the River Nile and is applied in the undergoing project of hydrographic surveying.

7. CONCLUSIONS

As a component of the undergoing project of updating the hydrographic and topographic maps of the Nile, a GPS control network have been established on both banks along the forth reach of the Nile with an average station separation equals 2.4 km. Ellipsoidal and orthometric heights have been determined for 130 control stations in the established 650-station network.

A comparison has been performed to justify the performance of some recent global geoid models, namely the PGM2000A and UCPH2002, in the study area. Geoidal undulations values of these models have been computed for 130 GPS/Levelling stations. The obtained results show that the EGM96 model produces less undulation differences in the study area, and then it can be concluded that it is still the “best” global geoid model. Therefore, it has been decided to model the irregularities between its geoid undulations and the observed estimates at GPS/Levelling stations in the study area. It has been concluded that a simple polynomial is not able to fit the irregular structure of the undulation differences. Thus, a correction or conversion surface has been developed to fit the undulation differences. The obtained results show that the accuracy of this surface is better than 0.04 m. Hence, a

precise geoid model, called NILE2004, is obtained covering the fourth reach of the River Nile and is applied in the undergoing project of hydrographic surveying. It can be concluded that the attained geoid model is the most precise one available in Egypt. Accordingly, it is recommended to apply the new geoid model in all surveying and mapping activities of the integrated water resources applications.

ACKNOWLEDGMENT

Special acknowledgments are given to Prof. Dr. Abd-Allah A. Saad, Shobra faculty of Engineering, Zagazig University, for his stimulating discussions and invaluable assistance.

REFERENCES

[1]. Abdel-Motaal, H., "Towards a precise geoid for Egypt", The IAG Third meeting of the International Gravity and Geoid Commission, Greece, Aug. 26-30, 2002.

[2]. Cressie, N., "Statistics for Spatial Data", John Wiley and Sons, Inc., New York, 900 pp,1991.

[3]. Dawod, G., and Abdel-Aziz, T., "Establishment of precise geodetic control networks for updating the River Nile maps", Proceedings of Al-Azhar Engineering Seventh International Conference (CD No. 3), Al-Azhar University, Cairo, April 7-10, 2003.

[4]. Fotopoulos, G., Featherstone, W., and Sideris, M., "Fitting a gravimetric model to the Australian height datum via GPS data", The IAG third meeting of the International Gravity and Geoid Commission, Greece, Aug. 26-30 , 2002.

[5]. Hassouna, R., "Modelling of outer gravity field in Egypt using recent available data", Ph.D. dissertation, Menoufia University, 2003.

[6]. How, E., Stenseng, L., and Tscherning, C., "Analysis of one month of CHAMP state vector and accelerometer data for the recovery of the gravity potential", *Advances in Geosciences*, No. 1, pp. 1-4, 2003.

[7]. Lemoine, F., Kenyon, S., Factor, J., Timmer, R., Pavils, N., Chinn, D., Cox, C., Rapp, R., and Olsen, T., "The development of the joint NASA GSFC and NIMA geopotential model EGM96", *NASA Technical Publication NASA/TP-1998-206861*, Goddard Space Flight Center, USA, 1998.

[8]. Pavils, N., Chinn, D., Cox, C., and Lemoine, F., "Geopotential model improvements using POCM4_B dynamic ocean topography information: PGM2000A", Presented at TOPEX/JASON science working team meeting, Miami, Florida, November, 2000.

[9]. Saad, A., and Dawod, G., "A Precise integrated GPS/Gravity geoid model for Egypt", *Civil Engineering Research Magazine (CERM)*, Al-Azhar University, V.24, No. 1, pp.391-405, 2002.

[10]. Wielgoz, P., Grjner-Brzezinska, D., and Kashani, I., "Regional ionospheric mapping with krigging and multiquadric methods", *Journal of Global Positioning System*, V.2, No.1, pp. 48-55, 2003.

FIRST
AIN SHAMS UNIVERSITY INTERNATIONAL CONFERENCE
ON
ENVIRONMENTAL ENGINEERING

April 9-11 2005

ASSESSMENT AND MODELLING OF SEA LEVEL RISE AND METROLOGICAL CHANGES IN EGYPT

Gomaa M. Dawod[1], Mamdouh M. Meligy[2], and Hoda F. Mohamed[1]

[1] Survey Research Institute, National Water Research Center, Cairo
TelFax: 02-5867174 E-Mail: dawod_gomaa@yahoo.com
[2] Marin Survey Department, Egyptian Naval Forces, Alexandria

ABSTRACT

Evaluating and formulating the rising rates of sea level and metrological parameters is a fundamental demand from engineering and environmental points of view. Daily tidal records and various metrological observations, at Alexandria, have been collected and analyzed covering the period from 1985 to 2003. The attained results show that the main metrological factors affecting the sea level rise are the air temperature, air pressure, and wind speed with correlation factors equal 0.60, -0.39, and -0.23 respectively. A relatively small relationship has been found between the sea level variations and the solar activities, as represented by the sun spot number. Additionally, it has been concluded that the 6th-order polynomial function, among five investigated types of mathematical formulas, is the optimum model describing the relationship between the sea level and the metrological parameters. Moreover, the annual rising rates of the studied quantities have been estimated as 0.20 cm/y for sea level, 0.04 ^{o}C/y for air temperature, -0.03 mb/y for air pressure, 0.05 knot/y for wind speed, and 1.07 y^{-1} for the number of sun spots. The sea level rise is one of the main elements that cause shoreline retreat and coastal erosion. Hence, it is recommended that the sea level rise should be taken into consideration in national development planes, particularly for coastal regions.

KEYWORDS: Sea level rise, Metrological changes, Tide gauge

INTRODUCTION

Measurements of sea level have a long history in several places all over the world, and have been utilized in a wide variety of scientific applications. Changes in the mean sea level are related to the changes in the volume of water in the oceans and to variations in the ocean currents. Sea level studies, in nowadays, concern with coastal erosion and protection, geological processes, and climate changes. Glacial melting, expansion of water due to heating, and changes in sea surface gradients are some factors leading to sea level change. This paper aims to investigate the relationship between the sea level changes and metrological variations in Egypt from both environmental and geodetic points of view.

The sea level rise is one of the main factors that cause shoreline retreat, coastal erosion, lowlands overflow, and increase the salinity of lakes and aquifers. Consequently, there exists a critical demand to explore, on geodetic and environmental basis, the consequences of sea level changes in Egypt. Moreover, an accurate multi-purpose monitoring system has to be established, over the Egyptian shores, to measure precisely the sea level rise.

GLOBAL SEA LEVEL RISE

The combination of sea level changes measured by several techniques shows a relatively rapid rise of sea level from 20,000 years ago, gradually slowing down 8,000 years ago when levels were some 15 meters below those of today. The increase then proceeded more gradually until present levels were reached some 4,000 years ago. Since that time, the changes have consisted of oscillations of small amplitude. Recent long-period sea level measurements at several stations show that there is a general increase of Mean Sea Level (MSL) of about 0.15-0.25 meter per century [e.g. IOC, 2002]. MSL is the average level of the sea, usually based on hourly values taken over a period of at least a year. The major effective causes for long-periodic sea level oscillations are [Vanicek and Krakiwsky, 1986]:

- Glacial melt is the main constitute of the secular water rise.
- Changes due to atmospheric pressure that may reach up to several decimeters.
- Changes due to wind stress, which could reach a few decimeters in some places.
- Thermal structure of sea water is an important source of long periodic changes.
- River discharge fluctuations can contribute significantly to long-term variations.

The issue of sea level rise has attained more concerns on a global base in the last few years. From a developmental point of view, the harmful effects of sea rise, especially in coastal areas, raise the attention to carry out detailed studies on this subject. Long-term tidal records may contribute significantly to precise determination of sea rise rate. It is evident that the sea rise rate on a global scale during the twentieth century has an average of 1.5-2.5 mm/year [IOC, 2002, and NOAA, 2001]. These real estimates are derived from analysis of actual long-term tide gauge data all over the world. On the other hand, other studies claim that the rising rate will be much higher in the next few decades and will lead to hazardous economical troubles [IPCC, 2001]. Most of these investigations are based on different scenarios and estimates of the air temperature rise due to the global warming phenomena. For example, recent environmental researches, based on business-as-usual scenario of greenhouse gas emission, expect that the sea rise on a global scale would be of 12 cm by the year 2030 and about 50 cm by the year 2100. This implies that the sea level rising rate would be doubled in the twenty-first century compared to the real rising rate of the twentieth century. Other expectations lead to a sea level rise of about 2 meters by the year 2100 when taken into

account the subsidence because of land movements and removal of ground water. However, it worth mentioning that many of these estimate has a great deal of uncertainties due to their extrapolation nature and suspected assumptions [Houghton, 1997]. Moreover, the sea level rise would differ from an area to another on the globe due to the different nature and amount of the leading factors such as the human and industrial activities. Therefore, the optimum realistic estimates of sea rise should result from analysis of real data sets, particularly long-term tidal records.

Meteorological residuals are the non-tidal part that remains after removing the tides by analysis. They are irregular, as are the variations in the weather. The term “surge residuals” is commonly used to describe non-tidal variations in the observed sea level. Physically, the atmosphere acts on the sea in two different manners. Changes in atmospheric pressure produce changes in the pressure acting vertically on the sea surface. One-millibar increase of atmospheric pressure decreases sea level by one centimeter. The drag of the wind on the sea surface increases as the square of the wind speed, to a first approximation. This drag sets the water in motion, where in shallow water the flow is in the direction of the wind, and in deeper water the transport is at right angles to the right in the Northern Hemisphere.

RECENT SEA LEVEL OBSERVING SYSTEM IN EGYPT

Although there are several agencies in Egypt operate measuring equipment for determining sea level changes, most of them suffer from several disadvantages in terms of structure, accuracy, and compatibility. For example, the installed out-of-date floating devices are not accurate enough to produce reliable results or estimates for the sea level rise rate. Additionally, there is no distinguishing between the relative and the absolute sea-level rise in these projects. Moreover, most of these activities are designed for a specific goal serving a specific area, with no national interest in mind.

The Survey Research Institute (SRI) has installed the recent state-of-the-art Sea Level Observing System (SLOS), inside the headquarter of the Naval Forces in Alexandria. That tide gauge station has been constructed and operated, by the hydrographic survey department, since 1993 for military marine applications. The gauge contained an old mechanical float-gauge device and several separated sensors for measuring meteorological conditions. This gauge station is located in the Western harbor, 800 meters north-west of the old tide gauge station operated by the Alexandria harbor authority. A precise levelling line has been carried out to connect the gauge staffs in both stations. Consequently, the constant datum shift was obtained and used, in later processing stages, to relate the tide readings of the new station to the old historical one. The research project has several objectives to fulfill both geodetic and environmental goals including among others (SRI, 2002):

- Precise monitoring of the sea-level rise in Egypt.
- Accurate realization of the vertical geodetic datum in Egypt.
- Studying the meteorological effects on the sea-level data.
- Development of computer strategy and models to re-define the vertical datum.
- Develop optimum models for meteorological effects on levelling measurements.

The new installed state-of-the-art SLOS consists of three devices integrated together in a unified scheme: a tide gauge, a meteorological unit, and a satellite-based GPS geodetic receiver (Figure 1). The utilized tide gauge is a high-accuracy temperature-compensated self-contained instrument for measuring and recording tide and wave data. This state-of-the-art

device, called Wave and Tide Gauge WTG904 Series 3, is a semi-conductor strain gauge pressure type that measures instantaneously the water column pressure, and converts it to height of water with respect to a specific user-defined location. The WTG904' measuring precision is ± 0.2 cm, and the tide is calculated continuously and recorded automatically every 10 minutes. The second device in this integrated system is the WMS-14 from Omega Inc., which is a microprocessor-based weather station. It features a combination wind vane and three-cup anemometer, a temperature and relative humidity sensor with sun shield, a solid state barometric pressure sensor, and, a self-emptying rain gauge. Hence, measurements of wind speed, wind direction, temperature, humidity, and precipitation are collected and processed by the control module of the station. In order to account for the land deformation at the tide gauge site, a geodetic instrumentation must be installed as part of the integrated SLOS. Hence, the Lieca GPS system 500 is installed which comprises GPS receiver, terminal and post-processing software. The SR520 dual-frequency GPS receiver has 12 L1 and 12 L2 continuous data tracking channels that track both codes and carrier phases of the transmitted satellite signals. It tracks up to 12 simultaneously satellites. Also, a high-precision AT504 choke-ring antenna is utilized to ensure high-quality reception of the satellites signals.

The new SLOS has been designed and installed based on the recent international specifications of such environmental and engineering systems. The collected precise homogenous data sets will enable an accurate monitoring of the sea level variations and the re-definition of the national geodetic vertical datum of Egypt. Hence, it is recommended that all tide gauge stations in Egypt should be upgraded to meet these objectives. Additionally, it is recommended that the SLOS installed at Alexandria must be incorporated in the Global Sea Level Observing System "GLOSS" program [Woodworth and Aarup, 2003] as well as in the proposed sea level observing system over Africa, which aims to establish an integrated coastal area management and early warning system [PSMSL, 2002].

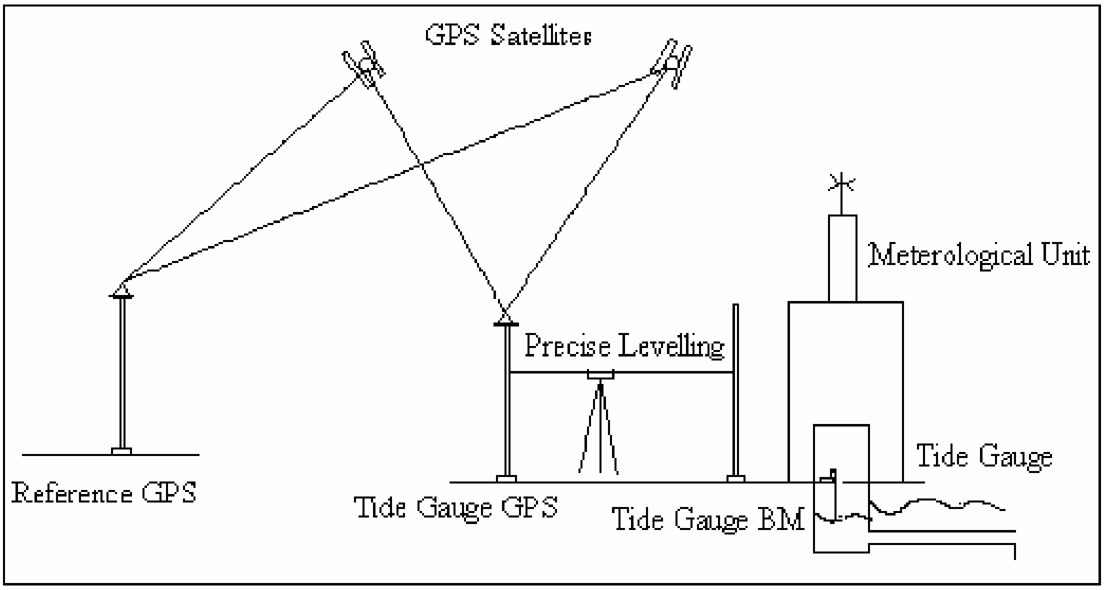

Figure 1: Modern Sea-Level Observing System

LONG-TERM SEA LEVEL RISE IN EGYPT

Previous local investigations revealed that the MSL in Egypt has increased by 12 cm from 1906 to 1980, which means a rate of approximately 1.5 mm per year [Nassar et al, 1998]. Also, Sharaf El-Din et al [1989] have estimated the MSL rise rate by 1.6 mm per year at Alexandria in the period from 1958 to 1988. Moreover, El Fishawi, et al [1991] studied the sea level characteristics along the Nile Delta Coast at Alexandria, Rosetta, Damietta, and Port Said. It has concluded that the mean sea level displays a significant lateral change along the coast; there is general increase from Alexandria to Damietta and marked decrease between Damietta and Port Said. Dawod [2001] has realized that the MSL at Alexandria, from 1944 to 1999, varies from 1.6 cm to 23.5 cm above the current national vertical geodetic datum, with a mean value of 11.1 cm. At Port Said, MSL changes between –1.7 cm to 24.0 cm, with an average of 9.0 cm. Also, it has been concluded that the sea level is rising by a rate of 1.7 mm/year at Alexandria, and 2.4 mm/year at Port Said.

AVAILABLE DATA

The daily tide averages have been collected at Alexandria for an eighteen-year period of time from 1985 to 2003. Additionally, monthly air pressure and air temperature values have been obtained for Alexandria covering the same period. Their statistics, as summarized in Table 1, reveal that the air pressure ranges from 1006.4 to 1022.7 with a mean of 1014.4, while the air temperature varies between 13.5^{o}C and 27.6 ^{o}C with an average equals 20.6 ^{o}C. Moreover, the wind speed varies from 2.6 knot to 11.0 knot, with a mean of 5.6 knot. For the same time interval, the monthly tide values range from 22.7 cm to 70.6 cm with a mean of 47.9 cm.

Recent research studies [e.g. Pararas-Carayannis, 2003] have shown that oscillations in global mean temperature are correlated with corresponding oscillations in solar activity. The traditional direct way to observe the Sun's activity is to look at the sunspot number (SSN). Sunspots are manifestations of magnetically disturbed conditions at the Sun's visible surface. The 11-year cycle of solar activities is the dominant pattern, where the current cycle has started in 1996 and has reached its maximum in 2000. The data of SSN can be obtained from several sources from the Internet [e.g. http://science.msfc.nasa.gov/]. Hence, SSN occurred from 1985 to 2003 have been collected. These numbers range from 1 spot to 200 spots with a mean of 73 spots.

Table 1: Statistics of tide and metrological data from 1985 to 2003

	Tide (cm)	Air Temperature (^{o}C)	Air Pressure (mb)	Wind Speed (knot)	Sun Spot Number
Minimum	22.7	13.5	1006.4	2.6	1
Maximum	70.6	27.6	1022.7	11.0	200
Mean	49.4	20.6	1014.4	5.6	73

TIDAL-WEATHER INTERRELATIONSHIP MODELLING

Although the tide usually dominates the spectrum of water level and current fluctuations, non-tidal variations are important for navigation. Atmospheric pressure and wind produce non-tidal rise in the sea water, usually known as surge. Therefore, the analysis of the interrelation between the tide and the meteorological conditions is a crucial procedure to estimate and more important to predict surges for navigation purposes. The first step is to describe the tide-metrological relationships by a simple linear mathematical model. The attained equations are:

$$T = 24.42 + 1.216\ AT \quad (1)$$

$$T = 1045.9 - 0.982\ AP \quad (2)$$

$$T = 49.08 + 0.051\ WS \quad (3)$$

$$T = 50.31 - 0.012\ SSN \quad (4)$$

where T is the tide in cm, AT is the air temperature in ^oC, AP is the air pressure in mb, WS is the wind speed in knot, and SSN is the sun spot number.

In addition, the annual rising rates of the studied quantities have been calculated. Their computed annual estimates are:

*	0.20	cm/year	for sea level,
*	0.04	^oC/year	for air temperature,
*	-0.03	mb/year	for air pressure,
*	0.05	knot/year	for wind speed, and
*	1.07	$year^{-1}$	for the number of sun spots.

In order to judge the quality of those formulas, the coefficient of determination (R^2) statistical factor has been chosen as the basis of comparison. R^2 is a ratio (or percentage) between the explained variation and the total variation of the regression model. It is an important indicator of how well the resulting regression equation explains the relationship among the variables. The bigger the value of R^2, the stronger the linear relationship between the observed and estimated values. The coefficient of determination is computed as:

$$R^2 = \text{Explained variation} / \text{Total variation}$$

$$= \Sigma\,(Y_{est} - Y_m)^2 / \ \Sigma\,(Y - Y_m)^2 \quad (5)$$

where Y is the observed dependant variable, Y_{est} is the estimated dependant variable; and Y_m is the mean of observed dependant variable

Based on the primary achieved findings, it has been noticed that the linear trend does not precisely fit the MSL variations of the collected data at Alexandria. Therefore, other regression polynomials have been tried out. Those mathematical models include exponential, logarithmic, power, and 6^{th}-order polynomial. The whole attained results are summarized in Table 2. From this table, it can be concluded that the 6^{th} order polynomial produce the highest coefficient of determination (86%) even though the improvements over the linear equation (82%) is not greatly significant. This result emphasizes that the 6^{th} order regression formula may be considered as the optimum mathematical model describing the variations of MSL at Alexandria.

Table 2: Statistical measures (R^2) of attained mathematical models

Tested parameters	Accomplished functions				
	Linear	Exponential	logarithmic	Power	6^{th} order
Air temperature	35	34	35	33	39
Air Pressure	16	15	16	15	25
Wind speed	0.03	0.1	0.1	0.1	11
SSN	0.5	0.9	0.3	0.6	6

CORRELATION ANALYSIS

Computing the correlation factors between the tested parameters is another significant analysis step to investigate the tide-metrological relationships. The attained results have been given in Table 3. From this table, it can be seen that the air temperature has a 60% positive correlation impact on the recorded tide, while the air pressure has a negative correlation of 40%. Also, it has been found that the wind speed and the SSN give negative correlations of 23% and 7% respectively. Figures 2 to 5 depicts the relationships between the tide and each element of the metrological parameters, where the correlation interactions can be recognized.

Table 3: Correlation matrix of tide-metrological parameters

	Tide	Air Temperature	Air Pressure	Wind Speed	SSN
Tide	1				
Air Temperature	60	1			
Air Pressure	-40	-80	1		
Wind Speed	-23	-49	28	1	
SSN	-7	5	2	17	1

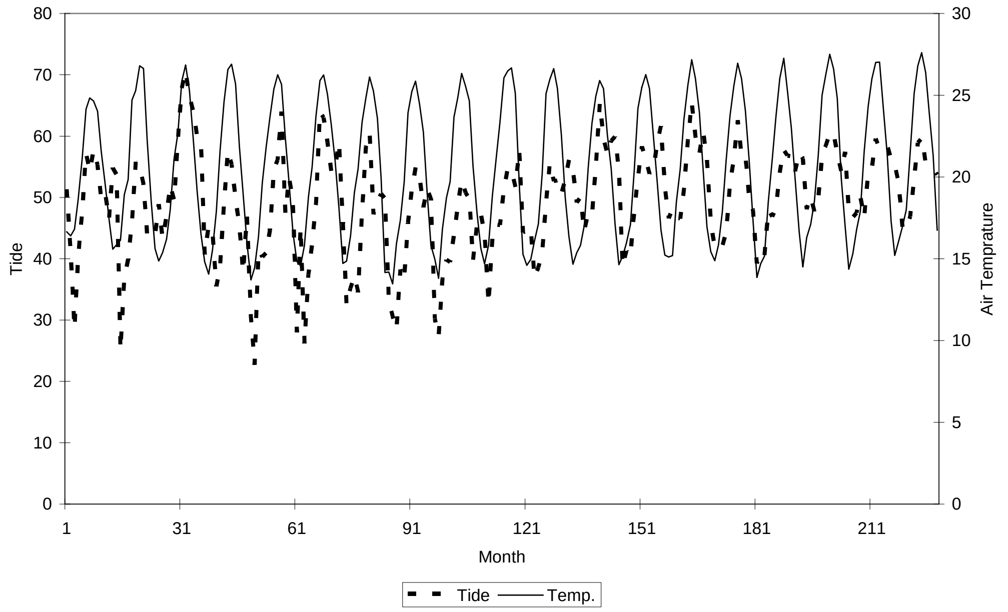

Figure 2: Inter-relationship between the tide and the air temperature

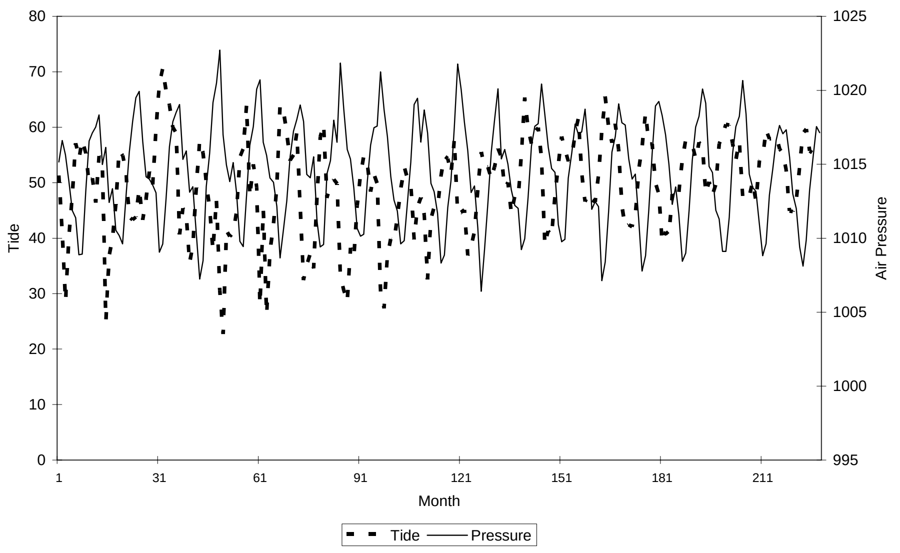

Figure 3: Inter-relationship between the tide and the air pressure

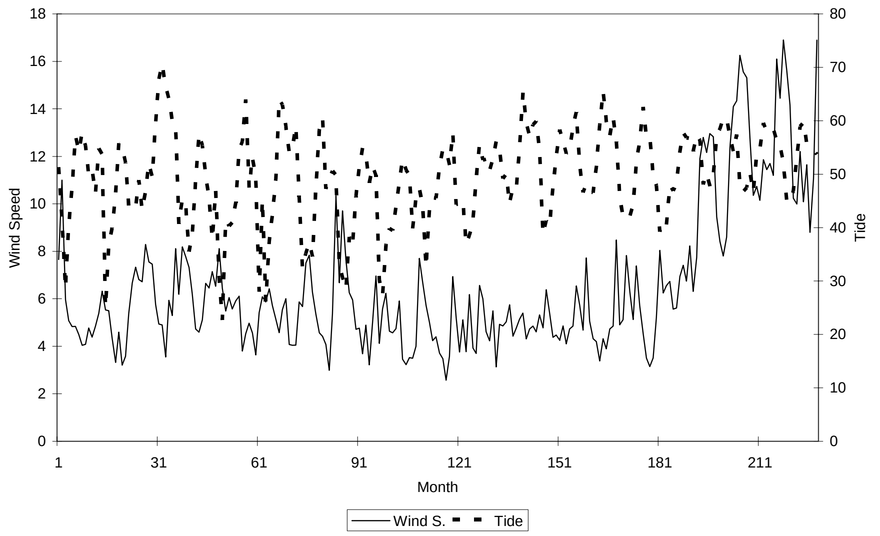

Figure 4: Inter-relationship between the tide and the wind speed

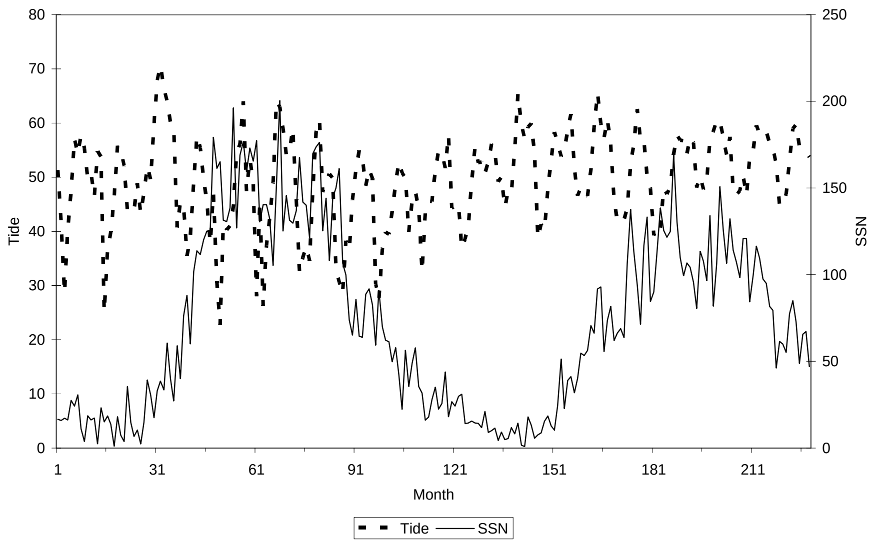

Figure 5: Inter-relationship between the tide and the sun spot number

CONCLUSIONS

Due to the global weather variations, the investigations of the rise of sea level and metrological parameters become an essential request from engineering and environmental perspectives. Daily tidal records and various metrological observations, at Alexandria, have been collected and analyzed covering the period from 1985 to 2003. The attained results show that the main metrological factors affecting the sea level rise are the air temperature, air pressure, and wind speed with correlation factors equal 0.60, -0.39, and -0.23 respectively. Additionally, the solar activities produce a relatively small relationship with the sea level variations. Among five investigated types of mathematical formulas, it has been concluded that the 6^{th}-order polynomial function is the optimum model describing the relationship between the mean sea level and the metrological parameters. Moreover, the annual rising rates of the studied quantities have been estimated as 0.20 cm/y for sea level, 0.04 ^{o}C/y for air temperature, -0.03 mb/y for air pressure, 0.05 knot/y for wind speed, and 1.07 y^{-1} for the number of sun spots.

A new state-of-the-art sea level observing system has been installed at Alexandria in 2001. Due to its reliability, integrity, and accuracy, it is recommended that all tide gauge stations in Egypt being upgraded by such a high-technology system in order to monitor the sea level changes in Egypt with a better level of accuracy. Additionally, it is recommended that the tide gauges in Egypt be incorporated in the international GLOSS program and the proposed regional sea level monitoring program in Africa. Since the sea level rise is one of the main elements that cause shoreline retreat and coastal erosion, it is recommended that the sea level rise should be taken into consideration in national development planes, particularly for coastal regions.

REFERENCES

El-Fishawi, N., Khafagy, A., 1991, Sea level characteristics along the Nile delta coast, MBSS Newsletter, No. 13, pp. 29-37.

Dawod, G., 2001, The magnitude and significance of long-term sea level rise in Egypt from a geodetic perspective, Proceedings of the Eleventh International Conference on Environmental Protection, Alexandria University, Alexandria, May 8-10, pp. 207-215

IOC (Intergovernmental Oceanographic Commission), 2002, Manual on sea level measurement and interpretation, Volume 3: Reappraisals and recommendations as of the year 2000, UNESCO.

IPCC (Intergovernmental Panel on Climate Change), 2001, Climate change 2001: The scientific basis, UN Technical report.

Houghton, J., 1997, Global warming: The complete briefing, Cambridge university press.

Pararas-Carayannis, G., 2003, Climate changes, natural and man-made disasters - Assessment of risks, preparedness and mitigation, Presented at the Climate change - disaster preparedness workshop, Kiev, Ukraine, October 26-30.

PSMSL, 2002, Enhancing sea level monitoring in Africa as a component of integrated coastal area management and early warning system, Proposal submitted to African Partnership Conference, Johannesburg, South Africa, August.

Nassar, M., Baraka, M., and El-Shazly, A., 1998, Modeling local sea surface topography in Egypt based on zero frequency response analysis, Scientific Bulletin of Faculty of Engineering, Ain Shams University, V. 33, No. 1.

NOAA (U.S. National Oceanic and Atmospheric Administration), 2001, Sea level variations of the United States 1854-1999, NOAA Technical Report NOS Co-OPS 36, 80 pp.

Sharaf El-Din, S., Ahmed, K., Khafagy, A., Fanos., A., and Ibrahim, A., 1989, Extreme sea level values on the Egyptian Medetteranean coast for the next 50 years, Proceedings of the International Seminar on Climate Fluctuations and Water Management, December 11-14, Cairo, Paper No. II-6.

SRI (Survey Research Institute), 2002, The establishment of a modern sea level monitoring system towards the re-definition of the geodetic vertical datum in Egypt, SRI Technical Report 2.

Vaníček, P. and Kraakiwsky, E., 1986, Geodesy: The concept, Elsevier Science Publishers B. V., The Netherlands.

Woodworth. P., and Aarup, T., 2003, A report on the status of the GLOSS program and a proposal for taking the program forward, Technical report No. IOC/INF 1190, 41 pp.

Published in: Water Science Magazine, Volume 38, October 2005, pp. 9-16

دراسة الفروق بين مناسيب رخامات الري و مناسيب روبيرات المساحة لمحطات قياس مناسيب المياه علي نهر النيل

جمعة محمد داود[1]

١. ملخص البحث:

من أهم الأدوات الفنية في منظومة الإدارة المتكاملة للموارد المائية في مصر توافر بيانات دورية لمناسيب المياه علي امتداد مجري نهر النيل و فرعيه وكافة المجاري المائية الأخرى. تبين أن مناسيب المياه المقاسة اعتمادا علي رخامات الري تختلف عن نفس المناسيب إذا تم قياسها اعتمادا علي روبيرات الهيئة العامة للمساحة والتي تحدد المرجع القومي الجيوديسي الرأسي المستخدم في كافة أعمال المساحة و إنتاج الخرائط. باستخدام بيانات ١٢ محطة معلوم عندها كلا من منسوب الري و منسوب المساحة - في الحبس الرابع من النيل الممتد لمسافة ٣٨٢ كيلومتر - تم تطبيق طريقتين لاستنباط معادلات ارتباط لنمذجة هذه التغيرات. تهدف معادلات الارتباط التي تم تطويرها الي الحصول علي قيمة الفرق بين منسوبي الري و المساحة عند أي موقع بحيث يمكن حساب قيمة المنسوب في أيا من النظامين بمعلومية قيمة المنسوب عند نفس الموقع في النظام الاخر ، وذلك حتي يمكن الاعتماد علي نظام واحد لقياس المناسيب في مشروعات الموارد المائية ومشروعات المساحة و الخرائط. هذا وقد تبين أن فروق المناسيب بين النظامين للمحطات المستخدمة يتراوح بين -٢٢.٨ سنتيمتر و +٣.٨ سنتيمتر. باستخدام بيانات ١٥ نقطة تحكيم خارجية أمكن استنتاج أن دقة نتائج الطريقة الأولى التي تعتمد علي استنتاج معادلة ارتباط واحدة لكامل الحبس الرابع تبلغ ± ٦.٨ سنتيمتر ، بينما تصل دقة الطريقة الثانية المبنية علي إيجاد معادلة ارتباط بين كل رخامتي ري إلى ± ٣.١ سنتيمتر. ومن ثم يمكن القول أن طريقة معادلة الارتباط بين كل نقطتين تعطي دقة أحسن من طريقة معادلة الارتباط لكل النقط الموجودة علي الحبس الرابع.

يوصي البحث بإعادة رصد مناسيب جميع رخامات الري علي نهر النيل و فرعيه من خلال عدة حلقات ميزانيات دقيقة بدءا من روبيرات الدرجة الأولى للهيئة العامة للمساحة مع تطبيق تقنية الرصد علي الأقمار الصناعية بنظام جي بي إس كوسيلة اختبار خارجية لاكتشاف أية أخطاء و الحكم علي أرصاد الميزانيات عند تحديد الفرق بين منسوبي الري و المساحة لرخامات الري. كما يوصي البحث - عند توافر الأرصاد الدقيقة – بأن يتم إعادة تحديد معادلات الارتباط لنمذجة هذه التغيرات في المناسيب بدقة أعلي.

٢. مقدمة:

تاريخيا كان مقدار منسوب المياه عند مقياس الروضة هو العامل الأساسي الذي يتم بناءا عليه تقدير حجم فيضان النيل ومن ثم تقدير استحقاقيه زكاة الزرع (الضرائب بلغة العصر الحالي) بالنسبة لسائر أنحاء القطر المصري. أما حاليا فتعد قياسات منسوب المياه أحد العوامل الحيوية المستخدمة في الأعمال الدورية لمنظومة إدارة الموارد المائية ضمن أنشطة وزارة الموارد المائية و الري. وتتم هذه القياسات بصفة يومية من خلال العديد من محطات القياس المقامة علي امتداد نهر النيل وكافة الترع الفرعية حيث

[1] أستاذ باحث مساعد - معهد بحوث المساحة – المركز القومي لبحوث المياه – dawod_gomaa@yahoo.com

Published in: Water Science Magazine, Volume 38, October 2005, pp. 9-16

يوجد بكل محطة تدريج لأقرب سنتيمتر مرسوم علي مقياس رأسي - غالبا مصنوع من الرخام - مثبت بصفة دائمة في جسم المنشأ المائي. وتعرف هذه المحطات باسم "رخامات الري".

يعد المرجع الجيوديسي الرأسي لجمهورية مصر العربية هو متوسط منسوب سطح البحر الأبيض عند المحطة المساحية الأساسية المقامة بميناء الإسكندرية والذي تم حسابه في عام ١٩٠٦. وعند هذه المحطة تم تحديد المنسوب "صفر" واعتمادا عليه وباستخدام أجهزة الميزان قامت الهيئة العامة للمساحة بإنشاء آلاف العلامات المساحية معلومة المنسوب (الروبيرات) التي تحدد قيم المناسيب والتي تغطي تقريبا كافة أنحاء الجمهورية. وهذا المرجع الرأسي هو المستخدم في كافة أعمال المساحة و إنشاء الخرائط علي مختلف أنواعها و دقتها في مصر.

تبين في الفترة الأخيرة أن هناك اختلافا في قيمة منسوب المياه عند نفس الموقع إذا تم قياس هذا المنسوب اعتمادا علي رخامات الري أو اعتمادا علي روبيرات هيئة المساحة. وتتسبب هذه الفروقات غير المنتظمة في بعض المشاكل الفنية مما يتتطلب بحث هذه المشكلة وايجاد حل مناسب لها. ومن الوهلة الأولى فأن الحل يتمثل في إعادة تثبيت رخامات الري في منسوبها الصحيح بعد تحديده بواسطة أرصاد الميزانيات الدقيقة اعتمادا علي روبيرات المساحة لضمان تجانس مناسيب محطات القياس مع المرجع القومي الجيوديسي. إلا أنه من الناحية العملية فربما لا يكون هذا هو الحل الأمثل ولكن يمكن إيجاد طريقة علمية لتمثيل هذه الفروق بمعادلات رياضية دقيقة لوضع أسلوب للتحويل بين كلا النظامين (مناسيب الري ومناسيب المساحة)، وهذا هو الدافع الأساسي للبحث الحالي. تهدف معادلات الارتباط المستنتجة الي الحصول علي قيمة الفرق بين منسوبي الري و المساحة عند أي موقع علي امتداد الحبس الرابع من النيل بحيث يمكن حساب قيمة المنسوب في أيا من النظامين بمعلومية قيمة المنسوب عند نفس الموقع في النظام الاخر ، وذلك حتي يمكن الاعتماد علي نظام واحد لقياس المناسيب في مشروعات الموارد المائية ومشروعات المساحة و الخرائط.

٣. المرجع القومي الجيوديسي الرأسي:

في النصف الثاني من القرن التاسع عشر توصل علماء المساحة والجغرافيا إلى حقيقة علمية مفادها أن شكل سطح مياه المحيطات و البحار هو الأقرب لتمثيل سطح الكرة الأرضية وذلك اعتمادا علي أن ثلاثة أرباع الأرض مغطي بالمياه ولا تمثل اليابسة إلا مقدار الربع تقريبا. ومع بدء وضع القواعد العلمية الحديثة لأعمال المساحة وإنشاء الخرائط في نهايات هذا القرن بدأت كل دولة في إنشاء محطة لقياس منسوب مياه البحر وتسجيله لمدة زمنية معينة لحساب متوسط هذه القياسات للوصول إلى قيمة دقيقة لهذا المنسوب بعد تلاشي التأثيرات الدورية للأمواج و المد والجزر. قامت هيئة المساحة المصرية بإنشاء محطة قياس بحرية داخل ميناء الإسكندرية (مكونة من بئر تدخله مياه البحر من خلال ماسورة و مثبت داخله مسطرة من الرخام مدرجة لأقرب سنتيمتر) واستمرت عملية تسجيل قياس منسوب مياه البحر من عام ١٨٩٨ إلى عام ١٩٠٦. وبحساب متوسط هذه القراءات أمكن تعريف المنسوب صفر علي المسطرة المدرجة ، ومن ثم تم إنشاء وحساب منسوب أول روبير علي الأرض بجوار هذه المحطة [١]. بتطبيق أسلوب الميزانية الطولية - الذي يستخدم جهاز الميزان لرصد وحساب فرق المنسوب بين نقطتين - تم إنشاء العديد من الروبيرات التي تكون ما يعرف باسم شبكة حلقات الروبيرات (شكل رقم ١) والتي تحدد المرجع القومي الجيوديسي الرأسي لجمهورية مصر العربية.

وجدير بالذكر أن الأبحاث العلمية الحديثة علي المستوي العالمي أثبتت أن متوسط منسوب سطح البحر يرتفع مع الوقت وخاصة في القرن الماضي نتيجة لعوامل متعددة أهمها التغيرات في الظروف المناخية للأرض. وفي مصر أمكن التوصل إلى أن متوسط منسوب سطح البحر عند الإسكندرية قد ارتفع بمقدار

Published in: Water Science Magazine, Volume 38, October 2005, pp. 9-16

١١.١ سنتيمتر في الفترة من عام ١٩٤٤ إلى عام ١٩٩٩ مما يتعين معه إعادة تعريف المرجع الجيوديسي الرأسي بطريق أدق [٢].

٤. البيانات المستخدمة:

تشمل البيانات التي تم استخدامها في هذا البحث مجموعتين من المناسيب لعدد ١٢ رخامة ري مثبتة علي الحبس الرابع من النيل وتغطي المنطقة من مقياس الروضة الواقع عند الكيلومتر صفر (المناظر للكيلومتر ٩٢٧.٠ خلف خزان أسوان) إلى مقياس خلف قناطر أسيوط الواقع عند الكيلومتر ٣٨٢.٣ خلف مقياس الروضة (المناظر للكيلومتر ٥٤٤.٧ خلف خزان أسوان) كما هو موضح بالشكل رقم ٢. تم عمل ميزانية دقيقة بدءا من أقرب روبير لرصد و حساب منسوب أعلي كل رخامة ري ومقارنته بالمنسوب الموجود علي الرخامة ذاتها ، ومن ثم أمكن حساب فرق المنسوب بين كلا النظامين لجميع المواقع الأثني عشر. ويعرض الجدول رقم ١ فروق المناسيب عند رخامات الري التي تم استخدامها في البحث بينما يقدم الجدول رقم ٢ الخصائص الإحصائية للبيانات المستخدمة ، والذي يمكن من خلاله التوصل إلى أن فروق المناسيب تتراوح بين -٢٢.٨ سنتيمتر و +٣.٨ سنتيمتر.

في إطار فعاليات المشروع القومي الرائد لإنشاء خرائط رقمية هيدروجرافية و طبوغرافية لنهر النيل و فرعيه الذي ينفذه معهد بحوث النيل أمكن الحصول علي مناسيب الري و مناسيب المساحة لعدد ١٥ موقع في المنطقة بين مدينة مغاغة الواقعة عند الكيلومتر ١٦٨ خلف مقياس الروضة و مدينة المنيا الواقعة عند الكيلومتر ٢٤١ خلف مقياس الروضة. هذا وقد تم حفظ هذه البيانات لاستخدامها كنقط تحكيم خارجية للدلالة علي جودة ودقة النماذج الرياضية التي تم تطويرها للتحويل بين كلا النظامين.

جدول رقم ١: فروق المناسيب عند رخامات الري المستخدمة

اسم مقياس الري	البعد الكيلومترى		منسوب الري (م)	منسوب المساحة (م)	الفرق (سم)
	من أسوان	من الروضة			
خلف قناطر اسيوط	٥٤٤.٧	٣٨٢.٣	٥٣.٥٠٠	٥٣.٤٧٩	٢.١
المندرة	٦١٢.١	٣١٤.٩	٤٨.٠٠٠	٤٧.٩٩٨	٠.٢
فلندول	٦٤٩.٤	٢٧٧.٦	٤٤.٠٠٠	٤٤.٠١٠	-١.٠
المنيا	٦٨٧.٥٥	٢٣٩.٤٥	٣٥.٠٠٠	٣٥.٠٩٠	-٩.٠
الشيخ فضل	٧٣٥.٢٥	١٩١.٧٥	٣٦.٠٠٠	٣٦.٠٣١	-٣.١
ببا	٧٨٩	١٣٨	٢٧.٥٠٠	٢٧.٤٦٢	٣.٨
بنى سويف	٨٠٨.٦	١١٨.٤	٢٤.٠٠٠	٢٤.٠٦٦	-٦.٦
الكريمات	٨٣٩.١	٨٧.٩	٢٥.٠٠٠	٢٤.٩٨٣	١.٧
الواسطى	٨٤٣.٨	٨٣.٢	٢٢.٥٠٠	٢٢.٥٤١	-٤.١
الليثى	٨٧٣.٧	٥٣.٣	٢٤.٥٠٠	٢٤.٤٦٧	٣.٣
الاخصاص	٨٨٨	٣٩	١٩.٥٠٠	١٩.٧٢٧	-٢٢.٧
الروضة	٩٢٧	٠	٢١.٠٠٠	٢١.٢٢٨	-٢٢.٨

Published in: Water Science Magazine, Volume 38, October 2005, pp. 9-16

جدول رقم ٢: إحصائيات البيانات المستخدمة

	الحد الأدنى	الحد الأقصى
مواقع رخامات الري المستخدمة (خلف مقياس الروضة) فروق المناسيب (منسوب الري – منسوب المساحة)	٠ كم -٢٢.٨ سم	٣٨٢.٣ كم +٣.٨ سم
مواقع نقاط التحكيم المستخدمة (خلف مقياس الروضة)	١٦٨ كم	٢٤١ كم

٥. الحسابات و النتائج:

تكونت أعمال الحسابات من مرحلتين ، تم في الأولى استنباط عدة نماذج رياضية للعلاقة بين النظامين باستخدام كافة البيانات علي امتداد الحبس الرابع بينما تم في مرحلة الحساب الثانية استنباط نموذج رياضي بين كل محطتي قياس متتاليتين.

في المجموعة الأولى من الحسابات تم استخدام نماذج رياضية متعددة الدرجات للوصول لتمثيل فروق المناسيب كدالة في البعد الكيلومتري من مقياس الروضة كالتالي:

ق = أ + ب ك (١)
ق = أ + ب ك + ت ك^{٢} (٢)
ق = أ + ب ك+ ت ك^{٢}+ ث ك^{٣} (٣)
ق = أ + ب ك+ ت ك^{٢}+ ث ك^{٣} + ج ك^{٤} (٤)
ق = أ + ب ك+ ت ك^{٢}+ ث ك^{٣}+ ج ك^{٤}+ ح ك^{٥} + خ ك^{٦}+ د ك^{٧} (٥)

حيث:
ق فرق المنسوب بين نظامي الري و المساحة (بالسنتيمتر)
ك البعد الكيلومتري للنقطة أمام مقياس الروضة (بالكيلومتر)
أ ، ب ، ت ، ث ، ج ، ح ، خ ، د المعاملات المجهولة المطلوب تحديدها (بالسنتيمتر)

وعند حل كل معادلة أمكن تكوين ١٢ معادلة رصد (للنقط المعلوم عندها فروق المناسيب). وحيث أن عدد معادلات الرصد لكل حالة أكثر من عدد المجاهيل – بحد أقصي ٧ مجاهيل للمعادلة رقم ٥ - فقد تم تطبيق نظرية أقل مجموع مربعات للوصول إلى أفضل قيم للعناصر المطلوب تحديدها. ويعرض الجدول رقم ٣ قيم المعاملات التي تم التوصل إليها في كل حالة.

جدول رقم ٣: نتائج معادلات الارتباط للحبس الرابع

المعادلة	أ	ب	ت	ث	ج	ح	خ	د
١	١٠.٩٠-	٠.٠٣٧٧						
٢	١٦.١٨-	٠.١٣١٣	٠.٠٠٠٢٥-					
٣	٢٣.٣٥-	٠.٣٨١١	٠.٠٠١٩٦-	٣×١٠$^{-٦}$				
٤	٢٥.٤٠-	٠.٥٤١٦	٠.٠٠٤١٤-	١.٢ ×١٠$^{-٥}$	١.٢- ×١٠$^{-٨}$			
٥	٢٣.٣١-	٠.٤٨٢٠-	٠.٠٣٣٢٠	٠.٠٠٠٥١-	٣.٦٤ ×١٠$^{-٦}$	١.٤- ×١٠$^{-٨}$	٢.٥٤ ×١٠$^{-١١}$	١.٩- ×١٠$^{-١٤}$

من أهم الخطوات في أعمال الهندسة المدنية بصفة عامة استخدام المعايير الاحصائية للحكم علي جودة نتائج أية عمليات حسابية. ومن أهم تلك المعايير الاحصائية تم اختيار المعاملين التاليين للتطبيق في هذا البحث:

(أ) معامل جودة الارتباط (ر٢):

يعد من أهم المؤشرات الإحصائية للحكم علي كفاءة معادلات الارتباط وهو يتراوح بين صفر وواحد حيث القيم القريبة من الصفر تدل علي أن معادلة الارتباط المستنبطة لا تعطي تمثيل حقيقي جيد بين المتغيرات الأولية بينما القيم القريبة من الواحد تدل علي أن المعادلات المستنتجة تمثل العلاقة بين المتغيرات بصورة جيدة. وبصورة أخري يمكن تمثيل معامل جودة الارتباط علي أنه يمثل النسبة المئوية من التغيرات بين القيم الأساسية التي أمكن تمثيلها بصورة جيدة من خلال معادلة الارتباط المستنبطة.

(ب) الخطأ التربيعي المتوسط:

يمثل الخطأ التربيعي المتوسط للأخطاء المتبقية مؤشر إحصائي هام للدلالة علي القيمة المتوسطة لفروق القيم التي لم يمكن التعبير عنها في معادلة الارتباط المستنبطة.

يعرض الجدول رقم ٤ قيم المعايير الإحصائية للمعادلات التي تم الحصول عليها. من هذا الجدول يمكن استنتاج أن:

- بصفة عامة كلما زادت درجة معادلة الارتباط تزداد قيمة معامل جودة الارتباط وتقل قيمة الخطأ التربيعي المتوسط.
- قيمة التحسن بين المعادلة رقم ٤ و المعادلة رقم ٥ ليست كبيرة مما يدل علي أن زيادة درجة معادلات الارتباط اكبر من الدرجة الرابعة غير محسوس النتيجة.
- المعادلة رقم ٥ هي الأنسب لتمثيل التغير في فروق المناسيب بين النظامين - علي امتداد الحبس الرابع - كدالة في البعد الكيلومتري للموقع أمام مقياس الروضة.
- أحسن قيمة لمعامل الارتباط للمعادلات المستنبطة (للمعادلة رقم ٥) تدل علي أن معادلة الارتباط لا تمثل إلا ٦٦% من قيم التغير في فروق المناسيب كدالة في البعد الكيلومتري ، وهذه القيمة بصفة عامة تعد مؤشر علي جودة معادلة الارتباط والتي يمكن القول أنها غير عالية الكفاءة.

جدول رقم ٤: معايير الحكم علي معادلات الارتباط للحبس الرابع

المعادلة	معامل جودة الارتباط (ر٢)	الخطأ التربيعي المتوسط (سنتيمتر)
١	٠.٢٤	٧.٧
٢	٠.٣٦	٧.١
٣	٠.٥٧	٥.٨
٤	٠.٦٠	٥.٦
٥	٠.٦٦	٥.٢

في الخطوة التالية وللحكم علي الدقة الخارجية لمعادلات الارتباط تم استخدام نقاط التحكيم – وعددهم ١٥ نقطة – حيث تم استخدام المعادلة رقم ٥ لحساب فرق المنسوب بين النظامين عند كل موقع ومقارنته بفرق المنسوب المعلوم. وقد تبين أن هذه الفروقات تراوحت بين ٢.٢ سنتيمتر و ١١.٤ سنتيمتر بمتوسط

يبلغ ٦.٨ سنتيمتر وانحراف معياري قيمته ٢.٩ سنتيمتر. ومن ثم يمكن استنتاج أن دقة إيجاد معادلة ارتباط واحدة لكامل الحبس الرابع تبلغ ± ٦.٨ سنتيمتر.

في المرحلة الثانية من الحسابات تم استنباط معادلة ارتباط خطية بين كل نقطتين من النقط المعلوم لها فرق المنسوب بين النظامين. في المسافة بين الكيلومتر ١١٨ و الكيلومتر ٢٤٥ أمام مقياس الروضة تم استنباط معادلة الارتباط التالية:

ق = - ٤.٢٥ - ٠.٠١٩٨ ك (٦)

وحيث أن عدد معادلات الرصد في هذه الحالة يساوي عدد الكميات المجهولة وكما هو متوقع لمثل هذه الحالة فان قيمة معامل جودة الارتباط (ر^{٢}) تساوي واحد وقيمة الخطأ التربيعي المتوسط تساوي صفر. ومن ثم فقد تم استخدام المعادلة ٦ لحساب قيم فرق المنسوب عند كل نقطة من نقاط التحكيم ومقارنته بالقيمة المعلومة ، حيث تبين أن الاختلافات تراوحت بين -١.٦ سنتيمتر و ٨.٠ سنتيمتر بمتوسط يبلغ ٣.١ سنتيمتر وانحراف معياري قيمته ٣.٠ سنتيمتر. وبذلك يمكن استنتاج أن دقة إيجاد معادلة ارتباط بين كل رخامتي ري تبلغ ± ٣.١ سنتيمتر. ويمثل الشكل رقم ٣ قيم الاختلافات عند نقاط التحكيم لكلتا الطريقتين. وبناء عليه يمكن استنتاج أن طريقة معادلة الارتباط بين كل نقطتين تعطي دقة أحسن من طريقة معادلة الارتباط لكل النقط الموجودة علي الحبس الرابع.

٦. الأسلوب المقترح لتحديد فروق المناسيب:

تعد النتائج التي تم الحصول عليها مشجعة لإيجاد حل علمي وعملي دقيق للاختلافات بين مناسيب الري و مناسيب المساحة لمحطات قياس مناسيب المياه علي امتداد نهر النيل ، إلا أن هذه النتائج تعتمد علي دقة و كثافة البيانات المتاحة. ويقترح البحث إعادة رصد مناسيب جميع رخامات الري علي نهر النيل و فرعيه من خلال عدة حلقات ميزانيات دقيقة بدءا من روبيرات الدرجة الأولى للهيئة العامة للمساحة. ومن المعلوم أنه توجد أخطاء تراكمية في أرصاد الميزانيات تعتمد علي طول المسافة بين الروبير المعلوم منسوبه و النقطة الجديدة المطلوب تحديد منسوبها. وبذلك فيجب توافر عنصر خارجي كوسيلة اختبار وتحكيم علي فروق المناسيب المطلوب تحديدها ، وهنا يبرز دور النظام العالمي للتوجيه (جي بي إس) كأدق تقنيات الرصد علي الأقمار الصناعية شائعة الاستخدام في كافة تطبيقات الهندسة المدنية بصفة عامة والمساحة و الخرائط بصفة خاصة. أثبتت تقنية جي بي إس فعالية هائلة ومميزات فنية واقتصادية ضخمة عند استخدامها في أعمال المساحة وإنشاء الخرائط سواء علي المستوي العالمي أو المستوي المحلي. ومن أمثلة هذه الاستخدامات لخدمة الإدارة المتكاملة للموارد المائية إنشاء خرائط رقمية طبوغرافية دقيقة لترعة الشيخ جابر الصباح بشمال سيناء [٧] وإنشاء شبكات الثوابت المساحية في إطار مشروع إنشاء خرائط رقمية هيدروجرافية لنهر النيل و فرعيه [٥].

يقترح البحث تطبيق أرصاد جي بي إس كوسيلة اختبار خارجية لاكتشاف أية أخطاء و الحكم علي أرصاد الميزانيات عند تحديد الفرق بين منسوبي الري و المساحة لرخامات الري. ومن المعلوم أن الارتفاعات المقاسة بتقنية جي بي إس تعد من نوع الارتفاع الجيوديسي (نسبة لسطح الالبسويد وهو المجسم الهندسي لشكل الأرض الأرضية) والذي يختلف عن الارتفاع الارثومتري أو المنسوب (المعتمد علي متوسط منسوب سطح البحر) كما هو موضح بالشكل رقم ٤ ، إلا أنه يمكن التحويل بين كلا النوعين عند توافر نموذج جيويد [٦] كالتالي:

م = ع - ن (٧)

و بين نقطتين يكون:

Δ م = Δ ع - Δ ن (٨)

حيث:

Δ م فرق المنسوب بين نقطتين

Δ ع فرق الارتفاع الجيوديسي بين النقطتين

Δ ن فرق شذوذ الجيويد بين النقطتين

يتم الحصول علي فرق شذوذ الجيويد من خلال نماذج الجيويد المعلومة سواء النماذج العالمية مثل نموذج EGM96 أو نماذج الجيويد القارية مثل الجيويد الأفريقي AGP2003 [٤] أو نماذج الجيويد المحلية مثل نموذج NILE2004 الذي تم تطويره حديثا للحبس الرابع من النيل وأثبتت نتائج اختباره أنه أعلي دقة من النماذج العالمية [٣].

عمليا يقترح البحث أن تتم أرصاد جي بي إس بحيث يتم رصد إشارات الأقمار الصناعية باستخدام أربعة أجهزة - علي الأقل - ثنائية الإشارة موزعين علي رخامتي ري و روبيرين متتاليين. ثم ينقل جهازين إلى رخامة ري و روبير آخرين مع بقاء الجهازين الآخرين ثابتين. يهدف هذا الأسلوب العملي إلى الحصول علي شبكة متجانسة من الأرصاد بين رخامات الري و الروبيرات لزيادة دقة وجودة الأرصاد وإمكانية تطبيق الطرق الإحصائية لاكتشاف الأخطاء. ومن ثم يمكن استخدام المعادلة رقم ٧ لحساب فرق المنسوب من فرق الارتفاع الجيوديسي الناتج من أرصاد جي بي إس. وبذلك تكون قيم فروق المناسيب التي يتم حسابها بهذا الأسلوب وسيلة تأكيد علي قيمة فروق المناسيب المرصودة سواء بين روبير و رخامة ري أو بين روبيرين أو بين رخامتي ري ، مما يتيح أرصاد دقيقة يمكن من خلالها تحديد أدق معادلات الارتباط التي تحدد العلاقة بين مناسيب الري و مناسيب المساحة لجميع محطات قياس منسوب المياه علي امتداد نهر النيل.

٧. الخلاصة و التوصيات:

تعد أعمال قياس منسوب المياه بصفة دورية من الأدوات الهامة في منظومة الإدارة المتكاملة للموارد المائية في مصر. تبين أن مناسيب رخامات الري لمحطات قياس منسوب المياه تختلف عن مناسيب الرخامات إذا تم قياسها من روبيرات الهيئة العامة للمساحة والتي تحدد المرجع القومي الجيوديسي الرأسي. باستخدام بيانات ١٢ محطة معلوم عندها كلا من منسوب الري و منسوب المساحة في الحبس الرابع من النيل تم تطبيق طريقتين لاستنباط معادلات ارتباط بين فروق المناسيب و البعد الكيلومتري للموقع عن مقياس الروضة. وتبين أن فروق المناسيب بين النظامين لهذه المحطات يتراوح بين - ٢٢.٨ سنتيمتر و +٣.٨ سنتيمتر. كذلك تم استخدام بيانات ١٥ موقع في المنطقة بين مدينة مغاغة و مدينة المنيا كنقط تحكيم خارجية للدلالة علي جودة ودقة معادلات الارتباط المستنتجة.

في المجموعة الأولى من الحسابات تم استخدام نماذج رياضية متعددة الدرجات للوصول لتمثيل فروق المناسيب كدالة في البعد الكيلومتري من مقياس الروضة وذلك بتطبيق بيانات جميع المحطات المعلومة علي امتداد الحبس الرابع. من نتائج الحسابات أمكن استنتاج أن معادلة الدرجة السابعة هي الأنسب لتمثيل التغير في فروق إلا أن قيمة معامل الارتباط التي تساوي ٦٦% تعد مؤشر علي أنها غير عالية الكفاءة. وباستخدام بيانات نقاط التحكيم أمكن استنتاج أن دقة إيجاد معادلة ارتباط لكامل الحبس الرابع تبلغ ± ٦.٨ سنتيمتر.

في المرحلة الثانية من الحسابات تم استنباط معادلة ارتباط خطية بين كل نقطتين من النقط المعلوم لها فرق المنسوب بين النظامين. وبناء علي النتائج التي تم الحصول عليها أمكن استنتاج أن دقة إيجاد معادلة ارتباط بين كل رخامتي ري تبلغ ± ٣.١ سنتيمتر. ومن ثم يمكن القول أن طريقة معادلة الارتباط بين كل نقطتين تعطي دقة أحسن من طريقة معادلة الارتباط لكل النقط الموجودة علي الحبس الرابع.

وبناء عليه أمكن استخلاص التوصيات التالية:

١- استخدام معادلات الارتباط التي تم تطويرها في حساب قيمة المنسوب في أيا من النظامين بمعلومية قيمة المنسوب عند نفس الموقع في النظام الاخر ، وذلك بهدف توحيد نظم قياس المناسيب في مشروعات الموارد المائية ومشروعات المساحة و الخرائط.
٢- إعادة رصد مناسيب جميع رخامات الري علي نهر النيل و فرعيه من خلال عدة حلقات ميزانيات دقيقة بدءا من روبيرات الدرجة الأولى للهيئة العامة للمساحة.
٣- تطبيق أرصاد جي بي إس كوسيلة اختبار خارجية لاكتشاف أية أخطاء و الحكم علي أرصاد الميزانيات عند تحديد الفرق بين منسوبي الري و المساحة لرخامات الري.
٤- استخدام نموذج الجيويد المحلي NILE2004 الذي تم تطويره حديثا للحبس الرابع من النيل في تحويل فرق الارتفاعات الجيوديسية إلى فرق منسوب حتى يمكن استخدام أرصاد جي بي إس كوسيلة تأكيد علي قيمة فروق المناسيب المرصودة.
٥- عند توافر الأرصاد الدقيقة يتم إعادة تحديد معادلات الارتباط المستنبطة في هذا البحث و التي تحدد العلاقة بين مناسيب الري و مناسيب المساحة لجميع محطات قياس منسوب المياه علي امتداد نهر النيل.

المراجع:

[1] Cole, J., 1939, Revision of first order levelling lower Egypt, Survey Department Paper No. 44, Egyptian Survey Authority, Giza, Egypt.

[2] Dawod, G., 2001, The magnitude and significance of long-term sea level rise in Egypt from a geodetic perspective, Proceedings of the Eleventh International Conference on Environmental Protection, Alexandria University, Alexandria, May 8-10, pp. 207-215.

[3] Dawod, G., 2005, Developing a precise geoid model for hydrographic surveying of the River Nile, Al-Azhar University Engineering Journal (AUEJ), V. 8, No. 1, January, pp. 96 - 107.

[4] Merry, C., 2003, The African geoid project and its relevance to the unification of African vertical reference frames, Proceedings of the second FIG regional conference, Marrakech, Morocco, December 2-5.

[5] NRI (Nile Research Institute), 2003, The geodetic control networks along the fourth reach of the Nile, Unpublished technical report.

[6] Roman, D., Wang, Y., Henning, W., and Hamilton, J., 2004, Assessment of the new national geoid height model, GEOID03, Proceedings of the ACSM Conference, Tennessee, USA, April 16-21.

[7] SRI (Survey Research Institute), 2001, Producing digital topographic maps for constructing a spell way on Sheikh Gaber canal, North Sinai, Unpublished technical report.

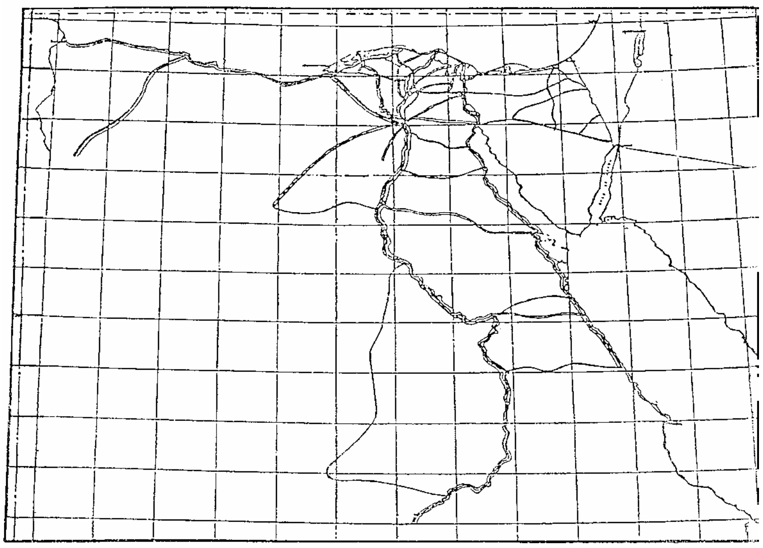

شكل رقم ١: شبكة حلقات الروبيرات في مصر

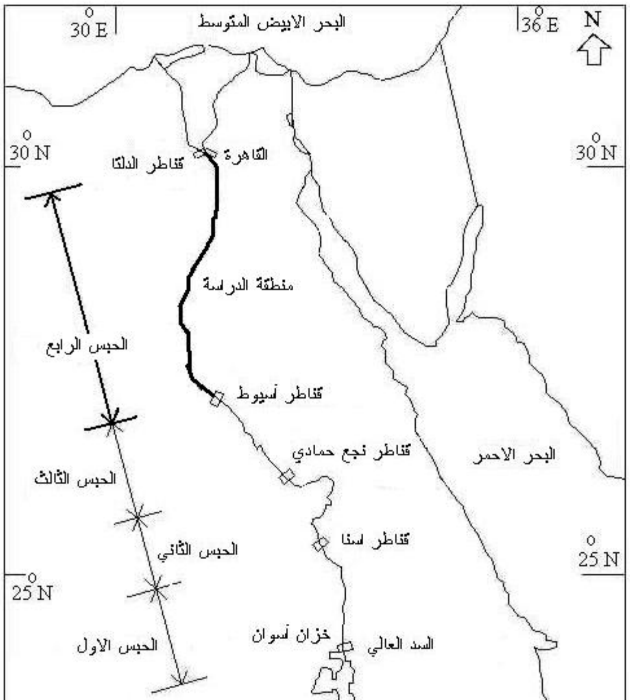

شكل رقم ٢: منطقة الدراسة

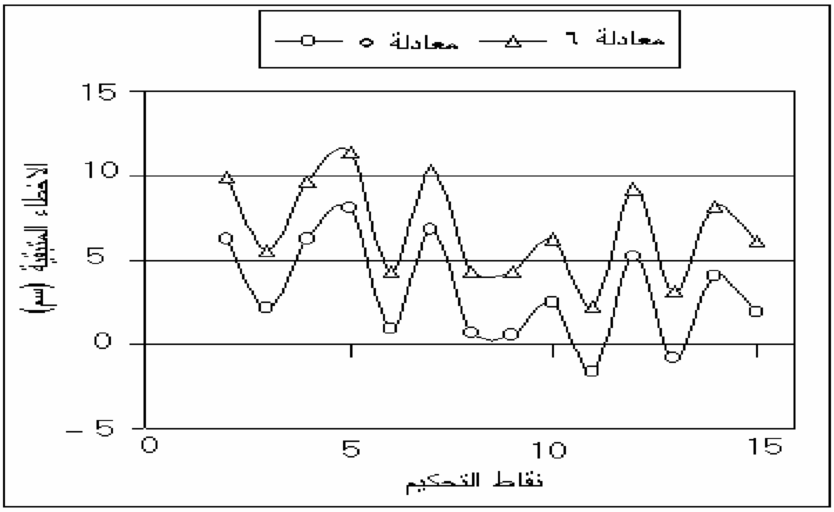

شكل رقم ٣: قيم الاختلافات عند نقاط التحكيم للطريقتين المستخدمتين

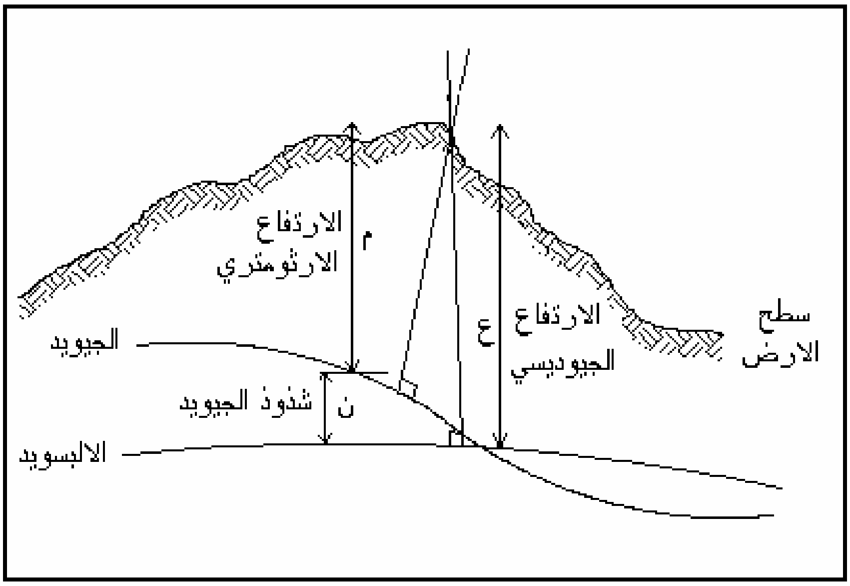

شكل رقم ٤: أنواع الارتفاعات

Summary

Published in: Water Science Magazine, Volume 38, October 2005, pp. 9-16

The periodical measurements of water levels along the Nile constitute one of the major factors in the integrated water management process in Egypt. Significant variations have been reported for the water levels measured based on the tide gauge stations' datum and the surveying national datum. This paper aims to describe the level differences by mathematical models based on a spatial basis. Two modeling approaches have been performed based on the data of 12 stations, located along the forth reach of the Nile that extends for about 382 km, at which both values of water levels are known. It has been found that the water level differences vary between -22.8 cm and +3.8 cm. Another data set, of 15 common stations, has been reserved as check points to judge the quality of the developed mathematical formulas.

Utilizing the entire data set of the known points in the study area produces an optimum polynomial of order 7. The coefficient of determination of this formula, as a precision measure, is 0.66. This equation, when tested on the available check points, gives an external accuracy measure of ± 6.8 cm. The second approach is based on developing a regression formula between each two successive known stations. When tested on the existing check sites, the attained model yields an external accuracy measure of ± 3.1 cm. Therefore, it can be concluded that, from a statistical point of view, the second modeling criterion gives better precision and accuracy values.

It is recommended that the levels of all tide gauges be re-observed by precise leveling starting from national first-order benchmarks. Furthermore, it is recommended that the satellite-based Global Positioning System (GPS) technology be employed as an external source of precise data to check the integrity and accuracy of the observed level differences. Having collected new observations, the modeling process should be re-performed to obtain more reliable mathematical formulas describing the relationship between the irrigation and surveying levels along the river Nile.

Enhancing the Integrity of the National Geodetic Data Bases in Egypt

Gomaa M. DAWOD and Sherine S. ISMAIL, Egypt

Key words: GPS, Geodetic control networks, Geoid.

SUMMARY

Egypt has recentely established a new precise geodetic framework based on the global WGS84 datum to furnish a national GPS-based reference system. For agricultural development along the Nile valley, the National Agricultural Cadastral Network (NACN) has been established with a precision of 1 part per million. However, the orthometric heights of the 112-station network have been computed utilizing the OSU91A global geopotential model. Previous studies have shown that the accuracy of this model over Egypt is almost 1.5 meter. Even the new global models, such as EGM96, PGM2000, and UCPH2002, do not represent the gravitational field over Egypt better than 0.80 meter.

Currently, accurate GPS networks are being constructed along the Nile to serve various undergoing surveying and mapping activities. Recent two local geoid models, SRI2001 and NILE2004, have been integrated to generate a new model mainly for the Nile valley. Accordingly, more reliable orthometric heights have been computed for 15 NACN stations. Over 5 known check points, the obtained heights have produced errors in the range between 0.06 meter and 0.42 meter with an average of 0.18 meter, which is seven times more accurate than the heights published by ESA right now. From an economical point of view, the developed approach can be performed as an alternative to the relatively expensive and time-consuming spirit levelling method. Thus, this scheme yields a considerable cost reduction in surveying and mapping applications in Egypt.

ملخص

للدخول في القرن الحادي و العشرين أنشأت مصر هيكل جيوديسي جديد عالي الدقة اعتمادا علي المرجع الجيوديسي العالمي لعام 1984 ليكون النظام المرجعي القومي المبني علي جي بي إس. أقيمت الشبكة القومية للكادستر الزراعي المكونة من 112 محطة جيوديسية بدقة جزء في المليون لخدمة التنمية الزراعية في وادي النيل. إلا أنه لم يتم رصد مناسيب نقاط هذه الشبكة وتم حساب المناسيب باستخدام نموذج الجيويد العالمي لعام 1991. وقد أثبتت دراسات سابقة أن دقة هذا النموذج في مصر تبلغ حوالي 1.5 متر ، وحتى نماذج الجيويد العالمية الأحدث لا تمثل طبيعة مجال الجاذبية الأرضية في مصر بدقة أحسن من 0.8 متر. يتم حاليا إنشاء شبكات جي بي إس دقيقة علي نهر النيل لخدمة العديد من تطبيقات المساحة و الخرائط لأغراض الإدارة المتكاملة للموارد المائية في مصر. وعلي صعيد آخر فقد تم دمج أحدث نموذجي جيويد محليين لإنتاج نموذج جيويد دقيق لمنطقة وادي النيل. ومن ثم فقد أمكن حساب مناسيب أدق لخمسة عشر نقطة من نقاط الشبكة القومية للكادستر الزراعي. وعند اختبار الطريقة الجديدة عند خمسة نقاط معلومة فقد أثبتت النتائج أن الدقة المتوقعة للمناسيب تتراوح بين 0.06 متر و 0.42 متر بمتوسط 0.18 متر مما يعادل سبعة أضعاف دقة المناسيب المستخدمة حاليا. ومن ثم يخلص البحث إلى أن هذا الأسلوب يزيد من دقة و تكامل وتجانس قواعد البيانات الجيوديسية في مصر ، كما أنه من وجهة النظر الاقتصادية يمكن استخدامه كبديل لطريقة الميزانيات الارضية المكلفة مما يساعد في خفض تكلفة مشروعات المساحة و الخرائط في مصر.

Enhancing the Integrity of the National Geodetic Data Bases in Egypt

Gomaa M. DAWOD and Sherine S. ISMAIL, Egypt

1. INTRODUCTION

At the end of the twentieth century, the necessity to develop new precise geodetic systems has been a crucial demand by the geodetic communities worldwide e.g. Kasser and Breton, (2003) . With the rapid growth of GPS utilization in Egypt since 1985, the WGS84 global geodetic datum has been selected to be the new geodetic framework. In 1995, two national GPS geodetic control networks have been established, by the Egyptian Survey Authority (ESA), to furnish a nationwide GPS skeleton for surveying and mapping applications. The first network is the High Accuracy Reference Network (HARN) that covers the entire Egyptian territories and consists of 30 stations with approximate separation of 200 Km. The relative precision level of HARN is 1:10,000,000. The second network is the National Agricultural Cadastral Network (NACN) that is mainly covers the Nile valley and the Delta. NACN consists of 112 stations, with a station separation of 50 Km approximately, whose relative precision is 1:1,000,000. Both networks are depicted in Figure 1. Other GPS geodetic control networks have been established for some specific projects, but do have neither a national coverage nor such accuracy limits e.g. Saad, (1998) .

A vital drawback for both networks concerns the orthometric heights of almost all stations. Because of the site selection of the stations to be on high places such as the top of buildings, the spirit levelling technique could not be used to observe those orthometric heights. Instead, the OSU91A global geopotential model has been employed to convert the ellipsoidal heights to the orthometric ones. It has been proved that the accuracy of the OSU91A model over Egypt is in the order of 1.5 meter Saad and Dawod, (2002) . Furthermore, new global geoid models, such as the EGM96, PGM2000A, and UCPH2002, do not represent the gravitational field over Egypt better than 0.8 meter Dawod, (2005) . Hence, this paper aims to develop a new efficient scheme to estimate precise orthometric heights of national GPS geodetic control networks in order to increase the integrity and completeness of the national geodetic databases in Egypt.

2. RECENT PRECISE GEOID MODELS IN EGYPT

Saad and Dawod (2002) have developed two precise geoid models for the entire Egyptian territory. The first geoid, called SRI2001A, is a gravimetric geoid model utilizing the most recent and accurate first-order gravity measurements, and is based on the GRS80 reference datum. The EGM96 global geopotential spherical harmonic model is used to provide the long wavelength of the Earth gravitational field, along with a local DEM in the remove-compute-restore FFT processing technique. The obtained geoid undulations range from 5.42 m to 22.40 m with a mean value of 14.54 m and RMS equals 2.96 m. A GPS/Levelling data set of 195 precise stations has been used to generate a geometric-satellite geoid model. A second-order polynomial, as a function of the distance from the network origin, is found to be the

best fitting function to integrate gravimetric undulations and GPS/Levelling undulations. Therefore, a combined GPS/Gravity geoid for Egypt, SRI2001B, has been generated. This geoid model, depicted in Figure 2, has a minimum undulation value of 9.437 m and a maximum value of 21.39 m with an average of 13.62 m and RMS of 2.62 m. The values of the estimated undulations from the SRI2001B model have been compared against the pure GPS undulation of some independent GPS/Levelling stations. The differences range between –0.01 m and –0.28 m, with an average equals –0.10 m, and RMS of 0.49 m.

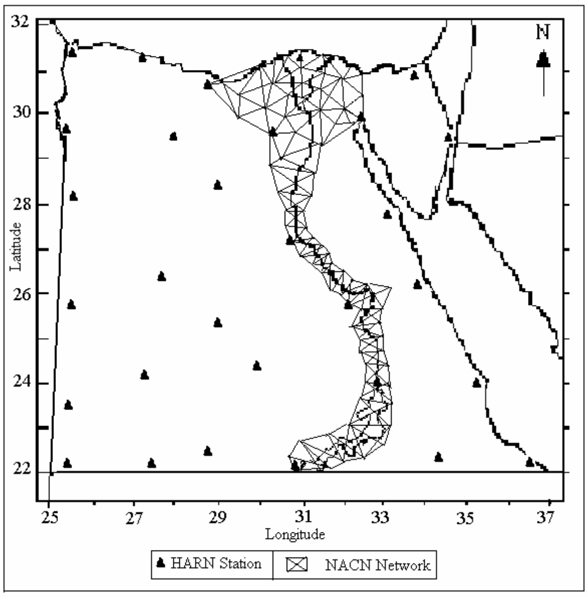

Figure 1: Recent precise GPS geodetic control networks in Egypt

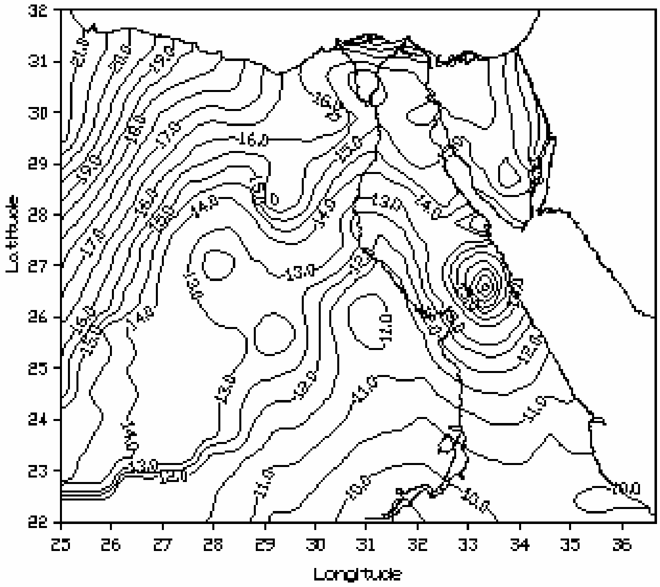

Figure 2: SRI2001 Geoid Model of Egypt

Dawod (2005) has proved that the EGM96 model, compared to other global geoid models, is the optimum global geoid model to deal with in Egypt. Therefore, it has been decided to model the irregularities between its geoid undulations and the observed estimates at GPS/Levelling stations in the study area, that covers 408 km along the Nile from Delta barrage to Assiut barrage. It has been conclueded that a simple polynomial is not able to fit the irregular structure of the undulation differences. Thus, a correction or conversion surface has been developed to fit the undulation differences. The obtained results show that the accuracy of this surface is better than 0.04 m. Hence, a precise geoid model, called NILE2004, has been obtained covering the fourth reach of the River Nile and is applied in the undergoing project of hydrographic surveying.

3. HYDROGRAPHIC SURVEYS ALONG THE NILE

Hydrographic and topographic maps play a crucial role in the management of water resources. Since the Nile constitutes the main source of fresh water in Egypt, its precise maps are a key element in the context of integrated water resources management policy. In order to study the recent morphological and hydrological changes of the Nile, the Nile Research Institute (NRI) has initiated a four-year national project to produce precise digital hydrographic and topographic maps covering the river and its two branches. The main core of this pioneer project is a multi-fold precise geodetic control network utilizing the state-of-the-art GPS instrumentation and techniques. The network consists of approximately 600 control stations spacing 5 km apart on both banks of the Nile, which is almost 1435 km long. Orthometric heights of all control stations will also be determined. It is anticipated that this network will improve the reliability of the national geodetic networks, and have a great economical impact on surveying and mapping activities in Egypt.

4. AVAILABLE DATA AND PROCESSING

A precise GPS control network have been established on both banks along the forth reach of the Nile, that is from Delta barrage to Assiut barrage extending about 408 km. The network, depicted in Figure 3, consists of 168 control points, of them 130 stations have observed orthometric heights, which station separation ranges from 0.2 km to 9.2 km with an average equals 5.7 km. The network has been observed and processed in the optimum way to insure the quality of precise geodetic control networks, i.e., at least 1 ppm level of precision. It has been tied to the HARN and NACN national networks through 20 tie stations. The networks' statistics are summarized in Table 1. The distances from GPS stations to NACN points range from 4.5 km to 34.2 km with an average equals 19.7 km. As previously stated, those stations have no observed orthometric heights.

The issue of obtaining orthometric heights from GPS measurements attains a great deal of research work recently e.g. Hu et al, 2004, Wisloff, 2002, and Martensson, (2002) . The proposed strategy consists of two steps: (a) obtaining a precise estimate of the undulation differences for each observed baselines connecting a NACN station to the GPS network, and (b) combining the attained undulation differences to the ellipsoidal height differences to come

up with an accurate orthometric height difference, which added to the observed orthometric height of the GPS station to compute the orthometric height of an NACN point.

Table 1: Statistics of available geodetic data

	GPS Control Network	GPS/Levelling Stations
No. of stations	166	130
Minimum distance (km)	0.2	0.2
Maximum distance (km)	7.3	9.2
Mean distance (km)	4.5	5.7

Since the NILE2004 geoid is restricted to the Nile area with a width of approximately 4 Km only, the first procedure combines the two local geoid models to produce a more-precise one that covers the study area. Next, the kriging statistical method has been utilized to interpolate undulation differences for the observed GPS baselines. Kriging is a geostatistical interpolation technique that gives best-linear unbiased prediction estimates of unknown values of a random function or a random field. Due to its efficiency in modeling the variations of geospatial quantities, this method is widely applied in various geodetic applications in the last few years e.g. Smith et al, 2003, and Wielgoz et al, (2003) . Krigging attempts to express trends suggested in a specific data set by utilizing the spatial and temporal correlation properties of the underlying phenomenon and incorporating the measures of the error and uncertainties when determining the estimates. The mathematical principle underlines krigging is the variogram, which is a measure of how quickly things change on the average, so it is a function of the distance between two locations. For example, a linear weighting kriging scheme is given by Johnston, (2003) :

$$\gamma (h) = (1/2n) \Sigma \{ zi - zi\text{-}h\}2 \qquad (1)$$

where,

h is the lag distance (the distance between two points used to calculate the variance), n is the number of observations, γ is the average difference in the interested quantity at a specific lag distance, z is the attribute of interest – in this case geoidal undulation, and i and i-h are index notations denoting the location of z. Applying an ordinary kriging, the geoidal undulation variations have been represented in a two-dimensional manner, that enables precise interpolation of undulations at the required unknown NACN points. Hence,

$$\Delta Ni,j = Nj - Ni \qquad (2)$$

where,

Nj is the known undulation at the GPS point j, and Ni is estimated or interpolated undulation at the NACN point i.

Similarly, the height difference can be written:

$$\Delta hi,j = hj - hi \qquad (3)$$

where,

hj and hi are the ellipsoidal heights for both the GPS point j, and the NACN point i.

Since,

$$Hi = hi - Ni \qquad (4)$$

where Hi denotes the orthometric heights of the required point, and the other two quantities are defined above. A similar equation (4) can be written also for station j. So, in a relative sense, it can be written:

$$\Delta Hi,j = \Delta hi,j - \Delta Ni,j \qquad (5)$$

Having obtaining the orthometric height difference between the GPS and the NACN points, the level of the NACN station can be computed as:

$$Hi = Hj + \Delta Hi,j \qquad (6)$$

If the NACN point is connected to several GPS stations, a least-squares adjustment is performed to come up with the optimum orthometric height estimate. Applying such a strategy, the orthometric heights of 20 HARN and NACN stations, depicted in Figure 3, have been attained. Finally, in order to judge the achieved results, 5 HARN stations with known observed orthometric heights (T2, E7, M3, F1, and O1) are utilized. The differences, or errors, in orthometric heights at those check points range from 0.06 meter and 0.42 meter with an average of 0.18 meter. Hence, it can be concluded that orthometric heights of 15 NACN national GPS stations, given in Table 2, have been estimated with a mean precision of ± 0.20 m.

Table 2: Computed orthometric heights of NACN stations

Station	Orthometric Height	Station	Orthometric Height
Z64	200.48	Z76	70.72
Z65	93.55	Z78	115.69
Z66	77.44	Z81	156.06
Z67	59.07	Z82	47.83
Z69	133.74	Z87	220.86
Z73	140.61	Z88	122.49
Z74	196.75	Z96	42.24
Z75	54.02		

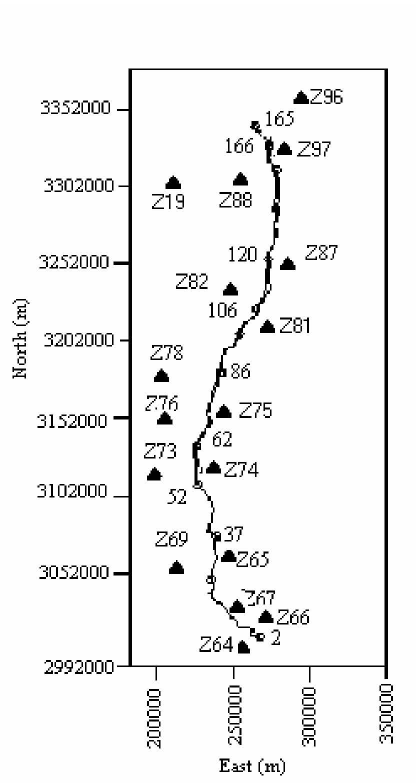

Figure 3: Utilized GPS networks

5. ACCURACY AND ECONOMICAL BENIFITS

From a technical point of view, it can be noticed that the developed procedure produces orthometric heights that are almost seven times more-accurate than the OSU91A-based heights published by ESA right now. Also, the results are even four times the accuracy of the EGM96-based (and those based on new global models such as PGM2000A and UCPH2002) orthometric heights. Recall that the average distance between the GPS and the NACN stations is 20 km, it can be concluded that the computed orthometric heights are within 1 cm/km level of relative precision. As the GPS national project over the Nile River continues, all NACN stations can obtain their precise and reliable orthometric heights utilizing the same procedure.

It is a matter of fact that the spacing between the NACN stations is 50 km in average, while that of the Nile GPS network is only 5 km approximately. Following the developed strategy, all GPS networks along the Nile valley can have an accurate estimate of orthometric heights. Hence, for any new GPS survey connected to an NACN station, orthometric heights can be estimated by converting the ellipsoidal heights. Economically speaking, the developed strategy can be used as an optional manner to get ride of the relatively expensive and time-consuming spirit levelling method. Thus, this scheme yields a considerable cost reduction in surveying and mapping applications in Egypt.

6. CONCLUSIONS

A critical shortcoming for the Egyptian national GPS networks (HARN and NACN) is the lack of observed orthometric heights of almost all stations. ESA has employed the OSU91A global geopotential model to convert the ellipsoidal heights to the orthometric ones. It has been proved that the accuracy of the OSU91A model over Egypt is in the order of 1.5 meter. This paper has developed an efficient scheme to estimate precise orthometric heights of national GPS geodetic control networks based on utilizing the recent national geoid models and the GPS network currently being established along the Nile.

It has been concluded that the accuracy of the estimated orthometric heights ranges from 0.06 meter and 0.42 meter with an average of 0.18 meter, which is seven times more-accurate than the OSU91A-based heights published by ESA right now. In a relative sense, the computed orthometric heights are within the 1 cm/km level. As the GPS national project over the Nile River carries on, all NACN stations can obtain their precise and reliable orthometric heights utilizing the same technique. Consequently, the developed procedure enhances the reliability and integrity of the national geodetic database in Egypt. Moreover, new GPS surveys can gain orthometric heights by converting the ellipsoidal heights. From an economical point of view, the developed approach can be performed as an alternative to the relatively expensive and time-consuming spirit levelling method. Thus, this scheme produces significant cost saving in surveying and mapping applications in Egypt.

REFERENCES

Dawod, G., 2005, Developing a precise geoid model for hydrographic surveying of the River Nile, Al-Azhar Engineering Al-Azhar University Engineering Journal (AUEJ), V. 8, No. 1, January, pp. 96 – 107

Hu, W., Gao, Q., Fidis, C., and Kuang, S., 2004, Research on GPS-derived orthometric height: A case study, The annual ACSM meeting, Tennessee, USA, April 16-21.

Johnston, S., 2003, Uncertainty in bathymetric surveys, The U.S. Army Corps of Engineers, Technical Report No. ERDC/CHL CHTEN-IV-59, March, 22 pp.

Kasser, M., and Breton, J., 2003, Necessity to work in a reference frame in France, FIG working week 2003, Paris, France, April 13-17.

Martensson, S., 2002, Height determination by GPS: Accuracy with respect to different geoid models in Sweden, The FIG XXII International Congress, Washington, D.C., USA, April 19-26.

Saad, A., 1998, Unifications of the GPS work in Egypt, Civil Engineering Research Magazine (CERM), Al-Azhar University, V.20, No.4, pp.462-470.

Saad, A., and Dawod, G., 2002, A Precise Integrated GPS/Gravity Geoid Model for Egypt, Civil Engineering Research Magazine (CERM), Al-Azhar University, V.24, No. 1, pp.391-405.

Smith, S., Holland, D., and Longley, P., 2003, The effect of changing grid size in the creation of laser scanner digital surface models, Proceedings of the Seventh International Conference on Geo Computations, University of Greenwich, U.K., September 8-10.

Wielgoz, P., Grjner-Brzezinska, D., and Kashani, I., 2003, Regional ionospheric mapping with krigging and multiquadric methods, Journal of Global Positioning System, V.2, No.1, pp. 48-55.

Wisloff, S., 2002, Deriving orthometric height from GPS measurements using a height reference surface, The FIG XXII International Congress, Washington, D.C., USA, April 19-26.

BIOGRAPHICAL NOTES

Gomaa M. Dawod received his Master of Geodetic Science and Surveying from the Ohio State University, Columbus, Ohio, USA in 1991 and his Ph.D. of Surveying Engineering from Shobra Faculty of Engineering, Zagazig University, Egypt in 1998. Since 1987, he is affiliated with the Survey Research Institute (SRI), the National Water Research Center (NWRC), Egypt, mainly in the field of Geodesy. He has participated in several national surveying and mapping projects and has established many geodetic control networks by GPS. He, also, has been fully involved in establishing the Egyptian National Gravity Standardization Network (ENGSN97). From 2002 to 2004, he has moved to the Nile Research Institute (NRI) and participated in the project of updating the hydrographic and topographic maps of the Nile River.

Sherine S. Ismail has obtained a BSC of Surveying Engineering from Shobra Faculty of Engineering, Zagazig University, Egypt in 1991. She also has obtained both MSC and Ph.D. of Hydraulic and Irrigation Engineering from Ain Shams University, Egypt in 1997 and 2001 respectively. She is a researcher at NRI, NWRC, Egypt, and she is involved in the undergoing project for updating the topographic and hydrographic maps of the River Nile, where dense GPS control networks are being established.

CONTACTS

Gomaa Mohamed Dawod
Survey Research Institute
308 Al-Ahram Street, Talbia, Giza 12111
EGYPT
Tel. + 20 2 5867174 / +20 12 3683541
Fax + 20 2 5867174
Email: dawod_gomaa@yahoo.com
Web site: http://www.nwrc.gov.eg

Published in: Civil Engineering Research Magazine (CERM), Al-Azhar University, Egypt, V. 29, No. 1 (Jan.), pp. 292-310.

NEW STRATEGIES IN THE UTILIZATION OF GPS TECHNOLOGY FOR MAPPING AND GIS ACTIVITIES IN EGYPT

Dr. Gomaa Mohamed Dawod

Survey Research Institute, National Water Research Center.
E-mail: dawod_gomaa@yahoo.com

ABSTRACT

GPS has been widely utilized since 1985 for extensive varieties of surveying, mapping, and GIS activities world-wide and in Egypt. Until the beginning of the twenty-first century, the employment of a single receiver to capture the satellite signals yielded coordinates' accuracy that was not good enough for surveying applications. The Selective Availability (SA) degradation has been terminated On May 1, 2000. This study tries to estimate recent Single Point Positioning (SPP) accuracy based on real data in Egypt, and to investigate its suitability for mapping and GIS activities. It has been found that the 3D SPP accuracy estimates have a mean value of 5.20 meters. Hence, it can be concluded that the SPP mode meets the requirements of medium-scale maps. On the other hand, even though there are two national GPS geodetic control networks in Egypt, a vital defect is that they are not dense enough to cover the areas of new development projects. Thus, the necessity for establishing new geodetic networks yet exists. Recent GPS positioning methodologies, such as the Precise Point Positioning (PPP) approach, have been inspected, and new strategies are explored in order to increase the accuracy and reliability of new precise GPS control networks in such remote regions. It has been found that utilizing global IGS stations to tie a local GPS network, and employing the IGS precise satellites' orbits considerably improves the precision of the geodetic networks, particularly for high-precision GPS applications such as deformation and crustal movement monitoring. Economically speaking, such processing approaches produce considerable cost reduction in the surveying and mapping projects in Egypt.

1- INTRODUCTION

The satellite-based Global Positioning System (GPS) has been extensively employed in Egypt since 1985 for a wide range of surveying and mapping applications. The major application of GPS was the establishment of precise geodetic networks that furnish a framework for other activities. In such a scenario, two or more GPS receivers were operated in a differential static mode. That was due to the fact that utilizing a single receiver to capture the satellite signals, which is called Single Point Positioning (SPP) mode, yields horizontal coordinates' accuracy within ±100 meters. Of course this accuracy is not good enough for surveying and even the Geographic Information System (GIS) activities. It is a matter of reality that the main source of error in the civilian SPP was the Selective Availability (SA) degradation imposed intentionally by the US government in order to prevent other-military users from gaining high accuracy in real time. On May 1, 2000 the US government has turned the SA off. Since then, several world-wide studies had been carried out to investigate the accuracy of the SPP. Hence, the first objective of this research study is to estimate recent SPP accuracy and to investigate if it is suitable for mapping and GIS applications in Egypt.

Moreover, the rapid growth of GPS utilization in Egypt has encouraged the utilization of the WGS84 global geodetic datum as a new national geodetic framework. In 1995, two national GPS geodetic control networks have been established, by the Egyptian Survey Authority (ESA), to furnish a nationwide GPS skeleton for surveying and mapping applications. The first network is the High Accuracy Reference Network (HARN) that covers the entire Egyptian territories and consists of 30 stations with approximate separation of 200 Km. The relative precision level of HARN is 1:10,000,000. The second network is the National Agricultural Cadastral Network (NACN) that is mainly covers the Nile valley and the Delta. NACN consists of 112 stations, with a station separation of 50 Km approximately, whose relative precision is 1:1,000,000. Both networks are depicted in Figure 1. One vital defect in these national data sets is that they are not dense enough to cover the areas of new development projects, e.g. the South Valley development project (south-west of Egypt) and the North Sinai development project (north-east of Egypt). Hence, the necessity for establishing new geodetic networks is yet existing for many surveying and mapping activities. Therefore, new strategies are explored in order to increase the accuracy and reliability of GPS geodetic networks in such remote regions. Consequently, the second goal of the current study comprises two issues: (1) the potential of utilizing the global International GNSS Service (IGS) stations as tie stations instead of the national

GPS stations; and (2) the precision improvements attained when utilizing the precise computed GPS satellites' orbits instead of the broadcasted ones.

Section two presents a brief on the recent GPS status and the available international services. The data used are summarized in section three, while section four presents the processing methodologies and the attained results. The achieved conclusions and drawn recommendations are given in section five.

2- CURRENT GPS STATUS AND INTERNATIONAL SERVICES

Although the instantaneous accuracy of using a single GPS receiver, whatever it is a hand-held or geodetic type, was limited by many error sources including satellite ephemeris error, satellite clock error, atmospheric effects, receiver noise and multipath, SA had been the dominant error since its introduction on 25 March 1990 [Rizos and Satirapod, 2001]. Hence, the SPP accuracy was degraded to about 100 meters in the horizontal components, and approximately 156 meters in the vertical component at the 95% confidence level. On midnight of 1 May 2000, the US President has declared to turn off SA. Since then, the improvements in the accuracy of SPP have been commented on by several investigators world wide. Table 1 presents some estimates of SPP accuracy reported from many researchers. It worth mentioning that the work of Saad and El-tokhy [2002] has investigated several items affecting the GPS attained accuracy; one of them is the termination of the SA. Additionally, other researchers have investigated new applications of Hand-Held GPS receivers for precise data collection through time synchronization between a base and rover handy receivers [Ali, 2004].

Within the context of the current discussion of the attained GPS accuracy, it is a matter of fact the undergoing GPS modernization plan will significantly afford more accuracy, reliability, and powerful signals from GPS satellites. For example, the first Block IIR-M satellite has been launched 26 September 2005. This type of modernized GPS satellites will broadcast the improved L2C code instead of the current C/A code, which in turn will enable civilian GPS users to better account for ionosphereic error. For more details on the GPS modernization plan, refer to e.g. Rizos [2006].

Table 1: Previous Estimates of SPP Horizontal Accuracy (95% confidence level)

Reference	SPP Accuracy (m)	Remarks
Saad and Al-tokhy, 2001	8.2	SPP accuracy of 3-hours observations
Rizos and Satirapod, 2001	6.0 5.7 5.4 5.1 4.7	Single-epoch accuracy Averaged 5-minutes's accuracy Averaged 15-minutes's accuracy Averaged 30-minutes's accuracy Averaged 60-minutes's accuracy
Milbert, 2001	9.3	Single-epoch accuracy
Ruppercht, 2001	7.0	Single-epoch accuracy
Snay, 2000	6.3 7.2 4.1	Averaged 24-hours's accuracy Averaged 12-hours's accuracy Averaged 6.5-hours's accuracy

Several international organizations provide significant and high-precision GPS services free of charge on the Internet. The famous organization is the IGS service.
The IGS, started in 1994, is a voluntary federation of more than 200 worldwide agencies that puts high-quality GPS data and data products on line in near real time to meet the objectives of a wide range of scientific and engineering applications and studies [IGS, 2006]. The IGS collects, archives, and distributes GPS observation data sets of sufficient accuracy to meet the objectives of a wide range of scientific and engineering applications and studies. These data sets are used to generate the following products:

- Three types of GPS ephemeris, clock and earth orientation solutions are computed. They are:
  - Final: The final combinations are available at 12 days latency.
  - Rapid: Rapid product is available with 17 hours latency.
  - Ultra Rapid: Ultra Rapid combinations are released 4 times a day.
- GLONASS satellite ephemerides
- Earth rotation parameters
- IGS tracking station coordinates and velocities (379 stations)
- GPS satellite and IGS tracking station clock information
- Zenith tropospheric path delay estimates
- Global ionospheric maps

Recently, new practical treatments have been proposed world-wide based on the utilization of IGS products. A new procedure has been developed, which is called Precise Point Positioning (PPP), and has been utilized for high-precision geodetic applications using a single GPS Receiver. PPP derives high precision positioning solutions by processing un-differenced carrier phase observations from a single GPS receiver assisted with IGS precise orbit and clock products. It has been employed for high precision kinematic positioning, at centimeter to decimeter level, using a single GPS receiver through the employment of precise GPS satellite orbit and clock data in real-time. This approach offers a significant cost saving since base stations do not need to be deployed [Nankali, 2006, Gao and Wojciechowski, 2004].

3- THE DATA USED

In order to investigate the three points of the current research studies, two groups of real recent data have been utilized. The source of these datasets is the undergoing national project of Nile Research Institute (NRI) that aims to produce precise digital hydrographic and topographic maps covering the Nile River and its two branches. The main core of this pioneer project is a multi-fold precise geodetic control network utilizing the state-of-the-art GPS instrumentation and techniques. The entire network consists of approximately 600 control stations spacing 5 km apart on both banks of the Nile, which is almost 1435 km long. The network is being tied to the HARN and NACN networks to ensure the integration and consistency of national GPS geodetic networks in Egypt [Dawod and Ismail, 2005].

The first dataset, used herein to investigate the obtained SPP accuracy, consists of 32 GPS static observation files over 22 NACN stations. This dataset cover an area extending about 450 Km in the North-South direction ($27^{o}\ 8^{'}$ N < latitude < $31^{o}\ 12^{''}$ N) and about 135 Km in the East-West direction($30^{o}\ 30^{'}$ E < longitude < $31^{o}\ 52^{''}$ E), as depicted in Figure 2. Since those static observations served to tie the Nile GPS networks to the national GPS datum, long observation sessions have been applied, and the sessions range from 115 to 303 minutes [Dawod and Abdel-Aziz, 2003]. Based on the satellites' geometry for the observed sessions, the number of collected epochs ranges from 458 to 2235 on a 15-seconds observation interval and 15-degree mask angle basis.

The second dataset, utilized in this study to inspect the potential of using IGS tie stations and precise satellite orbits, constitutes a GPS network along the forth reach of the Nile from Assiut to Al-Minia. This high-precision geodetic network covers an area extending about 130 Km in the North-South direction ($27^{o}\ 8^{'}$ N < latitude <

28^{o} $11^{''}$ N) and about 32 Km in the East-West direction (30^{o} $30^{'}$ E < longitude < 30^{o} $49^{''}$ E). It has been observed in 2004 by NRI, consisting of 54 new stations on both sides of the river with approximately 5-Km station separation, and tied to 6 NACN stations.

4- PROCESSING AND RESULTS

The processing procedures have been carried are divided into main categories, each set supports a main goal of the research study objectives as following.

4-1 RECENT ACCURACY ESTIMATES OF SPP

In order to investigate the recently obtained SPP accuracy, the collected 32 GPS static observation files, over 22 NACN stations, have been processed. The GeoGenius 2000 integrated surveying software has been utilized. It is a multi-folded processing and adjustment program for processing GPS, GLONASS, total station, and levelling data types [Spectra Precision, 2000]. This software, also, has a powerful tool for SPP processing for GPS data. Since all the utilized stations have their high-precision ground coordinates, the computed SPP coordinates for each station have been compared to the corresponding "true" coordinates. The positional errors in each coordinate component (dX, dY, and dZ) are computed, and furthermore, the length of the 3D error vector has been also computed as a resultant of the three error components. Through this procedure, real estimates of the SPP accuracy, not precision, are achieved. The obtained results are presented in Table 2, which shows that the 3D SPP accuracy estimates range from 1.94 meters to 7.93 meters, with a mean of 5.20 meters.

In order to investigate the frequencies of the SPP accuracy at several confidence levels, the obtained estimates have been grouped in a frequency distribution as presented in Table 3. From this table, it can be seen that 75 % of the obtained SPP accuracies are less than 6 meters.

Table 2: Accuracy estimates of SPP over NACN stations

	dX (m)	dY (m)	dZ (m)	3D (m)
Minimum	6.33	0.73	11.60	1.94
Maximum	11.22	11.25	18.52	7.93
Mean	4.82	4.47	4.65	5.20

Table 3: Frequency histogram of accuracy estimates of SPP

3D Error Range	No. of Stations	Percentage of Occurrence	Accumulated Percentage
< 2 m	2	6 %	6
2 – 3 m	4	13 %	19 %
3 – 4 m	1	3 %	22 %
4 – 5 m	6	19 %	41 %
5 – 6 m	11	34 %	75 %
6 – 7 m	1	3 %	78 %
> 7 m	7	22 %	100 %

Furthermore, the relationship between the obtained SPP accuracy and the number of collected epochs has been inspected, as depicted in Figure 3. A correlation analysis shows that the correlation coefficient between those two variables equals -0.49. The negative sign of the correlations means that the more number of observed epochs, the better the SPP accuracy. The correlation value itself shows that there is a moderate correlation relationship between the two variables under study. As mention before, the SPP even after the termination of the SA still suffers from several other sources of errors such as satellite ephemeris error, satellite clock error, atmospheric effects, receiver noise and multipath.

Moreover, the same 32 available GPS data files have been utilized to perform a regression analysis in order to simply describe the relationship between the SPP accuracy in meters (A) and the number of collected GPS epochs (B). The obtained regression equation is as following:

$$A = 7.186 - 0.0019 * B \qquad (1)$$

In order to provide some broad guidelines for GPS users, several simulated scenarios could be formulated based on this equation. For example, if the number of collected epochs is 100, the anticipated SPP 3D accuracy will be about 7 meters. If the desired SPP accuracy is 5 meters, 1150 epochs are needed. If the collected epochs reach 1675, the expected SPP accuracy is better than 4 meters, and if the required accuracy is about 2 meters, then 2730 epochs should be collected.

The question that is raised now is the potential of using SPP in surveying and GIS activities based on the attained SPP real accuracy estimates. Recall from Table 2 that the average SPP accuracy in 3D is 5.2 meters. It is a matter of fact that there are a wide range of mapping and GIS applications that do not require high accuracy

levels. It is a role that the field data collection of maps is of accuracy that is corresponding to 0.3 mm multiplied by the map scale. For example the field data collection of maps with scale 1:50,000 should be of accuracy better than 15 meters. Also, the field data collection of maps with scale 1:25,000 should be of accuracy better than 7.5 meters. Consequently, it can be concluded that the SPP accuracy meets the requirements of maps with scale 1:50,000 and 1:25,000. Hence from an economic point of view, using a GPS receiver in the SPP mode as a field data collection system, in mapping and GIS applications, will have a significant reduction of costs compared to the traditional surveying methods.

4-2 INCREASING ACCURACY OF GPS GEODETIC NETWORKS

As stated before, a critical weakness in the national GPS data sets in Egypt is that they are not dense enough to cover the areas of new development projects, e.g. the South Valley development project (south-west of Egypt) and the North Sinai development project (north-east of Egypt). Hence, the necessity for establishing new geodetic networks is yet existing for many surveying and mapping activities. Therefore, new strategies are explored in order to increase the accuracy and reliability of high-precision GPS geodetic networks in such remote regions. The second goal of the current study comprises two issues: (1) the potential of utilizing the global International GNSS Service (IGS) stations as tie stations instead of the national GPS stations; and (2) the precision improvements attained when utilizing the precise computed GPS satellites' orbits instead of the broadcasted ones.

The second available dataset constitutes a high-precision GPS network from Assiut to Al-Minia that consists of 54 new stations. The network has been observed utilizing static GPS techniques, where dual-frequency geodetic GPS receivers have collected data in observation sessions, that range from 2 to 5 hours. Additionally, This network has been tied to 6 NACN stations, which are Z64, Z65, Z66, Z69, Z73, and Z74. The corresponding raw observation files of two IGS stations, named MATE and BAHR, have been downloaded from the IGS web site, and incorporated in the GPS processing project. Firstly, the raw GPS observations of a sub-network that constitutes those 8 stations (the 2 IGS and the 6 NACN points) have been processed and adjusted using the Lieca SKI-Pro software. The aim of this procedure is to present an alternative in GPS network tie, particularly in areas where there are no close national GPS stations. Hence, the ITRF coordinates of both IGS stations have been held fixed in the over-constrained least-squares adjustment procedure. The obtained precision of the NACN stations, as expressed by the 3D standard deviations, range from ±0.6 cm to ±3.3 cm with a mean value of ±1.4 cm. These figures, presented in Table 4, indicate that utilizing IGS stations, as

ties to a new established precise GPS network, is a significant option especially in remote regions of Egypt where no HARN or NACN national GPS points exist. Recall that the IGS raw data files and the IGS stations' coordinates are obtained free of charge. Hence, from an economical perspective such a routine yields considerable reduction in the project costs since two GPS receivers will not be needed in the observation campaign.

Table 4: Standard deviations of NACN stations tied to the IGS network

St.	3D Standard Deviation (cm)
Z64	0.8
Z65	3.3
Z66	0.7
Z69	2.5
Z73	0.6
Z74	0.6
Minimum	0.6
Maximum	3.3
Mean	1.4

The second processing step in this section tries to estimate the improvements gained when utilizing IGS precise satellite orbits instead of the broadcasted orbits exist in the raw collected GPS observations. This sort of processing is dedicated to GPS applications require high level of precision, such as the deformation surveys, crustal movement monitoring, and establishment of local GPS reference networks. Hence, the corresponding precise orbit files for the observation campaign (the entire 54 GPS stations) have been downloaded from the IGS web site. Furthermore, two processing steps have been carried out for the entire GPS network, one with the broadcast orbits and the other with the precise orbits. It is expected that using the precise GPS satellites orbits will results in more precise GPS base lines vectors. After that, two least-squares adjustment runs have been carried out for adjusting the results of each processing scenarios. The standard deviations for latitude, longitude, and geodetic height, as measures of precision, for each GPS network' station have been computed in both cases, and the percentages of improvements have been work out. The attained results are summarized in Table 5, and depicted in Figures 4, 5, and 6. From these tables and figures, it can be seen that the standard deviation's mean of the latitude coordinates (σ_ϕ) has been decreased from ±1.4 cm to ±1.0 cm. For the longitude coordinates, the standard deviation's mean (σ_λ) has been

decreased from ±2.2 cm to ±1.3. For the geodetic heights, the standard deviation's mean (σ_h) has been decreased from ±5.3 cm to ±3.0 cm. Based on these findings, it can be concluded that utilizing IGS precise GPS orbits considerably improves the precision of GPS geodetic networks, particularly for GPS applications requiring high level of accuracy. Again, it worth mentioning that such significant improvements have no additional project' costs, since the IGS orbits are obtained free of charges.

Table 5: Precision improvements of utilizing IGS precise GPS orbits
(values are in cm)

	Case 1' Standard Deviations			Case 2' Standard Deviations		
	σ_ϕ	σ_λ	σ_h	σ_ϕ	σ_λ	σ_h
Minimum	0.5	0.5	2.9	0.5	0.5	1.9
Maximum	5.3	4.6	12.6	2.6	2.8	6.1
Mean	1.4	2.2	5.3	1.0	1.3	3.0

Case 1: Using broadcast satellites orbits
Case 2: Using precise satellites orbits

5- CONCLUSIONS

This research has investigated three principal issues concerning the utilization of GPS technology in surveying and GIS applications in Egypt: (1) to estimate recent SPP accuracy and to inspect its suitability, (2) to consider the potential of utilizing the global IGS stations as tie stations instead of the national GPS stations; and (3) to analyze the precision improvements attained when utilizing the precise computed GPS satellites' orbits instead of the broadcasted ones. The accomplished results can be summarized as following:

- Using 32 GPS static observation files, over 22 NACN stations, the 3D SPP accuracy estimates range from 1.94 meters to 7.93 meters, with a mean of 5.20 meters.
- Additionally, it has been found that 75 % of the obtained SPP accuracies are less than 6 meters.
- A correlation analysis shows that the correlation coefficient between the SPP accuracy and the number of collected GPS epochs equals -0.49. Then, the more collected observations, the better SPP accuracy obtained.

- It can be concluded that the SPP accuracy meets the requirements of maps with scale 1:50,000 and 1:25,000.
- From an economic point of view, using a GPS receiver in the SPP mode as a field data collection system, in mapping and GIS applications, will produce a significant reduction of costs compared to the traditional surveying methods.
- Utilizing two IGS stations to tie a local GPS network yields 3D standard deviations, range from ±0.6 cm to ±3.3 cm with a an average value equals ±1.4 cm.
- Economically speaking, such a routine yields considerable reduction in the project costs since two GPS receivers will not be needed in the observation campaign.
- Utilizing IGS precise GPS satellites orbits in the GPS network processing considerably improves the precision of GPS geodetic networks. It worth mentioning that such significant improvements have no additional project' costs, since the IGS orbits are obtained free of charges.

Based on the achieved results, the following recommendations can be drawn:

- The GPS SPP mode is an appropriate data collection tool in mapping activities for medium-scale maps, e.g. 1:50,000 and 1:25,000.
- Also, SPP could be applied in various GIS applications, which will produce a significant reduction of costs and still meets the required accuracy specifications.
- Utilizing IGS tie stations is an optimum alternative in establishing GPS geodetic networks in remote areas in Egypt where there are no existing national GPS control points.
- Employing IGS precise satellites' orbits in the GPS network processing should be a regular procedure in processing high-precision GPS geodetic control networks in Egypt.

REFERENCES

Ali, M., 2004, Application of Handy GPS Sets for Precision Data, Proceedings of the Map Asia 2004 Conference, August 26 - 29, 2004, Beijing, China.

Gao, Y., and Wojciechowski , A., 2004, High precision kinematic positioning using single dual-frequency GPS receiver, Proceedings of the XXth ISPRS Congress, 12-23 July, Istanbul, Turkey.

Dawod, G., and Abdel-Aziz, T., 2003, Establishment of precise geodetic control networks for updating the River Nile maps, Proceedings of Al-Azhar

Engineering Seventh International Conference (CD No. 3), Al-Azhar University, Cairo, April 7-10.

Dawod, G., and Ismail, S., 2005, Enhancing the integrity of the national geodetic data base in Egypt, CD Proceedings of the FIG working week and GSDI-8 international conference, Cairo, Egypt, April 16-21.

IGS, 2006, The International GNSS Service, http://igscb.jpl.nasa.gov/, Accessed August 2006.

Milbert, Dennis, 2001, Accuracy of hand-held GPS receivers after SA off, http://mywebpages.comcast.net/dmilbert/handacc/accur.htm, Accessed August 2006.

Nankali, N., 2006, GPS Precise Point Positioning Technique: A Case Study in Iranian Permanent GPS Network for Geodynamics, GIS Development, V. 10, No. 6, May, http://www.gisdevelopment.net/technology/gps/techgps_003b.htm, Accessed August 2006.

Rizos, C., 2006, New GNSS developments and their impact on the geospatial industry, GIS Development, V. 10, No. 6, June, pp. 34-36.

Rizos, C., and Satirapod, C., 2001, GPS with SA off: How good is it? Part 2, Measure and Map, No. 12, pp. 19-21.

Ruppercht, Wolfgang, 2001, Post SA accuracy measurements, http://www.wsrcc.com/wolfgang/gps/accuracy.html, Accessed August 2006.

Saad, A., and Al-tokhy, M., 2001, Precision investigation of the GPS results based on practical observations, Civil Engineering Research Magazine (CERM), Al-Azhar University, V. 23, No. 2.

Snay, Richard, 2000, Accuracy comparison with and without SA, http://www.ngs.noaa.gov/FGCS/info/sans_SA/, Accessed August 2006.

Spectra Precision, 2000, GeoGenius 2000 software user manual, Hoehenkirchen, Germany.

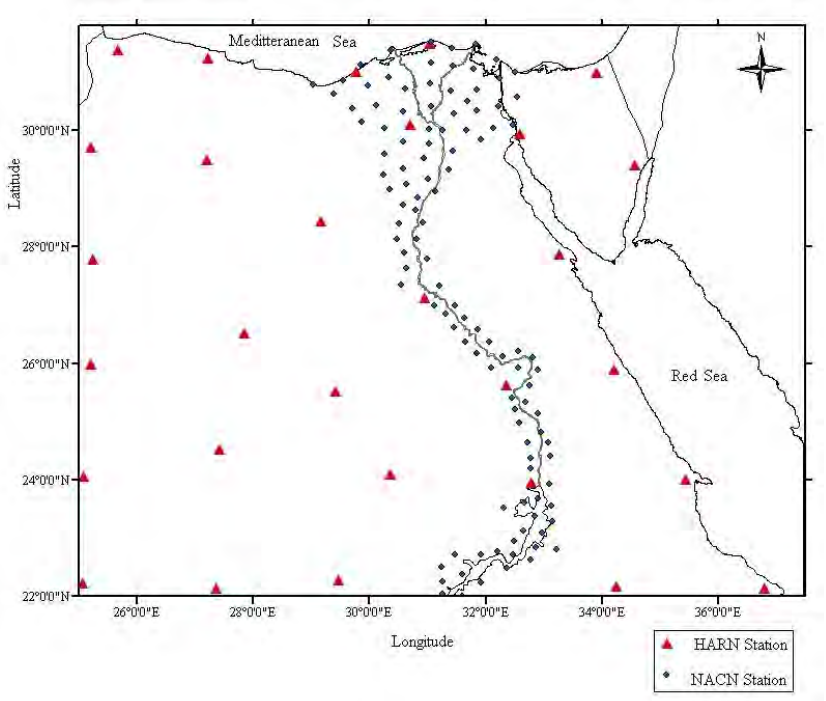

Figure 1: Recent precise GPS geodetic control networks in Egypt

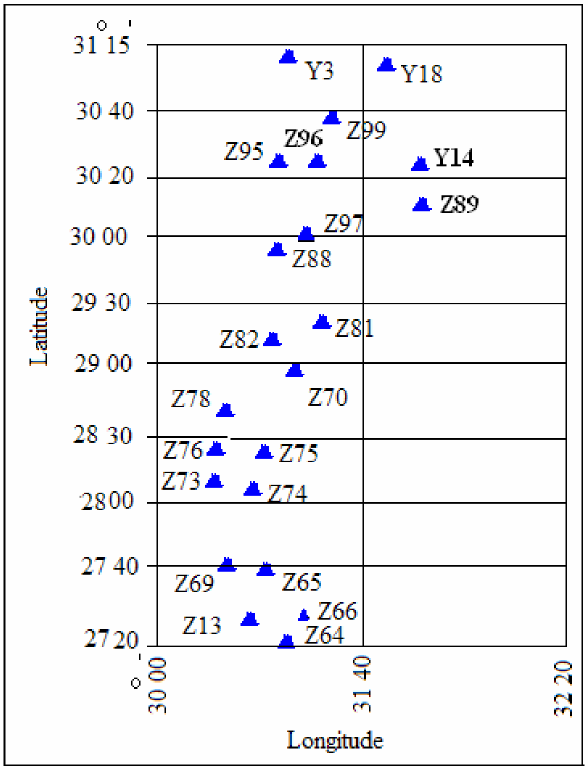

Figure 2: Utilized GPS national stations

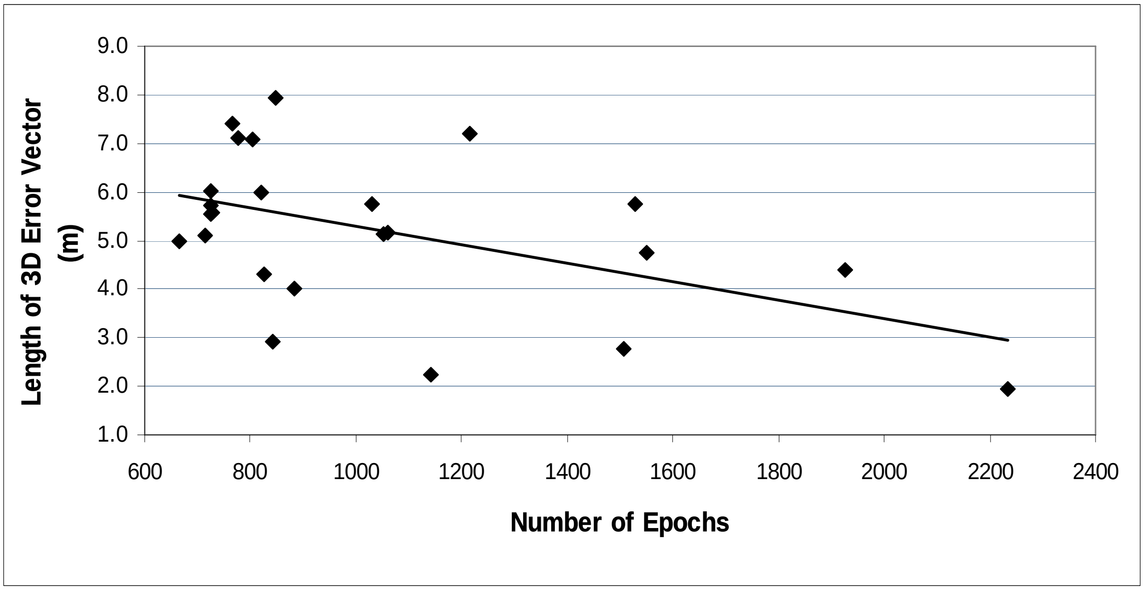

Figure 3: The relationship between SPP accuracy and number of epochs

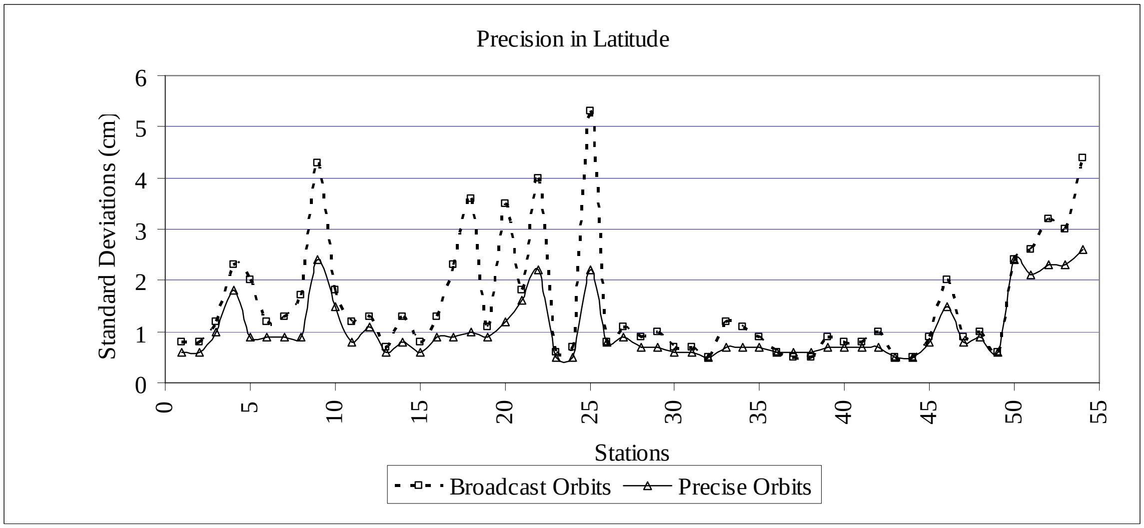

Figure 4: Improvements in latitude' standard deviations using precise orbits

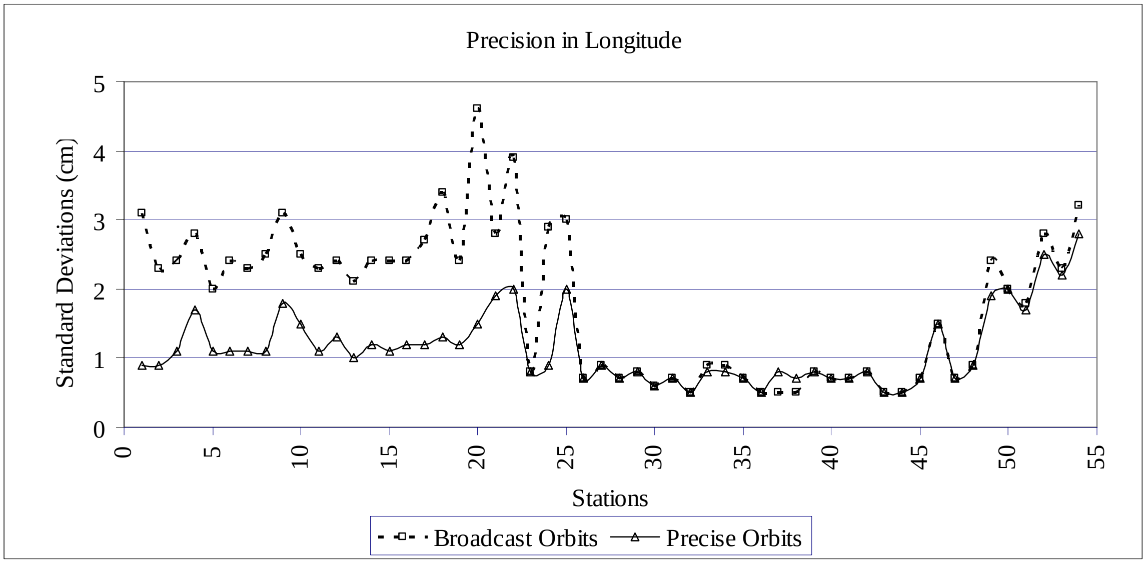

Figure 5: Improvements in longitude' standard deviations using precise orbits

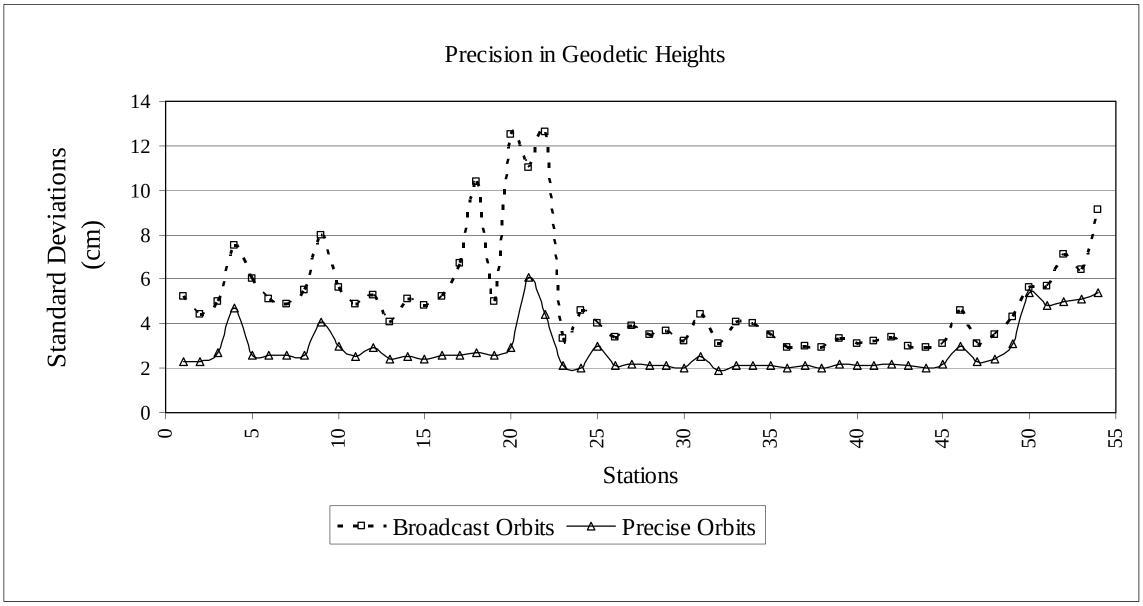

Figure 6: Improvements in geodetic height' standard deviations using precise orbits

تقييم مخاطر الفيضانات العالية لنهر النيل باستخدام نظم المعلومات الجغرافية

د. شيرين شوقي إسماعيل
معهد بحوث النيل – المركز القومي لبحوث المياه – مصر

د. هدي فيصل محمد
معهد بحوث المساحة – المركز القومي لبحوث المياه – مصر

د. جمعة محمد داود
معهد بحوث المساحة – المركز القومي لبحوث المياه – مصر
حاليا بجامعة أم القرى – مكة المكرمة – المملكة العربية السعودية
dawod_gomaa@yahoo.com

ملخص البحث:
يخضع نهر النيل لفيضانات تتغير في قيمتها بدرجة كبيرة من عام لآخر. ومع أن الفيضانات المنخفضة لها العديد من التأثيرات الجانبية علي الموارد المائية المتاحة مثل انخفاض كمية المياه والمشاكل الملاحية في النهر ، إلا أن الفيضانات العالية لها تأثيراتها الخطرة و الضارة جدا. حديثا تزايدت فيضانات نهر النيل مما يسبب ارتفاعا كبيرا في مناسيب المياه المنصرفة من خلف السد العالي. من المعلوم أن إنشاء السد العالي لعب دورا حيويا عظيما في منع إمرار مياه الفيضانات العالية خلفه (حيث تتجمع المياه في بحيرة ناصر) ، إلا أن قيم الفيضان في بعض السنوات سجلت زيادة أعلي من المتوسط مثل فيضانات عامي ١٩٩٨/١٩٩٩ و ١٩٩٩/٢٠٠٠. لذلك فأنه من المهم جدا إعداد مجري النهر و جانبيه لإمرار كميات من المياه (تصرفات) أعلي من القيم المتوسطة حاليا.

تبحث هذه الدراسة في تقييم تأثير مخاطر الفيضانات العالية لنهر النيل وتأثير إمرار كميات كبيرة من المياه وذلك باستخدام تقنية نظم المعلومات الجغرافية. تم تطوير برنامج حاسب آلي (بواسطة الباحثة الأولي) لحساب مقاطع المياه السطحية في أي جزء من نهر النيل. تم استخدام بيانات متاحة علي امتداد الحبس الرابع من نهر النيل والذي يمتد من قناطر أسيوط حتى قناطر الدلتا بطول حوالي ٤١٠ كيلومتر. تم تطوير أسلوب حاسوبي للدمج بين الحسابات الهندسية ونظم المعلومات الجغرافية لاستنباط تصورات لتأثير الفيضانات العالية. أظهرت نتائج الدراسة أن الأراضي الواقعة خلف حدود النهر ستكون في مأمن من مخاطر الفيضانات ، بينما وجدت حاجة ماسة لإعادة تأهيل الأراضي المنخفضة المنسوب. كما أثبتت النتائج أن تقنية نظم المعلومات الجغرافية تلعب دورا حيويا وأصبحت أداة تقنية عالية الجودة في تحليل و تقييم السيناريوهات المختلفة للفيضانات الخطرة وتقديم المعلومات المستنتجة – في صورة خرائط رقمية – لمتخذي القرار لوضع الخطوط الأساسية لعمليات التنمية في مصر.

Second National Symposium on GIS in Saudi Arabia
Al Khober, April 23-25, 2007

EVALUATION OF RIVER NILE HIGH FLOOD EFFECTS BY GEOGRAPHIC INFORMATION SYSTEM

Sherine S. Ismail
Nile Research Institute, National Water Research Center, Egypt
E-mail: sherine_shawky@yahoo.com

Hoda F. Mohamed
Survey Research Institute, National Water Research Center, Egypt
E-mail: hoda_faisal@yahoo.com

Gomaa M. Dawod
Survey Research Institute, National Water Research Center, Egypt
Currently at Um Al-Quraa University, Holly Makkah, Saudi Arabia
E-mail: **dawod_gomaa@yahoo.com**

ABSTRACT

River Nile is subjected to different floods with considerably high variations ranging from very low to very high floods. Even though low floods yield some side effects on the availability of water resources, low water levels, and navigation problems, high floods have many other critical outcomes. Recently, River Nile floods have relatively increased, which causes quite high water level upstream the High Aswan Dam. It is a matter of fact that construction of the High Aswan Dam, in 1968, has played a significant role in preventing downstream flooding. However, considerable floods have been recorded after the construction of the dam; such as the floods of 1998/1999 and 1999/2000. Therefore, it is extremely important to prepare the main Nile and its two branches for passing high releases more than the maximum current releases. This study evaluates the impacts of high water releases on the Nile water levels and bank line (terrace line) through a GIS application. A one-dimensional computer model program has been developed, by the authors, to compute water surface profiles along any river reach and, then, passes the results to a GIS package for further detailed analysis. The study area constitutes the fourth reach of the River Nile, which extends from Asyut

Barrage to Delta Barrage with a length about 410 Km. The achieved results showed that the entire lands behind the high bank, at this computed discharge, are safe against flood threats, while the low lands between the terrace and channel lines need to be developed. It has been concluded that GIS is quite an effective tool in analyzing such a hazardous scenario, produces valuable pieces of information for decision makers, and also presents guidelines for development planes.

Key Words: Nile River, Water Resources, Floods Impacts, GIS

1. INTRODUCTION

River Nile is considered a very unique river since it is one of the longest rivers in the world (about 6500 kilometers long) and its discharge is very limited compared with its length (Figure 1). River Nile flood has a very great variation due to the different characteristics of the Nile Basin. The Nile flood can be as high as 150 billion cubic meters per year (year 1878/1879) and as low as 42 billion cubic meters per year (year 1913/1914). Both extreme cases, very low and very high, floods have their own side effects. While the low floods have their own consequences such as of water supply un-sufficiency, navigation difficulties, and some local sedimentation problems, high floods produce very important side effects. Some of these impacts are the flooded areas, their effects on river banks, beds an hydraulic structures. River Nile is divided into different reaches between main hydraulic structures. The river length between down stream Old Aswan Dam to upstream of Delta Barrage is divided into four reaches according to the major hydraulic structures such as Old Aswan Dam, Esna Barrage, Naga Hammadi, Assiut Barrage, and Delta Barrage. The fourth reach located from Assiut Barrage to Delta Barrage is selected to be simulated during this study. The fourth reach length is about 410.00 kilometer length from kilometer 544.00 down stream Aswan Dam (Assiut Barrage) to kilometer 954.00 down stream Aswan Dam (Assiut Barrage). This reach is selected since it has suffered from many human interventions and its banks are relatively low compared with other reaches and it contains many populated islands.

The utilization of Geographic Information System (GIS) and Remote Sensing technologies has been spread in water resources management in the last two decades. GIS models can help people understand the problems they are facing

and help stakeholders to make decisions. It can be an important tool of communication and sharing knowledge, attributes which are now of high interest to international organizations. For example, in 1998 the United Nation Environmental Program (UNEP) started a project on water sharing in the Nile River basin. This project was set up to prepare an experimental methodology to identify the potential water-related issues in a watershed. Its first stage consisted of the compilation of available geo-referenced data sets for the Nile valley region to be used as inputs for water balance modelling, where these geo-referenced data sets have been stored in Arc/Info-ArcView environment [UNEP, 2000]. In Egypt, several researches have highlighted the role of GIS in a wide range of applications within the context of integrated water resources management [e.g. Yakoub and El-Kady, 1998, and Dawoud et al, 2005]. Moreover, the Nile River's flood management issue, has been investigated by many researchers [e.g. El-Sersawy et al, 2003] presenting approaches for producing digital floodplain maps, where GIS was used in the development of the base map imagery, redefinition of floodplains, manipulation of data, development of metadata, and the production of map panels.

2. OBJECTIVES

The objective of this paper is to study the effect of high floods on River Nile banks and islands using the most available recent techniques and data. Numerical model is developed and utilized, and selected study area' maps and Geographic Information Systems (GIS) have been used to identify areas subjected to flooding. Two flood values, for this study, were selected: the maximum future discharges, and the emergency flood of 7000 cubic meters per second, to indicate the effect of these damaging floods on a populated area.

3. MATERIALS AND DATA

Conventionally, three factors have to be analyzed in investigating the floods' harmful influences. These factors include: floodplain geometry (topography), flood discharge (hydrology), and flood stage (hydraulics). Topographic data describe the geometry of the physical system while hydraulic data are used to establish model boundary conditions, and to calibrate and test the model.

Figure 1. shows the Nile River and its selected fourth reach. For this specific area, many data are required. Some actual measurements were required to be able to calibrate the model. The particular inspected flow has never passed since the construction of the High Aswan Dam during the sixties. Hence, the measured records of the gauging stations for the period before the construction of the High Aswan Dam have been utilized. In order to study the flood effects on a populated area, a populated island (namely the Quarateen Island) has been chosen. This island has many buildings and factories and some other buildings. The island area is about 2 squared kilometers with a length of 3.8 kilometer.

4. PROPOSED MATHEMATICAL MODEL

Mathematical models are used to predict water levels for different flood conditions. For the current research, a mathematical model was derived based on solving the flow equations to compute water levels corresponding to different discharges. This model was developed, by the first author, using the Fortran computer language. Details of the computations are presented in the next sub-section.

Water Surface Profile Computations

Water surface profile computations for the developed model are based on solving the energy and the flow equations. The energy equation is described as follows:

$$\frac{V_1^2}{2g} + Y_1 + S_o \Delta L = \frac{V_2^2}{2g} + Y_2 + S_f \Delta L \quad (1)$$

Where:

V_1 = Average velocity at section (1)
V_2 = Average velocity at section (2)
Y_1 = Water depth at section (1)
Y_2 = Water depth at section (2)
S_o = Bed slope
S_f = Energy slope
ΔL = Distance between sections (1) and (2)

The Manning flow equation is described as follows:

$$Q = \frac{1}{n} R^{\frac{2}{3}} S^{\frac{1}{2}} A \quad .... \quad (2)$$

Where:

Q	=	Flow discharge,
n	=	Manning roughness,
R	=	Hydraulic radius (A / P),
S	=	Energy slope,
A	=	Cross sectional area, and
P	=	Wetted Perimeter.

The energy equation is solved numerically using Standard Step Method iterative procedure [Chow, 1957] The downstream boundary condition is pre-determined from the actual measurements and the water surface profile computations are processed from downstream to upstream.

5. MODEL CALIBRATION

The model calibration is a very essential task in any mathematical model computations. The first step for the model calibration is to determine the actual measurements related to the analyzed discharges at the gauging stations. Different gauging stations along the reach are used for this calibration water. These gauging stations are shown on Table 1.

The measured water levels related to the studied discharge (7000 cubic meters per second) are used for the selected gauging station and they are shown in Table 2 [NRI, 2007].

6. ACOMPLISHED RESULTS AND ANALYSIS

The model calibration and results are depicted in Figure 2. This figure shows the model results compared with the measured water levels for the selected discharge of 7000 cubic meters per second. It can be concluded, form this figure, that predicted simulation is very close to the measured data and the simulated results can be used for further analysis. Figure 3 shows the water

level for the whole fourth reach of the River Nile, and the study island is highlighted. It can be concluded, from this figure, that the water level due to the emergency discharge is estimated by 18.00 m at the southern end of the island and 17.72 m at the northern end of the island.

Table 1. Selected water level gauging stations.

No.	Site Name	Km
R4-1	Ds Assiut	544.78
R4-2	Maaabda	576.2
R4-3	Mandra	612.1
R4-4	Menia	687.55
R4-5	Fadl	735.25
R4-6	Beba	789
R4-7	Baniswafe	808.6
R4-8	Korimate	839.1
R4-9	Lethy	873.7
R4-10	Eksas	887
R4-11	Roda	927
R4-12	Usdelta	953

Table 2. Recorded levels for elected water level gauging stations.

Site Name	Km	Water Level
Ds Assiut	544.78	51.65
Maaabda	576.2	49.01
Mandra	612.1	45.71
Menia	687.55	39.26
Fadl	735.25	35.00
Beba	789	30.57
Baniswafe	808.6	28.98
Korimate	839.1	26.34
Lethy	873.7	23.69
Eksas	887	22.57
Roda	927	19.50
Usdelta	953	17.58

The ArcGIS software has been utilized to build a GIS for flood impacts of the study area. Digital topographic and cadastral maps have been incorporated in this system. Additionally, the attained flooding results have been displayed as a specific layer. Comprehensive GIS analysis, through merging, intersecting and buffering GIS tools, shows a very alarming result indicating that almost the whole island is subjected to flooding due to this condition. The detailed map of the study island is shown in figure 4. These findings can be confirmed by reviewing the levels on the study area map and similar conclusion can be reached that almost the whole island will be flooded during the emergency flood conditions. From this map, it is clear that the island contains houses, different types of buildings and even some factories.

Maximum future discharges

During the previous analysis it was shown that the whole study island is subjected to flooding under emergency discharge. However, the emergency discharge is a very rare event and extreme damages could be expected during this condition. The emergency flood is only considered in Egypt for hydraulic structures. The evaluation of flooded lands in Egypt is usually performed using the maximum future discharges. The maximum future discharges in Egypt are estimated by the flood of 350 million cubic meters per day which is equivalent to 4051 cubic meters per second. These discharges are used also to define the management lines for the river. Terrace line for the river bank is defined by the line that allow to pass a flow of the maximum future discharges and it is the line of slope change of the bank. Hence another analysis step has to be carried out.

Model results for the maximum future discharges

The model results for the maximum future discharges are obtained, and being analyzed. From the model results, it has been found that the water level due to the maximum future discharge is estimated by a level equals 16.68 m at the southern end of the island and 16.46 m at the northern end of the island. Furthermore, these results have been added, as a new layer, to the developed GIS of the study area. The comprehensive examination shows that the island is safe from flooding higher than the previously defined terrace line. So it can be concluded, for this part of the research, that the study area is safe from flooding for areas with levels higher than the terrace lines. The narrow strip

located between the terrace line and the water level is subjected to overtopping and under any condition, no buildings should be allowed in this strip.

7. CONCLUSIONS

The effects of high floods on River Nile banks and islands have been investigated. A numerical model was developed, by the first author, and utilized to compute and analyze the water levels related to the studied discharges. The model calibration procedure shows close computed results compared with the measured data. A study area has selected in this research to evaluate the effect of very high floods. This area consists of an Island located in the fourth reach with a length of 3.8 km and an overall area of about 2 squared km. The current emergency flood (a very rare event) was simulated by the model and the results were applied to the study area using GIS. The analysis results show that almost the whole island will be flooded during emergency flood. Another scenario has been also considered in this analysis, which is the maximum future discharges. The attained results correspond to the maximum future discharges show that the study area is safe against flooding higher than the terrace lines. More detailed analysis is recommended for the whole length of the river.

GIS utilization in such kind of studies related to water resources management is greatly valuable in capturing and communicating a great amount of information in a digital environment. A fundamental role of working in digital forms is that it allows the floodplain data to be easily incorporated with several other digital data types, such as digital orthophotos and GIS coverage of infrastructure, buildings, and land parcels. It has been concluded that GIS is quite an effective tool in analyzing such a hazardous scenario, produces valuable pieces of information for decision makers, and also presents guidelines for development planes.

REFERENCES

Chow, V. T. 1957, Open Channel Hydraulics, McGraw-Hill Book Co., New-York, pp. 680.

Dawoud, M., Darwish., M., and El-Kady, M., 2005, GIS-Based Groundwater Management Model for Western Nile Delta, Water Resources Management, V. 19, N. 5, pp. 585-604.

El-Sersawy, H., Aziz, M., and Ahmed, A.F., 2003, GIS Application for Developing Digital Floodplain Maps of the Nile River, Proceedings of Al-Azhar Seventh International Engineering Conference (CD No. 3), Al-Azhar University, Cairo, April 7-10.

NRI (Nile Research Institute), 2007, NRI Discharge Database, National Water research Center, El-Qanater, Egypt.

UNEP (United Nation Environmental Program), 2000, Project GNV011: Using GIS/Remote Sensing for the sustainable use of natural resources, Water sharing in the Nile Valley, A report by Diana Karyabwite.

Yakoub, N., and El-Kady, M., 1998, Using GIS for planning and water management of southern Egypt development project, Proceedings of the ESRI User Conference, San Diego, USA, http://www.wca-infonet.org/servlet/BinaryDownloaderServlet?filename=1059982781763_WRGIS_KO42.pdf&refID=96080 (Accessed Feb. 2007).

Figure 1: The River Nile Map

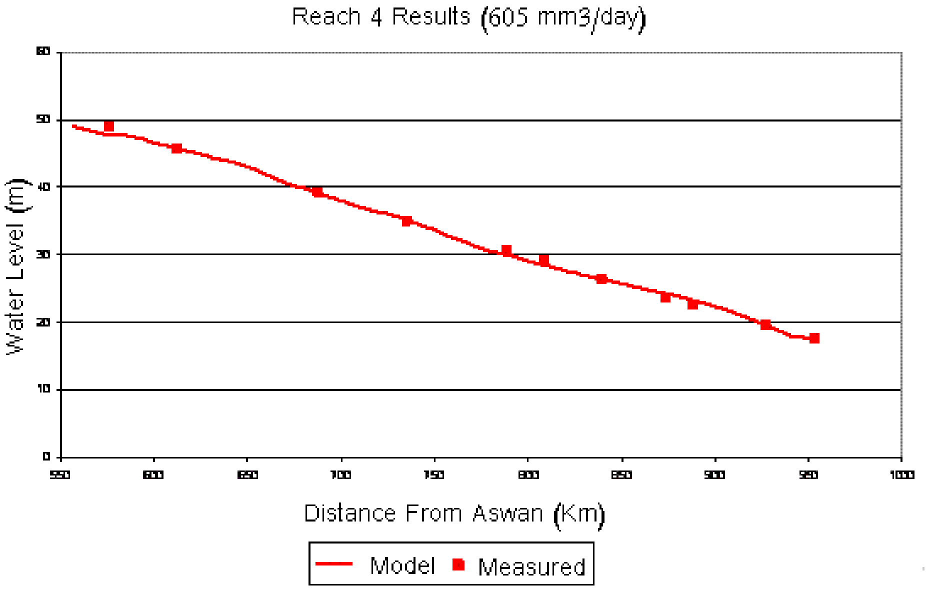

Figure 2: Model calibration and results

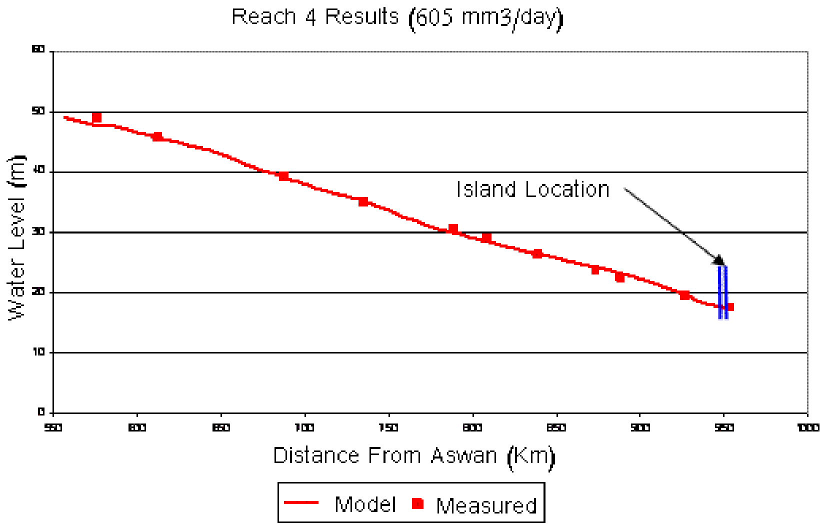

Figure 3. Model results for the study island

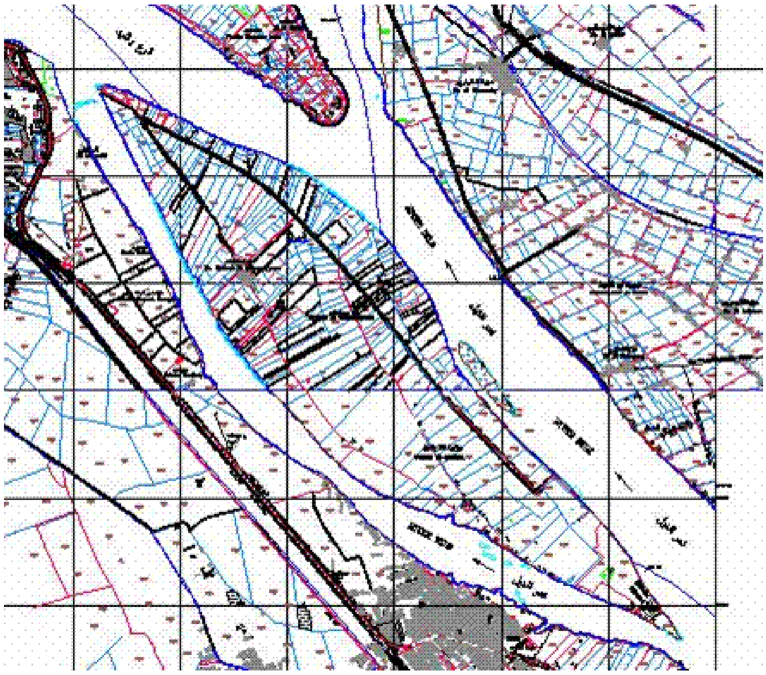

Figure 4: Map of the selected island

Published in: Civil Engineering Research Magazine (CERM), Al-Azhar College of Engineering, Cairo, Egypt, V. 29, No. 2, April 2007

ASSESSMENT OF A COST-EFFECTIVE GPS DATA PROCESSING ALTERNATIVE IN EGYPT UTILIZING INTERNATIONAL ON-LINE PROCESSING SERVICES

Hoda F. Mohamed [(1)], Sherine S. Ismail [(2)], and Gomaa M. Dawod [(1)]

[(1)] **Survey Research Institute, National Water Research Center**,
E-mail: dawod_gomaa@yahoo.com
[(2)] **Nile Research Institute, National Water Research Center Building,**
El Qanater, Egypt, P.O. 13621, Email: sherine_shawky@yahoo.com

Abstract

River Nile is one of the natural rivers that are subjected to erosion and sedimentation and accordingly to the change of its bed levels and contours. These changes in bed levels may affect different river usages and characteristics such as navigation, bank stability and morphology. Nile research Institute (NRI) is performing a continuous river hydrographic and topographic survey starting from 1979 up till recent survey of the river (on going now). The recent maps are now produced by NRI in cooperation with the Egyptian Survey Authority using the most advanced techniques of Global Positioning Systems (GPS).

Over the last few years, a number of free of charge on-line GPS processing services have been established and being available over the Internet. In order to judge two of these processing services; namely the PPP and AUSPOS services, static GPS observations that have been collected over 10 national GPS stations have been uploaded to both websites. The attained results show that the PPP service produces 3D standard deviations that have a mean of 0.090 m, and an accuracy average, when compared to the published coordinates, equals 0.209 m. Similarly, the accomplished outcomes of the AUSPOS service yield standard deviations with a mean of 0.026 m, and an accuracy average equals 0.240 m in the 3D space. Concerning the differences to the ESA stations' coordinates, the comparison reveals that the PPP results are better than the AUSPOS results by approximately 13%.

Investigating the on-line GPS processing services demonstrates several merits: (1) they are free of charge, (2) there is no need to purchase a processing software package, (3) those services are very useful for beginners GPS users who do not have a great experience in GPS processing strategies; and (4) using IGS stations to tie local GPS networks implies that receivers over base stations are not needed to be deployed in the field campaigns, and hence the time needed to collect data is considerably reduced. These advantages yield a substantial cost-saving in GPS surveying and mapping projects, and thus, on-line GPS processing services are recommended to be employed particularly for GPS campaigns in national development projects in Egypt.

1. Introduction

The Global Positioning Systems (GPS) is forming an essential tool for hydrographic and topographic survey for the River Nile and its banks. Nile Research Institute (NRI) has used this tool to develop the topographic and hydrographic maps to River Nile and its two branches with a total length of 1440 Km. The hydrographic survey for the River Nile and the topographic survey for River Nile banks are performed using GPS. Moreover, the hydrographic survey of Lake Nasser is performed by GPS since 1998 till now. Nile Research Institute has formed a huge data base of topographic and hydrographic GPS data (NRI, 2006).

Increasingly the spatial information sector is turning to the Internet as a tool to aid their activities. Both public and private sector organizations are developing, promoting and delivering their services and products using the Internet as a medium. Recently, several international organizations have developed on-line Global Positioning System (GPS) processing services. These services receive the user GPS observation files, in the RINEX format, and return back processing results free of charge. Organizations that provide these free services include: Geo-hazards Division of Geo-science of Australia, the Geodetic Survey Division (GSD) in Canada, the United States' National Geodetic Survey (NGS), Scripps Orbit and Permanent Array Center (SOPAC) at the University of California; and the Jet Propulsion Laboratory (JPL) at the US National Aeronautics and Space Administration (NASA).

The objective of this research study is to evaluate some of these online services, based on real GPS data, and compare their position results with expected values, as published by the Egyptian Survey Authority (ESA), in order to highlights the benefits of those international services particularly for surveying and mapping activities in Egypt. A brief description of each processing service is presented in section 2, while section 3 supplies the results of similar studies that have been carried out worldwide. Section 4 describes the available GPS data set that has been utilized to judge two of these on-line processing services. The achieved results are presented in section 5, and the concluded remarks are given in section 6.

2. Overview of online GPS processing services

There are a number of online GPS processing services that provide GPS processing results to the user free of charge and with unlimited access. These services provide solutions for a user-submitted Receiver Independent Exchange Format (RINEX) file based on differential methods using reference stations or precise point positioning using precise GPS orbit and clock data. Organizations that provide these free services include: Geohazards Division of Geoscience Australia, the Geodetic Survey Division (GSD) in Canada, the United States' National Geodetic Survey (NGS), Scripps Orbit and Permanent Array Center (SOPAC) at the University of California and the Jet Propulsion Laboratory (JPL) at National Aeronautics and Space Administration (NASA). An overview and a brief comparison are presented, herein, for a number of these global services [For more details, refer to Dare, 2006].

AUSPOS Service

The Geo-science Australia [formerly the Australian Surveying and Land Information Group's (AUSLIG)] Online GPS Processing Service (AUSPOS) was officially launched in late 2000,

and has been in continuous operation since then processing data for dual frequency geodetic GPS receivers located anywhere on earth. AUSPOS was designed and implemented with the following features and design goals: an easy to use web page interface, dual frequency geodetic GPS data processing capability, standard web-browser direct upload or ftp, highest quality global GPS processing standards, 24 hour 7 days a week service, rapid processing turnaround, < 15 minutes/file, results returned by email and ftp server, applicable anywhere on Earth; and GDA94 compliant for Australian users, ITRF elsewhere. The AUSPOS positioning is by differential GPS to the nearest three International GNSS Service (IGS) stations and uses the IGS precise orbit information. The AUSPOS design facilitates its use for a variety of applications, including: DGPS reference station positioning, remote GPS station positioning, ultra-long baseline positioning, GPS connections to IGS stations, high accuracy positioning; and GPS network quality control. This service is accessible via the Geo-science Australia website at: http://www.ga.gov.au.

PPP Service

The Geodetic Survey Division (GSD), Canada, developed the Canadian Spatial Reference System (CSRS) Precise Point Positioning (PPP) service. The PPP service provides post-processed position estimates over the Internet from GPS observation files submitted by the user. Precise position estimates are referred to the North American Datum of 1983 as well as the International Terrestrial Reference Frame (ITRF). Single station position estimates are computed for users operating in static or kinematic modes using precise GPS orbits and clocks. The online PPP positioning service is designed to minimize user interaction while providing the best possible solution for the given observation availability. Users need only specify the mode of processing, static or kinematic, and the reference frame for position output, NAD83 or ITRF. The observations processed are selected from the submitted RINEX file in the following order: (a) L1 and L2 pseudo-range and carrier phase observations, (b) L1 pseudo-range observation. Compared to uncorrected point positioning using broadcast GPS orbits, this application can improve results by a factor of 2 to 100, depending on user equipment, dynamics and duration of the observing session. This service is available via the GSD website at: http://www.geod.nrcan.gc.ca.

SCOUT Service

The Scripps Coordinate Update Tool (SCOUT) was developed by the Scripps Orbit and Permanent Array Center (SOPAC). This service also uses by default the three nearest IGS stations. However, this service allows the user to choose up to four different reference stations. The service's website is: http://sopac.ucsd.edu/

OPUS Service

The United States' National Geodetic Survey developed the Online Positioning User Service (OPUS). This service generates coordinate results by using data from three Continuously Operating Reference Stations (CORS). The CORS sites are chosen not according to closest proximity but picked according to compatibility between the user's data and the CORS site. There is also an option that allows the user to choose the CORS stations to be used. The service can be found at: http://www.ngs.noaa.gov.

Auto-GIPSY Service

Auto-GIPSY is an e-mail/FTP interface to the GPS Inferred Positioning System (GIPSY) developed by JPL. This service performs single point positioning, and is therefore not dependent on the proximity or availability of CORS/IGS data. The FTP address of user's data should be submitted by email to: ag@cobra.jpl.nasa.gov. For more details, visit the service's website at: http://milhouse.jpl.nasa.gov/ag/

A comparison of online services

There are general factors to consider in the evaluation of services; these include: the method of sending and receiving the data, the time delay in receiving the results; available options and limitations. An overall assessment of each service (summarizing the above-mentioned aspects) can be seen in Table 1. As can be seen in Table 1, the services use either uploading of the data or an FTP site in order to access the user's RINEX file. However, all of the services send an e-mail to the user either including the results or the FTP address of where the results can be obtained. Time delay on receiving the results depends on several factors including the traffic on the Internet and the number of users accessing the service at the same time. The displayed times in the Fourth column of Table 1 are only a rough indicator in order to compare the speed of each service and were obtained by submitting the same 6-h data set to each service [Dare, 2006].

3. Results of previous studies

In order to build a clear outlook about on-line GPS processing services and their merits, results of several research studies are presented herein. Soler, et al. [2006] have processed 30 consecutive days of GPS data using the OPUS service to determine how the accuracy of derived three-dimensional positional coordinates depends on the length of the observing session, ranging from 1 to 4 hours, over five Continuously Operating Reference Stations (CORS). The results emphasis that recommended session time for static data should be with a minimum of 2 hours in order to obtain a root mean square error better than five centimeters. Additionally, Witchayangkoon [2000] has investigated the accuracy of the precise point positioning (PPP) approach utilizing six-hour dual-frequency GPS data sets from four stations. It has been found the static solutions agree to within 10 cm with published coordinates, while the kinematic solutions show a discrepancy of less than one meter, mostly around half a meter. Moreover, Featherstone and Dent [2002] have performed a similar study utilizing the AUSPOS service in order to use this web-based service, along with a geoid model for Australia, to obtain orthometric heights utilizing only one GPS receiver. They have found that the computed coordinates of the check points differ from the published values by a total (geodesic) distance of 63 mm.

Furthermore, new modifications of the current processing models and strategies are being carried out in order to achieve more accurate results from such on-line services. For example, Chen et al. [2006] have analyzed the contribution of all major errors in the PPP observation models to the positioning accuracy and have developed new programs for static and kinematic PPP data processing. A new PPP algorithm based on parameter elimination method which separates time-variable parameters (i.e. position coordinates and receiver clock) and ambiguity

and tropospheric delays has been proposed for data processing. The positioning accuracy of 1 cm has been achieved with this static PPP method after the solution converges.

4. Utilized national GPS data

The available GPS data set consists of dual-frequency static GPS observation files that have been collected over 10 national GPS networks established by the Egyptian Survey Authority (ESA). This data set, depicted in Figure 1, has been observed by the Nile Research Institute (NRI) within the activities of the pioneer project for updating the topographic and hydrographic maps of the Nile River. The study area covers the region that extends in the North-South direction from 22 ^{o} 25$^{'}$ N to 31 ^{o} 12$^{'}$ N, and extends in the East-West direction from 30 ^{o} 37$^{'}$ E to 31 ^{o} 34$^{'}$ E. Those GPS observations have been used to tie the new established GPS Nile networks to the national GPS frame in order to assure the integrity of the achieved maps. The utilized GPS sessions, observed during the period 2002-2004, span a time ranging from 2.7 to 6.2 hours with an average of 3.8 hours.

5. Processing and results

Two of the previously mentioned on-line GPS processing services have been selected to deal with. The Canadian PPP and the Australian AUSPOS services are chosen due to two reasons: (1) PPP represents a category of services that is based on utilizing precise IGS GPS satellites orbits and clock corrections to estimate precise coordinates of the needed stations, while the AUSPOS is a candidate of the second category where, in addition, the IGS stations are used to tie the new ones in the ITRF2000 reference frame, (2) Both services are easy-to-use with minimum user interface needed, and based on upload the RINEX files instantaneously to the service website.

It worth to mention that the users of these on-line GPS processing services should be aware of a significant feature, that might lead to inaccurate results. Although the information on the antenna height and type are included in the RINEX files, the users must enter this piece of information in the appropriate website fields before uploading the RINEX files to the processing services. Otherwise, the antenna height will be considered as zero which, of course, will produce an error in the estimated station coordinates.

The first step in the processing stage was to convert the original GPS observation files to the RINEX format. It has been performed using the Lieca' SKI-Pro software since all the data have been collected using Lieca System 500 GPS receivers. Hence, those files have been sent to both on-line processing services. The attained processing results are presented in the following sub-sections.

5.1 Results of utilizing the PPP service

One of the merits of PPP is its richness of statistical information included in the output file. For example, it produces graphical representation of the standard deviations (SD) of each coordinate component (latitude, longitude, and geodetic height) as a function of the observation time span. Figure 2 is a typical example of such graphics for one of the utilized GPS stations. It can be seen, from this figure and other figures for all stations, that

approximately forty minutes of collected satellite signals is needed to reach a centimeter level in the standard deviations. The statistics of the attained standard deviations, as a measure of precision of the ten used GPS stations, are summarized in Table 2. From this table it can be noticed that the horizontal SD vectors range from 0.018 to 0.064 m with a mean of 0.043 m, while the 3D vectors of SD range from 0.032 to 0.141 m with an average of 0.090 m.

Furthermore, the obtained coordinates of each station have been compared against their published ESA coordinates in order to estimate the accuracy of the achieved PPP results. The statistics of the attained coordinates' differences are summarized in Table 3. From this table it can be noticed that the horizontal error vectors range from 0.079 to 0.266 m with a mean of 0.190 m, while the 3D error vectors range from 0.120 to 0.268 m with an average of 0.209 m.

5.2 Results of utilizing the AUSPOS service

The same RINEX files of the available 10 dual-frequency static GPS observations have been uploaded to the AUSPOS on-line GPS processing service. As mentioned previously, AUSPOS used the nearest 3 IGS stations to tie each new station and estimates its coordinates in the ITRF2000 frame. Additionally, the AUSPOS uses the EGM96 global geopotential model to estimate the geoid undulation, and hence can compute the orthometric height of each submitted station. Details of the GPS processing parameters, presented in Appendix 1, are included in the output file of each station. The statistics of the attained standard deviations, as a measure of precision of the ten used GPS stations, are summarized in Table 4. From this table it can be noticed that the horizontal SD vectors range from 0.009 to 0.037 m with a mean of 0.024 m, while the 3D vectors of SD range from 0.011 to 0.040 m with an average of 0.026 m. These figures are close to the results of a previous research study that has been performed on a local PC processing environment, not dealing with on-line processing service, and has utilized the basics of such an approach of employing the IGS precise orbits and IGS tie stations [Dawod, 2006].

Moreover, the obtained coordinates of each station have been compared against their published ESA coordinates in order to estimate the accuracy of the achieved AUSPOS results. The statistics of the attained coordinates' differences are summarized in Table 5. From this table it can be noticed that the horizontal error vectors range from 0.183 to 0.300 m with a mean of 0.230 m, while the 3D error vectors range from 0.196 to 0.302 m with an average of 0.240 m.

5.3 An assessment of achieved results from both services

A comparison between the coordinate differences of both PPP and AUSPOS results, as compared against the ESA published values, has been performed. Table 6 presents the attained statistics, which shows that the 2D error vector between the two services' results range from 0.044 to 0.157 m with an average of 0.086 m. In the 3D space, the error vector between the two services' results range from 0.049 to 0.175 m with an average of 0.098 m. These differences are basically due to the processing strategies applied in each service. As mentioned earlier, the AUSPOS service uses the nearest three IGS stations to tie the new station and estimates its coordinates, which does not applied in the PPP service. It is a matter of fact that fixing more than one GPS station, in a GPS network adjustment, creates an over-constraints

least-squares adjustment scenario which causes the accuracy of the estimated coordinates being a function of the accuracy of the fixed coordinates. Concerning the differences to the ESA stations' coordinates, the comparison reveals that the PPP results are better than the AUSPOS results by approximately 13% in the three-dimensional sense.

The results of the comparison of both services' results state that there is two key issues need further detailed investigations from the geodetic community in Egypt. Firstly, the results of some research studies, as mentioned in section 3, found that the expected accuracy results of on-line processing services are within the 10 cm level, while the achieved 3D results of the current study, when compared against the ESA coordinates, are 21 and 24 cm for the utilized two services. Unfortunately, there are no published processing details about the HARN national GPS network of Egypt. For example, it is not known, as far as the authors concerns, to which version of the ITRF reference frames the HARN coordinates are referred. The second crucial issue is the estimation of the effects of crustal movements on the GPS stations' coordinates since the establishment of the HARN network in 1995. Badawy [2005] has investigated present-day seismicity and crustal deformation of Egypt based on a comprehensive earthquake catalog from 1900 to 2004 by focal mechanism stress inversion and by recent GPS observations. He has found that the average horizontal velocity of GPS stations in Egypt is 5.15 ± 1.1 mm/year in mostly NNW direction. El-Fiky [2005] has analyzed five GPS measurements collected in campaign mode during the period 1997-2002 in order to derive velocity vectors and principal components of crustal strains along the Gulf of Suez and in the southern part of the Sinai Peninsula, Egypt. He has estimated horizontal velocity vectors, of this region, in the ITRF2000 reference frame in the range of 29-35 mm/yr. Additionally, analyzing the GPS-derived velocity field, over 1988–2005, for the zone of interaction of the Arabian, African, and Eurasian plates indicates counterclockwise rotation relative to Eurasia at rates in the range of 20–30 mm/yr [Reilinger, et al, 2006]. Hence, it is recommended that these two issues and their effects of the Egyptian national GPS HARN stations' coordinates should be investigated in details.

6. Conclusion

Recently, a number of on-line GPS processing services that provide GPS processing results to the user free of charge have been established. An overview and a brief comparison have been presented for a number of these global services. Dual-frequency static GPS observation that have been collected over 10 national GPS networks have been used to assist two of these processing services; namely the Canadian PPP and the Australian AUSPOS.

The attained results show that the PPP service produces horizontal standard deviations, as a measure of precision, that have a mean of 0.043 m, while the 3D average value is 0.090 m. Additionally, the accuracy of the achieved PPP results, when compared against the ESA published coordinates, show a mean of 0.190 m in the 2D sense and an average of 0.209 m in the 3D space. Similarly, the accomplished outcomes of the AUSPOS service yield horizontal standard deviations with a mean of 0.024 m, while the 3D average value is 0.026 m. Also, the accuracy of the achieved AUSPOS results, when judged against the ESA coordinates, reveal a mean of 0.230 m in the 2D sense and an average of 0.240 m in the 3D space. Concerning the differences to the ESA stations' coordinates, the comparison reveals that the PPP results are better than the AUSPOS results by approximately 13% in the three-dimensional sense. The

achieved findings, also, recommend that further detail investigations should be carried out specifically on the effects of crustal deformations on the Egyptian national GPS HARN stations' coordinates.

The main merits of on-line GPS processing services available over the Internet are: (1) they are free of charge, (2) there is no need to purchase a processing software package, (3) those services are very useful for beginners GPS users who do not have a great experience in GPS processing strategies; and (4) using IGS stations to tie local GPS networks imply that base stations are not needed to be deployed in the field campaigns. These advantages yield a significant cost-reduction in GPS surveying and mapping projects, and hence, on-line GPS processing services are recommended to be utilized particularly for GPS campaigns in national development projects in Egypt.

References

Badawy, A., 2005, Present-day seismicity, stress field and crustal deformation of Egypt, Journal of Seismology, V. 9, No. 3, pp. 267-276.

Chen W, Chen Y, and Ding X, 2006, GNSS applications in Deformation monitoring, Intelligent transport systems, Precise Point Positioning and Atmosphere study, GIS Development, June Issue, (http://www.gisdevelopment.net/magazine/years/2006/june/38_1.htm).

Dare P., 2006, Online GPS processing services: an initial study, GPS Solutions, No. 10, pp. 12–20

Dawod, G., 2006, New strategies in the utilization of GPS technology for mapping and GIS activities in Egypt, Submitted to CERM.

El-Fiky, g., 2005, GPS-derived Velocity and Crustal Strain Field in the Suez-Sinai Area, Egypt, Bulletin of Earthquake Research Institute, University of Tokyo, V. 80, pp. 73-86.

Featherstone, W., and Dent, V., 2002, Transfer of vertical geodetic control using only one GPS receiver: a case study, The Australian Surveyor, V. 47, No. 1.

NRI, Nile Research Institute hydrographic survey Database Nile Research Institute, National Water Research Center, El-Qanater, Egypt, 2006.

Reilinger, R., McClusky, S., Vernant, P., Lawrence, S., Ergintav, S., Cakmak, R., Ozener, H., Kadirov, F., Guliev, I., Stepanyan, R., Nadariya, M., Hahubia, G., Mahmoud, S., Sakr, K., ArRajehi, A., Paradissis, D., Al-Aydrus, A., Prilepin, M., Guseva, T., Evren, E., Dmitrotsa, A., Filikov, S., Gomez, F., Al-Ghazzi, R., and Karam, G., 2006, GPS constraints on continental deformation in the Africa-Arabia-Eurasia continental collision zone and implications for the dynamics of plate interactions, Journal of Geophysical Research, V. 111.

Soler, T. , Michalak, P. , Weston, N., Snay, R., Foote, R., and Michalak, P., 2006, Accuracy of OPUS solutions for 1-to 4-h observing sessions, GPS Solutions, No. 12, pp. 45-55

Witchayangkoon B., 2000, Elements of GPS precise point positioning, PhD Dissertation, University of Maine, USA.

Table 1: An overall assessment of online GPS processing services

Service name	Data transfer Method	Available options	Elapsed time to receive results (min)	Limitations of GPS data
AUSPOS	Uploading FTP	Antenna height Antenna type	>25	Min of 1 h Dual frequency static Max 7 RINEX files
PPP	Uploading	Mode of processing 2 Reference system	<3	No minimum Static or kinematic Max 6-day long Less than100 MB
SCOUT	FTP	Antenna height Antenna type Selection of reference stations	>15	Minimum of 1 h Dual frequency static
OPUS	Uploading	Antenna height Antenna type	>4	Minimum of 2 h Dual frequency static Max 24 h Static Only available for use in Central and North America
Auto-GIPSY	Sending the Anonymous FTP	None	<3	At least an hour

Table 2: Statistics of standard deviations of PPP service' results
(values are in meters)

	Obs. Time (hours)	$\sigma\ \phi$	$\sigma\ \lambda$	σ h	σ 2D	σ 3D
Minimum	2.7	0.005	0.017	0.027	0.018	0.032
Maximum	6.2	0.030	0.063	0.129	0.064	0.141
Mean	3.8	0.015	0.040	0.078	0.043	0.090

Table 3: Statistics of accuracy estimates of PPP service' results
(values are in meters)

	d_X	d_Y	d_Z	d_{2D}	d_{3D}
Minimum	-0.265	-0.130	0.012	0.079	0.120
Maximum	-0.077	0.136	0.149	0.266	0.268
Mean	-0.173	0.018	0.070	0.190	0.209

Table 4: Statistics of standard deviations of AUSPOS service' results
(values are in meters)

	σ_X	σ_Y	σ_Z	σ 2D	σ 3D
Minimum	0.005	0.008	0.005	0.009	0.011
Maximum	0.020	0.031	0.016	0.037	0.040
Mean	0.016	0.017	0.011	0.024	0.026

Table 5: Statistics of accuracy estimates of AUSPOS service' results
(values are in meters)

	d_X	d_Y	d_Z	d_{2D}	d_{3D}
Minimum	-0.299	-0.082	-0.021	0.183	0.196
Maximum	-0.179	0.078	0.093	0.300	0.302
Mean	-0.224	0.022	0.055	0.230	0.240

Table 6: Statistics of coordinates differences of PPP and AUSPOS services
(values are in meters)

	d_X	d_Y	d_Z	d_{2D}	d_{3D}
Minimum	-0.130	-0.089	-0.076	0.044	0.049
Maximum	0.060	0.055	0.060	0.157	0.175
Mean	-0.052	0.003	-0.016	0.086	0.098

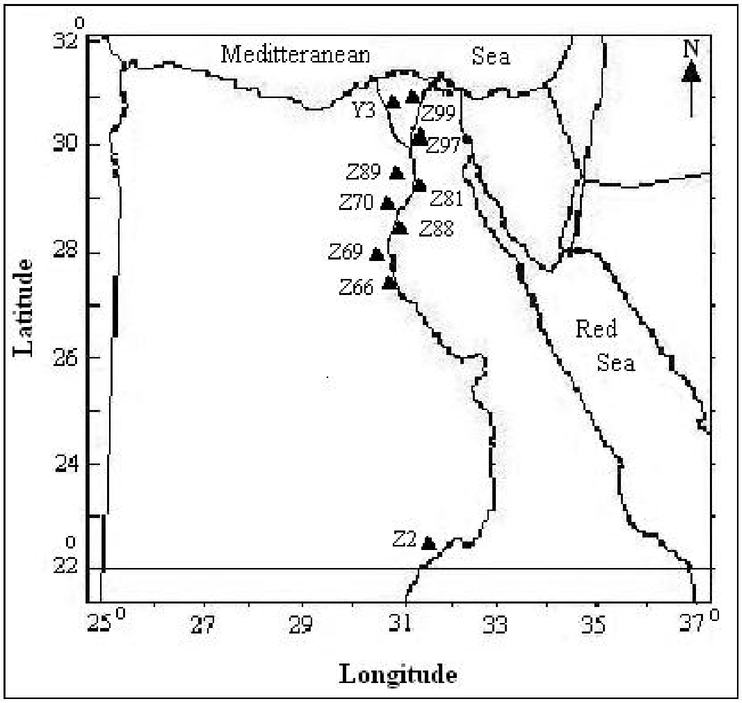

Figure 1: The utilized national GPS Stations

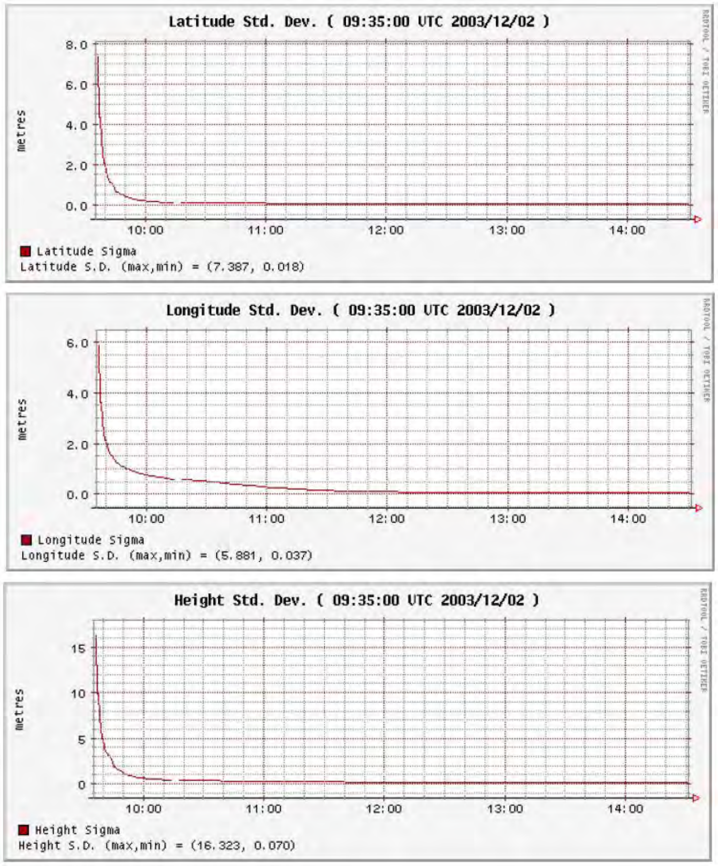

Figure 2: An example of Processing Standard Deviations of PPP results

Appendix 1

GPS Processing parameters used by the AUSPOS service

Observables	Ionosphere corrected L1 double difference carrier phase, Pseudo-range only used for receiver clock estimation, Elevation cut-off 15^o, Sampling rate 30 seconds, Weighting 1.0 cm for double difference, elevation dependent 1 / sin (E).
Troposphere	Hopfield, Niell mapping function
Preprocessing	Receiver clocks estimated using pseudo-range information
Satellite center of mass correction	Block II x,y,z: 0.2794, 0.0000, 1.0259 m Block IIA x,y,z: 0.2794, 0.0000, 1.2053 m
Ground Antenna phase centre calibrations	Elevation-dependent phase centre corrections are applied according to the model IGS01, the NGS antenna calibrations are used when the antenna used is not a recognized IGS type. The corrections are given relative to the Dorne Margolin T antenna.
Atmospheric Drag	Jachhia Model
Earth's Gravitational (Static) Potential Model	EGM96 -degree and order 12
Solid Earth Tides (Dynamic) Potential	Love Model
Ocean Tide (Dynamic) Potential	Christodoulidis
Third Body Perturbations	Sun, Moon and Planets. Values for physical constants -AU, Moon/Earth mass ratio, GM (moon, sun and planets) from JPL DE403 Planetary Ephemeris.
Geodesic Nutation	As in IERS TN 21, P. 37
Polar Motion	IGS Earth Orientation Parameters (Ultra-rapid, Rapid, Final) - apriori
Earth Rotation (UT1)	IGS Earth Orientation Parameters (Ultra-rapid, Rapid, Final) - apriori
Plate Motion	IGS Cumulative SSC
Reference Frame	IGS Cumulative SSC

JKAU: Eng. Sci., Vol.20 No.1, pp: 47-59 (2009 A.D. / 1430 A.H.)

Fitting Gravimetric Local and Global Quasi-Geoids to GPS/Levelling Data: The Role of Geoid/Quasi-Geoid Variations

Gomaa M. Dawod[1, 2] and **Hoda F. Mohamed**[1]

[1] *Survey Research Institute, National Water Research Center, Egypt*
[2] *Currently at Umm Al-Quraa University, Holy Makkah, Saudi Arabia*
dawod_gomaa@yahoo.com

Abstract. The Global Positioning System (GPS) has been extensively utilized in surveying and mapping applications worldwide and in Egypt, which results in a crucial need for precise geoid models. Traditionally, global and local gravimetric quasi-geoid models are determined and, then, fitted to GPS/leveling data. In the context of precise geoid determination, a quasi-geoid determination has to be converted to a geoid model prior to fitting process. Neglecting such a transforming process leads to the absorption of these effects in the fitting residuals that, hence, may produce misleading results and interpretations. The geoid/quasi-geoid separations in Egypt have been computed and found to range from –0.074 m to 0.367 m, with an average of 0.060 m. Additionally, when the quasi-geoid to geoid conversion is performed, it has been found that the undulation of the EIGEN-CG01C global quasi-geoid model when compared to true undulations of HARN stations, have been decreased, in the mean sense, from 0.52 m to 0.46 m. That means an average improvement of accuracy of about 11%. Based on the obtained results, it can be concluded that the conversion of the quasi-geoid to the geoid is quite significant and it should be a regular step in precise geoid determination in Egypt.

Keywords: Quasi-geoid, Geoid Model, Global Geopotential Model, GPS Surveying.

1. Introduction

Developing a precise nation-wide geoid model becomes a crucial geodetic task in Egypt in recent decades. It is mainly due to the extensive

utilization of the Global Positioning System (GPS) technique. The geoid is used to transform the GPS-derived ellipsoidal heights to orthometric heights used in surveying and mapping. Geoid development in Egypt has been addressed by a variety of researchers[1, 2, 15]. The geoid solution of Alnaggar[2] is considered the pioneering nation-wide (22°N<latitude <32°N, 25°E<longitude<37°E) geoid, developed using a least-squares collocation technique and heterogeneous geodetic data including terrestrial gravity, astronomic deflections of the vertical, and Doppler/levelling undulations. A generation of geoid models for Egypt on a five-minute grid has been developed by Saad and Dawod[15] : SRI2001A is a gravimetric geoid computed using local gravity, a local Digital Terrain Model (DTM) and the EGM96 GGM, using a remove-compute-restore Fast Fourier Transform (FFT) processing methodology. SRI2001B is a geoid based on surface-fitting of the SRI2001A model to GPS/levelling[15]. Abdelmotaal[2] developed and applied a high-degree tailored reference model by merging the available gravity anomalies with the EGM96 Global Geopotential Model (GGM) in order to obtain better residual gravity anomalies. Moreover, there are other studies that have developed geoid models for particular areas of interest in Egypt[19].

Most of gravimetric Egyptian geoids are based on the FFT technique in a remove-restore strategy that utilizes a GGM to represent the long wavelengths of the Earth gravity field. Furthermore, these geoid models are fitted to GPS/levelling data to enhance their integrity and accuracy. A key issue in the utilization of GGMs is that their direct results are the height anomalies (not the geoid undulations) representing a quasi-geoid surface, not the geoid itself. Neglecting the geoid/quasi-geoid separation, among other factors, affect the fitting process between the gravimetric local or global quasi-geoids and the GPS/levelling data[7]. This geoid/quasi-geoid transforming step has not been considered in most geodetic literature in Egypt, leading to the fact that the effects of such a correction being absorbed in the fitting residuals that, hence, may produce misleading results and interpretations. The main objectives of the current research study are: (1) the assessment of the geoid/quasi-geoid separations, based on real data; and (2) investigating the expected increase of accuracy in fitting quasi-geoids to GPS/levelling data towards the development of a precise geoid model for Egypt.

2. Geoid/Quasi-Geoid Separations

The well-known Stocks' integral for computing geoid undulations from gravity anomalies is [11]:

$$N = (R / 4 \pi G) \iint_{\sigma} \Delta g \, S(\psi) \, d\sigma \quad (1)$$

Where:

N	=	the geoid undulation
Δg	=	the gravity anomaly
R	=	a mean radius of the earth
$d\sigma$		denotes the surface element of the unite sphere
G	=	a mean gravity value over the earth
$\iint_{\sigma}$	=	represents an integral extended over the whole unit sphere
$S(\psi)$	=	the Stoles' function given by[11]:

$$S(\psi) = [1/(\sin \psi/2)] - 6 \sin(\psi/2) + 1 - 5 \cos \psi$$
$$- 3 \cos (\psi/2) \ln [(\sin (\psi/2) + \sin2 (\psi/2))] \quad (2)$$

where

ψ	=	the spherical distance between the computational point and the running point.

The remove-restore technique separates three different frequency contributions in the gravity anomalies, so that it may be written that[16]:

$$\Delta g = \Delta g_{FA} + \Delta g_{GGM} + \Delta g_{H} \quad (3)$$

and

$$N = N_{\Delta g} + N_{GGM} + N_{H} \quad (4)$$

where

Δg_{FA}	=	the medium wavelength contribution of the local free-air gravity anomalies.
Δg_{GGM}	=	the long wavelength contribution as represented by a GGM model.
Δg_{H}	=	the short wavelength contribution as represented by the topography or a DTM.
$N_{\Delta g}$	=	the local gravity medium wavelength component
N_{GGM}	=	the GGM long wavelength contribution.

N_H = the topography short wavelength component.

The long wavelength component, as represented by a GGM, can be evaluated in the FFT spherical approximation by[16]:

$$N_{GGM} = \sum_{n=2}^{n=ma} \sum_{m=0}^{n} R\,[C_{nm} \cos m\lambda + S_{nm} \sin m\lambda\,]\, P_{nm} (\sin \phi) \quad (5)$$

Where:

C_{nm} , S_{nm} = the fully normalized harmonic coefficients,
P_{nm} = the fully normalized associated Legendre polynomial
n, m = the degree and order of the GGM model respectively
ϕ , λ = the geocentric latitude and longitude respectively

GGMs, when used in a spherical harmonic expansion, produce quasi-geoid (sometimes called co-geoid) not geoid solutions since the processing yields height anomalies not geoid undulations[7,10,20]. Consequently, the conversion of the obtained quasi-geoid (height anomaly) to the geoid (geoidal undulation) is a regular step in precise geoid determination worldwide[6,8,9,12]. Neglecting this procedure, among other factors, affect the fitting process between the gravimetric local or global quasi-geoids and the GPS/levelling data[7]. Several researchers have considered this issue and have presented solutions to convert height anomalies to geoid heights. Rapp[13] suggested that potential coefficient models be used first to calculate a height anomaly and then a correction term, represented by a high degree spherical harmonic expansion, be applied to give the geoid undulation. Heiskanen and Moritz[11] provide a formula for computing the geoid/quasi-geoid separation as:

$$N = \xi + [\,(g' - \gamma') / \gamma'\,]\, H \quad (6)$$

Where:

N = the geoid undulations.
ξ = the height anomaly or undulations of quasi-geoid.
g' = the mean gravity along the plumb line between geoid and ground.
γ' = the mean normal gravity along the normal plumb line between ellipsoid and telleroid.
H = the orthometric height

For an average density = 2.67 g/cm3, g' can be computed as[11]:

$$g' = g \text{ (in gal)} + 0.0424\, H \text{ (in km)} \quad (7)$$

where: g = the measured surface gravity.

Additionally, the quantity γ' may be replaced by a constant average value[11]. The maximum geoid/quasi-geoid separation (N-ξ) can be up to 2 m[17]. In the Mt. Blanc area in the Alps, where the height equals 4877 m, this separation equals 1.8 m[11]. Consequently, applying such a transformation is crucial in the context of developing a precise geoid model for Egypt.

3. Available Data

The local geodetic data used in this study was held in two databases (Table 1). Firstly, terrestrial gravity values have been measured at 1138 points (Fig 1). The date of these observations and their accuracy vary greatly between the most recent Egyptian National Gravity Standardization Network of 1997 (ENGSN97) that was established by the Survey Research Institute[3] and older gravity surveys carried out by many private organizations several decades ago. The accuracy of ENGSN97 gravity values is 0.022 mGal, while the accuracy estimate for older gravity data is 0.5 mGal on average[4]. Even though the accuracy of the older gravity data is not of high-precision, this data set is used in this research study since it covers areas where no other gravity sources are available. As can be seen from Fig. 1, gravimetric data distribution is not homogeneous over Egypt, with significant gaps, particularly in the Eastern and Western deserts[4]. However, this data set almost constitute all the published gravity data in Egypt. An evaluation of the existing gravity data, based on comparing the gravity value of each point to values at the nearest four stations, was carried out to identify any large discrepancies. This process identified 58 points (about 5%) as suspected outliers and these were subsequently removed. The statistics of the remaining 1080 gravity stations are presented in Table 2.

The second compiled geodetic data base consists of 15 GPS/levelling points (Fig. 2). This data set belongs to the High Accuracy Reference Network (HARN), which furnishes the national Egyptian GPS datum established by the Egyptian Survey Authority (ESA) in 1995. The precision of the HARN network is 0.1 part per million (ppm), which can be written in another form as 1: 10,000,000. Although the HARN network consists of 30 stations, only those 15 points have observed real orthometric heights, and consequently true geoid undulations. The

precision of geoid undulations at these stations may be estimated as 1 cm or better[3]. It is worth mentioning that this data set is quite few in number, but it is of special importance since it is the most accurate and officially-published GPS/levelling data in Egypt. Other existing GPS/levelling data do not reach such a precision level, and hence may not be appropriate for the comparison in the current research study. The statistics of the geoid undulations over these stations are presented in Table 3.

Table 1. Available local geodetic data.

Data type	No. of points
Terrestrial Gravity: 1. ENGSN97 Network 2. Older gravity points	 150 988
GPS/levelling HARN	15

Table 2. Statistics of the available 1080 gravity stations.

Item	Min	Max	Mean
Observed Gravity (mGal)	978588.29	979509.69	979089.18
Orthometric Heights (m)	–253.23	1433.52	169.34

Table 3. Statistics of the available 15 GPS/Levelling stations.

Item	Min	Max	Mean
Orthometric Heights (m)	11.76	556.42	146.49
True Undulations (m)	10.86	21.14	15.47

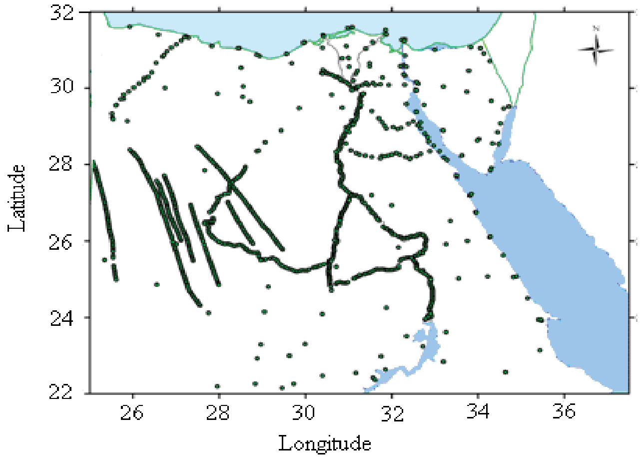

Fig. 1. Available local gravity stations.

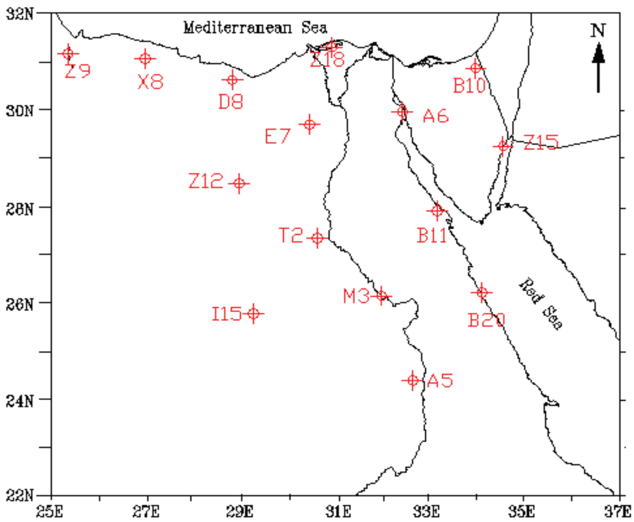

Fig. 2. Available stations with known geoid undulations.

4. Processing and Results

The main objectives of the current research study in the assessment of the geoid/quasi-geoid separations, and investigating the expected increase of accuracy in fitting quasi-geoids to GPS/levelling data towards the development of a precise geoid model for Egypt Therefore, the data processing involves two steps. Firstly, the geoid/quasi-geoid separations, through Equations 6 and 7, have been computed at the available known 1080 gravity stations. The attained results are presented in Table 4, and a contour map is depicted in Fig. 3. It can be seen that the geoid/quasi-geoid separations range from –0.074 m to 0.367 m, with an average of 0.060 m and a standard deviation equals 0.049 m. That means that such a correction to the gravimetric quasi-geoids can reach up to 37 centimeters at mountainous areas in Egypt (actually this value occurred at Saint Katreen area, south of Sinai peninsula). Moreover, although the topography of Egypt is fairly flat in general, the geoid/quasi-geoid correction has an average value of 6 centimeters. This value is quite significant when a precise geoid model is concerned.

Table 4. Statistics of geoid/quasi-geoid separations at known 1080 gravity stations (m).

Min	Max	Mean	RMS
–0.074	0.367	0.060	0.049

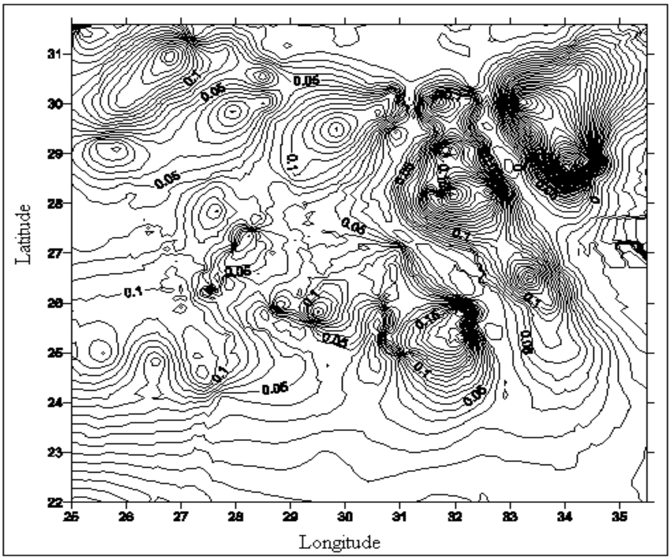

Fig. 3. Geoid/quasi-geoid separation contour map.

The second step in the data processing is the assessment of the expected accuracy of fitting quasi-geoids to GPS/levelling data. It should be emphasized that neglecting the geoid/quasi-geoid separations will be absorbed in the residuals of the fitting process, which causes misleading results. Dawod[5] concluded that, out of eight tested recent GGMs, the EIGEN-CG01C model[14] is best at representing the long and medium wavelengths of the gravity field in Egypt. Therefore, the height anomaly at the known 15 HARN GPS/levelling stations has been computed using the EIGEN-CG01C GGM, through the SHS360 program (Spherical Harmonic Solution to degree and order 360 computer program[18]. The corresponding geoid/quasi-geoid separations at these stations have been interpolated from the contour map. Furthermore, the geoid undulations have been computed by adding the geoid/quasi-geoid separations to the EIGEN-CG01C height anomalies. Two comparisons, of both height anomalies and GGM-based geoid undulations against known geoid undulations (N=h-H), have been carried out. The achieved results are tabulated in Table 5.

Table 5. Statistics of height anomaly and geoid undulations at the known 15 GPS/levelling stations (m).

Item	Min	Max	Mean	RMS
EIGEN-CG01C height anomaly	10.98	20.26	14.95	2.43
True geoid undulation – EIGEN-CG01C height anomaly	–4.82	4.86	0.52	2.42
Geoid/quasi-geoid separation	0.002	0.16	0.06	0.05
EIGEN-CG01C geoid undulation	11.00	20.28	15.01	2.42
True geoid undulation – EIGEN-CG01C geoid undulation	–4.84	4.86	0.46	2.41

It can be seen that the height anomalies of the EIGEN-CG01C GGM range have a mean value equals 14.95 m and a standard deviation of 2.43 m. When compared against true geoid undulations, the differences' s average equals 0.52 m and a standard deviation equals 2.42 m. The interpolated geoid/quasi-geoid separations at those stations range have a mean value equals 0.06 m and a standard deviation of 0.05 m. After the quasi-geoid to geoid conversion, the corresponding EIGEN-CG01C-based geoid undulations have a mean value of 15.01 m and a standard deviation equals 2.42 m. The computed undulation differences, between the GGM and true values, now have a an average of 0.46 m and a standard deviation equals 2.41 m. Consequently, the mean difference value of geoid undulation, of the EIGEN-CG01C GGM, has been decreased from 0.52 m to 0.46 m, which means an average improvement of accuracy of 11% approximately. Additionally, as presented in Table 4, the geoid/quasi-geoid separations can reach up to 37 centimeters at mountainous areas and their average value, over Egypt, is 6 centimeters which is quite significant when a precise geoid model is concerned. Thus, it should be realized that the utilized known HARN stations exist mostly at flat or moderate-topography areas, and it is expected that the attained findings may be greatly changed for mountainous areas in Egypt. As mentioned previously, the main objective of the current research study is assessing the role of geoid/quasi-geoid separations within the context of developing a precise geoid model. In many geodetic literature, particularly in Egypt, this surface transformation process is not applied in geoid determination. Hence, the attained results highlights, even in a relative sense, the importance of such a processing step that must be taken into account in geoid solutions.

5. Summary and Conclusions

The extensive utilization of GPS in surveying and mapping applications in Egypt has necessitated the development of a precise geoid model. Global and local gravimetric geoid determinations utilize GGMs, in the FFT spherical approximation processing, produce height anomalies representing a quasi-geoid surface, not the geoid itself. The geoid/quasi-geoid transforming step has not been considered in most geodetic literature in Egypt, leading to the fact that the effects of such a correction being absorbed in the fitting residuals that, hence, may produces misleading results and interpretations. In order to evaluate the geoid/quasi-geoid separation in Egypt, 1080 gravity stations have been utilized. Although, the gravimetric data distribution is not homogeneous over Egypt, with significant gaps, this data set almost constitute all the published gravity data in Egypt. The orthometric height of these stations, which is the key factor in geoid/quasi-geoid conversion, vary from –253.23 m to 1433.52 m, with a mean value of 169.34 m. The attained results show that the values of the quasi-geoid-to-geoid transformation range from –0.074 m to 0.367 m, with an average of 0.060 m and a standard deviation equals 0.049 m. It should be highlighted that this maximum value is quite significant in precise geoid modelling. Hence, it can be concluded that this conversion step is substantial when a precise Egyptian geoid model is concerned.

The second utilized dataset consists of 15 HARN GPS/levelling points, whose true geoid undulations are known. Even though, this data set is quite few in number, but it is of special importance since it is the most accurate and officially-published GPS/levelling data in Egypt. Other existing GPS/levelling data do not reach such a precision level, and hence may not be appropriate for the comparison in the current research study. This data set has been used to investigate the expected accuracy of fitting a global quasigeoid GGM model to GPS/levelling points. The EIGEN-CG01C has been found to be the best GGMs at representing the long and medium wavelengths of the gravity field in Egypt[5]. The EIGEN-CG01C height anomalies at those stations have been computed and the corresponding geoid/quasi-geoid separations have been interpolated. Two comparisons, of both GGM-based height anomalies and geoid undulations against known geoid undulations, have been carried out. The results show that when compared the quasi-geoid GGM against true geoid undulations, the differences have an average of 0.52 m.

After the quasi-geoid to geoid conversion, the corresponding undulation differences have been decreased, in the mean sense, to 0.46 m, which means an average improvement of accuracy of 11% approximately. Nevertheless, it should be recognized that the exploited HARN stations exist generally at flat or moderate-topography areas, and it is anticipated that the accomplished findings may be greatly changed for mountainous areas. Based on the available utilized data sets and the obtained results, it can be concluded, in a sense, that the conversion of the quasi-geoid to the geoid is quite significant and it should be a regular step in precise geoid determination in Egypt.

References

[1] **Abdelmotaal, H.**, High-Degree Geopotential Model Tailored to Egypt, Presented at *The 1st International Symposium of the International Gravity Field Service (IGFS), Istanbul, Turkey, August 28 – September 1* (2006).

[2] **Alnaggar, D.**, Determination of the Geoid in Egypt Using Heterogeneous Geodetic Data, *Ph.D. Dissertation*, Cairo University, Egypt (1986).

[3] **Dawod, G.**, A national gravity standardization network for Egypt, *Ph.D. Dissertation*, Shoubra Faculty of Engineering, Banha Branch, Zagazig University, Cairo, Egypt (1998).

[4] **Dawod, G.** and **Alnaggar, D.**, Quality control measures for the Egyptian National Gravity Standardization Network (ENGSN97), *Proceedings of the Second International Conference on Civil Engineering*, *Helwan University, Cairo, Egypt, April 1-3*, pp: 578-587 (2000).

[5] **Dawod, G.**, Towards the redefinition of the Egyptian geoid: Performance analysis of recent global geoid and digital terrain models, *Journal of Spatial Science*, **53**(1): 31-42, June (2008).

[6] **Denker, H.**, Evaluation and Improvement of the EGG97 Quasigeoid Model for Europe by GPS and Leveling Data, In: M. Vermeer, and J. Adam (Ed.), *Proceedings of the Second Continental Workshop on the Geoid in Europe*, Budapest, Hungary, March 10-14 (1998).

[7] **Featherstone, W.**, Fitting geoids to GNSS-levelling: You're fooling yourself and fooling others, *The Geodetic Week 2006*, *The International Congress Center Munich (ICM), October 10-12. Munich, Germany* (2006).

[8] **Featherstone, W., Claessens, S., Kuhn, M. , Kirby, J.** and **Sproule, D.**, Progress towards the new Australian geoid-type model, *Proceedings of SSC the National Biennial Conference of the Spatial Sciences Institute*, Hobart, Australia, May (2007).

[9] **Iliffe, J., Ziebart, M., Cross, P. Forsberg, R. Strykowski, G.** and **Tscherning, C.**, OSGM02: A new model for converting GPS-derived heights to local height datums in Great Britain and Ireland, *Survey Review*, **37**(290): 276-293 (2003).

[10] **Ivan, M.**, On the difference between quasi-geoid height and geoid undulation, *International Geoid Service Bulletin*, **8**(December): 53-64 (1998).

[11] **Heiskanen, W. A.** and **Moritz, H.**, *Physical Geodesy*, Freeman, San Francisco (1967).

[12] **Prijatna, K.**, A local quasigeoid determination approach for Jawa Island, Indonesia, Presented at the *Third FIG Regional Conference, Jakarta, Indonesia, October 3-7* (2004).

[13] **Rapp, R.**, Use of potential coefficient models for geoid undulation determinations using a spherical harmonic representation of the height anomaly/geoid undulation difference, *Journal of Geodesy*, **71**(5): 282-289 (1997).

[14] **Reigber, C., Schwintzer, P., Stubenvoll, R., Schmidt, R., Flechtner, F., Meyer, U., König, R., Neumayer, H., Förste, C., Barthelmes, F., Zhu, S., Balmino, G., Biancale,**

R., Lemoine, J. M., Meixner, H. and **Raimondo, J.**, A high resolution global gravity field model combining CHAMP and GRACE satellite mission and surface data: EIGEN-CG01C; *Scientific Technical Report STR06/07*, GeoForschungsZentrum Potsdam (2006).

[15] **Saad, A.**, and **Dawod, G.**, A precise integrated GPS/gravity geoid model for Egypt, *Civil Engineering Research Magazine (CERM)*, *Al-Azhar University*, **24**(1): 391-405 (2002).

[16] **Sideris, M.** and **Footopoulus, M.**, Geoid determination by FFT, *The International Geoid School, Budapest, Hungary, Jan. 31-Feb. 4* (2005).

[17] **Tenzer, R., Vanicek, P., Santos, M., Featherstone, W.** and **Kuhn, M.**, The rigorous determination of orthometric heights, *Journal of Geodesy*, **79**(1-3): 82-92 (2005).

[18] **Tscherning, C.C.**, On the chain-rule method for computing potential derivatives, *Manuscripta Geodaetica*, **1**: 125-141 (1976).

[19] **Tscherning, C.C. Radwan, A, Tealeb, A., Mahmoud, S., Mohamed, A., Hassan, R., Issawy, E.** and **Saker, K.**, Local geoid determination combining gravity disturbances and GPS/levelling: A case study in the Lake Naser area, Aswan, Egypt, *Journal of Geodesy*, **75**: 343-348 (2001).

[20] **Tscherning, C.C., Arabelos, D.** and **Strykowski, G.**, The 1-cm geoid after GOCE, In: M. Sideris (Ed.): *The IAG Symposia*, V. 12, pp: 267-270, Springer Verlag (2001).

توافق نماذج الجيويد وشبيه الجيويد المحلية والعالمية مع قياسات النظام العالمي لتحديد المواقع والميزانيات: دور التغيرات بين الجيويد وشبيه الجيويد

جمعة محمد داود[١،٢] و هدي فيصل محمد[١]

[١]*معهد بحوث المساحة – المركز القومي لبحوث المياه – مصر*

[٢] *جامعة أم القرى – مكة المكرمة – المملكة العربية السعودية*

المستخلص . مع انتشار تطبيقات النظام العالمي لتحديد المواقع في مشروعات المساحة والخرائط عالميا، فقد تزايدت الحاجة في مصر للحصول على نموذج دقيق لسطح الجيويد، وخاصة لتحويل الارتفاعات الجيوديسية إلي المناسيب المناظرة. يتم استنباط نماذج "شبيه الجيويد" تقليديا باستخدام قياسات الجاذبية الأرضية، ثم يتم ضبطها لتتوافق مع نقاط معلوم عندها قيم حيود الجيويد الناتجة من النظام العالمي لتحديد المواقع والميزانيات الأرضية. لكن يجب قبل إجراء عملية التوافق أن يتم تحويل نموذج شبيه الجيويد إلى نموذج جيويد حقيقي، وهذه الخطوة لم تؤخذ في الاعتبار في معظم الدراسات الجيوديسية في مصر. وبناء على قياسات جيوديسية حقيقية عند ١٠٨٠ نقطة فقد تم حساب المسافات بين شبيه الجيويد و الجيويد ووجد أن قيمها تتراوح بين -٠,٠٧٤ متر و ٠,٣٦٧ متر بمتوسط يبلغ ٠,٠٦٠ متر. وبعد إجراء هذا التحويل فان الدقة المتوسطة لأحد نماذج الجيويد العالمية – التي تم اختبارها ووجد أنه أحسن نموذج عالمي لتمثيل مجال الجاذبية في مصر – قد تحسنت من ٠,٥٢ متر إلى ٠,٤٦ متر بتحسن يبلغ ١١ ٪ في المتوسط. وتدل النتائج التي تم الحصول عليها على أن عملية التحويل من نماذج شبيه الجيويد إلي نماذج الجيويد تعد خطوة مؤثرة ويجب أخذها في الاعتبار في أية محاولة مستقبلية لتطوير نموذج جيويد دقيق في مصر.

The Third National GIS Symposium in Saudi Arabia
Al-Khobar, April 7 - 9, 2008

Gomaa Mohamed Dawod
Associate Professor, Survey Research Institute, Egypt
Currently at Um Al-Quraa University, Holly Makkah, Saudi Arabia
E-mail: dawod_gomaa@yahoo.com

Hoda Faisal Mohamed
Researcher, Survey Research Institute, Egypt
E-mail: hoda_faisal@yahoo.com

ESTIMATION OF SEA LEVEL RISE HAZARDOUS IMPACTS IN EGYPT WITHIN A GIS ENVIRONMENT

ABSTRACT

The global warming, and other, environmental phenomena have led to a global rise trend of sea level. Recent estimates of projected sea level rise at year 2100 expect that it can reach more than a meter. Several hazards are anticipated due to the rise of sea level, including shoreline retreat and loss of populated areas particularly in coastal regions. This research study assess those impacts on the Egyptian coastal areas of the Nile Delta, that extend approximately over 170 x 90 Km. Since there is no available precise national Digital Elevation Models (DEM) for this area, four global DEMs have been obtained and utilized. First, these DEMs have been examined, based on real terrestrial data points, to determine the optimal DEM that precisely represents the Egyptian topography. Next, the precise DEM (SRTM 3") has been represented in a Geographic Information System (GIS) environment containing 2206381 data points. Furthermore, several scenarios of the projected sea level rise (ranging from 0.25 to 1.5 m) have been investigated. It has been found that the estimated loss of populated lands varies from 292 to 2731 square kilometers. The spatial distributions of the loss of lands have been graphically mapped for each scenario. The effectiveness of utilizing the GIS technology in such an environmental assessment research has been confirmed. The achieved results should be employed, by the decision makers, in the development policies of coastal regions in Egypt.

Key Words: GIS, Sea Level Rise, Digital Elevation Model, Environmental Impacts, Egypt.

1. INTRODUCTION

Several types of environmental threats have been recognized, on the global scale, as results of the global warming phenomena. The increasing emission of carbon dioxide gas, CO_2, into the atmosphere and the burning of large areas of tropical forests, along with other factors, have led to altering the global energy budget and, thus, resulted in a global increase of the mean temperature of the Earth. Sea level rise is a vital aspect of the environmental hazards due to its potential impacts on human population living in coastal regions and on islands. Sea level rise results in coastal floods, salt water intrusion, excessive erosion, soil salinization, deterioration of coastal ecosystems.

The rate of the mean global sea level rise (GSLR) in the twentieth century have been estimated, based on two different data types as: (1) based on tide gauge data, GSLR equals 1.8 mm/year; (2) based on satellite altimetry data, GSLR equals 3.1 mm/year (Solomon et al., 2007). However, it should be mentioned that these average rates of the sea level rise are not geographically uniform, and there are regions of the Earth have relatively larger values. Projecting the sea level rise at the end of the twenty-first century reveals that the expected rise of the sea level varies between 0.18 m and 0.59 m (ibid). Other studies (e.g. Dasgupta et al. 2007) expect that global warming can promote GSLR of 1-3 m, and unexpected rapid breakup of the Greenland and West Antarctic ice sheets might produce a 5-m GSLR in this century. In Egypt, the rate of sea level rise in the twentieth century has been recently estimated as 1.7 mm/year at Alexandria (e.g. Dawod et al, 2005, and Mohamed, 2005).

Recently, the Geographic Information System (GIS) technology has been extensively utilized to evaluate the hazardous impacts of the environmental changes, particularly the effects of sea level rise. Numerous merits of utilizing GIS in such assessment studies have been attained, such as the capability of spatial representation of the anticipated effects, the integration of several data types in a unique environment, and the ability of modelling the expected flood scenarios (e.g. Dasgupta et al., 2007, Sposito 2007, Lee 2005, Szlafsztein 2005, Koohzare et al., 2004, and Marfai 2003).

2. OBJECTIVES

In Egypt, the issue of sea level rise and its anticipated harmful impacts has been addressed by several researchers. Assessment studies integrating the GIS and remote sensing technologies have been carried out for several regions such as: Marsa Matrouh (El Raey et al, 2006), Alexandria and Rossetta (El Raey, 2005), Abu Qir bay (El Raey et al., 2005), and Nile Delta (Agrawala et al., 2004, and El Raey, 2004). Most of these studies are restricted to small regions since they depend on the utilization of remote sensing images to construct a Digital Elevation Model (DEM), which constitute a major item in the data processing stages.

The current research suggests a new approach, which is the adaptation of global high-resolution DEMs in such environmental assessment studies. The objectives of this study are:

1- Evaluation of available high-resolution DEMs to determine the "optimum" model in representing the topography of the study area;
2- The integration of global DEMs into a GIS environment;
3- The determination of total areas subjected to floods under several sea level rise scenarios; and
4- Mapping the spatial distribution of these regions' threats.

3. THE STUDY AREA

The study area constitutes a major part of the Nile Delta, the main area in Egypt with expected environmental hazards following the sea level rise. The study area, shown in Figure 1, extends in the north direction from latitude 30.5^o N to 31.6^o N (about 90 Km), and extends in the east direction from longitude 30.5^o E to 32.6^o E (about 170 Km). This area combines regions belong to 8 different governorates. A main reason that the study area does not involve the entire Nile Delta region is the huge data sets dealing with high-resolution global DEMs (particularly the 90-meter resolution model) and the technical specification limitations of a normal PC computer. However, it is highly recommended to use the suggested processing strategy for the entire Egyptian coastal areas using a high-specification workstation computer that can handles a huge amount of data.

4. EVALUATION OF GLOBAL HIGH-RESOLUTION DEMS

Since there is no accessible precise national DEM for the study area, four global DEMs have been obtained and utilized. These DEMs are: the Shuttle Radar Topography Mission (SRTM) model of 3" and 30" resolution, the DTM2002 model of 30" resolution, and the ETOPO2v2 model of 2' resolution. Except the DTM2002, all other DEMs are available free of charge and can be downloaded from the Internet.

The SRTM, flown on Space Shuttle Endeavour in February 2000, was a joint project of the National Aeronautics and Space Administration, the National Geospatial Intelligence Agency (NGA) (formerly National Imagery and Mapping Agency, NIMA) of the U.S. Department of Defense (DoD), and DLR. The SRTM objective was to acquire a digital elevation model of all land between about 60° north latitude and 56° south latitude, about 80 percent of Earth's land surface. Three DEM have been derived from SRTM data: (1) a 1-arc second (approximately 30 meters) version, which is only for USA, (2) a global 3-arc second (approximately 90 meters) version, and (3) a global 30-arc second (approximately 900 meters) version. (For more information about SRTM, see e.g. Farr et al, 2004, and USGS 2007). The SRTM3 DEM has been evaluated and utilized in several research studies. For example, Denker (2005) compared the SRTM 3 against a 1-second DEM in Germany, and

estimated the standard deviation of the differences that equals 7.9 m. Moreover, Ghoneim and El-Baz (2007) have applied the SRTM 3 to construct a complete drainage map of the entire Tushka area, south of Egypt. The DTM2002 global DEM has been developed based on several sources of data, such as: the GTOPO30 and GLOBE global 30″ DEMs; the ACE 30″ DEM; Near ocean-wide bathymetric information predicted from altimetry data and constrained by ship-borne depth soundings; the Generic Mapping Tools (GMT) high-resolution global shoreline and land type database; new 5-km grids of ice surface elevations from altimetry data and the JGP95E geoid model over Antarctica and Greenland; revised ice thickness data over Antarctica and Greenland; and depth data (30″) for the Great Lakes (Saleh and Pavlis 2002). DTM2002 was compiled in a 30″ version that provides surface elevations and ocean depths only, and in 2′ and 5′ versions that include depth data for certain large lakes and ice thickness information (ibid). A part of DTM2002 (the 30" version) corresponding to the Egyptian territories has been obtained (Saleh 2004) and utilized in this research. The ETOPO2v2 global gridded 2-minute dataset has been released in 2006 by the U.S. National Geophysical Data Center (NGDC), the US NOAA Satellite and Information Service. ETOPO2v2 is a global relief for both land and ocean (available from http://www.ngdc.noaa.gov/mgg/fliers/06mgg01.html)

First, these four DEMs have been examined, based on a terrestrial dataset of 127 points with known orthometric heights, to determine the optimal DEM that precisely represents the Egyptian topography. Even though the study area is almost flat and the number of the available check points is small, this judgment step is considered as a proportional performance comparison of these DEMs in a relative sense. The attained results are presented in Table 1, with SRTM3" produced the smallest standard deviation value of 3.0 m. Thus, it is suggested that the SRTM 3" DEM may be considered the optimum global DEM representing the topography variations in the study area. Figures 2, 3, and 4 present a shaded-relief, a contour, and a 3D views, respectively, of the SRTM 3" DEM correspond to the study area.

5. DETERMINATION OF SEA LEVEL RISE IMPACTS USING GIS

Two computer packages have been utilized in the data processing stage. First, the Global Mapper 9.01 (TM) software has been used to combine, then transform, the downloaded SRTM 3" files from the raster format to XYZ text files. Second, the ESRI Arc GIS 9.2 (TM) has been used to build a Triangular Irregular Network (TIN), a contour map, and a 3D surface of this combined dataset. Additionally, the computations have been carried out using the 3D Analyst extension of the ARC GIS package.

First, it has been noticed that there are large regions of the study area that are already under the zero mean sea level. These low lands, shown in Figure 5, sum an area of 2466 square kilometers. Furthermore, the areas surrounded between contour lines equals 0.25, 0.5, 0.75, 1.0, 1.25, 1.5 m have been computed. Table 2 and Figure 6 present the achieved results. It can be seen that a sea level rise of

0.25, 0.5, 0.75, 1.0, 1.25, 1.5 m will led to loss of lands equal 292, 587, 885, 2023, 2378, and 2731 square kilometers respectively. These figures are quite significant since these areas losses constitute, in the same order, 2%, 5%, 7%, 17%, 19%, and 22% of the total area. It is a matter of fact that loosing such areas will lead to several other harmful impacts on the population and economy of the country. The population of those eight governorates (under study) constitute about 32.8% of the total population of Egypt, as of the January-2006's published official census (e.g. http://www.capmas.gov.eg/). Thus, the anticipated environmental threats can not only being justified based on the areas of the loss of lands, but also have to tack into consideration all other types of threats from the physical and the socio-economic points of view (El Raey, 2004 and Agrawala et al., 2004).

A major advantage of utilizing GIS is its capability of representing the spatial distribution of the results. Figures 7, 8, 9, and 10 depicts the geographical patterns of the expected loss of lands under the scenarios of sea level rise equals 0.25, 0.5, 1.0, and 1.5 m respectively. It can be noticed that the Kafr El-Sheikh is the most suffered governorate

6. CONCLUSIONS

The present-day rapid climate changes cause potential environmental threats, particularly the faster rise of sea level on a global basis. The projected sea level rise in the twenty-first century can reach a meter or more. The coastal areas in Egypt and the Nile Delta are expected to several hazardous impacts due to the sea level rise. This study utilize the high-precision SRTM 3" global DEM, within a GIS environment, to asses the loss of lands in the Nile Delta under several sea level rise scenarios ranging from 0.25 m to 1.5 m. The estimated results show that the anticipated loss of low lands range between 292 and 2731 square kilometers, that constitute about 2-22 % of the total area under consideration. These figures are extremely crucial, and call for an immediate national plane for coastal protection taking into considerations the faster sea level rise trend. Additionally, the spatial distributions of the expected loss of lands have been geographically represented through GIS. It has been shown that that Kafr El-Sheikh is the most suffered governorate in the study area. The suggested processing strategy, integrating global high-precision DEM and GIS, is quite significant in such an environmental assessment research, at least until a precise national DEM for Egypt be available.

REFERENCES

Agrawala, S., Moehner, A., El Raey, M., Conway, D., van Aalst, M., Hagenstad, M., and Smith, J., 2004, Development and climate change in Egypt: Focus on coastal resources and the Nile, A report published by the Organization for Economic Co-operation and Development (OECD), Paris. France.

Dasgupta, S., Laplante, B., Meisner, C., Wheeler, D., and Yan, J., 2007, The impact of sea level rise on developing countries: A comparative analysis, World Bank Policy Research Working Paper No. 4136, February.

Dawod, G., Meligy, M., and Mohamed, H., 2005, Assessment and modelling of sea level rise and metrological changes in Egypt, Proceedings of the Ain-Shams First International Conference on Environmental Engineering (ASCEE-1), Cairo, Egypt, April 11-12, pp. 573-582.

Denker, H., 2005, Evaluation of SRTM3 and GTOPO30 terrain data in Germany, In IAG International Symposium on Gravity, Geoid and Space Missions (GGSM2004), Ed. C Jekeli, L Bastos, and J Fernandes, V. 129, pp. 218-223.

El Raey, M., and Mohammed; W. 2006, Impact of Sea Level Rise on Marsa Matruh City – Egypt: A Spatial Approach, Presented in the Conference of Earth Observation and Geoinformation Sciences in Support of Africa's Development, Oct. 30 – Nov. 2, Cairo, Egypt.

El Raey, M., Nasr, S., Frihy, O., Fouda, Y., El-Hattab, M., Elbadawy, O., Shalaby, A., and Mohammed, W., 2005, Remote sensing and GIS for sustainable development of the coastal area of Abu Qir bay, Egypt, Sea to Sea Regional Forum, pp. 275-280, Cairo, Egypt.

El Raey, M., 2005, Mapping Areas Affected by Sea-level Rise due to Climate Change in the Nile Delta until 2100, Presented at the First World International Studies Conference, Istanbul, Turkey, August 24- 27.

El Raey, M., 2004, Adaptation to Climate Change for Sustainable Development in the Coastal Zone of Egypt, Presented at the global forum on sustainable development: Development and climate change, The Organization for Economic Co-operation and Development (OECD), Paris. France.

Farr, T, Rosen, P., Caro, E., Crippen, R., Duren, R., Hensley, S., Kobrick, M., Paller, M., Rodriguez, E., Roth, L., Seal, D., Shaffer, S., Shimada, J., Umland, J., Werner, M., Oskin, M., Hill, C., Burbank, D., Barbara, S., and Alsdorf, D., 2004, The Shuttle Radar Topography Mission, Rev. Geophys., 45, RG2004, Jet Propulsion Laboratory, California Institute of Technology, USA. Available from: http://www2.jpl.nasa.gov/srtm/SRTM_paper.pdf

Ghoneim, E. and El-Baz, F., 2007, The application of radar topographic data to mapping of a mega-paleodrainage in the Eastern Sahara, Journal of Arid Environments, V. 69, pp. 658–675.

Koohzare, A., Vanícek, P., and Santos, M., 2004, Spatial analysis and treatment of tide gauge records using GIS, Presented at the GEOIDE Sixth Annual Scientific Conference, May 30 -June 1, Gatineau, QC, Canada.

Lee, E., 2005, GIS modeling of wetlands elevation change in response to projected sea level rise, Trinity Bay, Texas., MSC Thesis, University of North Texas, Texas, USA.
Marfai, M., 2003, GIS modelling of river and tidal flood hazards in a waterfront city: A case study of Semarang city, Indonesia, MSC Thesis, The international institute for geo-information science and earth observation (ITC), Enschede, The Netherlands.
Mohamed, H.F., 2005, Realization and redefinition of the Egyptian vertical datum based on recent heterogeneous observations, PhD Dissertation, Shoubra faculty of engineering, Benha university, Egypt.
Saleh, J. ,2004, Personal communications.
Saleh, J., and Pavlis, N. ,2002, The development and evaluation of the global digital terrain model DTM2002, Presented at the 3rd Meeting of the International Gravity and Geoid Commission, GG2002, August 26 - 30, Thessaloniki, Greece.
Solomon, S., D. Qin, M. Manning, R.B. Alley, T. Berntsen, N.L. Bindoff, Z. Chen, A. Chidthaisong, J.M. Gregory, G.C. Hegerl, M. Heimann, B. Hewitson, B.J. Hoskins, F. Joos, J. Jouzel, V. Kattsov, U. Lohmann, T. Matsuno, M. Molina, N. Nicholls, J. Overpeck, G. Raga, V. Ramaswamy, J. Ren, M. Rusticucci, R. Somerville, T.F. Stocker, P. Whetton, R.A. Wood and D. Wratt, 2007, Technical Summary. In: Climate Change 2007: The Physical Science Basis. Contribution of Working Group I to the Fourth Assessment Report of the Intergovernmental Panel on Climate Change [Solomon, S., D. Qin, M. Manning, Z. Chen, M. Marquis, K.B. Averyt, M. Tignor and H.L. Miller (eds.)]. Cambridge University Press, Cambridge, United Kingdom and New York, NY, USA. (Available on-line from: http://www.ipcc.ch/pdf/assessment-report/ar4/wg1/ar4-wg1-ts.pdf)
Sposito, V., 2007, A strategic approach to climate change impacts and adaptation, Applied GIS, V. 2, No. 3, pp. 23.1–23.26, Published online: March 2007, Source: http://publications.epress.monash.edu/doi/full/10.2104/ag060023?cookieSet=1S , Accessed December 2007.
Stormst, J., and Kroonenbergt, S., 2007, The impact of rapid sea level changes on recent Azerbaijan beach ridges, Journal of Coastal Research, V. 23, No. 2, pp. 521- 527.
Szlafsztein, C., 2005, Climate change, Sea-level rise and Coastal Natural Hazards: A GIS-Based Vulnerability Assessment, State of Pará, Brazil, Proceedings of the International workshop on human security and climate change, Asker, Brazil, June 21–23.
Ustun, A., Bildirici, I., Selvi, H. Zahit , and Abbak, R., 2006, An evaluation of SRTM3 DTM data: validity, problems and solutions, The International Conference on Cartography and GIS, January 25-28, Borovec, Bulgaria.
USGS (The US Geological Survey), 2007, The Seamless Shuttle Radar Topography Mission (SRTM): Finished 3 Arc Second, http://seamless.usgs.gov/website/seamless/products/srtm3arc.asp, Accessed Dec. 2007.

Table 1: Statistics of height differences of global DEMs compared to known check points (in meters)

Item	DEM			
	SRTM3"	DTM2002	SRTM30"	ETOPO2v2
Minimum	-5	-12	-14	-16
Maximum	5	6	5	7
Mean	0.2	-0.5	-1.4	-2.2
Standard Deviation	3.0	4.2	5.3	5.8

Table 2: The expected loss of lands under several sea level rise scenarios

Sea Level Rise	Loss of Areas (sq.km)	% of Total Areas
0.25 m	292	2 %
0.50 m	587	5 %
0.75 m	885	7 %
1.00 m	2023	17 %
1.25 m	2378	19 %
1.50 m	2731	22 %

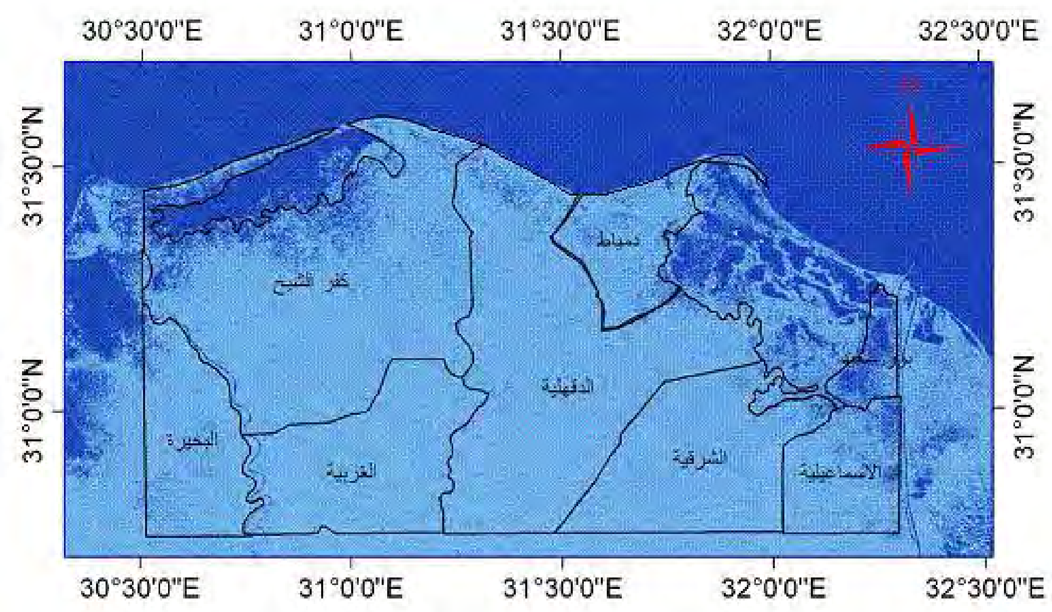

Figure 1: The study area

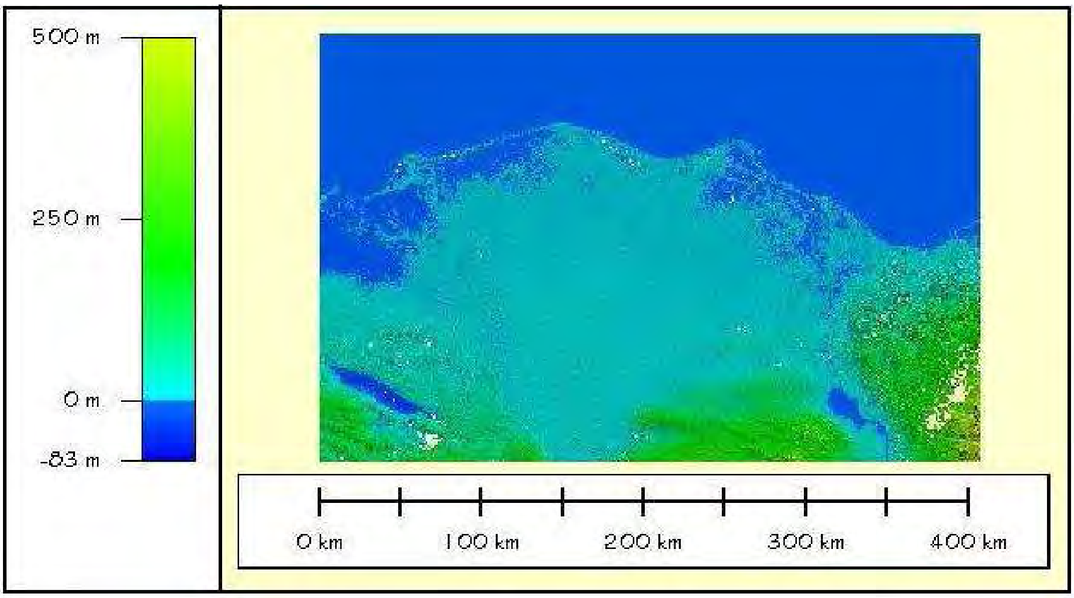

Figure 2: A shaded-relief representation of the study area using the SRTM 3" DEM

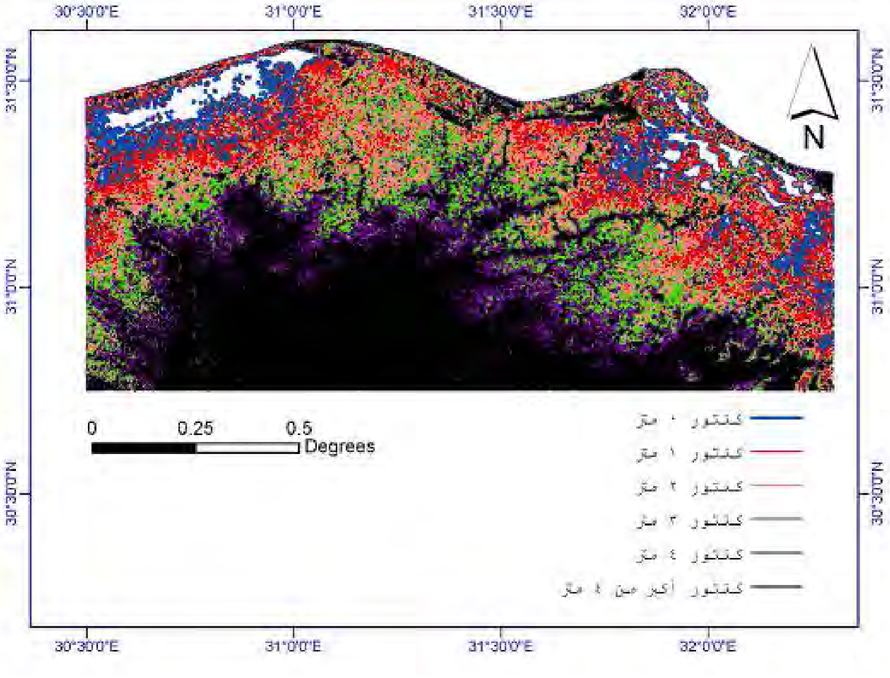

Figure 3: A contour representation of the study area using the SRTM 3" DEM

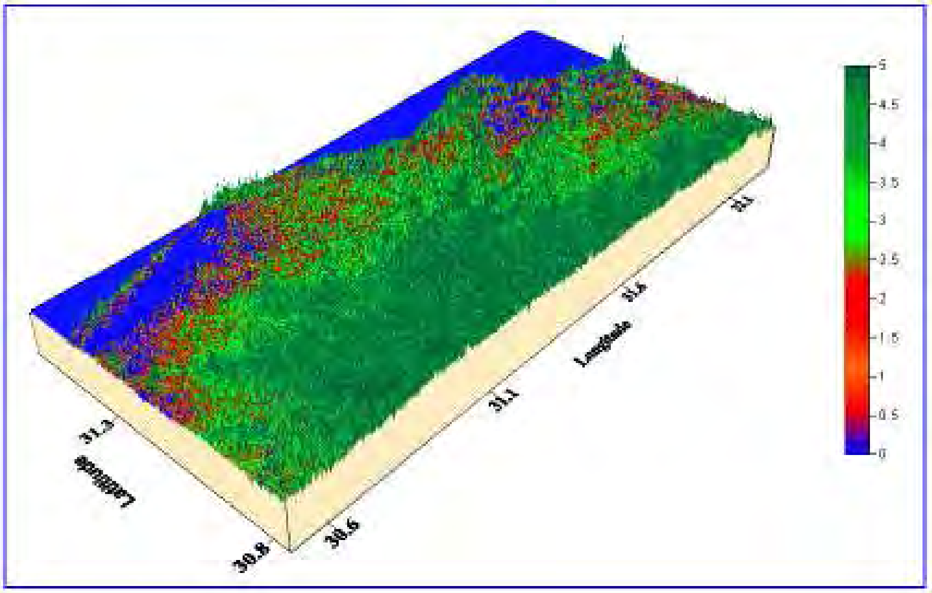

Figure 4: A 3D representation of the study area using the SRTM 3" DEM

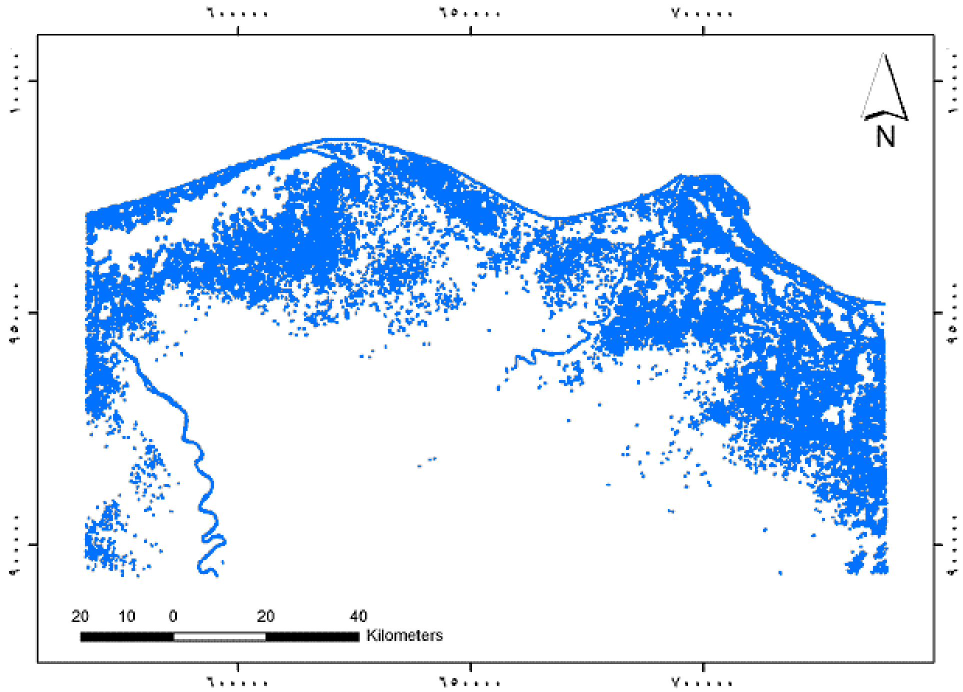

Figure 5: Regions corresponds to zero heights within the study area

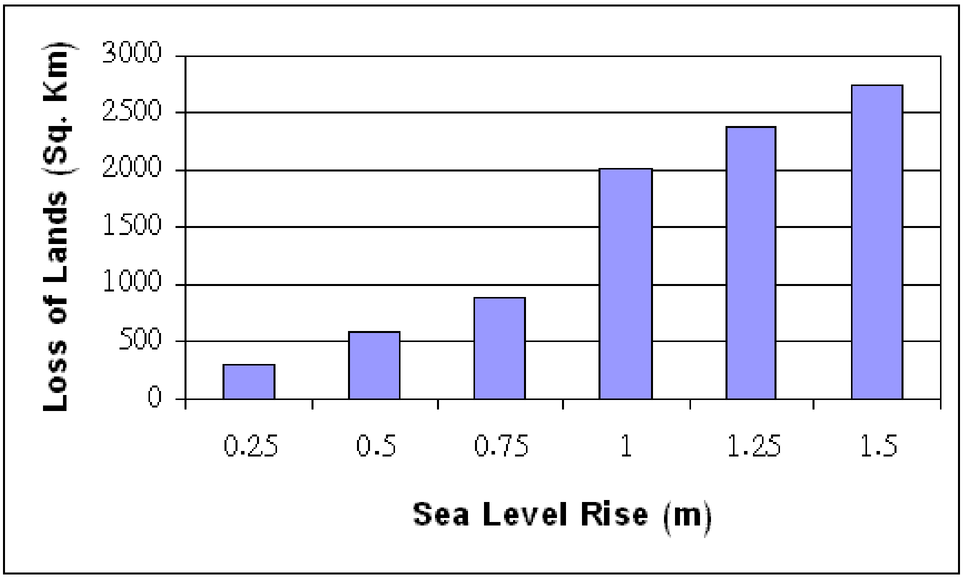

Figure 6: The expected loss of lands under several sea level rise scenarios

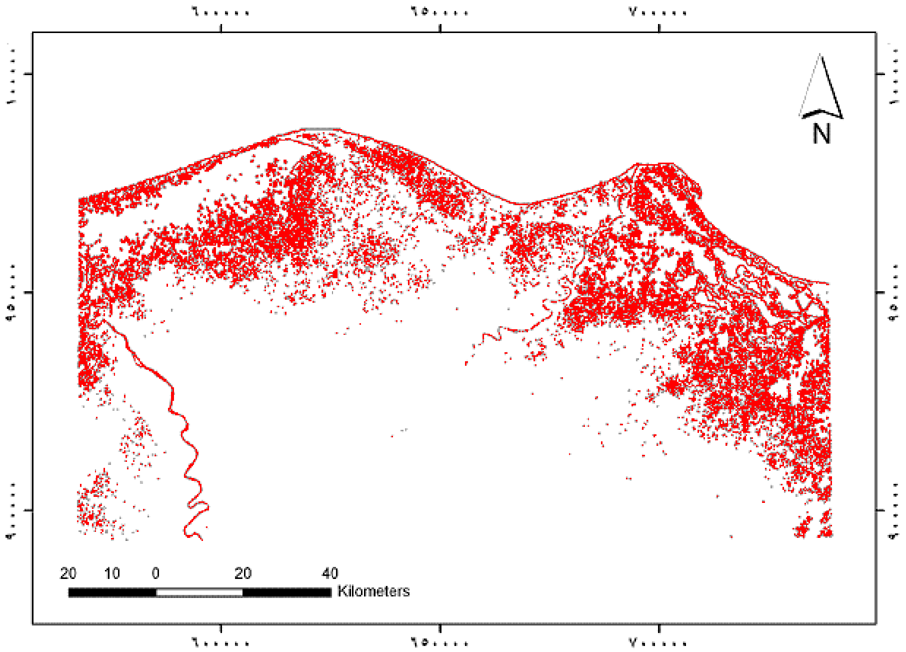

Figure 7: The expected loss of lands corresponds to sea level rise of 0.25 m

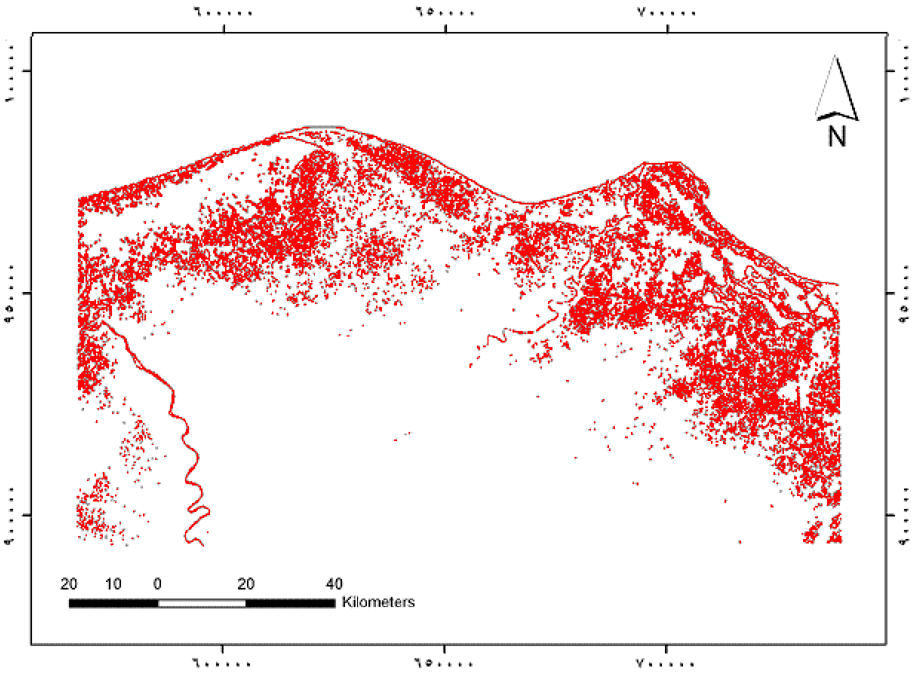

Figure 8: The expected loss of lands corresponds to sea level rise of 0.50 m

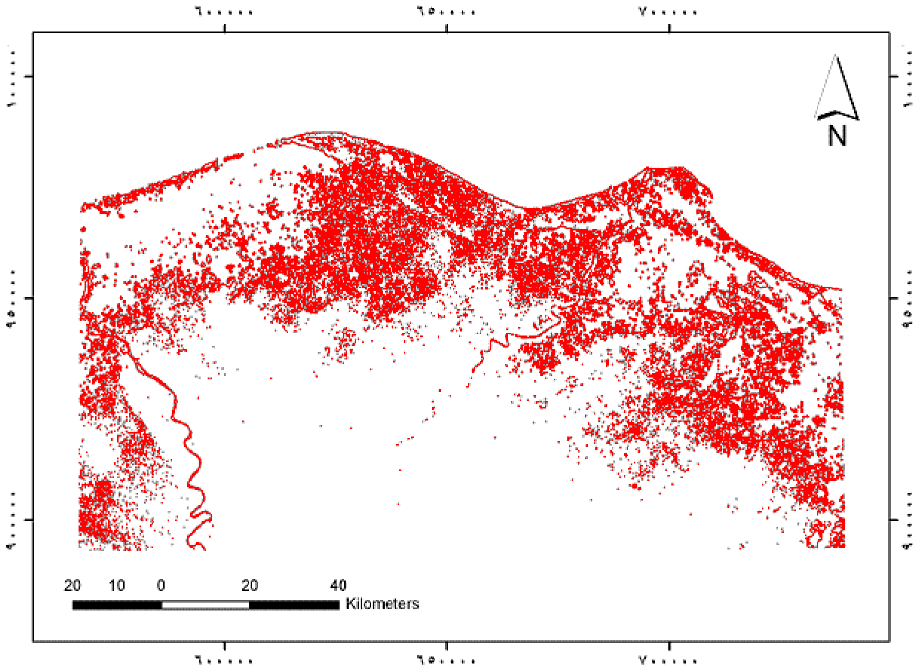

Figure 9: The expected loss of lands corresponds to sea level rise of 1.00 m

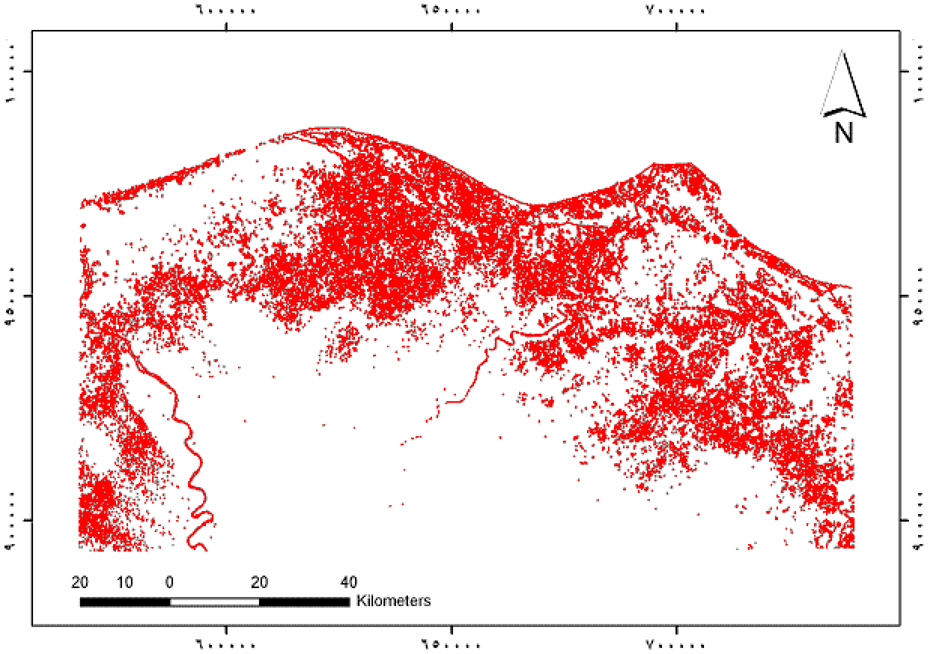

Figure 10: The expected loss of lands corresponds to sea level rise of 1.50 m

تقدير مخاطر ارتفاع منسوب سطح البحر في مصر داخل إطار نظم المعلومات الجغرافية

جمعة محمد داود[١ ، ٢] و هدي فيصل محمد[٢]

[١] جامعة أم القرى – مكة المكرمة – المملكة العربية السعودية
بريد الكتروني: dawod_gomaa@yahoo.com
[٢] معهد بحوث المساحة – المركز القومي لبحوث المياه – مصر
بريد الكتروني: hoda_faisal@yahoo.com

الملخص العربي:

تؤدي الظواهر المناخية – ومنها ظاهرة الاحتباس الحراري – لزيادة في منسوب سطح البحر علي المستوي العالمي. أشارت الدراسات و التوقعات العالمية الحديثة لقيم ارتفاع منسوب سطح البحر إلي أن هذه الزيادة قد تبلغ أكثر من متر بحلول عام ٢١٠٠م. يؤدي ارتفاع منسوب سطح البحر إلي عدة مخاطر بيئية منها تراجع الشواطئ وفقد مناطق سكنية خاصة في المدن الشاطئية. يهدف هذا البحث لتقدير و تقييم هذه المخاطر في المناطق الساحلية في دلتا النيل بمصر وهي المنطقة البالغ أبعادها حوالي ١٧٠ × ٩٠ كيلومتر. ولعدم توفر نموذج ارتفاعات رقمي وطني فقد اختبرت الدراسة الحالية أربعة من نماذج الارتفاعات الرقمية العالمية الحديثة لاختيار الأنسب لتمثيل طبوغرافية منطقة الدراسة وذلك باستخدام نقاط تحكم أرضية. ثم مثلت الدراسة أنسب نموذج ارتفاعات رقمي عالمي (ووجد أنه نموذج "SRTM3 ذا القدرة المكانية الأفقية حوالي ٩٠ متر) في إطار نظام معلومات جغرافي مكونا من ٢٢٠٦٣٨١ نقطة. تم دراسة عدة سيناريوهات لارتفاع منسوب سطح البحر تتراوح بين ٠.٢٥ متر إلي ١.٥ متر ، ووجد أن مساحة المناطق المعرضة للغرق تتراوح بين ٢٩٢ إلي ٢٧٣١ كيلومتر مربع. كما تم تمثيل التوزيع المكاني لهذه المخاطر في كل سيناريو متوقع لتطوير خرائط رقمية للمناطق المهددة. أثبتت نظم المعلومات الجغرافية فعالية هائلة ومميزات تقنية كبيرة في مثل هذا النوع من الدراسات البيئية. توصي الدراسة بأخذ النتائج – التي تم استنباطها – في الاعتبار بواسطة متخذي القرار في وضع خطط تنمية المناطق الساحلية في مصر.

كلمات مرجعية: نظم المعلومات الجغرافية ، ارتفاع منسوب سطح البحر ، نماذج الارتفاعات الرقمية، التأثيرات البيئية ، مصر.

This article was downloaded by: *[Umm Al-Qura University]*
On: *28 November 2010*
Access details: *Access Details: [subscription number 926970865]*
Publisher *Taylor & Francis*
Informa Ltd Registered in England and Wales Registered Number: 1072954 Registered office: Mortimer House, 37-41 Mortimer Street, London W1T 3JH, UK

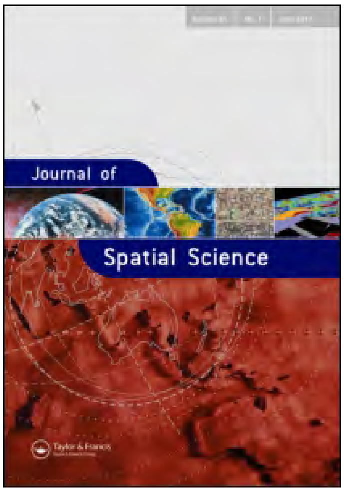

Journal of Spatial Science
Publication details, including instructions for authors and subscription information:
http://www.informaworld.com/smpp/title~content=t921253450

Towards the redefinition of the Egyptian geoid: Performance analysis of recent global geoid and digital terrain models

G. M. Dawod[a][b]
[a] Survey Research Institute, Egypt [b] Umm Al-Quraa University, Makkah, Saudi Arabia

Online publication date: 13 August 2010

To cite this Article Dawod, G. M.(2008) 'Towards the redefinition of the Egyptian geoid: Performance analysis of recent global geoid and digital terrain models', Journal of Spatial Science, 53: 1, 31 — 42
To link to this Article: DOI: 10.1080/14498596.2008.9635133
URL: http://dx.doi.org/10.1080/14498596.2008.9635133

PLEASE SCROLL DOWN FOR ARTICLE

Full terms and conditions of use: http://www.informaworld.com/terms-and-conditions-of-access.pdf

This article may be used for research, teaching and private study purposes. Any substantial or systematic reproduction, re-distribution, re-selling, loan or sub-licensing, systematic supply or distribution in any form to anyone is expressly forbidden.

The publisher does not give any warranty express or implied or make any representation that the contents will be complete or accurate or up to date. The accuracy of any instructions, formulae and drug doses should be independently verified with primary sources. The publisher shall not be liable for any loss, actions, claims, proceedings, demand or costs or damages whatsoever or howsoever caused arising directly or indirectly in connection with or arising out of the use of this material.

Towards the Redefinition of the Egyptian Geoid: Performance Analysis of Recent Global Geoid and Digital Terrain Models

G. M. Dawod

Launches of the CHAMP (CHAllenging Mini-satellite Payload) and GRACE (Gravity Recovery And Climate Experiment) satellite missions have produced a new generation of global geopotential models (GGMs). The performance of seven recent GGMs has been analyzed using a local geodetic dataset (terrestrial gravity and GPS/levelling points) in Egypt. The results show that the EIGEN-CG01C model is best at representing the long and medium wavelengths of the gravity field in Egypt. Its average accuracy, in terms of geoid undulations, when compared to known points, is estimated to be 0.36 m. Additionally, four digital terrain models (GTOPO30, SRTM, DTM2002, LDTM) have been investigated, leading to the conclusion that DTM2002 should be utilized in computing the terrain corrections for gravimetric geoid development in Egypt. When combined with local geodetic data, these two global models (EIGEN-CG01C and DTM2002) will support the production of a precise local geoid model, to be used in conjunction with Global Positioning System-based surveying and mapping projects in Egypt.

KeyWords: Global Geopotential Models, Geodesy, Regional Gravimetric Geoid, Digital Terrain Models, GPS/levelling, Egypt.

G. M. Dawod
Survey Research Institute
Egypt; currently at
Umm Al-Quraa University
Makkah
Saudi Arabia
dawod_gomaa@yahoo.com

INTRODUCTION

The rapid growth of Global Positioning System (GPS) utilisation in Egypt in recent decades necessitates having a nation-wide precise geoid model in order to transform the GPS-derived ellipsoidal heights to orthometric heights used in surveying and mapping. Global Geopotential Models (GGMs) produce a quasi-geoid, not the geoid itself. Since the height system used in Egypt is orthometric, GGM-based quasi-geoid heights have to be converted to true geoid undulations by adding a correction term, before GPS ellipsoidal heights can be converted to orthometric heights (Heiskanen and Moritz, 1967, p.326; Rapp, 1997). Neglecting such a correction may be misleading in fitting gravimetric quasi-geoids to GPS/Levelling data (Featherstone, 2006). Nevertheless, in order to improve local geoid modeling, the choice of an optimum GGM for a particular region is crucial (Kiamehr and Sjöberg, 2005a), which is one of the main objectives of this investigation.

Geoid development in Egypt has been addressed by a variety of researchers (e.g. Alnaggar, 1986; Abdelmotaal, 2002; Saad and Dawod, 2002). The geoid solution of Alnaggar (1986) is considered the pioneering nation-wide ($22^{o}N < latitude < 32^{0}N$, $25^{o}E < longitude < 37^{o}E$) geoid, developed using a least-squares collocation technique and heterogeneous geodetic data including terrestrial gravity, astronomic deflections of the vertical and Doppler/levelling undulations. Abdelmotaal (2002) has developed an Egyptian gravimetric

Downloaded By: [Umm Al-Qura University] At: 08:02 28 November 2010

geoid model, based on available free-air gravity anomalies and a local DTM, fitted to local GPS/levelling data. Another geoid solution, called EGGG2003, has been developed by Abdelmotaal (2003) using a technique (called the *Window* technique) to create an adapted version of the EGM96 global model to get a better fit to the Egyptian gravity field in a Fast Fourier Transform (FFT) process. Abdelmotaal (2006) developed and applied a high-degree tailored reference model by merging the available gravity anomalies with EGM96. Such a process gave better residual gravity anomalies than the original EGM96, and the variance was reduced by one third (*ibid*). A recent generation of geoid models for Egypt on a five-minute grid has been developed by Saad and Dawod (2002): SRI2001A is a gravimetric geoid computed using local gravity, a local Digital Terrain Model (DTM) and the EGM96 GGM, using a remove-compute-restore FFT processing methodology. SRI2001B is a geoid based on surface-fitting of the SRI2001A model to GPS/levelling (*ibid*). Moreover, there are other studies that have developed geoid models for particular areas of interest in Egypt (e.g. Tscherning *et al.,* 2001).

Practical studies have proved that, when comparing the GGM-based undulations to local geodetic datasets, none of the GGMs fit well to the Egyptian gravity field (e.g. Abdelmotaal, 2006; Saad and Dawod, 2002). In the last few years, several factors have given rise to the need for a new precise geoid model for Egypt, particularly the release of new GGMs and the compilation of more local geodetic datasets. This paper aims to provide guidelines for processing a new geoid for Egypt through analyzing the performance and accuracy of recent GGMs and DTMs.

RECENT GLOBAL GEOPOTENTIAL MODELS

The launch of the CHAMP (CHAllenging Mini-satellite Payload) in 2000 and the twin satellites GRACE (Gravity Recovery and Climate Experiment) in 2002, and the probable launch of GOCE (Gravity field and steady-state Ocean Circulation Explorer) in 2008 have introduced a new era in global gravity field determination (e.g. Featherstone, 2003). The CHAMP and GRACE satellite missions improve knowledge of the long and medium wavelength features of the gravity field. The future GOCE satellite will improve knowledge of the short-wavelength components up to degree 300. These new satellite missions allow the computation of a new generation of GGMs, which will significantly improve upon, and thus supersede, existing GGMs (e.g. Reigber *et al.,* 2006; Bilker, 2005; Featherstone, 2003). The International Center for Global Gravity Field Models (ICGEM, Potsdam, Germany) makes available a number of GGMs in the form of fully-normalized spherical harmonic coefficients that can be used to compute geodetic and gravitational quantities (http://icgem.gfz-potsdam.de/ICGEM/ICGEM.html).

It should be noted that GGMs, when used in a spherical harmonic expansion, produce quasigeoid not geoid solutions since the processing yields height anomalies not geoid undulations. Several researchers have considered this issue and have presented solutions to convert height anomalies to geoid heights (e.g. Heiskanen and Moritz, 1967, p.326, Eq. 8-100). Rapp (1997) suggested that potential coefficient models be used first to calculate a height anomaly, and then a correction term, represented by a high degree spherical harmonic expansion, be applied to give the geoid undulation. The geoid/quasigeoid separation is not the main focus of the current study, but such a conversion is an important step in the development of a precise geoid model for Egypt (particularly to convert GPS ellipsoidal heights to orthometric heights), and should be taken into consideration in due course.

In the last five years, several GGMs have been developed and released for world-wide use. Out of the most-recently released GGMs, a group of seven have been selected for this study and are briefly described in Table 1. The choice of these GGMs was made to cover a variety of models that have various degree and order (e.g. 140, 200, and 360), and various combinations of input data (satellite tracking data, terrestrial gravity data and altimetry data). The EGM96 model has been included in this study, even though it is older than the other GGMs, since it is broadly utilised worldwide and in Egypt (e.g. Saad and Dawod, 2002; Abdelmotaal, 2006).

Downloaded By: [Umm Al-Qura University] At: 08:02 28 November 2010

Model	Year	Degree	Data	Reference
EIGEN-GL04C	2006	360	S,G,A	Förste *et al.* (2006)
EIGEN-CG03C	2005	360	S,G,A	Förste *et al.* (2005)
GGM02C	2004	200	S,G,A	Tapley *et al.* (2005)
EIGEN-CG01C	2004	360	S,G,A	Reigber *et al.* (2006)
EIGEN-3P	2003	140	S	Reigber *et al.* (2005)
EIGEN-2	2003	140	S	Reigber *et al.* (2003)
EGM96	1996	360	S,G,A	Lemoine *et al.* (1998)

Table 1. *GGMs to be evaluated in this study*

Data: S=Satellite Tracking Data, G = Terrestrial Gravity Data, A = Altimetry Data

The EIGEN-CG01C global geoid model has an overall accuracy of 20 cm and 5 mgal, in terms of geoid heights and gravity anomalies respectively (Reigber *et al.*, 2006). The model benefits significantly from recently released gravity anomaly compilations over polar regions. In general, the accuracy of EIGEN-CG01C over the oceans is better than over the continents, reflecting the higher quality of the available satellite altimetry data (*ibid*).

The EIGEN-CG03C global mean gravity field model is a combination of data from the GRACE mission (376 days in the periods: February-May 2004; July-December 2003 and February-July 2004) and the CHAMP mission (860 days in the period October 2000-June 2003), plus altimetric and gravimetric surface data (Förste *et al.*, 2005). This model has an overall accuracy in terms of geoid heights and gravity anomalies of 30 cm and 8 mgal, respectively (*ibid*).

The EIGEN-GL04C gravity field model is an upgrade of EIGEN-CG03C. This model combines data from GRACE and LAser GEOdynamics Satellite (LAGEOS) missions plus 0.5 x 0.5 degree gravimetry and altimetry surface data (Förste *et al.*, 2006). The satellite data have been analyzed by two organizations: GFZ Potsdam and Groupe de Recherche de Geodesie Spaciale (GRGS) Toulouse. The processing standards used by both analysis centres were identical, with the exception of the ocean model used for correcting short-term mass variations. The surface data used were identical to the EIGEN-CG03C solution except for the geoid undulations over the oceans, which have been derived from a new GFZ mean sea surface height (MSSH) model (e.g. Förste *et al.*, 2006; and ICGEM page http://www.gfz-potsdam.de/pb1/op/grace/results/grav/g005_eigen-gl04c.html#t0).

The GGM02S satellite-only GGM was derived using approximately 14 months of GRACE data from April 2002 to December 2003 (Tapley *et al.* 2005). The satellite-only GGM02S solution (complete to degree/order 160) has been combined with the terrestrial gravity information used in EGM96, to obtain GGM02C (complete to degree/order 200) preserving the strength of the GRACE information at longer wavelengths and the surface information contained in EGM96 at shorter wavelengths. Calibrated error estimates for the GGM02 generation of models (either GGM02S or GGM02C) indicate a global geoid height RMS error of approximately 7 mm to degree/order 70, with no discrimination between land and ocean (Tapley *et al., 2*005). At low and mid degrees (approximately degree 5-70), this improvement is nearly two orders of magnitude better than pre-GRACE models, and more than a factor of two improvement over the earlier GGM01 generation (e.g. http://www.csr.utexas.edu/grace/gravity/ggm02/GGM02_Notes.pdf).

EIGEN-2 is a CHAMP-only gravity field model derived from CHAMP GPS satellite-to-satellite and accelerometer data for the period July to December 2000, and September to December 2001 (Reigber *et al.* 2003). Although higher-degree/order terms exist in EIGEN-2, the solution has full power only up to about degree/order 40 due to signal attenuation because of the satellite's altitude. The accuracy of EIGEN-2 is 10 cm and 0.5 mgal in terms of geoid heights and gravity anomalies, respectively, at a half wavelength resolution of 550 km. This is an improvement by almost one order of magnitude compared to any multi-satellite pre-CHAMP satellite-only gravity field model (*ibid*).

EIGEN-3P (EIGEN-3 preliminary) is a CHAMP-only gravity field model derived from CHAMP GPS satellite-to-satellite and accelerometer data for the period July 2000 through June 2003 (Reigber *et al.,* 2005). At the time of its release, this GGM was considered a preliminary model since its final processing had not been completed. EIGEN-3P differs from EIGEN-2 not only by the six times larger amount of CHAMP data but also by a different parameterisation

Downloaded By: [Umm Al-Qura University] At: 08:02 28 November 2010

Gravity Model	USA 6169 points	Canada 1930 points	Europe 186 points	Australia 201 point	Weighted Mean 8486 points
EIGEN-GL04C	0.363	0.261	0.332	0.262	0.337
EIGEN-CG01C	0.374	0.277	0.412	0.281	0.351
EIGEN-CG03C	0.367	0.311	0.397	0.277	0.353
EGM96	0.402	0.366	0.487	0.314	0.394
GGM02C	0.491	0.381	0.492	0.390	0.464
EIGEN-3P	0.830	0.862	1.333	0.856	0.849
EIGEN-2	0.971	1.082	1.620	1.072	1.013

Table 2. *Root mean square (RMS) differences of GPS-levelling minus GGM derived quasi-geoid heights (m) (after ICGEM)*

Downloaded By: [Umm Al-Qura University] At: 08:02 28 November 2010

of the accelerometer calibration. Although higher-degree/order terms exist in EIGEN-3P, the solution has full power only up to about degree/order 65, once again due to signal attenuation (for more details, see: http://www.gfz-potsdam.de/champ/results/index_RESULTS.html).

To evaluate the performance of the GGMs described above, their estimated height anomalies have been compared against geoid undulations at known GPS/levelling stations in USA, Canada, Europe, and Australia (for more details on this comparison and its results, see http://icgem.gfz-potsdam.de/ICGEM/evaluation/evaluation.html). The results of this comparison are presented in Table 2. The final column of Table 2 shows the weighted mean difference, computed using the number of points in each region as the relevant weighting factor.

It can be seen from Table 2, that despite the incorporation of recent satellite and terrestrial gravity data in the development of the newer GGMs, only three, namely EIGEN-GL04, EIGEN-CG01C, and EIGEN-CG03C, perform better – and that only marginally – than the older EGM96 model.

In this context, it is worth mentioning that a new GGM (the Earth Geopotential Model 2007/8 or EGM07/8) is under development by the US National Geospatial Intelligence Agency (NGA) (NGA, 2007) and will take advantage of updated satellite, surface gravity, elevation and altimetry data. EGM07/8 will be complete to degree and order 2160, with 5′ x 5′ resolution and 15 cm RMS expected accuracy (Forsberg, 2007). EGM07/8 is expected to be released to the public in early 2008 (NGA, 2007).

RECENT DIGITAL TERRAIN MODELS

Digital Terrain Models (DTM) are essential for gravity data processing and geoid model development, particularly for the computation of terrain corrections to observed terrestrial gravity data, and for downward continuation computations. Topographic height, bathymetry, and ice thickness data support the computation of analytical continuation terms, and the development of models to convert height anomalies to geoid undulations (e.g. Heiskanen and Moritz, 1967, p. 326). The effect of the topography (represented by a DTM) is accounted for in the calculation of reduced gravity anomalies as (*ibid*):

$$\Delta g = \Delta g_F - \Delta g_h - \Delta g_{Ref} \qquad (1)$$

where Δg_F is the free-air anomaly, Δg_h is the effect of the topography, and Δg_{Ref} is the effect of reference gravity field represented by a GGM. The full geoid undulation N is then computed as:

$$N = N_{\Delta g} + N_h + N_{Ref} \qquad (2)$$

where $N_{\Delta g}$ is the contribution of the reduced gravity anomalies computed by Stokes's integral, N_h is the contribution of the topography or the terrain effect, and N_{Ref} is the contribution of the reference gravity field computed by the spherical harmonic expansion (For more information on the FFT technique, see Sideris and Footopoulus, 2005).

Recently, global topographic and bathymetric databases have been compiled and released,

leading to the development of a new, more detailed global model called DTM2002. DTM2002 combines (Saleh and Pavlis, 2002):

(1) The GTOPO30 and GLOBE global 30Ð DEMs (Hastings and Dunbar, 1999);
(2) The ACE 30Ð DEM (Johnson et al., 2001);
(3) Near ocean-wide bathymetric information predicted from altimetry data and constrained by ship-borne depth soundings (Smith and Sandwell, 1997);
(4) The Generic Mapping Tools (GMT) high-resolution global shoreline and land type database (Wessel and Smith, 1996);
(5) New 5 km grids of ice surface elevations from altimetry data and the JGP95E geoid model over Antarctica and Greenland;
(6) Revised ice thickness data over Antarctica (on a 50 km grid) and Greenland (5Ðx10Ð);
(7) Depth data (30Ð) for the Great Lakes (Ekholm, 1996).

DTM2002 was compiled in a 30Ð version that provides surface elevations and ocean depths only, and in 2Ð and 5Ð versions that include depth data for certain large lakes and ice thickness information (*ibid*). A part of DTM2002 (the 30″ version) corresponding to the Egyptian territories has been obtained (Saleh, 2004) and utilized in this research.

GTOPO30 is a global DTM, completed in late 1996, with a horizontal grid spacing of 30″ (approximately 1 km). GTOPO30, developed over a three-year period through a collaborative effort led by the US Geological Survey's EROS Data Center (EDC), was derived from several raster and vector sources of topographic information. The vertical accuracy of GTOPO30 is quoted to be ± 30 m at the 90 percent confidence level (for more details, see http://edcdaac.usgs.gov/gtopo30/README.html#h31). GTOPO30 can be downloaded from http://edcdaac.usgs.gov/. The window of GTOPO30 that corresponds to the Egyptian territories has been extracted and utilized in this research.

The Shuttle Radar Topography Mission (SRTM) global DTM is a joint project between the US National Imagery and Mapping Agency (NIMA) and the National Aeronautics and Space Administration (NASA) (see http://www2.jpl.nasa.gov/strm/). A 90 m SRTM DTM for many parts of the world has been compiled and released (*ibid*). SRTM has been used in geoid modelling for several regions, particularly for topographic and downward continuation corrections (e.g Kiamehr and Sjöberg, 2005b). The window of the SRTM DTM corresponding to the Egyptian territories has been downloaded and has been considered in this study.

Even though DTM2002, GTOPO30 and SRTM are the only global DTMs that have been presented and evaluated in the current study, other DTMs (e.g. the Global Land One-km Base Elevation, GLOBE DTM) should also be evaluated in any future attempt to develop a precise Egyptian geoid model.

AVAILABLE EGYPTIAN GEODETIC DATABASES

The local geodetic data used in this study was held in two databases (Table 3). Firstly, terrestrial gravity values have been measured at 1138 points (Figure 1). The date of these observations and their accuracy vary greatly between the most recent Egyptian National Gravity Standardisation Network of 1997 (ENGSN97) (Dawod, 1998) and older gravity surveys carried out several decades ago. The accuracy of ENGSN97 gravity values is 0.022 mgal, while the accuracy estimate for older gravity data is 0.5 mgal on average (Dawod and Alnaggar, 2000). As can be seen from Figure 1, gravimetric data distribution is not homogeneous over Egypt, with significant gaps, particularly in the Eastern and Western deserts (*ibid*). An evaluation of the existing gravity data, based on comparing the gravity value of each point to values at the nearest four stations, was carried out to identify any large discrepancies. This process identified 58 points (about 5 percent) as suspected outliers and these were subsequently removed.

The second compiled geodetic data base consists of 202 GPS/levelling points (Figure 2), where geoid undulations have been directly computed. The majority of this data set comes from GPS campaigns carried out by the Nile Research Institute (NRI) for updating the hydro-topographic maps of the Nile (Dawod and Abdel-Aziz, 2003). The accuracy of the derived geoid undulations has been estimated to be ± 5 centimetres (*ibid*). Once again, an examination of the data was carried out by comparing the geoid undulation at each point to corresponding values at the nearest four stations. This

Downloaded By: [Umm Al-Qura University] At: 08:02 28 November 2010

examination revealed that 18 points (about 9 percent) were possible outliers and these data points were removed from the dataset.

Data Type	No. of points	Precision
Terrestrial Gravity:		
1- ENGSN97 Network	150	± 0.022 mgal
2- Older gravity points	988	± 0.500 mgal
GPS/levelling	202	± 0.05 m

Table 3: *Available local geodetic data*

Additionally, a local 5′ x 5′ DTM has been utilized for comparison of the global DTMs over Egypt (El Sagheer, 1995). This nationwide Egyptian LDTM has been developed using digitized hard copy topographic maps as well as scattered height data points (*ibid*).

It should be noted at this point that the number and the distribution of the available terrestrial gravity data over Egypt is not ideal for reliable geoid computation using the traditional FFT process. It may be necessary, therefore, to apply either an isostatic compensation model, or independent knowledge on the density distribution, e.g. from seismic data, to take into account the influence of the crust-mantle interface on the geoid. Abdelmotaal and Kühtreiber (2003) proposed the use of seismic Moho depths, representing the actual compensating masses, with variable density anomalies. The results showed that such a strategy gives better geoid accuracy compared to the GPS/levelling geoid (*ibid*). This work should be investigated in any future development of a precise geoid model for Egypt, but has not been considered further in the current study.

PERFORMANCE OF GGMS OVER EGYPT

Amos and Featherstone (2003) have argued that terrestrial gravity anomalies do not form a very good test of GGMs, because these terrestrial data are highly susceptible to medium- and

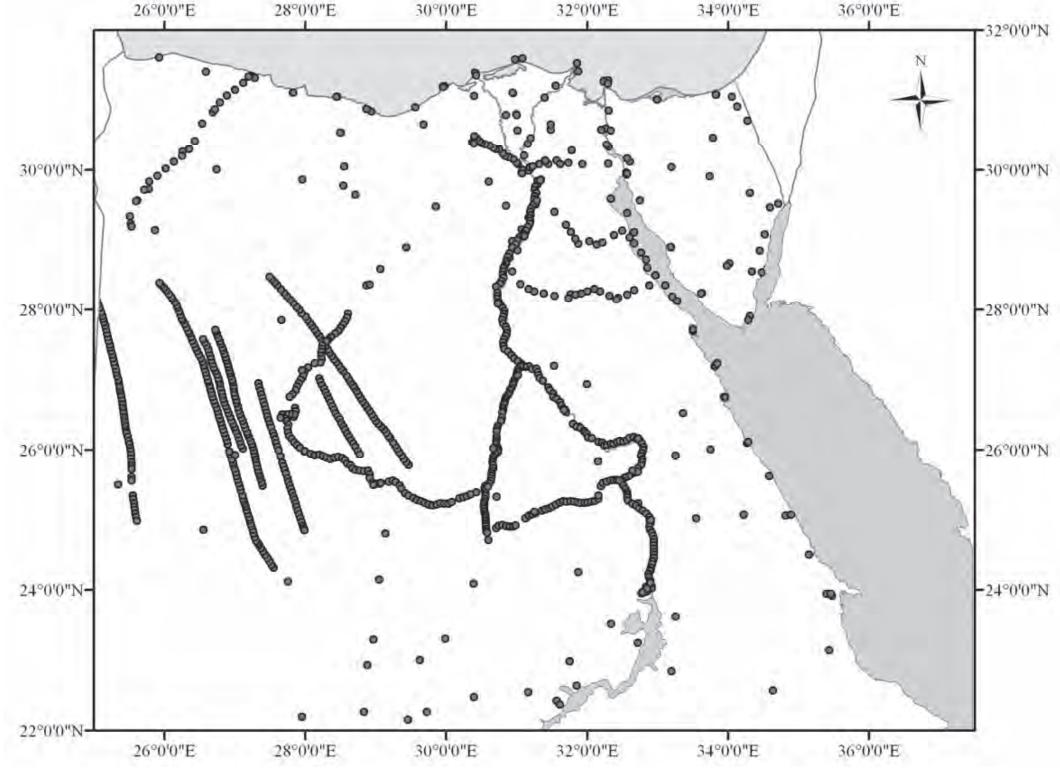

Figure 1. *Available local gravity stations*

Downloaded By: [Umm Al-Qura University] At: 08:02 28 November 2010

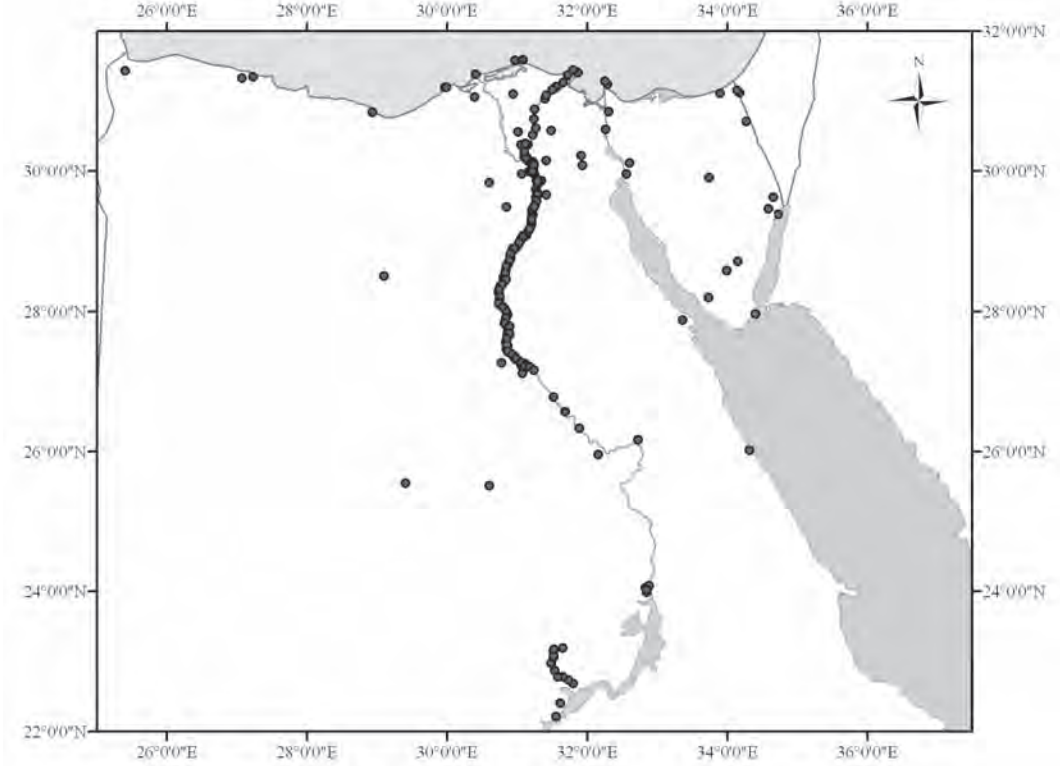

Figure 2. *Available stations with known geoid undulations*

long-wavelength errors due to factors such as distortions in the vertical geodetic datum and gravimeter drift. Additionally, they have pointed out that GPS/levelling data are also ambiguous not only because of potential datum errors, but also due to the fact that such datasets are usually collected over a long period of time, while processing algorithms and data availability (particularly precise GPS orbits) have matured.

However, a comparative analysis between GGMs and terrestrial data will reveal valuable information in the context of developing a local geoid for Egypt, particularly in terms of choosing a GGM that optimally maps the long- and medium-wavelength gravitational field in the area. It is a matter of fact that the local terrestrial gravity data, when combined with a GGM will enhance its performance, so that this addition should be the rational approach for developing a precise local geoid for Egypt.

The process of determining the *best* GGM for Egypt, consisted of two steps. Firstly, the spherical harmonic expansion coefficients of the GGMs (Table 1) were downloaded from the ICGEM website. Also, a new GGM has been created in this current study (named GGM02C/EGM96) by extending the GGM02C model to degree 360 through adding the EGM96 coefficients >200 to GGM02C. This step aims to see if such an extension has a significant effect on the final results (e.g. Tapley *et al.*, 2005; Featherstone, 2005).

Secondly, the program SHS360 (Spherical Harmonic Solution to degree and order 360) (Tscherning, 1976) has been used to compute gravity anomalies and quasi-geoid undulations at all points shown in Figures 1 and 2, respectively. The results have been compared with the measured values, and are presented in Tables 4 and 5 in order of increasing mean.

Table 4 reveals several important points about the performance of GGMs in terms of gravity field representation in Egypt. Concerning the RMS values, the EIGEN-CG01C and the EGM96 models give the same RMS, and the EIGEN-GL04C is also very close to this value.

Downloaded By: [Umm Al-Qura University] At: 08:02 28 November 2010

GGM (degree)	Min	Max	Mean	RMS
EIGEN-CG01C (360)	-146.4	102.6	-20.85	25.9
EIGEN-GL04C (360)	-143.6	103.3	-20.94	26.0
GGM02C/EGM96 (360)	-160.3	113.1	-21.97	28.2
EGM96 (360)	-135.4	98.7	-22.08	25.9
GGM02C (200)	-179.8	114.1	-23.01	27.4
EIGEN-3P (140)	-214.6	109.5	-25.74	30.1
EIGEN-CG03C (360)	-212.3	111.9	-26.92	30.0
EIGEN-2 (140)	-226.6	131.7	-27.71	32.8

Table 4. *Gravity anomaly differences (observed - model) at 1080 check points (mgal)*

GGM (degree)	Min	Max	Mean	RMS
EIGEN-CG01C (360)	-0.98	2.05	-0.07	0.36
GGM02C (200)	-1.24	1.87	-0.25	0.44
GGM02C/EGM96 (360)	-1.61	2.32	-0.28	0.54
EIGEN-CG03C (360)	-1.38	1.79	-0.43	0.36
EIGEN-GL04C (360)	-1.62	1.73	-0.57	0.38
EGM96 (360)	-1.60	1.41	-0.74	0.39
EIGEN-3P (140)	-3.63	3.10	-0.92	1.04
EIGEN-2 (140)	-4.12	4.79	-2.71	1.30

Table 5. *Geoid undulation differences (observed - model) at 184 check points (m)*

Downloaded By: [Umm Al-Qura University] At: 08:02 28 November 2010

The new generated model GGM02C/EGM96 does not offer an improvement over the original GGM02C solution, which may be attributed to the long and medium wavelength features being dominant in this case. Also, it can be seen that the EGM96 is better than CGM02C and CGM02C/EGM96 which identifies EGM96 as the marginally superior GGM and shows that supplementing CGM02C with the higher order coefficients does not improve its resolution. Moreover, it can be concluded that the lower the degree and order of the GGM, the lower the expected accuracy and precision (e.g. Bilker, 2005). This can be seen from Table 4, where the satellite-only GGMs EIGEN-3P and EIGEN-2 (degree and order equal 140) gave larger RMS values than the GGMs of degree and order 360, which is expected due to the omission errors. The only exception is EIGEN-CG03C, with degree and order 360, which produced a slightly worse RMS than GGM02C (degree and order 200).

Furthermore, several remarks can be made, based on the results presented in Table 5, concerning the performance of GGMs in terms of computing geoid undulations in Egypt. The most important point is that the EIGEN-CG01C produced the smallest mean undulation difference. Along with EIGEN-CG01C, GGM02C, EIGEN-CG03C, EIGEN-CLO4C and EGM96, all produced mean undulation differences less than half a metre. As expected, the satellite-only GGMs, EIGEN-3P and EIGEN-2, produced the largest mean undulation differences, which again can be attributed to their relatively low degree and order and, hence, their limited capacity to model the short wavelength variations of the gravity field (i.e. the omission errors). In terms of the RMS values, EIGEN-CG01C and EIGEN-CG03C performed the best, followed by EIGEN-GL04C, EGM96, and GGM02C. However the mean undulation differences were larger in the latter four cases.

It follows from the models tested and in terms of modeling known gravity anomalies and geoid undulations over Egypt, EIGEN-CG01C is the GGM that most accurately represents the gravity field. It is worth mentioning that the EIGEN-CG01C has been used to develop local gravimetric geoid models for Bolivia (Corchete *et al.*, 2006) and Iberia (Corchete *et al.*, 2005). Although it is one of the older models, EIGEN-CG01C was the second best of the GGMs compared against GPS/levelling data worldwide (see Table 2). Furthermore, it is likely that the performance of different GGMs varies from one region to another, particularly in areas where local gravimetric data have not been incorporated in the development of those GGMs. For example, Kiamehr (2006) used 260 GPS/levelling points to test the performance of several GGMs (CGM02S, CGM02C, EIGEN-02S, EIGEN-CG01, GPM98C, EGM96, and a tailored CGM02/EGM96) over Iran, and found that the satellite-only CGM02S fitted the GPS/levelling data best in both relative and absolute terms.

PERFORMANCE OF DTMS OVER EGYPT

Table 6 presents the statistics of the height differences for the four DTMs when compared to the local geodetic datasets. From the mean and RMS values it is clear that DTM2002 was superior to both the global DTMs (GTOPO30 and SRTM) and the local DTM (LDTM). It can be concluded therefore that DTM2002 will improve the development of a new gravimetric geoid for Egypt, particularly in the computation of the terrain corrections.

CONCLUSIONS

A significant step in the development of a precise geoid model for Egypt is the utilisation of a global geoid model that accurately maps the gravity field variations in this area, along with a DTM that represents the topographic variations with a considerable level of reliability.

The performance of eight recent GGMs has been compared against the local geodetic data over parts of Egypt. The results show that the EIGEN-CG01C is the best GGM in terms representing the gravity anomalies (with a mean difference of -20.9 mgal and an RMS of 25.9 mgal), and also in representing the geoid undulations (with a mean difference of -0.07 m and an RMS of 0.36 m). From these findings it is anticipated that the EIGEN-GC01C GGM will yield considerable enhancements within the FFT process for developing a local precise geoid model for Egypt.

Additionally, the DTM2002 has shown to be the more accurate terrain model, than either the global DTMs (GTOPO30 and SRTM) or the local DTM, in representing the topography variations in Egypt, with a mean height difference (as compared against known orthometric heights) of 0.6 m and an RMS of 20.7 m.

Therefore, it can be concluded that EIGEN-CG01C is the optimum global geoid model, and the DTM2002 is the optimum digital terrain model for use in Egypt. It is recommended that these two models should be utilised in the development of a new precise geoid for Egypt.

REFERENCES

Abdelmotaal, H. (2002) Towards a Precise Geoid for Egypt, In Tziavos: *Gravity and Geoid 2002*, 3rd Meeting of the International Gravity and Geoid Commission, Thessaloniki, Greece, August 26-30, pp. 120-125.

Abdelmotaal, H. (2003) The Egyptian Geoid EGGG2003, *Presented at the 23rd General Assembly of the International Union of Geodesy and Geophysics IUGG*, Sapporo, Japan, June 30 - July 11.

DTM	Min	Max	Mean	RMS
GTOPO30	-332.0	214.2	-80.7	93.3
LDTM	-97.3	97.5	-3.0	25.9
SRTM	-132.5	94.0	-0.9	25.1
DTM2002	-80.8	73.9	0.6	20.7

Table 6. *Statistics of the height differences (observed - DTM) at 1264 check points (m)*

Downloaded By: [Umm Al-Qura University] At: 08:02 28 November 2010

Abdelmotaal, H. (2006) High-Degree Geopotential Model Tailored to Egypt, *Presented at the 1st International Symposium of The International Gravity Field Service (IGFS)*, Istanbul, Turkey, August 28 – September 1.

Abdelmotaal, H. and Kühtreiber, N. (2003) Geoid determination using adopted reference field, seismic Moho depths and variable density contrast, *Journal of Geodesy*, Vol. 77, No. 1-2, pp. 77-85.

Alnaggar, D. (1986) Determination of the Geoid in Egypt Using Heterogeneous Geodetic Data, *Ph.D. Dissertation*, Cairo University, Egypt.

Amos, M. and Featherstone, W. (2003) Comparisons of recent global geopotential models with terrestrial gravity field data over New Zealand and Australia, *Geomatics Research Australia*, No. 79, pp. 1-20.

Bilker, M. (2005) Evaluation of the new global gravity field models from CHAMP and GRACE with GPS/levelling data in Fennoscandia, XXII *Geophysical Society of Finland Conference*, Helsinki, May 19-20.

Corchete V., Chourak, M. and Khattach D. (2005) The high-resolution gravimetric geoid of Iberia: IGG2005, *Geophys. J. Int.*, 162, pp. 676–684.

Corchete, V., Flores, D. and Oviedo, F. (2006) The first high-resolution gravimetric geoid for the Bolivian tableland: BOLGEO, *Phys. Earth Planet. Inter.*, No. 157, pp. 250-256.

Dawod, G. (1998) A national gravity standardization network for Egypt, *Ph.D. Dissertation*, Shoubra Faculty of Engineering, Banha Branch, Zagazig University, Cairo, Egypt.

Dawod, G. and Abdel-Aziz, T. (2003) Establishment of precise geodetic control networks for updating the River Nile maps, *Proceedings of Al-Azhar Engineering Seventh International Conference (CD No. 3)*, Al-Azhar University, Cairo, Egypt, April 7-10.

Dawod, G. and Alnaggar, D. (2000) Quality control measures for the Egyptian National Gravity Standardization Network (ENGSN97), *Proceedings of The Second International Conference on Civil Engineering*, Helwan University, Cairo, Egypt, April 1-3, pp. 578-587.

Denker, H. (1998) Evaluation and Improvement of the EGG97 Quasigeoid Model for Europe by GPS and Leveling Data, In: Vermeer, M. and Adam, J. (Eds.), *Proceedings of the Second Continental Workshop on the Geoid in Europe*, Budapest, Hungary, March 10-14.

Ekholm, S. (1996) A full coverage, high-resolution, topographic model of Greenland computed from a variety of digital elevation data, *Journal of Geophysical Research*, Vol. 21, B 10, pp. 961-972.

El Sagheer, A. (1995) Development of a digital terrain model for Egypt and its application for a gravimetric geoid determination, *Ph.D. Thesis*, Shoubra Faculty of Engineering, Zagazig University, Egypt.

Featherstone, W. (2003) Improvement to long-wavelength Australian gravity anomalies expected from the GRACE, CHAMP and GOCE dedicated satellite gravimetry missions, *Exploration Geophysics*, Vol. 34, No. 1-2, pp. 69-76.

Featherstone, W. (2005) Long-wavelength discrepancies between the Australian gravity field and EIGEN-2 CHAMP data, In: Sanso, F. (ed) *A Window on the Future of Geodesy*, Springer, Berlin, pp. 300-305.

Featherstone, W. (2006) Fitting geoids to GNSS-levelling: You're fooling yourself and fooling others, Presented at *The Geodetic Week 2006, The International Congress Center Munich (ICM)*, October 10-12. Munich, Germany.

Forsberg, R. (2007) The International Gravity Field Service and GGOS, *Presented at the GGOS Retreat 2007 and Eighth Steering Committee Meeting*, California, USA, February 19-21.

Förste, C., Flechtner, F., Schmidt, R., Meyer, U., Stubenvoll, R., Barthelmes, F., König, R., Neumayer, K., Rothacher, M., Reigber, C., Biancale, R., Bruinsma, S., Lemoine, J.-M. and Raimondo, J. (2005) A new high resolution global gravity field model derived from combination of GRACE and CHAMP mission and altimetry/gravimetry surface gravity data, *Poster presented at EGU General Assembly 2005*, Vienna, Austria, April 24-29.

Förste, C., Flechtner, F., Schmidt, R., König, R., Meyer, U., Stubenvoll, R., Rothacher, M., Barthelmes, F., Neumayer, K.H., Biancale, R., Bruinsma, S. and Lemoine, J.-M. (2006) A mean global gravity field model from the

Downloaded By: [Umm Al-Qura University] At: 08:02 28 November 2010

combination of satellite mission and altimetry/gravimetry surface gravity data, *Poster presented at EGU General Assembly 2006*, Vienna, Austria, April 2-7.

Hastings, D. and Dunbar, P. (1999) *GLOBE Digital Elevation Model Documentation*, Volume 1.0. NOAA, NGDC, Boulder, Colorado.

Heiskanen, W. A. and Moritz, H. (1967) *Physical geodesy*, Freeman, San Francisco.

Johnson, C., Berry, P. and Hilton, R. (2001) *Report on ACE Generation*, Geomatics Unit, DeMontfort University, Leicester, UK.

Kiamehr, R. (2006) Precise gravimetric geoid model for Iran based on GRACE and SRTM data and the least-squares modification of Stokes' formula with some geodynamic interpretations, *Ph.D. Dissertation*, Division of Geodesy, Department of Transport and Economics, Royal Institute of Technology, Stockholm, Sweden.

Kiamehr, R. and Sjöberg, L. E. (2005a) Comparison of the qualities of recent global and local gravimetric geoid models in Iran, *Studia Geophysica et Geodaetica*, V. 49, No. 3, pp.289-304.

Kiamehr, R. and Sjöberg, L. E. (2005b) Effect of the SRTM global DEM on the determination of a high-resolution geoid model: a case study in Iran, *Journal of Geodesy*, Volume 79, No. 9, pp.540-551.

Lemoine, F., Kenyon, S., Factor, J., Trimmer, R., Pavlis, N., Chinn, D., Cox, C., Klosko, S., Luthcke, S., Torrence, M., Wang, Y., Williamson, R., Pavlis, E., Rapp, R. and Olson, T. (1998) The development of the Joint NASA GSFC and the National IMagery and Mapping Agency (NIMA) geopotential model EGM96, *NASA Technical Paper NASA/TP1998206861*, Goddard Space Flight Center, Greenbelt, USA.

NGA (the US National Geospatial Intelligence Agency) (2007) *http://earth-info.nga.mil/GandG/wgs84/gravitymod/new_egm/*, Accessed June 2007.

Rapp, R. (1997) Use of potential coefficient models for geoid undulation determinations using a spherical harmonic representation of the height anomaly/geoid undulation difference, *Journal of Geodesy*, Vol. 71, No. 5, pp. 282-289.

Reigber, C., Schwintzer, P., Stubenvoll, R., Schmidt, R., Flechtner, F., Meyer, U., König, R., Neumayer, H., Förste, C., Barthelmes, F., Zhu, S., Balmino, G., Biancale, R., Lemoine, J.-M., Meixner, H. and Raimondo, J. (2006) A high resolution global gravity field model combining CHAMP and GRACE satellite mission and surface data: EIGEN-CG01C; *Scientific Technical Report STR06/07*, GeoForschungsZentrum Potsdam.

Reigber, C., Jochmann, H., Wünsch, J., Petrovic, S., Schwintzer, P., Barthelmes, F., Neumayer, K.-H., König, R., Förste, C., Balmino, G., Biancale, R., Lemoine, J.-M., Loyer, S. and Perosanz, F. (2005) Earth gravity field and seasonal variability from CHAMP; In: Reigber, C., Lühr, H., Schwintzer, P., and Wickert, J. (eds.), *Earth observation with CHAMP - Results from three years in orbit*, Springer, Berlin, p. 25-30.

Reigber, C., Schwintzer, P., Neumayer, K.-H., Barthelmes, F., König,R., Förste, C., Balmino, G., Biancale, R., Lemoine, J.-M., Loyer, S., Bruinsma, S., Perosanz, F. and Fayard, T. (2003) The CHAMP-only Earth gravity field model EIGEN-2; *Advances in Space Research,* Vol. 31, No. 8, pp. 1883-1888.

Saad, A. and Dawod, G. (2002) A precise integrated GPS/gravity geoid model for Egypt, *Civil Engineering Research Magazine (CERM)*, Al-Azhar University, V.24, No. 1, pp.391-405.

Saleh, J. (2004*) Personal communications*.

Saleh, J. and Pavlis, N. (2002) The development and evaluation of the global digital terrain model DTM2002, *Presented at the 3rd Meeting of the International Gravity and Geoid Commission*, GG2002, August 26 - 30, Thessaloniki, Greece.

Sideris, M. and Footopoulus, M. (2005), Geoid determination by FFT, Presented in *the International Geoid School*, Budapest, Hungary, Jan. 31-Feb. 4.

Smith, W. and Sandwell, D. (1997) Global sea floor topography from satellite altimetry and ship depth soundings, *Science*, 277, pp. 1956-1962.

Tapley, B., Ries, J., Bettadpur, S., Chambers, D., Cheng, F., Condi, F., Gunter, B., Kang, Z., Nagel, P., Pastor, R., Pekker, T., Poole, S., and Wang, F. (2005) GGM02: An improved Earth gravity

Downloaded By: [Umm Al-Qura University] At: 08:02 28 November 2010

field model from GRACE, *Journal of Geodesy*, Vol. 79, No. 8, pp. 467-478.

Tscherning, C.C., (1976), On the chain-rule method for computing potential derivatives, *Manuscripta Geodaetica*, Vol.1, pp. 125-141, 1976.

Tscherning, C.C. Radwan, A, Tealeb, A., Mahmoud, S., Mohamed, A., Hassan, R., Issawy, E., and Saker, K., (2001), Local geoid determination combining gravity disturbances and GPS/levelling: A case study in the Lake Naser area, Aswan, Egypt, *Journal of Geodesy*, V. 75, pp 343-348

Wessel, P. and Smith, W. (1996), A global self-consistent hierarchical high-resolution shoreline database, *Journal of Geophysical Research*, 101, B4, pp. 8741-8743.

Downloaded By: [Umm Al-Qura University] At: 08:02 28 November 2010

Evaluation and Adaptation of the EGM2008 Geopotential Model along the Northern Nile Valley, Egypt: Case Study

Gomaa M. Dawod[1]; Hoda F. Mohamed[2]; and Sherine S. Ismail[3]

Abstract: The performance of the new EGM2008 global geopotential model (GGM), over the northern Nile valley and delta in Egypt, has been evaluated. Over 305 global positioning system (GPS)/levelling stations, the standard deviation of the undulation differences has been estimated to be 0.23 m. Thus, it can be concluded that the EGM2008 is superior to earlier GGMs over the northern area of Egypt by a factor of 1.6. Moreover, four mathematical models have been investigated in order to incorporate local data sets with the EGM2008, leading to the conclusion that the first-order polynomial is the optimum one. An improvement of about 26% has been obtained after applying that regression model, and the standard deviation has been decreased to 0.17 m. As a result, the EGM2008 produces a crucial influence on integrated GPS surveys where the orthometric heights can be obtained without any additional costs. Such a practice presents a suitable alternative, from an economical point of view, to substitute the expensive traditional levelling technique particularly for topographic mapping.

DOI: 10.1061/(ASCE)SU.1943-5428.0000002

CE Database subject headings: Geodetic surveys; Global positioning; Leveling; Egypt; Case studies.

Author keywords: Geoid; Geodetic surveys; Global positioning; Leveling; Egypt.

Introduction

Geoid models are used in GPS surveys in order to convert the GPS-based geodetic heights to orthometric heights usually used in surveying and mapping applications. A large number of global geopotential models (GGMs) have been released and used in geoid modeling all over the world. A basic utilization of GGMs is to represent the long wavelength component of the Earth gravitational field in modeling geoidal undulations [e.g., Daho et al. (2008) and Krynski and Lyszkowicz (2006)]. Combining GGMs and local geodetic data sets has been investigated extensively in order to increase the performance precision in local regions through minimizing the long-wavelength geoid errors and the datum inconsistencies between local height data and GPS data [e.g., Benahmeddaho and Fairhead (2007) and Reguzzoni et al. (2005)]. Such a procedure offers an appropriate alternative, from an economical point of view, to substitute the expensive traditional levelling technique.

Regarding Egypt, several researchers have investigated the utilization of GGMs in developing geoid models. For example, Ghanem (2001) has developed a 2.5×2.5 in. grid gravimetric national geoid for Egypt, based on the EGM96 GGM. When compared against (only) 10 GPS/levelling points, that geoid produced a standard deviation of 0.47 m and the standard deviation after fitting that gravimetric geoid to the GPS/leveling points was better than 0.13 m. Additionally, Amin et al. (2005) has used a tailored GGM model, denoted as EGM96EGCT, that was estimated up to degree and order 599, based on the coefficients of the EGM96 and all the available terrestrial geodetic data in Egypt. Then, that model was used to develop a gravimetric geoid model for Toshka area (about 1000 km south of Cairo) and, when compared against (only) 29 GPS/levelling points, produced a standard deviation of 0.16 m. Moreover, a recent study by Dawod (2008) has analyzed the performance of eight recent GGMs using local geodetic data sets (terrestrial gravity and GPS/levelling points) in Egypt. The results show that the EIGEN-CG01C model is best at representing the long and medium wavelengths of the gravity field in Egypt. Its average accuracy, in terms of geoid undulations, when compared to known points, is estimated to be 0.36 m. The objectives of this paper are to evaluate the performance of the most-recent released GGM (EGM2008) and to investigate the incorporation of local geodetic data sets in order to increase its precision in integrated GPS surveys in the Nile valley and delta area, Egypt. Moreover, the utilization of this new GGM in the African continent, in general, is also discussed.

EGM2008 Geopotential Model

The Earth Gravitational Model EGM2008 has been publicly released by the U.S. National Geospatial-Intelligence Agency (NGA) in mid-2008 (http://earth-info.nima.mil/GandG/wgs84/gravitymod/egm2008). This model is complete to degree and order 2,160, and contains additional spherical harmonic coefficients extending to degree 2,190 and order 2,159. Full access to the model's coefficients and other processing programs is available from the NGA site at http://earth-info.nima.mil/GandG/

[1]Research Professor, Survey Research Institute, National Water Research Center, 13411 Cairo, Egypt; presently, Umm Al-Quraa Univ., Makkah, P.O. Box 5477 Al-Shisha, Saudi Arabia (corresponding author). E-mail: dawod_gomaa@yahoo.com

[2]Researcher, Survey Research Institute, National Water Research Center, 13411 Cairo, Egypt.

[3]Researcher, Survey Research Institute, National Water Research Center, 13411 Cairo, Egypt.

Note. This manuscript was submitted on August 19, 2008; approved on December 15, 2008; published online on March 20, 2009. Discussion period open until July 1, 2010; separate discussions must be submitted for individual papers. This paper is part of the ***Journal of Surveying Engineering***, Vol. 136, No. 1, February 1, 2010. ©ASCE, ISSN 0733-9453/2010/1-36–40/$25.00.

Table 1. RMS Differences of GPS-Levelling Minus GGM Derived Quasigeoid Heights (m) (after ICGEM)

Region	United States	Canada	Europe	Australia	All
Number of points	6,169	1,930	186	201	8,486
Gravity model (Year, degree)	RMS differences between GPS/leveling and GGM derived geoid undulations (in meters)				
EGM2008 (2008, 2,190)	0.25	0.13	0.19	0.22	0.22
EIGEN-05C (2008, 360)	0.34	0.25	0.29	0.24	0.32
EIGEN-GL04C (2006, 360)	0.34	0.25	0.34	0.25	0.32
EIGEN-CG03C (2005, 360)	0.35	0.31	0.39	0.26	0.34
EIGEN-CG01C (2004, 360)	0.35	0.27	0.41	0.26	0.33
EGM96 (1996, 360)	0.38	0.36	0.48	0.30	0.37

wgs84/gravitymod/index.html. Even before its official release, a primarily version of this model was distributed and being used in various researches [e.g., Felus et al. (2008) and Merry 2003: http://www.eepublishers.co.za/view.php?sid=13532]. EGM2008 model is a unique GGM representing the Earth gravitational field by spherical harmonic coefficients, since it precedes any earlier GGM by reaching degree and order equals 2,160.

The EGM2008 is based on the satellite-only gravity ITG-GRACE03S GGM combined with a recent global 5×5 in. terrestrial gravity anomaly data set. The EGM2008 does not include any GPS/levelling or astronomic deflection of the vertical data. Remarkable improvements have been obtained when EGM2008 has been compared against GPS/levelling in United States, where the weighted standard deviation has been decreased from 18.2 cm (for the EGM96) to 4.8 cm in case of removing a linear trend (Pavlis et al. 2008: http://earth-info.nima.mil/GandG/wgs84/gravitymod/egm2008/NPavlis&al_EGU2008.ppt).

The International Center for Global Gravity Field Models (ICGEM) (Potsdam, Germany) makes available a number of GGMs in the form of fully normalized spherical harmonic coefficients that can be used to compute geodetic and gravitational quantities (http://icgem.gfz-potsdam.de/ICGEM/ICGEM.html). To evaluate the performance of GGMs, their estimated height anomalies have been compared against geoid undulations at known GPS/levelling stations in United States, Canada, Europe, and Australia (for more details on this comparison and its results, see http://icgem.gfz-potsdam.de/ICGEM/evaluation/evaluation.html). Considering the number of GPS/levelling stations as the weights, a weighted mean of RMS, for all stations, has been computed for each GGM. The results are presented in Table 1, where the computed weighted RMS mean values are given in the last column. Obviously, the EGM2008 shows better precision than all other GGMs by a factor of at least 1.5, which indicates that it the most precise available GGM in this moment.

Additionally, the EGM2008 has produced significant improvements when compared to 1,542 GPS/levelling points in Greece, where the standard deviation decreased to about 0.14 m after a least square bias fit (Kotsakis et al. 2008). Another test of the EGM2008 GGM in Croatia has shown that its overall precision estimate is 0.088 m after removing a shift of 0.899 m (Liker et al. 2008).

Data Used

In order to assess the performance of the EGM2008 GGM over Egypt, a local geodetic data has been used. This recent database consists of 305 GPS/levelling points (Fig. 1), where geoid undulations have been directly computed. The majority of this data set comes from GPS campaigns carried out by the Nile Research Institute for updating the hydrotopographic maps of the Nile. It is a matter of fact that about 90% of the population of Egypt live in the Nile valley and delta region, and thus most of the surveying and geodetic activities, and thus data, exit in this area. Regarding this geodetic data set, both the GPS and the spirit levelling networks have been observed, through subsections, applying the first-order standards and specifications, and have adjusted using the least-square adjustment techniques. The orthometric heights of the stations have been obtained through tying the first-order levelling loops to the national vertical datum of Egypt that is based on the mean sea level at Alexandria tide gauge of 1906. The accuracy of the derived geoid undulations has been estimated to be ±5 cm (Dawod and Ismail 2005). The entire network has been used, in this study, in order to get reliable results about the performance of the EGM2008 using all available recent precise data.

Processing and Results

The first step in the processing strategy was to compute the EGM2008-based geoid undulations over the known points. The hsynth_WGS84.exe program, along with the two data files: EGM2008_to2190_TideFree.gz and Zeta-to-N_to2160_egm2008.gz have been downloaded from the NGA website. Then, the observed geoid undulations have been compared against the EGM2008 corresponding values at known points. The attained results are tabulated in Table 2, from which it can be noticed that the standard deviation of the undulation differences is 0.23 m. This precision measure of the EGM2008 GGM over Egypt is almost identical to its global precision value presented in Table 1.

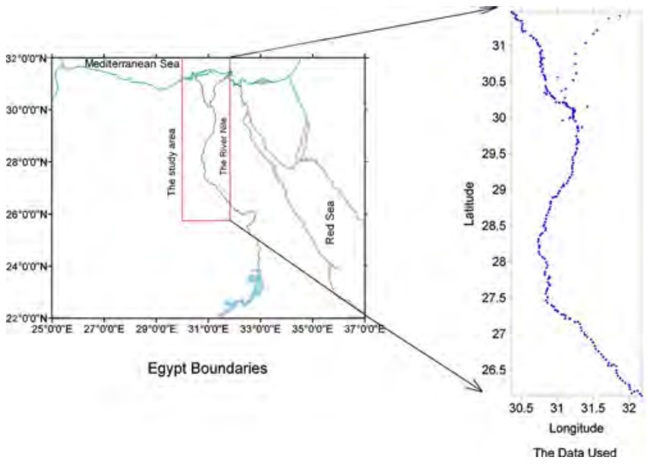

Fig. 1. GPS/levelling known stations

Table 2. Known and EGM2008 Geoid Undulations over Check Points (m)

	Minimum	Maximum	Mean	Standard deviation
Known undulations	12.00	16.84	14.33	1.15
EGM2008 undulations	11.91	17.40	14.55	1.26
Undulation differences	−0.76	0.41	−0.23	0.23

Dawod (2008) has found out that the best GGM that represent the gravitational field over Egypt is the EIGEN-CG01C, which produced a standard deviation of the undulation differences that equals 0.36 m. Consequently, it can be concluded that the EGM2008 GGM is superior to earlier GGMs over Egypt by a factor of 1.6.

The second stage of processing was to modify the EGM2008 GGM to the local geodetic data in order to increases its precision performance. Several mathematical models have been proposed in such integration step [e.g., Tranes et al. (2007) and You (2006)]. In the current study, four models have been tested: a bias and a tilt, a first-order regression, a second-order regression, and the Kriging model. The attained bias and tilt's model has been found to be

$$N^1_{\mathrm{EGM2008}} - N_{\mathrm{EGM2008}} = 1.271413252 - 0.102945895 \times N_{\mathrm{EGM2008}} \qquad (1)$$

where N_{EGM2008} = original geoid undulation of the EGM2008 GGM and N^1_{EGM2008} = modified corresponding value (both in meters).

The first-order regression model was computed as

$$N^2_{\mathrm{EGM2008}} - N_{\mathrm{EGM2008}} = -5.529490551 - 0.05161249\varphi + 0.219581806\lambda \qquad (2)$$

where N^2_{EGM2008} = modified geoid undulation of the EGM2008 GGM (in meters); φ = geodetic latitude in decimal degrees; and λ = geodetic longitude in decimal degrees.

The coefficients of both latitude and longitude (φ and λ) in Eq. (2) represent slopes of the undulation differences between the observed and the EGM2008 undulations. It is suggested that these slopes are due to the errors associated with the GPS/levelling data and the inconsistence between the associated geodetic datums.

Table 3. Results of Models Relating the EGM2008 Undulations to Known Undulations over Check Points (m)

	Minimum	Maximum	Mean	Standard deviation
$\Delta N^1 = N_{\mathrm{obs}} - N^1_{\mathrm{EGM2008}}$	−0.53	0.44	−0.0004	0.19
$\Delta N^2 = N_{\mathrm{obs}} - N^2_{\mathrm{EGM2008}}$	−0.53	0.57	−0.0002	0.17
$\Delta N^3 = N_{\mathrm{obs}} - N^3_{\mathrm{EGM2008}}$	−0.50	0.57	−0.0003m	0.18
Kriging corrector surface	−0.53	0.57	−0.0003	0.17

The second-order regression model was computed as

$$N^3_{\mathrm{EGM2008}} - N_{\mathrm{EGM2008}} = 72.70656003 - 0.585861292\varphi - 4.214098131\lambda + 0.009003071\varphi^2 + 0.069825898\lambda^2 \qquad (3)$$

The fourth tested model was using the Kriging technique to develop a correction surface that spatially distributes the EGM2008 undulation difference in the study area. The Surfer software was used where the linear semivariogram method (Barnes 1991) was applied. Fig. 2 depicts the attained undulation difference residuals due to the above four methods. It can be seen, from this figure, that there is no specific spatial pattern in the distribution of the residuals. That is due to the existing inconsistencies between the datums implied by both the GPS and levelling data sets. For example, one of the major defects of the Egyptian national control networks (1906–1945) is that they have been adjusted section-by-section not in a unique rigorous least-square adjustment (Mohamed 2005). Additionally, the vertical datum of Egypt has been defined, in 1906, based on a single tide gauge station located at Alexandria harbor on the Mediterranean sea (ibid).

The achieved results, presented in Table 3, show that significant improvements have been obtained. The standard deviation of the EGM2008-based GGM has been decreased by about 0.26%. Also, the similarities exist between those models' residuals (Fig. 2) show that no large differences between the four tested math-

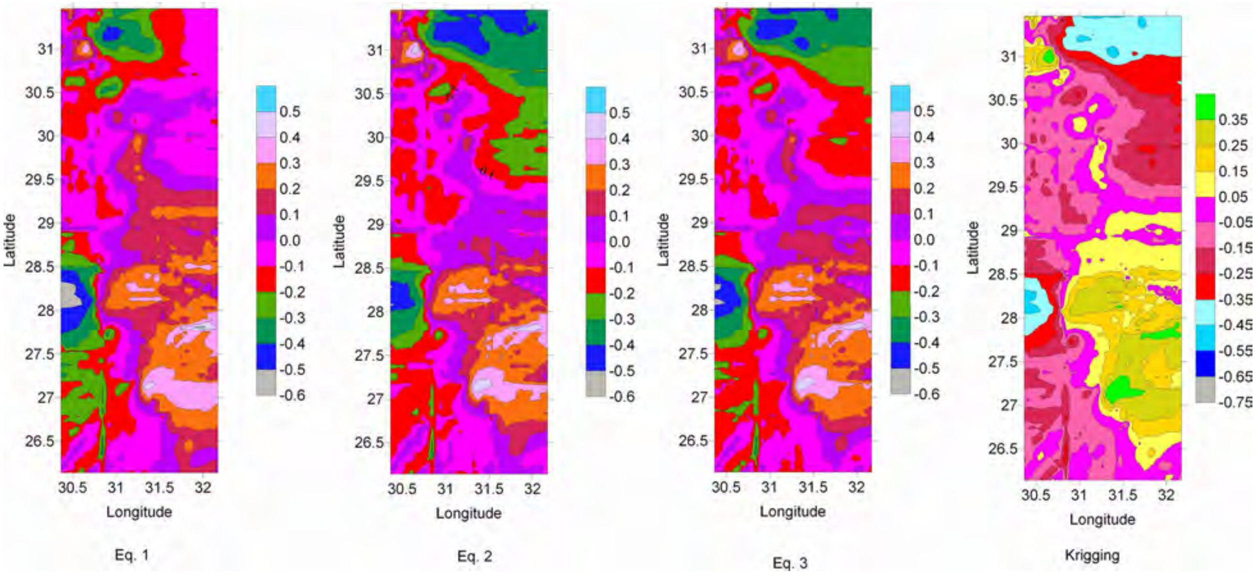

Fig. 2. Undulation difference residuals clue to the four used methods

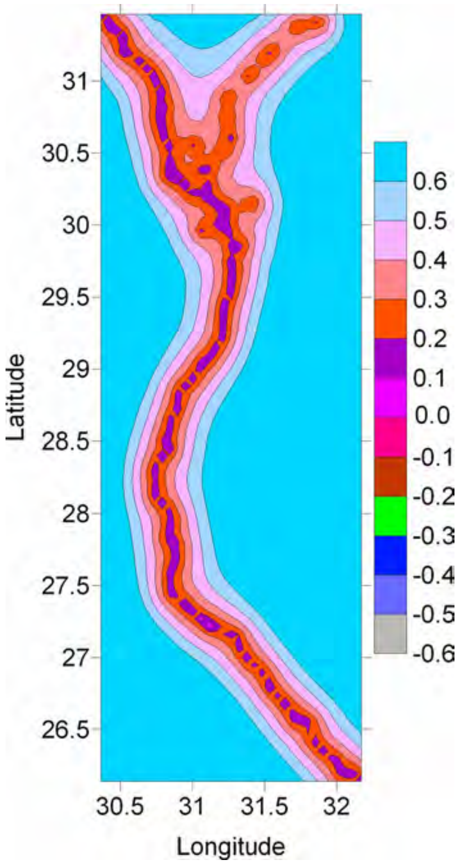

Fig. 3. Standard deviations of the Kriging method

ematical models. Moreover, it is clearly seen that the large residuals exist outside the area of the available data, where the extrapolation takes place. However, the first-order regression and the Kriging models produce relatively smaller standard deviation of the undulation differences (0.17 m). Hence, these two models are the suitable candidates in adapting the original EGM2008 undulations to local geodetic data in the study area. Fig. 3 presents the standard deviations of the Kriging output. It worth mentioning that such a surface is significantly applicable within the area where available data exist, since the extrapolation outside this area may introduce large errors. This can be clearly seen from Fig. 3 where the standard deviations within the data area is almost less than 0.2 m while it is increased to about 0.5 m in the outer area.

For integrated GPS surveys, the orthometric heights of the surveyed stations can be computed with a "reasonable" level of precision with no additional costs. This can be achieved by computing the EGM2008 geoid undulation values, using the NGA programs, and then compute the corresponding undulation corrections either by using Eq. (2) or by interpolating the corrector surface. The precision of this strategy in obtaining orthometric heights can be estimated to be 0.17 m. Even though this precision may not be suitable for high-precision surveying applications such as the augmentation of the national Egyptian vertical datum, it is acceptable in various surveying and mapping applications such as topographic mapping. Consequently, a considerable cost reduction is accomplished in GPS surveying projects in Egypt.

Additionally and on a continental basis, the precision of the EGM2008 suggests that it would be an appropriate GGM to be used in the on-going project for developing a geoid of Africa. This continental geoid is being developed as a component of the African Reference Frame project to define a continental reference system for Africa to be fully consistent and homogeneous with the global reference frame of the ITRF (Wonnacott 2006). A gravimetric geoid model called the African Geoid Project was developed based on the EGM96 GGM, and when compared against 8 GPS/levelling data in Egypt produced a standard deviation of 0.80 m (Merry 2003).

Conclusions

The release of the EGM2008 GGM, early this year, is a millstone step in enhancing gravitational and geoidal modeling on a global scale. Based on several comparisons against GPS/levelling data sets, the precision level of the EGM2008 is estimated to 0.22 m. In Egypt, it has been found that the best GGM that represent the gravitational field is the EIGEN-CG01C, which produced a standard deviation of the undulation differences that equals 0.36 m. This study has evaluated the performance of EGM2008 over 305 GPS/levelling points in the northern Nile valley and delta, Egypt, and has found that its precision is 0.23 m. Consequently, it can be concluded that the EGM2008 GGM is superior to earlier GGMs over this part of Egypt by a factor of 1.6. Furthermore, incorporating local geodetic data sets, in the study area, decrease this standard deviation figure to 0.17 m. Additionally, it has been found that the first-order regression model is the best mathematical relationship in modeling the undulation differences in the study area. Although this precision may not be appropriate for high-precision surveying applications such as the augmentation of the national Egyptian vertical datum, it is adequate in various surveying and mapping applications such as topographic mapping. Hence, it can be concluded that EGM2008 can play an essential role in integrated GPS surveys where the orthometric heights can be obtained without any additional costs. The presented methodology may be re-applied in the future having new GGMs released, or new local Egyptian geodetic data sets being collected in other regions. On a continental basis, the precision of the EGM2008 suggests that it would be the appropriate GGM, for the time being, to be used in the on-going effort for developing a geoid of Africa.

Notation

The following symbols are used in this paper:

N_{EGM2008} = original geoid undulation of the EGM2008 GGM (meter);

N^1_{EGM2008}, N^2_{EGM2008}, and N^3_{EGM2008} = modified geoid undulation of the EGM2008 GGM due to several regression models (meter);

λ = geodetic longitude (decimal degrees); and

φ = the geodetic latitude (decimal degrees).

References

Amin, M., El-Fatairy, S., and Hassouna, R. (2005). "A precise geoidal map of the southern part of Egypt by collocation: Toshka geoid." *FIG Working Week 2005 and GSDI-8 Conf.*, International Federation of Surveyors, Cairo, Egypt.

Barnes, R. (1991). "The variogram sill and the sample variance." *Math.*

Geol., 23(4), 673–678.
Benahmeddaho, S., and Fairhead, J. (2007). “Accuracy assessment of the available geoid models in Algeria.” *Comput. Geosci.*, 33, 76–82.
Daho, S., et al. (2008). “New investigation on the choice of the tailored geopotential model for Algeria.” *J. Geodyn.*, 45, 154–162.
Dawod, G. (2008). “Towards the redefinition of the Egyptian geoid: Performance analysis of recent global geoid models and digital terrain models.” *Journal of Spatial Science*, 53(1), 31–42.
Dawod, G., and Ismail, S. (2005). “Enhancing the integrity of the national geodetic data base in Egypt.” *Proc., FIG Working Week and GSDI-8 Int. Conf.*, International Federation of Surveyors, Cairo, Egypt.
Felus, Y., Steinberg, G., and Tuchin, Y. (2008). “On the augmentation of Isreaeli GPS-BM data with a global earth geoid model.” *Proc., FIG Working Week 2008*, International Federation of Surveyors, Stockholm, Sweden.
Ghanem, E. (2001). “GPS-gravimetric geoid determination in Egypt.” *Geo-spatial Information Science*, 4(1), 19–23.
Kotsakis, C., Katsambalos, K., and Ampatzidis, D. (2008). “Evaluation of EGM2008 using GPS and leveling heights in Greece.” ⟨http://users.auth.gr/~kvek/Crete_Paper_2008.pdf⟩.
Krynski, J., and Lyszkowicz, A. (2006). “Regional quasi-geoid determination in the area of Poland.” *Proc., 5th FIG Regional Conf.*, International Federation of Surveyors, Accra, Ghana.
Liker, M., Lucic, M., Barisic, B., Repanic, M., and Grgic, I. (2008). “How most recent global geopotential models fit the Croation territory.” ⟨http://www.cgi.hr/radovi/how%20most%20recent%20global%20geopotential%20models%20fit%20the%20croatian%20territory.pdf⟩.
Merry, C. (2003). “The African geoid project and its relevance to the unification of African vertical reference frames.” *Proc., 2nd FIG Regional Conf.*, International Federation of Surveyors, Marrakech, Morocco.
Mohamed, H. (2005). “Realization and redefinition of the Egyptian vertical datum based on recent heterogeneous observations.” Ph.D. dissertation, Shoubra Faculty of Engineering, Benha Univ., Cairo, Egypt.
Pavlis, N., Holmes, S., Kenyon, S., and Factor, J. (2008). “An earth gravitational model to degree 2160.” EGM2008, Proc., European Geosciences Union general assembly, Vienna.
Reguzzoni, M., Sanso, F., and Venuti, G. (2005). “The theory of general kriging, with applications to the determination of a local geoid.” *Geophys. J. Int.*, 162(2), 303–314.
Tranes, M., Meyer, T., and Massalski, D. (2007). “Comparisons of GPS-derived orthometric heights using local geometric geoid models.” *J. Surv. Eng.*, 133(1), 6–13.
Wonnacott, R. (2006). “The AFREF Project: Background, rationale and progress.” *Proc., 5th FIG Regional Conf.*, International Federation of Surveyors, Accra, Ghana.
You, R. (2006). “Local geoid improvement using GPS and leveling data: Case study.” *J. Surv. Eng.*, 132(3), 101–107.

DATA MANAGEMENT OF DIFFERENT HEIGHT SYSTEMS WITHIN GPS/GIS INTEGRATED SPATIAL TECHNOLOGY

GOMAA M. DAWOD

SURVEY RESEARCH INSTITUTE, CAIRO, EGYPT, CURRENTLY AFFILIATED WITH UMM AL-QURAA UNIVERSITY, MAKKAH, P.O. BOX 5477 AL-SHISHA, SAUDI ARABIA.

E-MAIL: dawod_gomaa@yahoo.com

WISAM E. MOHAMMED

INSTITUTE OF GRADUATE STUDIES AND RESEARCH, ALEXANDRIA UNIVERSITY, EGYPT, CURRENTLY AFFILIATED WITH THE PUBLIC COMMISSION FOR THE PROTECTION OF MARINE RESOURCES, ENVIRONMENT & WILDLIFE, P.O. BOX 32657, KINGDOM OF BAHRAIN.

E-MAIL: wisam.mohammed@gmail.com

ABSTRACT

The integration between both GPS and GIS technologies has proved to be precious in collecting, managing, analyzing, and presenting spatial data. A problematic aspect of dealing with GPS-based datasets is that their heights are ellipsoidal type in nature, while the traditional height type used in civil engineering and mapping activities is the orthometric height. A height conversion methodology is needed, through the so-called geoid modelling, in GPS/GIS data integration. This paper develops a conversion scheme, within a GIS environment, that transforms ellipsoidal into orthometric heights of collected GPS data survey utilizing the most-recent EGM2008 global geoid model. Results of testing the proposed technique, using 300 ground control stations along the Nile river in Egypt, reveals that the excepted accuracy is less than quarter a meter. Performing the height transformation process inside a GIS environment enables efficient and faster management of GPS data collected for GIS projects and assets in producing DEM and contour maps effectively, which in turns reduce the costs of spatial applications.

KEYWORDS

GPS, GIS, Height Systems, Geoid, Egypt

1 Introduction

Recently, the applications of the Geographic Information Systems (GIS) have covered a wide range of engineering disciplines particularly in the Arab countries. For example, Gaber et al. (2009) has utilized the GIS and remote sensing technologies to study the geological structures exist in Sinai, Egypt. Also, El-Mowafy et al. (2008) have developed a scheme for improving the pavement maintenance activities in Abu Dhabi based on GIS. Additionally, Aljenid and Mohamed (2007) has utilized GIS to assess the ecological characteristics of a region in Egypt. In Jordan, the GIS has been used to analyze the impact of modern practices and polices of urban planning (Al-Kheder et al. 2009). In Bahrain, the GIS was applied for documenting historical cities (Tolba 2007). Moreover, GIS has been applied for investigating agricultural development scenarios in the Egyptian deserts (Effat and Hegazy, 2009) and in sustainable development of coastal areas (El Raey et al. 2005).

The integration between the Global Positioning System (GPS) and the GIS technologies has become a major task for the surveying and mapping community in the last decade. GPS/GIS integrated technology has been utilized in a wide range of engineering applications. For example, Shalaby and Tateishi (2007) has used GPS/GIS for mapping and monitoring land cover and land-use changes in Egypt. Al-Musawa and El-Mowafy (2008) has applied GIS/GPS integration for machine automation in construction projects in Dubai. GPS/GIS can be a new tool for road traffic data collection (Owusu et al. 2006). A unique GIS was designed for manipulating various types of geodetic networks in Algeria (Derkaoui et al, 2008). Moreover, the integration of three technologies (namely GIS, GPS, and remote sensing) has been proposed for updating digital maps (Okuno and Shikada, 2004).

However, most GPS/GIS applications has focused only on the different horizontal coordinate systems, and how to convert features' coordinates from one geodetic datum to another. The problem of dealing with different height systems has not been addressed intensely, and hence, it is the main objective of the current study.

2 Height Systems and Geoid Models

Two main height systems are used in engineering and GIS applications: (1) the geodetic height, and (2) the orthometric height. The geodetic or the ellipsoidal height (h) is the height of a point above the surface of an ellipsoid. It worth mention that the GPS-based height is a geodetic height referenced to the World Geodetic System 1984 (WGS84) ellipsoid. On the other hand, the orthometric height (H) is the height of a point above the geoid (approximated by the Mean Sea Level; MSL). Most heights used in surveying and mapping applications are orthometric heights. The difference between the two height types is called the geoid undulation or geoidal height (N), which can be described by (Figure 1):

$$N = h - H \quad (1)$$

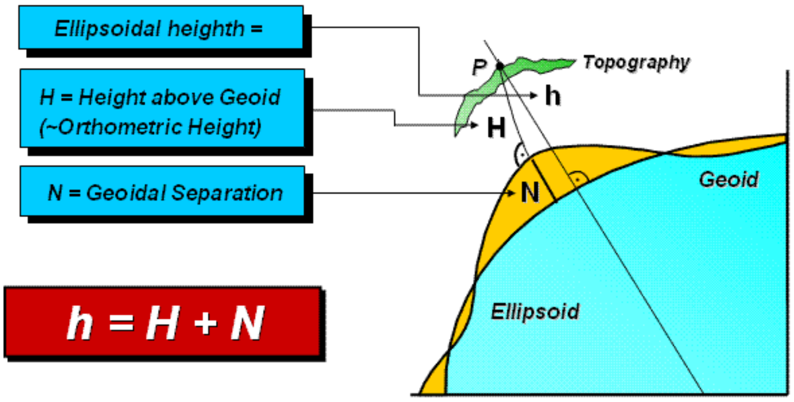

Figure 1: Height Systems

This equation implies that in order to convert the GPS-based geodetic height (h) into the map-based orthometric height (H), the undulation term (N) should be known at every point, in other words, a geoid model is needed. Geoid modelling is an old task of geodesy, which has become a crucial need in all countries since the spread of GPS utilization. Geoid may be developed locally (called local geoid models) or globally (global geoid models). An example of a local geoid model for Egypt is the SRI2002 developed by Saad and Dawod (2002). Regarding global geoids, it worth to mention that the International Center for Global Gravity Field Models (ICGEM) makes available a number of global geoid models, in the form of fully-normalized spherical harmonic coefficients, that can be used to compute geodetic and gravitational

quantities (http://icgem.gfz-potsdam.de/ICGEM/ICGEM.html). The most-recent released global geoid model is the Earth Gravitational Model 2008 (EGM2008) published by the U.S. National Geospatial-Intelligence Agency (NGA) in mid 2008 ((Pavlis et al. 2008). The EGM2008 has been utilized for height conversion in several countries and was found to be superior, in terms of accuracy, to all preceded global geoid models (e.g. Femandes 2009, Sadiq and Ahmad, 2009, and Claessens et al. 2009). Comparable investigations have been carried out in Arabic countries. For example, Daho (2009) has evaluate the performance of EGM2008 in Algeria, and has found that its standard deviation equals 0.21 meter over known GPS/levelling points. In Egypt, the overall accuracy of EGM2008 in Egypt was found to be 0.23 meter, and could be decreased to 0.17 meter (Dawod et al, 2009).

3 Data Utilized

In order to assess the GIS-Based height conversion process, utilizing EGM2008 in Egypt, a local geodetic dataset has been utilized. This recent database consists of 300 GPS/levelling points (Figure 2), where geoid undulations have been directly computed. The majority of this data set comes from GPS campaigns carried out by the Nile Research Institute (NRI) for updating the hydro-topographic maps of the Nile. Regarding this geodetic dataset, both the GPS and the spirit levelling networks have been observed, through sub-sections, applying the first-order standards and specifications, and have adjusted using the least-square adjustment techniques. The orthometric heights of the stations have been obtained through tying the first-order levelling loops to the national vertical datum of Egypt, that is based on the MSL at Alexandria tide gauge of 1906. The accuracy of the derived geoid undulations has been estimated to be ± 5 centimeters (Dawod 2008).

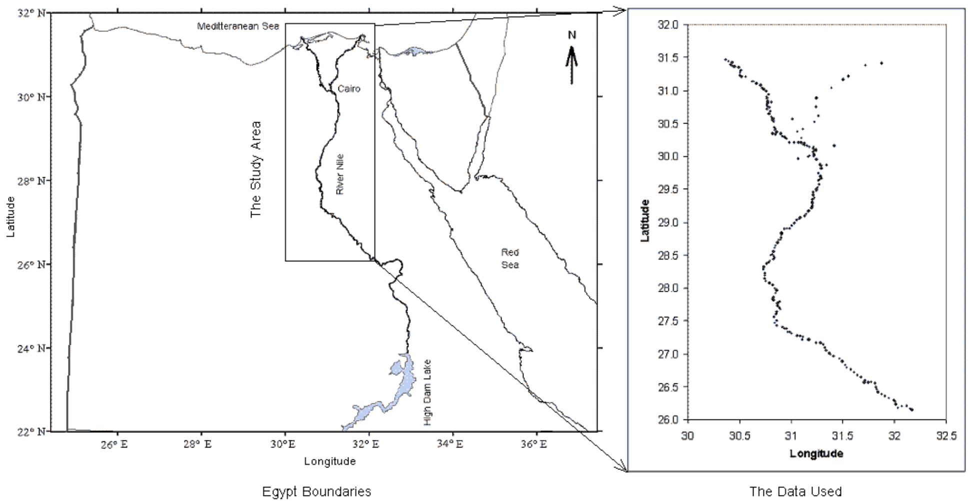

Figure 2: GPS/Levelling Known Stations

4 Methodology

The EGM2008 global geoid model constitutes the chief tool, in the current research study, to convert the GPS-based geodetic heights into the MSL-based orthometric heights. The EGM2008 is available, free of charge, at: http://earth-info.nga.mil/GandG/wgs84/gravitymod/egm2008/. Three methods have been investigated in such process.

4.1 Point-by-point conversion

The original version of the EGM2008, released in April 2008, was in the format of fully-normalized harmonic coefficients' file along with a program that computes the undulation values for some points knowing their geodetic coordinates (latitude and longitude).

4.2 Grid-wise conversion

In July 2008, the NGA has released 2.5-minute world raster grids of the EGM2008 geoid (Fig. 3). Each grid covers an area extending 45 degrees in both latitude and longitude. An interpolation program has been released, too, in order to interpolate points' geoidal undulation values from the corresponding grid.

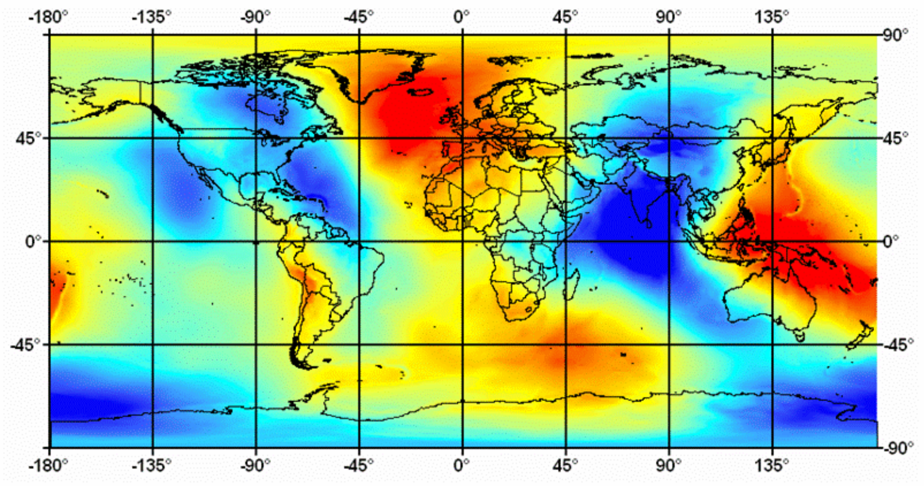

Figure 3: The World Raster Grids of the EGM2008

4.3 GIS-based grid conversion

More recently, in February 2009, the NGA has released a new 2.5-minute GIS-based geoid grid for the Middle East. This ESRI-format grid (Fig. 3) covers the area extending from 20°E to 90°E longitude and from 5° S to 60° N in latitude.

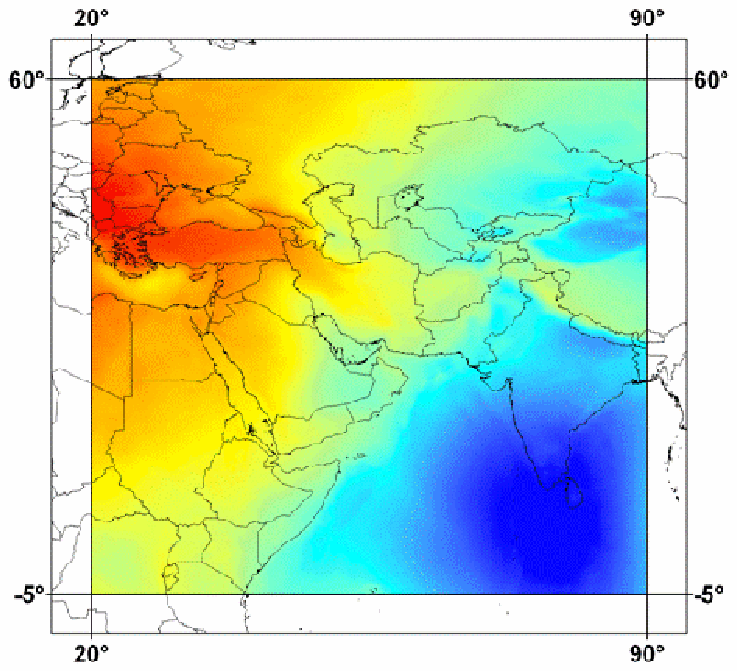

Figure 4: The Middle-East GIS Grid of the EGM2008

5 Processing and Results

In the first stage before starting the actual computations, a comparison has been carried out between the available three different representation means of the EGM2008 geoid. Such a comparison reveals the general characteristics of each method.

The point-wise technique may be considered the most-precise method since it compute the EGM2008 geoidal heights for each point based on the original EGM2008 harmonic coefficients. Hence, it may considered as the optimum mean for geoid computations in high-precision GPS surveying applications. However, it can expect that this method will be the slower one particularly for large geodetic datasets.

The grid-wise conversion method can be expected to be more faster than the point-wise technique, since the interpolation mathematical process will take less processor time than the harmonic expansion computations. That reason has encouraged many commercial GPS data processing software to include those world raster grids in order to perform the height conversion process. However, a main point need to be addressed about the precision of interpolating 2.5' grids, where a cell of 2.5'x2.5' (approximately 4.5x4.5 km) has the same unique geoid undulation.

The main advantage of the third EGM2008 representation technique is its compatibility with the GIS environment, where the height conversion process can take place within the GIS software. The question of interpolation' process is still applicable for this method too.

Secondly, the available geodetic dataset has been utilized to test the three methods of height conversion. In the point-wise scenario, the NGA's hsynth_wgs84.exe program has been run to compute the geoidal undulation for the 300 known geodetic stations. In order to judge the performance of the EGM2008 geoid, the computed undulations have been compared against the known corresponding values. This precision measure of the EGM2008, over Egypt, concludes that the EGM2008 is superior to earlier global geoids by a factor of 1.6 (Dawod et al. 2009).

The grid-wise method has been, then, performed using the NGA's interp_2p5min.exe program to interpolate the undulation at the known

check points out of the raster 2.5' grid. The last step was to utilize the GIS-based middle-east ESRI grid, within the Arc GIS software, to interpolate the EGM2008 geoid undulations at the check points.

The attained results, of the three methods, are tabulated in Table 1. The first remark, from this table, is that the overall precision of the EGM2008 global geoid model is, in terms of standard deviation, is 0.23 m. This is an indication about the accuracy of utilizing global geoid models in converting the GPS-based geodetic heights into the MSL-based orthometric heights. In some high-precision GPS surveying, such an accuracy level may not be acceptable, and thus a local precise geoid model should be developed and applied in height transformation. However, that accuracy may be suitable for several GIS and mapping applications. Thus the global geoid models, particularly the EGM2008, provide an optimum free-of-charge candidate for height conversion. The second remark, drawn from Table 1, is that there are no significant differences between the point-wise and the grid-wise interpolation using the NGA's programs. Thus, the time-consumer point-wise method can be avoided in GIS applications, where the grid interpolation will be optimum. Surprisingly, significant differences have been found between the grid-wise interpolation using the NGA's program and the interpolation carried out within the Arc GIS software. The standard deviation of the undulation differences between both programs is about 0.05 m. The main reason may be due to the interpolation mathematical model utilized in each case. The NGA's interpolation program depends on a 6x6 spline interpolation method, while the ArcGIS interpolation (in the surface spot command) is based on the linear interpolation technique. But, the five-centimeter precision level is quite suitable for GIS and mapping projects. However, performing the height transformation within the GIS environment has extra merits.

Table 1: Known and EGM2008 Geoid Undulations over Check Points (m)

	Minimum	Maximum	Mean	Standard Deviation
Known undulations	9.92	18.36	14.22	2.23
EGM2008 point-wise undulations	10.25	18.44	14.33	2.20
Known minus point-wise undulation differences	-0.48	0.32	-0.11	0.23
EGM2008 grid-wise undulations	10.27	18.37	14.33	2.18
Known minus grid-wise undulation differences	-0.48	0.32	-0.11	0.23
Point-wise minus grid-wise undulation differences	-0.001	0.000	0.0001	0.0003
Grid-wise minus GIS-grid undulation differences	-0.08	0.09	-0.001	0.05

Performing the height transformation within the GIS environment not only convert geodetic to orthometric heights, but also produce other significant products. For example, a geoid surface map and a contour geoid map have been developed for Egypt (Figures 5 and 6). Moreover, all the GIS project's processing steps will be carried out within the same environment. If the project uses hand-held navigation GPS receivers, the data can be downloaded directly to the Arc GIS software. If geodetic GPS receivers were utilized, most GPS data processing software have the capability to export their final results in the shapefile format. For both cases, the transformation process is performed within the GIS package in order to convert the GPS-based geodetic heights into the MSL-based orthometric heights using the third discussed method. Furthermore, Digital Elevation Model (DEM), surface and contour maps can be developed for the study area. Even more, cut and fill computations can be also carried out within the GIS environment.

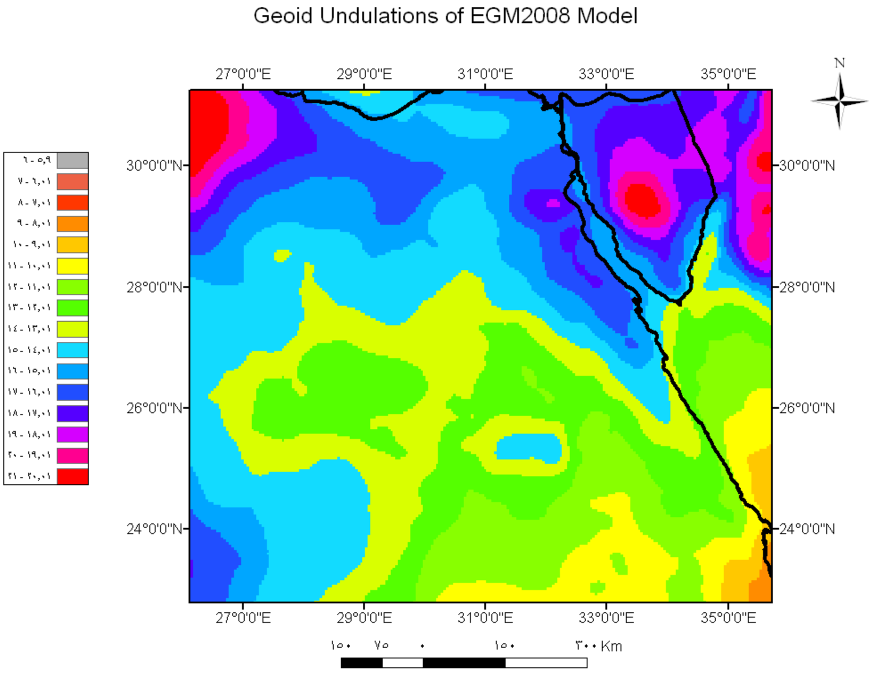

Figure 5: The EGM2008 Undulations over Egypt

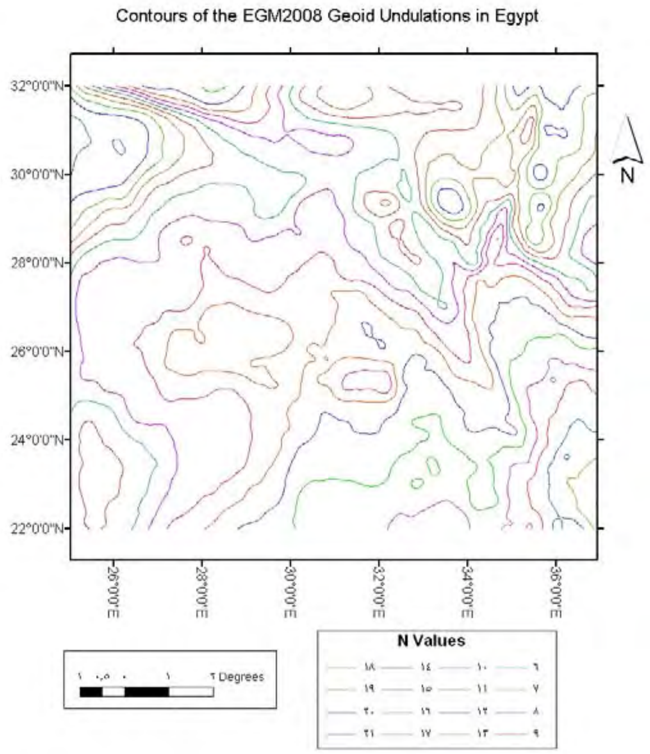

Figure 6: Contours of the EGM2008 Undulations over Egypt

6 Conclusions

The geodetic height obtained from GPS receivers must be converted to MSL-based orthometric height, which is the basic height type used for engineering, mapping, and GIS activities. Height transformation requires a local or a global geoid model. The most-recent and most-precise global geoid model is the EGM2008 released, by the US geospatial intelligence agency, in April 2008. In the current research study, three methods have been investigated for performing height conversion using the EGM2008 geoid. The point-wise height conversion technique is the most-precise but most-slower scenario, which might be suitable for high-precession GPS surveying. Both, the point-wise and the grid-wise methods are stand-alone and further procedures are required to convey the results into the GIS environment. The third conversion scenario, namely the EGM2008 ESRI grid, is the optimum one since it is completely carried out inside the ArcGIS software. But, it produces 0.05 precision differences compared with the previous two methods, which is not significant in many GIS applications. However, performing the height transformation within the GIS environment not only convert geodetic to orthometric heights, but also produce other significant products such as DEM, geoid surface maps, and contour geoid maps. Moreover, cut and fill computations can be also carried out in the GIS environment. Thus, all the processing steps of the GPS/GIS integrated spatial technology' applications will be carried out within the same environment. Furthermore, a cost reduction is anticipated for such projects.

References

Aljenid, S., and Mohamed, W. (2007). Developing a GIS to assess the ecological characteristics of El-Daba'a region, Egypt, *Middle East Spatial Technology (MEST2007)*, Kingdom of Bahrain: Bahrain Society of Engineers.

Al-kheder, S., Haddad, N., Fakhoury, L., and Baqaen, S. (2009). A GIS analysis of the impact of modern practices and polices on the urban heritage of Irbid, Jordan, *Cities*, (26), 81-92.

El-Mowafy, A., Abo-Hashema, M., and Ba-Obaid, A. (2008), Improvement of Pavement Maintenance Activities using Geographic

Information Systems in Abu Dhabi, *Map Middle East 2008*, Dubai, United Arab Emirates.

Al-Musawa, M., and El-Mowafy, S. (2008). Utilization of GIS and RTK GPS reference networks for machine automation, *Map Middle East 2008*, Dubai, United Arab Emirates.

Claessens, S.J., W.E. Featherstone and I.M. Anjasmara (2009). Is Australian data really validating EGM2008, or is EGM2008 just in/validating Australian data? In: Mertikas, S. (ed.) *Gravity Geoid and Space Missions*, Springer, Berlin Heidelberg New York.

Daho, S. (2009). Evaluation of EGM2008 Earth Gravitational Model in Algeria using gravity and GPS/levelling data, *The European Geosciences Union (EGU)General Assembly*, Vienna, Austria.

Dawod, G. (2008). Towards the redefinition of the Egyptian geoid: Performance analysis of recent global geoid models and digital terrain models, *Spatial Science*, 53 (1), 31-42.

Dawod, G., Mohamed, H., and Ismail, S. (2009). Evaluation and Adaptation of the EGM2008 Geopotential Model along the Northern Nile Valley, Egypt: Case Study, Accepted for publications in the *ASCE J. Surveying Engineering*.

Derkaoui, A., Ghezali, B.m and Courine, B. (2008). Contribution of GIS for the geodetic network management, *The FIG working week 2008*, Stockholm, Sweden.

El Raey, M., Nasr, S., Frihy, O., Fouda, Y., El-Hattab, M., Elbadawy, O., Shalaby, A., and Mohammed, W. (2005). Remote sensing and GIS for sustainable development of the coastal area of Abu Qir bay, *Sea to Sea Regional Forum* (pp. 275-280), Cairo Egypt.

Effat, H., and Hegazy, M. (2009). Application of spatial multi-criteria evaluation for an agricultural development scenario in the Egyptian deserts, *The 16th International GIS Symposium*, Ostravam Czech Republic.

Femandes, R. (2009). Precise determination of the orthometric height of Mt. Kilimanjaro, *The FIG working week 2009*, Eilat, Israel.

Gaber, A., Ghoniem, E., Khalaf, F., and El-Baz, F. (2009). Delineation of paleolakes in the Sinai Peninsula, Egypt, using remote sensing and GIS, *Arid Environments*, (73) 127–134.

Okuno, A., and Shikada, M. (2004). Application of real-time GIS using remote sensing and RTK-GPS for local government, *The ISPRS Congress*, Istanbul, Turkey.

Owusu, J., Afukaar, F., and Prahm B. (2006). Towards improving road traffic data collection: The use of GPS/GIS, *The 5th FIG regional conference*, Accra, Ghana.

Pavlis, N., Holmes, S., Kenyon, S., and Factor, J. (2008). An earth gravitational model to degree 2160: EGM2008, *The European Geosciences Union (EGU) general Assembly*, Vienna, Austria.

Saad, A., and Dawod, G. (2002). A precise integrated GPS/gravity geoid model for Egypt, *Civil Engineering Research Magazine*, 24 (1) 391-405.

Sadiq, M., and Ahmad, Z. (2009). On the selection of optimal global geopotential model for geoid modeling: A case study in Pakistan. *Advances in Space Researches*, doi:10.1016/j.asr.2009.05.004

Shalaby, A., and Tateishi, R. (2007). Remote sensing and GIS for mapping and monitoring land cover and land-use changes in the Northwestern coastal zone of Egypt, *Applied Geography*, (27) 28-41.

Tolba, O. (2007). The role of GIS in documenting Bahrain's historic cities, *The 3rd International ASCAAD Conference* (pp. 517-526). Alexandria, Egypt: Arab Society of Computer Aided Architectural Design.

Simple Precise Coordinates Transformations for Geomatics Applications in Makkah Metropolitan Area, Saudi Arabia

Gomaa M. DAWOD, Egypt, Meraj N. MIRZA, and Khalid A. AL-GHAMDI, Saudi Arabia

Key words: GPS, GIS, Datum transformation, Geomatics applications, Saudi Arabia.

SUMMARY

With the rapid growth of utilizing the Global Positioning System (GPS) technology in Saudi Arabia, the issue of transforming GPS-based coordinates to the local coordinates system becomes a crucial concern for geodetic and geomatics applications. Traditional similarity mathematical models for datum conversion (such as Molodensky-Badekas formula) do not take into account the systematic errors exist in national geodetic networks. This paper aims to develop simple, still precise, coordinate transformation algorithms particularly for Geographic Information Systems (GIS) applications. A dataset of high-precision geodetic control points with known GPS and the Saudi geodetic datum (Ain El-Abd 1970) coordinates, within the metropolitan area of Makkah city, has been compiled and utilized in data processing. Results of classical 7-parameters similarity transformation are presented. Additionally, four regression formulas have been developed to convert GPS coordinates (geographic and projected sets) to their local values just by using a calculator. Precision estimates of these regression equations have been anticipated to be within 0.30 meter. Compared with the accuracy of pre-defined transformation parameters utilized in commercial GIS software (which is about 10 meters), the obtained accuracy is quite reasonable for geomatics activities. The proposed approach is practical and decreases both costs and time of engineering surveying, integrated GPS/GIS projects, and topographic mapping.

Simple Precise Coordinates Transformations for Geomatics Applications in Makkah Metropolitan Area, Saudi Arabia

Gomaa M. DAWOD, Meraj N. MIRZA, and Khalid AL-GHAMDI, Saudi Arabia

1. INTRODUCTION

Global Navigation Satellite Systems (GNSS) furnish the principal technology for geomatics and geodetic activities in Kingdom of Saudi Arabia (KSA). The rapid growth of utilizing the Global Positioning System (GPS) in KSA has necessitated the definition of the mathematical relationship between global and national geodetic datums. Traditional datum transformation formulas, such as Bursa-Wolf (Bursa, 1962) and Molodensky-Badekas (Badekas, 1969), have some disadvantages particularly that they do not account for systematic errors exist in old triangulation geodetic networks, which is the case in many countries established their geodetic skeleton in the first half of the twenty century. Hence, different datum conversion techniques have been propose, e.g. finite elements (Kohli and Jenni, 2008), least squares by different weights (Shaker et al, 2007), least-squares collocation (You and Hwang, 2006), and total least-squares estimation (Felus, and Burtch, 2009). GNSS networks are currently being established to cover the entire Arabian Peninsula to realize a new reference geodetic frame (Al-Sahhaf et al, 2010). Consequently, the datum conversion from the World Geodetic System 1984 (WGS84) to the national Saudi geodetic datum has to be defined. That is an important demand in the undergoing research project of estimating flood hazardous impacts in Makkah city (Mirza et al., 2011). This paper aims to investigate a classical similarity transformation model, and to develop regression models to convert GPS-based coordinates to the Ain El-Abd 1970 national Saudi geodetic datum.

2. AVAILABLE DATA

Makkah city is located in the south-west part of KSA, about 80 Km east of the Red Sea (Fig. 1). It extends from $39^o\ 35^{'}$ E to $40^o\ 02^{'}$ E, and from $21^o\ 09^{'}$ N to $21^o\ 37^{'}$ N. The old (still used) Saudi geodetic datum is called Ain El-Abd 1970, which depends on the International (Hayford 1909) ellipsoid utilizing the Universal Transverse Merecator (UTM) as a map projection. A new Saudi Geodetic Datum (SGD2000) is proposed to ease the GPS data utilization for surveying and mapping (Yanar, 2009). Defining parameters of Ain El-Abd 1970 and SGD2000 datums are tabulated in Table 1. A dataset of thirteen first-order GPS stations, with known WGS84 and local coordinates, has been compiled and utilized in the current research (Fig. 2). Ten points have been used in data processing; while the remaining three stations (No. 7, 8, and 9) have been reserved as check points.

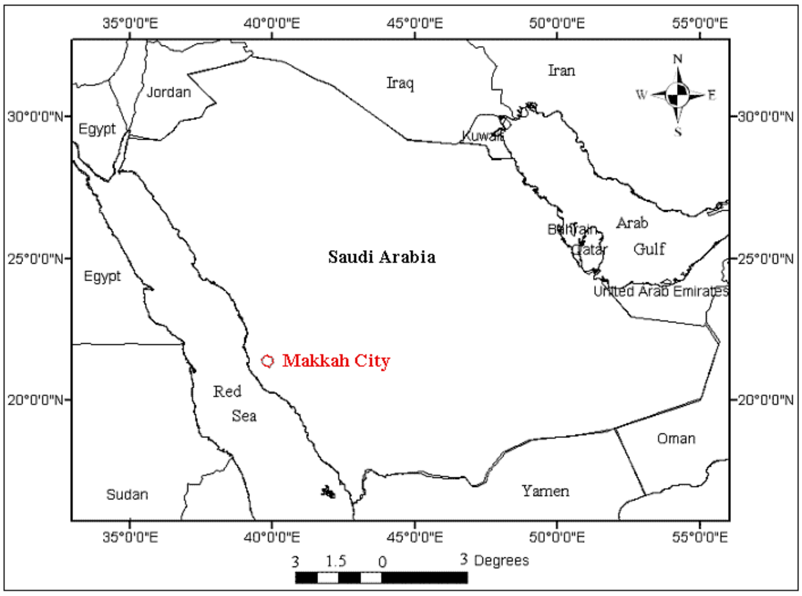

Figure 1: Study Area

Table 1: Parameters of the Saudi Geodetic Datums

Datum Name	Ain El-Abd 1970	SGD2000
Reference Frame	N/A	International Terrestrial Reference Frame (ITRF2000)
Coordinates Epoch	N/A	2004.0
Ellipsoid	Hayford 1909	Geodetic Reference System (GRS80)
Semi-major axes	6378388.0 meter	6378137.0 meter
Inverse Flattening (1/f)	297.0	298.257222101
Map Projection	Universal Transverse Merecator (UTM)	Universal Transverse Merecator (UTM)

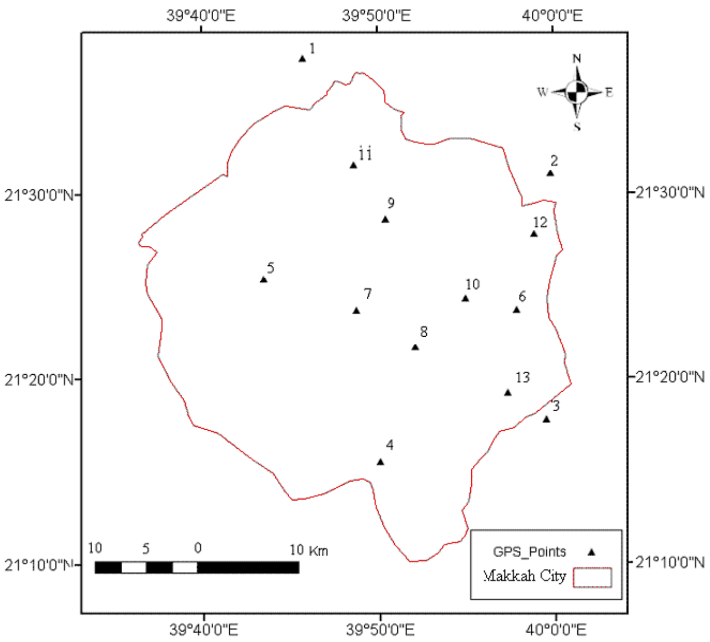

Figure 2: Available GPS Stations

It worth mentioning that several commercial software have implicit estimates of datum transformation parameters between WGS84 and Ain El-Abd 1970 geodetic datums. Usually typical geomatics users utilize these values without giving attention to their accuracy. Table 2 presents values and precision of published datum transformation parameters for KSA (Mugnier, 2008). It can be noticed that the precision of these transformation parameters is within 10 meters, which implies that they are not precise enough for geodetic applications.

Table 2: Values of General Similarity Transformation Parameters

System A	WGS 84
System B	Ain El-Abd 1970
Shift X	- 143 ± 10 m
Shift Y	- 236 ± 10 m
Shift Z	+ 7 ± 10 m

3. PROCESSING AND RESULTS

The first stage of the data processing applied the Molodensky-Badekas similarity transformation model to define the transformation parameters between WGS84 and Ain El-Abd 1970 datums. The accomplished results are presented in Table 3. The accuracy estimates of these parameters

have been computed at the three check points, where the average standard deviations of coordinate's difference equals ± 0.212 meter.

Table 3: Results of Molodensky-Badekas Similarity Transformation Parameters

System A	WGS 84
System B	Ain El-Abd 1970
Rotation Origin	
X_o	4559545.892 m
Y_o	3808252.221 m
Z_o	2314350.329 m
Translation Parameters	
Shift X	41.650 m
Shift Y	286.321 m
Shift Z	89.132 m
Rotation Parameters	
Rotation X	-1.91577 "
Rotation Y	10.28662 "
Rotation Z	-14.08571 "
Scale	
Scale Factor	-7.1256 part per million (ppm)

It is known that traditional datum transformation formulas have some weaknesses mainly that they do not account for systematic errors exist in old triangulation geodetic networks. Moreover, simple coordinates transformation models are needed for geomatics applications, e.g. Geographic Information Systems (GIS) data collection. Regression models offer a suitable candidate for developing simple, still precise, transformation formulas that takes into consideration the precision and errors' conditions of the old triangulation geodetic networks (e.g. Dawod and Alnaggar 2000, and Mossa 2009). Theoretically, these models are superior to the conformal transformation models since they can account for non-linear distortions between the terrestrial and satellite datums (Featherstone, 1997). Moreover, regression models have been utilized in many geodetic applications, particularly for fitting gravimetric quasi-geoid to GPS/Levelling data (e.g. Tranes et al, 2007 and Dahoa et al, 2008) and fitting Global Geoid Models (GGMs) to national geodetic data (e.g. Rabah, 2009). Furthermore, the U.S. Defense Mapping Agency (DMA) has published numerous regression models to convert GPS-based coordinates to a variety of local geodetic datums (DMA, 1991).

Several regression models have been developed to define simple relationships between the WGS84 and Ain El-Abd 1970 datums. Derivatives of regression models can be found in many statistical literatures (e.g. Stephens, 1998) and can be summarized as:

A linear regression general form is:

$$y = b_o + b_l\,x \qquad (1)$$

where (x, and y) are coordinates of some known points,
b_o and b_l are unknown regression coefficients; represent the intercept and slope of a line, to be estimated.

The estimates b_o and b_l are determined, so that the sum of squares of deviations about the line is minimized, as:

$$b_1 = S_{xy} / S_{xx} \qquad (2)$$

$$S_{xx} = \Sigma\, x^2 – (\Sigma x)^2/n \qquad (3)$$

$$S_{xy} = \Sigma\, xy –(\Sigma x)(\Sigma y)/n \qquad (4)$$

$$b_o = y' - b_1\, x' \qquad (5)$$

where x' and y' represent the mean of x and y coordinates respectively, and n is the number of data points.

Accordingly, equations 2 to 5 have been applied to develop 4 regression formulas (in the form of equation 1), where the x, and y represent the latitude, longitude, easting, and northing coordinates of the known GPS stations. The first (geographic) group of the developed regression formulas, for Makkah metropolitan area, are:

$$\Delta\varphi = - 0.001043117 + 0.0000208\ \ \varphi_{84} \qquad (6)$$

$$\Delta\lambda = - 0.003703158 + 0.0000462\ \ \lambda_{84} \qquad (7)$$

where,

$\Delta\varphi$ is the difference in latitude, in degrees, between the WGS84 and Ain El-Abd 1970 datums.
$\Delta\lambda$ is the difference in longitude, in degrees, between the WGS84 and Ain El-Abd 1970 datums.
φ_{84} is the WGS84 latitude, in degrees.
λ_{84} is the WGS84 longitude, in degrees.

Equations 6 and 7 will be used to compute the local geodetic coordinates from the observed GPS coordinates. The accuracy estimates of these transformation equations have been evaluated at the three check points, where the average coordinate difference equals 0.039 ± 0.256 meter.

The second (projected) group of the developed regression models deal with the UTM projected coordinates (Zone 37) as:

$$E_{local} = - 199.224 + 0.00000490 \; E_{84} \quad (8)$$

$$N_{local} = - 112.363 + 0.00000623 \; N_{84} \quad (9)$$

where,

E_{local} is the UTM East coordinate, in meters, based on Ain El-Abd 1970 datum.
N_{local} is the UTM North coordinate, in meters, based on Ain El-Abd 1970 datum.
E_{84} is the UTM East coordinate, in meters, based on WGS84 datum.
N_{84} is the UTM North coordinate, in meters, based on WGS84 datum.

Hence, equations 8 and 9 can be used to compute the local UTM coordinates from the projected UTM GPS coordinates in a straightforward way. Similarly, the accuracy estimates of these transformation equations have been evaluated at the three check points, where the average coordinate difference equals 0.052 ± 0.267 meter.

Regarding the developed regression models, it is obvious that they are related only for Makkah metropolitan area since they implicitly depend on local GPS datasets. However, this approach can be simply implemented in any other region in Saudi Arabia, or anywhere else, as long as GPS datasets are in hand. For example, similar regression models for Jeddah city have been estimated (Mossa, 2009). Hence, the regression approach is recommended as a coordinate transformation tool for other regions in KSA.

4. CONCLUSION

Coordinates transformations are needed to convert the WGS84-based GPS coordinates to local Saudi mapping system. Obtaining an accurate-consistent transformation parameters set, utilizing the classical similarity transformation models, is not an easy task because of the inaccuracy and inconsistency in the local geodetic networks. In this research, two groups of regression models have been developed to transform geodetic and projected GPS coordinates to their national values for Makkah metropolitan area. The main advantages, of such regression models, are simplicity and accuracy (within 0.3 meter). These models are extremely more accurate than the transformation parameters implicitly found in most commercial GPS software. Moreover, they can be utilized in field surveying works just by using a calculator, which overcomes the complexity of the traditional similarity transformation formulas. Such models are efficient for several types of geomatics activities, for example GIS data collection, engineering surveying, and topographic mapping.

ACKNOLWDGEMENTS

The authors would like to acknowledge the financial support offered by the Center of Research Excellence in Hajj and Omrah (Hajjcore), Um Al-Qura university, Saudi Arabia.

REFERENCES

Al-Sahhaf, N., Fernandes, R., and Alhamidi, S., 2010, The ArabRef project: A new geodetic network for Arabia, FIG congress 2010, Sydney, Australia, 11-16 April.

Badekas, J. (1969) Investigations related to the establishment of a world geodetic system, Report 124, Department of Geodetic Science, Ohio State University, Columbus, OH, USA.

Bursa, M. (1962) The theory for the determination of the non-parallelism of the minor axis of the reference ellipsoid and the inertial polar axis of the Earth, and the planes of the initial astronomic and geodetic meridians from observations of artificial Earth satellites, Studia Geophysica et Geodetica, No. 6, pp. 209-214.

Dahoa, S., Fairhead, J., Zeggaia, A., Ghezali, B., Derkaoui, A., Gourine, B., and Khelifa, B., 2008, New investigation on the choice of the tailored geopotential model for Algeria, Geodynamics, 45, pp.154–162.

Dawod, G., and Alnaggar, D., 2000, Optimum geodetic datum transformation techniques for GPS surveys in Egypt, Proceedings of Al-Azhar Engineering Sixth International Engineering Conference, Al-Azhar University, September 1-4, Volume 4, pp. 709-718.

DMA (Defense Mapping Agency), 1991, Department of Defense World Geodetic System 1984: its definition and relationships with local geodetic systems (second edition). Technical Report no. 8350.2, Defense Mapping Agency, Washington, USA.

Featherstone, W., 1997, A comparison of existing co-ordinate transformation models and parameters in Australia, Cartography, Vol. 26, No. 1, pp. 13-26.

Felus, Y. and Burtch, R., 2009, On symmetrical three-dimensional datum conversion, GPS Solution, No. 13, pp. 65–74.

Kohli, A. and Jenni, L., 2008, Transformation of cadastral data between geodetic reference frames using finite element method, FIG working week 2008, Stockholm, Sweden, 14-19 June.

Mirza, M., Dawod, G., and Al-Ghamdi, K., 2011, Assessment of global and national digital elevation models for geodetic and geomorphologic applications in Makkah metropolitan area, Saudi Arabia, Submitted to the XXV IUGG General Assembly, 28 June - 7 July, Melbourne, Australia.

Mugnier, C., 2008, Datums and coordinates systems: Kingdom of Saudi Arabia, ASPRS Journal, pp. 949-951.

Mossa, A., 2009, Coordinates systems and the Jeddah's governorate mapping system, Unpublished technical report, Surveying Department, Jeddah governorate, Saudi Arabia.

Rabah, M., 2009, Using RTK tides on the northern coast of Egypt: Undulation model corrections from EGM2008, Civil Engineering Surveyor, September, pp. 43-47.

Shaker, A., Saad, A., El-Sayed, M., and Ali, A., 2007, Remove-restore technique for improving the datum transformation process, FIG Working Week 2007, Hong Kong SAR, China, 13-17 May.

Stephens, L., 1998, Schaum's outline of theory and problems of statistics, McGraw-Hill, Inc, New York, USA, 371 pp.

Tranes, M., Meyer, T., and Massalski, D., 2007, Comparisons of GPS-derived orthometric heights using local geometric geoid models, Surveying Engineering, February, pp. 6-13.

Yanar, R., 2009, Coordinates systems, datums, and map projections in Saudi Arabia, Forth annual workshop of surveying departments in KSA governorates, Jeddah, Saudi Arabia, January 28.

You, R. and Hwang, H., 2006, Coordinate transformation between two geodetic datums of Taiwan by least-squares collocation, Surveying Engineering, pp. 64-70.

BIOGRAPHICAL NOTES

Gomaa M. Dawod received his Master of Geodetic Science and Surveying from the Ohio State University, Columbus, Ohio, USA in 1991 and his Ph.D. of Surveying Engineering from Shobra Faculty of Engineering, Zagazig University, Egypt in 1998. Since 1987, he is affiliated with the Survey Research Institute (SRI), the National Water Research Center (NWRC), Egypt, mainly in the field of Geodesy. Since 2005, he is affiliated with Umm Al-Quraa university, Makkah city, Saudi Arabia.

Meraj N. Mirza received his Master degree from the Michigan University, USA in 1979 and his Ph.D. from Khartoum University, Sudan in 1995. Since 1975, he is affiliated with Umm Al-Quraa university, Makkah city, Saudi Arabia. In 1997, he was one of the initiators of the GIS/Remote Sensing unit in Umm Al-Qura university, which is the pioneer GIS unit in Saudi universities. He is also an active associate of the Center of Research Excellence in Hajj and Omrah (Hajjcore), Um Al-Qura university. He has published several technical papers, and has attended numerous scientific conferences in KSA and abroad.

Khalid A. Al-Ghamdi received his Master degree from Clark University, Worcester, Massachusetts, USA in 2002, and his Ph.D. from University of Fribourg, Fribourg, Switzerland in 2008. Since 1993, he is affiliated with Umm Al-Quraa university, Makkah city, Saudi Arabia. Since 2009, he is the supervisor of the GIS/Remote Sensing unit in Umm Al-Qura university. He has taught several geomatics courses, and has attended many scientific conferences in KSA and abroad.

CONTACTS

Gomaa M. Dawod
P.O. Box 715, Makkah 21955, Saudi Arabia
Tel. +966551402093
Fax. +96625534113
Email: dawod_gomaa@yahoo.com
Web site:http://gomaa.dawod.googlepages.com/

Meraj N. Mirza
Centre of Research Excellence in Hajj and Omrah (Hajjcore)**,** Umm Al-Qura University,
P.O. Box 6247, Makkah 21955, Saudi Arabia
Tel. +966505509935
Fax. +96625571561
Email: meraj@mmirza.com
Web site: http://www.mmirza.com

Khalid Al-Ghamdi
P. O. Box 138474, Jeddah 21323, Saudi Arabia
Tel. +966541740090
Fax. +96625534113
Email: kaghamdi@uqu.edu.sa
Web site: http://www.uqu.edu.sa/kaghamdi

INTERNATIONAL JOURNAL OF GEOMATICS AND GEOSCIENCES
Volume 1, No 4, 2011

© Copyright 2010 All rights reserved Integrated Publishing services

Research article ISSN 0976 – 4380

Accuracy and relevance of Digital Elevation Models for Geomatics applications - A case study of Makkah Municipality, Saudi Arabia

Mirza.M [1,2], Dawod.G. [2,3], and Al-Ghamdi.K [2]
1- Center of Research Excellence in Hajj and Omrah, Umm Al-Qura University, Makkah, Saudi Arabia
2- Geography Department, Umm Al-Qura University, Makkah, Saudi Arabia
3- Survey Research Institute, Giza, Egypt
meraj@mmirza.com

ABSTRACT

Several geomatics applications depend on utilizing Digital Elevation Models (DEMs), such as geomorphologic applications of watershed management and flood hazard determination. Additionally, DEMs play a crucial role in geodetic applications, particularly for the determination of topographic effects in quasi-geoid modelling. This study aims to investigate the accuracy performance of several global and national DEMs in order to define the suitability of them in engineering applications in Kingdom of Saudi Arabia (KSA). Two global DEMs have been exploited, namely the Advanced Spaceborne Thermal Emission and Reflection Radiometer (ASTER) and the Shuttle Radar Topographic Mission (SRTM3), along with two national DEMs, belong to the center of research excellence in Hajj and Omrah, with 5 and 10 meter resolution. A dataset of 200 first-order Global Positioning System (GPS) ground control points, that covers the Makkah (Mecca) metropolitan area in the western region of KSA, has been compiled and employed to judge the accuracy of all DEMs in a Geographic Information Systems (GIS) environment. The attained results showed that the 5-meter resolution national DEM is the most accurate one, that produces mean height difference and standard deviations equal 0.01 ± 2.95 m respectively. That national DEM is more accurate by factors of 3 and 2 over the global ASTER and SRTM3 DEMs respectively. Guidelines have been drawn to apply each DEM in geodetic, topographic mapping, and geomorphologic studies in KSA.

Keywords: DEM, Accuracy analysis, GPS controls, Geomatics activities, Saudi Arabia.

1. Introduction

Digital Elevation Models (DEMs) are essential for both geodetic and geomorphologic applications. DEMs are utilized in gravity data processing and geoid model development, particularly for the computation of terrain corrections at observed terrestrial gravity data, and for downward continuation computations. Watersheds management and flood hazard assessment are typical morphometry and geomorphologic activities utilize DEMs (Subyani et al. 2010, and Mendas 2010). In the last few decades, several global DEMs have been compiled and released. This study aims to investigate the accuracy

INTERNATIONAL JOURNAL OF GEOMATICS AND GEOSCIENCES
Volume 1, No 4, 2011

© Copyright 2010 All rights reserved Integrated Publishing services

Research article ISSN 0976 – 4380

performance of several global and national DEMs in order to define the suitability of them in engineering and geomatics applications in Kingdom of Saudi Arabia (KSA).

2. Study Area

Makkah city is located in the south-west part of KSA, about 80 Km east of the Red Sea (Figure.1). It extends from 39° 35' E to 40° 02' E, and from 21° 09' N to 21° 37' N. The area of the metropolitan region (the study area) equals 1593 square kilometers. The topography of Makkah is complex in nature, and several mountainous areas exist inside its metropolitan area.

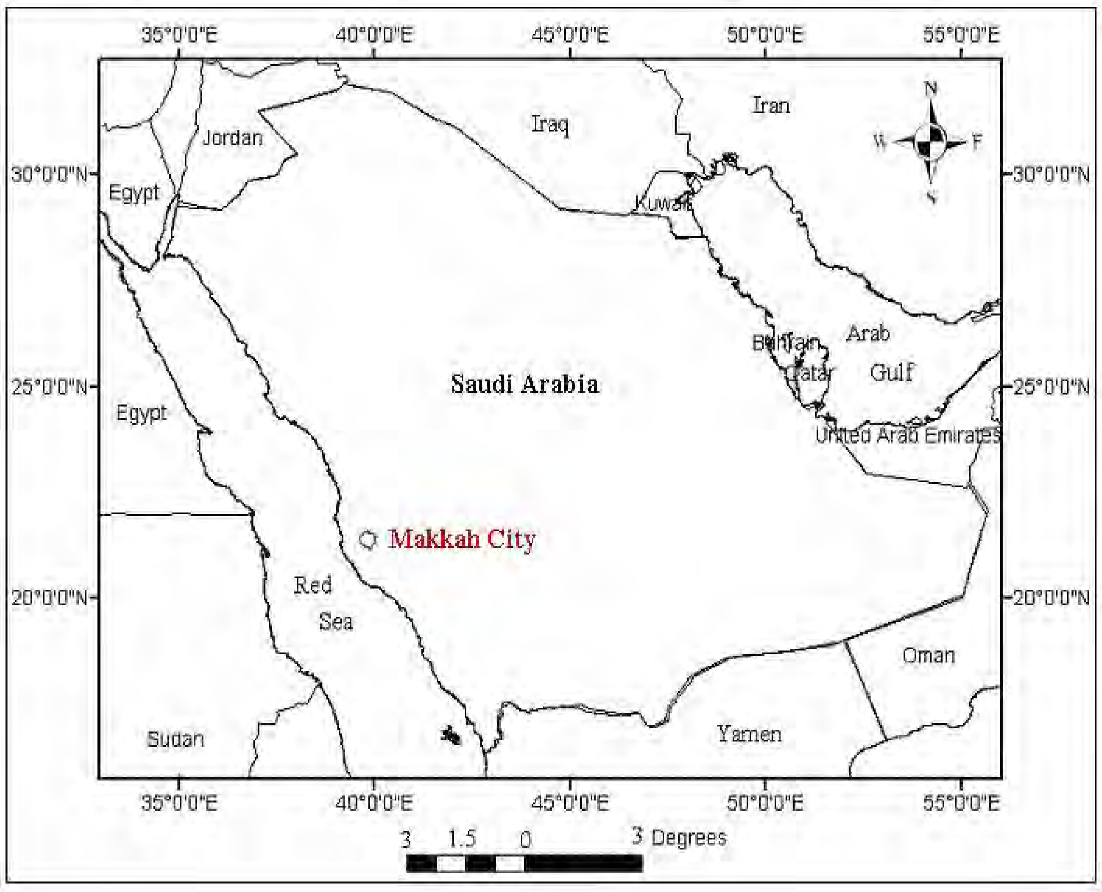

Figure 1: Study Area

2.1 Digital Elevation Models (DEMs)

Two global DEMs, along with two KSA national DEMs, have been exploited in this research, and they will be briefly described.

© Copyright 2010 All rights reserved Integrated Publishing services

Research article ISSN 0976 – 4380

2.2 Global DEMs

The Ministry of Economy, Trade, and Industry (METI) of Japan and the United States National Aeronautics and Space Administration (NASA) have jointly released Version 1 of the Advanced Spaceborne Thermal Emission and Reflection Radiometer (ASTER) Global Digital Elevation Model (GDEM). ASTER horizontal resolution equals 1 arc second, that is 30 meters approximately, and it is available free of charge. ASTER DEM has been utilized in many research studies (Dowerah 2010, Abdeen et al. 2009, and Mousavi et al. 2007). The window of the ASTER DEM corresponding to Makkah metropolitan area has been downloaded (http://www.gdem.aster.ersdac.or.jp/) and has been considered in this study (Figure. 2).

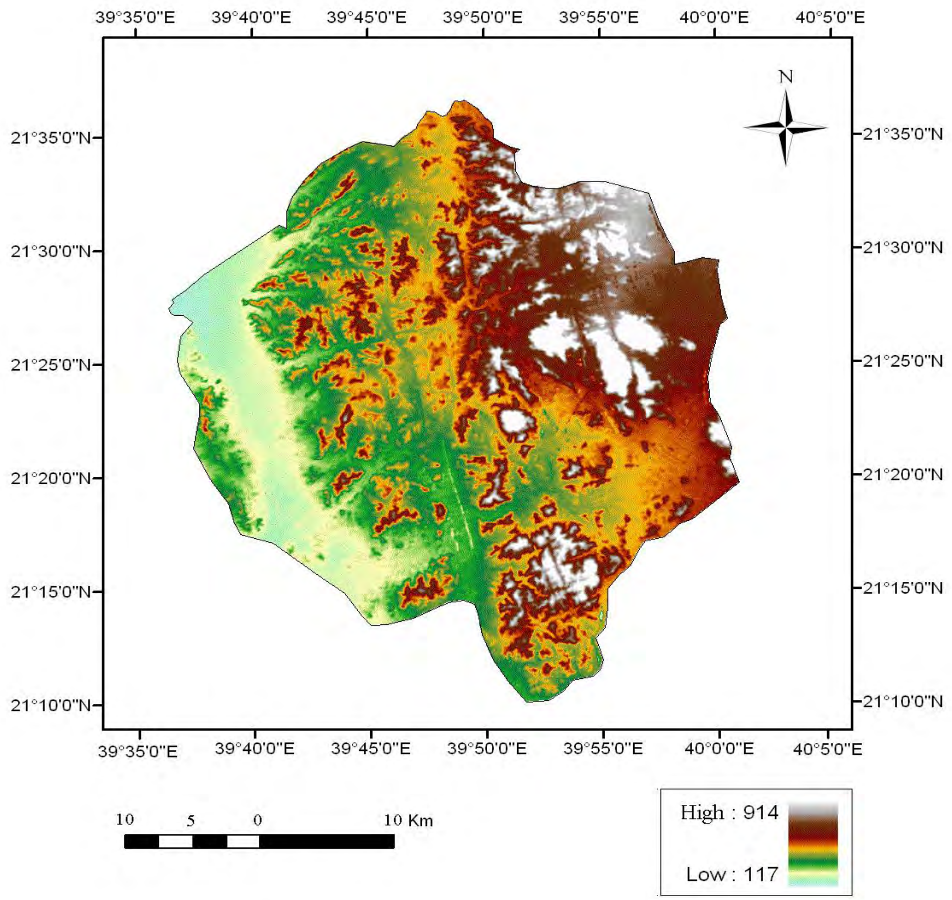

Figure 2: ASTER DEM for Makkah

The Shuttle Radar Topography Mission (SRTM) global DTM is a joint project between the U.S. National Imagery and Mapping Agency (NIMA) and the National Aeronautics and Space Administration (NASA). A 90 meters (3 arc seconds) SRTM DTM for many parts of the world has been compiled and released (Called SRTM3) and being available free of charge. SRTM3 has been used in geoid odeling for several regions, particularly

© Copyright 2010 All rights reserved Integrated Publishing services

Research article ISSN 0976 – 4380

for topographic and downward continuation corrections (Kiamehr and Sjöberg 2005) and also for morphometric studies (Bubenzer and Bolten 2008, and El Bastawesy 2007). The window of the SRTM DEM corresponding to Makkah territories has been downloaded (http://www2.jpl.nasa.gov/strm/) and has been considered in this study (Figure. 3).

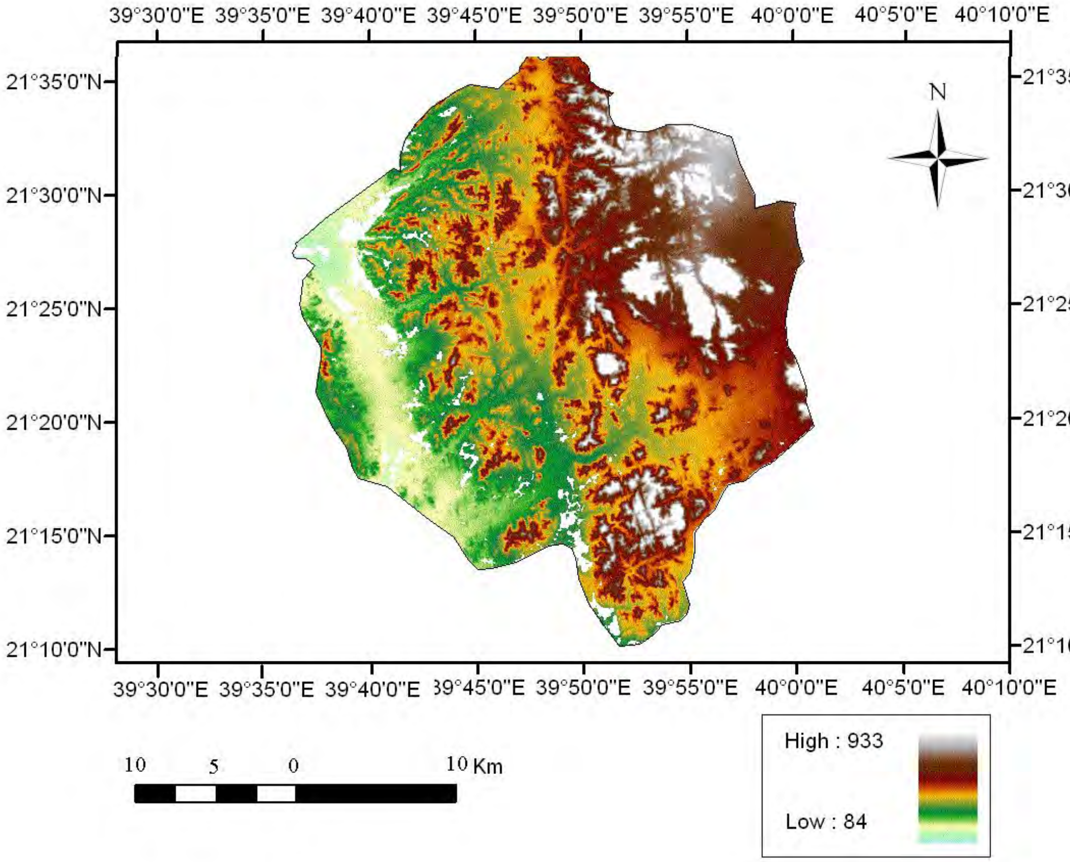

Figure 3: SRTM3 DEM for Makkah

2.3 National DEMs

Two national DEMs have been acquired, with resolution of 5 and 10 meters, developed by King Abdulaziz City of Sciences and Technology (KACST). Windows cover Makkah metropolitan area has been provided through the Center of Excellence in Hajj and Omrah, Umm Al-Qura University. The ASTER and SRTM3 are rectified relative to the World Geodetic System 1984 (WGS84). Since the available GPS data are relative to that geodetic datum too, the national 5-m (Figure. 4) and 10-m DEM has been projected from the national Saudi geodetic datum (Ain El-Abd 1970) to WGS84. That process, and consecutive procedures, has been performed using the Arc GIS software.

© Copyright 2010 All rights reserved Integrated Publishing services

Research article ISSN 0976 – 4380

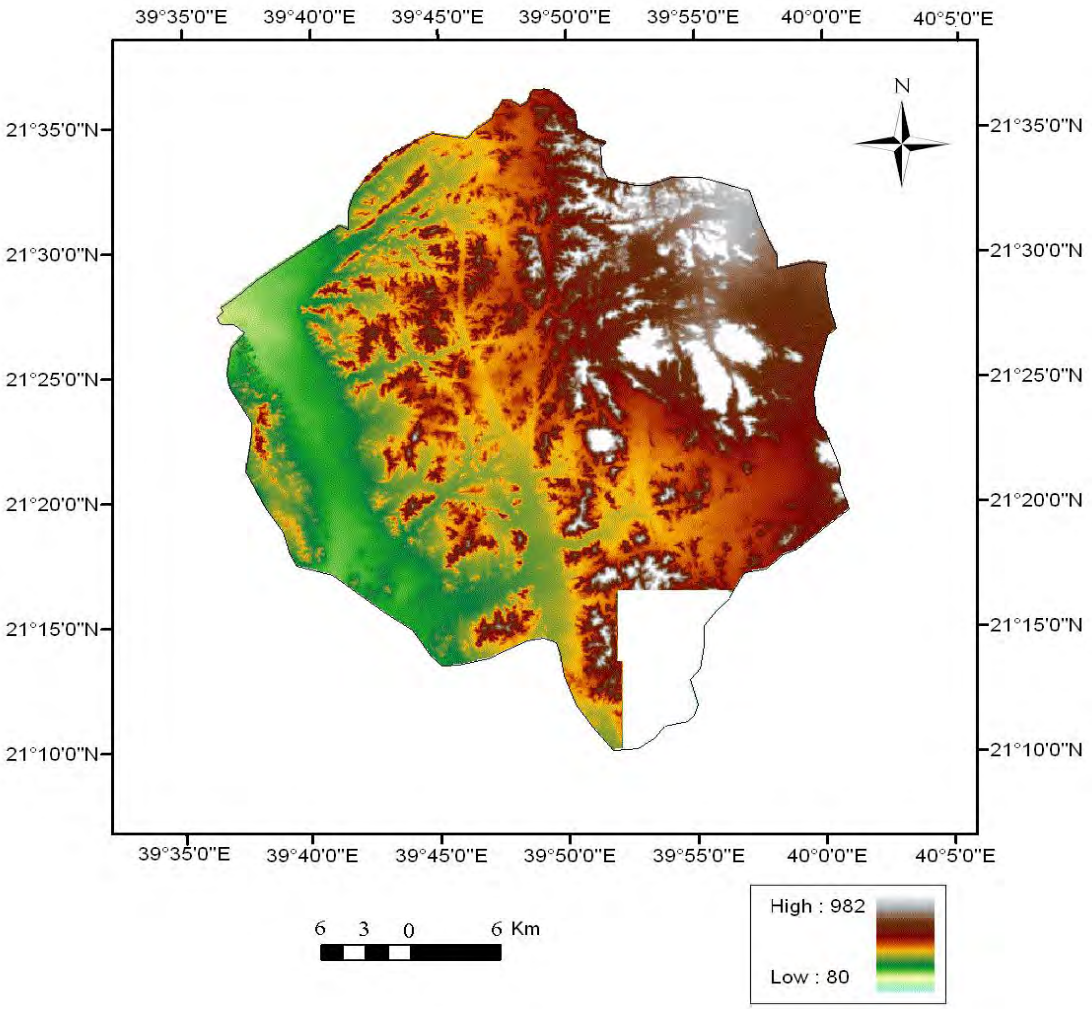

Figure 4: National 5-m DEM for Makkah

3. Data and Processing

3.1 Available data

A dataset of 200 first-order Global Positioning System (GPS) terrestrial control points, with known orthometric heights, has been compiled and used to judge the accuracy of DEMs. That dataset covers the entire Makkah metropolitan region as seen in Figure 5.

3.2 Processing methodology

GIS provides an efficient technical tool for spatial and attribute data storage, manipulation, processing and analysis. Utilizing GIS technology in GPS surveying activities facilitate the data processing for a number of applications (Dawod and

INTERNATIONAL JOURNAL OF GEOMATICS AND GEOSCIENCES
Volume 1, No 4, 2011

© Copyright 2010 All rights reserved Integrated Publishing services

Research article ISSN 0976 – 4380

Mohamed 2009). The GIS processing procedures, carried out in this research, consist of several steps (Figure. 6).

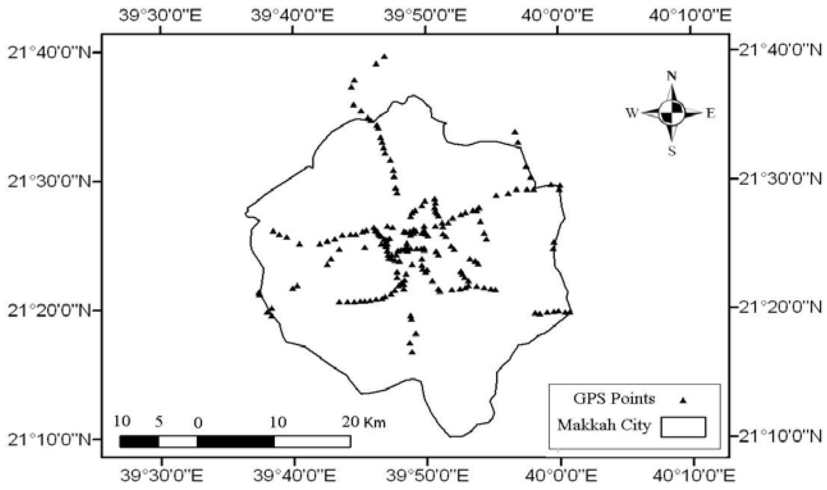

Figure 5: Available GPS Stations

Firstly, all available DEMs and the GPS dataset have been imported within the Arc GIS software. That program has a lot of spatial analysis tools within its Arc Toolbox component. That component, in the second procedure, has been utilized to interpolate the DEMs' heights of the available GPS points. Thirdly, the obtained DEMs' heights have been compared against the known heights of the 200 terrestrial control points cover the Makkah metropolitan area. Finally, statistical analysis has been performed to investigate the accomplished results.

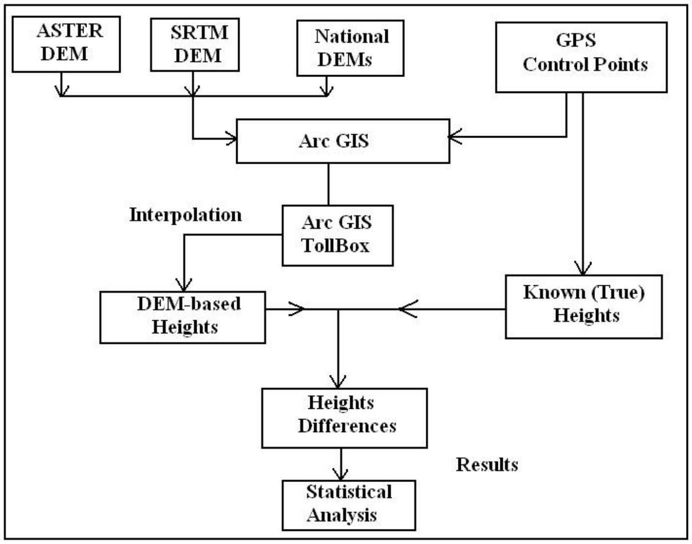

Figure 6: GIS Processing Steps

© Copyright 2010 All rights reserved Integrated Publishing services

Research article ISSN 0976 – 4380

4. Results, discussion, and conclusions

4.1 DEM accuracy

For the global DEMs, the published accuracy levels are 7-14 and 6-10 meters for ASTER and SRTM3 respectively (Abrams et al. 2008 and Rodriguez et al. 2005 respectively). These accuracy levels are on a global scale, hence, the main task of the current research is to assess their accuracy within Makkah metropolitan area. DEMs accuracy assessment studies have been performed in several regions in the world (Denker 2005, Kiser and Kelly 2010, and Dawod 2008). Clearly, it can be noticed from figures 1 and 2 that there are some differences between ASTER and SRTM3 DEMs over Makkah. ASTER produces height values range from 117 to 914 meters, while the SRTM3's heights range vary from 84 to 933 meters. From Figure 3, the corresponding heights of the 5-m national DEM range from 80 to 982 meters.

Tables 1 and 2 present the accomplished results of heights comparison. From Table 1, it can be seen that the ASTER DEM yields height differences range from -20.34 m to 19.30 m, with a mean value of 2.59 m and a standard deviations equals ± 8.66 m. On the other hand, the SRTM3 DEM produces height differences vary from -20.12 m to 9.07 m, with an average of -5.20 m and standard deviations equals ± 5.85 m. Therefore, it can be concluded that the 90-m resolution SRTM3 DEM is more accurate than the 30-m resolution ASTER DEM by a factor of 1.5 approximately, over Makkah city. Comparable results over Australia have been reported (Hirt et al. 2010).

Table 1: Statistics of Global DEMs' Height Differences over Check Points

	Heights Differences of ASTER	Heights Differences of SRTM3
Minimum	-20.34	-20.12
Maximum	19.30	9.07
Mean	2.59	-5.20
Standard Deviation	8.66	5.85

Regarding the available national DEMs, it can be seen, from Table 2, that the 10-m resolution DEM generates height differences range from -7.60 m to 7.36 m, with a mean value of 0.01 m and a standard deviations equals ± 2.96 m. Conversely, the 5-m resolution DEM produces height differences vary from -7.54 m to 7.07 m, with an average of 0.01 m and standard deviations equals ± 2.95 m. Therefore, it can be concluded that there are no significant differences between the accuracy of both DEMs even though their horizontal resolutions are different. This conclusion is quite important in computer data processing since the file size of the 5-m resolution DEM is almost twice that of the 10-m DEM. Hence, utilizing the 10-m DEM will be faster in performing processing tasks of surveying, mapping, and geomorphologic studies.

INTERNATIONAL JOURNAL OF GEOMATICS AND GEOSCIENCES
Volume 1, No 4, 2011

© Copyright 2010 All rights reserved Integrated Publishing services

Research article ISSN 0976 – 4380

Table 2: Statistics of National DEMs' Height Differences over Check Points

	Heights Differences of National 10m-DEM	Heights Differences of National 5m-DEM
Minimum	-7.60	-7.54
Maximum	7.36	7.07
Mean	0.01	0.01
Standard Deviation	2.96	2.95

Another comparison between global and national DEMs reveals that both national DEMs are more accurate, in representing the topography of Makkah city, by factors of 3 and 2 over the global ASTER and SRTM3 DEMs respectively.

4.2 DEM relevance

A chief concern in utilizing DEMs is to select a DEM that is appropriate, in terms of precision, for a specific geodetic, mapping, or morphometric task. Three example issues, in this regard, will be considered. Firstly, creating contour maps from a DEM mainly depends on the DEM accuracy. The United States Geological Survey (USGS) standards state that: "for topographic maps, the vertical accuracy standard, for all map scales, requires that the elevation of 90 percent of all points tested must be correct within half of the contour interval" (USGS 1999). Hence, the tested two national DEMs can be used to develop topographic maps with a contour interval equals 6 m, while SRTM3 and ASTER DEMs can yield 12-m and 18-m interval contour maps, respectively. Secondly, the rigid topography of Makkah metropolitan area emphasis the fact that a precise DEM is needed in estimating the terrain corrections in quasi-geoid modelling. Hence, the 5-m resolution national DEM is the optimum candidate in developing gravimetric co-geoid of Makkah city. Thirdly, for hydrological analysis and water resources management, DEM spatial resolution affects flood simulation and the computations of inundation areas from flood simulations (Li and Wong 2010 and Dixon and Earls 2009).

5. Conclusions

DEMs play a crucial role in geodetic, geomorphologic, and mapping applications. This study has investigated the accuracy of two national DEMs, with 5m and 10m resolutions, along with the ASTER and SRTM3 global DEMs. A dataset of 200 first-order GPS ground control points, that covers the Makkah (Mecca) metropolitan area in the western region of Saudi Arabia, has been utilized to judge the accuracy of these DEMs. The attained results showed that the 5-meter resolution national DEM is the most accurate one and produces mean height difference and standard deviations equal 0.01 ± 2.95 m respectively. That national DEM is more accurate by factors of 3 and 2 over the global ASTER and SRTM3 DEMs respectively. Recommendations have been drawn to apply each DEM in the geodetic, topographic mapping, and geomorphologic activities in Saudi Arabia.

© Copyright 2010 All rights reserved Integrated Publishing services

Research article ISSN 0976 – 4380

Acknowledgements

The authors would like to acknowledge the financial support offered by the Center of Research Excellence in Hajj and Omrah, Umm Al-Qura University, Saudi Arabia.

6. References

1. Abdeen, M. El-Kazzaz, Y., Attia, G., Yehia, M., and Hassan, S. (2009), "Mapping geological structures in Wadi Ghoweiba area, northwest gulf of Suez, Egypt, using ASTER Spot data fusion and ASTER DEM", Egypt Journal Remote Sensing and Space Sciences, 12, pp 101-126.

2. Abrams, M., Hook, S., and Ramachandran, B. (2008), "ASTER user handbook: Version 2", Jet Propulsion Laboratory, Pasadena, CA, USA.

3. Bubenzer, O. and Bolten, A. (2008), "The use of new elevation data (SRTM/ASTER) for the detection and morphometric quantification of Pleistocene megadunes (Draa) in the eastern Sahara and the southern Namib", Geomorphology, 102, pp 221–231.

4. Dawod, G. (2008), "Towards the redefinition of the Egyptian geoid: Performance analysis of recent global geoid and digital terrain models", Journal of Spatial Science, 53(1), pp 31-42.

5. Dawod, G., and Mohamed, W. (2009), "Data management of different height systems within GPS/GIS integrated spatial technology", Middle East Spatial Technology Conference (MEST2009), December 7-9, Kingdom of Bahrain.

6. Denker, H. (2005), "Evaluation of SRTM3 and GTOPO30 terrain data in Germany", The International Association of Geodesy's Symposium on Gravity, Geoid and Space Missions, 129, pp 218-223.

7. Dixon, B. and Earls, J. (2009), "Resample or not? Effects of resolution of DEMs in watershed modelling", Hydrological Processes, 23, pp 1714–1724.

8. Dowerah, B. (2010), "ASTER DEM based studies for geological investigation around Singhbhum Shear Zone (SSZ) in Jharkhand, India", Journal of Geographic Information System, 2, pp 11-14.

9. El Bastawesy, M. (2007), "Influence of DEM source and resolution on the hydrographical simulation of Wadi Keed catchment, Sinai, Egypt", Egypt Journal of Remote Sensing and Space Sciences, 10, pp 53-62.

10. Hirt, C. Filmer, M., and Featherstone, W. (2010), "Comparison and validation of the recent freely available ASTER-GDEM ver1, SRTM ver4.1 and GEODATA

© Copyright 2010 All rights reserved Integrated Publishing services

Research article ISSN 0976 – 4380

DEM-9S ver3 digital elevation models over Australia", Australian Journal of Earth Sciences, 57, pp 337–347.

11. Kiamehr, R. and Sjöberg, L. E. (2005), "Effect of the SRTM global DEM on the determination of a high-resolution geoid model: a case study in Iran", Journal of Geodesy, 2005, 79(9), pp 540-551.

12. Kiser, L. and Kelly, M. (2010), "GPS- vs. DEM-derived elevation estimates from a Hardwood dominated forest watershed", Journal of Geographic Information System, 2, pp 147-151.

13. Li, J. and Wong, D. (2010), "Effects of DEM sources on hydrologic applications", Journal of Computers, Environment and Urban Systems, 34, pp 251–261.

14. Mendas, A. (2010), "The contribution of the digital elevation models and geographic information systems in a watershed hydrologic research", Applied Geomatics, 2, pp 33–42.

15. Mousavi, S., Fallah, A., Abbasnejadc, R., Mousavi, S. R., and Shabani, M. (2007), "The ASTER DEM generation for geomorphometric analysis of central Alborz mountains, Iran", Proceedings of the Asian Association of Remote Sensing Conference, Nov. 12-16, Kuala Lumpur, Malaysia.

16. USGS (U.S. Geological Survey) (1999), "Map accuracy standards", USGS Fact Sheet 171-99, November.

17. Rodriguez, E., Morris, C., Belz, J., Chapin, E., Martin, J., Daffer, W., and Hensley, S. (2005), "An assessment of the SRTM topographic products", Technical Report JPL D-31639, Jet Propulsion Laboratory, Pasadena, California, USA.

18. Subyani, A., Qari, M., and Matsah, M. (2010), "Digital elevation model and multivariate statistical analysis of morphometric parameters of some wadis, western Saudi Arabia", Arab Journal Geosciences, Published on line May 11.

Assessment of Global and National Digital Elevation Models for Geodetic and Geomorphologic Applications in Makkah Metropolitan Area, Saudi Arabia

M. N. Mirza [1,2], G. M. Dawod [2, 3] , and K. Al-Ghamdi [2]

[1] Center of Research Excellence in Hajj and Omrah, Umm Al-Qura university, Makkah, Saudi Arabia;
[2] Geography Department, Umm Al-Qura university, Makkah, Saudi Arabia;
[3] Survey Research Institute, Giza, Egypt.

ABSTRACT

Digital Elevation Models (DEMs) are essential in geodetic applications, particularly for the determination of topographic effects in quasi-geoid modelling. On the other hand, DEMs play a crucial role in geomorphologic applications such as watershed management and flood hazard determination. DEMs vary in both horizontal resolution and accuracy of their heights' estimates. This study aims to investigate the accuracy of several global and national DEMs in order to define the suitability of them in engineering applications in Kingdom of Saudi Arabia (KSA). Two global DEMs have been exploited, namely the Advanced Spaceborne Thermal Emission and Reflection Radiometer (ASTER) and the Shuttle Radar Topographic Mission (SRTM3), along with two national DEMs, belong to the center of research excellence in Hajj and Omrah, with 5 and 10 meter resolution. A dataset of 200 first-order Global Positioning System (GPS) ground control points, that covers the Makkah (Mecca) metropolitan area in the western region of KSA, has been compiled and employed to judge the accuracy of all DEMs in a Geographic Information Systems (GIS) environment. The attained results showed that the 5-meter resolution national DEM is the most accurate one, that produces mean height difference and standard deviations equal 0.01 ± 2.95 m respectively. That national DEM is more accurate by factors of 3 and 2 over the global ASTER and SRTM3 DEMs respectively. Guidelines have been drawn to apply each DEM in geodetic, topographic mapping, and geomorphologic studies in KSA.

1. INTRODUCTION

Digital Elevation Models (DEMs) are essential for both geodetic and geomorphologic applications. DEMs are utilized in gravity data processing and geoid model development, particularly for the computation of terrain corrections at observed terrestrial gravity data, and for downward continuation computations. Watersheds management and flood hazard assessment are typical morphometry and geomorphologic activities utilize DEMs (e.g. Subyani et al, 2010 and Mendas 2010). In the last few decades, several global DEMs have been compiled and released. Two global DEMs have been utilized in this research study, and they will be briefly described.

The Ministry of Economy, Trade, and Industry (METI) of Japan and the United States National Aeronautics and Space Administration (NASA) have jointly released Version 1 of the Advanced Spaceborne Thermal Emission and Reflection Radiometer (ASTER) Global Digital Elevation Model (GDEM). ASTER horizontal resolution equals 1 arc second, that is 30 meters approximately, and it is available free of charge. ASTER DEM has been utilized in many research studies (e.g. Dowerah 2010, Abdeen et al, 2009 and Mousavi et al, 2007). The window of the ASTER DEM corresponding to Makkah metropolitan area has been downloaded (http://www.gdem.aster.ersdac.or.jp/) and has been considered in this study (Fig. 1).

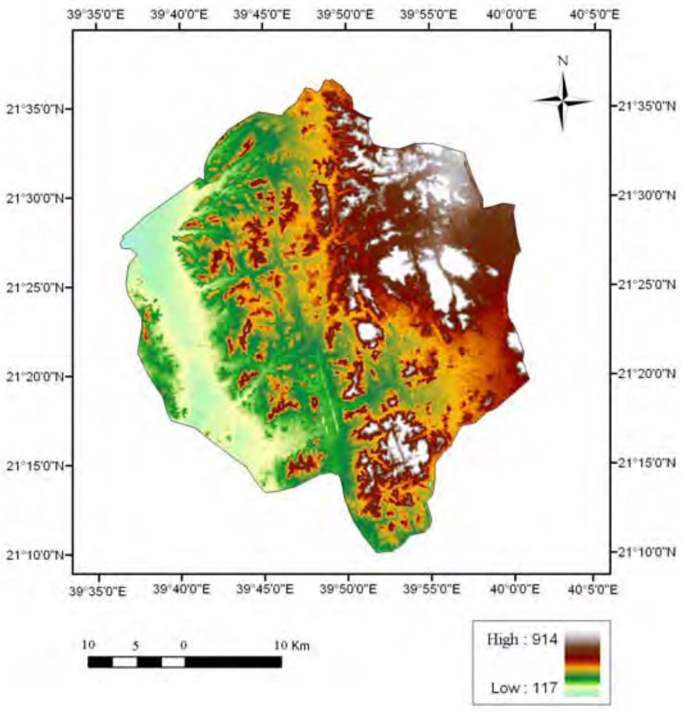

Figure 1: ASTER DEM for Makkah

The Shuttle Radar Topography Mission (SRTM) global DTM is a joint project between the U.S. National Imagery and Mapping Agency (NIMA) and the National Aeronautics and Space Administration (NASA). A 90 meters (3 arc seconds) SRTM DTM for many parts of the world has been compiled and released (Called SRTM3) and being available free of charge. SRTM3 has been used in geoid modelling for several regions, particularly for topographic and downward continuation corrections (e.g. Kiamehr and Sjöberg 2005) and also for morphometric studies (e.g. Bubenzer and Bolten 2008, and El Bastawesy, 2007). The window of the SRTM DEM corresponding to Makkah territories has been downloaded (http://www2.jpl.nasa.gov/strm/) and has been considered in this study (Fig. 2).

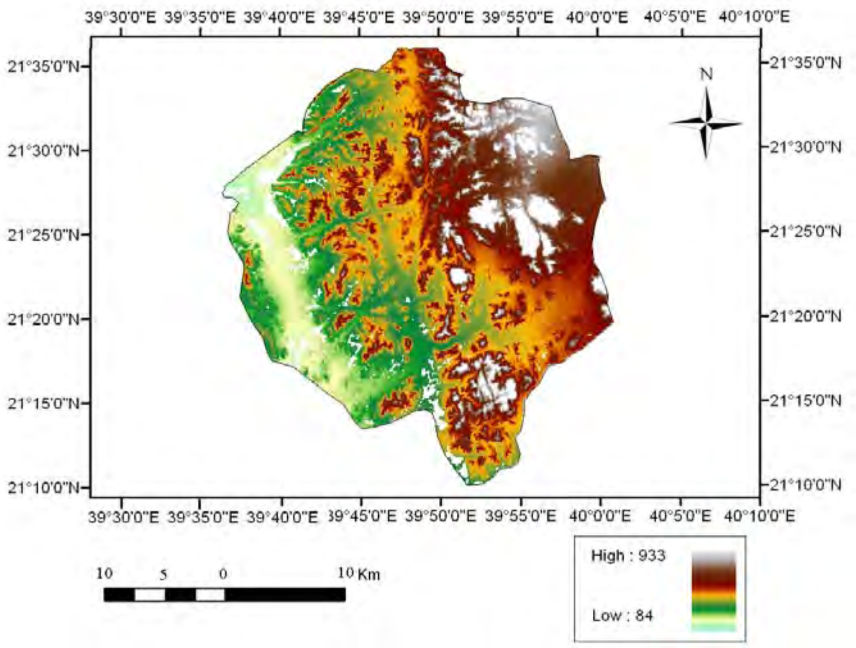

Figure 2: SRTM3 DEM for Makkah

2. AVAILABLE DATA

The first available dataset constitutes two national DEMs, with resolution of 5 and 10 meters, developed by King Abdulaziz City of Sciences and Technology (KACST). Windows cover Makkah metropolitan area have been provided through the Center of Excellence in Hajj and Omrah, Umm Al-Qura university. The ASTER and SRTM3 are rectified relative to the World Geodetic System 1984 (WGS84). Since the available GPS data are relative to that geodetic datum too, the national 5-m (Fig. 3) and 10-m DEM has been projected from the national Saudi geodetic datum (Ain El-Abd 1970) to WGS84. That process, and consecutive procedures, have been performed using the Arc GIS software. The second available dataset consists of 200 first-order Global Positioning System (GPS) terrestrial control points with known orthometric heights (Fig. 4).

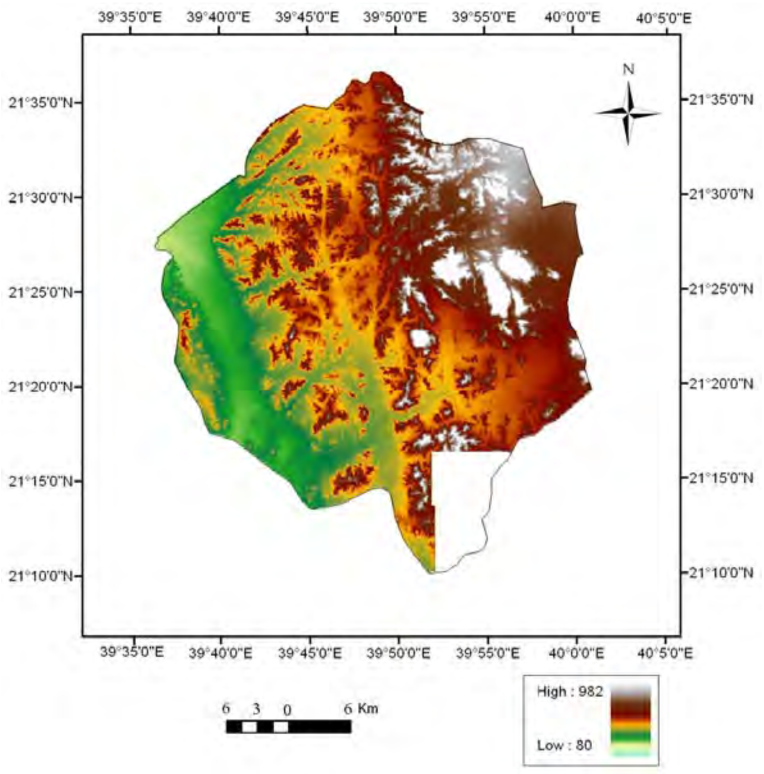

Figure 3: National 5-m DEM for Makkah

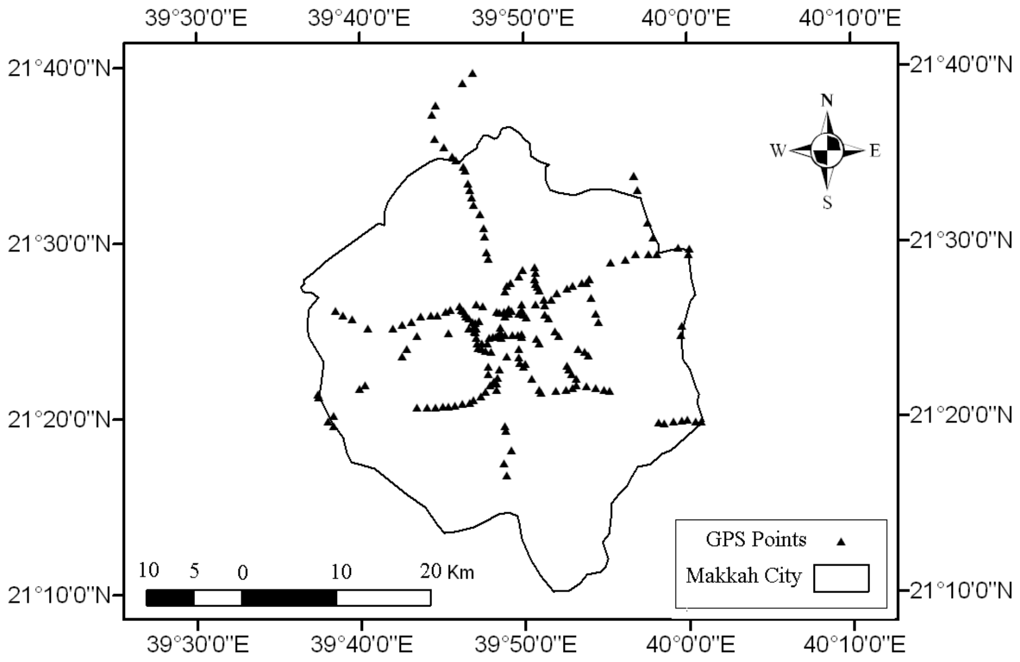

Figure 4: Available GPS Stations

3. PROCESSING AND RESULTS

For the global DEMs, the published accuracy levels are 7-14 and 6-10 meters for ASTER and SRTM3 respectively (Abrams et 2008, and Rodriguez et al, 2005 respectively). These accuracy levels are on a global scale, hence, the main task of the current research is to assess their accuracy within Makkah metropolitan area. DEMs accuracy assessment studies have been performed in several regions in the world (e.g. Denker 2005, Kiser and Kelly 2010, and Dawod 2008). Clearly, it can be noticed from figures 1 and 2 that there are some differences between ASTER and SRTM3 DEMs over Makkah. ASTER produces height values range from 117 to 914 meters, while the SRTM3's heights range vary from 84 to 933 meters. From Figure 3, the corresponding heights of the 5-m national DEM range from 80 to 982 meters.

The Arc GIS software has been utilized to interpolate the DEMs' heights of the available GPS points. Utilizing GIS technology in GPS surveying activities facilitate the data processing for a number of applications (Dawod and Mohamed 2009). The obtained DEMs' heights have been compared against the known heights of the 200 terrestrial control points cover the Makkah metropolitan area. Tables 1 and 2 present the accomplished results of heights comparison. From Table 1, it can be seen that the ASTER DEM yields height differences range from -20.34 m to 19.30 m, with a mean value of 2.59 m and a standard deviations equals ± 8.66 m. On the other hand, the SRTM3 DEM produces height differences vary from -20.12 m to 9.07 m, with an average of -5.20 m and a standard deviations equals ± 5.85 m. Therefore, it can be concluded that the 90-m resolution SRTM3 DEM is more accurate than the 30-m resolution ASTER DEM by a factor of 1.5 approximately, over Makkah city. Comparable results over Australia have been reported (Hirt et al, 2010).

Table 1: Statistics of Global DEMs' Height Differences over Check Points

	Heights Differences of ASTER	Heights Differences of SRTM3
Minimum	-20.34	-20.12
Maximum	19.30	9.07
Mean	2.59	-5.20
Standard Deviation	8.66	5.85

Regarding the available national DEMs, it can be seen, from Table 2, that the 10-m resolution DEM generates height differences range from -7.60 m to 7.36 m, with a mean value of 0.01 m and a standard deviations equals ± 2.96 m. Conversely, the 5-m resolution DEM produces height differences vary from -7.54 m to 7.07 m, with an average of 0.01 m and a standard deviations equals ± 2.95 m. Therefore, it can be concluded that there are no significant differences between the accuracy of both DEMs even though their horizontal resolutions are different. This conclusion is quite important in computer data processing since the file size of the 5-m resolution DEM is almost twice that of the 10-m DEM. Hence, utilizing the 10-m DEM will be faster in performing processing tasks of surveying, mapping, and geomorphologic studies.

Table 2: Statistics of National DEMs' Height Differences over Check Points

	Heights Differences of National 10m-DEM	Heights Differences of National 5m-DEM
Minimum	-7.60	-7.54
Maximum	7.36	7.07
Mean	0.01	0.01
Standard Deviation	2.96	2.95

Another comparison between global and national DEMs reveals that both national DEMs are more accurate, in representing the topography of Makkah city, by factors 0f 3 and 2 over the global ASTER and SRTM3 DEMs respectively.

A chief concern in utilizing DEMs is to select a DEM that is appropriate, in terms of precision, for a specific geodetic, mapping, or morphometric task. Three example issues, in this regard, will be considered. Firstly, creating contour maps from a DEM mainly depends on the DEM accuracy. The United States Geological Survey (USGS) standards state that: "for topographic maps, the vertical accuracy standard, for all map scales, requires that the elevation of 90 percent of all points tested must be correct within half of the contour interval" (USGS 1999). Hence, the tested two national DEMs can be used to develop topographic maps with a contour interval equals 6 m, while SRTM3 and ASTER DEMs can yield 12-m and 18-m interval contour maps, respectively. Secondly, the rigid topography of Makkah metropolitan area emphasis the fact that a precise DEM is needed in estimating the terrain corrections in quasi-geoid modelling. Hence, the 5-m resolution national DEM is the optimum candidate in developing gravimetric co-geoid of Makkah city. Thirdly, for hydrological analysis and water resources management, DEM spatial resolution affects flood simulation and the computations of inundation areas from flood simulations (Li and Wong, 2010 and Dixon and Earls, 2009).

4. CONCLUSIONS

DEMs play a crucial role in geodetic, geomorphologic, and mapping applications. This study has investigated the accuracy of two national DEMs, with 5m and 10m resolutions, along with the ASTER and SRTM3 global DEMs. A dataset of 200 first-order GPS ground control points, that covers the Makkah (Mecca) metropolitan area in the western region of Saudi Arabia, has been utilized to judge the accuracy of these DEMs. The attained results showed that the 5-meter resolution national DEM is the most accurate one and produces mean height difference and standard deviations equal 0.01 ± 2.95 m respectively. That national DEM is more accurate by factors of 3 and 2 over the global ASTER and SRTM3 DEMs respectively. Recommendations have been drawn to apply each DEM in the geodetic, topographic mapping, and geomorphologic activities in Saudi Arabia.

REFERENCES

Abdeen, M. El-Kazzaz, Y., Attia, G., Yehia, M., and Hassan, S., 2009, Mapping geological structures in Wadi Ghoweiba area, northwest gulf of Suez, Egypt, using ASTER Spot data fusion and ASTER DEM, Egypt. Journal Remote Sensing and Space Sciences, v.12, pp. 101-126.

Abrams, M., Hook, S., and Ramachandran, B., 2008, ASTER user handbook: Version 2, Jet Propulsion Laboratory, Pasadena, CA, USA, 135 pp.

Bubenzer, O. and Bolten, A., 2008, The use of new elevation data (SRTM/ASTER) for the detection and morphometric quantification of Pleistocene megadunes (Draa) in the eastern Sahara and the southern Namib, Geomorphology, No. 102, pp. 221–231.

Dawod, G., 2008, Towards the redefinition of the Egyptian geoid: Performance analysis of recent global geoid and digital terrain models, Journal of Spatial Science, V. 53, No. 1, pp. 31-42.

Dawod, G., and Mohamed, W., 2009, Data management of different height systems within GPS/GIS integrated spatial technology, Middle East Spatial Technology Conference (MEST2009), December 7-9, Kingdom of Bahrain.

Denker, H., 2005, Evaluation of SRTM3 and GTOPO30 terrain data in Germany, The IAG International Symposium on Gravity, Geoid and Space Missions, V. 129, pp. 218-223.

Dixon, B. and Earls, J., 2009, Resample or not? Effects of resolution of DEMs in watershed modeling, Hydrological Processes, No. 23, pp. 1714–1724.

Dowerah, B., 2010, ASTER DEM based studies for geological investigation around Singhbhum Shear Zone (SSZ) in Jharkhand, India, Journal of Geographic Information System, No. 2, pp. 11-14.

El Bastawesy, M., 2007, Influence of DEM source and resolution on the hydrographical simulation of Wadi Keed catchment, Sinai, Egypt, Egypt. J. Remote Sensing and Space Sciences, V.10, pp. 53-62.

Hirt, C. Filmer, M., and Featherstone, W. 2010, Comparison and validation of the recent freely available ASTER-GDEM ver1, SRTM ver4.1 and GEODATA DEM-9S ver3 digital elevation models over Australia, Australian Journal of Earth Sciences, No. 57, pp. 337–347.

Kiamehr, R. and Sjöberg, L. E., 2005, Effect of the SRTM global DEM on the determination of a high-resolution geoid model: a case study in Iran, Journal of Geodesy, 2005, Volume 79, No. 9, pp.540-551.

Kiser, L. and Kelly, M., 2010, GPS- vs. DEM-derived elevation estimates from a Hardwood dominated forest watershed, Journal of Geographic Information System, No. 2, pp. 147-151.

Li, J. and Wong, D., 2010, Effects of DEM sources on hydrologic applications, Journal of Computers, Environment and Urban Systems, No. 34, pp. 251–261.

Mendas, A., 2010, The contribution of the digital elevation models and geographic information systems in a watershed hydrologic research, Applied Geomatics, No. 2, pp. 33–42.

Mousavi, S., Fallah, A., Abbasnejadc, R., Mousavi, S. R., and Shabani, M., 2007, The ASTER DEM generation for geomorphometric analysis of central Alborz mountains, Iran, Proceedings of the Asian Association of Remote Sensing Conference, Nov. 12-16, Kuala Lumpur, Malaysia.

Rodriguez, E., C.S. Morris, J.E. Belz, E.C. Chapin, J.M. Martin, W. Daffer, S. Hensley, 2005, An assessment of the SRTM topographic products, Technical Report JPL D-31639, Jet Propulsion Laboratory, Pasadena, California, USA, 143 pp.

Subyani, A., Qari, M., and Matsah, M., 2010, Digital elevation model and multivariate statistical analysis of morphometric parameters of some wadis, western Saudi Arabia, Arab Journal Geosciences, Published on line May 11.

USGS (U.S. Geological Survey), 1999, Map accuracy standards, USGS Fact Sheet 171-99, November, 3 pp.

ACKNOLWDGEMENTS

The authors would like to acknowledge the financial support offered by the Center of Research Excellence in Hajj and Omrah, Um Al-Qura university, Saudi Arabia.

Arab J Geosci (2013) 6:985–993
DOI 10.1007/s12517-011-0405-5

ORIGINAL PAPER

Assessment of several flood estimation methodologies in Makkah metropolitan area, Saudi Arabia

Gomaa M. Dawod · Meraj N. Mirza · Khalid A. Al-Ghamdi

Received: 26 February 2011 / Accepted: 18 September 2011 / Published online: 6 October 2011
© Saudi Society for Geosciences 2011

Abstract Estimation of floods in a hydrological basin is essential for efficient flood management and development planning. Several approaches have been proposed to estimate flood peak discharge based on topographic and morphometric characteristics of ungauged hydrological basins. Two global approaches, namely the rational and the curve number methods, along with four national regression models have been compared over Makkah metropolitan area, Saudi Arabia. The curve number methodology has been taken as the basis of comparison due to its precision and wide utilization. Results show that the rational method produces differences equal to 44% in terms of peak discharges. Moreover, the best national regression model gives difference in the order of 18% with respect to the curve number results. Other national models give results very far away from those of the curve number (up to 95%), which can be considered as measures for their awful accuracy. Hence, the curve number is recommended as an optimum methodology for flood estimation, in Makkah city, in case of availability of geological, metrological, land use, and topographic datasets. Otherwise, a specific national regression model (Al-Subai) may be utilized in a simple way.

Keywords Flood assessment · Rainfall–runoff models · Ungauged catchments · Saudi Arabia

G. M. Dawod
Survey Research Institute,
Giza, Egypt

M. N. Mirza
Center of Research Excellence in Hajj and Omrah,
Umm Al-Qura University,
Makkah, Saudi Arabia

K. A. Al-Ghamdi
Geography Department, Umm Al-Qura University,
Makkah, Saudi Arabia

Present Address:
G. M. Dawod (✉)
Umm Al-Qura University,
P.O. Box 715, Makkah 21955, Saudi Arabia
e-mail: dawod_gomaa@yahoo.com

Introduction

Hazards of flash floods are vital in terms of human lives loss and economical damages. Flash floods affect local residents in a dangerous way particularly in developing countries, and flood hazard maps should be available and updated (Hagen and Lu 2011). Economically speaking, floods produce significant financial loss so that a flood assessment model should include the estimation of economic damages (Hsu et al. 2011). Utilization of recent technologies, such as the geographic information systems (GIS) and remote sensing (RS), in developing flood hazard maps is gaining increasing attention in the last couple of decades (e.g., Forkuo 2011; Mouri et al. 2011; Parker et al. 2011; Dang et al. 2011; and Soussa et al. 2010). A reliable estimation of floods in a hydrological basin is crucial for efficient flood management and surface water resources planning. On a national level, a precise flood assessment is considered as an important demand in Makkah metropolitan area, Kingdom of Saudi Arabia (KSA) due to the unexpected nature of rainfall that often produces hazardous flash floods. It is worth mentioning that the southwest part of KSA contains almost 60% of the volume of wadi flow, particularly in the terrain situated between the Red Sea coast and the adjacent mountains (Nouh 2006). Extensive flood estimation studies have been carried out in KSA in

the last few years chiefly with the utilization of GIS and RS techniques (e.g., Dawod et al. 2011; Dawod and Koshak 2011; Al Saud 2010; and Metwaly et al. 2010).

It is economically costly and physically difficult to gauge all streams in a region, particularly in a large country such as KSA (Şen and Al-Suba'l 2002). For ungauged hydrological catchments, where measured flood discharge data records are missing, the flood estimation becomes more complicated. Countless approaches have been proposed globally trying to estimate flood peak discharge quantities based on topographic and morphometric characteristics of hydrological regions. Such approaches may be grouped into three categories: simple, medium, and complex models (Mihalik 2007). Simple hydrological models can produce estimates of flood peak discharge, and other hydrological quantities, fast and with little amount of required data. Rational and regression can be classified as simple models. Ordinary and other regression models have been utilized in hydrological modeling all over the world (e.g., Ishak et al. 2011; Liu et al. 2011; Subyani 2011; and Meddi et al. 2010). Medium hydrological models, e.g., the curve number approach, utilize more parameters in modeling the rainfall–runoff relationship. Complex models, e.g., the Soil and Water Assessment Tool, are able to identify the causes of problems rather than producing a simple description of overall conditions.

The rainfall–runoff relationship plays a fundamental role in many aspects of watershed management such as the determination of the available and sustainable water resources, the design of flood operations and protective measures, and drought management (Sen 2008b). On a national scale, some regression models have been developed to perform that task. For example, Şen and Al-Suba'l (2002) and Al-Subai (1992) have developed empirical formulas to model the precipitation–runoff relationship in the southwest region of KSA. However, understanding the nature and limitations of those estimation models is necessary before utilizing any specific method. This paper aims to present and justify some global and national models for estimating flood discharge in Makkah metropolitan area.

Flood estimation models

Simple flood estimation methods usually employ empirical relationships between rainfall and runoff that allow estimation of design discharges on ungauged watersheds by the development of parameters describing the watershed. Moreover, other models are presented in case of availability of measured discharge datasets such as ordinary regression, Bayesian regression, artificial neural networks, fuzzy logic, and genetic algorithms (e.g., Tayfur and Singh 2010; Kim and Lee 2010; Singh et al. 2010).

On a national level, some regression models have been developed in Saudi Arabia in order to compute flood discharge. Other methods have presented non-computational different approaches to accomplish this task, such as utilizing hydrographs (e.g., Sen 2008a) and geostatistical method (e.g., Subyani and Al-Dakheel 2009). However, only the computational methods are considered herein, and they are briefed in the next sections. It is a matter of reality that the accuracy of the input data in flood modeling seriously influences the precision of the estimated quantities (Moel and Aerts 2011).

General flood estimation models

There are countless hydrologic flood estimation methodologies that have been proposed in the last decades. In this paper, only two approaches are considered, namely the rational method and the U.S. National Resources Conservation Services (NRCS) method.

The rational method was first introduced in 1889. Although it is often considered simplistic, it still is appropriate for estimating peak discharges for small drainage areas of up to about 200 acres (80 ha) in which no significant flood storage appears. A main assumption in this method is that the rainfall is assumed uniform over the area of interest, which is a valid assumption for small areas (US TDoT 2009). The metric form of the rational method reads:

$$Q_p = C\,I\,A/360 \tag{1}$$

where,

- Q_p is the peak discharge (cubic meters per second)
- I is the rainfall intensity for the design storm (millimeters per hour)
- A is the drainage area (square kilometer), and
- C is a dimensionless runoff coefficient assumed to be a function of the cover of the watershed and often the frequency of the flood being estimated. Tables which provide values of this constant are provided in several hydraulic literatures (e.g., US DoT 2002).

It worth mentioning that Sen (2008b) reported that the estimation of the C value is difficult and is the major source of uncertainty in many water resources projects. This coefficient must account for all the significant factors affecting the peak flow to average rainfall intensity, not restricted to area and response time.

The NRCS, formerly known as the Soil Conservation Service (SCS), utilizes geological information to assign a unique curve number (CN) coefficient value for each area that will be further used to estimate the surface runoff depth and the peak discharge magnitude. The NRCS method is quite utilized in engineering design and flood management

Table 1 Coefficient discharge values of modified Talbot formula (after Quraishi and Al-Hassoun 1996)

Constant	Value	Usage
C_1	0.30	Mountainous areas
	0.20	Semi-mountainous areas
	0.10	Low land areas
C_2	0.50	$S>15\%$
	0.40	$10<S<15\%$
	0.30	$5<S<10\%$
	0.25	$2<S<5\%$
	0.20	$1<S<2\%$
	0.15	$0.5<S<1\%$
	0.10	$S<0.5\%$
C_3	0.30	$W=L$
	0.20	W=0.4 L
	0.10	W=0.2 L

S slope, *W* width, and *L* length of the drainage area

projects in several countries (e.g., Al-Jabari et al. 2009; Adebayo et al. 2009; Elaji 2010; Xianzhao and Jiazhu 2008; and Gul et al. 2009), and particularly in USA (e.g., US ACE 2004; US DoT 2002). The basic formulas of the NRCS approach are (e.g., US NRCS 1986):

$$Q = (P - 0.2S)^2/(P + 0.8S) \quad (2)$$

where,

Q=depth of direct runoff (millimeter)
P=depth of precipitation for a specific return period (millimeter)
S=maximum potential retention (millimeter):

$$S = 25.4((1,000/\mathrm{CN}) - 10) \quad (3)$$

where CN is the curve number. Tables which provide values of CN are presented in several hydraulic literatures (e.g., Sen 2008b, pp. 165).

$$\mathrm{qp} = \mathrm{qu}\,A\,Q \quad (4)$$

where,

qp=peak discharge (cubic meters per second)
A=drainage area (square kilometer)
Q=depth of runoff (millimeter)
qu=unit peak discharge (cubic meters per second per kilometer per millimeter) that can be interpolated from specific charts (e.g., US NRCS 1986) or computed from corresponding tables (e.g., US DoT 2002, pp. 5–28).

The time of concentration constitutes an important factor in flood assessment studies since it is the time required by runoff to travel from the most distant point to the basin's outlet point. There are several formulas to compute the concentration time; one of them is the NRCS equation which is given as:

$$\mathrm{tc} = 1.67\left[L^{0.8}(S+1)^{0.7}\right]/\left[1,900 \times \mathrm{SL}^{0.5}\right] \quad (5)$$

where L is the basin length (expressed in units of meters), tc is the concentration time (minutes), and SL is the average watershed land slope in percentage.

National flood regression models

Al-Subai (1992) has determined, from actual field measurements in the southwest part of KSA, that average peak discharge can be estimated for the Arabian Peninsula as the power relation of classic regression technique as (Sen 2008b, Eq. 4.33, pp. 135):

$$Q_p = 43\,A^{0:522} \quad (6)$$

where Q_p is the average discharge (cubic meters per second) of a given Area A (square kilometer).

The mean annual flood discharge for the wadi being considered has to be known in order to use the method, and empirical methods can also be applied to estimate this from catchment properties. Nouh 1987 has presented a regression formula based on data from 26 gauging stations in the southwest part of KSA:

$$\mathrm{MAF} = 0.365\,A^{0.83}\mathrm{ELEV}^{0.47} \quad (7)$$

where:

MAF is the mean annual flood peak discharge (cubic meters per second)
A is the catchment area (square kilometer), and
ELEV is the mean catchment elevation (meter).

It is worth to mention that another slightly different regression formula has been developed by Nouh (2006) similar to Eq. 7, but the geographic area includes the southwest KSA and Yemen.

Farquharson et al. (1992) also developed general relationships, which only depend on catchment area, for eight separate world regions using catchment area only, as follows:

$$\mathrm{MAF} = \mathrm{constant}\ A\ \mathrm{exponent} \quad (8)$$

Table 2 Design storm frequency factor of modified Talbot formula (after Quraishi and Al-Hassoun 1996)

Frequency in years	F_f
5	0.60
10	0.80
25	1.00
50	1.20
100	1.40

In Saudi Arabia and Yemen, the developed formula is (Steenbergen 2010):

$$\mathrm{MAF} = 0.991\,A^{0.701} \tag{9}$$

Quraishi and Al-Hassoun (1996) reported a method called modified Talbot that is used in the Saudi Ministry of Communication on a national level. The basic modified Talbot formula is:

$$Q_{\mathrm{p}} = K\,C\,A^{n}R_{\mathrm{f}}F_{\mathrm{f}} \tag{10}$$

where,

- K is a constant which has values of 0.557, 3.561, and 10.166 for medium, large, and regional watersheds, respectively. The catchment area categories are: medium for size 400–1,258 ha, large for size 1,258–35,944 ha, and regional for size more than 35,944 ha
- A is the drainage area in hectares
- N is an exponent which depends on the size of the drainage area, and has values of 0.75, 0.50, and 0.40 for medium, large, and regional watersheds, respectively.
- C is a coefficient of discharge which was suggested to be the summation of C_1, C_2, C_3, where C_1 is the coefficient of terrain condition, C_2 is the coefficient of slope of drainage area, and C_3 is the coefficient of shape of drainage area. Table 1 shows the values of these constants.
- R_{f} is a rainfall factor suggested to be 1.5 for medium watersheds and 1.4 for both large and regional watersheds.
- F_{f} is a frequency factor which depends on the desired storm frequency, and is shown in Table 2.

Study area and available data

Makkah city is located in the southwest part of KSA, about 80 km east of the Red Sea (Fig. 1). It extends from 39° 35′ E to 40° 02′ E and from 21° 09′ N to 21° 37′ N. The area of the metropolitan region (the study area) equals 1,593 km^2 approximately. The topography of Makkah is complex in nature, and several mountainous areas exist inside its metropolitan area. Winter is considered as the main rainy season in Saudi Arabia. The annual rain over Makkah city, for a period extending from 1966–2009, varies from 3.8 to 318.5 mm, with an average of rainfall

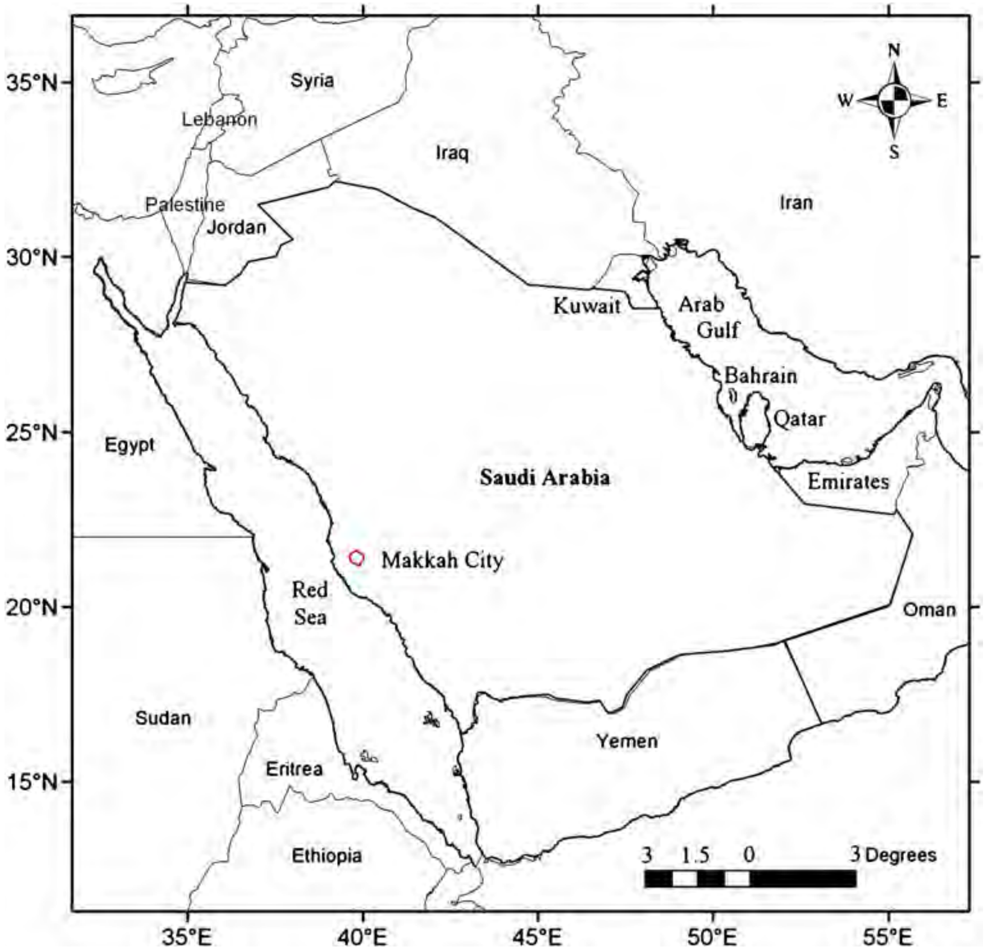

Fig. 1 Study area

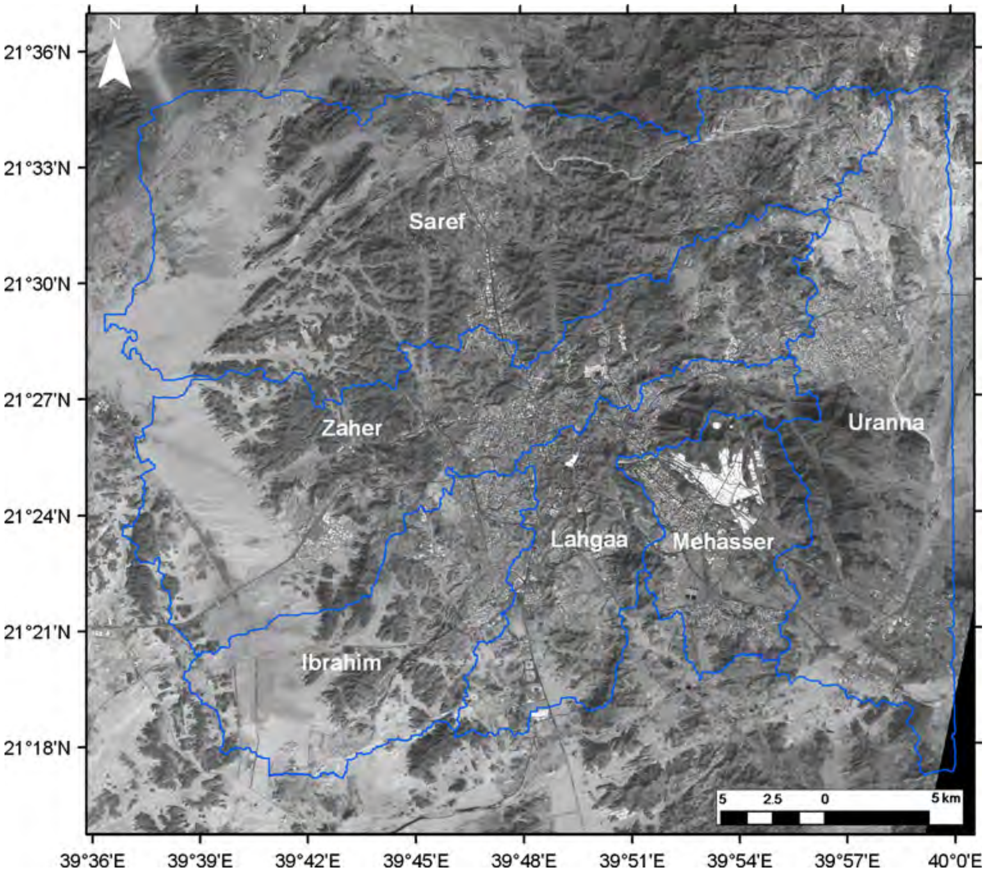

Fig. 2 The main basins in Makkah metropolitan area

equal to 101.2 mm (Mirza et al. 2011a). Due to the complexity of Makkah's topography, flash floods occur periodically with significant variations in magnitude. The rain intensity in a single extreme storm may exceed the annual rain average in that year.

Several datasets have been collected for the cause of flood assessment. The main data piece is a digital elevation model (DEM) for the study area. The acquired DEM produced by the by King Abdulaziz City of Sciences and Technology had a spatial resolution of 5 m. A window covering Makkah metropolitan area has been provided through the Center of Research Excellence in Hajj and Umrah, Umm Al-Qura University. Mirza et al. (2011b) confirm that that national DEM is three times more accurate than published global DEMs. The other collected datasets include digital geological, soil, and land use maps of the study area. The Arc GIS software has been utilized to delineate the main catchments in Makkah based on the available DEM (Dawod et al. 2011). Six main basins are identified whose area ranges from 74.3 to 360.6 km^2, and lengths of their main streams vary from 16.50 to 48.55 km (Fig. 2). Table 3 presents statistics of some hydrological parameters of these catchments. A comprehensive GIS-based morphometric analysis of these basins has been carried out (Koshak and Dawod 2011).

Table 3 Statistics of morphometric quantities

Item	C1	C2	C3	C4	C5	C6
Basin area (km^2)	252.7	122.3	74.3	109.9	360.6	200.2
Basin premier (km)	134.6	69.13	50.23	89.09	134.76	102.03
Length of main stream (km)	42.48	23.64	16.50	29.70	48.55	38.13
Relief ratio (m/km)	12.6	14.1	40.4	25.9	13.0	18.7

C1 Zaher wadi, *C2* Ibrahim wadi, *C3* Mehasser wadi, *C4* Lahgaa wadi, *C5* Sareef wadi, *C6* Uranna wadi

Table 4 NRCS flood results (for a 10-year return period)

Item	C1	C2	C3	C4	C5	C6
Time of concentration (h)	6.00	4.00	1.98	3.24	2.51	4.60
CN	84	84	93	89	84	83
Runoff depth (mm)	71.5	71.5	94.2	83.7	71.5	69.2
Peak discharge (m^3/s)	733	501	689	620	2,116	705

Table 5 Rational flood results (for a 10-year return period)

Item	C1	C2	C3	C4	C5	C6
Peak discharge (m^3/s)	642	311	189	279	916	508
Difference to NRCS-based peak discharge (m^3/s)	91	190	500	341	1,200	196
Difference percentage to NRCS-based peak discharge	12%	38%	73%	55%	57%	28%
Difference mean percentage	44%					

Table 7 Nouh's model flood results

Item	C1	C2	C3	C4	C5	C6
Mean catchment elevation (ELEV in m)	278	225	460	324	289	395
Peak discharge (m^3/s)	507	251	207	273	694	493
Difference to NRCS-based peak discharge (m^3/s)	226	250	481	347	1,422	212
Difference percentage to NRCS-based peak discharge	31%	50%	70%	56%	67%	30%
Difference mean percentage	51%					

Accomplished results

The recent extensive utilization of the NRCS method on a global basis (e.g., Reshma et al. 2010; Ebrahimian et al. 2009; Soussa et al. 2010) has led the authors of the current paper to believe that it may be considered as an optimum tool for estimating flood discharge for ungauged hydrological basins. Consequently, this method is considered as a base of comparison to the other investigated hydrological methods. The NRCS method has been performed for the available data of Makkah metropolitan area to compute the peak discharge value for the six basins. The return period has been chosen, herein, as 10 years, for which the rainfall intensity has been estimated, by applying the Log Pearson III statistical analysis, as 114.3 mm/h. Similar results have been reported for Makkah city (MPWH 2001). Based on the geological, soil, and land use characteristics, the curve number (CN) has been estimated for the study area catchments. Table 4 presents the results of the NRCS method.

Secondly, the rational method has been performed using appropriate values of the runoff coefficients C (Eq. 1). The *C* coefficient ranges from 0.05 to 0.95 based on land use, soil, and geology of the concerned regions. A detailed classification of these values can be found in several flood analysis literature (e.g., US ACE 1994, pp. 11–2). In the current research, the *C* value has been taken as 0.8 since the majority of the Makkah metropolitan area constitutes paved-street residential areas. Then, the achieved results have been compared to those of the NRCS method. Table 5 presents the accomplished results. It can be noticed that the overall agreement between the NRCS and rational methods is 45% only. That is expected due to the assumption behind the rational method, which is the equal distribution of rainfall over all the catchment areas. As mentioned earlier, the rational method is valid only for small basins with about 1 km^2 in area.

Thirdly, the national regression models have been carried out to compute peak discharge quantities in Makkah metropolitan area. Al-Subai's model (Eq. 6) is computed for the six hydrological catchments and then compared to the NRCS results (Table 6). It can be noticed that the overall differences agreement with the NRCS method reaches 18%, which means that this model produces 82% of the NRCS-based peak discharges in the study area. Recall that this model has been developed for the southwest region of KSA, where the study area is located.

Next, the Nouh's formula (Eq. 7) has been utilized in the same manner (Table 7). The mean catchment elevation has been obtained from the DEM using the Arc GIS software. It can be noticed that the overall differences agreement with the NRCS method reaches 51%, which means that this model produces 49% of the NRCS-based peak discharges in the study area. It should be considered that the results of this model are in a mean scene as stated in Eq. 7.

Next, Farquharson's model (Eq. 9) has been performed and, as usual, was compared to the NRCS results (Table 8). It can be seen that the general differences agreement with the NRCS method reaches 95%, which means that this model produces only 5% of the NRCS-based peak discharges in the study area. Such extraordinary results are due to the fact that this model covers a huge geographic

Table 6 Al-Subai's model flood results (for a 10-year return period)

Item	C1	C2	C3	C4	C5	C6
Peak discharge (m^3/s)	772	529	408	500	929	684
Difference to NRCS-based peak discharge (m^3/s)	−39	−27	281	120	1,176	21
Difference percentage to NRCS-based peak discharge	−5%	−5%	41%	19%	56%	3%
Difference mean percentage	18%					

Table 8 Farquharson's model flood results

Item	C1	C2	C3	C4	C5	C6
Peak discharge (m^3/s)	48	29	20	27	61	41
Difference to NRCS-based peak discharge (m^3/s)	685	472	668	593	2,055	664
Difference percentage to NRCS-based peak discharge	93%	94%	97%	96%	97%	94%
Difference mean percentage	95%					

Table 9 Modified Talbot's model flood results

Item	C1	C2	C3	C4	C5	C6
Peak discharge (m^3/s)	444	309	309	334	606	395
Difference to NRCS-based peak discharge (m^3/s)	289	192	379	285	1,510	310
Difference percentage to NRCS-based peak discharge	39%	38%	55%	46%	71%	44%
Difference mean percentage	49%					

area (Saudi Arabia and Yemen) utilizing only 26 gauge stations in its development, which in turns makes it impractical in nature.

Lastly, the modified Talbot model (Eq. 10) has been carried out and again compared to the NRCS results (Table 9). It can be noticed that the general differences agreement with the NRCS method reaches 49%, which means that this model produces only 51% of the NRCS-based peak discharges in the study area. Similar results have been reported by Quraishi and Al-Hassoun (1996).

As a conclusion, Table 10 presents a brief comparison of all the test models. Clearly, it can be concluded that Al-Subai's regression model is the closer method to the NRCS approach. On the other hand, it is obvious that Farquharson's regression model produces results very far from those of the NRCS hydrologic methodology.

Conclusions

Rainfall–runoff modeling plays a vital role in several watershed management phases, particularly for the determination of the available and sustainable water resources and for flood management. The southwest part of KSA contains almost 60% of the volume of wadi flow, and hence, precise flood assessment is important in planning and development. There are a lot of flood modeling approaches at hand, and their simplicity and accuracy are significantly different. This study has examined two global flood modeling approaches, namely the rational and SCS methodologies.

Table 10 Summary of all flood estimation models

Model	Percent of produced discharge as compared to the NRCS method (%)
NRCS	NA
Rational	56
Al-Subai	82
Nouh	49
Farquharson	5
Talbot	51

On a national levels, some regression models have been developed in Saudi Arabia in order to compute flood discharge. Other methods have presented non-computational different approaches to accomplish this task, such as utilizing hydrographs and geostatistical method. Four regression models have been also justified in the current research to compute flood discharge in Makkah metropolitan area based on the available precise datasets. The curve number methodology has been taken as the basis of comparison due to its precision and wide utilization in engineering and environmental projects in several countries. The accomplished results show that the rational method produces differences equal to 44% in terms of peak discharges. That is expected due to the assumption behind the rational method, which is the equal distribution of rainfall over all the catchment areas. Previous hydrological studies recommended this approach only for estimating peak discharges in small drainage areas of up to about 200 acres (80 ha).

Regarding the national flood regression models, it has been found that Al-Subai, Nouh, Farquharson, and the modified Talbot methods provide peak discharge values that equal 82%, 49%, 5%, and 51%, respectively, with respect to the curve number results. These differences may be attributed to the fact that the accuracy of the input data in flood modeling greatly affects the precision of the computed output. Furthermore, it can be obviously realized that the catchment C3 (Mehasser wadi) produced almost the biggest difference in the utilized national regression models. That can be attributed to the fact that these models depend only upon the catchment area and its mean elevation, and ignore all other topographic and morphometric characteristics of the basin. Mehasser wadi, even though it is the smallest wadi in terms of area, has specific natural properties that make it the most dangerous basin in Makkah city. For example, its terrain slope (relief ratio in Table 3) is the maximum one in this area that extensively increases the hazards of flash floods. That is an important conclusion since this basin covers the holy shrines (Mina and Muzdalifa), in which millions of Muslims are gathered for few days during the pilgrim (Hajj) seasons.

It is concluded that Al-Subai's model is the most precise national hydrological model in Makkah area. This is due to the fact that this model has been developed based on actual precise field measurements in the southwest part of KSA. The other national empirical function aimed to estimate annual flood peak discharge in a mean sense. However, in case of availability of topographic, metrological, land use, and geological datasets, the curve number method should be considered as the optimum flood modeling approach.

Acknowledgments The authors would like to acknowledge the financial support offered by the Center of Research Excellence in Hajj and Umrah (Hajjcore), Umm Al-Qura University, Makkah, Saudi Arabia.

References

Adebayo W, Solomon O, Ayanniyi M, Sikiru F (2009) Evaluation of synthetic unit hydrograph methods for the development of design storm hydrographs for rivers in South-West, Nigeria. Journal of American Science 5(4):23–32

Al-Jabari S, Abu Sharakh M, Al-Mimi Z (2009) Estimation of runoff for agricultural watershed using SCS curve number and GIS. Proceedings of the Thirteenth International Water Technology Conference, Hurghada, Egypt, pp. 1213–1229

Al Saud M (2010) Assessment of flood hazard of Jeddah area 2009, Saudi Arabia. Journal of Water Resource and Protection 2:839–847

Al-Subai K (1992) Erosion-sedimentation and seismic considerations to dam sitting in the central Tihamat Asir region. Ph.D dissertation, Faculty of Earth Science, King Abdulaziz University, Saudi Arabia

Dang N, Babel M, Luong H (2011) Evaluation of food risk parameters in the Day River flood diversion area, Red River delta, Vietnam. Natural Hazards 56:169–194

Dawod G, Koshak N (2011) Developing GIS-based unit hydrographs for flood management in Makkah metropolitan area, Saudi Arabia. J Geogr Inf Syst 3(2):153–159

Dawod G, Mirza M, Al-Ghamdi K (2011) GIS-based spatial mapping of flash flood hazards in Makkah city, Saudi Arabia. J Geogr Inf Syst 3(3):217–223

Ebrahimian M, See L, Abdul Malek I (2009) Application of Natural Resources Conservation Service—curve number method for runoff estimation with GIS in the Kardeh watershed, Iran. Eur J Sci Res 34(4):575–590

Elaji A (2010) Applications of Geographic Information Systems to construct databases of morphometric characteristics and their hydrologic meanings in Yalamlam basin (in Arabic). MSC thesis, Umm Al-Qura University, Makkah, Saudi Arabia

Farquharson K, Meigh R, Sutcliffe V (1992) Regional flood frequency analysis in arid and semi-arid areas. J Hydrol 138 (3–4):487–501

Forkuo E (2011) Flood hazard mapping using Aster image data with GIS. International Journal of Geomatics and Geosciences 1(4):932–950

Gul G, Harmancıoglu N, Gul A (2009) A combined hydrologic and hydraulic modeling approach for testing efficiency of structural flood control measures. Natural Hazards 54(2):245–260. doi:10.1007/s11069-009-9464-2

Hagen E, Lu X (2011) Let us create flood hazard maps for developing countries. Natural Hazards 58:841–843

Hsu W, Huang P, Chang C, Chen C, Hung D, Chiang W (2011) An integrated flood risk assessment model for property insurance industry in Taiwan. Natural Hazards 58:1295–1309

Ishak E, Haddad K, Zaman M, Rahman A (2011) Scaling property of regional floods in New South Wales, Australia. Natural Hazards. doi:10.1007/s11069-011-9719-6

Kim S, Lee K (2010) Regional low flow frequency analysis using Bayesian regression and prediction at ungauged catchment in Korea. KSCE J Civ Eng 14(1):87–98

Koshak, N. and Dawod, G. (2011) A GIS morphometric analysis of hydrological basins for flood management within Makkah Metropolitan Area, Saudi Arabia. International Journal of Geomatics and Geosciences (in press)

Liu Y, Chen Z, Wang J, Xu S, Hu B (2011) Fifty-year rainfall change and its effect on droughts and floods in Wenzhou, China. Natural Hazards 56:131–143

Meddi M, Assani A, Meddi H (2010) Temporal variability of annual rainfall in the Macta and Tafna catchments, Northwestern Algeria. Water Resour Manag 24:817–3833

Metwaly M, El-Awadi E, Al-Arifi N (2010) Flooding risk analysis of the central part of western Saudi Arabia using remote sensing data. Proceedings of the Fifth National GIS Symposium in Saudi Arabia, Al-Khobar, April 26–28

Mihalik E (2007) Watershed characterization and runoff modelling of the Chapel Branch Creek, Orangeburg county, South Carolina. MSC thesis, College of Charleston, USA

Mirza M, Dawod G, Al-Ghamdi K (2011a) Assessment of flood hazards on road network in Makkah city and holly areas using a 3D GIS (in Arabic), Un-published technical report, Center of research excellence in Hajj and Omrah, Umm Al-Qura University, Makkah, Saudi Arabia

Mirza M, Dawod G, Al-Ghamdi K (2011b) Accuracy and relevance of digital elevation models for geomatics applications—a case study of Makkah municipality, Saudi Arabia. International Journal of Geomatics and Geosciences 1(4):803–812

MPWH (Saudi Ministry of Public Works and Housing) (2001) Storm water drainage system for Muzdalifa and Arafat areas, Unpublished technical report, December 2001

Moel H, Aerts J (2011) Effect of uncertainty in land use, damage models and inundation depth on flood damage estimates. Natural Hazards 58:407–425

Mouri G, Kanae S, Oki T (2011) Long-term changes in flood event patterns due to changes in hydrological distribution parameters in a rural–urban catchment, Shikoku, Japan. Atmos Res. doi:10.1016/j.atmosres.2011.02.002

Nouh M (1987) A comparison of three methods for regional flood frequency analysis in Saudi Arabia. Water Resour 10:212–219

Nouh M (2006) Wadi flow in the Arabian Gulf states. Hydrolog Process 20:2393–2413

Parker D, Priest S, McCarthy S (2011) Surface water flood warnings requirements and potential in England and Wales. Appl Geogr 31:891–900

Quraishi A, Al-Hassoun S (1996) Use of Talbot formula for estimating peak discharge in Saudi Arabia. Journal of King Abdulaziz University–Engineering Sciences 8:73–85

Reshma T, Kumar P, Babu M, Kumar K (2010) Simulation of runoff in watersheds using SCS-CN and Muskingum-Cunge methods using remote sensing and geographical information systems. International Journal of Advanced Science and Technology 25:31–42

Şen Z, Al-Suba'l K (2002) Hydrological considerations for dam siting in arid regions: a Saudi Arabian study. Hydrol Sci J 47(2):173–186

Şen Z (2008a) Modified hydrograph method for arid regions. Hydrolog Process 22:356–365

Şen Z (2008b) Wadi hydrology. CRC Press, New York

Singh K, Pal M, Singh V (2010) Estimation of mean annual flood in Indian catchments using back-propagation neural network and m5 model tree. Water Resour Manag 24:2007–2019

Soussa H, El Feel A, Alfy S, Yousif M (2010) Flood hazard in wadi Rahbaa area, Egypt. Arabian Journal of Geosciences. doi:10.1007/s12517-010-0144-z

Steenbergen F (ed) (2010) Guidelines on spate irrigation, FAO (Food and Agriculture Organization of the United Nations) irrigation and drainage paper 65. Food and Agriculture Organization of the United Nations, Rome

Subyani A, Al-Dakheel A (2009) Multivariate geostatistical methods of mean annual and seasonal rainfall in southwest Saudi Arabia. Arab Journal of Geosciences 2. doi:10.1007/s12517-008-0015-z

Subyani A (2011) Hydrologic behavior and flood probability for selected arid basins in Makkah area, western Saudi Arabia. Arab J Geosci 4:817–824

Tayfur G, Singh V (2010) Predicting mean and bankfull discharge from channel cross-sectional area by expert and regression methods. Water Resour Manag. doi:10.1007/s11269-010-9741-6

US ACE (US Army Corps of Engineers) (1994) Flood-runoff analysis manual. United States Army Corps of Engineers. Davis, California, USA.

US ACE (US Army Corps of Engineers) (2004) Physical stream assessment. United States Army Corps of Engineers. Davis, California, USA.

US DoT (US Department of Transportation) (2002) Highway hydrology manual, Publication No. FHWA-02-001.

US NRCS (US National Resources Conservation Services) (1986) Urban hydrology for small watersheds, Technical Manual TR55.

US TDoT (US Texas Department of Transportation) (2009) Hydraulic design manual.

Xianzhao L, Jiazhu L (2008) Application of SCS model in estimation of runoff from small watershed in Loess plateau of China. Chin Geogr Sci 18(3):235–241

Journal of Geographic Information System, 2011, 3, 153-159
doi:10.4236/jgis.2011.32012 Published Online April 2011 (http://www.SciRP.org/journal/jgis)

Developing GIS-Based Unit Hydrographs for Flood Management in Makkah Metropolitan Area, Saudi Arabia

Gomaa M. Dawod[1,2], Nabeel A. Koshak[3]
[1]*Survey Research Institute, Giza, Egypt*
[2]*Umm Al-Qura University, Makkah, Saudi Arabia*
[3]*Center of Research Excellence in Hajj and Omrah, Umm Al-Qura University, Makkah, Saudi Arabia*
E-mail: *dawod_gomaa@yahoo.com*, *nakoshak@uqu.edu.sa*
Received March 6, 2011; *revised March* 31, 2011; *accepted April* 2, 2011

Abstract

Unit hydrographs (UH) are either determined from gauged data or derived using empirically-based synthetic unit hydrograph procedures. In Saudi Arabia, the discharge records may not be available either for several locations or for long time scales, and therefore synthetic unit hydrographs are crucial in flood and water resources management. Available metrological, geological, and land use datasets have been utilized in order to apply the US National Resources Conservative Services (NRCS) methodology in a Geographic Information Systems (GIS) environment. Furthermore, NRCS unit hydrographs have been developed for six watersheds within Makkah metropolitan area, southwest Saudi Arabia. The accomplished results show that the UH time to peak discharge vary from 1.15 hours to 4.47 hours, and the UH peak discharge quantities range from 10.14 m^3/s to 16.74 m^3/s. It is concluded that the third basin in Makkah city may be considered as the most hazardous catchment. Hence, it is recommended that careful flood protection procedures should be taken in this area within Makkah city.

Keywords: GIS, Unit Hydrograph, NRCS, Flood Management, Saudi Arabia

1. Introduction

Flood modeling usually involves approximate descriptions of the rainfall-runoff transformation processes, based on empirical, or physically-based, or combined descriptions of the physical processes involved. The resulting models are quite useful in practice since they are simple and provide adequate estimates of flood hydrographs. Sherman [1] first proposed the unit hydrograph (UH) concept. The UH of a watershed is defined as the direct runoff hydrograph resulting from a unit volume of excess rainfall of constant intensity and uniformly distributed over the drainage area. The UH approach is applied for several engineering designs and environmental studies [2,3] Detailed descriptions of UH types and formulas can be found in several literatures [4,5]. Moreover, the Geographic Information Systems (GIS) technology has been applied for flood management based on utilizing unit hydrographs [6-8].

2. Objectives

The current research study aims to:

- Utilize the unite hydrograph approach for flood characterizing in Makkah city, Saudi Arabia.
- Compute the requited quantities of unit hydrographs for six hydrological basins within the study area.
- Apply the US National Resources Conservative Service (NRCS) methodology to develop unit hydrographs, for the first time in Saudi Arabia.
- Perform flood assessment computations within a GIS environment as a precise, effective, and fast technological tool.

3. Previous Works

Sets of observations of effective rainfall and direct runoff are required for the derivation of unit hydrographs. When no direct observations are available, or when UH's for other locations on the stream in the same watershed or for nearby watersheds of similar characteristics are required, Synthetic, or conceptual, Unit Hydrograph (SUH) procedures must be used [9]. SUH procedures can be categorized as [10]: 1) those based on models of watershed storage; 2) those relating hydrograph characteristics

Copyright © 2011 SciRes.

to watershed characteristics [11]; and 3) those based on a dimensionless unit hydrograph [12,13].

In Kingdom of Saudi Arabia (KSA) the Snyder UH is the most common method in a variety of geomorphologic and flood literatures [14,15]. However, a crucial issue in this model is the existence of two parameters (namely: C_t a coefficient represents variations in watershed slopes and storage characteristics; and C_p a coefficient represents the effects of retention and storage) that need to be determined from actual observations for the specific watershed or can be taken from some other watersheds that have similar topographic and morphometric characteristics. Hence, empirical approach is suggested as an alternative for constructing a dimensionless UH for ungauged basins in southwest region of KSA [16,17]. The Soil Conservative Service (SCS) method is seldom utilized, particularly in few academic studies in KSA [18].

4. Materials and Methods

4.1. NRCS Hydrographs' Method

The National Resources Conservative Service (NRCS), formally SCS, UH approach represents an optimum dimensionless UH method, that are extensively utilized in the last few years in several countries [19-22]. The NRCS dimensionless UH was developed based on an extensive analysis of measured data for a large number of actual watersheds and then made dimensionless by dividing all discharge ordinates by the peak discharge and the time ordinates by the time to peak. The time base of the dimensionless UH was approximately 5 times the time to peak, and approximately 3/8 of the total volume occurred before the time to peak; the inflection point on the recession limb occurs at approximately 1.7 times the time to peak, and the UH has a curvilinear shape [23]. The discharge ratios for selected values of the time ratios are given in **Table 1**.

The mathematical formulas of the requited parameters, to construct the NRCS UH for watersheds, are:

$$qp = qu\ A\ Q \tag{1}$$

where,

qp = peak discharge (m^3/s)

A = drainage area (km^2)

Q = depth of runoff (mm)

qu = unit peak discharge ($m^3/s/km^2/mm$) that can be interpolated from a specific charts (e.g. NRCS, 1986) or computed from corresponding tables [23, pp. 5-28].

The time of concentration, tc, is the time needed for a drop of water to move from the most distant point in the watershed to the design point downstream (taken as the basin outlet in the current study). There are numerous

Table 1. Some ratios for NRCS dimensionless UH.

Time Ratio t/T_p	Discharge Ratio q/q_p	Time Ratio t/T_p	Discharge Ratio q/q_p
0	0.000	0.9	0.990
0.1	0.030	1.0	1.000
0.2	0.100	1.5	0.680
0.3	0.190	2.0	0.280
0.4	0.310	3.0	0.055
0.5	0.470	3.6	0.021
0.6	0.660	4.0	0.011
0.7	0.820	4.5	0.005
0.8	0.930	5.0	0.000

After [23, p. 6-59].

empirical equations to calculate tc, such as: Jaton formula [24], kirpich formula [25], and kirpich/Ramser formula [8]. However, the NRCS formula for time of concentration [18] is given by [26, pp. 3-9]:

$$tc = 1.67\left[L^{0.8}\left(S+1\right)^{0.7}\right]\Big/\left[1900 * SL^{0.5}\right] \tag{2}$$

where,

tc = concentration time (minutes),

L = length of basin main stream (feet)

SL = average watershed land slope in percentage.

$$Q = \left(P - 0.2S\right)^2 \Big/ \left(P + 0.8S\right) \tag{3}$$

where,

Q = depth of direct runoff (mm)

P = depth of precipitation for a specific return period (mm)

S = maximum potential retention (mm):

$$S = 25.4\left(\left(1000/\text{CN}\right) - 10\right) \tag{4}$$

where CN is the curve number, a coefficient determined based on geological, soil, and land use properties for each basin.

4.2. Materials

Makkah city is located in the south-west part of KSA, about 80 Km east of the Red Sea (**Figure 1**). It extends from 39˚35'E to 40˚02'E, and from 21˚09'N to 21˚37'N. The area of the metropolitan region (the study area) equals 1593 square kilometers approximately. The topography of Makkah is complex in nature, and several mountainous areas exist inside its metropolitan area. The winter is considered as the main rainy season in Saudi Arabia. The annual rain over Makkah city, for a period

Copyright © 2011 SciRes.

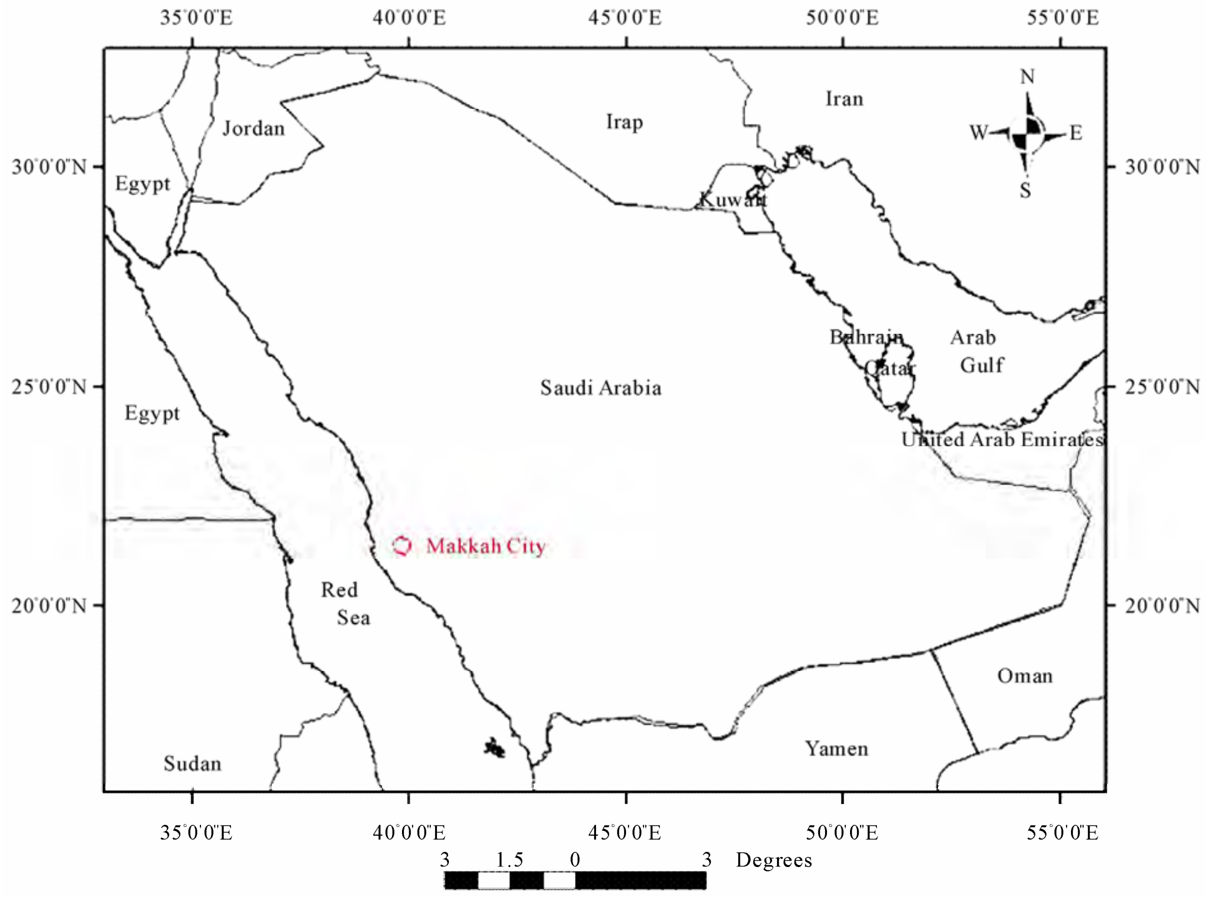

Figure 1. Study area.

extends from 1966 to 2009, varies from 3.8 mm to 318.5 mm, with an average of rainfall equals 101.2 mm. Due to the complexity of Makkah's topography, flash floods occurs periodically with significant variations in magnitude [27]. The rain intensity in a single extreme storm may exceed the annual rain average in that year.

Several datasets have been collected for the cause of flood assessment. The main data set, of the current study, is a Digital Elevation Model (DEM) for the study area. The acquired DEM produced by the by King Abdulaziz City of Sciences and Technology (KACST) with a spatial resolution equals 5 meters. A window covers Makkah metropolitan area has been provided through the Center of Excellence in Hajj and Omrah, Umm Al-Qura university. Mirza *et al.* [28] confirm that that national DEM is 3 times more accurate than published global DEMs (ASTER and SRTM 3). The other collected datasets include digital geological, soil, and land uses maps of the study area. The Arc GIS v.10 software has been utilized, in the current study, to delineates the main catchments in Makkah based on the available DEM. Six main basins are identified those area ranged from 74.3 to 360.6 square kilometers, and lengths of their main streams vary from 16.50 to 48.55 kilometers (**Figure 2**). **Table 2** presents statistics of some accomplished hydrological parameters of these catchments.

5. Results

Dawod *et al.* [29] computed CN, runoff depth, peak discharge, and time of concentration for the six basins in Makkah metropolitan area. In that study, a GIS-based methodology has been developed for quantifying and spatially mapping the flood characteristics. The core of that approach is integrating several topographic, metrological, geological, and land use datasets in a GIS environment that utilizes the NRCS method of flood modelling for ungauged arid catchments. The computations have performed using the depth of precipitation (P) equals 200 mm for a return period of 50 years. Additionally, the calculations of flood quantities, such as depth and volume of runoff (Equations 3 and 4), were performed in the attribute tables of GIS layers, in order to assemble all results in the same environment. **Table 3** presents these quantities.

The NRCS UH methodology, as described above, has

Copyright © 2011 SciRes.

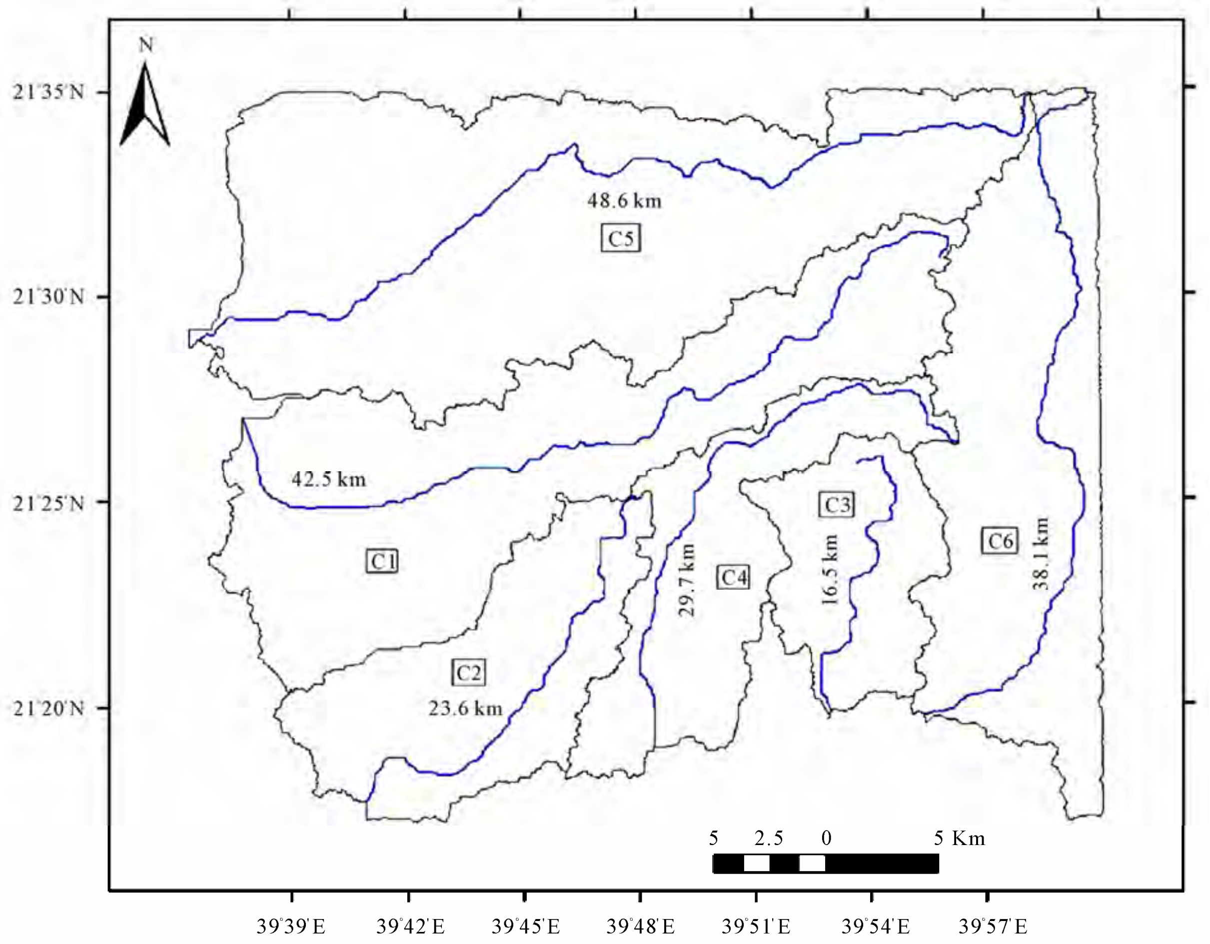

Figure 2. Catchments and their main streams in Makkah.

Table 2. Statistics of morphometric quantities.

Item	C1	C2	C3	C4	C5	C6
Basin Area (km^2)	252.7	122.3	74.3	109.9	360.6	200.2
Basin Premier (km)	134.6	69.13	50.23	89.09	134.76	102.03
Length of Main Stream (km)	42.48	23.64	16.50	29.70	48.55	38.13

Table 3. NRCS-based hydrological results in the study area.

Item	C1	C2	C3	C4	C5	C6
CN	84	84	93	89	84	83
Time of concentration (hours)	5.69	3.76	1.73	2.63	6.72	4.17
Runoff depth (mm)	152	152	179	167	152	149
Peak discharge (m3/s)	1554	1063	1307	1234	4489	1514

been applied, for the first time in Saudi Arabia, for the six watersheds of Makkah metropolitan area. The accomplished results are presented in **Table 4** and depicted in **Figure 3**. It can be seen that the elapsed time from rainfall start to peak discharge vary from 1.15 hours (in catchment C3) to 4.47 hours (for catchment 6). Secondly, it has been found that the UH peak discharge quantities range from 10.14 m^3/s (for catchment 2) to 16.74 m^3/s

Copyright © 2011 SciRes.

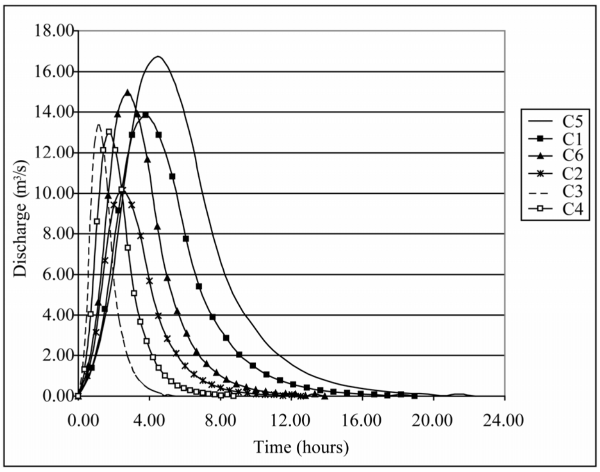

Figure 3. NRCS Unit Hydrographs of Makkah' Catchments.

(for catchment 5). Furthermore, the total runoff time varies from 5.75 hours (for catchment 3) to 22.34 hours (for catchment 5). The same results can be visualized graphically from **Figure 3**.

Moreover, a correlation analysis has been performed between the main morphometric and NRCS UH parameters of the six basins. The results (**Table 5**) showed that the basin area, with a positive correlation equaling to 0.74, is the most effective element that influences the UH peak discharges. In addition, the time of concentration also resulted in moderate positive correlation values, 0.55.

6. Discussion

Results in **Table 4** indicate that the smallest elapsed time is 1.15 hours (in catchment C3). Recall from **Table 3**,

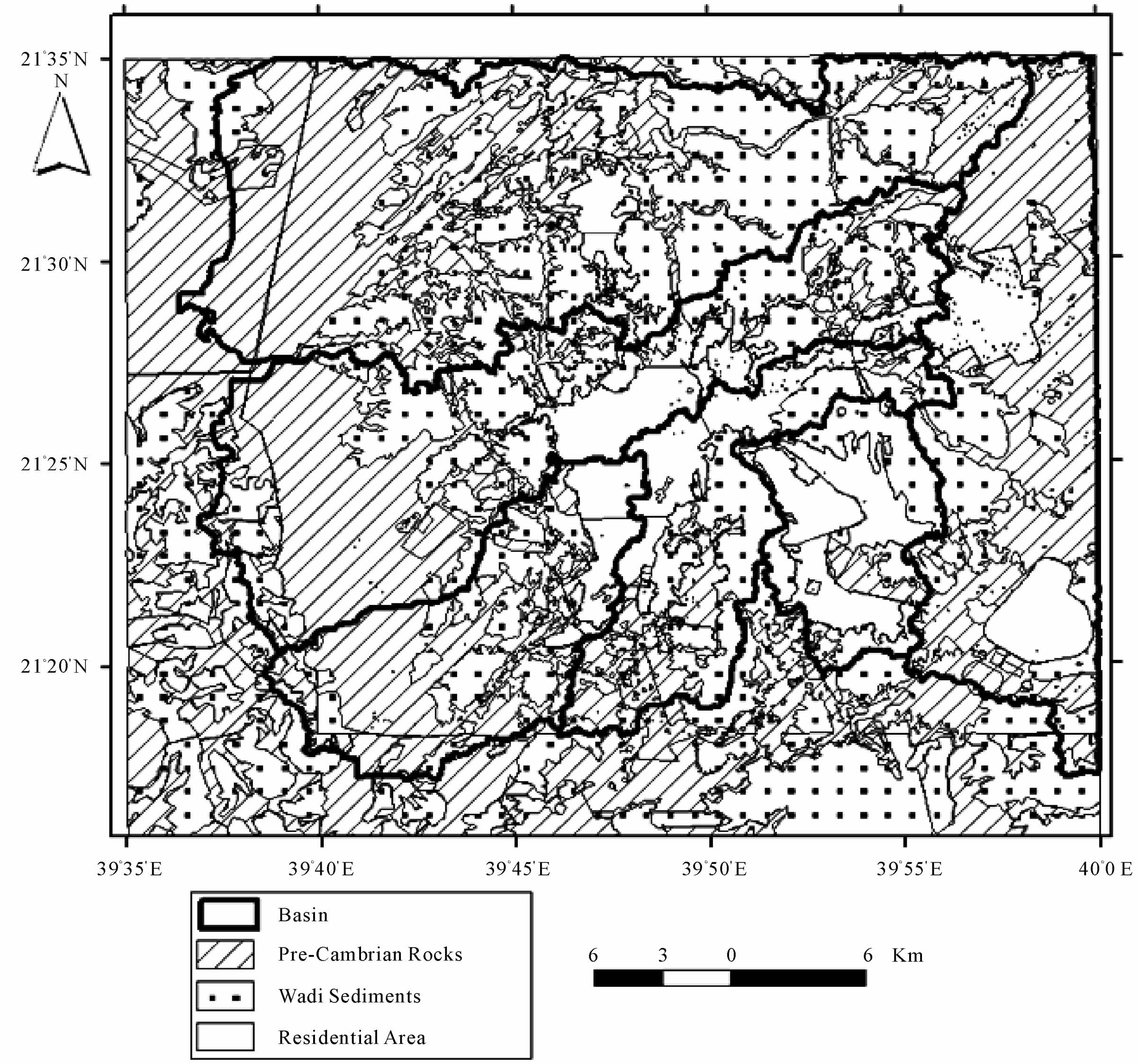

Figure 4. Geology and land use of Makkah' catchments.

Table 4. NRCS UH quantities for Makkah' catchments.

Item	C1	C2	C3	C4	C5	C6
Time to Peak (hours)	3.78	2.50	1.15	1.75	4.47	2.78
UH Peak discharge (m^3/s)	13.86	10.14	13.40	13.04	16.74	14.96
Total Time (hours)	18.92	12.51	5.75	8.74	22.34	13.88

Table 5. Correlation between main morphometric and UH parameters.

Item	UH Peak Discharge	Basin area	Time of concentration
UH Peak Discharge	1		
Basin area	0.74	1	
Time of concentration	0.55	0.97	1

this catchment has the higher CN value, since it mainly constitutes of residential areas (**Figure 4**) which have the least permeability property. Hence, it can be concluded that the third basin in Makkah city may be considered as the most hazardous catchment. Also, the total runoff time for this basin reaches 5.75 hours, which is another evident that the third basin in Makkah city may be considered as the most hazardous catchment. The same conclusions can be drawn from the inspection of **Figure 3**, where the UH of this particular basin has the least time-to-peak and total runoff time. That leads to the fact that there is no enough time, in case of floods, for both the residents and the governmental authorities to evacuate people or apply precaution procedures. Hence, careful flood protection policies should be taken in this area within Makkah city. Moreover, it has been found that the maximum UH peak discharge equals 16.74 m^3/s (for catchment 5). Although this catchment produces the highest peak discharge, its time to peak is relatively large (4.47 hours), which might gives suitable enough time for residents to get ready and receive some governmental assistance.

7. Conclusions

Unit hydrographs graphically represent the direct runoff resulted from a unit volume of excess rainfall of constant intensity and uniformly distributed over the drainage area. Out of several methods of unit hydrographs developments, the NRCS represent an optimum approach for ungauged watersheds, since it incorporates several data types of the area of interest. The current research study has utilized a high-resolution DEM in order to apply the NRCS approach for flood assessment. NRCS- based unit hydrographs have been developed for basins within Makkah metropolitan area, southwest of Saudi Arabia. The attained results show that the time to peak discharge vary from 1.15 hours to 4.47 hours, and the UH peak discharge quantities range from 10.14 m^3/s to 16.74 m^3/s. It is concluded that the third basin in Makkah city may be considered as the most hazardous catchment, since it has the least UH time-to-peak and total runoff time. Hence, it is recommended that careful flood protection procedures should be taken in this area within Makkah city.

8. Acknowledgements

The authors would like to acknowledge the financial support offered by the Center of Research Excellence in Hajj and Omrah, Um Al-Qura university, Saudi Arabia.

9. References

[1] L. Sherman, "Stream Flow from Rainfall by the Unit Graph Method," *Engineering News Record*, No. 108, 1932, pp. 501-505.

[2] D. Roy and D. Banerjee, "Performance Analysis of the Proposed Reservoir Project in the State of West Bengal," *Hydrology and Earth System Sciences Discussions*, Vol. 7, No. 1, 2010, pp. 1373-1405. doi:10.5194/hessd-7-1373-2010

[3] T. Reshma, P. Kumar, M. Babu and K. Kumar, "Simulation of Runoff in Watersheds Using SCS-CN and Muskingum-Cunge Methods Using Remote Sensing and Geographical Information Systems," *International Journal of Advanced Science and Technology*, Vol. 25, 2010, pp. 31-42.

[4] T. Davie, "Fundamentals of Hydrology," 2nd Edition, Rout- ledge Inc., New York, 2008.

[5] H. Raghunath, "Hydrology: Principles, Analysis, and Design," 2nd Edition, New Age International Limited, New Delhi, 2006.

[6] S. Al-Jabari, M. Abu Sharakh and Z. Al-Mimi, "Estimation of Runoff for Agricultural Watershed Using SCS Curve Number And GIS," *Proceedings of the thirteenth International Water Technology Conference*, Hurghada, 2009, pp. 1213-1229.

[7] J. Lee, J. Yang and J. Choi, "Development of Integrated GIS Interface For Characteristics of Regional Daily Flow," *World Academy of Science, Journal of Engineering and Technology*, Vol. 28, 2007, pp. 180-185.

Copyright © 2011 SciRes.

[8] Y. Sherief, "Flash Floods and Their Effects on the Development in El-Qaá Plain Area in South Sinai, Egypt, a Study in Applied Geomorphology Using GIS and Remote Sensing," PhD Dissertation, Mainz University, Germany, 2008.

[9] J. Wilkerson, "Regional Regression Equations to Estimate Synthetic Unit Hydrograph Parameters for Indiana," MSC thesis, Purdue University, USA, 2009.

[10] J. Ramírez, "Prediction and Modeling of Flood Hydrology and Hydraulics," In: E. Wohl, Ed., *Inland Flood Hazards: Human, Riparian and Aquatic Communities*, Cambridge university press, New York, 2000.

[11] F. F. Snyder, "Synthetic Unit Graphs," *Transactions American Geophysics Union*, Vol. 19, 1938, pp. 447-454.

[12] SCS (US Soil Conservation Service), "Sec. 4 of National Engineering Handbook," Soil Conservation Service, U.S. Department of Agriculture, Washington, D.C., 1972.

[13] NRCS (US National Resources Conservation Services), "Urban Hydrology for Small Watersheds," *Technical Manual TR55*, 1986.

[14] F. Al-Juaidi, "Hydro-Morphometric and Flow Characteristics of the Suggested Dams Basins in Ulaya wadis, Al-Kharj (in Arabic)," *Research Papers in Geography*, Vol. 84, Riyadh, 2008.

[15] H. Al-Ghilan, "The Role of GIS in Sustainable Development (In Arabic)," *Proceedings of the Fifth Arab Geographers*, Kuwait, 5-7 April 2009, pp. 1332-1413.

[16] Z. Sen, "Modified Hydrograph Method for Arid Regions," *Journal of Hydrological Processes*, Vol. 22, 2008, pp. 356-365. doi:10.1002/hyp.6601

[17] S. Sirdas and Z. Sen, "Determination of Flash Floods in Western Arabian Peninsula," *ASCE Journal of Hydrologic Engineering*, Vol. 12, No. 6, 2007, pp. 676-581. doi:10.1061/(ASCE)1084-0699(2007)12:6(676)

[18] H. Al-Nofai, "Estimating Runoff and Flood Hazards in the Upper Basin of Oranah Valley, East Makkah, through Remote Sensing and Geographic Information Systems (In Arabic)," MSC Thesis, Umm Al-Qura University, Makkah, 2010.

[19] W. Adebayo, O. Solomon, M. Ayanniyi and F. Sikiru, "Evaluation of Synthetic Unit Hydrograph Methods for the Development of Design Storm Hydrographs for Rivers in South-West, Nigeria," *Journal of American Science*, Vol. 5, No.4, 2009, pp. 23-32.

[20] G. Gul¸ N. Harmancıoglu and A. Gul, "A Combined Hydrologic and Hydraulic Modeling Approach for Testing Efficiency of Structural Flood Control Measures," *Journal of Natural Hazards*, 2009.

[21] A. Bradley, L. Wehmeyer and L. Chen, "Evaluation of Design Flood Frequency Methods for Iowa Streams," Report No. TR-533, Iowa Department of Transportation, Iowa State, 2009.

[22] A. Salami, "Evaluation of Methods of Storm Hydrograph Development," *International Egyptian Engineering Mathematical Society (IEEMS)*, Vol. 6, 2009, pp. 17-28.

[23] US DoT (US Department of Transportation), "Highway Hydrology," 2nd Ed., U.S. Department of Transportation Federal Highway Administration, 2002.

[24] M. Mirza and M. Barodi, "Geological Basis and Their Role in Surface Feature Development in Haram Area, Makkah," *Social Science Researches*, Vol. 56, 2004.

[25] E. Daniil and S. Michas, "Use of Digital Elevation Models for the Determination of Storm Water Discharges for Highway and Railway Projects," *Proceedings of the 33rd Congress of the International Association of Hydraulic Engineering and Research*, Vancouver, 9-14 August 2009, pp. 2771-2778.

[26] MHP (Maryland Hydrology Panel), "Applications of Hydrologic Methods in Maryland," Technical Manual, 2nd Editon, Maryland Hydrology Panel, Maryland State, 2005.

[27] A. Shehata and N. Koshak, "Using 3D GIS to Assess Environmental Hazards in Built Environments, Case Study: Mina," *Al-Azhar Engineering Journal*, Vol. 2, No. 2, 2007, pp. 1-13.

[28] M. Mirza, G. Dawod and K. Al-Ghamdi, "Assessment of Global and National Digital Elevation Models for Geodetic and Geomorphologic Applications in Makkah Metropolitan Area, Saudi Arabia," *XXV IUGG General Assembly*, Melbourne, 28 June - 7 July 2011.

[29] G. Dawod, M. Mirza and K. Al-Ghamdi, "A GIS-Based Approach for Estimating Flash Flood Hazards in Makkah Metropolitan Area, Saudi Arabia," *International Journal of Geographical Information Science*, Vol. 25, No. 1, 2011, pp. 51-64.

Copyright © 2011 SciRes.

Journal of Geographic Information System, **2011, 3, 217-223**
doi:10.4236/jgis.2011.33019 Published Online July 2011 (http://www.SciRP.org/journal/jgis)

GIS-Based Spatial Mapping of Flash Flood Hazard in Makkah City, Saudi Arabia

Gomaa M. Dawod[1], Meraj N. Mirza[2], Khalid A. Al-Ghamdi[3]
[1]*Survey Research Institute, Giza, Egypt. Currently: Umm Al-Qura University, Makkah, Saudi Arabia*
[2]*Center of Research Excellence in Hajj and Omrah, Umm Al-Qura University, Makkah, Saudi Arabia*
[3]*Geography Department, Umm Al-Qura University, Makkah, Saudi Arabia*
E-mail: dawod_gomaa@yahoo.com, meraj@mmirza.com, kaghamdi@uqu.edu.sa
Received March 29, 2011; *revised May* 12, 2011; *accepted May* 20, 2011

Abstract

Flash floods occur periodically in Makkah city, Saudi Arabia, due to several factors including its rugged topography and geological structures. Hence, precise assessment of floods becomes a more vital demand in development planning. A GIS-based methodology has been developed for quantifying and spatially mapping the flood characteristics. The core of this new approach is integrating several topographic, metrological, geological, and land use datasets in a GIS environment that utilizes the Curve Number (CN) method of flood modelling for ungauged arid catchments. Additionally, the computations of flood quantities, such as depth and volume of runoff, are performed in the attribute tables of GIS layers, in order to assemble all results in the same environment. The accomplished results show that the runoff depth in Makkah, using a 50-years return period, range from 128.1 mm to 193.9 mm while the peak discharge vary from 1063 m^3/s to 4489 m^3/s. The total flood volume is expected to reach 172.97 million m^3 over Makkah metropolitan area. The advantages of the developed methodology include precision, cost-effective, digital outputs, and its ability to be re-run in other conditions.

Keywords: Flood Assessment, Rainfall-Runoff Model, NRCS, GIS, Saudi Arabia

1. Introduction

Hazards of flash floods are vital in terms of human lives loss and economical damages. Makkah city, west of Kingdom of Saudi Arabia (KSA), exhibits two unique features that increase the hazardous flood consequences: (1) its topography is very complex; (2) about three million Muslims are gathered annually in Makkah to perform Hajj over a two-weeks period in the winter, which is the main rainfall season in Saudi Arabia. Due to the increasing interest in flood impacts over the last couple of decades, extensive flood estimation studies have been carried out in different countries, such as USA [1], Egypt [2,3], Nigeria [4], South Korea [5], China [6], and Saudi Arabia [7,8]. This paper aims to develop a GIS approach for assessing the flash flood hazards for Makkah metropolitan area, utilizing the most up-to-date and precise available data sets.

2. Flood Estimation

Flood estimation methods aim to model the rainfall-runoff relationships, and can be categorized into three groups according to their complexity. Simple approaches, such as the rational method and empirical formulas, estimate the peak discharge quickly and with little number of inputs. The Curve Number (CN) is an example of moderate flood estimation methods. Detailed, or complex, models are able to identify the causes of problems rather than producing a simple description of overall conditions [9]. The CN method is quite used in engineering design and flood management projects, particularly in the USA [10-13].

Geographic Information Systems (GIS) and Remote Sensing (RS) techniques have been utilized as efficient tools in flood risk assessment [14,15]. For example, Change *et al.* [16] applied GIS to study the time-based

Copyright © 2011 SciRes.

relationship between flood hazards and land use changes. Also, Jasrotia and Singh [17] uutilized the CN method to study the runoff and soil erosion within a GIS environment. Moreover, Chen *et al.* [18] tested a GIS model, which consists of a storm–runoff model and an inundation model, to model flood hazards. In addition, Dongquan *et al.* [19] developed a GIS batch process to delineate catchments and compute their geomorphologic parameters. Furthermore, Guptaa, and Panigrahya [20] has utilized several data sources and two runoff models in a GIS platform to investigate the flood characteristics and variations of large basins in India. Additionally, Gogoase *et al.* [21] utilized GIS to develop inundation maps foe extreme flood events. Moreover, Karmakar *et al.* [22] proposed a methodology for six major damage centers in the Upper Thames River watershed, Canada to assess the flood risks, i.e. flood probability of occurrence, vulnerability to flood, and exposures of land use and soil type to flood.

3. Flash Floods in Makkah City

Makkah city is located in the south-west part of KSA, about 80 Km east of the Red Sea (**Figure 1**). It extends from 39˚35’ E to 40˚02’ E, and from 21˚09’ N to 21˚37’ N. The area of the metropolitan region (the study area) equals 1593 square kilometres. The topography of Makkah is complex in nature, and several mountainous areas exist inside its metropolitan area. The winter is considered as the main rainy season in Saudi Arabia. The annual rain over Makkah city, for a period extending from 1966 to 2009, varies from 3.8 mm to 318.5 mm, with an average of rainfall equals 101.2 mm (**Figure 2**). Due to the complexity of Makkah’s topography, flash floods occur periodically with significant variations in magnitude. Mirza and Ahmed [23] have reported that the extreme flood type is repeated with a return period of 46 years, while a second-order flood takes place occasionally with a return period of 33 years, and a low-dangerous flood comes about every 13 years. Using the magnitude of the annual rain average (which equals 101.2 mm) as a rain intensity factor might not be optimum in flood estimation process. The rain intensity of a single extreme storm may exceed the annual rainfall average for a year. For example, the 1969 storm records (**Figure 3**) showed that the rain intensity reaches 107.5 mm/hour during the first 10 minutes of that storm. Based on records of a single rainfall station, this extreme storm resulted in a runoff volume of more than 41 million cubic meters in the central area of Makkah city, with results of severe damages and human loses [23].

Analyzing the flood series frequency, the return period or recurrence interval can be computed. That period defines the average number of years during which a flood of a given magnitude will be equalled or exceeded once. The Welbull method, among several other formulas, computes the return period T as [24]:

$$T = (n+1)/m \tag{1}$$

where: n is the number of events, or number of records, m is the order or rank of the event (flood item) when flood magnitudes ranked in descending order.

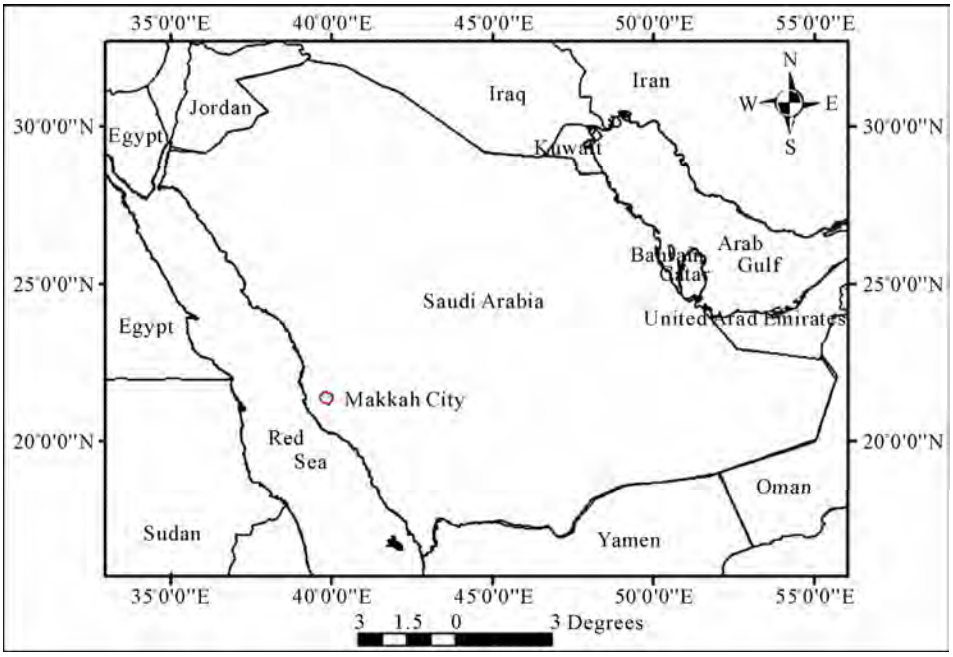

Figure 1. Study area.

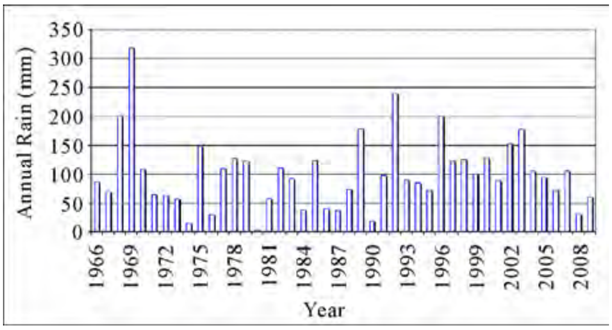

Figure 2. Annual rains in Makkah city from 1966 to 2009.

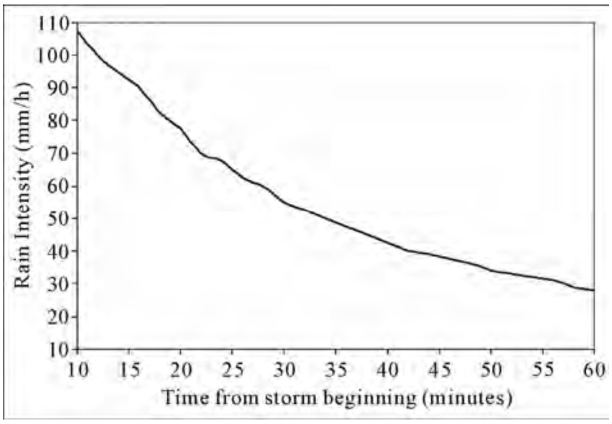

Figure 3. Rain intensity of the 1969 storm in Makkah city.

The computed return period of the 1969's flood has been estimated to 44 years. That piece of information is quite helpful in flood assessment studies, as it means that: 1) that flood magnitude is expected to occur by about 2013; and 2) selected return period value for flood management projects should be equal or greater than 44 years. The rainfall intensity for a 50-years return period has been estimated as 200 mm/h [25] and is used in the current research study.

4. Data and Methodology

Several datasets have been collected for flood assessment in Makkah city. The main data set is a Digital Elevation Model (DEM) over the study area. This DEM was produced by the by King Abdulaziz City of Sciences and Technology (KACST) with a spatial resolution equals to 5 meters. A window covering Makkah metropolitan area (**Figure 4**) has been provided through the Center of Excellence in Hajj and Omrah, Umm Al-Qura university. Mirza *et al.* [26] confirm that this national DEM is 3 times more accurate than previously published global DEMs (e.g. ASTER and SRTM) over Makkah area. From **Figure 4**, it can be noticed that the heights of Makkah metropolitan area range from 80 to 982 meters. The other datasets include digital geological, soil, and land use maps of the study area.

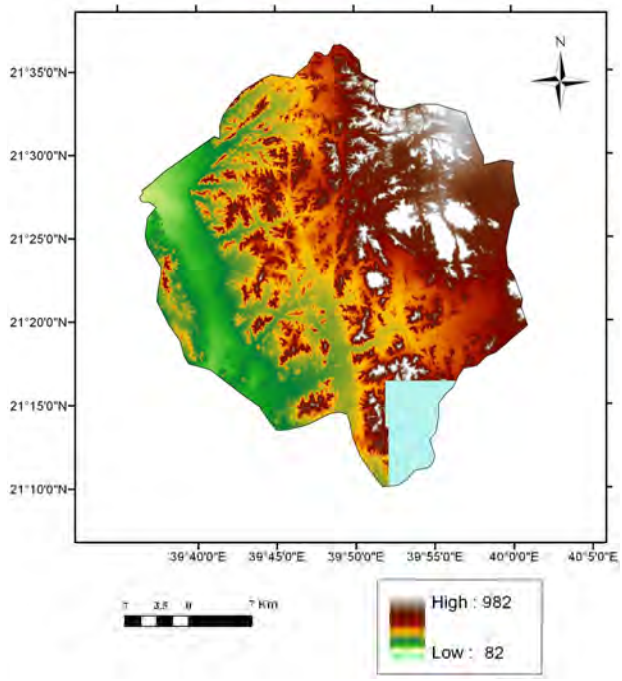

Figure 4. The national 5-m DEM for Makkah city.

The developed GIS-based flood assessment methodology consists of several stages. **Figure 5** depicts an overview flow chart of that scheme. In the first stage, the Arc GIS software along with the Arc Hydro extension are used to obtain several shapefiles describing the geomorphology of the study area. These shapefiles include: the main basins and the sub-basins of each main catchment, along with drainage network using Strahler method (a simple widely-utilized network order method), and the longest stream path in each catchment. The second stage of the developed methodology is based on the flood assessment method developed by the US Natural Resources Conservation Service (NRCS), formerly known as the Soil Conservation Service (SCS). It worth mentioning that there are several hydrologic methods used for flood estimation, but the SCS method has been applied in the current research study. This method, also known as the Curve Number (CN), makes use of geological information to assign a unique CN value for each area, which will be further used to estimate the surface runoff depth and the peak discharge magnitude. VBA is used to compute the required flood defining parameters that consists of [27]:

$$Q = (P - 0.2S)2/(P + 0.8S) \quad (2)$$

$$S = 25.4((1000/CN) - 10) \quad (3)$$

$$QT = QA \quad (4)$$

$$qp = quAQ \quad (5)$$

Copyright © 2011 SciRes.

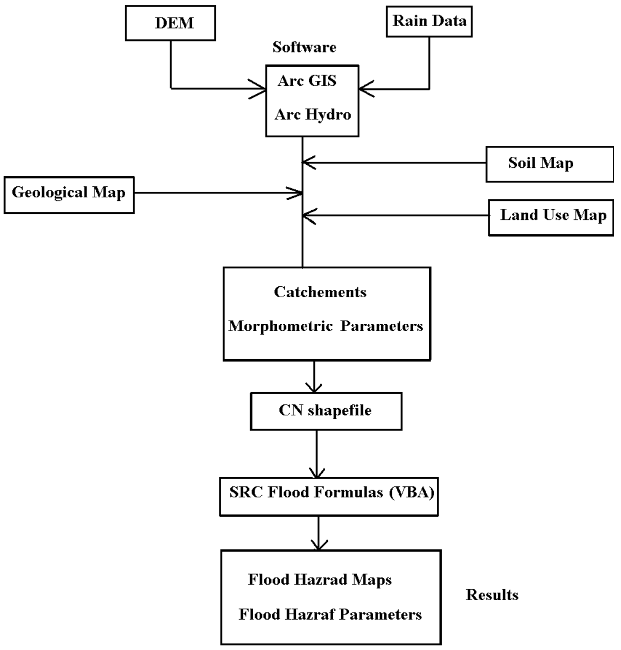

Figure 5. The developed GIS-based flood assessment methodology.

where: Q is the depth of direct runoff (mm), P is the depth of precipitation for a specific return period (mm), S is the maximum potential retention (mm), CN is the curve number, QT is the volume of runoff (m^3), A is the Area of basin (Km^2), Q is the depth of direct runoff (m), qp is the peak discharge (m^3/s), and qu is the unit peak discharge ($m^3/s/km^2/mm$) that can be interpolated from a specific charts [28] or computed from corresponding tables [13, pp. 5-28].

It worth mentioning that P was computed through statistical analysis of rainfall records (e.g. by Log Pearson III method) to determine the expected rainfall depth for a specific storm to be occurred again with the same magnitude.

Other hydrological parameters include:

$$v = 0.2279L/tc \quad (6)$$

$$tc = 1.67\left[L^{0.8}(S+1)^{0.7}\right] / \left[1900 * SL^{0.5}\right] \quad (7)$$

$$Sd = 0.133Tc \quad (8)$$

where: v is the flow velocity (m/s), L is the basin length (expressed in units of meters), tc is the concentration time (minutes) that can be estimated using several formulas, one of them (NRCS method) is given in Equation (7), SL is the average watershed land slope in percentage, and Sd is the storm duration (hours).

5. Results

The developed GIS-based methodology has been carried out using the available datasets of Makkah metropolitan area. Results of the first stage include several maps and the estimation of many morphometric parameters. It has been found that there are 6 main catchments in Makkah, whose areas range from 74.3 to 360.6 square kilometres, and lengths of their main streams vary from 16.50 to 48.55 kilometres (**Figure 6**). **Table 1** presents statistics of some morphometric parameters of the six catchments.

The second stage of the developed approach results is the determination of flood characteristics in Makkah city. The computations have performed using the depth of precipitation (P) equals 200 mm for a return period of 50 years. That value is the result of the Log Pearson III statistical analysis for the available rainfall datasets of Makkah city. Additionally, the unit peak discharge (qu in Equation (4)) has been computed through the equation and tables provided in [13, Equation 5-26, pp. 5-28]. **Table 2** and **Figure 7** present the flood estimated parameters.

Moreover, the peak discharge values found to vary from 1063 m^3/s (for catchment C2) to 4489 m^3/s (for catchment C5). Additionally, the runoff depths of the six basins vary from 151.7 mm to 178.8 mm. The flood volume range between 13.28 m^3 (for catchment 3) and 54.69 m^3 (for catchment 3), with a total of 172.97 million m^3 over Makkah metropolitan area.

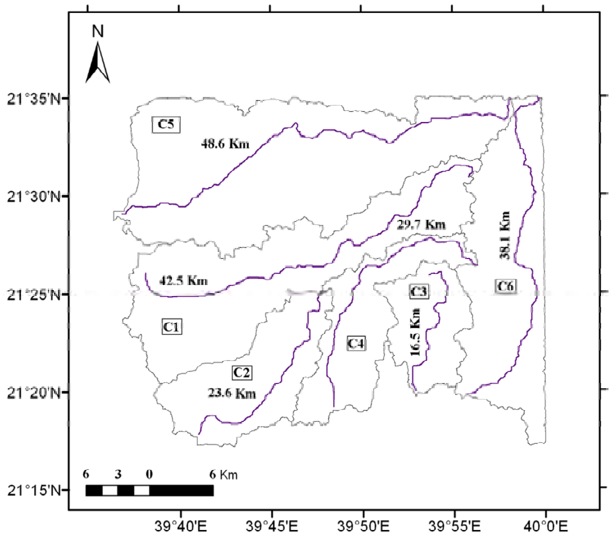

Figure 6. Catchments and their main streams.

Table 1. Statistics of morphometric quantities.

Item	C1	C2	C3	C4	C5	C6
Basin Area (km^2)	252.7	122.3	74.3	109.9	360.6	200.2
Basin Premier (km)	134.6	69.13	50.23	89.09	134.76	102.03
Basin Length (km)	42.48	23.64	16.50	29.70	48.55	38.13

Copyright © 2011 SciRes.

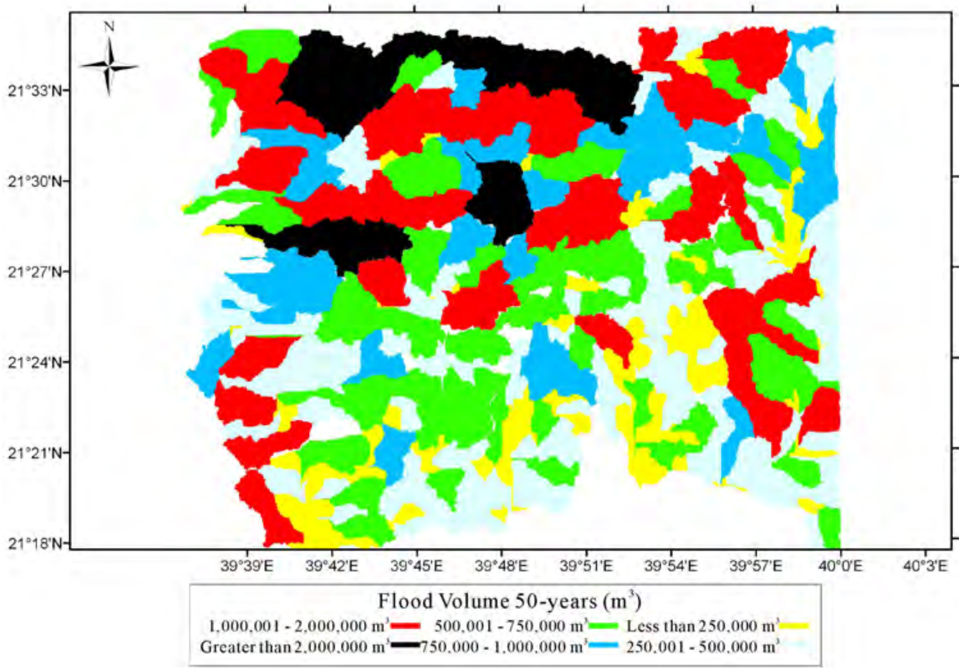

Figure 7. Flood spatial variations in Makkah.

Table 2. Flood characteristics in Makkah city (for a 50-years return period).

Item	C1	C2	C3	C4	C5	C6
Time of concentration (hours)	5.69	3.76	1.73	2.63	6.72	4.17
CN	84	84	93	89	84	83
Runoff depth (mm)	151.7	151.7	178.8	166.7	151.7	148.8
Peak discharge (m^3/s)	1554	1063	1307	1234	4489	1514
Storm duration (hour)	0.76	0.50	0.23	0.35	0.89	0.56
Flow velocity (m/s)	28.34	23.86	36.19	42.87	27.44	34.68
Volume of runoff (million m^3)	38.34	18.55	13.28	18.32	54.69	29.79
	Total = 172.97 million m^3					

6. Discussion

First, it can be noticed that catchment C3 has the lowest concentration time (1.98 hours), which is the time for runoff to travel from the most distant point to the outlet point. The lower time of concentration, the more hazardous is the runoff. Additionally, catchment C3 is expected to have minimum storm duration (0.26 hours) while catchment C1 has the maximum value (0.80 hours). Concerning the flow velocity of the six basins, it has been found that the values range from 22.44 m/s (for catchment C2) to 73.37 m/s (for catchment C5).

Keeping in mind that the lower concentration time, the more hazardous is the runoff, it has been found that catchment C3 has the lower concentration time That is an excepted result, since catchment C3 has the highest relief ratio (40.43 m/km) even though it does not have the highest flow velocity. Additionally, catchment C3 is expected to have minimum storm duration (0.26 hours) while catchment C1 has the maximum value (0.80 hours). It is worth mentioning that the storm duration is a function of the concentration time as seen in Equation (8).

A coloration analysis was performed between the main flood factors. The correlation matrix is presented in **Table 3**. Concerning the flow velocity of the six basins, it has been found that the minimum velocity belongs to catchment C2 while the maximum velocity is for catchment C5. Equation (5) shows that the flow velocity is directly proportional to the catchment stream length, and is inversely proportional to the concentration time. The same conclusion is drawn from Table 4 where the peak discharge, total flood volume, basin area, and basin stream length have positive strong correlations with the flow velocity (0.97, 0.76, 0.74, and 0.61 respectively), while the concentration time has a negative moderate correlation (–0.48).

Second, catchment C3 also has the highest CN value of 93. The higher CN values, in the study area, is attributed to two factors: 1) the residential area of Makkah city, paved streets, was assigned CN of 98 that reflects the low permeability of rains; 2) a great portion of Makkah's geology consists of Pre-Cambrian igneous and metamorphic rocks, that get relatively high CN according to

Table 3. Correlation between main flood characteristics.

	CN	*tc*	*A*	*L*	*Q*	*QT*	*v*
CN	1						
tc	–0.65	1					
A	–0.66	0.21	1				
L	–0.72	0.39	0.94	1			
Q	–0.30	–0.33	0.85	0.70	1		
QT	–0.62	0.18	0.9987	0.94	0.87	1	
v	–0.14	–0.48	0.74	0.61	0.97	0.76	1

where: *CN* is the curve number, *tc* is the time of concentration, *A* is the basin area, *L* is the basin stream length, *Q* is runoff depth, *QT* is the runoff volume, and v is the runoff velocity.

the SRC classification.

Moreover, it can be noticed that four catchments (C1, C2, C5, and C6) have similar CN values, but C2 has the least basin area. That leads to this catchment produces the minimum peak discharge. As expected, catchment C5 produces the highest peak discharge because of its big basin area. **Table 3** concludes the same result since the basin area and basin stream length has strong correlations (0.85 and 0.70) with the peak discharge.

Additionally, it can be concluded that the highest runoff depth belong to catchment C3, which has the highest CN value. Regarding the flood volume, it can be seen that catchment C5 produces the biggest value due to the fact that it has the biggest area (360.6 km^2). The correlation between flood volume and basin area is strong (0.9987) as seen in **Table 3**.

The GIS-based CN flood estimation methodology has several advantages. First, it incorporates many input datasets including metrological, geological, soil, land use, and DEM. Other approaches (e.g. the rational method) employ less input items, while some national regression models used in Saudi Arabia depend only on the basin area to estimate expected flood. Dawod *et al.* [29] concluded that the CN method is more precise than some other flood estimation methods over Makkah region. Moreover, this paper presents a GIS-based implementation of the CN methodology where computations have been performed in the attribute tables within the GIS environment (using VBA). So, the flood estimation process is efficient, faster, and can be easily performed for several scenarios and even for several regions in Saudi Arabia once the required input layers are available.

7. Conclusions

Makkah metropolitan area, south west of Saudi Arabia, is distinguished by two items (a complex topography and the gathering of about three million Muslims to perform Hajj over a specific short time period annually) that greatly raises awareness of flood hazards impacts. This research develops a GIS-based approach for mapping and quantifying flood assessment measures. The developed methodology is based on integrating several datasets in a GIS environment utilizing the SRC CN flood modelling method. Results show that the main factors affect the total flood volumes, in Makkah metropolitan area, are the catchment area, the basin stream length, and the peak discharge. Additionally, it has been concluded that the higher CN value (for low permeability soil, geological, and land use features), the higher runoff and flood hazards. Merits of that methodology include precision, cost-effective, digital outputs, and its ability to be re-run for other scenario (e.g., other design return period). Hence, it is recommended that the attained results be utilized in governmental planning in Makkah city, and that approach should be applied to all other cities in Saudi Arabia.

8. Acknowledgements

The authors would like to acknowledge the financial support offered by the Center of Research Excellence in Hajj and Omrah (Hajjcore), Umm Al-Qura university, Saudi Arabia.

9. References

[1] USGS (U.S. Geological Survey). "Watershed models for decision support for inflows to Potholes reservoir", Washington scientific investigations report 2009-5081, 2009.

[2] M., Azab. "Assessment and management of natural hazards and disasters along Qena-Safaga road, central eastern desert, Egypt", Egypt. Journal of Remote Sensing and Space Science, 12, 2009, pp. 55-70.

[3] M. El Bastawesy, K., White, and A. Nasr,. "Integration of remote sensing and GIS for modelling flash floods in Wadi Hudain catchment, Egypt", Hydrological Process, 23, 2009, pp. 1359-1368.

[4] S. Yahaya, N. Ahmad, and R. Abdalla. "Multicriteria analysis for flood vulnerable areas in Hadejia-Jama'are river basin, Nigeria", European Journal of Scientific Research, 42(1), 2010, pp. 71-83.

[5] N. Kim, J.W. Lee, J., Lee, and J.E. Lee,. "SWAT application to estimate design runoff curve number for South Korean conditions", Hydrological Process,. 24, 2010, pp. 2156-2170.

[6] W. Liang, C. Yongli, C. Hongquan, D. Daler, Z. Jingmin, and Y. Juan. "Flood disaster in Taihu Basin, China: causal chain and policy option analyses", Environmental Earth Science, DOI 10.1007/s12665-010-0786-x, Published on line October 19, 2010.

[7] M. Al Saud. "Assessment of flood hazard of Jeddah area 2009, Saudi Arabia", Journal of Water Resource and Protection, 2, 2010, pp. 839-847.

[8] E. Fred, and B. Mostafa. "Flood risk modeling for holy sites in Makkah", Proc. of the symposium on National GIS application in Saudi Arabia, Al-Kober city, Saudi Arabia, 2008.

[9] E. Mihalik. "Watershed characterization and runoff modelling of the Chapel branch creek, Orangeburg county, South Carolina", MSC thesis, College of Charleston, South Carolina State, USA, 2008.

[10] IDoT (Iowa state Department of Transportation). "Iowa storm water management manual", 2009.

[11] US ACE (US Army Corps of Engineers). "Physical stream assessment", 2004.

[12] NH DoT (New Hampshire Department of Transportation). "Drainage design manual for highways", 1998.

[13] US DoT (US Department of Transportation). "Highway hydrology manual", Publication No. FHWA-02-001, 2002.

[14] A. Youssef, B. Pradhan, and A. Hassan. "Flash flood risk estimation along the St. Katherine road, southern Sinai, Egypt using GIS based morphometry and satellite imagery", Environmental Earth Science, DOI 10.1007/ s12665-010-0551-1, Published on line April 27, 2010.

[15] A. Saleh, and S. Al-Hatrushi. "Torrential flood hazards assessment, management, and mitigation, in wadi Aday, Muscat area, Sultanate of Oman, a GIS & RS approach", Egypt. Journal of Remote Sensing and Space Sciences., 12, 2010, pp. 71-86.

[16] H. Chang, J., Franczyk, and C. Kim. "What is responsible for increasing flood risks? The case of Gangwon Province, Korea", Natural Hazards, (48), 2009, pp. 339-354.

[17] A. Jasrotia, and R. Singh. "Modeling runoff and soil erosion in a catchment area, using the GIS, in the Himalayan region, India", Environmental Geology, (51), 2006, pp 29-37.

[18] J. Chen, A. Hill, and L. Urbano. "A GIS-based model for urban flood inundation", Journal of Hydrology, 373, 2010, pp. 184-192.

[19] Z. Dongquan, C. Jining, W. Haozheng, T. Qingyuan, C. Shangbing, and S. Zheng. "GIS-based urban rainfall-runoff modeling using an automatic catchment-discretization approach: a case study in Macau", Environmental Earth Sciences, (59), 2009, pp. 465-472.

[20] P. Guptaa, and S. Panigrahya. "Geo-spatial modeling of runoff of large land mass: Analysis, approach and results for major river basins of India", Proceedings. Of the international archives of the photogrammetry, remote sensing and spatial information sciences. Vol. XXXVII. Part B2. Beijing, 2008.

[21] D. Gogoase, I. Armaş, and C. Ionescu. "Inundation Maps for Extreme Flood Events at the Mouth of the Danube River", International Journal of Geosciences, (2), 2011, pp. 68-74.

[22] S. Karmakar, S. Simonovic, A. Peck, and J. Black. "An information system for risk-vulnerability assessment to flood", Journal of Geographic Information System, No. 2, 2010, pp. 129-146.

[23] M. Mirza, and B. Ahmed. "Winter weather and climate conditions in Makkah (in Arabic)", Geographic Messages, 253, Kuwait Geographic Association, Kuwait, 2001.

[24] H. Raghunath. "Hydrology: Principles, Analysis, and Design", New Age International Ltd., New Delhi, India, 2006.

[25] KSA MoPWH (Saudi Ministry of Public Works and Housing). "Storm water drainage system for Muzdalifah and Arafat areas", Unpublished technical report, 2001.

[26] M. Mirza, G. Dawod, and K. Al-Ghamdi. "Assessment of global and national digital elevation models for geodetic and geomorphologic applications in Makkah metropolitan area, Saudi Arabia", The XXV IUGG General Assembly, Melbourne, Australia, 28 June - 7 July, 2011.

[27] Z. Sen. "Wadi hydrology", CRC Press, New York, 2008.

[28] US NRCS (US National Resources Conservation Services). "Urban hydrology for small watersheds", Technical Manual TR55, 1986.

[29] G. Dawod, M. Mirza, and K. Al-Ghamdi. "Assessment of several flood estimation methodologies in Makkah metropolitan area, Saudi Arabia", Under review, Arabian Journal of Geosciences 2011.

Copyright © 2011 SciRes.

مركز التميز
في أبحاث الحج والعمرة
Center of Research Excellence in Hajj and Omrah

تطوير نظام معلومات جغرافي لتقدير مخاطر السيول في مدينة مكة المكرمة و المشاعر المقدسة

د. معراج بن نواب مرزا

أ.د. جمعة بن محمد داود

د. خالد بن عبد الرحمن الغامدي

مركز التميز في أبحاث الحج و العمرة - جامعة أم القرى

أهداف الدراسة

1. بناء قاعدة بيانات رقمية دقيقة للخصائص الهندسية و المورفومترية والجيومورفولوجية والمناخية لأودية مكة المكرمة و المشاعر المقدسة.
2. التحديد الدقيق للأخطار المتوقعة للسيول.
3. إنتاج خرائط رقمية تفصيلية لمكة المكرمة والمشاعر المقدسة والمخاطر المتوقعة للسيول بها.
4. تقديم توصيات محددة للتدابير البيئية الواجب اتخاذها للحفاظ علي شبكة الطرق في المشاعر المقدسة.

مخاطر السيول في مكة المكرمة

مكة المكرمة بطبيعتها الجغرافية تتكون من:

– جبال وثنايا

– سفوح وشعاب

– أودية ومجاري السيول

- **تتميز مدينة مكة المكرمة عن غيرها من المدن أنه *لا تأتيها السيول من خارجها*.**
- **أحواض أوديتها محدودة : من داخل حدود الحرم .**

طبوغرافية المشاعر المقدسة

طبوغرافية المشاعر المقدسة

أودية مكة المكرمة

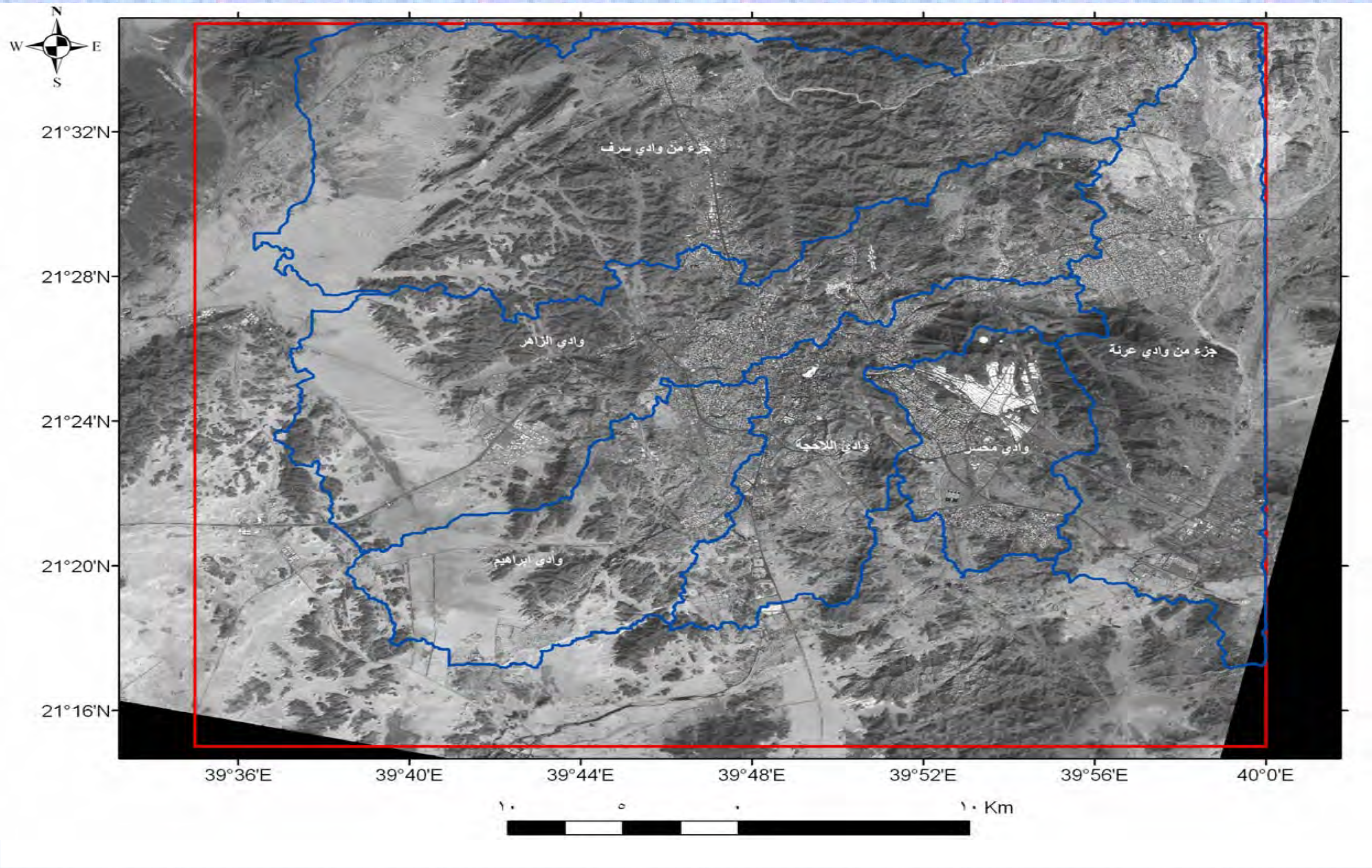

سيول مكة المكرمة

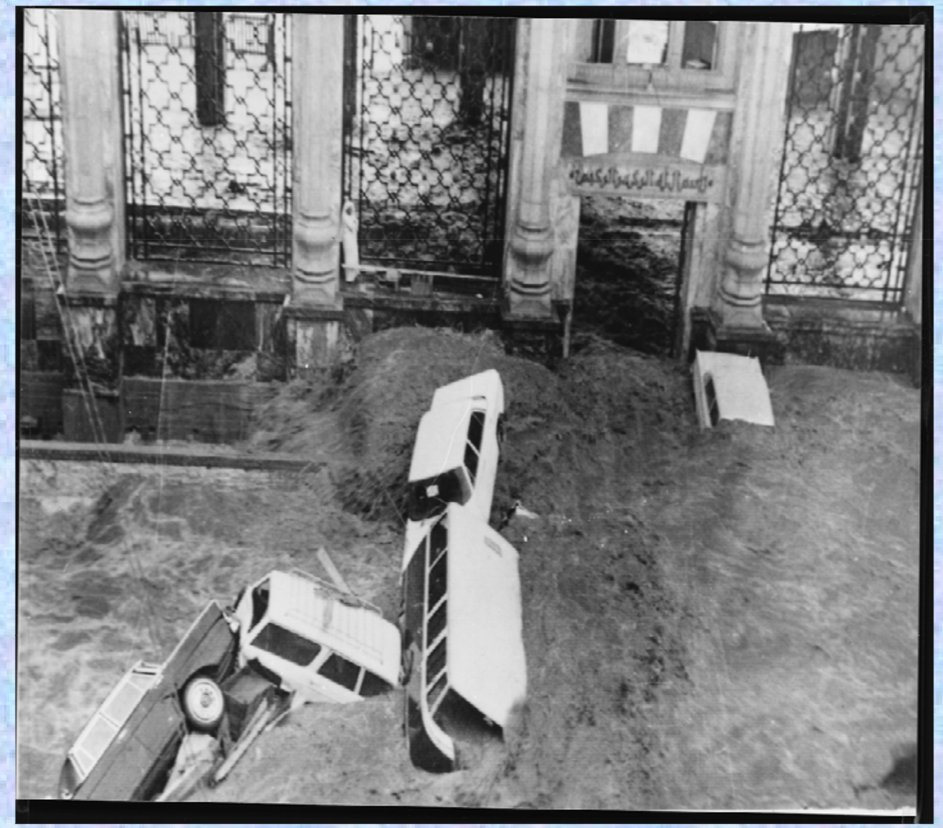

منهج الدراسة (1)

مدخلات:

- مجموعة متعددة من قواعد البيانات الهيدرولوجية و الجيولوجية و المورفولوجية لمكة المكرمة
- نموذج ارتفاعات رقمية عالي الدقة.
- بيانات الأمطار و السيول بمكة المكرمة لفترة خمسة وأربعين عاما.

التقنيات المستخدمة:

- نظم المعلومات الجغرافية
- الاستشعار عن بعد
- الطريقة الامريكية لتحديد مخاطر السيول NRCS

منهج الدراسة (2)

الحسابات:

- التحليل الاحصائي لبيانات الامطار لاختيار فترة الرجوع.
- التحليل المورفومتري لخصائص الاودية.
- خرائط رقمية لاستخدامات الاراضي و التراكيب الجيولوجية
- تقدير خصائص السيول المتوقعة (عمق و سرعة و حجم الجريان السطحي)
- التوزيع المكاني لدرجات خطورة السيول في مكة المكرمة.

النتائج:

- جداول للقيم + خرائط رقمية توضح خصائص السيول في أجزاء مدينة مكة المكرمة و المشاعر المقدسة.

الامطار في مكة المكرمة

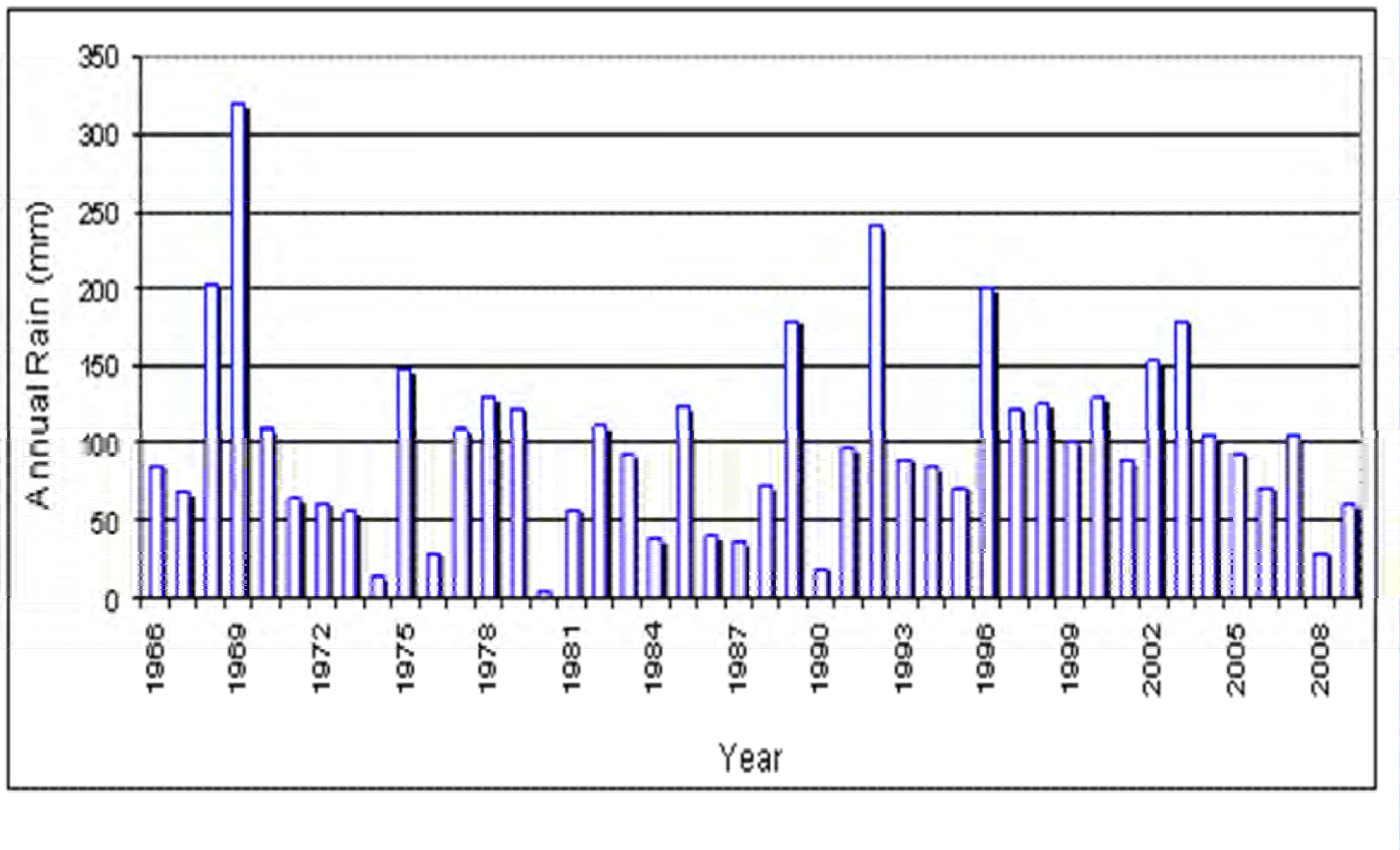

السيول في مكة المكرمة

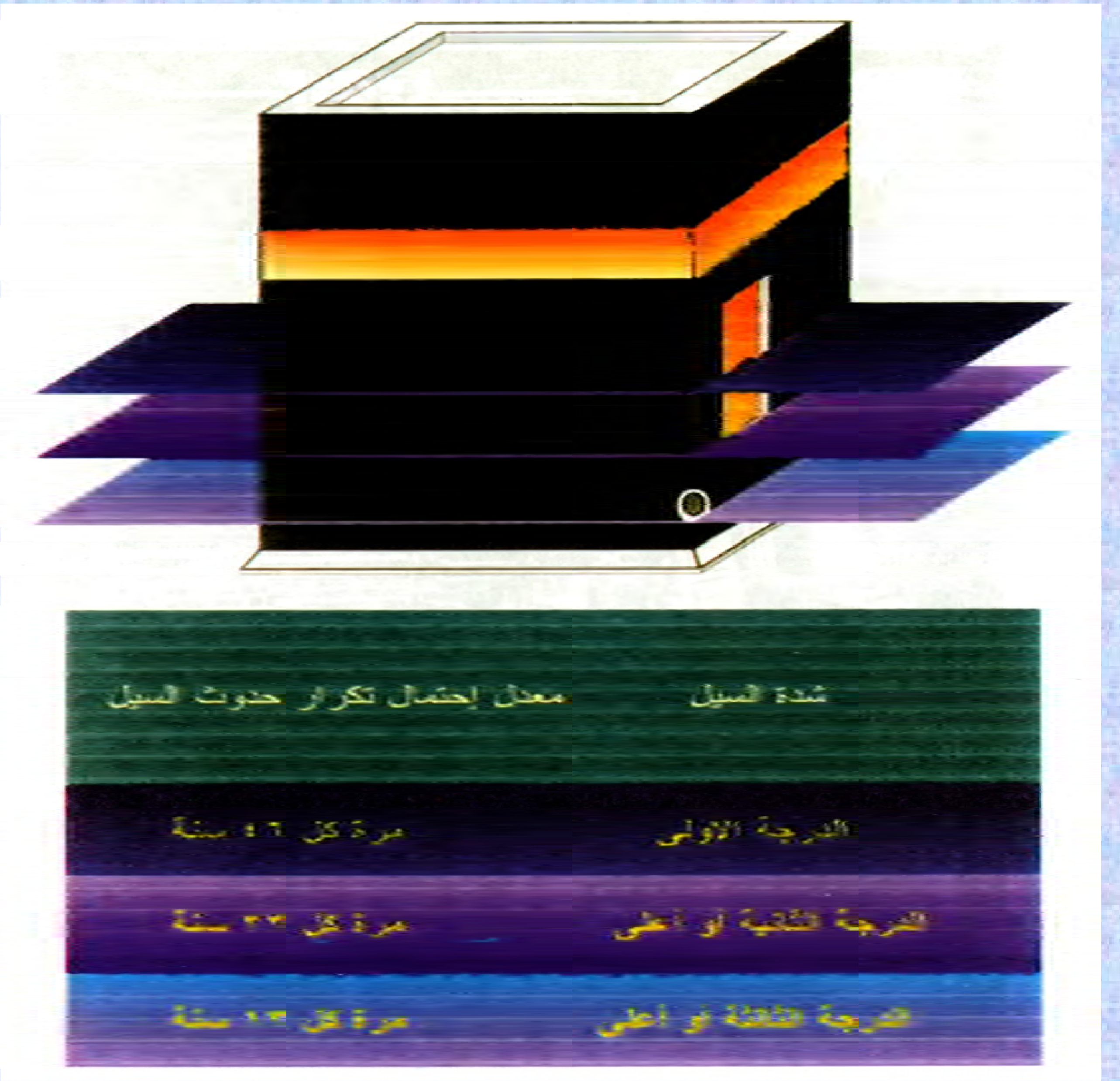

السيول العنيفة في مكة المكرمة

كثافة أمطار سيل 1388 هـ / 1969 م

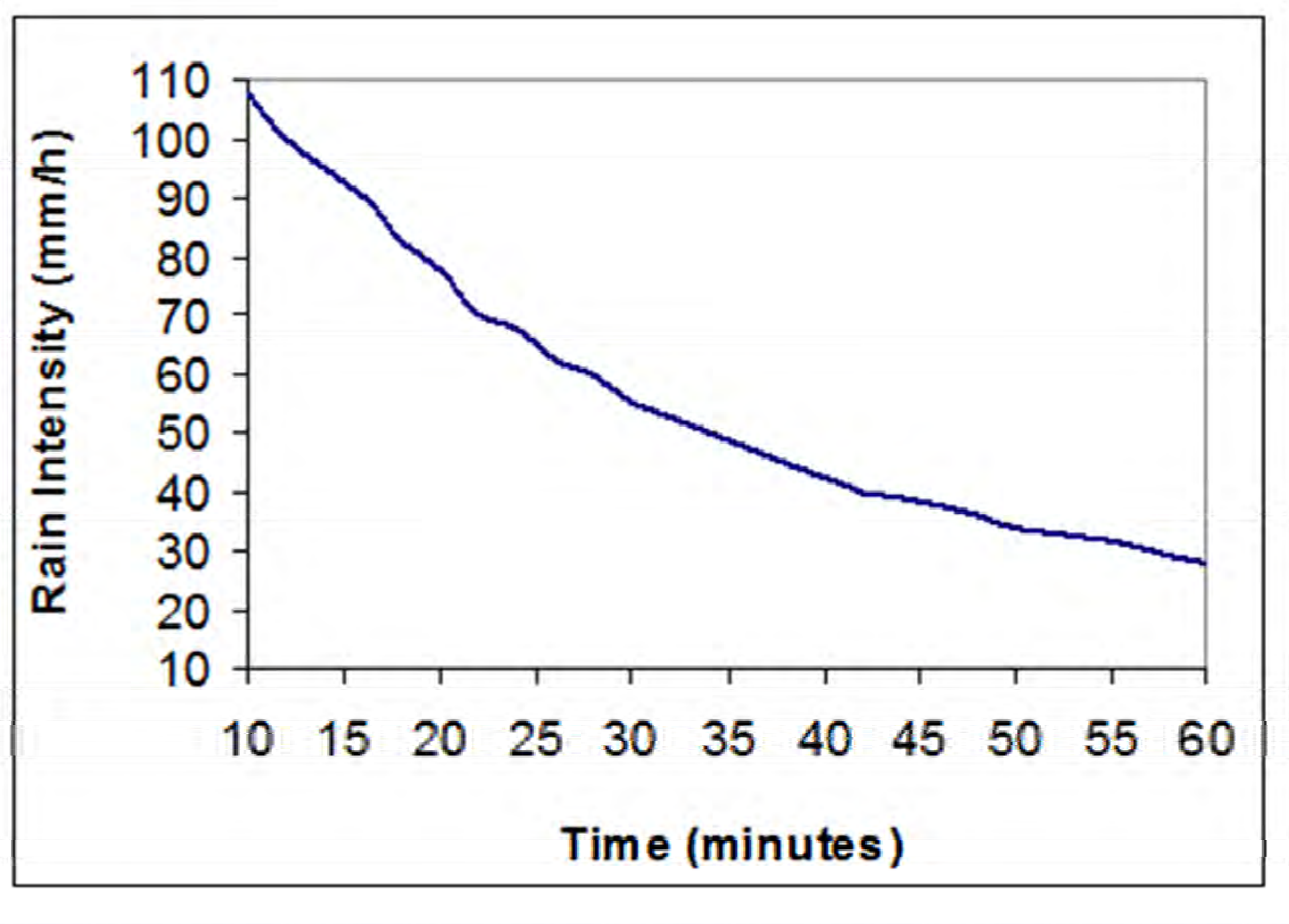

الحسابات

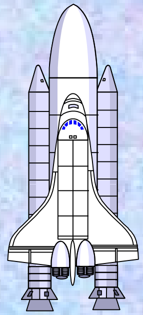

للوصول الى نتائج دقيقة:

1. لا يجب الاعتماد علي المتوسط السنوي للمطر في تقدير حجم السيول
2. التحديد الاحصائي لأنسب فترة رجوع يتوقع عندها – لا قدر الله – أن تتكرر السيول العنيفة
3. استخدام نماذج رياضية دقيقة ومنتشرة التطبيق علي المستوي العالمي
4. استخدام التقنيات الحديثة

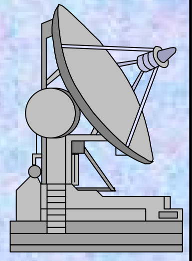

التطبيق

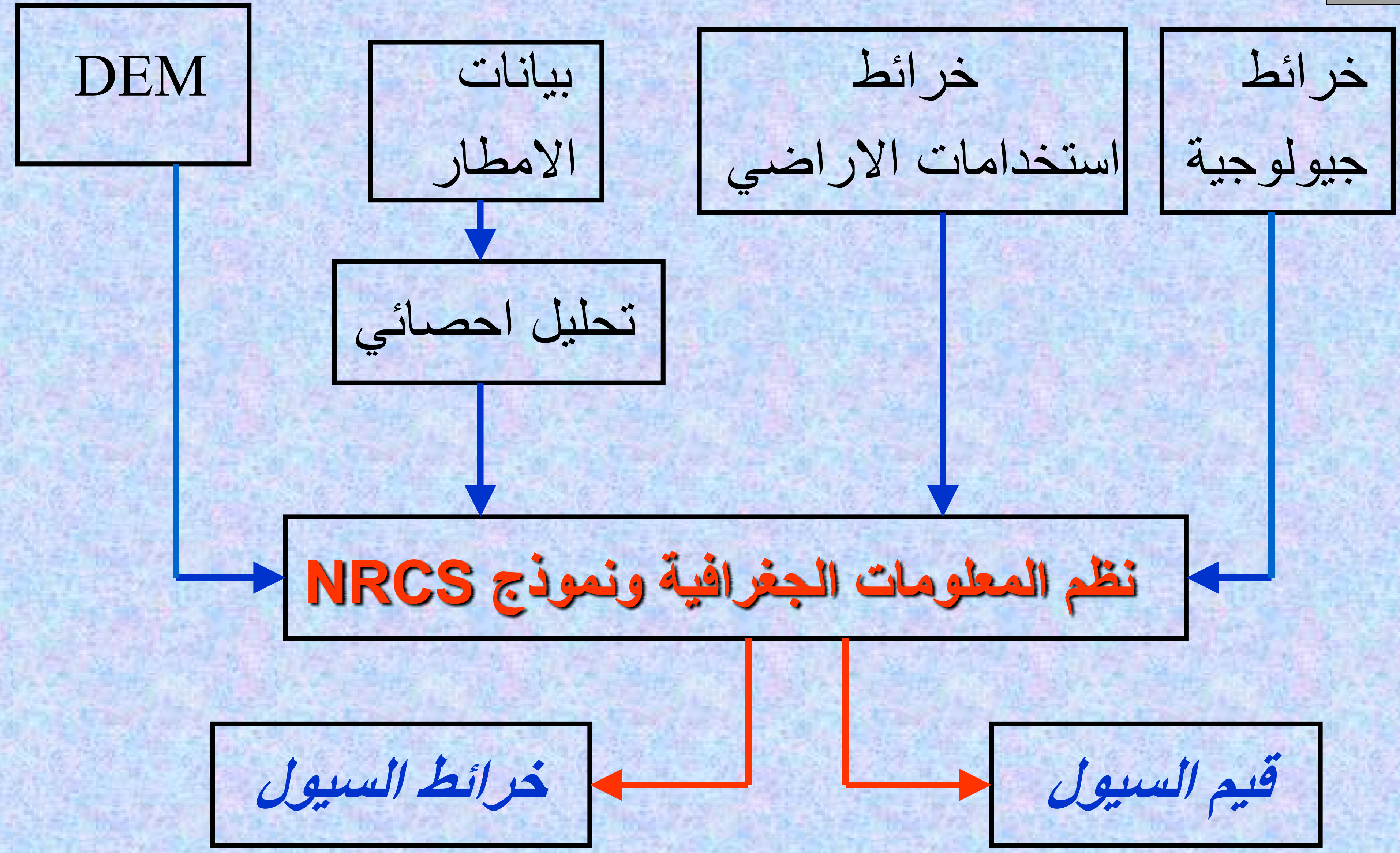
DEM
بيانات الامطار
خرائط استخدامات الاراضي
خرائط جيولوجية
تحليل احصائي
نظم المعلومات الجغرافية ونموذج NRCS
خرائط السيول
قيم السيول

النتائج

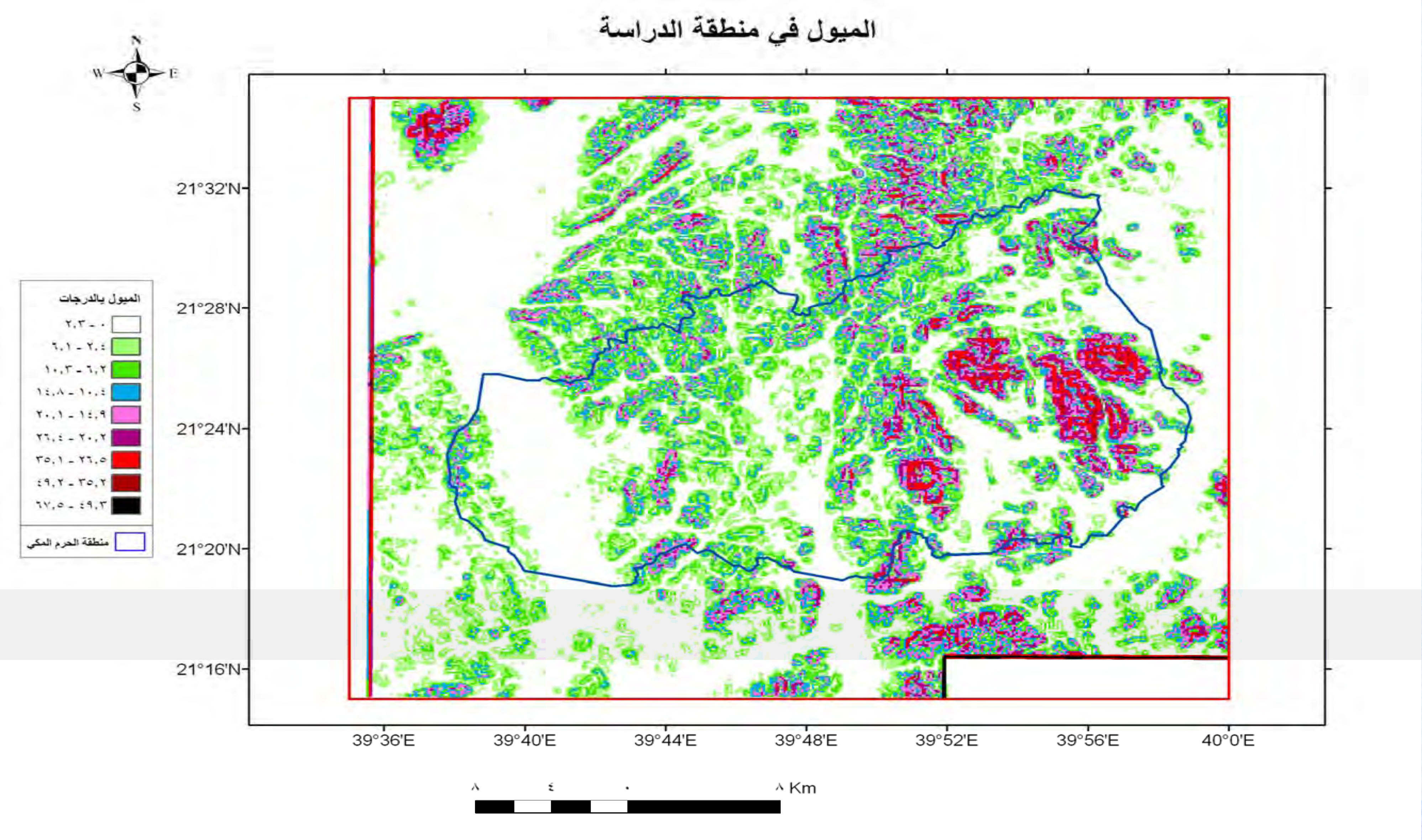
الميول في منطقة الدراسة
N
W
E
S
الميول بالدرجات
٠ - ٢,٣
٢,٤ - ٦,١
٦,٢ - ١٠,٣
١٠,٤ - ١٤,٨
١٤,٩ - ٢٠,١
٢٠,٢ - ٢٦,٤
٢٦,٥ - ٣٥,١
٣٥,٢ - ٤٩,٢
٤٩,٣ - ٦٧,٥
منطقة الحرم المكي
21°32'N
21°28'N
21°24'N
21°20'N
21°16'N
39°36'E
39°40'E
39°44'E
39°48'E
39°52'E
39°56'E
40°0'E
٨
٤
٠
٨ Km

النتائج

الأحواض الفرعية لأودية مدينة مكة المكرمة و المشاعر المقدسة

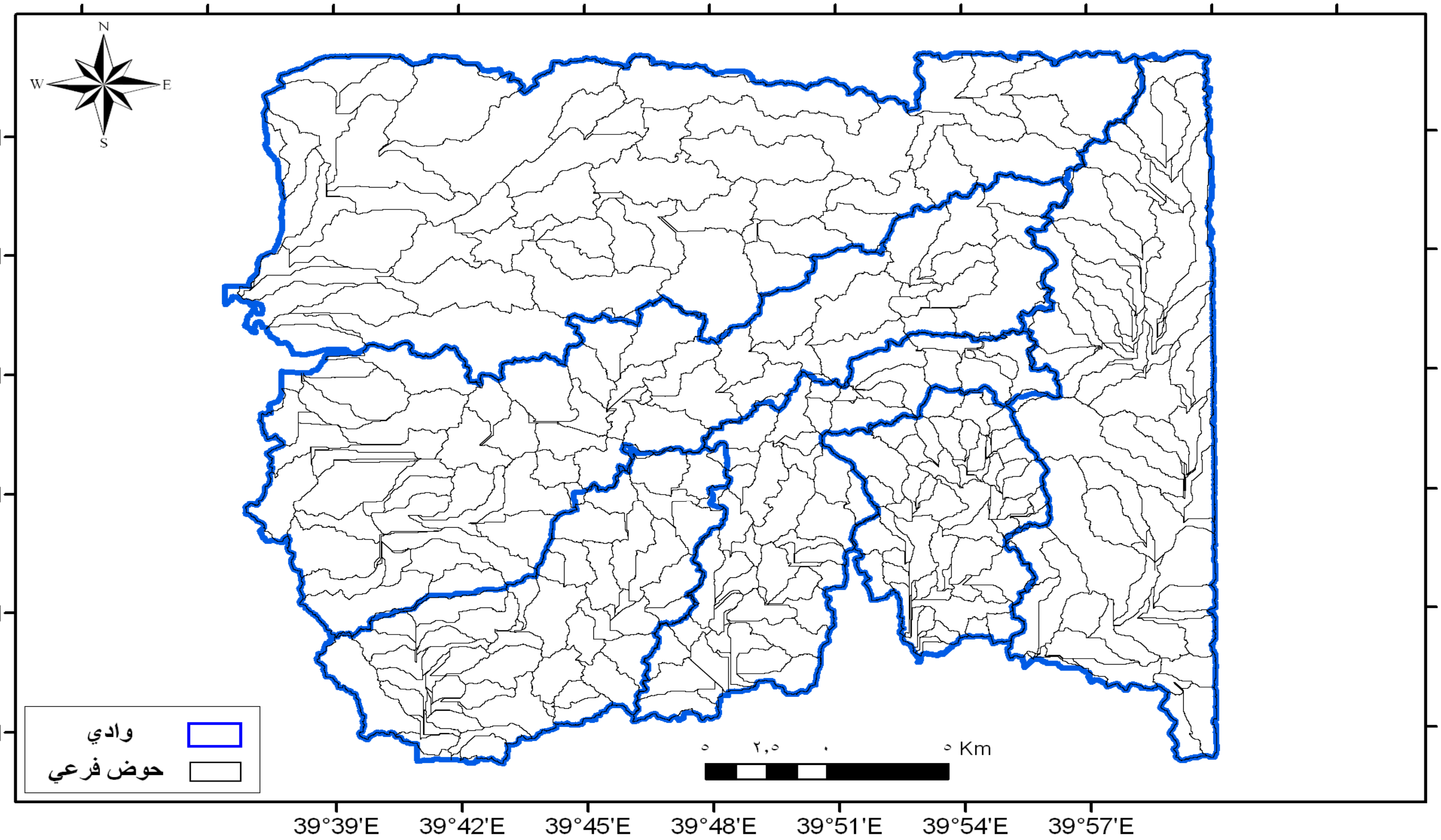

النتائج

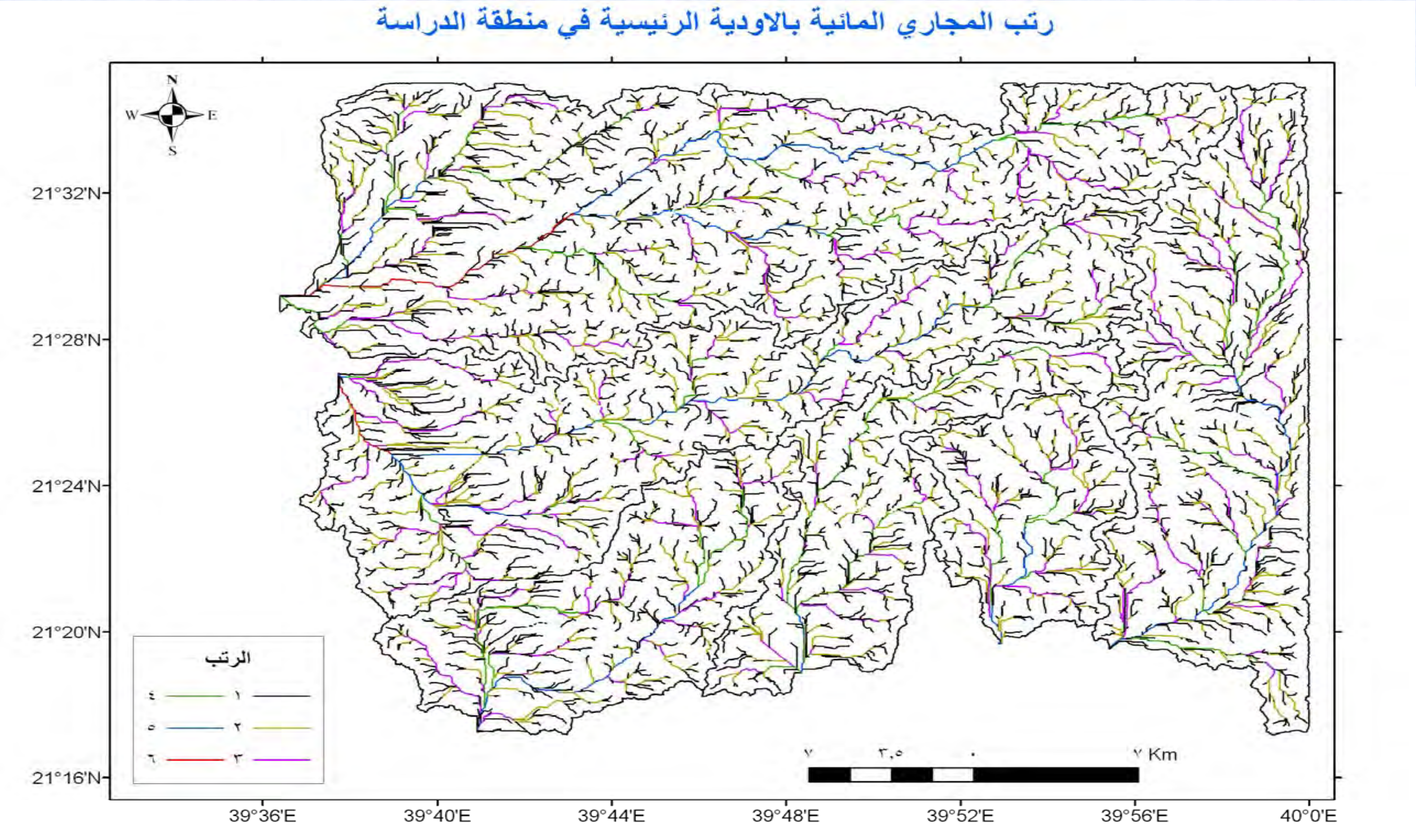

رتب المجاري المائية بالاودية الرئيسية في منطقة الدراسة
N
W
E
S
21°32'N
21°28'N
21°24'N
21°20'N
21°16'N
39°36'E
39°40'E
39°44'E
39°48'E
39°52'E
39°56'E
40°0'E
الرتب
١
٢
٣
٤
٥
٦
٧
٣,٥
٠
٧ Km

النتائج

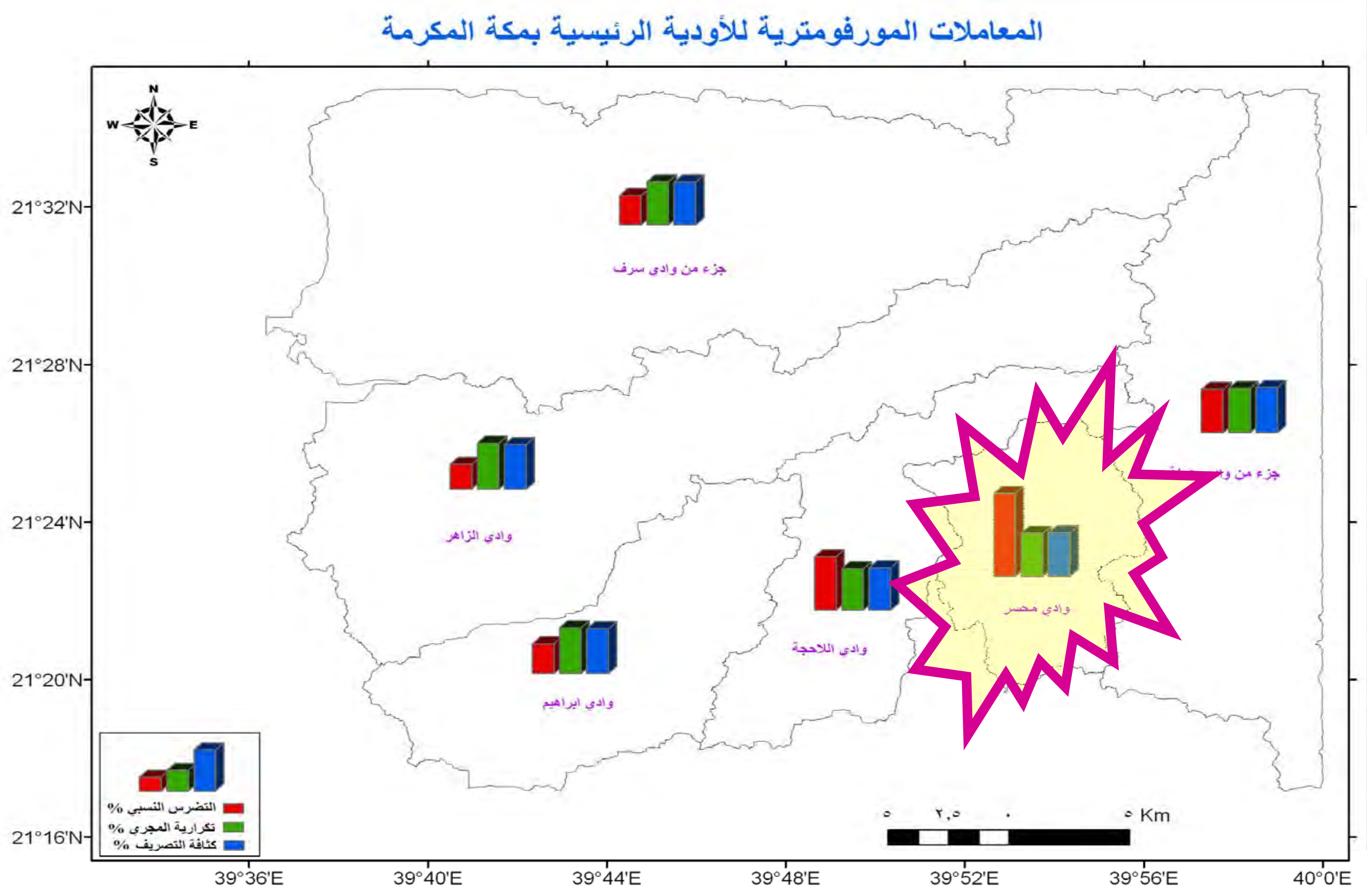
المعاملات المورفومترية للأودية الرئيسية بمكة المكرمة
N
W
E
S
21°32'N
21°28'N
21°24'N
21°20'N
21°16'N
39°36'E
39°40'E
39°44'E
39°48'E
39°52'E
39°56'E
40°0'E
جزء من وادي سرف
وادي الزاهر
وادي ابراهيم
وادي اللاحجة
وادي محسر
التضرس النسبي %
تكرارية المجرى %
كثافة التصريف %
٥ ٢,٥ ٠ ٥ Km

النمو العمراني و مخاطر الفيضان

شكرا لحسن استماعكم

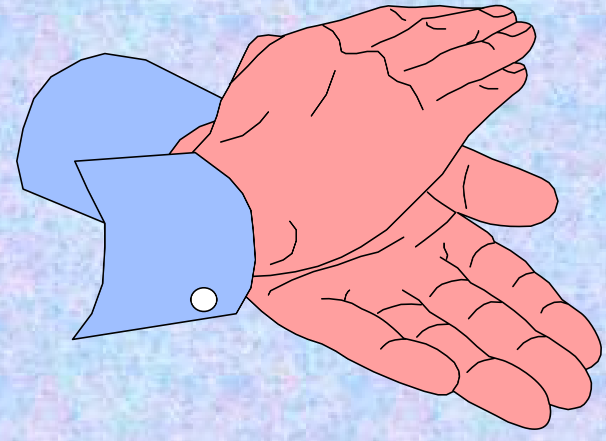

INTERNATIONAL JOURNAL OF GEOMATICS AND GEOSCIENCES
Volume 2, No 2, 2011

© Copyright 2010 All rights reserved Integrated Publishing services

Research article ISSN 0976 – 4380

A GIS morphometric analysis of hydrological catchments within Makkah Metropolitan area, Saudi Arabia

Koshak.N [1], Dawod.G [2]
1 Center of Research Excellence in Hajj and Omrah, Umm Al-Qura University, Makkah, Saudi Arabia.
2 Survey Research Institute, Giza, Egypt, Currently affiliated with Umm Al-Qura University, P.O. Box 6247, Makkah 21955, Saudi Arabia
nakoshak@uqu.edu.sa

ABSTRACT

Spatial information technologies, particularly the Geographical Information Systems (GIS), represent efficient tools in determination of drainage basin morphometric properties for water resources management and environmental planning. GIS and a high-resolution Digital Elevation Model (DEM) have been utilized for the morphometric analysis of six basins exist within Makkah metropolitan area, southwest Saudi Arabia. Several morphometric parameters have been computed and analyzed,such as total relief, relative relief, relief ratio, ruggedness number, texture ratio, elongation ratio, circularity ratio, form factor ratio, drainage density, stream frequency, sinuosity factor, and bifurcation ratio. Impacts of morphometric parameters on flash flood characteristics have been also investigated. It has been found that the catchment no. 3 has the least time of concentration, the highest runoff depth. Such hydrological hazards are mainly due to the basin's small area and its highest relief ratio, relative relief, and ruggedness factor. Hence, it is concluded that this specific catchment might be considered as the most hazardous area in Makkah city in terms of flash flood impacts. Therefore, it is recommended that the attained results be utilized in water resources management and environmental planning in Makkah city.

Keywords: GIS, DEM, morphometry, water resources, Saudi Arabia.

1. Introduction

The hydrological and physical characteristic description of a watershed constitutes an essential task for hydrologic and water resource management projects. Delineation of hydrologic basins and determination of their morphometric parameters has been considered as regular geomorphologic tasks. Spatial information technologies, particularly Geographic Information Systems (GIS) and remote sensing (RS), have proved to be efficient tools in delineation of drainage pattern and water resources planning. GIS has been widely used in several geomorphologic, morphometric, flood management, and environmental applications (e.g. Dawod and Mohamed, 2009, El Bastawesy et al., 2010, Rao, et al., 2010, Dawod and Mohamed, 2008, and Dongquan et al., 2009). In Kingdom of Saudi Arabia (KSA), several morphometric and hydrological investigations have been carried out using different datasets and methodologies. Dawod et al. (2011) has developed a GIS-based flood management approach, including delineation of catchments, for Makkah metropolitan area. Dawod and Koshak (2011) utilized GIS to develop unit hydrographs for flood and water resources management within Makkah city. Also, Al Suad (2009) has applied topographic maps, IKONOS and ASTER remote sensed images, and GIS to delineate more than 20 sub-basin in wadi Auranh, southwest KSA. Elaji (2010) also utilized a number of GIS software along with

ASTER Digital Elevation Model (DEM) to construct a morphometric and hydrologic databases for Yalamlam basin. Moreover, Al-Ghamdi (2004) has utilized IRS and LandSat-5 remote sensing images to extract drainage networks in Nomaan mountainous area, southwest KSA. In addition, Shehata and Koshak (2007) have constructed a 3D GIS to understand and analyze the locations, types, and sizes of the possible natural risks in Mina, near Makkah city.

2. Study Area

Makkah city is located in the south-west part of KSA, about 80 Km east of the Red Sea (Fig. 1). It extends from 39° 35' E to 40° 02' E, and from 21° 09' N to 21° 37' N. The area of the metropolitan region (the study area) equals 1593 square kilometers approximately. The topography of Makkah is complex in nature, and several mountainous areas exist inside its metropolitan extent.

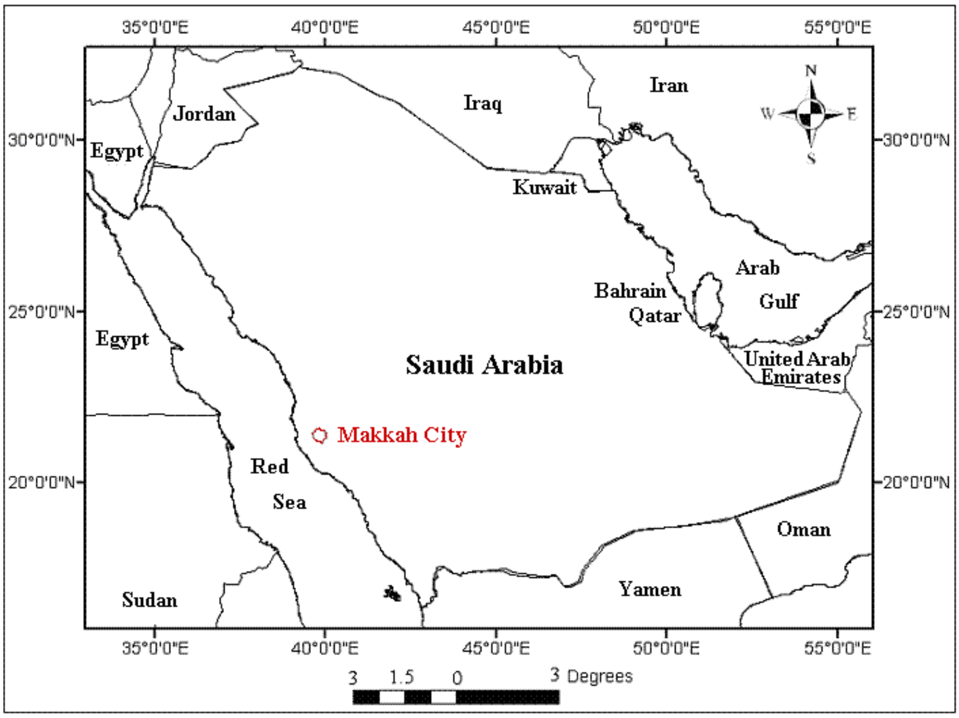

Figure 1: Study area map

The winter is considered as the main rainy season in Saudi Arabia. The annual rain over Makkah city, for a period extends from 1966 to 2009, varies from 3.8 mm to 318.5 mm, with an average of rainfall equals 101.2 mm (Dawod et al., 2011). Due to the complexity of Makkah's topography, flash floods occur periodically with significant variations in magnitude. Regarding the geology of Makkah metropolitan area, Precambrian volcanic rocks constitute the main geological features that define the general topography framework, particularly the mountainous structures, in this area. These rocks may be classified into several categories, but the most widespread types are: the precambrian layered rocks, e.g. unassigned amphibolites, tonalities, and diorite, that constitute about 65% of the area; and the Precambrian intrusive rocks that occupy approximately 20% of the area (Mirza and Barodi, 2004). The second main geological feature in Makkah is the quaternary deposits, e.g. sands and pebbles, exist in lower streams of the basins.

3. Morphometric Parameters

A number of common parameters are usually utilized in order to describe the morphometric and geomorphologic properties of a watershed. Such parameters can be grouped in four categories: topographic, areal, relief, and network properties. Although details can be found in several literature (e.g. Huggett, 2007, and Horton, 1945), table 1 presents mathematical formulas for computing morphometric parameters of a watershed.

3.1 Data and Methodology

The main utilized data piece is a Digital Elevation Model (DEM) for the study area. The acquired DEM produced by the by King Abdulaziz City of Sciences and Technology (KACST) with a horizontal spatial resolution equals 5 meters.

Table 1: Morphometric Parameter Mathematical Formulas

Parameter	Formula
Topographic properties	
Area of basin (km^2)	A
Perimeter of basin (km)	P
Maximum length: L_{max}	The maximum basin length
Relief properties	
Basin relief: ΔH	$\Delta H = H_{max} - H_{min}$
Relative relief: R_{hp}	$R_{hp} = \Delta H / P$
Relief ratio: R_h	$R_h = \Delta H / L_{max}$
Ruggedness number: N	$N = \Delta H . D$
Areal properties	
Texture ratio: T	$T = N_1 / P$
Elongation ratio: R_l	$R_l = 2 [\sqrt{} (A / \prod)] / L_u$
Circularity ratio: R_c	$R_c = 4 \prod A / P^2$
Form factor ratio: R_f	$R_f = A / L_b^2$
Network properties	
Drainage density (km/km^2): D	$D = L_u / A$
Stream frequency: F_s	$F_s = N_u / A$
Sinuosity Factor: S	$S = L_b / L_{min}$
Bifurcation Ratio: R_{b-m}	R_b = Number of streams of an order / number of streams of the next order. A mean value of this coefficient (R_{b-m}) is usually used for a watershed.
where: L_u = Total stream length of all orders, N_u = Total number of streams of all orders, N_1 = Total number of streams of 1st order, L_b = Basin length (km), H_{max} = The elevation of the highest point in the basin , H_{min} = The elevation of the lowest point in the basin , L_{min} = shortest distance between spring and outlet, and $\prod$ = 22 / 7	

A window covers Makkah metropolitan area (Fig. 2) has been provided through the Center of Excellence in Hajj and Omrah, Umm Al-Qura university. Mirza et al (2010) confirm that that national DEM is 3 times more accurate than published global ASTER and SRTM3 DEMs. From Fig. 2, it can noticed that the heights of Makkah metropolitan area range from 80 to 982 meters. In order to precisely determine morphometric parameters in Makkah metropolitan area, GIS technology has been utilized. The Arc GIS, Arc Hydro, and Tau DEM software have been applied in the current research to determine the morphometric parameters of Makkah city' basins. Additionally, some programming steps have been performed within the attribute tables to compute necessary morphometric quantities.

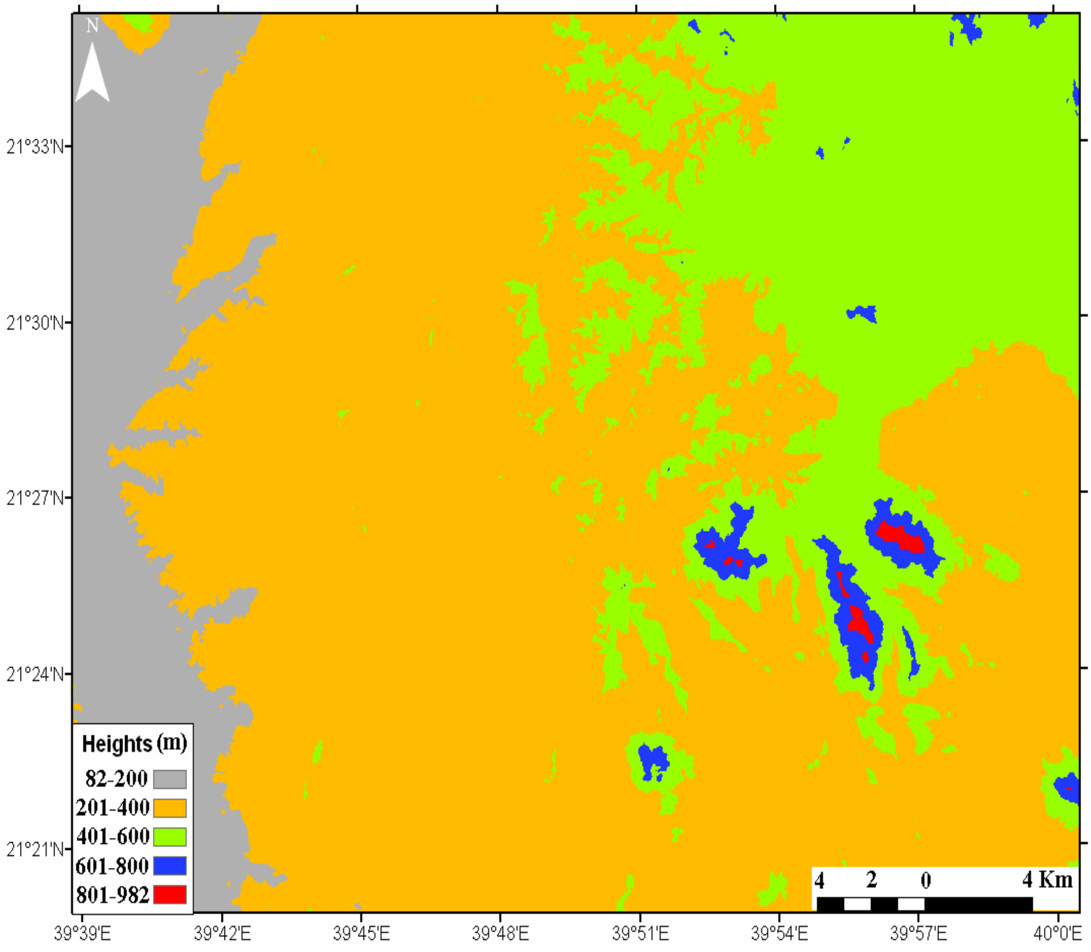

Figure 2: The National 5-m DEM for Makkah city

4. Results and Discussion

Utilization of the Arc GIS software, along with some other associated extensions, has resulted in delineating six watersheds within Makkah metropolitan area (Fig. 3). Four catchments are entirely located within the study area, while basins C5 and C6 represent sub-basins that exits within Makkah metropolitan extent but belong to some large basins surround Makkah city. Table 2 presents the topographic properties of these watersheds. Basin areas range from 74.3 to 360.6 square kilometers, while the basin perimeters vary from 50.2 to 134.9 kilometer. The maximum length of stream, which is a significant morphometric parameter, varies from 16.5 to 48.6 kilometer.

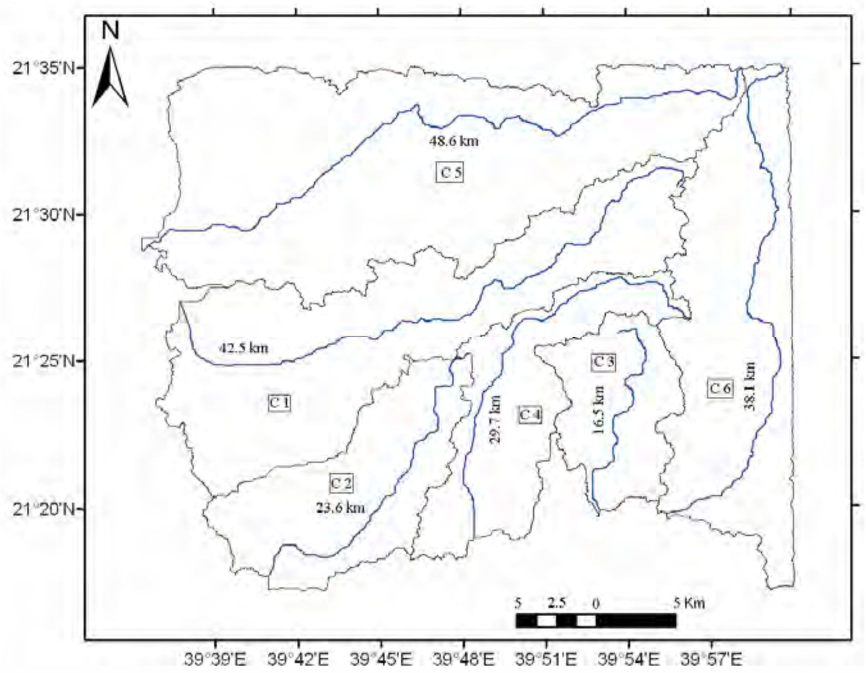

Figure 3: Watersheds and their main streams

Table 2: Statistics of topographic properties

Item	C1	C2	C3	C4	C5	C6
Basin Area (km^2)	252.7	122.3	74.3	109.9	360.6	200.2
Basin Premier (km)	134.6	69.1	50.2	89.1	134.9	102.0
Length of Main Stream (km)	42.5	23.6	16.5	29.7	48.6	38.1

Concerning the relief properties of the study area' watersheds, Table 3 presents the accomplished results. The total relief varies from 333 meters to 769 meters, while the relief ration, in m/km, range between 12.6 and 40.4. Additionally, the relative relief ranges from 4.0 to 13.3 meters, while the ruggedness value vary from 33.7 to 104.3.

Table 3: Statistics of relief properties

Item	C1	C2	C3	C4	C5	C6
Total Relief (m)	546	333	667	769	632	714
Relief ratio (m/km)	12.6	14.1	40.4	25.9	13.0	18.7
Relative relief (m)	4.0	4.8	13.3	8.6	4.7	7.0
Ruggedness value	33.7	38.1	104.3	66.4	33.8	51.1

It has been found that catchment no. 3 has the maximum relief ratio, relative relief, and ruggedness factor even though it does not have the maximum height difference (total relief). That might be due to the smallest basin area of that catchment (only 74.3 square kilometers as seen in Table 2). Hence, that catchment can be considered the most topographical-complex basin in the study area, which will result in more steep morphometric characteristics as will

be seen later on. Table 4 presents the attained results of the aerial properties of the catchments within Makkah metropolitan area. The circularity ratio is the ratio of the basin area to the area of a circle has the same circumference. It is influenced by the length and frequency of streams, geological structures, land use, and the slope of the watershed. Catchment no. 3 has the highest circularity ratio (0.37) and catchment no. 2 has a closer value (0.32). It can be seen from Fig. 2 that these two basins are the closer to a circular shape. Again, catchment no. 3 has the highest circularity ratio even though it is the smallest watershed, which is considered as a hazardous indication since it means that the flash floods could reach great volume over a small area. On the other hand, the elongation ratio represents how close a basin to a rectangular shape. From table 4, it can be seen that two basins have rectangular ratio grater than 0.5, while the other four have elongation ratios less than 0.4. Hence, the six catchments in Makkah metropolitan area are far from a complete rectangular shape (see Fig. 2). Moreover, the form factor ratio is another indication of the basin circularity. Its value is always less than 0.785, for a perfectly circular basin (Horton, 1945). The attained form factor ratios for the study area vary from 0.12 to 0.27, which also means that six basins don't represent a circular shape. Additionally, the texture ratio of the six basins vary from 3.46 to 7.86, which indicates that it may be classified as a medium texture. It is known that the basins have similar geological, structural, and hydrological conditions will nearly have the same category of texture ratio (Sherief, 2008). It is concluded that the complex topography of the study area plays a major factor affecting the aerial characteristics of those watersheds.

Table 4: Statistics of aerial properties

Item	C1	C2	C3	C4	C5	C6
Texture ratio: T	5.69	5.58	4.20	3.46	7.86	5.98
Elongation ratio: R_l	0.42	0.53	0.59	0.40	0.44	0.42
Circularity ratio: R_c	0.18	0.32	0.37	0.17	0.25	0.24
Form factor ratio: R_f	0.14	0.22	0.27	0.12	0.15	0.14

The network properties are considered the major morphometric characteristics of watersheds. Stream order is used to denote the hierarchical relationship between stream segments and allows drainage basins to be classified according to size. Several stream-ordering systems exist, the most commonly used being those devised by Arthur N. Strahler and by Ronald L. Shreve. In Strahler's ordering system (which is used in the current research), a stream segment with no tributaries that flows from the stream source is denoted as a first-order segment.

A second order segment is created by joining two first-order segments, a third-order segment by joining two second order segments, and so on. It has been found that the maximum stream order in the six watersheds, in the study area, equals 5 for the four small sub-basins (No. C2, C3, C4, and C6) and reaches order 6 in the other two sub-basins (C1 and C5), which have the maximum basin areas (Table 5). Figure 4 depicts the stream order spatial variations in Makkah metropolitan area. Analyzing the variations of streams' length, Table 6 concludes that there is an inversely proportional relationship between stream lengths and stream orders.

Table 5: Statistics of basin stream orders

Catchment	C1	C2	C3	C4	C5	C6
No. of streams of Order 1	766	386	211	308	1059	610
No. of streams of Order 2	257	109	65	85	318	171
No. of streams of Order 3	45	23	13	25	53	40
No. of streams of Order 4	10	4	4	5	14	9
No. of streams of Order 5	3	1	1	1	3	1
No. of streams of Order 6	1	NA	NA	NA	1	NA
Total No. of streams	1082	523	294	424	1448	831

Table 6: Statistics of basin stream lengths' percentage

Catchment	C1	C2	C3	C4	C5	C6
Order 1	51.0%	54.3%	50.4%	54.1%	53.0%	51.5%
Order 2	26.2%	23.4%	23.8%	24.6%	22.7%	23.2%
Order 3	12.3%	11.7%	14.9%	8.6%	12.3%	14.1%
Order 4	4.3%	6.3%	7.1%	11.6%	5.8%	7.4%
Order 5	5.4%	4.4%	3.8%	1.1%	4.7%	3.7%
Order 6	0.8%	N/A	N/A	N/A	1.5%	N/A

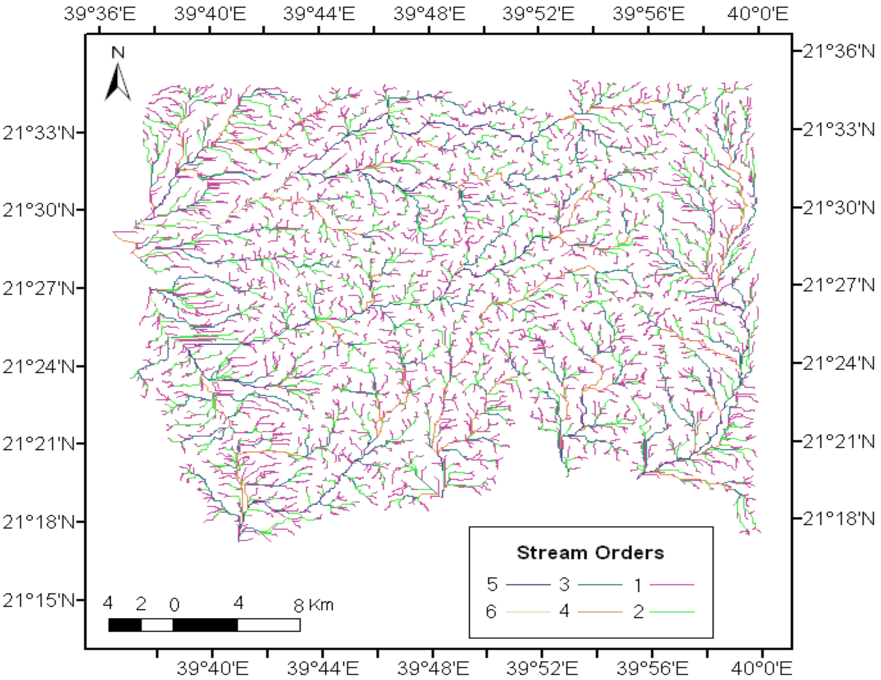

Figure 4: Stream orders of watersheds

Drainage density is a measure of how frequently streams occur on the land surface. It indicates the closeness of spacing between channels and is a measure of the total length of the stream segment of all orders per unit area. It reflects a balance between erosive forces and the resistance of the ground surface, and is therefore related closely to climate, lithology, and vegetation. Drainage densities can range from less than 5 km/km2 when slopes are gentle,

rainfall low, and bedrock permeable, to much larger values of more than 500 km/km2 in upland areas where rocks are impermeable, slopes are steep, and rainfall totals are high (Huggett, 2007). Table 6 that the drainage density for Makkah's sub-basin range from 2.56 to 2.73 km/km^2. So, that can classified, in general, as a medium drainage density pattern. Moreover, the stream frequency for Makkah's sub-basin vary between 3.86 and 4.28 streams/km^2 (Table 7). Generally, the stream frequency has positive correlation with the drainage density of all sub-watersheds, suggesting increase in stream population with respect to increase in drainage density. Also, the sinuosity factor of the basins within Makkah metropolitan area range from 1.21 to 1.42. Thus, those streams can be classified as from transitional to regular streams, which is due to the steep slopes in the topography of the study area.

Another commonly used topological property is the bifurcation ratio, that is, the ratio between the number of stream segments of one order and the number of the next-highest order. A mean bifurcation ratio is usually used because the ratio values for different successive basins will vary slightly. With relatively homogeneous lithology, the bifurcation ratio is normally not more than five or less than three. However, a value of ten or more is possible in very elongated basins where there are narrow, alternating outcrops of soft and resistant strata. The values of mean bifurcation ratios, in the study area, slightly vary between 3.87 to 5.32 (Table 7). Similar results for some small sub-watersheds have been reported (Altın and Altın, 2011, and Javad et al., 2009).

Table 7: Statistics of network properties

Item	C1	C2	C3	C4	C5	C6
Drainage density: D (km/km^2)	2.67	2.71	2.58	2.56	2.59	2.73
Stream frequency: F_s (stream/km)	4.28	4.28	3.96	3.86	4.02	4.15
Sinuosity Factor: S	1.26	1.21	1.26	1.42	1.25	1.30
Bifurcation Ratio: R_{b-m}	3.90	4.51	3.87	4.26	4.16	5.32

A correlation analysis has been performed between the main morphometric parameters of the six sub-basins. The results (Table 8) showed that the basin area, with a positive correlation equals 0.999, is the most effective element that influences the sum of stream lengths of all orders. Moreover, the basin width and length also resulted in high positive correlation values, 0.95 and 0.91 respectively. On the other hand, the total relief, or height difference, has a non-significant negative impact, -0.02, to the sum of stream lengths of all orders. Similar results have been reported by Subyani et al. (2010) for major basins in western Saudi Arabia.

Table 8: Correlation between main morphometric parameters

Item	$\sum L_n$	A	ΔH	L	W
$\sum L_n$	1				
A	0.999	1			
ΔH	-0.02	-0.01	1		
L	0.91	0.92	-0.22	1	
W	0.95	0.94	0.14	0.74	1
where: $\sum L_n$ = sum of stream length of all orders, A = basin area, ΔH = total relief, L = length of main stream of the basin, and W = basin width.					

In order to study the relationship between the morphometric properties of watersheds and their hydrological impacts, Table 9 summarizes some flood hazard factors. The time of concentration is the time elapsed of a water drop to travel from the farthest point of a basin to its outlet. The catchment no. 3 has the least time of concentration (1.73 hours), the highest runoff depth (178.8 mm). Such hydrological vulnerabilities are mainly due to the basin's small area and its highest relief ratio, relative relief, and ruggedness factor. Again, that catchment might be considered as the most hazardous area in Makkah city in terms of flash flood impacts.

Table 9: Flood characteristics in Makkah city

Item	C1	C2	C3	C4	C5	C6
Time of concentration (hours)	5.69	3.76	1.73	2.63	6.72	4.17
Runoff depth (mm)	151.7	151.7	178.8	166.7	151.7	148.8

After Dawod et al., 2011

5. Conclusions

Delineation of hydrologic basins and determination of their morphometric parameters are standard geomorphologic tasks. GIS has been utilized to compute several morphometric parameters for six basins within Makkah city, southwest Saudi Arabia, for water resources management and environmental planning. The accomplished results show that the basins' areas range from 74.3 to 360.6 square kilometers, while the maximum length of stream varies from 16.5 to 48.6 kilometer. Additionally, the total relief varies from 333 meters to 769 meters, while the relief ration range between 12.6 and 40.4 m/km. In addition, the relative relief ranges from 4.0 to 13.3 meters, while the ruggedness value vary from 33.7 to 104.3. It has been found that catchment no. 3 has the maximum relief ratio, relative relief, and ruggedness factor even though it does not have the maximum height difference (total relief). That might be due to the smallest basin area of that catchment (only 74.3 square kilometers. Hence, that catchment can be considered the most topographical-complex basin in the study area, which will result in more steep morphometric characteristics.

Also, it has been found that the maximum stream order in the six watersheds, in the study area, equals 5 for the four small sub-basins and reaches order 6 in the other two sub-basins The correlation results showed that the basin area is the most effective element that influences the sum of stream lengths of all orders. The drainage density for Makkah's sub-basin range from 2.56 to 2.73 km/km^2. So, that can classified, in general, as a medium drainage density pattern. Dawod et al. (2011) have found out that the catchment no. 3 has the least time of concentration, the highest runoff depth. Such hydrological hazards are mainly due to the basin's small area and its highest relief ratio, relative relief, and ruggedness factor. Again, it is concluded that this particular catchment may be regarded as the most hazardous area in Makkah city in terms of flash flood impacts. Therefore, it is recommended that the attained results be utilized in hydrological, water resources, and environmental management in Makkah city, Saudi Arabia.

Acknowledgements

The authors would like to acknowledge the financial support offered by the Center of Research Excellence in Hajj and Omrah, Um Al-Qura university, Saudi Arabia.

6. References

1. Al Saud, M (2009), Watershed characterization of wadi Aurnah, western Arabian Peninsula, Journal of Water Resource and Protection, 1, pp 316-324.

2. Al-Ghamdi, S (2004), The extraction of drainage network using image processing of digital satellite data, case study: Noman mountainous area (in Arabic), Journal of Umm Al-Qura University of Social Sciences, 16(2), pp 287-316.

3. Altın, T. and Altın, B (2011), Development and morphometry of drainage network in volcanic terrain, Central Anatolia, Turkey, Geomorphology, 125, pp 485–503.

4. Elaji, A. (2010), Applications of Geographic Information Systems to construct databases of morphometric characteristics and their hydrologic meanings in Yalamlam basin , MSC thesis, Umm Al-Qura university, Makkah, Saudi Arabia.

5. El Bastawesy, M., Faid, A., and El Gammal, E. (2010), The Quaternary development of tributary channels to the Nile River at Kom Ombo area, Eastern Desert of Egypt, and their implication for groundwater resources , Journal of Hydrological Processes, 24, pp 1856–1865.

6. Dawod, G., Mirza, M., and Al-Ghamdi, K. (2011), A GIS-based approach for estimating flash flood hazards in Makkah metropolitan area, Saudi Arabia, Journal of Geographical Information System, 3(3), pp 217-223..

7. Dawod, G., and Koshak, N. (2011), Developing GIS-Based Unit Hydrographs for Flood Management in Makkah Metropolitan Area, Saudi Arabia, Journal of Geographic Information System, 3(2), pp 153-159.

8. Dawod, G., and Mohamed, W. (2009), Data management of different height systems within GPS/GIS integrated spatial technology, Middle East Spatial Technology Conference (MEST2009), December 7-9, Kingdom of Bahrain.

9. Dawod, G. and Mohamed, H. (2008), Estimation of Sea Level Rise Hazardous Impacts in Egypt within a GIS Environment, Proceedings of the Third National GIS Symposium in Saudi Arabia, April 7 – 9, Al-Khobar City, Saudi Arabia.

10. Dongquan, Z., Jining, C., Haozheng, W., Qingyuan, T., Shangbing, C., and Zheng, S. (2009), GIS-based urban rainfall-runoff modeling using an automatic catchment-discretization approach: a case study in Macau, Journal of Environmental Earth Sciences, 59, pp 465–472.

11. Huggett, R. (2007), Fundamentals of geomorphology, Second edition, Routledge, New York, USA, pp 464 .

12. Horton, R. (1945), Erosional development of streams and their drainage basins: Hydrological approach to quantitative morphology, Geological Society Bulletin, 56, pp 275-370.

13. Javad, A., Khanday, M., and Ahmed, R. (2009), Prioritization of sub-watersheds based on morphometric and land use analysis using remote sensing and GIS techniques, Journal of Indian Society of Remote Sensing, 37, pp 261-274.

14. Mirza, M., and Barodi, M. (2004), "Geological basis and their role in surface feature development in Haram area, Makkah", Social Science Researches, No. 56, Umm Al-Qura University, Saudi Arabia, pp 133.

15. Mirza, M., Dawod, G., and Al-Ghamdi, K. (2011), Accuracy and Relevance of Digital Elevation Models for Geomatics Applications - A case study of Makkah Municipality, Saudi Arabia, International Journal of Geomatics and Geosciences, 1(4), pp 803-812..

16. Rao, N., Latha, S., Kumar, A., and. Krishna, H. (2010), Morphometric Analysis of Gostani river basin in Andhra Pradesh state, India using spatial information technology, International Journal of Geomatics and Geosciences, 1(2), pp 179-187.

17. Shehata, A. and Koshak, N. (2007), Using 3D GIS to assess environmental hazards in built environments; Case study: Mina, Al-Azhar Engineering Journal, 2(2), pp 1-11.

18. Sherief, Y. (2008), Flash floods and their effects on the development in El-Qaá plain area in south Sinai, Egypt, a study in applied geomorphology using GIS and remote sensing, PhD Dissertation, Mainz University, Germany.

19. Subyani, A., Qari, M., and Matsah, M. (2010), Digital elevation model and multivariate statistical analysis of morphometric parameters of some wadis, western Saudi Arabia, Arabian Journal of Geosciences, DOI 10-1007/s12517-010-0149-7.

International Journal of Water Resources and Environmental Engineering Vol. 4(2), pp. 23-34, February 2012
Available online at http://www.academicjournals.org/IJWREE
DOI: 10.5897/IJWREE11.128
ISSN 1991-637X ©2012 Academic Journals

Full Length Research Paper

Impacts of urban growth on flood hazards in Makkah City, Saudi Arabia

Khaled A. Al-Ghamdi[1], Ramze A. Elzahrany[1], Meraj N. Mirza[1,2] and Gomaa M. Dawod[1,3]*

[1]Geography Department, Umm Al-Qura University, Makkah, Saudi Arabia.
[2]Center of Research Excellence in Hajj and Omrah, Umm Al-Qura University, Makkah, Saudi Arabia.
[3]Survey Research Institute, Egypt.

Accepted 23 January, 2012

Flash floods are the most dangerous type of natural disasters in arid regions, such as Saudi Arabia. The effects of urban growth, witnessed between 1990 and 2010, in Makkah city, Saudi Arabia, on runoff volume and peak discharge are investigated using the curve number (CN) flood-modelling methodology. Shapefiles of residential areas are compiled and integrated in a unique geographic information system (GIS) environment. Datasets of geological structures, soil types, and a digital elevation model (DEM) have been collected and utilized. Peak discharges have been computed on the wadi scale, while the total flood volume have been estimated on the sub-basin scale for residential sub-basins in order to get a detailed view of urbanization impacts on flood hazards. The results obtained show that the residential regions of Makkah city have been increased, over the period 1990 to 2010, by 197%, while the total flood volumes have been enlarged by 248%. The spatial distribution of high-flood urban regions is mapped. Furthermore, the results show significant positive correlations between urbanization and both peak discharge and flood volume. Accordingly, these findings should be taken into account in future urbanization, sustainable development and flood management plans of Makkah metropolitan area.

Key words: Flood hazards, rainfall-runoff, curve number (CN), geographic information system (GIS), Saudi Arabia.

INTRODUCTION

The dispersed development along highways or surrounding a city and in rural countryside is called urban sprawl. Geomatics technologies, such as remote sensing (RS) and geographic information system (GIS), furnish exceptional technical tools for urban modelling and planning. Extensive studies have been carried out to investigate the utilization of RS images, in particular, in the assessment of land use and land cover changes over time (Prakasam, 2011; Arunachalam et al., 2011; Liu et al., 2011; Kioko and Okello, 2011). In addition, GIS has been widely employed as a valuable precise tool in monitoring urban sprawl for land use planning (Kelarestaghi and Jeloudar, 2011; Su et al., 2011; Antipova et al., 2011). The integration of both GIS and RS presents an exceptional technique in monitoring and prediction of urban growth (Park et al., 2011).

Generally, floods are natural returning hydrological phenomena that significantly affect human lives. The hazards of flash floods, chiefly in urban regions, are vital from both human settlement and economical perspectives. Recently, the estimation of flood hazardous impacts and the development of GIS-based flood inundation maps have been considered a crucial demand. For example, Sagala (2006) carried out a detailed vulnerability assessment study to investigate physical flood hazards, particularly buildings' damages, in a residential area depending upon a mobile GIS. Fernandez and Lutz (2010) described a GIS-based research produced flood hazard maps for two cities in Argentina based on a multi-criteria design analysis. Park

*Corresponding author. E-mail: dawod_gomaa@yahoo.com.

and Hur (2011) have utilized GIS for the development of flood simulation system for Namgang watershed, South Korea. In addition, a similar methodology was proposed and rested in Georgia, USA (Qi and Altinakar, 2011). Hagen et al. (2011) presented a simple methodology for developing a nation-wide flood hazard maps in Afghanistan as an example of developing countries.

In the Kingdom of Saudi Arabia (KSA), a great attention has been paid recently to the issue of flood assessment and flood hazards estimation. For example, Al Saud (2010) has utilized GIS and RS to assess the hazardous impacts of the flash flood that occurred in November 2009 in Jeddah city. It was concluded that flood-urbanization relationship should be considered in order to avoid further urban expansions in areas under flood risk. Dawod et al. (2011) developed a GIS-based process to quantify the flood parameters, for example, peak discharge and runoff volume, and in Makkah city based on the US National Resources Conservation Service (NRCS)'s flood modelling method (known also as the curve number (CN) methodology. Moreover, Subyani (2011) investigated the flood probability for arid basins in Makkah administrative area. Dawod and Koshak (2011) developed NRCS-based unit hydrographs for the six basins within Makkah metropolitan area as a tool for rainfall-runoff modelling and flood management. Sen (2008a) proposed modified Snyder unit hydrographs for flood modeling in Wadi Baysh, a major Wadi in the southwestern part of KSA.

With the development of urbanization, flood disaster in urban areas threatens regional sustainable development. Human encroachment on urban regions made these urban communities more vulnerable to floods, which necessitates continues updating of flood management strategies (Zheng and Qi, 2011). Land use plays a critical role in the hydrological behavior of basins, and changing land uses may influence the local hydrological cycle. The land use changing scenarios should be continuously integrated with flood hazard maps (Barredo and Engelen, 2010).

The relationship between urban growth and floods has been investigated in many countries. Paquier (2010) emphasized that the eventual change in flood discharges could be one among other factors of the changes in flood risks in the Agly River, city of Marseille, France. That study showed that flood vulnerability increased a lot because of the development of urbanization mainly in connection with recreation activities or because of the proximity of a large city. Olang and Furst (2011) studied the impacts of historical land cover changes witnessed between 1973 and 2000 on the hydrologic response of the Nyando River Basin, Kenya. The study utilized RS images, land cover change maps, a digital elevation model (DEM), and soil datasets of the basin. Their results revealed significant and varying increases in the runoff peak discharges and volumes within the basin. The study carried out by Ronfort et al. (2011) reported that the runoff volume is affected by the crop types in an agricultural watershed in upper Normandy, France. Elfert and Bormann (2011) have also studied the relation between land use and runoff in Germany. Douglas et al. (2007) pointed out that the land cover throughout London city continues to be greatly modified by urbanization, changing the response to rainfall and flood peaks and extent are becoming higher. Furthermore, it has been confirmed that the main driving force of increased flood risk is found in new urban developments in flood-prone areas in the Pordenone province in northern Italy (Barredo and Engelen, 2010). A GIS-based research showed that runoff might be increased, due to the expected urbanization in Lai Nullah basin in Pakistan, by 52 to 100% (Ali et al., 2011). In the great lake region in USA, the land use changes increased the total runoff by 10 to 40% over the period 1950 to 2000 (Mao and Cherkauer, 2009). Similarly, Im et al. (2009) reported that changes of 10% non-urban area to urban area, between 1980 and 2000, has resulted in 5.5% increase in total runoff within the Gyeongancheon watershed in Korea. Significant increase in total runoff was also reported due to the land use changes in the Golestan watershed, Iran (Saghafian et al., 2008). Another study, in New York city USA, has emphasized that suburban development and its associated impervious surfaces accelerate the transport of storm runoff (Burns et al., 2005). Moreover, Pizzuto et al. (2007) have studied the impacts of land use and climate changes on riverbeds in Maryland, USA. The results of a study in the Los Angeles metropolitan region have shown the potential increase in flood risk for various watersheds as a result of growing population. It was found that urban watersheds, on average, convert 90% of rainfall to runoff, whereas the non-urban forested watersheds retain 25% of the rainfall (Sheng and Wilson, 2009). In addition, Sherief (2008) has concluded that land use and road networks are key factors affect flood runoff volume and path in south Sinai, Egypt. The study carried out by Wang et al. (2010) presented a GIS-based process for assessing lake impairment status and identifying which human disturbances have the greatest impact on each lake for all lakes in the state of Michigan, USA. Moel et al. (2011) showed that the total amount of urban area, in the Netherlands, that can potentially become inundated due to floods from the sea or main rivers has increased six-fold during the 20th century, and may double again during the 21st century.

The current research aims to investigate and quantify the relationship between urban sprawl and flood hazards in Makkah city.

STUDY AREA

Makkah city is located in the south-west part of KSA, about 80 km east of the Red Sea (Figure 1). It extends from longitudes 39° 35' E to 40° 02' E, and from latitudes

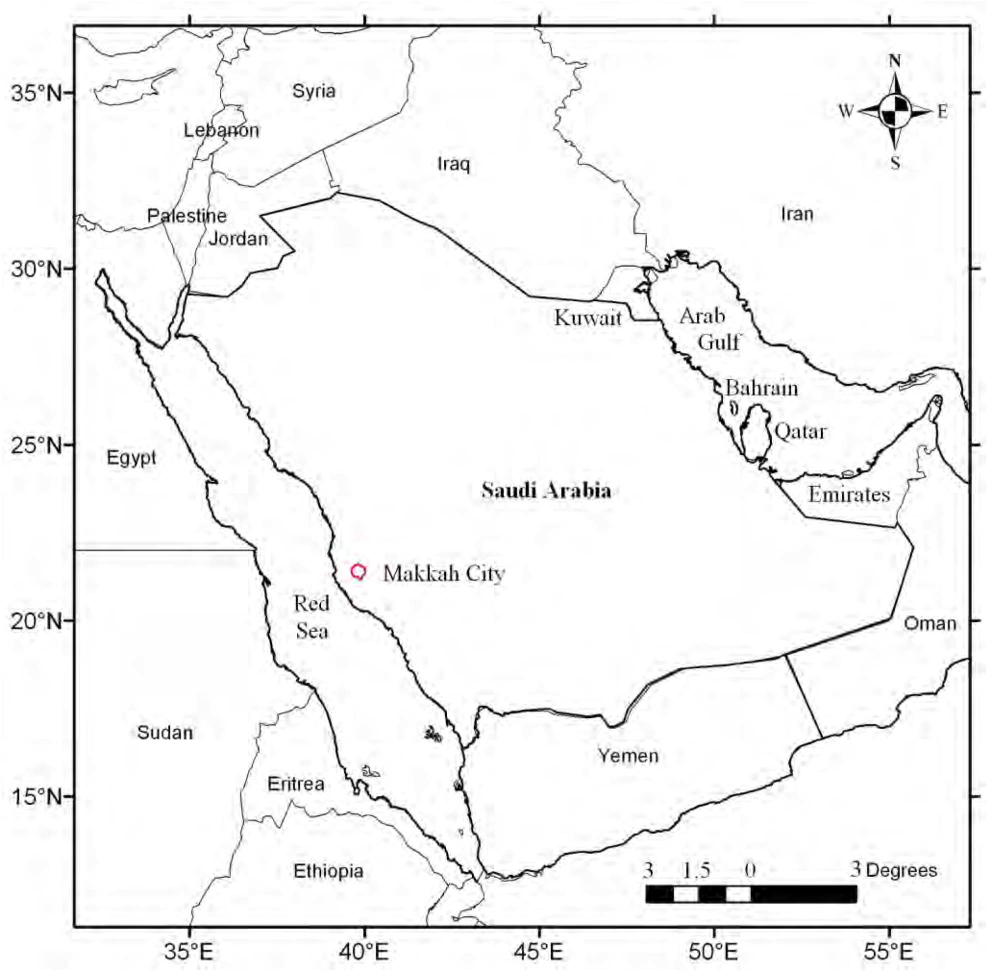

Figure 1. Location of the study area.

21° 09' N to 21° 37' N. Makkah city is a unique city for Muslims all over the world, since it contains the holly mosque. From a religious point of view, a Muslim should perform pilgrimage (called Hajj, which means visiting Makkah in specific days in the year) once in his/her life. Thus, several millions Muslims gather in Makkah yearly. In addition, Muslims prefer to perform a religious tourism plane, called Omarh, to Makkah all over the years. This is an important factor to be considered in analysing the urban growth of this city. Moreover, the topography of Makkah is complex in nature, and several mountainous areas exist inside its metropolitan area. That is also a vital element in investigating the spatial pattern of Makkah sprawl and its impacts on flood hazards.

On a national level, precise flood assessment is considered as an important demand in the Makkah metropolitan area due to the unexpected nature of rainfall that often produces hazardous flash floods. It worth mentioning that the southwest part of KSA contains almost 60% of the volume of wadi flow, particularly in the terrain situated between the Red Sea coast and the adjacent mountains (Nouh, 2006). The annual rain over Makkah city, for a period extending from 1966 to 2010, varies from 3.8 to 318.5 mm, with an average of rainfall equals 102.6 mm (Figure 2). Due to the complexity of Makkah's topography, flash floods occur periodically with significant variations in magnitude. Mirza and Ahmed (2001) reported that the extreme flood type is repeated with a return period of 46 years, while a second-order flood takes place occasionally with a return period of 33 years, and a low-dangerous flood comes about every 13 years. Using the magnitude of the annual rain average (which equals 101.2 mm) as a rain intensity factor might not be optimum in flood estimation process. The rain intensity of a single extreme storm may exceed the annual rainfall average for a year. For example, the 1969 storm records showed that the rain intensity reaches 107.5 mm/h during the first 10 min of that storm. Based on records of a single rainfall station, this extreme storm resulted in a runoff volume of more than 41 million m^3 in the central area of Makkah city, with results of severe damages and human loses (ibid). The topography of the

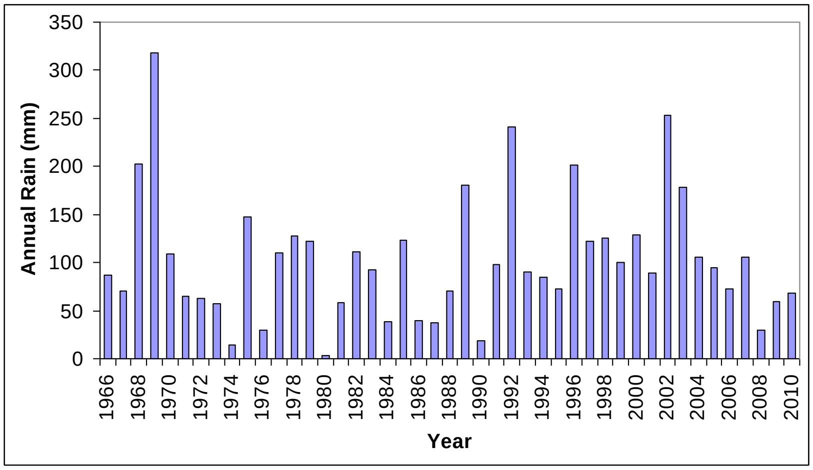

Figure 2. Annual rainfall in Makkah city from 1966 to 2010.

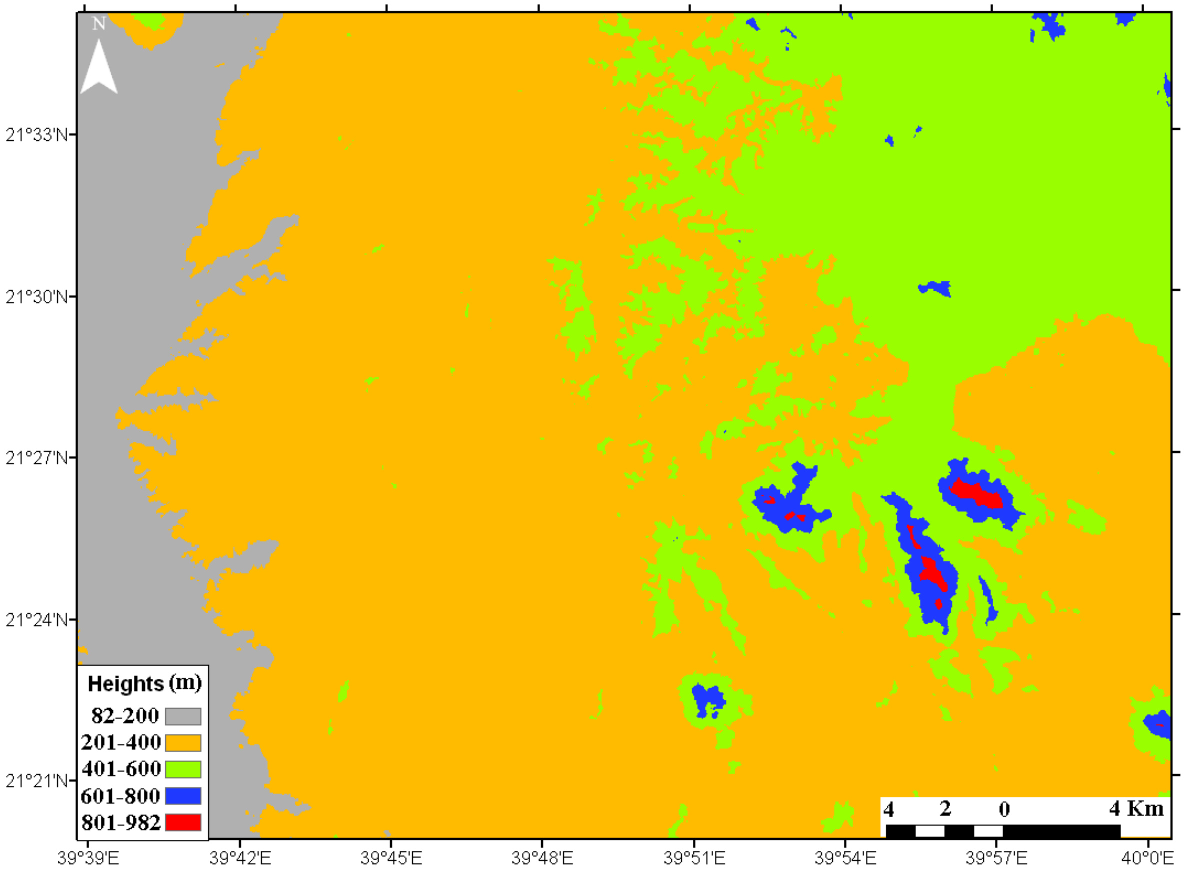

Figure 3. Terrain heights, above mean sea level, in Makkah city.

Makkah metropolitan area is complex, where several mountainous regions exist within the urban boundaries of the city. Terrain heights in Makkah (Figure 3) range from 82 to 982 m above sea level (Mirza et al., 2011). It is known that the growth in Makkah city spreads out along the valleys and stays away from the mountainous areas for economical reasons. It worth mentioning that almost 50% of Makkah's geology contains igneous rocks, mainly granite, that massively increase the development costs in mountainous areas.

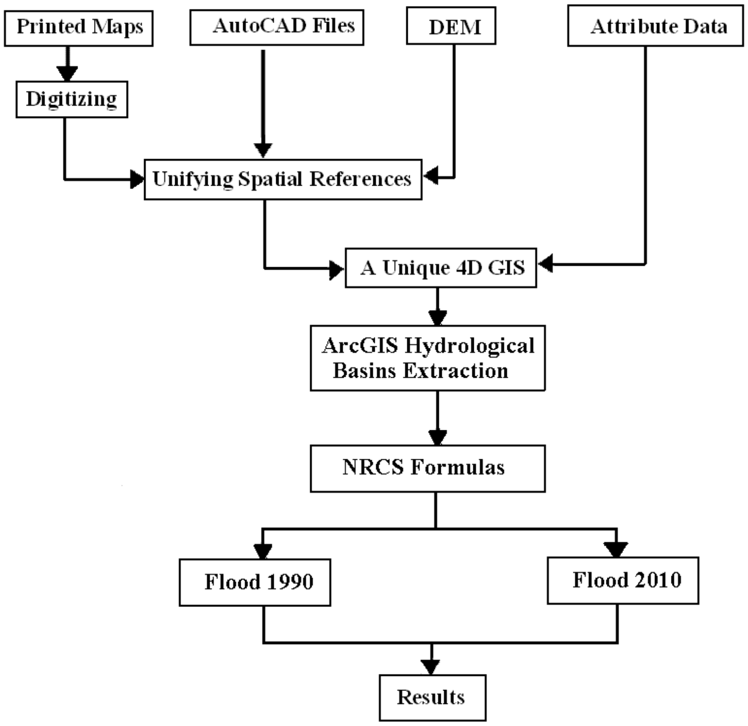

Figure 4. Summary of the employed processing procedures**.**

MATERIALS AND METHODS

The compiled available spatial datasets constitute of two categories for 1990 and 2010. The first element consists of 105 cadastral maps in AutoCAD format for 1990, obtained from the Makkah governorate. The second constituent consists of a land use map developed by the Saudi geological survey authority dated 2010. Additionally, a national 5-m resolution DEM for the study area (Figure 3) has been obtained from King Abdulaziz City of Sciences and Technology (KACST). The Arc GIS software (v. 10) has been used in the present study to combine all obtainable data in a unique environment. The processing phase includes (Figure 4): rectifying the printed maps, digitizing shapefiles for residential, converting AutoCAD files to GIS shapefiles, unifying the spatial reference frames for all datasets, estimating flood characteristics, particularly the flood volume, through the curve number methodology, and comparing the attained quantitative for 1990 and 2010. The ArcGIS and ArcHydro programs were utilized to extract the main hydrological basins in the study area, and their sub-basins. The spatial analysis tools have been utilized to assign the CN value of each sub-basin based on its geological, soil, and land use properties. Visual basic application (VBA) was utilized to compute sub-basins' flood characteristics, for 1990 and 2010, within the attribute table of GIS shapefiles.

Countless approaches have been proposed globally for estimating flood characteristics based on topographic and morphometric properties of hydrological regions. The NRCS, formerly known as the soil conservation service (SCS), might be considered as the most widely-utilized flood modelling methodology. It utilizes geological information to assign a unique CN coefficient value for each area that will be further used to estimate the surface runoff depth and the peak discharge magnitude. The NRCS method is utilized in engineering design and flood management projects in several countries (Masoud, 2011; Al-Jabari et al., 2009; Adebayo et al., 2009; Elaji, 2010; Xianzhao and Jiazhu, 2008; Gul et al., 2009), and particularly in USA (US ACE, 2004; US DoT, 2002). The basic formulas of the NRCS approach are (US NRCS, 1986):

$$Q = (P – 0.2 S)^2 / (P + 0.8 S) \quad (1)$$

Where,
Q = depth of direct runoff (mm)
P = depth of precipitation for a specific return period (mm)
S = maximum potential retention (mm):

$$S = 25.4 ((1000 / CN) – 10) \quad (2)$$

Tables providing values of CN, for soil and geological types, are presented in several hydraulic literatures (Sen, 2008b: 165). Table 1 presents some of these CN values.

$$qp = qu\ A\ Q \quad (3)$$

Where,
qp = peak discharge (m^3/s)
A = drainage area (km^2)
Q = depth of runoff (mm)
qu = unit peak discharge ($m^3/s/km^2/mm$) that can be interpolated from a specific charts (e.g. US NRCS, 1986) or computed from corresponding tables (US DoT, 2002: 5-28).

$$Q_T = Q\ A \quad (4)$$

Where Q_T = Flood volume (m^3)

$$Q_P = qu\ A \quad (5)$$

Table 1. Examples of runoff CN values.

Cover type	Hydrological soil types			
	A	B	C	D
Fully developed urban areas (vegetation established):				
Good condition; grass cover on 75% or more of the area	39	61	74	80
Fair condition; grass cover on 50 to 75% of the area	49	69	79	84
Poor condition; grass cover on 50% or less of the area	68	79	86	89
Streets and roads:				
Paved with curbs and storm sewers (excl. right-of-way)	98	98	98	98
Gravel (incl. right-of-way)	76	85	89	91
Industrial districts (72% average impervious)	81	88	91	93
Commercial and business areas (85% average impervious)	89	92	94	95

Where: Group A soils have low runoff potential and high infiltration rates even when thoroughly wetted, Group B soils have moderate infiltration rates when thoroughly wetted, Group C soils have low infiltration rates when thoroughly wetted, Group D soils have high runoff potential and low infiltration rates when thoroughly wetted. After US NRCS, 1986.

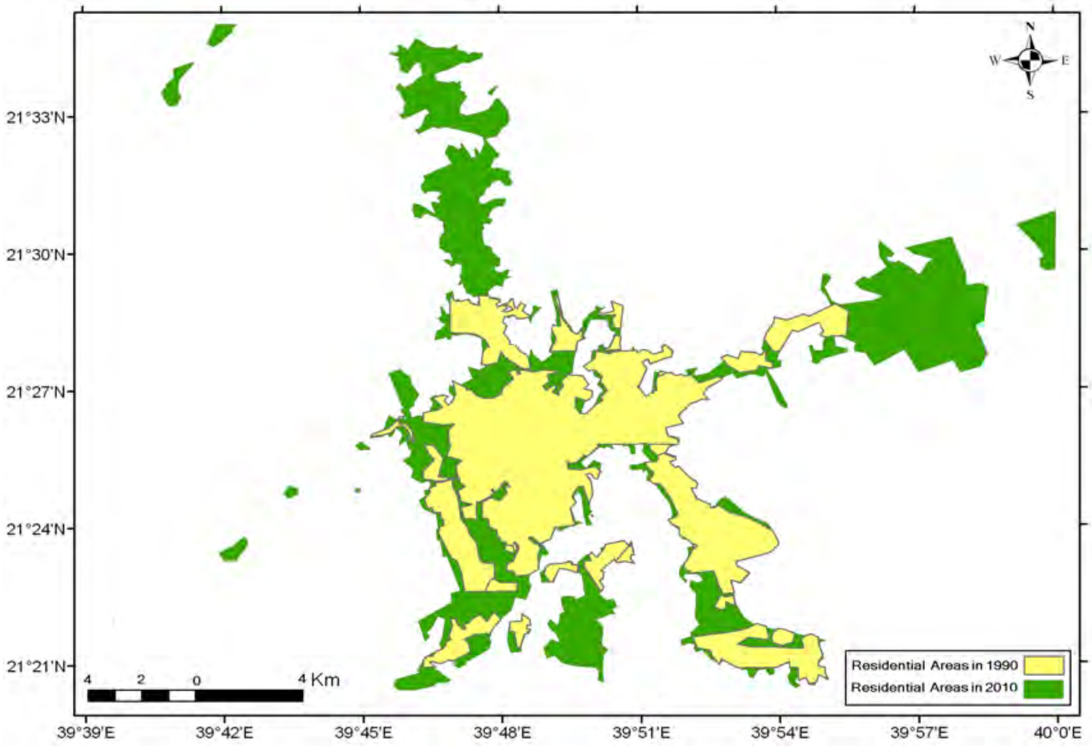

Figure 5. Urban sprawl patterns of Makkah city for 1990 and 2010.

Where Q_P = peak discharge (m3/s).

RESULTS AND DISCUSSION

In the first processing step, shapefiles of Makkah metropolitan area for 1990, and 2010 have been integrated in a GIS project (Figure 5). The total residential area has been computed and found to be 80.021 and 157.564 km^2 for 1990 and 2010 respectively. This means that the residential areas in Makkah city have been grown by about 97% from 1990 to 2010 (with a 4.8% annual rate). The most important reason behind the huge urban sprawl in mid-20th century might be the enormous national income expansion due to oil exploration in the Gulf region. This economical enlargement caused an

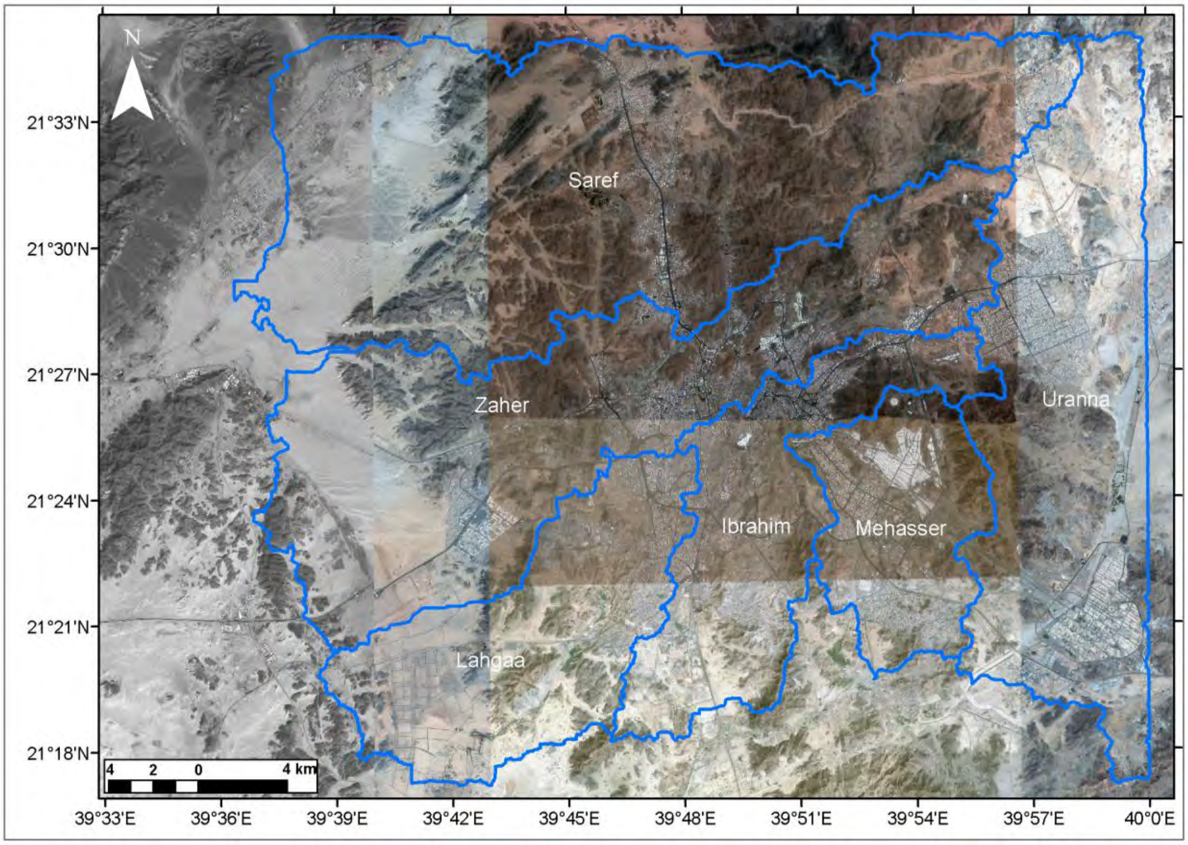

Figure 6. The main basins in the Makkah metropolitan area.

Table 2. Statistics of morphometric quantities of the main basins in the Makkah metropolitan area.

Item	C1	C2	C3	C4	C5	C6
Basin area (km^2)	252.7	122.3	74.3	109.9	360.6	200.2
Basin Premier (km)	134.6	69.13	50.23	89.09	134.76	102.03
Length of main stream (km)	42.48	23.64	16.50	29.70	48.55	38.13
Relief ratio (m/km)	12.6	14.1	40.4	25.9	13.0	18.7

Where C1: Zaher wadi, C2: Ibrahim wadi, C3: Mehasser wadi, C4: Lahgaa wadi, C5: Sareef wadi; and C6: Uranna wadi.

urban development revolution not just in Makkah city but also in almost all towns within Saudi Arabia. Secondly, the official planning rules and governmental authority have been started in 1955 in order to regulate the urban development of Makkah city (HAMDD, 2004).

Secondly, six main hydrological basins have been identified, in Makkah city, with areas ranging from 74.3 to 360.6 km^2, and lengths of their main streams varying from 16.50 to 48.55 km (Figure 6). Table 2 presents the statistics of some of the hydrological parameters of these basins. A comprehensive GIS-based morphometric analysis of these basins has been carried out (Koshak and Dawod, 2011). A number of 60 sub-basins have been recognized within these six basins.

Furthermore, the NRCS method has been performed for the available data of Makkah metropolitan area to compute the peak discharge value for the six basins for the 1990 and 2010 datasets. The return period has been chosen, herein, as 50 years, for which the rainfall intensity (P in Equation 1) has been estimated, by applying the Log Pearson III statistical analysis, as 200 mm/h (Dawod et al., 2011).

The first stage of the flood hazard estimation has been performed on the main-basin level. In this phase, the peak discharges have been computed (Equation 5) for the six main basins of the study area for both 1990 and 2010. The differences, in peak discharges of six basins, range from 11 to 88 m^3/s. In a relative sense, this is an

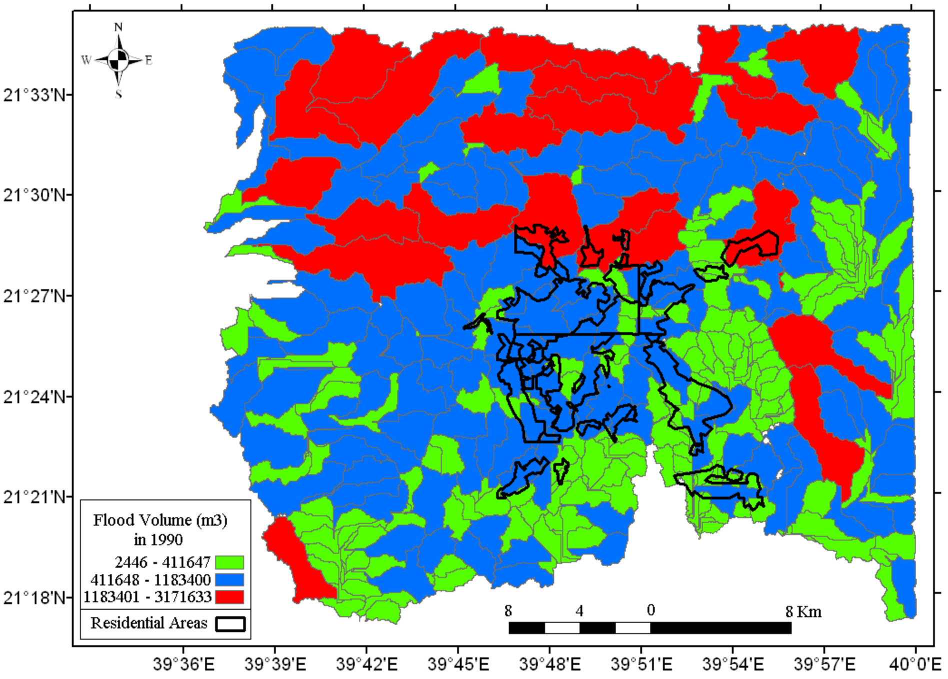

Figure 7. Floods over residential areas in 1990.

Table 3. Statistics of floods over residential areas in 1990 and 2010.

Item	1990	2010
Number of sub-basins contain residential areas	25	64
Total area of residential areas (km^2)	80.021	157.564
Minimum flood volumes (m^3)	79,623	45,487
Maximum flood volumes (m^3)	1,809,701	2,928,694
Total flood volumes (m^3)	11,849,980	41,282,085

increase of 1.1 to 3.5% relative to the 1990 peak discharge values. Such results only provide an overall view of the inter-relationship between urbanization and flood hazards. The mean increase of flood peak discharge, 1.8%, might not the optimum mathematical element to revalue the impact of urban growth in Makkah city. It worth mentioning that the urban areas only constitute 7.3 and 14.4% out of the total area of the six watersheds (which is 1095 km^2). Hence, their effects on the peak-discharge increase are small, but they give a general indication that urbanization increases flood hazardous impacts.

In the second phase of data processing, the total flood volumes have been computed on the sub-basin scale, only for those sub-basins which contain residential areas. A total of 25 sub-basins, that include residential areas in 1990, have been identified within the study area (Figure 7). Table 3 presents the statistical properties of the flood properties in residential areas in 1990. The area of these sub-basins range from 0.478 to 10.663 km^2, with a sum of 71.587 km^2. The flood volumes of these sub-basins have been estimated (equation 4) for 1990 and found to vary from 79.6 to 1809.7 thousands m^3 with a total of 11849.9 thousands m^3.

Then, utilization of the 2010 datasets revealed that there are 64 sub-basins that include residential areas (Figure 8). Table 3 also presents the attained statistical properties of the 2010 flood properties. The area of these sub-basins range from 0.223 to 18.569 km^2, with a sum of 157.564 km^2. The flood volumes of these sub-basins have been estimated for 2010 and found to vary from 45.5 to 2928.7 thousands m^3 with a total of 41282.1 thousands m^3.

Comparing the results of flood estimation for both 1990 and 2010 reveals critical points. First, the residential areas of Makkah city have been increased, over the twenty year period, from 80.0 to 157.6 km^2, with 197% increase (with an annual rate of 9.8%). Second, the total

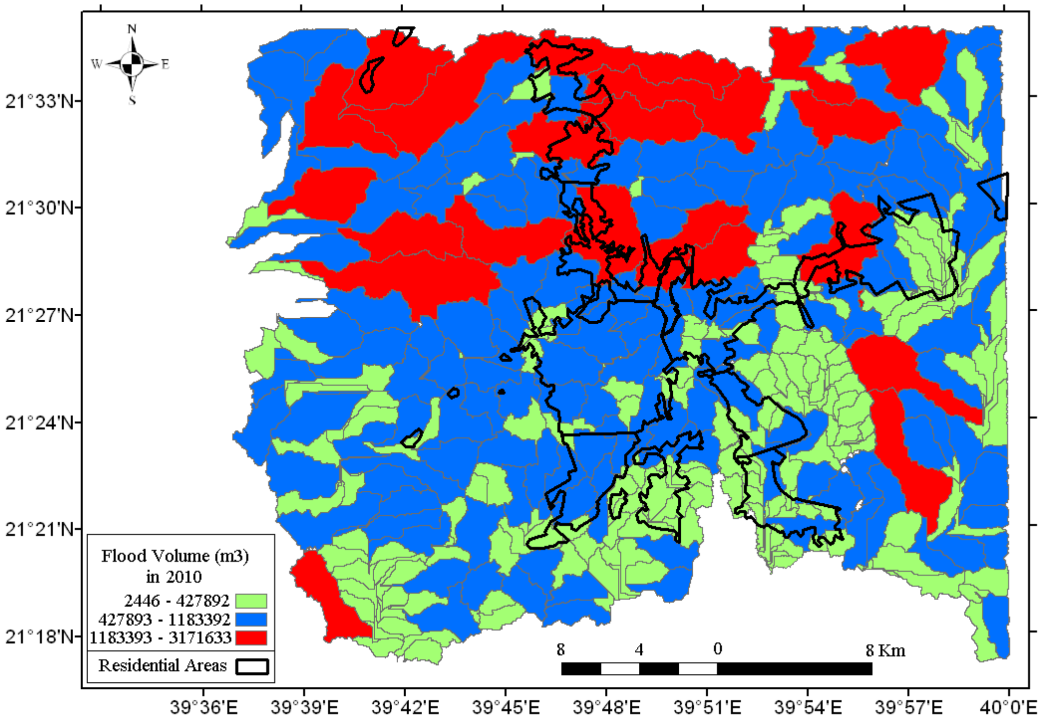

Figure 8. Floods over residential areas in 2010.

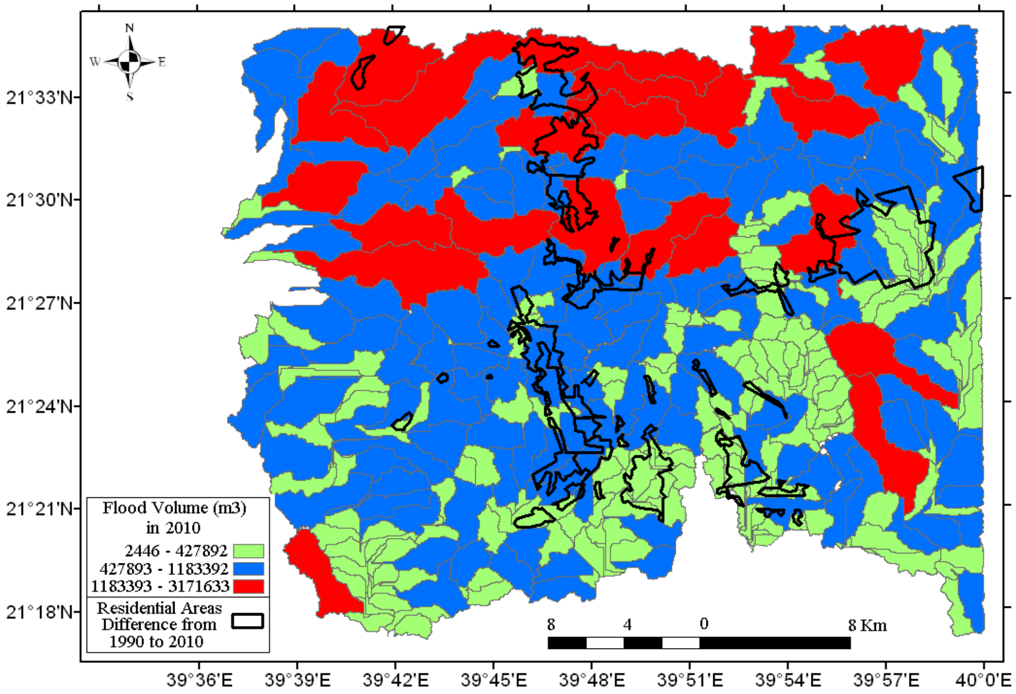

Figure 9. Floods over new residential areas built between 1990 and 2010.

flood volumes have been increased from 11.8 to 41.3 million m^3, i.e. 248%. The spatial distribution of the new residential areas (built between 1990 and 2010) is depicted in Figure 9. It can be seen that there are several

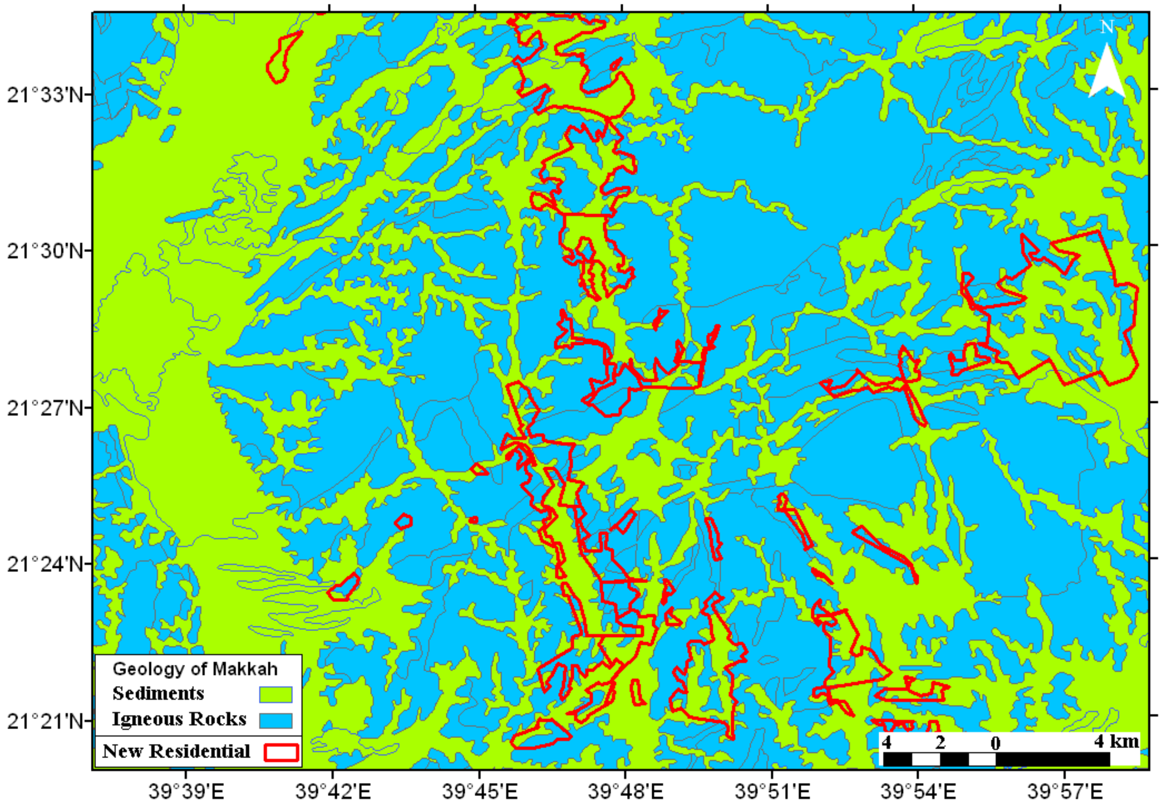

Figure 10. Geology of new residential areas built between 1990 and 2010.

new areas, particularly in the north of Makkah city, located in high-flood sub-basins. It has been found that even though the new residential areas within the Saref wadi constitute only 26.5% of the total urbanization, they are responsible for 51.8 % of the flood increase. Furthermore, it has been found that most of the new residential areas have been established on sediment soils (Figure 10). From an economical point of view, that geological type is cost-effective than constructing building on solid igneous rock geology. However, that urbanization significantly decreases the permeability of the soil and, thus, leads to a crucial increase in hazardous water surface runoff. For example, the CN of sediment geology type equals 76, while it equals 98 for paved residential areas (Sen, 2008b; US NRCS, 1986). These two factors might be the major reasons for severe augmentation of flood volume in the Makkah metropolitan area.

Lastly, a correlation analysis has been carried out on the wadi level for residential area increase, peak discharge increase, and total flood volume changes in the six main basins in the study area (Figure 6) between 1990 and 2010. The relationship between these three factors is depicted in Figure 11, and results of correlation are tabulated in Table 4. Figure 11 shows a positive proportional trend, in general, between the increase of residential areas, peak discharge, and flood volume. The correlation, between urbanization and peak discharge augmentation equals 0.70, and that between urbanization and total flood volume increase equals 0.51. These values might be considered as a significant positive correlation between urbanization and enlarged flood hazards.

Conclusions

The NRCS curve number approach has been used in this study, utilizing available topographic, geological, and land use datasets, to estimate flood hazards in Makkah city in 1990 and 2010. The results showed that the residential regions of Makkah city have been increased by 197%, while the total flood volumes have been enlarged by 248%. Two factors might be considered possible reasons leading to the rise in significant flood hazard. First, establishment of new residential areas in regions that already posse high flood impacts. Second, building up new suburban areas on sediment soil significantly decreases the permeability of the soil and thus, leads to a crucial increase in hazardous water surface runoff. Results showed significant positive correlations between urbanization and both peak discharge and flood volume.

Such findings should be taken into account in future urbanization and flood management plans of Makkah

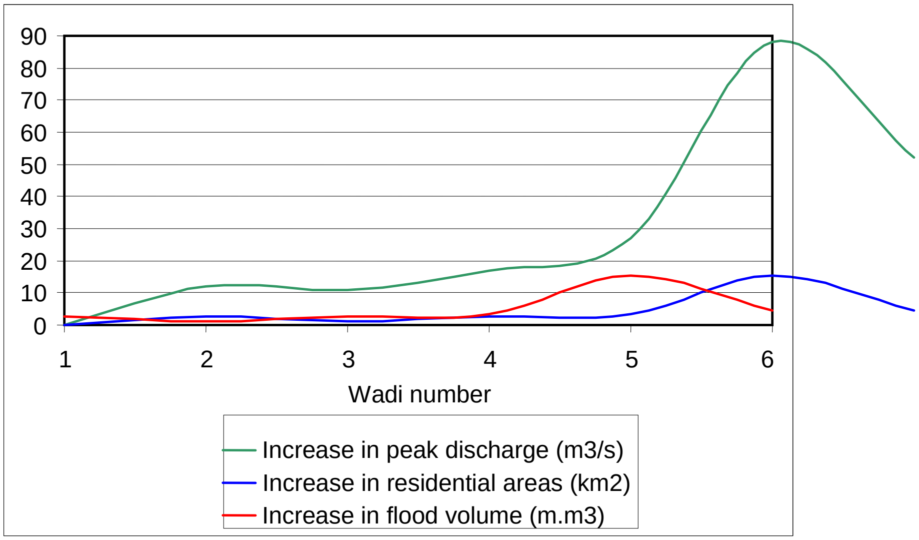

Figure 11. Variations of peak discharges, residential areas, and total flood volumes from 1990 to 2010.

Table 4. Correlation values.

	A	B	C
A	1		
B	0.70	1	
C	0.51	0.94	1

Where: A = Increase in residential areas (km^2), B = Increase in peak discharge (m^3/s), and C = Increase in flood volume (m.m^3).

city, Saudi Arabia.

ACKNOWLEDGMENT

The authors would like to acknowledge the partial financial support offered by the Center of Research Excellence in Hajj and Omrah, Um Al-Qura university, Saudi Arabia (Project PR12/2011).

REFERENCES

Adebayo W, Solomon O, Ayanniyi M, Sikiru F (2009). Evaluation of synthetic unit hydrograph methods for the development of design storm hydrographs for Rivers in South-West, Nigeria. J. Am. Sci., (5)4: 23-32.

Ali M, Khan S, Aslam I, Khan Z (2011). Simulation of the impacts of land-use change on surface runoff of Lai Nullah Basin in Islamabad, Pakistan, Landscape and Urban Planning. 102: 271-279.

Al-Jabari S, Abu Sharakh M, Al-Mimi Z (2009). Estimation of runoff for agricultural watershed using SCS curve number and GIS, Proceedings of the thirteenth International Water Technology Conference, Hurghada, Egypt. 1213-1229.

Al Saud M (2010). Assessment of flood hazard of Jeddah area 2009, Saudi Arabia. J. Water Res. Prot., 2: 839-847.

Antipova A, Wang F, Wilmot C (2011). Urban land uses, socio-demographic attributes and commuting: A multilevel modeling approach, Applied Geography. 31: 1010-1018.

Arunachalam S, Maharani K, Chidambaram S, Prasanna M, Manivel M, Thivya C (2011). A study on the Land use pattern change along the coastal region of Nagapattinam, Tamil Nadu. Int. J. Geom. Geosci., (1)4: 700-720.

Barredo J, Engelen G (2010). Land use scenario modeling for flood risk mitigation, Sustainability. 2: 1327-1344.

Burns D, Vitvar T, McDonnell J, Hassett J, Duncan J, Kendall C (2005). Effects of suburban development on runoff generation in the Croton River basin, New York, USA. J. Hydrol., 311: 266-281.

Dawod G, Koshak N (2011). Developing GIS-based unit hydrographs for flood management in Makkah metropolitan area, Saudi Arabia, J. Geogr. Inform. System. (3)2: 153-159.

Dawod G, Mirza M, Al-Ghamdi K (2011). GIS-based spatial mapping of flash flood hazards in Makkah city, Saudi Arabia, J. Geogr. Inform, System. (3)3: 217-223.

Douglas I, Kobold M, Lawson N, Pasche E, White I (2007). Characterization of urban streams and urban flooding, In: Advances in urban flood management, Ashley, R. (ed), Taylor and Francis group, London, UK. pp. 29-58.

Elaji A (2010). Applications of Geographic Information Systems to construct databases of morphometric characteristics and their hydrologic meanings in Yalamlam basin (in Arabic), MSC thesis, Umm Al-Qura University, Makkah, Saudi Arabia.

Elfert S, Bormann H (2011). Simulated impact of past and possible future land use changes on the hydrological response of the Northern German lowland 'Hunte' catchment, J. Hydrol., (383): 245-255.

Im S, Kim H, Kim C, Jang C (2009). Assessing the impacts of land use changes on watershed hydrology using MIKE SHE, Environmental Geology. 57: 231-239.

Fernandez D, Lutz M (2010). Urban flood hazard zoning in Tucumán Province, Argentina, using GIS and multicriteria decision analysis, Engineering Geology. 111: 90-98.

Gul G, Harmancıoglu N, Gul A (2009). A combined hydrologic and hydraulic modeling approach for testing efficiency of structural flood control measures, J. Nat. Hazard. DOI 10.1007/s11069-009-9464-2.

Hagen E, Shroder J, Lu X, Teufert J (2011). Reverse engineered flood hazard mapping in Afghanistan: A parsimonious flood map model for developing countries, Quaternary International. 226: 82-91.

HAMDD (Higher Authority for Makkah District Development) (2004) Master planning of Makkah city till 2028, Technical report (in Arabic), Makkah. Saudi Arabia.

Kelarestaghi A, Jeloudar Z (2011). Land use/cover change and driving force analyses in parts of northern Iran using RS and GIS techniques, Arab J. Geosci., 4: 401-411.

Kioko J, Okello M (2011). Land use cover and environmental changes in a semiarid rangeland, Southern Kenya, J. Geogr. Regional Plan., (3)11: 322-326.

Koshak N, Dawod G (2011). A GIS morphometric analysis of hydrological basins for flood management within Makkah Metropolitan Area, Saudi Arabia. Int. J. Geom. Geosci., 2(2): 502-511.

Liu D, Li B, Liu X, Warrington D (2011). Monitoring land use change at a small watershed scale on the Loess Plateau, China: applications of landscape metrics, remote sensing and GIS, Environmental Earth Science, DOI 10.1007/s12665-011-1051-7.

Mao D, Cherkauer K (2009). Impacts of land-use change on hydrologic responses in the great lakes region, J. Hydrol., 374: 71-82.

Masoud A (2011). Runoff modeling of the wadi systems for estimating flash flood and groundwater recharge potential in Southern Sinai, Egypt. Arab J. Geosci., 4: 785-801.

Mirza M, Ahmed B (2001). Winter weather and climate conditions in Makkah (in Arabic), Geographic Messages, 253, Kuwait Geographic Association, Kuwait.

Mirza M, Dawod G, Al-Ghamdi K (2011). Accuracy and relevance of digital elevation models for geomatics applications - A case study of Makkah municipality, Saudi Arabia, Int. J. Geom. Geosci., (1)4: 803-812.

Moel H, Aerts J, Koomen E (2011). Development of flood exposure in the Netherlands during the 20th and 21st century, Global Environmental Change. 21: 620-627.

Nouh M (2006). Wadi flow in the Arabian Gulf states, Hydrological Process. 20: 2393-2413.

Olang L, Furst J (2011). Effects of land cover change on flood peak discharges and runoff volumes: model estimates for the Nyando River Basin, Kenya, Hydrological Processes. 25: 80-89.

Paquier A (2010). Flood studies and effects of climate change: two examples. Presented in the International Workshop on Impacts of Global Warming from Hydrological and Hydraulics Issues, March 16, Kyoto, Japan.

Park J, Hur Y (2011). Development and application of GIS based K-DRUM for flood runoff simulation using radar rainfall, J. Hydro-environ. Res., doi:10.1016/j.jher.2011.05.005.

Park S, Jeon S, Kim S, Choi C (2011). Prediction and comparison of urban growth by land suitability index mapping using GIS and RS in South Korea, Landscape and Urban Planning, 99: 104-114.

Pizzuto J, Moglen G, Palmer M, Nelson K (2007). Two model scenarios illustrating the effects of land use and climate change on gravel riverbeds of suburban Maryland, USA, A technical Report, University of Maryland, USA.

Prakasam C (2011). Land use and land cover change detection through remote sensing approach: A case study of Kodaikanal taluk, Tamil nadu. Int. J. Geom. Geosci., (1)2: 150-158.

Qi H, Altinakar M (2011). A GIS-based decision support system for integrated flood management under uncertainty with two dimensional numerical simulations, Environmental Modelling and Software. 26: 817-821.

Ronfort C, Souchère V, Martin P, Sebillotte C, Castellazzi M, Barbottin, Meynard J, Laignel B (2011). Methodology for land use change scenario assessment for runoff impacts: A case study in a north-western European Loess belt region (Pays de Caux, France), Catena. 86: 36-48.

Saghafian B, Farazjoo H, Bozorgy B, Yazdandoost F (2008). Flood intensification due to changes in land use, Water Resources Management, 22:1051-1067.

Sagala S (2006). Analysis of flood physical vulnerability in residential areas, Case study: Naga city, the Philippines, Master thesis, International Institute for Geo-information Science and Earth Observation, The Netherlands.

Sen Z (2008a). Modified hydrograph method for arid regions, Hydrological Process. 22: 356-365.

Sen Z (2008b). Wadi Hydrology, CRC Press.

Sheng J, Wilson J (2009). Watershed urbanization and changing flood behavior across the Los Angeles metropolitan region, Nat. Hazard. 48: 41-57.

Sherief Y (2008). Flash floods and their effects on the development in El-Qaa plain area in south Sinai, Egypt, PhD Dissertation, University of Mainz, Germany.

Su S, Jiang Z, Zhang Q, Zhang Y (2011). Transformation of agricultural landscapes under rapid urbanization: A threat to sustainability in Hang-Jia-Hu region, China. Appl. Geogr., 31: 439-449.

Subyani A (2011). Hydrologic behavior and flood probability for selected arid basins in Makkah area, western Saudi Arabia. Arab J. Geosci., 4: 817-824.

US ACE (US Army Corps of Engineers) (2004). Physical stream assessment.

US DoT (US Department of Transportation) (2002). Highway hydrology manual, Publication No. FHWA-02-001.

US NRCS (US National Resources Conservation Services) (1986). Urban hydrology for small watersheds, Technical Manual TR55.

Wang L, Wehrly K, Breck J, Kraft L (2010). Landscape-based assessment of human disturbance for Michigan lakes. J. Environ. Manage., 46: 471-483.

Xianzhao L, Jiazhu L (2008). Application of SCS model in estimation of runoff from small watershed in Loess plateau of China. J. Chinese Geogr. Sci., (18)3: 235-241.

Zheng Z, Qi S (2011). Potential flood hazard due to urban expansion in the Karst mountainous region of North China, Regional Environmental Change. 11: 439-440.

Environ Earth Sci (2012) 67:2205–2215
DOI 10.1007/s12665-012-1660-9

ORIGINAL ARTICLE

GIS-based estimation of flood hazard impacts on road network in Makkah city, Saudi Arabia

Gomaa M. Dawod · Meraj N. Mirza · Khalid A. Al-Ghamdi

Received: 18 May 2011 / Accepted: 27 March 2012 / Published online: 12 April 2012
© Springer-Verlag 2012

Abstract Makkah city, Saudi Arabia, is periodically exposed to flash floods that result in major human and economical damages. That is due to several factors including its rugged topography and geological structures. Hence, precise assessment of floods becomes a more vital demand in development planning. A GIS-based methodology has been developed for quantifying and spatially mapping the flood characteristics. The core of this new approach is integrating several topographic, metrological, geological, and land use data sets in a geographic information system (GIS) environment that utilizes the curve number method of flood modelling for ungauged arid catchments. Based on the estimated flood volume of sub-basins, a hazard factor has been developed to quantify the expected hazard level for each road. Applying this proposed approach reveals that 21 % of the road network in Makkah city is subjected to low flood hazards, 29 % is facing medium hazards, and 50 % of roads are exposed to harsh flood impacts. The developed approach may be considered a digital precise method that can be easily re-run, in other situations or regions, to estimate flood hazards on roads.

Keywords Flood assessment · Rainfall-runoff model · Road network · GIS · Saudi Arabia

G. M. Dawod (✉)
Survey Research Institute, Giza, Egypt
e-mail: dawod_gomaa@yahoo.com

Present Address:
G. M. Dawod
Umm Al-Qura University, P.O. Box 715,
Makkah 21955, Saudi Arabia

M. N. Mirza
Center of Research Excellence in Hajj and Omrah,
Umm Al-Qura University, P.O. Box 6247,
Makkah 21955, Saudi Arabia
e-mail: meraj@mmirza.com

K. A. Al-Ghamdi
Geography Department, Umm Al-Qura University,
P. O. Box 138474, Jidda 21323, Saudi Arabia
e-mail: kaghamdi@uqu.edu.sa

Introduction

Hazards of flash floods are vital in terms of human lives loss and economical damages. Roads, in particular, are affected seriously by flash floods. Makkah city, west of Kingdom of Saudi Arabia (KSA), exhibits two unique features that increase the hazardous flood consequences: (1) its topography is very complex; (2) about three million Muslims are gathered annually in Makkah to perform Hajj over a 2-week period in the winter, which is the main rainfall season in Saudi Arabia. The topography of Makkah, which in general can be considered as a plateau rises about 300 m above mean sea level, is not entirely flat. Several mountains, whose elevations reach more than 900 m, exist within the metropolitan extents of the city. Hence, a number of hydrological catchments, with significant natural ground slopes, have been formed inside the city, leading to an increasing probability that rainfall could be converted to dangerous runoff. Surface runoff generally affects the road network in Makkah city in terms of serious traffic problems, road destruction, mudflow, and landslides. Due to the increasing interest in flood impacts over the last couple of decades, extensive flood estimation studies have been carried out in different countries, such as USA (e.g., USGS 2009), Egypt (e.g., Azab 2009; El Bastawesy et al. 2009), Nigeria (e.g., Yahaya et al. 2010), South Korea

(e.g., Kim et al. 2010), China (e.g., Liang et al. 2010), and Saudi Arabia (e.g., Dawod and Koshak 2011; Al Saud 2010; Fred and Mostafa 2008). Also, geographic information system (GIS) is utilized for road maintenance (e.g., Yunus and Hassan 2010). This paper aims to utilize a GIS approach for assessing the flash flood hazards on road networks within Makkah metropolitan area, utilizing the most up-to-date and precise data sets.

Flood estimation

Flood estimation deals with modelling the rainfall-runoff relationship. This relationship plays a key role in numerous human activities such as flood risk evaluation of floodplains, flood damage evaluation for project planning, design of hydraulic structures for flood control, flood-runoff forecasting for project operations, and water resources planning and maintenance projects. Moreover, flood estimations on small urban drainage basins are required for a number of engineering structures such as dams, levees, culverts, and soil conservation purposes. Defining the rainfall-runoff relationship leads to estimation of several flood properties such as runoff depth, runoff speed, peak discharge, and total flood volume. Evaluating flood characteristics is essential for planners and decision makers. For example, such quantities assist municipalities in preparing urban expansion strategies, and they are critical for civil defence organizations in developing rescue plans.

It is economically costly and physically difficult to gauge all streams in a region, particularly in a large country such as KSA (Sen and Al-Suba'l 2002). For ungauged hydrological catchments, where measured flood discharge data records are missing, the flood estimation becomes more complicated. Countless approaches have been proposed globally trying to estimate flood peak discharge quantities based on topographic and morphometric characteristics of hydrological regions. Such approaches may be categorized into three groups according to their complexity. The first group, or simple approaches, includes the so-called rational method and empirical formulas. Even though those methods estimate the peak discharge quickly and simply with little number of inputs, they did not take into account important parameters particularly the land use and land cover of the catchment area. The curve number (CN) is an example of the second, or moderate, flood estimation methods, where more input factors are needed to estimate the flood characteristics. CN is a rainfall-runoff coefficient that depends on geological, soil, and land use properties of a catchment. The third group consists of detailed or complex models that are able to identify the causes of problems rather than producing a simple description of overall conditions. The soil and water assessment tool (SWAT) is an example of those process-based complex models (Mihalik 2008). The CN method is quite used in engineering design and flood management projects, particularly in the USA (e.g., IDoT 2009; US ACE 2004; NH DoT 1998; and US DoT 2002).

GIS and remote sensing (RS) techniques have been utilized as efficient tools in flood risk assessment (e.g., Saleh and Al-Hatrushi 2009). Remote sensing images provide a significant source of extensive geospatial data particularly when the ground surveys or recent topographic maps are not available or not updated. For example, road networks can be extracted precisely from a high-resolution RS images. In addition, post-flood RS images can be used to calibrate developed floodplains in a hydrological basin. In addition, soil and geological maps, needed for flood estimation, can be developed based on RS imageries. GIS-based software can delineate hydrological catchments having a digital elevation model (DEM) being available. Global DEMs provide a free-of-charge terrain representation to be used in flood estimation. The Shuttle Radar Topography Mission (SRTM) is one of the most famous global DEMs, which is a joint project between the US National Imagery and Mapping Agency (NIMA) and the National Aeronautics and Space Administration (NASA). Chang et al. (2009) applied GIS to study the time-based relationship between flood hazards and land use changes. Furthermore, Jasrotia and Singh (2006) have utilized the CN method to study the runoff and soil erosion within a GIS environment. Moreover, Chen et al. (2010) tested a GIS model, which consists of a storm-runoff model and an inundation model, to model flood hazards. In addition, Dongquan et al. (2009) developed a GIS batch process to delineate catchments and compute their geomorphologic parameters. Furthermore, Guptaa and Panigrahya (2008) have utilized several data sources and two runoff models in a GIS platform to investigate the flood characteristics and variations of large basins in India. Additionally, Gogoase et al. (2011) utilized GIS to develop inundation maps foe extreme flood events. Moreover, Karmakar et al. (2010) proposed a methodology for six major damage centers in the Upper Thames River watershed, Canada to assess the flood risks, i.e., flood probability of occurrence, vulnerability to flood, and exposures of land use and soil type to flood.

Regarding flood impacts on roads, some researchers have investigated this aspect in several countries. Blanton and Marcus (2009) have documented the geographic distribution of roads and railroads in the alluvial floodplains of the continental United States and the regional variability of their potential impacts on lateral connectivity and resultant channel and floodplain structure and function. Youssef et al. (2010) have presented the utilization of remote sensing data; SRTM DEM coupled with geological,

geomorphological, and field data in a GIS environment for the estimation of the flash flood risk along the Feiran–Katherine road, southern Sinai, Egypt. In this study, morphometric parameters were computed and classified, such as basin area, circulation ratio, relief, relief ratio, drainage density, drainage frequency, number of orders, total drainage number, total drainage length, and slope. Each morphometric parameter, then, is converted to a flood risk parameter based on a statistical method. Then all parameters were summed and normalized in order to obtain a unique morphometric number for each sub-basin. The basic idea in this research study is that the higher the morphometric number, the higher is the flood hazard rank for a sub-basin and for its existing road. However, those two studies are based on flood hazards estimation thorough analyzing morphometric characteristics of basins in which roads exist. That means that the flash floods, themselves, have not being estimated. In the current paper, GIS has been utilized to quantify some flood characteristics in Makkah city and then estimate dangerous impacts on the road network.

Flash floods in Makkah city

Makkah city is located in the southwest part of KSA, about 80 km east of the Red Sea (Fig. 1). It extends from 39°35′E to 40°02′E, and from 21°09′N to 21°37′N. The area of the metropolitan region (the study area) equals 1,593 km^2. The topography of Makkah is complex in nature, and several mountainous areas exist inside its metropolitan area. Table 1 presents statistics of the terrain slopes' categories of Makkah city. About 4.6 % of the study area posses highly slopes greater than 20°. Such areas increase the probability of rainfall conversion to immediate runoff.

The winter is considered as the main rainy season in Saudi Arabia. The annual rain over Makkah city, for a period extending from 1966 to 2010, varies from 3.8 to 318.5 mm, with an average of rainfall equals 101.2 mm (Fig. 2). It worth mentioning that this data set has been combined from several metrological stations' records varying in geographical locations (inside and close to Makkah city) and in time span. It is considered the most recent and longest metrological information available for Makkah. Due to the complexity of Makkah's topography, flash floods occur periodically with significant variations in magnitude, and cause serious damages particularly on road network (Fig. 3). Mirza and Ahmed (2001) have reported that the extreme flood type is repeated with a return period of 46 years, while a second-order flood takes place occasionally with a return period of 33 years, and a low-dangerous flood comes about every 13 years. Using the magnitude of the annual rain average (which equals 101.2 mm) as a rain intensity factor might not be optimum in flood estimation process. The rain intensity of a single extreme storm may exceed the annual rainfall average for a year. For example, the 1969 storm records (Fig. 4) showed that the rain intensity reaches 107.5 mm/h during the first 10 min of that storm. Analyzing the flood series frequency, the return period or recurrence interval can be computed. That period defines the average number of years during which a flood of a given magnitude will be equalled or exceeded once. The Welbull method, among several other formulas, computes the return period T as (Raghunath 2006):

$$T = (n + 1)/m \quad (1)$$

where, n is the number of events, or number of records, m is the order or rank of the event (flood item) when flood magnitudes ranked in descending order.

The computed return period of the 1969s flood has been estimated to 45 years. That piece of information is quite helpful in flood assessment studies, as it means that: (a) that flood magnitude is expected to occur by about 2014; and (b) selected return period value for flood management projects should be equal or >44 years. The rainfall intensity for a 50-years return period has been estimated, through the Log Pearson II statistical method, as 200 mm/h.

Additionally, floods are affected by the geology of the area in question, since infiltration rate differs from a geology structure to another. The geology of Makkah metropolitan area consists mainly of three geological structures (Table 2). The Precambrian igneous rocks occupy about 809 km^2 (with 51 % approximately of the total area). That rock type implicitly implies a low-permeability property that increases the ability of rainfall to be converted into dangerous surface runoff. The deposits, or wadi alluvium, exist mainly along the wadis streams, constitute about 48 %, with an area equals 770 km^2 approximately. The rest of Makkah area, about 12 km^2 only, represent the tripartite rocks. Soils of Makkah city are chiefly shallow clay soils over nearly impervious material, i.e., they have high runoff potential and very slow infiltration rates. Thus, these soils belong to group 4 (or the D type) in the curve number's hydrologic soil categories.

Data and methodology

Several data sets have been collected for flood assessment in Makkah city. The main data set is a national DEM produced by the by King Abdulaziz City of Sciences and Technology (KACST) with a spatial resolution equals to 5 m. A window covering Makkah metropolitan area (Fig. 5) has been provided through the Center of

Fig. 1 Study area

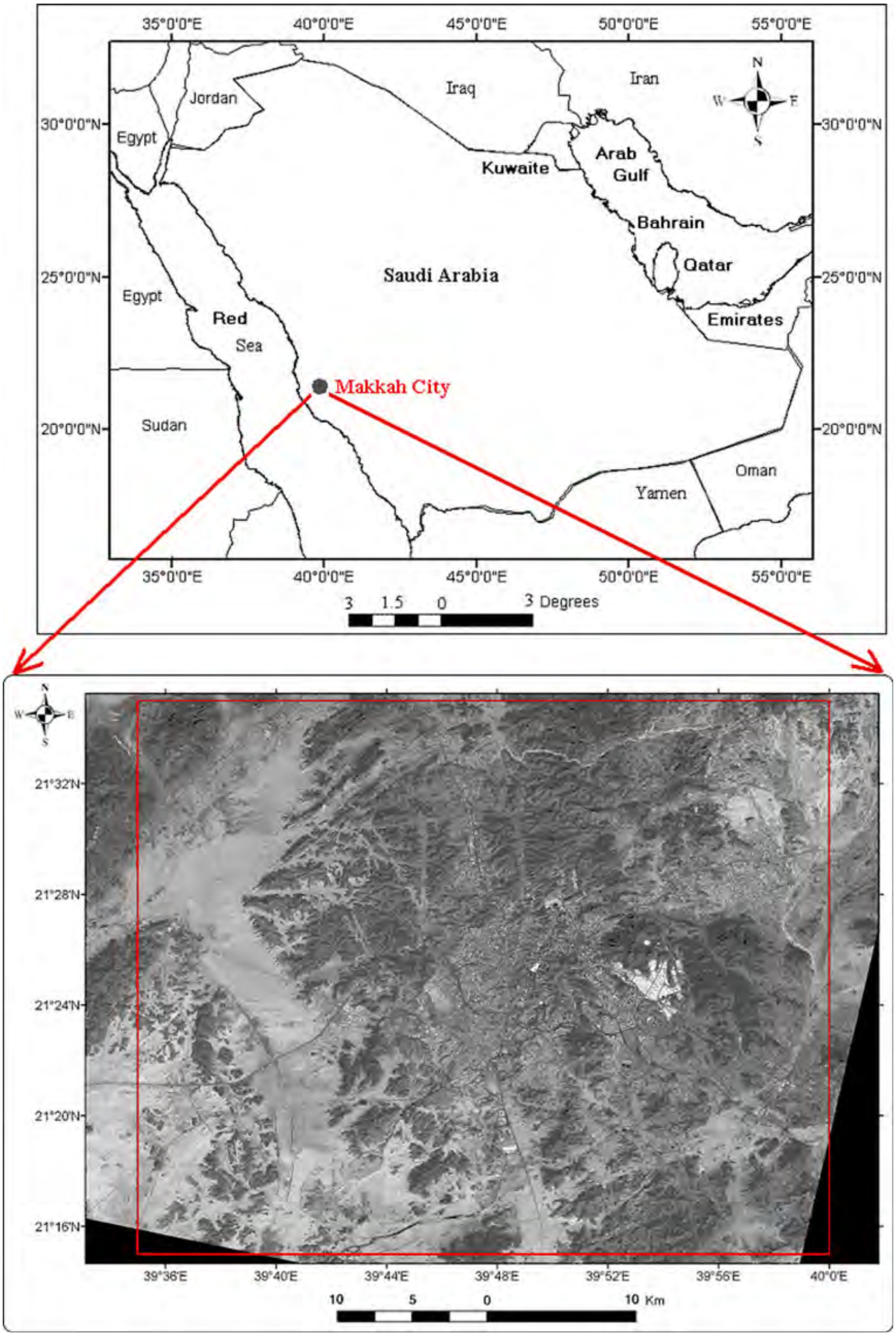

Excellence in Hajj and Omrah, Umm Al-Qura University. From Fig. 5, it can be noticed that the heights of Makkah metropolitan area range from 80 to 982 m. The other data sets include digital geological, soil, and land use maps of the study area.

The utilized GIS-based flood assessment methodology consists of several stages. Figure 6 depicts an overview

Table 1 Makkah slopes' categories

Slope (°)	Area (%)
<10	79.7
10–20	15.7
20–30	3.7
>30	0.9

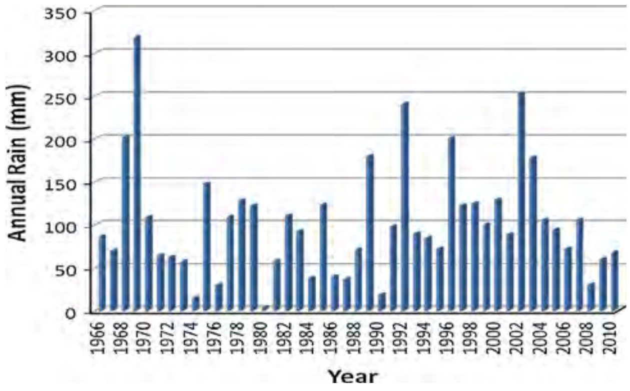

Fig. 2 Annual rains in Makkah city from 1966 to 2010

flow chart of that scheme. In the first stage, the Arc GIS software along with the Arc Hydro extension is used to obtain several shapefiles describing the geomorphology of the study area. These shapefiles include: the main basins and the sub-basins of each main catchment, along with drainage network using Strahler method (a simple widely-utilized network order method), and the longest stream path in each catchment. The second stage of the utilized methodology is based on the flood assessment method developed by the US Natural Resources Conservation Service (NRCS), formerly known as the Soil Conservation Service (SCS). It worth mentioning that there are several hydrologic methods used for flood estimation, but the SCS method has been applied in the current research study. This method, also known as the curve number (CN), makes use of geological information to assign a unique CN value for each area, which will be further used to estimate the surface runoff depth and the peak discharge magnitude. The visual basic applications (VBA), a programming environment within the Arc GIS software, is used to compute the required flood defining parameters that consist of (Sen 2008):

$$Q = (P - 0.2S)2/(P + 0.8S) \quad (2)$$

$$S = 25.4((1{,}000/\mathrm{CN}) - 10) \quad (3)$$

$$\mathrm{QT} = \mathrm{QA} \quad (4)$$

Fig. 3 Flood hazards on road network in Makkah city in 2010

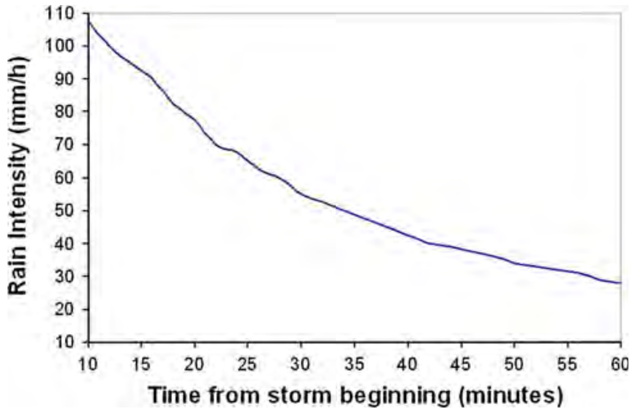

Fig. 4 Rain intensity of the 1969 storm in Makkah city

Table 2 Makkah geological categories

Geological structure	Area (km^2)	Area (%)
Precambrian igneous rocks	809	50.8
Wadi alluvium	770	48.4
Tripartite rocks	12	0.8

$$q_p = q_u A Q \tag{5}$$

$$t_c = 1.67L^{0.8}(S+1)^{0.7}/1{,}900\,Y^{0.5} \tag{6}$$

$$S_d = 0.133 t_c \tag{7}$$

$$v = 0.2278 L/t_c \tag{8}$$

where: Q is the depth of direct runoff (mm), P is the depth of precipitation for a specific return period (mm), S is the maximum potential retention (mm), CN is the curve number, QT is the volume of runoff (m^3), A is the area of basin (km^2), Q is the depth of direct runoff (m), q_p is the peak discharge (m^3/s), q_u is the unit peak discharge ($m^3/s/km^2/mm$) that can be interpolated from a specific charts (e.g., US NRCS 1986) or computed from corresponding tables (e.g., US DoT 2002, pp. 5–28), t_c is the time of concentration (min), L is the basin length (km), Y is the slope (m/km %), S_d is the storm duration (h), and v is the flow velocity (m/s).

Computing the morphometric parameters of a catchment provides a useful tool in understanding the basins natural properties and their roles in flood hazards. A number of common parameters are usually utilized in order to describe the morphometric and geomorphologic properties of a watershed. Although details can be found in several literature (e.g., Huggett 2007; Horton 1945), the utilized morphometric parameters of basins are computed by the following formulas.

$$\Delta H = H_{max} - H_{min} \tag{9}$$

$$R_{hp} = \Delta H/P \tag{10}$$

$$R_l = 2[\sqrt{(A/\Pi)}]/L_u \tag{11}$$

$$R_c = 4\Pi A/P^2 \tag{12}$$

$$D = L_u/A \tag{13}$$

where, ΔH is the basin total relief, H_{max} is the elevation of the highest point in the basin, H_{min} is the elevation of the lowest point in the basin, R_{hp} is the relative relief, P is the perimeter of basin (km), R_l is the elongation ratio, A is the basin's area (km^2), L_u is the total stream length of all orders, R_c is the circularity ratio, $\Pi = 22/7$, and D is the drainage density (km/km^2).

In the third stage of the proposed GIS approach, an estimation has been developed to quantify flood impacts on

Fig. 5 The National 5-m DEM for Makkah city

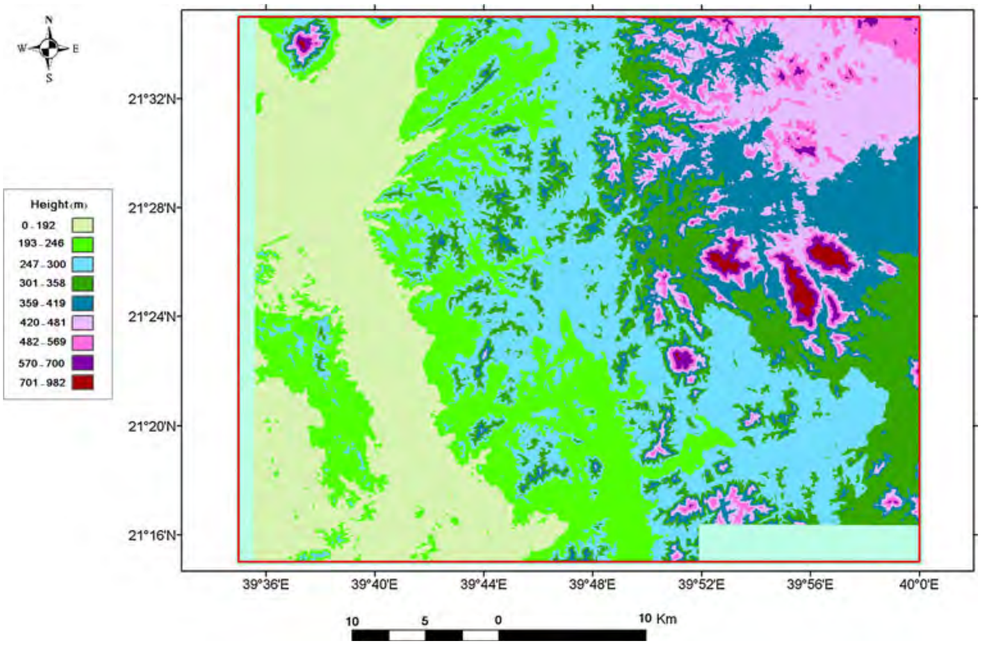

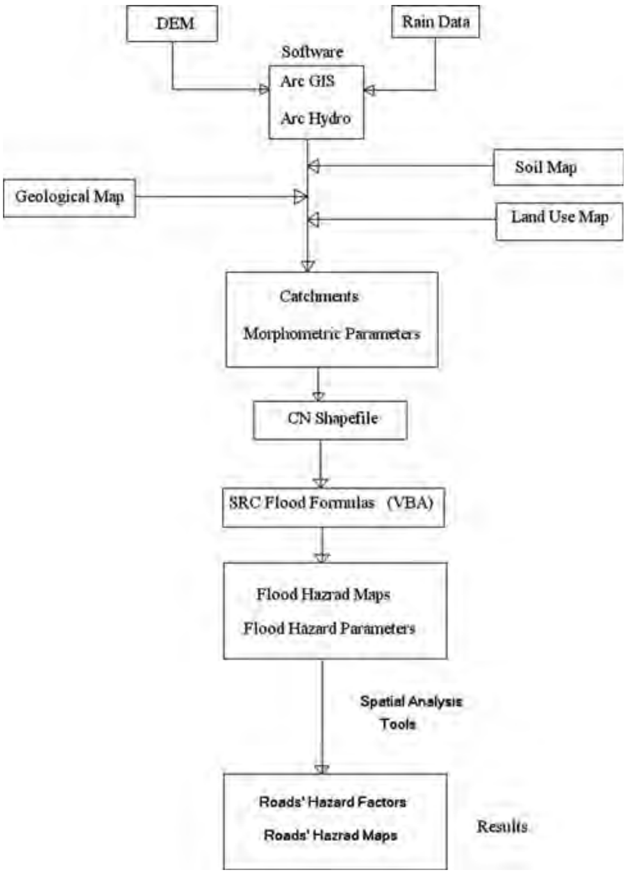

Fig. 6 The developed GIS-based methodology for flood assessment on road network

roads. It is implicitly based on an idea that the large flood volume in a sub-basin, the more hazards on roads within that sub-basin. Since the flood computations have been performed on a sub-basin level, the flood volume of each sub-basin may be considered as the most effectual factor that affects the flood impact. Hence, the spatial analysis tools of the Arc GIS software are utilized to re-classify flood volumes in ten categories, and each category is assigned a unique number. That number, called the hazard factor, will be assigned to the road exist in a particular sub-basin. By this approach, each road in the transportation network gets a unique hazard factor that represents the flood hazard level.

Results

The utilized GIS-based methodology has been carried out using the available data sets of Makkah metropolitan area. The attained results of the first stage include quantities of several many significant morphometric parameters (Table 3). It has been found that there are six main catchments in Makkah, whose areas range from 74.3 to 360.6 km^2, and lengths of their main streams vary from 16.50 to 48.55 km (Fig. 7). The total relief varies from 333 to 769 m, while the relief ration, in m/km, range between 12.6 and 40.4. The circularity ratio is the ratio of the basin area to the area of a circle has the same circumference. It is influenced by the length and frequency of streams, geological structures, land use, and the slope of the watershed. Catchment no. 3 has the highest circularity ratio (0.37) and catchment no. 2 has a closer value (0.32). It can be seen from Fig. 7 that these two basins are the closer to a circular shape. On the other hand, the elongation ratio represents how close a basin to a rectangular shape. From Table 3, it can be seen that two basins have rectangular ratio greater than 0.5, while the other four have elongation ratios <0.4. Hence, the six catchments in Makkah metropolitan area are far from a complete rectangular shape (see Fig. 7).

The network properties are considered the major morphometric characteristics of watersheds. Stream order is used to denote the hierarchical relationship between stream segments and allows drainage basins to be classified according to size. Several stream-ordering systems exist, the most commonly used being those devised by Arthur N. Strahler and by Ronald L. Shreve. In Strahler's ordering

Table 3 Statistics of morphometric quantities

Item	C1	C2	C3	C4	C5	C6
Basin area (km^2)	252.7	122.3	74.3	109.9	360.6	200.2
Basin premier (km)	134.6	69.13	50.23	89.09	134.76	102.03
Basin length (km)	42.48	23.64	16.50	29.70	48.55	38.13
Total relief (m)	546	333	667	769	632	714
Relief ratio (m/km)	12.6	14.1	40.4	25.9	13.0	18.7
Elongation ratio	0.42	0.53	0.59	0.40	0.44	0.42
Circularity ratio	0.18	0.32	0.37	0.17	0.25	0.24
Maximum stream order	6	5	5	5	6	5
Total no. of streams	1,082	523	294	424	1,448	831
Drainage density (km/km^2)	2.67	2.71	2.58	2.56	2.59	2.73

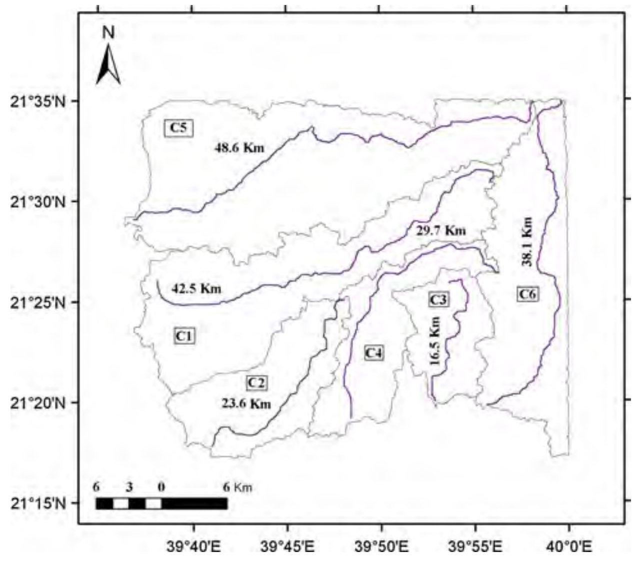

Fig. 7 Catchments and their main streams

system (which is used in the current research), a stream segment with no tributaries that flows from the stream source is denoted as a first-order segment. A second order segment is created by joining two first-order segments, a third-order segment by joining two second order segments, and so on. It has been found that the maximum stream order in the six watersheds, in the study area, equals 5 for the four small sub-basins (No. C2, C3, C4, and C6) and reaches order 6 in the other two sub-basins (C1 and C5), which have the maximum basin areas. The drainage density is a measure of how frequently streams occur on the land surface. It indicates the closeness of spacing between channels and is a measure of the total length of the stream segment of all orders per unit area. It reflects a balance between erosive forces and the resistance of the ground surface, and is therefore related closely to climate, lithology, and vegetation. Drainage densities can range from <5 km/km^2 when slopes are gentle, rainfall low, and bedrock permeable, to much larger values of more than 500 km/km^2 in upland areas where rocks are impermeable, slopes are steep, and rainfall totals are high (Huggett 2007). The drainage density for Makkah's sub-basin range from 2.56 to 2.73 km/km^2. So, it can be classified, in general, as a medium drainage density pattern.

The second stage of the applied approach results is the determination of flood characteristics in Makkah city. The computations have performed using the depth of precipitation (P) equals 200 mm for a return period of 50 years. That value is the result of the Log Pearson III statistical analysis for the available rainfall data sets of Makkah city. Additionally, the unit peak discharge (q_u in Eq. 5) has been computed through the equation and tables provided in US DoT (2002) (Equation 5–26, pp. 5–28). Table 4 presents the flood estimated parameters on the catchment's level. First, it can be noticed that the peak discharge values found to vary from 1,063 m^3/s (for catchment C2) to 4,489 m^3/s (for catchment C5). Additionally, the runoff depths of the six basins vary from 151.7 to 178.8 mm. The flood volume range between 13.28 m^3 (for catchment 3) and 54.69 m^3 (for catchment 3), with a total of 172.97 million m^3 over Makkah metropolitan area. Additionally, catchment C3 is expected to have minimum storm duration (0.26 h) while catchment C1 has the maximum value (0.80 h). Concerning the flow velocity of the six basins, it has been found that the values range from 22.44 m/s (for catchment C2) to 73.37 m/s (for catchment C5).

Furthermore, the utilized approach has been performed at the sub-basin level in order to get more detailed flash flood analysis. Table 5 and Fig. 8 present the accomplished results. It can be seen that the six main catchments contain 350 sub-basins whose area vary between 0.019 and 20.676 km, with an average equals 3.092 km. Additionally, the sub-basin runoff depth varies between 128 and 194 mm with an average equals 157 mm. Also, the runoff volume on the sub-basin level (QT in Eq. 4) range from 2,446 and 3,171,609 m^3 with a mean of 478,925 m^3. Moreover, it can be noticed that the highest runoff depth and runoff volume values exist in sub-basins with high CN values. Such high CN values are attributed to the fact that those sub-basins belong to either a residential land use type or an igneous-rocks geological category. Hence, these maps should be considered in future development planning of that area in Makkah city.

Table 4 Catchments flood characteristics in Makkah city (for a 50-years return period)

Item	C1	C2	C3	C4	C5	C6
Runoff depth (mm)	151.7	151.7	178.8	166.7	151.7	148.8
Peak discharge (m^3/s)	1,554	1,063	1,307	1,234	4,489	1,514
Time of concentration (min)	5.69	3.76	1.73	2.63	6.72	4.17
Storm duration (h)	0.76	0.50	0.23	0.35	0.89	0.56
Flow velocity (m/s)	28.34	23.86	36.19	42.87	27.44	34.68
Volume of runoff (million m^3)	38.34	18.55	13.28	18.32	54.69	29.79
	Total = 172.97 million m^3					

Table 5 Sub-basins flood characteristics in Makkah city (for a 50-year return period)

Item	Minimum	Maximum	Average
No. of all sub-basins		350	
Sub-basin area (km^2)	0.019	20.676	3.092
CN	76	98	86
Runoff depth (mm)	128	194	157
Total volume of runoff (m^3)	2,446	3,171,609	478,925

Regarding the flood impacts on roads, a shapefile has been first constructed containing the road network of Makkah city. It was decided to work with main roads only, whose lengths are >1,000 m, just for simplicity in the current research. So, that road network consists of 511 roads whose lengths range from 1,003 to 20,530 m, with a mean of 2,348 m. The Arc GIS spatial analysis tools have been utilized to: (a) divide the sub-basins' runoff volumes into ten groups using the natural-break classification method, which identifies break points by picking the class breaks that best group similar total flood volume values, (b) re-classify those flood volume groups to unique label values ranging from 1 to 10, just for simplicity, which will be considered as the hazard factor, (c) convert that shapefile into a raster format; and (d) project that raster onto the road network in order to assign each road with the corresponding unique hazard factor. By this approach, the flood hazard impact on each road is assigned on a scale from 1 to 10 (based on the total flood volume for the corresponding sub-basin), that is a simple scale to be interpreted. This quantitative classification is presented in Table 6. Next, the flood hazards on roads have been classified into three groups, just for simplicity too, as seen in and Table 7 and Fig. 9. Obviously, a great part of the road network in Makkah city is subjected to high dangerous flood impacts. That category constitutes 260 roads, representing 51 % of the network, with a total length of 528 km.

Discussion

Analyzing the morphometric parameters, it has been found that the catchment C3 has the maximum relief ratio even though it does not have the maximum height difference (total relief). That might be due to the smallest basin area of that catchment (only 74.3 km^2). Hence, that catchment can be considered the most topographical-complex basin in the study area, which will result in more steep morphometric characteristics. Also, it has been found that this catchment has the highest circularity ratio even though it is the smallest watershed, which is considered as a hazardous indication since it means that the flash floods could reach great volume over a small area. Furthermore, it can be noticed that catchment C3 has the lowest concentration time (1.98 h), which is the time for runoff to travel from the most distant point to the outlet point. That is an excepted result, since this catchment has the highest relief ratio (40.43 m/km) even though it does not have the highest flow velocity. Additionally, this catchment has the minimum storm duration (0.26 h) while catchment C1 has the maximum value (0.80 h). It is worth mentioning that

Fig. 8 Flood spatial variations in Makkah city

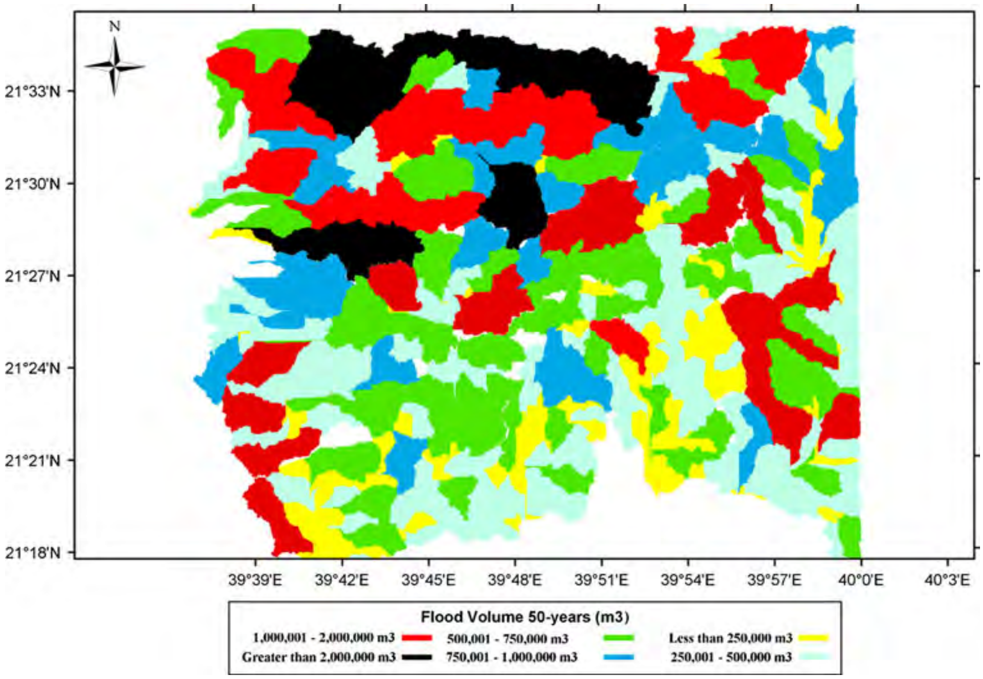

Table 6 Flood hazard estimation on road network in Makkah city

Item	No. of roads	Percentage of roads	Total length of roads (km)
Hazard factor = 1	12	2.3	20.890
Hazard factor = 2	31	6.1	74.974
Hazard factor = 3	42	8.2	80.746
Hazard factor = 4	20	3.9	70.418
Hazard factor = 5	24	4.7	70.591
Hazard factor = 6	44	10.7	115.824
Hazard factor = 7	68	13.3	134.497
Hazard factor = 8	75	14.6	144.588
Hazard factor = 9	89	17.4	205.089
Hazard factor = 10	96	18.8	178.210

Table 7 Categories of flood hazard on road network in Makkah city

Hazard category	Hazard factor	No. of roads	Percentage of roads	Total length of roads (km)
Low	1–4	105	20.5	247.028
Medium	5–7	147	28.7	320.912
High	8–10	260	50.8	527.887

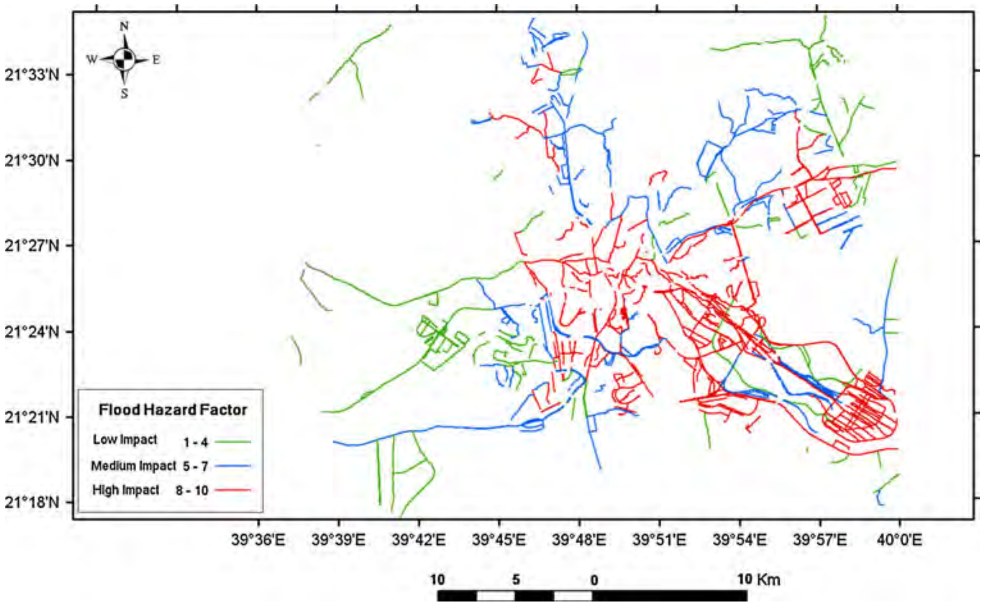

Fig. 9 Flood impacts on road network in Makkah city

the storm duration is a function of the concentration time as seen in Eq. 8.

The higher CN values, in the study area, are attributed to two factors: (a) the residential area of Makkah city, paved streets, was assigned CN of 98 that reflects the low permeability of rains; (b) a great portion of Makkah's geology consists of igneous and metamorphic rocks, which get relatively high CN according to the SRC classification. Moreover, it can be noticed that four catchments (C1, C2, C5, and C6) have similar CN values, but C2 has the least basin area. That leads to this catchment produces the minimum peak discharge. As expected, catchment C5 produces the highest peak discharge because of its big basin area. Additionally, it can be concluded that the highest runoff depth belong to catchment C3, which has the highest CN value. Regarding the flood volume, it can be seen that catchment C5 produces the biggest value due to the fact that it has the biggest area (360.6 km^2). The proposed approach of estimating flood impacts on roads is based on the computed flood volumes of sub-basins. So, it might be considered more appropriate than the other approaches that are based only on analysing morphometric characteristics of the basins themselves. That is due to the fact that the runoff volume is the chief factor distinguishes

the expected flood damages on roads. The attained results reveal that almost half of Makkah's road network is subjected to severe flood impacts. Consequently, certain precautions should be taken by the governmental authorities to protect such roads.

Conclusions

Makkah metropolitan area, southwest of Saudi Arabia, is distinguished by two items: a complex topography; and the gathering of about three million Muslims to perform Hajj over a specific short time period annually. This research utilizes a GIS-based approach for mapping and quantifying flood assessment measures particularly on road network. The used methodology is based on integrating several data sets in a GIS environment utilizing the SRC CN flood modelling method. A hazard factor has been developed to quantify the expected flood hazards on roads. Results show that 50.8 % of Makkah's road network, with a total length of 528 km, is subjected to high or serious flood impacts. Properties of this GIS-based methodology include precision, cost-effective, digital outputs, and its ability to be re-run for other scenario (e.g., other design return period). Hence, it is recommended that the attained results be utilized in governmental planning in Makkah city, and that approach should be applied to all other cities in Saudi Arabia.

Acknowledgments The authors would like to acknowledge the financial support offered by the Center of Research Excellence in Hajj and Omrah (Hajjcore), Umm Al-Qura University, Saudi Arabia.

References

Al Saud M (2010) Assessment of flood hazard of Jeddah area 2009, Saudi Arabia. J Water Resour Prot 2:839–847

Azab M (2009) Assessment and management of natural hazards and disasters along Qena–Safaga road, central eastern desert, Egypt. Egypt J Remote Sens Space Sci 12:55–70

Blanton P, Marcus A (2009) Railroads, roads and lateral disconnection in the river landscapes of the continental, United States. Geomorphology 112:12–227

Chang H, Franczyk J, Kim C (2009) What is responsible for increasing flood risks? Case Gangwon Prov Korea Nat Hazards 48:39–354

Chen J, Hill A, Urbano L (2010) A GIS-based model for urban flood inundation. J Hydrol 373:84–192

Dawod G, Koshak N (2011) Developing GIS-based unit hydrographs for flood management in Makkah metropolitan area, Saudi Arabia. J Geogr Inf Syst 3(2):153–159

Dongquan Z, Jining C, Haozheng W, Qingyuan T, Shangbing C, Zheng S (2009) GIS-based urban rainfall-runoff modeling using an automatic catchment-discretization approach: a case study in Macau. Environ Earth Sci 59:65–472

El Bastawesy M, White K, Nasr A (2009) Integration of remote sensing and GIS for modelling flash floods in Wadi Hudain catchment, Egypt. Hydrol Process 23:1359–1368

Fred E, Mostafa B (2008) Flood risk modeling for holy sites in Makkah. In: Proceedings of the symposium on national GIS application in Saudi Arabia, Al-Kober City, Saudi Arabia

Gogoase D, Armaş I, Ionescu C (2011) Inundation maps for extreme flood events at the mouth of the Danube River. Int J Geosci 2:8–74

Guptaa P, Panigrahya S (2008) Geo-spatial modeling of runoff of large land mass: analysis, approach and results for major river basins of India. In: Proceedings of the international archives of the photogrammetry, remote sensing and spatial information sciences, vol. XXXVII. Part B2. Beijing

Horton R (1945) Erosional development of streams and their drainage basins: hydrological approach to quantitative morphology. Geol Soc Bull 56:275–370

Huggett R (2007) Fundamentals of geomorphology, 2nd edn. Routledge, New York

IDoT (Iowa state Department of Transportation) (2009) Iowa storm water management manual

Jasrotia A, Singh R (2006) Modeling runoff and soil erosion in a catchment area, using the GIS, in the Himalayan region, India. Environ Geol 51:9–37

Karmakar S, Simonovic S, Peck A, Black J (2010) An information system for risk-vulnerability assessment to flood. J Geogr Inf Syst 2:29–146

Kim N, Lee JW, Lee J, Lee JE (2010) SWAT application to estimate design runoff curve number for South Korean conditions. Hydrol Process 24:156–2170

Liang W, Yongli C, Hongquan C, Daler D, Jingmin Z, Juan Y (2010) Flood disaster in Taihu Basin, China: causal chain and policy option analyses. Environ Earth Sci. doi:10.1007/s12665-010-0786-x

Mihalik E (2008) Watershed characterization and runoff modelling of the Chapel branch creek, Orangeburg county, South Carolina, MSC thesis, College of Charleston, South Carolina State, USA

Mirza M, Ahmed B (2001) Winter weather and climate conditions in Makkah (in Arabic), Geographic Messages, vol 253. Kuwait Geographic Association, Kuwait

NH DoT (New Hampshire Department of Transportation) (1998) Drainage design manual for highways

Raghunath H (2006) Hydrology: principles, analysis, and design. New Age International Ltd., New Delhi

Saleh A, Al-Hatrushi S (2009) Torrential flood hazards assessment, management, and mitigation, in Wadi Aday, Muscat area, Sultanate of Oman, a GIS and RS approach, Egypt. J Remote Sens Space Sci 12:1–86

Sen Z (2008) Wadi hydrology. CRC Press, New York

Şen Z, Al-Suba'l K (2002) Hydrological considerations for dam siting in arid regions: a Saudi Arabian study. Hydrol Sci J 2(47):173–186

US ACE (US Army Corps of Engineers) (2004) Physical stream assessment

US DoT (US Department of Transportation) (2002) Highway hydrology manual, Publication No. FHWA-02-001

US NRCS (US National Resources Conservation Services) (1986) Urban hydrology for small watersheds, Technical Manual TR55

USGS (2009) (U.S. Geological Survey) Watershed models for decision support for inflows to Potholes reservoir, Washington scientific investigations report 2009–5081

Yahaya S, Ahmad N, Abdalla R (2010) Multicriteria analysis for flood vulnerable areas in Hadejia–Jama'are river basin, Nigeria. Eur J Sci Res 42(1):1–83

Youssef A, Pradhan B, Hassan A (2010) Flash flood risk estimation along the St. Katherine road, southern Sinai, Egypt using GIS based morphometry and satellite imagery. Environ Earth Sci. doi:10.1007/s12665-010-0551-1

Yunus M, Hassan H (2010) Managing road maintenance using geographic information system application. J Geogr Inf Syst 2:15–219

THIS IS A PEER REVIEWED PAPER
FIG Working Week 2012

GIS EVALUATION OF URBAN GROWTH AND FLOOD HAZARDS: A CASE STUDY OF MAKKAH CITY, SAUDI ARABIA

Khalid A. AL-GHAMDI, Meraj N. MIRZA, , Ramze A. ELZAHRANY Saudi Arabia, and Gomaa M. DAWOD, Egypt

SUMMARY

Four-dimensional Geographic Information System (4D GIS) furnishes a noteworthy technical tool for precisely mapping 3D-space growth of urban municipality over time. It can be augmented to estimate flood hazardous impacts due to urban sprawl. In the current study, a 4D GIS has been developed to analyze and quantify both urban growth and flood hazard changes in Makkah city, Saudi Arabia, over the last twenty years. It has been found that the urban growth in 1990 took the north-east and south-west directions, while it took the north-west and south-east directions in 2010. Additionally, investigating the city topography reveals that the urban sprawl mostly exist in low- and moderate-elevation regions. Attained results showed, also, that the residential regions of Makkah city have been increased by 197%, while the total flood volumes have been enlarged by 248%. This is due to two factors: (1) establishment of new residential areas in regions that already posse high flood impacts; and (2) building up new suburban areas on sediment soil that significantly decreases the permeability of the soil and, thus, leads to a crucial increase in hazardous water surface runoff. It is concluded that the utilization of GIS in urban growth and flood hazard estimation studies is quit powerful and provides a successful technical tool that helps in analyzing and understanding such phenomena. It is recommended that the achieved findings should be taken into account by decision-makers in development planning and resources management policies for Makkah metropolitan area.

Keywords: GIS, Spatial analysis, Urban growth, Flood hazards, Rainfall-Runoff, Saudi Arabia.

GIS EVALUATION OF URBAN GROWTH AND FLOOD HAZARDS: A CASE STUDY OF MAKKAH CITY, SAUDI ARABIA

Khalid A. AL-GHAMDI, Meraj N. MIRZA, , Ramze A. ELZAHRANY Saudi Arabia, and Gomaa M. DAWOD, Egypt

1. INTRODUCTION

Urbanization is an outcome of natural and socio-economic factors and their utilization by man in time and space. The dispersed development along highways, or surrounding a city and in rural countryside is called urban sprawl. Geomatics technologies, such as Remote Sensing (RS) and GIS, furnish exceptional technical tools for urban modelling and planning. Mapping the spatial (three-dimensional) growth of a city over time, i.e. a four-dimensional scenario, is a central aspect in developing city planning strategies. Several researchers have examined this issue particularly with utilization of GIS and RS. Mishra et al. (2011) carried out a research project for detecting urban growth (1930-2005) and land use changes (2000-2005) in Bhubaneswar city, India. Also, Saravanan and Ilangovan (2010) used GIS to investigate the nature and pattern of urban expansion of Madurai city over its surrounding region during the period 1991-2006. Similarly, Feng (2009) used GIS and RS to quantifying the urban sprawl in China over the period 1980-2003. Moreover, Alabi (2009) integrated RS and GIS data to examine the sprawl of Lokoja region, Nigeria over the period 1987-2007. Abd-Allah (2007) utilized GIS and RS in modelling urban dynamics, particularly for quantifying the loss in agricultural lands in the greater Cairo region, Egypt, for 1972-2005.

On the other hand, floods are natural returning hydrological phenomena that affect human lives. Hazards of flash floods, chiefly in urban regions, are vital from both human settlement and economical perspectives. Recently, the estimation of flood hazardous impacts and the development of GIS-based flood inundation maps have been considered a crucial demand. For example, Sagala (2006) carried out a detailed vulnerability assessment study to investigate physical flood hazards, particularly buildings' damages, in a residential area depending upon a mobile GIS. Fernandez and Lutz (2010) described a GIS-based research produced flood hazard maps for two cities in Argentina based on a multi-criteria design analysis. Park and Hur (2011) have utilized GIS for the development of flood simulation system for Namgang watershed, Korea. In addition, a similar methodology was proposed and rested in Georgia, USA (Qi and Altinakar, 2011). Hagen et al. (2011) presented a simple methodology for developing a nation-wide flood hazard maps in Afghanistan as an example of developing countries.

A special attention was given to the interrelationship between urbanization and flood hazardous impact in the last few decades. He and Hogue (2011) integrated hydrologic modelling and land use projections to predict long-term impacts of urbanization on hydrologic behavior and water supply in Los Angeles, USA. Amini et al. (2011) concluded that changes in land-use will increase the peak stream flow, and the increase is directly proportional to the rate of urbanization in Damansara watershed, Malaysia. Additionally, Zheng and Qi (2011) highlighted that serious natural hazards, particularly flood impacts, are increased due to

urbanization in Chinese mountainous cities. 3D GIS models are proposed for simulating flood spreading in urban areas in order to decide optimum urban protection levels (e.g. Wang et al., 2010, and Merwade et al., 2008). Moreover, GIS was used for assessing economic impacts of flood damages in Korea (Yi et al., 2010) and in France (Vinet 2008).

In Kingdom of Saudi Arabia (KSA), GIS and RS have been utilized in a variety of planning and development tasks such as: urban-rural land use change detection (e.g. Belaid, 2003), change detection in coastal areas (e.g. Al-Otaibi et al., 2006), traffic planning in Makkah city (Koshak 2006), modelling urban growth dynamics (e.g. Al-Ahmadia et al., 2008), analysis of population distribution variations (Elzahrany 2007), developing maps from RS images (AlSultan et al., 2008), groundwater exploration (e.g. El-Hames et al., 2001, and Al Saud 2010), and morphometric analysis (Subyani et al., 2010). Moreover, a great attention has been paid recently to the issue of flood assessment and flood hazards estimation in KSA. For example, Dawod et al. (2011) developed a GIS-based process to quantify the flood parameters, e.g. peak discharge and runoff volume, in Makkah city based on the US National Resources Conservation Service (NRCS)'s flood modelling method (known also as the curve number methodology). Moreover, Subyani (2011) investigated the flood probability for arid basins in Makkah administrative area. Dawod and Koshak (2011) developed NRCS-based unit hydrographs for the six catchments within Makkah metropolitan area as a tool for rainfall-runoff modelling and flood management. This paper aims to monitor and quantify the spatial urban sprawl of Makkah metropolitan area and the anticipated flood hazards' increase over the period 1947-2010 within a GIS environment.

2. STUDY AREA

Makkah city is located in the south-west part of Kingdom of Saudi Arabia (KSA), about 80 km east of the Red Sea (Fig. 1). It extends from longitudes 39^{o} 35’ E to 40^{o} 02’ E, and from latitudes 21^{o} 09’ N to 21^{o} 37’ N. The current area of the metropolitan region (the study area) equals 1593 square kilometres. Makkah city is a unique city for Muslims all over the world, since it contains the holly mosque. From a religious point of view, a Muslim should perform pilgrimage (called Hajj, which means visiting Makkah in specific days in the year) once in his/her life. Thus, hundreds of thousands Muslims are gathered in Makkah yearly. Also, Muslims prefer to perform a religious tourism plane, called Omarh, to Makkah all over the years. This is an important factor to be considered in analyzing the urban growth of this city. Moreover, the topography of Makkah is complex in nature, and several mountainous areas exist inside its metropolitan area. That is also a vital element in investigating the spatial pattern of Makkah sprawl.

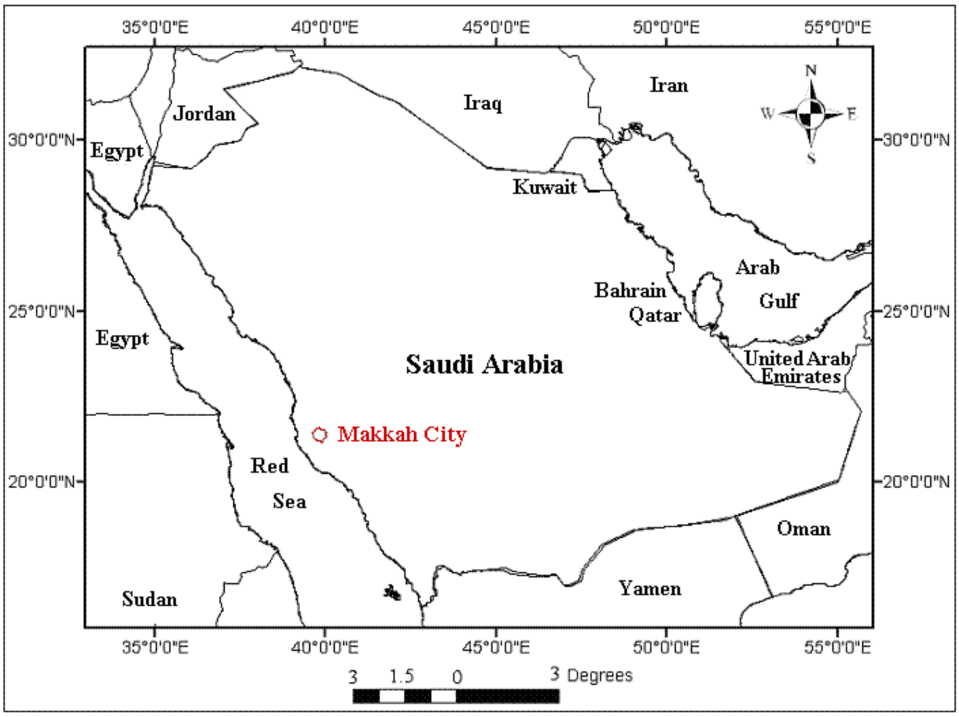

Figure 1: Study Area

On a national level, precise flood assessment is considered as an important demand in Makkah metropolitan area due to the unexpected nature of rainfall that often produce flash hazardous floods. The annual rain over Makkah city, for a period extending from 1966 to 2010, varies from 3.8 mm to 318.5 mm, with an average of rainfall equals 102.6 mm (Fig. 2). Due to the complexity of Makkah's topography, flash floods occur periodically with significant variations in magnitude. Mirza and Ahmed (2001) reported that the extreme flood type is repeated with a return period of 46 years, while a second-order flood takes place occasionally with a return period of 33 years, and a low-dangerous flood comes about every 13 years. The topography of the Makkah metropolitan area is complex, where several mountainous regions exist within the urban boundaries of the city. Terrain elevations in Makkah (Figure 3) range from 82 to 982 meters above sea level (Mirza et al., 2011).

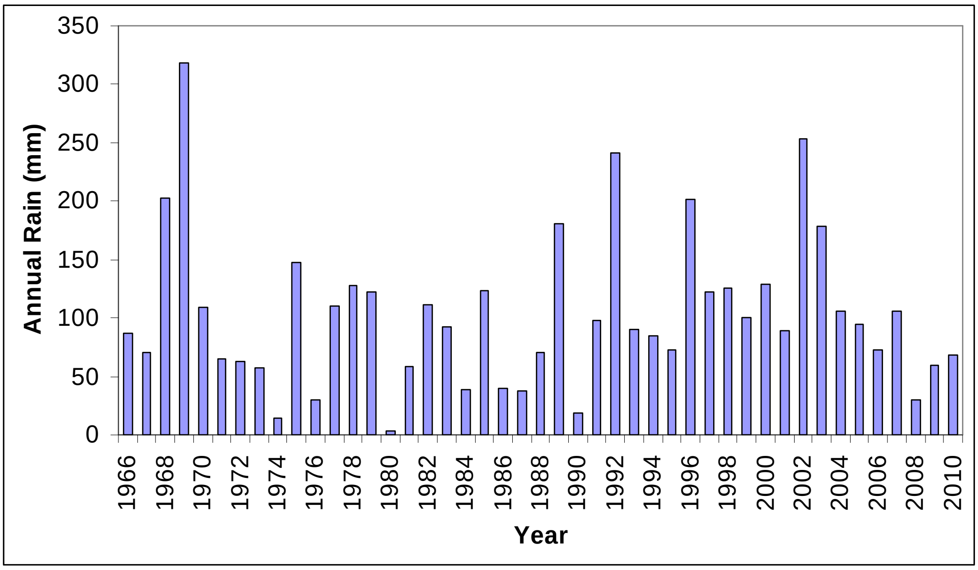

Figure 2: Annual Rains in Makkah city from 1966 to 2010

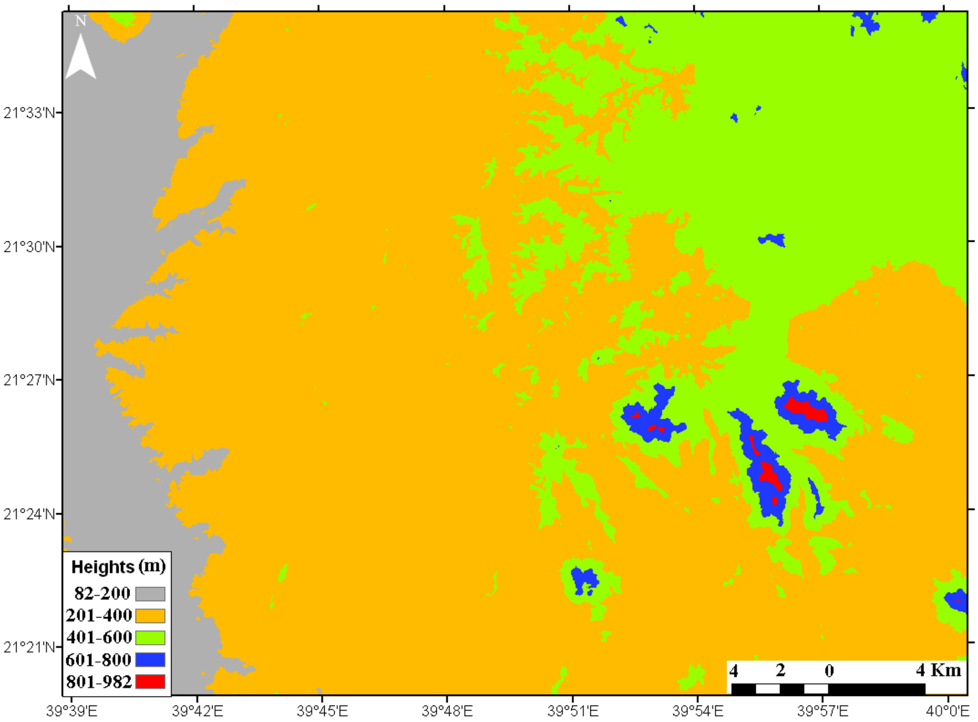

Figure 3: Elevations of Makkah city

3. DATA AND METHODOLOGY

The spatial compiled datasets constitute of three categories. The first element is a topographic map of Makkah city in 1947. The second group consists of 105 cadastral maps in AutoCAD file format for 1990. The third constituent consists of a land use map developed by the Saudi geological survey authority dated 2010. Additionally, a national 5-meter resolution Digital Elevation Model (DEM) for the study area has been obtained from King Abdulaziz City of Sciences and Technology (KACST). The Arc GIS software (v. 10), along with the Arc Hydro extension, has been used in the present study to combine all obtainable data in a unique environment, and to delineate the main hydrological basins, and their associated sub-basins, in the study area. The processing phase includes (Fig. 4): rectifying the printed maps, digitizing two shapefile for residential areas and roads for each dataset, converting AutoCAD files to GIS shapefiles, unifying the spatial reference frames for all datasets, performing statistical and spatial analysis; and flood estimation. The term 4D GIS in Fig. 4 indicates the integration and utilization of 3D spatial datasets for several time intervals in a unique GIS environment.

Regarding flood estimation, the NRCS, formerly known as the Soil Conservation Service (SCS), has been selected in this research study since it might be considered the most widely-utilized flood modelling methodology. It utilizes geological information to assign a unique Curve Number (CN) coefficient value for each area, that will be further used to estimate the surface runoff depth and the peak discharge magnitude. The NRCS method is quit utilized in engineering design and flood management projects (e.g. Masoud, 2011, Al-Jabari et al., 2009; Adebayo et al., 2009; Elaji, 2010; Xianzhao and Jiazhu, 2008; and Gul et al., 2009), and particularly in USA (e.g. US ACE, 2004; and US DoT, 2002). The basic formulas of the NRCS approach are (e.g. US NRCS, 1986):

$$Q = (P - 0.2 S)^2 / (P + 0.8 S) \qquad (1)$$

where,

Q = depth of direct runoff (mm)
P = depth of precipitation for a specific return period (mm)
S = maximum potential retention (mm):

$$S = 25.4 ((1000 / CN) - 10) \qquad (2)$$

where CN is the curve number. Tables provide values of CN are presented in several hydraulic literatures (e.g., Sen 2008b, pp. 165). Table 1 presents some of these CN values.

$$qp = qu\ A\ Q \qquad (3)$$

where,

qp = peak discharge (m^3/s)
A = drainage area (km^2)

Q = depth of runoff (mm)

qu = unit peak discharge ($m^3/s/km^2/mm$) that can be interpolated from a specific charts (e.g. US NRCS, 1986) or computed from corresponding tables (e.g. US DoT 2002, pp. 5-28).

$$Q_T = Q\ A \qquad (4)$$

where Q_T = Flood volume (m^3)

Table 1: Examples of runoff CN values

Cover Type	Hydrological Soil Types			
	A	B	C	D
Fully developed urban areas (vegetation established):				
- Good condition; grass cover on 75% or more of the area	39	61	74	80
- Fair condition; grass cover on 50% to 75% of the area	49	69	79	84
- Poor condition; grass cover on 50% or less of the area	68	79	86	89
Streets and Roads:				
- Paved with curbs and storm sewers (excl. right-of-way)	98	98	98	98
- Gravel (incl. right-of-way)	76	85	89	91
Industrial districts (72% average impervious)	81	88	91	93
Commercial and business areas (85% average impervious)	89	92	94	95
Where: Group A soils have low runoff potential and high infiltration rates even when thoroughly wetted, Group B soils have moderate infiltration rates when thoroughly wetted, Group C soils have low infiltration rates when thoroughly wetted, Group D soils have high runoff potential and low infiltration rates when thoroughly wetted.				

after US NRCS 1986.

Simply, the flood processing stage starts by assigning a CN value for each sub-basin based on its geological, soil, and land use properties. Then the maximum potential retention, S, is computed through eq. 2. The value of the depth of precipitation, P in eq. 1, is obtained through the Pearson Log III statistical analysis of the rainfall dataset for a specific return period (e.g., 50 years in the current study). The depth of runoff, Q in eq. 1, can then be computed. Next, the unit peak discharge, qu, being computed or interpolated from the corresponding specific diagrams. Finally, the peak discharge, qp, is evaluated through eq. 3, and the total flood volume for each sub-basin, Q_T, is obtained from eq. 4.

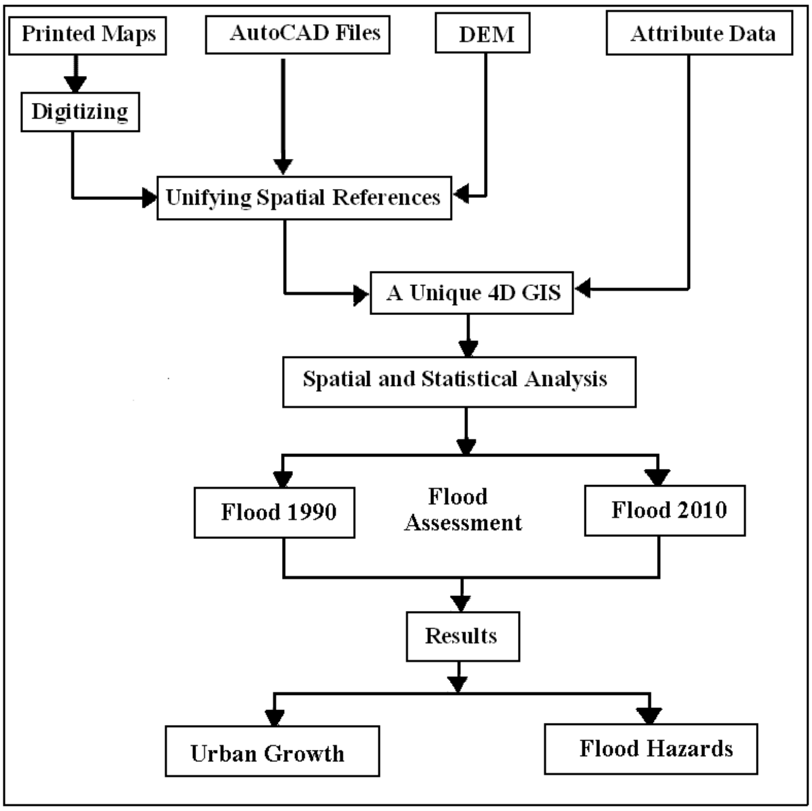

Figure 4: Processing Workflow

4. RESULTS AND DISCUSSION

The attained results may be divided into two main groups: (1) results related to urban growth; and (2) results related to flood hazards. For the first results' category, shapefiles of Makkah metropolitan area for 1947, 1990, and 2010 have been integrated in a GIS project (Fig. 5). The total residential area has been computed and found to be 5.168, 99.234, and 158.583 square kilometers for 1947, 1990, and 2010 respectively. Thus, the residential areas in Makkah city have been grown by about 1820% between 1947 and 1990 (with 42% annual rate), and by about 97 % from 1990 to 2010 (with 4.8 % annual rate). The most important reason behind the huge urban sprawl in mid 20^{th} century might be the enormous national income expansion due to the oil exploration in the Gulf region. That economical enlargement caused an urban development revolution not just in Makkah city but almost in all towns within Saudi Arabia. Secondly, the official planning rules and governmental authority have been started in 1955 in order to regulate the urban development of Makkah city (HAMDD 2004).

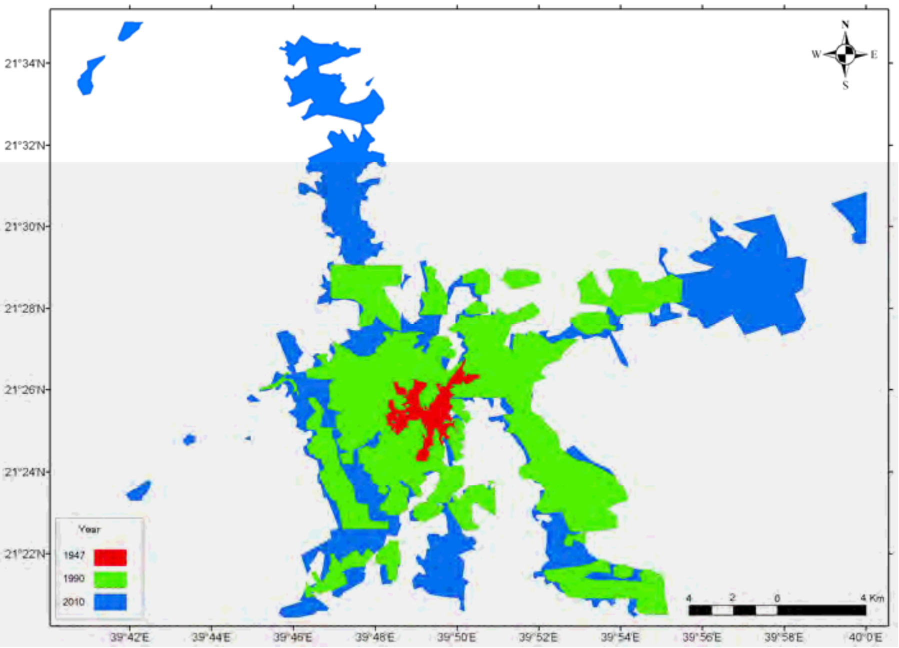

Figure 5: Urban Sprawl of Makkah City

It can be realized from figure 5 that the urban growth in Makkah city takes a radial (or spoke) pattern. That is logically understood knowing that the holly mosque is considered the center of the city, and the central area around it has the highest population density since residents and pilgrims prefer to stay close to this holly mosque.

Applying GIS spatial analysis tools produces more valuable pieces of information. The directional distribution tool supplies precious information about the spatial directional trend of the urban spread out. Directional distribution, or standard deviational ellipse, has been carried out for the three urban development stages of Makkah city (Fig. 6). Although a directional ellipse by itself gives a static perspective about the residential areas at a specific time, comparing several ellipses may give an idea about the changes took place over a time interval. The idea, herein, is that the changes occurred in the ellipses' orientation may portrait, to some extent, the variations of the residential areas' expansion or growth directions. From figure 6, it can be noticed that the azimuth of the major axes of the ellipse, in a clockwise from the North direction, has been found to be 35^o, 31^o, and 148^o for 1947, 1990, and 2010 respectively. Therefore, the urban growth in both 1947 and 1990 took the north-east and south-west directions, while it took the north-west and south-east directions in 2010. So, such results conclude that the growth general direction has been relatively fixed between 1947 and 1990, while it has been significantly changed between 1990 and 2010.

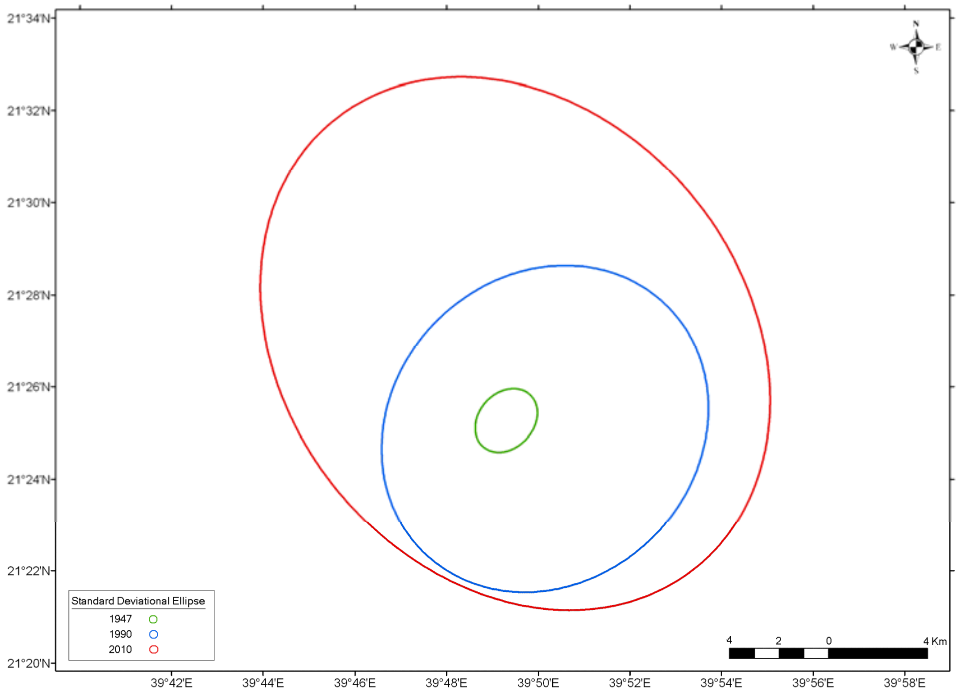

Figure 6: Standard Deviational Ellipses of Urban Sprawl of Makkah City

The available national 5-meter resolution DEM describes the rigid topography of Makkah metropolitan area. Several mountainous areas exist within Makkah city, and affect the spatial urban growth location and direction. Figure 7 depicts the topography of Makkah as divided into four categories. It can be seen that the urban sprawl mainly exist in low- and moderate-elevation regions. The growth spreads out along the valleys and stays away from the mountainous areas for economical reasons. It worth mentioning that almost 50% of Makkah's geology contains igneous rocks, mainly granite, that massively increase the development costs in mountainous areas.

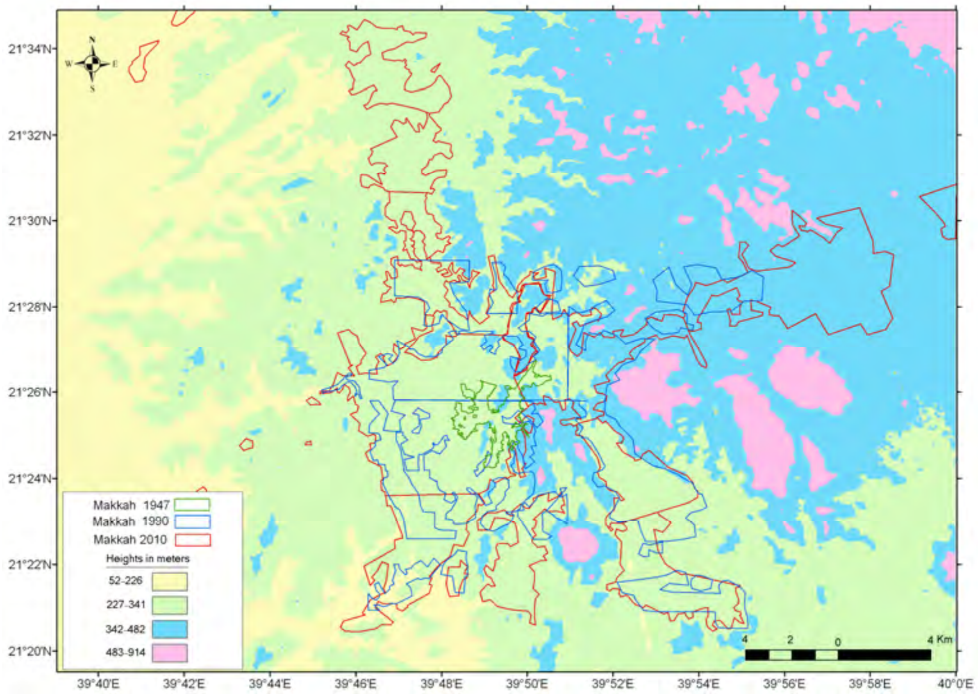

Figure 7: Topography of Residential Areas in Makkah City

Concerning the road network, it worth mention that Makkah has six regional highways that connect it to major Saudi city (Fig. 8). These roads are: Makkah-Madinah road (427 km), Makkah-Riyadh road (880 km), Makkah-Taif road (88 km), Makkah-Laith road (180 Km), and two Makkah-Jeddah roads (78 km). Inspecting both figures 3 and 7 concludes that the urban sprawl of Makkah city follows those regional roads. In the first phase (1947-1990) the urban growth has been concentrated mainly along Makkah-Riyadh and Makkah-Taif roads. Moreover, in the second phase (1990-210) the urban development has been intensive mostly along Makkah-Riyadh and Makkah-Madinah roads. That growth leads to the creation of new districts in Makkah city, such as: Sharee'h, Sharee'h Al Mojahdeen, Al Rashdia, and Al-Khadraa at the North-East corner, and Omraa, Nowaria, Al Bohayrat at the North corner of Makkah (Fig. 9). That conclusion consents with the values of the rotation angles of the standard deviational ellipses as argued earlier.

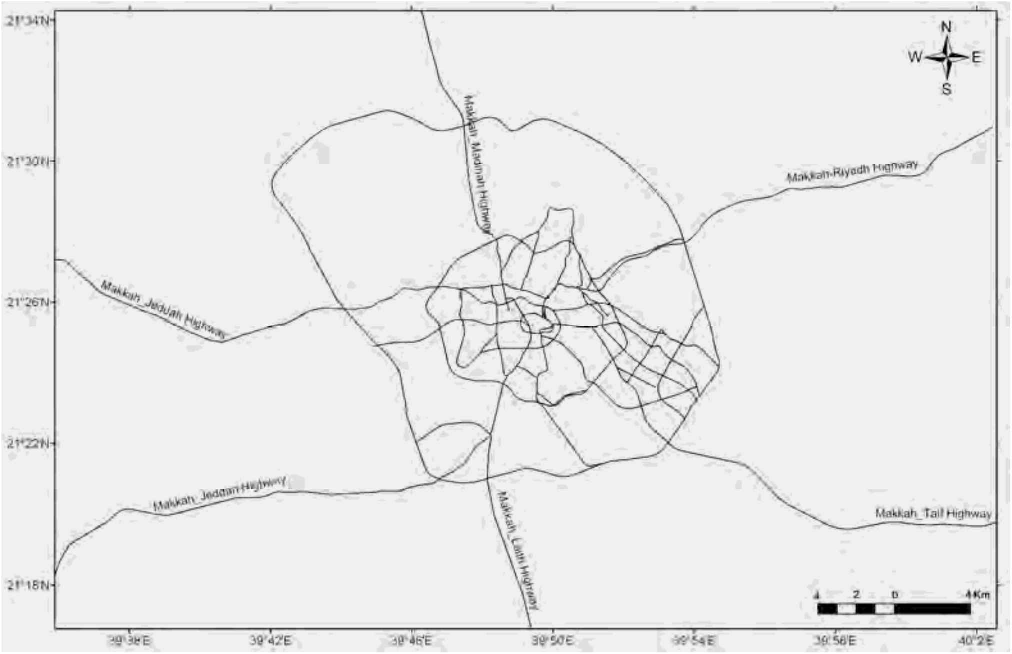

Figure 8: Main Roads in Makkah City

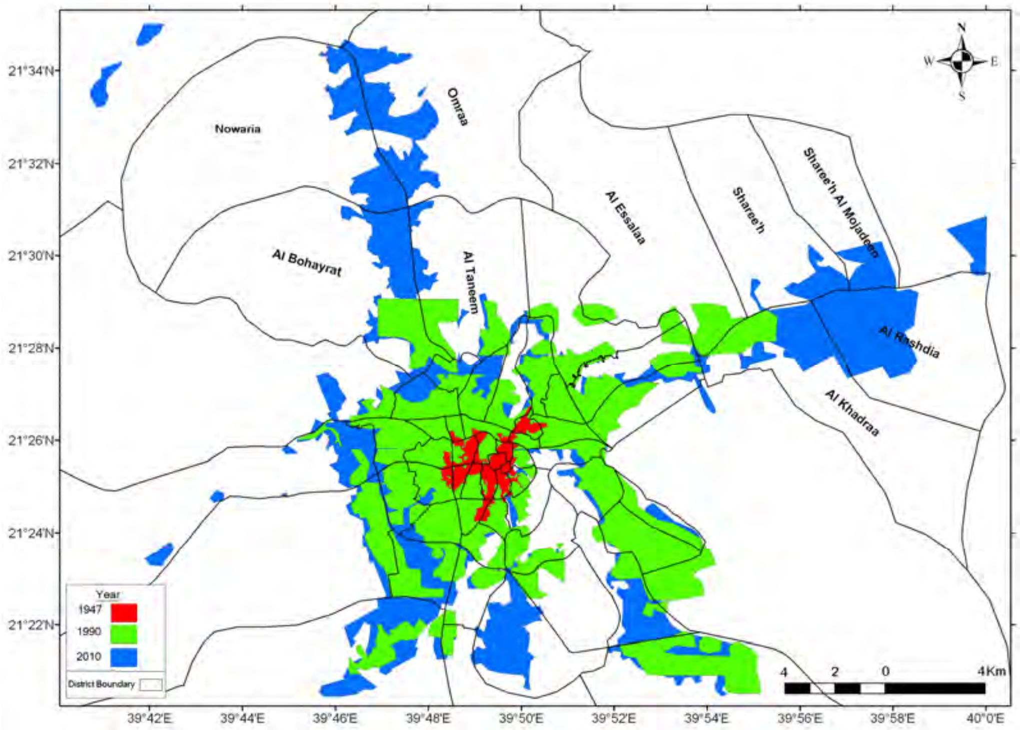

Figure 9: New Districts Within Makkah City

The second category of accomplished results deal with the estimation of flood hazards in Makkah city. The NRCS method has been performed for the available data of Makkah metropolitan area to compute the peak discharge value for the six basins for 1990 and 2010 datasets. The return period has been chosen, herein, as 50 years, for which the rainfall intensity (P in equation 1) has been estimated, by applying the Log Pearson III statistical analysis, as 200 mm/hour (Dawod et al., 2011). Table 2 presents statistics of the attained flood parameters, over residential areas, for 1990 and 2010. The runoff depth and the total flood volumes have been computed on the sub-basin scale, only for those sub-basins contain residential areas (Fig. 10). Twenty-five sub-basins that include residential areas, in 1990, have been identified within the study area. The area of these sub-basins range from 0.478 to 10.663 square kilometers, with a sum of 71.587 square kilometers. The flood volumes of these sub-basins have been estimated (equation 4) for 1990 and found to vary from 79.6 to 1809.7 thousands cubic meters with a total of 11849.9 thousands cubic meters. Then, utilization of the 2010 datasets revealed that there are 64 sub-basins that include residential areas (Fig. 11). The area of these sub-basins range from 0.223 to 18.569 square kilometers, with a sum of 157.564 square kilometers. The flood volumes of these sub-basins have been estimated for 2010 and found to vary from 45.5 to 2928.7 thousands cubic meters with a total of 41282.1 thousands cubic meters.

Table 2: Statistics of floods over residential areas in 1990 and 2010

Item	1990	2010
Number of sub-basins contain residential areas	25	64
Total area of residential areas (km^2)	80.021	157.564
Minimum flood volumes (m^3)	79,623	45,487
Maximum flood volumes (m^3)	1,809,701	2,928,694
Total flood volumes (m^3)	11,849,980	41,282,085

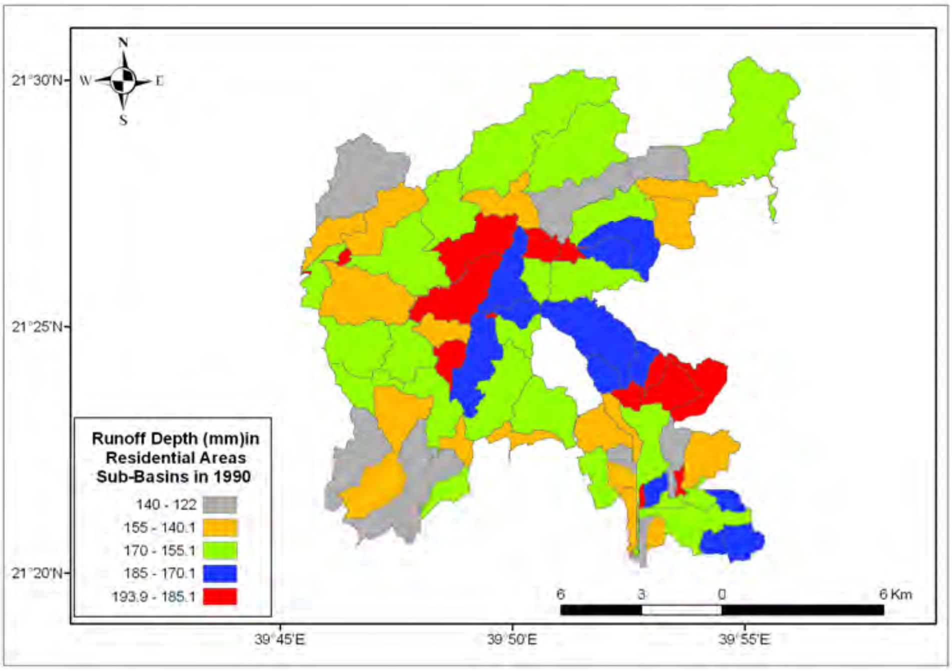

(a) Runoff Depth

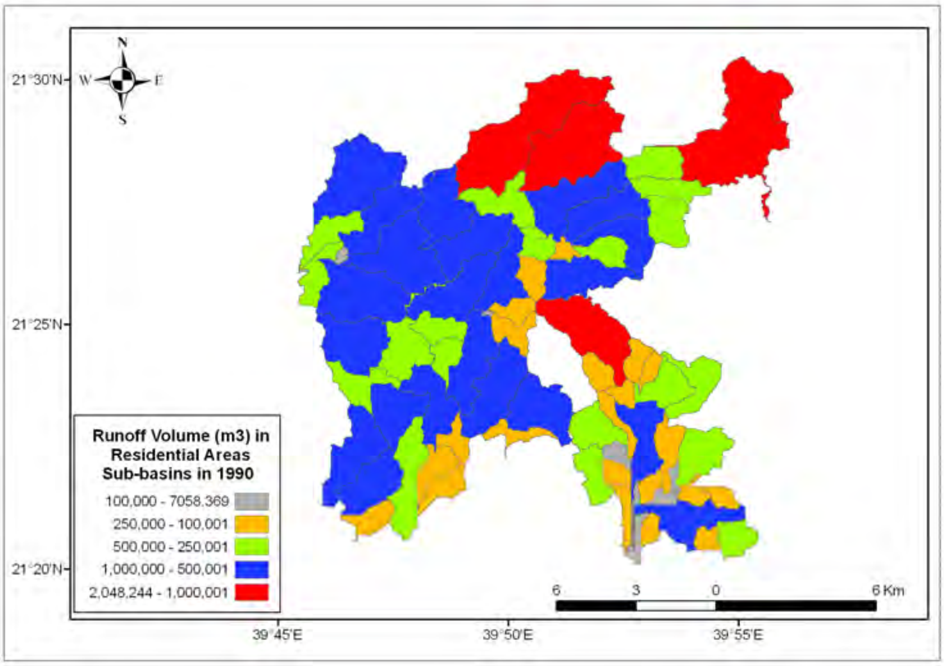

(b) Flood Volume

Fig 10: Floods over Residential Areas in 1990

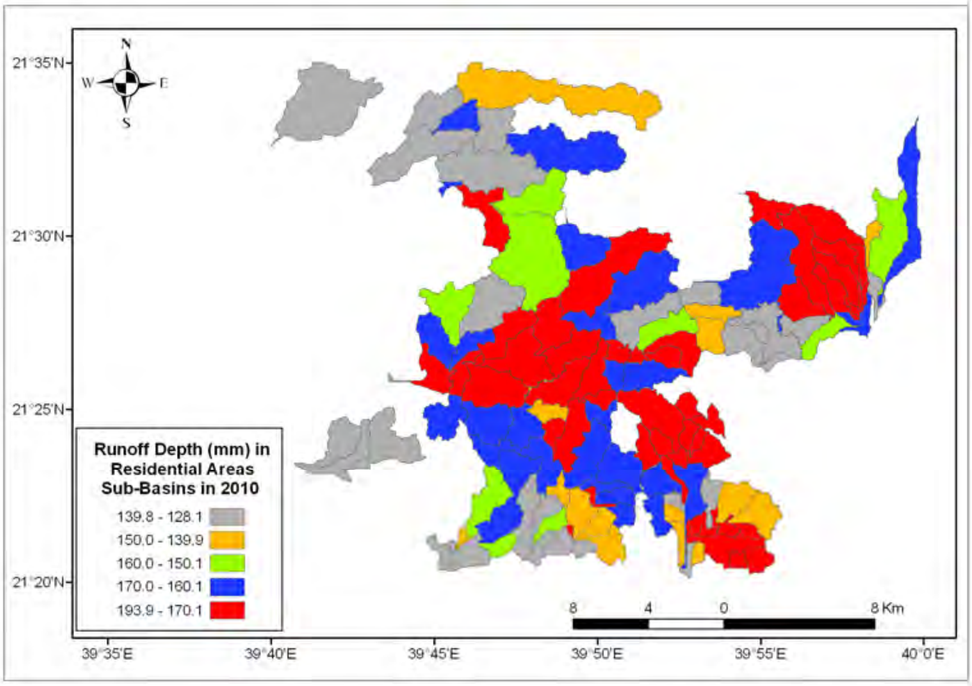

(a) Runoff Depth

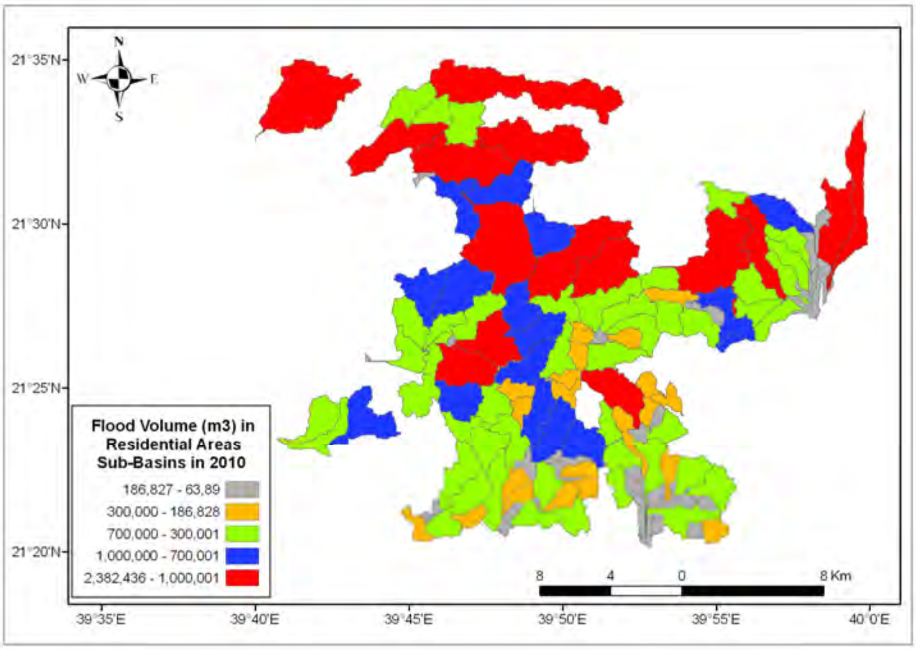

(b) Flood Volume

Fig 11: Floods over Residential Areas in 2010

Comparing the results of flood estimation for both 1990 and 2010 reveals critical points. First, the residential areas of Makkah city have been increased, over twenty years, from 80.0 to 157.6 km2, with 197% increase (with an annual rate of 9.8%). Second, the total flood volumes, of the entire study area, have been increased from 11.8 to 41.3 million cubic meters, i.e. 248%. The spatial distribution of the new residential areas (built between 1990 and 2010) is depicted in figure 12. It can be seen that there are several new areas, particularly in the north of Makkah city, located in high-flood sub-basins. Furthermore, it has been found that most of the new residential areas have been established on sediment soils (Figure 13). From an economical point of view, that geological type is cost-effective than constructing building on solid igneous rock geology. However, that urbanization significantly decreases the permeability of the soil and, thus, leads to a crucial increase in hazardous water surface runoff. For example, the curve number (CN in equation 2) of sediment geology type equals 76 while it equals 98 for paved residential areas (e.g. Sen 2008b, and US NRCS 1986). These two factors might be the major reasons resulted in that sever augmentation of flood volume in Makkah metropolitan area.

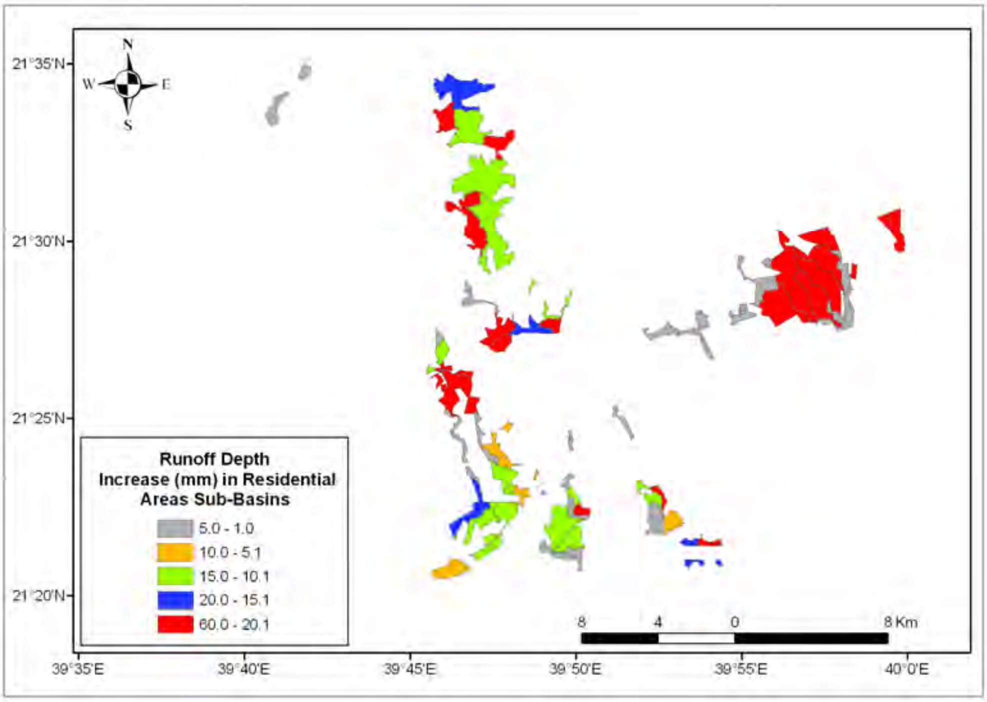

(a) Runoff Depth

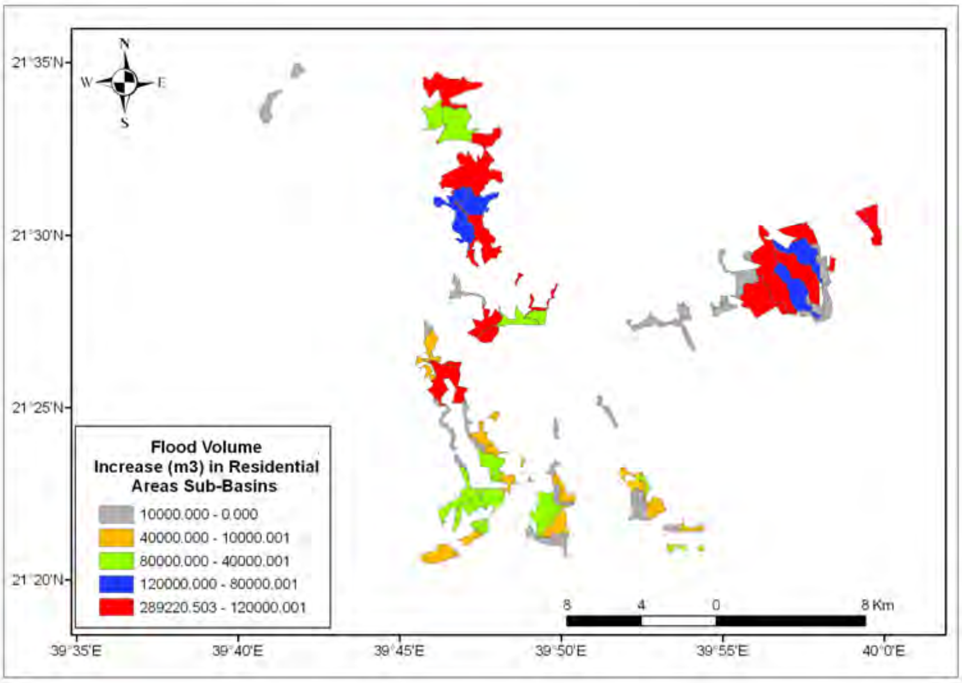

(b) Flood Volume

Fig 12: Floods over New Residential Areas

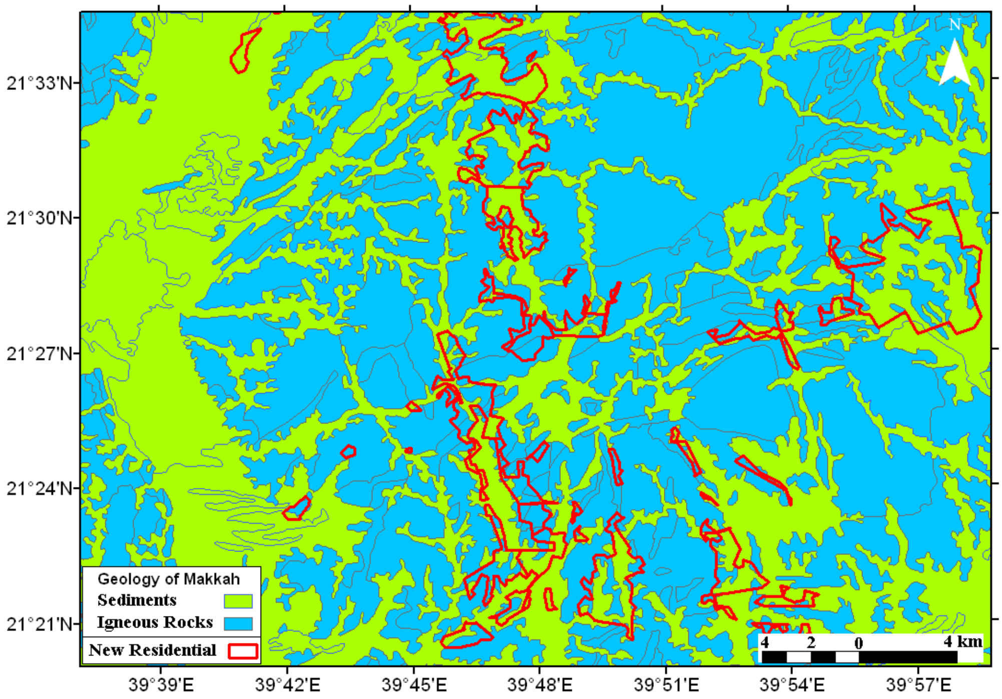

Fig 13: Geology of New Residential Areas

5. CONCLUSIONS

The urban sprawl is one of the human-induced potential threats to sustainable development where urban planning, with effective resource utilization and allocation, is a crucial concern. Thus, identification and analysis of the patterns of sprawl would help in effective land-use planning in an urban area. In the current study, a four-dimensional GIS has been developed to analyze and quantify the urban growth of Makkah city in the last sixty years. Makkah has witnessed a huge urban sprawl in mid 20^{th} century, that might be due the enormous national income expansion due to the oil exploration in the Gulf region. That economical growth commenced an urban development revolution for almost all towns within Saudi Arabia. Also, it has been found that the urban growth in Makkah city takes a radial pattern, which is logically understood knowing that the holly mosque is considered the center of the city, and the central area around it has the highest population intensity since residents and pilgrims prefer to stay close to this mosque. In the context of 4D GIS, it worth mentioning that GIS presents a valuable tool for developing 4D cadastre for land use and real estate of a city (Van Oosterom et al., 2006). Such a project is currently proposed for Makkah city, and can be linked to the GIS-based flood modelling developed in this research.

Applying GIS spatial analysis tools produces more valuable pieces of information. The azimuth of the major axes of the standard deviational ellipse has been found to be 35^o, 31^o, and 148^o for 1947, 1990, and 2010 respectively. Therefore, the urban growth in both 1947 and 1990 took the north-east and south-west directions, while it took the north-west and south-east

directions in 2010. Furthermore, inspecting the topography of Makkah city concluded that the urban sprawl mainly exist in low- and moderate-elevation regions. The growth spreads out along the valleys and avoid the mountainous areas for economical reasons. Moreover, it is concluded that the urban sprawl of Makkah city follows regional roads. In the first phase (1947-1990) the urban growth has been concentrated mainly along Makkah-Riyadh and Makkah-Taif roads. However, in the second phase (1990-210) the urban development has been intensive mostly along Makkah- Riyadh and Makkah-Madinah roads. Furthermore, accomplished results showed that the residential regions of Makkah city have been increased by 197%, while the total flood volumes have been enlarged by 248%. Two factors might be considered possible reasons led to that significant flood hazard raising. First, establishment of new residential areas in regions that already posse high flood impacts. Second, building up new suburban areas on sediment soil significantly decreases the permeability of the soil and, thus, leads to a crucial increase in hazardous water surface runoff.

It is concluded that the utilization of GIS in urban growth and flood hazard estimation researches is quit powerful and provides an effective technical tool that helps in analyzing and understanding such phenomena. It is recommended that the attained results should be taken into account by decision-makers in implementing new development planning of Makkah metropolitan area.

ACKNOWLEDGMENT

The authors would like to acknowledge the financial support offered by the Center of Research Excellence in Hajj and Omrah, Umm Al-Qura university, Saudi Arabia (Project PR12/2011).

REFERENCES

Abd-Allah, M., 2007, Modelling urban dynamics using geographic information systems, remote sensing and urban growth models, PhD Dissertation, Faculty of Engineering, Cairo university, Cairo, Egypt.

Al-Ahmadia, K., Heppenstallb, A., Seeb, L., and Hoggb, J., 2008, Modeling urban growth dynamics using cellular automata and GIS, Proceedings of the Third National GIS Symposium in Saudi Arabia, April 7 – 9, Al-Khobar, Saudi Arabia.

Alabi, M., 2009, Urban sprawl, pattern and measurement in Lokoja, Nigeria, Theoretical and Empirical Researches in Urban Management. 13(4) 158-164.

Al-Jabari S., Abu Sharakh M., and Al-Mimi Z., 2009, Estimation of runoff for agricultural watershed using SCS curve number and GIS, Proceedings of the thirteenth International Water Technology Conference, Hurghada, Egypt, 1213-1229.

Al-Otaibi, Y., Belaid, M., and Abdu, A, 2006, Impact assessment of human activities on coastal zones of eastern Saudi Arabia using remote sensing and geographic information systems techniques, Proceedings of the ISPRS Commission 7's workshop on Remote Sensing, May 8-11, Enschede, the Netherlands.

Al Saud, M., 2010, Mapping potential areas for groundwater storage in Wadi Aurnah Basin, western Arabian Peninsula, using remote sensing and geographic information system

techniques, Hydrogeology Journal, Published on-line April 13, DOI 10.1007/s10040-010-0598-9.

AlSultan, S., Lim, J., MatJafri, M., Abdullah, K. and Saleh, N., 2008, Innovative satellite image map of Alkhabrta area, Saudi Arabia using high resolution image, Proceedings of the ISPRS XXIst Congress. July 3-11. Beijing, China, Part B7, pp. 1355-1358.

Adebayo W., Solomon O., Ayanniyi M. and Sikiru, F., 2009, Evaluation of synthetic unit hydrograph methods for the development of design storm hydrographs for Rivers in South-West, Nigeria, Journal of American Science, (5)4: 23-32.

Amini, A., Ali, T., Ghazali, A., Aziz, A., and Akib, S., 2011, Impacts of Land-Use Change on stream flows in the Damansara Watershed, Malaysia, Arabian Journal Sciences and Engineering, 36:713–720.

Basawaraja, R., Chari, K., Mise, S., and Chetti, S., 2011, Analysis of the impact of urban sprawl in altering the land-use, land-cover pattern of Raichur City, India, using geospatial technologies, Journal of Geography and Regional Planning, 4(8) 455-462.

Belaid, M., 2003, Urban-rural land use change detection and analysis using GIS and RS technologies, Proceedings of the 2nd FIG regional conference, December 2-5, Marrakech, Morocco.

Dawod, G., Mirza, M., and Al-Ghamdi, K., 2011, GIS-based spatial mapping of flash flood hazards in Makkah city, Saudi Arabia, Journal of Geographic Information System, 3(3) 217-223.

Dawod, G., and Koshak, N., 2011, Developing GIS-Based Unit Hydrographs for Flood Management in Makkah Metropolitan Area, Saudi Arabia, Journal of Geographic Information System, 3(2) 153-159.

El-Hames, A. Al-Ahmadi, M. and Al-Amri, N., 2011, A GIS approach for the assessment of groundwater quality in Wadi Rabigh aquifer, Saudi Arabia, Environmental Earth Science, (63) 1319–1331.

Elaji A., 2010, Applications of Geographic Information Systems to construct databases of morphometric characteristics and their hydrologic meanings in Yalamlam basin (in Arabic), MSC thesis, Umm Al-Qura university, Makkah, Saudi Arabia.

Elzahrany, R., 2007, The geographical distribution of population and houses in provinces of the Kingdom of Saudi Arabia, 1425(2004), (in Arabic), Umm Al-Qura university's Journal of Social Sciences, 19(1) 12-66.

Feng, L., 2009, Applying remote sensing and GIS on monitoring and measuring urban sprawl. A case study of China, Revista Internacional de Sostenibilisas, Tecnologia y Humanismo, (4) 47-56.

Fernandez D. and Lutz M., 2010, Urban flood hazard zoning in Tucumán Province, Argentina, using GIS and multicriteria decision analysis, Engineering Geology, 111:90–98

Gul G., Harmancıoglu N., and Gul A., 2009, A combined hydrologic and hydraulic modeling approach for testing efficiency of structural flood control measures, Journal of Natural Hazards, DOI 10.1007/s11069-009-9464-2.

Hagen E., Shroder J., Lu X. and Teufert, J., 2011, Reverse engineered flood hazard mapping in Afghanistan: A parsimonious flood map model for developing countries, Quaternary International, 226:82–91.

HAMDD (Higher Authority for Makkah District Development), 2004, Master planning of Makkah city till 2028, Technical report (in Arabic), Makkah. Saudi Arabia.

He, M. and Hogue, T., 2011, Integrating hydrologic modeling and land use projections for evaluation of hydrologic response and regional water supply impacts in semi-arid environments, Environmental Earth Science, DOI 10.1007/s12665-011-1144-3.

Hegde, N., MuraliKrishna, I., and ChalapatiRao, K., 2008, Integration of cellular automata and GIS for simulating land use changes, Proceedings of the ISPRS 5th International Symposium, June 13-15, Enschede, The Netherlands.

Koshak, N., 2006, Developing a web-based GIS for Hajj traffic plan, Journal of Urban Planning Research, Cairo University, 6(6) 1-13.

Li, C., Hongbo, L., and Kemper, G., 2008, Monitoring urban development of small Chinese cities using innovative aerial surveying technologies, Proceedings of the ISPRS XXIst Congress, July 3-11. Beijing, China, Part B7, pp. 1667-1674.

Mishra, M., Mishra, K., Subudhi, A., and Phil, M., 2011, Urban sprawl mapping and land use change analysis using remote sensing and GIS: Case study of bhubaneswar city, orissa, Proceedings of the Geo-Spatial World Forum, January 18-21, Hyderabad, India.

Masoud A., 2011, Runoff modeling of the wadi systems for estimating flash flood and groundwater recharge potential in Southern Sinai, Egypt, Arab Journal of Geosciences, 4:785–801.

Merwade, V., Cook, A., and Coonrod, J., 2008, GIS techniques for creating river terrain models for hydrodynamic modeling and flood inundation mapping, Environmental Modelling and Software, 23:1300–1311.

Mirza M., Dawod G., and Al-Ghamdi K., 2011, Accuracy and relevance of digital elevation models for geomatics applications - A case study of Makkah municipality, Saudi Arabia, International Journal of Geomatics and Geosciences, (1)4:803-812.

Park J., and Hur Y., 2011, Development and application of GIS based K-DRUM for flood runoff simulation using radar rainfall, Journal of Hydro-environment Research, doi:10.1016/j.jher.2011.05.005.

Qi H. and Altinakar M., 2011, A GIS-based decision support system for integrated flood management under uncertainty with two dimensional numerical simulations, Environmental Modelling and Software, 26:817-821.

Saravanan, P. and Ilangovan, P., 2010, Identification of urban sprawl pattern for Madurai region using GIS, International Journal of Geomatics and Geosciences, 1(2) 141-149.

Sagala S., 2006, Analysis of flood physical vulnerability in residential areas, Case study: Naga city, the Philippines, Master thesis, International Institute for Geo-information Science and Earth Observation, The Netherlands.

Sen Z., 2008a, Modified hydrograph method for arid regions, Hydrological Process. 22:356–365.

Sen Z., 2008b, Wadi Hydrology, CRC Press.

Su, S. Xiao, R. and Zhang, Y., 2011, Multi-scale analysis of spatially varying relationships between agricultural landscape patterns and urbanization using geographically weighted regression, Applied Geography, (32) 360-375.

Subyani, A., Qari, M., and Matsah, M., 2010, Digital elevation model and multivariate statistical analysis of morphometric parameters of some wadis, western Saudi Arabia,

Arabian Journal of Geosciences, DOI 10.1007/s12517-010-0149-7, Published online May 11.

US ACE (US Army Corps of Engineers), 2004, Physical stream assessment.

US DoT (US Department of Transportation), 2002, Highway hydrology manual, Publication No. FHWA-02-001.

US NRCS (US National Resources Conservation Services), 1986, Urban hydrology for small watersheds, Technical Manual TR55.

Van Oosterom, P., Ploeger, H., Stoter, J., Thompson, R., and Lemmen, C., 2006, Aspects of a 4D cadastre: A First exploration, XXIII FIG Congress, Munich, Germany, October 8-13.

Vinet, F., 2008, Geographical analysis of damage due to flash floods in southern France: The cases of 12–13 November 1999 and 8–9 September 2002, Applied Geography 28:323–336.

Xianzhao L. and Jiazhu L., 2008, Application of SCS model in estimation of runoff from small watershed in Loess plateau of China, Journal of Chinese Geographical Science, (18)3:235–241.

Yi, C., Lee, J., and Shim, M., 2010, GIS-based distributed technique for assessing economic loss from flood damage: pre-feasibility study for the Anyang Stream Basin in Korea, Natural Hazards, 55:251–272.

Zhang, X., Tong, X., and Liu, M., 2008, Genetic algorithm optimized neutral network classification and overlapping pixel change detection based on remote sensing for urban sprawl: a case study in Jiading district of Shanghai, China, Proceedings of the ISPRS XXIst Congress, July 3-11, Beijing, China.

Zheng, Z. and Qi, S., 2011, Potential flood hazard due to urban expansion in the karst mountainous region of North China, Regional Environmental Change. 11:439–440.

Wang, C., Wan, T., and Palmer, I., 2010, Urban flood risk analysis for determining optimal flood protection levels based on digital terrain model and flood spreading model, Vis Comput, 26: 1369–1381.

BIOGRAPHICAL NOTES

Khalid A. Al-Ghamdi received his Master degree from Clark University, Worcester, Massachusetts, USA in 2002, and his Ph.D. from University of Fribourg, Fribourg, Switzerland in 2008. Since 1993, he is affiliated with Umm Al-Qura university, Makkah city, Saudi Arabia. Since 2009, he is the supervisor of the GIS/Remote Sensing unit in Umm Al-Qura university. He has taught several geomatics courses, and has attended many scientific conferences in KSA and abroad. Currently, he is the chairperson of the geography department in Umm Al-Qura university, Saudi Arabia.

Meraj N. Mirza received his Master degree from the Michigan University, USA in 1979 and his Ph.D. from Khartoum University, Sudan in 1995. Since 1975, he is affiliated with Umm Al-Qura university, Makkah city, Saudi Arabia. In 1997, he was one of the initiators of the GIS/Remote Sensing unit in Umm Al-Qura university, which is the pioneer GIS unit in Saudi universities. He is also an active associate of the Center of Research Excellence in Hajj and Omrah (Hajjcore), Umm Al-Qura university. Currently, he is a visiting professor at center of GIS in Harvard university, USA.

Ramze A. Elzahrany received his Master degree from the Eastern Michigan University, USA in 1983 and his Ph.D. from Kent State University, Ohio, USA in 1989. He works, now, as a professor of human geography in the geography department, Umm Al-Qura university, Saudi Arabia. Additionally, he is a member of Umm Al-Qura university's scientific council, and a member of the editorial board of Umm Al-Qura university's journal of social sciences, and a member of the editorial board of the Arabian journal of Geographical Information Systems, the Saudi geographical society. Furthermore, he published more than twenty nine papers; mainly in Arabic and few in English.

Gomaa M. Dawod received his Master of Geodetic Science and Surveying from the Ohio State University, Columbus, Ohio, USA in 1991 and his Ph.D. of Surveying Engineering from Shobra Faculty of Engineering, Zagazig University, Egypt in 1998. Since 1987, he is affiliated with the Survey Research Institute (SRI), the National Water Research Center (NWRC), Egypt, mainly in the field of Geodesy. Since 2005, he is affiliated with Umm Al-Qura university, Makkah city, Saudi Arabia. Dr. Dawod published more than forty papers related to GPS and GIS. Additionally, he has been chosen in the 2011-2012 edition of Who is Who encyclopedia in engineering and sciences.

CONTACTS

Khalid Abdel-Rahman Al-Ghamdi
Geography department, Umm Al-Qura University
P. O. Box 138474, Jeddah 21323, Saudi Arabia
Tel. +966541740090
Fax. +96625534113
Email: kaghamdi@uqu.edu.sa and alghamdik@hotmail.com
Web site: http://www.uqu.edu.sa/kaghamdi

Meraj Nawab Mirza
Centre of Research Excellence in Hajj and Omrah (Hajjcore), Umm Al-Qura University,
P.O. Box 6247, Makkah 21955, Saudi Arabia
Tel. +966505509935
Fax. +96625571561
Email: meraj@mmirza.com and mnmirza@uqu.edu.sa
Web site: http://www.mmirza.com

Ramze Ahmed Elzahrany
Geography department, Umm Al-Qura University
P.O. Box 715, Makkah 21955, Saudi Arabia
Tel. +966555510613
Fax. +96625534113
Email: raelzahrany@uqu.edu.sa and rzahrany@gmail.com
Web site: http://www.uqu.edu.sa/raelzahrany

Gomaa Mohamed Dawod
Geography department, Umm Al-Qura University
P.O. Box 715, Makkah 21955, Saudi Arabia
Tel. +966551402093
Fax. +96625534113
Email: dawod_gomaa@yahoo.com and gmmahmoud@uqu.edu.sa
Web site: http://www.uqu.edu.sa/gmmahmoud

Projected impacts of land use and road network changes on increasing flood hazards using a 4D GIS: A case study in Makkah metropolitan area, Saudi Arabia

Gomaa M. Dawod, Meraj N. Mirza, Khaled A. Al-Ghamdi & Ramze A. Elzahrany

Arabian Journal of Geosciences

ISSN 1866-7511
Volume 7
Number 3

Arab J Geosci (2014) 7:1139-1156
DOI 10.1007/s12517-013-0876-7

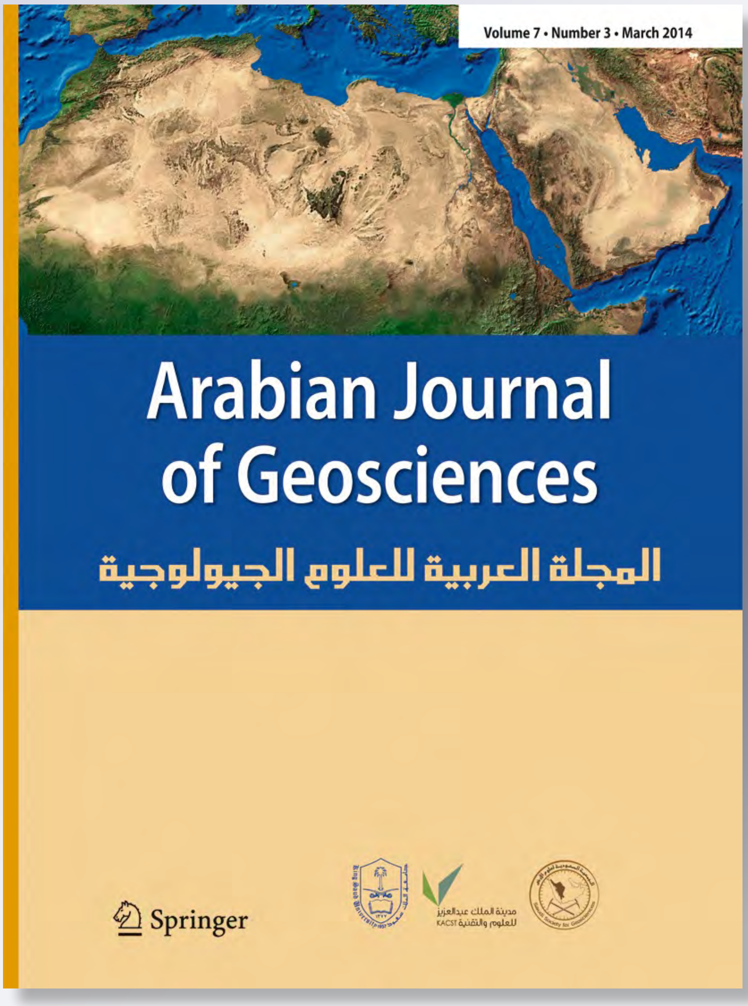

Springer

Arab J Geosci (2014) 7:1139–1156
DOI 10.1007/s12517-013-0876-7

ORIGINAL PAPER

Projected impacts of land use and road network changes on increasing flood hazards using a 4D GIS: A case study in Makkah metropolitan area, Saudi Arabia

Gomaa M. Dawod · Meraj N. Mirza · Khaled A. Al-Ghamdi · Ramze A. Elzahrany

Received: 28 November 2012 / Accepted: 25 January 2013 / Published online: 14 February 2013
© Saudi Society for Geosciences 2013

Abstract Makkah City, west of the Kingdom of Saudi Arabia, is considered the third main highly populated metropolitan area in the Kingdom of Saudi Arabia. It exhibits two unique features that increase the hazardous flood consequences: (1) its topography is very complex and (2) about three million Muslims are gathered annually in Makkah to perform Hajj over a 2-week period. Floods are natural returning hydrological phenomena that have been affecting human lives. The objectives of the current study are: (1) identification of land use types and road networks in Makkah, (2) hydrological modeling of flood characteristics in Makkah based on precise up-to-date databases, (3) examination of the relationship between land use, land cover changes, transportation network expansion, and the floods' prosperities and hazards, and (4) development of digital hydrological maps for present and near future flood hazards in Makkah. The attained results show that the mean runoff depth and the total flood volume are significantly increased from 2010 to 2030. Additionally, it has been found that a great part of the road network in Makkah City is subjected to high dangerous flood impacts. The overall length of flood danger-factor roads is increased from 481 km (with almost 37 %) to 1,398 km (with 74 % approximately) between 2010 and 2030. Thus, it is concluded that urbanization has a direct strong relationship with flood hazards. Consequently, it is recommended that the attained results should be taken into account by decision makers in implementing new development planning of the Makkah metropolitan area.

Keywords Flood management · Road networks · Urbanization · GIS · Makkah

G. M. Dawod (✉) · M. N. Mirza · K. A. Al-Ghamdi · R. A. Elzahrany
Technology Innovation Center on Geographic Information Systems, Umm Al-Qura University, Makkah, Saudi Arabia
e-mail: dawod_gomaa@yahoo.com

Introduction

Flash floods occur periodically in Makkah City, Saudi Arabia, due to several factors including its rugged topography and geological structures. Hazards of flash floods are vital in terms of human lives lost and economical damages. Hence, precise assessment of floods becomes a more vital demand in development planning (e.g., Subyani et al. 2010; Fred and Mostafa 2008). A Geographic Information System (GIS)-based methodology has been already developed to quantify and spatially map the flood characteristics (Dawod et al. 2011a). Utilization of a precise Digital Elevation Model (DEM) enables precise flood modeling in Makkah (Mirza et al. 2011a, b, c). Simple rainfall-runoff models (e.g., Snyder and regression models) did not take into account important parameters particularly the land use and land cover of the catchment area. Land use plays a central role in flood runoff and, consequently, in flood hazardous impacts. Generally, flood runoff reacts differently with respect to land covers and road network locations. Global and national flood modeling methodologies implicitly take into account the types of land use in the catchment area. One of the most popular flood model is the US National Resources Conservation Services (NRCS) curve number (CN), which has been applied globally for flood modeling (e.g., Chen et al. 2010; Mojaddadi et al. 2009).

The relationship between land use changes, road network expansion, and the increase of flood hazards has been investigated by a number of researchers. This issue may not have acquired the necessary awareness in Saudi Arabia although it is considered a major subject in hydrological and environmental planning, and many governmental organizations, in several countries, have focused on that dilemma. For example, research studies and practical projects have been carried out in: the USA (e.g., Wang et al. 2010; Sheng and Wilson 2009), France (e.g., Paquier 2010), and New Zeeland (e.g., Hansford 2010). Consequently, land use and road networks are

key factors affecting flood runoff volume and path (e.g., Sherief 2008).

Regarding the influences of land cover changes on flood peak discharge, Olang and Furst (2011) have studied the impacts of historical land cover changes witnessed between 1973 and 2000 on the hydrologic response of the Nyando river basin in Kenya. Physically based parameters of the models were estimated from the land cover change maps together with a digital elevation model and soil datasets of the basin. Results revealed significant and varying increases in the runoff peak discharges and volumes within the basin. A similar study has investigated the land use/flood dilemma in India, but from a different perspective (Kar et al. 2009). That research aimed to study the morphometric and hydrological properties of a watershed and tried to get benefits of those properties in enhancing land use sustainable planning. Other investigations have focused on the assessment of land uses and also population distribution on hydrological section properties. An approach was developed to quantify the landscape alterations resulting from human disturbances (e.g., urbanization, agriculture, roads, and population) on lake conditions in Michigan state, USA (Wang et al. 2010). More recently, the relationship between urbanization and flood hazards has been investigated extensively utilizing geomatics technologies particularly the GIS. Amini et al. (2011) concluded that land cover deterioration has increased the flood peak by up to 26.7 % in the Damansara watersheds, Malaysia. Similar results reveal that increasing development (in Los Angeles, CA, USA) increases total annual runoff and decreases groundwater recharge during both dry and wet seasons (He and Hogue 2011). Also, a special flood warning system is proposed for road networks in particular (e.g., Versini et al. 2010).

Based on results of related investigations worldwide, it can be concluded that inspecting the impacts of land use changes and road network expansion on flood hazards in Makkah metropolitan area becomes an obligation. It is worth mentioning that the metropolitan extent of Makkah City has been increased from 4,800 ha in 1983 to 9,457 ha in 2004 (Mirza 2009). Also, new circular highways and metro lines are planned in Makkah. Hence, the growing urbanization rate in Makkah nowadays emphasizes the necessity for conducting a scientific project, utilizing recent technical tools and models, to quantify the expected flood hazard increase in the present and near future, particularly in the holy shrines. This study will be the first of its kind to be carried out not just in Makkah City, but in the entire Saudi Arabia.

Study area

Makkah City is located in the southwest part of the Kingdom of Saudi Arabia, about 80 km east of the Red Sea (Fig. 1). The current area of the metropolitan region (the study area) extends about 37 km in the north and 43 km in the east; thus, it equals approximately 1,600 km^2. It extends from longitudes 39°35′E to 40°0′E, and from latitudes 21°15′N to 21°35′N. Makkah City is a unique city for Muslims all over the world, since it contains the holy mosque. From a religious point of view, a Muslim should perform pilgrimage (called Hajj, which means visiting Makkah in specific days in the year) once in his/her life. Thus, hundreds of thousands of Muslims are gathered in Makkah yearly. Moreover, the topography of Makkah is complex in nature, and several mountainous areas exist inside its metropolitan area. That is also a vital element in investigating the spatial pattern of Makkah sprawl.

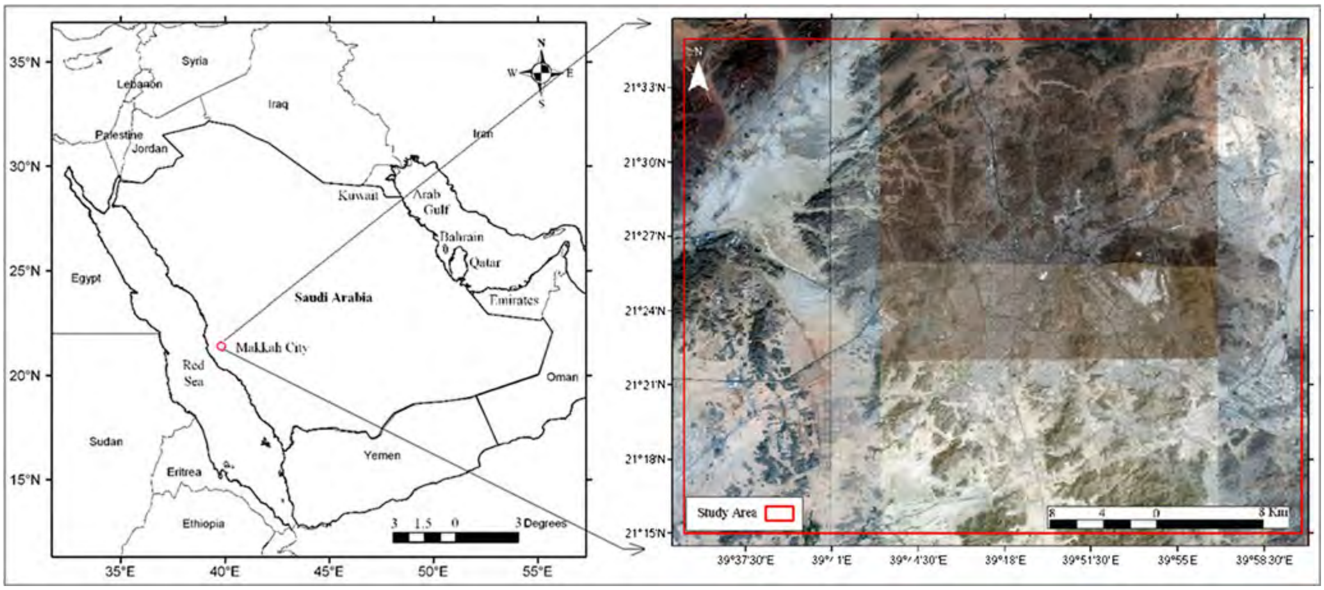

Fig. 1 Makkah City

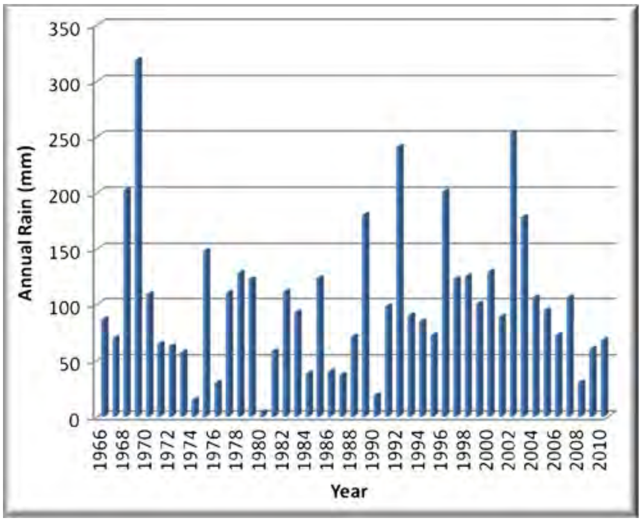

Fig. 2 Annual rains in Makkah City from 1966 to 2010

Makkah's hydrology

It is worth mentioning that the southwest part of the Kingdom of Saudi Arabia contains almost 60 % of the volume of wadi flow, particularly in the terrain situated between the Red Sea coast and the adjacent mountains. The annual rain over Makkah City, for a period extending from 1966 to 2010, varies from 3.8 to 318.5 mm, with the average rainfall equal to 102.6 mm (Fig. 2). Due to the complexity of Makkah's topography, flash floods occur periodically with significant variations in magnitude. Mirza and Ahmed (2001) have reported that the extreme flood type is repeated with a return period of 46 years, while a second-order flood takes place occasionally with a return period of 33 years, and a low-dangerous flood comes about every 13 years.

Makkah's topography

The topography of the Makkah metropolitan area is complex, where several mountainous regions exist within the urban boundaries of the city. Terrain heights in Makkah (Fig. 3) range from 82 to 982 m above sea level (Mirza et al. 2011a, b, c). The highest mountains in Makkah City are: Al-Tarki (987 m), Ahdaab (919 m), Thabeer (814 m), Thour (719 m), and Al-Noor mountain (620 m). Dividing Makkah's heights in groups (Table 1), it can be realized that 81.8 % of the heights are less than 400 m. In the second group, heights range from 400 to 600 m and occupy 17 % of Makkah's area, while 1.1 % has heights ranging from 600 to 800 m. The highest area, with values greater than 800 m, only occupies 0.1 % of Makkah City. Distributions of the topography slopes in Makkah City are also depicted in Fig. 4 and tabulated in Table 2. It can be noticed that about 80 % of Makkah territories have smart slopes of less than 10°, while 0.9 % of the study area represents hilly regions of slopes greater than 30°.

It is known that the growth in Makkah City spreads out along the valleys and stays away from the mountainous areas for economical reasons. It is worth mentioning that almost 50 % of Makkah's geology contains igneous rocks, mainly granite, that massively increase the development costs in mountainous areas.

Fig. 3 Topography of Makkah City

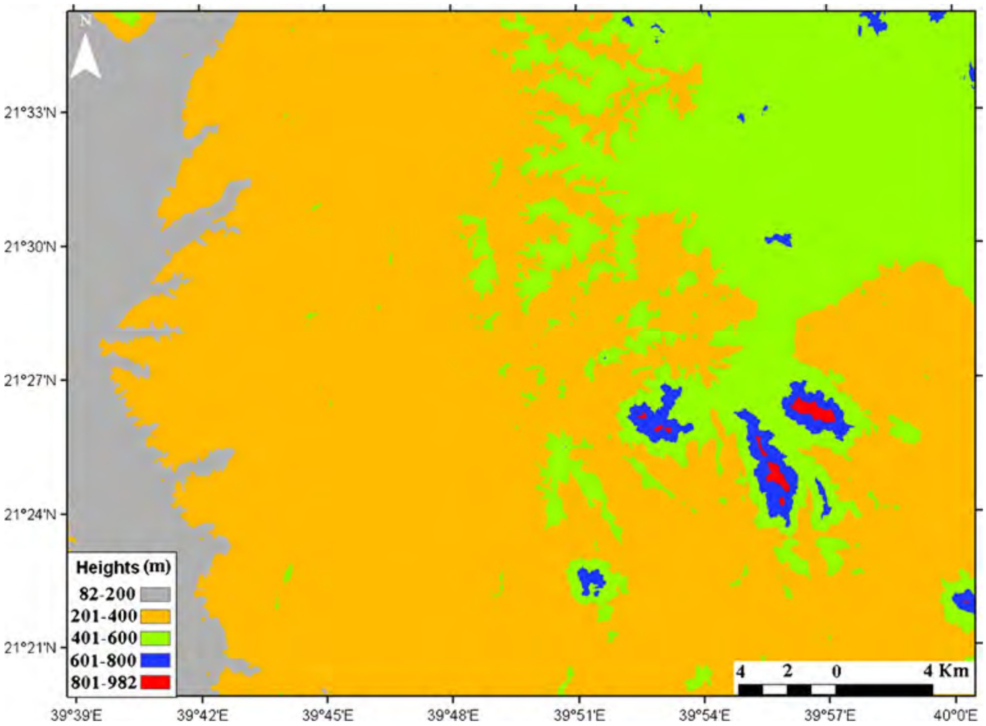

Table 1 Makkah height categories

Heights in meters (above mean sea level)	Area (%)
Less than 400 m	81.8
From 400 to 600 m	17.0
From 600 to 800 m	1.1
Greater than 800 m	0.1

Table 2 Makkah slope categories

Slope (°)	Area (%)
Less than 10°	79.7
From 10 to 20°	15.7
From 20 to 30°	3.7
Greater than 30°	0.9

Makkah's geology

The geology of Makkah metropolitan area consists mainly of three geological structures (Fig. 5 and Table 3). The Precambrian igneous rocks occupy about 809 km^2 (with 51 % approximately of the total area). Those rocks implicitly imply a low-permeability property that increases the ability of rainfall to be converted into dangerous surface runoff. The deposits, or wadi alluvium, exist mainly along the wadi streams and constitute about 48 %, with an area equal to 770 km^2 approximately. The rest of Makkah area, about 12 km^2 only, represents the tripartite rocks.

Available data

The collected databases consist of several data sets of different types, sources, and dates. They include:

- The spatial urban compiled datasets constituting two categories:
  - The first element consists of 105 cadastral maps in AutoCAD files for 1990.
  - The second constituent consists of a land use map developed by the Saudi Geological Survey Authority dated 2010.
  - The third category contains detailed cadastral maps that describe the future Makkah land use and road network in 1,450 H (HAMDD 2004).
- A national 5-m-resolution DEM for the study area has been obtained from the King Abdulaziz City of Sciences and Technology.
- A set of 1:50,000 topographic maps, produced by the Military Survey Department, Ministry of Defense and Aviation.
- A set of 1:50,000 geological maps, produced by the Saudi Geological Survey Authority.
- A set of Ikonos and Quick-Bird high-resolution satellite images.
- A hydrological database obtained from Institute of Hajj and Omrah, Umm Al-Qura University.

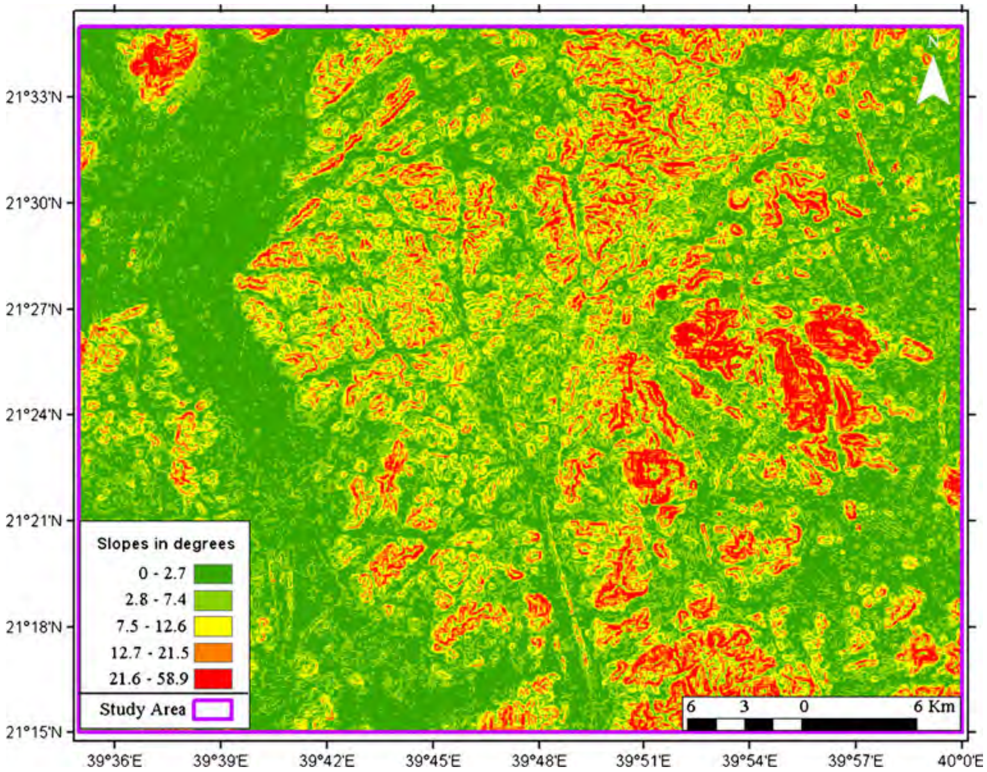

Fig. 4 Terrain slopes of Makkah City

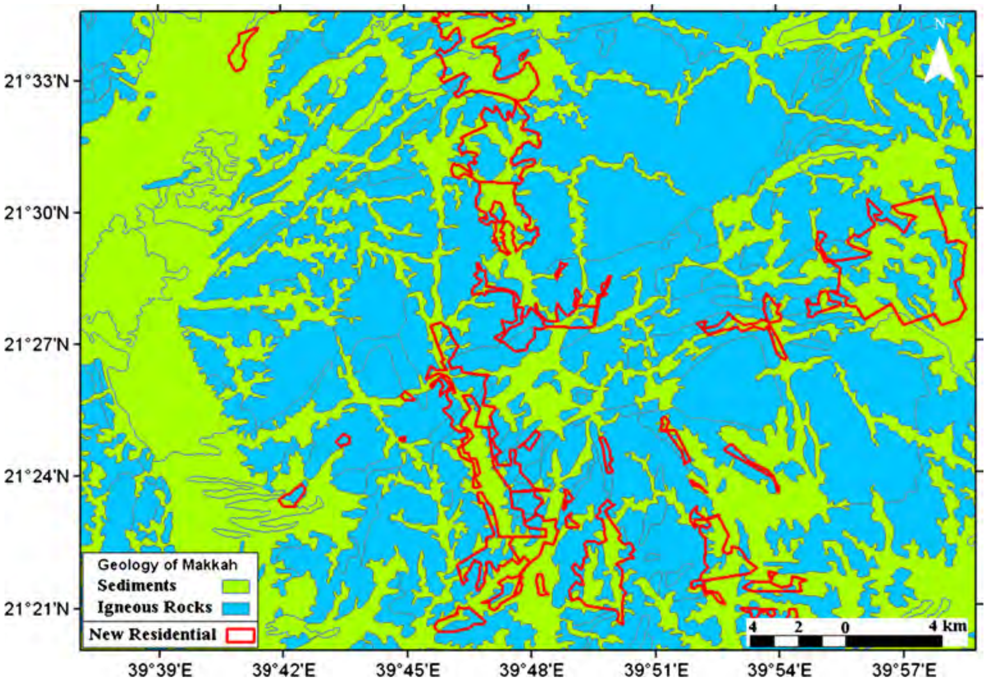

Fig. 5 Geology of Makkah City

Methodology and data processing

Accurate estimation of flood characteristics in Makkah metropolitan area is a vital demand in planning and resources management. The different collected datasets have been manipulated and stored in a digital form after unifying their geographic datums and coordinate systems. In order to extract the hydrological catchments in Makkah City, a morphometric analysis has been performed and utilized as an input step for flood estimation. Then, a unique GIS system has been built for quantifying and spatial mapping of flood hazards in Makkah in past, present, and future scenarios. Impacts of urban growth and flood hazard increase on the road networks in Makkah have been determined. The following sections describe, in detail, the utilized methodology and the procedures applied in data processing.

Building a unique 4D GIS

The developed GIS-based flood assessment methodology consists of several stages. The Arc GIS software (v. 10), along with the Arc Hydro extension, has been used in the present study to combine all obtainable data in a unique environment. The processing phase includes (Fig. 6): rectifying the printed maps, digitizing two shapefiles for residential areas and roads for each dataset, converting AutoCAD files to GIS shapefiles, unifying the spatial reference frames for all datasets, performing statistical and spatial analyses, and flood computations (Al-Ghamdi et al. 2012b). The Arc GIS software has been used to obtain several shapefiles describing the geomorphology of the study area. These shapefiles include: the main basins and the sub-basins of each main catchment, along with drainage network using the Strahler method (a simple widely utilized network order method), and the longest stream path in each catchment. The second stage of the developed methodology is based on the flood assessment method developed by the NRCS, formerly known as the Soil Conservation Service. Processing steps, and hence attained results, have been performed for past (1990), present (2010), and future (2030) scenarios.

Table 3 Makkah geological categories

Geological structure	Area (km^2)	Area (%)
Precambrian igneous rocks	809	50.8
Wadi alluvium	770	48.4
Tripartite rocks	12	0.8

Urban growth data processing

Shapefiles of residential areas, within Makkah City, for 1990, 2010, and 2030 have been developed and integrated in a GIS project. Surface areas have been computed and compared for the three dates, and growth rates have been obtained. Spatial statistics tools, in the Arc Tool Box component of the Arc GIS software, have been performed in order to investigate the spatial pattern of Makkah sprawl. Applying GIS spatial analysis tools produces more valuable pieces of information. Measuring the compactness of a distribution provides a single value representing the dispersion of features around the center (Al-Ghamdi et al. 2012a). The available national 5-m-resolution DEM describes the rigid topography of Makkah metropolitan area. Several mountainous areas exist within Makkah City and affect the spatial urban growth location and direction. Thus, the residential areas' layers have been compared against the DEM layer

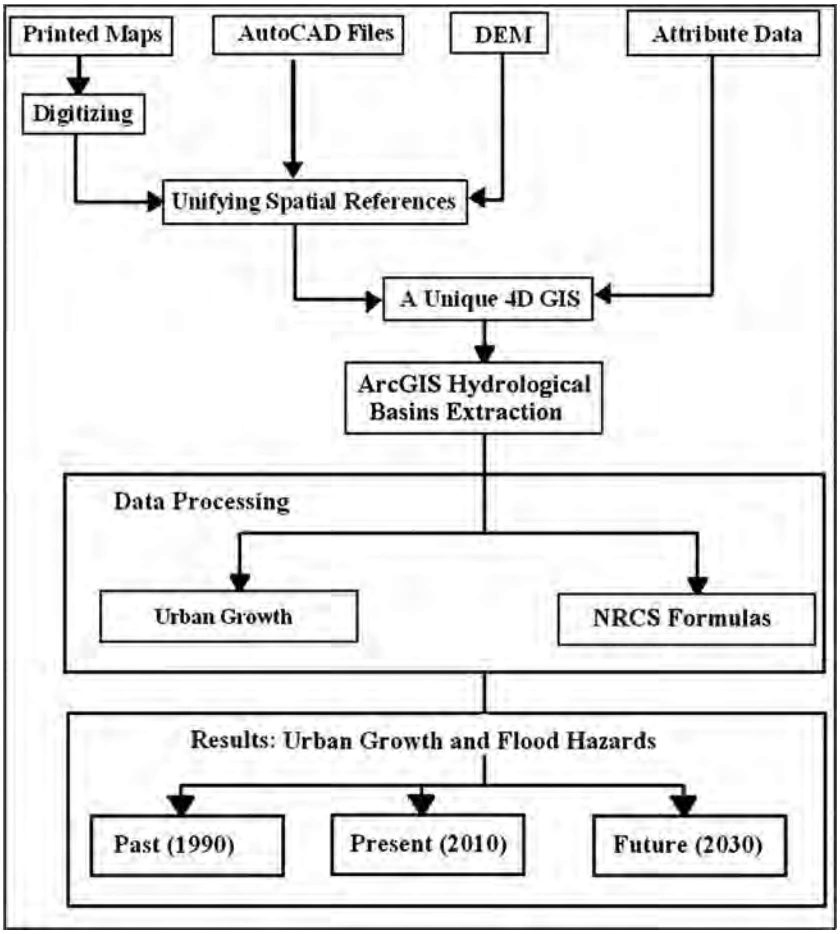

Fig. 6 The developed GIS-based flood assessment approach

in order to investigate the topography–urban development relationship. Additionally, residential areas' layers have been compared against the road network's layer in order to determine the relationship between urban growth and roads in the three scenarios under investigation. A similar task has been carried out, also, to define the relationship between urban expansion and the geology structures of the study area.

Flood data processing

First, analyzing the flood series frequency, the return period or recurrence interval can be computed. That period defines the average number of years during which a flood of a given magnitude will be equalled or exceeded once. The Welbull method, among several other formulas, computes the return period T as (Raghunath 2006):

$$T = (n + 1)/m \quad (1)$$

where n is the number of events or number of records, and m is the order or rank of the event (flood item) when flood magnitudes are ranked in descending order.

The computed return period of the 1969 flood has been estimated to be 45 years. That piece of information is quite helpful in flood assessment studies, as it means that: (a) flood magnitude is expected to occur by about 2014, and (b) the selected return period value for flood management projects should be equal or greater than 44 years. The rainfall intensity for a 50-year return period has been estimated, through the log Pearson II statistical method, as 200 mm/h.

The CN has been determined for each sub-basin in each scenario (1990, 2010, and 2030) based on the available soil and geological digital databases of Makkah metropolitan area. Dawod et al. (2011b) has performed a comparison study of several flood estimation techniques and concluded that the CN is the optimum one. Then, flood characteristics have been computed through Eq. 2, using VBA in the GIS environment. Additionally, the total flood volume of a basin is computed as:

$$QT = QA \quad (2)$$

where Q is the depth of direct runoff (in millimeter), QT is the volume of runoff (in cubic millimeter), and A is the area of the basin (in square kilometer).

Road network data processing

Regarding flood impacts on roads, some researchers have investigated this aspect in several countries. Blanton and

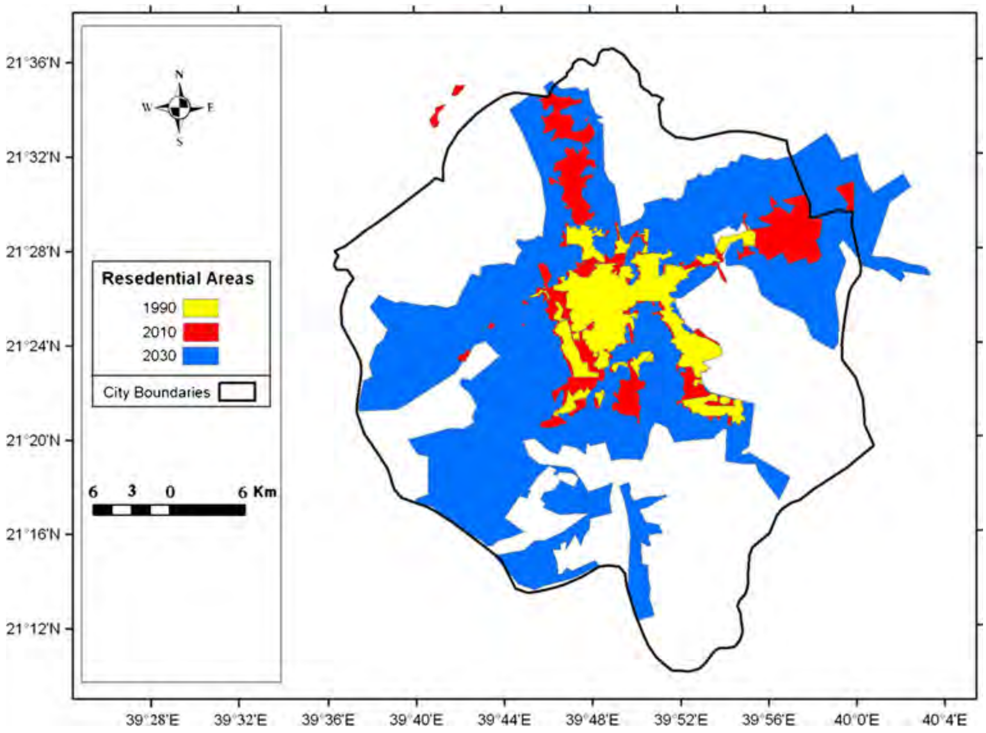

Fig. 7 Urban growth of Makkah City between 1990 and 2030

Marcus (2009) have documented the geographic distribution of roads and railroads in the alluvial floodplains of the continental USA and the regional variability of their potential impacts on lateral connectivity and resultant channel and floodplain structure and function. Youssef et al. (2010) have presented the utilization of remote sensing data, Shuttle Radar Topography Mission, coupled with geological, geomorphological, and field data in a GIS environment for the estimation of the flash flood risk along the Feiran–Katherine road, southern Sinai, Egypt. However, those two studies are based on flood hazard estimation by analyzing morphometric characteristics of basins in which roads exist. That means that the flash floods themselves have not been estimated. In the current paper, a GIS has been developed to quantify flood characteristics in Makkah City and then estimate dangerous impacts on the road network.

Next, an estimation has been developed to quantify flood impacts on roads. It is implicitly based on an idea that the higher the runoff depth in a sub-basin, the more hazards on roads within that sub-basin. Since the flood computations have been performed on a sub-basin level, the runoff depth of each sub-basin may be considered as the most effectual factor that affects the flood impact. Hence, the spatial analysis tools of the Arc GIS software are utilized to re-classify runoff depths in ten categories, and each category is assigned a unique number. That number, called the hazard, or danger, factor, will be assigned to the road existing in a particular sub-basin. By this approach, each road in the transportation network gets a unique hazard factor (in each scenario) that represents the flood hazard level.

Results and discussion

Several datasets have been compiled, processed, and analyzed in the current research study dealing with urban growth and flood hazard increase in Makkah City. The attained results can be divided in three main groups: (1) results of urbanization, (2) results of flood hazards, and (3) results of flood impacts on the road network. The results are presented in the next sections according to this classification.

Results of urban growth

For the first results' category, shapefiles of Makkah metropolitan area for 1990, 2010, and 2030 have been integrated in a GIS project (Fig. 7). Table 4 shows that the total residential area has been computed and found to be 80.012, 158.583, and 690.007 km^2 for 1990, 2010, and 2030, respectively. Thus, the residential areas in Makkah City have grown by about 98 % from 1990 to 2010 (with 4.9 % annual rate) and are expected to have grown by about 335 % from 2010 to 2030.

Table 4 Urban growth of Makkah City between 1990 and 2030

Year	Area (km^2)	Difference (km^2)	Difference (%)	Annual growth (%)
1990	80.012			
2010	158.583	78.571	98	4.9
2030	690.007	531.424	335	16.8

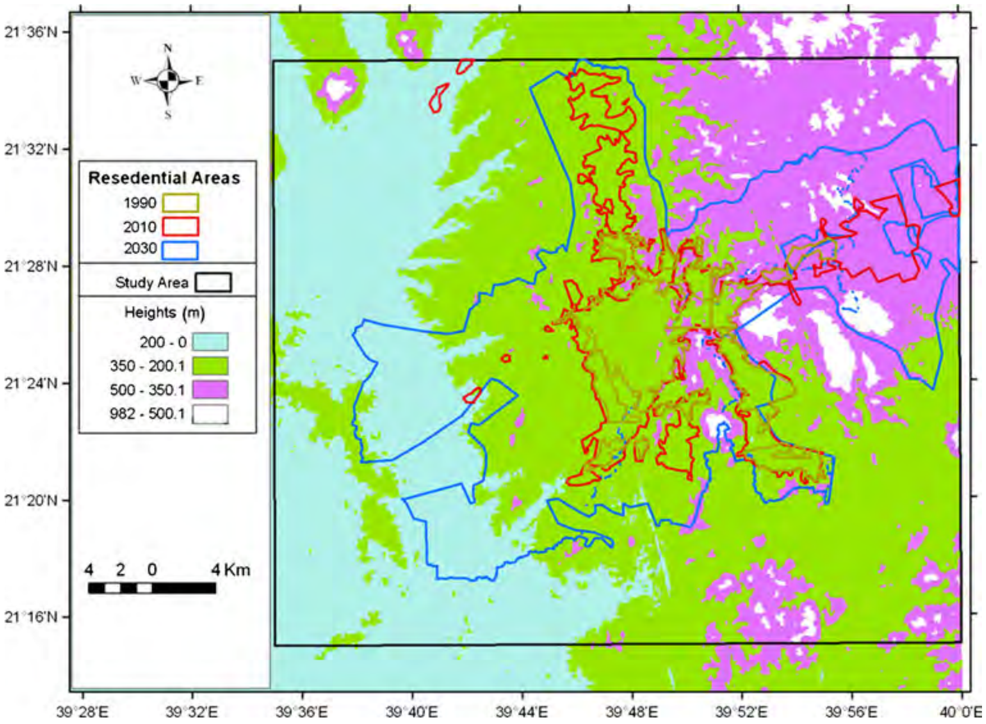

Fig. 8 Topography of residential areas in Makkah City

It can be realized from Fig. 7 that the urban growth in Makkah City takes a radial (or spoke) pattern. That is logically understood knowing that the holy mosque is considered the center of the city, and the central area around it

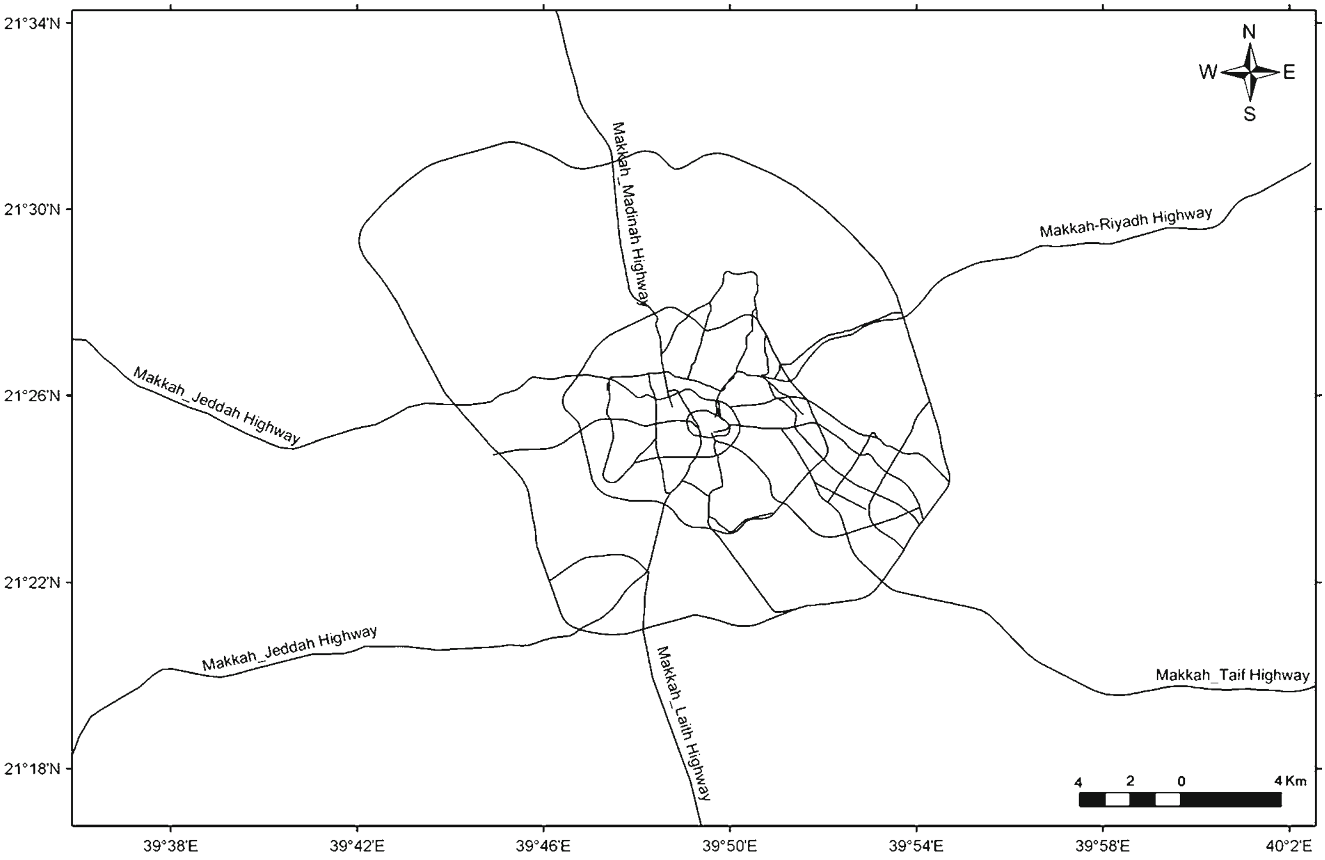

Fig. 9 Main roads in Makkah City

has the highest population density since residents and pilgrims prefer to stay close to this holy mosque.

The available national 5-m-resolution DEM describes the rigid topography of Makkah metropolitan area. Several mountainous areas exist within Makkah City and affect the spatial urban growth location and direction. Figure 8 depicts the topography of Makkah as divided into four categories. It can be seen that the urban sprawl mainly exists in low- and moderate-elevation regions. The growth spreads out along the valleys and stays away from the mountainous areas for economical reasons. It is worth mentioning that almost 50 % of Makkah's geology contains igneous rocks, mainly granite, that massively increase the development costs in mountainous areas.

Concerning the road network, it is worth mentioning that Makkah has six regional highways that connect it to a major Saudi city (Fig. 9). These roads are: Makkah–Madinah road (427 km), Makkah–Riyadh road (880 km), Makkah–Taif road (88 km), Makkah–Laith road (180 km), and two Makkah–Jeddah roads (78 km). Inspecting both Figs. 7 and 9, it can be concluded that the urban sprawl of Makkah City follows those regional roads. In the first phase (1990–210), urban development has been intensive mostly along Makkah–Riyadh and Makkah–Madinah roads. That growth leads to the creation of new districts in Makkah City, such as: Sharee'h, Sharee'h Al Mojahdeen, Al Rashdia, and Al-Khadraa at the northeast corner, and Omraa, Nowaria, and Al Bohayrat at the north corner of Makkah (Fig. 10). That conclusion consents with the values of the rotation angles of the standard deviational ellipses as argued earlier.

Results of flood hazard increase

The second results' group concerns the estimation of flood hazards in Makkah City. Six main hydrological basins have been identified in the study area, with areas ranging from 74.3 to 360.6 km^2 and lengths of their main streams varying from 16.50 to 48.55 km (Fig. 11). Table 5 presents the statistics of hydrological parameters of these basins (Koshak and Dawod 2011). Sixty sub-basins have been recognized within these six basins (Fig. 12). The NRCS method has been performed for the available data of Makkah metropolitan area to compute the peak discharge value for the six basins for the 1990, 2010, and

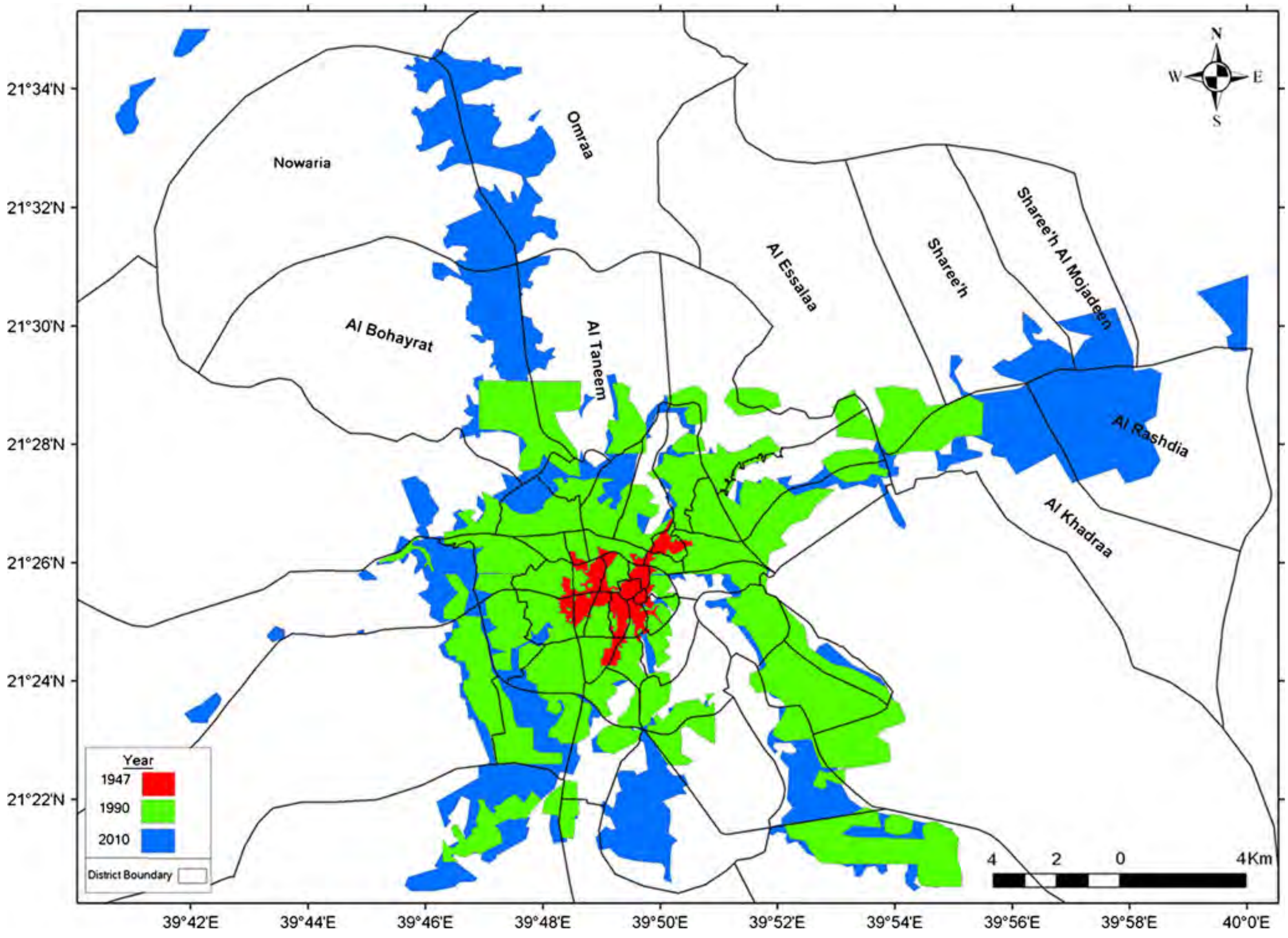

Fig. 10 New districts within Makkah City

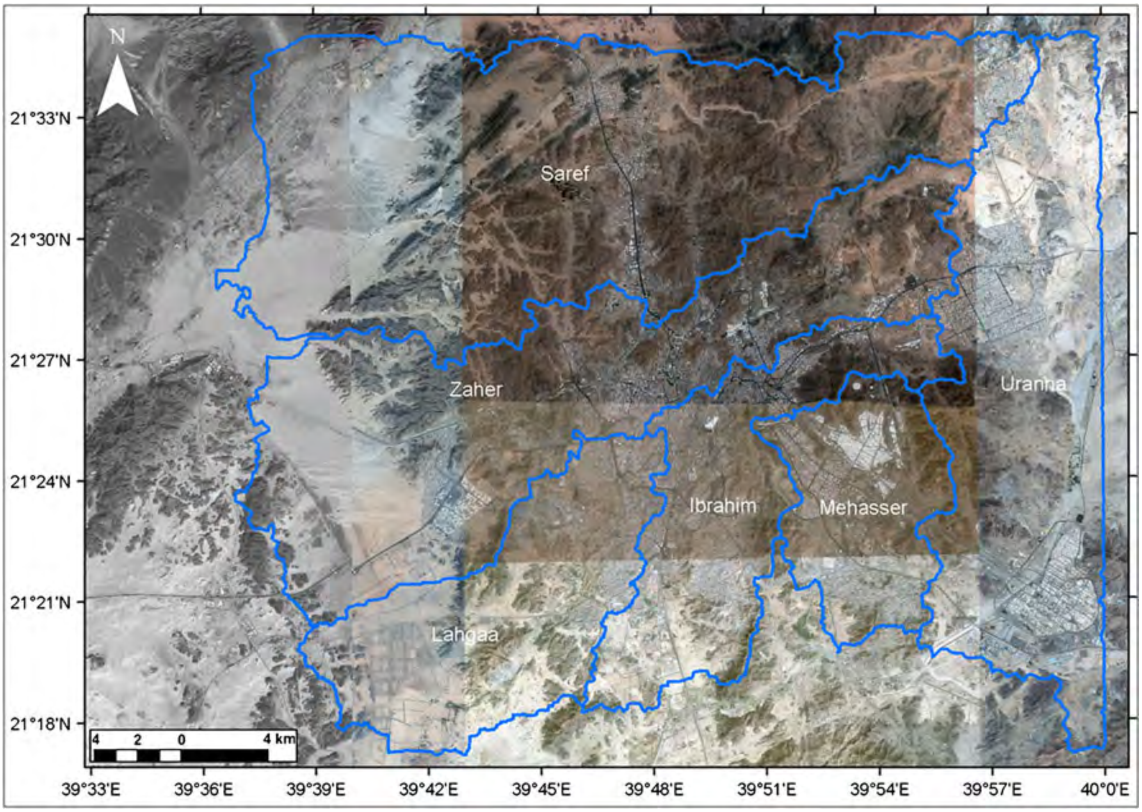

Fig. 11 The main basins in the Makkah metropolitan area

2030 datasets. The return period has been chosen, herein, as 50 years, for which the rainfall intensity has been estimated, by applying the log Pearson III statistical analysis, as 200 mm/h. The total flood volumes have been computed on the sub-basin scale, only for those sub-basins which contain residential areas. A total of 76 sub-basins, which include residential areas in 1990, have been identified within the study area. These sub-basins extended over an area of 194.726 km^2, which constitutes 17.5 % of the total area of the main hydrological basins in the study area. In 2010, the urban areas have been extended to cover 136 sub-basins, whose total areas equal 400.551 km^2. In 2030, it is expected that the urban extent of Makkah City will cover 264 sub-basins with an overall area of 780.388 km^2.

Regarding the runoff depth over the urban sub-basins, it has been found that its mean value has been increased from 165.3 mm in 1990 to 185.7 mm in 2030 (Figs. 13, 14, and 15). However, the most dangerous flood impact is the total flood volume (Figs. 16, 17, and 18). It has been found that the total flood volume (for urban sub-basins) equals 31.6, 64.6, and 141.9 million m^3 for 1990, 2010, and 2030, respectively. Hence, it is concluded that the augmentation of the total flood volume has been increased by almost 104 % from 1990 to 2010, and by almost 120 % from 2010 to 2030.

Table 5 Statistics of floods over residential areas in 1990 and 2010

Item	1990	2010	2030
Number of sub-basins containing residential areas	76	136	264
Total area of sub-basins of residential areas (km^2)	194.725	400.551	780.388
Percentage of these sub-basins' area to main basins' area	17.5 %	36.0 %	70.2 %
Minimum CN of these sub-basins	76	76	76
Maximum CN of these sub-basins	98	98	98
Mean CN of these sub-basins	88.5	88.5	95.3
Minimum runoff depth of these sub-basins (mm)	122.3	128.1	128.1
Maximum runoff depth of these sub-basins (mm)	193.9	193.9	193.9
Mean runoff depth of these sub-basins (mm)	165.3	165.3	185.7
Total flood volumes in these sub-basins (million m^3)	31.632	64.620	141.945

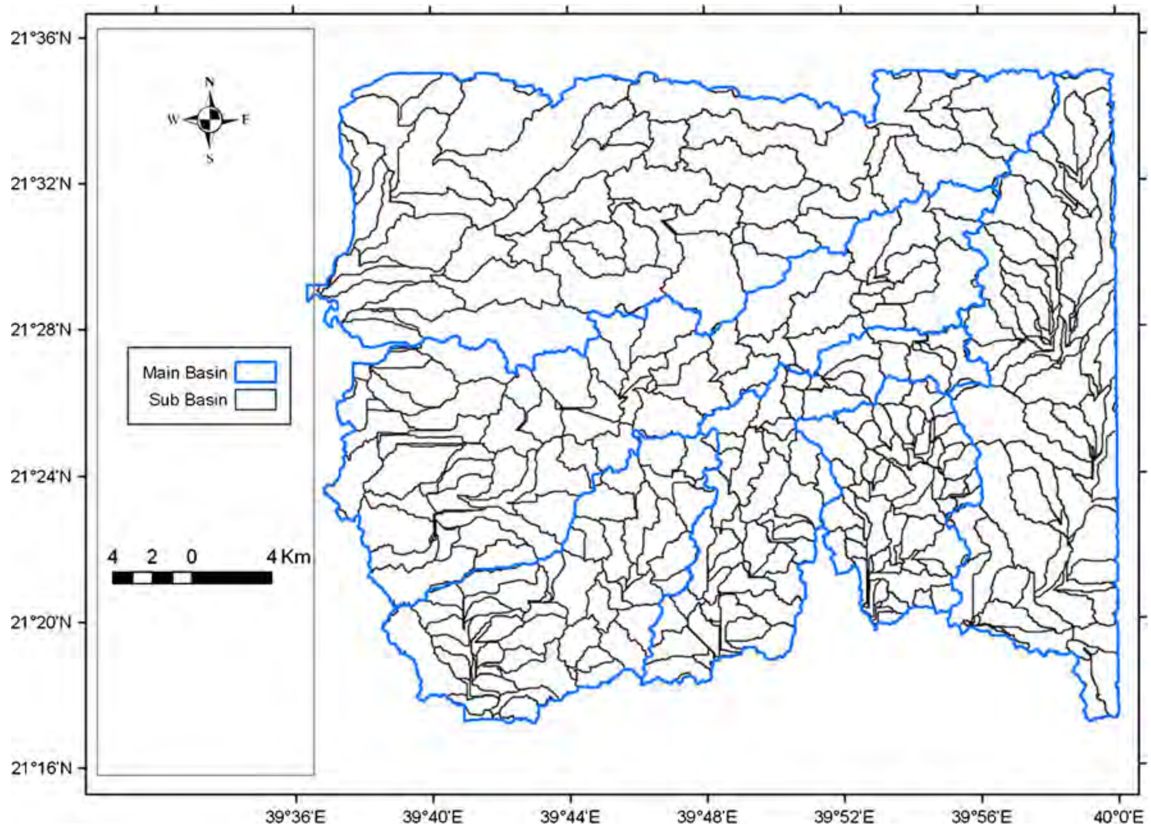

Fig. 12 The sub-basins in the Makkah metropolitan area

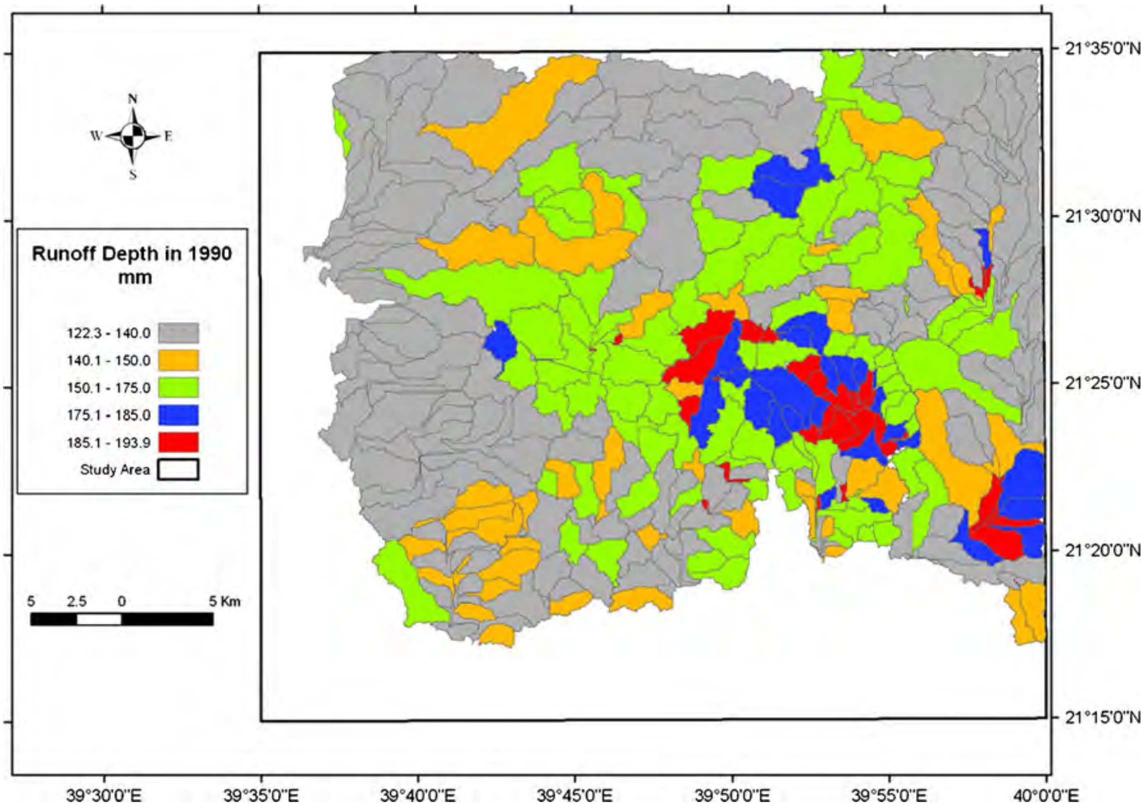

Fig. 13 Runoff depth in 1990

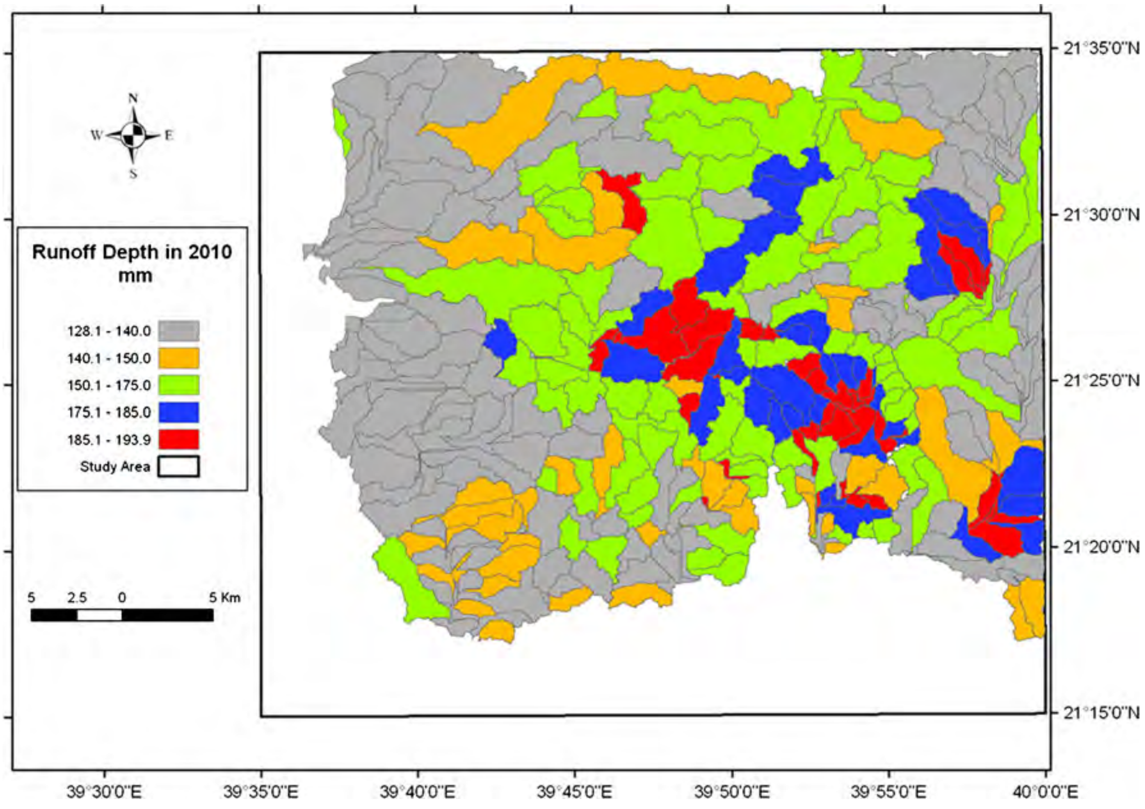

Fig. 14 Runoff depth in 2010

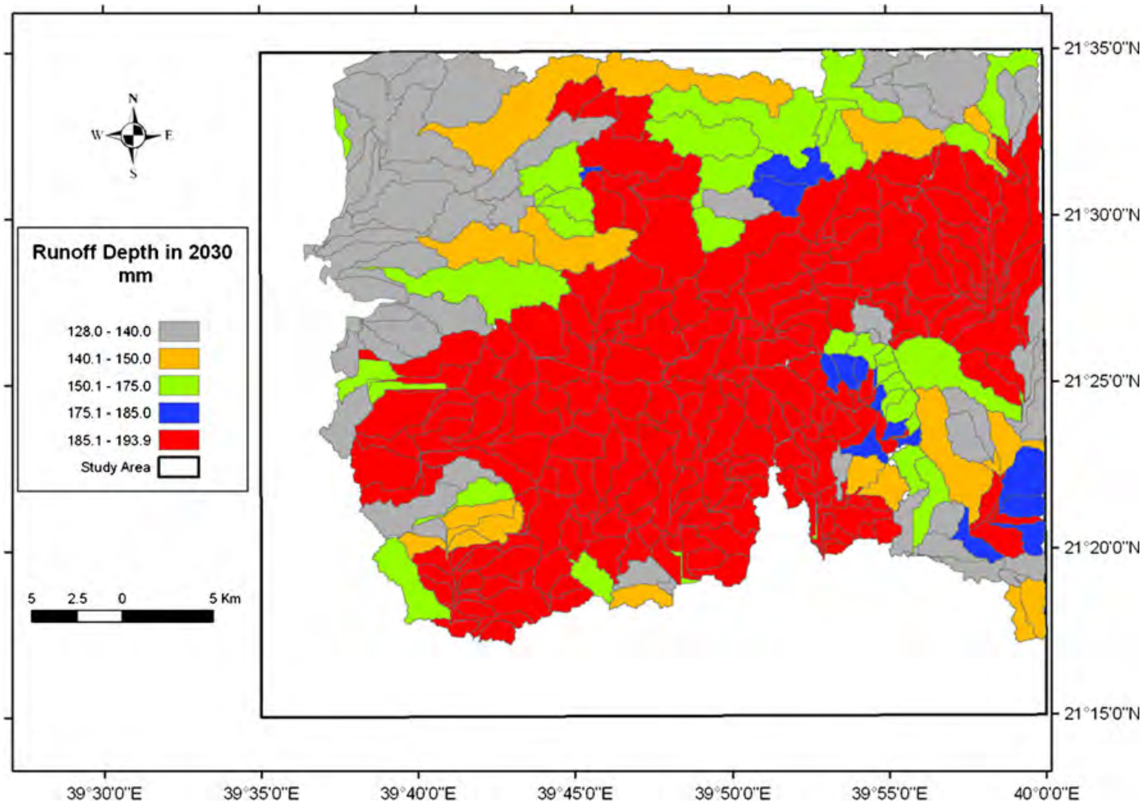

Fig. 15 Runoff depth in 2030

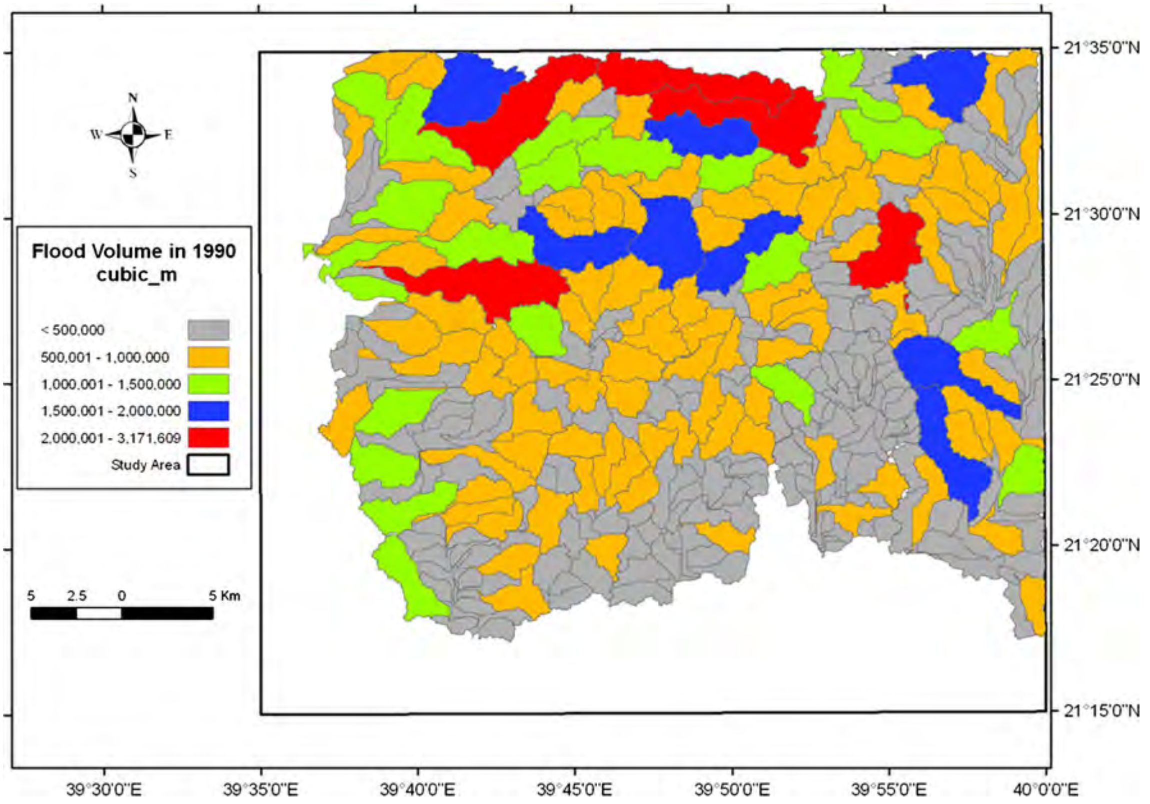

Fig. 16 Flood volume in 1990

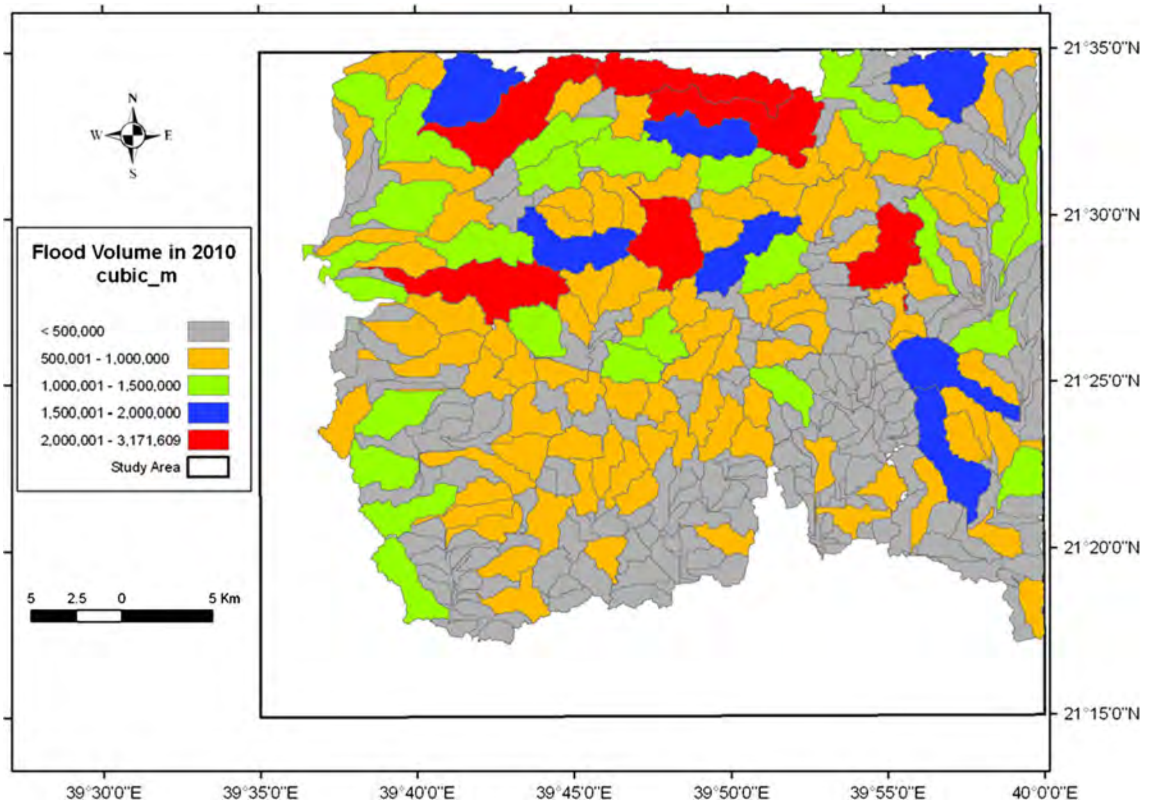

Fig. 17 Flood volume in 2010

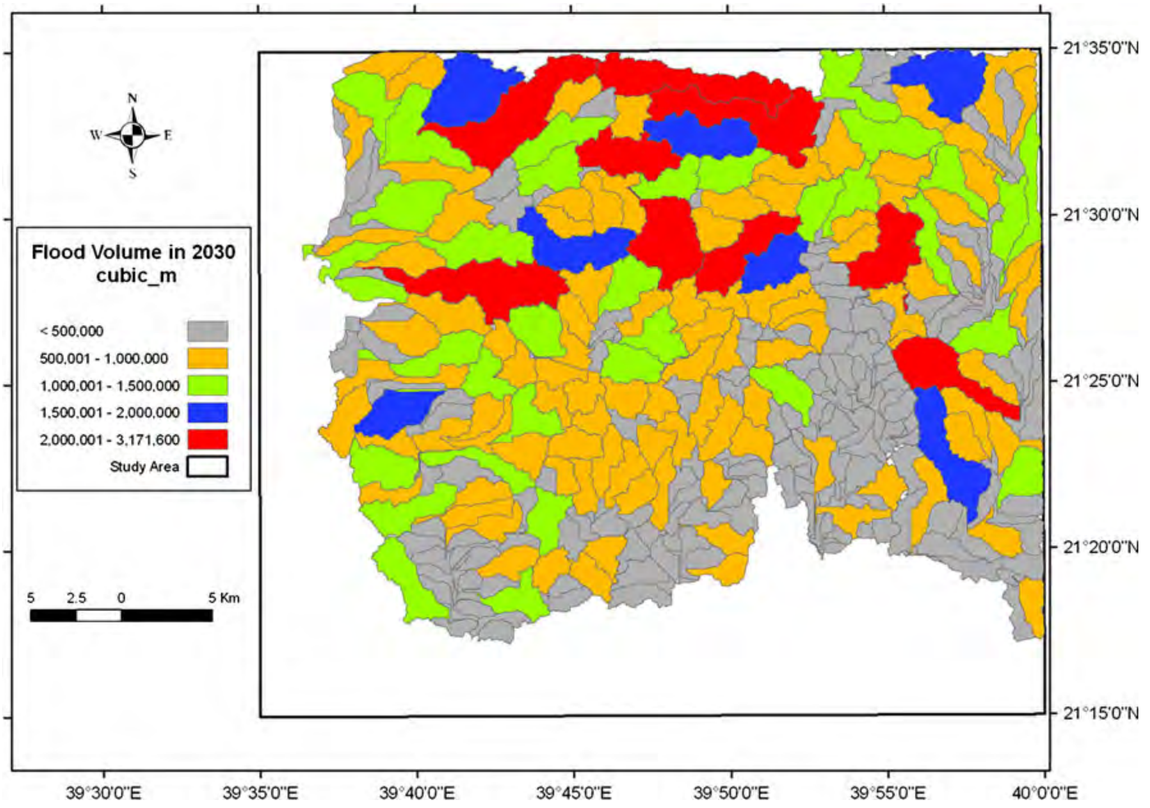

Fig. 18 Flood volume in 2030

Results of flood impacts on road network

Regarding the flood impacts on roads, two shapefiles have been constructed containing the road network of Makkah City in 2010 and 2030. It was decided to work with main roads only, whose lengths are greater than 1,000 m, just for simplicity in the current research. So, that road network, in 2010, consists of 566 roads whose lengths range from 1.004 to 20.531 km, with a mean of 2.311 km. The Arc GIS spatial analysis tools have been utilized to: (a) divide the sub-basins' runoff depth into ten groups using the equal-interval classification method; (b) re-classify those flood depth groups to unique label values ranging from 1 to 10, just for simplicity, which will be considered as the hazard factor; (c) convert that shapefile into a raster format; and (d) project that raster onto the road network in order to assign each road with the corresponding unique hazard factor. By this approach, the flood hazard impact on each road is assigned on a scale from 1 to 10 (based on the runoff depth for the corresponding sub-basin), which is a simple scale to be interpreted. This quantitative classification is presented in Table 6 and depicted in Fig. 19. Next, the flood hazards on roads have been classified into three groups, just for simplicity too, as seen in Table 6 and Fig. 20. Obviously, a great part of the road network in Makkah City is subjected to high dangerous flood impacts. That category constitutes 211 roads, representing 37 % of the network, with a total length of 481 km. It is worth noticing that roads of high flood impacts exist in the holy shrines particularly in the Arafat area. That finding is quite important and strongly necessitates the development of a specific surface water drainage network in this area to avoid flood hazards during the Hajj season.

Secondly, the same procedures have been performed on the future road networks of Makkah City in 2030. Again, it was

Table 6 Categories of flood hazard on road network in Makkah City in 2010

Hazard category	Hazard factor	No. of roads	Total length of roads (km)	Percentage of road length
Low	1–4	171	429.242	32.8 %
Medium	5–7	184	397.79	30.4 %
High	8–10	211	481.226	36.8 %

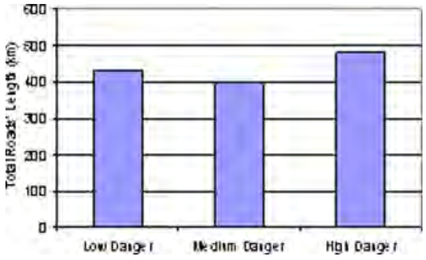

Fig. 19 Flood hazard categories on road network in Makkah City in 2010

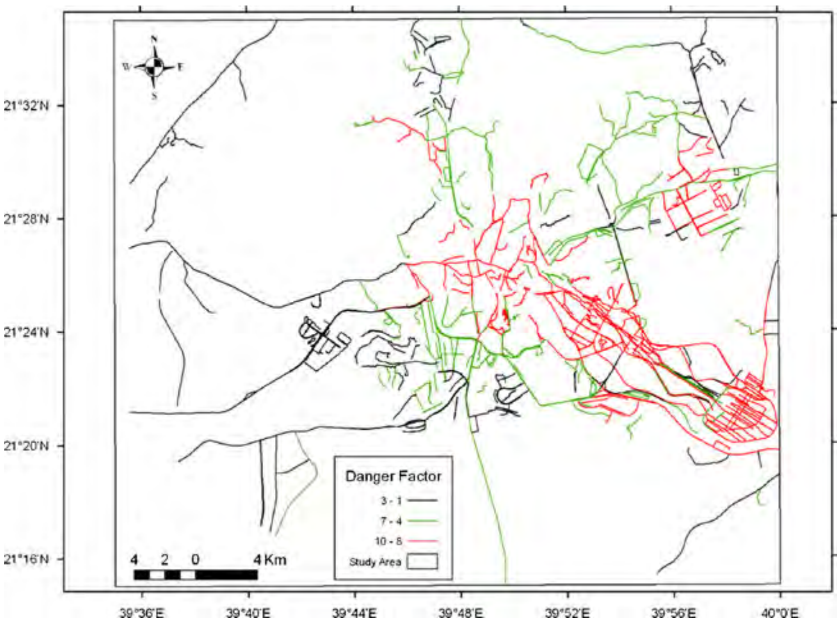

Fig. 20 Flood hazards on road network in Makkah City in 2010

decided to work with main roads only, whose lengths are greater than 1,000 m, just for simplicity in the current research. That road network consists of 705 roads whose lengths range from 1.004 to 23.70 km, with a mean of 2.691 km. The attained quantities of danger factor on roads are presented in Table 7 and depicted in Fig. 21. Additionally, the flood hazards on roads have been classified into three groups, as seen in Table 7 and Fig. 22. It is concluded that a major part of the road network in Makkah City, in 2030, is subjected to high dangerous flood impacts. That category constitutes 563 roads, representing 74 % of the network, with a total length of 1,398 km. Again, it is noticed that roads of high flood impacts exist in the holy shrines particularly in the Arafat area. That finding is quite important and strongly necessitates the development of a specific surface water drainage network in this area to avoid flood hazards during the Hajj season.

Comparing Tables 6 and 7, it can be noticed that there is a significant increase in the flood impacts on Makkah's road networks between 2010 and 2030. The overall length of flood danger-factor roads is increased from 481 km (with almost 37 %) to 1,398 km (with 74 % approximately). The main reason is the huge expected urban development of the city from 2010 to 2030, where the urban boundaries of Makkah will increase from 158 to 690 km^2. As a matter of fact, urbanization has a direct strong relationship with the flood hazards (Fig. 23). Urbanization leads to changing the land use of a region, changes its geological characteristics, and decreases its ability to absorb surface water which, in turn, increases the surface water runoff. Hence, it is concluded that the current surface water drainage network in Makkah City should be re-evaluated, in terms of its capacity and spatial distribution, in order to cope with the expected flood hazards in 2030.

Table 7 Categories of flood hazard on road network in Makkah City in 2030

Hazard category	Hazard factor	No. of roads	Total length of roads (km)	Percentage of road length
Low	1–4	71	271.355	14.3 %
Medium	5–7	69	228.329	12.0 %
High	8–10	563	1,397.964	73.7 %

Conclusions and recommendations

The current research study aims to: (1) identify land use types and road networks in Makkah, through recent high-resolution multi-band satellite images, and prepare corresponding digital maps; (2) perform hydrological modeling of flood characteristics in Makkah based on precise up-to-date metrological, geological, and topographic datasets; (3) build 4D geographic, topographic, geological, metrological, and hydrological digital databases for Makkah; (4) examine the relationship between land use, land cover changes, transportation network expansion, and the floods' prosperities and hazards, and (5)

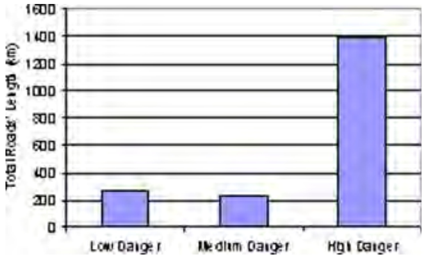

Fig. 21 Flood hazard categories on road network in Makkah City in 2030

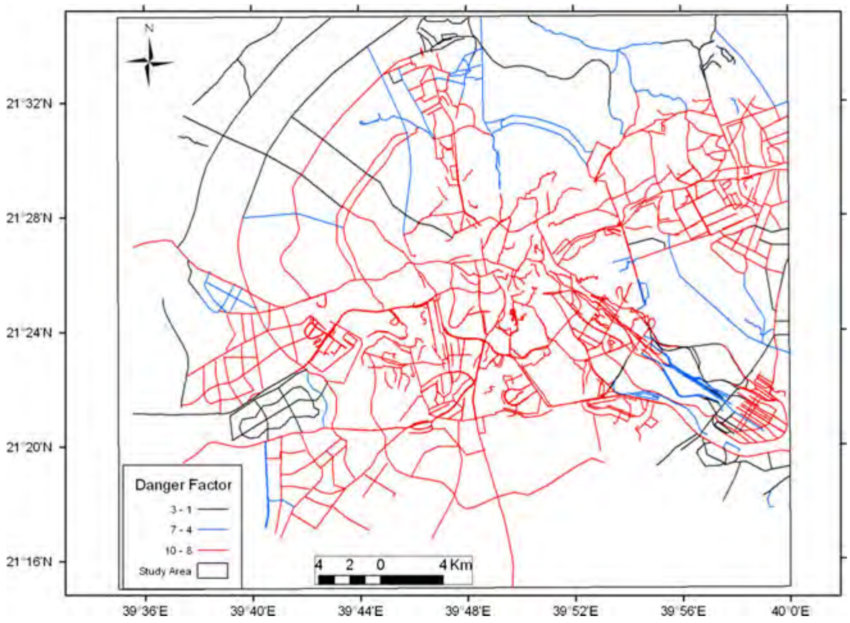

Fig. 22 Flood hazards on road network in Makkah City in 2030

develop digital hydrological maps for present and near future flood hazards in Makkah.

The main findings of the study are:

- The urban sprawl mainly exists in low- and moderate-elevation regions. The growth spreads out along the valleys and stays away from the mountainous areas for economical reasons. Almost 50 % of Makkah's geology contains igneous rocks, mainly granite, that massively increase the development costs in mountainous areas.
- Six main hydrological basins have been identified in the study area, with areas ranging from 74.3 to 360.6 km^2 and lengths of their main streams varying from 16.50 to 48.55 km. A number of 60 sub-basins have been recognized within these six basins. A total of 76 sub-basins, which include residential areas in 1990, have been identified within the study area. These sub-basins extended over an area of 194.726 km^2, which constitute 17.5 % of the total area of the main hydrological basins in the study area. In 2010, the urban areas have been extended to cover 136 sub-basins, whose total areas equal 400.551 km^2. In 2030, it is expected that the urban extent of Makkah City will cover 264 sub-basins with an overall area of 780.388 km^2.
- The mean runoff depth has been increased from 165.3 mm in 1990 to 185.7 mm in 2030. The total flood volume (for urban sub-basins) equals 31.6, 64.6, and 141.9 million m^3 for 1990, 2010, and 2030, respectively. The augmentation of the total flood volume has been increased by almost 104 % from 1990 to 2010, and by almost 120 % from 2010 to 2030.
- A great part of the road network in Makkah City is subjected to high dangerous flood impacts. That category constitutes 211 roads, representing 37 % of the network, with a total length of 481 km. Those roads of high flood impacts exist in the holy shrines particularly in the Arafat area. The future road network of Makkah City in 2030 consists of 705 roads whose lengths range from 1.004 to 23.70 km, with a mean of 2.691 km. A major part of the road network in Makkah City, in 2030, is subjected to high dangerous flood impacts. That category constitutes 563 roads, representing 74 % of the network, with a total length of 1,398 km.
- There is a significant increase in the flood impacts on Makkah's road networks between 2010 and 2030. The overall length of flood danger-factor roads is increased from 481 km (with almost 37 %) to 1,398 km (with 74 % approximately).
- Urbanization has a direct strong relationship with the flood hazards. Urbanization leads to change in the land use of a region, changes its geological characteristics, and decreases its ability to absorb surface water which, in turn, increases the surface water runoff.

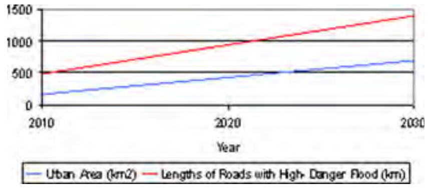

Fig. 23 Relationship between urbanization and flood impacts on roads in Makkah City

Based on the attained results, the following concluding remarks can be drawn:

– It is recommended that the attained results should be taken into account by decision makers in implementing new development planning of Makkah metropolitan area.

– The utilization of GIS in urban growth and flood hazard estimation researches is quit powerful and provides an effective technical tool which should be utilized in analyzing and understanding such phenomena.
– It is recommended that the developed flood hazard maps should be considered a chief aspect in allocating new residential areas within Makkah City.
– The current surface and flood drainage network in Makkah City should be continuously maintained and periodically cleaned, in order for them to work at maximum capacity when surface runoff starts.
– The current surface water drainage network in Makkah City should be re-evaluated, in terms of its capacity and spatial distribution, in order to cope with the expected flood hazards in 2030.
– The process of cutting mountainous portions for urbanization should be strongly controlled by decision makers, particularly during the execution stage, since some falling rocks may block the surface water drainage inlets.
– The integrated water resources management should be considered in order to optimally utilize surface and underground water resources in Makkah.
– A number of flood measurement metrological stations should be established in Makkah to measure, record, and analyze the flood characteristics more precisely.
– An on-line flood warning system should be developed in Makkah in order to issue warnings for the residents before the start of a real flood scenario.

Acknowledgments The authors would like to acknowledge the financial support offered by the Technology Innovation Center on Geographic Information System (TIC-GIS), Umm Al-Qura University, Saudi Arabia.

References

Al-Ghamdi K, Elzahrany R, Mirza M, Dawod G (2012a) Impacts of urban growth on flood hazards in Makkah City, Saudi Arabia. Int J Water Resour Environ Eng 4(2):23–34

Al-Ghamdi K, Mirza M, Elzahrany R, Dawod G (2012b) GIS evaluation of urban growth and flood hazards: a case study of Makkah City, Saudi Arabia. The International FIG Working Week 2012, Rome, Italy, May 6–10

Amini A, Ali T, Ghazali A, Aziz A, Akib S (2011) Impacts of land-use change on stream flows in the Damansara watershed. Malays Arab J Sci Eng 36:713–720

Blanton P, Marcus A (2009) Railroads, roads and lateral disconnection in the river landscapes of the continental. US Geomorphol 112:12–227

Chen J, Hill A, Urbano L (2010) A GIS-based model for urban flood inundation. J Hydrol 373:184–192

Dawod G, Mirza M, Al-Ghamdi K (2011a) GIS-based spatial mapping of flash flood hazards in Makkah City, Saudi Arabia. J Geogr Inf Syst 3(3):217–223

Dawod G, Mirza M, Al-Ghamdi K (2011b) Assessment of several flood estimation methodologies in Makkah metropolitan area, Saudi Arabia. Arab J Geosci. doi:10.1007/s12517-011-0405-5, Published online October, 6

Fred E, Mostafa B (2008) Flood risk modeling for holy sites in Makkah. Third National Conference of GIS Applications in Saudi Arabia, April 7–9, Al Khober City, Saudi Arabia

Hansford J (2010) Impact of land use changes on floods in the Upper Waikato, New Zeeland, Final Report, January 19, 16 pp

HAMDD (Higher Authority for Makkah District Development) (2004) Master planning of Makkah City till 2030. Technical report (in Arabic), Makkah. Saudi Arabia

He M, Hogue T (2011) Integrating hydrologic modeling and land use projections for evaluation of hydrologic response and regional water supply impacts in semi-arid environments. Environ Earth Sci. doi:10.1007/s12665-011-1144-3

Kar G, Kumar A, Singh R (2009) Spatial distribution of soil hydrophysical properties and morphometric analysis of a rainfed watershed as a tool for sustainable land use planning. Agr Water Manage 96:1449–1459

Koshak N, Dawod G (2011) A GIS morphometric analysis of hydrological basins for flood management within Makkah Metropolitan Area, Saudi Arabia, under review. Int J Geomatics Geosci 2 (2):544–554

Paquier A (2010) Flood studies and effects of climate changes: two examples. Presented in the International Workshop on Impacts of Global Warming from Hydrological and Hydraulics Issues, Kyoto, Japan

Mirza M, Ahmed B (2001) Winter weather and climate conditions in Makkah (in Arabic), Geographic Messages, 253, Kuwait Geographic Association, Kuwait

Mirza M (2009) Impacts of development on spatial variations in Makkah City, Saudi Arabia (in Arabic). Presented in the Fourth Arab Geographers Meeting, Rebate, Morocco

Mirza M, Dawod G, Al-Ghamdi K (2011a) Assessment of flood hazards on road network in Makkah City and holy areas using a 3D GIS (in Arabic). Unpublished technical report, Center of Research Excellence in Hajj and Omrah, Umm Al-Qura University, Makkah, Saudi Arabia

Mirza M, Dawod G, Al-Ghamdi K (2011b) Accuracy and relevance of digital elevation models for geomatics applications—a case study of Makkah municipality, Saudi Arabia. Int J Geomatics Geosci 1 (4):803–812

Mirza M, Dawod G, Al-Ghamdi K, Elzahrany R, Al-Harbi K, Shehata A (2011) Assessment of flood hazards on road network in Makkah City and holy areas using a 3D GIS. Unpublished technical report, Center of Research Excellence in Hajj and Omrah, Umm Al-Qura University, Makkah, Saudi Arabia

Mojaddadi H, Habibnejad M, Solaimani K, Abmadi M, Hadian-Amri M (2009) An investigation of efficiency of outlet runoff assessment models: Navroud watershed, Iran. J Appl Sci 9(1):105–112

Olang L, Furst J (2011) Effects of land cover change on flood peak discharges and runoff volumes: model estimates for the Nyando river basin, Kenya. Hydrol Process 25:80–89

Ragunath H (2006) Hydrology: principles, analysis, and design, 2nd edn. New Age International Limited Publications, New Delhi, India

Sheng J, Wilson J (2009) Watershed urbanization and changing flood behavior across the Los Angeles metropolitan region. Nat Hazards 48:41–57

Sherief Y (2008) Flash floods and their effects on the development in El-Qaa plain area in south Sinai, Egypt. PhD dissertation, University of Mainz, Germany

Subyani A, Qari M, Matsah M (2012) Digital elevation model and multivariate statistical analysis of morphometric parameters of some wadis, western Saudi Arabia. Arab J Geosci 5:147–157

Versini P, Gaume E, Andrieu H (2010) Application of a distributed hydrological model to the design of a road inundation warning system for flash flood prone areas. Nat Hazard Earth Syst Sci 10:805–817

Youssef A, Pradhan B, Hassan A (2010) Flash flood risk estimation along the St. Katherine road, southern Sinai, Egypt using GIS based morphometry and satellite imagery. Environ Earth Sci. doi:10.1007/s12665-010-0551-1

Wang L, Wehrly K, Breck J, Kraft L (2010) Landscape-based assessment of human disturbance for Michigan lakes. J Environ Manag 46:471–483

No. 47

Mirza, M., Dawod, G., Elzahrany, R., and Al-Ghamdi, K., **2013**, Utilizing GIS for the assessment of relationship between urban growth and flood hazard increase in Makkah city, Saudi Arabia, for the period 1990-2030, Presented in the flood hazard workshop of the Saudi Geographic Association, Prince Sultan University, Al-Kharj, Saudi Arabia, Feb. 26-28.

Unfortunately, this article's source is missing right now !!

المملكة العربية السعودية
وزارة التعليم العالي
جامعة طيبة
كلية الآداب والعلوم الإنسانية

جامعة طيبة
Taibah University

وزارة التعليم العالي
MINISTRY OF HIGHER EDUCATION

المؤتمر الجغرافي الدولي
(الجغرافيا والتغيرات العالمية المعاصرة)

٢٠-١٤٣٤/٥/٢٣هـ / ١-٢٠١٣/٤/٤م

الأبحاث

جامعة أم القرى

معهد خادم الحرمين الشريفين

لأبحاث الحج والعمرة

استخدام نظم المعلومات الجغرافية في تقدير أحجام السيول ومدى خطورتها عند المجرى الأدنى لوادي نعمان جنوب مدينة مكة المكرمة من خلال تطبيق نموذج سنايدر و اعتماد نموذج الارتفاعات الرقمية ASTER

الأستاذ الدكتور/ محمد سعيد البارودي....... باحث رئيسي

الأستاذ الدكتور/ معراج نواب مرزا...........باحث

الأستاذ الدكتور/ جمعة محمد داوود ....باحث

مكة المكرمة

١٤٣٣ / ٢٠١٢

{أَنزَلَ مِنَ السَّمَاء مَاء فَسَالَتْ أَوْدِيَةٌ بِقَدَرِهَا فَاحْتَمَلَ السَّيْلُ زَبَدًا رَّابِيًا}

سورة الرعد آية ١٧

تمهيد:

تقع مباني المدينة الجامعية لجامعة أم القرى في جنوب مدينة مكة المكرمة وذلك الى الغرب من مشعر عرفات. بينما تغطي منطقة البحث المجاري العليا والوسطى لوادي نعمان عند التقائها بالسد التحويلي للمدينة الجامعية.

و تضم المدينة الجامعية لجامعة أم القرى بضع عشرات الآلاف من الطلاب والإداريين والأكاديميين إضافة إلى المباني الجامعية التي استنزفت الكثير من الجهد والمال . وهي تقع في مواجهة السيول المتدفقة من وادي نعمان الذي يواجه المدينة الجامعية مباشرة.

وقد دفع هذا الموقع الحرج المسئولين في الجامعة الى بناء سد أمام مجرى وادي نعمان لتحويل المياه الى فتحة بعيداً عن الجامعة وبالتحديد بدلاً من دخوله الحرم الجامعي أصبح مجراه خلف الجامعة في اتجاه الحسينية ليلتقي بوادي عرنة عند الزاوية الشمالية الغربية للجامعة عند مدخل قرية الحسينية .

ونظراً لتخوف الكثير من مخاطر السيول والفيضان فقد أثار هذا الوضع عديد من التساؤلات والجدل حول مدى فعالية الإجراءات المتخذة ، وعن امكانية استيعاب المجرى الجديد للمياه التي يمكن أن تتجمع امام السد المذكور. ولعل أهمية هذا البحث تكمن في تحديد مدى كفاءة الاجراءات السالفة الذكر وتقييمها من خلال تقدير احجام السيول ومدى خطورتها عند سد الجامعة ، حيث قامت العديد من المزارع و المباني السكنية العشوائية والأنشطة البشرية الأخرى في مجرى الوادي وهو ما سيؤدي الى إعاقة الجريان وتفاقم المشكلة .

ويهدف هذا البحث إلى :

١- استخدام تقنية نظم المعلومات الجغرافية (ArcGis) في الاستخراج الآلي للخصائص المورفومترية لحوض تصريف منطقة البحث وذلك بالاعتماد على معالجة بيانات نموذج الارتفاعات الرقمية ASTER للعام ٢٠٠٩ م .

٢- تقدير أحجام السيول وتدفق الذروة وارتفاع السيول ومدى خطورتها عند نقطة محددة في منطقة البحث ، وذلك عن طريق تطبيق نموذج سنايدر Snyder's Model الأكثر ملائمة لمنطقة البحث ، وخاصة بعدما تم استنباط بعض المعاملات الخاصة بهذا النموذج لأول مرة في المملكة من خلال قياس عدد من السيول التي حدثت في وادي عرنة المجاور عقب عواصف مطرية .

٣- إعطاء مثال تطبيقي لعملية التكامل بين نظم المعلومات الجغرافية ونموذج الارتفاعات الرقمية والنماذج الرياضية من أجل تشجيع المهتمين بالدراسات الهيدرومورفومترية على تطبيق مثل هذه الطرق التكاملية في البحث العلمي .

٤- اثراء البحوث العلمية عن مكة المكرمة والمشاعر المقدسة بالدراسات الجيومورفومترية والهيدرومورفومترية التي تفتقر اليها .

وقد قام الباحث بطرح عدد من التساؤلات لجعل الإطار الموضوعي للبحث أكثر تحديداً، ومن أهم هذه التساؤلات التي يتوخى البحث الإجابة عليها:

١- مامدى كفاءة الاستخراج الآلي للخصائص الهيدرومورفومترية باستخدام نظم المعلومات الجغرافية والاعتماد على معالجة بيانات نموذج الارتفاعات الرقمية .

٢- مامدى خطورة السيول وأحجامها وارتفاعها (عمقها) عند سد الجامعة.

٣- هل يعتبر نموذج سنايدر لتقدير مخاطر السيول وأحجامها هو الأكثر ملائمة لمنطقة البحث من النماذج الأخرى .

٤- مامدى ملائمة المنشآت الهندسية كالجسور المقامة على وادي نعمان ، والسد التحويلي لمجرى وادي نعمان عند الجامعة والمجرى الجديد للوادي في مواجهة السيول العارمة للوادي المذكور .

ولتحقيق الأهداف المذكورة آنفاً وللإجابة على التساؤلات أعلاه قام الباحث بوضع طريقة للبحث – بعد التعريف بأهم الخصائص الطبيعية لمنطقة البحث – تضمنت الخطوات المرحلية لإنجاز البحث ومناقشة النتائج .

أولاً : الخصائص الطبيعية لمنطقة البحث :

سيتم استعراض أهم الخصائص الطبيعية لحوض وادي نعمان والتي لها علاقة مباشرة أو غير مباشرة بموضوع البحث والمتمثلة بكل من الخصائص التضاريسية والجيولوجية والجيومورفولوجية والمناخية .

ا-الخصائص التضاريسية :

تقع منطقة البحث إلى الجنوب والجنوب الشرقي من مدينة مكة المكرمة وتشغل الحوضين الأعلى والأوسط لوادي نعمان ، ويحدها فلكياً دائرتي عرض °21 02 و ٢٩ °٢١ شمالاً ، وخطي طول ٥٨ °٣٩ و ١٧ °٤٠ شرقاً (شكل ١) .

وتصل مساحة حوض وادي نعمان بحسب النقطة المحددة في المجرى الأدنى عند السد إلى ٦٨٥.١ Km^2 وذلك حسب نموذج الارتفاعات الرقمية ASTER .

ويستمد حوض وادي نعمان مياهه من المجاري العليا عند الجرف الإنكساري لمنطقة الهدا ، وذلك عند ارتفاعات يصل أقصاها إلى ٢٥٩٩ م ، وأدناها عند ٢٩٢ م عند سد الجامعة (شكل ٢) ،وتتكون الشبكة المائية لحوض وادي نعمان من أودية يعرج وعلق ومجاريش وعرعر ورهجان، أما طول المجرى الرئيسي لوادي نعمان فيصل إلى ٤١.٥ كم وهو ما أدى إلى شدة انحداره الذي وصل إلى ٠,٠٥٥ (جدول١)

الخصائص الشكلية لأودية البحث	نعمان السد
المساحة (كم)	٦٨٥.١
المحيط (كم)	١٤٩.٢
الارتفاع الادني (م)	٢٩٢
الارتفاع الاقصي (م)	٢٥٩٩
الارتفاع المتوسط (م)	٩٣٧
طول الحوض (كم)	٣٥.٦
عرض الحوض (كم)	٢٤.٩
طول المجري الرئيسي (كم)	٤١.٥
متوسط انحدار الحوض (%)	٣٢.٨
متوسط انحدار المجري الرئيسي (م/م)	٠.٠٥٥
المسافة بين مركز ثقل الحوض و المصب (كم)	٢٤
معامل الاستدارة	٠.٠٦٢
نسبة الاستطالة	٠.٣٠٩
عامل الشكل	٠.٥٤١

(جدول ١) الخصائص الشكلية والتضاريسية لحوض وادي نعمان (سد الجامعة)

اما انحدار سطح الحوض فقد وصل الى ٣٢.٨ % وهو ما يعكس بطبيعة الحال الارتفاعات الشاهقة للكتل الجبلية في حوض وادي نعمان،و بالإضافة الى جرف الهدى فان جميع الروافد الرئيسية في حوض وادي نعمان كأودية الكر ويعرج وعلق والشرى ومجاريش ورهجان وعرعر تضرب بمجاريها العليا نحو ارتفاعات شاهقة تتراوح بين ٢٠٠٠- ٢٥٠٠ م في الجرف الإنكساري

لمناطق الشفا والهدى والحساسنة اضافة الى جبل كبكب الذي لا يقل ارتفاعه كثيرا عن جبال الجرف الانكساري (شكل ٣) .

ب- الخصائص الجيولوجية :

يمكن من خلال الخريطة الجيولوجية المعدة لمنطقة البحث من مربع مكة (Moor and AL Rehaili,١٩٨٩) تمييز وحدتين رئيسيتين :أولاهما وحدة صخور ماقبل الكامبري ، وثانيهما وحدة رواسب الزمن الرابع الفتاتية (شكل ٤) .

١-وحدة صخور ماقبل الكامبري :

تنقسم صخور هذه الوحدة الى نوعين رئيسيين ، وهما الصخور النارية الباطنية المتبلورة ، ومتكونات ماقبل الكامبري الطباقية. ويشمل النوع الاول معقدات ما قبل الكامبري كمعقدات ملح والنعمان وجعرانة وشرقة والشامية ، حيث يتوزع معقد ملح في وادي نعمان في روافده كوادي مجاريش ورهجان وعرعر وعلق. ويتكون من الجابرو والديوريت والكوارتزديوريت. اما معقد النعمان فيتوزع في جميع مناطق الحوض وهو الاكثر انتشارا في منطقة البجث ويتكون من الجرانيت والجرانوديوريت في وادي نعمان ويظهر على التكوين النسيج الورقي بعد تعرضه للضغط في نطاق انكسار الدام بينما يتوزع معقد جعرانة في مناطق قمم جبال الهدى والكر وغيرها من المجرى الاعلى لوادي نعمان. ويتكون من التوناليت والجرانوديوريت اما معقد الشرقة فيتوزع في السفوح العليا لوادي الشرا و وادي يعرج رافدي نعمان.

أما متكونات ما قبل الكامبري الطباقية فهي في معظمها صخور نارية وفتاتية متحولة وتشمل مساحات صغيرة من متكون عباسة من مجموعة سمران في الحوض الاعلى لوادي نعمان وخاصة في اعالي رافده وادي مجاريش وتتكون من لابا متحولة ومن صخور فتاتية بركانية.ومما تجدر الاشارة اليه أن مجموع ماتشكله وحدة صخور ماقبل الكامبري بنوعيها من مساحة حوض منطقة البحث هي ٧٤% لحوض وادي نعمان (سد الجامعة) ، وهو مايعكس الدور الذي تلعبه هذه الصخور غير المنفذة عقب تساقط الامطار وحدوث الجريان .

٢-وحدة رواسب الزمن الرابع :

تتوزع رواسب الزمن الرابع في مجاري الاودية بالدرجة الاولى وخاصة في المجاري الوسطى والدنيا لوادي نعمان ، وتتكون من الرواسب الرملية والحصوية . كما تتوزع هذه الرواسب في المراوح الفيضية كمروحة وادي الكر ووادي علق ووادي يعرج وغيرها ، إضافة إلى رواسب المدرجات النهرية . وتشكل مساحات هذه الرواسب ما نسبته ٢٦% من مساحة

حوض وادي نعمان ، وهو ما ينعكس على الخصائص الهيدرولوجية للحوضين ، وخاصة على حجم الجريان وتصريف الذروة لسيول الحوض .

ويمكن من خلال العرض السابق للخصائص الجيولوجية والتضاريسية لحوض وادي نعمان إدراك مدى مساهمة الحوض في تحويل مياه الأمطار إلى جريان سطحي حيث تزداد فيه المساحات التي تشغلها الصخور النارية البلورية على حساب الرواسب الرباعية الفتاتية ما يعني قلة التسرب وزيادة الجريان ، وهو ما يمكن التوصل إليه بعد تطبيق النماذج الرياضية في تقدير الجريان السطحي لهذا الحوض .

ج- الخصائص الجيومورفولوجية والشكلية لمنطقة البحث :

يبدو من خلال الملاحظة المستمرة للجريان في أودية المناطق الجافة عموماً أنه لا يشغل سوى نظاماً ضيقاً من القطاع العرضي للمجرى الواسع باستثناء الحالات النادرة التي تسببها عواصف مطرية متباعدة سواء في زمانها أو مكانها.

ومن ثم فإن معظم الأودية الصحراوية إن لم تكن جميعها هي أودية ضامرة حالياً من فترات مطيرة كان فيها الجريان أعظم بكثير مما هو عليه الآن سواء في كمياته أو تكرار حدوثه. ومن ثم كان هذا الجريان هو من أنشأ هذه الأودية الواسعة والتي انحسرت في الوقت الحاضر لتجري في مجار ضيقة تاركة بقية القطاع العرضي للمجرى كسهول فيضية غالباً ما نشأت فوقها المزارع أو المنشآت المدنية الأخرى الناجمة عن النشاط البشري.

وعلى الرغم من ذلك فإن ظاهرة الفيضان المعروفة في المناطق المعتدلة لا تحدث إطلاقاً في المناطق الجافة بنفس الطريقة والكيفية نظرا لأن حدوث الفيضان في تلك المناطق يرتبط بتجاوز كميات المياه المتدفقة من جميع الروافد إلى المجرى الرئيسي طاقة هذا الأخير على استيعابها مما يجعله يفيض على جوانب قنوات المجاري غامراً بذلك السهول الفيضية على الجانين وهو ما لا يحدث في المناطق الصحراوية الجافة التي يقتصرفيها الفيضان على المجرى الرئيسي فقط .

وقد دفعت مشكلة السيول التي تشهدها المناطق الجافة إلى البحث عن طرق كمية تهدف إلى البحث عن العلاقة بين خصائص الأحواض وحدوث السيول عن طريق تحديد العوامل المؤثرة في المخطط المائي (الهيدروجراف) لهذه الأحواض ومن ثم التنبؤ بشكل دقيق بحجم وشكل هذه المخططات المائية بغية التحذير من السيول فيما يتعلق بوقتها أو شدتها أو لتصميم العبارات أو الجسور المناسبة لأقصى تصريف لها.

ونظراً لما تتطلبه عملية رسم المخطط المائي للأحواض من بيانات مطرية مسجلة أو بيانات عن التدفق قد لا تتوافر في المناطق الجافة فقد لجأ الهيدرولوجيين إلى بيانات خصائص الأحواض المعروفة بثباتها من أجل اشتقاق الهيدروجراف لهذه الأحواض.

والمعروف أنه بعد حدوث أي عاصفة مطرية فإن معدل كمية الجريان داخل الأحواض ستتأثر بعدة عوامل أهمها عمليات التبخر ورطوبة التربة وطريقة استغلال أراضي الأحواض والغطاء النباتي وغيرها من العوامل التي قد لا يمكن الحصول على بياناتها أيضاً. بينما نجد أن خصائص الأحواض تتحكم بشكل أوضح بوصول موجة الفيضان أو السيل إلى مخارج الأحواض أو محطات القياس ومن أهم هذه الخصائص الطبيعية المتمثلة بجيومورفولوجية الأحواض وخاصة المورفومترية منها كالمساحة والشكل والانحدار وطول المجرى الرئيسي نظراً لما تلعبه هذه الخصائص من دور في تحديد شكل مخطط الهيدروجراف وأهمها تحديد زمن الاستجابة أو الوقت الفاصل بين قمة الفترة الزمنية للعاصفة المطرية وقمة أو ذروة التصريف.

١- مساحة الحوض: **Basin Aria**

تلعب مساحة الحوض دورا كبيرا في تحديد كميات المياه المتلقاة من العواصف المطرية فالعلاقة طرديه بينهما، ومن ثم تزداد قمة التصريف ارتفاعاً مع ازدياد كميات الأمطار الساقطة على الحوض. وغالباً ما تدخل مساحة الحوض في جميع عمليات رسم مخطط الماء (الهيدروجراف) لهذه الأحواض. كما أن زيادة المساحة غالباً ما تؤدي إلى قلة انحدار الأحواض والعكس صحيح. إلا أن الخصائص الأخرى كالارتفاع تلغي مثل هذه الاستنتاجات وقد وصلت مساحة حوض وادي نعمان ٦٨٥كم^{٢} .

٢- انحدار الحوض: **Basin Slope**

يتحكم كل من الانحدار وارتفاع الأحواض بشكل مباشر وغير مباشر في قمة التصريف سواء أكان انحدار الأحواض أو انحدار المجرى الرئيسي ، وقد وصل ارتفاع حوض وادي نعمان ٢٥٩٩م فوق مستوى سطح البحر ووصل أدنى مستوى ٢٩٢ متراً، أما انحدار الحوض فقد وصل ٣٢.٨٠% في مقابل متوسط انحدار للمجرى الرئيسي ٥٥ م/ كم . وقد أثبتت قياسات المجرى الرئيسي قيمتها عند اشتقاق الهيدروجراف لحوض منطقة البحث .

٣- شكل الحوض: **Shape Factor**

يلعب شكل الحوض دوراً هاماً في تحديد قمة الجريان والكثير من الخصائص الهيدرولوجية الأخرى وخاصة من خلال مقارنته بالسمات الشكلية الأخرى كالاستدارة والاستطالة وغيرها. وتحكمها كلها بسرعة الجريان وقمة التصريف ويمكن حساب عامل الشكل من المعادلة التالية: (Horton,١٩٤٥)

معادلة (١) $$F= A/Lb^2$$

حيث أن :

F = عامل الشكل.

A = مساحة الحوض (كم٢)

Lb^2 = مربع طول الحوض .

ويتضح من خلال الجدول رقم (١) أن معامل الشكل قد وصل ٠.٥٤١ في حوض وادي نعمان (سد الجامعة) . ويتضح من خلال هذه القيمة للحوض أنه يقترب من القيمة المطلقة لعامل الشكل والبالغة (٠.٧٨٥). ومن ثم فهو يقترب من الشكل الكمثري الأكثر تناسقا في أشكال الأحواض النهرية .

٤- معامل الاستدارة : Basin circularity

يتم استخراج استدارة الأحواض من خلال قسمة مساحته على مساحة دائرة يساوي محيطها محيط الحوض نفسه وذلك حسب المعادلة التالية: (Strahler, ١٩٦٨)

معادلة (٢) $$R_c = \frac{A}{A_c}$$

حيث أن :

A = مساحة الحوض (كم٢) .

Ac= مساحة دائرة لها محيط يساوي محيط الحوض (كم٢)

Rc= معامل استدارة الحوض.

وعادة فإن اقتراب القيمة الناتجة من الرقم ١ يشير إلى زيادة استدارة الحوض والعكس صحيح . وقد وصل معامل الاستدارة إلى ٠.٦٢ في حوض وادي نعمان (سد الجامعة) وهو ما يشير إلى زيادة إستا درته وبالتالي فإن وصول مياه الجريان نحو المجرى الرئيسي يتم سريعا الأمر

الذي يجعل زمن الاستجابة قصيراً ومن ثم تزداد خطورته أثناء الفيضـــان . إلا أن وقـــوع معظـــم أحواضه عند المجاري العليا تجعله أقل خطورة من حوض وادي عرنـــة (البـــارودي ،٢٠١٢) ، حيث تجري المياه لمسافات أطول فبل وصولها إلى منطقة سد الجامعة وهو ما يعرضها إلى الكثير من التسرب أثناء الجريان.

٥- نسبة الاستطالة : Elongation Ratio

تعد نسبة الاستطالة من المعايير المستخدمة أيضاً في تحديد أشكال الأحواض وتحسب عادة من قسمة قطر دائرة تساوي مساحتها مساحة الحوض المائي (كم) على أقصى طول للحوض (كم) وذلك من المعادلة التالية (Schumm, ١٩٥٦):

معادلة (٣)

$$R_e = \frac{D_c}{L_b}$$

حيث أن :

Re = نسبة استطالة الحوض.

Dc = قطر دائرة لها مساحة تساوي مساحة الحوض (كم).

Lb = أقصى طول للحوض المائي (كم).

وغالباً ما تلعب زيادة الاستطالة (قرب الحوض من الشكل المستطيل) دوراً هاماً في تـــأخير كل من زمن الاستجابة وزمن التركيز Time of concentration والوصول إلى ذروة (قمـــة) التصريف للعديد من الأسباب. وقد أظهرت النتائج أن استطالة حوض وادي نعمان منخفضة نســبيا لقربه من الاستدارة حيث وصل إلى ٠.٣٠٩ وهو ما ينعكس أيضاً على خصائص الســيول فـــي الحوض والتي تجعله أكثر استجابة للجريان.

٦ - شبكة التصريف المائي :

تم تصنيف مجاري شبكة التصريف المائي لحوض وادي نعمان إلى رتب بحســب طريقـــة ستريلر Strahlar وتبين من الشكل وصول وادي نعمان إلى الرتبة السابعة (شكل ٥) ، أما أعداد مجاري الرتبة الأولى (وهي اللاعبة الأساسية في سرعة الاستجابة نظراً لانحداراتها الشديدة) فقـــد بلغت ١٧٥٠ مجرى في حوض وادي نعمان كما بلغ الطول الإجمالي للشبكة المائية ١٣٥٧ كم ، وهو ما انعكس على كثافة التصريف التي بلغت ٢.٠ كم/كم^2 .

ورغم كثرة الحديث عن دور الخصائص المورفولوجية لشبكات التصريف في التأثير على الجريان إلا أن عدد قليل من هذه الخصائص أثبت تأثيره المباشر على ذلك. وقد تم استنتاج أن سرعة استجابة أي حوض للوصول إلى ذروة التصريف هو دليل على تطور شبكته. وعلى العكس من ذلك فإن تأخير زمن الاستجابة يدل على عدم تطور الشبكة. بينما لم تثبت علاقة زمن الاستجابة بكل من رتبة المجرى أو نسبة التفرع أو كثافة التصريف، فإن طول المجرى الرئيسي كان له أكبر الأثر في تحديد قمة التصريف إذا ما ترافق مع زيادة في انحدار المجرى الرئيسي. وقد تبين من خلال حساب المتغيرات المذكورة أن طول المجرى الرئيسي لوادي نعمان ٥٤ كم ،ومن ثم فهو قصير نسبيا إذا ماعلمنا أن مجراه شديد الانحدار ٥٥ م/كم) ومن ثم يقل فيه زمن التباطؤ (زمن الاستجابة) وهو ما يعني أنه شديد الخطورة.

د- الخصائص المناخية :

تلعب الخصائص المناخية عادةً دوراً هاماً في عملية حساب الميزانية المائية لأحواض التصريف النهري ، إلا أن خصوصية البحث المتمثلة في تقدير تصريف الذروة وحجم الجريان عقب العواصف المطرية يجعل من كميات الأمطار الساقطة على الأحواض المدروسة خلال ساعات العاصفة المطرية ذو أولوية خاصة في هذا البحث ، فالعناصر المناخية رغم أهميتها إلا انه يمكن إهمالها في هذا المقام ، فالحرارة والرطوبة والرياح والإشعاع الشمسي ودورها كلها في عمليات التبخر يمكن إهمالها نظراً لأن كميات التبخر الحقيقي (يقصد به مايتم تبخيره خلال فترة العاصفة المطرية) لاتكاد تذكر ، ومن ثم يمكن اعتبار كل من التساقط وخصائص الأحواض هي العوامل الأساسية المؤثرة في الجريان السطحي .

وترتبط درجات السيول عادة بالأمطار المسببة لها مع الاخذ بعين الاعتبار القدرة التسريبية والتخزينية لأحواض التصريف . كما أنه من الصعوبة بمكان تقدير شدة ومدة وتوزيع الامطار على امتداد الاحواض نظرا لغياب مثل هذه القياسات في منطقة البحث ، إلا أن عملية الربط بين الوصول الى قمة التصريف وكثافة فترة العاصفة المطرية قد لاقت نجاحا في المخططات المائية (الهيدروجراف) للأحواض المقاسة في العديد من المناطق ، ومن ثم فهي بلا شك تنطبق على المخططات المائية المشتقة .

١- المعدلات السنوية للأمطار والقيم اليومية المتطرفة لها :

حيث أن معدلات الأمطار لا تعكس القيمة الحقيقية لمدى مساهمتها في الجريان السطحي كما تظهرها خرائط خطوط المطر المتساوي (شكل ٦) والتي يصل أقصاها عند المجاري العليا لمنطقة البحث (٢٠٠ملم) وأدناها عند المجاري الدنيا لها والتي لاتزيد عن ١٢٠ ملم

فان التساقطات المطرية المتطرفة والمرتبطة بالعواصف المطرية هي الأكثر فعالية في الجريان كما سجلته محطة مكة المكرمة .

وغالباً مانجم عن هذا الترابط بين القيم المتطرفة للتساقط المطري والجريان السطحي سيول عارمة ازهقت في الماضي العديد من الأرواح . وكانت بعض الدراسات (شومان ، سامر أحمد ، ١٤١٨ هـ) قد قسمت السيول في مدينة مكة المكرمة الى ثلاث مستويات ، حيث تكررت سيول الدرجة الأولى (العارمة) مرة كل ٤٦ عاماً ، بينما تكررت سيول الدرجة الثانية مرة كل ٣٣ عاماً . أما سيول الدرجة الثالثة فقد تكررت كل ١٣ عاماً . ويرى بعض الباحثين أن آخر سيل من الدرجة الأولى حدث عام ١٩٦٩م وهو مايعني أن بالإمكان تكرره خلال السنوات العشر القادمة ، وهو ماقد يمثل خطورة على الحجاج في المشاعر المقدسة (مرزا وأحمد ، ٢٠٠١ ، ص ٧٨) . وتمثل محطة مكة المكرمة كما هو معلوم المجاري الدنيا لمنطقة البحث والتي تعد تهامية الموقع ومن ثم فمن المتوقع أن تزيد الأمطار كثيرا في المناطق الجبلية . وبما أن محطة أم القرى تمثل قيم التساقط المطري على المجاري الدنيا لمنطقة البحث فإن الأمطار على المجاري العليا لأودية عرنة ونعمان ستكون مختلفة الى حد كبير (جدول ٢).

وقد سجلت محطات المجاري العليا لمنطقة البحث (المناطق الجبلية) امطاراً سنوية وصلت الى قيم متطرفة خلال الاعوام الثلاثين الماضية الممتدة بين عامي ١٩٧٠و٢٠٠٠ حيث سجلت ٣٤٢.٤ ملم عند حافة الهدا في عام ١٩٧٥.

المحطة	القيم العظمى	سنة التسجيل
الفرين	٣٦٤	١٩٧٩
مكة	٢٦٠	١٩٩٢
الكر السفلي	٣٩٣.٤	١٩٧٥
حافة الهدا	٣٤٢.٤	١٩٧٥
شفا بني سفيان	٤٣٢.٦	١٩٧٥
حافة الشفا	٤٩٤	١٩٧٢
شداد	٣٩٨.٩	١٩٧٥
رهجان	٢٧٩.٤	١٩٧٩
الطائف	٢٣٨.٤	١٩٨٢

(جدول ٢) القيم العظمى للأمطار (ملم في منطقة البحث للفترة ١٩٧٠ الى ٢٠٠٠ م)

وكما هو موضح في الجدول ٢ فقد سجل العام ١٩٧٥ أمطاراً مرتفعة وصلت الى ٤٣٢.٦ ملم في شفا بني سفيان ، و ٣٩٨.٩ ملم في شداد ، و ٣٩٣.٤ ملم في الكر السفلي ، و ٣٤٢.٤ ملم في حافة الهدا (عواري ، ابتسام ، ٢٠٠٥ ، ص ١٢٦) ،الا أن أعلى قيمة للأمطار وصلت ٤٩٤ ملم في عام ١٩٧٢عند حافة الشفا . ويبدو ان غياب البيانات اللحظية واليومية لسجلات هذه الأمطار لا يجعل منها سوى مؤشر على معدلات التساقط وليس على كثافته .

٢- السجلات اليومية القصوى للأمطار في منطقة البحث :

يشير الجدول ٣ الى كميات الأمطار اليومية الساقطة على محطة مكة المكرمة في الفترة الممتدة من عام ١٩٨٥وحتى عام ٢٠١٠ بين ١٠و٧١ملم (جدول ٣ أ) وهي غالبا ماتسقط خلال فترة زمنية تتراوح مابين ساعة وساعتين ، ومن ثم يمكن اعتبارها ممثلة لفترة العاصفة المطرية التي تتصف بها العواصف في مثل هذه المناطق .

وكما يتضح من الجدول(٣ ب) يمكن تكرار كمية المطر اليومي القصوى (العواصف المطرية) كل ٢٧ عاما في منطقة البحث والتي وصلت ٧١،٧ملم وهوماينجم عنه سيول عارمة ، كما يظهر من الجدول أيضا القيم الاحتمالية لسقوط الأمطار العاصفية في المنطقة .

السنة	ملم / يوم	السنة	ملم / يوم	السنة	ملم / يوم
١٩٨٥	٦٣	١٩٩٤	٢٥.١	٢٠٠٣	٢١.٤
١٩٨٦	٢٤	١٩٩٥	٢٩.٤	٢٠٠٤	٥٥
١٩٨٧	١٨	١٩٩٦	٣٢.٢	٢٠٠٥	٦٥.٢
١٩٨٨	٤٣.٨	١٩٩٧	٣٤.٦	٢٠٠٦	٥٤.٤
١٩٨٩	٧١.٧	١٩٩٨	٣٤.١	٢٠٠٧	١٧.٤
١٩٩٠	١٠	١٩٩٩	٢٤.٧	٢٠٠٨	٦١.١
١٩٩١	٢٢.٧	٢٠٠٠	٥٣.٧	٢٠٠٩	٢٤
١٩٩٢	٤٩.٤	٢٠٠١	٤٢	٢٠١٠	٥٥
١٩٩٣	٤٠	٢٠٠٢	٥٠		

(جدول ٣، أ) كميات المطر اليومية القصوى في مكة المكرمة بين عامي ١٩٨٥ – ٢٠١٠

السنة	ملم / يوم	الترتيب	فترة الرجوع	الاحتمالية
١٩٨٩	٧١.٧	١	٢٧	٠.٠٣٧
٢٠٠٥	٦٥.٢	٢	١٣.٥	٠.٠٧٤
١٩٨٥	٦٣	٣	٩	٠.١١١
٢٠٠٨	٦١.١	٤	٦.٧٥	٠.١٤٨
٢٠٠٤	٥٥	٥	٥.٤	٠.١٨٥
٢٠١٠	٥٥	٦	٤.٥	٠.٢٢٢
٢٠٠٦	٥٤.٤	٧	٣.٨٥	٠.٢٥٩
٢٠٠٠	٥٣.٧	٨	٣.٣٧	٠.٢٩٦
٢٠٠٢	٥٠	٩	٣	٠.٣٣٣
١٩٩٢	٤٩.٤	١٠	٢.٧	٠.٣٧٠
١٩٨٨	٤٣.٨	١١	٢.٤٥	٠.٤٠٧
٢٠٠١	٤٢	١٢	٢.٢٥	٠.٤٤٤
١٩٩٣	٤٠	١٣	٢.٠٧	٠.٤٨١
١٩٩٧	٣٤.٦	١٤	١.٩٢	٠.٥١٨
١٩٩٨	٣٤.١	١٥	١.٨	٠.٥٥٥

١٩٩٦	٣٢.٢	١٦	١.٦٨	٠.٥٩٢
١٩٩٥	٢٩.٤	١٧	١.٥٨	٠.٦٢٩
١٩٩٤	٢٥.١	١٨	١.٥	٠.٦٦٦
١٩٩٩	٢٤.٧	١٩	١.٤٢	٠.٧٠٣
١٩٨٦	٢٤	٢٠	١.٣٥	٠.٧٤٠
٢٠٠٩	٢٤	٢١	١.٢٨	٠.٧٧٧
١٩٩١	٢٢.٧	٢٢	١.٢٢	٠.٨١٤
٢٠٠٣	٢١.٤	٢٣	١.١٧	٠.٨٥١
١٩٨٧	١٨	٢٤	١.١٢٥	٠.٨٨٨
٢٠٠٧	١٧.٤	٢٥	١.٠٨	٠.٩٢٥
١٩٩٠	١٠	٢٦	١.٠٣	٠.٩٦٢

(جدول٣ ، ب) فترة الرجوع والاحتمالية للأمطار اليومية القصوى لمدينة مكة المكرمة بين عامي ١٩٨٥- ٢٠١٠

وبناء على قياس العاصفة المطرية والسيل الناجم عنها في ٢٠١٠/٢/١٣ والتي وصلت ٥٥ملم فوق حوض وادي عرنة المجاور فقد نجم عنها سيلا عارما وصلت ذروة تصريفه الى ٤٣١م٣/ ثا (البارودي ، ٢٠١٢) ويمكن اعتبار هذه النتيجة كأول عملية قياس لحجم تدفق الذروة للسيول في وادي عرنة والتي يمكن مقارنتها مع نتائج تطبيق النماذج النظرية كنموذج سنايدر من خلال البحث كما يمكن الاستعانة بها في تحديد المعاملات الضرورية لتطبيق النموذج المذكور.

ثانيا – الإطار النظري للبحث والدراسات السابقة :

ترجع عمليات الربط بين المطر والجريان السطحي باستخدام النماذج الرياضية الى العالم شيرمان Sherman ١٩٣٢ حيث قدم نظرية كان الهدف منها ايجاد العلاقة بين المطر والجريان السطحي : وتتمثل في تثبيت تأثير الأمطار والتي هي بالتأكيد في حالتها الطبيعية تكون متغيرة مع الزمن فجعلها تمثل وحدة عمق واحدة (١سم أو ١ إنش) في وحدة زمنية معينة (١ ساعة أو ١ يوم) وهكذا نتج التصريف عن هذه الأمطار وحدة واحدة أيضًا وهذا التصريف أطلق عليه وحدة الهيدروجراف وقد عرفت فيما بعد بنظرية وحدة الهيدروغراف Hydrograph Unit ، ونعني بمصطلح وحدة الهيدروغراف تغير تصريف النهر مع الوقت لفترة زمنية محددة من الأمطار عندما يكون عمق المطر المؤثر وحدة عمق واحدة (سنتيمترًا أو إنشاً واحدًا) ومن هنا جاءت تسمية وحدة الهيدروغراف ، وقد تنوعت هذه الطرق بتنوع البيانات والأنظمة المستخدمة في إيجاد العلاقة بين المطر والجريان . (الدليمي ، ٢٠٠٦ ، ص ١٣٨)

وقد تعددت الطرق في الوقت الحاضر وأصبحت متاحة بشكل أفضل لتحديد وتطبيق وحدة الهيدروجراف وتشترك جميع الطرق بمفهوم واحد عنها ، حيث أن نسبة قمة الجريان على حجم الجريان لوحدة الزمن هي ثابته للحوض نفسه .

وتعتبر وحدة مخطط الهيدروجراف التي تصورها Sherman ١٩٣٢ عبارة عن مجموعة من الاحداثيات (زمن – تصريف) ومستمدة مباشرة من أحواض مقاسة ، أما وحدة الهيدروجراف المشتقة للأحواض غير المقاسة فتستخدم معادلات بمعاملات مُعرفة وذلك لتحديد التصريف عند اي نقطة في الهيدروجراف ، وتملك هذه المعاملات المستخدمة قيمة هيدرولوجية ، كزمن الهيدروجراف للوصول لذروة التصريف ، ويمكن تقدير المعاملات من بيانات لأحواض مقاسة أو البيانات الطبيعية للأحواض . ويمكن تصنيف طرق اشتقاق وحدة الهيدروجراف بناء على نوعية البيانات المستخدمة والمتاحة ويمكن تلخيصها على النحو التالي :

- **طرق استخدمت بيانات حوض النهر فقط في اشتقاق وحدة الهيدروجراف ، مثل طريقة سنايدر snyder في سنة ١٩٣٨م .**
- **طرق استخدمت بيانات الأمطار والتصريف معًا في اشتقاق وحدة الهيدروجراف مثل طريقة المربع الأدنى المستخدمة من قبل الباحثين دوج Dooge وبرون Brune سنة ١٩٨٤م .**
- **طرق استخدمت بيانات التصريف فقط ، كطريقة انتقاء الجذور المقترحة من قبل الباحثين الثلاثة (Turner, Dooge, Bree) سنة ١٩٨٩م .**

- طرق استخدمت بيانات حوض النهر وبيانات الأمطار، أو بيانات حوض النهر وبيانات التصريف .(الدليمي، ١٩٩٥)

وعلى الرغم من أن طريقة سنايدر تعتبر رائدة في اشتقاق وحدة الهيدروجراف للأحواض غير المقاسة إلا أن هناك طرق أخرىالمستفيدين من نوعية البيانات كطريقة كلارك**Clark unit hydrograph** وطريقة **SCS Method** (طريقة خدمة حفظ التربة **Soil Conservation Service**) ، وتشترك جميع هذه الطرق بأنها توظف معاملات زمنية متشابهة ولكن غير متطابقة ، حيث أن طريقة **NRCS** تستخدم تعبير **lag time** للزمن ، وسنايدر استخدم **tp** ، و كلارك استخدم **Tc** . وكما هو واضح فان الاختلاف بين هذه المعاملات التي استخدمت من قبل الباحثين واختلاف اصطلاحاتها تجعل المطبقين أو المستفيدين من هذه الطرق في حيرة كبيرة .

وقد حقق نموذج سنايدر انتشارا واسعا بفضل التعديلات التي قام بها العديد من الباحثين والهيئات ومنهم سلاح المهندسين في الجيش الأمريكي ، وكل من شو **Chow et al** ١٩٨٨ وزنجبو يو **Zhongbo yo** ١٩٩٨ ، وراميرز **Ramerez**٢٠٠٠ ، وراجوناث **Raghunath** ١٩٩١ و ٢٠٠٦ والتي شملت تغيير قيم معاملات سنايدر بما يتناسب مع الوحدات المترية بدلا من الوحدات الانكليزية .

١- نموذج سنايدر **Snyder's model**:

قدم سنايدر طريقته للتطبيق على المناطق الجافة أو تلك التي تفتقر إلى بيانات مسجلة عن الجريان أو العواصف المطرية وتعد طريقته الأشهر في تقدير الجريان لأحواض المناطق الجافة على الرغم من وجود طرق عديدة لعلماء آخرين.

وكان سنايدر **Snyder** ١٩٣٨ قد قدم طريقته التجريبية لاشتقاق وحدة الهيدروجراف **unit Hydrograph** من خلال تحليله لهيدروجراف عدد كبير من أحواض تصريف منطقة جبال الأبالاش في الولايات المتحدة الأمريكية والتي لا يوجد لها سجلات جريان، وتتراوح مساحاتها بين ١٠- ١٠.٠٠٠ ميل مربع، واختار عاملين **parameters** أساسيين لتطوير وحدة الهيدروجراف، وهما عامل تدفق الذروة **peak flow factor**. وعامل زمن تدفق الذروة **time of peak flow** وهما اختصاراً **ct** و **cp**. والافتراض الرئيسي لهذه الطريقة أن الأحواض التي لها خصائص متشابهة (طبيعية وشكلية) وموجودة في نفس المنطقة سيكون لها قيم متشابهة للعاملين، وبالتالي فإن الأحواض غير المقاسة **ungaged** القريبة والمماثلة لأحواض مقاسة **gaged** تكون قيم معاملات **ct** وكذلك **cp** معلومة لها يمكن عندها استخدامها في تحديد معاملات الأحواض غير

المقاسة والأخذ بها، لأنه من المفترض أن يكون لها نفس القيمة. وبإدخالها ضمن النمــوذج مــع طول الحوض ومعاملات الشكل الأخرى لاستخراج عامل التباطؤ lag time (أو زمن الاستجابة) الخاص بالحوض ومن ثم لاستخراج وقت تدفق الذروة Peak flow time . والإضافة إلى ذلــك فإن شكل وحدة الهيدروجراف يمكن تعريفها بشكل أعمق عن طريق تطوير علاقات محليــة بــين تدفق الذروة لكل وحدة مساحية وبين عرض width مخطط وحدة الهيدروجراف (UH) عند ٥٠% وكذلك ٧٥% والتي تمثل نسبة مئوية من ذروة التدفق أو التصريف.

تبين من خلال العرض السابق لطريقة سنايدر وجود قيود هامة على تطبيق هــذه الطريقــة والتي أغفلها بعض الباحثين وأول هذه القيود هي وجود حوض تم قياسه من قبل (حوض مقــاس) gaged basin ومشابه في الخصائص الشكلية والطبيعية للحوض غيــر المقــاس ungaged basin والمراد تطبيق طريقة سنايدر عليه ونقل معاملات الحوض المقاس إليه ولابــد أن يكــون الحوضان المقاس وغير المقاس هدف الدراسة متشابهان بالشكل الكافي لنقل قيم عــاملا الــ ct والــ cp من أحدهما للآخر ومن أهم محددات هذا التشابه: التشابه الجيولــوجي والطبــوغرافي، والتربة وأنماط التصريف، والمساحة، والغطاء الأرضي. وفي ظل غياب مثل هذه المحــددات فــلا يمكن التأكد من ملاءمة نقل المعاملات المذكورة من الحوض المقاس إلى الحوض غير المقاس.

أما أهم البيانات المطلوبة لإيجاد أو استخراج معاملات ســنايدر ct و cp لحــوض مقــاس فتتضمن سجلات العواصف ومخططات الفيضان ومعلومات عن الحــوض كالمســاحة (A) وطــول المجرى (Lb) وقيمة Lca وهي طول المجرى الرئيسي من المصب أو المخرج وحتى نقطة تقابل مركز ثقل الحوض (centroid) ومن ثم لنقل وحدة الهيدروجراف للحوض الآخر (غير المقــاس) يجب قياس وتحديد كل من المساحة (A) وطول المجرى الرئيسي (Lb) بالإضافة إلى قيمــة Lca للحوض غير المقاس وكان سنايدر قد أطلق عليها معلم شــكل الحــوض watershed shape parameter وحسب ما جاء به مــاكوين ١٩٨٨مــن جامعــة مريلانــد (McCuen, ١٩٩٨, p.٥٤٠)

وفيما يلي عرض للمعادلات الأصلية التي استخدمها سنايدر في اشتقاق وحدة الهيدروجراف.

أ) حساب زمن التبــاطؤ أو الاســتجابة: TL أو t_p ويحســب مــن المعادلــة التاليــة : (Snyder,١٩٣٨)

من المعادلة (٤) $$Tlag = Ct(L \times Lca)^{٠.٣}$$

حيث أن :

Tlag = زمن التباطؤ القياسي لسنايدر بالساعات (hr).

Ct = معامل التباطؤ ويعتمد على خصائص الحوض ويتراوح بين ١.٨ – ٢.٢ حسب اعتقاد سنايدر.

L = طول المجرى الرئيسي من مخرج الحوض إلى حدود الحوض العليا (miles)

Lca = معلم شكل الحوض وهو (طول المجرى الرئيسي من المصب وحتى نقطة تقابل مركز جاذبية (ثقل) الحوض .

(ب) الفترة الزمنية والتي يتم تحديدها (حسابها) من المعادلة التجريبية التالية:

المعادلة (٥) $Td = Tlag/5.5$

(جـ) الفترة المحسوبة بالمعادلة (٢) قد لا تعطي نتيجتها الفترة الزمنية المطلوبة ولذلك استبدلها سنايدر بالمعادلة التالية لحساب الفترة البديلة التي يختارها الباحث أو تم خلالها سقوط أمطار محددة .

المعادلة (٦) $Tlag\ alt = Tlag + 0.25(Tda - Td)$.

حيث أن: Tlag alt = هي زمن التباطؤ البديل الذي قدمه سنايدر.

Td = هي الفترة المحسوبة من المعادلة (٢)

Tda = هي فترة جديدة يختارها المستخدم.

(د) حساب زمن الذروة T_p فهو كما في طريقة ScS حيث أن زمن الذروة يساوي زمن التباطؤ + نصف الفترة وتحسب من المعادلة التالية :

المعادلة (٧)

$$T_p = \frac{Td}{2} + Tlag$$

أو $T_p = Tlag + 0.5\ T_d$

حيث أن : T_p = زمن الوصول للذروة.

Td = زمن الفترة .

Tlag= زمن التباطؤ (الاستجابة).

(هــ) تصريف الذروة لوحدة الهيدروجراف يتم حسابه من المعادلة التالية :

المعادلة (٨)
$$Qp = \frac{640 \times A \times Cp}{Tlag}$$

حيث أن : Qp= تصريف الذروة (ft^3/sec)

Cp= معامل جريان الذروة، ويعتمد على خصائص الحوض ويتراوح بين ٠.٧-٠.٥

Tlag= التباطؤ القياسي لسنايدر (hr)

A = مساحة الحوض (ميل مربع).

وحتى هذه المرحلة فقد سمحت لنا طريقة سنايدر بحساب الفترة duration وزمن التبــاطؤ the lag time وزمن الوصول للذروة the time to peak وجريان الــذروة the peak flow لوحدة الهيدروجراف. إلا أن هذه الطريقة لم تقدم رسماً لوحدة الهيدروجراف ولا القاعدة الزمنيــة time base . وقدمت فقط قمة (ذروة) التصريف خلال وقت محدد بدون تحديد معالم شكل منحنى الهيدروجراف ومن ثم قدم سنايدر طريقته لحساب القاعدة الزمنية (زمن الأساس للسيل) .

(و) حساب زمن الأساس للسيل ويحسب من المعادلة التالية:

المعادلة (٩)
$$Tbase = 3 + \frac{Tlag}{8}$$

حيث أن: Tbase القاعدة الزمنية (زمن الأساس للسيل) بالأيام للأحواض الكبيرة ومن ثم فهو لا يناسب الأحواض الصغيرة حيث أن المعادلة السابقة تشير إلى أن أقل قاعدة زمنية تســاوي ٣ أيام. وكقاعدة عامة يمكن احتساب القاعدة الزمنية من ٣ – ٥ أضعاف زمن الوصول للــذروة ، فإذا كان زمن الذروة يساوي ٣ ساعات فإن القاعدة الزمنية تتراوح بين ٩ – ١٥ ســاعة. ومــن المفيد تحديد معامل الضرب (٣-٥ أضعاف) من خلال مقارنات لنتائج معروفة . أما شــكل رسـم وحدة هيدروجراف سنايدر فإن أكثر الطرق شيوعاً لرسمه فتتم بواسطة تحكم معلمين زمنيين وهما : W_{50} و W_{75} وهما يشكلان السعة الزمنية لوحدة الهيدروجراف عند تصريف ٥٠٪ و ٧٥٪ من قمة (ذروة) التصريف وتحسب بالمعادلتين التاليتين:

المعادلة (١٠) $W_{٥٠} = ٧٥٦ qa^{-١.٠٨١}$

والمعادلة (١١) $W_{٧٥} = ٤٥٠ qa^{-١.٠٨١}$

حيث أن : qa = تصريف الذروة لكل ميــل مربــع ($qa/A,\ ft^{3}/sec/m^{2}i$) أو التصــريف النوعي وكقاعدة عامة يمكن رسم شكل الهيدروجراف بالبعدين من المعادلتين السابقتين، بحيث أن الثلث يحدث قبل الوصول للقمة (للذروة) والثلثين يحدثان بعدها (McCuen,١٩٩٨) ومــن ثــم يمكن رسم الشكل مع اعتبار أنه لابد من ضمان وجود ١ بوصة أو وحدة جريــان تحــت وحــدة الهيدروجراف النهائي.

٢ - التعديلات على طريقة سنايدر:

سبقت الإشارة إلى أن وحدات القياس التي استخدمها سنايدر كانت الميــل المربــع والقــدم المكعب والانش إضافة إلى القيمة النموذجية التي يراها مناسبة لكل من الــ Ct والتي تتراوح بين ١.٨ – ٢.٢ والــ Cp والتي تتراوح بين ٠.٥ – ٠.٧ وكانت هذه الوحدات والقيم مــن شــروط سنايدر لتطبيق طريقته. إلا أن استخدام وحدات القياس المترية وانتشارها عالمياً دفع الباحثين إلى التحويل من نظام الوحدات الانكليزية إلى نظام الوحدات المترية ومن هؤلاء راميرز Ramirez من جامعة كلورادو و زنجبويو Zhongboyo ١٩٨٨ من جامعة نيقادا وشو وآخرون Chow et al ١٩٨٨م وسلاح المهندسين في الجيش الأمريكي وراجوناث Raghunath ٢٠٠٦م. مــن معهــد مانيبال في الهند،وسوف يتم الأخذبالتعديلات الأخيرة (لتفاصيل التعــديلات انظــر : البــارودي ، ٢٠١٢)

٣ - الدراسات السابقة:

اعتمدت الدراسات المهتمة بتقدير أحجام السيول ومدى خطورتها أو مساهمتها في مشاريع إقامة السدود، والتنمية على الطرق اليدوية في إجراء القياســات الخاصــة بــأحواض التصــريف المائي، وهو ما كان يستوجب الكثير من الجهد والوقت، كما تطلب استخدام عــدد مــن معــاملات الجريان التي تعد ضرورية في حساب الجريان من المتوسطات السنوية للأمطــار . وبــديلاً عــن الطرق اليدوية في الدراسة المورفومترية لشبكات التصريف المــائي فقــد تطــورت البرمجيــات الحاسوبية وانتشر تطبيقها في الآونة الأخيرة في مجال الدراسات التي تناولت اشتقاق واستخلاص شبكات التصريف السطحي من المعالجة الآلية لبيانات وصور الأقمار الصناعية، أو الاعتماد علــى

نماذج الارتفاعات الرقمية Dem وتوظيف نظم المعلومات الجغرافية GIS في الدراسات الهيدرومورفومترية. ولعل أهمها في هذا المجال:

- دراسة الغامدي ٢٠٠٤ لاستخلاص شبكة التصريف السطحي للمياه باستعمال المعالجة الآلية لبيانات صور الأقمار الصناعية في منطقة جبال نعمان بحوض وادي نعمان وخلصت الدراسة إلى أن المعالجة الآلية كانت أفضل بكثير من الطرق التقليدية وأنها حل بديل ناجح للقصور في الطرق التقليدية.
- دراسة الجعيدي ٢٠٠٥ حول استخدام صور الاستشعار عن بُعد الرقمية عالية الوضوح المكاني لتحديد امتداد فيضانات السيول في سهل الخرج جنوب شرق مدينة الرياض، واستطاعت هذه الدراسة توضيح امتداد الفيضان وتحديده والمناطق المعرضة للغمر بالمياه، كما اتضح من الدراسة وجود عدد من المعوقات الاصطناعية التي صرفت مياه السيول لتغمر شمال منطقة البحث.
- دراسة الغامدي ٢٠٠٦ حول توظيف نظم المعلومات في استخراج بعض القياسات المورفومترية من نماذج الارتفاعات الرقمية لحوض وادي ذرى (من الروافد المهمة لوادي الليث). وقد توصل الباحث إلى أن نماذج الارتفاعات الرقمية هي بديل ناجح للأساليب التقليدية المعتمدة على استخدام الخرائط الطبوغرافية سواء في استخلاص شبكات التصريف أو القياسات المورفومترية عموماً.
- دراسة الروسان والقرالة ٢٠٠٧ حول استخدام نظم المعلومات الجغرافية في دراسة خصائص حوض وادي شعيب في الأردن وقد هدفت الدراسة إلى استخلاص شبكة التصريف من خلال الطريقة الآلية المعتمدة على نموذج الارتفاعات الرقمية ومقارنتها بالوسائل الأخرى. وأظهرت الدراسة وجود تباين بين الطريقة الآلية والطرق الأخرى التقليدية وذلك في مجمل الخصائص المورفومترية إضافة إلى توفير الجهد والوقت.
- وقد تناولت دراسة الحربي ١٤٢٨ النمذجة الآلية لحوض وادي ملكان باستخدام نظم المعلومات الجغرافية ونماذج الارتفاعات الرقمية وقد أوصت الدراسة بضرورة بناء كود برمجي يستطيع حساب وتقييم جميع المتغيرات والمؤشرات لأحواض التصريف عوضاً عن التنقل بين البرامج المختلفة ومحاولة إيجاد صيغة تكاملية بينها بدلاً من ضياع الكثير من الوقت في تعلمها كما أوصت الدراسة بضرورة الاتجاه نحو استخدام التقنيات الحديثة والبعد عن نمط الدراسات التقليدية نظراً للمنافع التي تقدمها هذه التقنيات للباحثين .
- أما دراسة الحواس ١٤٢٨ فقد وظف فيها تقنيات الاستشعار عن بعد ونظم المعلومات الجغرافية لتحديد وتحليل الخصائص الهيدروموفومترية لأحواض التصريف الصحراوية كما

اعتمد على نموذج الارتفاعات الرقمي مع مجموعة من البرامج التقنية الأخرى في التحليل الهيدرومورفومتري.

أما في مجال الدراسات المورفوهيدرولوجية فقد تعددت في المملكة والمنطقة العربية مستخدمة العديد من النماذج والطرق الكمية في تقدير الجريان السطحي، إلا أنها غالباً ما تكون مناسبة للمناطق المعتدلة التي وضعت لها هذه النماذج وليس للمناطق الجافة. وقد بدأت بعض الدراسات بتطبيق نموذج سنايدر Snyder's Model المناسب أكثر من غيره للمناقط الصحراوية التي لا تتوفر فيها محطات قياس هيدرومترية ويعتمد على الخصائص المورفومترية والطبيعية للأحواض المائية ، إلا أن معظم هذه الدراسات قد اعتمدت في استخراج الخصائص المورفومترية للأحواض على الطرق التقليدية.

وعلى الرغم من استخدام هذا النموذج منذ عهد مبكر في أمريكا وبعض مناطق العالم الأخرى لتقدير تصريف الذروة للسيول the peak discharge، وزمن تباطؤ السيل lag time ورسم المخططات المائية (الهيدروجراف hydrograph) للتنبؤ بالسيول، إلا أن تطبيقه قد تأخر كثيراً في المنطقة العربية ومنها المملكة العربية السعودية، نظراً لاستخدامه الوحدات الإنكليزية والتي لا تتماشي مع الوحدات المترية المستخدمة في منطقتنا حتى تم تعديله على يد عدد من الباحثين مؤخراً وأهمهم راجوناث ١٩٩١ Raghunath وراميرز ٢٠٠٠ Ramirez.

- **وتعد دراسة الصبياني Subyani والبيومي ٢٠٠١ Bayumi حول الخصائص الهيدرولوجية والطبيعية لحوض وادي يلملم في منطقة جنوب مدينة مكة المكرمة من أوائل تلك الدراسات التي تعرضت لنموذج سنايدر Snyder's Model بعد أن قسمت الحوض إلى ثلاث أحواض فرعية، وقدمت قيماً افتراضية للنموذج نظراً لغياب كل من البيانات الهيدرولوجية للحوض ومحطات قياس المطر. كما قدمت ثلاث مخططات مائية للأحواض الفرعية وآخر للحوض الرئيسي الا أنها رسمت بطريقة SCS.**

ولعل من أهم الدراسات وأكثرها شهرة وانتشاراً ما قام به بوروبه من دراسات حول تقدير أحجام الجريان لعدد من الأودية في كل من الجزائر والمملكة العربية السعودية ومن أهم هذه الدراسات.

- **دراسة بوروبه ٢٠٠٧ حول تقدير حجم سيول وادي عتود في جنوب غرب المملكة، بعدما تعرض الوادي لسيلين كبيرين بتاريخ ١٩٨٢/١/١٤ و١٩٨٣/١/١٥. وقد استخدم في بحثه نموذج سنايدر لحساب تدفق الذروة الأقصى والأوسط والأدنى وحساب عدد من الخصائص الهيدرولوجية الأخرى مع تحديد التباينات الزمانية والمكانية لخصائص سيول الروافد الرئيسية للحوض. ونظراً لعدم تحديد القيمة المناسبة لمعاملات تدفق الذروة Peak**

(ct) flow factor وزمن تدفق الــذروة (cp) Time of peak flow فقــد اتصــفت الدراسة بالاحتمالية النظرية التي لا تستطيع تحديد قيم محددة يمكن فيها تقــدير مخــاطر السيول والتنبؤ بها.

- دراسة الجعيدي وبوروبه ٢٠٠٧ حول تقدير تدفق الذروة للسيول بحــوض وادي العــين بمحافظة الخرج باستخدام نموذج سنايدر اعتماداً على المتغيرات المورفومترية المستخلصة من صور القمر الصناعي سبوت ٥-Spot (٥متر) وتحليلها باستخدام نظــم المعلومــات الجغرافية، وقدمت الدراسة القيم القصوى والوسطى والدنيا لتدفق الذروة وأحجام الجريان، وهذه الدراسة كسابقتها لم تحدد القيم المناسبة لمعاملي الــ ct والــ cp التي يمكن علــى أساسها تحديد القيم الأقرب إلى الواقع للتنبؤ بخصائص السيول.
- دراسة الجعيدي ٢٠٠٨ عن الخصائص الهيدرومورفومترية وخصائص السيول في أحواض السدود المقترحة على أودية العين وماوان في محافظة الخرج. وقد خلصت الدراسة إلــى نتائج تقدير تدفق الذروة القصوى والوسطى والدنيا للواديين المــذكورين بالإضــافة إلــى حساب القيم ذاتها لبقية عناصر نموذج سنايدر، وعلى الرغم من أوجه الشبه المنهجية مع الدراسة السابقة إلا أنها أضافت مجموعــة مــن التوصــيات الهامــة حــول الخصــائص الهيدرولوجية لهذين الواديين نظراً لارتباطها بإقامة سدود مقترحة عليهما.
- دراسة فريد Fred ومصطفى Mostafa ٢٠٠٨ حول نمذجة مخاطر الفيضــان للمواقــع المقدسة في مكة المكرمة (وادي عرنة) وقد اعتمدت الدراسة على نموذج ارتفاعات رقمي مبني على ترقيم للخرائط الكنتورية وقد وتوصلت الدراسة التــي تمــت باســتخدام نظــم المعلومات الجغرافية في تحليل أكبر عاصفة مطرية بشدة ٣٠ملم/ ساعة وموزعــة علــى كامل الحوض ولفترة ساعة زمنية واحدة إلى أن تصريف الذروة يصل الى نقطة القيــاس عند بداية عرفات بعد ١٢ ساعة من بداية العاصفة وبحجم جريان يصل أقصاه ٥٠٠م³/ثا . وقد أغفلت الدراسة الفاقد أثناء الجريان المعتمد على كل من مســاحة القطــاع العرضــي للمجرى والخواص الطبيعية للرواسب الفتاتية ومن ثم معدل التسرب. وقد أوصت الدراسة باعتماد نموذج ارتفاعات رقمي دقيق وأخذ الفاقد أثناء الجريان بعــين الاعتبــار فــي أي دراسة مستقبلية.

- أما دراسة علاجي ٢٠١٠ حول تطبيق نظم المعلومات الجغرافية في بناء قاعــدة بيانــات للخصائص المورفومترية ومدلولاتها الهيدرولوجية في حوض وادي يلملم . وقد أظهــرت الدراسة مدى الارتباط بين الخصائص المورفومترية وبعض المتغيرات الهيدرولوجية كمــا توصلت الدراسة إلى أن الشكل الكمثري للحوض والاستطالة التي يتميز بها تقلل من احتمال حدوث الفيضان في أدنى الحوض كما أوصت الدراسة بالتحول إلــى اعتمــاد الخصــائص

المورفومترية للوصول إلى المدلولات الهيدرولوجية فـي ظـل غيـاب محطـات القيـاس الهيدرومترية وضرورة تنظيم التدفق في الأحواض التي ترتفع فيهـا احتمـالات حـدوث الفيضان.

- بينما أشارت دراسة مدخلي ٢٠١٠ حول مخاطر السيول بحوض وادي بيش بمنطقة جازان والتي اعتمدت فيها على نظام الارتفاعات الرقمي ونظم المعلومات الجغرافية إلى أن السيول الخطرة جداً يمكنها أن تتكرر مره واحدة كل عشرين عاماً كما تتعدد المخاطر السيلية في حوض وادي بيش لتشمل بعض الآثار السلبية المباشرة أو غير المباشرة والخسائر المادية والاقتصادية والتنموية . كما أوصت الدراسة بإنشاء محطات لقياس الجريان السطحي على طول حوض وادي بيش ، وبجعل مخططات المساكن العمرانية بعيدة عن مناطق الخطر ألسيلي .
- أما دراسة النفيعي ٢٠١٠ حول تقدير الجريان السطحي ومخاطره السيلية في الحوض الأعلى لوادي عرنة باستخدام تقنيتي الاستشعار ونظم المعلومات الجغرافية فقد أشارت إلى إن خصائص الحوض الطبيعية والبشرية قد أسهمت في رفع قيم الاصمات في الحوض وذلك بعد استخدام نموذج الأرقام المنحنية للجريان .كما أشارت إلى أنه من خلال تطبيق نموذج مخطط قمة التصريف أمكن تحديد الأماكن الأكثر عرضة لمخاطر السيول ، حيث بلغت قمة التصريف ٤٠٩٦ م^{٣}/ ثا وأوصت الدراسة بضرورة إنشاء محطات مطرية في الحوض لبناء قاعدة بيانات تفصيلية تساهم في تطوير الدراسات المناخية والهيدرولوجية ، كما أوصت الدراسة بالحد من التوسع العمراني في بعض أودية الحوض وإنشاء قنوات لتصريف مياه السيول في الأحياء السكنية التي نشأت في الحوض .

يبدو بعد العرض الموجز للدراسات السابقة التي استعانت بنموذج سنايدر Snyder's Model أن هناك عدة مآخذ على معظمها ويمكن تلخيصها في النقاط التالية:

- عدم اعتماد ها قيم محددة لكل من معاملي الــ ct والــ cp من أحواض مجاورة و مشابهة للأحواض المدروسة وهو ما أدى إلى قيم نظرية بحتة .
- استخدامها للحد الأدنى لزمن الأساس للسيل Tbوهو ٣ أيام دون تعديل لــيلائم الأحــواض الصغيرة.
- لم يظهر في تلك الدراسات حساب زمن الوصول للذروة Tp وهو الأمر الذي سيؤدي إلــى عدم تحديد دقيق لزمن الأساس للسيل وأيضاً إلى عدم دقة تحديد النقطة الحمراء التي تمثل زمن الوصول لذروة التصريف وهو ما يجعل حدوث الفيضان أسرع من الواقع.

وقد استدركت دراسة البارودي ٢٠١٢ لحوض وادي عرنة المآخذ السابقة في تطبيق نموذج سنايدر وهدفت الى تقدير أحجام السيول ومدى خطورتها عند المجرى الأدنى لوادي عرنة من خلال تطبيق نموذج سنايدر وتوصلت الى النتائج التالية :

١- أشارت نتائج قياس العاصفة المطرية في ٢٠١٠/٢/١٣ وقياس خصائص السيل الناجم عنها إلى إمكانية تحديد معاملي تدفق الذروة ct وزمن تدفق الذروة cp .وهو ما أتاح الفرصة لتحديد جميع القيم الأخرى في نموذج سنايدر الذي يشترط الحصول على قيمة هذين المعاملين من حوض مجاور أو قياسهما من عاصفة مطرية ، ومن ثم يمكن القول بأن تصريف الذروة الأقصى للسيول في حوض وادى عرنة ٥٠٠.٧م^{٣}/ ثا ، بتدفق نوعي قدره ٠.٨٨م^{٣}/ثا/ كم^{٢} ، وبحجم جريان سطحي قدره ٥٥.٤٧ مليون متر مكعب وبعمق جريان سطحي قدره ٩٨ملم.

٢- أظهرت القياسات الميدانية للسيل ارتفاعه إلى ١,٦ م ، وهو ارتفاع يقل ٠,٢٥ م فقط عن عارضة الجسور القديمة فوق المجرى وهو ما يمثل خطورة كبيرة في حال ارتفاع السيل ووصوله إلى عوارض هذه الجسور.

ثالثا – طريقة العمل :

شملت طريقة العمل كل مكن جمع بيانات البحث وطريقة معالجتها ، ويكن ايجاز ذلك على النحو التالي :

أ – جمع بيانات البحث : وقد اشتملت على خرائط طبوغرافية مقياس ١ :٥٠٠٠٠ ومقياس ١: ٢٥٠٠٠٠ لمربع مكة المكرمة ، وخريطة مكة الجيولوجية مقياس ١:٢٥٠٠٠٠ ،وبيانات الامطار السنوية واليومية ، ونموذج الارتفاعات الرقمية ASTER DEM .ويعد هذا النموذج من أهم البيانات التي تم الاعتماد عليها في هذا البحث ،وقد تم تطوير نموذج الارتفاعات الرقمية ASTER كتعاون مشترك بين وزارة الاقتصاد و التجارة والصناعة اليابانية METI ووكالة الفضاء الأمريكية NASA . وقد تم بناءه من قياسات القمر الصناعي المحمل بجهاز الراديومتر الانعكاسي الحراري المتقدم المحمول فضائيا ، والذي تم تصميمه و بناءه في اليابان ، وأطلق على احدى المركبات الفضائية الأمريكية في شهر ديسمبر من عام ١٩٩٩م كجزء من البرنامج العالمي لمراقبة التغيرات البيئية علي سطح الأرض . و تتعدد التطبيقات التي يخدمها نموذج ASTER لتشمل عدد من المجالات منها علي سبيل المثال: استخراج أحواض المجاري المائية ، و الفوالق الطبيعية ، واستنباط خرائط لتأثير الكوارث الطبيعية مثل الفيضانات والبراكين ، وإدارة الموارد المائية ، و دراسات استكشاف الموارد الطبيعية مثل النفط ، و تطوير الخرائط الهندسية لتمثيل تضاريس سطح الأرض ، والدراسات الجيولوجية و البيئية.

بدأ تجميع بيانات نموذج ASTER منذ عام ٢٠٠٠م و حتي الآن ، وفي ٢٩ يونيه من عام ٢٠٠٩م تم إطلاق النسخة الأولي من نموذج الارتفاعات الرقمية العالمي ASTER . و يغطي النموذج مناطق اليابسة في العالم بين دائرة عرض ٨٣ درجة شمالا و دائرة عرض ٨٣ درجة جنوبا من خلال ملفات يبلغ عددها ٢٢٦٠٠ ملف. أما مجال التغطية لنموذج ASTER فهوأكبر من مثيله نموذج الارتفاعات الرقمية الأمريكي SRTM الذي يغطي فقط المنطقة من ٥٦ درجة جنوبا إلي ٦٠ درجة شمالا. وقد أعد كل ملف من ملفات ASTER علي شبكة الانترنت – بصيغة GeoTIFF وهو يغطي منطقة تمتد ١ درجة من خطوط الطول و ١ درجة من دوائر العرض – أي يحتوي ٣٦٠١ خلية – و بقدرة تمييز مكانية Resolution تبلغ ١ ثانية أو ٣٠ متر تقريبا. هذه القدرة التمييزية العالية تجعل نموذج ASTER أفضل من أي نموذج آخر من نماذج الارتفاعات الرقمية العالمية المتاحة والتي لا تقل قدرتها التمييزية عن ٣ ثانية أو ٩٠ متر تقريبا (ASTER, ٢٠١٠).

ب – معالجة بيانات البحث :

تم اتباع الخطوات التالية في المعالجة :

١- تم تجهيز نموذج الارتفاعات الرقمية ASTER لمنطقة الدراسة من خلال الموقع السابق عن طريق تحديد احداثيات المنطقة أو باستخدام Shape File مجهز مسبقاً بحيث يكون نظام احداثياته معرف .
٢- تم نقل صورة الـــ DEM الى برنامج Global Mapper لاقتطاع منطقة الدراسة منها حسب خطوط الطول والعرض أو لدمج ملفين DEM من الموقع السابق والاقتطاع منهم معاً حيث يعطي الموقع السابق ملف واحد لكل منطقة ابعادها درجة * درجة وتصديره بصيغة Arc ASCII Grid لاستخدامه في برنامج Arc GIS .
٣-تم استخدام هذا النموذج الصادر الى برنامج Arc GIS والبدء بتطبيق خطوات اشتقاق المجرى.
٤-تحديد نظام الاحداثيات في بيئة العمل في Arc GIS .
٥-البدء بخطوات التحليل المكاني باستخدام أدوات Hydrology من Spatial Analyst Tools . وفي البداية يتم التأكد من أن الـــ DEM لا يحتوي نتؤات أومنخفضات pits / depression غير حقيقية من الممكن أن تؤثر علي جودة تمثيل المجاري المائية ، حيث أنه أثناء معالجة خرائط الارتفاعات الرقمية فإن هذه البرامج تفترض أن كل خلية (Pixel) تؤدي إلى خلية مجاورة لها حتى يتم الوصول إلى مخرج الحوض المائي Outlet والذي يجمع جميع الخلايا ولكن وجود هذه المنخفضات أو الحفر أو النتوءات والشذوذات سوف يؤدي إلى انقطاع المجرى المائي وعدم اتصاله مع ما هو أسفل منه. و يتم ذلك باستخدام الأمر Fill من قائمة Hydrology في صندوق

الأدوات. هذا الأمر يحسن من تمثيل ملف الارتفاعات الرقمية للمجرى المائي فيقوم بزيادة قيمة الخلايا الموجودة في الحفر والمنخفضات أو ينقصها في النتوءات والشذوذات بطريقة علمية تطبيقية تعطي نتائج دقيقة ، وفي حالة استخدام هذا الأمر فإن Arc GIS سوف يقوم بإنشاء ملف ارتفاعات جديد معدل خالي من الشذوذات .(شكل ٧)

٦-تم استخدام أمر حساب اتجاه الجريان Flow Direction من قائمة Hydrology والذي يقوم بحساب اتجاه الجريان في كل خلية من خلايا نموذج الارتفاعات الرقمية لخلق اتجاه جريان من الراستر من كل خلية إلى أعمق انحدار مجاور لها وذلك حسب طريقة D٨ حيث يحيط بكل خلية ثمان خلايا تأخذ ثماني قيم توازي الاتجاهات الأساسية والثانوية (شكل ٨).

٧-تم استخدام أمر حساب الجريان التراكمي Flow Accumulation أو تجميعات الجريان من قائمة Hydrology ، في هذه الخطوة يكون الملف المدخل هو ملف اتجاه الجريان والذي تم إنشاؤه في الخطوة السابقة . وفي هذا الأمر يقوم البرنامج بإنشاء ملف شبكي بالاعتماد علي اتجاه الجريان المحسوب لكل خلية من الخطوة السابقة ، وكل خلية في هذا الملف تحتوي على قيمة معينة ، وتمثل هذه القيم عدد الخلايا التي تعلو هذه الخلية وتصب (تتجمع) فيها ، ونتيجة لهذه الخطوة يكون الناتج صورة عامة للمجاري المائية في منطقة الدراسة (شكل ٩) .

٨- تم استخدام الأمر Times من قائمة Math من Spatial Analyst Tools لتحويل الملف الناتج من الخطوة السابقة الى ملف تعبر قيمه عن مساحة التصريف لكل من خلايا الــ DEM وذلك عن طريق ضرب قيمة كل خلية ناتجة من الخطوة السابقة في أبعاد هذه الخلية وهي في ASTER ٣٠ * ٣٠ .

٩- تم استخدام الأمر Log١٠ من قائمة Math لتحويل مساحة التصريف من الخطوة السابقة الى Log١٠ m٢ (شكل ١٠) .

١٠- تم استخدام الأمر Con من Conditional من Spatial Analyst Tools لتحديد قيمة التحسس التي ينتج عنها مجاري تصريف .حيث أنه كلما قلت قيمة معامل التحسس زادت تفاصيل المجاري المائية التي يمكن استنباطها للمنطقة والعكس بالعكس ، ويتم ذلك باستخدام الملف من الخطوة السابقة ، و ينتج لدينا شبكة تصريف الحوض على شكل راستر (شكل ١١) .

١١- تم ترتيب واستخراج المجاري المائية بصورة أكثر تفصيلا بالاعتماد علي الصورة العامة الناتجة من الخطوة السابقة. وذلك باستخدام أمر رُتب المجاري المائية Stream Orders من Hydrology ، في هذه الخطوة تم الاعتماد على نموذج Strahler في طريقة تصنيف رتب مجاري الأودية .

١٢- تم تحويل رتب المجاري المائية من الصيغة الخلوية أو الشبكية Raster والتي نتجت من الخطوة السابقة إلى الصيغة الخطية Vector لسهولة التعامل معها سواء في التمثيل الخرائطي أو

إجراء التعديلات أوللقيام بمزيد من الحسابات عليها ، وذلك من خلال الأمر Stream to Feature من Hydrology (شكل ٥).

١٣- تم تحديد نقطة Outlet للحوض المائي عن طريق انشاء Shape File في برنامج Arc Catalog من نوع Point وتحديد نظام الإحداثيات المتبع . وتحديد مكان النقطة بواسطة Sketch tool على المجرى المائي . وتعمل هذه النقطة على تحديد حدود الحوض المائي المغذي للمجرى عندها ، وهذه النقطة غالباً ما تكون في الدراسات الهيدرولوجية عبارة عن موقع سد ، أوطريق سريع أو أي نشاط بشري أو نهاية مجرى وادي معين .

١٤- تم استخراج حدود الحوض المغذي لهذه النقطة وهي عبارة عن منطقة محددة من المنطقة الكلية التي يغطيها نموذج الارتفاعات الرقمية ، من خلال الأمر Watershed من Hydrology .

١٥- تم تحويل الحوض المستخرج من صيغة Raster إلى مضلع Polygon (في الصيغة الخطية) لسهولة التعامل معه لاحقاً ، من خلال الأمر Raster to Polygon من قائمة أدوات Conversion Tools من From Raster ، وهكذا تكون منطقة حوضي الدراسة قد حددت.

١٦- ولاقتطاع المجاري المائية التي تقع فقط بداخل الحوض المستخرج من الخطوة السابقة تم استخدام الأمر Clip والمدخلات في هذه الخطوة هي الحوض بصيغة polygon من الخطوة السابقة مع رتب المجاري بالصيغة الخطية والتي نتجت من الخطوة (١٢) .

١٧- بعد أن أصبحت لدينا هذه الملفات من حدود أحواض ورتب مجاري نهرية أمكن بعد ذلك تطبيق أي طريقة من طرق القياس المتعددة في برنامج Arc GIS لحساب طول المجرى الرئيسي ، تحديد مركز ثقل الاحواض ، تحديد الرتب النهرية ، حساب مساحة الاحواض ، انحدار المجاري ، وانحدار الاحواض ... الخ ، اضافة الى العديد من الخرائط ومنها خرائط مظللة Shaded Relief (شكل ١٢) ، وخريطة انحدار Slope Map (شكل ١٣) ، وخريطة اتجاه المنحدرات Aspect (شكل ١٤) وذلك من خلال البيانات المتوفرة في الملفات التي ذكرت في الخطوات السابقة .

رابعا :تقدير تصريف السيول في حوض وادي نعمان (سد الجامعة):

تبين من خلال عرض طريقة أو نموذج سنايدر Snyder's Model أنها الطريقة المناسبة لتقدير تدفق السيول في منطقة البحث نظراً لكونها تعتمد على بيانات الأحواض ، وهي البيانات المتوفرة عادة للمناطق الجافة وغيرها من المناطق التي تفتقر إلى بيانات مسجلة عن الجريان أو العواصف المطرية.

ولتطبيق نموذج سنايدر لابد من المرور بخمسة مراحل أساسية لاشتقاق وحدة الهيدروجراف وتتلخص بحساب زمن التباطؤ أو زمن الاستجابة للحوض المائي TL أو tp،

وتصريف الذروة Qp، وزمن الأساس للسيل (القاعدة الزمنية) Tb، والفترة المثالية (القياسـية) لهطول الأمطار Td أو tr، وحساب الفترة الزمنية W٥٠ و W٧٥ المناسبة لعرض الهيدروجراف عند مستوى ٪٥٠ و ٪٧٥ من تدفق أو تصريف الذروة.

وقد اتبع الباحث في هذا البحث النموذج المعدل من قبل راجونـات Raghunath,١٩٩١ نظراً لسهولته واعتماده الوحدات المتريـة، واعتبـاره الأكثـر تطبيقـاً فـي المملكـة العربيـة السعودية(Raghunath, ٢٠٠٦) ، كما سيتم الاستعانة أيضاً بالآراء الأخرى ذات العلاقـة فـي بعض الحالات (الجعيدي و بوربه، ١٤٢٨) وخاصة فيما يتعلق بعدد من الخصائص الهيدرولوجيـة المتعلقة كحساب حجم السيول ومعامل قوتها وعمق الجريان.

وكان راجونات Raghunath قد أعطى قيماً مناسبة لعاملي الـ ct والـ cp تراوحت بين ٠.٢ و ٢.٢ للأول و ٢ و ٦.٥ للثاني.وهي قيم تشمل جميع نماذج الأحواض النهرية ، وفيما يلي عرض لتطبيق هذا النموذج مع الأخذ بعين الاعتبار بعض متغيرات أحواض منطقة البحث :

١- حساب زمن إستجابة الاحواض المائية لهطول الأمطار(مقاس بالساعات) للوصول الى ذروة التصريف (التدفق)tp أو T_Lعند سنايدر، ويعرف أيضا بزمن التباطؤ Lag Time (hr) لانه يمثل الفترة الزمنية الفاصلة بين ذروة هطول الامطار وذروة التدفق ويطلق عليه زمن الاستجابة الأولي ، ويستخرج ذلك من خلال تطبيق المعادلة التالية:
(Raghunath, ٢٠٠٦)

$$t_p\,(hr) = Ct\,(L_b\; L_{ca})^{0.3}$$

المعادلة (١٢)

حيث أن:

L_b: طول المجرى الرئيس (كلم).

L_{ca} : المسافة الفاصلة بين مصب الحوض المائي ومركز ثقله (كلم).

tp (hr) : فترة إستجابة الحوض المائي لهطول الأمطار (ساعات).

Ct : معامل زمن تدفق الذروة Peak Flow Time Factor أو معامل التباطؤ وهو خاص بطبيعة الحوض وإنحداره وتتراوح قيمته بين ٠.٢ و ٢.٢.

وادي نعمان (سد الجامعة)		
Ct	**tp**	**tr**
٠.٢	١.٥٨٦٧٤٧	٠.٢٨٨٥
٠.٤	٣.١٧٣٤٩٥	٠.٥٧٦٩٩٩
٠.٦	٤.٧٦٠٢٤٢	٠.٨٦٥٤٩٩
٠.٨	٦.٣٤٦٩٩	١.١٥٣٩٩٨
١	٧.٩٣٣٧٣٧	١.٤٤٢٤٩٨
١.٢	٩.٥٢٠٤٨٤	١.٧٣٠٩٩٧
١.٤	١١.١٠٧٢٣	٢.٠١٩٤٩٧
١.٦	١٢.٦٩٣٩٨	٢.٣٠٧٩٩٦
١.٨	١٤.٢٨٠٧٣	٢.٥٩٦٤٩٦
٢	١٥.٨٦٧٤٧	٢.٨٨٤٩٩٥
٢.٢	١٧.٤٥٤٢٢	٣.١٧٣٤٩٥
Min	١.٥٩	٠.٢٩
Max	١٧.٤٥	٣.١٧
Mean	٩.٥٢	١.٧٣

(جدول ٤) فترة الأستجابة فى حوض وادى نعمان و الفترة القياسية للأمطار (ساعة)

ويمثل الجدول ٤ فترة استجابة حوض وادي نعمان (سد الجامعة) لهطول الأمطار والتي تراوحت بين ١٧.٤٥ و١.٦ . ويتضح من خلال الجدول أيضا أنه كلما زادت قيمة ال Ct زاد زمن استجابة الحوض للوصول الى ذروة التدفق (tp) ، لأن هذه الزيادة تعني قلة الانحدار وزيادة الازمنة الاخرى، بينما قلتها تعني زيادة الانحدار وبالتالي تناقص القيم الزمنية الاخرى .

٢- حساب الفترة الزمنية القياسية standard duration لتمثيل ذروة هطول الأمطار (ساعات tr (أو T_d عند سنايدر) وذلك بتطبيق المعادلة التالية:المعادلة (١٣)

$$t_r(hr) = \frac{t_p(hr)}{5.5}$$

(Raghunath, ٢٠٠٦)

حيث أن:

t_p (hr) : زمن إستجابة الحوض المائي لهطول الأمطار(ساعات) المحسوبة من المعادلة (١٢).

t_r (hr) : الفترة الزمنية القياسية لتمثيل ذروة هطول الأمطار (ساعات)، وتعرف بالفترة الأولية.

وتستخدم هذه المعادلة عندما تكون فترة هطول الأمطار t_r(hr) لا تتجاوز زمن استجابة الحوض المائي **tp**. ولقد تم تطبيق هذه المعادلة لحساب قيمة الفترة الزمنية المثالية لتمثيل ذروة هطول الأمطار (ساعات) t_r (hr) نظرا لطبيعة الأمطار التي تتساقط في منطقة البحث على شكل عواصف مطرية كثيفة وقصيرة وقد لاتتعدى ساعة أو بضع ساعات.

ويشيرالجدول ٤ حساب الفترة الزمنية **duration**القياسية **standard** لتمثيل ذروة هطول الأمطار (ساعات) t_r(hr) في حوض وادي نعمان (سد الجامعة) والتي تراوحت بين ٣.١٧ و ٠.٢٩ ساعة . ويتضح من خلال الجدول أيضا أنه كلما زادت قيمة t_r(hr) زاد زمن استجابة الحوض، وكلما زاد الاخير زادت قيمة ال **Ct** ومن ثم مع زيادة الفترة t_r(hr) تزداد قيمة ال **Ct** او مايسمى معامل التباطؤ .

أما في حال ما إذاكانت الفترة المثالية لهطول الأمطار (الفترة الأولية) أقل من ساعة أو عدة ساعات، أو لتوحيد هذه الفترة مع فترة وحدة الهيدروجراف وأيضاً إذا كانت هناك فترة فعلية للأمطار يتم اختيارها من قبل المستخدم أو فترة مسجلة فيمكن عندها تطبيق المعادلة رقم (٦) وذلك بهدف تعديل الفترة الأولية إلى الفترة البديلة، و من ثم تعديل زمن الاستجابة الأولي إلى زمن الاستجابة البديل، أو زمن الوصول إلى الذروة والذي يمكن حسابه عن طريق زمن الاستجابة البديل مضافاً إليه نصف الفترة البديلة وذلك حسب المعادلة (٧).

٣- حساب كمية تدفق الذروة للسيول بنموذج سنايدر**Snyder** بتطبيق المعادلةالتالية (Raghunath, ٢٠٠٦) المعادلة(١٤):

$$Qp\,(m^3/s) = \frac{Cp\ A}{tp\ (hr)} \quad -٤$$

حيث أن:

Q_p : كمية التدفق الأقصى للسيول بالحوض المائي (م^3/ ثانية).

A : مساحة الحوض المائي (كلم^2).

C_p : معامل تدفق الذروة **Peak Flow Factor** و يرتبط بقابلية الحوض المائي لتخزين المياه وله علاقة بالنفاذية وتتراوح قيمته بين ٢.٠ و ٦.٥.

tp (hr) : فترة إستجابة الحوض المائي لهطول الأمطار (ساعة)

ويتناسب هذا النموذج مع العواصف المطرية التي بإمكانها أن تتسبب في حدوث جريان سطحي بعمق (سمك) لا يقل عن ٢٥- ٢٦ ملم (ما يعادل ١ بوصة)

	Ct			Cp			
		٢	٣	٤	٥	٦	٦.٥
Min	٠.٢	٨٦٣.٥٣	١٢٩٥	١٧٢٧.١	٢١٥٩	٢٥٩١	٢٨٠٦
٧٩	٠.٤	٤٣١.٧٦	٦٤٧.٦	٨٦٣.٥٣	١٠٧٩	١٢٩٥	١٤٠٣
Max	٠.٦	٢٨٧.٨٤	٤٣١.٨	٥٧٥.٦٨	٧١٩.٦	٨٦٣.٥	٩٣٥
٢٨٠٦	٠.٨	٢١٥.٨٨	٣٢٣.٨	٤٣١.٧٦	٥٣٩.٧	٦٤٧.٦	٧٠٢
Mean	١	١٧٢.٧١	٢٥٩.١	٣٤٥.٤١	٤٣١.٨	٥١٨.١	٥٦١
٥٢٤	١.٢	١٤٣.٩٢	٢١٥.٩	٢٨٧.٨٤	٣٥٩.٨	٤٣١.٨	٤٦٨
	١.٤	١٢٣.٣٦	١٨٥	٢٤٦.٧٢	٣٠٨.٤	٣٧٠.١	٤٠١
	١.٦	١٠٧.٩٤	١٦١.٩	٢١٥.٨٨	٢٦٩.٩	٣٢٣.٨	٣٥١
	١.٨	٩٥.٩٤٧	١٤٣.٩	١٩١.٨٩	٢٣٩.٩	٢٨٧.٨	٣١٢
	٢	٨٦.٣٥٣	١٢٩.٥	١٧٢.٧١	٢١٥.٩	٢٥٩.١	٢٨١
	٢.٢	٧٨.٥٠٢	١١٧.٨	١٥٧	١٩٦.٣	٢٣٥.٥	٢٥٥

(جدول ٥) كمية تدفق الذروة لحوض وادى نعمان (م^{3})

ويمثل الجدول ٥ كمية التدفق الأقصى للسيول بحوض وادي نعمان عند نقطة سد الجامعة ، ويتضح من خلاله أن أقصى تصريف يصل ٢٨٠٦م٣/ ث، ويصل أدنى تصريف إلى حوالي ٧٩م٣/ ث. وهو تفاوت يصل إلى أكثر من ٣٥ مرة بين القيمتين، الأمر الذي يجعل من عملية تحديد القيم الحقيقية لمعاملي الـــ Ct والـــ Cp أمراً حتمياً وذلك للوصول إلى تقدير أقرب إلى واقع الحال في الحوض بناء على خصائصهما الطبيعية، بينما نجد أن الواقع النظري يفيد بزيادة التصريف كلما زادت قيمة الـــ Cp وقلت قيمة الـــ Ct وسيتم مناقشة هذا الموضوع بعد استكمال عرض النموذج.

٥-حساب زمن الأساس للسيل (القاعدة الزمنية للهيدروجراف أو زمن السيل) (يوم) (days) Time base في نموذج سنايدر بتطبيق المعادلة التالية: (Raghunath, ٢٠٠٦)

المعادلة (١٥)

$$T_b\ (days) = 3 + \frac{t_p\ (hr)}{8}$$

حيث أن:

T_b(days) : زمن الأساس للسيل (يوم).وقد حددها سنايدر بثلاثة ايام للأحواض الكبيرة ، وبالامكان معايرة ذلك للاحواض الصغيرة على أساس أن القاعدة الزمنية (زمن الاساس) تساوي ٣-٥ أضعاف زمن الذروة ،وتتحول من أيام الى ساعات .أو مقارنتها بنتائج لاحواض معروفة .

t_p(hr) : فترة إستجابة الحوض المائي لهطول الأمطار(ساعات) المحسوبة من المعادلة (١٢)

Ct	Tb day	Tb Hours
٠.٢	٣.١٩٨٣٤٣	٦.٣٤٦٩٩
٠.٤	٣.٣٩٦٦٨٧	١٢.٦٩٣٩٨
٠.٦	٣.٥٩٥٠٣	١٩.٠٤٠٩٧
٠.٨	٣.٧٩٣٣٧٤	٢٥.٣٨٧٩٦
١	٣.٩٩١٧١٧	٣١.٧٣٤٩٥
١.٢	٤.١٩٠٠٦١	٣٨.٠٨١٩٤
١.٤	٤.٣٨٨٤٠٤	٤٤.٤٢٨٩٣
١.٦	٤.٥٨٦٧٤٧	٥٠.٧٧٥٩٢
١.٨	٤.٧٨٥٠٩١	٥٧.١٢٢٩١
٢	٤.٩٨٣٤٣٤	٦٣.٤٦٩٩
٢.٢	٥.١٨١٧٧٨	٦٩.٨١٦٨٩
Min	٣.٢٠	٦.٣٥
Max	٥.١٨	٦٩.٨٢
Mean	٤.١٩	٣٨.٠٨

(جدول ٦) زمن الأساس للسيل في وادي نعمان(يوم – ساعة)

ويتضح من الجدول ٦ أنه كلما زادت قيمة الـــ tp (زمن الاستجابة) زادت قيمة زمن الأساس للسيل Tb ومن ثم فإنه كلما زادت قيمة الـــ Ct (معامل التباطؤ) زادت قيمة زمن الأساس للسيل، وكما يبدو واضحاً من الجدول فإن أقصى وأدنى قيمة لزمن الأساس تتراوح بين ٣-٥ أيام وهو ما لا يتفق مع أحواض المنطقة ومن ثم تم استبدال ذلك حسب سنايدر بضرب زمن الوصول للذروة برقم ٤ وذلك من خلال المعادلة التالية والتي تتناسب وسعة الأحواض الصغيرة:

المعادلة (١٦) **Tb hr = Tp*٤**

حيث أن :

Tb hr : زمن الأساس للسيل (يوم).

Tp : زمن الوصول للذروة

ويتضح من الجدول ٦ أن أقصى وأدنى قيمة لزمن الأساس تراوحت بين ٦ و ٧٠ ساعة ، وهو ما سيؤثر بالتالي على قيم فترة الارتفاع التدريجي للسيل .

٥- حساب فترة الارتفاع التدريجي لتدفق السيل $T_m(hr)$ بتطبيق المعادلة التالية:

المعادلة (١٧)   (Raghunath, ٢٠٠٦)

$$T_m\ (hr) = \frac{1}{3} T_b\ (hr)$$

حيث أن:

$T_m(hr)$: فترة الإرتفاع التدريجي لتدفق السيل (ساعات) وهي الفترة الزمنية الممتدة من بداية جريان السيل إلى فترة ذروته على الهيدروغراف .

$T_b(hr)$: زمن الأساس (القاعدة) (ساعات) و يتم تقديره بواسطة المعادلة (١٥).

نعمان (سد الجامعة)		
Ct	Tm hour	Tm hour
٠.٢	٢٥.٥٨٦٧٥	٢.١١٥٦٦٣
٠.٤	٢٧.١٧٣٤٩	٤.٢٣١٣٢٦
٠.٦	٢٨.٧٦٠٢٤	٦.٣٤٦٩٩
٠.٨	٣٠.٣٤٦٩٩	٨.٤٦٢٦٥٣
١	٣١.٩٣٣٧٤	١٠.٥٧٨٣٢
١.٢	٣٣.٥٢٠٤٨	١٢.٦٩٣٩٨
١.٤	٣٥.١٠٧٢٣	١٤.٨٠٩٦٤
١.٦	٣٦.٦٩٣٩٨	١٦.٩٢٥٣١
١.٨	٣٨.٢٨٠٧٣	١٩.٠٤٠٩٧
٢	٣٩.٨٦٧٤٧	٢١.١٥٦٦٣
٢.٢	٤١.٤٥٤٢٢	٢٣.٢٧٢٣
Min	٢٥.٥٩	٢.١٢
Max	٤١.٤٥	٢٣.٢٧
Mean	٣٣.٥٢	١٢.٦٩

(جدول ٧) فترة الارتفاع التدريجى لتدفق السيل في وادي نعمان (يوم- ساعة)

ويلاحظ من الجدول ٧ أنه كلما زادت قيمة معامل التباطؤ Ct زادت فترة الارتفاع التدريجي للوصول إلى ذروة التدفق، وبما أن زمن الارتفاع التدريجي للسيل محسوب من القاعدة الزمنية (زمن الأساس) التي لا يقل حدها الأولي عن ثلاثة أيام فقد أثر ذلك على القيمة العظمى والدنيا لزمن الارتفاع التدريجي لتدفق السيل والتي تراوحت بين ٤١ و ٢٥ ساعة ومن ثم تم حساب الارتفاع التدريجي لتدفق السيل اعتماداً على زمن الأساس للسيل بالساعات حسب المعادلة التالية:

المعادلة (١٨) **Tm hours = Tb hr /٣**

وهو ما أدى الى تناقص القيمة العظمى والدنيا لزمن الارتفاع التدريجي لتدفق السيل الى ١٢ و٢ ساعة فقط .

٦- حساب فترة الإنخفاض التدريجي لتدفق السيل (ساعات) T_d(hr) بتطبيق المعادلة التالية:

المعادلة (١٩)

$$T_d\,(hr) = \frac{2}{3} T_b\,(hr)$$ **(Raghunath,٢٠٠٦)**

حيث أن:

T_d (hr):فترة الإنخفاض التدريجي لتدفق السيل (ساعات) وهي الفترة الزمنية الممتدة من ذروة التدفق إلى نهايته على الهيدروغراف.

T_b (hr): زمن الأساس (القاعدة) (ساعات) وقد يتم تقديره بواسطة المعادلة (١٥).

نعمان (سد الجامعة)			
Ct	Td hour	Td hour	i
٠.٢	٥١.١٧٣٤٩	٤.٢٣١٣٢٦	٣.٤٦٦٢١
٠.٤	٥٤.٣٤٦٩٩	٨.٤٦٢٦٥٣	١.٧٣٣١٠٥
٠.٦	٥٧.٥٢٠٤٨	١٢.٦٩٣٩٨	١.١٥٥٤٠٣
٠.٨	٦٠.٦٩٣٩٨	١٦.٩٢٥٣١	٠.٨٦٦٥٥٣
١	٦٣.٨٦٧٤٧	٢١.١٥٦٦٣	٠.٦٩٣٢٤٢
١.٢	٦٧.٠٤٠٩٧	٢٥.٣٨٧٩٦	٠.٥٧٧٧٠٢
١.٤	٧٠.٢١٤٤٦	٢٩.٦١٩٢٨	٠.٤٩٥١٧٣

١.٦	٧٣.٣٨٧٩٦	٣٣.٨٥٠٦١	٠.٤٣٣٢٧٦
١.٨	٧٦.٥٦١٤٥	٣٨.٠٨١٩٤	٠.٣٨٥١٣٤
٢	٧٩.٧٣٤٩٥	٤٢.٣١٣٢٦	٠.٣٤٦٦٢١
٢.٢	٨٢.٩٠٨٤٤	٤٦.٥٤٤٥٩	٠.٣١٥١١
Min	٥١.١٧	٤.٢٣	٠.٣١
Max	٨٢.٩١	٤٦.٥٤	٣.٤٦
Mean	٦٧.٠٤	٢٥.٣٩	١.٨٩

(جدول ٨) فترة الأنخفاض التدريجى لتدفق السيل (يوم – ساعة) و تركيز الأمطار المناسبة لتدفق الذروة في وادي نعمان.

ويلاحظ أيضاً من الجدول ٨ نفس الملاحظة السابقة عن زمن الارتفاع التدريجي للسيل وهو زيادة هذه المدة الزمنية نظراً لحسابها أيضاً كما في الأحواض الكبيرة، وبما أنها أيضاً محسوبة من زمن الأساس للسيل فقد بدت أكبر من قيمتها والتي تراوحت بين ٨٢ و ٥١ ساعة . ومع احتساب زمن الأساس للسيل بالساعات تبين من خلال الجدول ٨ المنتج منها قصر الفترة الزمنية للانخفاض التدريجي لتدفق السيل لتتراوح بين٤٦ و٤ ساعات.

ويستنتج أيضاً مما سبق أنه كلما زادت قيمة معامل التباطؤ Ct زادت فترة الانخفاض التدريجي لتدفق السيل. ويمكن استنتاج أن علاقة معامل التباطؤ Ct في الأحواض علاقة طردية مع جميع قيم الزمن أي بزيادته يزداد زمن استجابة الأحواض للوصول إلى ذروة التدفق tp كما تزداد الفترة المثالية (القياسية) لهطول الأمطار tr وزمن الأساس للسيل Tb إضافة إلى ارتفاع زمني ارتفاع السيل Tm وانخفاض السيل Td

٧- حساب قيمة تدفق الذروة النوعي للحوض المائي ($q_p(m^3/s/km^2)$ بتطبيق المعادلة التالية:

المعادلة (٢٠) **(Raghunath,٢٠٠٦)**

$$q_p\ (m^3/s/km^2) = \frac{Q_p\ (m^3/s)}{A\ (km^2)}$$

حيث أن:

$A(km^2)$: مساحة الحوض المائي (كلم٢).

$Q_p(m^3/s)$: قيمة تدفق الذروة للسيل (م٣/ثانية) المحسوب من المعادلة (١٤).

	Ct			Cp			
		٢	٣	٤	٥	٦	٦.٥
Min	٠.٢	١.٢٦٠٤	١.٨٩٠٦٦	٢.٥٢٠٨٨	٣.١٥١١	٣.٧٨١٣٢	٤.٠٩٦٤٣
٠	٠.٤	٠.٦٣٠٢	٠.٩٤٥٣٣	١.٢٦٠٤٤	١.٥٧٥٥٥	١.٨٩٠٦٦	٢.٠٤٨٢١٥
Max	٠.٦	٠.٤٢٠١	٠.٦٣٠٢٢	٠.٨٤٠٢٩٣	١.٠٥٠٣٦٧	١.٢٦٠٤٤	١.٣٦٥٤٧٧
٤	٠.٨	٠.٣١٥١	٠.٤٧٢٦٦٥	٠.٦٣٠٢٢	٠.٧٨٧٧٧٥	٠.٩٤٥٣٣	١.٠٢٤١٠٨
Mean	١	٠.٢٥٢١	٠.٣٧٨١٣٢	٠.٥٠٤١٧٦	٠.٦٣٠٢٢	٠.٧٥٦٢٦٤	٠.٨١٩٢٨٦
١	١.٢	٠.٢١٠١	٠.٣١٥١١	٠.٤٢٠١٤٧	٠.٥٢٥١٨٣	٠.٦٣٠٢٢	٠.٦٨٢٧٣٨
	١.٤	٠.١٨٠١	٠.٢٧٠٠٩٤	٠.٣٦٠١٢٦	٠.٤٥٠١٥٧	٠.٥٤٠١٨٩	٠.٥٨٥٢٠٤
	١.٦	٠.١٥٧٦	٠.٢٣٦٣٣٣	٠.٣١٥١١	٠.٣٩٣٨٨٨	٠.٤٧٢٦٦٥	٠.٥١٢٠٥٤
	١.٨	٠.١٤	٠.٢١٠٠٧٣	٠.٢٨٠٠٩٨	٠.٣٥٠١٢٢	٠.٤٢٠١٤٧	٠.٤٥٥١٥٩
	٢	٠.١٢٦	٠.١٨٩٠٦٦	٠.٢٥٢٠٨٨	٠.٣١٥١١	٠.٣٧٨١٣٢	٠.٤٠٩٦٤٣
	٢.٢	٠.١١٤٦	٠.١٧١٨٧٨	٠.٢٢٩١٧١	٠.٢٨٦٤٦٤	٠.٣٤٣٧٥٦	٠.٣٧٢٤٠٣

(جدول ٩) قيمة تدفق الذروة النوعى في وادي نعمان (م^{٣} / ثا / كم^{٢})

وتبين من خلال الجدول أن أقصى وأدنى كمية لتدفق الذروة النوعي أقصى وأدنى كمية وصلت ٤ و ٠.١١م٣/ ث/ كم٢ لحوض وادي نعمان

٨- حساب الفترة الزمنية W_{50} و W_{75} المناسبتين لعرض منحنى السيل (الهيدروغراف) عند مستوى ٥٠ % و ٧٥ % على التوالي من تدفق الذروة بتطبيق المعادلتين التاليتين: (Raghunath,٢٠٠٦)

المعادلة (٢١)
$$W_{50}(\mathrm{hr}) = \frac{5.6}{(q_p)^{1.08}}$$

(٢٢)
$$W_{75}(\mathrm{hr}) = \frac{3.21}{(q_p)^{1.08}}$$

حيث أن:

W_{50} (hr) و W_{75} (hr) : الفترة الزمنية المناسبة لقيمة ٥٠ % و ٧٥ % من التدفق الأقصى للسيل (م^{٣}/ثانية).

q_p : تدفق الذروة النوعي للحوض المائي (م^{٣}/ثانية/كلم^{٢}) وقد تم تقديره من المعادلة (٢٠).

	Ct			Cp			
		٢	٣	٤	٥	٦	٦.٥
Min	٠.٢	٤.٣٦١٣٨١	٢.٨١٤٧٨٧	٢.٠٦٣٠٥٩	١.٦٢١٢٤٦	١.٣٣١٤٧٥	١.٢٢١٢٠٩
١	٠.٤	٩.٢٢٠١١٧	٥.٩٥٠٥٦١	٤.٣٦١٣٨١	٣.٤٢٧٣٧٢	٢.٨١٤٧٨٧	٢.٥٨١٦٨
Max	٠.٦	١٤.٢٨٦١٤	٩.٢٢٠١١٧	٦.٧٥٧٧٥٨	٥.٣١٠٥٥٤	٤.٣٦١٣٨١	٤.٠٠٠١٩٣
٥٨	٠.٨	١٩.٤٩١٦٦	١٢.٥٧٩٧	٩.٢٢٠١١٧	٧.٢٤٥٥٨٨	٥.٩٥٠٥٦١	٥.٤٥٧٧٦٥
Mean	١	٢٤.٨٠٣٤٣	١٦.٠٠٧٨٥	١١.٧٣٢٧٤	٩.٢٢٠١١٧	٧.٥٧٢١٧٦	٦.٩٤٥٠٨٦
١٦	١.٢	٣٠.٢٠١٤٢	١٩.٤٩١٦٦	١٤.٢٨٦١٤	١١.٢٢٦٧	٩.٢٢٠١١٧	٨.٤٥٦٥٥٣
	١.٤	٣٥.٦٧٢٢	٢٣.٠٢٢٤٤	١٦.٨٧٣٩٨	١٣.٢٦٠٣٤	١٠.٨٩٠٢٨	٩.٩٨٨٤
	١.٦	٤١.٢٠٦٠٧	٢٦.٥٩٣٩٤	١٩.٤٩١٦٦	١٥.٣١٧٤٣	١٢.٥٧٩٧	١١.٥٣٧٩١
	١.٨	٤٦.٧٩٥٧	٣٠.٢٠١٤٢	٢٢.١٣٥٧٢	١٧.٣٩٥٢٥	١٤.٢٨٦١٤	١٣.١٠٣٠٤
	٢	٥٢.٤٣٥٣٤	٣٣.٨٤١١٨	٢٤.٨٠٣٤٣	١٩.٤٩١٦٦	١٦.٠٠٧٨٥	١٤.٦٨٢١٦
	٢.٢	٥٨.١٢٠٣٤	٣٧.٥١٠٢٢	٢٧.٤٩٢٦	٢١.٦٠٤٩٣	١٧.٧٤٣٤١	١٦.٢٧٣٩٩

(جدول ١٠) الفترة الزمنية W٥٠ المناسبة لعرض منحنى السيل فى وادى نعمان.

ويظهر من خلال الجدول ١٠ أن أدنى فترة زمنية مناسبة لعرض منحنى السيل أو الهيدروجراف عند مستوى ٥٠% من تدفق الذروة وصلت ٢،١ ساعة لوادي نعمان ، بينما وصلت أقصى فترة زمنية مناسبة لعرض منحنى السيل عند نفس المستوى ٥٨ ساعة.

	Ct			Cp			
		٢	٣	٤	٥	٦	٦.٥
Min	٠.٢	٢.٥٠٠٠٠٦	١.٦١٣٤٧٦	١.١٨٢٥٧٥	٠.٩٢٩٣٢١	٠.٧٦٣٢٢١	٠.٧٠٠٠١٤
١	٠.٤	٥.٢٨٥١٠٣	٣.٤١٠٩٤٦	٢.٥٠٠٠٠٦	١.٩٦٤٦١٩	١.٦١٣٤٧٦	١.٤٧٩٨٥٦
Max	٠.٦	٨.١٨٩٠٢٢	٥.٢٨٥١٠٣	٣.٨٧٣٦٤٣	٣.٠٤٤٠٨٥	٢.٥٠٠٠٠٦	٢.٢٩٢٩٦٨
٣٣	٠.٨	١١.١٧٢٩	٧.٢١٠٨٦٤	٥.٢٨٥١٠٣	٤.١٥٣٢٧٥	٣.٤١٠٩٤٦	٣.١٢٨٤٦٩
Mean	١	١٤.٢١٧٦٨	٩.١٧٥٩٣	٦.٧٢٥٣٧١	٥.٢٨٥١٠٣	٤.٣٤٠٤٧٩	٣.٩٨١٠٢٣
٩	١.٢	١٧.٣١١٨٩	١١.١٧٢٩	٨.١٨٩٠٢٢	٦.٤٣٥٣٠٦	٥.٢٨٥١٠٣	٤.٨٤٧٤١٧
	١.٤	٢٠.٤٤٧٨٢	١٣.١٩٦٧٩	٩.٦٧٢٤٠٧	٧.٦٠١٠١٧	٦.٢٤٢٤٦٣	٥.٧٢٥٤٩٣
	١.٦	٢٣.٦١٩٩١	١٥.٢٤٤٠٣	١١.١٧٢٩	٨.٧٨٠١٧٢	٧.٢١٠٨٦٤	٦.٦١٣٦٩٦
	١.٨	٢٦.٨٢٣٩٦	١٧.٣١١٨٩	١٢.٦٨٨٥١	٩.٩٧١٢٠٨	٨.١٨٩٠٢٢	٧.٥١٠٨٤٧

	٢	٣٠.٠٥٦٦٨	١٩.٣٩٨٢٥	١٤.٢١٧٦٨	١١.١٧٢٩	٩.١٧٥٩٣	٨.٤١٦٠٢٥
	٢.٢	٣٣.٣١٥٤١	٢١.٥٠١٣٩	١٥.٧٥٩١٥	١٢.٣٨٤٢٦	١٠.١٧٠٧٨	٩.٣٢٨٤٨٥

(جدول ١١) الفترة الزمنية ٧٥ W المناسبة لعرض منحنى السيل فى حوض وادى نعمان.

بينما أظهر الجدول١١أن أدنى فترة زمنية مناسبة لعرض منحنى السيل أو الهيدروجراف عند مستوى ٧٥% من تدفق الذروة وصلت ٠.٧٠ ساعة ، بينما وصلت أقصى فترة زمنية مناسبة لعرض منحنى السيل عند نفس المستوى ٣٣ ساعة لوادي نعمان.

٩- حساب تركيز الأمطار المناسبة لتدفق الذروة بتطبيق المعادلة التالية: (Raghunath,٢٠٠٦)

المعادلة (٢٣)

$$i\,(cm/hr) = \frac{1}{t_r\ (hr)}$$

حيث أن:

i (cm/hr) : تركيز (كثافة) الأمطار في الزمن (سم/ ساعة).

t_r (hr) : الفترة الزمنية القياسية لهطول الأمطار (ساعات) وقد تم تقديرها بواسطة المعادلة (١٣).

وتبين من خلال الجدول ٨ أن أدنى تركيز (كثافة) أمطار مناسبة لتدفق الذروة وصلت ٠.٣١ سم/ ساعة في حوض وادي نعمان ، بينما وصل أقصى تركيز للأمطار مناسب لتدفق الذروة ٣.٤٦ سم / ساعة في الحوض. ويمكن استخلاص العلاقة بين قيمة الفترة الزمنية للأمطار tr وقيمة تركيز أو كثافة الأمطار i بأن العلاقة عكسية بينهما ، أي إذا زادت قيمة tr ومعها أيضاً فترة وحدة الهيدرجراف قلت قيمة التركيز للأمطار i والعكس صحيح أيضاً ، فاذا قلت وحدة الهيدروجراف زاد تركيز الأمطار وهو ما يعني أن علاقة تركيز الأمطار بعامل التباطؤ Ct علاقة عسكية أيضاً.

١٠- حساب حجم السيل بتطبيق المعادلة الآتية: (PNUD-OPE,١٩٨٧)

المعادلة (٢٤)

$$AL\,(Hm^3)\,(10^6 m^3) = Q_p\ (m^3/s)\left[T_m\ (sec.)10^{-6}\right]$$

حيث أن:

(Hm^3) ($10^6 m^3$) AL: حجم التدفق للسيل على مستوى الحوض المائي (مليون م^3).

Q_p (m^3/s) : التدفق الأقصى للسيل (م^3/ثانية) وقد تم تقديره من المعادلة (١٤).

T_m (hr) : فترة الارتفاع التدريجي لتدفق السيل (ساعات) وقد تم تقديرها من المعادلة (١٧).

	Ct			Cp			
		٢	٣	٤	٥	٦	٦.٥
Min	٠.٢	٧٩.٥٤	١١٩.٣١	١٥٩.٠٨	١٩٨.٨٥	٢٣٨.٦٢	٢٥٨.٥١
١٢	٠.٤	٤٢.٢٤	٦٣.٣٦	٨٤.٤٧	١٠٥.٥٩	١٢٦.٧١	١٣٧.٢٧
Max	٠.٦	٢٩.٨٠	٤٤.٧٠	٥٩.٦٠	٧٤.٥١	٨٩.٤١	٩٦.٨٦
٢٥٩	٠.٨	٢٣.٥٨	٣٥.٣٨	٤٧.١٧	٥٨.٩٦	٧٠.٧٥	٧٦.٦٥
Mean	١	١٩.٨٥	٢٩.٧٨	٣٩.٧١	٤٩.٦٤	٥٩.٥٦	٦٤.٥٣
٥٦	١.٢	١٧.٣٧	٢٦.٠٥	٣٤.٧٤	٤٣.٤٢	٥٢.١٠	٥٦.٤٤
	١.٤	١٥.٥٩	٢٣.٣٩	٣١.١٨	٣٨.٩٨	٤٦.٧٧	٥٠.٦٧
	١.٦	١٤.٢٦	٢١.٣٩	٢٨.٥٢	٣٥.٦٥	٤٢.٧٨	٤٦.٣٤
	١.٨	١٣.٢٢	١٩.٨٣	٢٦.٤٥	٣٣.٠٦	٣٩.٦٧	٤٢.٩٧
	٢	١٢.٣٩	١٨.٥٩	٢٤.٧٩	٣٠.٩٨	٣٧.١٨	٤٠.٢٨
	٢.٢	١١.٧٢	١٧.٥٧	٢٣.٤٣	٢٩.٢٩	٣٥.١٥	٣٨.٠٧

(جدول ١٢) أحجام السيول فى وادى نعمان .

ويظهر من الجدول ١٢ أن أدنى حجم للسيول في حوض وادي نعمان وصل ١١.٧ مليون / م٣ ، بينما قدر الحجم الأقصى للسيول في الحوض ٢٥٨ مليون / م٣ .

١١- حساب سمك (عمق) الجريان السطحي المناسب لذروة تدفق السيل بإستخدام المعادلة التالية:

المعادلة (٢٥) $$E(mm) = Q_p max\ (m^3/s) \left[(T_m(sec.) \times 10^{-3})\ (S^{-1}(km^2) \right]$$

حيث أن:

E (mm): عمق (سمك) الجريان السطحي (ملم).

T_m (sec.) : فترة الإرتفاع التدريجي لتدفق السيل (ثانية) وقد تم تقديره من المعادلة (١٧).

	Ct			Cp			
		٢	٣	٤	٥	٦	٦.٥
Min	٠.٢	١١٦.١٠	١٧٤.١٥	٢٣٢.٢٠	٢٩٠.٢٦	٣٤٨.٣١	٣٧٧.٣٣
١٧	٠.٤	٦١.٦٥	٩٢.٤٨	١٢٣.٣٠	١٥٤.١٣	١٨٤.٩٥	٢٠٠.٣٧
Max	٠.٦	٤٣.٥٠	٦٥.٢٥	٨٧.٠٠	١٠٨.٧٥	١٣٠.٥٠	١٤١.٣٨
٣٧٧	٠.٨	٣٤.٤٣	٥١.٦٤	٦٨.٨٥	٨٦.٠٦	١٠٣.٢٨	١١١.٨٨
Mean	١	٢٨.٩٨	٤٣.٤٧	٥٧.٩٦	٧٢.٤٥	٨٦.٩٤	٩٤.١٩
٨٢	١.٢	٢٥.٣٥	٣٨.٠٣	٥٠.٧٠	٦٣.٣٨	٧٦.٠٥	٨٢.٣٩
	١.٤	٢٢.٧٦	٣٤.١٤	٤٥.٥١	٥٦.٨٩	٦٨.٢٧	٧٣.٩٦
	١.٦	٢٠.٨١	٣١.٢٢	٤١.٦٣	٥٢.٠٣	٦٢.٤٤	٦٧.٦٤
	١.٨	١٩.٣٠	٢٨.٩٥	٣٨.٦٠	٤٨.٢٥	٥٧.٩٠	٦٢.٧٣
	٢	١٨.٠٩	٢٧.١٤	٣٦.١٨	٤٥.٢٣	٥٤.٢٧	٥٨.٧٩
	٢.٢	١٧.١٠	٢٥.٦٥	٣٤.٢٠	٤٢.٧٥	٥١.٣٠	٥٥.٥٨

(جدول ١٣) عمق الجريان السطحى المناسب لذروة تدفق السيل فى وادى نعمان.

ويتبين من الجدول ١٣ أن أقل سمك للجريان السطحي المناسب لذروة تدفق السيول في حوض وادي نعمان يصل ١٧ ملم ، بينما يصل أكبر سمك للجريان في الحوض المذكور ٣٧٧ ملم.

١٢- حساب قوة السيل "A" بتطبيق المعدلة التالية: (Pardé, ١٩٦١).

المعادلة (٢٦)

$$A = \frac{Q_p\,(m^3/s)}{\sqrt{S\,(km^2)}}$$

حيث أن:

$Q_{p\ (m^3/s)}$: تصريف ذروة السيل (م٣/ثانية) وقد تم تقديره من المعادلة (١٤).

S (km٢): مساحة الحوض المائي (كلم٢).

A : معامل قوة السيل.

	Ct			Cp			
		٢	٣	٤	٥	٦	٦.٥
Min	٠.٢	٣٣.٠	٤٩.٥	٦٦.٠	٨٢.٥	٩٩.٠	١٠٧.٢
٣	٠.٤	١٦.٥	٢٤.٧	٣٣.٠	٤١.٢	٤٩.٥	٥٣.٦
Max	٠.٦	١١.٠	١٦.٥	٢٢.٠	٢٧.٥	٣٣.٠	٣٥.٧
١٠٧	٠.٨	٨.٢	١٢.٤	١٦.٥	٢٠.٦	٢٤.٧	٢٦.٨
Mean	١	٦.٦	٩.٩	١٣.٢	١٦.٥	١٩.٨	٢١.٤
٢٠	١.٢	٥.٥	٨.٢	١١.٠	١٣.٧	١٦.٥	١٧.٩
	١.٤	٤.٧	٧.١	٩.٤	١١.٨	١٤.١	١٥.٣
	١.٦	٤.١	٦.٢	٨.٢	١٠.٣	١٢.٤	١٣.٤
	١.٨	٣.٧	٥.٥	٧.٣	٩.٢	١١.٠	١١.٩
	٢	٣.٣	٤.٩	٦.٦	٨.٢	٩.٩	١٠.٧
	٢.٢	٣.٠	٤.٥	٦.٠	٧.٥	٩.٠	٩.٧

جدول ١٤) معامل قوة السيول فى وادى نعمان.

ويظهر من خلال الجدول ١٤ أن أدنى قيمة لمعامل قوة السيول في حوض نعمان ٣ بينما ، بينما وصلت أعلى قيمة للمعامل المذكور ١٠٧ .

وكما هو موضح فإنه بالإمكان تطبيق نموذج سنايدر على أي حوض كان، وفي أي منطقة تفتقر إلى بيانات متيوهيدرولوجية ، إلا أن النتائج المستخرجة ستبقى نظرية بحتة، ولا يمكن الرجوع إليها أو الاعتماد عليها سوى في تحديد الحدود القصوى والوسطى والدنيا لقيم خصائص السيول في هذه الأحواض. وهو ما يعني أن القيم المشتقة من النموذج تبقى رياضية بحتة ، وهو ماتوضحه قيم الجدول التالي :

حوض وادي نعمان (سدالجامعة)			المتغير
Qp Min.	Qp Mean.	Qp Max.	
٢٤	٢٤	٢٤	Lca (Km)
٤١.٥	٤١.٥	٤١.٥	Lb (Km)
٢.٢	١.٢	٠.٢	Ct
٢	٤.٢٥	٦.٥	Cp

tp (hr)	١٧.٤٥	٩.٥٢	١.٥٩
tr (hr)	٣.١٧	١.٧٣	٠.٢٩
Qp (m^3 / S)	٢٨٠٦	٥٢٤	٧٩
Tb(day)	٥.١٨	٤.١٩	٣.٢٠
Tm (hr)	٤١.٤٥	٣٣.٥٢	٢٥.٥٩
Td (hr)	٨٢.٩١	٦٧.٠٤	٥١.١٧
qp (m^3/S/Km^2)	٤.٠٩	١	٠.١١
(hr)W_{50}	٥٨.١	١٦	١.٢
(hr)W_{75}	٣٣.٣١	٩	٠.٧٠
i (cm/hr)	٣.٤٦	١	٠.٣١
AL (10^6 m^3)	٢٥٨.٥١	٥٦	١١.٧٢
E (mm)	٣٧٧.٣	٨٢	١٧.١
“A”	١٠٧	٢٠	٣

(جدول ١٥) القيم الكمية والزمنية لتصريف السيول في حوض نعمان حسب القيم العظمى والوسطى والدنيا لمعاملي ال ct وال cp

حيث بالإمكان اشتقاق جميع الأزمنة المتعلقة بالنموذج من خلال زمن الاستجابة للحوض أو الأحواض tp، وهو المرتبط أساساً بثوابت لا تتغير مثل طول المجرى الرئيسي Lb ومركز ثقل الحوض Lca أو المساحةA، وهو ما يعني الخروج بنتائج تشمل جميع الأنواع المحتملة لخصائص الأحواض المائية، سواء تلك عديمة النفاذية بالمطلق، وحتى تلك ذات النفاذية العالية جداً، وأيضاً من الأحواض شبه المستوية إلى تلك شديدة الانحدار، وهو ما يعطي عشرات من نماذج الأحواض المائية. بحسب قيم معاملات زمن تدفق الذروة (التباطؤ) ct أو تدفق الذروة cp. ومن ثم تبقى القيمة الفعلية لأي تطبيق لهذا النموذج مرهونة بما اشترطه سنايدر نفسه عن نقل بيانات عاملي زمن تدفق الذروة peak flow time factor (ct) أو معامل تدفق الذروة peak flow factor (cp) من حوض مقاس geged basin ومشابه في الخصائص الطبيعية ومجاور للحوض غير المقاس ungaged basin المراد تطبيق النموذج عليه.

وكما سبقت الإشارة إليه في الدراسات السابقة فقد تم الحصول على بيانات حول تقدير حجم الجريان وقيمة زمن الاستجابة والمستخرجة من بيانات مسجلة لعاصفة مطرية في حوض وادي عرنة (البحث ص) ومن ثم أصبح بالإمكان الحصول على قيمة الـ ct والـ cp لحوض وادي

عرنة ممكنة بعد الحصول على قيمة زمن الاستجابة tp ومن ثم نقلها إلى حوض وادي نعمان وتطبيق النموذج على الحوضين.

كما أن القيمتين يمكن معايرتهما أيضاً عند نقلهما إلى حوض وادي نعمان والذي تختلف خصائصه الطبيعية عن وادي عرنة. وللوصول إلى قيم واقعية لعاملي الـ ct و cp لكل من حوض وادي عرنة وحوض وادي نعمان ومن ثم البناء عليها للوصول إلى نتائج مرضية لنموذج سنايدر تجدر العودة إلى التعرف على مميزات الحوضين basin characteristics والمقارنة بينهما.

وبداية نجد أن حوض وادي نعمان يتميز عن حوض وادي عرنة بأنه الأشد انحداراً سواء في مجراه الرئيسي الذي يزيد عن مجرى وادي عرنة، أو في متوسط انحدار الحوض (البحث ص).كما يتبين بالرجوع إلى الجدول ١ تفوق وادي نعمان بجميع الخصائص الطبيعية الأخرى كالارتفاع الأقصى للحوض وطول المجرى (في هذه الحالة هو الأقصر) وغيرها...أما الخصائص الشكلية للحوض فهي الأكثر تفوقاً أيضاً من وادي عرنة، سواء أكان ذلك في معامل الاستدارة Circularity Index أو نسبة الاستطالة Elongation Ratio ومعامل الشكل Factor Form ، الا أن شكله الكمثري وتموضع أحواضه عند المجرى الأعلى له وهو عكس الحال في وادي عرنة الذي تتموضع أحواضه قرب المصب ، فان كل ذلك يدفعنا إلى التقليل من عامل زمن تدفق الذروة (ct) لوادي نعمان إلى ١ وهي القيمة التي حددت لوادي عرنة.

أما بالنسبة لعامل تدفق الذروة (cp) فإن الخصائص المحددة له والمتعلقة بالنفاذية بالدرجة الأولى تجعل وادي نعمان الأعلى قيمة نظراً لخصائصه الجيولوجية المتمثلة بنسبة الصخور غير المنفذة التي تشغل حوضه والتي تزيد عن حوض وادي عرنة بمقدار ١.٣ مرة (البحث ص) ومن ثم فلو أعطينا وادي عرنة قيمة قصوى لعامل (cp) وهي ٦ فإن هذه القيمة يجب أن تتعدى القيمة المعطاة لهذا العامل لوادي نعمان ،الا أنه ولنفس الأسباب المذكورة لتموضع الأحواض الجزئية يمكن الأخذ بالقيم المناسبة لهذين العاملين في الحوض حسب ما ورد في تطبيق نموذج سنايدر أي أن قيمة الـ ct والـ cp لحوض وادي عرنة هي عند ٨،. و ٦ على التوالي،وهي قيم يجب أن تنقل لحوض وادي نعمان للمعاملين حسب نموذج سنايدر. وبناء عليه يمكن تحديد جميع قيم النموذج لرسم هيدروجراف أقرب إلى الواقع ابتداء من زمن استجابة الأحواض tp وحتى تحديد عرض منحنى الهيدروجراف عند مستوى ٥٠% و٧٥% من ذروة التصريف.

ويمكن الآن بعد اعتماد المعاملات المذكورة أعلاه تحديد قيم تطبيق نموذج سنايدر والتي ظهرت نتائجها من خلال الجدول ١٦ الذي يمثل القيم الكمية والفترات الزمنية لتصريف الذروة للسيول في حوض وادي نعمان (سد الجامعة) .

المتغير	حوض وادي نعمان (سدالجامعة)
	Qp Max.
Ct	٠.٨
Cp	٦
tp (hr)	٦.٣٤
tr (hr)	١.١٥
Qp (m^3 / S)	٦٤٧.٦
Tb (hr)	٢٥.٣٨
Tm (hr)	٨.٤٦
Td (hr)	١٦.٩٢
qp (m^3/S/Km^2)	٠.٩٤
(hr)W_{50}	٧
(hr)W_{75}	٤
i (cm/hr)	٠.٨٦
AL (10^6 m^3)	٧٠.٧٥
E (mm)	١٠٣.٢٨
"A"	٢٤.٧

(جدول ١٦) القيم الكمية والزمنية لتصريف الذروة في حوض وادي نعمان بعد تحديد قيمتي ال ct وال cp

خامساً: مناقشة النتائج:

تبين من خلال ما سبق أن الاعتماد على خصائص الأحواض لتقدير الجريان أو اشتقاق الهيدروجراف (المخطط المائي) بدون نقل معاملات ال ct وال cp من أحواض مقاسة الى الحوض هدف البحث قد أعطى قيماً نظرية قد لا يكون لها أي قيمة فعلية في تقدير الجريان للحوض المدروس، نظراً لأن معاملات الـ ct والـ cp إنما تعكس خصائص الحوض المقاس (الانحدار والنفاذية والشكل والمساحة وغيرها....) والتي يجب أن تتشابه مع الحوض غير المقاس

حتى يمكن الوصول إلى تقدير صحيح لهذا الجريان. نظراً إلى أن القيم العظمى التي غالباً ما تظهر عند تطبيق النماذج النظرية إنما تعكس الخصائص الطبيعية للحوض، والتي نشـأت فـي فتـرات مناخية مختلفة تماماً عما هو عليه الحال في الوقت الحاضر. إذ أن الجريان خلال هـذه الفتـرات السابقة هو من قام بنحت أحواض هذه الأودية والتي تعد موروثة عن الماضي.

وإذا ما أخذنا هذه القيم العظمى للتصريف المحسوبة من نماذج نظرية بعين الاعتبار فإنها سوف تتسبب بجريان يملأ جميع أجزاء الوادي بما فيه السهول الفيضية على جانبي المجرى، كما يمكن أن يرتفع السيل إلى مستويات لا معقولة. وهو تماماً ما حدث في الماضي عند نشـأة هـذه الأودية. ومما يؤكد ذلك أن القطاع الجيولوجي للرواسب الفيضية التي تشكل حشوة المجرى تشير إلى عملية تصنيف تبدأ من الجلاميد الكبيرة (أكثر من ٢٥ سم) التي تشكل قاعدة القطاع و تتدرج نحو الأعلى إلى جلاميد أصغر ثم حصباء وحصى وجميعها جيدة الاستدارة، وهو ما يشير إلى تطبق متوازن **Grade bedding** ناجم عن تراجع منتظم للفيضانات التي مرت بالوادي منذ نشأته. كما أن الطبقة العليا التي تفترش سطح المجاري والمكونة من الرمال الخشنة والناعمة غالباً تشير إلى استقرار الفيضانات الحالية عند مستوى منخفض من التصريف (التـدفق)، مقارنـة بالمسـتويات العالية للفيضانات عندما ترسبت الجلاميد في أسفل القطاع.وهكذا نخلص إلى أن القيمـة الحقيقيـة للنماذج التي تعتمد على خصائص الأحواض ومنها نمـوذج سـنايدر **Snyder's model** هـي تطبيقها ضمن الظروف المناخية الحالية ، وبما تتصف به هذه الأحواض من خصـائص طبيعيـة يمكن تقديرها من خلال أحواض مقاسة ومجاورة، مع الاستعانة بالسجلات التاريخيـة للعواصـف المطرية إن وجدت.

وفيما يلي مقارنة لنتائج القيم الكمية والزمنية لتصريف السيول في حـوض وادي نعمـان حسب القيم العظمى والدنيا لمعاملي الـ **ct** والـ **cp** (جدول ١٥) والقيم الكميـة والزمنيـة لتصريف الذروة للسيول في حوض وادي نعمان بعد تحديد قيمتي الـ **ct** والـ **cp** (جدول ١٦).

١- وصل تصريف الذروة الأقصى للسيول في الحوض (جدول ١٥) ٢٨٠٦م³/ ثا ، بتـدفق نوعي قدره ٤.٠٩م³/ثا/كم² ، وبحجم جريان سطحي قدره ٢٥٨مليون متر مكعب ، وبعمق جريان سطحي قدره ٣٧٧ملم.بينما وصل تصريف الذروة الأدنى للسيول في حوض نعمـان ٧٩م³/ثـا ، بتدفق نوعي قدره ٠.١١م³/ثا/كم² ، وبحجم جريان سطحي قدره ١١.٧ مليون متر مكعب ، وبعمق جريان سطحي قدره ١٧ملم.

ويتضح من خلال مقارنة القيم القصوى والدنيا لتصريف ذروة السيول في حوض منطقة البحث أن القيم القصوى تزيد بنسبة ٣٦ مرة عن القيم الدنيا لكل من تصريف الذروة وتصريف الذروة النوعي، كما تزيد القيم القصوى بنسبة ٢٢ مرة عن القيم الدنيا لكل من الحجم الكلي للسيول وعمق الجريان السطحي . وتتفق هذه النتائج مع جميع نتائج دراسات السيول التي اعتمدت تطبيق نموذج سنايدر دون تحديد قيمة معاملي الـ ct والـ cp (بوروبه٢٠٠٧، الجعيدي ٢٠٠٨).

وتبدو القيم القصوى للتصريف المذكورة أعلاه بعيدة جداً عن الواقع وهي بطبيعة الحال تبقى قيم نظرية كما سبقت الإشارة إليه. وهو ما يؤكد ما تم التوصل إليه من أن هذه القيم القصوى للتصريف إنما تعكس القيم الافتراضية لحوض وادي نعمان والمستمدة من خصائص الحوض. والتي لا يمكن الاعتماد عليها أو الأخذ بها لتقدير القيم القصوى لتصريف السيول أو حجمها ومن ثم لتخطيط الجسور أو العبارات أو السدود بناء عليها.

٢- يصل تصريف الذروة الأقصى للسيول في حوض وادي نعمان (جدول ١٦) ٦٤٧.٦م^3/ ثا ، بتدفق نوعي قدره ٠.٩٤م^3/ثا/كم^2 ، وبحجم جريان سطحي قدره ٧٠.٧٥مليون متر مكعب ، وبعمق جريان سطحي قدره ١٠٣.٢٨ملم.وقد تم حساب هذه القيم بعد تحديد معاملي الـ ct والـ cp للحوض وذلك عند ٠.٨ و٦ لحوض وادي نعمان بعد أن تم نقلها من حوض وادي عرنة المجاور.وتبدو هذه القيم أقرب إلى واقع الحال. وخاصة إذا ما قارنا هذه القيم بقيم لأحواض مقاسة في جنوب غرب المملكة كأودية بيش وضمد وجيزان وخلب.

فقد وصل متوسط الحجم الكلي للجريان السنوي بين سنتي ١٩٧٠ و١٩٨٥ إلى ٧٦ و ٤٠ و ٥٧ و ٣٢ مليون متر مكعب للأحواض المذكورة على التوالي .وتزيد مساحات الأحواض السابقة بعدة مرات عن مساحات حوض منطقة البحث ، كما أن متوسط كمية التساقط السنوي تزيد عن حوض منطقة البحث مع العلم أن الحجم الأقصى للجريان خلال جميع السنوات المقاسة لم يتعد ضعف الأرقام المشار إليها (sen,٢٠٠٨).كما تبين من خلال حساب حجم الجريان الكلي الناجم عن التساقط السنوي أنه يتراوح بين ٥ و ١٤% من الحجم الكلي للتساقط .وعلى افتراض تساقط مطري متطرف يصل حتى ٤٠٠ فان الحجم الكلي له سيصل ٢٧٤مليون متر مكعب في حوض وادي نعمان . وبتطبيق نسبة حجم الجريان من حجم التساقط الكلي فإن حجم الجريان يجب ألا يزيد ٤١ مليون متر مكعب في حوض وادي نعمان أي بنسبة ١٥% ، وهي قيم لا تبتعد كثيراً عن النتائج التي تم التوصل إليها من خلال القيم المعطاة لمعاملي الـ ct والـ cp. مع الأخذ بالاعتبار تباين الخصائص الطبيعية للحوضين.

وما يفسر ذلك (إضافة إلى خصائص الحوض) أن العواصف المطرية في حوض منطقة البحث غالباً ما تتجه من المجرى الادنى الى المجرى الاعلى للحوض، ويرى البعض أن القيم سابقة الذكر يمكن أن تنعكس فيما لو اتجهت حركة العواصف المطرية من المجاري العليا نحو المجاري الدنيا (Sen,٢٠٠٨). ويمكن تفسير الحالة الأولى بأن حالة عدم الاستقرار في الأحوال الجوية تزداد ويتجدد نشاطها مع زيادة الارتفاع القهري للكتل الهوائية على السفوح الجبلية شبه القائمة لمنطقة الهدا وهومايؤدي الى زيادة التساقط.

بينما تميل الحالة الجوية للاستقرار أكثر فأكثر في الحالة الثانية، حيث يزداد زمن استجابة الأحواض، كما تزداد الفترة الزمنية للوصول إلى ذروة التصريف، وتقل كميات تصريف الذروة، ويزداد طول القاعدة الزمنية للسيل، حيث أن على المياه الجارية الناجمة عن العاصفة قطع المسافة من الحدود العليا للحوض وحتى الحدود الدنيا له أو نقطة القياس، وهو ما يؤدي إلى شبه تساوي قيمة زمن الاستجابة **tp** مع قيمة زمن التركيز **time of concentration (Tc)**.

ملخص النتائج والتوصيات:

ويمكن تلخيصها بالنقاط التالية:

١- تمت الاستفادة من عملية قياس ميدانية للعاصفة المطرية التي حدثت في٢٠١٠/٢/١٣ ودراسة خصائص السيل الناجم عنها في وادي عرنة ، اضافة الى اشتقاق معاملات الـ **ct** والـ **cp**الهامة لنموذج سنايدر واستعارتها لوادي نعمان ، واعتمادها مستقبلا في دراسة الأحواض المجاورة والمشابهة لحوض وادي عرنة .

٢- تم تقدير قيم تصريف الذروة وحجم السيول اعتماداً على الخصائص المورفومترية والطبيعية للحوض حسب نموذج سنايدر **Snyder Model** وذلك باعتماد قيمة مناسبة لمعاملي الـ **ct** والـ **cp** بحيث تعكس القيم القصوى المرجحة لأية سيول تحدث في مجاري أودية منطقة البحث ، وتبين منها أن تصريف الذروة للسيول يصل ٦٤٧.٦م^{٣}/ثا. بينما يصل الحجم الكلي للسيول ٧٠.٧٥ مليون متر مكعب. أما معامل قوة السيول فقد وصل ٢٤.٧ في وادي منطقة البحث.

٣ – تم بناء على قيم تصريف الذروة لوادي نعمان حساب ارتفاع السيل عند الفتحة التحويلية المجاورة للسد والبالغة ٨٠ مترا اعتمادا على مساحة القطاع العرضي وسرعة الجريان باستخدام طريقة مانتج **manning method** ، وقد تبين منها ارتفاع السيل الى مستوى ٣ أمتار .

٤ – إهمال مناقشة القيم الدنيا لتصريف السيول لعدم أهميتها من الناحية العملية أولا ولأهداف البحث ثانيا ، كما تم إهمال القيم الدنيا لأحجام السيول للأسباب ذاتها.

٥ – تم اشتقاق مخطط مائي (هيدروجراف) لوادي نعمان لحالتين : احداهما لقاعدة زمنية للسيل تساوي اربعة أضعاف زمن الذروة (الحالة رقم ١ ، شكل ١٥) والثانية تساوي ثلاثة أضعاف زمن الذروة (الحالة رقم ٢ شكل ١٦) وكلاهما حسب نموذج سنايدر ن كما يمكن الاعتماد عليهما في التنبؤ بزمن تصريف الذروة للسيول في الوادي وخاصة في حال حدوث عاصفة مطرية ذات شدة محددة إضافة إلى التنبؤ بالزمن الذي تستمر فيه هذه السيول بالجريان.

٦ – تتمثل خطورة سيول منطقة البحث في عدة نقاط يمكن تلخيصها فيما يلي:

أ) أهمها عملية إشغال مجاري الأودية بالأنشطة البشرية (المزارع المسورة سواء بالعقوم الترابية أو الأبنية) وهو ما يؤدي إلى خطر تدمير المنشآت المقامة فيها لوقوعها في مواجهة السيول أولاً، ولدورها في إعاقة سرعة الجريان ثانياً. وهو ما ينجم عنه تباطؤ في تصريف السيول وتجميع للمياه مما يرفع من منسوبها وفيضانها إلى مستويات أكثر ارتفاعاً مما يزيد من مساحة المناطق المتضررة بهذه السيول.

ب) اهمال عملية تنظيف عبارات السيول أو أنفاق الجسور من الرواسب أو مجروفات السيول والتي تؤدي إلى ضيق مساحة القطاع العرضي لهذه العبارات أو الأنفاق (كما لوحظ ذلك أسفل عدد من الجسور وخاصة جسري طريق الخواجات التي تكاد تسد بهذه المجروفات) وهو ما يؤدي إلى قصور في تصريف الماء وارتفاعه إلى مستويات قد تؤدي إلى تدمير هذه الجسور بسبب الفعل الهيدروليكي لمياه هذه السيول كما حدث في عقبة ضلع عندما رفعت مياه السيول جسور المجاري وألقتها على جوانب الوادي في عامي ١٩٨٢ و١٩٨٣.

ت) ليس هناك ما يشير إلى أي خطورة من سيول وادي نعمان على سد الجامعة التحويلي (أشكال ١٧ ، ١٨،١٩) نظراً للمساحة الواسعة للقطاع العرضي له قبل سد الجامعة التحويلي وهو ما يساهم في تخفيض مستوى ارتفاع السيول إلى حدودها الدنيا شريطة استمرار عملية تنظيف وتجريف الرواسب

من أسفل عبارات الجسور المقامة على الوادي ، وتوسعة المجرى الجديد للوادي المجاور للسد لزيادة مساحة القطاع العرضي للمجرى وتخفيض مستوى ارتفاع السيل أمام السد.

شكل (١)

موقع حوض وادي نعمان من مدينة مكة المكرمة

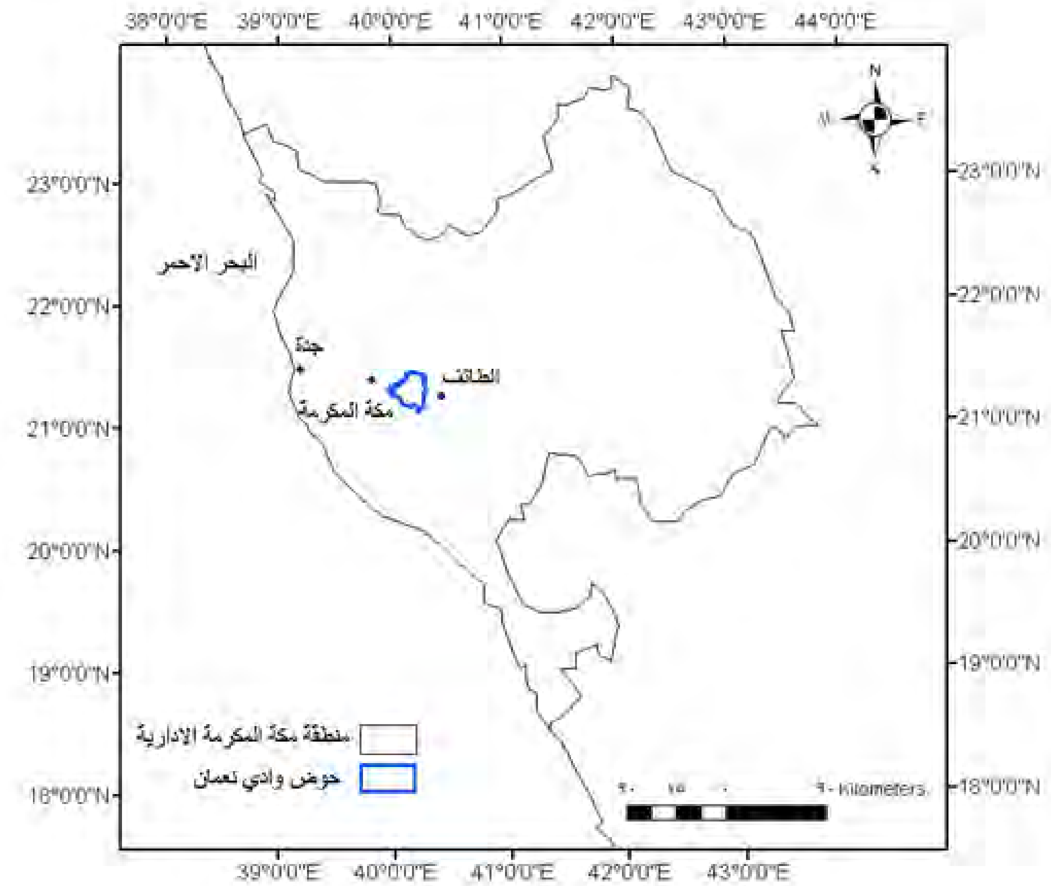

(شكل ٢)

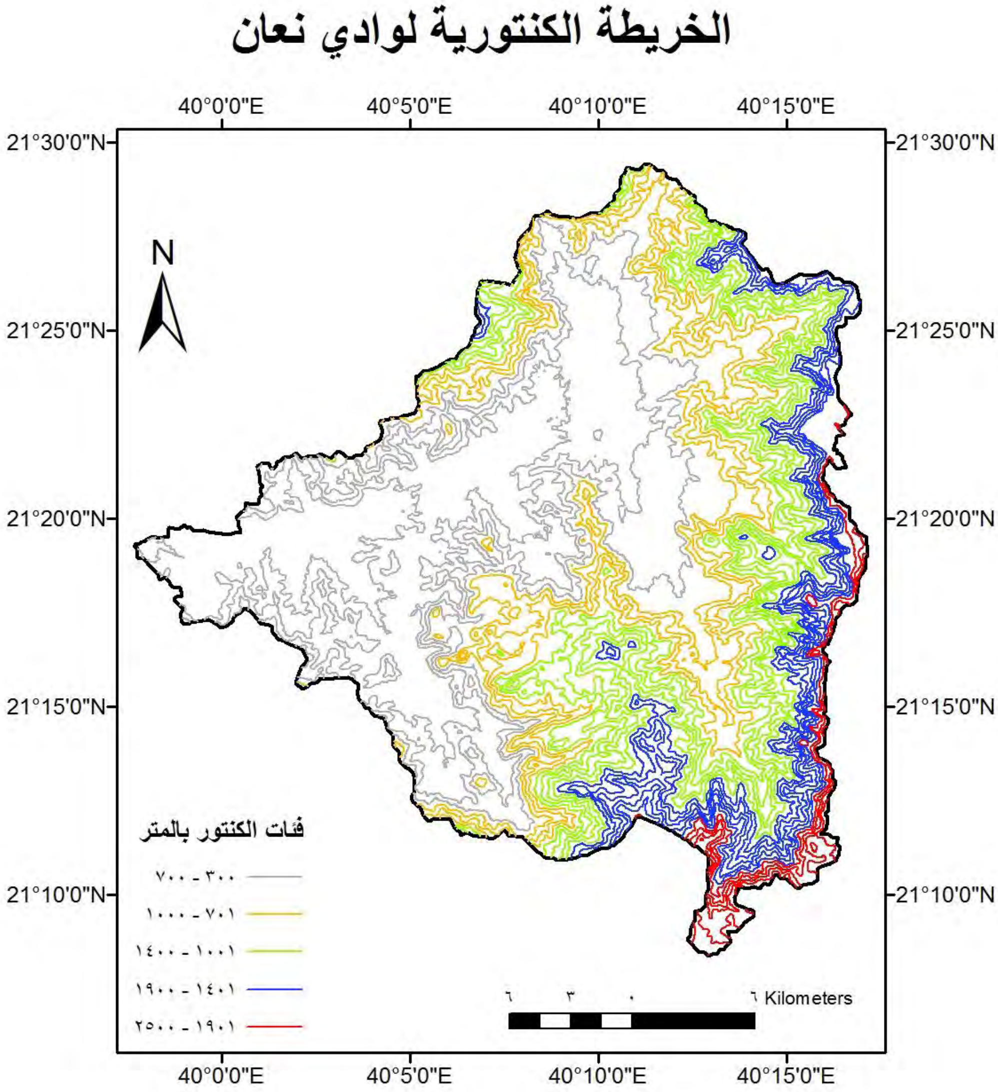

الخريطة الكنتورية لوادي نعان
40°0'0"E
40°5'0"E
40°10'0"E
40°15'0"E
21°30'0"N
21°25'0"N
21°20'0"N
21°15'0"N
21°10'0"N
N
فئات الكنتور بالمتر
٣٠٠ - ٧٠٠
٧٠١ - ١٠٠٠
١٠٠١ - ١٤٠٠
١٤٠١ - ١٩٠٠
١٩٠١ - ٢٥٠٠
٦ ٣ ٠ ٦ Kilometers

(شكل ٣)

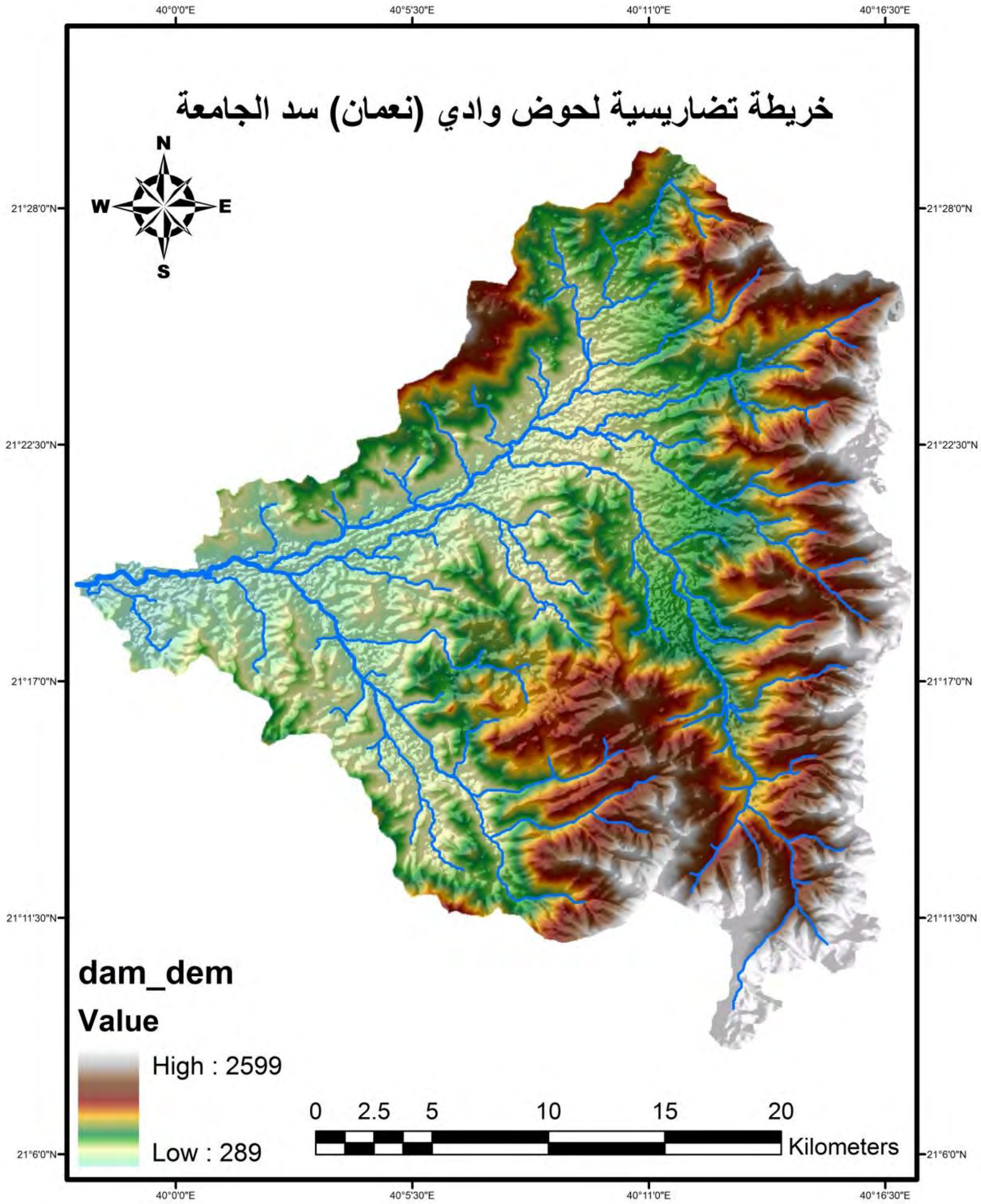

40°0'0"E
40°5'30"E
40°11'0"E
40°16'30"E
خريطة تضاريسية لحوض وادي (نعمان) سد الجامعة
N
W
E
S
21°28'0"N
21°22'30"N
21°17'0"N
21°11'30"N
21°6'0"N
dam_dem
Value
High : 2599
Low : 289
0 2.5 5 10 15 20
Kilometers

(شكل ٤)

الخريطة الجيولوجية لمنطقة حوض نعمان (سد الجامعة)

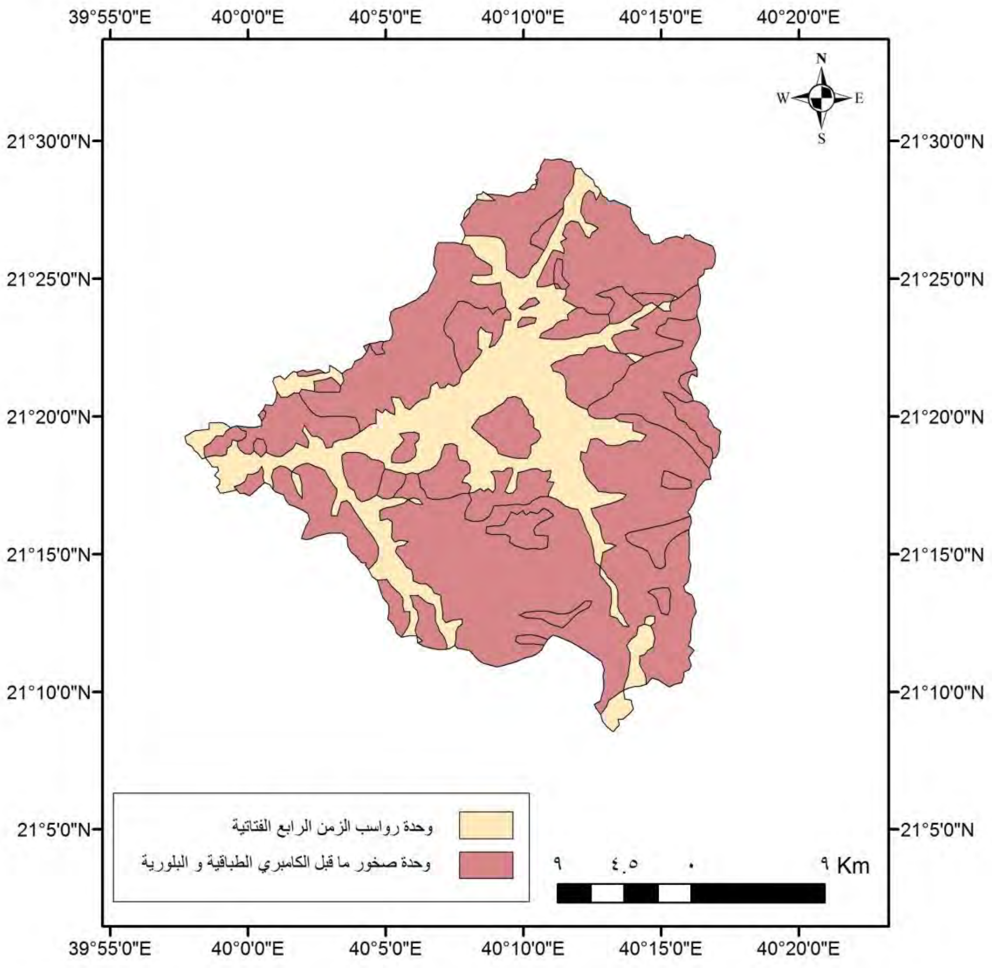

(شكل ٥)

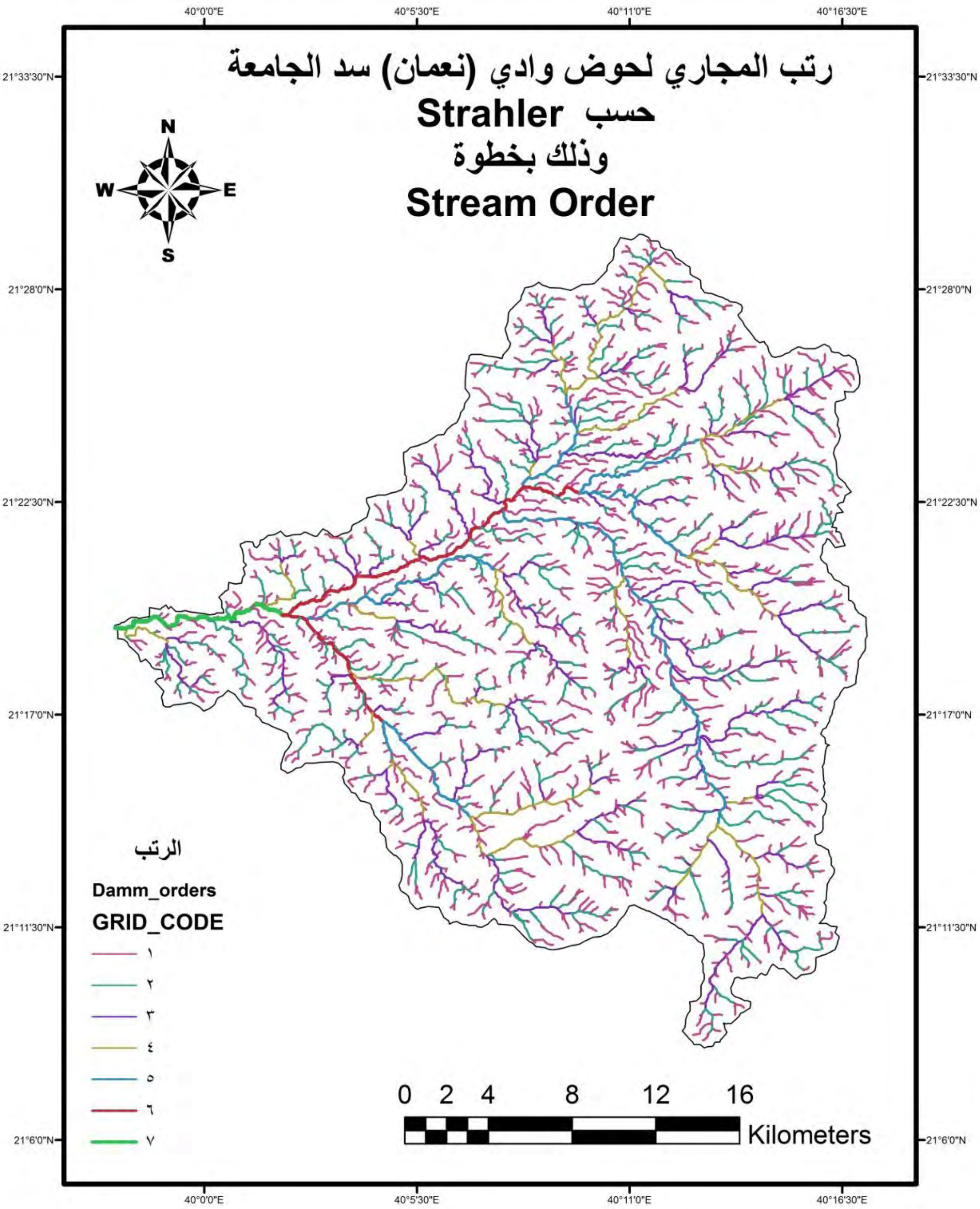

رتب المجاري لحوض وادي (نعمان) سد الجامعة
حسب Strahler
وذلك بخطوة
Stream Order
N
S
E
W
الرتب
Damm_orders
GRID_CODE
١
٢
٣
٤
٥
٦
٧
0 2 4 8 12 16
Kilometers
40°0'0"E
40°5'30"E
40°11'0"E
40°16'30"E
21°33'30"N
21°28'0"N
21°22'30"N
21°17'0"N
21°11'30"N
21°6'0"N

(شكل ٦)

معدل الامطار السنوية لحوض وادي عرنة

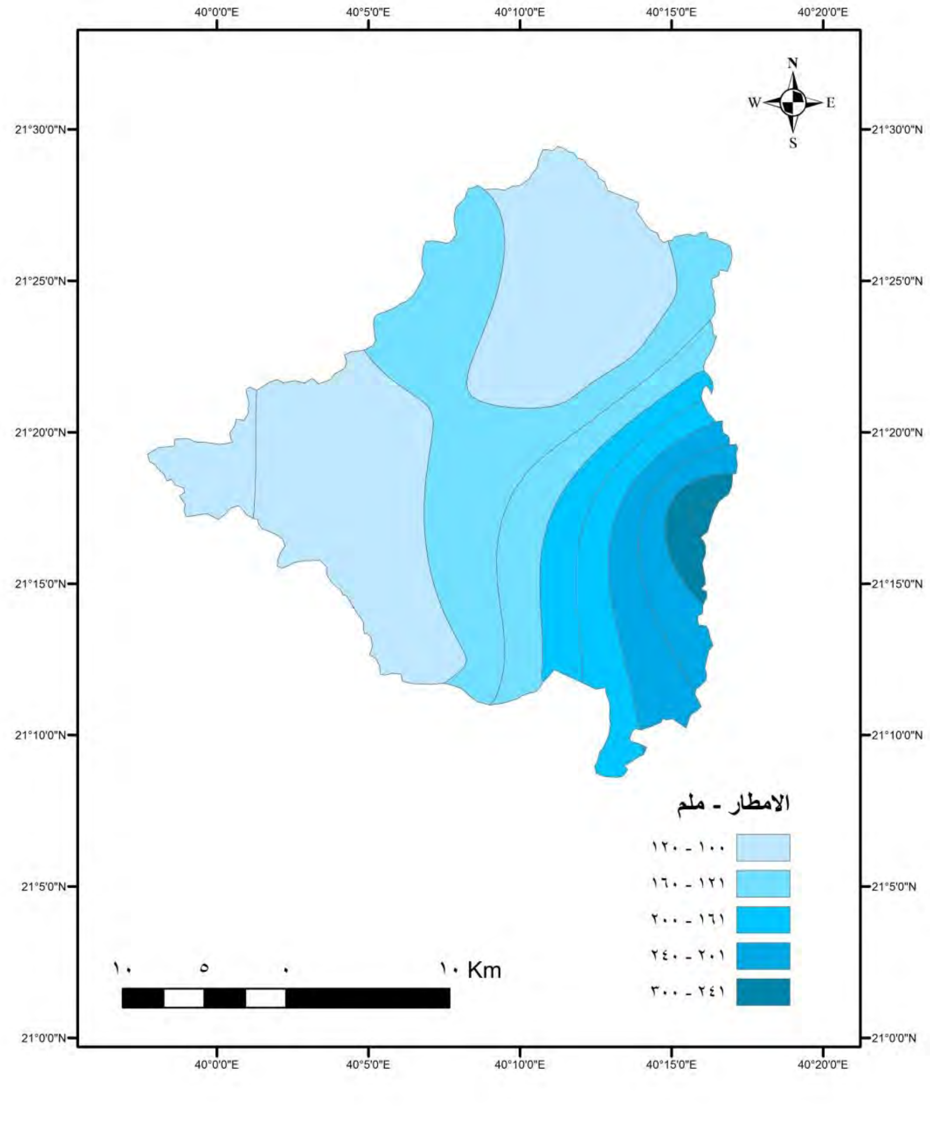

(شكل ٧)

منطقة حوض سد الجامعة المقتطعة من نموذج الارتفاعات الرقمية ASTER DEM

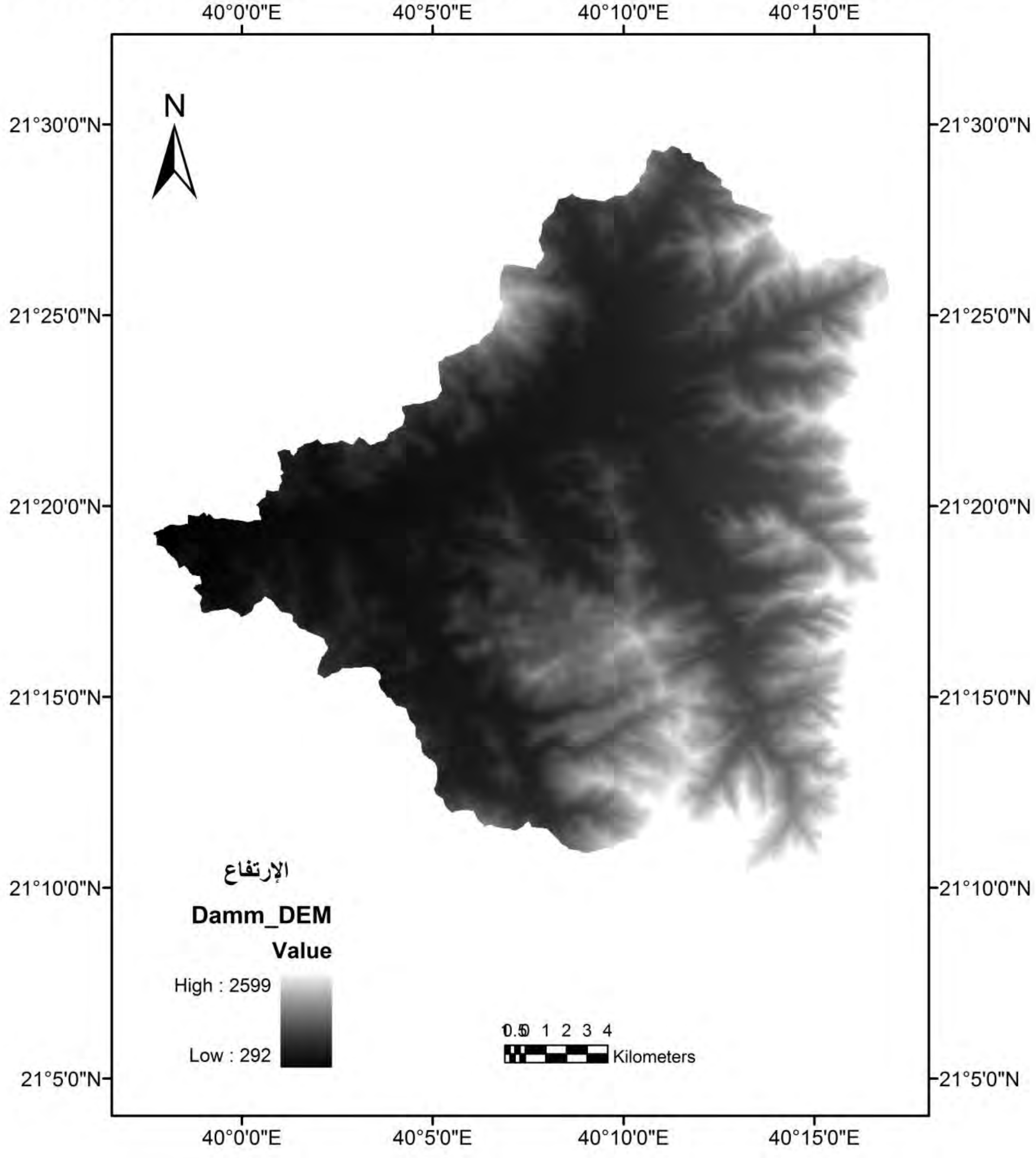

(شكل ٨)

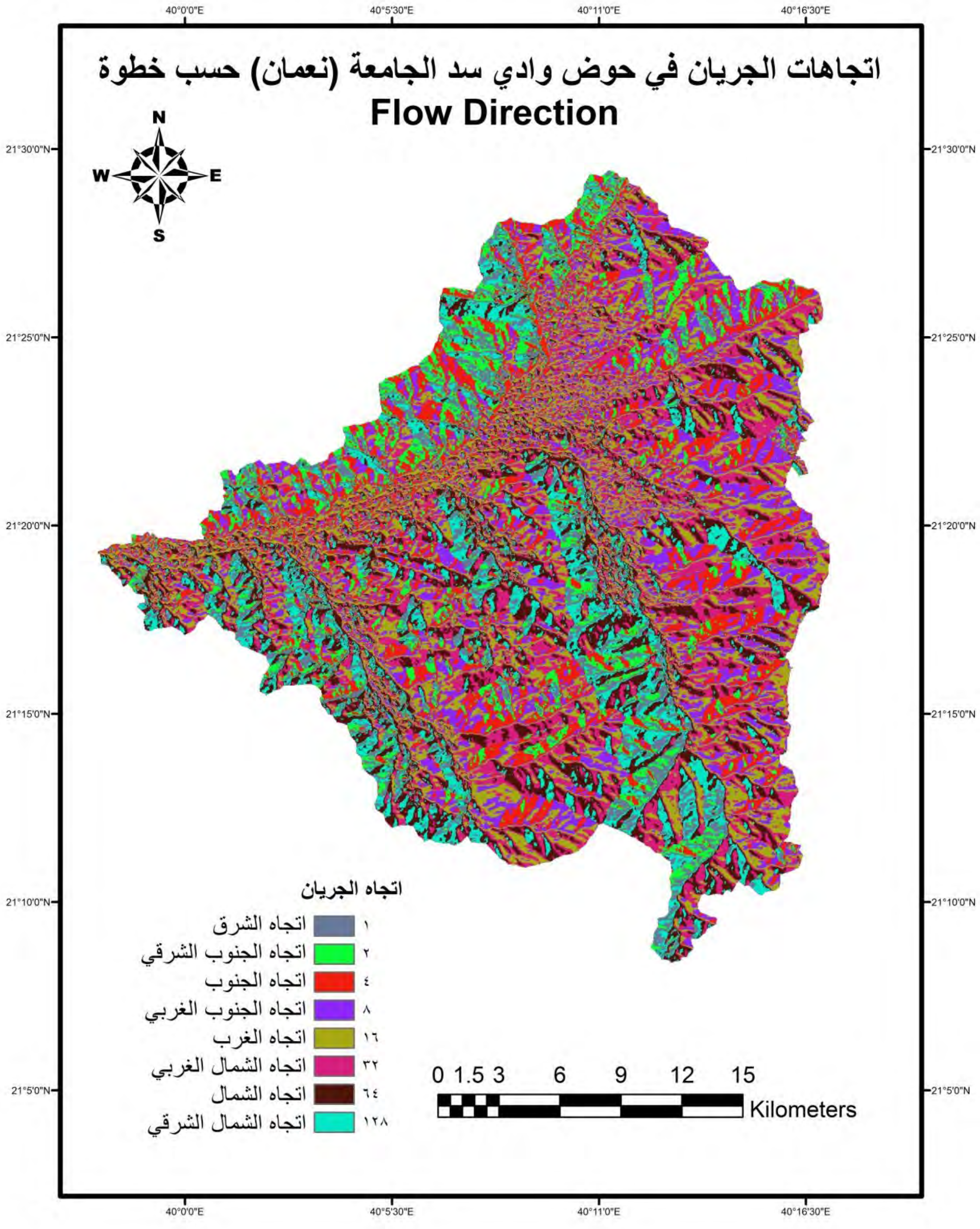

اتجاهات الجريان في حوض وادي سد الجامعة (نعمان) حسب خطوة
Flow Direction
N
W
E
S
40°0'0"E
40°5'30"E
40°11'0"E
40°16'30"E
21°30'0"N
21°25'0"N
21°20'0"N
21°15'0"N
21°10'0"N
21°5'0"N
اتجاه الجريان
١ اتجاه الشرق
٢ اتجاه الجنوب الشرقي
٤ اتجاه الجنوب
٨ اتجاه الجنوب الغربي
١٦ اتجاه الغرب
٣٢ اتجاه الشمال الغربي
٦٤ اتجاه الشمال
١٢٨ اتجاه الشمال الشرقي
0 1.5 3 6 9 12 15
Kilometers

(شكل ٩)

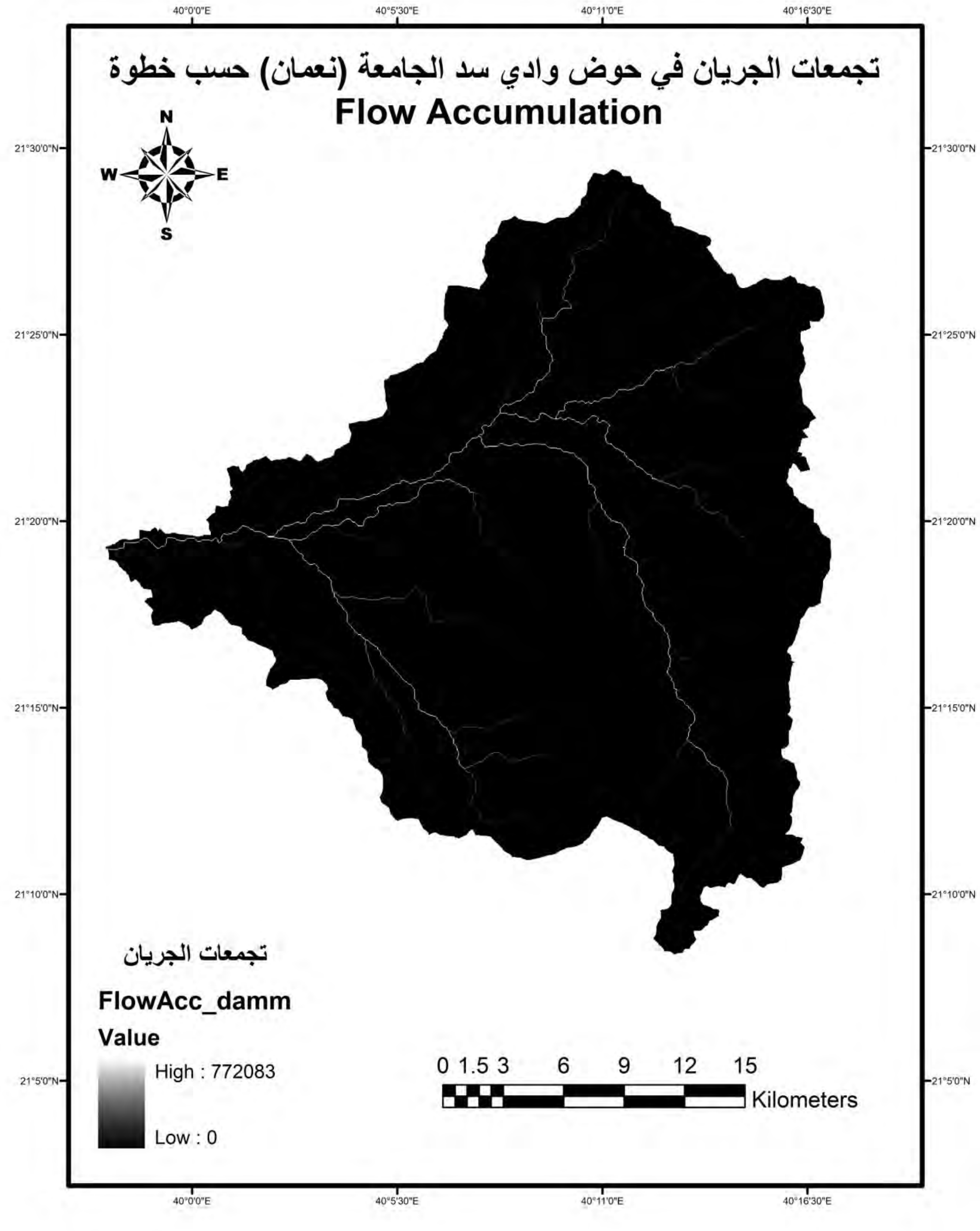

تجمعات الجريان في حوض وادي سد الجامعة (نعمان) حسب خطوة
Flow Accumulation
N
W
E
S
40°0'0"E
40°5'30"E
40°11'0"E
40°16'30"E
21°30'0"N
21°25'0"N
21°20'0"N
21°15'0"N
21°10'0"N
21°5'0"N
تجمعات الجريان
FlowAcc_damm
Value
High : 772083
Low : 0
0 1.5 3 6 9 12 15
Kilometers

(شكل ١٠)

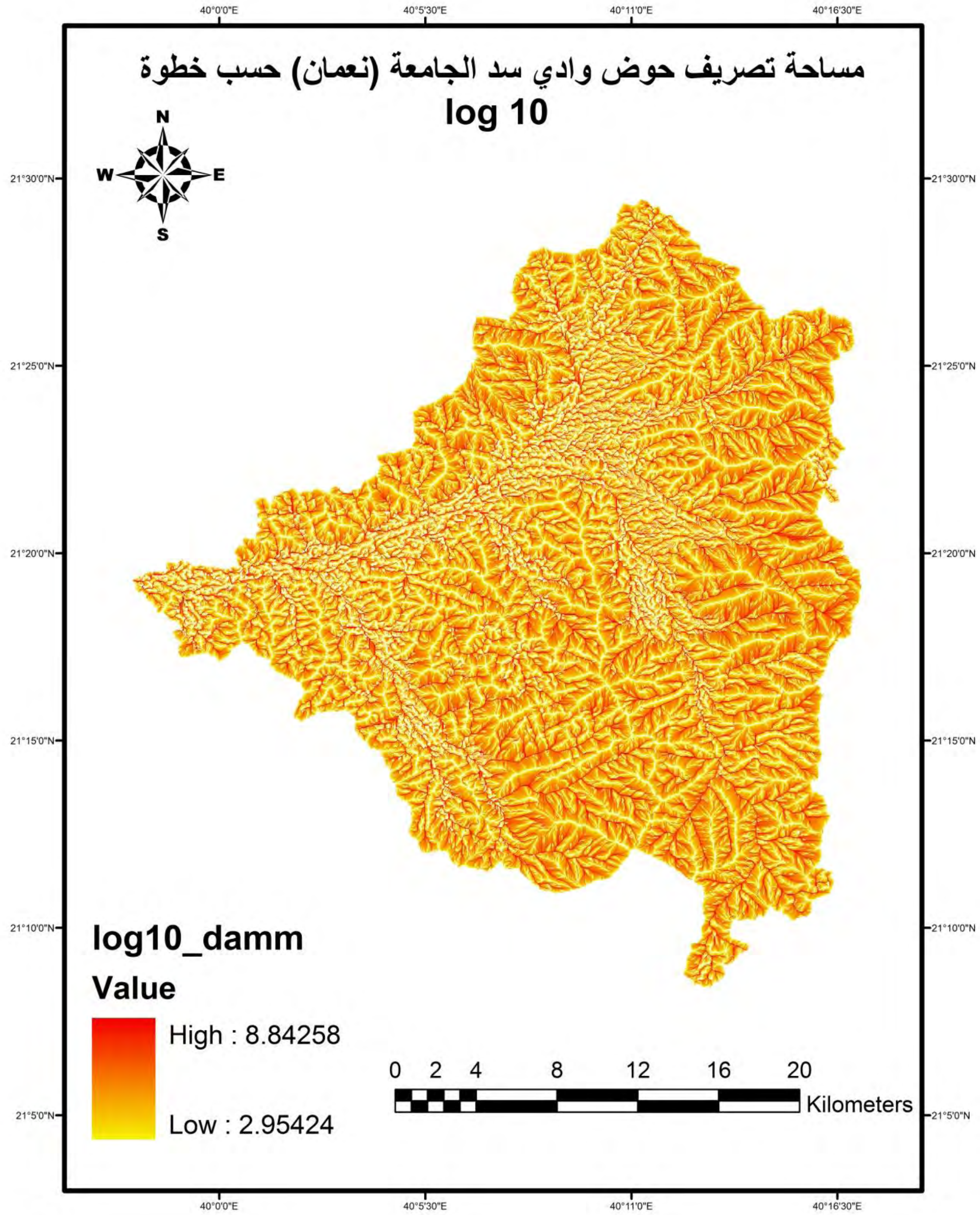

مساحة تصريف حوض وادي سد الجامعة (نعمان) حسب خطوة
log 10
N
W
E
S
40°0'0"E
40°5'30"E
40°11'0"E
40°16'30"E
21°30'0"N
21°25'0"N
21°20'0"N
21°15'0"N
21°10'0"N
21°5'0"N
log10_damm
Value
High : 8.84258
Low : 2.95424
0 2 4 8 12 16 20
Kilometers

(شكل ١١)

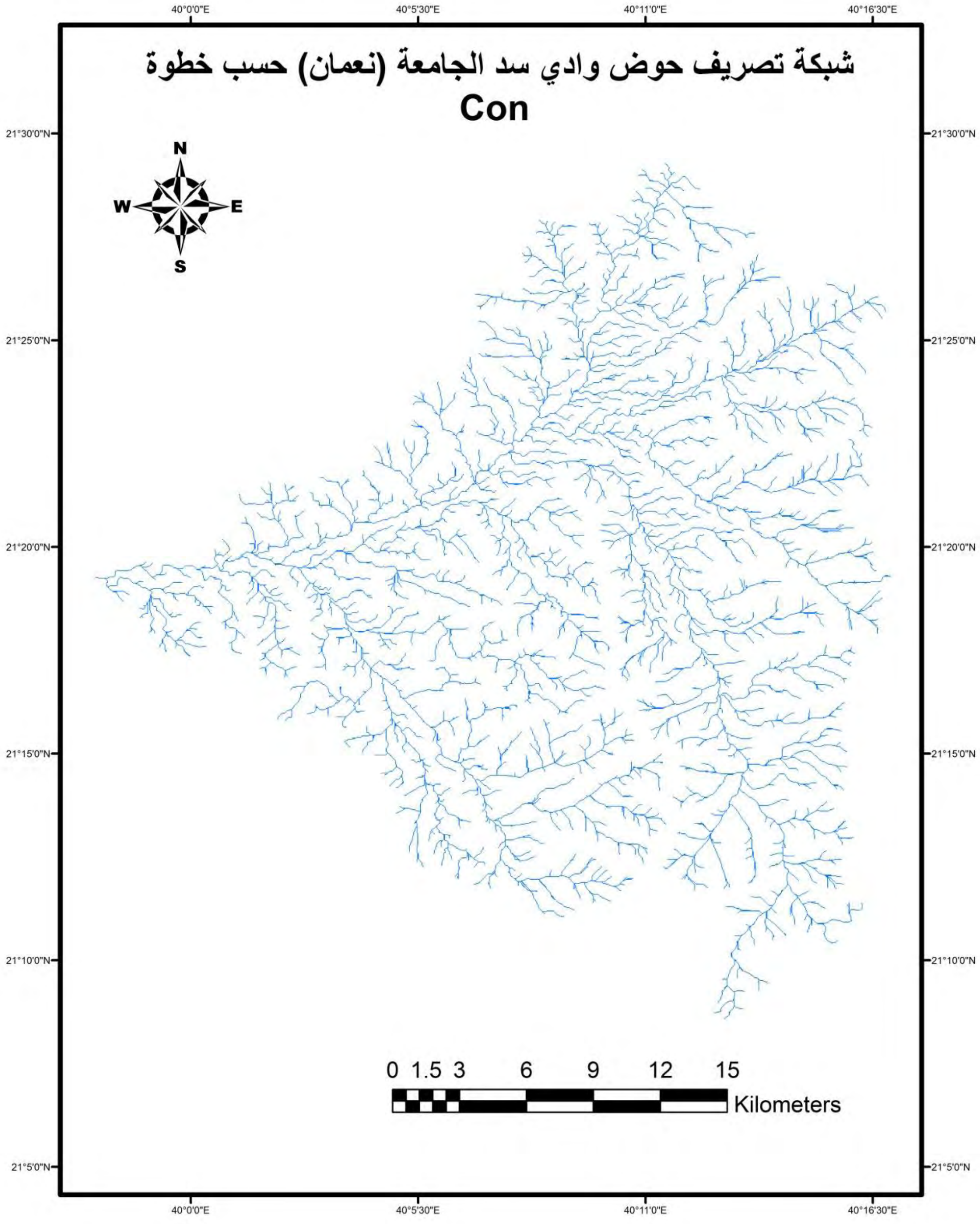
40°0'0"E
40°5'30"E
40°11'0"E
40°16'30"E
شبكة تصريف حوض وادي سد الجامعة (نعمان) حسب خطوة
Con
N
W
E
S
21°30'0"N
21°25'0"N
21°20'0"N
21°15'0"N
21°10'0"N
21°5'0"N
0 1.5 3 6 9 12 15
Kilometers

(شكل ١٢)

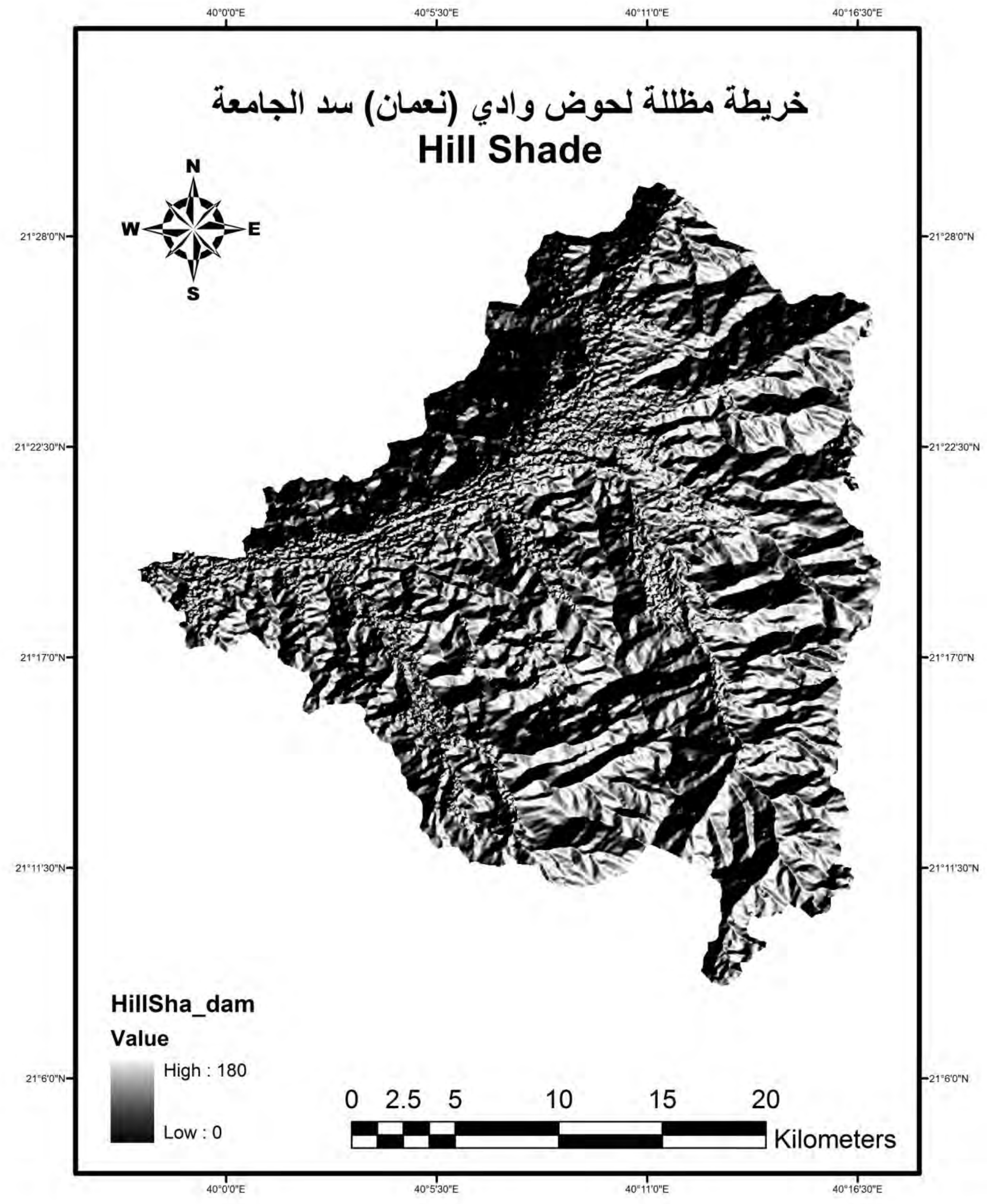
خريطة مظللة لحوض وادي (نعمان) سد الجامعة
Hill Shade
N
W
E
S
40°0'0"E
40°5'30"E
40°11'0"E
40°16'30"E
21°28'0"N
21°22'30"N
21°17'0"N
21°11'30"N
21°6'0"N
HillSha_dam
Value
High : 180
Low : 0
0 2.5 5 10 15 20
Kilometers

(١٣)

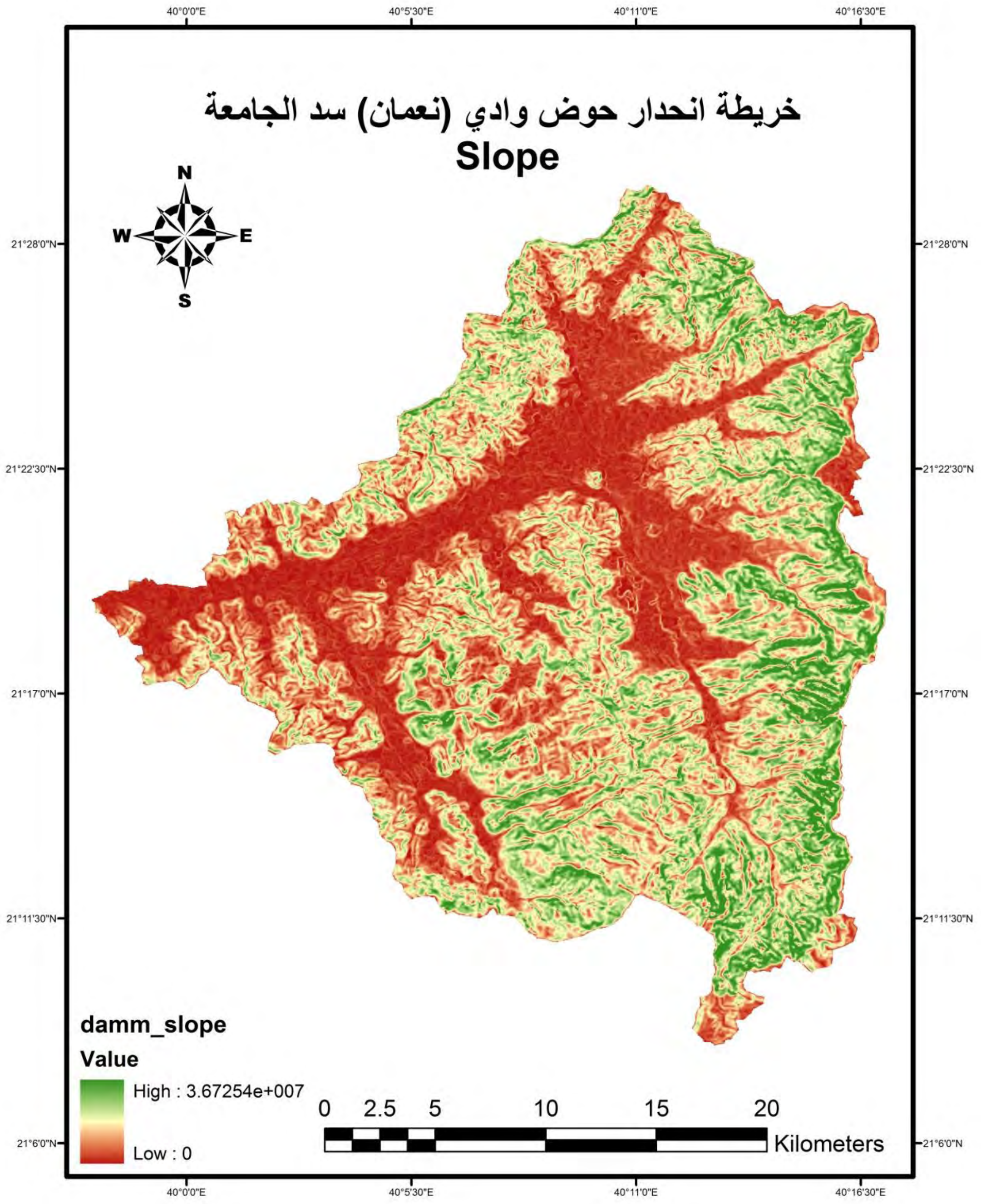

خريطة انحدار حوض وادي (نعمان) سد الجامعة
Slope
N
W
E
S
40°0'0"E
40°5'30"E
40°11'0"E
40°16'30"E
21°28'0"N
21°22'30"N
21°17'0"N
21°11'30"N
21°6'0"N
damm_slope
Value
High : 3.67254e+007
Low : 0
0 2.5 5 10 15 20
Kilometers

(شكل ١٤)

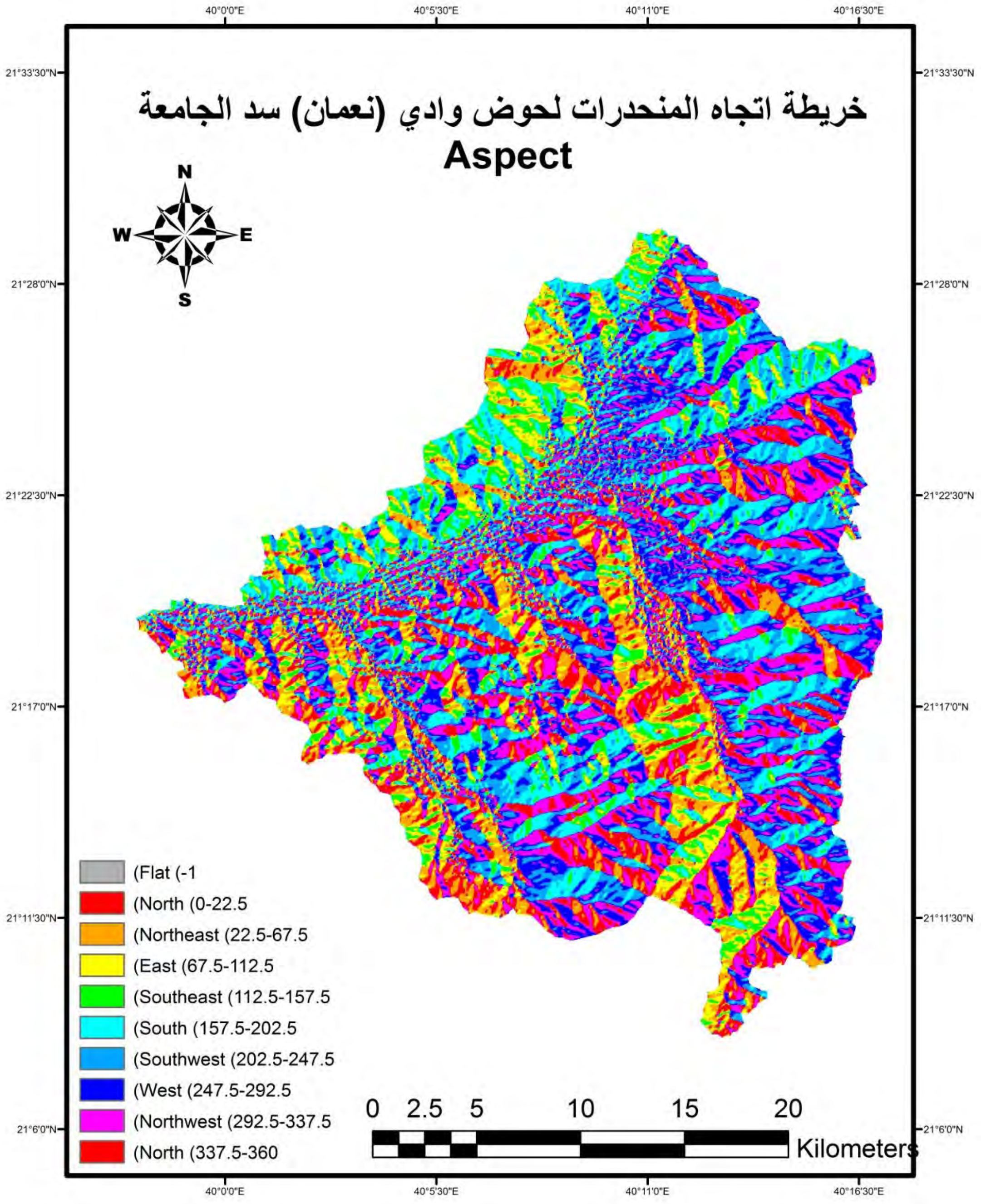

40°0'0"E
40°5'30"E
40°11'0"E
40°16'30"E
21°33'30"N
21°28'0"N
21°22'30"N
21°17'0"N
21°11'30"N
21°6'0"N
خريطة اتجاه المنحدرات لحوض وادي (نعمان) سد الجامعة
Aspect
N
W
E
S
(Flat (-1
(North (0-22.5
(Northeast (22.5-67.5
(East (67.5-112.5
(Southeast (112.5-157.5
(South (157.5-202.5
(Southwest (202.5-247.5
(West (247.5-292.5
(Northwest (292.5-337.5
(North (337.5-360
0 2.5 5 10 15 20
Kilometers

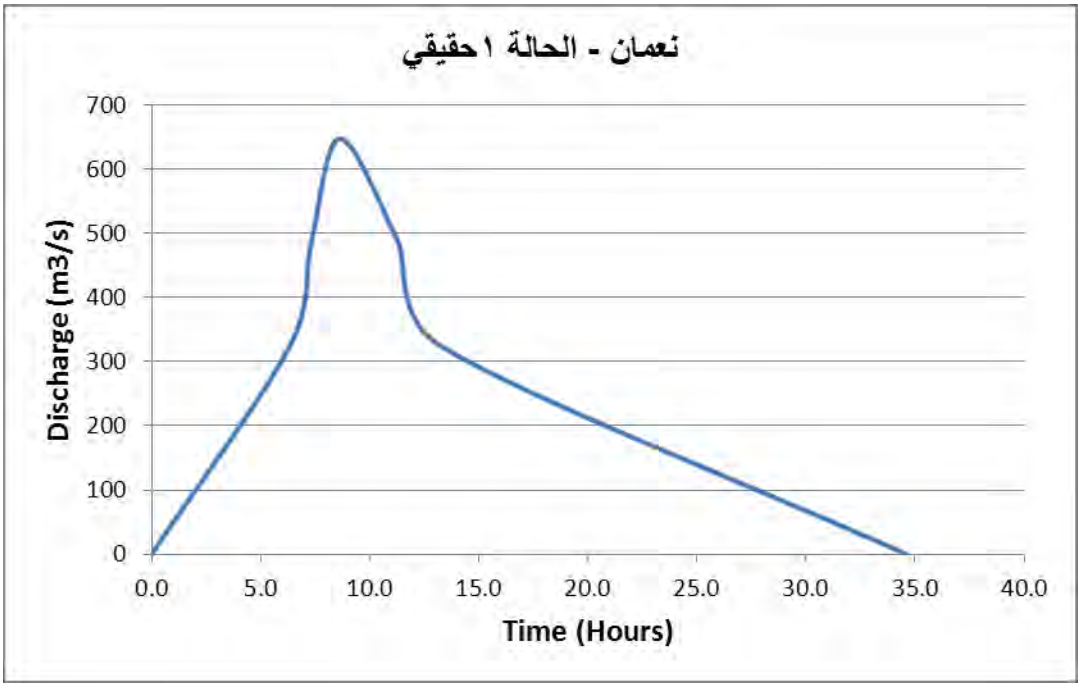

(شكل ١٥) هيدروجراف حوض وادي عرنة حسب نموذج سنايدر **حالة** ١

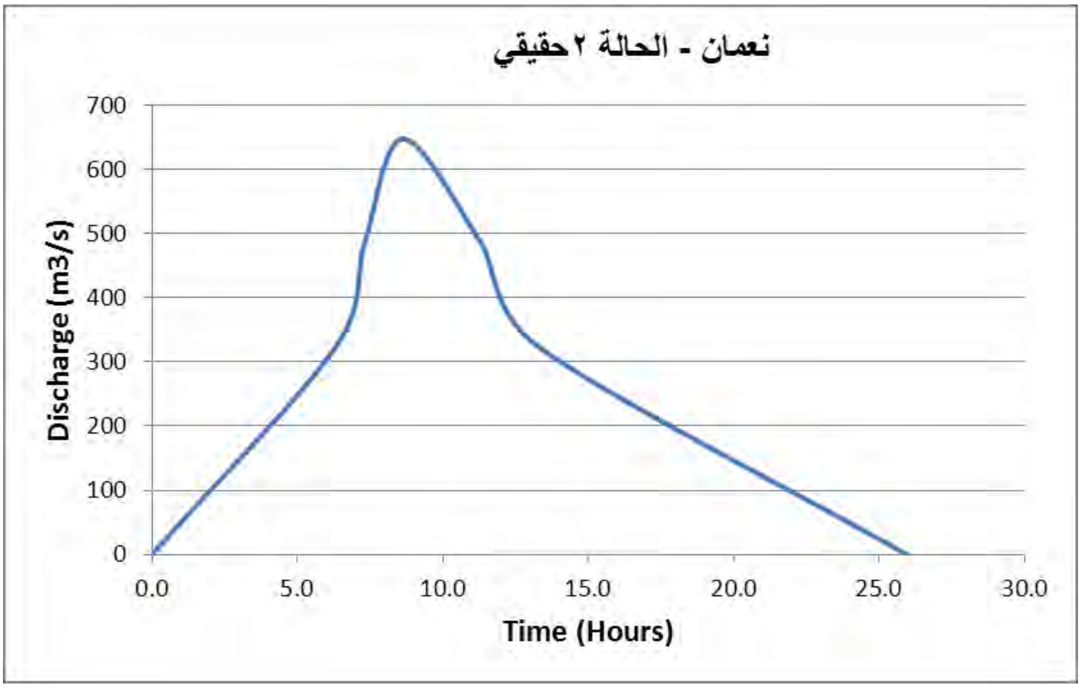

(شكل ١٦)هيدروجراف حوض وادي عرنة حسب نموذج سنايدر **حالة** ٢

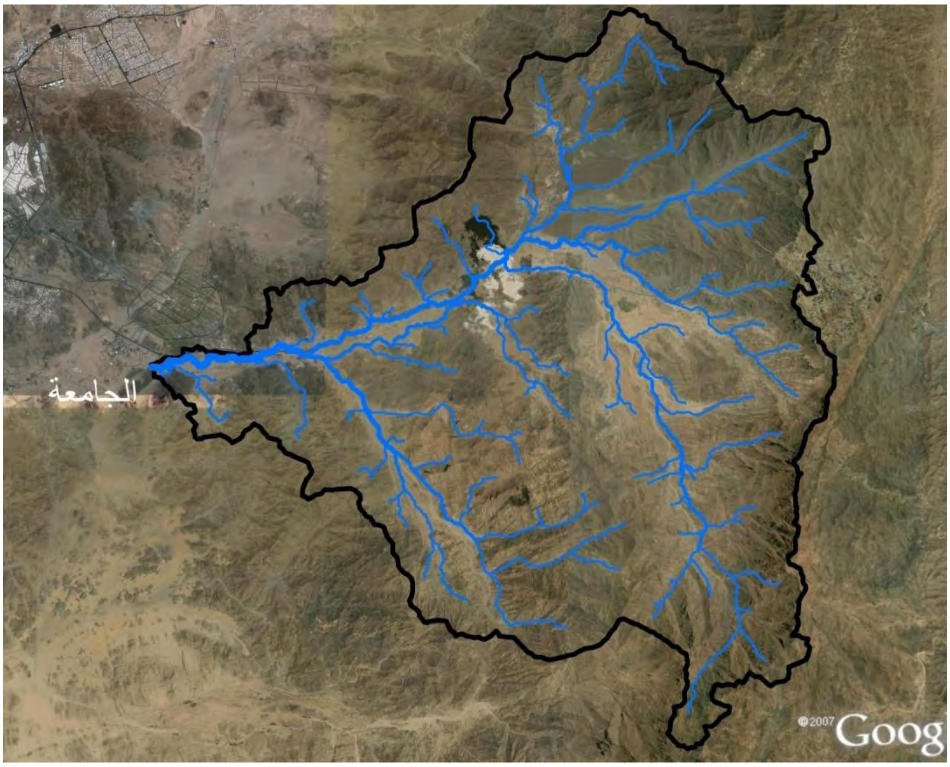

(شكل ١٧) التقاء وادي نعمان مع المدينة الجامعية لأم القرى

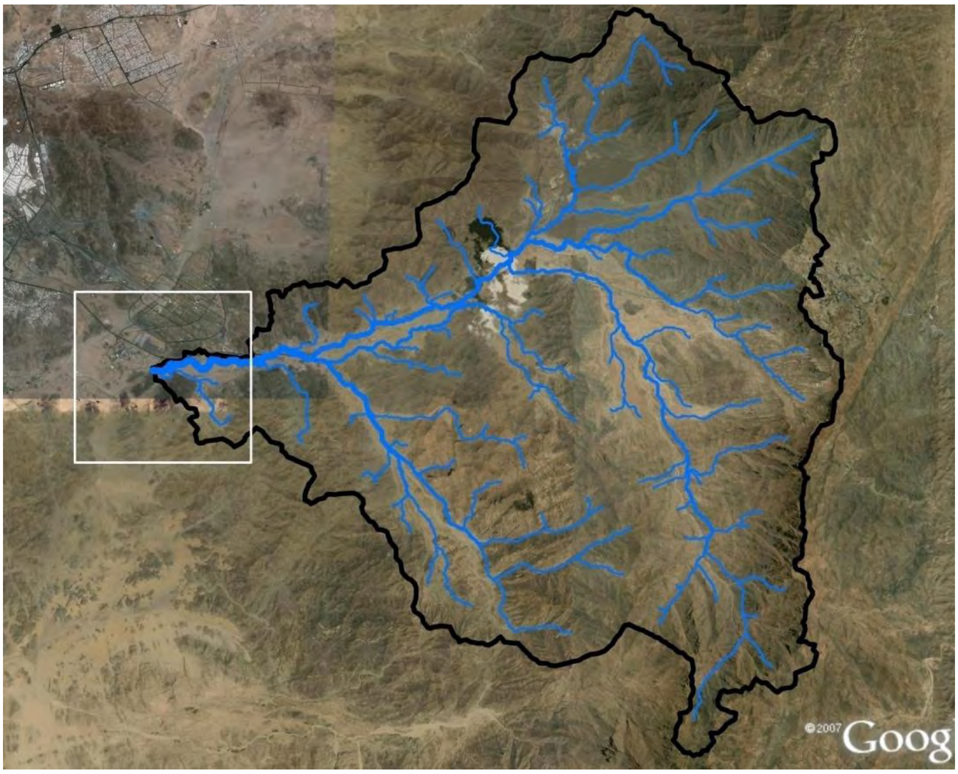

(شكل ١٨) تحديد منطقة التقاء وادي نعمان مع سد الجامعة

(شكل ١٩) تكبير منطقة التقاء وادي نعمان مع سد الجامعة

<u>فهرس الجداول</u>

١- الخصائص الشكلية والتضاريسية لمنطقة البحث.

٢- كميات المطر اليومية القصوى في مكة المكرمة بين عامي ١٩٨٥ – ٢٠١٠

٣- فترة الرجوع والاحتمالية للأمطار اليومية القصوى لمدينة مكة المكرمة بين عامي ١٩٨٥- ٢٠١٠

٤- فترة الاستجابة و الفترة القياسية للأمطار (ساعة).

٥- كمية التدفق الأقصى للسيول في حوض وادي نعمان.

٦- زمن الأساس للسيل في منطقة البحث (يوم – ساعة).

٧- فترة الارتفاع التدريجي لتدفق السيل (يوم - ساعة).

٨- فترة الانخفاض التدريجي لتدفق السيل اعتماداً على زمن الأساس (يوم – ساعة) و تركيز الأمطار المناسبة لتدفق الذروة في حوض نعمان .

٩- حساب تدفق الذروة النوعي لحوض وادي نعمان.

١٠- حساب الفترة الزمنية W٥٠ المناسبة لعرض في الهيدروجراف عند مستوى ٥٠% لحوض وادي نعمان.

١١- حساب الفترة الزمنية W٧٥ المناسبة لعرض في الهيدروجراف عند مستوى ٧٥% لحوض وادي نعمان.

١٢- حساب حجم السيل في حوض وادي نعمان.

١٣- حساب عمق الجريان السطحي المناسب لذروة التدفق في حوض نعمان.

١٤- حساب قوة السيل لحوض وادي نعمان.

١٥- القيمة الكمية والزمنية لتدفق السيول في حوض نعمان حسب القيم العظمى والوسطى والدنيا لمعاملي ال ct وال cp .

١٦- القيم الكمية والزمنية لتصريف الذروة في حوض نعمان بعد تحديد قيمتي ال ct والcp .

<u>فهرس الأشكال</u>

١-موقع حوض وادي نعمان من مدينة مكة المكرمة
٢-الخريطة الجيولوجية لحوض وادي نعمان
٣-الخريطة الكنتورية لحوض وادي نعمان
٤-الخريطة التضاريسية لحوض وادي نعمان
٥-رتب التصريف النهري لشبكة حوض وادي نعمان
٦-خريطة خطوط المطر المتساوي لحوض وادي نعمان
٧-خريطة نظام الارتفاعات الرقمي لحوض وادي نعمان
٨-خريطة اتجاهات الجريان في حوض وادي نعمان
٩-خريطة تجمعات الجريان في حوض وادي نعمان
١٠- مساحات تصريف حوض وادي نعمان حسب خطوة log١٠
١١- شبكة تصريف حوض وادي نعمان حسب خطوة con
١٢- خريطة مظللة لحوض وادي نعمان
١٣- خريطة انحدار حوض وادي نعمان slope
١٤- خريطة اتجاه المنحدرات لحوض وادي نعمان Aspect
١٥- هيدروجراف حوض وادي عرنة حسب نموذج سنايدر حالة ١
١٦- هيدروجراف حوض وادي عرنة حسب نموذج سنايدر حالة ٢
١٧- التقاء وادي نعمان مع المدينة الجامعية لأم القرى
١٨- تحديد منطقة التقاء وادي نعمان مع سد الجامعة
١٩- تكبير منطقة التقاء وادي نعمان مع سد الجامعة

المراجع :

- الدليمي،أحمدعامر(١٩٩٥)تطوير طريقة انتقاء الجذور لاشتقاق الهيدروجراف القياسي،رسالةماجستير،كلية الهندسة ، جامعة الموصل .
- الغامدي، سعد (٢٠٠٤): استخلاص شبكة التصريف السطحي للمياه باستعمال المعالجة الآلية لبيانات الأقمار الصناعية: دراسة على منطقة جبل نعمان، مجلة جامعة أم القرى للعلوم التربوية والاجتماعية والإنسانية، م١٦، (٢) ص ص ٢٨٧-٣١٦.
- الغامدي، سعد (٢٠٠٦): توظيف نظم المعلومات الجغرافية في استخراج بعض القياسات المورفومترية من نماذج الارتفاعات الرقمية. دراسة حالة وادي ذرى في المملكة العربية السعودية، الجمعية الجغرافية الكويتية، رسائل جغرافية عدد ٣١٧. الكويت.
- الروسان، نايف والقرالة، محمد (٢٠٠٨) استخدام نظم المعلومات الجغرافية في دراسة خصائص حوض وادي شعيب في الأردن، جامعة مؤتة، الأردن...
- الجعيدي، فرحان (٢٠٠٥). استخدام صور الاستشعار عن بُعد الرقمية عالية الوضوح المكاني لتحديد امتداد فيضانات السيول في سهل الخرج . الجمعية الجغرافية، السعودية، سلسلة رقم ٧١، جامعة الملك سعود،الرياض.
- مرزا، معراج والبارودي، محمد (٢٠٠٥) السمات المورفولوجية والخصائص المورفومترية والهيدرولوجية لأودية الحرم المكي، مجلة جامعة أم القرى للعلوم التربوية والاجتماعية والإنسانية، م١٧ العدد ٣، مكة المكرمة.
- مرزا، معراج نواب، وأحمد، بدر الدين يوسف(٢٠٠١)، أحوال الطقس والمناخ في الشتاء بمكة المكرمة، الجمعية الجغرافية الكويتية، قسم الجغرافيا بجامعة الكويت، العدد٢٥٣، الكويت.
- الجعيدي، فرحان (٢٠٠٨) الخصائص الهيدرومورفومترية وخصائص السيول في أحواض السدود المقترحة على أودية علية في محافظة الخرج، الجمعية الجغرافية السعودية، بحوث جغرافية العدد ٨٤، جامعة الملك سعود، الرياض.
- بوروبه، محمد (٢٠٠٧) دراسة هيدرومورفومترية لتقدير حجم سيول حوض وادي عتود بالمملكة العربية السعودية ، سلسلة، الإصدارات الخاصة، عدد(٢١)،مركز دراسات الخليج والجزيرة العربية، الكويت.

- الجعيدي، فرحان وبوروبه، محمد (١٤٢٨) تقدير تدفق الذروة للسيول بحوض وادي العين بمحافظة الخرج في المملكة العربية السعودية،مركز البحــوث، كليـــة الآداب، جامعة الملك سعود، عدد ١٢١، الرياض.
- أحمد، بدر الدين يوسف (٢٠٠٦) تطرق العناصر المناخية فـــي المملكـــة العربيـــة السعودية. سلسلة الإصدارات الخاصة. مركز دراسات الخليج والجزيرة العربية، العدد ١٦ الكويت
- أحمد، بدر الدين يوسف (١٩٩٢م) مناخ مكة المكرمـــة، سلســـلة بحـــوث العلـــوم الاجتماعية ١٥ معهد البحوث العلمية وإحياء التراث الإسلامي، مركز بحوث العلـــوم الاجتماعية، مكة المكرمة.
- الصالح، محمد عبدالله (١٩٩٢) بعض طرق قياس المتغيرات في أحواض التصريف، مركز بحوث كلية الآداب، جامعة الملك سعود، الرياض.
- الحواس ، علي عساف (١٤٢٨) توظيف تكاملي لتقنيات الاستشعار عن بعد ونظم المعلومات الجغراية لتحديد وتحليل الخصائص الهيدرومورفومترية لأحواض التصريف الصحراوي ، بحوث جغرافية (٨١) ، الجمعية الجغرافية السعودية ، الرياض.
- شومان ، سامر أحمد سمير (١٤١٨) السجل التاريخي للسيول في وادي ابراهيم وأثرها على المسجد الحرام ، مركز أبحاث الحج ، جامعة أم القرى ، مكة المكرمة.
- البارودي ، محمد سعيد (٢٠١٢) تقدير أحجام السيول ومخاطرها عند المجرى الادنى لوادي عرنة جنوب شرق مدينة مكة المكرمة باستخدام نظم المعلومات الجغرافية ، سلسلة بحوث جغرافية ، العدد ٤٨ ، الجمعية الجغرافية المصرية ، القاهرة .
- ASTER, ٢٠١٠, ASTER Web site at: http://www.ersdac.or.jp/GDEM/E/١.html , Accessed January ٢٠١٠.
- Chow, V.T., Maidment, D., and Mays, L. W., (١٩٨٨). Applied Hydrology. McGraw Hill.
- Clark, C.O. (١٩٤٥). Storage and The Unit Hydrograph. Proc. Am. Soc. Civ. Eng., vol. ٩, pp١٣٣٣-١٣٦٠.
- Dooge, J. C. I. (١٩٥٩). A General Theory of the Unit Hydrograph. Journal of Geophysical Research, ٦٤(٢): ٢٤١-٢٥٦.

- Hadley, R. F.,(١٩٨٦). Fluvial transport of sediment in arid and semi-arid regions. Proc. Int. Symp. on Erosion and Sedimentation in Arab Countries. Iraqi J. Water Res., Vol. ٥, ٣٣٥–٣٤٨.
- Horton, R. E.,(١٩٤٥). Erosional development of stream and their drainage basins: Hydrophysical applications of quantitative morphology. Bull. Geol. Soc. Am., Vol. ٥٦, ٢٧٥–٣٧٠. Hudson,
- Maidment, D. R.,(١٩٩٣). Handbook of Hydrology. McGraw-Hill Book, ١٢.١–١٢.٦١
- Saudiconsult,(١٩٨٧). Sedimentation control project for Jizan dam reservoir. Draft feasibility report. Saudi Arabian Minist. Agric. Wat., Unpublished Report.
- Sen, Zekâi (٢٠٠٨)Wadi hydrology , CRC Press is an imprint of Taylor & Francis Group, an Informa business
- Sen, Z. and Al-Suba'i, K.,(٢٠٠٢). Hydrologic considerations for dam siting in arid regions: A Saudi Arabian study. Hydrol. Sci. J., ٤٧ (١), ١–١٩.
- Snyder, F.F. (١٩٣٨). Synthetic Unit Graphs. Trans. Am. Geophys. Union, ١٩, ٤٤٧–٤٥٤.
- Sherman, L. K. (١٩٣٢). Streamflow from Rainfall by the Unit Graph Method. Eng. News Rec., ١٠٨, ٥٠١–٥٠٥.
- Soil Conservation Service, Hydrology, (١٩٧٢). Sec. ٤ of National Engineering Handbook, Soil Conservation Service, U.S. Department of Agriculture, Washington, D.C.
- Ramírez, J. A.,(٢٠٠٠) . Prediction and Modeling of Flood Hydrology and Hydraulics. Chapter ١١ of Inland Flood Hazards: Human, Riparian and Aquatic Communities Eds. Ellen Wohl; Cambridge University Press.
- U. S. Army Corps of Engineers, (١٩٧٢). Program Description and User's Manual for SSARR Model Streamflow Synthesisi and Reservoir Regulation. Program ٧٢٤-K٥G٠٠١٠.

- Subyani,A and Bayumi, t.(٢٠٠١) Physiographical and Hydrological Analysis of Yalamlam Basin, Makkah Al-Mukarramah Area, JKAU: Earth Sci., vol. ١٣,pp١٥١-١٧٧. Jeddah, Saudi Arabia.
- Fred, E and Mostafa, B., (٢٠٠٨) Flood Risk Modeling for Holy Sites in Makkah,
  Development Commission of Makkah, Madinah and Holy Sites.

INTERNATIONAL JOURNAL OF GEOMATICS AND GEOSCIENCES
Volume 1, No 4, 2011

© Copyright 2010 All rights reserved Integrated Publishing services

Research article ISSN 0976 – 4380

Accuracy and relevance of Digital Elevation Models for Geomatics applications - A case study of Makkah Municipality, Saudi Arabia

Mirza.M [1,2], Dawod.G. [2,3], and Al-Ghamdi.K [2]
1- Center of Research Excellence in Hajj and Omrah, Umm Al-Qura University, Makkah, Saudi Arabia
2- Geography Department, Umm Al-Qura University, Makkah, Saudi Arabia
3- Survey Research Institute, Giza, Egypt
meraj@mmirza.com

ABSTRACT

Several geomatics applications depend on utilizing Digital Elevation Models (DEMs), such as geomorphologic applications of watershed management and flood hazard determination. Additionally, DEMs play a crucial role in geodetic applications, particularly for the determination of topographic effects in quasi-geoid modelling. This study aims to investigate the accuracy performance of several global and national DEMs in order to define the suitability of them in engineering applications in Kingdom of Saudi Arabia (KSA). Two global DEMs have been exploited, namely the Advanced Spaceborne Thermal Emission and Reflection Radiometer (ASTER) and the Shuttle Radar Topographic Mission (SRTM3), along with two national DEMs, belong to the center of research excellence in Hajj and Omrah, with 5 and 10 meter resolution. A dataset of 200 first-order Global Positioning System (GPS) ground control points, that covers the Makkah (Mecca) metropolitan area in the western region of KSA, has been compiled and employed to judge the accuracy of all DEMs in a Geographic Information Systems (GIS) environment. The attained results showed that the 5-meter resolution national DEM is the most accurate one, that produces mean height difference and standard deviations equal 0.01 ± 2.95 m respectively. That national DEM is more accurate by factors of 3 and 2 over the global ASTER and SRTM3 DEMs respectively. Guidelines have been drawn to apply each DEM in geodetic, topographic mapping, and geomorphologic studies in KSA.

Keywords: DEM, Accuracy analysis, GPS controls, Geomatics activities, Saudi Arabia.

1. Introduction

Digital Elevation Models (DEMs) are essential for both geodetic and geomorphologic applications. DEMs are utilized in gravity data processing and geoid model development, particularly for the computation of terrain corrections at observed terrestrial gravity data, and for downward continuation computations. Watersheds management and flood hazard assessment are typical morphometry and geomorphologic activities utilize DEMs (Subyani et al. 2010, and Mendas 2010). In the last few decades, several global DEMs have been compiled and released. This study aims to investigate the accuracy

INTERNATIONAL JOURNAL OF GEOMATICS AND GEOSCIENCES
Volume 1, No 4, 2011

© Copyright 2010 All rights reserved Integrated Publishing services

Research article ISSN 0976 – 4380

performance of several global and national DEMs in order to define the suitability of them in engineering and geomatics applications in Kingdom of Saudi Arabia (KSA).

2. Study Area

Makkah city is located in the south-west part of KSA, about 80 Km east of the Red Sea (Figure.1). It extends from 39° 35' E to 40° 02' E, and from 21° 09' N to 21° 37' N. The area of the metropolitan region (the study area) equals 1593 square kilometers. The topography of Makkah is complex in nature, and several mountainous areas exist inside its metropolitan area.

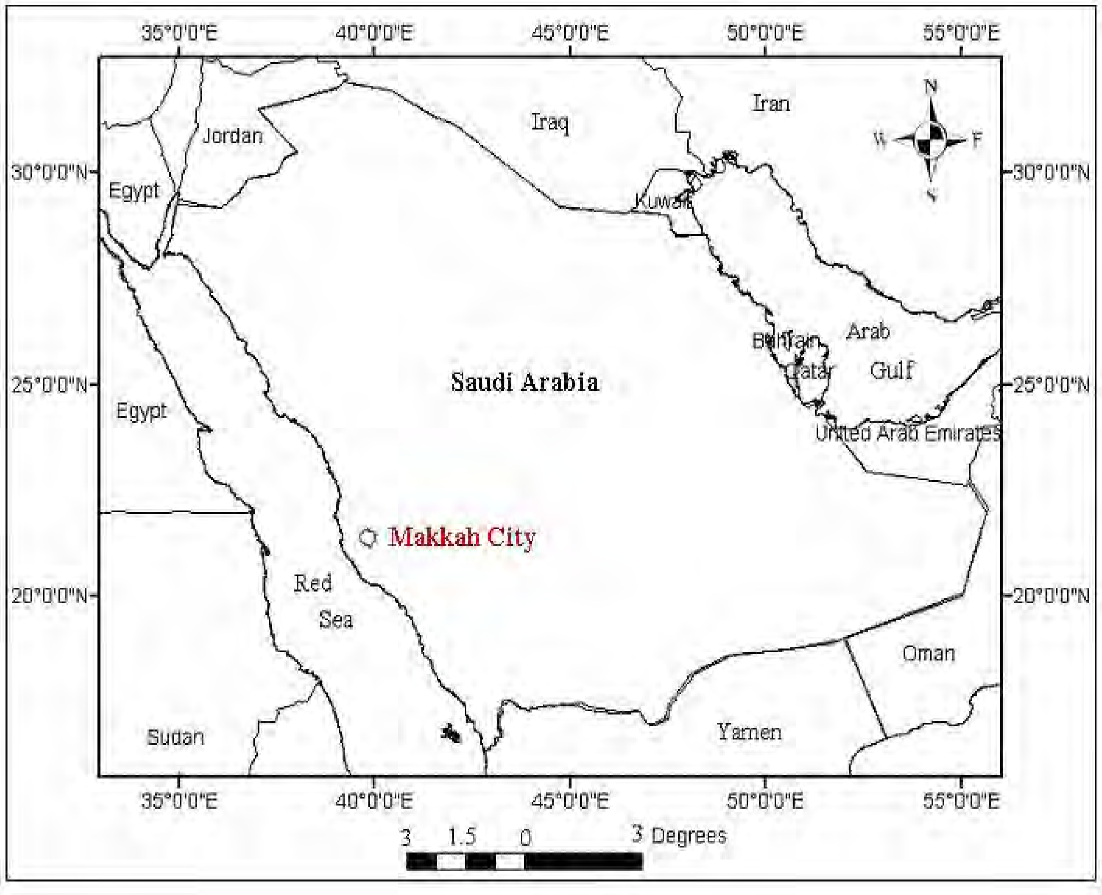

Figure 1: Study Area

2.1 Digital Elevation Models (DEMs)

Two global DEMs, along with two KSA national DEMs, have been exploited in this research, and they will be briefly described.

INTERNATIONAL JOURNAL OF GEOMATICS AND GEOSCIENCES
Volume 1, No 4, 2011

© Copyright 2010 All rights reserved Integrated Publishing services

Research article ISSN 0976 – 4380

2.2 Global DEMs

The Ministry of Economy, Trade, and Industry (METI) of Japan and the United States National Aeronautics and Space Administration (NASA) have jointly released Version 1 of the Advanced Spaceborne Thermal Emission and Reflection Radiometer (ASTER) Global Digital Elevation Model (GDEM). ASTER horizontal resolution equals 1 arc second, that is 30 meters approximately, and it is available free of charge. ASTER DEM has been utilized in many research studies (Dowerah 2010, Abdeen et al. 2009, and Mousavi et al. 2007). The window of the ASTER DEM corresponding to Makkah metropolitan area has been downloaded (http://www.gdem.aster.ersdac.or.jp/) and has been considered in this study (Figure. 2).

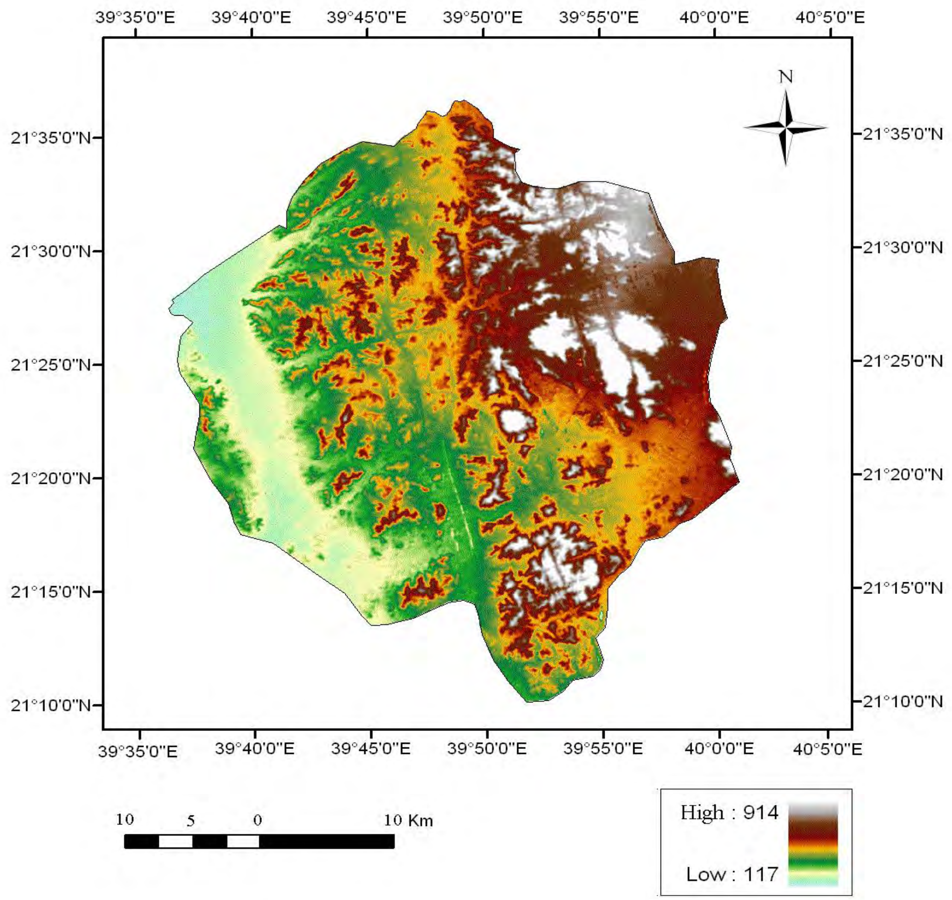

Figure 2: ASTER DEM for Makkah

The Shuttle Radar Topography Mission (SRTM) global DTM is a joint project between the U.S. National Imagery and Mapping Agency (NIMA) and the National Aeronautics and Space Administration (NASA). A 90 meters (3 arc seconds) SRTM DTM for many parts of the world has been compiled and released (Called SRTM3) and being available free of charge. SRTM3 has been used in geoid odeling for several regions, particularly

INTERNATIONAL JOURNAL OF GEOMATICS AND GEOSCIENCES
Volume 1, No 4, 2011

© Copyright 2010 All rights reserved Integrated Publishing services

Research article ISSN 0976 – 4380

for topographic and downward continuation corrections (Kiamehr and Sjöberg 2005) and also for morphometric studies (Bubenzer and Bolten 2008, and El Bastawesy 2007). The window of the SRTM DEM corresponding to Makkah territories has been downloaded (http://www2.jpl.nasa.gov/strm/) and has been considered in this study (Figure. 3).

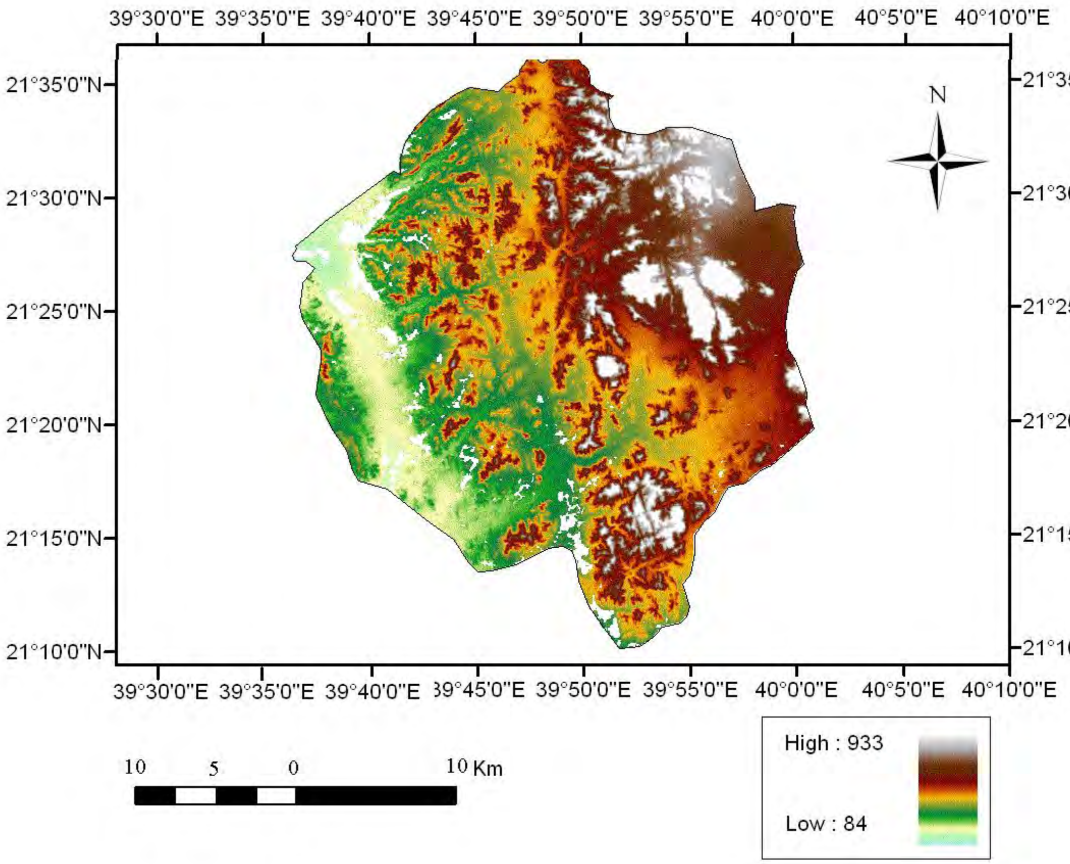

Figure 3: SRTM3 DEM for Makkah

2.3 National DEMs

Two national DEMs have been acquired, with resolution of 5 and 10 meters, developed by King Abdulaziz City of Sciences and Technology (KACST). Windows cover Makkah metropolitan area has been provided through the Center of Excellence in Hajj and Omrah, Umm Al-Qura University. The ASTER and SRTM3 are rectified relative to the World Geodetic System 1984 (WGS84). Since the available GPS data are relative to that geodetic datum too, the national 5-m (Figure. 4) and 10-m DEM has been projected from the national Saudi geodetic datum (Ain El-Abd 1970) to WGS84. That process, and consecutive procedures, has been performed using the Arc GIS software.

© Copyright 2010 All rights reserved Integrated Publishing services

Research article ISSN 0976 – 4380

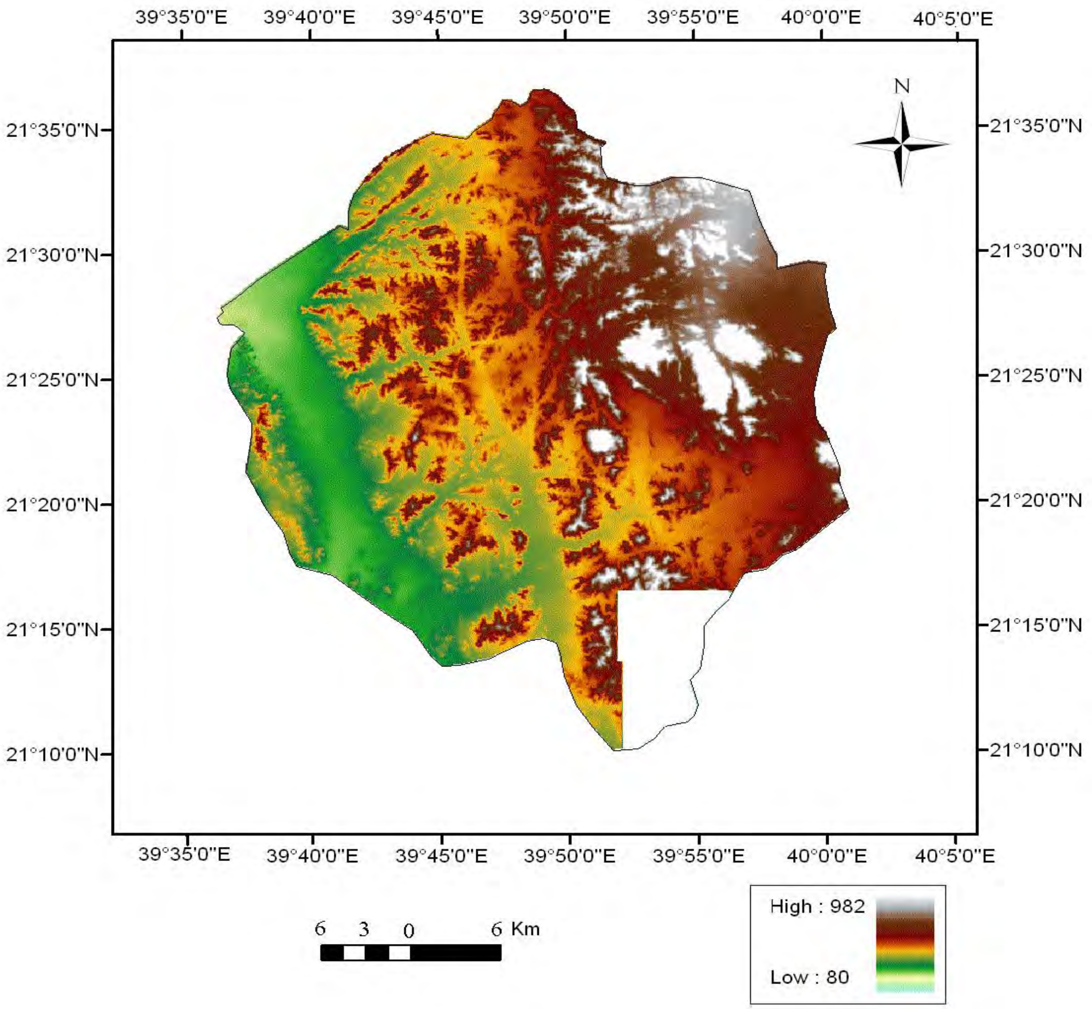

Figure 4: National 5-m DEM for Makkah

3. Data and Processing

3.1 Available data

A dataset of 200 first-order Global Positioning System (GPS) terrestrial control points, with known orthometric heights, has been compiled and used to judge the accuracy of DEMs. That dataset covers the entire Makkah metropolitan region as seen in Figure 5.

3.2 Processing methodology

GIS provides an efficient technical tool for spatial and attribute data storage, manipulation, processing and analysis. Utilizing GIS technology in GPS surveying activities facilitate the data processing for a number of applications (Dawod and

INTERNATIONAL JOURNAL OF GEOMATICS AND GEOSCIENCES
Volume 1, No 4, 2011

© Copyright 2010 All rights reserved Integrated Publishing services

Research article ISSN 0976 – 4380

Mohamed 2009). The GIS processing procedures, carried out in this research, consist of several steps (Figure. 6).

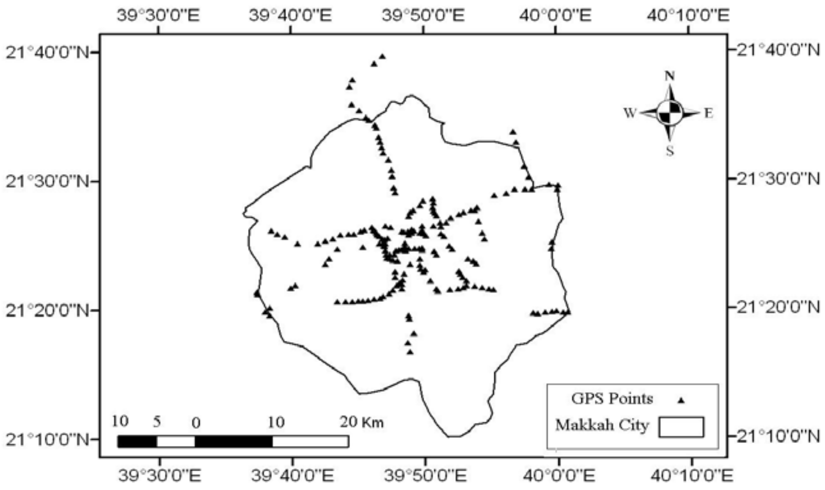

Figure 5: Available GPS Stations

Firstly, all available DEMs and the GPS dataset have been imported within the Arc GIS software. That program has a lot of spatial analysis tools within its Arc Toolbox component. That component, in the second procedure, has been utilized to interpolate the DEMs' heights of the available GPS points. Thirdly, the obtained DEMs' heights have been compared against the known heights of the 200 terrestrial control points cover the Makkah metropolitan area. Finally, statistical analysis has been performed to investigate the accomplished results.

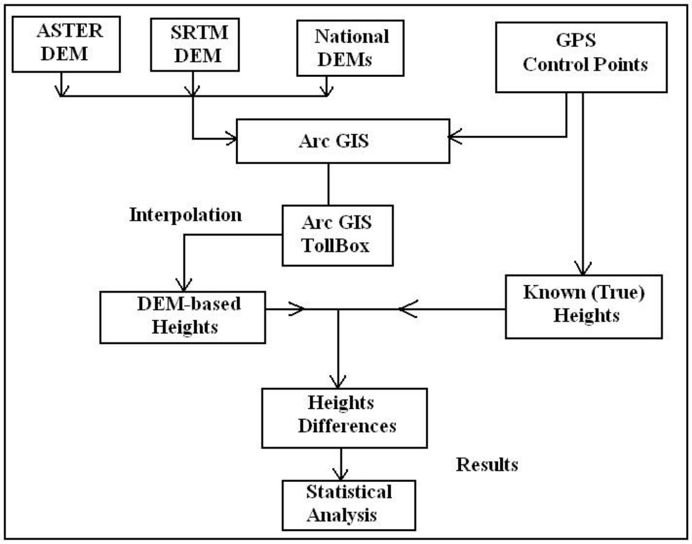

Figure 6: GIS Processing Steps

INTERNATIONAL JOURNAL OF GEOMATICS AND GEOSCIENCES
Volume 1, No 4, 2011

© Copyright 2010 All rights reserved Integrated Publishing services

Research article ISSN 0976 – 4380

4. Results, discussion, and conclusions

4.1 DEM accuracy

For the global DEMs, the published accuracy levels are 7-14 and 6-10 meters for ASTER and SRTM3 respectively (Abrams et al. 2008 and Rodriguez et al. 2005 respectively). These accuracy levels are on a global scale, hence, the main task of the current research is to assess their accuracy within Makkah metropolitan area. DEMs accuracy assessment studies have been performed in several regions in the world (Denker 2005, Kiser and Kelly 2010, and Dawod 2008). Clearly, it can be noticed from figures 1 and 2 that there are some differences between ASTER and SRTM3 DEMs over Makkah. ASTER produces height values range from 117 to 914 meters, while the SRTM3's heights range vary from 84 to 933 meters. From Figure 3, the corresponding heights of the 5-m national DEM range from 80 to 982 meters.

Tables 1 and 2 present the accomplished results of heights comparison. From Table 1, it can be seen that the ASTER DEM yields height differences range from -20.34 m to 19.30 m, with a mean value of 2.59 m and a standard deviations equals ± 8.66 m. On the other hand, the SRTM3 DEM produces height differences vary from -20.12 m to 9.07 m, with an average of -5.20 m and standard deviations equals ± 5.85 m. Therefore, it can be concluded that the 90-m resolution SRTM3 DEM is more accurate than the 30-m resolution ASTER DEM by a factor of 1.5 approximately, over Makkah city. Comparable results over Australia have been reported (Hirt et al. 2010).

Table 1: Statistics of Global DEMs' Height Differences over Check Points

	Heights Differences of ASTER	Heights Differences of SRTM3
Minimum	-20.34	-20.12
Maximum	19.30	9.07
Mean	2.59	-5.20
Standard Deviation	8.66	5.85

Regarding the available national DEMs, it can be seen, from Table 2, that the 10-m resolution DEM generates height differences range from -7.60 m to 7.36 m, with a mean value of 0.01 m and a standard deviations equals ± 2.96 m. Conversely, the 5-m resolution DEM produces height differences vary from -7.54 m to 7.07 m, with an average of 0.01 m and standard deviations equals ± 2.95 m. Therefore, it can be concluded that there are no significant differences between the accuracy of both DEMs even though their horizontal resolutions are different. This conclusion is quite important in computer data processing since the file size of the 5-m resolution DEM is almost twice that of the 10-m DEM. Hence, utilizing the 10-m DEM will be faster in performing processing tasks of surveying, mapping, and geomorphologic studies.

INTERNATIONAL JOURNAL OF GEOMATICS AND GEOSCIENCES
Volume 1, No 4, 2011

© Copyright 2010 All rights reserved Integrated Publishing services

Research article ISSN 0976 – 4380

Table 2: Statistics of National DEMs' Height Differences over Check Points

	Heights Differences of National 10m-DEM	Heights Differences of National 5m-DEM
Minimum	-7.60	-7.54
Maximum	7.36	7.07
Mean	0.01	0.01
Standard Deviation	2.96	2.95

Another comparison between global and national DEMs reveals that both national DEMs are more accurate, in representing the topography of Makkah city, by factors of 3 and 2 over the global ASTER and SRTM3 DEMs respectively.

4.2 DEM relevance

A chief concern in utilizing DEMs is to select a DEM that is appropriate, in terms of precision, for a specific geodetic, mapping, or morphometric task. Three example issues, in this regard, will be considered. Firstly, creating contour maps from a DEM mainly depends on the DEM accuracy. The United States Geological Survey (USGS) standards state that: "for topographic maps, the vertical accuracy standard, for all map scales, requires that the elevation of 90 percent of all points tested must be correct within half of the contour interval" (USGS 1999). Hence, the tested two national DEMs can be used to develop topographic maps with a contour interval equals 6 m, while SRTM3 and ASTER DEMs can yield 12-m and 18-m interval contour maps, respectively. Secondly, the rigid topography of Makkah metropolitan area emphasis the fact that a precise DEM is needed in estimating the terrain corrections in quasi-geoid modelling. Hence, the 5-m resolution national DEM is the optimum candidate in developing gravimetric co-geoid of Makkah city. Thirdly, for hydrological analysis and water resources management, DEM spatial resolution affects flood simulation and the computations of inundation areas from flood simulations (Li and Wong 2010 and Dixon and Earls 2009).

5. Conclusions

DEMs play a crucial role in geodetic, geomorphologic, and mapping applications. This study has investigated the accuracy of two national DEMs, with 5m and 10m resolutions, along with the ASTER and SRTM3 global DEMs. A dataset of 200 first-order GPS ground control points, that covers the Makkah (Mecca) metropolitan area in the western region of Saudi Arabia, has been utilized to judge the accuracy of these DEMs. The attained results showed that the 5-meter resolution national DEM is the most accurate one and produces mean height difference and standard deviations equal 0.01 ± 2.95 m respectively. That national DEM is more accurate by factors of 3 and 2 over the global ASTER and SRTM3 DEMs respectively. Recommendations have been drawn to apply each DEM in the geodetic, topographic mapping, and geomorphologic activities in Saudi Arabia.

© Copyright 2010 All rights reserved Integrated Publishing services

Research article ISSN 0976 – 4380

Acknowledgements

The authors would like to acknowledge the financial support offered by the Center of Research Excellence in Hajj and Omrah, Umm Al-Qura University, Saudi Arabia.

6. References

1. Abdeen, M. El-Kazzaz, Y., Attia, G., Yehia, M., and Hassan, S. (2009), "Mapping geological structures in Wadi Ghoweiba area, northwest gulf of Suez, Egypt, using ASTER Spot data fusion and ASTER DEM", Egypt Journal Remote Sensing and Space Sciences, 12, pp 101-126.

2. Abrams, M., Hook, S., and Ramachandran, B. (2008), "ASTER user handbook: Version 2", Jet Propulsion Laboratory, Pasadena, CA, USA.

3. Bubenzer, O. and Bolten, A. (2008), "The use of new elevation data (SRTM/ASTER) for the detection and morphometric quantification of Pleistocene megadunes (Draa) in the eastern Sahara and the southern Namib", Geomorphology, 102, pp 221–231.

4. Dawod, G. (2008), "Towards the redefinition of the Egyptian geoid: Performance analysis of recent global geoid and digital terrain models", Journal of Spatial Science, 53(1), pp 31-42.

5. Dawod, G., and Mohamed, W. (2009), "Data management of different height systems within GPS/GIS integrated spatial technology", Middle East Spatial Technology Conference (MEST2009), December 7-9, Kingdom of Bahrain.

6. Denker, H. (2005), "Evaluation of SRTM3 and GTOPO30 terrain data in Germany", The International Association of Geodesy's Symposium on Gravity, Geoid and Space Missions, 129, pp 218-223.

7. Dixon, B. and Earls, J. (2009), "Resample or not? Effects of resolution of DEMs in watershed modelling", Hydrological Processes, 23, pp 1714–1724.

8. Dowerah, B. (2010), "ASTER DEM based studies for geological investigation around Singhbhum Shear Zone (SSZ) in Jharkhand, India", Journal of Geographic Information System, 2, pp 11-14.

9. El Bastawesy, M. (2007), "Influence of DEM source and resolution on the hydrographical simulation of Wadi Keed catchment, Sinai, Egypt", Egypt Journal of Remote Sensing and Space Sciences, 10, pp 53-62.

10. Hirt, C. Filmer, M., and Featherstone, W. (2010), "Comparison and validation of the recent freely available ASTER-GDEM ver1, SRTM ver4.1 and GEODATA

© Copyright 2010 All rights reserved Integrated Publishing services

Research article ISSN 0976 – 4380

DEM-9S ver3 digital elevation models over Australia", Australian Journal of Earth Sciences, 57, pp 337–347.

11. Kiamehr, R. and Sjöberg, L. E. (2005), "Effect of the SRTM global DEM on the determination of a high-resolution geoid model: a case study in Iran", Journal of Geodesy, 2005, 79(9), pp 540-551.

12. Kiser, L. and Kelly, M. (2010), "GPS- vs. DEM-derived elevation estimates from a Hardwood dominated forest watershed", Journal of Geographic Information System, 2, pp 147-151.

13. Li, J. and Wong, D. (2010), "Effects of DEM sources on hydrologic applications", Journal of Computers, Environment and Urban Systems, 34, pp 251–261.

14. Mendas, A. (2010), "The contribution of the digital elevation models and geographic information systems in a watershed hydrologic research", Applied Geomatics, 2, pp 33–42.

15. Mousavi, S., Fallah, A., Abbasnejadc, R., Mousavi, S. R., and Shabani, M. (2007), “The ASTER DEM generation for geomorphometric analysis of central Alborz mountains, Iran”, Proceedings of the Asian Association of Remote Sensing Conference, Nov. 12-16, Kuala Lumpur, Malaysia.

16. USGS (U.S. Geological Survey) (1999), "Map accuracy standards", USGS Fact Sheet 171-99, November.

17. Rodriguez, E., Morris, C., Belz, J., Chapin, E., Martin, J., Daffer, W., and Hensley, S. (2005), "An assessment of the SRTM topographic products", Technical Report JPL D-31639, Jet Propulsion Laboratory, Pasadena, California, USA.

18. Subyani, A., Qari, M., and Matsah, M. (2010), "Digital elevation model and multivariate statistical analysis of morphometric parameters of some wadis, western Saudi Arabia", Arab Journal Geosciences, Published on line May 11.

Journal of Geographic Information System, **2013, 5, 378-395**
doi:10.4236/jgis.2013.54036Published Online August 2013 (http://www.scirp.org/journal/jgis)

GIS-Based Public Services Analysis Based on Municipal Election Areas: A Methodological Approach for the City of Makkah, Saudi Arabia

Gomaa M. Dawod, Meraj N. Mirza, Ramze A. Elzahrany, Khalid A. Al-Ghamdi
Deaprtment of Geography, Umm Al-Qura University, Makkah, Saudi Arabia
Email: gmmahmoud@uqu.edu.sa

Received May 23, 2013; revised June 25, 2013; accepted July 15, 2013

Copyright © 2013 Gomaa M. Dawod *et al.* This is an open access article distributed under the Creative Commons Attribution License, which permits unrestricted use, distribution, and reproduction in any medium, provided the original work is properly cited.

ABSTRACT

The spatial fairness of public services is a major aspect in offering a healthy and cheerful living environment in a city. The Geographic Information System (GIS) technology has been applied to investigate the spatial distribution of some selected public services over the municipal election areas within Makkah city, Saudi Arabia. These services include education, health, security, religious, commercial, and sports services. The attained results show that except for religious services, other public services are not quantitatively proportional with the population variations in Makkah. It has been found that the third election area posses almost one third of five public services and two thirds of the sport services. That might be attributed to the fact that the third election area possesses almost a one quarter of the city population. But, although the first election area has a closer percentage of the total population, it does not include a comparable percentage of public services. On a spatial basis, results of GIS spatial analysis (particularly the Euclidian distance, the mean distance band to a neighbor, the standard distance, the directional distribution ellipse, and the average nearest neighbor ratio tools) have concluded that there is inequity in the services distribution over municipal election areas in Makkah city. Consequently, it is recommended that local planners and decision makers should take the obtained results into consideration to achieve fair and better distribution of public services in the city.

Keywords: Public Services; Spatial Analysis; GIS; Saudi Arabia

1. Introduction

Public services and facilities are essential for residents in any city all over the world in general, and in developing countries in particular. Governments start to rethink the delivery of public services in order to enhance their quality and quantity, to meet public's needs and expectations [1]. Improving efficiency of basic public services for residents has been recognized as one of the major ways of promoting sound human settlements, good health, and appropriate and decent living conditions. Assessing efficiency of public services is multidimensional and includes several factors such as geographic and financial accessibility, availability, quantity, distribution, quality, and clients' satisfaction. However, spatial distribution is of great importance. Thus, spatial analysis of public services distribution gains an increasing attention in the last decades from both geographic and environmental perspectives [2]. Moreover, the issue of spatial equity of urban public facilities has proliferated recently from both planning and geographic points of view, trying to arrive to the so-called spatial justice [3]. Diagnosing the current situation of a public service is quite essential in planning its new spatial locations in order to increase the service availability and accessibility to residents [4]. Geographic Information System (GIS) plays an important technical role in spatial analysis of geographic features. GIS has been utilized in a wide range of mapping and analysis applications all over the world in general, and in Kingdom of Saudi Arabia (KSA) in particular. Such GIS applications include, for instance, urban growth monitoring [5], flood management [6], and health services' spatial analysis [7]. Concerning services spatial analysis, GIS has been applied in several studies. For example, Zhou *et al.* [8] have utilized GIS to identify and map the distribution pattern of public and community facilities in a study area in four neighboring sub-districts in Beijing, China and to analyze their spatial equity. Moreover, Mavo *et al.* [9] investigated the utilization of GIS to assess accessibility of public transit in New Zealand. Similarly, GIS

was used to develop a site suitability model for social services in Atlanta city [10]. In addition, GIS has been applied to identify spatio-temporal gaps in public transportation services in Belgium [11]. In Saudi Arabia, public services are mainly provided by the government with significant attention to the holy city of Makkah. During the period 1990 to 2010, Makkah total residential area had been increased from 99.23 to 158.58 square kilometers, with 4.8% annual rate [5]. In addition, the annual population growth rate in KSA is almost 2.9%. Both growing rates emphasize the need for new public services in terms of quantities and spatial distribution. This paper utilizes GIS for mapping and analyzing the distribution of existing public services based on municipal election areas in Makkah.

2. The Study Area

Makkah city is located in the western region of the Kingdom of Saudi Arabia (KSA), about 80 km east of the Red Sea (**Figure 1**). It extends from longitudes 39˚35'E to 40˚02'E, and from latitudes 21˚09'N to 21˚37'N. Makkah city is a sacred city for all Muslims; since it houses Al-Masjid Al-Haram (the Holy Mosque). All Muslim are expected to perform Hajj "pilgrimage" to Makkah once in their life time if they can afford it. Thus, million Muslims gather in Makkah yearly. Also, Muslims perform Omrah "a religious visit to Makkah" all over the years. The religious functionality of Makkah is an important factor to be considered when analyzing its services distribution. For instance, there are several seasonal allocations of public services, e.g. health and security services, in the holy sites. The seasonal services have been excluded in the current research. Moreover, the topography of Makkah is complex, and several mountainous areas exist inside its metropolitan area. That is a vital element in investigating the spatial pattern of Makkah sprawl and service spatial locations. Terrain elevations in Makkah (**Figure 2**) range from 82 to 982 meters above sea level [12]. Al-Ghamdi *et al.* [5] have concluded that the urban growth in Makkah city (between 1947 and 2010) take a radial (or spoke) pattern. That is logically understood knowing that the holy mosque is considered the center of the city, and the central area around it has the highest population density since residents and pilgrims prefer to stay close to this holy mosque.

Makkah city is composed of 60 districts, one of them is a special area containing the holy sites of Mina, Muzdalifa, and Arafat. This last district is excluded from the

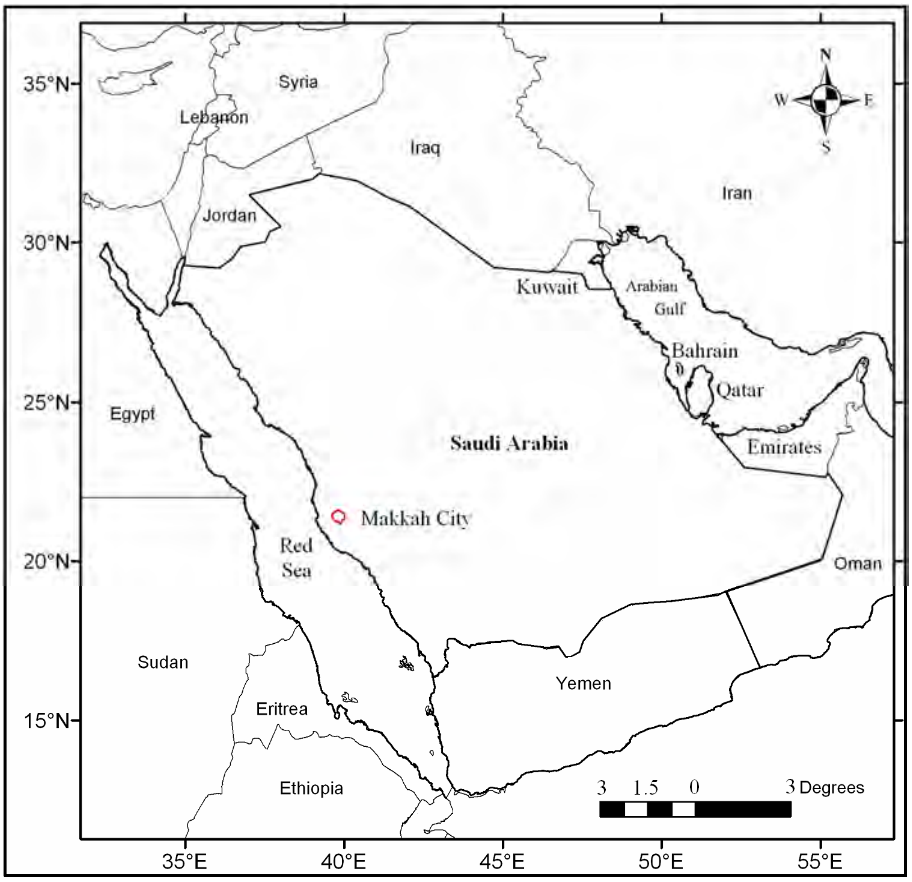

Figure 1. Study area.

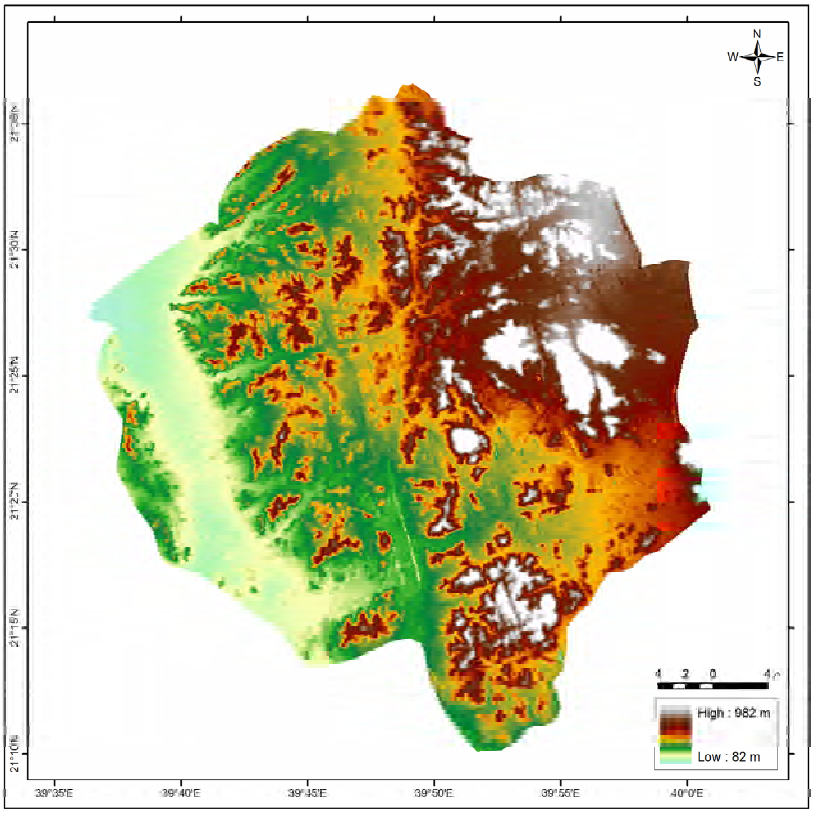

Figure 2. Topography of Makkah city.

current study, since its public services are seasonal in nature and operate only during the pilgrimage seasons. There are seven municipal election areas in Makkah, where the seventh area contains the western villages outside the urban extents of the city. Hence, only the six urban municipal election areas within the city have been considered in this study (**Figure 3**). **Table 1** and **Figure 4** present the population relative distribution over the municipal election areas of Makkah city. It can be seen the third election area posses the highest population percentage, and it contains more than a quarter of the city total population. The first election area, which is the central area of the city, ranks second. The fifth and sixth municipal election areas contain the least population portions, since they are newly urbanized areas.

3. Available Data

The quantity and spatial distribution of six types of public services have been investigated in this study. They include: general education services, security services, health services, commercial services, religious services, and sport services. The corresponding GIS shapefiles have been obtained from the Holy City Municipality's base map released in 2012. However, these shapefiles depict both existing and planned services. In order to limit the current study to the existing services only, several editing process using ArcGIS 10.0 have been carried out to eliminate non-existing features on recent IKONOS satellite imageries of Makkah city. Education services have been grouped into four sub-types; kindergarten, primary schools, intermediate schools, and secondary or high schools (**Figure 5**). Also, security services have been divided into fire stations, police stations, and traffic facilities (**Figure 6**). Health services include both governmental and private facilities (**Figure 7**). Three sub-types of religious services have been assessed (**Figure 8**). Similarly, commercial services, markets in particular, have been divided into three sub-groups (**Figure 9**), and sports services have been divided into three sub-types too (**Figure 10**).

Table 1. Distribution of population percentage on municipal election areas.

Municipal Election Area	1	2	3	4	5	6
No. of Districts	11	14	15	9	5	5
Percentage of Population	24.1%	20.4%	26.4%	12.3%	9.2%	7.5%

4. Methodology and Data Processing

The analysis of public services distribution has been car-

Copyright © 2013 SciRes.

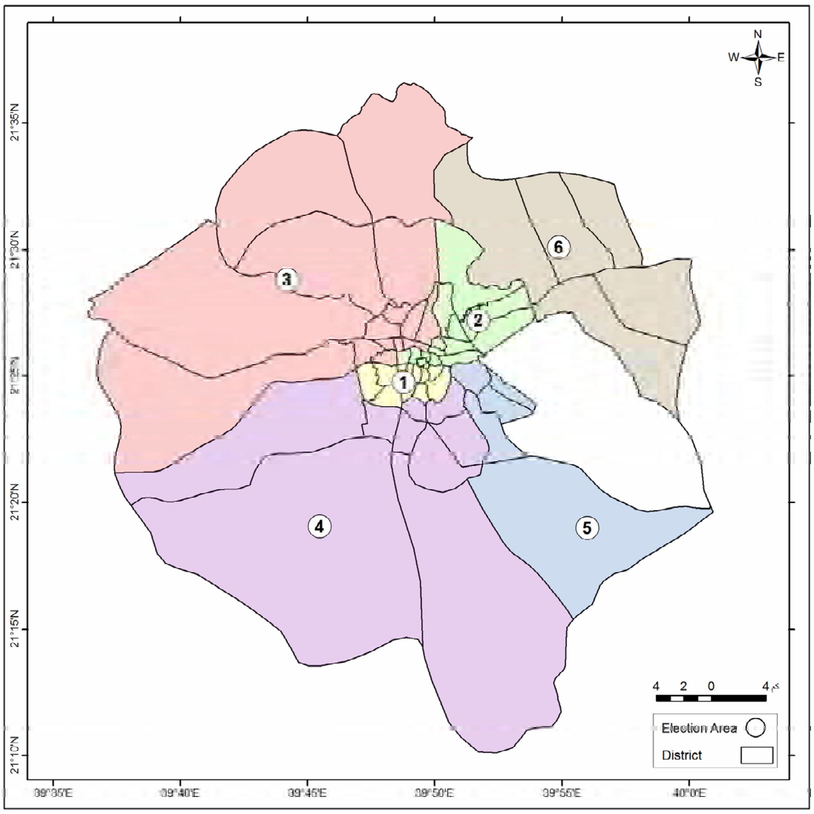

Figure 3. Districts and municipal election areas.

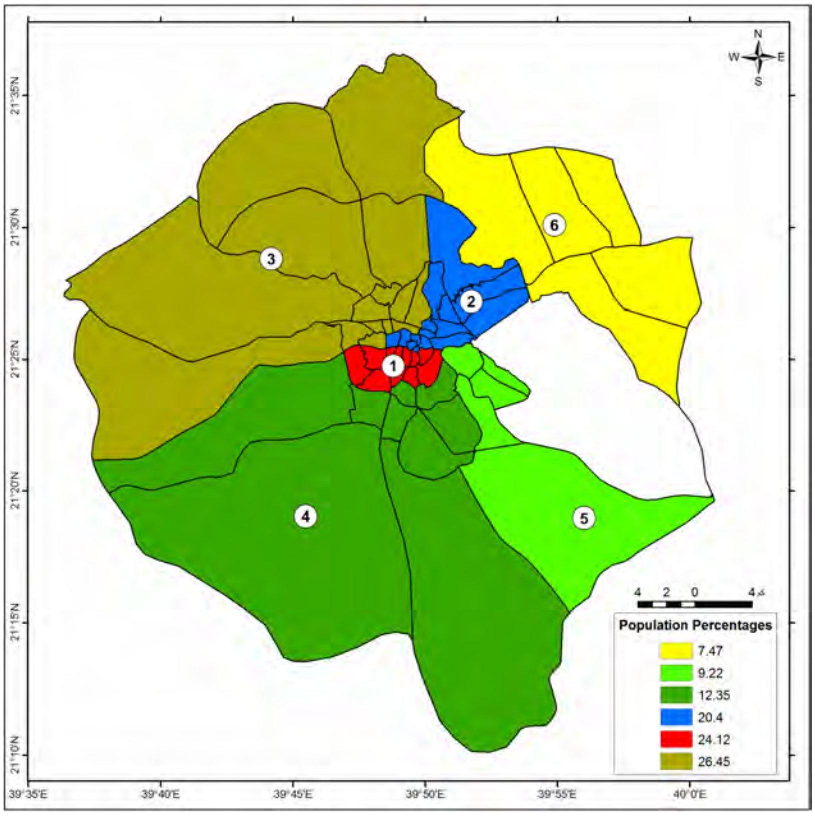

Figure 4. Population relative distribution.

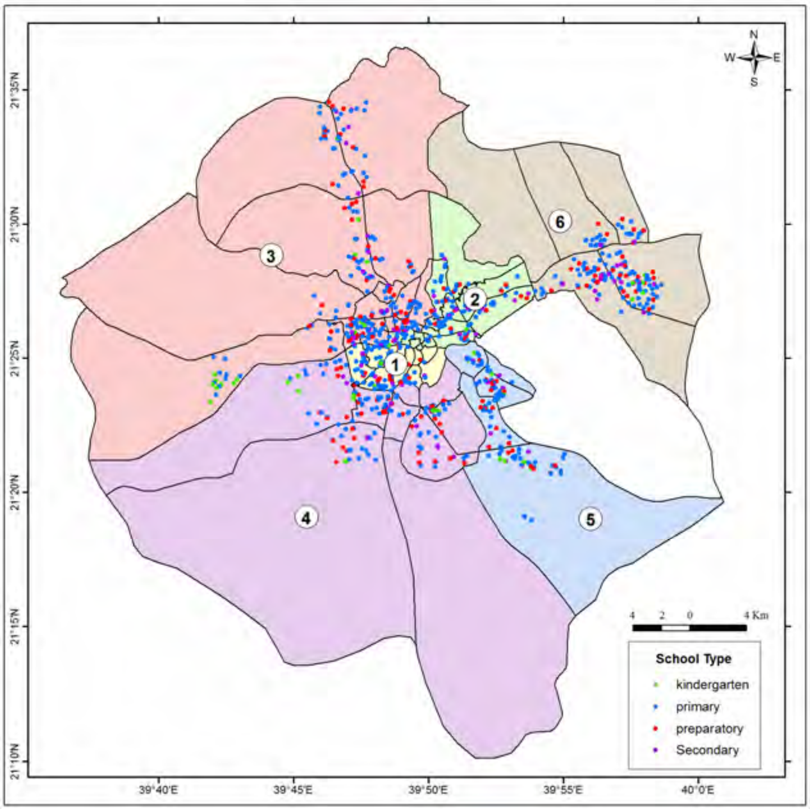

Figure 5. Education services.

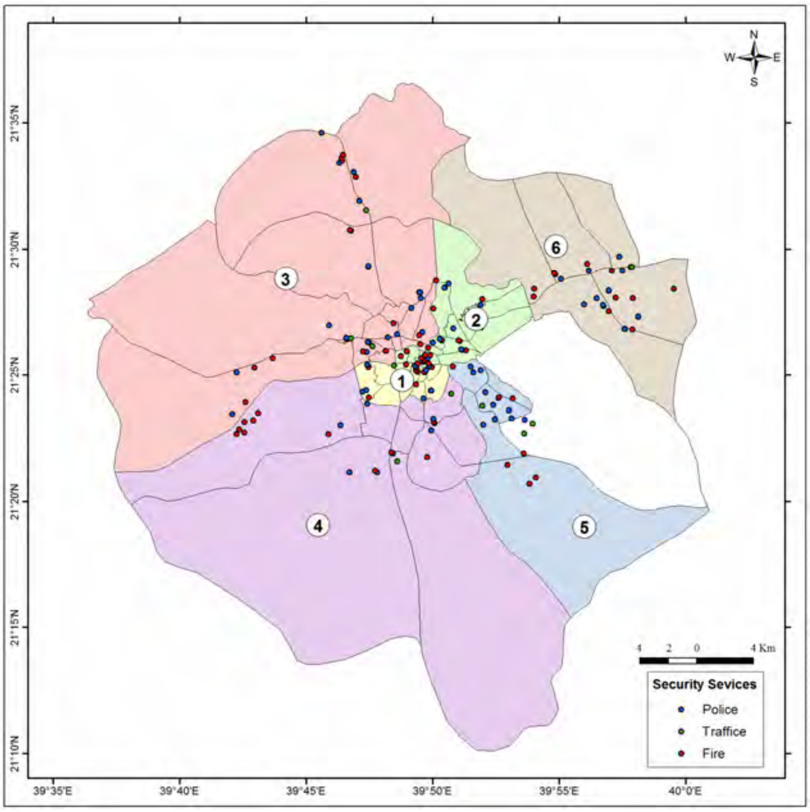

Figure 6. Security services.

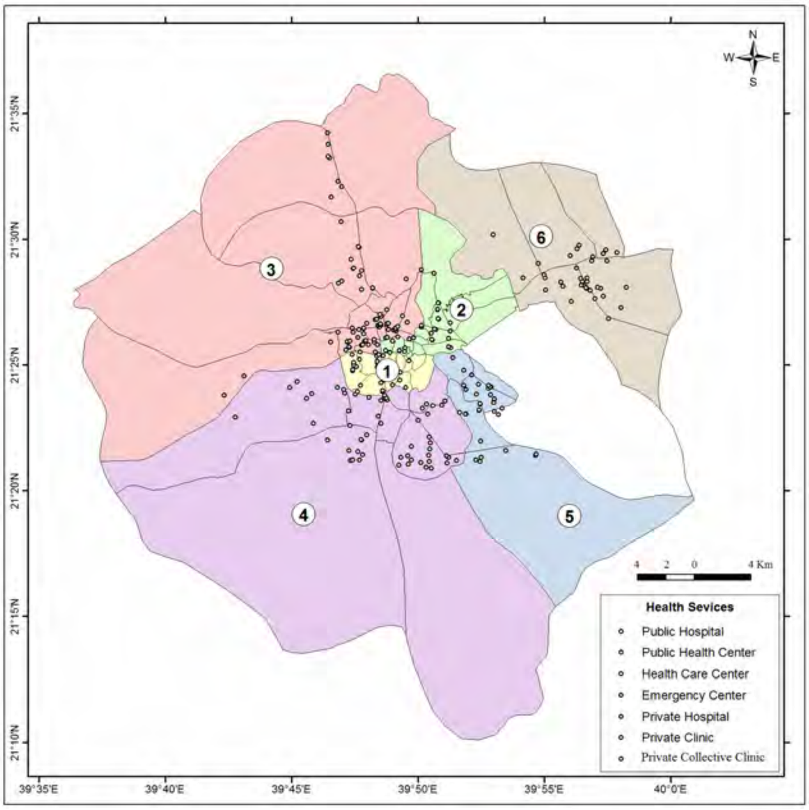

Figure 7. Health services.

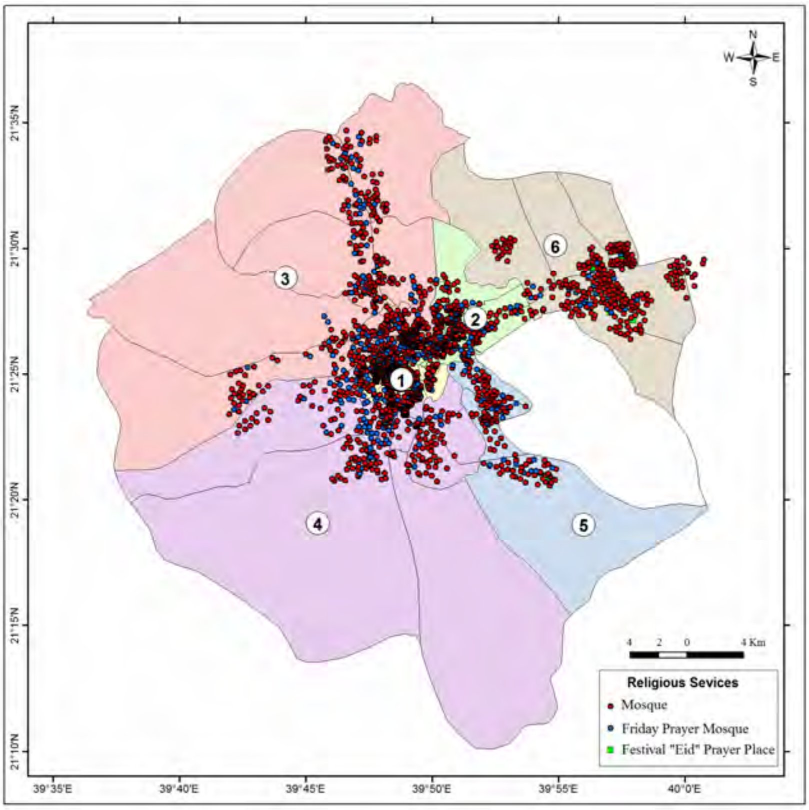

Figure 8. Religious services.

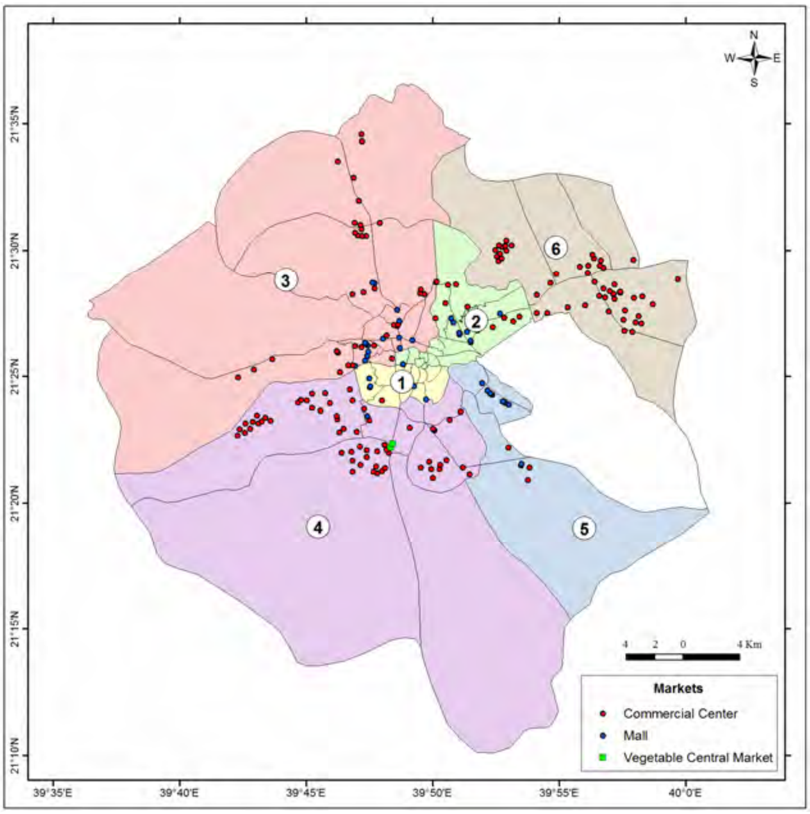

Figure 9. Commercial services.

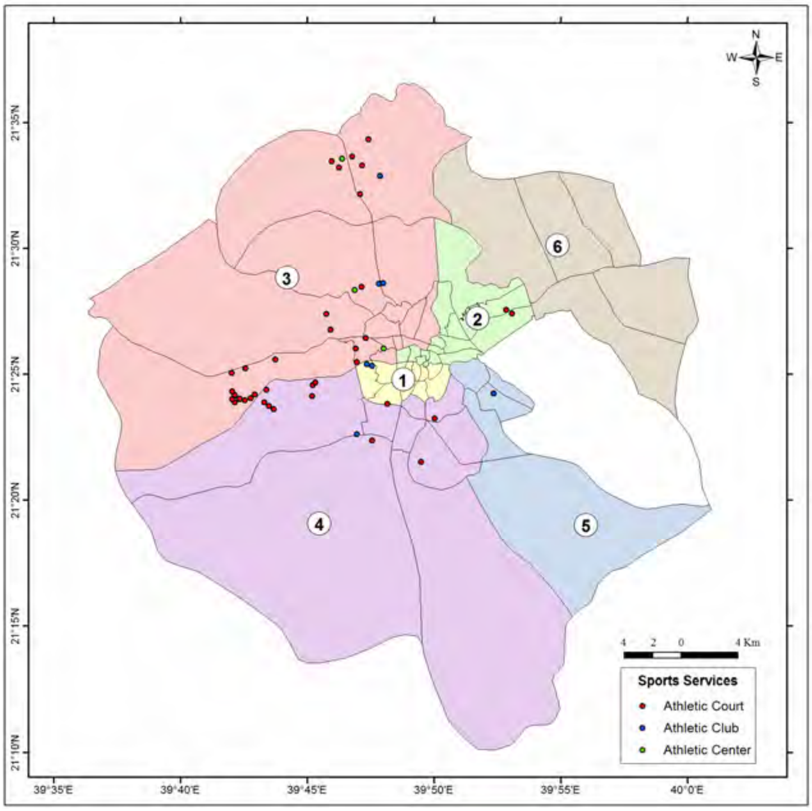

Figure 10. Sports services.

ried out on both statistical and spatial scales within the municipal election areas of Makkah. First, ArcGIS has been used to split each service's spatial distribution over the municipal election areas. Thus, the quantity of each sub-type of the utilized public services has been obtained. So, a percentage portion has been computed for each sub-category of a specific service for each election area. For more simplicity, these percentage figures have been scaled by 10 in order to obtain a simple measure on a scale ranges from 1 to 10. Let us denote such a scale Ri, j, where i denotes a public service, and j denotes sub-types within that service. So, i in our study ranges from 1 to 6 (number of available public services types), and j varies from 1 to 7 according to numbers of sub-categories in each public service. Another factor, Ti, has been computed that represents, on a scale from 1 to 10, the relative portion of each public service located within each election area. That means that Ti accounts generally for a specific service, while Ri, j accounts for sub-types within each service. Next, an overall indicator has been computed to describe the availability and relative distribution of public services over the municipal election areas in Makkah city. This indicator is called Public Services Index (PSI) as:

$$\text{PSI} = \left(1/\text{m}\right)\sum_{i=1}^{6}\sum_{j=1}^{7}\text{Ri, j} \tag{1}$$

where m equals the total numbers of public services' sub-types (that is 24 in the current study). PSI, also, has a value ranges from 0 to 10 for simplicity, and the sum of PSI's indices equals 10 for a certain public service. Thus, it can be though of as a measure of justifiable distribution of public services over municipal election areas in Makkah city.

In the next processing stage, the equity issue of public services distribution, with respect to population variations, has been investigated. In this regard, the Lorenz curve and the Gini index have been utilized. The Gini index or coefficient is based on the Lorenz curve, a cumulative frequency curve that compares the distribution of a specific variable with the uniform distribution that represents equality. This equality distribution is represented by a diagonal line, and the greater the deviations of the Lorenz curve from this line, the greater the inequality. By putting commutative proportion of a particular public service in the y axis and commutative proportion of population of the election area in the x axis, the area of equality is being calculated. A low Gini coefficient indicates a more equal distribution, with 0 corresponding to complete equality. While higher Gini coefficients indicate more unequal distributions, with 1 corresponding to complete inequality. In addition, correlation and geographically weighted regression analysis have been performed to investigate the statistical characteristics between the public services quantity and distribution and the population variations in the municipal election areas. Then, a prediction has been attained to estimate the required public services in Makkah city in 2020. The spatial analysis stage includes the utilization of selected four main spatial tools available in ArcGIS. The Euclidian distance, the standard distance, the directional distribution ellipse, and the average nearest neighbor ratio. The Euclidian distance tool calculates for each cell or feature the zone of the closest source location in Euclidean distance. Hence, the attained raster represents the spatial variation of a specific public service over the municipal election areas of Makkah city. The standard distance and the directional distribution ellipse are spatial analysis tools measure the geographic distribution. On the other hand, the directional distribution tool measures whether a distribution of features exhibits a directional trend, *i.e.* whether features are farther from a specified point in one direction than in another direction.

5. Results and Discussion

Starting with the statistical analysis, **Table 2** and **Figure 11** present the index of relative portion of each public

Table 2. Relative distribution of public services (on a scale 0 to 10).

Public Service	Municipal election areas					
	1	2	3	4	5	6
Education	1.2	1.5	2.9	1.6	1.3	1.6
Health	1.1	1.3	2.9	2.2	1.1	1.4
Security	1.4	2.0	2.6	1.3	1.1	1.7
Religious	1.9	1.7	2.7	1.6	0.8	1.4
Commercial	0.3	0.9	2.5	3.1	0.7	2.5
Sports	0.6	0.4	6.5	2.3	0.2	0.0
Overall Average Scale (PSI index)	1.1	1.2	3.5	1.8	1.1	1.3

Copyright © 2013 SciRes.

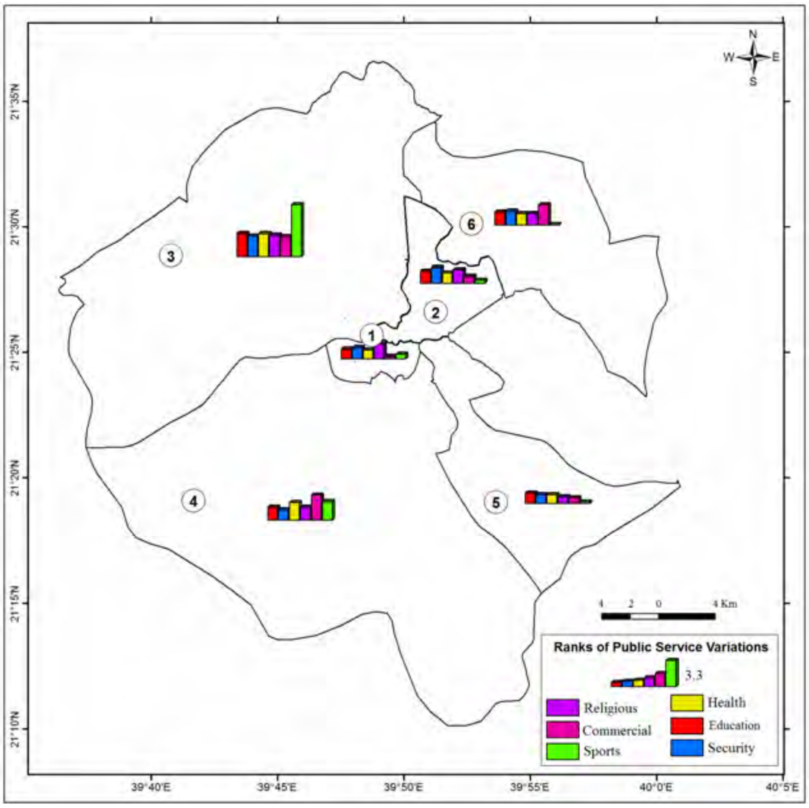

Figure 11. Public services variations.

services over the municipal election area (on a scale 0 - 10). From this table, it can be noticed that the third election area posses almost one third of five public services and two thirds of the sport services. This election area comes in the first rank in all public services distribution except commercial services, where the forth municipal election area becomes first. This result might be attributed to the fact that the third election area possess almost a one quarter of the city population (**Table 1**). But, although the first election area has a close percentage of the total population, it does not include a comparable percentage of the public services. So, and as a general remark, it can be concluded that there is inequity in the services distribution over municipal election areas in Makkah city. The overall indicator (PSI is Equation (1)) is shown in the last column of **Table 2**, and depicted in **Figure 12**. PSI describes the availability and relative distribution of public services over the municipal election areas in Makkah city. It can be concluded that the third election area is the first-ranked area regarding public services availability and quantity. On the other hand, both first and fifth municipal election area comes in the last, or least, rank in this regard. Again, the values of PSI index prove the unfairness nature of public service distribution in Makkah city.

Next, the Lorenz curves and the Gini indices have been developed. **Figure 13** and **Table 3** present the attained results. It can be seen from these table and figure that the inequality of service distribution is significant for both the commercial and sports services. On the other hand, the religious and security services seem to have a reasonable fairness in distribution over the municipal election areas. Both health and education services have a medium equality in their distribution over the city municipal election areas.

Table 3. Gini index of public services.

Public Service	Gini Index
Education	0.38
Health	0.40
Security	0.34
Religious	0.31
Commercial	0.50
Sports	0.47

Similar conclusions can be drawn from the correlation factors between public services and population of the municipal election areas (**Table 4**). It can be seen that the religious services show a strong positive correlation with population of municipal election areas, while the unequal distribution of the commercial services produces a weak negative correlation. That might be attributed to the fact

Copyright © 2013 SciRes.

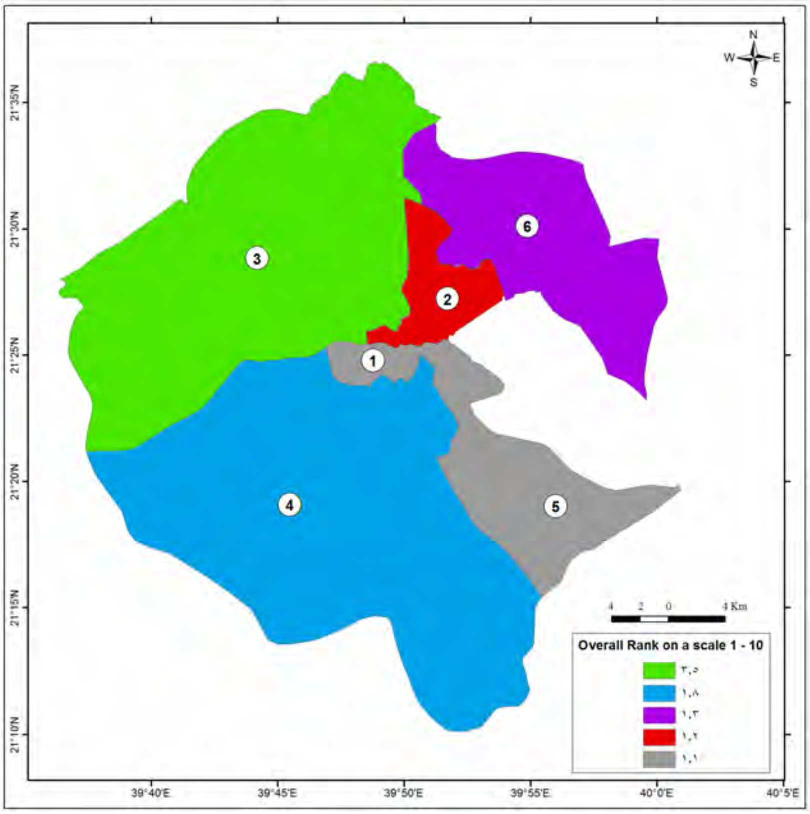

Figure 12. Public services overall index.

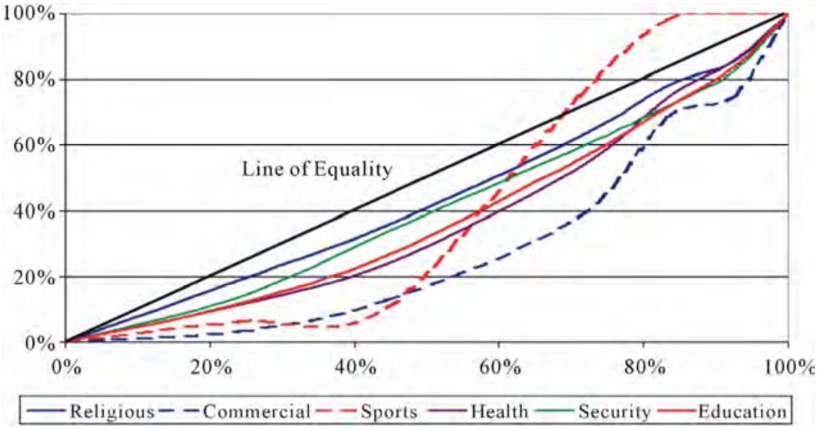

Figure 13. Lorenz curves of public services.

Table 4. Correlation between population and public services quantities.

Public Service	Correlation
Education	0.46
Health	0.37
Security	0.60
Religious	0.83
Commercial	−0.22
Sports	0.58

that the government of KSA and many other Islamic countries are responsible for providing religious services to residents. The inequality in commercial services distribution in Makkah city might be owing to that such private sites are concentrated mainly in the districts that have a large number of hotels, since a large proportion of commercial services depend, to a large extent, on visitors.

The results of the geographically weighted regression, with respect to population, are presented in **Table 5**. The R2 coefficient of regression represents the goodness of

Table 5. Geographically weighted regression between population and public services quantities.

Public Service	Regression Intercept	Regression Coefficient	R2 Coefficient
Education	101.83	0.000272	0.21
Health	28.36	0.000065	0.14
Security	16.32	0.000053	0.36
Religious	121.45	0.001000	0.70
Commercial	45.34	−0.000050	0.05
Sports	−6.31	0.000065	0.34

the attained regression equation since it determines the percentage of the variations in the input data that can be modeled by the regression formula. Thus, it can concluded that the attained regression equations are of little goodness for all public services except for religious services only. Again, this is another statistical evidence that there is dissimilarity of public services distribution over the municipal election areas in Makkah city. So, such regression equations could not be appropriate for computing projected numbers of public services in Makkah city. In this regard, another concept has been utilized. First, the number of individuals correspond to a single public service in each election area is computed. The average of these figures, over all municipal election areas, is then obtained. Based on the average population growth rate in KSA (which is 2.9% annually), the population of Makkah city in year 2020 has been computed and was found to be 1,947,330. Next, the average public service/ capita is utilized to estimate total number of each public service type in year 2020. As a conclusion, it has been found that 135, 31, 25, 417, 59, and 74 new services are needed for education, security, health, religious, commercial, and sports services respectively. However, the distribution of these new public services should be on a justice basis regarding population of the municipal election areas in Makkah.

The second group of the accomplished results express the GIS-based spatial analysis of public service distribution. First, the results of the Arc GIS Euclidian-distance tool are shown in **Figures 14(a)-(f)** for each investigated public service. Additionally, the results of the distance-band-from-neighbor tool are tabulated in **Table 6**.

Analyzing **Table 6** reveals that the sports public services have the maximum mean distance neighbors, while the religious services show the minimum value. Inspecting the figures of Euclidian distance variation between neighbors conclude that the interval 0 - 1000 meters (the yellow interval) is dominant for all public services except for sports services. The inequality of the services spatial distribution, over the municipal election areas, is obviously seen in these figures.

Furthermore, the results of the Arc GIS standard distance, deviational distribution ellipse (both at one standard-deviation level), and nearest neighbor ratio tools are presented in **Table 7** and depicted in **Figures 15(a)-(f)** for each investigated public service. It can be noticed that the standard circles for all public service are centered on the city central area (the holy mosque area), which is quit logical since this area has the highest population and tourists density. The only exception is found in the spatial distribution of the sports services where the centers of both the standard circle and the deviational ellipse have been moved northwest (**Figure 15(f)**). The attained results of the nearest neighbor ration have been computed using the total area of the urbanized extents of Makkah city, which equals 291.45 square kilometers. That means that these results are realistic rather than using the sum area of the six election regions. The less-than-one values of the nearest neighbor ratios indicate that the spatial pattern of distribution of all public service is the clustered pattern. That concludes the previously-achieved remark that the public services in Makkah city are not uniformly distributed in space, due to its topography.

Table 6. Distance to a neighbor for public services.

Public Service	Maximum Distance to a Neighbor (m)	Average Distance to a Neighbor (m)
Education	2944	223
Health	6045	440
Security	2046	289
Religious	3901	205
Commercial	1861	496
Sports	11715	1061

Table 7. Spatial statistics for public services.

Public Service	Standard Distance (m)	Deviational Ellipse			Nearest Neighbor Ratio
		Semi Major Axis (m)	Semi Minor Axis (m)	Rotation Angle	
Education	7889	8748	6924	74.60	0.73
Health	7394	8172	6521	61.70	0.73
Security	8332	9509	6958	76.10	0.65
Religious	7638	8717	6378	65.30	0.98
Commercial	9184	11021	6874	61.90	0.87
Sports	8126	9518	6438	23.60	0.75

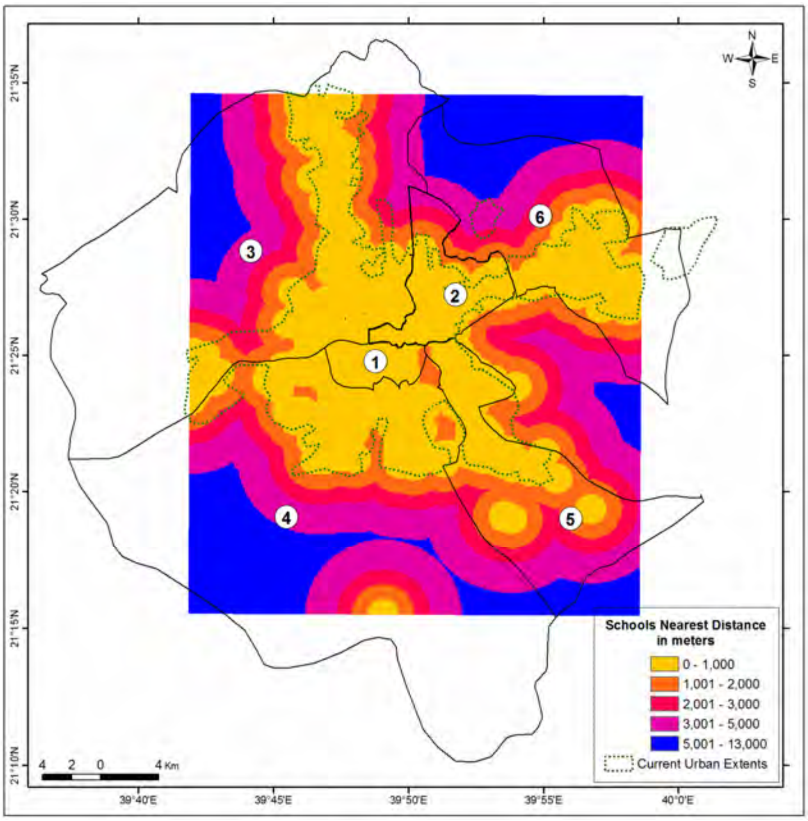

(a)

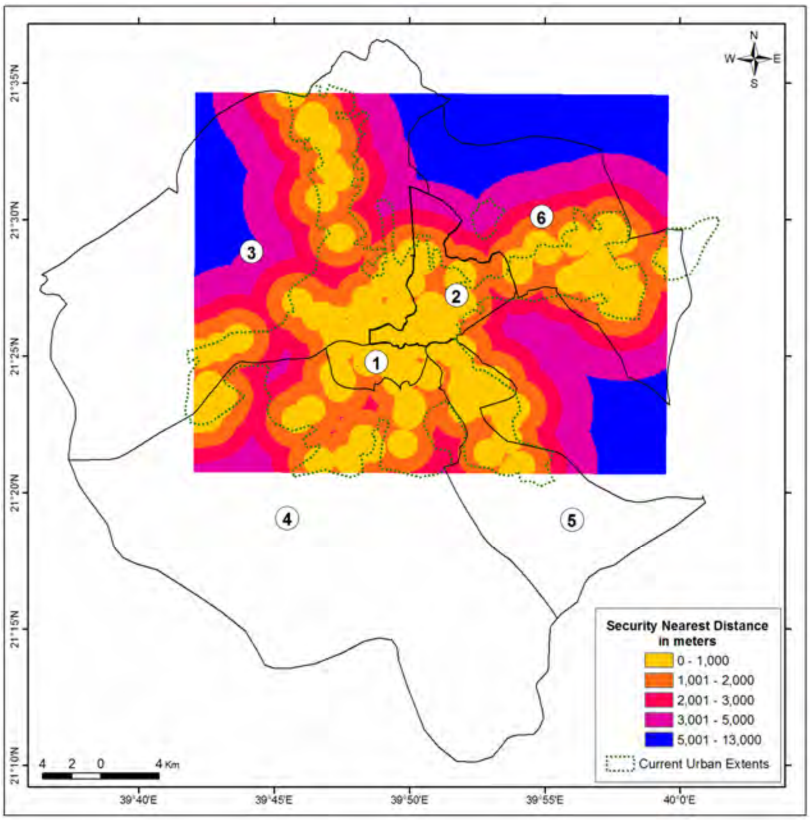

(b)

Copyright © 2013 SciRes.

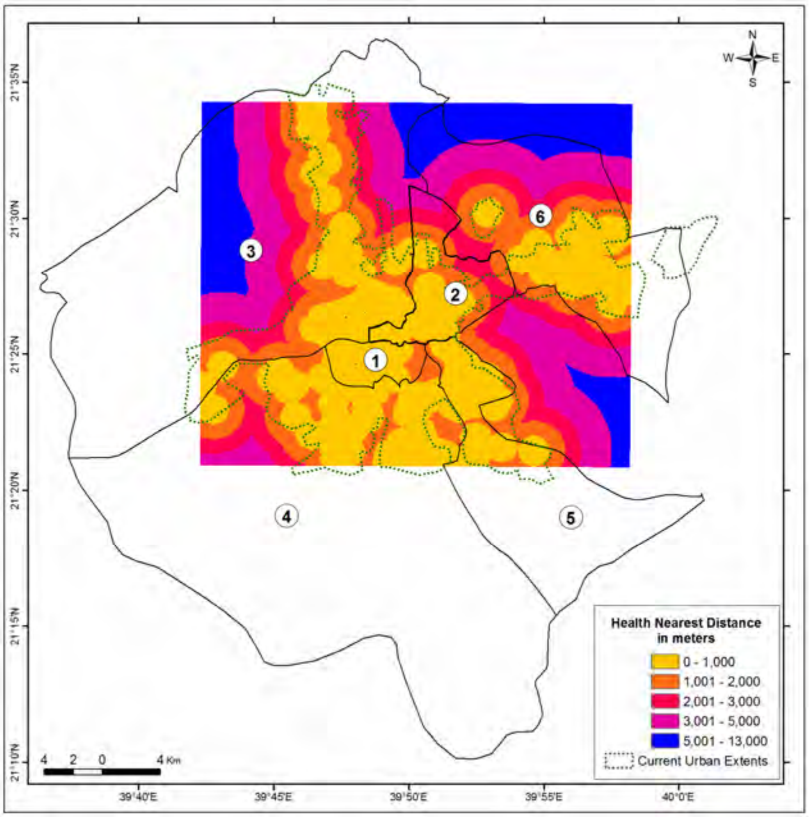
Health Nearest Distance in meters
0 - 1,000
1,001 - 2,000
2,001 - 3,000
3,001 - 5,000
5,001 - 13,000
Current Urban Extents
39°40'E
39°45'E
39°50'E
39°55'E
40°0'E
21°35'N
21°30'N
21°25'N
21°20'N
21°15'N
21°10'N
4 2 0 4 Km
N
W
E
S
1
2
3
4
5
6

(c)

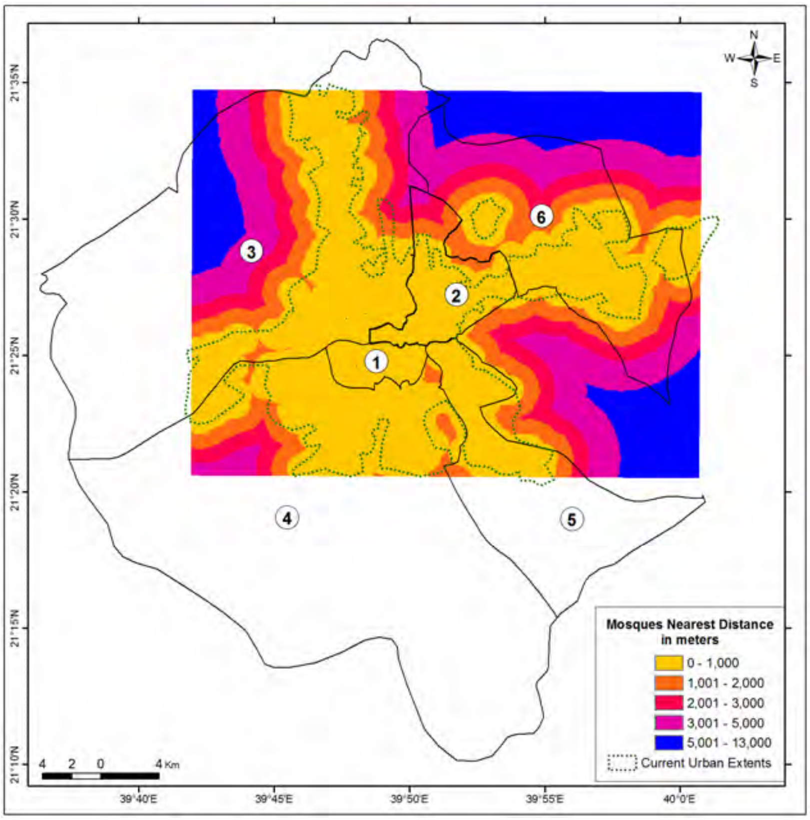
Mosques Nearest Distance in meters
0 - 1,000
1,001 - 2,000
2,001 - 3,000
3,001 - 5,000
5,001 - 13,000
Current Urban Extents
39°40'E
39°45'E
39°50'E
39°55'E
40°0'E
21°35'N
21°30'N
21°25'N
21°20'N
21°15'N
21°10'N
4 2 0 4 Km
N
W
E
S
1
2
3
4
5
6

(d)

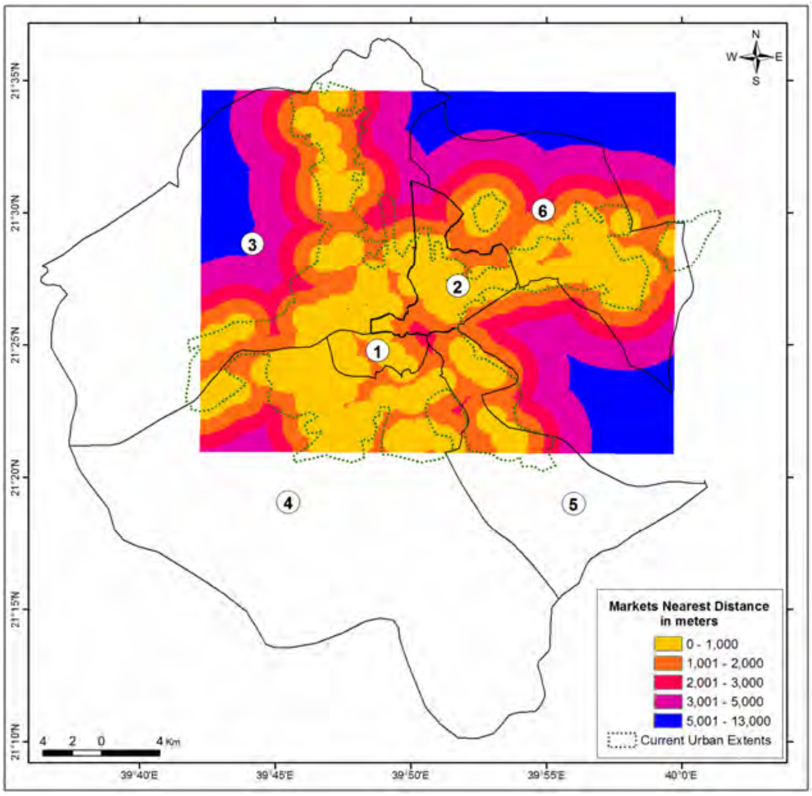

(e)

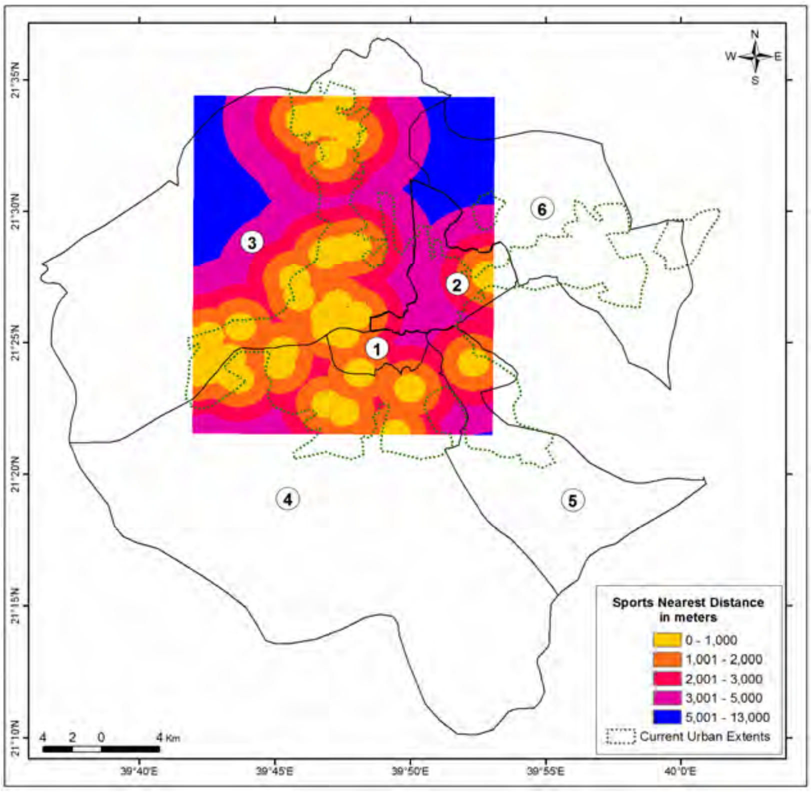

(f)

Figure 14. Distance variation of public services. (a) Education services; (b) Security services; (c) Health services; (d) Religious services; (e) Commercial services; (f) Sports services.

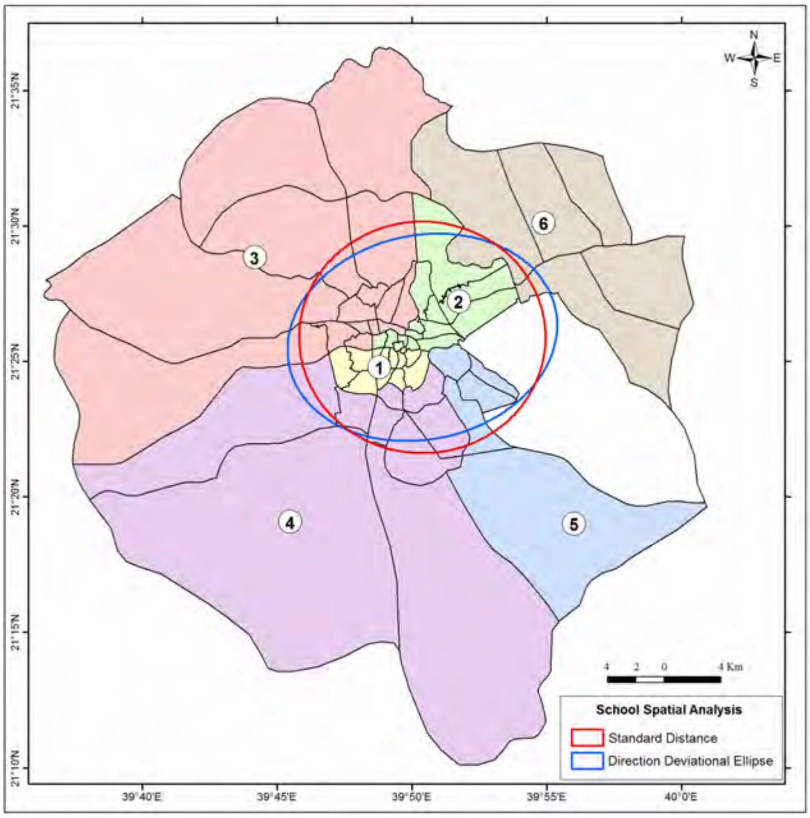

(a)

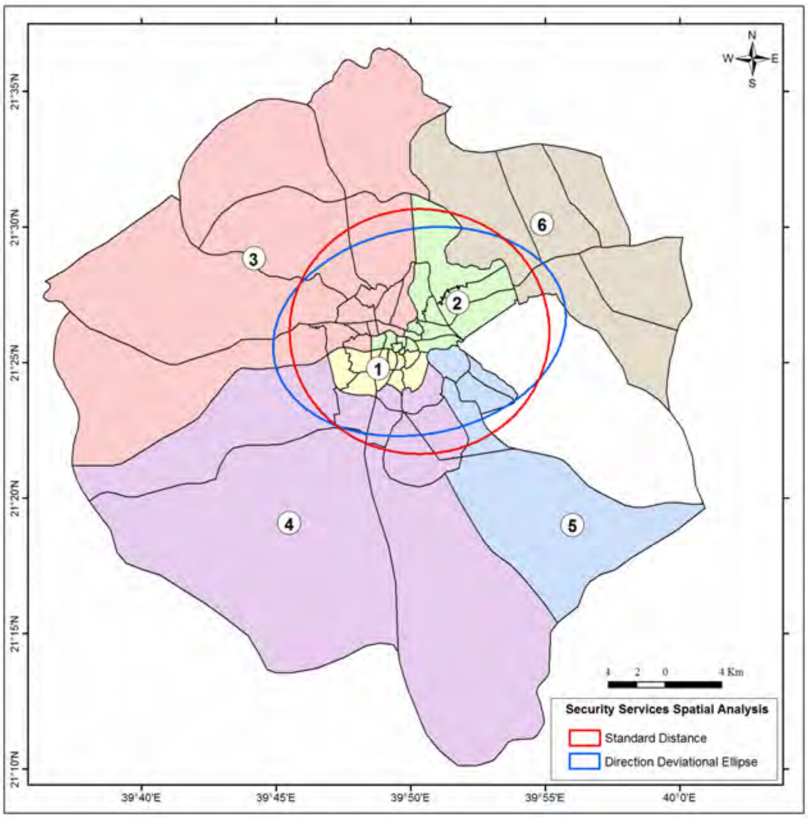

(b)

Copyright © 2013 SciRes.

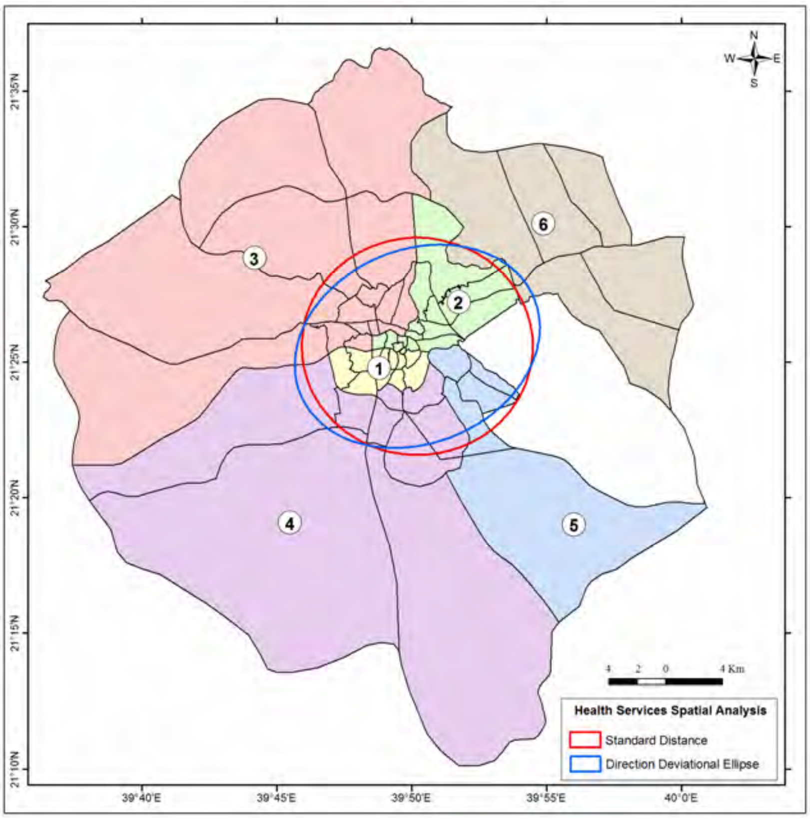

(c)

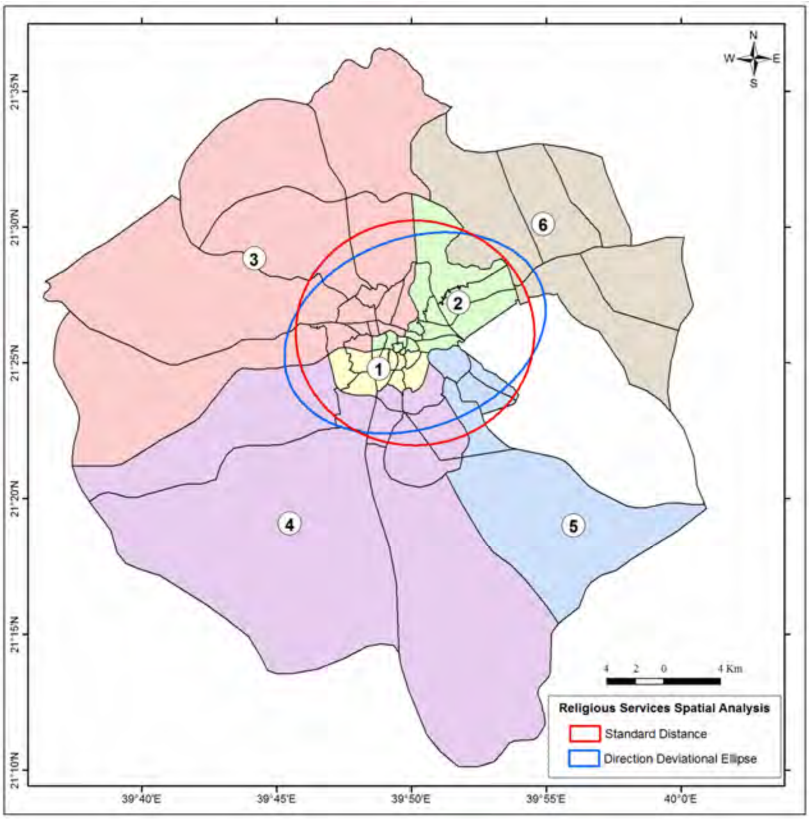

(d)

Copyright © 2013 SciRes.

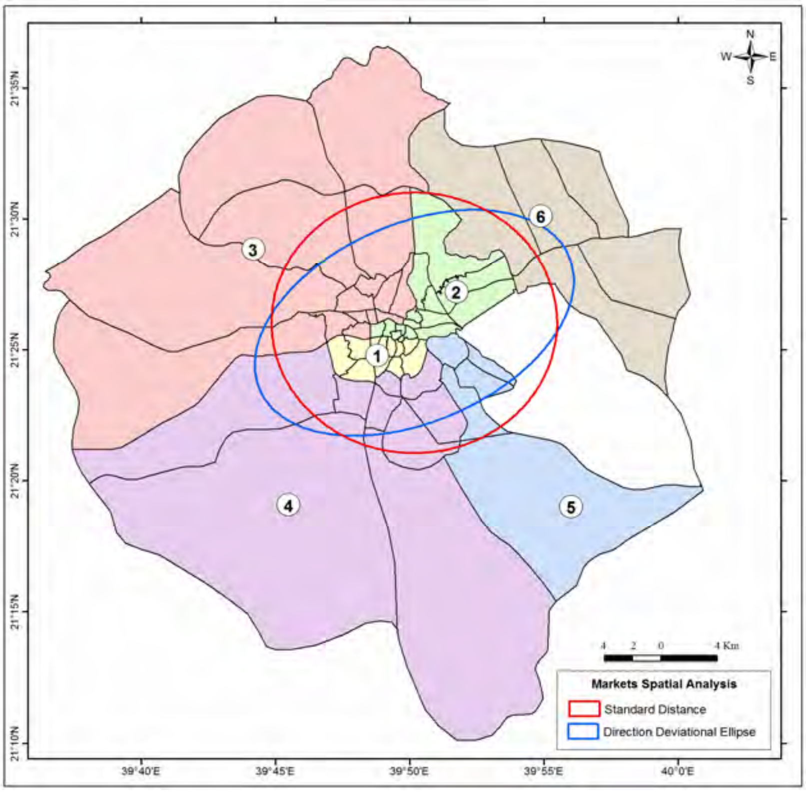

(e)

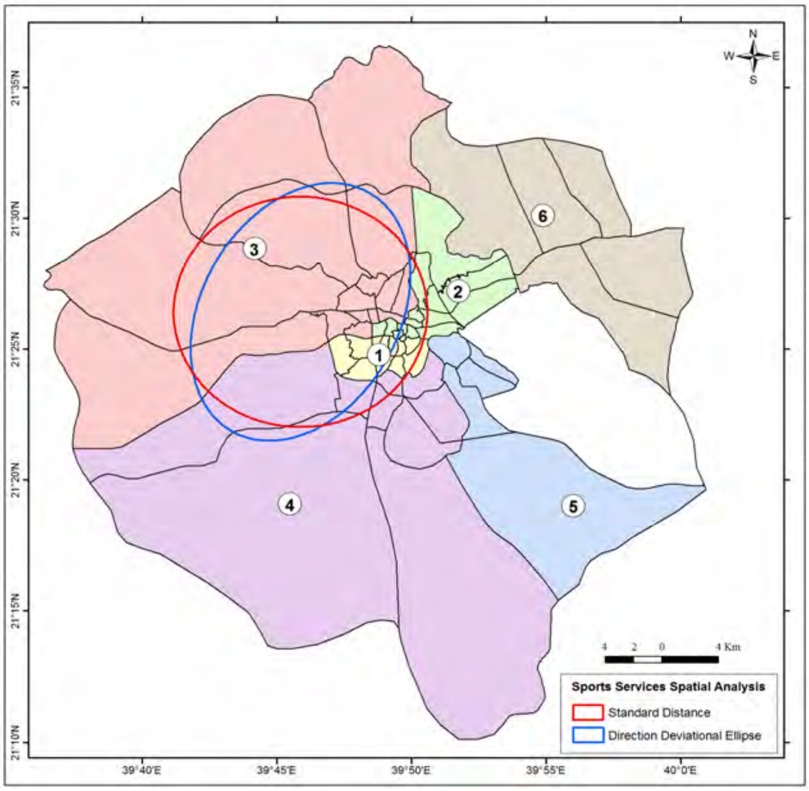

(f)

Figure 15. Spatial variation of public services. (a) Education services; (b) Security services; (c) Health services; (d) Religious services; (e) Commercial services; (f) Sports services.

6. Conclusion

Improving the availability of public services to residents is a key element of the Saudi government development plans. Makkah city is inhibited by more than a million. It is also considered the most important city for all Muslims; millions of Muslims visit it annually. This paper has applied GIS technology to investigate the statistical and spatial distributions of some selected public services of municipal election areas in Makkah. Several GIS spatial analysis tools, along with statistical tests, have been utilized to precisely depict the current situation of public services variations and to project the needed public services in the year 2020. Several accomplished results emphasis the inequality nature of the current public service distribution over municipal election areas. For example, most public services show weak correlation with population distribution, and the general spatial pattern of the services distribution was found to be clustered. In particular, the sports services show unfairness in their spatial distribution over current the urbanized extents of Makkah. This study presents a methodological approach for analyzing the spatial distribution of public services in a city based on municipal election areas. Consequently, such a new GIS-based approach could stimulate researchers and planners in other Saudi cities. Thus, it is recommended that the accomplished results should be considered, by local decision makers, in the future city planning in order to afford more justice availability of public services.

REFERENCES

[1] C. Carvalho, C. Brito, and J. Cabral, "Towards a Conceptual Model for Assessing the Quality of Public Services," *International Review on Public and Nonprofit Marketing*, Vol. 7, No. 1, 2010, pp. 69-86.

[2] R. Elzahrany, "Geographical Distribution of Health Care Services in Makkah Al-Mukarramah Province (in Arabic)," *Research Papers in Geography, Saudi Geographical Society*, No. 55, 2003, 58 p.

[3] H. Dadashpoor and F. Rostami, "Measurement of Integrated Index of Spatial Justice in the Distribution of Urban Public Services Based on Population Distribution, Accessibility and Efficiency in Yasuj City," *Urban-Regional Studies and Research Journal*, Vol. 3, No. 10, 2011, pp. 1-4.

[4] A. Singh and Kaish, "Exploring the Provision and Accessibility to Urban Basic Services in the Slums of a Medium Sized City of India," *Global Advanced Research Journal of Geography and Regional Planning*, Vol. 2, No. 2, 2013, pp. 19-28.

[5] K. Al-Ghamdi, M. Mirza, R. Elzahrany and G. Dawod, "GIS Evaluation of Urban Growth and Flood Hazards: A Case Study of Makkah City, Saudi Arabia," *FIG Working Week*, Rome, 6-10 May 2012.

[6] G. Dawod, M. Mirza and K. Al-Ghamdi, "GIS-Based Spatial Mapping of Flash Flood Hazards in Makkah City, Saudi Arabia," *Journal of Geographic Information System*, Vol. 3, No. 3, 2011, pp. 217-223. doi:10.4236/jgis.2011.33019

[7] R. Elzahrany, "Auto Spatial Correlation of Health Services Distribution in Jeddah City (in Arabic)," *Journal of Gulf and Arabian Peninsula Studies*, No. 123, 2005, pp. 193-267.

[8] S. Zhou, Y. Cheng, M. Xiao and X. Bao, "Assessing the Location of Public-and-Community Facilities for the Elderly in Beijing, China," *GeoJournal*, Vol. 78, No. 3, 2012, pp. 539-551. doi:10.1007/s10708-012-9450-1

[9] S. Mavoa, K. Witten, T. McCreanor and D. O'Sullivan, "GIS Based Destination Accessibility via Public Transit and Walking in Auckland, New Zealand," *Journal of Transport Geography*, Vol. 20, No. 1, 2012, pp. 15-22.

[10] C. Case and T. Hawthorne, "Served or Unserved? A Site Suitability Analysis of Social Services in Atlanta, Georgia Using Geographic Information Systems," *Applied Geography*, Vol. 38, 2013, pp. 96-106. doi:10.1016/j.apgeog.2012.11.012

[11] T. Neutens, M. Delafontaine, D. Scott and P. De Maeyer, "A GIS-Based Method to Identify Spatiotemporal Gaps in Public Service Delivery," *Applied Geography*, Vol. 32, No. 2, 2012, pp. 253-264.

[12] M. Mirza, G. Dawod and K. Al-Ghamdi, "Accuracy and Relevance of Digital Elevation Models for Geomatics Applications: A Case Study of Makkah Municipality, Saudi Arabia," International Journal of Geomatics and Geosciences, Vol. 1, No. 4, 2011, pp. 803-812.

Copyright © 2013 SciRes.

INTERNATIONAL JOURNAL OF GEOMATICS AND GEOSCIENCES
Volume 4, No 2, 2013

© Copyright by the authors - Licensee IPA- Under Creative Commons license 3.0
Research article ISSN 0976 – 4380

Suitability analysis for tourist infrastructures utilizing multi-criteria GIS: A case study in Al-Hada city, Saudi Arabia

Gomaa M. Dawod
Umm Al-Qura University, Makkah 21955, Saudi Arabia
gmmahmoud@uqu.edu.sa

ABSTRACT

Nowadays, GIS is widely recognized as a valuable decision support system that enables the determination of suitable spatial locations for a specific objective based on a group of criteria. This paper aims to utilize such a comprehensive approach for delineating suitable sites to set up future tourist infrastructures in Al-Hada city, southwest Saudi Arabia. Several recent databases have been gathered, integrated, processed, and analyzed for that city. Six criteria have been designed and applied for finding safe, homogenously-distrusted, and economical optimal locations for potential tourist facilities in the study area. A suitability map has been developed based on a weighted integration of the chosen six criteria. The accomplished results show that there exist 124 candidate sites with a suitability index ranges from 5 to 10 on a 10-point scale. It is recommended that these findings being considered in the development plan of Al-Hada city, and the developed GIS mutlicriteria suitability analysis being applied for all Saudi tourist cities.

Keywords: GIS, multi criteria analysis, site suitability, tourism land use, Saudi Arabia.

1. Introduction

Geographic Information Systems (GIS) technology has been utilized in the last two decades in a wide range of geographic, engineering, planning, and environmental applications. Examples of such utilizations include: flood hazard monitoring (Dawod et al. 2012), urban planning (e.g. Arnous 2013), underground water quality (e.g. Alqadi et al. 2013), transportation networks analysis (e.g. Aljoufie et al. 2013), water resources management (e.g. Dawoud 2013), land degradation monitoring (e.g. Mohamed and Saleh 2012), tourism management (Abomeh et al. 2013), and agriculture sustainability (Abdel Kawy 2011).

One of the major characteristics of GIS is its capability to integrate heterogeneous datasets in a unique framework, that leads to the performance of multi-criteria analysis. Thus, suitability models can be developed for the determination of appropriate spatial locations for specific objectives. The site suitability has been a novel regular GIS practice in various disciplines nowadays. Kumar and Shaikh (2013) has applied mutlicriteria GIS analysis for the determination of suitable sites for urban development. On another scale, Bagdanaviciute and Valiuliunas have performed a study to identify potential pollution sources based on sixteen different environmental factors for the sack of land use planning. Additionally, GIS mutlicriteria has been utilized in identifying optimal landfill sites in several countries (e.g. Khamehchiyan et al. 2011, and Al-Rehaili 2010). Suitable sites for public parks are, also, identified based on GIS suitability analysis (e.g. Chandio et al. 2011). Moreover, a similar investigation has been carried out to delineate the development zones of educational infrastructure facilities based on mutlicriteria analysis (e.g. Bhunia et al. 2012). Krishnaveni (2012) has applied GIS-based suitability analysis for the determination of optimal wastewater

treatment plants. Furthermore, a GIS-based location-allocation method has been applied for the optimal distribution of smoking cessation centers in relation to the spatial distribution of the smoking population (e.g. Ajebon and Asikhia, 2013). The current research study aims to identify optimal geographic locations for establishing new tourist infrastructures in Al-Hada tourist area, southwest Saudi Arabia, based on mutlicriteria GIS approach.

2. Study area

Al-Hada city is a tourist area located in Makkah administrative area southwest Saudi Arabia, on the road from Makkah city to Al-Taif city. It is bounded by latitude 21o 20' and 21o 23'N, and by longitude 40o 15' and 40o 18' E (Figure 1). The main geographic feature of Al-Hada city is its high elevation above mean sea level compared with eastern neighboring cities such as Makkah and Jeddah. That city is located on the cliff of Al-Hejaz mountainous series. So, the average level of Al-Hada area is about 2000, which is 1700 and 2000 meters higher than that of Makkah and Jeddah cities respectively (Figure 2).

Figure 1: The study area

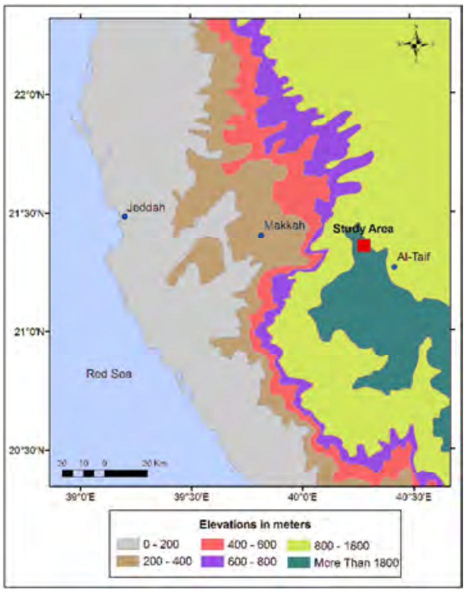

Figure 2: Topography of Southwest Saudi Arabia

Thus, the air temperature in Al-Hada is lower than its neighboring cities by almost ten degrees, particularly in the summer season (Organgi et al 2013). Consequently, Al-Hada is traditionally considered as a summer resort for residents, not just for Saudi but for tourists come from many gulf countries. The topography of Al-Hada range from 1900 to 2165 meters above mean sea level, with an average equals 2000 meters (Figure 3).

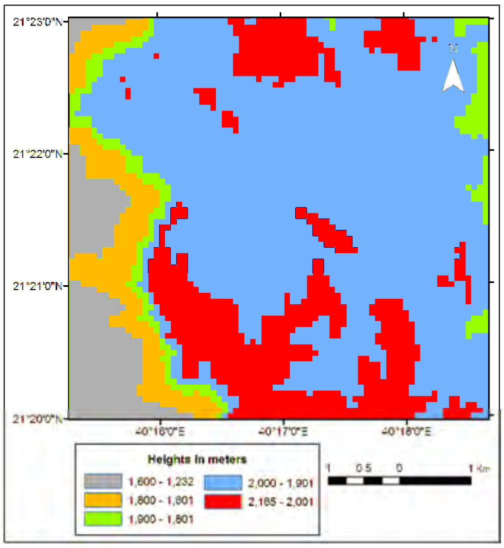

Figure 3: Topography of Al-Hada City

3. Methodology

The data processing has been performed in several stages in order to acquired up-to-data spatial datasets regarding the study area. In the first step, a recent high-resolution satellite image has been obtained, and then digitized through the Arc GIS 10 software. Secondly, a field campaign has been organized to collect field data about land use types for the recognized 1357 parcels. Integrating such attribute data into the study area shapefile enables the categorizing of available land uses in Al-Hada city. A total of 31 land use sub-types has been obtained for the urban boundaries of Al-Hada city that extend over more than 8 million square meters. The chief land use kinds are depicted in Figure 4. Farms constitute 28% of the study area, while empty parcels comprise 27%. The existing tourist infrastructures occupy 747823 square meters, which represents only 9% of the overall land uses.

Regarding the existing tourist infrastructures, it has been found that 4 types of tourist facilities are available: (1) resorts that constitute 69% of the entire area of tourist land uses; (2) hotels, which occupy 27% of the tourist total areas; (3) furnished apartments representing only 4%; and (4) rest houses occupy less than 0.5% of the area of tourist facilities in the study area (Figure 5). It can be obviously realized that the spatial distribution of these infrastructures is not homogenous over the study area. The standard distance, at one-standard-deviation level, has been presented in Figure 6. It can noticed that this circle lies in the west region of Al-Hada city, with a radius equals 1281 meters. Thus, there is a vital need to establish new tourist infrastructures that are homogeneously distributed over the city. Since it is quit important that new infrastructures being safe regarding flood hazards, the ARC GIS hydrological analysis tools have been utilized to delineate the hydrological stream network in the study area (Figure 7).

The multi-criteria site suitability analysis is performed to identify appropriate spatial locations based on a group of criteria or constraints. In the recent study six criteria have been designed to construct a tourist infrastructure' suitability model. These conditions aim to (1) identify safe locations against flood hazards, (2) fulfill spatial homogenous distribution over the city, (3) reduce construction' costs by allocating sites close to an existing road, being in a flat or small-slope areas, and currently being empty parcels, and (4) select appropriate locations with areas fit tourist infrastructures. Accordingly, these criteria composite of:

1. Criteria 1: at least 100-meter away from hydrological streams.
2. Criteria 2: less than 10 degrees terrain slopes.
3. Criteria 3: The land use type must be an empty parcel.
4. Criteria 4: Away from an existing tourist infrastructure by at least 200 meters.
5. Criteria 5: Away from an existing road by no more than 100 meters.
6. Criteria 6: The area of the proposed site is larger than 1000 square meters.

Lastly, a weighted multi-criteria analysis is performed to spatially integrate the first five conditions in a weighted manner. The designed weights have been selected to be: a weight of 0.25 for the first three conditions, and a weight of 0.125 for the next two constraints. The last criteria has been performed separately after the site suitability model is obtained, in order to define appropriate sites.

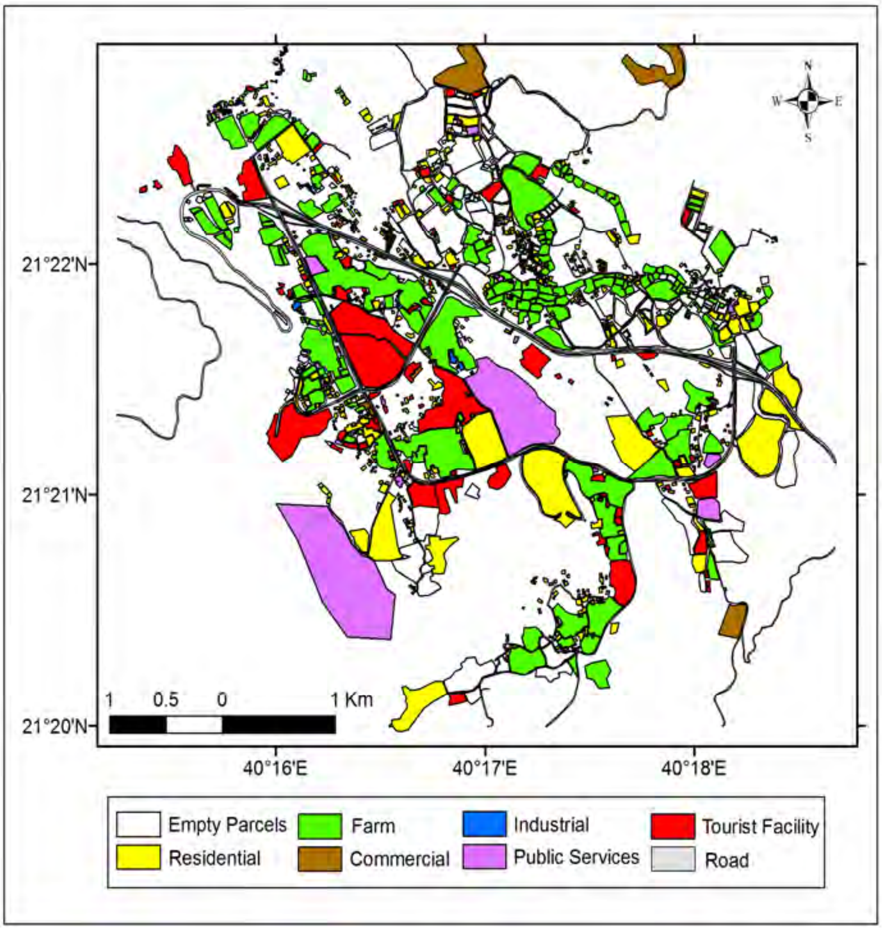

Figure 4: Main Land Uses in Al-Hada City

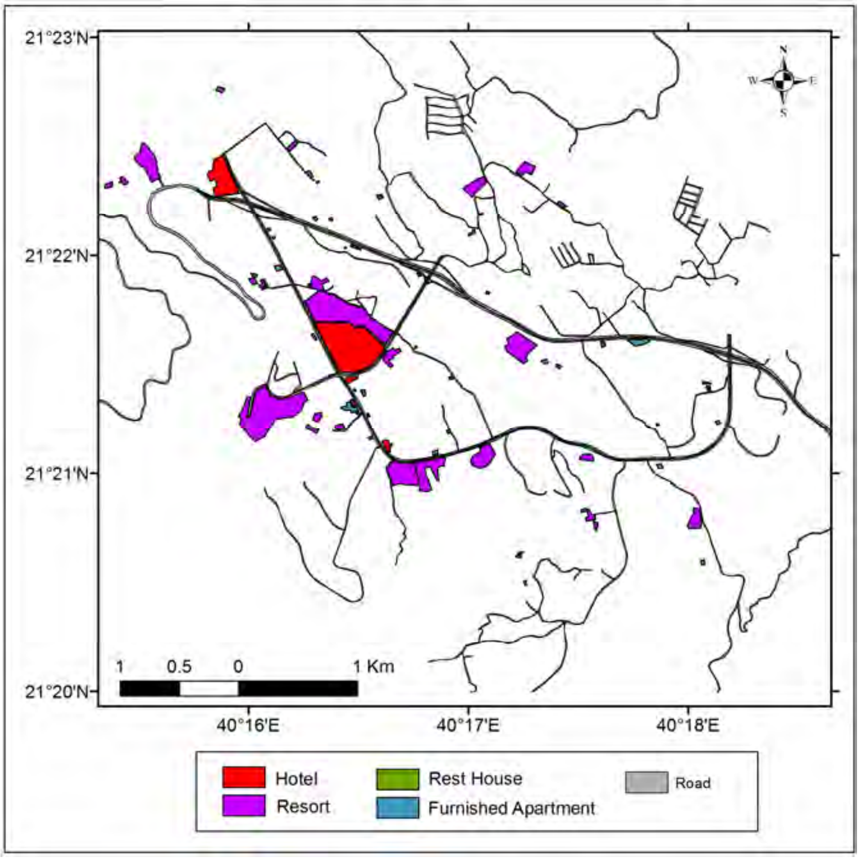

Figure 5: Tourist Land Uses in Al-Hada City

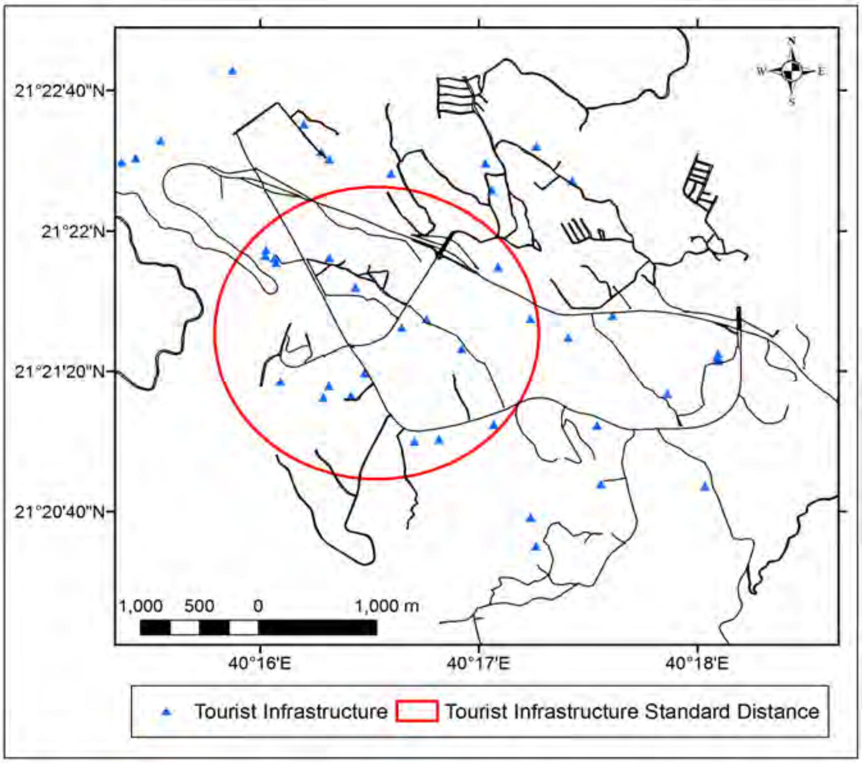

Figure 6: Spatial Distribution of Tourist Infrastructures

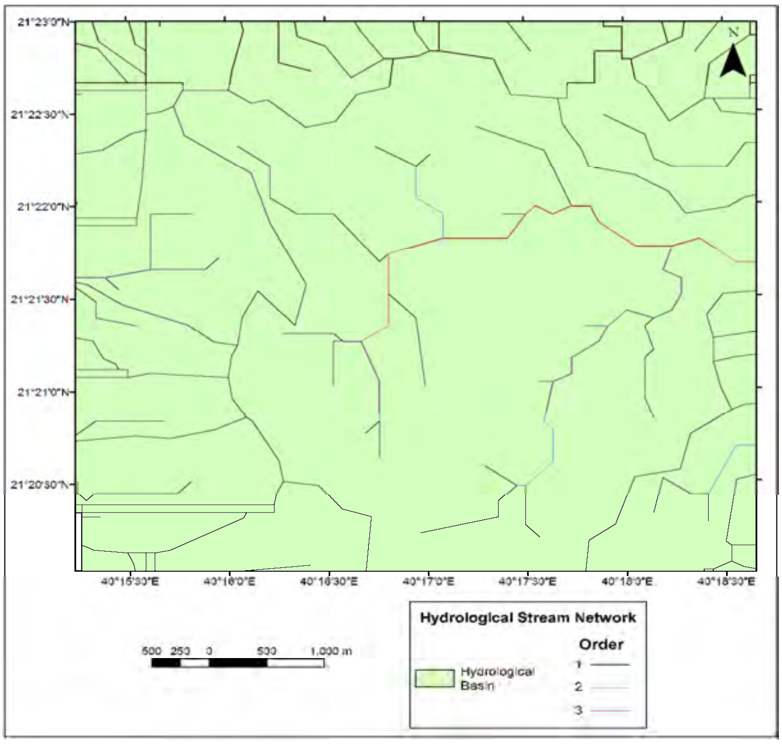

Figure 7: Hydrological Stream Network

4. Results and analysis

Firstly, the ArcGIS spatial analysis tools have been applied for each criterion individually. Thus, 5 distinct suitability models have been obtained, one for each specified constraint. The spatial results of each attained model have been divided into three categories: low, medium, and high suitability. The only exception are the terrain slope and the empty land use suitability models, which are divided only into two categories: suitable or not suitable. Such results are depicted in figures 8 to 12.

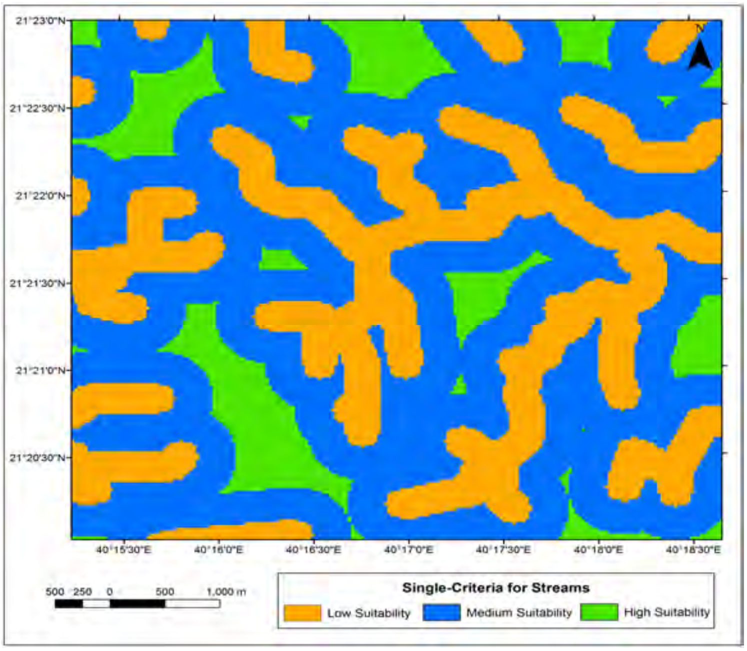

Figure 8: Hydrological Streams Suitability Model

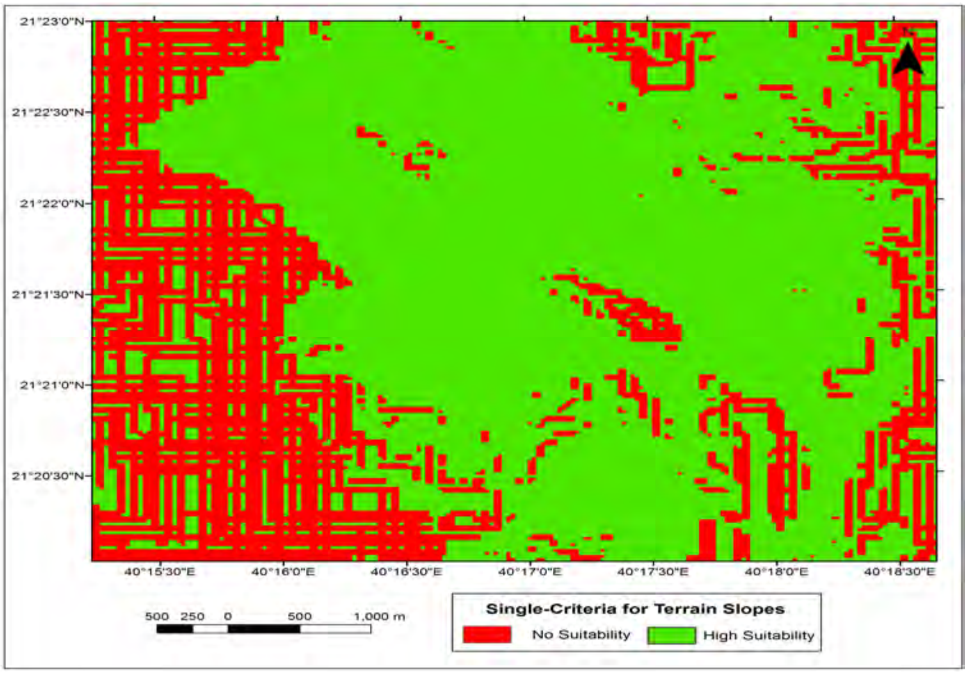

Figure 9: Terrain Slopes Suitability Model

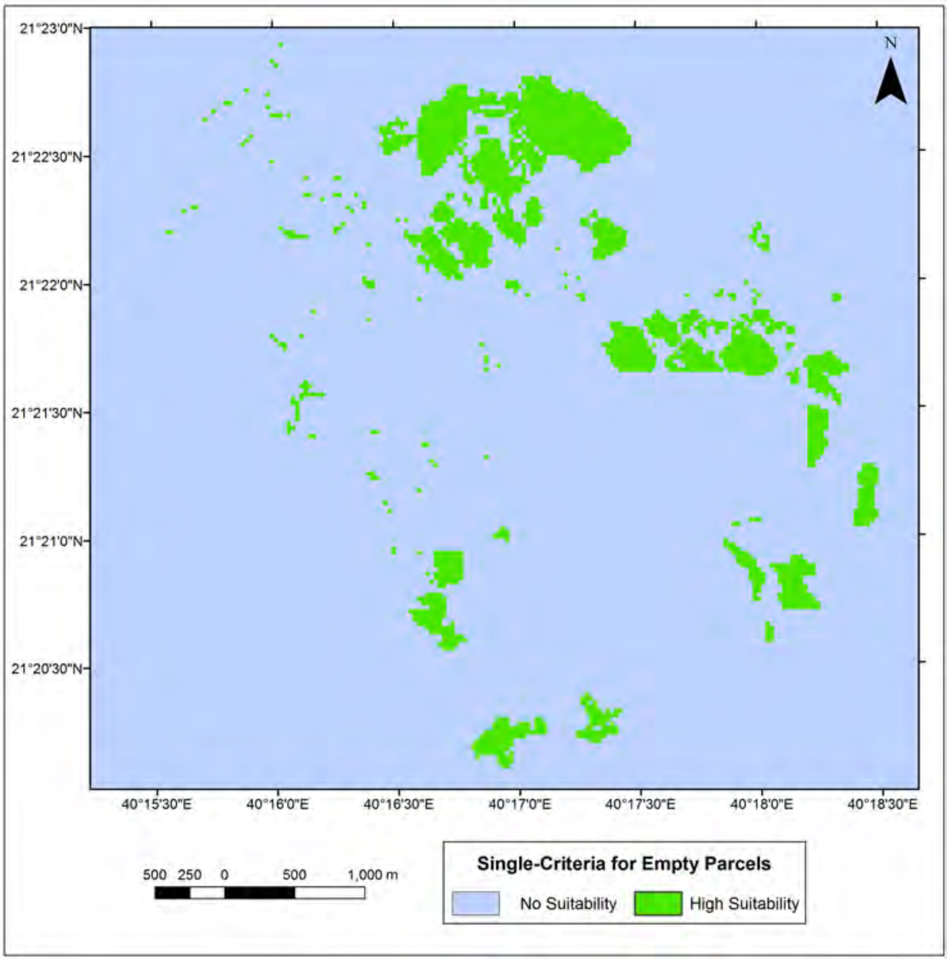

Figure 10: Land Uses Suitability Model

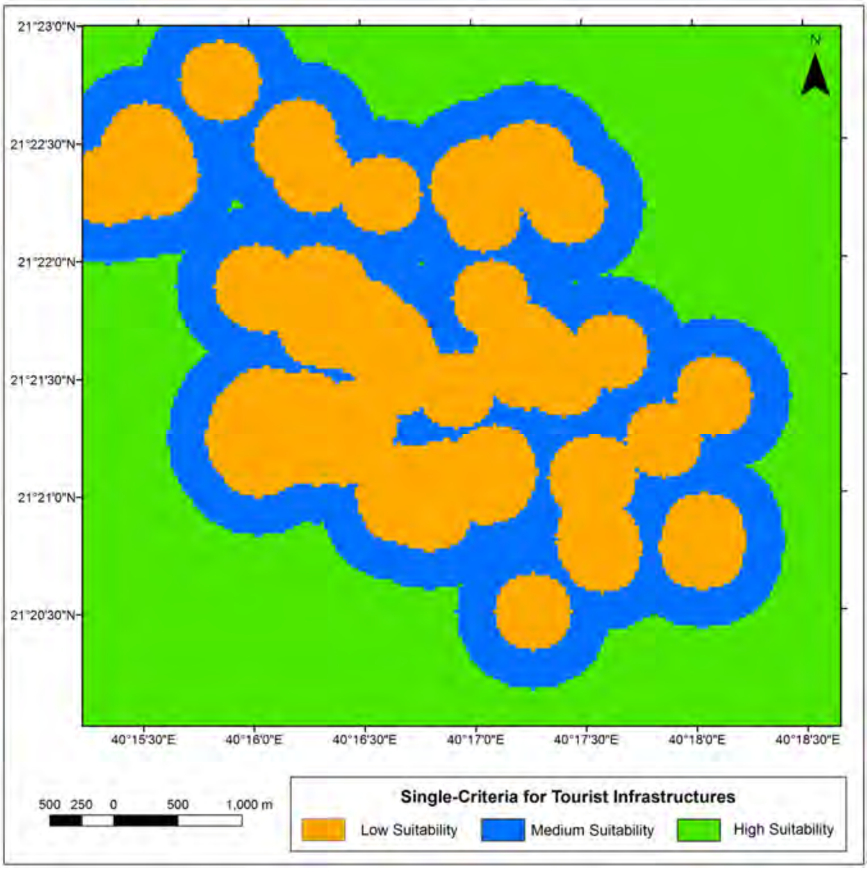

Figure 11: Tourist Infrastructures Suitability Model

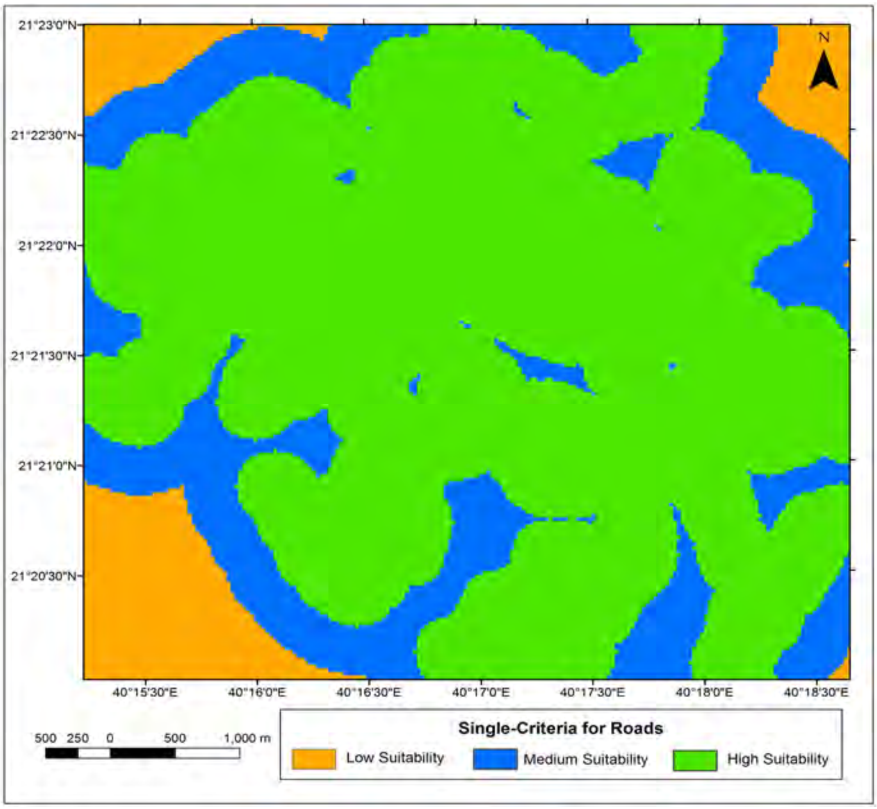

Figure 12: Road Distance Suitability Model

It can be noticed that the five single-condition result in different spatial locations that satisfy each single constraint. The multi-criteria GIS analysis integrates such conditions in a distinctive way to produce a unique appropriate spatial solution. Thus, in the second processing stage the five raster images corresponding to the five criteria, have been spatially integrated in a weighted manner. The weights have chosen as 0.25 for terrain slopes, hydrological streams, and land uses, and 0.125 for both roads and tourist infrastructures. That results in a new weighted suitability model that identifies suitable geographic sites for establishing new tourist infrastructures in the study area. For simplicity, the suitability model has been ranked on a scale from 1 to 10, as seen in Figure 13. Clearly, it can be seen that the most-suitable locations exist in the center of the study area, and the suitability index is deceased as we move to the borders. The sixth criterion has been applied in the last processing step. The suitability index has been interpolated for empty parcels, so that each parcels gets a unique suitability index. Then, parcels with areas less than 1000 square-meters have been excluded. The suitability index for the remaining 124 empty parcels range from 5 to 10, on a scale of 10. The final output is depicted in Figure 14. It has been found that there exist 6 locations with a medium suitability index, that ranges from 5 to 6, and 45 sites have a good suitability index ranges from 7 to 8, and 73 sites with excellent suitability index equals 9 or 10. These results conclude that there exist several geographic locations within the study area that are appropriate for establishing new tourist infrastructures.

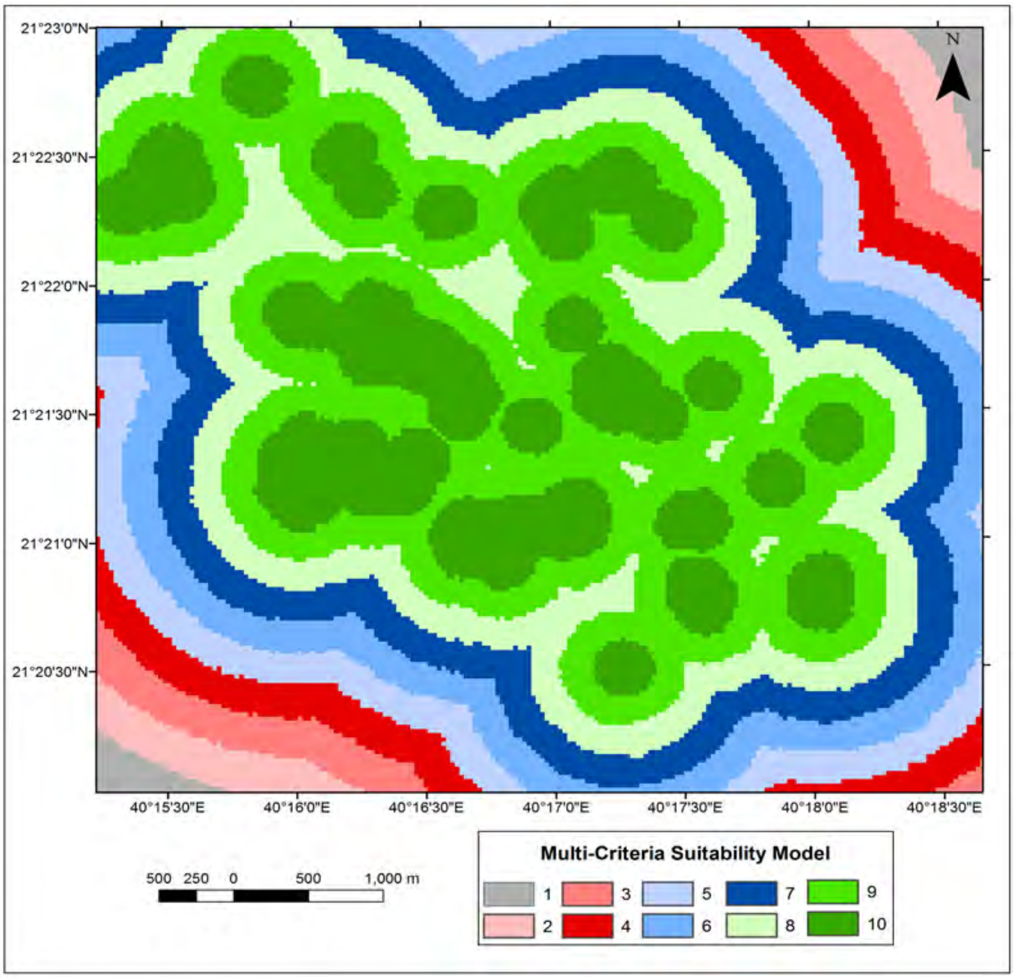

Figure 13: Five-Criteria Suitability Model

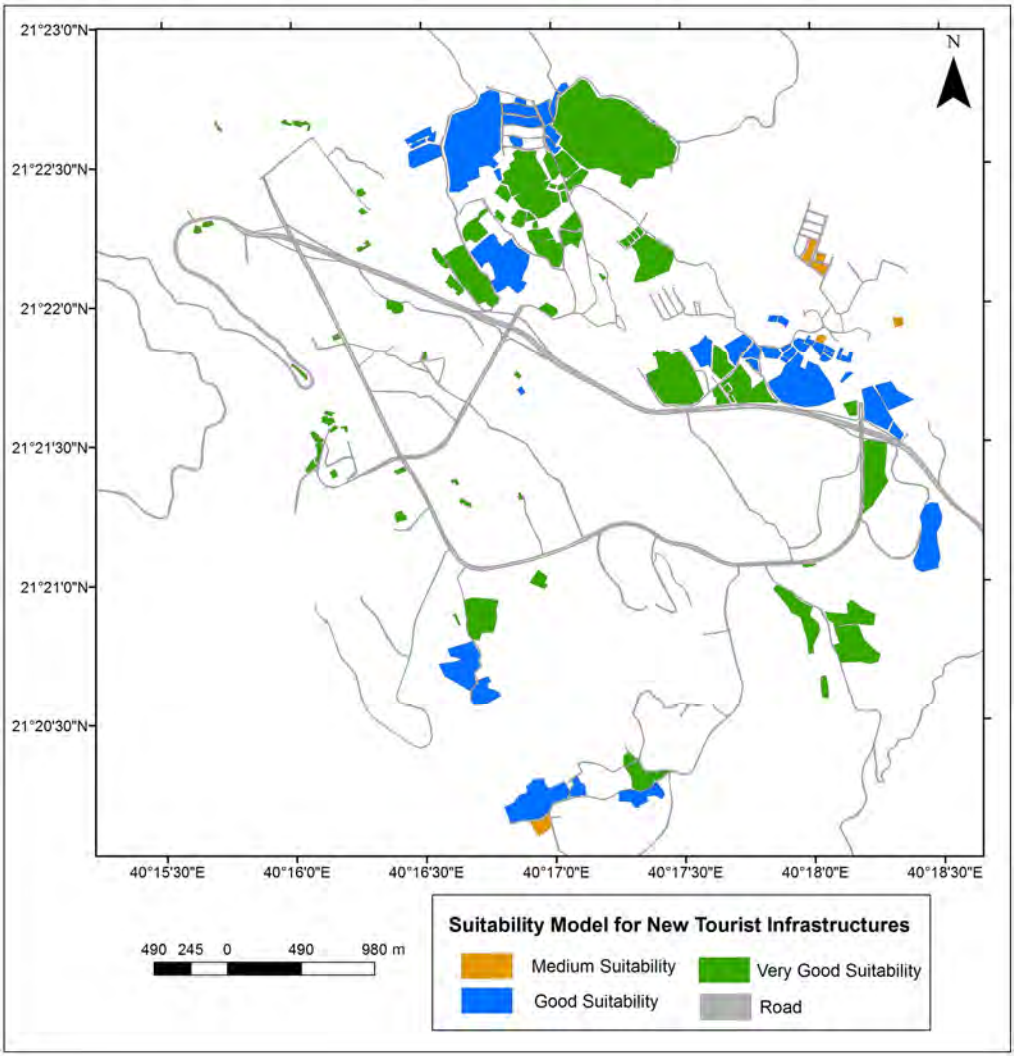

Figure 14: Suitable Locations for New Tourist Infrastructures

5. Conclusions

With advances in information technologies, computer-based decision support models have been developed for a wide range of development applications. In this research, the GIS mutlicriteria analysis, as a decision support system, has been performed to identify appropriate sites for establishing future tourist infrastructures in Al-Hada city, southwest Saudi Arabia. Results show that there exist 124 empty parcels that represent proper candidate sites, with a suitability index varies from 5 to 10, on a scale of 10. Hence, it is recommended that the accomplished results being considered by the local decision makers in Al-Hada city in any future city planning. In addition, it is recommended that city and regional planning activities, within Saudi Arabia, should regularly apply the GIS multi-criteria analysis for efficient resources management.

Acknowledgment

The author acknowledges the financial support provided by the Scientific Researches Institute of Umm Al-Qura university, Makkah, Saudi Arabia.

6. References

1. Abdel Kawy, W., (2011), Using GIS modeling to assess the agricultural sustainability in Kafr El-Sheikh governorate, Nile Delta, Egypt, Arab journal geosciences, DOI 10.1007/s12517-011-0377-5.

2. Abomeh, O., Nuga, O., and Blessing, I., (2013), Utilization of GIS technology for tourism management in Victoria island Lagos, European scientific journal, 9(3), pp 1857–7881.

3. Ajebon, M. and Asikhia, M., (2013), Geographical analysis of smoking in Leeds: A GIS-based location-allocation technique for the optimal location of smoking cessation services, Journal of geographic information system, 5, pp 269-280.

4. Aljoufie, M., Zuidgeest, M., Brussel, M. and Maarseveen, M., (2013), Spatial–temporal analysis of urban growth and transportation in Jeddah City, Saudi Arabia, Cities, 31, pp 57–68.

5. Alqadi, K., Kumar, L., and Khormi, H., (2013), Mapping hotspots of underground water quality based on the variation of chemical concentration in Amman, Zarqa and Balqa regions, Jordan, Environ earth sciences, DOI 10.1007/s12665-013-2632-4.

6. Al-Rehaili, O., (2010), The use of GIS in determining the most appropriate landfill sites in Al- Madinah city, MSC thesis, Geography department, Umm Al-Qura University, Makkah, Saudi Arabia.

7. Arnous, M., (2013), Geotechnical site investigations for possible urban extensions at Suez City, Egypt using GIS, Arab journal of geosciences, 6, pp 1349–1369.

8. Bagdanaviciute, I. and Valiuliunas, J., (2013), GIS-based land suitability analysis integrating multi-criteria evaluation for the allocation of potential pollution sources, Environ earth sciences, 68, pp 1797–1812.

9. Bhunia, G., Shit, P., and Duary, S., (2012), Assessment of school infrastructure at primary and upper primary level: A geospatial analysis, Journal of geographic information system, 4, pp 412-424.

10. Chandio, I., Matori, A., Lawal, D., and Sabri, S. (2011) GIS-based land suitability analysis using AHP for public parks planning in Larkana city, Modern applied science, 5(4), pp177-189.

11. Dawod, G., Mirza, M., and Al-Ghamdi, K., (2012), GIS-based estimation of flood hazard impacts on road network in Makkah city, Saudi Arabia, Environ earth sciences, 67, pp 2205–2215.

12. Dawoud, M., (2013), The development of integrated water resource information management system in arid regions, Arab journal of geosciences, 6, pp 1601–1612.

13. Khamehchiyan, M., Nikoudel, M., and Boroumandi, M., (2011), Identification of hazardous waste landfill site: a case study from Zanjan province, Iran, Environ Earth Sciences, DOI 10.1007/s12665-011-1023-y.

14. Kumar, M. and Shaikh, V. (2013) Site suitability analysis for urban development using GIS based mutlicriteria evaluation technique: A case study of Mussoorie municipal area, Dehradun district, Uttarakhand, India, Journal of indian society of remote sensing, 41(2), pp 417–424.

15. Krishnaveni, K., (2012), Suitable site selection of decentralized treatment plants Using mutlicriteria approach in GIS, Journal of geographic information system, 4, pp 254-260.

16. Organgi, F., Barodi, M., and Dawod, G., (2013), The future of urban land uses in Al-Hada city utilizing GIS (in Arabic), Un-published technical report, Center of Scientific Researches, Umm Al-Qura University, Makkah, Saudi Arabia.

17. Mohamed, E. and Saleh, B., (2012), Assessment of land degradation east of the Nile Delta, Egypt using remote sensing and GIS techniques, Arab journal of geosciences, DOI 10.1007/s12517-012-0553-2.

Towards an Accurate Definition of the Local Geoid Model in Egypt using GPS/Leveling Data: A Case Study at Rosetta Zone

Essam M. Al-Krargy, Mohamed I. Doma, Gomaa M. Dawod

Abstract— Nowadays the Global Positioning System (GPS) is one of the most favorite techniques in practical geodesy. A major dilemma in GPS surveying lies in its ellipsoidal-based type of heights, while in engineering practice orthometric heights are usually utilized. Thus, it is important to convert GPS heights into orthometric heights through applying an accurate geoid model. The objectives of this paper are to model a local geoid in the study area using GPS/levelling technique, and to evaluate the performance of several Global Geopotential Models (GGMs) particularly the OUS-91A, EGM96 and EGM2008 in the study area, which is located in the northern Egypt at Rosetta zone area. The accomplished results show that the EGM 2008 represents the most precise global geopotential model to be used for geoid determination in Egypt. Furthermore, the achievable accuracy of local geoid determination in the study area after using regression method models is ranges between 0.059 meter to -0.083 meter, with an average -0.01 meter and standard deviation of ± 0.05 meter. It is concluded that increasing the number of control points with well spatial distribution will result in developing a precise geoid model for Egypt.

Index Terms— Global Geopotential Models (GGMs), Global Positioning System (GPS), Local geoid. Orthometric height.

I. INTRODUCTION

During the last decades, GPS has been used in many applications of geodesy, geophysics, and surveying. GPS technique provides surveyors with three-dimensional coordinates including the height relative to a best fitting ellipsoid that is called the ellipsoidal height (h). On the other hand, many applications in civil engineering, such as topographic mapping, engineering design, and construction projects, depend upon the so-called orthometric height (H), which is the height above the geoid as approximated by the Mean Sea Level (M.S.L). The geoid fits the actual Earth surface more accurately than the geometric representation of the earth by the ellipsoid. Because of these facts ellipsoidal heights can't satisfy the needs of practical surveying engineering or geophysical application as they have no physical meaning and must be transformed to orthometric height. In order to accomplish this height transformation, there is a need to calculate the difference between ellipsoidal and orthometric heights, which is called the geoid undulation N.

Manuscript Received on October 2014.

Eng. Essam Mohamed Farag ALkrargy, Asst. Researcher of Survey Research Institute, Department of Physical Geodesy, National Water Research Center, Cairo, Egypt.

Dr. Mohamed Ismail Ali Doma, Assoc. Prof. of Surveying and Geodesy, Department of Civil Engineering, Faculty of Engineering, Menoufia University, Egypt.

Prof. Gomaa Mohamed Dawod, Department of Physical Geodesy, Survey Research Institute, National Water Research Center, Cairo, Egypt.

These undulations can be determined using several techniques such as: Global Geopotential Models (GGMs) such as the OSU-91A, EGM 96, EGM 2008 models, gravimetric method using surface gravity data, and geometric method using GPS/leveling data (Erol and Çelik, 2004). The present research aims to develop a precise local geoid using GPS/levelling data, and to compare the attained geoid undulations against some GGMs in order to evaluate their precision performance in the study area. The paper is organized as follows; first, an overview of geoid modeling is presented. Then, the most used GGMs in Egypt are summarized. Thirdly, a numerical case study is outlined and the accomplished results are discussed. Finally, conclusions and recommendations are given.

II. GEOID MODELING

The geoid is the equipotential surface of the Earth's gravity field approximating Mean Sea Level (MSL) in an optimum way, and extended under the continents. The geoid is determined using several techniques based on a wide variety of using one or more of the different data sources such as: the gravimetric method using surface gravity data, satellite positioning based on measuring both ellipsoidal heights for stations with known orthometric heights (Al-Ghamdi and Dawod, 2013):

$$N = h - H \qquad (1)$$

Where N is the geoidal heights or geoidal undulations, h is the ellipsoidal or GPS-based height, and H is the orthometric or MSL-based height. Fig. (1) shows the relationship between ellipsoidal, orthometric and geoid heights.

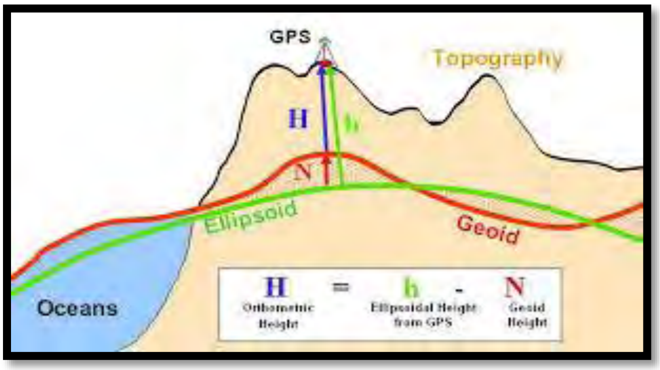

Fig. 1: The Relation between Ellipsoid Height and Geoid Height

According to the geometric method, there are several factors that affect the accuracy of the determined geoid model, such as (Kaloop and Rabah, 2008).

- Distribution and number of reference stations (GPS/leveling stations). These points must be distributed homogeneously to the coverage area of the model and have to be chosen to Fig. out the changes of

Published By:
Blue Eyes Intelligence Engineering
& Sciences Publication Pvt. Ltd.

geoid surface.

- The accuracy of GPS derived ellipsoidal heights (h) and the heights derived from leveling measurements (H).
- Used method while modeling the geoid.

Several techniques are used for determination of geoid surface surround the data points, for example, interpolation, finite elements, numerical differential solution, one-dimensional datum transformation. Interpolation methods are the most common approaches utilized for modeling the geoid heights (N) for a local area. There are different interpolation algorithms, such as (Maher et al, 2012):

- Inverse Distance Weighting to Power
- Kriging
- Minimum Curvature
- Nearest Neighbor
- Polynomial regression

In this study, the last method (polynomial regression) has been chosen to model the geoid undulations in the study area. This method is described as:

$$N(\varphi,\lambda) = \sum_{i=0}^{n}\sum_{j=0}^{m} a_{ij}\phi_i\lambda_j \qquad (2)$$

Where a_{ij} are the coefficients of the polynomial regression, n, m are the polynomial orders, φ is the geocentric latitude, and λ is the geocentric longitude. This method is used to define large-scale trends and patterns in data, and there are several options to define the type of the trend surface. Such options are presented in equations 3, 4, 5, and 6.

Simple Planar Surface:

$$N = a_o + a_1\varphi + a_2\lambda \qquad (3)$$

Bi-Linear Saddle:

$$N = a_o + a_1\varphi + a_2\lambda + a_3\varphi\lambda \qquad (4)$$

Quadratic Surface:

$$N = a_o + a_1\varphi + a_2\lambda + a_3\varphi^2 + a_4\lambda^2 + a_5\varphi\lambda \qquad (5)$$

Cubic Surface:

$$N = a_o + a_1\varphi + a_2\lambda + a_3\varphi^2 + a_4\lambda^2 + a_5\varphi\lambda + a_6\varphi^3 + a^7\lambda^3 + a_8\varphi^2\lambda + a_9\varphi\lambda^2 \qquad (6)$$

Where *$a_0, a_1, a_2, \ldots\ldots a_n$ are the* coefficients of polynomial regression, φ is the geocentric latitude, λ is the geocentric longitude. In practice, for surfacing with polynomial regression, selection of polynomial degree is very important. The surface can be lost its reality and suitability due to wrong selection of coefficient and polynomial degree. In surfacing with polynomial regression methods, degree of polynomial is depending on number of points and degree of freedom. As possible as it must be started with the highest degree and the most suitable coefficient must be determined by using statistical tests (Schut, 1976, Yanalak, 1991).

III. GLOBAL GEOPOTENTIAL MODELS (GGMs)

During the last 30 years, numerous GGMs have been computed by various groups. For an extensive description of existing model refer to the web pages of international center for Global Earth Models (ICGEM 2014), and the references therein. Examples of the most common GGMs applied for geoid modeling computations are The Earth Geopotential Models (EGM 2008), (EGM 96), and the OhioStateUniversity (OSU-91A). The quality of the selected GGMs used greatly affects the accuracy of the computed geoid. These global models have been developed from the combination of satellite perturbation analysis with both surface gravity and satellite altimetry data. A brief description for three GGMs the most common worldwide, and also in Egypt, is follows:

A) Ohio State University (OSU-91A) Model

To cater for the needs of the GPS system, the department of geodetic sciences and surveying of the Ohio state university established the model OSU-91A, from the model GEM-T2 and from available gravity data (for more detailed of OSU-91A see Rapp et al., 1991).The OSU-91A geopotential model was for long time the most accurate reference model in geodesy and other geosciences. This model provides the spherical harmonics up to degree and order 360. Therefore, the shortest wavelength of this model is one degree in latitude and longitude, and its resolution is one-half degree (about 50 km). OSU-91A did not incorporate enough data from the Middle East, and consequently it may not be able to represent it very well. The geoid undulations of OSU-91A over Egypt area are represented as a contour map in Fig. (2a) (Saad and Dawod, 2002).

B) Earth Geopotential Model 1996 (EGM 96)

The Earth Geopotential Model 1996 (EGM 96) is a GGM produced through a collaborative effort of the NASA Goddard Space Flight Centre (GSFC), the National Imagery and Mapping Agency (NIMA), and the Ohio State University (OSU). EGM 96 was improved the data holding over many of the world's land area. Furthermore, it has been calculated using a new set of 30′ × 30′ mean free-air gravity anomalies obtained from several ocean gravimetric missions which took place from 1975 to 1990 (Catlao and Sevilla, 1999). In addition, EGM96 incorporated improved surface gravity data, altimeter-derived anomalies from ERS-1 and from the GEOSAT Geodetic Mission, extensive satellite tracking data, the GPS NASA's Tracking and Data Relay Satellite System (TDRSS), the French DORIS system, the US Navy TRANSET Doppler tracking system, as well as direct altimeter ranges from TOPEX/POSEIDON (T/P), ERS-1, and GEOSAT. The distribution and extent of the surface gravity data in EGM 96 is a major improvement on the data available for the OSU-91A. The geoid undulations of EGM 96 GGM over Egypt are represented as a contour map in Fig. (2b) (Saad and Dawod, 2002).

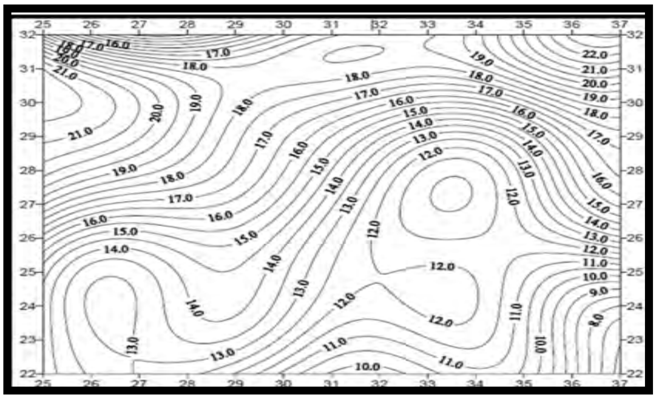

(a)

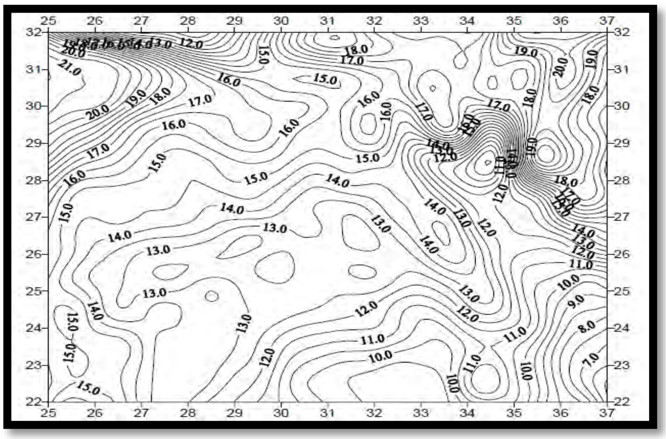

(b)

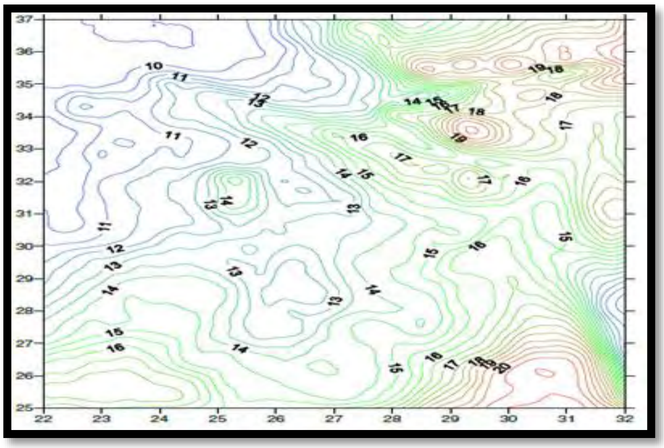

(c)

Fig. 2: (A) A Contour Map of Geoid Undulations of OSU9-1A (Saad and Dawod, 2002), (B) A Contour Map of Geoid Undulations of EGM 96 (Saad and Dawod, 2002), and (C) A Contour Map of Geoid Undulations of EGM2008 in Egypt (Rabah and Kaloop, 2013)

C) Earth Geopotential Model 2008 (EGM 2008)

EGM 2008 is the most recent earth geopotential model developed by least squares combination of the ITG-GRACEEO35 gravitational model and its associated error covariance matrix, with the gravitational information obtained from a global set of area –mean free-air gravity anomalies defined on a 5-arc-minute grid. This grid was formed by merging terrestrial, altimetry-derived, and airborne gravity data. Over areas where available, their spectral content was supplemented with gravitational information implied by the topography (Pavlis et al, 2008; Avlis et al, 20120) It does not incorporate any GPS/Leveling or Astronomic deflections of the vertical data (Dawod et al, 2010). For the first time, this gravitational model is complete to spherical harmonic degree and order 2159, and contains additional coefficients extending to degree 2190 and order 2159. The spatial resolution (half wavelength) of EGM2008 is (nominally) 9.3x9.3 km on the equator, which is 6 times higher than that of EGM996. Over EGM96 and older GGMs, EGM 2008 represents improvement by a factor of six in resolution, and by factors of three to six in accuracy depending on gravitational quantity and geographic area. EGM2008 represents a milestone and a new paradigm in global gravity field modeling, by demonstrating for the first time ever, that given accurate and detailed gravimetric data, a single global model may satisfy the requirements of a very wide range of applications (Pavlis et a;; 2012). The geoid undulations of Egypt as computed from EGM 2008 are shown in Fig. (2c) (Rabah and Kaloop, 2013).

IV. STUDY AREA AND AVAILABLE DATA

The study area is located in the northern Egypt from Rosetta to Brullous Fishing port along the Mediterranean coast (Fig. 3).It extends from longitude 30º22.40' E to 30º55.15' E, and from latitude 31º 27.8' N to 31º 33.9' N. The current area of the study area covers 198 square kilometers approximately. The study have been carried out using 31 GPS/leveling data points as shown in Fig. (4). 24 of these points were used as control points in the development of a geoid model for the Rosetta area, while 7 points were used as check points. The selection of control points set was based upon maintaining homogeneous distribution taking into consideration the topography of the region. The majority of this data set comes from research project carried out by the Survey Research Institute (SRI). The spirit levelling observations were performed as closed loops that run between known high-precision benchmarks established by Egyptian survey Authority (ESA) based on the national vertical datum of Egypt, whose origin is based on Mean Sea Level (MSL) at Alexandria tide gauge of 1906. In addition, GPS measurements were carried out relative to the ESA national geodetic reference framework of Egypt

Fig. 3: The Study Area

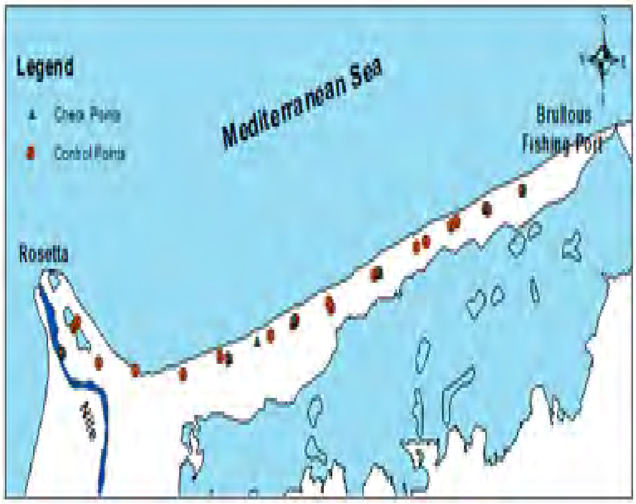

Fig. 4: Distribution of Control and Check Points in the Study Area

Published By:
Blue Eyes Intelligence Engineering & Sciences Publication Pvt. Ltd.

V. EVALUATION OF GGMS IN THE STUDY AREA

In order to evaluate the performance of selected GGMs in the study area: first geoid undulations at all GPS/leveling points (Nobs) have been computed using equation 1, secondly the Trimble Business Center program (TBC) was used to calculate geoid undulations (NGGMs) at the same points for OSU-91A, E9M96, and EGM2008, and thirdly a comparison of results has been performed in order to choose the optimum GGM to be utilized in Rosetta zone.

$$dN = N_{obs} - N_{GGMs} \qquad (7)$$

where:

N_{ObS} is the difference between ellipsoidal heights "h" and orthometric heights "H"

N_{GGMs} is geoid undulations for Geoid Global Models (OSU-91A, EGM 96, EGM 2008)

The obtained results are presented in Tables (I) and (II). Fig. (5) shows the geoid undulations (NGGMs) for the OSU-91A, EGM96, and EGM2008 and (Nobs.) from GPS/Levelling observation. Fig. (6) shows the geoid undulation differences (dN) between (Nobs) and (NGGMs). It can be noticed that, the EGM 2008 is the closer GGMs to the observed local geodetic dataset, in terms of difference of geoid undulation that have a maximum of 0.691 meter, a minimum of 0.430 meter, an average of 0.571 meter, and a standard deviation of ±0.060.

Table I: Difference of Geoid Undulation (dN) between GPS/Leveling and GGMs

St.	dN			St.	dN		
	OSU-91A	EGM 96	EGM 2008		OSU-91A	EGM 96	EGM 2008
R1	1.715	0.714	0.577	R14	2.182	0.885	0.652
R2	1.843	0.797	0.651	R15	2.117	0.816	0.582
R3	1.710	0.667	0.523	R16	2.160	0.830	0.586
Ch 1	1.746	0.701	0.554	Ch 4	2.076	0.776	0.542
R4	1.808	0.728	0.575	R17	2.262	0.879	0.624
R5	1.744	0.656	0.503	R18	2.302	0.912	0.650
R6	1.865	0.744	0.583	Ch 5	2.242	0.895	0.647
R7	1.818	0.697	0.538	R19	2.269	0.839	0.572
Ch 2	1.991	0.805	0.615	R20	2.242	0.823	0.536
R8	1.910	0.776	0.612	R21	2.262	0.778	0.481
R9	1.867	0.681	0.490	Ch 6	2.259	0.876	0.620
R10	1.966	0.780	0.590	R22	2.334	0.848	0.544
R11	1.953	0.762	0.570	R23	2.218	0.736	0.430
R12	2.100	0.846	0.630	Ch 7	2.330	0.947	0.691
Ch 3	2.056	0.755	0.524	R24	2.274	0.774	0.467

Table II: Statistical Function for Geoid Undulations Difference (dN) Computed usingOSU-91A, EGM96, and EGM2008

Statistical function	dN		
	OSUA91	EGM 96	EGM 2008
Minimum	1.710	0.656	0.430
Maximum	2.334	0.947	0.691
Range	0.624	0.291	0.261
Average	2.051	0.789	0.571
St. Deviation	0.208	0.074	0.060

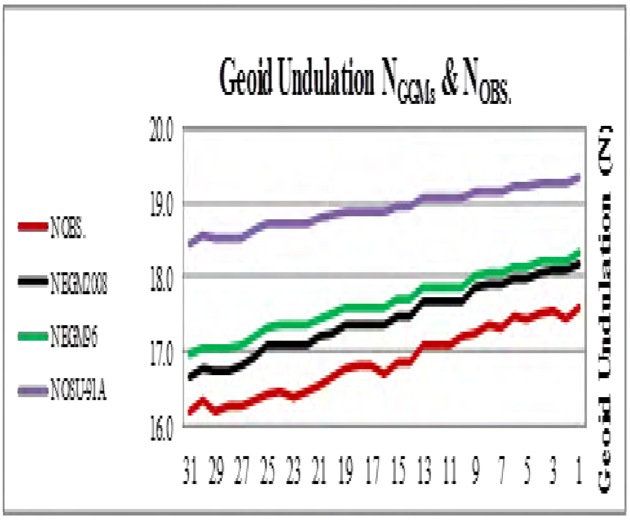

Fig. 5: Result of the Comparison of (NEGM2008), (NEGM96), (NOSU-91A), and (NObS)

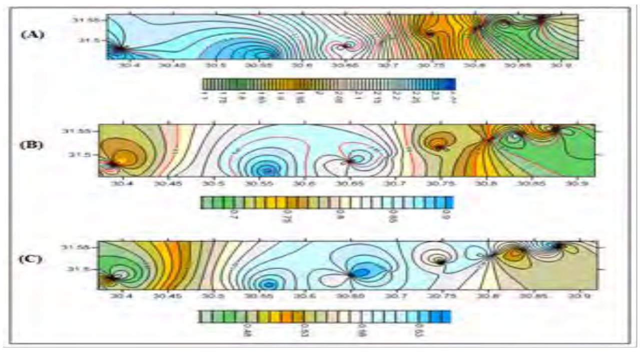

Fig. 6: (A) A Contour Map of dN between (NOSU-91A, NObs.), (B) A Contour Map of dN between (NEGM96, NObs.), and(C) (Contour Map of dN between (NEGM2008, NObs.)

VI. DEVELOPMENT OF A LOCAL GPS/LEVELLING GEOID MODEL

The second step of the processing stage of the current study is to develop the local geoid model over the study area by using GPS/leveling observations. Many surface modeling techniques can be used to improve the accuracy of the model. In this study, the polynomial regression approach is utilized since is the most common method for local geoid surface modeling. The computational steps are outlined as follows Fig. (7):

Published By:
Blue Eyes Intelligence Engineering & Sciences Publication Pvt. Ltd.

-Four cases are processed by using 6, 12, 18 and 24 data points respectively in order to investigate the effect of point distribution.

-Additionally, three types of polynomial order (1, 2, and 3) have been performed in order to investigate the optimum polynomial order in geoid modeling. Of course, in the first case (6 control points) the 2rd, and 3rd order polynomial regression have not been applied because the number of unknowns is more than the number of equations.

-Thus, 10 local geoid models have been obtained as a combination of all possible cases.

-Finally, a comparison has been carried out between the values of geoid undulations of each local model (NLocal_Model), and geoid undulations of the GPS/Levelling (NObs) at the check points.

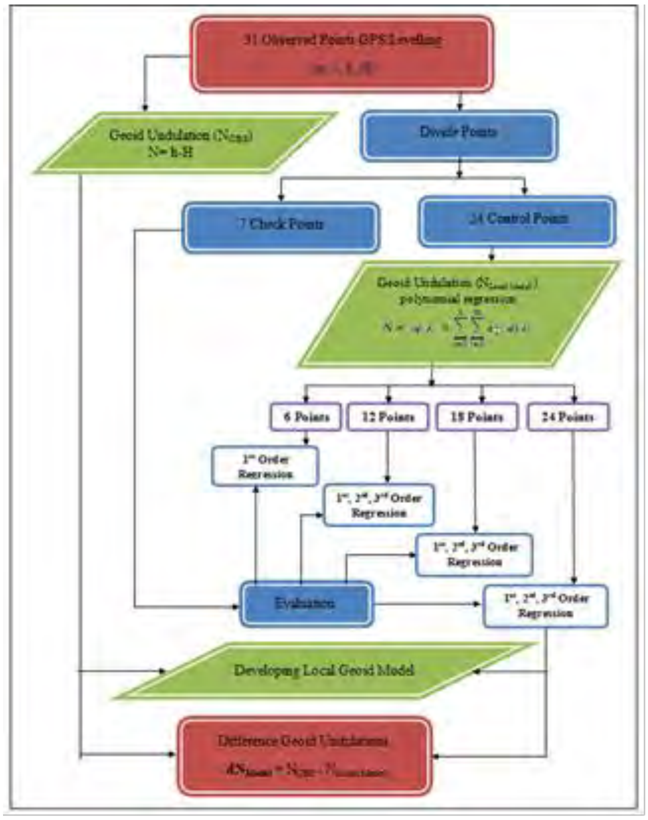

Fig. 7: A flowchart of the Utilized Methodology

Fig. (8), and (9) along with Table (III) depict the accomplished results.

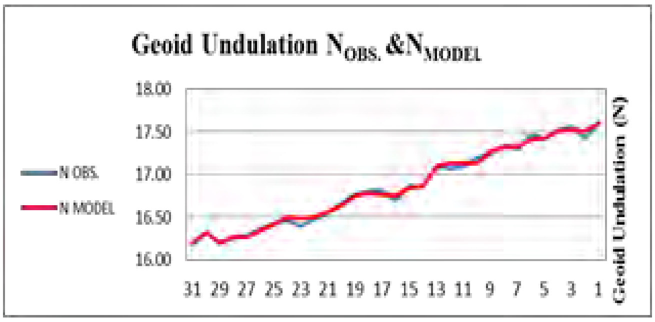

Fig. 8: Result of the Comparison of (NOBS) and (NLocal -Model)

The accomplished results show that the best model for local geoid in the study area is that of the 2rd-order polynomial degree in the fourth case (24 control points).

The attained geoid undulation of that model (NLocal_Model) is computed by:

$$N_{local_model} = -73856.5 + 5661.6\phi - 1008.1\lambda + 42.33\phi\lambda + 0.6668h - 110.32\phi^2 - 5.299\lambda^2 - 0.016h^2 \quad (8)$$

Table III: Statistical Parameters of Geoid Undulations Difference ($dN_{Local\text{-}Model}$) between ($N_{Local\text{-}Model}$) and (N_{Obs}) for Four Cases in Meters

Case 1 (6) Control Points

Models			Statistical Parameters
Model 1 1st Order	Model 2 2nd Order	Model 3 3rd Order	
0.049	–	–	Max
-0.219	–	–	Min
0.268	–	–	Range
-0.063	–	–	Average
0.097	–	–	STDEV

Case 2 (12) Control Points

Models			Statistical Parameters
Model 1 1st Order	Model 2 2nd Order	Model 3 3rd Order	
0.028	0.120	0.114	Max
-0.167	-0.034	-0.014	Min
0.195	0.154	0.129	Range
-0.045	0.028	0.047	Average
0.072	0.059	0.052	STDEV

Case 3 (18) Control Points

Models			Statistical Parameters
Model 1 1st Order	Model 2 2nd Order	Model 3 3rd Order	
0.045	0.051	0.030	Max
-0.137	-0.101	-0.123	Min
0.182	0.152	0.154	Range
-0.034	-0.020	-0.033	Average
0.062	0.053	0.055	STDEV

Published By:
Blue Eyes Intelligence Engineering
& Sciences Publication Pvt. Ltd.

Case 4 (24) Control Points			
Models			Statistical Parameters
Model 1 1st Order	Model 2 2nd Order	Model 3 3rd Order	
0.054	0.059	0.051	Max
-0.117	-0.083	-0.094	Min
0.170	0.142	0.145	Range
-0.023	-0.010	-0.016	Average
0.057	0.050	0.051	STDEV

When compared against observed undulations, this model produces differences range from 0.059 meter to -0.083 meter, with average of -0.010 meter, and a standard deviation equals ± 0.050 meter. This level of precision exceeds that of all tested GGMs models over the study area.

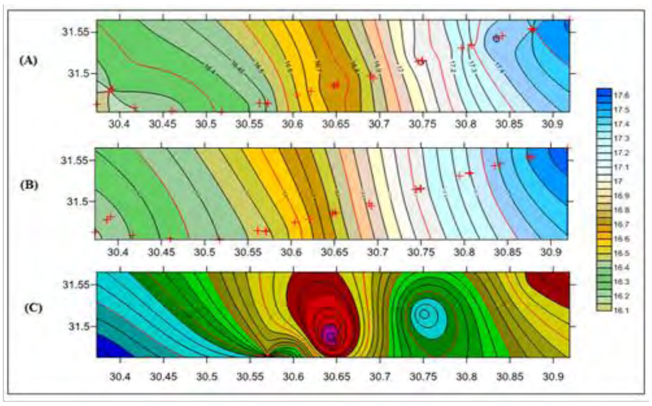

Fig. 9: (A) A Contour Map of Geoid Undulation (NObs), (B) A Contour Map of Geoid Undulation (NLocal_Model), and (C) Contour Map of Difference Geoid Undulations (dNLocal-Model)

VII. CONCLUSION AND RECOMMENDATION

A geoid model is very important to convert the GPS-based ellipsoidal heights into MSL-based orthometric heights usually used in mapping, geomatics, GIS, and surveying applications. So far, there is no national precise geoid model covers the entire Egyptian territories. The current study has investigated GPS/levelling geoid modelling technique and improving its precision through polynomial regression. Additionally, an evaluation of the performance of GGMs in the study area has been carried out. The attained results and concluding remarks can be summarized as following:

- The EGM 2008 represents the most precise global geopotential model to be used for geoid determination in Egypt. it has been found that this model produce geoid undulation differences, in the study area, range from 0.43 meter to 0.691 meter, with an average of 0.57 meter and a standard deviation equals ± 0.06 meter.
- The achievable accuracy of local geoid determination in the study area after using regression method models is ranges between 0.059 meter to -0.083 meter, with an average -0.01 meter and Standard Deviation± 0.05 meter.
- Increasing the number of control points with well spatial distribution, and increasing the polynomial regression order for the same number of control points improves precision of geoid determination model.
- It is highly recommended in future to use GPS/levelling all over Egypt with sufficient and well distributed points to improve the accuracy of geoid determination with cooperation of all surveying authorities in Egypt.
- It is recommended to apply other surface modeling techniques (such as, Kriging, Inverse Distance to a Power, Nearest Neighbor, and Natural Neighbor) in order to check their validity and performance in geoid modeling in Egypt.

REFRENCES

[1] Al-Ghamdi K., and Dawod G. (2013) Accuracy assessment of global geopotential models for GIS and geomatics applications in Makkah metropolitan area, *The Eighth National GIS Symposium in Saudi Arabia*, April 2013, pp. 1-13.

[2] Catalao J. C., and Sevila M. J.(1999) Comparison between EGM96 and FCUL96B tailored geopotential model for the north-east Atlantic, *Bollettino di Geofisica Teorica ed Applicata*, Vol. 40, No. 3-4, Sep.-Dec.1999, pp. 255-259

[3] El-Hallaq M. (2012) Development of a local GPS/leveling geoid model for the Gaza strip area, *International Journal of Emerging Technology and Advanced Engineering*, ISSN 2250-2459, Volume 2, Issue 3, March 2012, pp. 268-273

[4] Erol B., and Çelik R.(2004) Precise local geoid determination to make GPS technique more effective in practical applications of geodesy, *FIG Working Week*, Athens, Greece, May 22-27.

[5] Dawod, G., Mohamed, H., and Ismail, S. (2010) Evaluation and adaptation of the EGM2008 geopotential model along the northern Nile valley, Egypt: A case study, *Journal of Surveying Engineering*, Vol. 136, No. 1, February 2010, pp. 36-40.

[6] Golden Software Surfer Win-XP Software 'Help menus'

[7] Hong-Sic Yun (1999) Precision geoid determination by spherical FFT in and around the Korean peninsula , *Earth Planets and Space*, Volume 51, issue 1, pp.13–18.

[8] IECGM (2014), available: http://icgem.gfzpotsdam.de/ICGEM/ICGEM.html, accessed Sept. 2014.

[9] Kaloop M., Rabah M. and EL-Shmbaky H. (2008) High Accurate Local Geoid in Egypt, *FIG Working Week*, Stockholm, Sweden 14-19 June.

[10] Pavlis, N.K., Holmes S.A., Kenyon S.C., and Factor J.K.,(2008) Earth Gravitational Model to degree 2160: EGM2008, *European Geosciences Union general assembly*, Vienna, Austria, April 2008, pp.13-18.

[11] Pavlis, N.K., Holmes S.A., Kenyon S.C., and Factor J.K., (2012) The development and evaluation of the Earth Gravitational Model 2008 (EGM2008), *Journal of Geophysical Research: Solid Earth* (1978–2012), April, Volume 117 Issue B4.

[12] Rabah M. and Kaloop M. (2013) The use of minimum curvature surface technique in geoid computation processing of Egypt, *Arabian Journal of Geosciences*, April, Volume 6, Issue 4, pp. 1263-1272.

[13] Saad A., and Dawod G. (2002) A Precise integrated GPS/gravity geoid model for Egypt, *Civil Engineering Research Magazine (CERM)*, Al-Azhar University, Volume 24, No. 1, pp.391-405.

[14] Schut G.H. (1976) Review of Interpolation Methods for Digital Terrain Models, *The Canadian Surveyor*, December, Volume 30, No.5

[15] Yanalak M. (1991) Digital terrain models and interpolation methods. *Master thesis, Yıldız Technical University*, Civil Engineering Faculty Geodesy and Photogrammetry Engineering,

Eng. Essam Mohamed Farag ALkrargy, Asst. Researcher of Survey Research Institute, Department of Physical geodesy, National Water Research Center, Cairo, Egypt.

Dr. Mohamed Ismail Ali Doma, Assoc. Prof. of Surveying and Geodesy, Department of Civil Engineering, Faculty of Engineering, Menoufia University, Egypt.

Prof. Gomaa Mohamed Dawod, Department of Physical geodesy, Survey Research Institute, National Water Research Center, Cairo, Egypt.

Published By:
Blue Eyes Intelligence Engineering & Sciences Publication Pvt. Ltd.

Investigating the Precision of Recent Global Geoid Models and Global Digital Elevation Models for Geoid Modelling in Egypt

Essam M. Al-Krargy, Magdy M. Hosny, and Gomaa M. Dawod

Survey Research Institute
National Water Research Center, Egypt
essamalkrargy@yahoo.com

Abstract

A national geoid model is crucial for a wide range of surveying and civil engineering applications worldwide, with Egypt being of no exception. Although there are many researchers attempted to develop a national Egyptian geoid model, the limitations of available geodetic data sized the precision of such models. In order to increase the accuracy of a geoid model, a precise Global Geopotential Model (GGM) along with a precise Digital Elevation Model (DEM) is needed. This papers aims to quantify the precision of most-recent released GGM and global DEM models based on a precise local geodetic dataset (gravity and GPS/Levelling data) covers the Egyptian territories. The attained results show that, out of seven investigated recent GGMs, the EGM2008 is the most precise global models over Egypt, that produces a mean standard deviation of geoid undulation differences equals ± 0.23 meter over observed 1074 GPS/Levelling stations. Additionally, the EGM2008 model gives a mean standard deviation of gravity differences that equals ± 25.1 mGal when examined over 941 observed gravity points. Furthermore, it has been shown that the SRTM3 DEM produces a mean standard deviation of ± 4.3 meter when compared over 1227 points of observed orthometric heights. Consequently, it is recommended to apply these two specific models in the undergoing development of a national geoid model of Egypt.

Keywords: Geoid, Gravity, GPS, GGM, DEM, Egypt

1. Introduction

A precise geoid model constitutes one of the most challenging research subjects of geodesy, particularly since 1980s. Geoid modelling deal with the determination of geoid undulations between the geodetic heights obtained from the Global Navigation Satellite Systems (GNSS) techniques and the orthometric heights, or levels, relative to the Mean Sea Level (MSL). Thus, geoid models are crucial for the utilization of GNSS (particularly the Global Positioning System: GPS) in civil engineering projects. Over the last two decades, national precise geoids have been developed all over the world, e.g. in Indonesia (Pahlevi et al. 2015), Uganda (Ssengendo et al. 2015), Korea (Lee and Kim, 2012), New Zealand (Classens et al. 2011), Sudan (Abdalla and Fairhead, 2011), and Italy (Corchete 2011).

In Egypt, since the development of the first pioneer national-scale geoid (Alnaggar 1986), several geoid researches have been carried out. For example, Dawod (1998) has developed a national geoid model based on the data of the Egyptian National Standardization Network of 1997 (ENGSN97) along with GPS/levelling data. Saad and Dawod (2002) have developed a national geoid model

based on the EGM96 global geopotential model along with GPS/levelling datasets. In addition, Abd-Elmotaal (2008) has developed a gravimetric geoid model utilizing high-degree tailored reference geopotential model. Recently, Rabah and Kaloop (2013) have developed a local geoid model utilizing the minimum curvature surface technique. and Al-Karargy et al. (2014) have investigated the utilization of GPS/levelling in developing geoid models for small areas in Egypt.

The geoid undulation (N) can be computed from gravity data by the well-known Stokes' formula (e.g. Heiskanen and Moritz 1967):

$$N = R/_{4\pi\gamma} \iint_{\sigma} S(\psi) \Delta g d\sigma \tag{1}$$

where: R is the mean Earth radius, γ is the normal gravity on the reference ellipsoid, Δg is the gravity anomaly, $d\sigma$ is an infinitesimal surface element on the unit sphere σ, and $S(\psi)$ is the Stokes' function which can be expressed as a series of Legendre polynomial $P_n(\cos\psi)$ over the sphere:

$$S(\psi) = \sum_{n=2}^{\infty} (2n+1/_{n-1}) P_n(\cos\psi) \tag{2}$$

Stokes' formula (Eq. 1) need to be applied over the whole Earth, however in practice gravity datasets of the whole Earth are not available. Thus the gravimetric geoid modelling methods break up the gravity anomalies (Δg) into three components:

$$\Delta g = +\Delta g_{REF} + \Delta g_F + \Delta g_h \tag{3}$$

where: Δg_F represents the free-air gravity anomalies, Δg_h is the effect of topography, and Δg_{REF} represents the gravity anomalies of a reference gravity field represented by a GGM.

Therefore, the full geoid undulation (N) is decomposed into three components too:

$$N = N_{REF} + N_{\Delta g} + N_h \tag{4}$$

where: $N_{\Delta g}$ is the contribution of the reduced gravity anomalies computed by Stokes's integral, N_h is the contribution of the topography, and N_{REF} is the contribution of the reference gravity field.

Consequently, geoid modelling techniques require the utilization of a GGM to represent the global variations or long wavelengths of the Earth gravitational field, along with a DEM to depicts the topography of the local area and determine its effects on the developed geoid model. Hence, the precision of the utilized GGM and DEM influences the attained precision of the geoid models. Several research studies (e.g. Mahmoud 2012, Dawod 2008, Arabelos and Tscherning 2010, and Erol et al. 2009) have investigated the precision of several GGM and DEM as an initial procedure for precise geoid modelling. This paper aims to explore the accuracy of several most-recent GGM and DEM models in representing the gravity and topography fields over Egypt in order to select which models to be utilized in developing a precise national geoid model.

2. Global Geopotential Models (GGM)

The geoid undulations (N) may be computed using the following spherical harmonic expansion:

$$N = (GM/r\gamma)\sum_{n=2}^{n\max}(a/r)^n - \sum_{m=0}^{n}((C_{nm}^{-}\cos m\lambda) + (S_{nm}^{-}\sin m\lambda))P_{nm}\sin\varphi) \quad (5)$$

where: n is the degree of the GGM model, n max is the maximum degree of the GGM model, m is the maximum order of the model, γ is the normal gravity of the reference ellipsoid, r is the geocentric radial distance of the computation point projected on the ellipsoid, G is the Newtonian gravitational constant, M is the mass of the Earth, a is the semi-major axis, ϕ is the geocentric latitude, λ is the geocentric longitude, C^{-}_{nm} and S^{-}_{nm} are the fully normalized harmonic coefficients, and P_{nm} is the fully normalized associated Legendre polynomial.

GGM models have been developed since the 1960s as an important tool for geoid modelling on a regional or local scales. So far, there are more than 150 GGM available at the website of the International Center for Global Earth Models (http://icgem.gfz-potsdam.de/ICGEM/ICGEM.html). In developing GGM models, datasets from several sources might be utilized such as: satellite-based gravity data, terrestrial gravity data, satellite altimetry data, and terrestrial geodetic data. Therefore, the maximum degree and the precision of GGM models vary significantly.

This paper utilizes seven GGM models and evaluates their accuracy when compared against precise local geodetic datasets in Egypt. Those models are:

- EIGEN-6C4: A model released in 2014, that utilizes satellite tracking data (from both LAGEOS, GRACE, and GOCE missions) along with a global surface gravity anomaly grid. The model is up to 2190 degree. It was developed by both the Germany GFZ research center and the French CNES research center.
- GO_CONS_GCF_DIR_R5: A satellite-only GGM up to degree 300, developed by the European Space Agency (ESA), and released in 2014. It utilizes data from LAGEOS, GRACE, and GOCE satellite missions.
- GO_CONS_GCF_TIM_R5: Another satellite-only ESA model dated 2012 with a maximum degree of 250. It utilizes data from only GOCE satellite mission.
- DGM-1S: A model developed by Delft university, Netherlands, that was released in 2012. Also, it is a satellite-only GGM based on data from both GOCE and GRACE missions.
- EGM2008: An integrated GGM developed by the US National Geospatial-Intelligence Agency (NGA) up to 2190 degree. It was developed in 2008 based on satellite tracking data, terrestrial gravity data, and altimetry data. It was a millstone in GGM development, since its preceding model did not exceed 360 maximum degree.
- EIGEN-5C: A traditional integrated GGM (i.e. up to maximum degree of 360) developed by the Germany GFZ research center.
- EGM96: One of the most famous GGM that was developed, in 1996, by the US National Aeronautics and Space Administration (NASA) up to maximum degree of 360. It was based on a previous satellite-only GGM (EGM96S) combined with terrestrial and altimetry datasets.

Table 1 summarizes the main characteristics of those GGM models. From this table, it can be realized that the selection of such models depicts a variety in their nature in terms of development year, maximum model degree, and the types of data utilized in the development of each model.

Table 1: Characteristics of Utilized GGM Models

GGM Model	Year	Max Degree	Data Type
EIGEN-6C4	2014	2190	S (GOCO, GRACE, LAGEOS), G, A
GO_CONS_GCF_2_DIR_R5	2014	300	S (GOCO, GRACE, LAGEOS)
GO_CONS_GCF_2_TIM_R5	2014	280	S (GOCO)
DGM-1S	2012	250	S (GOCO , GRACE)
EGM2008	2008	2190	S (GRACE), G, A
EIGEN-5C	2008	360	S (GRACE , CHAMP), G, A
EGM96	1996	360	EGM96S, G, A
where: S = Satellite tracking data, G = Terrestrial gravity data, A = Altimetry data, GOCE, GRACE, and LAGEOS are gravity satellite missions.			

The International Center for Global Earth Models (ICGEM) continuously analyzes the performance of every new released GGM model over several GPS/Levelling check points worldwide. Table 2 presents the statistics of evaluation of the selected seven GGM models in terms of the Root Mean Square error (RMS) of the undulation differences. It can be seen that the overall accuracy of EGM2008 over the entire 12036 check points indicates that it is the most precise GGM.

Table 2: RMS of Differences of GGM-Based Geoid Undulations over GPS/Levelling Check Points (m)

Test Area	USA	Canada	Europe	Australia	Japan	Brazil	ALL
No. of Check Points	6169	2691	1047	201	816	1112	12036
GGM Model							
EIGEN-6C4	0.247	0.126	0.121	0.212	0.079	0.446	0.236
GO_CONS_GCF_2_DIR_R5	0.405	0.299	0.345	0.327	0.447	0.507	0.392
GO_CONS_GCF_2_TIM_R5	0.398	0.310	0.343	0.336	0.450	0.505	0.390
DGM-1S	0.441	0.348	0.413	0.366	0.513	0.517	0.432
EGM2008	0.248	0.128	0.125	0.217	0.083	0.460	0.240
EIGEN-5C	0.341	0.278	0.266	0.244	0.339	0.524	0.342
EGM96	0.379	0.353	0.493	0.298	0.364	0.730	0.427

source: http://icgem.gfz-potsdam.de/ICGEM/ICGEM.html

3. Digital Elevation Models (DEM)

DEM models depict the topography of a spatial area in a digital format, and have been utilized for a wide range of applications including, for instance, topographic mapping, hydrologic modelling, water resources management, and hazards assessment. Several global DEM have been developed and released in the last two decades. Nevertheless, the spatial resolution and the precision of global DEM models vary significantly. In this research, three global DEM models have been tested in order to evaluate their accuracy in depicting the topography of Egypt. Those models are:

- Shuttle Radar Topography Mission (SRTM): SRTM is a joint project between the U.S. National Imagery and Mapping Agency (NIMA) and the National Aeronautics and Space Administration (NASA) (http://www2.jpl.nasa.gov/strm/). A 3-arce-second SRTM DEM (SRTM3) for many parts of the world has been compiled and released.
- GTOPO30: It is a global DEM, completed in late 1996, with a horizontal grid spacing of 30" (approximately 1 km). GTOPO30, developed over a three-year period through a collaborative effort led by the U.S. Geological Survey's EROS Data Center (EDC), and was derived from several raster and vector sources of topographic information.
- Advanced Spaceborne Thermal Emission and Reflection Radiometer (ASTER): The Ministry of Economy, Trade, and Industry (METI) of Japan and the United States National Aeronautics and Space Administration (NASA) have jointly released Version 1 of the Advanced Spaceborne Thermal Emission and Reflection Radiometer (ASTER) Global DEM. ASTER horizontal resolution equals 1 arc second, that is 30 meters approximately, and it is available free of charge (http://www.gdem.aster.ersdac.or.jp/).

The window of each DEM that corresponds to the Egyptian territories has been downloaded and utilized in this research. For example, the SRTM3 DEM of Egypt (Figure 1) show that the elevations range from -134 m to 2476 m with a mean of 304 m. On the other hand, the GTOPO30 DEM show that the terrain elevations vary between -174 m and 2575 m with an average of 302 m. Moreover, the ASTER DEM show that the terrain elevations vary between -154 m and 2495 m with an average of 300 m.

4. Available Data

The available geodetic dataset contains 1074 GPS/Levelling stations, along with 941 observed terrestrial gravity points(Figures 2 and 3). The GPS/levelling stations have been observed by the Survey Research Institute (SRI) in several surveying projects mainly in the last five years. Their orthometric heights have been observed by precise levelling while their geodetic heights have been observed by dual-frequency GPs receivers. Thus, an observed geoid undulation is computed at each station. The terrestrial gravity dataset consists of the most-precise data of the Egyptian National Gravity Standardization Network of 1997 (ENGSN97) along with older gravity measurements carried out in 1960s. For the DEM evaluation, known elevations at 1227 points have been utilized (Figure 4).

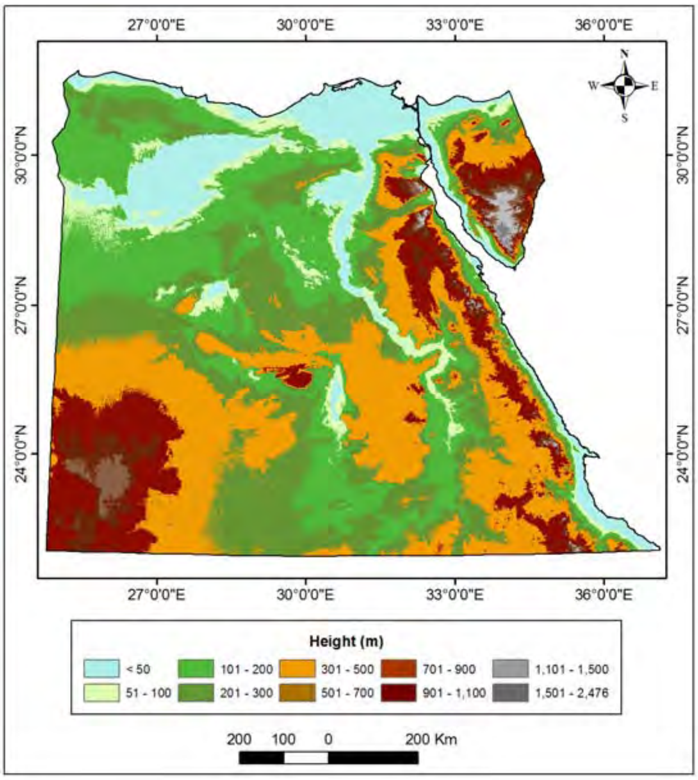

Figure 1: SRTM3 DEM of Egypt

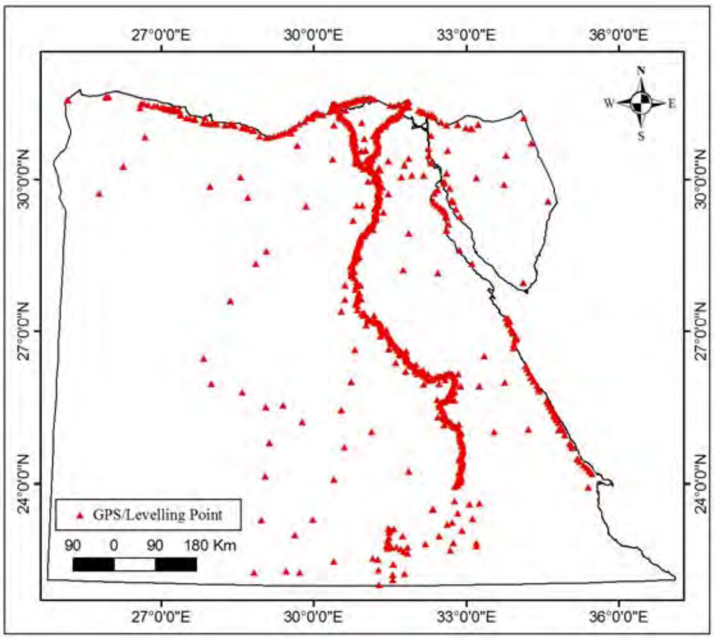

Figure 2: Available Known GPS/Levelling Points

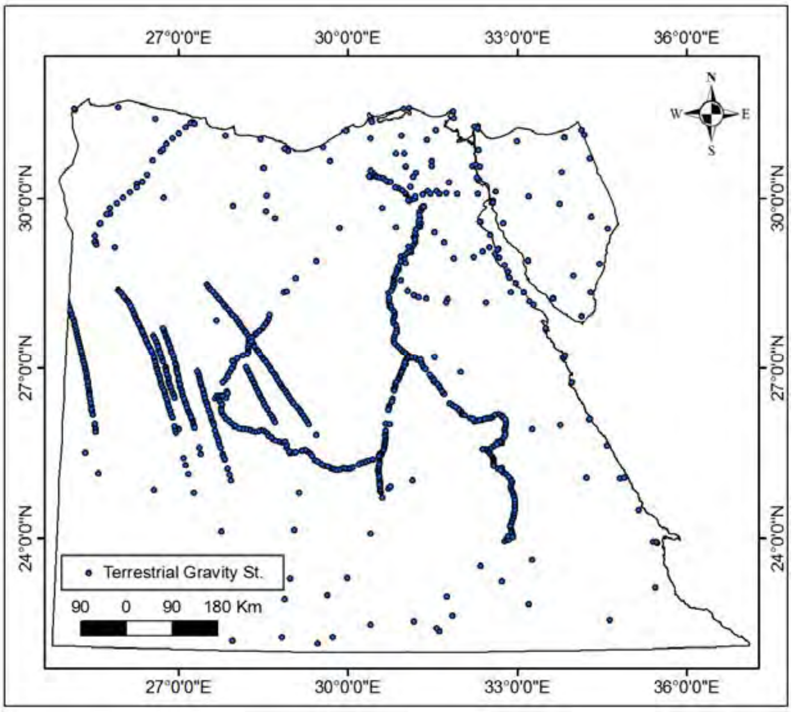

Figure 3: Available Known Terrestrial Gravity Points

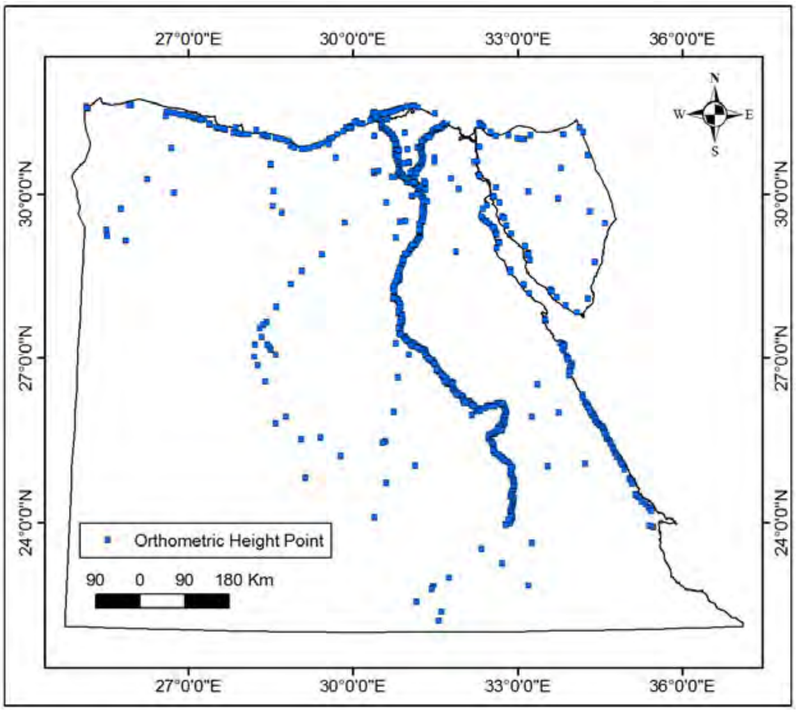

Figure 4: Available Known Elevation Points

5. Data Processing and Attained Results

The performed data processing consists of two stages: (1) evaluation of GGM models, and (2) evaluation of DEM models. The attained results are discussed in the two following sub-sections.

5.1 GGM Evaluation Results

The performance analysis of the GGM seven models consists of two procedures: (1) comparing the observed N values against the estimated GGM-based N for each GGM model, and (2) comparing the observed free-air gravity anomaly values against the corresponding GGM-based for each GGM model. The GRAVSOFT 2.9 package (Forsberg and Tscherning 2008) has been utilized in computing geoid undulations and free-air gravity anomalies of the selected GGM models at the 941 check points. The accomplished results are presented in Table 3. It can be realized, from this table, that the EGM2008 GGM produces the smallest differences (in terms of RMS values) compared to the observed terrestrial free-air gravity values. The EIGEN-6C4 GGM came in the second place with a close RMS value, while the GO_CONS_GCF_2 TIM_R5 GGM give the largest differences. As seen in Table 1, both EGM2008 and EIGEN-6C4 have maximum degree of 2190, while GO_CONS_GCF_2_DIR_R5 has maximum degree of only 300. That might explain the attained results, since the higher degree of a model, the smaller spatial resolution in representing the gravity field.

Table 3: Performance of GGM Models in terms of Gravity Anomalies

GGM Models	Differences between observed and GGM-Based Free-Air Gravity Anomalies (mGal)			
	Minimum	Maximum	Average	RMS
EIGEN-6C4	-55.2	91.9	23.8	25.5
GO_CONS_GCF_2_DIR_R5	-83.4	92.0	18.1	27.6
GO_CONS_GCF_2 TIM_R5	-82.9	91.7	18.4	28.1
DGM-1S	-50.6	84.2	17.7	27.9
EGM2008	-52.73	80.26	24.75	25.1
EIGEN-5C	-45.7	77.1	18.4	26.7
EGM96	-55.2	122.4	16.9	27.3

Table 4 presents the geoidal undulations comparison between the observed or known undulations and the GGM-based corresponding values at the 1074 GPS/Levelling check points. It can be seen that the EGM2008 GGM, again, produces the smallest RMS for the differences with a value of ±0.23 m. The EIGEN-5C came in the second place with an RMS of ±0.32 m. In the last place, the EGM96 GGM came with a value of ±0.52 m. The higher precision of EGM2008 might be attributed to the amount and quality of the terrestrial dataset utilized in the model development.

Table 4: Performance of GGM Models in terms of Geoid Undulations

GGM Models	Differences between observed and GGM-Based Geoidal Undulations (m)			
	Minimum	Maximum	Average	RMS
EIGEN-6C4	-1.69	0.78	-0.67	0.36
GO_CONS_GCF_2_DIR_R5	-1.51	1.44	-0.29	0.38
GO_CONS_GCF_2_TIM_R5	-1.50	1.49	-0.27	0.38
DGM-1S	-1.93	0.70	-0.71	0.37
EGM2008	-0.59	0.31	-0.22	0.23
EIGEN-5C	-1.50	0.56	-0.68	0.32
EGM96	-1.77	1.77	-0.81	0.52

Based on the attained results, it can be concluded that the EGM2008 is the most precise GGM model in representing the gravity field of Egypt in terms of free-air gravity anomalies and geoidal undulations too. Figures 5 and 6 depicts the long-wavelength contribution of the gravity field over the entire Egyptian territories based on the EGM2008 GGM. Such spatial variations of both geoidal undulations and gravity anomalies should be considered in developing a national precise geoid model.

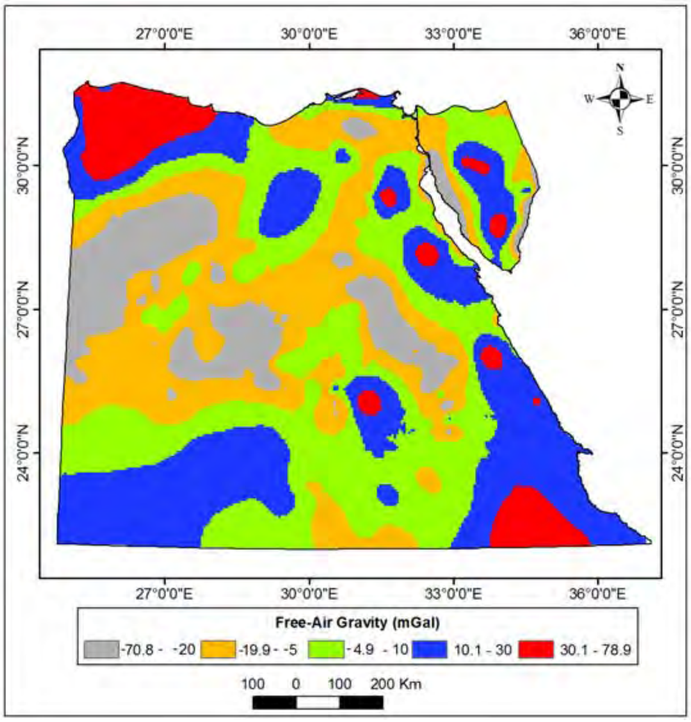

Figure 5: EGM2008 Free-Air Gravity Anomalies of Egypt

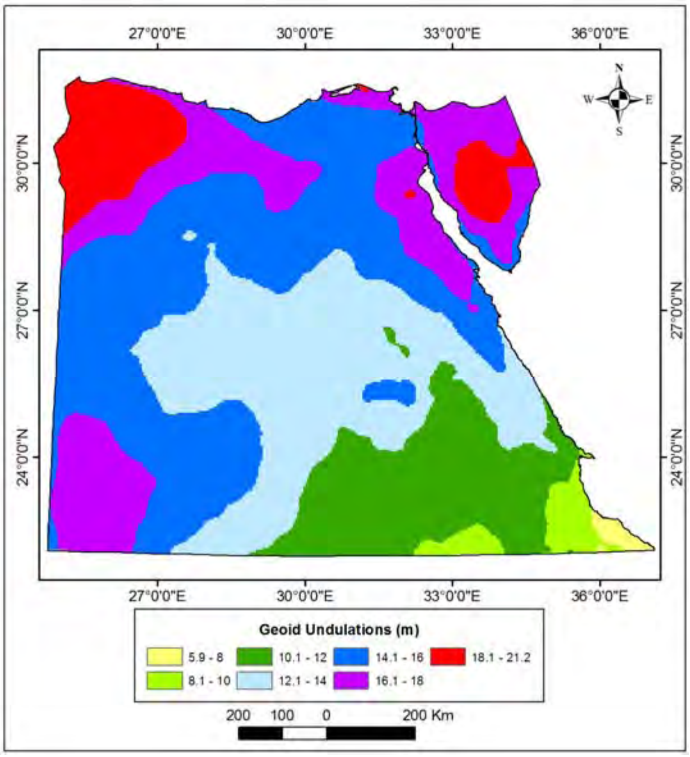

Figure 6: EGM2008 Geoid Undulations of Egypt

5.2 DEM Evaluation Results

For the DEM evaluation, the ArcGIS 10.2 package has been utilized to interpolate the levels of the 1227 available data points based on their geodetic coordinates, and then compare them to the observed orthometric heights. The statistics of the estimated height differences are presented in Table 5. Clearly, it can be realized that the SRTM DEM produces the smallest differences (both in average and RMS values), while the GTOPO30 gave the biggest differences. Similar results have been reported in different countries, such as Nigeria (Amans et al., 2013) and Saudi Arabia (Mirza et al., 2011). Hence, it can be concluded that SRTM is the most precise global DEM model in representing the topography of Egypt.

Table 5: Performance of DEM Models in terms of Orthometric Heights

DEM Models	Differences between observed and DEM-Based Orthometric Heights (m)			
	Minimum	Maximum	Average	RMS
SRTM	-9.0	14.8	1.1	4.3
ASTER	-25.8	25.4	2.0	8.1
GTOPO30	-163.9	205.6	4.9	25.2

6. Conclusions

A geoid model is fundamental for converting the GPS-based ellipsoidal heights into MSL-based orthometric heights usually used in geomatics, GIS, surveying, geodetic, and mapping applications. So far, there is no available published precise national geoid model that covers the entire territories of Egypt. Thus, this research study has compared seven of the most-recent released GGM (namely EIGEN-6C4, GO_CONS_GCF_DIR_R5, GO_CONS_GCF_TIM_R5, DGM-1S, EGM2008, EIGEN-5C, and EGM96) over most-recent precise GPS/levelling points and terrestrial gravity stations, in order to decide the most precise one that precisely represent the Earth's gravitational field over Egypt. On the other hand, DEM is needed in geoid development in order to compute the topographic effects. Hence, three global DEM (SRTM, ASTER, and GTOPO30) have been investigated, too, over a precise geodetic dataset of Egypt.

The accomplished results show that the EGM2008 GGM produces the smallest differences (in terms of RMS values) compared to the observed terrestrial free-air gravity values. The EIGEN-6C4 GGM came in the second place with a close RMS value, while the GO_CONS_GCF_2 TIM_R5_2014 GGM give the largest differences. Regarding the geoid undulations, it has been found that the EGM2008 GGM, again, produces the smallest RMS for the differences , and the EIGEN-5C came in the second place. Consequently, it can be concluded that the EGM2008 is the most precise GGM model in representing the gravity field of Egypt in terms of free-air gravity anomalies and geoidal undulations too. Concerning the global DEM evaluation, the attained findings show that the SRTM produces the smallest differences (both in average and RMS values), while the GTOPO30 gave the largest differences. As a result, it is recommended that the EGM2008 GGM and the SRTM DEM should be considered in the undergoing developing of a precise national Egyptian geoid model.

References

Abdalla, A. and Fairhead, D. (2011) A new gravimetric geoid model for Sudan using the KTH method, Journal of African Earth Sciences, No. 60, pp. 213-221.

Abd-Elmotaal, H. (2008) Gravimetric geoid for Egypt using high-degree tailored reference geopotential model, NRIAG Journal of Geophysics special issue. pp. 507-531.

Al-Karagy, E., Doma, M., and Dawod, G. (2014) Towards an accurate discrimination of the local geoid model in Egypt using GPS/levelling data: A case study at Rosetta area, The International Journal of Innovative Science and Modern Engineering, V. 2, No. 11, pp.10-15.

Alnaggar, D. (1986) Determination of the geoid in Egypt using heterogeneous geodetic data, PhD dissertation, Faculty of Engineering, Cairo University, Egypt.

Amans, O., Beiping, W., and Ziggah, Y. (2013) Assessing vertical accuracy of SRTM ver 4.1 and ASTER GDEM ver. 2 using differential GPS measurements: Case study in Ondo state, Nigeria, International Journal of Scientific and Engineering Research, V. 4, No. 12, pp. 523-531.

Arabelos, D. and Tscherning, C. (2010) A comparison of recent earth gravitational models with emphasis on their contribution in refining the gravity and geoid at continental or regional scale, Journal of Geodesy, DOI 10.1007/s00190-010-0397-z.

Classens, S., Hirt, C., Amos, M., Featherstone, W., and Kirby, J. (2011) The NSGEOID09 model of New Zealand, Survey Review, No. 43, pp. 2-15.
Corchete, V. (2011) The high-resolution gravimetric geoid of Italy: ITG2009, Journal of African Earth Sciences, No. 58, pp. 580-584.
Dawod, G. (1998) A national gravity standardization network for Egypt, PhD dissertation, Faculty of Engineering at Shoubra, Zagazig University, Egypt.
Dawod, G. (2008) Towards the redefinition of the Egyptian geoid: Performance analysis of recent global geoid and digital elevation models, Journal of Spatial Science, No. 53, pp. 31-42.
Erol, B., Sideris, M. and Celik, R. (2009) Comparison of global geopotential models from the CHAMP and GRACE missions for regional geoid modelling in Turkey, Journal of Studies in Geophysics and Geodesy, No. 53, pp. 419-441.
Forsberg, R. and Tscherning, C. 2008) An overview manual for the GRAVSOFT geodetic gravity field modelling programs, University of Copenhagen, Denmark.
Heiskanen, W. and Moritz, H. (1967) Physical Geodesy, W.H. Freeman and Company, London.
Mahmoud. S. (2012) Assessment of the gravitational global models in Egypt, MSC thesis, Faculty of Engineering, Al-Azhar university, Egypt.
Mirza, M., Dawod, G., and Al-Ghamdi, K. (2011) Accuracy and relevance of digital elevation models for geomatics applications: A case study of Makkah metropolitan area, Saudi Arabia, International Journal of Geomatics and Geosciences, V. 1, No. 4, pp. 803-812.
Rabah, M. and Kaloop, M. (2013) The use of minimum curvature surface technique in geoid computation processing of Egypt, Arabian Journal of Geosciences, N, 6, pp. 1263-1272.
Lee, S. and Kim, C. (2012) Development of regional gravimetric geoid model and comparison with EGM2008 gravity field model over Korea, Scientific Research and Essay, V. 7, No. 3, pp. 387-397.
Pahlevi, A.,, Pangastuti, D., Sofia, N., Kasendi, A., and Prijatna, K. (2015) Determination of gravimetric geoid model in Sulawesi, Indonesia, Presented in the FIG Working Week Conference, Sofia, Bulgaria, May 17-21.
Saad, A. and Dawod, G. (2002) A precise integrated GPS/gravity geoid model for Egypt, Civil Engineering Research Magazine, V. 24, No. 1, pp. 391-405.
Ssengendo, R., Sjoberg, L, and Gidudu, A. (2015) Computation of the gravimetric quasigeoid model over Uganda using the KTH method, Presented in the FIG Working Week Conference, Sofia, Bulgaria, May 17-21.

High-Precision GPS Monitoring of the Land Subsidence in the Nile Delta: Status and Preliminary Results

Hoda F. Mohamed, Bahaa A. Shaheen, Magdy M. Hosny, and Gomaa M. Dawod

Survey Research Institute
National Water Research Center, Egypt
hoda.faisal@yahoo.com

Abstract

Land subsidence is a crucial spatial phenomena harmfully affects dens populated areas. Several delta regions of rivers worldwide suffer from noteworthy land subsidence and deformation. In the Nile delta, quite a few researches have been carried out to estimate the land subsidence rates and spatial distribution. However, results have been shown that the Nile delta encounters a substantial subsidence in the last few decades. Out of many geodetic monitoring methods (e.g. tide gauge data analysis, repeated levelling data, radar remote sensing imageries) GPS proves to be the most precise approach for land subsidence and deformation, that can fulfill the millimeter level of accuracy. This paper summarizes the undergoing research study to utilize high-precision GPS geodetic techniques to monitor land subsidence and horizontal deformation in the Nile delta area. Repeated GPS observations for six stations over the Delta covering the period 2012-2015 have been compiled, processed, and analyzed. Preliminary results, in terms of vertical and horizontal land deformations rates, patterns, and spatial coverage, are presented. It has been found that the vertical land movements at these six locations range from +4.9 to -6.5 mm/year, while the horizontal ground movements vary from 4.2 to 6.6 mm/year in the north-east direction. It is recommended that further detailed multi-disciplinary studies should be performed to explore the relationships between land subsidence and other environmental factors such as soil compaction and variations of groundwater levels. Finally, it is recommended that the accomplished results should be taken into consideration by decision makers in any existing and upcoming development plans of the Nile Delta.

Keywords: Ground deformation, Land subsidence, GPS, Nile Delta, Egypt

Introduction

Land subsidence is a natural hazard affects several large urban areas all over the world, particularly in coastal and rivers' delta regions. Geometrically, land subsidence can be defined as the downward displacement of land surface relative to a specific reference surface, such as the Mean Sea Level (MSL), the geoid, or a reference ellipsoid, or relative to a certain assumed stable point outside the prone subsidence area. Such natural hazard phenomena can be attributed to natural and/or human activities, such as tectonic activities (e.g. earthquake and faulting), volcanic activities, landslide, underground mining activities, excessive groundwater or oil/gas extraction, natural consolidation of alluvium soil, and load of huge constructions. Impacts of land subsidence might be categorized into infrastructure, environmental, economic, and social impacts (e.g. Abidin et al, 2015). In some cases, such a phenomena results in catastrophic effects as what happened in Cairo, particularly in El-Dewica area, where landslide of large blocks of rocks from Mokattam mountain has led to the destruction of almost 50 houses in 2008 (Poscolieri et al. 2011).

Crustal movements and land subsidence can be monitored by several techniques including levelling, Global Navigation Satellite Systems (GNSS) such as the Global Positioning System (GPS), and the Synthetic Aperture Radar (SAR) such as the Interferometry SAR (InSAR). Several studies have utilized such techniques for land subsidence all over the world (e.g. Atanasova 2015, DEPI 2014, Kalkan 2014, and Serpelloni et al. 2007). InSAR provides the capability of subsidence monitoring over large areas in a cost effective manner on a few-millimeters level of precision. On the other hand, levelling can reach a millimeter level of accuracy in monitoring huge infrastructure, e.g. dams, but it becomes time consuming in monitoring large areas. Thus, GNSS techniques would be the optimum and most accurate geodetic tool regarding deformation and subsidence over large areas.

In Egypt, geodetic deformation monitoring activities have begun in the 1980s, particularly after the occurrence of Aswan earthquake in 1981. For example, Rayan et al. (2010) have analyzed observations of a network of 11 GPS stations around lake Nasser in south Egypt, and have found that the horizontal crustal movements are in the order of 20 mm/year. Additionally, Aly et al. (2009) and Poscolieri et al. (2011) have utilized InSAR images covering the grater Cairo area during the period 1993-2000, and have found that the average rate of land subsidence is approximately 7 mm/year. Similar results with a rate of subsidence of 2-8 mm/year have been recently reported also for the Nile Delta region over the period 1992-1999 (Zaid et al., 2014). It has been shown that highest subsidence occurred at Damietta branch of the Nile, while moderate rates observed around Manzala lagoon (Becker and Sultan, 2009). In Sinai peninsula, the average velocity of crustal motion has been estimated, from GPS surveys, as 31 mm/year northward (El-Fiky 2005). Mohamed (2005) has analyzed continuous GPS observations at the Alexandria tide gauge station over the period 2001-2003 and has estimated land subsidence to be 0.47 mm/year.

The Nile delta area posses a complex geological and hydrological structures so that land subsidence and land uplift are existed interchangeably on the spatial coverage of the area. Fugate (2014) has reported vertical ground motions ranging from uplift of approximately 7.5 mm/year to subsidence of almost 8.5 mm/year over the northern region of the Nile Delta in the period 1993-2000. Within the central Delta area, vertical land movements of ± 5 mm/year have been reported for the period 1993-2000 (e.g. Aly 2006). Additionally, the vertical movements in the Greater Cairo metropolitan area were estimated in the range from -7 mm/year to +3.8 mm/year in the period 2003-2009 (Poscolieri et al., 2011). Similar situations of integrated complex land subsidence/uplift have been reported in other geographic locations(e.g. Sneed et al., 2002).

It worth mentioning that no recent precise geodetic measurements have been conducted within the entire Nile delta to capture present-day subsidence (Aly 2006). This paper demonstrate a precise GPS-based strategy for monitoring land subsidence in the Nile delta region, and presents the accomplished preliminary results.

The Nile Delta

The study area, as shown in Figure 1, extends from longitude 29.6^{o} E to longitude 32.3^{o} E, and from latitude 29.8^{o} N to latitude 31.6^{o} N. The study area extends more than 300 kilometer along the Mediterranean costs from Port Said on the east to Alexandria on the west, and extends almost 200 kilometers perpendicular south to the coastline to Cairo. Thus, its total area equals approximately 25,000 square kilometers. With more than fifty million people, the Nile delta might be considered as one of the most densely populated areas worldwide. The topography of the study area (Figure 2)

ranges from elevation -72 meter to 197 meter, with an average of 5.9 meter. As can be seen from that figure that the dominant elevation is less than 10 meter in the northern and middle parts of the delta. Moreover, it can be realized that the northern region of the delta area has an elevation less than almost 5 meter. That fact necessitates performing vulnerability analysis studies regarding the sea rise global phenomena and its hazardous impacts on the Nile delta region (Dawod and Mohamed, 2008). However, researchers emphasis the fact that land subsidence in the Nile Delta might be more environmentally hazardous than the sea level rise phenomena (e.g. Zaid et al., 2014).

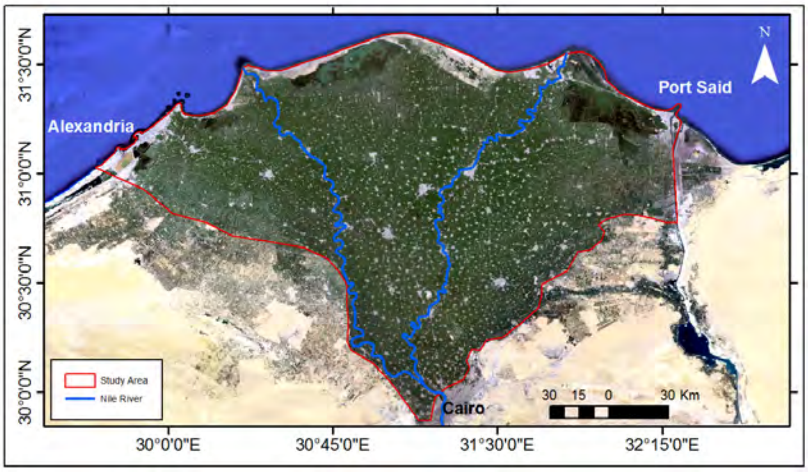

Figure 1: The Study Area

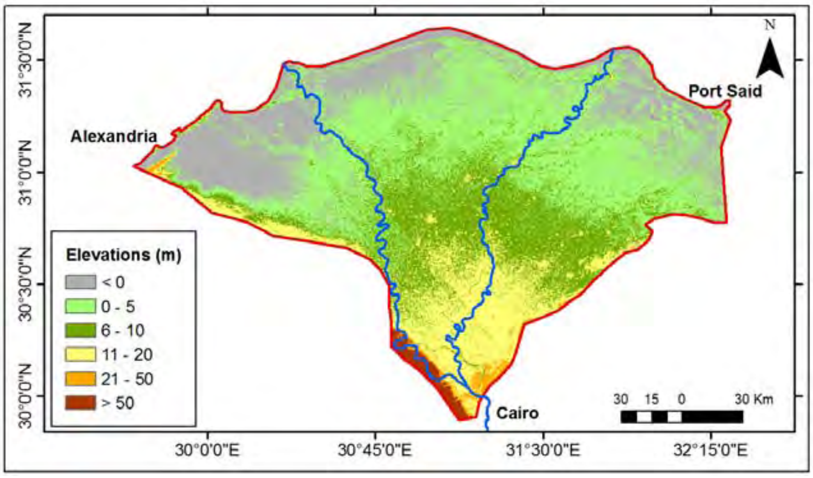

Figure 2: Topography of the Study Area

Available Data

The utilized dataset compresses GPS raw data of 6 stations of the Virtual Reference Stations (VRS) belong to the Egyptian Survey Authority (ESA). ESA has established these 40 Continuously Operating Reference Systems (CORS) in 2010. Each station is equipped with a dual-frequency GPS receiver fixed on the top of an ESA building, and every station sends its raw data in real time to the central ESA office in Cairo. The utilized stations are: Cairo, Tanta, Baltim, Port Said, Abu

El-Matameer, and Abu Kebeer (Fig. 3). The stations and the dataset have been chosen according to the availability and continuity of GPS data. Therefore, three sessions have been selected for each station in the period 2012-2015, where each session contains a 48-hour continuous GPS dataset in the RINEX (Receiver-INdependent EXchange) format (Table 1).

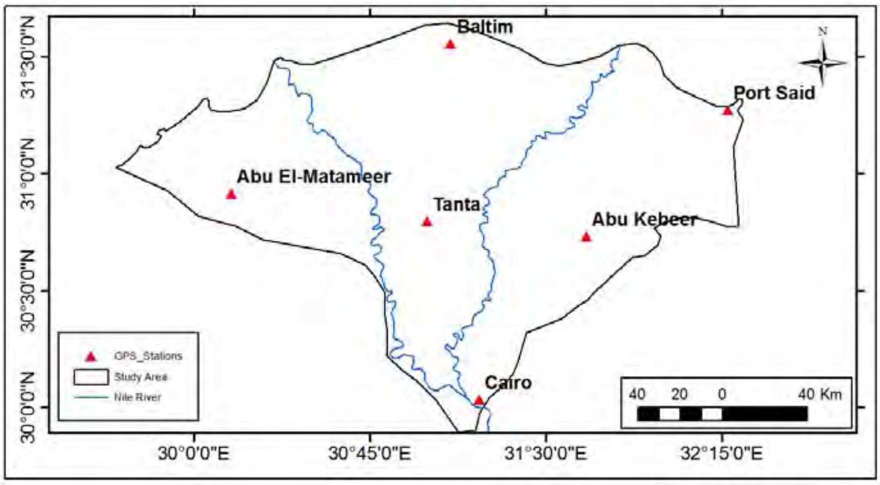

Figure 3: The Utilized GPS VRS Stations

Table 1: The Available GPS Data

Station	1-2012	1-2013	7-2013	1-2014	7-2014	1-2015
Cairo	X				X	X
Port Said	X				X	X
Abu Kebeer	X		X		X	X
Tanta	X	X	X			
Baltim	X		X	X		
Abu El-Matameer	X	X		X		

Processing and Results

The Precise Point Positioning (PPP) technique was applied in this research in order to achieve the most-precise coordinates, particularly heights, for each GPS station. The basic idea behind PPP is the estimation of precise satellites orbits and satellite clock errors based on observations from a high quality global fiducial network, and then the utilization of such information to solve the station parameters of any site world-wide (Seeber, 2003). The PPP position determination is based on the processing of the following ionosphere-free combination of the un-differenced code and phase observations (Xu, 2007):

$$\lambda\Phi = \rho - (\delta t_r - \delta t_k)c + \lambda N + \delta_{trop} + \delta_{tide} + \delta_{rel} + \varepsilon_{pc} \quad (1)$$

$$R = \rho - (\delta t_r - \delta t_k)c + \delta_{trop} + \delta_{tide} + \delta_{rel} + \varepsilon_{cc} \quad (2)$$

where

$$N = f_1 N_1 - f_2 N_2 \quad (3)$$

$$\lambda = \frac{c}{(f_1^2 - f_2^2)} \tag{4}$$

where,

R	is the pseudorange,
ρ	is the geometric range,
c	is the speed of light,
f_1 and f_2	are the GPS L1 and L2 frequencies,
N_1 and N_2	are the phase ambiguity terms on L1 and L2 frequencies,
Φ	is the carrier phase,
λ	is the wavelength of the combination,
δt_r, δt_k,	are the clock errors of the receiver and satellite respectively,
δ_{trop}, δ_{tide}, δ_{rel}	are the troposheric, tidal, and relativistic effect respectively,
ε_{cc} and ε_{pc}	denote the residuals after the combination of code and phase respectively.

The above equations show that the unknown parameters to be estimated in PPP include position coordinates, phase ambiguity terms, receiver clock offset, and the troposheric effect. Precise satellite orbits and clock products with the centimeter-level accuracy needed for PPP are now widely available from a number of public organizations. One of these well-known organizations is the International GNSS Service (IGS). Consequently, the processing workflow consists of several steps (Figure 4). First, in each session, the raw GPS data of an IGS station have been downloaded as a control point. Second, Precise satellite orbits, for both GPS and GLONASS satellites, have been obtained too. Next, using PPP strategy, precise geodetic heights have been estimated for each station in each session in the International Terrestrial Reference Frame (ITRF2008) epoch 2012. Lastly, comparing station's heights enables the determination of vertical movement rate between two successive sessions at each station (e.g. Sneed et al., 2002).

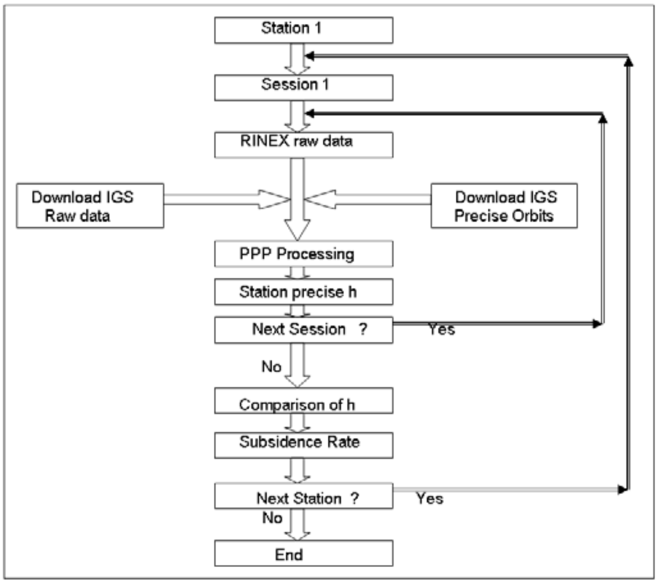

Figure 4: The Data Processing Workflow

Using the Trimble TBC 3.2 GPS data processing package, ellipsoidal heights have been computed for each station at each session with a precision of ± 0.002 m. The rates of vertical land movements

have been, then, estimated through linear regression. The attained results are represented in Table 2 and depicted in Figure 5. It can be realized that subsidence exist in Port Said and Tanta, while the remaining four stations show uplift. Additionally, it is observed that the vertical deformation at both Baltim and Abu El-Matameer are relatively small compared to the rate of the other stations. Moreover, it can be seen that the GPS station at Tanta shows the maximum subsidence annual rate with almost 7 mm/year. The last column of Table 2 shows the value of coefficient of determination (R^2), which constitutes a statistical measure about the amount of variations in the original data that the regression formula could explain. The higher the value of that coefficient, the more-precise the regression equation developed. It can be realized that R^2 value of four stations (namely Cairo, Tanta, Baltim, and Port Said) are close to one, which means that the linear regression model precisely describe the land vertical movements at these locations. On the other hand, stations Abu El-Matameer, and Abu Kebeer produce moderate R^2 values, which indicates that their vertical movements might not follow a precise linear pattern with respect to time. These concluded remarks could be also visualized clearly in Figure 5.

Furthermore, a spatial model of vertical movements in the Nile Delta (Figure 6) area has been developed using the Krigging statistical method within the Arc GIS software. From this figure, it can be concluded that the average vertical movement, over the study area, equals -0.74 mm/year. Additionally, it can be realized that the middle region of the Delta suffer from land subsidence, particularly at its eastern borders, while the north-western and the south-eastern areas show an uplift. These findings agree, on a general basis, with those reported by earlier studies (e.g. Fugate 2014 and Aly 2006). However, detailed research studies should be carried out in order to investigate the relationship between the attained preliminary results and the soil compaction and groundwater extraction characteristics in the Nile Delta region. Recent research studies have utilized an integration of GPS, InSAR, spirit levelling, and groundwater-level data to monitor land subsidence (e.g. USGS 2013). Additionally, the correlation between geological characteristics and land vertical movements in the study area should be explored in details. For example, Becker and Sultan (2009) suggested that higher land subsidence in the north-east borders of the Delta might have a casual relationship with the distribution of young (<3500 year old) sediments that were deposited during recent development of the Damietta branch of the Nile and have been compacted since then.

Table 2: Vertical Land Movements Rates 2012-2015

Station	Vertical Movement Rate (mm/year)	R^2
Cairo	+ 4.94	0.92
Port Said	- 4.72	0.94
Abu Kebeer	+ 3.69	0.73
Tanta	- 6.51	0.99
Baltim	+ 0.71	0.99
Abu El-Matameer	+ 0.55	0.41

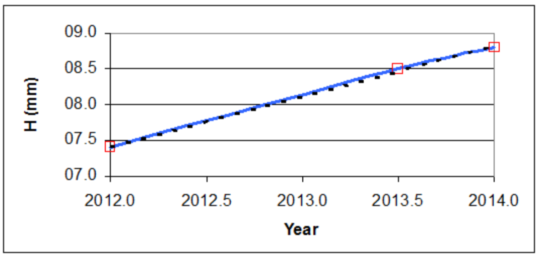

Baltim

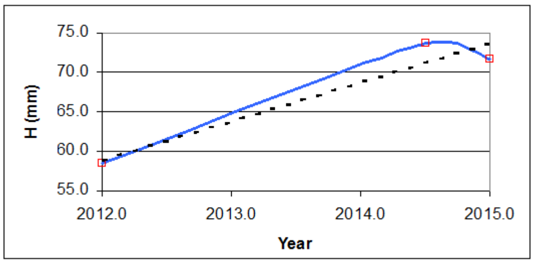

Cairo

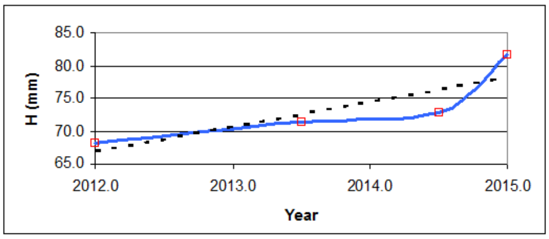

Abu Kebeer

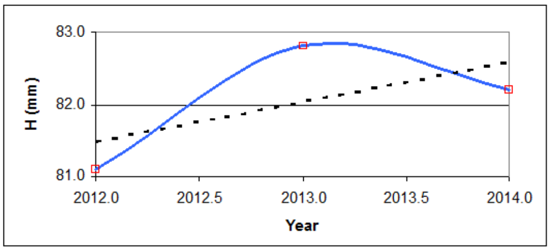

Abu El-Matameer

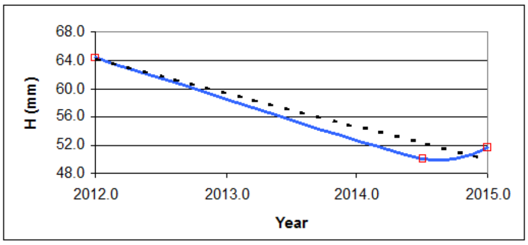

Port Said

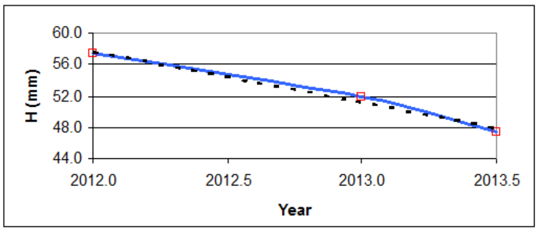

Tanta

Figure 5: Linear Trends of Vertical Movements

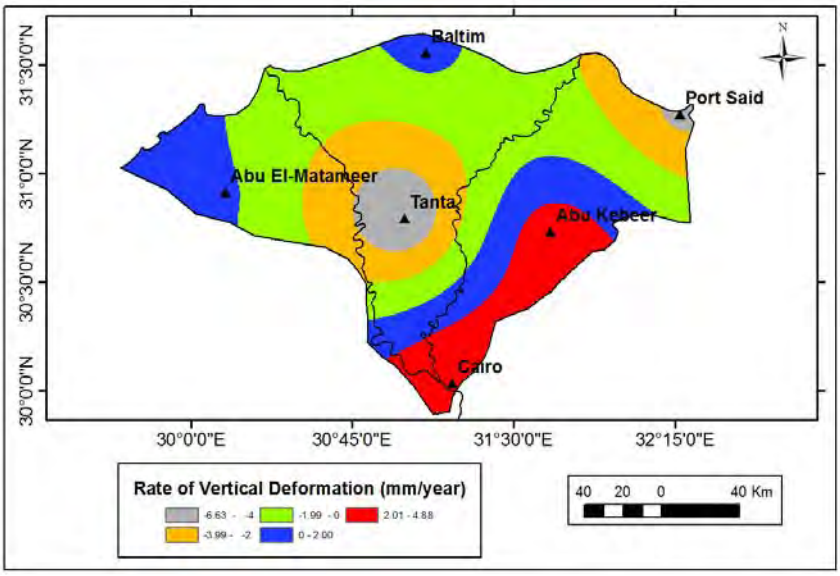

Figure 6: Vertical Ground Movements Annual Rates

Next, the horizontal land movements in the study area have been investigated as well. For each GPS station, the projected 2D coordinates (UTM east and north) have been computed at each session with a precision of ± 0.001 m. The changes in horizontal coordinates have been estimated, and the rate of horizontal movements have been obtained (in terms of amount and direction), as presented in Table 3. As well, a spatial model of horizontal movements in the Nile Delta area has been developed (Figure 7). From the accomplished findings, it can be realized that the horizontal ground movement at Tanta station is relatively small compared to the other stations. The horizontal deformation rates are in the range of 4-7 mm/year with a mean equals 5.6 mm/year, which still can be classified as small horizontal movements. Similar results have been reported by Rayan (2003). Again, further detailed research studies should be performed to explore the relationship between these attained preliminary results and the geological characteristics of the Nile Delta region.

Table 3: Horizontal Land Movements Rates 2012-2015

Station	Horizontal Movement Rate (mm/year)
Cairo	5.37 NE
Port Said	5.83 NE
Abu Kebeer	6.62 NE
Tanta	4.22 NE
Baltim	5.85 NE
Abu El-Matameer	6.04 NE

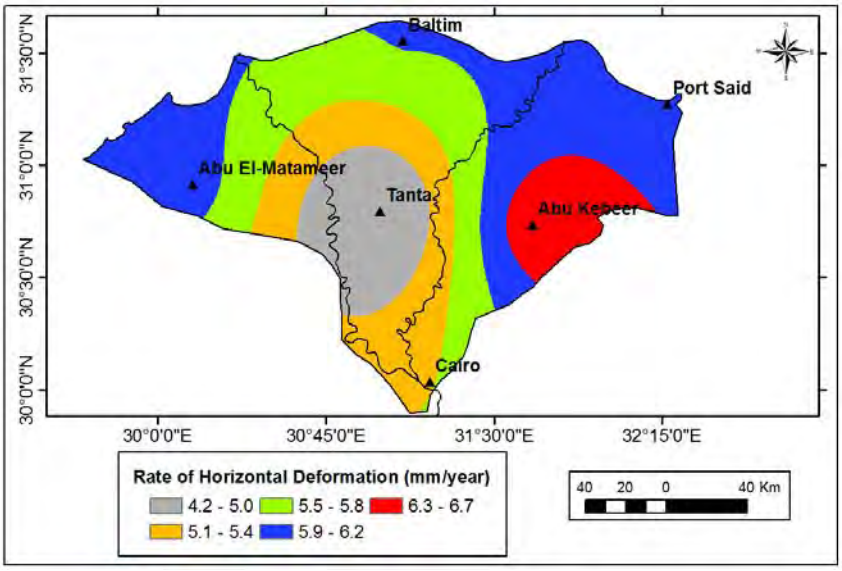

Figure 7: Horizontal Ground Movements Annual Rates

Conclusions

Ground deformation in general and land subsidence in particular significantly influence urban areas on environmental, development, and human basis. This research study has applied recent high-precision GPS datasets for monitoring and detecting both vertical and horizontal ground movements in the Nile Delta region. Repeated GPS observations for six stations over the Delta covering the period 2012-2015 have been compiled, processed, and analyzed. Ellipsoidal heights have been computed for each station at each session with a precision of ± 0.002 m. The attained results show that subsidence exist in Port Said and Tanta, while the remaining four stations show uplift. Additionally, it is observed that the vertical deformation at both Baltim and Abu El-Matameer are relatively small compared to the rate of the other stations. Furthermore, it can be seen that the GPS station at Tanta shows the maximum subsidence annual rate with almost 7 mm/year. On the other hand, the estimated horizontal land movements are in the range of 4-7 mm/year, which still can be classified as small horizontal movements. It should be highlighted that six GPS stations over the entire Nile Delta area might not be the optimum number of stations to precisely monitor ground deformation over that large area. More GPS monitoring stations are recommended to fulfill a homogenous spatial distribution. The proposed stations should agree completely with the international geodetic standards for such a high-precision activity. In addition, further investigations should be carried out in the future utilizing longer time-span datasets in order to accurately map the time-dependant vertical movements in the study area.

Based on the attained primarily findings, few recommendation could be made. Firstly, although geodetic techniques, such as GPS, can monitor and detect ground deformation by a high-accuracy level, they observe such deformation at specific point locations. Performing GPS monitoring at large number of points over a large area might be time-consuming and expansive. Hence, for the Nile Delta region, it is recommended to integrate GPS with SAR satellite imagery method in order to spatially portray the ground deformation pattern with adequate precision. Furthermore, it is a matter of fact that ground deformations are often caused by human activities such as water and oil pumping, and are influenced by natural characteristics particularly the geological, hydrological, and soil conditions. Hence, it is recommended that further detailed multi-disciplinary studies

should be carried out to detect the soil compaction features of the Nile Delta, along with the recent variations of groundwater levels. Finally, the accomplished results should be taken into consideration by decision makers in any future development plans of the Nile Delta.

References

Abidin, H., Andreas, H., Gumilar, I. , Sidiq, T., and Gamal, M. (2015) Environmental impacts of land subsidence in urban areas of Indonesia, Presented at the FIG Working Week 2015, Sofia, Bulgaria, 17-21 May.

Aly, M. (2006) Radar interferometry for monitoring land subsidence and coastal change in the Nile delta, Egypt, PhD Dissertation, Texas A&M University, USA.

Aly, M., Zebker, H., Giardino, J., and Klein, A. (2009) Permanent scatterer investigation of land subsidence in grater Cairo, Egypt, Geophysical Journal International, No. 178, pp. 1238-1245.

Atanasova, M. (2015) Study of deformation and movements on the Earth's crust of techogenic character based on repeated geodetic measurements, Presented at the FIG Working Week 2015, Sofia, Bulgaria, 17-21 May.

Becker, R. and Sultan, M. (2009) Land subsidence in the Nile Delta: Inferences from radar interferometry, The Holocene, V.19, No. 6 , pp. 949–954.

Dawod, G. and Mohamed, H. (2008) Estimation of sea level rise hazardous impacts in Egypt within a GIS environment, Presented at the Third National GIS Symposium in Saudi Arabia, Al-Khober, Saudi Arabia, April 7-9.

DEPI (Department of Environment and Primary Industries) (2014) Trial of satellite radar Interferometry (InSAR) to monitor subsidence along the Gippsland coast, State of Vectoria's technical report, Melbourne, Australia.

El-Fiky, G. (2005) GPS-derived velocity and crustal strain field in the Suez-Sinai area, Egypt, Bulletin of Earthquake Research Institute, University of Tokyo, V. 80, pp. 73-86.

Fugate, J. (2014) Measurements of land subsidence rates on the north-western portion of the Nile Delta using radar interferometry techniques, MSC thesis, University of Toledo, Ohio, USA.

Kalkan, Y. (2014) Geodetic deformation monitoring of Ataturk dam in Turkey, Arabian Journal of GeoSciences, No. 7, pp. 397-405.

Poscolieri, M., Parchardis, I., Foumelis, M., and Rafanelli, C. (2011) Ground deformation monitoring in the greater Cairo metropolitan region (Egypt) by SAR interferometry, Journal of Environmental Semeiotics, V. 4, No. 3, pp. 17-45.

Mohamed, H. (2005) Realization and redefinition of the Egyptian vertical datum based on recent heterogeneous observations, PhD Dissertation, Shoubra faculty of engineering, Benha university, Egypt.

USGS (United States Geological Survey) (2013) , Land subsidence along the Delta-Mendota canal in the northern part of the San Joaquin valley, California, 2003-2010, Scientific investigations report no. 2013-5142.

Rayan, A. (2003) Regional dynamic studies of greater Cairo area using geodetic techniques, PhD Dissertation, Surveying Engineering department, Shoubra Faculty of Engineering, Zagazig university, Egypt.

Rayan, A., Fernandes, R., Khalil, H., Mahmoud, S., Mirandam J., and Tealab, A. (2010) Evaluation of the crustal deformations in the northern region of Lake Nasser (Egypt) derived from 8 years of GPS campaign observations, Journal of Geodynamics, No. 49, pp. 210-215.

Seeber, G. (2003) Satellite geodesy, 2nd ed., Walter de Gruyter, New York, USA.

Serpelloni, E., Vannucci, G., Ponderlli, S., Argnani, A., Casula, G., Anzideo, M., Baldi, P., and Gasperini, P. (2007) Kinematics of the western African-Eurasia plate boundary from local mechanisms and GPS data, Geophysical Journal International, No. 169, pp. 1180-1200.

Sneed, M., Stork, S., and Lkehrara, M. (2002) Detection and measurement of land subsidence using global positioning system and interferometric synthetic aperture radar Coachella valley, Californium 1998-2000, US Geological Survey Water Resources Investigations Report 02-4239, California, USA.

Xu, G. (2007) GPS theory, algorithms, and applications, Springer, Berlin, Germany.

Zaid, S., Mamoun, M., and Al-Mobark, N. (2014) Vulnerability assessment of the impact of sea level rise and land subsidence on north Nile Delta region, World Applied Sciences Journal, V. 32, No. 3, pp 325-342

Building a Historical GIS for the City of Makkah, Saudi Arabia

Meraj N. Mirza[1, 2,3], Gomaa M. Dawod[4], Ramaze A. Elzahrany[1,2], and Mohammad M. Mirza[5]

[1] Umm Al-Qura University, Makkah, Saudi Arabia, meraj@mmirza.com
[2] KACST GIS Technology Innovation Center, Makkah, Saudi Arabia
[3] Center for Geographic Analysis, Harvard University, USA
[4] Survey Research Institute, Giza, Egypt
[5] Colorado State University, Denver, Colorado, USA

Abstract

A Historical Geographic Information System (HGIS) is a way to create a time-variable spatial representation of geographic features, which is considered as a bridging technology between geography and history in a digital framework. The history of Makkah (Mecca), Saudi Arabia covers several thousand years, with numerous sites representing important historical landmarks. As Makkah is the most important city in Islamic history, developing a HGIS for it would have significant meaning for the more than a billion Muslims around the world. A state-of-the-art HGIS has been developed for Makkah through acquiring, integrating, manipulating, and analyzing an extensive collection of spatial and non-spatial datasets. This research has resulted in the publishing of a bi-lingual atlas of historical sites in Makkah that contains more than seventy historical locations and covers almost a thousand years (500s to 1500s). Work is underway to also build an online HGIS on the Harvard WorldMap platform, so that materials in the atlas and beyond will be made available for researchers and the general public from any part of the world through a web-based dynamic mapping site. Future work may propel the system into an augmented reality innovation. This paper introduces the background and historical-geographic materials, summarizes the technical challenges and solutions, and presents milestones and perspectives for this on-going effort.

Keywords: Geographic Information System (GIS), Historical GIS, Atlas, Makkah, Saudi Arabia, WorldMap

Introduction

The concept of documenting and mapping historical data is an old practice in geography and in field of mapping. Maps showing historical information are used in a simple manner for visualizing and even analyzing geographical data which refers to the past. There are many examples of printed atlases which have been developed representing the geographic patterns of specific events over space and time. Concerning Islam, several atlases have been published covering the geographic and historical expansion of the Islamic empire (e.g. Ruthven and Nanji

2004, Mones1987, and Abu Khalil 2005b). However, such maps have certain limitations compared with modern day geographic information systems. For instance, due to the large extent of the subject in both geographic coverage (almost half of the world) and historical time span (about fourteen centuries), such atlases can only give a general picture of the subject. In addition presenting historical data on regular printed maps in a non-digital format, is restricted by map size, scale, and quality. In such an environment, combining and/or comparing different maps is not a simple task mainly due to the great variation in mathematical projection and spatial reference of the maps involved (Mirza 2013).

Geographic Information System (GIS) represent a computer-based technology for collecting, storing, archiving, querying, analyzing, visualizing, and presenting large amounts of spatial and non-spatial data.. GIS has been used in a wide range of applications world-wide, with the Kingdom of Saudi Arabia (KSA) being no exception. Some examples of GIS applications in KSA include urban growth monitoring (Al-Ghamdi et al. 2012), flood management (Dawod et al. 2011), soil management (El Bastawesy et al. 2012), and the spatial monitoring of disease (Khormi et al. 2012).

Historical Geographic Information System (HGIS) is a discipline within GIS which deals with historical events, data, and geographic locations (Bol, 2013). HGIS provides a new approach for studying history that allows for spatial historical analysis and the linking of historical data to specific geographical locations (Schlichting, 2008). HGIS can be considered a potentially revolutionary approach linking both geography and history together to study patterns of changes over space and time (Bailey and Schick, 2009). A major application of HGIS is urban history analysis in an integrated digital framework that comprises heterogeneous data sources (Raymond 2011). HGIS has many merits such as the spatial-referencing of all data which allows for rapid map production , and the ability to perform geographic analysis of past events (DeBats and Gregory, 2011).

HGIS is utilized in a wide range of applications. For example, at the city or local level, Ayhan and Cubukcu (2010) applied a 4D spatial analysis to explore urban changes of the city of Izmer, Turkey based on the historical distribution of mosques. HGIS was also utilized in the construction of a historical heterogeneous database for Macedonia, Northern Greece for the purpose of locating hundreds of unknown buried ancient constructions (Kaimarisa et al., 2011). Another HGIS has investigated historical spatial occurrences of soil liquefaction as a measure for earthquake hazards in Greece since 1509, which could be valuable for urban planners (Papathanassiou and Pavlides, 2011). Additionally, HGIS can be used as a platform for public participation in historical site usage and preservation, and offers new understandings of the landscape of such historical locations (Algeo et al., 2011). A unique HGIS has been utilized to analyze visitation patterns for commercial hotels in three small places in central Pennsylvania, USA during the late 19th century (Fyfe et al., 2009). Moreover, HGIS has been used for modeling drought and population change in Canada (McLeman et al., 2010).

Several national HGIS projects have been carried out in the last years or decade. Some of them are available online. Examples of such activities include the US national historical GIS (https://www.nhgis.org/), the Canadian national historical sites (http://www.pc.gc.ca/eng/index.aspx), the US national register of historical places (http://www.nps.gov/nr/), the Great Britain HGIS (http://www.port.ac.uk/research/gbhgis/), and the China historical GIS developed by Harvard University (http://www.fas.harvard.edu/~chgis/). Other HGIS projects have been established at smaller scales, state or county for instance, such as the one for the Goodhue county of Minnesota, USA (http://maps.co.goodhue.mn.us/historicplaces/), and the Ohio state online historical mapping system (http://www.ohiohistory.org/ohio-historic-preservation-office/online-mapping-system).

This research aims to use GIS to integrate several data types (maps, aerial photographs, satellite imageries, and non-spatial data) within a framework representing the geographic locations of historical events in Makkah city. The first product of the study will be an atlas of historical locations within Makkah. Work is underway to also build an online HGIS on the WorldMap platform, so that materials in the atlas and beyond will be made available for researchers and the general public from any part of the world through a web-based dynamic mapping site. Future work may propel the system into an augmented reality implementation (Elzahrany and Mirza, 2011).

Study Area

The city of Makkah (Mecca) is located in the southwest of KSA, about 80 km east of the Red Sea (Fig. 1). It extends from longitudes 39o 35’ E to 40o 02’ E, and from latitudes 21o 09’ N to 21o 37’ N. Makkah is a unique city for Muslims around the world, since it contains the holy mosque. From a religious point of view, a Muslim should perform a pilgrimage (called Hajj, which means visiting Makkah during the 8th - 12th days of the 12th month in the Lunar year) once in his/her life. Thus, hundreds of thousands Muslims gather in Makkah yearly. Also, Muslims perform a religious journey, called Omrah, to Makkah year-round. From an Islamic perspective, Makkah is the first place created on the Earth’s surface and the holy mosque in Makkah is the first "God House" for worship on Earth. Thus, the history of Makkah has been unfolding even before the start of the Islam itself. However, the main historical event in Makkah was the commencement of the Islamic religion in year 610 AD. It is known that Prophet Muhammad stayed 13 years in Makkah trying to convert people to Islam before he was obligated to leave for Al-Madinah (about 400 kilometers north of Makkah). Even though the Prophet Muhammad established Makkah eight years later, Al-Madinah stood as the capital of the new Islamic state. However, Makkah has remained the religious capital of the Islamic world and the most-important city for Muslims throughout the last fourteen centuries.

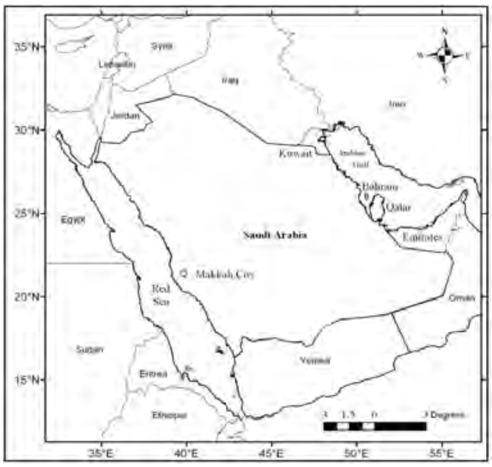

Figure 1: The study area in relation to the Arabic Peninsula

It is amazing to know that there was an attempt to make historical maps two centuries ago. That was when the Turkish officer Ayoub Sabry, in his book "A Mirror of Makkah" in 1872, drew an imaginary sketch showing Makkah’s landscape in the pre-Islam period (i.e., before the 5th Georgian century), as seen in Fig. 2d. He constructed this 3D image based on the historical description of Makkah as set by Kosaii Ibn Kalab (the 5th grandfather of Prophet Muhammad) when he ordered residents to leave some open spaces around the holy Kaaba and regulated buildings to be in circles around it with some radial streets to ease the access to it (ibid).

Recently, several atlases have been published concerning the Islamic history including the city of Makkah. For example, Abu Khalil published an atlas regarding the geographic places mentioned in the teachings of Prophet Muhammad (2005a). He also produced another atlas about geographic sites mentioned in the holy Qur'an (2003). The nature of these two atlases is general, with no details about the geography of Makkah itself. Mirza and Shawoosh (2011) published an illustrated atlas for Makkah and its holy shrines.

GIS was utilized in Makkah as a platform for four dimensional analyses over time, which can be seen as a specific application of HGIS. For example, Shehata (2007) carried out a 4D GIS to investigate the urban and landscape changes in the central region of Makkah in the last three decades. Similarly, Al-Ghamdi et al. (2012) constructed a GIS to estimate the urban growth of Makkah, and the corresponding flood hazards, over the period of 1947-2010.

Additionally, a large amount of historical geographic information about Makkah can be found in literature. Such historical data describing geographic sites could be extremely valuable for developing an HGIS about the holy city. For example, Al-Azraqi wrote one of the most famous geographic books about Makkah in 864 (Al-Azraqi, 2003). The two-volume book dealt with both the history and geography of the holy city, with a detailed verbal description of the famous geographic sites. Similarly, Al-Mekki developed a six-volume book about the history, geography,

and people of Makkah (Al-Mekki, 2000). In addition, Snouck Hugronje published a two-volume book about Makkah in 1888 (that was translated into Arabic in 2012). Furthermore, many historical landmarks within Makkah have been also mentioned in the geographic encyclopedia by Yakoot Al-Hamoy in the early 1200s (Al-Hamoy 1977). The challenge is to convert these rich texts into digital structured spatiotemporal information.

(a) A Simplified Sketch of Al-Estakhri World Map

(b) The Turkish Empire Map

(b) Makkah detailed map By Burkhart

(d) Makkah before Islam as drawn by Ayoub Sabry

Figure 2: Examples of Ancient Maps Showing Makkah

Building the Historical Geodatabase

Developing a GIS-based atlas for historical sites within Makkah is the first step in building a HGIS for the city. The effort presents several technical challenges. The key issues are the availability of spatial and attribute data and the linkage between past and present. Much effort has been put into source data collection, including maps of different scales (some dated a few centuries ago), aerial photos (for many decades), and satellite imageries. Attribute data presenting textual descriptions about specific geographic locations in the past are also gathered. Such attribute tables could be helpful in positioning some historical sites in modern geographic coordinate systems. Additionally, historical attribute data, particularly historical textbooks,

provide "recent or known" names of some old geographic locations (gazetteers). For instance, Al-Hudaibia village in which the famous peace treaty was signed in year 628 is currently known as Al-Shemesy. Figure 3 depicts the input data types to the spatiotemporal database. In the current research study, the geographic experience (of the first author) played a vital role in matching past and present names of historical sites, and required much field geographic experience and historical knowledge. It is known that Makkah has been expanding rapidly in the last two or three decades. Prior to that period many historical sites still existed though they were known by different names. Thus, defining the geographic locations of historical landmarks depends heavily on geographic experience acquired from field study before the rapid expansion of the city.

Another technical challenge in building the HGIS is the georeferencing of some historical spatial data. Some valuable old maps may be available but we do not know their spatial reference or datum, thus they can only be georeferenced through spatial adjustment or rubber sheeting. Scanned historical maps were systematically georeferenced, and spatial features digitized from them in order to create vector GIS layers of the historical geodatabase. These were then used to produce the atlas (Fig, 4).

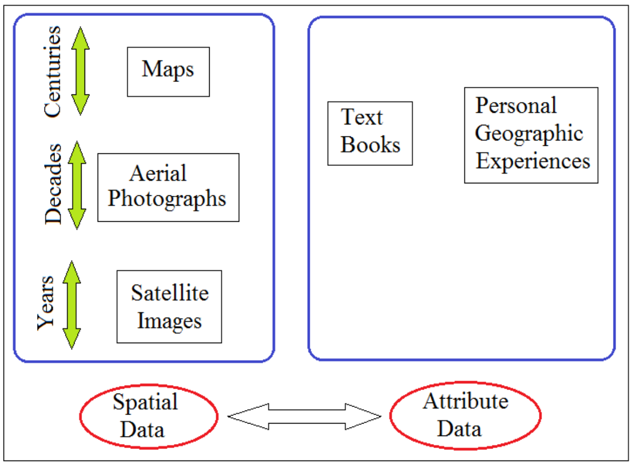

Figure 3: Utilized Input Data Types

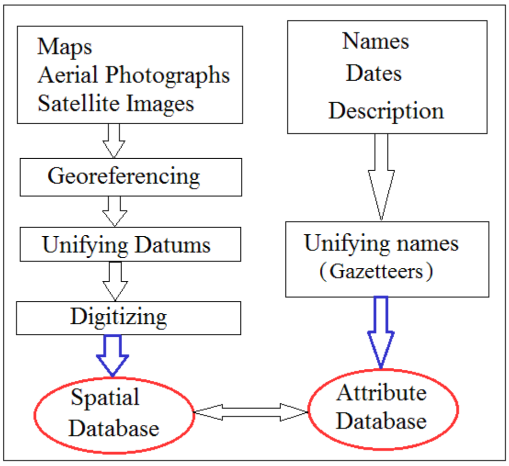

Figure 4: Historical Geodatabase Construction Process

Designing the Historical Atlas

The design of the historical geodatabase supported the development of the atlas as the first product of this project. The atlas consists of two pages for each historical landmark. The first page comprises the attribute data of a location in both Arabic and English, including: Name, Type, Geographic location, Direction from holy Kaaba, Distance from holy Kaaba, Description, and Historical remarks. Since the Kaaba is the center of the holy mosque (the most important Islamic site in the world), the distances and directions of a specific site are measured from the

Kaaba to show the location of the landmark with respect to this central object.. On the opposite page of a historical landmark, its geographic location is presented on both map and satellite images.

The resulting atlas of historical sites in Makkah city contains more than seventy locations. The locations are grouped into nine types:

- Holy Kaaba
- History of the holy mosque
- Holy shrines
- Historical mosques
- Historical locations
- Historical mountains
- Historical events
- Ancient sites
- Pilgrimage and Omrah mikats

The first chapter of the atlas presents the main features existing within the holy mosque, particularly the holy Kaaba, Ismail Hijr, and the Zamzam well. The second chapter depicts the historical expansions of the holy mosque over almost fourteen centuries (Fig. 5). The area of the holy mosque has been enlarged from 2061 square meters in the pre-Islamic period (the 5th Georgian century) to 9844 square meters by year 710, and would be 1,225,000 square meters after the completion of the undergoing expansion project. Such information could not be represented well without HGIS. The third chapter includes five sites belonging to the holy shrines in Makkah, while the forth chapter contains fifteen historical mosques. Another fifteen sites, mostly related to the Prophet Muhammad, are depicted in the fifth chapter of the atlas. The famous mountains, where famous historical events occurred, are presented in the sixth chapter. The seventh chapter includes geographic locations of some famous historical events, i.e. battles and peace treaties. The ancient sites, in the eighth chapter, contain some historical locations that are not exactly related to the life time of Prophet Muhammad. An example of these ancient sites is the dam constructed between 692 and 694 by Al-Hagag Al-Thakafy, the ruler of Makkah by that time, to protect the city from flood water. The last chapter presents the geographic locations of the so-called "mikats". From an Islamic point of view, a mikat is a geographic location from which pilgrims declare "the intention" to start pilgrimage or Omrah before entering Makkah city. There are 5 mikat locations surround Makkah from all directions. Examples of the published atlas pages are presented in Figures 6 to 8 in the appendix.

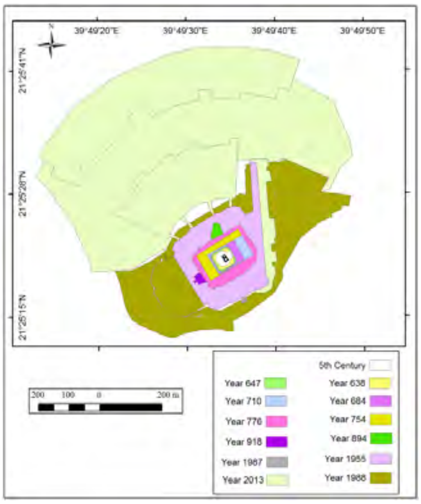

Figure 5: The historical expansions of the holy mosque

Creating the Online Historical GIS for Makkah on WorldMap

The demand in history and the humanities for searchable online maps, online mapping utilities, historical GIS, and user participation in mapping data has been evident for at least a decade. WorldMap (http://worldmap.harvard.edu) is an attempt to meet this demand. It is an open-source, web-based, map-centric data exploration and visualization platform (Guan et al, 2012). WorldMap is designed to be publicly accessible, simple to use for nontechnical scholars, fast in search and mapping, and rich in geographic content. It is being built by and hosted by the Center for Geographic Analysis at Harvard University and is open to users around the world for both viewing and editing data (Lewis and Guan 2011). The platform is particularly useful for technology-challenged humanities scholars for it lowers the cost of entry to the spatial humanities. WorldMap eliminates the wasteful duplication of efforts for elementary and routine spatial tasks such as finding a base map as locational reference or overlaying multiple layers of spatial data and examining their locational relationships. In providing a working platform for spatial investigation, WorldMap also grants a powerful new and permanent life to the spatial research of any scholar in the world who shares their data using the system. Rather than resting inertly and often forgotten on their computer's hard drive once the research is published, the data shared on WorldMap becomes part of a global online library of new evidence and analyses. Through such a process, humanists are encouraged to follow the example of scientists in sharing their data and the interpretive thinking upon which their work is founded. In putting the tools developed by geographic information science in the service of the humanities, WorldMap makes it possible for historians and humanities scholars to develop multiple and competing spatial visualizations, to collaborate, and work cumulatively.

The historical geodatabase and historical atlas for Makkah lay a foundation for creating an online historical GIS for the city of Makkah on WorldMap

(http://worldmap.harvard.edu/makkahhistorical/). This online dynamic map combines modern-day base maps with historical satellite images and aerial photos, historical topographic maps, historical GIS data layers, historical photos, and modern-day social media streams such as geo-tagged photos from Flickr, giving users the freedom to turn on or off any of these layers, zoom in or out at any scale, "drill down" to any spot to find out more information behind the visible map symbols, or even embed the interactive map in their own website such as personal blogs. As of October 2013, this Makkah Historical Map contains two dozen GIS data layers, many of them are first-hand datasets developed by the first author, such as wells in 1947, urban boundary in 1880 and 1947, building foot prints in 1880 and 1947, etc. . This is a living map that is being edited and improved continuously, while viewable by the world (Fig. 6).

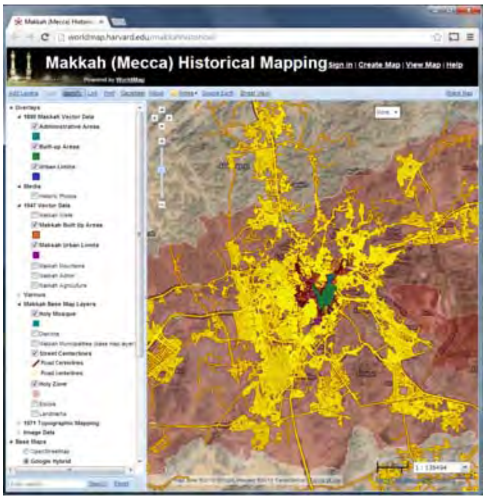

Figure 6: Makkah Historical Mapping on WorldMap

Conclusions

Historical GIS plays a primary role in connecting the history and geography of a particular location by introducing time as the fourth coordinate. Since Makkah is the most important and ancient city in the Islamic history, developing a HGIS for it is critically important for more than a billion Muslims. A comprehensive geodatabase of historical data has been acquired, scanned, digitized, and processed, including historical maps at different scales, aerial photos, and satellite imagery. Attribute datasets have been collected and organized in a HGIS framework, thus forming the first HGIS for Makkah. The first product of this HGIS is a bi-language atlas of historical sites that contains more than seventy historical locations within Makkah. The time span covered by this atlas is almost a thousand year (500s to 1500s). Work is underway to also build an online HGIS on the WorldMap platform, so that materials in the atlas and beyond will be made available for researchers and the general public from any part of the world through a web-based dynamic mapping site. Future work may propel the system into an augmented reality innovation.

References

Abu Khalil, S. (2003) Atlas of Qur'an: Places and people (in Arabic), 2nd edition, Dar Al Fekr, Damascus, Syria, 336 pp.

Abu Khalil, S. (2005a) Atlas of prophetic novels: Places and people (in Arabic), 4th edition, Dar Al Fekr, Damascus, Syria, 440 pp.

Abu Khalil, S. (2005b) Atlas of the Arabic Islamic history (in Arabic), 12th edition, Dar Al Fekr, Damascus, Syria, 336 pp.

Al-Azraqi, M. (2003) News of Makkah and its traces (in Arabic), Edited by Abdel-Malek Bin Dehesh, Al-Asdi publishing house, Makkah, Saudi Arabia, 1195 pp.

Al-Ghamdi, K., Mirza, M., Elzahrany, R., and Dawod, G. (2012) GIS evaluation of urban growth and flood hazards: A case study of Makkah city, Saudi Arabia, FIG Working Week 2012, Rome, Italy, May 6-10.

Al-Hamoy, Y. (1977) Encyclopedia of places (in Arabic), Sader publishing house, Beirut, Lebanon, 5 volumes.

Al-Mekki, T. (2000) The straight history of Makkah (in Arabic) Edited by Abdel-Malek Bin Dehesh, Kheder publishing house, Beirut, Lebanon,6 volumes.

Algeo, K., Epperson, A., and Brunt, M., (2011) Historical GIS as a platform for public memory at Mammoth Cave national park, International Journal of Applied Geospatial Research, (2) 4: 19-37.

Ayhan, I., and Cubukcu, K. (2010) Explaining historical urban development using the locations of mosques: A GIS/spatial statistics-based approach, Applied Geography, 30:229–238.

Bailey, T., and Schick, J. (2009) Historical GIS: Enabling the collision of history and geography, Social Science Computer Review, (27)3:291-296.

Bol, Peter K. (2013) On the Cyberinfrastructure for GIS-Enabled Historiography Space-Time Integration in Geography and GIScience, Annals of the Association of American Geographers, (103) 5:1087-1092.

Dawod, G., Mirza, M., and Al-Ghamdi, K. (2011) GIS-based spatial mapping of flash flood hazards in Makkah city, Saudi Arabia, Journal of Geographic Information System, (3) 3: 217-223.

DeBats, D. and Gregory, I. (2011) Introduction to historical GIS and the study of urban history, Social Science History, (35)4: 455-463.

El Bastawesy, M., Ali, R., and Al Harbi, K. (2012) Impact of the geomorphology and soil management on the development of waterlogging in closed drainage basins of Egypt and Saudi Arabia, Environ Earth Science, DOI 10.1007/s12665-012-1826-5.

Elzahrany, R. and Mirza, M. (2011) Using augmented reality to introduce historical sites in Makkah "Mecca", Saudi Arabia: Conceptual framework, The UGI 2011 Geography Regional Conference, Santiago, Chile, Nov. 14-18.

Fyfe, D., Holdsworth, D., and Weaver, C. (2009) Historical GIS and visualization insights from three hotel guest registers in central Pennsylvania, 1888–1897, Social Science Computer Review, (27) 3: 348-362.

Guan, W., P. K. Bol, B. G. Lewis, M. Bertrand, M. L. Berman and J. C. Blossom (2012): WorldMap – a geospatial framework for collaborative research, Annals of GIS, 18:2, 121-134

Horkhronee, S. (2012) Pages from the history of Makkah: Volume 1 (in Arabic), The center of Makkah history, Makkah, Saudi Arabia, 796 pp.

Kaimarisa, D. Sylaioub, S., Georgoulac, O. and Patias, P. (2011) GIS of landmarks management, Cultural Heritage, 12:65–73.

Khormi, H., Elzahrany, R., and Kumar, L. (2012) The benefits and challenges of scaling up dengue surveillance in Saudi Arabia from a GIS perspective, Dengue Bulletin, 36:1-11.

Lewis, B. and W. Guan (2011) Jump-starting the next level of online geospatial collaboration: Lessons from AfricaMap, in Advances in Web-based GIS, Mapping Services and Applications, Li, Dragic´ evic´ & Veenendaal (eds), London: Taylor & Francis Group, 255:276.

McLeman, R., Herold, S., Reljic, Z., Sawada, M., and McKenney, D. (2011) GIS-based modeling of drought and historical population change on the Canadian Prairies, Historical Geography, 36:43–56.

Mirza, M. (2005) Atlas of Makkah maps (in Arabic), First edition, Saudi geological survey, Jeddah, Saudi Arabia, 263 pp.

Mirza, M. and Shawoosh, A. (2011) The illustrated atlas of Makkah and the holy environs, The center of Makkah history, Makkah, Saudi Arabia, 260 pp.

Mirza, M. (2013) Historical city GIS projects and resources, Presented at the historical GIS workshop, Jeddah, Saudi Arabia, January 5.

Mones, H. (1987) Atlas of the history of Islam (in Arabic), 1st edition, Al-Zahraa for Arab Mass Media, Cairo, Egypt, 527 pp.

Papathanassiou, G. and Pavlides, S. (2011) GIS-based database of historical liquefaction occurrences in the broader Aegean region, DALO v1.0, Quaternary International, 242:115-125.

Raymond, A. (2011) Denny Regrade, 1893-2008: A Case study in historical GIS, Social Science History, (35)4:571-597.

Ruthven, M. and Nanji, A. (2004) Historical atlas of Islam, Harvard University Press, 208 pp.

Schlichting, K. (2008) Historical GIS: New ways of doing history, Historical Methods, (41) 4:191-194.

Shehataa, A. (2007) A 4D GIS model to predict the urban changes: Makkah city centre as a case study (in Arabic), Presented in the 3rd International Symposium of Computer-Aided Architectural Design, Alexandria, Egypt, Nov. 28-30.

Appendix 1: Examples of the developed atlas pages

Name:	Zamzam Well	بئر زمزم	الاسم:
Type:	A water well	بئر ماء	النوع:
Geographic Location:	21° 25' 21' North 39° 49' 35" East	٢١" ٢٥' ٥٢١شمالا ٣٥" ٤٩' ٥٣٩ شرقا	الموقع الجغرافي:
Direction from Holy Kaaba:	South East	جنوب شرق	الاتجاه من الكعبة المشرفة:
Distance from Holy Kaaba: (Euclidian Distance)	30 Meters	٣٠ متر	البعد عن الكعبة المشرفة: (المسافة الهوائية)
Description:	It is located inside the Tawaf area within the holy mosque. Currently, it is covered to ease the Tawaf around the holy Kaaba. It is known that the water of Zamzam is the best water ever on the Earth.	تقع بئر زمزم في صحن المطاف بالمسجد الحرام، وفي العصر الحاضر عمل لها مجمع خارج صحن المطاف توسعة على الطائفين ويدخل لها عبر نفق من خارج المطاف، وماؤها خير ماء على وجه الأرض، طعام طعم وشفاء سقم .	الوصف:
Historical Remarks:	This well was first flow to prophet Ismail, the son of prophet Abraham, and his mother. It has been filled up for several decades, until Abdel-Motaleb, the grandfather of prophet Mohamed peace upon him, dig it again.	هي البئر المباركة التي نبعت آية من الله لإسماعيل بن إبراهيم عليهما السلام وأمه هاجر في صحن مطاف الكعبة المشرفة، وقد ردمتها قبيلة جرهم عند خروجهم من مكة، وبقيت هكذا حتى حفرها عبد المطلب جد الرسول صلى الله عليه و سلم.	نبذة تاريخية:

Figure A-1: Zamzam Well

Name:	Mina Holy Shrine	مشعر منى	الاسم:
Type:	An holy shrine	مشعر	النوع:
Geographic Location:	Midpoint: 21° 24' 49" North 39° 53' 13" East	نقطة المنتصف: ٤٩" ٢٤' ٢١° شمالا ١٣" ٥٣' ٣٩° شرقا	الموقع الجغرافي:
Direction from Holy Kaaba:	East	شرق	الاتجاه من الكعبة المشرفة:
Distance from Holy Kaaba: (Euclidian Distance)	4.7 Kilometers to its western border.	٤.٧ كيلومتر إلي الحد الغربي للمشعر	البعد عن الكعبة المشرفة: (المسافة الهوائية)
Description:	Mina is located within the Haram area, with an area about 7.8 square kilometers. It is a small valley between Thobyer and Al-Da'eh mountains. Its name is due to that pilgrims slaughtering animals as a pilgrimage' procedure in this place.	يقع مشعر مني داخل حدود منطقة الحرم المكي، وتبلغ مساحة المشعر ٧.٨ كيلومتر مربع تقريبا. مني شعب بين جبلي ثبير و الضائع. ومن أسباب تسميتها أنها تمني (أي تراق) فيها دماء الأضاحي.	الوصف:
Historical Remarks:	This is the holy place where pilgrims stay the three Tashreeq' days during pilgrimage process. Mina includes the Jamarat and the famous Al-Khaif mosque.	هو المشعر الذي يقضي به الحجاج أيام التشريق الثلاثة، وبه يرمي الحجاج الجمرات. ومن أهم معالم مشعر مني الجمرات و مسجد الخيف.	نبذة تاريخية:

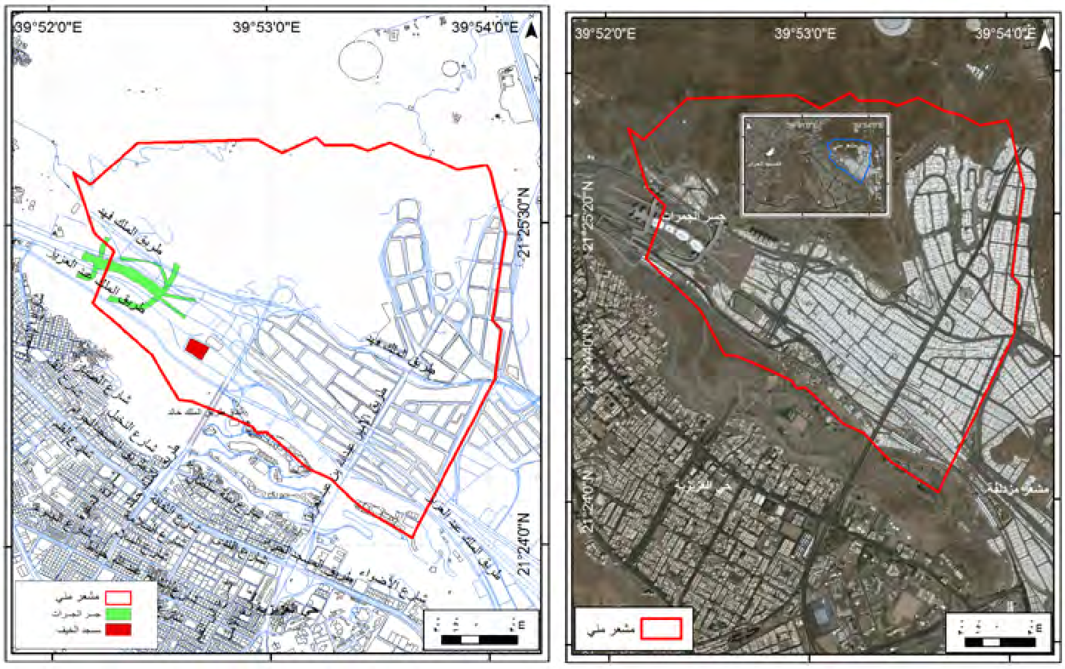

Figure A-2: Mina Holy Shrine

Name:	Heraa	حراء	الاسم:
Type:	A mountain and a cave	جبل و غار	النوع:
Geographic Location:	21° 27' 32' North, 39° 51' 30" East	٣٢" ٢٧' ٢١° شمالا ، ٣٠" ٥١' ٣٩° شرقا	الموقع الجغرافي:
Direction from Holy Kaaba:	North East	شمال شرق	الاتجاه من الكعبة المشرفة:
Distance from Holy Kaaba: (Euclidian Distance)	5.5 Kilometers	٥.٥ كيلومتر	البعد عن الكعبة المشرفة: (المسافة الهوائية)
Description:	Heraa mountain, now called Al-Noor mountain, is the place where prophet Mohamed, peace upon him, used to spend sometimes before being a prophet.	جبل حراء و يسميه أهل مكة جبل النور لكثرة مجاورة النبي صلى الله عليه وسلم و تعبده فيه، وقد سمي الحي كله بحي جبل النور.	الوصف:
Historical Remarks:	Prophet Mohamed, peace upon him, used to spend a mouth every year in this place meditate on God and the live. In this mountain, the Holy Qur'an has been started to be revealed to the prophet.	جبل حراء هو الجبل الذي به غار حراء حيث كان رسول الله صلى الله عليه و سلم يتعبد به مدة شهرا في كل سنة وبه نزل الوحي عليه.	نبذة تاريخية: 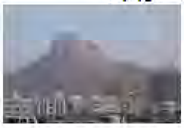

Figure A-3: Heraa Mountain and Cave

The New Cairo Capital Mega Development Project from Geodetic and Environmental Perspectives

Gomaa M. Dawod

Survey Research Institute
National Water Research Center, Egypt
dawod_gomaa@yahoo.com

Abstract

The Egyptian government has recently announced the starting of a mega development project to establish a new administration capital. The proposed site is located about 30 kilometers east of the current capital, and 70 kilometers approximately west of Red sea and Suez canal. The project is likely be finished within five years. As a contribution of the academic and research communities in this pioneer national mission, this paper describes and analyzes the overall spatial location of such a massive development activity from geodetic and environmental points of view. Several geospatial databases have been compiled and evaluated within a Geographic Information System (GIS) environment. It is recommended that the accomplished results, the developed maps and spatial databases being taken into consideration by decision makers in the undergoing development phases of this national mega project.

Keywords: Cairo Capital, GIS, Spatial Databases, Environmental planning, Egypt

1. Introduction

Often, a capital of a country is a very populated city where much history has been made due to high-level political and economic activities that occur there. However, sometimes governments decide to move the capital from one city to another or build a new capital due to tremendous changes in terms of population growth and urbanization. Capital reallocation has been done hundreds of times throughout history. Examples of such countries include: Nigeria in 1992, Myanmar in 2005, Russia in 1918, Pakistan in 1959, Brazil in 1955, Kazakhstan in 1997, Tanzania in 1985, and Ivory Coast in 1983.

City, community, and regional planning deal with spatial information to monitor multiple urban and regional indicators, forecast future needs, and plan accordingly to help improve the quality of life in a community. Objectives of urban planning include, for instance, promotion of sustainable development, achieving integrated planning, developing appropriate planning tools, and integrating plans with budgets. Proper planning is a major key to make cities inclusive, environmentally friendly, economically vibrant, culturally meaningful, and safe for all (Un-HABITAT 2010). Within the activities of city and regional planning, GIS has proven to be an effective technical tool and has been utilized for a wide range of applications worldwide, with Egypt being of no exception. Examples of such GIS applications include: transportation planning (e.g. LA-DCP 2014), flood management (e.g. Dawod et al. 2011), land use planning (e.g. Mohammed and Al-Jenaid 2012), urban growth monitoring (e.g. Al-Ghamdi et al. 2012), optimum site selection for dams (e.g. Salih and Al-Tarif 2012), soil mapping (e.g. Labib and Nashed, 2013), groundwater mapping (e.g. Abdalla 2012), monitoring social conditions in slum areas (e.g. Khadr et al. 2010).

This paper aims to utilize GIS to develop and analyze geospatial databases regarding the new Cairo Capital mega project from geodetic and environmental perspectives.

2. The Cairo Capital Mega Project

Traditionally, Cairo has been the Egyptian capital for almost 1000 years. However, the Greater Cairo metropolitan area, has a population of almost 18 million people, and is expected to grow to 40 million people by 2050. Thus, it is considered one of the most densely regions all over the world. That fact might be an important motive for the Egyptian government to think about constructing a new capital. On March 2015 during the economic development conference, the government has announced the Cairo-Capital large-scale development project. It aims to built a national spirit, foster consensus global city with smart infrastructure for future. The project area, Figure 1, located east of Cairo outside the second greater Cairo ring road, halfway to the sea port of Suez. It is anticipated that the new city would become the new administrative and financial capital, housing the main government departments and ministries, as well as foreign embassies.

The new capital will take advantage of the sustainable technologies of today as well as be adaptable to future technologies, further enhancing its resource-efficiency. The main features of that mega project comprises (Cairo Capital, 2015):

- 700 km^2 gross land area
- 490 km^2 land available for development
- 5,000,000 population
- 250,000 city center's population
- 21 residential districts
- 5.6 km^2 central business district
- 16 km^2 airport area
- 4,200,000 m^2 large retail malls
- 91 km^2 energy farms
- 4 km^2 theme park
- 140 km^2 major and minor streets
- 1,100,00 residential units
- 1250 religious buildings
- 700 kindergartens
- 1,750,000 permanent jobs
- 40,000 hotel rooms

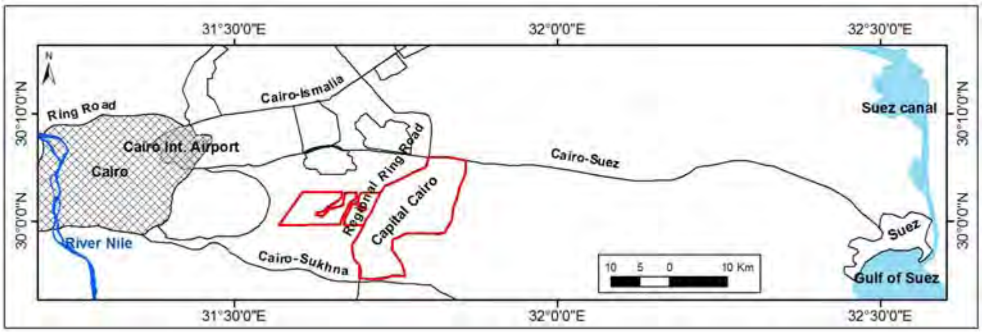

Figure 1: General Location of the Cairo Capital Project

3. Data and Processing Strategy

In the current study, it has been focused only on the area of the first phase of that mega project. That region (Figure 2) has a total area of approximately 245 square kilometers. Several datasets have been acquired and analyzed. Firstly, a Digital Elevation Model (DEM) representing the topography of the study area has been downloaded from the SRTM3 global DEM website (e.g. http://srtm.csi.cgiar.org). Secondly, two geological maps of scale 1 : 500,000 (namely: Cairo and Beni-Suef) have been obtained, scanned, georeferenced, digitized, and clipped in order to construct a digital geological database for the study area. Additionally, meteorological data for four stations around the study area (namely: Cairo Airport, Helwan, Ras Seder, and Ismalia) have been acquired, and then utilized to create spatial environmental data. Moreover, a map of the proposed transportation networks has been acquired and digitized.

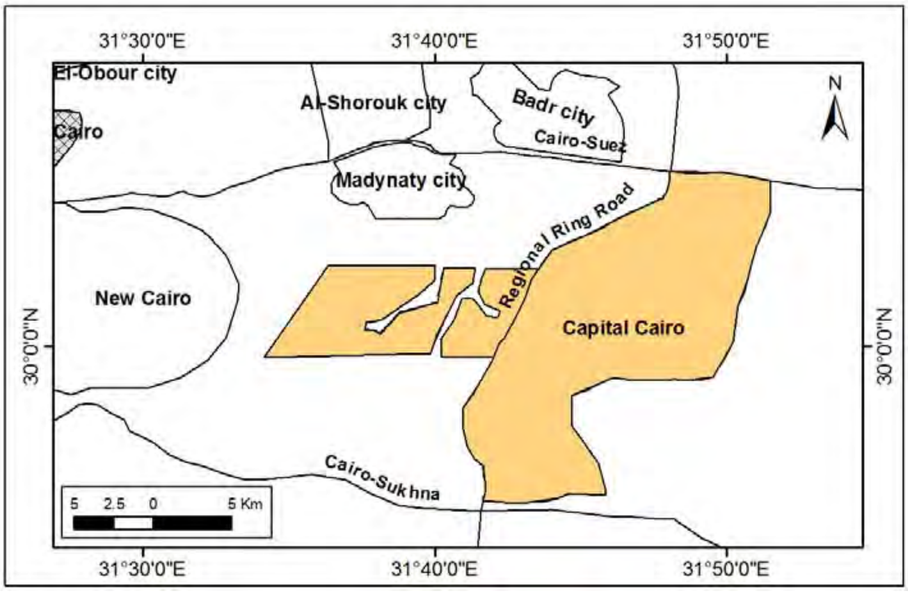

Figure 2: Phase 1 of the Cairo Capital Project

The Arc GIS 10 software has been utilized as the main tool for developing and analyzing digital geospatial databases. The processing has consists of several procedures as represented in Figure 3. The DEM has been processed in two separate stages: to create spatial representations of the topography in several forms, and to delineate the hydrological basins existed in the study area. The metrological data have been converted to raster format in order to clip the metrological characteristics of the study area. Additionally, the geological maps and the transportation network have been vectorized. Based on that procedures, several geospatial databases have been developed. Such datasets enable performing an integrated analysis for the Cairo Capital project from geodetics and environmental points of view.

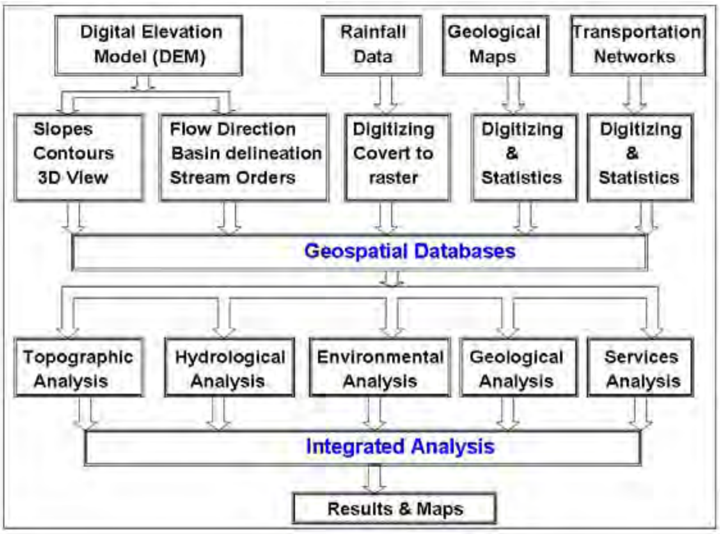

Figure 3: Workflow of Data Processing

4. Attained Results

4.1 The Topographic Analysis Results

The topography of the study area has been depicted in several forms as presented in Figures 4 to 7. It can be seen that the terrain elevations range from 216 to 451 meter, with an average of 314 meter. The highest elevations exist only in the southern and south-western borders of the area, while the majority of the elevations are less than 360 meter. Concerning the terrain slopes, it has been found that slopes vary from 0 to 17.8 degree, with a mean of 1.4 degree. Also, in units of percentage the slopes range from 0% to 32.1%, with an average of 2.4%. Accordingly, it can be concluded that the topography of the study area is almost of gentle slopes, except few locations mostly in its western edges. From an economical point of view, that is an important remark since it will significantly reduces the construction costs in this national project.

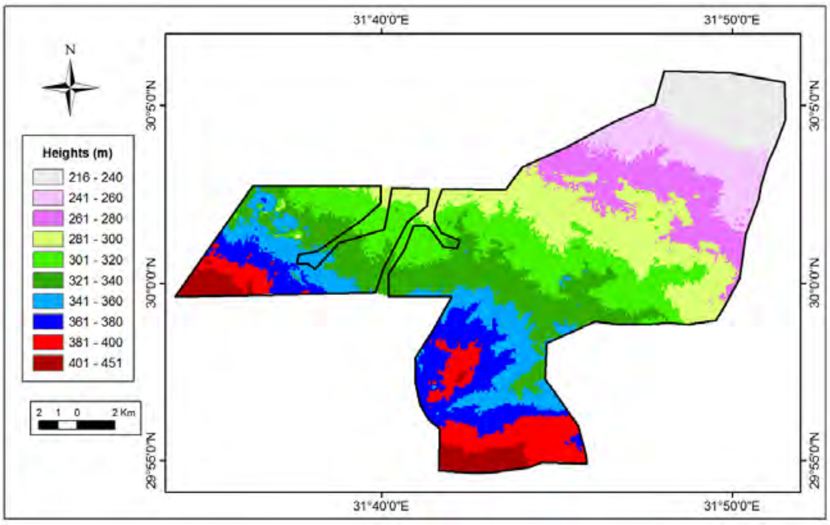

Figure 4: Topography of the Study Area

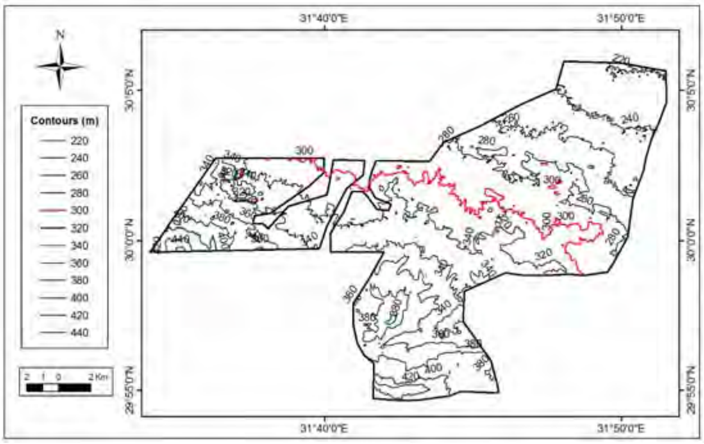

Figure 5: A Contour Map of the Study Area

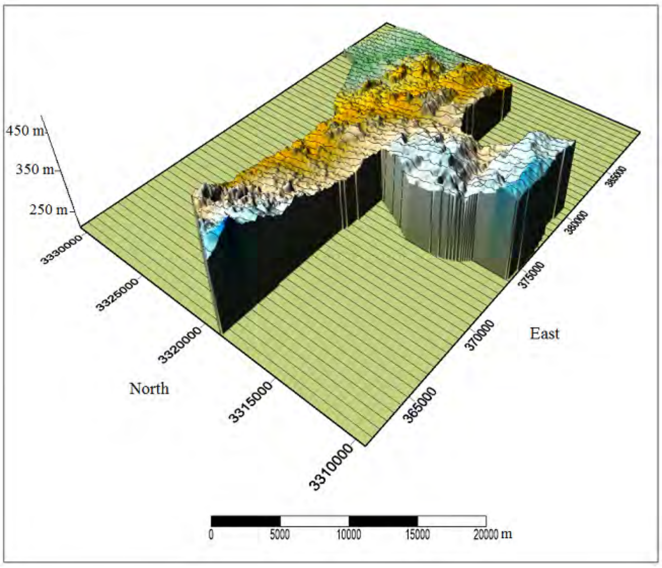

Figure 6: 3D View of the Study Area

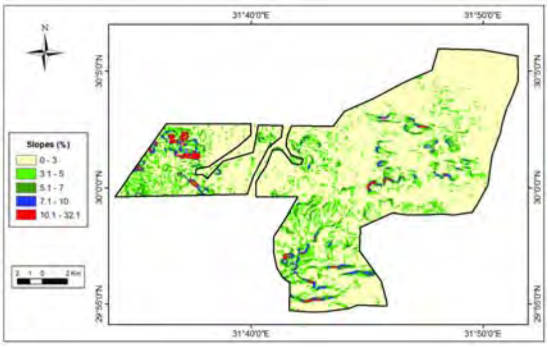

(a) slopes percentage

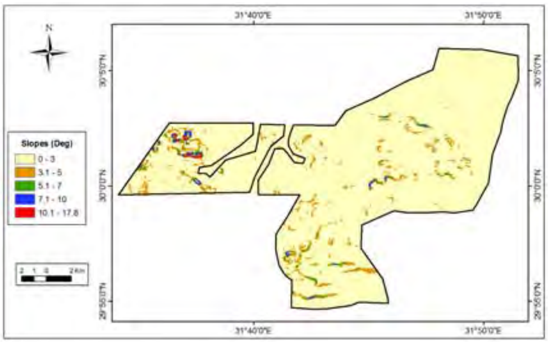

(b) slopes in degrees

Figure 7: Terrain Slopes of the Study Area

4.2 The Hydrological Analysis Results

The Hydrology toolbox of the Arc GIS package has been utilized in order to construct a hydrological geospatial database for the study area. Flow direction, flow accumulation, basin, and stream orders functions have been carried out. Eight main hydrological watersheds, that cover the study area, have been extracted. Table 1 summarizes these basins' characteristics, while Figure 8 depict them spatially. It can be realized that almost two thirds of the study area is covered by basin no. 1, with a total area of almost 167 square kilometers.

Table 1: Hydrological Basins Statistics

Basin	Area (km^2)	Area%
1	167.445	68.4
2	33.984	13.9
3	12.434	5.1
4	16.328	6.7
5	8.46	3.5
6	1.142	0.3
7	1.381	0.6
8	3.78	1.5
Sum	245	100%

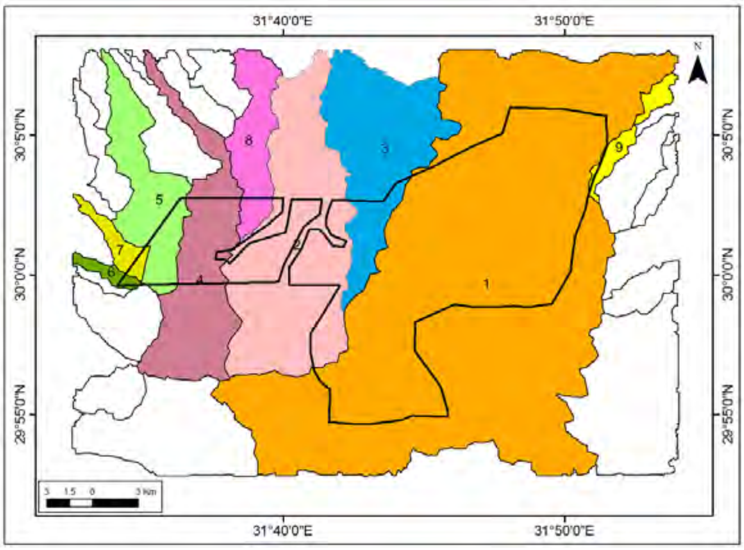

Figure 8: Hydrological Basins of the Study Area

Next, the stream orders of the surface drainage networks have been computed based on the Stralher method. It has been found that the streams have orders from 1 to 4, with a total length of 219.2 kilometer approximately (Table 2 and Figure 9). From Figure 9, it can be noticed that the main stream, of order 4, crosses the study area at the north-east border. Therefore, a great care should be taken into account in the design stage of the Cairo Capital landscape. This path should not have any infrastructure or surface utilities on its path, since it might be the most hazardous location in case of surface water runoff.

Table 2: Stream Orders Statistics

Stream Order	Count	Length (m)	Length%
1	96	117228.4	53.5
2	42	54510.6	24.9
3	38	39716.8	18.1
4	5	7713.3	3.5
Sum		219169.1	100%

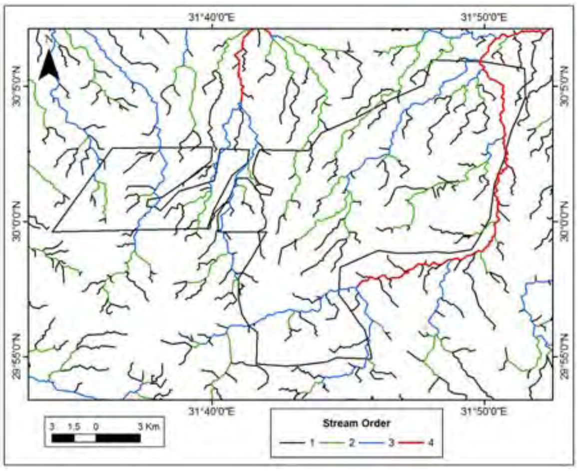

Figure 9: Hydrological Stream Orders of the Study Area

4.3 The Geological Analysis Results

Concerning the geology of the study area, sex main geological structures exist. The main geological feature is the Hagul formation, that occupies more than half of the study area. The Hagul formation consists mainly from fluviatile sand and gravel, and is locally underline by white limestone with marl. The second main geological structure, Gabel el-Ahmar formation, consists of continental vividly colored sands, quartzite and gravel. Wadi deposits constitutes about 15% of the study area. Therefore, this is an imperative finding from an economical point of view since it will significantly reduces the construction costs in this national development project.

Structure	**Area (km^2)**	**Area%**
Hagul formation	128.544	52.5
Gebel el-Ahmar formation	48.049	19.6
Wadi deposits	37.765	15.4
Maadi formation	25.157	10.3
Mokattam group	3.235	1.3
Basalt	2.204	0.9
Sum	245	100%

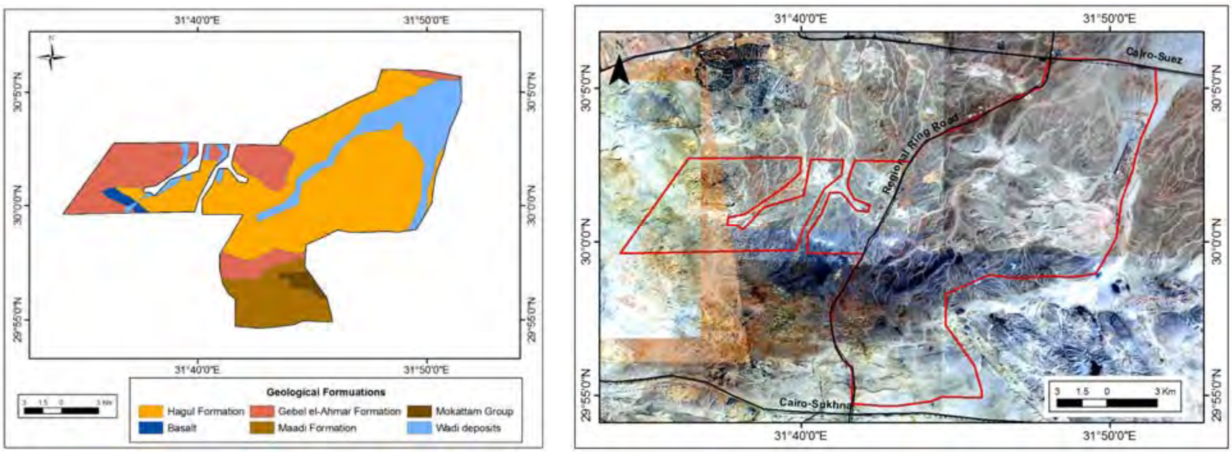

Figure 10: Geology of the Study Area

4.4 The Environmental Analysis Results

Regarding the rainfall, the study area posses an average annual rain varies from 20 to 39 millimeter/year, with an average value of 28 millimeter/year. It increases northward as can be noticed from Figure 11. It is a matter of fact that the biggest amount of rainfall in Egypt occurs in the autumn and winter sessions (from November to March). Although this can be considered as a small rainfall rate, care should be considered in the design process of the project, particularly for the pathway of surface drainage network of order 4, just to avoid any possible hazardous impacts of surface water runoff.

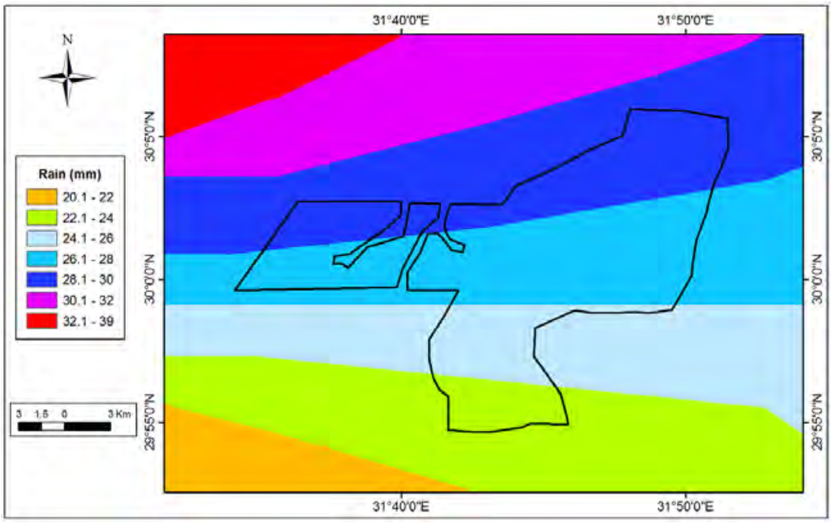

Figure 11: Average Annual Rains of the Study Area

4.5 The Transportation Analysis Results

Figure 12 depicts the current and future transportation networks in the study area. Currently, the Cairo Capital project area is connected by two highways: Cairo-Suez, and Cairo-Sukhna, that run from the traditional Cairo city to Suez city and Red Sea. Another highway that cross the study area is the regional ring road, which connects several governorates around Cairo. The future

transportation road networks in the first phase of the project contains major roads with a total length of 193 kilometer approximately. Also, it has been found that the proposed network of the future expansion phase of the project will include main roads with a total of 158 kilometer length approximately. Furthermore, the transportation network will contain an international airport at the north-east of the project region.

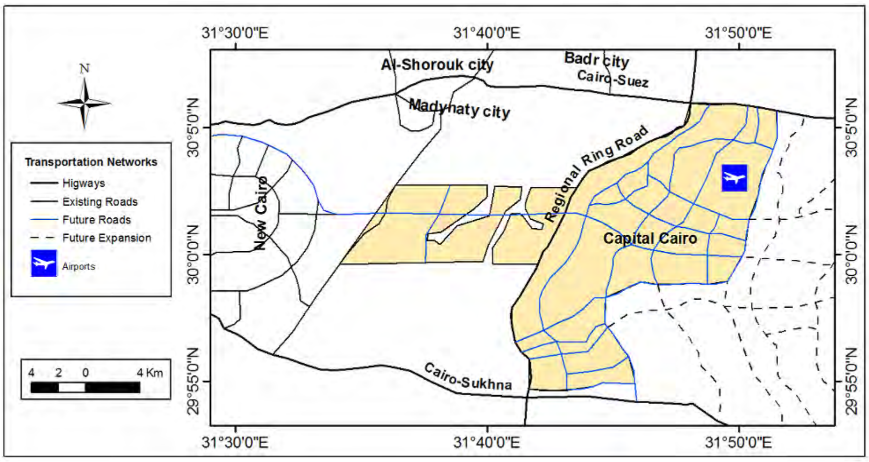

Figure 12: Transportation Networks of the Study Area

5. Conclusions

A mega development project has been initiated in Egypt to establish a new capital located about 30 kilometers east of the current capital, and 70 kilometers approximately west of Red sea and Suez canal. This research analyzes the overall spatial location of such a massive development activity from geodetic and environmental points of view. The attained topographic results show that the heights range from 216 to 451 m, with an average equals 314 m above sea level. The surface terrain slopes vary between 0 and 18 degrees, with an average equals 1.4 degree, which indicates a gentle-slope pattern. From a hydrologic perspective, the new capital location extends over six hydrologic sub-basins, with stream orders up to the fourth order. It has been found that the main hydrological streams almost run out of the study area expect in few specific locations. In order to minimize the possible flood hazards, it is recommended that such sites should be highlighted in the landscape design of the new capital, and probably left as preserved areas. The developed geological database show that there are six existing geological structures in the study area. The main structure was found to be the Hagul formation, which consists mainly from fluviatile sand and gravel. Several topographic, geological, and hydrological digital maps have been developed for the new capital general location. It is recommended that those maps and spatial databases being taken into consideration by decision makers in the development stages of this national mega project.

6. References

Abdalla, F. (2012) Mapping of groundwater prospective zones using remote and GIS techniques: A case study from the central eastern desert, Egypt, Journal of African Earth Sciences, No. 70, pp. 8-17.

Al-Ghamdi, K. Mirza, M., Elzahrany, R. and Dawod, G., (2012) GIS evaluation of urban growth and flood hazards: A case study of Makkah city, Saudi Arabia, Presented in the FIG working week, Rome, Italy, May 6-10.

Cairo Capital (2015) http://thecapitalcairo.com, accessed June 2015.

Dawod, G., Mirza, M., and Al-Ghamdi, K. (2011) GIS-based spatial mapping of flash flood hazard in Makkah city, Saudi Arabia, Journal of Geographic Information System, No. 3, pp. 217-223.

Khadr, Z., Nour el Dein, M., and Hamed, R. (2010) Using GIS in constructing area-based physical deprivation index in Cairo governorate, Egypt, Habitat International, No. 34, pp. 264-272.

Labib, M. and Nashed, A. (2013) GIS and geotechnical mapping of expansive soil in Toshka region, Ain Shams Engineering Journal, http://dx.doi.org/10.1016/j.asej.2012.11.005.

LA-DCP (Los Angeles Department of City Planning) (2014) Mobility plan 2035, A technical report, Los Angeles, USA, 193 pp.

Mohammed, W. and Al-Jenaid, S. (2012) Sustainable planning for environmental sensitive area using multi criteria / multi objective spatial analysis: Case study El-Dabaa, Egypt, The Arab Gukf Journal of Scientific Research, No. 2/3, pp. 78-87.

Salih, S. and Al-Tarif, A. (2012) Using GIS spatial analyses to study the selected location for dam reservoir on Wadi Al-Jirnaf, west of Shirqat area, Iraq, Journal of Geographic Information System, No. 4, pp. 117-127.

UN-HABITAT (The United Nations Human Settlement Program) (2010) Planning sustainable cities: Un-HABITAT practices and perspectives, A report, UN-HABITAT, Kenya, 50 pp.

Optimum Sites for Solar Energy Harvesting in Egypt Based on Multi-Criteria GIS

Gomaa M. Dawod
Survey Research Institute
National Water Research Center
Cairo, Egypt
dawod_gomaa@yahoo.com

Mosaad S. Mandoer
Geography Department
Mansoura University
Mansoura, Egypt
mosaad_3_70@hotmail.com

***Abstract*— Egypt faces an electricity sacristy recently, since it depends mainly on fossil fuels in electricity production. Thus, it initiated an ambitious plan to increase the renewable energy share from 2% (now) to 20% of the total demand by year 2020. This study focuses on utilizing the Multi-Criteria Analysis (MCA) within a Geographic Information Systems (GIS) environment to locate optimum locations for solar energy projects. Several physical and environmental spatial databases have been built up and an integrated GIS system have been developed. Ten different criteria have been selected and weighted to represent the favorite conditions for solar energy new investments. The attained suitability model represents the optimum locations for solar energy harvesting on a national scale. It has been found that the entire Egyptian territories is almost suitable for solar energy harvesting with varying suitability index. The suitability value range from 4.5 to 9.3, with an average equals 7.4 on a scale of 10. Moreover, areas of suitability index more than 80% have identified, and found to have a total area of 25310 square kilometer, which is a significant indicator about the potential of solar energy harvesting in Egypt. It is recommended that the developed suitability model being considered by decision makers in the future plans of energy development in Egypt.**

Keywords—Solar energy, Geographic Information Systems, Multi-criteria analysis, Egypt

I. Introduction

The global requirement for sustainable energy provision becomes increasingly significant over the next years as the environmental effects of fossil fuels become apparent. Additionally, the rapid growth of population in developing countries increase the need for electric generation and distribution. Renewable energy, such as solar energy, wind energy, biofuel energy, ...etc, is becoming a fundamental source for green energy worldwide. Solar power technologies are advancing and making a strong argument to be considered the next step towards the future of renewable energy production. On a national scale, the Egyptian Cabinet has approved, in 2012, an ambitious plan to increase the percentage of renewable energy to 20% by 2020 [1]. Some current solar energy projects include the solar water heaters project for hotels in Red Sea and south Sinai governorate, the Kurimat 140 MW (mega watt) integrated solar power plant, and the 100 MW solar thermal power plant at Kom Ombo [1].

However, selecting appropriate sites for harvesting solar energy is not a single-criteria task. Basically, it is based on several sets of physical, environmental, and socio-economical criteria in order to decide optimum geographic locations. GIS has been utilized extensively in the last decades for sighting optimum locations for a variety of objects, such as groundwater [2], touristic infrastructures [3], urban development [4], earthquake refugee camps [5], water harvesting [6], solid waste disposal [7], and wind turbine [8]. Finding a suitable location for solar energy development affects purchase price, solar power efficiency, and environmental impacts. The GIS-based multi-criteria approach has proven to be an efficient decision-support tool for locating optimum spatial sites particularly for solar energy harvesting. For example, Wanerer and Herle [9] has developed a web-based spatial decision support system based on a multi-criteria analysis in Spain. Also, Tahri et al. [10] combined GIS and multi-criteria method to assess the suitability of some locations in Morocco to carry out a renewable energy project. Similarly, Brewer et al. [11] utilized the GIS-based multi-criteria approach to determine socially acceptable and economically viable locations for utility-scale solar projects in Idaho, USA. Moreover, Matejicek [12] utilized multi-criteria GIS approach to locate optimum sites of renewable energy projects in Czech republic. This paper aims to locating appropriate sites for solar energy harvesting in Egypt utilizing the GIS-based multi-criteria scheme.

II. Multi-Criteria GIS

A criterion is a measureable phase of a judgment, that makes it achievable to differentiate and quantify choices in the decision-making process. Decision makers can use multi-criteria approach to judge various subjective and conflicting criteria whereas evaluating the suitability of a specific area with regards to a certain development. The method is often utilized within a GIS environment where the suitability of an area is represented with visual aids.

Several GIS-based multi-criteria approaches have been proposed and utilized, such as binary overlay (Boolean logic), Analytic Hierarchy Process (APH), and the weighted linear combination. The first method can be though of as overlaying many transparencies each represents a certain condition or criterion. In a GIS software, this method is adopted as a grid analysis procedure using an AND function to combine all layers of criteria. The result of this method comprises the sites that meet the whole set of the required conditions. On the other hand, the AHP multi-criteria method involves several steps including: calculation of the criteria scores, calculation of the criteria weights, local priorities and consistency of comparisons, and the determination of suitable alternatives [e.g. 18, and 11] The weighted linear addition method is based on the concept of computing a weighted average for each cell in a raster. In order to obtain the suitability map, the following summation is obtained:

$$S = \sum_{i=1}^{n} w_i x_i / \sum w \tag{1}$$

where S denotes the suitability index, wi is the weight of criteria i, xi is the criterion of factor i, n is the number of criteria. A simplified form of equation 1 may be obtained if the weights are scaled so that their sum equals one. Finally, the attained suitability model assigns a suitability index for each cell representing its suitability degree regarding the designed set of criteria.

Finding a suitable location for solar energy development affects purchase price, solar power efficiency, and environmental impacts. The GIS-based multi-criteria approach has proven to be an efficient decision-support tool for locating optimum spatial sites particularly for solar energy harvesting. For example, Castillo et al. [18] evaluated the potential of solar power generation within the European Union utilizing a multi-criteria assessment approach. In addition, Wanerer and Herle [19] has developed a web-based spatial decision support system based on a multi-criteria analysis in Spain. Also, Tahri et al. [20] combined GIS and multi-criteria method to assess the suitability of some locations in Morocco to carry out a renewable energy project. Similarly, Brewer et al. [21] utilized the same approach to determine socially acceptable and economically viable locations for utility-scale solar projects in Idaho, USA. Moreover, Matejicek [22] applied the multi-criteria GIS method to locate optimum sites of renewable energy projects in Czech republic.

III. INPUT MATERIALS

In the current research, a number of processing procedures have been performed in order to apply the multi-criteria approach within a GIS environment. Basically, multi-criteria analysis aims to optimize spatial locations to meets a number of conditions or limiting factors. Hence, the input datasets consist of several geospatial databases, each represents a specific criterion. In the current research, the acquired input data contain a Digital Elevation Model (DEM) for Egypt, annual average of solar radiation map, and several topographic and remote sensing imageries. The first step in the data processing stage include data manipulation, such as slope extraction from the available DEM, digitization of required datasets including the road and electricity distribution networks, and unification of geodetic datums for all raster and vector data types. Figure 1 depicts the processing scheme in this primary step in order to construct a number of digital spatial databases.

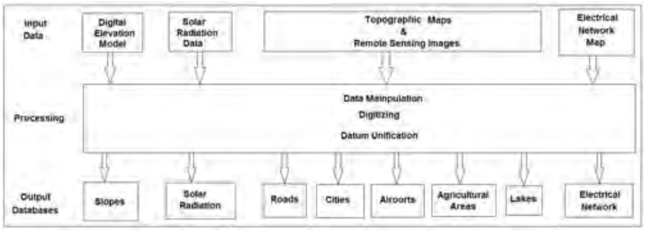

Fig 1: Input Data Processing Methodology

The utilized SRTM (Shuttle Radar Topography Mission) global DEM indicates that the terrain heights of Egypt range from -135 m to 2603 m with an average of 300 m (Fig. 2). The Arc GIS v. 10 software has been applied to extract terrain slopes, that is found to vary from 0 to 71 degree, with a mean of 2 degree (Fig. 3). Shapefiles for main urban features, particularly main cities and airports, have been also constructed utilizing the available topographic maps and remote sensing imageries (Fig. 4). A total of 98 major city and 15 major civilian airports have been exploited. Furthermore, the road and electrical distribution networks have been developed (Fig. 5). The total length of main road network has found to be more than 10 thousand kilometers, while the main electrical distribution network has a total length of 8500 km approximately.

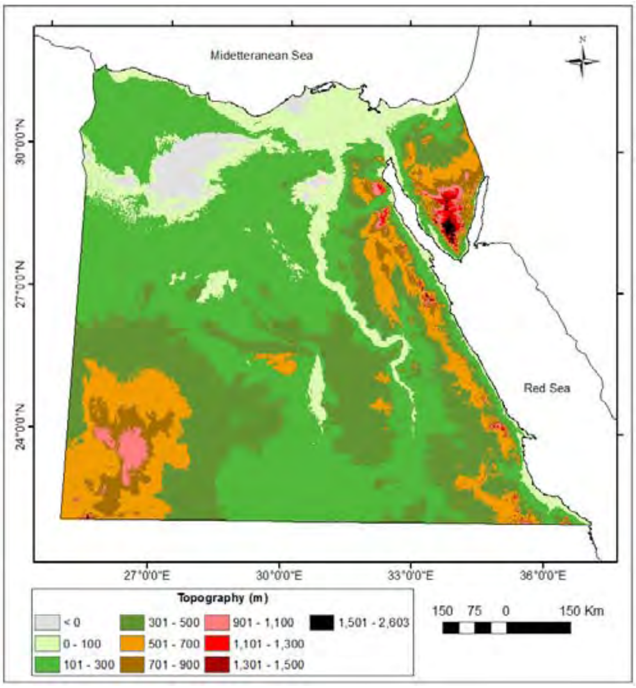

Fig. 2: Topography of Egypt

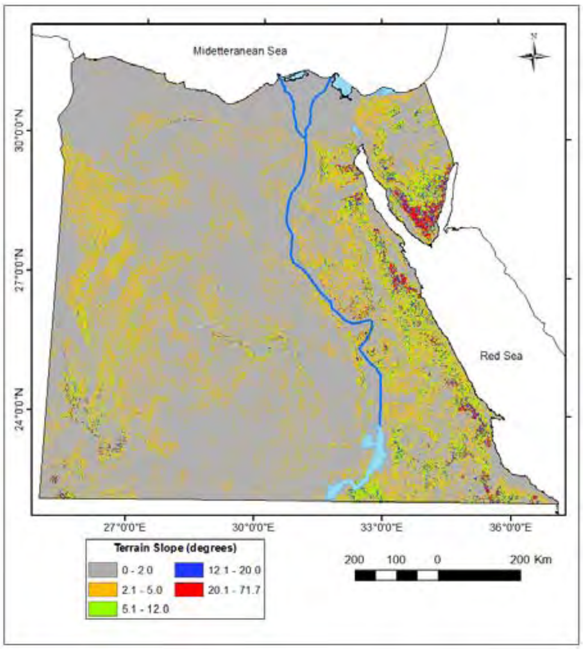

Fig. 3: Slopes of Egypt

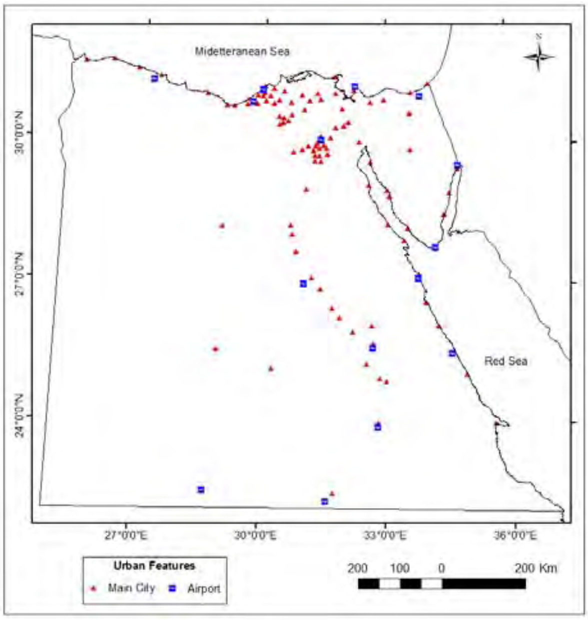

Fig. 4: Cities and Airports Distribution

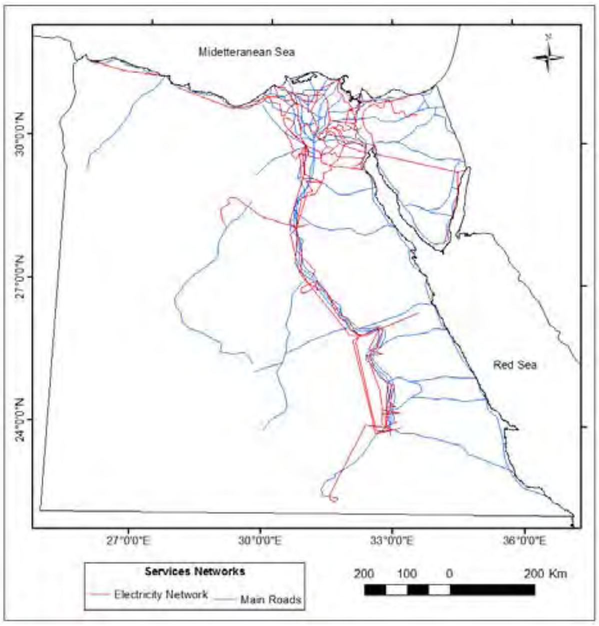

Fig. 5: Electrical And Roads Networks

The solar atlas of Egypt, issued in 1991, showed that the annual average of direct solar radiation range between 5.5 kWh (kilowatt-hour)/m^2/year to 9.3 kWh/m^2/year (NREA, 2013). These data, depicted in Figure 6, have been converted to a raster dataset and have been utilized in the current research study.

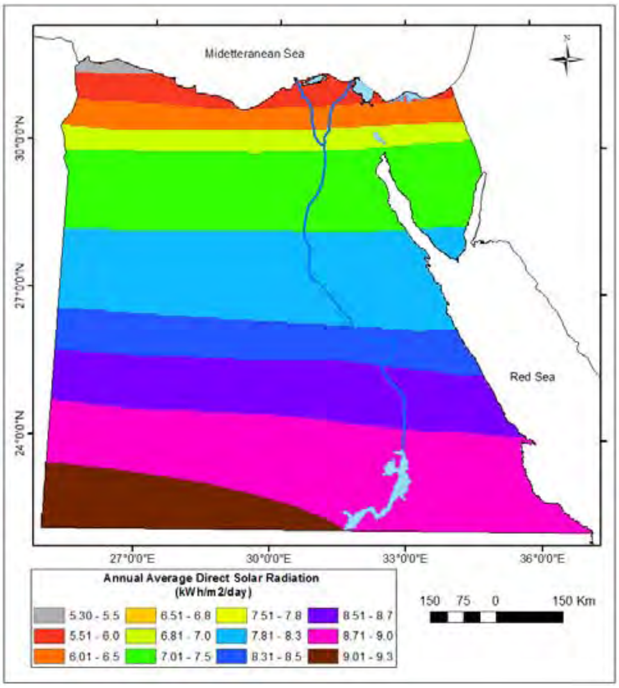

Fig. 6: Annual Average Solar Radiation

Furthermore, digital spatial databases for protected areas including the agricultural lands, lakes, and valleys have been created (Fig. 7). Their total area exceeds almost 61 thousands of square kilometers. The agricultural areas contain both the traditional lands in the Nile valley and Delta along with the lands of the undergoing development project for reclaiming a million faddans (a faddan is approximately 4200 square meters).

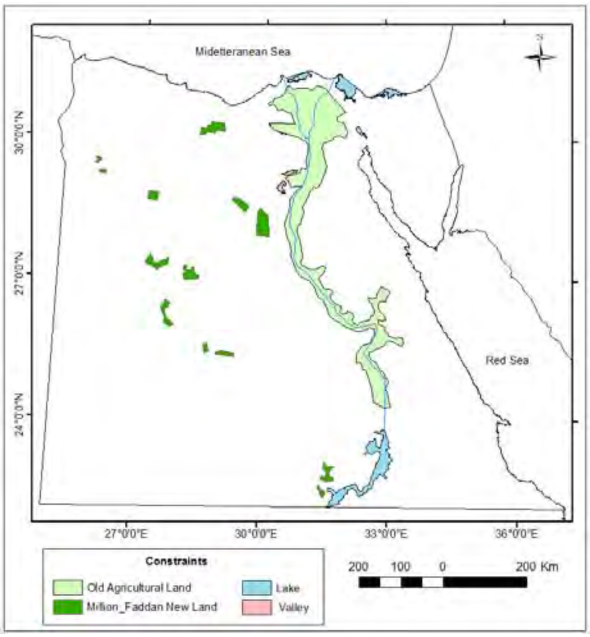

Fig. 7: Protected Areas

IV. Processing Methodology

Based on several literatures and case studies concerning solar energy harvesting, ten criteria have been selected to be processed in the current research [e.g. 18, 25, 26, and 27]. Table 1 presents the adopted criteria, that can be divided generally into two groups: technical criteria (potential of solar radiation, terrain slopes, and distances from the electrical distribution network); and economical criteria (distances from roads, coastlines, cities, and airports). Additionally, the protected areas' type have been imposed as constraints in the processing multi-criteria stage. For each criterion, a reclassification has been performed in order to evaluate its particular suitability for solar energy harvesting. A specific weight strategy has been applied in treating the utilized criteria while processing the final suitability model (Figure 8). The selected weights, as shown in the last column of Table 1, assign a sum of 60% to the technical criteria and a total of 40% to the economical conditions.

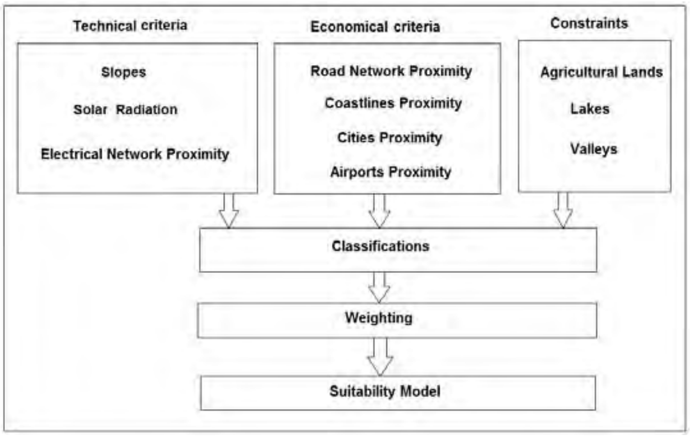

Fig. 8: Multi-Criteria Processing Algorithm

TABLE 1: UTILIZED CRITERIA AND WEIGHTS

Criteria Type	Criterion	Categories	Suitability	Weight
Technical	Solar Radiation (kWh/m2/day)	> 8 6 - 8 4.5 - 6 < 4.5	High Medium Low NA	0.30
	Slope (degree)	0 - 3 3 - 5 5 - 10 > 10	High Medium Low NA	0.15
	Distance from Electrical Network (km)	0 - 5 5 - 10 10 - 20 > 20	High Medium Low NA	0.15
Economical	Distance from Roads (km)	> 5 < 5	Suitable NA	0.10
	Distance from Coastlines (km)	> 5 < 5	Suitable NA	0.10
	Distance from Cities (km)	> 5 < 5	Suitable NA	0.10
	Distance from Airports (km)	> 3 < 3	Suitable NA	0.10
Constraints	Land Use	Agricultural Other	NA Suitable	NA
	Lakes	Lakes	NA	
	Valleys	Valleys	NA	

V. RESULTS AND DISCUSIONS

Proximity-to-feature raster datasets have been constructed for each selected limiting factor. So, several primarily suitability models have been developed according the classification schemes applied. Re-classification function has been carried out to convert values of each raster on a scale of 10 points, where 10 represents the highest suitability index. Figures 9, 10, and 11 depicts examples of such models particularly for the terrain slopes, distances from electrical distribution network, and distances from the road network respectively.

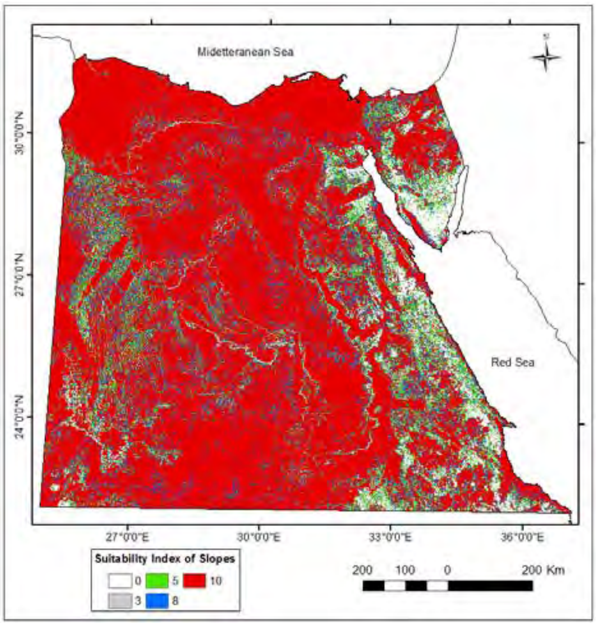

Fig. 9: Suitability of Terrain Slopes

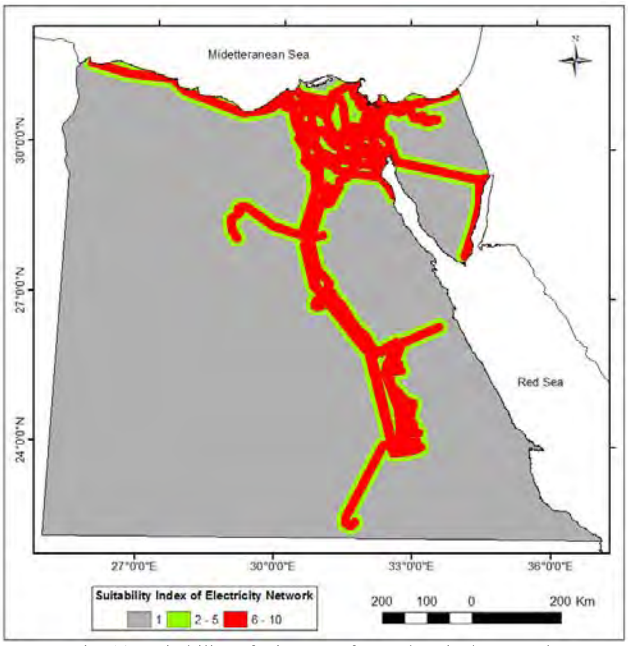

Fig. 10: Suitability of Distances from Electrical Network

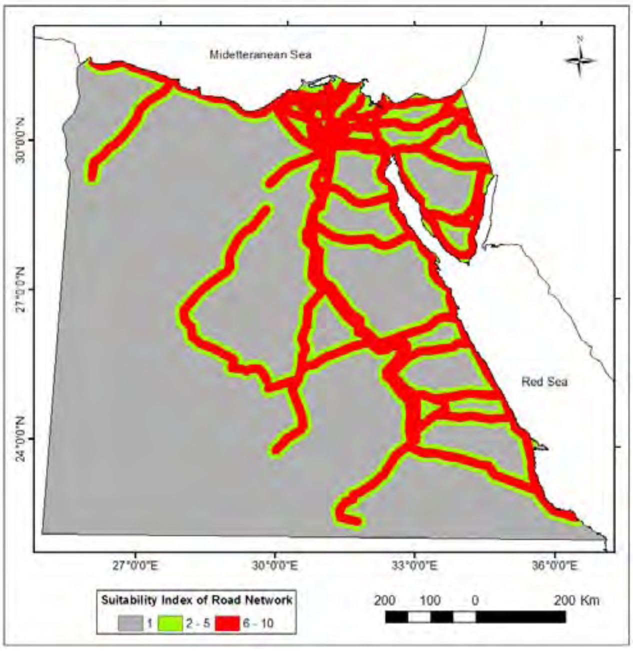

Fig. 11: Suitability of Distances from Roads Network

Lastly, all raster suitability models representing the whole criteria have been combined in a weighted scheme according to the designed weights. The resulted model multiplies the weighted value by each raster layer value that sums each corresponding cell. Again, a reclassification function was applied in order to scale the attained weighted-sum model on a 10-point scale. The accomplished final suitability model, depicted in figure 12, shows that the entire Egyptian territories is almost suitable for solar energy harvesting with varying suitability index. The suitability value range from 4.5 to 9.3, with an average equals 7.4.

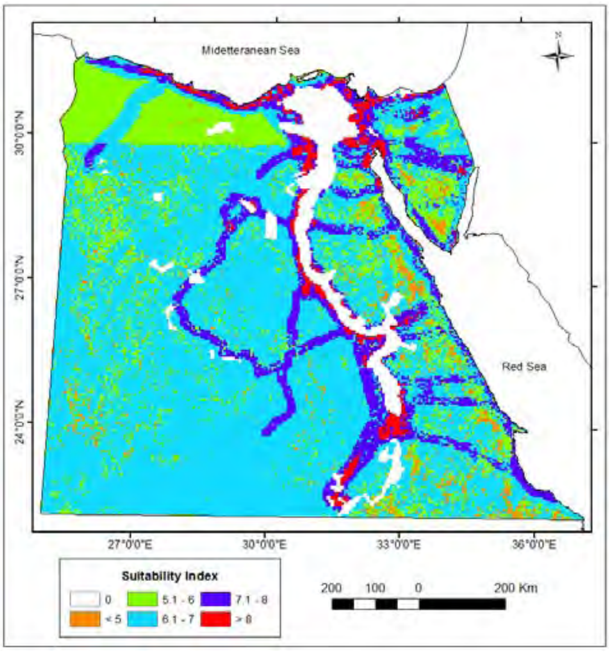

Fig. 12: Final Suitability Model

Moreover, areas of suitability index more than 80% have identified and represented in figure 13. It has been concluded that these high-suitability sites have a total area of 25310 square kilometer, which is a great indicator about the potential of solar energy harvesting in Egypt. Table 2 represents the major areas of high-suitability according to governorates. It can be seen that the New Valley governorate contains 20 % of these promising locations, while Aswan governorate posses 15 %. Hence, it is recommended that priority of future plans for solar energy projects should be given to these two specific governorates.

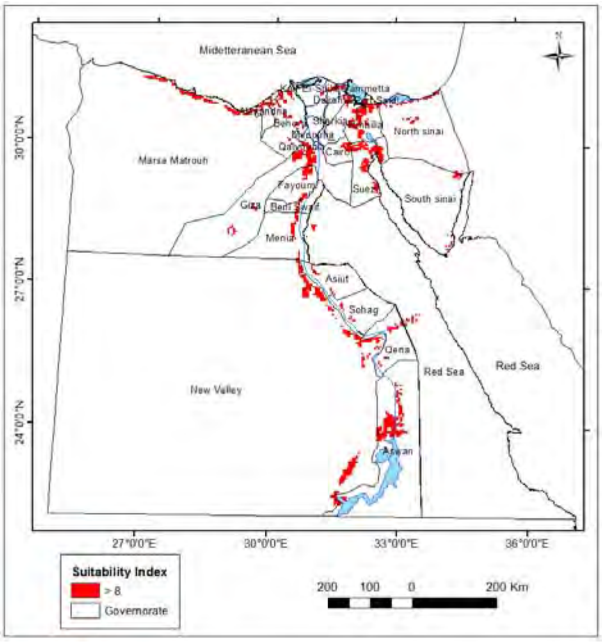

Fig. 13: High-Suitability Sites

TABLE 2: HIGH-SUITABILITY AREAS BY GOVERNORATES

Governorates	High-Suitable Locations	
	Area (km2)	Percentage
New Valley	5090	20 %
Aswan	3838	15 %
Suez	2940	12 %
Marsa Matrouh	2872	11 %
Giza	1917	8 %
Others Governorates	8653	34 %
Sum	25310	100 %

VI. CONCLUSIONS

Energy is fundamental force that affects all aspects of development social, economic, and environmental issues. Renewable energy, particularly solar energy, becomes an essential clean energy source worldwide. This paper focused on the utilization of multi-criteria GIS approach for locating optimum sites for solar energy harvesting in Egypt. Based on ten technical and economical criteria, a suitability model has been developed representing the spatial variation of solar energy potential over the Egyptian territories. It has been found that almost all the Egyptian lands are promising in solar energy harvesting with variable suitability index. High-suitability locations have been identified with a total area of more than 25 thousand square kilometers. The New Valley, Aswan, and Suez governorates posses almost half of such promising locations. Hence, it is recommended that the accomplished suitability model being considered by decision makers in the future plans of energy development in Egypt.

REFERENCES

[1] NREA (Egypt's New and Renewable Energy Authority) (2013) Annual report, 2012-2013, 56 pp.

[2] Cradden, L. , Kalogeri, C. , Martinez Barrios, I., Galanis, G., Ingram, D. and Kallos, G., (2016) Multi-criteria site selection for offshore renewable energy platforms, Renewable energy, No. 87, pp. 791-806.

[3] Lemana, N., Ramlia, M., and Khirotdinb, P., (2016) GIS-based integrated evaluation of environmentally sensitive areas (ESAs) for land use planning in Langkawi, Malaysia, Ecological indicators, No. 61, pp. 293–308.

[4] Fraile, A., Larrodé, E., Magrenan, A., and Sicilia, J. (2016) Decision model for siting transport and logistic facilities in urban environments: A methodological approach, Computational and applied mathematics, No. 291, pp. 478–487.

[5] Hofer, T., Sunak, Y., Siddique, H., and Madlener, R. (2016) Wind farm siting using a spatial analytic hierarchy process approach: A case study of the Stadteregion Aachen, Applied energy, No. 163, pp. 222–243.

[6] Colantoni, A., Delfanti, L., Recanatesi, F., Tolli, M., and Lord, R. (2016) Land use planning for utilizing biomass residues in Tuscia Romana (central Italy): Preliminary results of a multi criteria analysis to create an agro-energy district, Land use policy, No. 50, pp. 125–133.

[7] Dawod, G., 2013, Suitability analysis for tourist infrastructures utilizing multi-criteria GIS: A case study in Al-Hada city, Saudi Arabia,

International journal of geomatics and geosciences, V. 4, No. 2, pp. 313-24.

[8] Inamdar, P., Cook, S., Sharma, A., Corby, N., Connor, J., and Perera, B. (2013) A GIS based screening tool for locating and ranking of suitable storm water harvesting sites in urban areas, Environmental management, No. 128, pp. 363-370.

[9] Pradhan, J. and Samanta, K. (2015) Site suitability analysis using remote sensing and GIS for proper selection of solid waste disposal ground within Rajarhat, Gopalpur municipal area, Kolkata, West Bengal, International journal of geomatics and geosciences, V. 5, No. 4, pp. 640-654.

[10] Mahmoud, S., Adamowski, J., Alazba, A., and El-Gindy, A. (2016) Rainwater harvesting for the management of agricultural droughts in arid and semi-arid regions, Paddy and Water Environment, No.14, pp. 231–246.

[11] Abudeif, A., Abdel Moneim, A., and Farrag, A. (2015) Multicriteria decision analysis based on analytic hierarchy process in GIS environment for siting nuclear power plant in Egypt, Annals of nuclear energy, No. 75, pp. 682–692.

[12] Shaker, A. and Mahmoud, S. (2015) Towards a good urban development plan in Sinai through land site suitability maps, Presented at the regional conference on surveying and development, Sharm El-Sheikh, Egypt, October 3-6.

[13] Saleh, A., Belal, A., and Mohamed, E. (2015) Land resources assessment of El-Galaba basin, south Egypt for the potentiality of agriculture expansion using remote sensing and GIS techniques, Egyptian journal of remote sensing and space sciences, No. 18, pp. S19–S30.

[14] Hassaan, M. (2015) A GIS-based suitability analysis for sitting a solid waste incineration power plant in an urban area case study: Alexandria governorate, Egypt, Geographic information system, No. 7, pp. 643-657.

[15] Effat, H. (2014) Spatial modeling of optimum zones for wind farms using remote sensing and geographic information system: Application in the Red Sea, Egypt, Geographic information system, No. 6, pp. 358-374.

[16] Kaiser, M. and Ahmed, S. (2013) Optimal thermal water locations along the Gulf of Suez coastal zones, Egypt, Renewable Energy, No. 55, pp. 374-379.

[17] Salim, M. (2012) Selection of groundwater sites in Egypt using geographic information systems for desalination by solar energy in order to reduce greenhouse gases, Advanced research, No. 3, pp. 11-19.

[18] Castillo, C., Silva, F., and Lavalle, C. (2016) Assessment of the regional potential for solar power generation in EU-28, Energy policy, No. 88, pp. 86-99.

[19] Wanerer, T. and Herle, S. (2015) Creating a spatial multi-criteria decision support system for energy related integrated environmental impact assessment, Environmental impact assessment review No. 52, pp. 2-8.

[20] Tahri, M., Hakdaoui, M., and Maanan, M. (2015) The evaluation of solar farm locations applying geographic information system and multi-criteria decision-making methods: Case study in southern Morocco, Renewable and sustainable energy review, No. 51, pp. 1354-1362.

[21] Brewer, J., Ames, D., Solan, D., Lee, R. and Carlisle, J. (2015) Using GIS analytics and social preference data to evaluate utility-scale solar power site suitability, Renewable energy, No. 81, pp. 825-836.

[22] Matejicek, L. (2015) Multi-criteria analysis for sources of renewable energy using data from remote sensing, Presented at the 36th international symposium on remote sensing of environment, Berlin, Germany, May 11-15.

[23] Watson, J. and Hudson, M. (2015) Regional scale wind farm and solar farm suitability assessment using GIS-based multi-criteria evaluation, Landscape and urban planning, No. 138, pp. 20-31.

[24] Recanatesi, F., Tolli, M., and Lord, R. (2014) Multi criteria analysis to evaluate the best locations of plants for renewable energy by forest biomass: A case study in central Italy, Applied mathematical sciences, V. 8, No. 129, pp. 6447-6458.

[25] Aydin, N., Kentel, E., and Duzgun, S. (2013) GIS-based site selection methodology for hybrid renewable energy systems: A case study from western Turkey, Energy conversion and management, No. 70, pp. 90-106.

[26] Sanchez-Lozano, J., Teruel-Solano, J., Soto-Elvira, P., and Garcia-Cascales, S. (2013) Geographic information systems (GIS) and multi-criteria decision making (MCDM) methods for the evaluation of solar farms locations: Case study in south-eastern Spain, Renewable and sustainable energy review, No. 24, pp. 544-556.

[27] Uyan, M. (2013) GIS-based solar farms site selection using analytic process in Karapinar region, Konya, Turkey, Renewable and sustainable energy reviews, No. 28, pp. 11-17.

National Water Research Center (NWRC) Conference on:
Research and Technology Development for Sustainable Water Resources Management
Cairo, Egypt. December 4-6, 2017

A HIGH-PRECISION GEOID FOR WATER RESOURCES MANAGEMENT: A CASE STUDY IN MENOFIA GOVERNORATE, EGYPT

Essam M. Al-Krargy, Hoda F. Mohamed, Magdy M. Hosney, and Gomaa M. Dawod
Survey Research Institute, National Water Research Center, Egypt

Abstract

The Global Positioning System (GPS) has been utilized, as a positioning technique, in various water resources management applications in Egypt since the mid 1980s. However, up till now there is no an official published national geoid model to convert the GPS-based heights into Mean Sea Level (MSL) elevations. On the other hand, the accuracy level of the global geoid models could not satisfies the requirements of civil engineering projects. Recently, the Survey Research Institute (SRI) has initiated a research project to establish a prototype centimeters-level geoid utilizing heterogeneous geodetic datasets. A new vertical geodetic network has been established in Menofia governorate using the precise levelling technique, and 47 new Bench Marks (BM) have been established with an average spacing of 4 kilometers apart. The entire network has been positioning by GPS applying the international geodetic standards and specifications, and tied to the national geodetic datum of Egypt. The least-squares adjustment method has been carried out for both networks. The geoidal heights have been achieved with a few centimeters level of precision, and a precise geoid model has been developed for the study area, enabling expanded utilization of GPS, time reduction, and cost saving in water resources management projects. It is recommended that the exploited field procedures and processing strategies being followed as national geodetic standards. Additionally, It is highly recommended that a nation-wide high-precision geoid model for Egypt has to be established.

Keywords:
Geoid; GPS; BM; MSL; Heights; Menofia governorate.

1. Introduction

A geoid model is a three-dimensional (3D) geospatial model defines the relationship between the ellipsoid and the geoid surfaces at a specific area. In a sense, geoid models have been one of the main activities of the geodetic community a long time ago. However, a geoid model became an essential task since the spread of Global Navigation Satellite Systems (GNSS) utilizations in 1980s. Since GNSS-based heights are referred to the surface of an ellipsoid, a geoid model converts them to the MSL-based orthometric elevations used in civil engineering applications. On a global basis, the separations between the geoid and ellipsoid surfaces are in the range of ± 100 meters (Fig. 1)

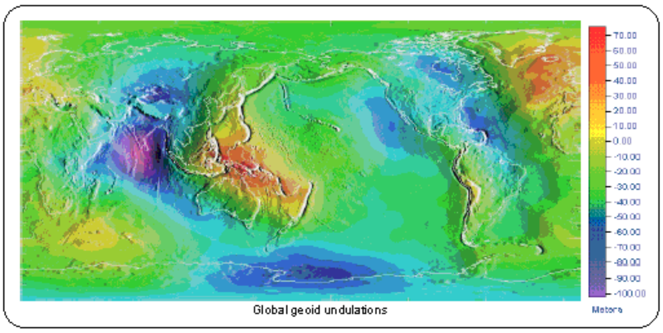

Fig. 1: Global Geoid/Ellipsoid Separations

Geoid models are developed on a global, regional, or national basis. For civil engineering and surveying projects, certain geoid models could be developed at a smaller scale. Over the last two decades, several precise geoids have been developed all over the world, e.g. in Japan (Matsuo et al., 2016), Turkey (Karaaslan et al. 2016), Sudan (Abdalla and Green, 2016), Indonesia (Pahlevi et al. 2015), Uganda (Ssengendo et al. 2015), and Latvia (Balodis et al., 2015).

In Egypt, since the development of the first pioneer national-scale geoid (Alnaggar 1986), several geoid researches have been carried out. For example, Dawod (1998) has developed a national geoid model based on the data of the Egyptian National Standardization Network of 1997 (ENGSN97) along with GPS/levelling data. Saad and Dawod (2002) have developed a national geoid model based on the EGM96 global geopotential model along with GPS/levelling datasets. In addition, Abd-Elmotaal (2008) has developed a gravimetric geoid model utilizing high-degree tailored reference geopotential model. Recently, Rabah and Kaloop (2013) have

developed a local geoid model utilizing the minimum curvature surface technique. and Al-Karargy et al. (2014) have investigated the utilization of GPS/levelling in developing geoid models for small areas in Egypt.

The vertical geodetic network of Egypt has been established between 1906 and 1945, where thousands of BM lines have been observed to cover the urban areas on a national base. However, it has been found that great damages have been occurred to such locations and almost 80% of those BM have been destroyed (SRI, 2016). SRI has initiated a research study to re-construct and observe the vertical geodetic network in Menofia governorate along with GNSS measurements over BM in order to develop a prototype high-precision geoid model. This paper discuses such a study in details and presents the performed processing and adjustments procedures, along with the attained results.

2. Geoid Modelling

Geoid modelling is performed using several types of geodetic measurements. Gravity observations are applied to develop gravimetric geoid utilizing the well-known Stokes' formula in a spherical harmonic expansion way (e.g. Heiskanen and Moritz, 1967):

$$N = \frac{R}{4\Pi\gamma} \iint_{\sigma} \Delta g S(\Psi) d\sigma \qquad (1)$$

where,

N is the geoidal undulation, R is the average radius of the Earth, γ is the normal gravity on the ellipsoid, Δg represents the gravity anomaly, and

S(ψ) is called the Stokes' function computed as:

$$S(\Psi) = \frac{1}{\sin(\Psi/2)} - 6\sin(\Psi/2) + 1 - 5\cos(\Psi) - 3\cos(\Psi)\ln[\sin(\Psi/2) + \sin^2(\Psi/2)] \qquad (2)$$

The second method of geoid modelling overcomes the problem of the Stokes' formula that needs gravity measurements all over the Earth in order to evaluate the double integral in Equation 1. This method concerns the utilization of heterogeneous geodetic datasets to develop a Global Geopotential or Geoid Model (GGM) as:

$$N = (\frac{GM}{r\gamma}) \sum_{n=2}^{n_{\max}} (\frac{a}{r}) \sum_{m=0}^{n} ((\bar{C}_{nm} \cos m\lambda) + (\bar{S}_{nm} \sin m\lambda)) P_{nm} \sin \phi) \qquad (3)$$

where: n is the degree of the GGM model, n_{max} is the maximum degree of the GGM model, m is the maximum order of the model, γ is the normal gravity of the reference ellipsoid, r is the geocentric radial distance of the computation point projected on the ellipsoid, G is the Newtonian gravitational constant, M is the mass of the Earth, a is the semi-major axis, ϕ is the geocentric latitude, λ is the geocentric longitude, $\bar{C}_{nm}$ and $\bar{S}_{nm}$ are the fully normalized harmonic coefficients, and P_{nm} is the fully normalized associated Legendre polynomial.

GGM development incorporates the integration of heterogeneous geodetic datasets, including terrestrial gravity observations, satellite-based gravity measurements, altimetry measurements, and terrestrial geodetic data. As a result, the coefficients of C's and S's in equation 3 are evaluated based on the required maximum degree and order of the model. GGM models have been developed since the 1960s, and there are more than 150 GGM available at the website of the International Center for Global Earth Models (http://icgem.gfz-potsdam.de/ICGEM/ICGEM.html). Table 1 presents few examples of the most recently released GGM and their characteristics. However, it has been concluded that the precision of utilizing any GGM alone did not reach the two-decimeter level of accuracy (e.g. Al-Krargy et al., 2015, and Eshagh and Zoghi, 2016).

Table 1: Characteristics of Recent Global Geopotential Models

GGM Name	Year	Degree	Data Type
GGM05C	2016	360	S (Goce, Grace, Lageos)
GECO	2015	2190	S (Goce, Grace), G, A
EIGEN-6C4	2014	2190	S (Goce, Grace, Lageos), G, A
EIGEN-6C3stat	2014	1949	S (Goce, Grace, Lageos), G, A
EIGEN-6C	2011	1420	S (Goce, Grace, Lageos), G, A
EGM2008	2008	2190	S (Grace), G, A
where: S = satellite tracking data, G = Gravity data, and A = Altimetry data			

The third geoid modelling strategy breaks the geoid undulation (N) into three components:

$$N = N_{REF} + N_{\Delta g} + N_h \tag{4}$$

where: $N_{\Delta g}$ is the contribution of the reduced gravity anomalies computed by Stokes's integral, N_h is the contribution of the topography, and N_{REF} is the contribution of the reference gravity field from a GGM. This implies that the gravity anomaly Δg is decomposed, too, into three parts:

$$\Delta g = +\Delta g_{REF} + \Delta g_F + \Delta g_h \quad (5)$$

where: Δg_F represents the residual free-air gravity anomalies, Δg_h is the effect of local topography, and Δg_{REF} represents the long-wavelength gravity anomalies of a reference gravity field represented by a GGM.

The geometric geoid is the forth way to develop a geoid model, particularly in small to medium areas. It computes the geoid undulation (N) directly from GPS-based ellipsoidal height (h) and the corresponding orthometric elevation (H) at the same locations (Fig. 2):

$$N = h - H \quad (6)$$

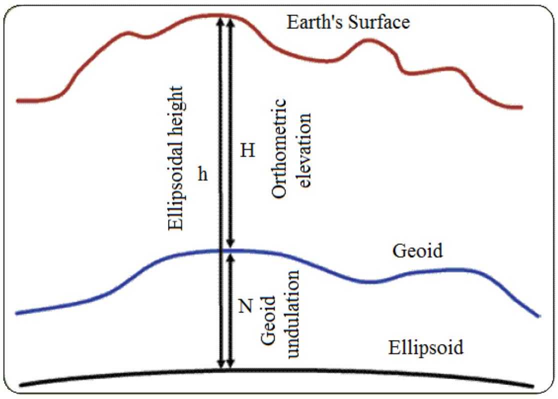

Fig. 2: Types of Heights

Due to existing datum inconsistencies, random errors, systematic distortions in the different height datasets in equation 6, a combined least-squares adjustment is needed (e.g. Fotopoulos 2005, Kiamehr and Eshagh, 2008). Thus, the last equation is extended, in a matrix form, to:

$$l = A\,x + v \quad (7)$$

where, A is the coefficients matrix, x is the vector of unknowns, v is the vector of un-modeled residual effects, and l is the vector of observations: l = h - H - N. The solution of equation 7 is obtained as:

$$x^{\wedge} = (A^T PA)^{-1}(A^T Pl) \quad (8)$$

where, *P* represents the weight matrix.

3. Available Data

SRI has initiated a research study aiming to develop a national high-precision geoid for Egypt for the first time. The Menofia governorate has been selected as the study area, that represents a guided primary area in which a prototype geoid will be modeled and, later, could be generalized for the entire Egyptian territories. The study has many objectives including:

- Evaluating the current status of the vertical geodetic (BM) network,
- Designing and establishing a new BM network, applying the international standards and specifications,
- GPS observing of the new BM networks in order to obtain the precise three-dimensional geodetic coordinates,
- Developing and evaluating a high-precision geometric geoid model utilizing the least-squares integrated adjustment technique of all available geodetic observations,
- Building a geospatial database of new geodetic stations using the Geographic Information Systems (GIS).

The study area extends over four urban centers of Menofia governorate; namely: Menouf, Ashmoun, Al-Bagoor, and Sers El-Layan (Fig. 3). Its area equals 700 square kilometers approximately. At the first stage of the study, a reconnaissance survey has been carried out. It has been found that only 12 BM (out of 85 BM) exist, which in other words means that the lost BM points constitute about 86%. A new BM network has been designed, established, and observed by the first-order spirit levelling technique fulfilling the international standards and specifications in terms of utilized equipments, field measurements, and field computational checks ad quality control measures. This network contains 47 new BM along with 11 old BM (Fig. 4). A number of 61 levelling lines have been observed in dual directions, forming 14 closed levelling loops. Dual-frequency GPS receivers have been utilized to observe 3D baselines connecting these BM. A total of 296 vectors have been determined, whose lengths vary between 1.3 km and 33.1 km with an average of 9.2 km. Table 2 summarizes the statistics of both levelling and GPS networks.

Table 2: Statistics of the New BM Network

	Number	Minimum (Km)	Maximum (Km)	Average (Km)
Levelling Lines	61	1.1	7.7	3.4
Levelling Loops	14	11.3	34.6	17.0
GPS Baselines	296	1.3	33.1	9.2

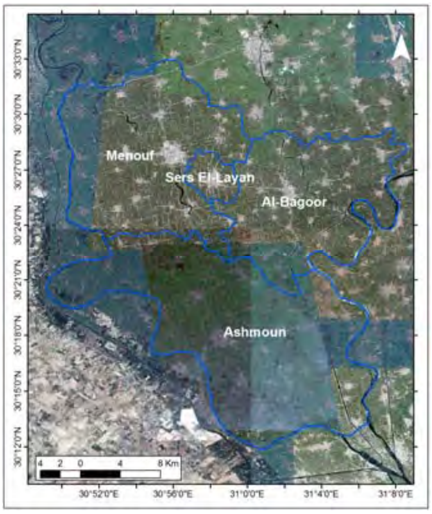

Fig. 3: The Study Area

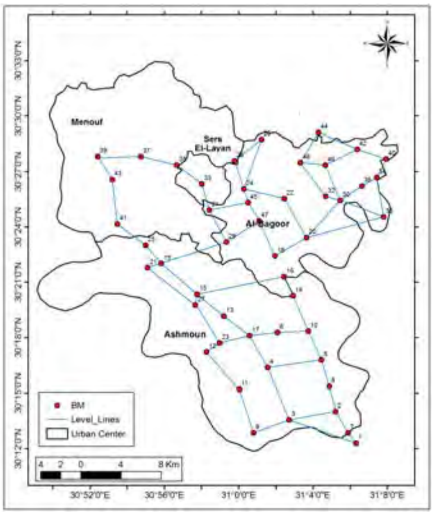

Fig. 4: The New Established BM Network

4. Results and Discussions

The first stage of the data processing concerns the analysis of the systematic errors influencing precise levelling measurements. The main sources of systematic effects are the gravity effect, the astronomical tide effect, and the refraction effect. The most significant error source is the gravity effect, which had not performed during the computations of the national vertical network of Egypt (Saad 1993). Since the determination of that systematic error requires the gravity value at each BM, the gravity field of the Egyptian National Gravity Standardization Network (ENGSN97) has been utilized to interpolate the gravity values at the established BM stations. It has been found that the gravity at the study area ranges from 979315.2 mGal to 979335.8 mGal (1 mGal = 1×10^{-5} m/s^2). Then, the gravimetric effect on levelling lines, known as the Orthometric correction, has been evaluated as:

$$OC_{AB} = \sum_{i=A}^{B-1} \frac{\bar{g}_{ij} - G}{G} dh_{ij} + \frac{\bar{g}_A - G}{G} H_A - \frac{\bar{g}_B - G}{G} H_B \qquad (9)$$

where, G represents the gravity at the mid-latitude of the country, dh_{ij} is the observed height difference between points 1 and j, g_{ij} is the average gravity between i and j, H_A and H_B are the elevations of A and B, g_A and g_B are the average gravity along the plumb line at A and B respectively.

Results show that the computed orthometric corrections vary from -0.81 mm to 0.88 mm, with a mean of 0.06 mm. Although such values are small, due to the short observed levelling lines, the orthometric correction is essential in computing the orthometric heights of BM (e.g. Mohamed, 2005).

A least-square adjustment program has been, then, utilized to adjust the entire levelling network. It should be mentioned that the vertical geodetic network of Egypt has been adjusted loop by loop, which affects its overall quality (e.g. Saad, 1993). The results of the least-square adjustment show that the standard deviations of the BM elevations range from ± 2 mm to ± 17 mm, with an average equals ± 9 mm. Therefore, it can be concluded that the established BM network satisfies the accuracy and standards of high-precision vertical geodetic network.

Regarding the GPS measurements, the Trimble Business Center (TBC) software has been utilized to process and adjust the observed GPS network. The attained findings reveal that the

standard deviations of the horizontal coordinates vary from ± 6 mm and ± 11 mm, with an average of ± 8 mm. The ellipsoidal heights' standard deviation have been found to range from ± 12 mm and ± 27 mm, with an average of ± 22 mm. Figure 5 depicts the precisions of the GPS networks over BM stations.

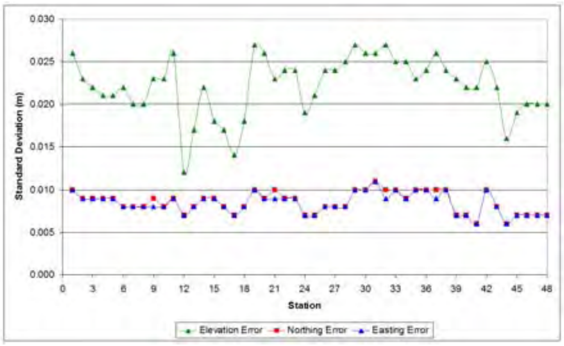

Fig. 5: The Standard Deviations of the GPS Network

Afterward, equation 6 has been performed to compute the geoid undulations at the 48 observed points. The computed geoidal heights range from 14.475 m to 15.092 m, with a mean of 14.753 m. Firstly, those values have been compared against the Earth Geopotential Model EGM2008-based undulations in order to judge the accuracy of this GGM at the study area. The estimated geoidal differences range from -0.143 m to 0.401 m, with an average of 0.271 m and a standard deviation equals ± 0.131 m (Table 3). Such findings emphasis the fact that the utilization of a GGM alone does not satisfy the required accuracy level for precise orthometric heights determination, and a local precise geoid model is a must in first-order surveying measurements.

Table 3: Statistics of the Estimated Different Heights at BM stations

	Minimum (m)	Maximum (m)	Average (m)
Ellipsoidal heights	26.809	35.020	29.880
Orthometric heights	12.122	20.063	15.075
EGM2008 geoidal heights	14.890	15.325	15.076
Observed geoidal heights	14.475	15.092	14.753
EGM2008 geoidal errors	-0.143	0.401	0.271

Finally, 7 out of the observed 48 GPS/levelling stations have been reserved as check points, and the Arc GIS software has been applied to develop a spatial geoid model over the study area. Next, the geoidal undulations have been interpolated at the check points and compared against their known values. It has been found that the differences range from -0.052 m to 0.049 m, with a mean of 0.0024 m and a standard deviation equals ± 0.038 m. Accordingly, it can be concluded that the developed geoid model in the study area (Fig. 6) has an accuracy level of almost four centimeters. Such a high-accuracy state-of-the-art geoid model is the first of its kind in Egypt.

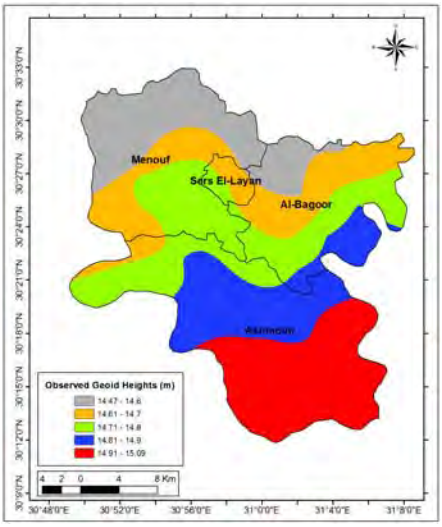

Fig. 6: The Developed Final Geoid Model

5. Conclusion and Future Work

Nowadays, satellite-based positioning technologies, particularly the Global Positioning System (GPS), have been extensively utilized in surveying and mapping activities in Egypt. One of the central factors in such applications is the difference between the GPS-based measured height (geodetic height) and that used in civil and surveying engineering projects (orthometric height). A geoid model, describing the spatial relationship between both height systems, is mandatory in order to efficiently utilize GPS in surveying projects. Although geoid modelling has been carried out by several researchers in Egypt, the accuracy level has not satisfied the requirements of precise surveying and mapping.

SRI has carried out a research study aiming to develop a national high-precision geoid for Egypt for the first time. The Menofia governorate has been selected as the study area, that represents a guided primary area in which a prototype geoid will be modeled and, later, be generalized for the entire Egyptian territories. It has been found that the lost BM points constitute about 86% in this area, due to urbanization and non-maintenance of the national vertical control network. Then, a new BM network has been established, that contains 47 new BM along with 11 old BM. A number of 61 levelling lines have been observed in dual directions, forming 14 closed levelling loops. Dual-frequency GPS receivers have been utilized to observe 3D baselines connecting these BM. The least-squares adjustment technique has been applied to adjust both control networks, and the attained results have been utilized in determining geoid undulation at all stations. These geoidal heights range from 14.475 m to 15.092 m, with a mean of 14.753 m. Comparing the observed undulations against the EGM2008-based corresponding values reveal that the utilization of any GGM alone does not satisfy the required accuracy level for precise orthometric heights determination. The Arc GIS software has been applied to develop a spatial geoid model over the study area. Validating this model over some observed check points reveals that it has an accuracy level of almost four centimeters. Therefore, it can be concluded that the attained state-of-the-art accurate geoid model is the first of its kind in Egypt.

Finally, it worth mentioning that a national accurate geoid model for Egypt has to be developed as a central component of the currently undergoing project for establishing a national spatial data infrastructure. Economically speaking, such a geoid model will reduce the costs of GPS surveying projects by a considerable amount compared to the traditional surveying techniques. It is a matter of reality that such a national geoid model will advance the surveying and mapping activities in Egypt.

6. References

Abdalla, A. and Green, C., 2016. Utilization of fast Fourier transform and least-squares modification of Stokes formula to compile a gravimetric geoid model over Khartoum State, Sudan, Arabian Journal of Geosciences, DOI 10.1007/s12517-015-2117-8

Abd-Elmotaal, H., 2008. Gravimetric geoid for Egypt using high-degree tailored reference geopotential model, NRIAG Journal of Geophysics special issue. pp. 507-531.

Al-Karagy, E., Doma, M., and Dawod, G., 2014. Towards an accurate discrimination of the local geoid model in Egypt using GPS/levelling data: A case study at Rosetta area, The International Journal of Innovative Science and Modern Engineering, V. 2, No. 11, pp.10-15.

Al-Krargy, E., Hosny, M. and Dawod, G., 2015. Investigating the precision of recent global geoid models and global digital elevation models for geoid modelling in Egypt, Regional Conference on Surveying and Development, Sharm El-Sheikh, Egypt, Oct. 3-6.

Alnaggar, D., 1986. Determination of the geoid in Egypt using heterogeneous geodetic data, PhD dissertation, Faculty of Engineering, Cairo University, Egypt.

Balodis, J., Silabriedis, G., Haritonova, D., Kaļinka, M., Janpaule, I., Morozova, K., Jumāre, I., Mitrofanovs, I., Zvirgzds, J., Kaminskis, J., and Liepiņs, I., 2015. Development of the one centimeter accuracy geoid model of Latvia for GNSS measurements, IOP Conference Series: Materials Science and Engineering, No. 96, DOI:10.1088/1757-899X/96/1/012037

Dawod, G., 1998. A national gravity standardization network for Egypt, PhD dissertation, Faculty of Engineering at Shoubra, Zagazig University, Egypt.

Dawod, G., Mohamed, H., and Ismail, S., 2010. Evaluation and adaptation of the EGM2008 geopotential model along the Northern Nile valley, Egypt: Case study, ASCE Journal of Surveying Engineering, V. 136, No. 1, pp. 36-40, Feb. 2010.

Eshagh, M. and Zoghi, S., 2016. Local error calibration of EGM08 geoid using GNSS/levelling data, Journal of Applied Geophysics, No. 130, pp. 209–217.

Fotopoulos, G., 2005. Calibration of geoid error models via a combined adjustment of ellipsoidal, orthometric and gravimetric geoid height data, Journal of Geodesy, No.79, pp. 111–123.

Heiskanen, W. and Moritz, H., 1967. Physical Geodesy, W.H. Freeman and Company, London.

Karaaslan, O., Kayikcr, E., and Asik, Y., 2016. Comparison of local geoid height surfaces in the province of Trabzon, Arabian Journal of Geosciences, DOI 10.1007/s12517-016-2470-2.

Kiamehr, R and Eshagh, M., 2008. Estimating variance components of ellipsoidal, orthometric and geoidal heights through the GPS/levelling Network in Iran, Journal of the Earth and Space Physics. V. 34, No. 3, pp. 1-13

Pahlevi, A., Pangastuti, D., Sofia, N., Kasendi, A., and Prijatna, K., 2015. Determination of gravimetric geoid model in Sulawesi, Indonesia, Presented in the FIG Working Week Conference, Sofia, Bulgaria, May 17-21.

Matsuo, K., Miyazaki, T., and Kuroishi, Y., 2016. Development of a new gravimetric geoid model for Japan, Presented at the FIG working week, New Zealand, May 2-6.

Rabah, M. and Kaloop, M., 2013. The use of minimum curvature surface technique in geoid computation processing of Egypt, Arabian Journal of Geosciences, N, 6, pp. 1263-1272.

Saad, A., 1993. Towards the redefinition of the Egyptian vertical control network, Ph.D. Dissertation, Shoubra Faculty of Engineering, Zagazig University, Cairo, Egypt.

Saad, A. and Dawod, G., 2002. A precise integrated GPS/gravity geoid model for Egypt, Civil Engineering Research Magazine, V. 24, No. 1, pp. 391-405.

SRI (Survey Research Institute), 2016. Developing a prototype geoid model for Egypt: A guided area in Menofia governorate, Unpublished technical report.

Ssengendo, R., Sjoberg, L, and Gidudu, A., 2015. Computation of the gravimetric quasigeoid model over Uganda using the KTH method, Presented in the FIG Working Week Conference, Sofia, Bulgaria, May 17-21.

تحديد أفضل المواقع لتجميع الطاقة الشمسية في منطقة مكة المكرمة الادارية باستخدام نظم المعلومات الجغرافية متعددة المعايير

جمعة محمد داود [١]، خالد بن عبد الرحمن الغامدي [٢]، مسعد سلامة مندور [٣]

[١] معهد بحوث المساحة، المركز القومى لبحوث المياه، القاهرة، جمهورية مصر العربية
dawod_gomaa@yahoo.com
[٢] قسم الجغرافيا، كلية العلوم الاجتماعية، جامعة أم القرى، مكة المكرمة، المملكة العربية السعودية
kaghamdi@uqu.edu.sa
[٣] قسم الجغرافيا، كلية الاداب، جامعة المنصورة، المنصورة، جمهورية مصر العربية
mosaad_3_70@hotmail.com

الملخص:

تعد الطاقة الشمسية أحد أهم مكونات الطاقة المتجددة التي تشكل مصدرا هاما من مصادر الطاقة النظيفة في العديد من المجالات خاصة تحلية المياه و توليد الكهرباء. ومع زيادة استهلاك الكهرباء في المملكة العربية السعودية بمعدل سنوي ٥% فقد تم اطلاق المبادرة الوطنية لإنتاج المياه و الكهرباء والتي تسعى للحصول علي ما يقارب ٤١ جيجا واط من الكهرباء بحلول عام ١٤٥٣ هـ. تهدف الدراسة الحالية الي تطبيق أسلوب نظم المعلومات الجغرافية متعددة المعايير لتحديد أنسب المواقع المكانية لتجميع الطاقة الشمسية في منطقة مكة المكرمة الادارية، اعتمادا على مجموعة من الشروط و المعايير المطلوبة سواء الجغرافية أو الفنية أو البيئية أو الاقتصادية للحصول علي نموذج ملائمة رقمي يوضح أفضل مواقع انشاء محطات الطاقة الشمسية. قامت الدراسة بتحديد المعايير المطلوبة طبقا للمواصفات العالمية و انشاء قاعدة بيانات جغرافية رقمية لهذه الاشتراطات ومن ثم دمج هذه الاشتراطات في نظام معلومات جغرافي متكامل بهدف الحصول علي نموذج الملائمة المكانية المطلوب. وتشير نتائج الدراسة الي أن كل منطقة مكة المكرمة مناسبة لمشروعات تجميع الطاقة الشمسية بنسب ملائمة تتراوح بين ٤٧% و ٩٧% وبمتوسط يبلغ ٨٠%، وتبلغ مساحة الأراضي التي تتميز بنسبة ملائمة أكبر من ٩٠% حوالي ٧ آلاف كيلومتر مربع بنسبة ٥% من اجمالي الاراضي المناسبة. و تتركز هذه الاراضي عالية الملائمة في محافظة مكة المكرمة بنسبة ٢٢% تليها محافظتى رابغ و خليص بنسبة ١٩% لكلا منهما ثم محافظة جدة بنسبة ١٣%. وتم عمل خريطة رقمية توضح التوزيع المكاني للأراضي الملائمة لمشروعات حصاد الطاقة الشمسية بمنطقة مكة المكرمة الادارية. وتوصي الدراسة بوضع النتائج التي تم الحصول عليها أمام متخذي القرار لتطبيقها في الخطة الوطنية لمصادر الطاقة المتجددة في المملكة العربية السعودية.

كلمات مفتاحيه: نظم المعلومات الجغرافية، أسلوب المعايير المتعددة، الطاقة الشمسية، منطقة مكة المكرمة الادارية.

Abstract:

Kingdom of Saudi Arabia (KSA) depends mainly on fossil fuels in electricity generation, desalination, and heating. With the growing electricity consumption, KSA has initiated an ambitious plan to increase the share of renewable energy sources, e.g. solar and wind, to reach 41 Giga Watt by year 2032. This study focuses on utilizing the Multi-Criteria Analysis (MCA) within a Geographic Information Systems (GIS) environment to locate optimum sites for solar energy projects within Makkah administrative area. Several physical and environmental spatial databases have been built up and an integrated GIS system has been developed. It has been found that the entire region is almost suitable for solar energy harvesting with varying suitability index. The suitability value range from 4.7 to 9.7, with an average equals 8.0 on a scale of 10. Moreover, areas of suitability index more than 90% have been identified, and found to have a total area of 7,000 square kilometers, which is a significant indicator about the potential of solar energy harvesting in Makkah. It is recommended that the developed suitability model being considered by decision makers in the future plans of energy development.

مقدمة:

تعد الكهرباء أحد أهم أسباب التطور و النمو السريع في جميع مجالات الحياة علي المستوى العالمي و في المملكة العربية السعودية في العقدين الأخيرين. ففي الفترة ما بين عام ١٩٩٠ م و ٢٠٠٩ م زادت قدرة التوليد الفعلية للكهرباء في المملكة من ١٥٢١٢ ميجا واط الى ٥١٣٠٢ ميجا واط بمعدل زيادة متوسطة تتعدي ٧% سنويا، كما زاد نصيب المشترك الواحد من ٢٣٩٢٨ كيلو واط/ساعة الي ٣٣٩٣٦ كيلو واط/ساعة في نفس الفترة الزمنية (وزارة المياه و الكهرباء ١٤٣١ هـ).

ان الطاقة الشمسية هي أحد مصادر الطاقة المتجددة التي يمكن استغلالها في أي مكان و تشكل مصدرا مجانيا لا ينضب لكافة الاحتياجات. ومن مميزات هذا النوع من الطاقة المتجددة أنه طاقة نظيفة لا ينتج عنها أية ملوثات للبيئة أو أية أضرار علي صحة البشر، كما أنها طاقة مجانية و متجددة ومن مصدر لا ينضب علي الاطلاق بخلاف أنواع الطاقة التقليدية المحدودة. ويمكن استخدام الطاقة الشمسية في العديد من المجالات التي تشمل تسخين و تحلية المياه والتدفئة و الانارة و معالجة مياه الصرف الصحي بالإضافة الي توليد الكهرباء. وفي العقدين الأخيرين زاد الاهتمام علي المستوي العالمي بتقنيات و أساليب و طرق تجميع الطاقة الشمسية و تحويلها الي كهرباء. وبلغ معدل النمو السنوي لإنتاج الطاقة الشمسية ٢٣% خلال الفترة من عام ١٩٨٠ حتى عام ٢٠٠١، بينما شهد انتاج الطاقة الشمسية نموا بقيمة ١٥% خلال عام ٢٠٠٧ فقط (غرفة الشرقية ٢٠١٠). وتجدر الاشارة الي أن التوسع في انتاج الكهرباء من الطاقة الشمسية قد ساهم في خفض أسعارها بنسبة ٤% سنويا في الخمسة عشرة الأخيرة (غرفة الشرقية ٢٠١٠). وتتمتع المنطقة العربية و الشرق الأوسط بصفة عامة بمعدلات عالية من الاشعاع الشمسي الذي يمكن تحويله الي طاقة شمسية، ومن ثم فقد اتجهت دول هذا المنطقة في الفترة الأخيرة الي تكثيف جهود التطوير و الابتكار و الاستثمار في الطاقة الشمسية (Darwish and Shaaban 2016). هذا وقد بدأ الاهتمام بالطاقة الشمسية في المملكة العربية السعودية منذ حوالي أربعة عقود عندما قام فريق فرنسي بتشغيل نظام ملاحي في مطار المدينة المنورة اعتمادا علي امداده بالطاقة المولدة من الخلايا الكهروضوئية، ثم بدأت مدينة الملك عبد العزيز للعلوم والتقنية في عام ١٩٧٧ بإدخال مجال الطاقة الشمسية ضمن أنشطتها البحثية (Hepbasli and Alsuhaibani, 2011). وتمثلت أهم الخطوات العلمية في عام ١٩٩٤ مع زيادة الاهتمام بالحاجة لإجراء قياسات دقيقة للإشعاع الشمسي في أنحاء المملكة ومن ثم تم اطلاق مشروع "أطلس الطاقة السعودي" بين كلا من معهد بحوث الطاقة بمدينة الملك عبد العزيز للعلوم و التقنية و المعهد الوطني الأمريكي لبحوث الطاقة. وفي عام ٢٠٠٨ أعرب وزير البترول السعودي عن سعي المملكة لتكون مركزا علميا رائدا في مجال الطاقة الشمسية وأن تستطيع أن تصدر الطاقة الشمسية في خلال ٣٠-٥٠ عاما (Hepbasli and Alsuhaibani, 2011).

يعد الوقود الأحفوري والغاز الطبيعي هما المصدرين الرئيسيين لتوليد الكهرباء و انتاج المياه المحلاة في المملكة في الوقت الراهن بنسبة ٦٥% و ٢٧% علي الترتيب (Nizami et al. 2015, and Tlili 2015). ومع المخزون الكبير للموارد الهيدروكربونية إلا الخطة المستقبلية الطموحة للطاقة في المملكة تسعى للوصول الي انتاج ٥٠% من احتياجات المملكة بحلول عام ٢٠٣٢ م من مصادر الطاقة المتجددة. ومن أهداف هذه الخطة الطموحة الوصول الي انتاج ٤١ جيجا واط من الطاقة الشمسية فقط و باستثمارات ضخمة للغاية (AlYahya and Irfan, 2016). ومن ثم فقد تم انشاء مدينة الملك عبد الله للطاقة الذرية و المتجددة في عام ١٤٣١ هـ بهدف بناء مستقبل مستدام للمملكة من خلال ادراج مصادر الطاقة الذرية و المتجددة ضمن منظومة الطاقة المحلية. وتشمل أنواع الطاقة المتجددة المنشودة كلا من (مدينة الملك عبد الله للطاقة الذرية و المتجددة ١٤٣٧ هـ):

- طاقة الرياح
- الطاقة المحولة من النفايات
- الطاقة الجوفية الحرارية
- الطاقة الشمسية وتشمل كلا من:
  - الطاقة الكهروضوئية
  - الطاقة الشمسية المركزة

وفي هذا الاطار أطلقت المدينة أطلس مصادر الطاقة المتجددة علي شبكة الانترنت (http://rratlas.kacare.gov.sa/RRMMPublicPortal/) والذي يعد مشروعا وطنيا رائدا لقياس مصادر الطاقة المتجددة علي مستوى المملكة بهدف بناء قاعدة بيانات يستفاد منها في تنفيذ مشاريع الطاقة المتجددة لإنتاج الكهرباء و تحلية المياه. كما أن الأطلس يهدف أيضا لتوفير البيانات المطلوبة للباحثين و الأكاديميين العاملين في مجال الطاقة للاستفادة منها في تطوير التقنيات و الحلول المناسبة لأجواء المملكة و مناخها المختلف في مناطقها المتعددة.

تجدر الاشارة الي أن بعض الدراسات في المملكة قد أشارت الي أن تكلفة انتاج الكهرباء من الطاقة الشمسية تقل عن تكلفتها من انتاج البترول اذا ما تم الأخذ في الاعتبار القيمة الاقتصادية للمخاطر البيئية و الصحية لاستخدام البترول (Almsoud and Gandayh, 2015). كما أن استخدام مركب من أكثر من مصدر من مصادر الطاقة المتجددة قد يكون أفضل و أوفر اقتصاديا في المملكة (Eltamaly et al., 2014). أما علي المستوي الاقليمي فقد بدأت دول مجلس التعاون الخليجي كلها في السنوات الأخيرة الي الاستثمار في مصادر الطاقة المتجددة وخاصة الطاقة الشمسية (Bhutto et al. 2014). فعلي سبيل المثال فقد حددت الكويت أنها تستهدف الحصول علي ١٥%، من احتياجاتها بحلول عام ٢٠٢٠ من الطاقة الشمسية، بينما بلغت نسبة هذا الهدف في سلطنة عمان ١٠% و في مملكة البحرين ٥% و في دولة قطر ٢% (Darwish and Shaaban 2016).

وعلي الجانب التقني فأن نظم المعلومات الجغرافية (GIS) هي الوعاء المثالي لجمع و تخزين و معالجة و تحليل و عرض البيانات المكانية و غير المكانية لاستنباط حلول تقنية لقضايا متعددة المجالات. وفي المملكة العربية السعودية يعد الزهراني (١٤١٢ هـ) أول من تناول هذا العلم المكانى داعيا لتطبيقه والاستفادة من مميزاته الهائلة في المملكة. و تهدف طريقة نظم المعلومات الجغرافية متعددة المعايير الي دراسة امكانية توافر عدد من المعايير الطبيعية و الاقتصادية و البيئية في بقعة مكانية محددة ومن ثم التوصل الي مجموعة من البدائل أو الحلول التي توضع أمام متخذى القرار. ولا يقتصر تطبيق هذا الأسلوب علي نطاق محدد من المجالات بل أنه استخدم في تحديد أفضل المواقع لعدة أهداف منها: الطاقة المتجددة (Cradden et al. 2016) ، تخطيط استخدامات الأرض (Colantoni et al. 2016)، الحصاد المائي (Inamdar et al. 2013)، محطات معالجة مياه الصرف الصحي (Pradhan and Samanta 2015)، محطات الطاقة النووية (Abudeif et al. 2015)، التوسع الزراعي (Saleh et al. 2015)، محطات معالجة النفايات الصلبة (Hassaan 2015)، و تدفئة المياه (Kaiser and Ahmed 2013). وفي المملكة العربية السعودية فقد تم تطبيق هذا الأسلوب في عدة مجالات، فعلي سبيل المثال قامت الدعدي (١٤٣٥ هـ) بتطبيق هذه الطريقة في اختيار أفضل المواقع لإنشاء سدود حصاد مياه الأمطار و السيول في منطقة القصيم. أيضا استخدمت الرحيلي (١٤٣١ هـ) هذا الأسلوب في اختيار أنسب مواقع دفن النفايات في المدينة المنورة. كما طبق (Dawod 2013) أسلوب تعدد المعايير في تحديد أفضل مواقع اقامة المنشئات السياحية بمنطقة الهدا شرق مكة المكرمة. أما دراسة (Zaidi et al. 2015) فقد طبقت طريقة المعايير المتعددة في تحديد أفضل مناطق اعادة شحن خزان المياه الجوفية في المنطقة الشمالية الغربية من المملكة. تتعلق الدراسة الحالية بتطبيق أسلوب نظم المعلومات الجغرافية متعددة المعايير في تحديد أنسب المواقع المكانية لإقامة مشروعات تجميع الطاقة الشمسية في منطقة مكة المكرمة الادارية بالمملكة العربية السعودية.

تمثل مواقع مشروعات الطاقة الشمسية أمرا بالغ الأهمية في كفاءة الطاقة المولدة و سعرها بالإضافة الي التأثيرات البيئية لهذه المشروعات. وفي هذا الاطار فقد أثبت أسلوب نظم المعلومات الجغرافية متعددة المعايير كفاءة كبيرة كنظام لمساعدة متخذي القرار من خلال تحديد أفضل مواقع تجميع الطاقة الشمسية. قام (Castillo et al. 2016) بتقييم امكانيات تجميع الطاقة الشمسية في دول الاتحاد الأوروبي باستخدام أسلوب نظم المعلومات الجغرافية متعددة المعايير. بينما قام كلا من (Wanerer and Herle 2015) بتطوير موقع علي شبكة الانترنت لدراسة أفضل مواقع تجميع الطاقة الشمسية في أسبانيا بناءا علي التحليل متعدد المعايير. كذلك طبق كلا من Dawod and Mandoer (2016), و Matejicek (2015) و Tahri et al. (2015) أسلوب المعايير المتعددة لتحديد أنسب مواقع تجميع الطاقة الشمسية في كلا من جمهورية مصر العربية و جمهورية التشيك و المملكة المغربية علي الترتيب.

المنهجية و منطقة الدراسة:

يهدف أسلوب المعايير المتعددة الي دراسة مدى توافر مجموعة من الشروط أو المعايير في منطقة مكانية محددة وتوفير عدة اختيارات أو بدائل أمام متخذى القرار. وعادة ما يتم تطبيق هذا الأسلوب في بيئة نظم المعلومات الجغرافية لما توفره من امكانيات تحليل و معالجة البيانات و أيضا عرض النتائج من خلال عدة وسائل بصرية. وهناك ثلاثة طرق لتطبيق المعايير المتعددة وهي: التراكب overlay، و طريقة التحليل التسلسلي الهرمى Analytic Hierarchy Process، و طريقة التركيب الخطي الموزون weighted linear combination. تعتمد الطريقة الاولي علي فكرة ايجاد منطقة التداخل بين مجموعة من الطبقات (التي تمثل كل طبقة منهم معيارا معينا) بهدف الوصول الي المناطق المكانية التي تتحقق فيها كل هذه المعايير أو الشروط. أما طريقة التحليل التسلسلي الهرمي فتتكون من عدة خطوات تشمل حساب مجموعة النقاط لكل معيار و حساب وزن كل معيار وتحديد أولويات المعايير ومن ثم الوصول الي تحديد أنسب البدائل (Castillo et al. 2016, and Abudeif et al. 2015). وعلي الجانب الآخر فأن طريقة التركيب الخطي الموزون (المستخدمة في هذه الدراسة) مبنية علي مبدأ حساب المتوسط الموزون لمجموعة من المعايير في كل خلية للوصول الي نموذج ملائمة طبقا للمعادلة:

$$S = \sum_{i=1}^{n} w_i x_i / \sum w \qquad (١)$$

حيث:

S معامل الملائمة،

w_i الوزن لكل معيار،

x_i معامل المعيار رقم i،

n عدد المعايير المطبقة.

تقع منطقة مكة المكرمة الادارية في وسط القطاع الغربي من المملكة العربية السعودية حيث تشمل مساحة شاسعة تمتد بين دائرتي عرض ١٩° و ٢٤° شمالا و خطي طول ٣٩° و ٤٤° شرقا (شكل رقم ١). وتتكون المنطقة من ١١ محافظة بخلاف امارة المنطقة وتأتي في الترتيب الرابع من بين مناطق المملكة من حيث المساحة الجغرافية حيث تبلغ مساحتها نحو ١٤٠.١ ألف كيلومتر مربع وهو ما يعادل ٦.٤ من اجمالي مساحة المملكة (إمارة منطقة مكة المكرمة ١٤٣٣ هـ). وتعد منطقة مكة المكرمة أكبر مناطق المملكة من حيث عدد السكان و تضم ما يزيد عن ربع سكان المملكة حيث اقترب عدد سكانها من سبعة ملايين نسمة طبقا للتعداد العام للسكان و المساكن في عام ١٤٣١ هـ. ومن المتوقع أن يرتفع هذا العدد ليبلغ ٩.٧ مليون نسمة بحلول عام ٢٠٢٥ م (مصلحة الاحصاءات العامة و المعلومات ١٤٣٧ هـ).

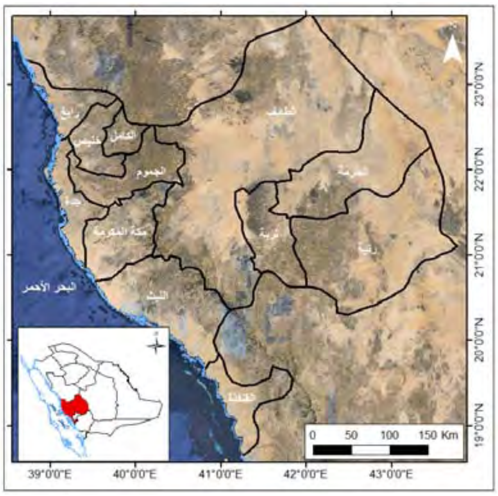

شكل رقم (١): منطقة مكة المكرمة الادارية

اعتمدت الدراسة علي عدة مصادر للحصول علي البيانات الأولية المطلوبة و تحويلها الي صورة رقمية في اطار نظم المعلومات الجغرافية و من ثم انشاء قواعد البيانات اللازمة (شكل رقم ٢). وتمثلت البيانات الأولية في نموذج ارتفاعات رقمي عالمي من نوع SRTM 3 وعدد من الخرائط الطبوغرافية و المرئيات الفضائية الحديثة بالإضافة الي بيانات الاشعاع الشمسي و خريطة توزيع شبكة الكهرباء و اللذان تم الحصول عليها من أطلس مصادر الطاقة المتجددة.

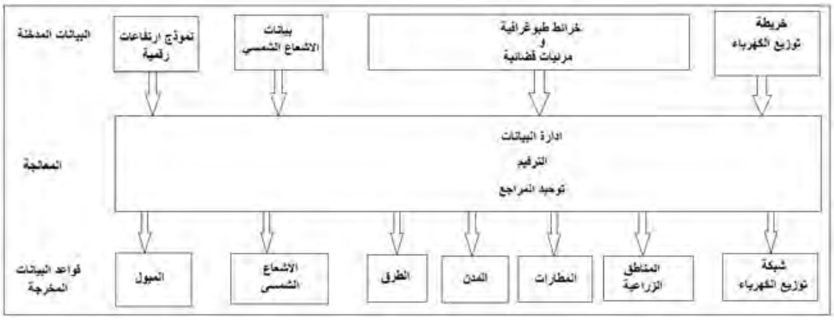

شكل رقم (٢): منهجية اعداد قواعد البيانات المستخدمة

باستخدام نموذج الارتفاعات الرقمية العالمي SRTM 3 تبين أن مناسيب سطح الأرض في منطقة مكة المكرمة الادارية تتراوح بين -٩ متر و ٢٥٨٦ متر بمتوسط يبلغ ٨٤٣ متر (شكل رقم ٣). ومن أمثلة جبال المنطقة جبل الحدب في ميسان بلحارث و هو الأعلى ارتفاعا (٢٥٠٠ متر تقريبا فوق سطح البحر) و جبل المصطبة في الدار الحمراء (٢٤٠٠ متر) و جبل دكا في الشفا جنوب الطائف (٢٤٠٠ متر) و جبل كرا في الهدا الي الغرب من الطائف (٢١٧٧ متر) وجبل طويرق (١٨٦٣ متر). كما تتميز تضاريس سطح الأرض في منطقة مكة المكرمة الادارية بوجود مجموعة من الهضاب التي تمتد مع امتداد جبال السروات - الحجاز من الشمال الغربي الي الجنوب الشرقي ومنها هضبة شرق السروات الممتدة من حدود منطقة الباحة جنوبا و حتى مدينة الطائف شمالا و هضبة سهل ركبة الممتدة لحوالي ٢٠٠ كيلومتر شمال-جنوب و حوالي ٤٠٠ كيلومتر نحو الشمال الشرقي. كما تشمل طبوغرافية المنطقة مجموعة من السهول الساحلية علي شكل نطاق يوازي ساحل البحر الأحمر و باتساع يتراوح ما بين ١٥ و ٢٥ كيلومتر (هيئة تطوير مكة المكرمة و المشاعر المقدسة، ١٤٢٧ هـ).

كذلك قامت الدراسة الحالية بتطبيق أداة حساب الميول في برنامج نظم المعلومات الجغرافية Arc GIS 10 للحصول علي سطح شبكي يمثل ميول الأرض في منطقة الدراسة، حيث تبين أن الميول تتراوح ما بين الصفر و ٢٨.٥ درجة بمتوسط يبلغ ١.١ درجة (شكل رقم ٤).

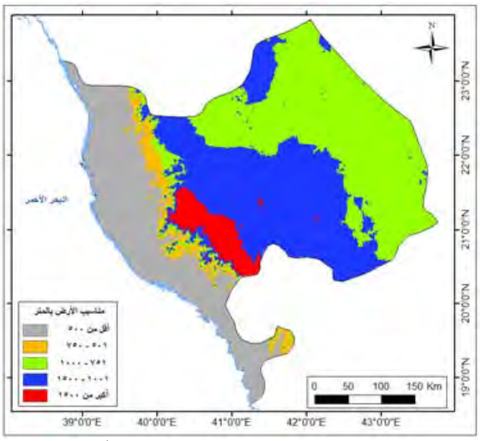

شكل رقم (٣): مناسيب سطح الأرض في منطقة مكة المكرمة

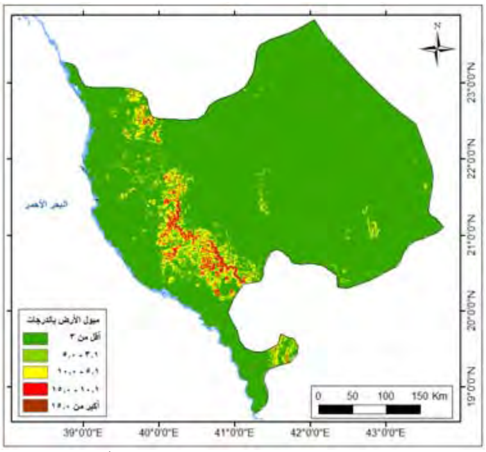

شكل رقم (٤): ميول سطح الأرض في منطقة مكة المكرمة

أيضا تم استخدام مجموعة الخرائط الطبوغرافية و المرئيات الفضائية المتعددة في ترقيم عدة طبقات خطية تمثل مواقع المدن الرئيسية و المطارات في منطقة مكة المكرمة الادارية (شكل رقم ٥) و شبكتي الطرق الرئيسية و خطوط توزيع الكهرباء (شكل رقم ٦). وأشارت النتائج الي أن مجموع أطوال شبكة الطرق الرئيسية بمنطقة مكة المكرمة يبلغ حوالي سبعة آلاف كيلومتر، بينما يبلغ مجموع أطوال شبكة توزيع الكهرباء الرئيسية حوالي تسعمائة كيلومتر. كذلك بلغ مجموع أطوال شبكة الأودية و المجاري المائية ما يزيد عن ٢٩ ألف كيلومتر.

شكل رقم (٥): المدن الرئيسية و المطارات في مكة المكرمة الادارية

شكل رقم (٦): شبكتي الطرق و توزيع الكهرباء في منطقة مكة المكرمة

بترقيم بيانات الاشعاع الشمسي التي تم الحصول عليها من أطلس مصادر الطاقة المتجددة تبين أن المتوسط السنوي للإشعاع الشمسي في منطقة مكة المكرمة الادارية يتراوح بين ٤.٧٥ كيلو وات/متر مربع/يوم و ٦.٧٥ كيلو وات/متر مربع/يوم بمتوسط يبلغ ٦.٠ كيلو وات/متر مربع/يوم. ويشير الشكل رقم ٧ الي أن الاشعاع الشمسي يبلغ قيمه العظمي في الشريحة المتوسطة من المنطقة وخاصة في بعض مرتفعات محافظة الطائف.

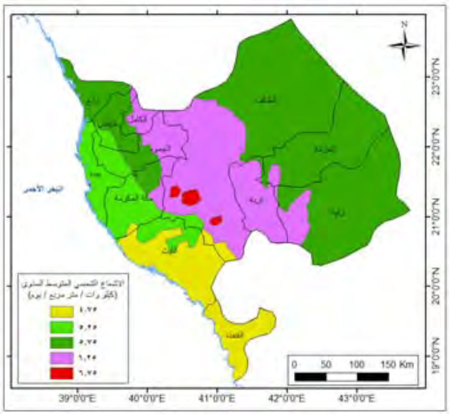

شكل رقم (٧): المتوسط السنوى للإشعاع الشمسي في منطقة مكة المكرمة

معالجة البيانات:

تمثلت أولي خطوات معالجة البيانات في التوصل الي مجموعة المعايير المطلوب توافرها في أنسب المواقع المكانية لمشروعات تجميع الطاقة الشمسية. وفي هذا الاطار تم تجميع عدد من الدراسات و البحوث العالمية المتعلقة بذات الموضوع ودراسة المعايير المطبقة في كل دراسة للتوصل الي أدق المعايير التي تؤدي لكفاءة هذه المواقع المكانية في اقامة مشروعات تجميع الطاقة الشمسية بها (Castillo et al. 2016, Watson and Hudson 2015, Recannatesi et al. 2014, Aydin et al. 2013, Sanchez-Lozano et al. 2013, and Uyan 2013). وتعد قيمة الاشعاع الشمسي التي تصل الي سطح الأرض هي المعيار الأول في تجميع الطاقة الشمسية، ثم يأتي بعده معيار ميول سطح الأرض الذي يؤثر علي تجهيزات و تركيب الأجهزة اللازمة لهذه المشروعات. أيضا فأن البعد عن شبكة توزيع الكهرباء يعد عاملا هاما حيث كلما زادت هذه المسافة كلما زادت كمية الطاقة المفقودة أثناء عملية النقل وأيضا زادت تكلفة نقل الطاقة. أما من الناحية البيئية فأن البعد من المدن الرئيسية و المطارات والطرق و الشواطئ تعد أيضا عوامل هامة في اختيار أنسب مواقع مشروعات الطاقة الشمسية. ومن ثم فقد تم اختيار سبعة معايير فنية و اقتصادية (الجدول رقم ١) يجب توافرها في أنسب مواقع مشروعات الطاقة الشمسية بالإضافة الي تحديد قيدين لتجنب اقامة هذه المشروعات داخل التجمعات العمرانية أو علي أراضي زراعية. أيضا تم تحديد الأوزان النسبية لكل معيار من هذه المعايير كما هو موضح في العمود الأخير من الجدول التالي. وتكونت خطوات معالجة البيانات (شكل رقم ٨) من اشتقاق طبقة شبكية لكل معيار من المعايير المحددة تمثل تصنيف قيم المعيار الي فئات ثم اعادة التصنيف الي درجات علي مقياس يتراوح من ١ الي ١٠ لسهولة العرض و التحليل، ثم تطبيق الأوزان المحددة (المعادلة رقم ١) للوصول الي نموذج الملائمة النهائي. وتعرض الأشكال أرقام ٩، ١٠، ١١ نماذج لطبقات تصنيف المعايير التي تم استنباطها بالنسبة للبعد عن كلا من المدن الرئيسية و شبكة الكهرباء و شبكة الطرق الرئيسية.

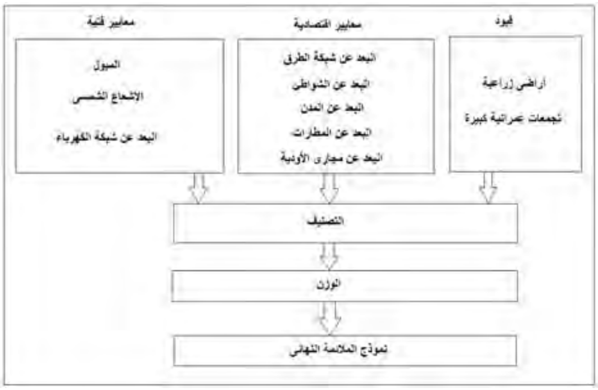

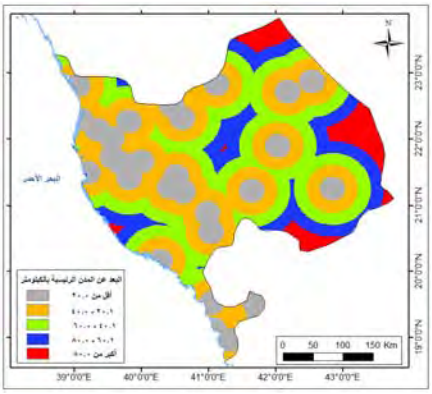

شكل رقم (٨): منهجية استنباط نموذج الملائمة **شكل رقم (٩): البعد عن المدن الرئيسية**

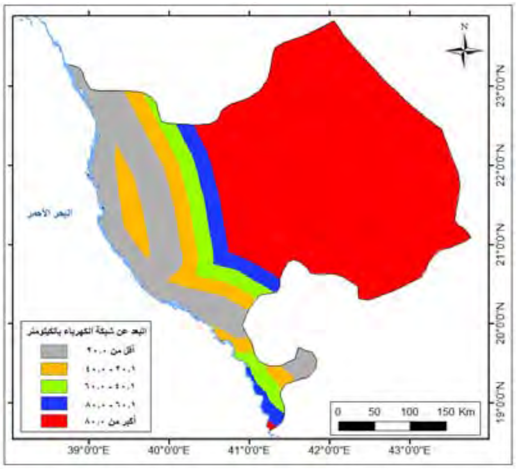

شكل رقم (١٠): البعد عن شبكة الكهرباء

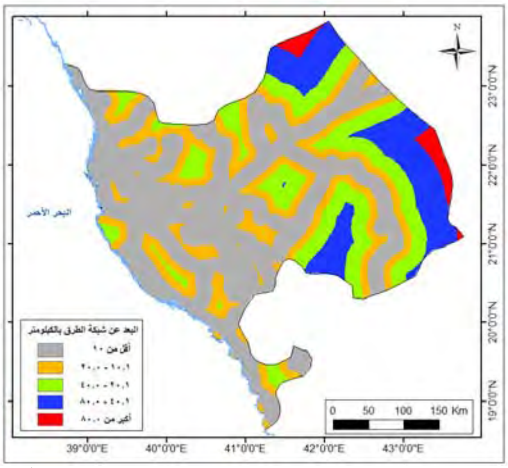

شكل رقم (١١): البعد عن الطرق الرئيسية

جدول رقم (١): معايير أنسب مواقع تجميع الطاقة الشمسية

نوع المعيار	المعيار	الفئات	الملائمة	الوزن
تقني	الاشعاع الشمسي (كيلو وات/متر مربع/يوم)	< ٨ ٦ - ٨ ٤.٥ - ٦ > ٤.٥	عالية متوسطة قليلة غير ملائمة	٠.٣٠
	ميل سطح الأرض (درجة)	٠ - ٣ ٣ - ٥ ٥ - ١٠ < ١٠	عالية متوسطة قليلة غير ملائمة	٠.١٥
	البعد عن شبكة توزيع الكهرباء (كم)	٠ - ٥ ٥ - ١٠ ١٠ - ٢٠ < ٢٠	عالية متوسطة قليلة غير ملائمة	٠.١٥
اقتصادي/بيئي	البعد عن شبكة الطرق (كم)	> ٥ < ٥	ملائم غير ملائم	٠.١٠
	البعد عن الشواطئ (كم)	< ٥ > ٥	ملائم غير ملائم	٠.١٠
	البعد عن المدن (كم)	< ٥ > ٥	ملائم غير ملائم	٠.١٠
	البعد عن المطارات (كم)	< ٣ > ٣	ملائم غير ملائم	٠.١٠
قيود	حدود التجمعات العمرانية	-	غير ملائم	-
	الأراضي الزراعية	-		

النتائج و المناقشة:

تم تحويل طبقات قيم كل معيار من المعايير الي طبقات تمثل مدي الملائمة المكانية لكل معيار منفردا، أي أنه تم التوصل الي عدة نماذج ملائمة أولية. فعلي سبيل المثال يعرض الشكل رقم (١٢) نموذج الملائمة المكانية لمعيار البعد عن شبكة توزيع الكهرباء، حيث نلاحظ أن المواقع عالية الملائمة هي التي لا تبعد بأكثر من ٥ كيلومترات عن خطوط توزيع هذه الشبكة. ويدل الشكل أيضا الي أن هذه المواقع الملائمة لهذا المعيار تتركز فقط علي الجزء الغربي من منطقة الدراسة و القريب من ساحل البحر الأحمر. أما نموذج الملائمة المبدئي لمعيار البعد عن الطرق الرئيسية (شكل رقم ١٣) فيظهر

مواقع مكانية أكثر حيث أن شبكة الطرق تمتد تقريبا في كامل أرجاء المنطقة الادارية. أما بالنسبة لميول سطح الأرض فقد أظهر نموذج الملائمة المبدئي لهذا المعيار (شكل رقم ١٤) أن معظم أنحاء المنطقة الادارية لها درجات ملائمة جيدة ما عدا الشريحة الوسطي من المنطقة التي لها ميول كبيرة و من ثم كانت درجات الملائمة عندها متوسطة و أحيانا ضعيفة في قمم المرتفعات.

يمثل الشكل رقم (١٥) أماكن القيود التي لا يجب أن يتم عندها اقامة مشروعات تجميع الطاقة الشمسية وهي حدود التجمعات العمرانية و الاراضي الزراعية. ومن ثم فقد تم تطبيق هذه القيود أثناء عملية اشتقاق نموذج الملائمة النهائي الممثل في الشكل رقم ١٦.

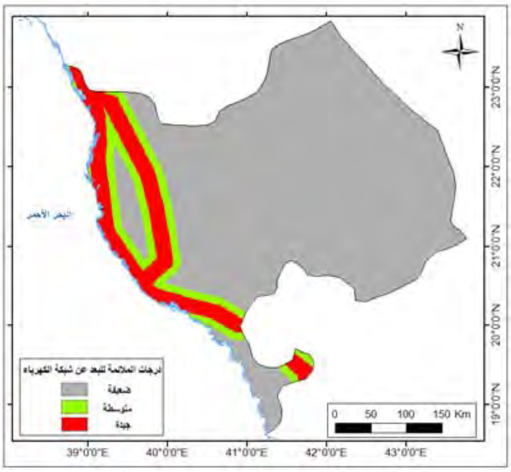

شكل رقم (١٢): درجات الملائمة لمعيار البعد عن شبكة الكهرباء

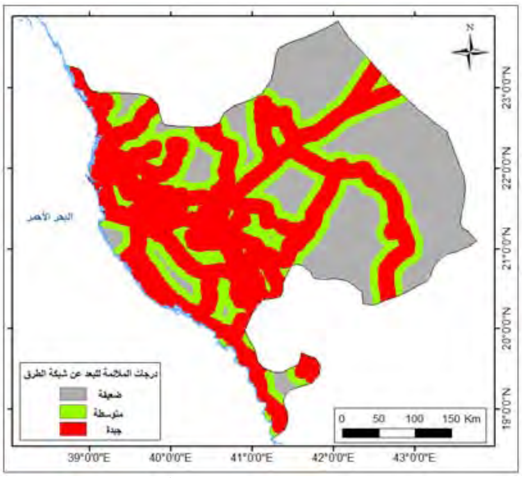

شكل رقم (١٣): درجات الملائمة لمعيار البعد عن شبكة الطرق

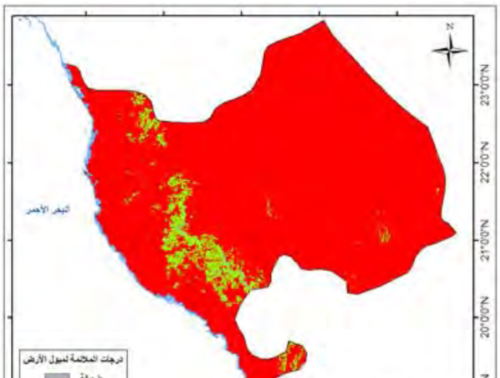

شكل رقم (١٤): درجات الملائمة لمعيار ميول الأرض

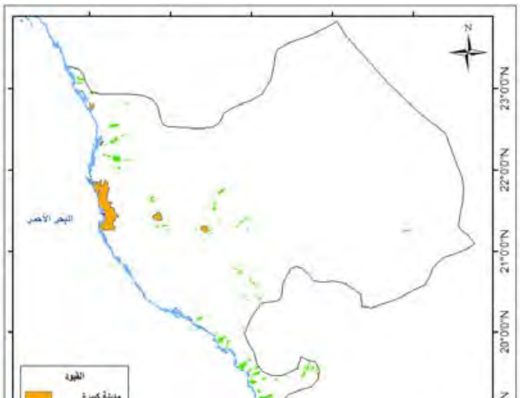

شكل رقم (١٥): القيود المكانية المفروضة علي نموذج الملائمة

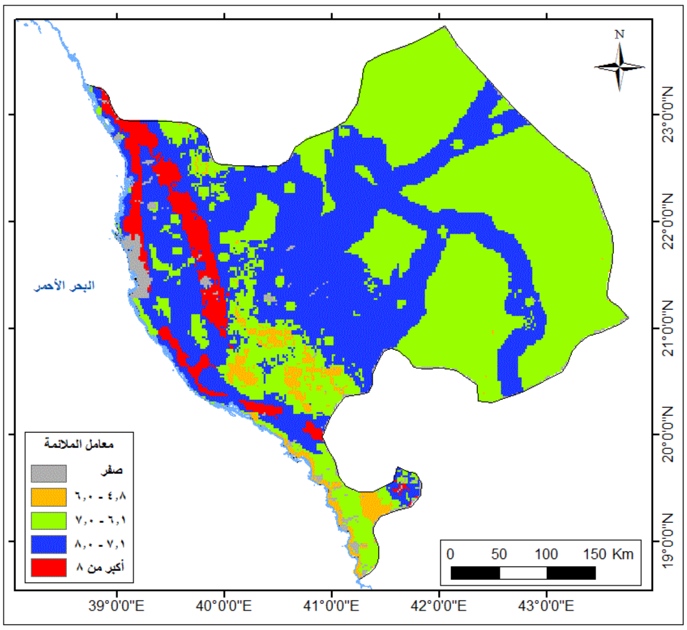

شكل رقم (١٦): نموذج الملائمة النهائي لمواقع حصاد الطاقة الشمسية

تشير نتائج نموذج الملائمة النهائي الي أن كل منطقة مكة المكرمة مناسبة لمشروعات تجميع الطاقة الشمسية بنسب ملائمة تتراوح بين ٤٧% و ٩٧% وبمتوسط يبلغ ٨٠%. وهذه النتائج واعدة و مبشرة لقطاع الطاقة المتجددة في منطقة مكة المكرمة ويجب أخذها في الاعتبار. وبالتحليل الدقيق لهذه المواقع المكانية و درجة ملائمتها تبين أن الأراضي التي تتميز بنسبة ملائمة أكبر من ٩٠% تبلغ مساحتها حوالي ٧ آلاف كيلومتر مربع بنسبة ٥% من اجمالي الاراضي المناسبة (شكل رقم ١٧). ويبين الجدول رقم (٢) والشكل رقم (١٨) توزيع هذه المناطق عالية الملائمة علي محافظات منطقة مكة المكرمة الادارية، حيث تأتي محافظة مكة المكرمة في المركز الأول بنسبة ٢٢% من اجمالي مساحة هذه المناطق تليها محافظتي خليص و رابغ بنسبة ١٩% لكلا منهما. وعلي الجانب الآخر فأن محافظات رنية، تربة، الخرمة، الطائف ليس بها أية مناطق بدرجة ملائمة أكبر من ٩٠%.

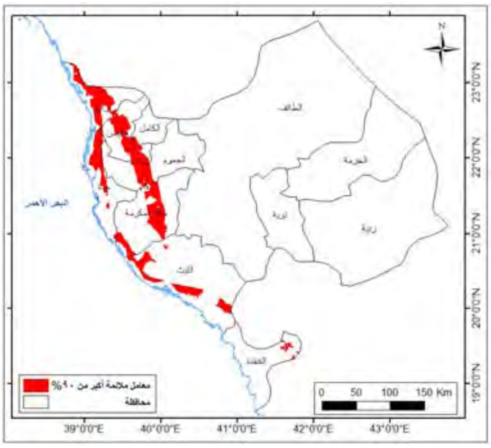

شكل رقم (١٧): مواقع ذات معامل ملائمة أكبر من ٩٠%

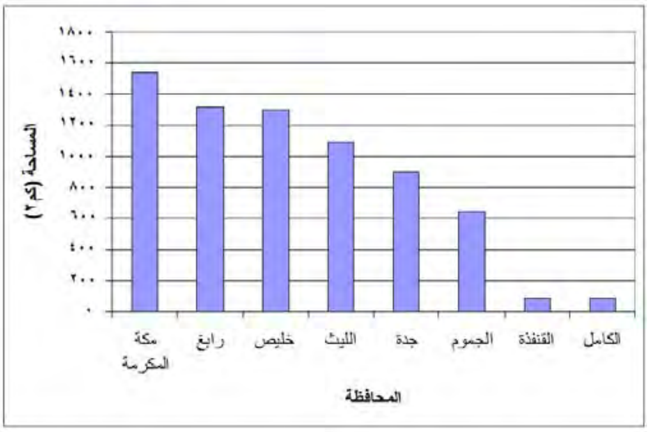

شكل رقم (١٨): احصائيات المواقع ذات معامل ملائمة أكبر من ٩٠%

جدول رقم (٢): توزيع المواقع ذات معامل ملائمة أكبر من ٨٠% علي المحافظات

المحافظة	المساحة (كيلومتر مربع)	النسبة المئوية
مكة المكرمة	١٥٤٠	٢٢ %
خليص	١٢٩٧	١٩ %
رابغ	١٣١٨	١٩ %
الليث	١٠٩٥	١٦ %
جدة	٩٠٢	١٣ %
الجموم	٦٣٩	٩ %
الكامل	٨٥	١ %
القنفذة	٨٣	١ %
رنية - تربة - الخرمة - الطائف	٠	٠
المجموع	٦٩٥٩	١٠٠ %

الخلاصة و التوصيات:

تعد الطاقة قوة أساسية مؤثرة علي كافة مناحى الحياة سواء الاقتصادية أو الاجتماعية أو البيئية، ومن ثم فأن استخدام مصادر الطاقة المتجددة وخاصة الطاقة الشمسية أضحت قضية هامة علي المستوي العالمي. ركزت الدراسة الحالية علي تطبيق أسلوب نظم المعلومات الجغرافية متعددة المعايير في تحديد أنسب المواقع الملائمة لإقامة مشروعات تجميع الطاقة الشمسية في منطقة مكة المكرمة الادارية. وبناءا علي عدد من المعايير الفنية و الاقتصادية و البيئية تم بناء مجموعة من قواعد البيانات المكانية لمنطقة الدراسة ثم استخدمت في استنباط نموذج الملائمة الرقمي. وأشارت النتائج التي تم الحصول عليها الي أن معظم أنحاء منطقة مكة المكرمة الادارية مناسبة لإقامة مشروعات تجميع الطاقة الشمسية و ان كانت بدرجات ملائمة مختلفة تتراوح ما بين ٤٧% و ٩٧% وبمتوسط يبلغ ٨٠%. وبإجراء تحليلات مكانية تفصيلية تبين أن هناك ما يقرب من ٧ آلاف كيلومتر مربع من أراضي المنطقة يبلغ معامل الملائمة فيها أكثر من ٩٠%، حيث تأتي علي محافظة مكة المكرمة في المركز الأول بنسبة ٢٢% من اجمالي مساحة هذه المناطق تليها محافظتي خليص و رابغ بنسبة ١٩% لكلا منهما. وتوصي الدراسة بوضع نموذج الملائمة الذي تم تطويره أمام متخذي القرار لأخذه في الاعتبار في الخطط المستقبلية لمشروعات الطاقة الجديدة في منطقة مكة المكرمة. كما توصي الدراسة أيضا بتعميم أسلوب نظم المعلومات الجغرافية متعددة المعايير في كافة خطط التنمية في قطاع الطاقة في المملكة العربية السعودية.

المراجع:

المراجع العربية:

إمارة منطقة مكة المكرمة (١٤٣٣ هـ) المخطط الاقليمي لمنطقة مكة المكرمة: تفعيل المخطط الاقليمي و الخطة العشرية، تقرير لإمارة منطقة مكة المكرمة، المملكة العربية السعودية.

أطلس مصادر الطاقة المتجددة (١٤٣٧ هـ) http://rratlas.kacare.gov.sa/RRMMPublicPortal/ ، تاريخ الدخول: أكتوبر ٢٠١٦.

الدعدي، ماجدة بنت عبد الله (١٤٣٥ هـ) استخدام تقنية الاستشعار عن بعد و نظم المعلومات الجغرافية لدراسة الحصاد المائي لمياه السيول في منطقة القصيم، رسالة ماجستير، قسم الجغرافيا، جامعة أم القرى، مكة المكرمة، المملكة العربية السعودية.

الرحيلي، عهود بنت عائض (١٤٣١ هـ) استخدام نظم المعلومات الجغرافية في تحديد أنسب مواقع دفن النفايات بالمدينة المنورة ، رسالة ماجستير، قسم الجغرافيا، جامعة أم القرى، مكة المكرمة.

الزهرانى، رمزى بن أحمد (١٤١٢ هـ) نظم المعلومات الجغرافية: مكوناتها و بعض استعمالاتها، سلسلة بحوث العلوم الاجتماعية رقم ١٧، معهد البحوث العلمية و احياء التراث الاسلامي، جامعة أم القرى، مكة المكرمة، المملكة العربية السعودية.

غرفة الشرقية (٢٠١٠) اقتصاديات الطاقة الشمسية في المملكة العربية السعودية، تقرير لمركز الدراسات و البحوث بغرفة الشرقية، المنطقة الشرقية، المملكة العربية السعودية.

وزارة المياه و الكهرباء (١٤٣١ هـ) الكهرباء في المملكة العربية السعودية: نموها و تطورها، تقرير من مركز المعلومات و الاحصاء بوكالة الوزارة للتخطيط و التطوير، المملكة العربية السعودية.

مدينة الملك عبد الله للطاقة الذرية و المتجددة (١٤٣٧ هـ) الطاقة المتجددة، https://www.kacare.gov.sa/ar/futureenergy/renewableenergy/ ، تاريخ الدخول: أكتوبر ٢٠١٦.
مصلحة الاحصاءات العامة و المعلومات (١٤٣٧ هـ) تقديرات السكان للمناطق الادارية و المحافظات خلال الفترة من ٢٠١٠ الي ٢٠٢٥، http://www.cdsi.gov.sa/socandpub/resd ، تاريخ الدخول: أكتوبر ٢٠١٦.
هيئة تطوير مكة المكرمة و المشاعر المقدسة (١٤٢٧ هـ) المخطط الاقليمي لمنطقة مكة المكرمة، الجزء الثاني: المعلومات الأساسية و الأوضاع الراهنة، مكة المكرمة، المملكة العربية السعودية.

المراجع الانجليزية:

Abudeif, A., Abdel Moneim, A., and Farrag, A. (2015) Multicriteria decision analysis based on analytic hierarchy process in GIS environment for siting nuclear power plant in Egypt, Annals of nuclear energy, No. 75, pp. 682–692.
Almsoud, A. and Gandayh, H. (2015) Future of solar energy in Saudi Arabia, Journal of King Saud University – Engineering Sciences, No. 27, pp. 153–157.
Altamaly, A., Addoweesh, K., Bawa, U., and Mohamed, M. (2014) Economic modeling of hybrid renewable energy system: A case study in Saudi Arabia, Arabian Journal of Sciences and Engineering, No. 39, pp. 3827–3839.
AlYahya, S. and Irfan, M. (2016) The techno-economic potential of Saudi Arabia's solar industry, Renewable and Sustainable Energy Reviews, No. 55, pp. 697–702.
Aydin, N., Kentel, E., and Duzgun, S. (2013) GIS-based site selection methodology for hybrid renewable energy systems: A case study from western Turkey, Energy conversion and management, No. 70, pp. 90-106.
Bhutto, A., Bazmi, A., Zahedi, G., and Klemes, J. (2014) A review of progress in renewable energy implementation in the Gulf Cooperation Council countries, Journal of Cleaner Production, No. 71, pp. 168-180.
Castillo, C., Silva, F., and Lavalle, C. (2016) Assessment of the regional potential for solar power generation in EU-28, Energy policy, No. 88, pp. 86-99.
Colantoni, A., Delfanti, L., Recanatesi, F., Tolli, M., and Lord, R. (2016) Land use planning for utilizing biomass residues in Tuscia Romana (central Italy): Preliminary results of a multi criteria analysis to create an agro-energy district, Land use policy, No. 50, pp. 125–133.
Cradden, L. , Kalogeri, C. , Martinez Barrios, I., Galanis, G., Ingram, D. and Kallos, G., (2016) Multi-criteria site selection for offshore renewable energy platforms, Renewable energy, No. 87, pp. 791-806.
Darwish, A. and Shaaban, S. (2016) Solar and wind energy: Present and future energy prospects in the Middle East and North Africa, In: Sayigh, A. (ed.), Renewable Energy in the Service of Mankind Volume II, Springer International Publishing, Switzerland.
Dawod, G., and Mandoer, M. 2016, Optimum sites for solar energy harvesting in Egypt based on multi-criteria GIS, The first Future University international conference on new energy and environmental engineering, April 11-14, Cairo, Egypt, pp. 450-456.
Dawod, G., 2013, Suitability analysis for tourist infrastructures utilizing multi-criteria GIS: A case study in Al-Hada city, Saudi Arabia, International journal of geomatics and geosciences, V. 4, No. 2, pp. 313-24.
Hassaan, M. (2015) A GIS-based suitability analysis for sitting a solid waste incineration power plant in an urban area case study: Alexandria governorate, Egypt, Geographic information system, No. 7, pp. 643-657.

Hepbasli, A. and Alsuhaibani, Z. (2011) A key review on present status and future directions of solar energy studies and applications in Saudi Arabia, Renewable and Sustainable Energy Reviews, No. 15, pp. 5021– 5050.

Inamdar, P., Cook, S., Sharma, A., Corby, N., Connor, J., and Perera, B. (2013) A GIS based screening tool for locating and ranking of suitable storm water harvesting sites in urban areas, Environmental management, No. 128, pp. 363-370.

Kaiser, M. and Ahmed, S. (2013) Optimal thermal water locations along the Gulf of Suez coastal zones, Egypt, Renewable Energy, No. 55, pp. 374-379.

Matejicek, L. (2015) Multi-criteria analysis for sources of renewable energy using data from remote sensing, Presented at the 36th international symposium on remote sensing of environment, Berlin, Germany, May 11-15.

Nizami, A., Ouda, O/., Rehan, M., El-Maghraby, A., Gardy, J., Hassanpour, A., Kumar, S., and Ismail, I. (2015) The potential of Saudi Arabian natural zeolites in energy recovery technologies, Energy, DOI: 10.1016/j.energy.2015.07.030.

Pradhan, J. and Samanta, K. (2015) Site suitability analysis using remote sensing and GIS for proper selection of solid waste disposal ground within Rajarhat, Gopalpur municipal area, Kolkata, West Bengal, International journal of geomatics and geosciences, V. 5, No. 4, pp. 640-654.

Uyan, M. (2013) GIS-based solar farms site selection using analytic process in Karapinar region, Konya, Turkey, Renewable and sustainable energy reviews, No. 28, pp. 11-17.

Recanatesi, F., Tolli, M., and Lord, R. (2014) Multi criteria analysis to evaluate the best locations of plants for renewable energy by forest biomass: A case study in central Italy, Applied mathematical sciences, V. 8, No. 129, pp. 6447-6458.

Saleh, A., Belal, A., and Mohamed, E. (2015) Land resources assessment of El-Galaba basin, south Egypt for the potentiality of agriculture expansion using remote sensing and GIS techniques, Egyptian journal of remote sensing and space sciences, No. 18, pp. S19–S30.

Sanchez-Lozano, J., Teruel-Solano, J., Soto-Elvira, P., and Garcia-Cascales, S. (2013) Geographic information systems (GIS) and multi-criteria decision making (MCDM) methods for the evaluation of solar farms locations: Case study in south-eastern Spain, Renewable and sustainable energy review, No. 24, pp. 544-556.

Tahri, M., Hakdaoui, M., and Maanan, M. (2015) The evaluation of solar farm locations applying geographic information system and multi-criteria decision-making methods: Case study in southern Morocco, Renewable and sustainable energy review, No. 51, pp. 1354-1362.

Tlili, I. (2015) Renewable energy in Saudi Arabia: current status and future potentials, Environ Dev Sustain, No. 17, pp. 859–886.

Wanerer, T. and Herle, S. (2015) Creating a spatial multi-criteria decision support system for energy related integrated environmental impact assessment, Environmental impact assessment review No. 52, pp. 2-8.

Watson, J. and Hudson, M. (2015) Regional scale wind farm and solar farm suitability assessment using GIS-based multi-criteria evaluation, Landscape and urban planning, No. 138, pp. 20-31.

Zaidi, F., Nazzal, Y., Ahmed, I., Naeem, M., and Jafri, M. (2015) Identification of potential artificial groundwater recharge zones in Northwestern Saudi Arabia using GIS and Boolean logic, Journal of African Earth Sciences, No. 111, pp. 156-169.

Available online www.jsaer.com

***Journal of Scientific and Engineering Research*, 2017, 4(10):312-319**

Research Article

ISSN: 2394-2630
CODEN(USA): JSERBR

Toward a Centimeter-Geoid Model for Engineering Surveying in Egypt: Status and Projected Activities

Gomaa M. Dawod*, Magdy M. Hosny

Survey Research Institute, National Water Research Center, 308 Al-Ahram St., Talbiam Giza 12111, Egypt

Abstract With the broad spread of Global Navigation Satellite Systems (GNSS) utilization in geomatics and engineering surveying in Egypt in the last two decades, a precise geoid model becomes an essential demand. This paper investigates the possibilities of using global or local geoid models for height conversion in engineering activities. It has been found that most Global Geopotential Models (GGMs) could not depict the gravitational field over Egypt with a precision level less than 0.20 meter. On the other hand, recent available local geoid models still suffer from several factors and their accuracy still in the range of 0.10-0.15 meters. Precise surveying projects necessitate a more-accurate geoid model. As a result, the Survey Research Institute (SRI) has initiated a national collaborative effort to develop a centimeter-level hybrid geoid model for Egypt. So, three new geodetic networks; namely GNSS, levelling, and gravity, will be established on a national basis with first-order geodetic specifications and a reasonable grid spacing. The project aims to develop a national geoid model with a few-centimeter accuracy in the first phase, which can be modified later to achieve the one-centimeter accuracy level. Status of geodetic infrastructures and geoid modelling in Egypt, along with the projected geospatial activities are presented in details in this paper.

Keywords GNSS Surveying, Gravity, Levelling, Geoid, Egypt

1. Introduction

Geoid modelling is looking for the precise determination of geoid undulations between the geodetic heights obtained from the Global Navigation Satellite Systems (GNSS) techniques and the orthometric heights, or levels, relative to the Mean Sea Level (MSL). Consequently, geoid models are essential for the utilization of gnss (particularly the Global Positioning System: GPS) in civil engineering projects. geoid models could be developed globally, regionally, nationally, or on a local scale. in the last few years, many countries all over the world have developed their national geoid models for a variety of engineering applications, e.g. Japan [1], Argentina [2], Latvia [3], Nigeria [4], and Tanzania [5].

In Egypt, since the development of the first pioneer national-scale geoid [6], several geoid researches have been carried out. For example, Dawod [7] has developed a national geoid model based on the data of the Egyptian National Standardization Network of 1997 (ENGSN97) along with GPS/levelling data. Saad and Dawod [8] have developed a national geoid model based on the EGM96 global geopotential model along with GPS/levelling datasets. In addition, Abd-Elmotaal [9] has developed a gravimetric geoid model utilizing high-degree tailored reference geopotential models. Recently, Al-Karargy [10] has developed a national geoid model for Egypt based on recent accurate geodetic databases. Additionally, Al-Ashqar [11] has investigated the integration of Global Geopotential Models (GGMs) with local databases for the development of a hybrid geoid model for Egypt.

The major complications affecting the development of a precise geoid model for Egypt could be: (1) the availability of geodetic data, (2) the accuracy and datum conflict of available data, and (3) the non-homogeneous spatial distribution of available data over the Egyptian territories. This paper aims to investigate the geodetic infrastructures in Egypt, and to analyze the current geoid modeling activities. Furthermore, a new strategy of precise geoid development is proposed and discussed in details.

2. Geoid Modelling

The geoid undulation (N) can be computed from gravity data by the well-known Stokes' formula (e.g. Heiskanen and Moritz [12]):

$$N = R/4\pi\gamma \iint_{\sigma} S(\psi)\Delta g d\sigma \tag{1}$$

where: R is the mean Earth radius, γ is the normal gravity on the reference ellipsoid, Δg is the gravity anomaly, $d\sigma$ is an infinitesimal surface element on the unit sphere σ, and $S(\psi)$ is the Stokes' function which can be expressed as a series of Legendre polynomial $Pn(\cos\psi)$ over the sphere:

$$S(\psi) = \sum_{n=2}^{\infty} (2n+1/n-1) P_n(\cos\psi) \tag{2}$$

Stokes' formula (Eq. 1) needs to be applied over the whole Earth; however in practice gravity datasets of the whole Earth are not available. Thus the gravimetric geoid modelling methods break up the gravity anomalies (Δg) into three components:

$$\Delta g = +\Delta g_{REF} + \Delta g_F + \Delta g_h \tag{3}$$

where: ΔgF represents the free-air gravity anomalies, Δgh is the effect of topography, and Δg_{REF} represents the gravity anomalies of a reference gravity field represented by a GGM.

Therefore, the full geoid undulation (N) is decomposed into three components too:

$$N = N_{REF} + N_{\Delta g} + N_h \tag{4}$$

where: $N\Delta g$ is the contribution of the reduced gravity anomalies computed by Stokes's integral, N_h is the contribution of the topography, and N_{REF} is the contribution of the reference gravity field.

Globally, the geoid undulations (N) may be computed using the following spherical harmonic expansion:

$$N = (GM/r\gamma) \sum_{n=2}^{n\max} (a/r)^n - \sum_{m=0}^{n} ((C_{nm}^{-} \cos m\lambda) + (S_{nm}^{-} \sin m\lambda)) P_{nm} \sin\varphi) \tag{5}$$

where: n is the degree of the GGM model, n max is the maximum degree of the GGM model, m is the maximum order of the model, γ is the normal gravity of the reference ellipsoid, r is the geocentric radial distance of the computation point projected on the ellipsoid, G is the Newtonian gravitational constant, M is the mass of the Earth, a is the semi-major axis, ϕ is the geocentric latitude, λ is the geocentric longitude, C-nm and S-nm are the fully normalized harmonic coefficients, and Pnm is the fully normalized associated Legendre polynomial.

GGM models have been developed since the 1960s as an important tool for geoid modelling on a regional or local scales. So far, there are more than 150 GGM available at the website of the International Center for Global Earth Models (*http://icgem.gfz-potsdam.de/ICGEM/ICGEM.html*). In developing GGM models, datasets from several sources might be utilized such as: satellite-based gravity data, terrestrial gravity data, satellite altimetry data, and terrestrial geodetic data. Therefore, the maximum degree and the precision of GGM models vary significantly.

3. Geoid Status in Egypt

Geoid modelling is a scientific task by nature, and the governmental surveying organizations, in many developing countries, are interested in utilizing a geoid model not developing one. So, the availability of required datasets might be a major problem facing researchers in such countries. The traditional geodetic data

infrastructures in Egypt have major drawbacks in terms of precision, availability, datum conflict, and spatial distribution, as will be discussed herein.

Gravity observations have been carried out in Egypt since 1908, primarily for oil and mineral exploration [13]. The earliest absolute gravity observations in Egypt have been carried out in 1908 at Helwan observatory, south of Cairo. Between 1922 and 1950, some foreign geophysical exploration companies have carried out second-order gravimetric survey mainly in the western desert. Within an international gravity program, 21 stations have been established in Egypt in 1950-1951 and tied to the Potsdam gravity reference system. Moreover, as a part of the International Gravity Standardization Network 1971 (IGSN-71), 11 gravity stations have been measured in Egypt. A ten-year project (1974 - 1984) for compilation of gravity maps of Egypt has resulted in the National Gravity Standard Base Net (NGSBN-77). The project was executed and supervised by the General Petroleum Company (GPC) under the auspices of the Egyptian Academy of Sciences and Technology. The NGSBN-77 consists of 66 stations (Figure 1) and has tied to IGSN-71. More recently, the Survey Research Institute (SRI) has established the most-recent most-accurate Egyptian National Gravity Standardization Network (ENGSN97) between 1994 and 1997. It consists of 5 absolute gravity stations and 145 relative gravity stations (Fig. 1). Several recent studies (e.g. Al-Ashqar, [11] and Al-Karargy, [10]) have concluded that the second-order gravity measurements, in the western desert, are not precise enough for geoid modelling in Egypt, and emphasized that only NGSBN-77 and ENGSN-97 should be utilized to represent precisely the gravitational field of Egypt. Thus, the precise gravity stations in Egypt are not quit enough, in terms of number and distribution, for accurate gravimetric geoid modelling.

Regarding the geodetic vertical datum and reference networks in Egypt, it is a matter of reality that the national MSL has been determined in 1906. It was based on collecting and averaging daily sea level data at the Alexandria tide gauge between 1898 and 1906. However, it is evident that MSL has been significantly changed due to global warming on a global basis. Mohamed [14] has concluded that the relative rising rate of MSL at Alexandria equals 1.7 mm/year. Additionally, it has been found that the linear velocity estimate of the tide gauge GPS station height equals -0.47 mm/year. Therefore, it is concluded that the absolute sea level rise at Alexandria has been computed as 2.17 mm/year (ibid). On the other hand, the Egyptian first-order levelling network (Fig. 2) had been carried out from 1906 to 1936, in order to establish fundamental benchmarks over the cultivated lands of Egypt to control the levelling works that was performed by the irrigation departments and to unify a precise vertical datum for the irrigation system in Egypt. Concerning the systematic error sources in the Egyptian precise levelling network, the effect of refraction has been treated by field observational procedures in order to reduce it as much as possible. However, the correction for other sources of systematic errors, namely orthometric and tidal corrections, have not been considered in the computation of the network [15]. Another defect of that network is that no integrated least-square adjustment has been carried out, but it was adjusted loop by loop, which decreased its overall precision (ibid).

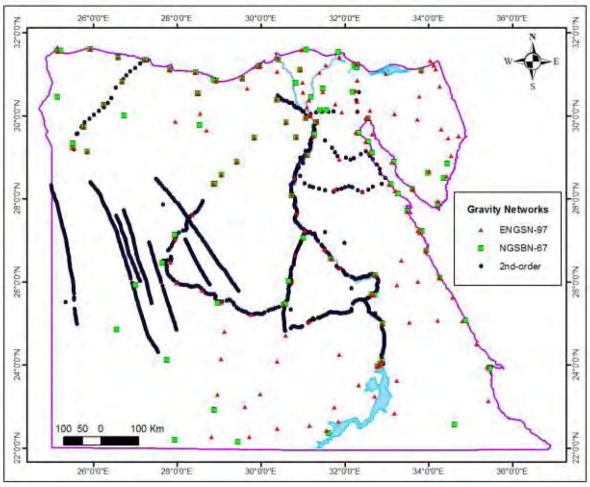

Figure 1: Traditional Gravity Stations in Egypt

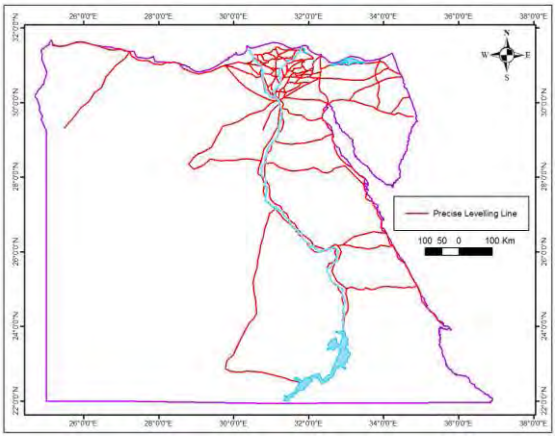

Figure 2: The Precise Levelling Network in Egypt

The Egyptian Survey Authority (ESA) has established the GPS-based High Accuracy Reference Network (HARN) in 1995. It consists of 30 stations with an almost 200 kilometer spacing covering Egypt. Next, ESA has established the National Agriculture Control Network (NACN) consisting of 112 stations along the Nile valley and Delta (Fig. 3). Both networks have been referenced to the International Terrestrial Reference Frame of 1994 (ITRF94). It worth mentioning that only 16 stations of the HARN and NACN have measured orthometric heights, and thus could be utilized in geoid modelling. Moreover, in 2010 ESA has established 40 Continuous Operating Reference Stations (CORS) to provide corrections to GNSS users in Egypt. Those stations, referenced to ITRF2008, have been established on the top of ESA buildings, and thus have no orthometric heights.

On the other hand, the utilization of GGMs only does not meet the accuracy limits required for GNSS surveying for engineering projects in Egypt. Many research studies have been performed to investigate the accuracy of GGMs in representing the gravitational field over Egypt. For example, Dawod et al. [13] have tested the Earth Geopotential Model 2008 (EGM2008) over known 305 GPS/levelling stations and found that the undulation differences range from -0.76 m to 0.41 m, with a mean of -0.23 m and a standard deviation equals ± 0.23 m. Al-Karargy et al. [16] showed that EGM2008 gave a mean standard deviation of gravity differences equals ± 25.1 mGal when examined over 941 observed gravity points in Egypt. Even when integrating GGMs with the available geodetic datasets, the developed hybrid geoid models produce accuracy levels in the order of ± 0.10 to 0.15 m approximately on a national scale (e.g. Al-Ashqar, [11] and Al-Karargy, [10]). Again, such a precision limit is not appropriate for GNSS engineering surveying applications.

Analyzing the status of geodetic data infrastructures in Egypt reveals critical challenges regarding precise geoid modelling. First, the vertical geodetic datum determined in 1906 has been changed significantly due to the global warming evidence in the twentieth century. Secondly, the available precise gravity stations are quite little and do not homogeneously cover the country. Additionally, it is a matter of fact that a large percentage of the first-order Bench Mark (BM) stations has been destroyed due to the urban growth in Egypt in the last few decades [17]. Also, field reconnaissance has revealed that some GPS and ENGSN97 gravity stations have been lost in several places due to urban development. Furthermore, the spatial separation and distribution of GPS and gravity networks, as depicted in the last figures, do not support the requirements of precise geoid modelling over Egypt. Hence, a new strategy is needed to cope with those serious problems of the national geodetic infrastructures.

4. Undergoing National Geoid Activities

Recently, SRI has completed a prototype research study for densification of geodetic networks and development of a precise geoid model in the Minufiya governorate, north of Cairo. A network of 47 new BM has been established with an average spacing of 4 kilometers apart. That entire network has been positioning by GPS applying the international geodetic standards and specifications, and tied to the national geodetic datum of Egypt. The least-squares adjustment method has been carried out for both networks. The geoidal undulations have been achieved with a few centimeters level of precision (Fig. 4), and a precise geoid model has been

developed for the study area [18-19]. This case study has motivated SRI to propose the development of a precise geoid model for entire Egypt.

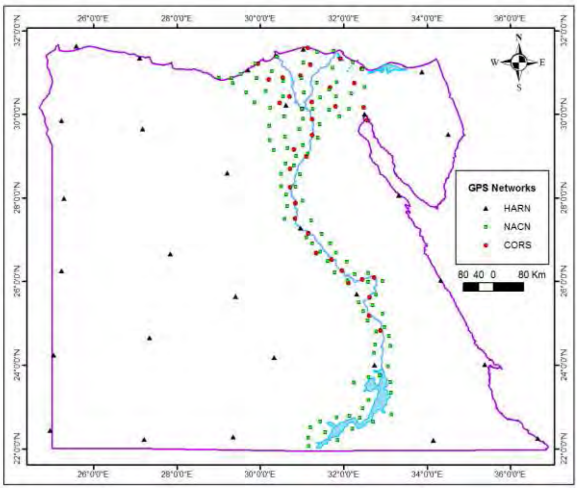

Figure 3: The GPS Networks in Egypt

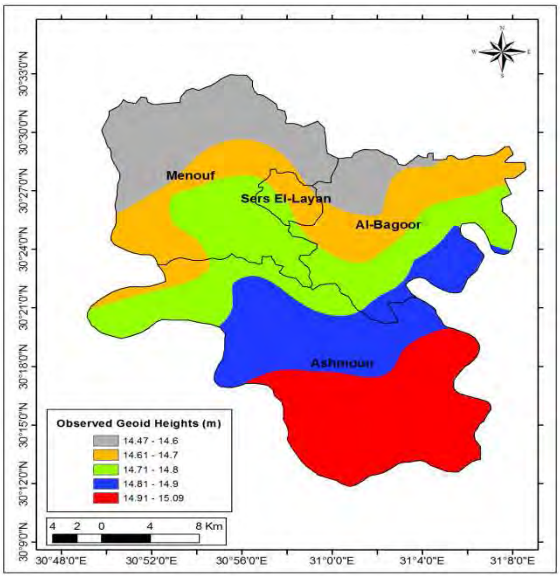

Figure 4: The Local Geoid of Minufiya Governorate

During the second half of 2016, SRI has organized many workshops, attended by professional from many governmental organizations, in order to discuss the geoid modelling future activity. Those organizations include: the Egyptian Surveying Authority (ESA), the Egyptian Commission of Surveying and Mapping (ECSM), the National Research Institute for Astronomy and Geophysics (NRIAG), the Egyptian Mineral Resources Authority (EMRA), the Nuclear Materials Authority (NMA), the Egyptian General Petroleum Corporation (EGPC), the National Authority for Remote Sensing and Space Sciences (NARSS), and many university professionals. The workshops reveal essential facts about the national resources, in terms of existing data and capabilities, that could be participated in a national effort to develop a precise geoid model for Egypt. For example, it has been recognized that NMA acquires an aircraft equipped with an airborne gravity meter, among other sensors. Also, EMRA has recent gravity databases in different regions of Egypt, while NRIAG has collected gravity and GPS measurements in the southern region, particularly around lake Nasser. Moreover, SRI has acquired a recent precise GPS/levelling database of more than 500 stations mainly along the coastlines (Fig. 5). Hence, it is a matter of reality that the unification and integration of all available resources and efforts will be supportive in national geoid modelling.

Based on the comprehensive deliberations in the organized workshops, a proposal of national geoid modelling has been accomplished. The objectives and strategy of that proposal, in the first phase, could be summarized as (Fig. 6):

- Collecting, analyzing, and validating all available measurements in a unique information system.
- Redefining the MSL datum based on recent heterogeneous data at available tide gauge stations.
- Establishing three high-accuracy geodetic reference networks (terrestrial gravity, GPS, and precise levelling) on a national base with homogenous spatial distribution using 10x10 kilometer interval.
- Measuring airborne gravity in remote areas of Egypt, where terrestrial gravity can not accomplished.
- Developing a national gravimetric geoid model, then fitting it to GPS/levelling data.
- Capacity building and professional training of junior engineers in geoid modelling.

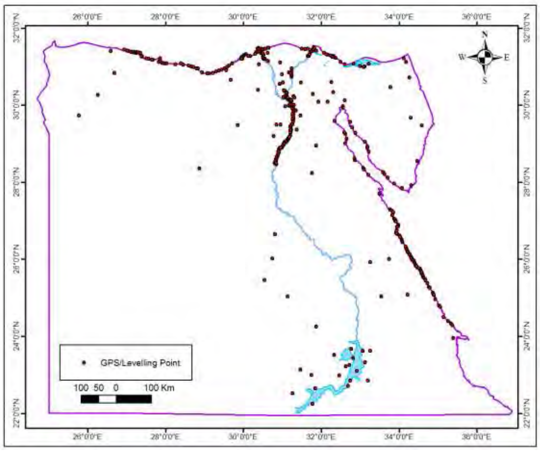

Figure 5: The Available SRI GPS/Levelling Stations

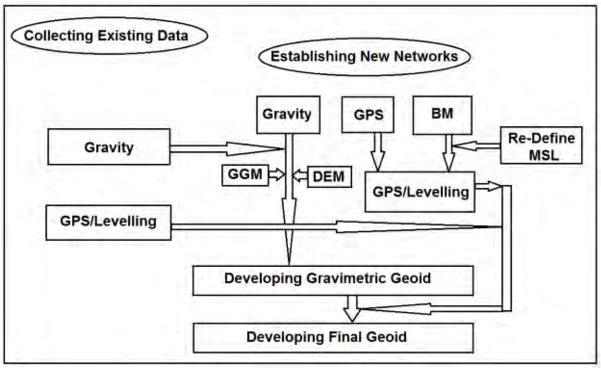

Figure 6: The Main Steps for Developing a Geoid Model For Egypt

The proposed geoid modelling task could be divided into two phases: (a) a two-year first phase that could result in a national geoid model with an approximate accuracy of 3-4 cm; and (b) the second phase that deals with densification of geodetic measurement permitting the development of a centimeter level of accuracy geoid for Egypt. The budget of that proposal could be financed through the current undergoing national project for establishing the Spatial Data Infrastructure (SDI) for Egypt. Economically speaking, such a geoid model will broaden the utilization of GNSS positioning techniques in engineering applications, which in turn will considerably decrease their costs comparing with the usage of terrestrial surveying methods.

5. Conclusions

In engineering surveying, the transformation of GNSS-based geodetic heights to the MSL-based orthometric heights requires a precise geoid model. On a national basis over Egypt, the most available geoid models produce an accuracy levels of 0.10-0.15 m. On the other hand, the utilization of GGM models gives errors in the order of more than 0.20 m. That accuracy is, by default, not appropriate for engineering activities. The main reason behind this situation is the lack of precise and homogeneously-distributed geodetic database over the country. Based on several workshops organized by SRI, it has been found that the optimum strategy is the unification and

integration of all available resources and capabilities in carrying out a national project for developing a geoid model for Egypt. In this paper, the proposal is discussed in details including the strategy and technical procedures for conducting that effort. The anticipated project intends to develop a national geoid model with a few-centimeter accuracy in the first phase, which can be modified later to achieve the one-centimeter accuracy level. From an economic perspective, a national geoid model will broaden the utilization of GNSS positioning techniques in engineering applications in Egypt, and significantly decrease their costs compared with the time-consuming and expensive terrestrial surveying methods.

References

[1]. Matsuo, K., Miyazaki, T., and Kuroishi, Y. (2016). Development of a new gravimetric geoid model for Japan, The FIG working week 2016, New Zeeland, May 2-6.

[2]. Pinon, D. (2016). Development of a precise gravimetric geoid model for Argentina, MSC thesis, RMIY university, Millburn, Australia.

[3]. Balodis, J., Morozova, K., Silabriedis, G., Jäger, R., Kälber, S., Haritonova, D., Janpaule, I., and Kaminskis, J. (2016). Case Study: One centimeter precision regional quasi-geoid, International Journal of Engineering Science and Innovative Technology, V. 5, No. 1, pp. 66-75.

[4]. Odumosu, J., Kelly, K., Omogunloye, O., Adejare, Q., Adeleke, O., and Olaniyi, A. (2016). Empirical geoid modelling using classical gravimetric method, The FIG working week 2016, New Zeeland, May 2-6.

[5]. Ulotu, P. (2016). Integeration of Tanzania new gravity network and database into vertical spatial reference system, International Journal of Engineering Science and Computing, V. 6,No. 8, pp. 2619-2622.

[6]. Alnaggar, D. (1986). Determination of the geoid in Egypt using heterogeneous geodetic data, PhD dissertation, Faculty of engineering, Cairo University, Egypt.

[7]. Dawod, G. (1998). A national gravity standardization network for Egypt, Ph.D. dissertation, Shoubra faculty of engineering, Zagazig University, Cairo, Egypt.

[8]. Saad, A. and Dawod, G. (2002). A precise integrated GPS/gravity geoid model for Egypt, Civil Engineering Research Magazine, V. 24, No. 1, pp. 391-405.

[9]. Abd-Elmotaal, H. (2008). Gravimetric geoid for Egypt using high-degree tailored reference geopotential model, NRIAG Journal of Geophysics special issue, pp. 507-531.

[10]. Al-Karargy, E. (2016). Development of a national geoid fir Egypt using recent surveying data, Ph.D. dissertation, Minufiya University, Egypt.

[11]. Al-Ashqar, M. (2017). An improved hybrid local geoid model for Egypt, Ph.D. dissertation, Zagazig University, Egypt.

[12]. Heiskanen, W. and Moritz, H. (1967). Physical Geodesy, W.H. Freeman and Company, London.

[13]. Dawod, G., Mohamed, H. and Ismail, S. (2010). Evaluation and adaptation of the EGM2008 geopotential model along the northern Nile valley, Egypt: Case study, ASCE Journal of Surveying Engineering, V. 136, No. 1, pp. 36-40.

[14]. Mohamed, H. (2006). Realization and redefinition of the Egyptian vertical datum based on recent heterogeneous observations, Ph.D. dissertation, Shoubra faculty of engineering, Benha University, Egypt.

[15]. Saad, A. (1993). Towards the redefinition of the Egyptian vertical control network, Ph.D. dissertation, Shoubra faculty of engineering, Zagazig university, Cairo, Egypt.

[16]. Al-Krargy, E., Hosny, M. and Dawod, G. (2015). Investigating the precision of recent global geoid models and global digital elevation models for geoid modelling in Egypt, The regional conference on surveying and development, Sharm El-Sheikh, Egypt, Oct. 3-6.

[17]. SRI (Survey Research Institute) (2016a). Development of a geoid model for Egypt: Case study: Minufiya governorate, Internal technical report.

[18]. Al-Krargy, E., Mohamed, H., Hosney, M., and Dawod, G. (2017). A high-precision geoid for water resources management: a case study in Minufiya governorate, Egypt, The National Water Research

Center (NWRC) Conference on: Research and Technology Development for Sustainable Water Resources Management, Cairo, Egypt. December 4-6.

[19]. SRI (Survey Research Institute) (2016b). A proposal for developing an accurate geoid model for Egypt, Internal technical report.

Journal of Geographic Information System, 2017, 9, 685-698
http://www.scirp.org/journal/jgis
ISSN Online: 2151-1969
ISSN Print: 2151-1950

Reliability of Recent Global Digital Elevation Models for Geomatics Applications in Egypt and Saudi Arabia

Gomaa Dawod[1], Khaled Al-Ghamdi[2]

[1]Survey Research Institute, National Water Research Center, Giza, Egypt
[2]Umm Al-Qura University, Makkah, KSA
Email: dawod_gomaa@yahoo.com, kaghamdi@uqu.edu.sa

How to cite this paper: Dawod, G. and Al-Ghamdi, K. (2017) Reliability of Recent Global Digital Elevation Models for Geomatics Applications in Egypt and Saudi Arabia. *Journal of Geographic Information System*, **9**, 685-698.
https://doi.org/10.4236/jgis.2017.96043

Received: October 30, 2017
Accepted: November 28, 2017
Published: December 1, 2017

Copyright © 2017 by authors and Scientific Research Publishing Inc.
This work is licensed under the Creative Commons Attribution International License (CC BY 4.0).
http://creativecommons.org/licenses/by/4.0/
Open Access

Abstract

Global Digital Elevation Models (DEMs) have been utilized in various geomatics activities worldwide. Recently, there exist several available DEMs vary significantly in terms of spatial resolution and release dates. This paper examines the reliability of eight recent global DEMs, namely the EarthEnv-D90, SRTM 1, SRTM 3, ASTER, GMTED2010, GLOBE, GTOPO30, and AW3D30, in two study areas in Egypt and Saudi Arabia representing different topography patterns. Known ground control points with measured accurate coordinates and precise elevations have been utilized in evaluating the performance of those DEMs. It has been concluded that such a judgment procedure should not be carried based on a single statistical measure. First, five statistical measures, specifically the range, standard deviation, correlation, kurtosis, and skewness, have been evaluated separately for each DEM's errors. Then, a new reliability index is introduced based on the weighted average concept. The accomplished results show that global DEMs perform differently in different topography patterns. It has been concluded that the EarthEnv-D90 and SRTM1 models attain high reliability indexes in the Nile delta region that represents a flat topography, while the GMTED2010 and EarthEnv-DEM90 models came in the first places for the second study area, Makkah, which represents mountainous topography.

Keywords

DEM, Geomatics, Reliability, Egypt, Saudi Arabia

1. Introduction

Digital Elevation Models (DEMs) play an essential role in various geomatics, geo-

detic, Geographic Information Systems (GIS) environmental, surveying, and mapping applications. Some of such utilizations include, for instance, planner and topographic mapping [1] [2], hydrological modelling [3] [4] [5], seismic hazard assessment [6], morphometric analysis [7], cost distance modelling [8], landslide monitoring [9], landform classification [10], and climate change impacts monitoring [11] [12].

Although there are many available free global DEMs, their accuracy and reliability should be quantified prior to actual implementation [13] [14] [15] [16]. This paper investigates the accuracy and reliability of eight existing global DEMs based on several statistical measures. **Table 1** summarizes the characteristics of those selected global DEMs, including:

– SRTM: The Shuttle Radar Topography Mission (SRTM) is a global DEM that has two versions: SRTM1 with a spatial resolution of 1 arc second, *i.e.*, approximately 30 meter, and SRTM3 model with a 3 arc second resolution (download from e.g. https://earthexplorer.usgs.gov/).
– ASTER: The Advanced Spaceborne Thermal Emission and Reflection Radiometer (ASTER) is 1 arc second global DEM. The ASTER version 2 has been publically released in 2011 (download from e.g. https://asterweb.jpl.nasa.gov/gdem.asp).
– EarthEnv-DEM90: A global DEM derived from processing and merging SRTMv4 and ASTER v2 data products to provide continuous coverage of 91% of the globe (download from http://www.earthenv.org/DEM)
– GMTED2010: The Global Multi-resolution Terrain Elevation Data 2010 (GMTED 2010) is a global DEM available with three levels of spatial resolution: 7.5, 15, and 30 arc seconds (download from e.g. https://earthexplorer.usgs.gov/).
– GLOBE: The Global Land One-km Base Elevation (GLOBE) is a global DEM with a spatial resolution of 30 arc seconds, *i.e.* almost 1 kilometer (download from e.g. https://earthexplorer.usgs.gov/).
– GTOPO30: The Global 30 arc-second (GTOPO30) is global DEM derived from several sources of topographic information (download from e.g. https://earthexplorer.usgs.gov/).

Table 1. Characteristics of the utilized global DEM.

DEM	Released Year	Spatial Resolution	
		arc second	m
ALOS AW3D30	2015	1"	~30
SRTM 1	2015	1"	~30
ASTER v.2	2011	1"	~30
EarthEnvi-90 m	2014	3"	~90
SRTM 3	2009	3"	~90
GMTED2010	2011	7.5"	~225
GLOBE	2000	30"	~900
GTOPO30	1996	30"	~900

– AW3D30: The Advanced Land Observing Satellite (ALOS), is a Japanese satellite mission resulted in the development of ALOS World 3D - 30 m (AW3D30); a global free DEM with a spatial resolution of 1 arc second (download from http://www.eorc.jaxa.jp/ALOS/en/aw3d30/).

2. Data and Study Areas

Two study areas have been utilized in this research: the Nile delta region, Egypt and Makkah metropolitan area, Kingdom of Saudi Arabia (KSA). These two test areas have been selected so that the first one represents flat topography environment, while the second area is representing a hilly or complex topography region. The first study area covers most of the Nile delta region north of Egypt from Alexandria at the west (29.6˚E) to Port Said at the east (32.3˚E) on the Mediterranean coasts (Figure 1(a)). It is bounded by the two branches of the Nile River, and extending a little bit from both sides to cover coastal areas with existing ground data, with an overall area of approximately 13,000 square kilometers. The topography of the region smoothly slopes northwards towards the Mediterranean coast, where the difference in elevation between its southern peak, at Cairo, and northern coastal fringes is approximately 18 meter. 416 control points with measured GPS coordinates along with precise elevations (relative to the Mean Sea Level: MSL datum) have been utilized in this research study. Those points lay mainly on the two Nile branches and on the coasts of the Mediterranean, with an average spacing of 5 kilometers (Figure 1(a)).

The second study area is located at south west of KSA, about 80 kilometers east of the Red sea and extending from latitude 21˚09'N to 21˚37'N and from longitude 39˚35'E to 40˚02'E, covering 1301 square kilometers approximately (Figure 1(b)). Its elevations vary from almost 100 meters in the west to more than 960 meters in the west. It is a matter of reality that the topography of Makkah is complex in nature, and several mountainous areas exist inside its metropolitan area. Within this region, 137 ground control points with precise MSL-based elevations and GPS coordinates are known and utilized in the research study.

3. Methodology and Data Processing

For global DEM accuracy assessment, the measured elevation of each control point (H_m) has been compared against its corresponding DEM-based elevation (H_{DEM}), and the height differences or DEM errors (ΔH) is then estimated:

$$\Delta H = H_m - H_{\text{DEM}} \quad (1)$$

The outlier detection procedure took place before any further analysis in order to detect and remove erroneous observations or gross errors. An outlier is, simply, an observation that appears to depart significantly from the remaining observation in the sample. There are many statistical approaches for outlier detection, but the traditional method is the Z score statistical test as:

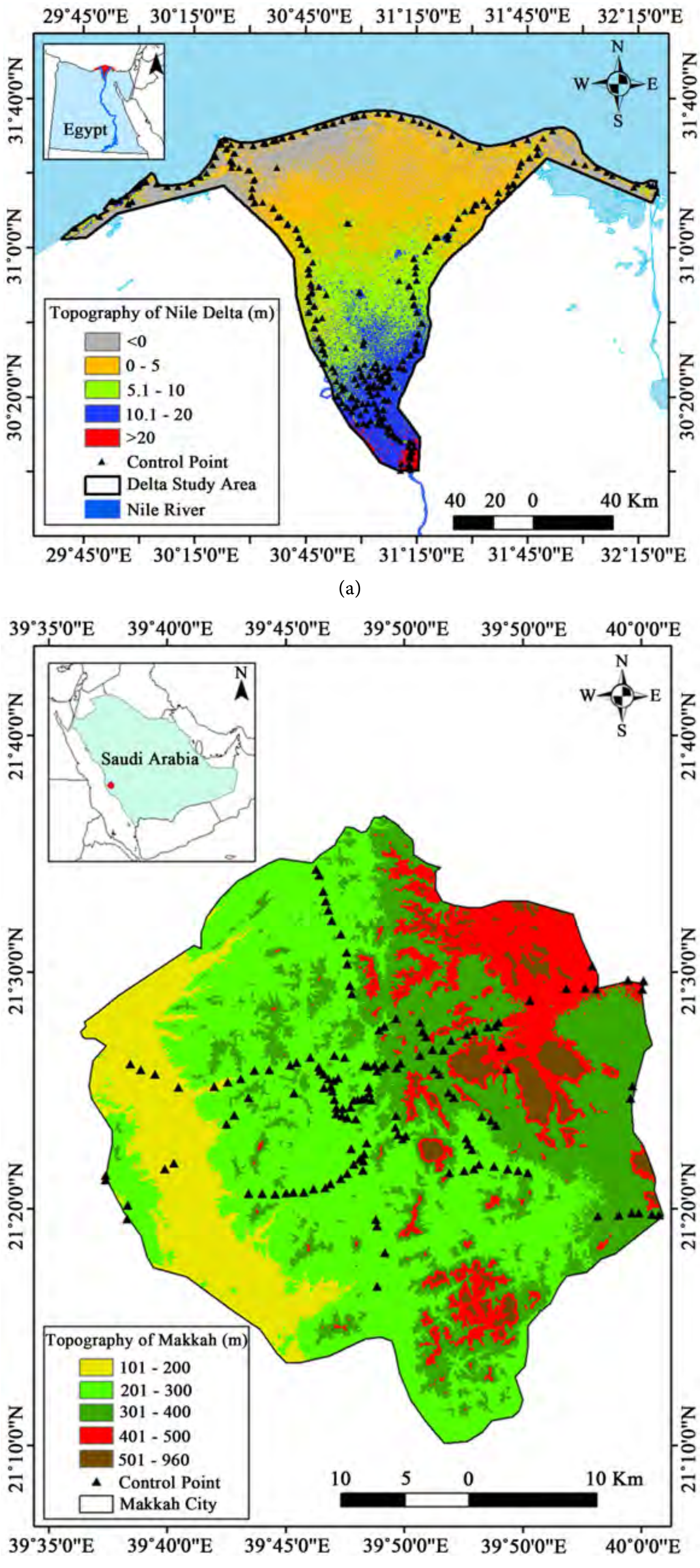

(a)

(b)

Figure 1. Study areas. (a) Nile delta, Egypt; (b) Makkah, Saudi Arabia.

$$Z_i = \left(Y_i - Y^{-}\right)/s \tag{2}$$

where, Y_i is an observation, Y^{-} denotes the sample mean, and *SD* is the sample standards deviation. The computed Z_i score, for each observation, is compared against the values obtained from normal distribution table. If the score exceeds the given limits, it is considered as a possible outlier and should be removed.

Next, five statistical measures have been evaluated individually [17], and then a unique reliability index has been proposed and computed. The correlation between observed elevations of the control points (X or H_M) and their respective elevation from a particular DEM (Y or H_{DEM}) is computed as:

$$COR = \frac{S_{XY}}{\sqrt{S_{XX} S_{YY}}} \tag{4}$$

where,

$$S_{XX} = \sum X^2 - \frac{\left(\sum X\right)^2}{n} \tag{5}$$

$$S_{YY} = \sum Y^2 - \frac{\left(\sum Y\right)^2}{n} \tag{6}$$

$$S_{XY} = \sum XY - \frac{\left(\sum X\right)\left(\sum Y\right)}{n} \tag{7}$$

where *COR* represents the correlation between X and Y, $\sum X$, $\sum Y$, $\sum XY$ are the summation of X, Y, and XY respectively, and n is the total number of available sample points.

Subsequently, the range of height difference is evaluated as the difference between the maximum and minimum computed differences for each DEM. Thirdly, the standard deviation (*SD*) of height differences is computed as:

$$SD = \sqrt{\frac{\sum_1^n \Delta H^2}{n}} \tag{8}$$

where n is the number of the utilized control points. It is expected that the larger the standard deviation, the flatter the normal distribution curve. The smaller the standard deviation, the higher the peak of the curve. Several research studies [18] [19] depend primly on the standard deviation measure in evaluating DEMs performance, which is not the case in this study. Afterward, a histogram of each DEM errors is plotted, and the skewness and kurtosis statistical measures are evaluated. The skewness is computed as:

$$sk = \frac{m_3}{m_2^{3/2}} \tag{9}$$

where

$$m_3 = \frac{\sum \left(Y - \bar{Y}\right)^3}{n} \tag{10}$$

and,

$$m_2 = \frac{\sum\left(Y - \bar{Y}\right)^2}{n} \tag{11}$$

The kurtosis, as another measure of the shape of the histogram or the normal distribution curve, is computed as:

$$K = \frac{m_4}{m_2^2} \tag{12}$$

where

$$m_4 = \frac{\sum\left(Y - \bar{Y}\right)^4}{n} \tag{13}$$

Having those five statistical measures attained for each DEM, they are categorized in a certain manner and a rank is assigned to each DEM in each measure (R_i). For the correlation, range, and standard deviation measures, the ranks vary from 1 to 8 based on the ascending order of those measures for each DEM. For the skewness measure the assigned rank is 8 if its value range between +0.5 and −0.5 (approximately symmetric), 5 if the value range from −1 to −0.5 or from +0.5 and +1 (moderately skewed), and 3 if the skewness is between −1 and +1 (highly skewed). For the kurtosis measure the assigned rank is 8 if the kurtosis equals 3, 5 if the kurtosis is greater than 3, and 3 if the kurtosis is less than 3.

In the last step, a new reliability index (*RI*) is introduced and computed for each DEM, based on the weighted mean approach. It ranges from zero as the lowest reliability of a DEM, to value of 10 represents the highest reliability. This concept is similar to the optimization approach utilized in GIS applications (e.g. [20]). The selected weights (W_j) are: a value of 4 for the standard deviation, 2 for both the range and the correlation, and 1 for both kurtosis and skewness. The reliability index measure is computed as:

$$RI = \frac{\sum R_i W_j}{\sum W} \tag{14}$$

where $\sum W$ denotes the sum of the utilized weight, *i.e.* 10.

4. Results and Discussion

The eight selected DEMs have been downloaded, from their respective websites, for both study areas and the elevation of each control has been interpolated using the ARC GIS 10 software package. The statistics of the attained results are presented in Table 2. It can be realized from that table that the AW3D30 and EARTHEnv-DEMM90 have the biggest correlation to the observed values in both study areas respectively. Next, the outlier detection procedure has been applied using the Z-score approach. Table 3 presents the accomplished findings, that emphasis that a significant improvement has been gained. For the first study area, the improvements, or the reduction of the standard deviation, range from 0% to 16.5% with an average equals 8.6%, and for Makkah area the improvements range from 0% to 42.2% with a mean of 10.1%. Thus, the outlier detection

Table 2. (a) Statistical measures of DEM elevations in delta area; (b) Statistical measures of DEM elevations in Makkah area.

(a)

	Min	Max	Mean	Correlation
Observed H	−1.9	22.3	8.7	NA
SRTM 1	−4.8	24.0	7.2	0.92
SRTM 3	−3.0	25.9	7.1	0.89
EarthEnv-DEM90	−4.0	28.2	6.7	0.94
GTOPO30	−6.6	35.9	10.7	0.47
GMTED2010	−5.1	29.1	7.1	0.90
ASTER	−4.4	34.5	11.1	0.57
GLOBE	−6.3	30.4	10.2	0.47
AW3D30	−4.0	39.2	8.0	0.94

(b)

	Min	Max	Mean	Correlation
Observed H	147.1	420.9	269.4	NA
SRTM 1	140.5	424.4	273.5	0.996
SRTM 3	146.4	424.4	273.4	0.997
EarthEnv-DEM90	148.2	425.0	274.0	0.997
GTOPO30	133.8	432.2	278.9	0.958
GMTED2010	149.0	426.0	274.1	0.997
ASTER	142.6	421.2	269.4	0.989
GLOBE	132.8	419.0	265.5	0.979
AW3D30	149.2	425.5	275.9	0.995

Table 3. (a) Statistical characteristics of DEM errors in Delta area; (b) Statistical characteristics of DEM errors in Makkah area.

(a)

DEM	SD Before Removing Outliers	SD After Removing Outliers	Improvement%
SRTM 1	±2.6	±2.4	7.7%
SRTM 3	±2.8	±2.4	16.5%
EarthEnv-DEM90	±2.1	±1.9	9.4%
GTOPO30	±6.8	±6.7	0.9%
GMTED2010	±2.7	±2.4	11.4%
ASTER	±5.7	±5.2	8.5%
GLOBE	±6.6	±6.6	0%
AW3D30	±2.4	±2.0	14.8%

(b)

DEM	SD Before Removing Outlier	SD After Removing Outliers	Improvement%
SRTM 1	±6.8	±6.5	4.4%
SRTM 3	±5.2	±5.1	1.9%
EarthEnv-DEM90	±5.0	±4.7	6.0%
GTOPO30	±21.9	±18.6	15.1%
GMTED2010	±4.9	±4.6	6.1%
ASTER	±9.9	±9.4	5.1%
GLOBE	±21.8	±12.6	42.2%
AW3D30	±6.8	±6.5	4.4%

should be applied in similar studies in order to detect and remove gross errors prior to further analysis. From Table 3, it can be seen that, after removing outliers, the EarthEnv-DEM90 and GMTED2010 models attain the smallest standard deviation in both study areas as ±1.9 and ±4.6 m respectively. Therefore, the difference in these two values implicitly implies that global DEMs perform better in flat area than in hilly or complex topography. Similar results have been reported by other researchers [18] [19] [21] particularly for SRTM and ASTER models. In addition, those accuracy measures confirm the known fact that global DEMs should not be the first option to be utilized in high-precision geomatics activities.

Next, the height differences or DEMs' errors have been computed, for all utilized models, at both study areas (Figures 2(a)-(h) and Figures 3(a)-(h)). Knowing that the elevations in the Delta region decrease from north to east and that in the Makkah region increase from east to west, it can be seen from these two figures that all global DEMs do not follow that particular schemes. Hence, it can be concluded that those errors do not spatially depend on geographic locations in both case study areas.

The statistical measures for utilized DEMs have been computed and presented in Table 4, and their histograms are plotted in Figure 4(a) and Figure 4(b), Figure 5(a) and Figure 5(b). From Table 4(a) it can be realized that the AW3D30 model has the lowest mean value of the DEM errors in the first area, while ASTER has it in the second area. However, both models did not get the smallest error range. Additionally, the EarthEnv-DEM90 model has the smallest error range in both case studies respectively, even though it does not attain the smallest mean error value. Consequently, it can be said that judgment of DEMs performance cannot be evaluated based on just one statistical quantity.

Figure 4(a) and Figure 4(b), Figure 5(a) and Figure 5(b) also reveal noteworthy remarks, from which it can be recognized that in both study regions, ASTER, GTOPO30, and GLOBE models present histograms spread over larger area with lower peaks. That generally implies that the error distributions of those global DEMs are relatively far away from the normal distribution and spread over wider ranges. This remark can be also recognized from the bigger errors range values presented in Table 4 for both study areas.

The last procedure computes the reliability index of each DEM in each study in each study areas as a weighted mean (Equation (14)) based on the ranks of the models in the five statistical measures, and the accomplished results are tabularized in Table 5(a) and Table 5(b). Hence, it can be seen that, in a relative sense, the EarthEnv-D90 and SRTM1 models attain high reliability indexes in the Nile delta region that represents a flat topography. On the other study area, Makkah representing hilly or mountainous topography, the GMTED2010 and EarthEnv-DEM90 models came in the first places on a reliability scale of 10. It can be realized, from Table 1, that those DEMs vary in their spatial resolution, which indicates that the accuracy and reliability do not depend primarily on the

Table 4. (a) Statistical measures of DEM errors in delta area; (b) Statistical measures of DEM errors in Makkah area.

(a)

DEM	Min	Max	Range	Mean	Kurtosis	Skewness
SRTM 1	−11.6	9.4	21.0	1.6	1.5	−0.01
SRTM 3	−16.2	11.7	27.9	1.6	4.7	−0.1
EarthEnv-DEM90	−7.6	9.5	17.1	2.0	1.4	−0.1
GTOPO30	−21.3	19.0	40.3	−2.0	0.6	0.6
GMTED2010	−10.5	9.4	19.9	1.6	1.4	0.1
ASTER	−29.1	17.6	46.7	−2.4	2.1	−0.4
GLOBE	−16.0	17.0	33.0	−1.5	0.3	0.6
AW3D30	−16.9	8.9	25.8	0.7	8.3	−1.4

(b)

DEM	Min	Max	Range	Mean	Kurtosis	Skewness
SRTM 1	−18.7	11.1	29.8	−4.2	0.4	−0.2
SRTM 3	−17.1	8.4	25.5	−4.1	0.2	−0.5
EarthEnv-DEM90	−17.5	5.3	22.8	−4.6	0.1	−0.5
GTOPO30	−52.1	32.6	84.7	−9.6	−0.9	−0.2
GMTED2010	−18.6	5.7	24.2	−4.7	0.2	−0.4
ASTER	−28.3	20.3	48.6	−0.01	0.6	−0.7
GLOBE	−27.1	28.5	55.7	3.9	0.05	−0.8
AW3D30	−24.1	6.9	31.0	−6.3	0.5	−0.9

Table 5. (a) Reliability index of Global DEM in delta area; (b) Reliability index of global DEM in Makkah area.

(a)

Global DEM	RI	Category
EarthEnv-DEM90	7.7	High Reliable
SRTM1	6.5	
GMTED2010	6.3	
AW3D30	6.0	Moderate Reliable
SRTM3	4.9	
Aster	3.5	Low Reliable
GLOBE	3.0	
GTOPO30	2.4	Very Low Reliable

(b)

Global DEM	RI	Category
GMTED2010	7.5	High Reliable
EarthEnv-DEM90	7.3	
SRTM3	6.5	Moderate Reliable
SRTM1	5.7	
AW3D30	4.6	
ASTER	3.8	Low Reliable
GLOBE	3.0	
GTOPO30	2.5	Very Low Reliable

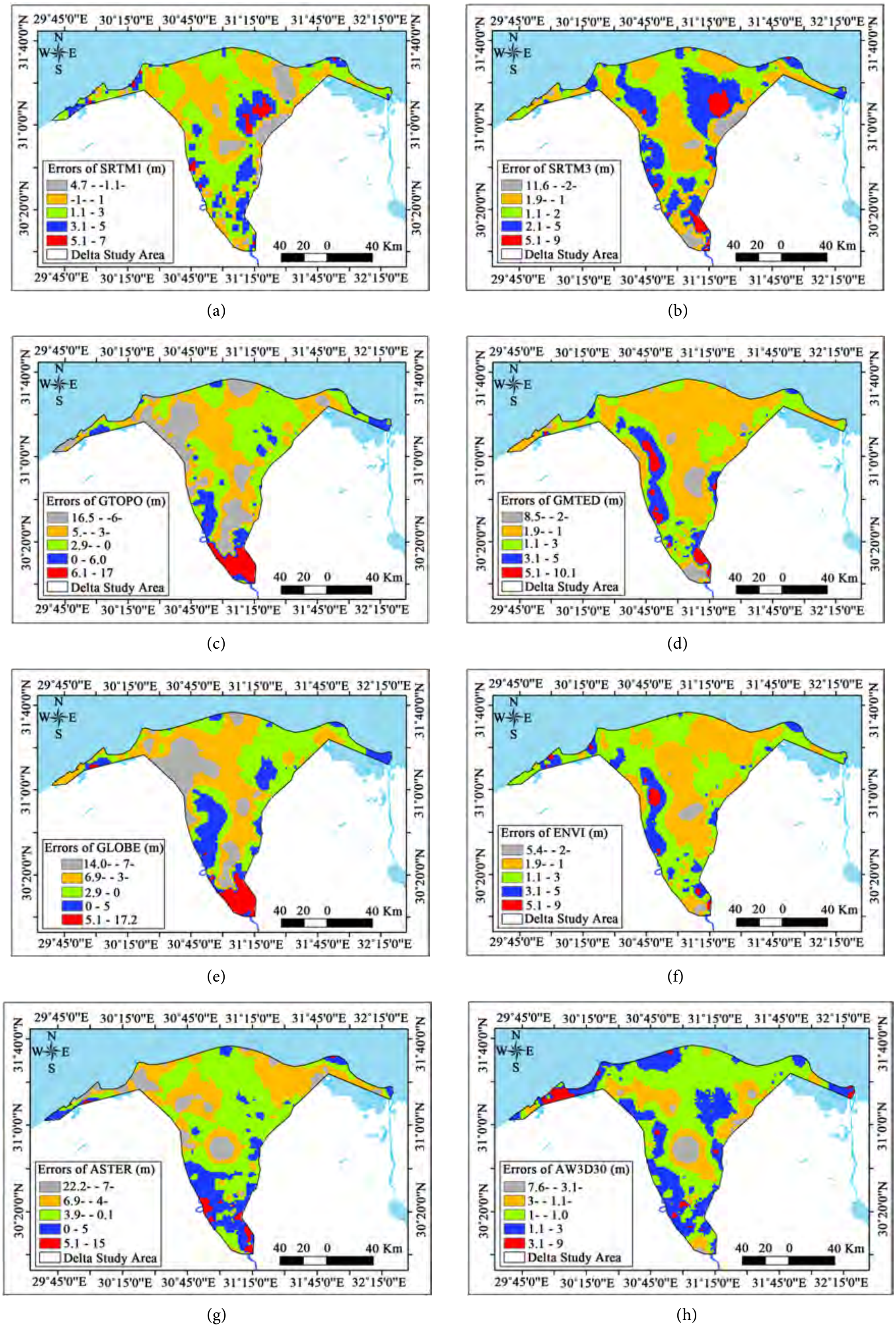

Figure 2. Errors of global DEM in Nile delta study area. (a) SRTM 1 DEM; (b) SRTM 3 DEM; (c) GTOP30 DEM; (d) GMTED DEM; (e) GLOBE DEM; (f) ENVI DEM; (g) ASTER DEM; (h) AW3D30 DEM.

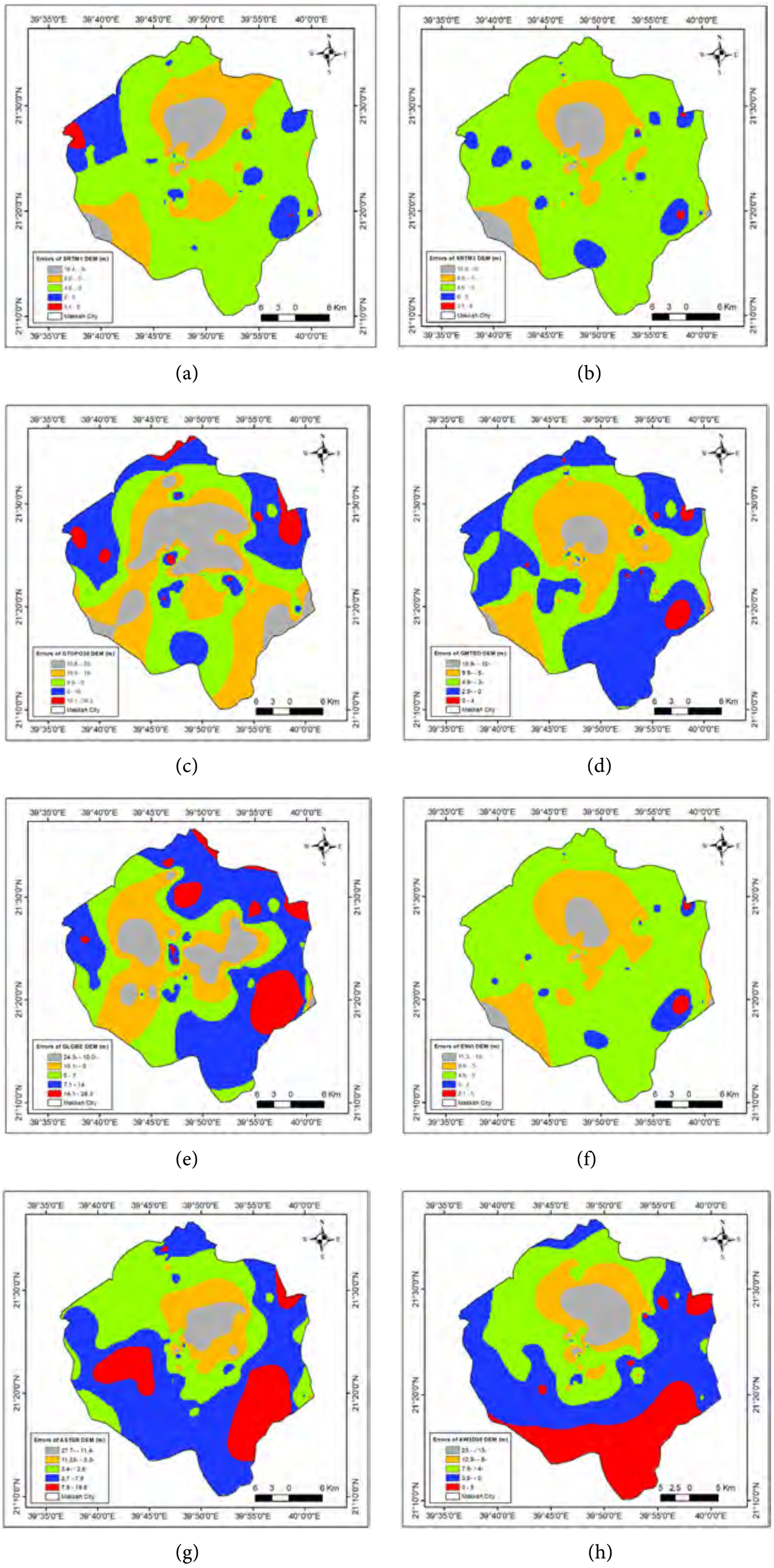

Figure 3. Errors of global DEM in Makkah study area. (a) SRTM 1 DEM; (b) SRTM 3 DEM; (c) GTOP30 DEM; (d) GMTED DEM; (e) GLOBE DEM; (f) ENVI DEM; (g) ASTER DEM; (h) AW3D30 DEM.

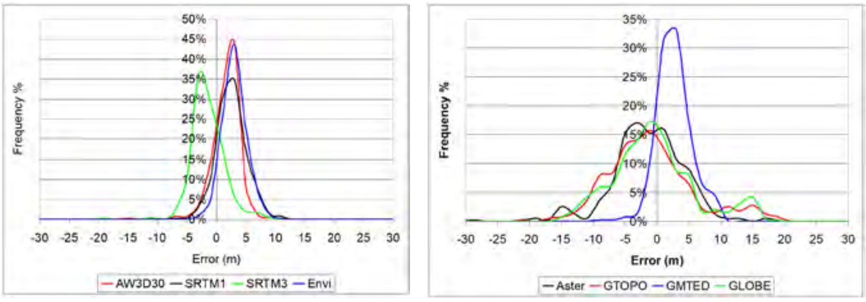

(a) (b)

Figure 4. Histograms of DEM errors in Nile delta study area.

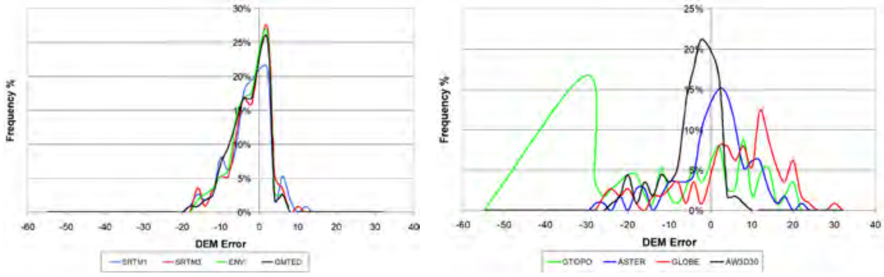

(a) (b)

Figure 5. Histograms of DEM errors in Makkah study area.

resolution of a DEM. Additionally, it can be seen that the GMTED2010, AW3D30 present a moderate reliability index in the first study area and SRTM1 and SRTM 3 gave the same result in the second area. Moreover, the older models, namely GLOBE and GTOPO30, came in the last places, from the reliability point of view, in both study areas. That might be due to the recent development attained, in the last few years, in both sensor development and data processing techniques.

5. Conclusions

This research study has investigated the reliability of eight recent global digital elevation models for geomatics and GIS applications. Those models include EarthEnv-D90, SRTM 1, SRTM 3, ASTER, GMTED2010, GLOBE, GTOPO30, and AW3D30. The evaluation has been carried out over two study areas: the Nile delta region, Egypt, representing a flat topography, and Makkah metropolitan area, Saudi Arabia representing a hilly or complex topography region. 416 and 137 control points with measured GPS coordinates along with precise elevations have been utilized in both areas respectively. First, the outlier detection procedure has been applied using the Z-score approach in order to increase the accuracy and integrity of the datasets. It has been concluded that the improvements, or the reduction of the standard deviation, have averages of 8.6% and 10.1% for both study areas respectively. Accordingly, the outlier detection should be a regular routine applied in similar studies.

Based on the accomplished results, it has been concluded that such a judgment procedure should not be carried based on a single statistical measure. A novel re-

liability index is introduced based on the weighted average concept and has been applied in two study areas in both Egypt and Saudi Arabia. The attained results showed that the EarthEnv-D90 and SRTM1 models attain high reliability indexes in the Nile delta region that represents a flat topography. In addition, for the second study area, Makkah, which represents mountainous topography, the GMTED 2010 and EarthEnv-DEM90 models came in the first places on the relative reliability scale of ten. Moreover, the accomplished findings reveal that global DEMs perform better in flat area than in hilly or complex topography. Furthermore, it is concluded that even though the accuracy measures of global DEMs are not high, they present a good candidate when accurate local models are not available.

References

[1] Elaksher, A. (2017) Automatic Correction of DEM Surface Errors. *Journal of Geographic Information System*, **9**, 326-338. https://doi.org/10.4236/jgis.2017.93020

[2] Ouerghi, S., Elsheikh, R., Achour, H. and Bouazi, S. (2015) Evaluation and Validation of Recent Freely-Available ASTER-GDEM V.2, SRTM V.4.1, and DEM Derived from Topographic Maps over SW Grombalia (Test Area) in North East of Tunisia. *Journal of Geographic Information System*, **7**, 266-279. https://doi.org/10.4236/jgis.2015.73021

[3] Reddy, G., Kumar, N., Sahu, N. and Singh, S. (2017) Evaluation of Automatic Drainage Extraction Thresholds Using ASTER GDEM and Cartosat-1 DEM: A Case Study from Basaltic Terrain of CENTRAL India. *The Egyptian Journal of Remote Sensing and Space Sciences*. https://doi.org/10.1016/j.ejrs.2017.04.001

[4] Fernandeza, A., Adamowskib, J. and Petrosellic, A. (2016) Analysis of the Behavior of Three Digital Elevation Model Correction Methods on Critical Natural Scenarios. *Journal of Hydrology: Regional Studies*, **8**, 304-315. https://doi.org/10.1016/j.ejrh.2016.09.009

[5] Dawod, G., Mirza, M. and Al-Ghamdi, K. (2011) GIS-Based Spatial Mapping of Flash Flood Hazards in Makkah City, Saudi Arabia. *Journal of Geographic Information System*, **3**, 217-223. https://doi.org/10.4236/jgis.2011.33019

[6] Ahmed, R. and Singh, R. (2017) Seismic Hazard Assessment of Syria Using Seismicity, DEM, Slope, Active Faults, and GIS. *Journal of Remote Sensing Applications: Society and Environment*, **6**, 59-70. https://doi.org/10.1016/j.rsase.2017.04.003

[7] Farahan, Y. (2017) Morphometric Assessment of Wadi Wala Watershed, Southern Jordan Using ASTER (DEM) and GIS. *Journal of Geographic Information System*, **9**, 158-190. https://doi.org/10.4236/jgis.2017.92011

[8] Becker, D., de Andrés-Herrero, M., Willmes, C., Weniger, G. and Bareth, G. (2017) Investigating the Influence of Different DEMs on GIS-Based Cost Distance Modeling for Site Catchment Analysis of Prehistoric Sites in Andalusia. *International Journal of Geo-Information*, **6**, 1-28.

[9] Du, Y., Xu, Q., Zhang, L., Feng, C. and Lin, C. (2017) Recent Landslide Movement in Tsaoling, Taiwan Tracked by TerraSAR-X/TanDEM-X DEM Time Series. *Journal of Remote Sensing*, **9**, 353. https://doi.org/10.3390/rs9040353

[10] Mokarrama, M. and Hojati, M. (2016) Landform Classification Using a Sub-Pixel Spatial Attraction Model to Increase Spatial Resolution of Digital Elevation Model (DEM). *The Egyptian Journal of Remote Sensing and Space Sciences*. https://doi.org/10.1016/j.ejrs.2016.11.005

[11] Hasan, E., Khan, S. and Hong, Y. (2015) Investigation of Potential Sea Level Rise Impact on the Nile Delta, Egypt Using Digital Elevation Models. *Journal of Environmental Assessment Monitoring*, **187**, 649. https://doi.org/10.1007/s10661-015-4868-9

[12] Al-Ghamdi, K., Mirza, M., Elzahrany, R. and Dawod, G. (2012) GIS Evaluation of Urban Growth and Flood Hazards: A Case Study of Makkah City, Saudi Arabia. *FIG Working Week* 2012, Rome, 6-10 May 2010.

[13] Elkhrachy, I. (2017) Vertical Accuracy Assessment for SRTM and ASTER Digital Elevation Models: A Case Study of Najiran City, Saudi Arabia. *Ain Shams Engineering Journal*. https://doi.org/10.1016/j.asej.2017.01.007

[14] Al-Karargy, E., Hosny, M. and Dawod, G. (2015) Investigating the Precision of Recent Global Geoid Models and Global Digital Elevation Models for Geoid Modelling in Egypt. *The Regional Conference on Surveying and Development*, Sharm El-Sheikh, 3-6 October 2015.

[15] Mukherjee, S., Joshi, P., Mukherjee, S., Chosh, A., Garg, R.D. and Mukhopadhyay, A. (2013) Evaluation of Vertical Accuracy of Open Source Digital Elevation Model (DEM). *International Journal of Applied Earth Observation and Geoinformation*, **21**, 205-217. https://doi.org/10.1016/j.jag.2012.09.004

[16] Mirza, M., Dawod, G. and Al-Ghamdi, K. (2011) Accuracy and Relevance of Digital Elevation Models for Geomatics Applications—A Case Study of Makkah Municipality, Saudi Arabia. *International Journal of Geomatics and Geosciences*, **1**, 803-812.

[17] NIST (US National Institute of Standards and Technology) (2012) Engineering Statistics Handbook. http://www.itl.nist.gov/div898/handbook/toolaids/pff/E-Handbook.pdf

[18] Althumania, D. and Achour, H. (2014) External Validation of the ASTER GDEM2, GMTED2010 and CGIAR-CSI-SRTM v4.1 Free Access Digital Elevation Models (DEMs) in Tunisia and Algeria. *Journal of Remote Sensing*, **6**, 4600-4620.

[19] Patel, A., Katiyar, S. and Prasas, V. (2016) Performance Evaluation of Different Open Source DEM Using Differential Global Positioning System (DGPS). *The Egyptian Journal of Remote Sensing and Space Sciences*, **19**, 7-16. https://doi.org/10.1016/j.ejrs.2015.12.004

[20] Dawod, G., Al-Ghamdi, K. and Mandoer, M. (2017) Optimum Sites for Solar Energy Harvesting in Makkah Metropolitan Area Based on Multi-Criteria GIS. *The* 11*th National Conference on GIS Applications*, Imam Abdul Rahman Bin Faisal University, Dammam, Saudi Arabia, 11-13 April 2017. (In Arabic)

[21] Ghaieb, A., Rebai, N. and Bouaziz, S. (2016) Vertical Accuracy Assessment of SRTM Ver 4.1 and ASTER GDEM Ver 2 Using GPS Measurements in Central West of Tunisia. *Journal of Geographic Information System*, **8**, 57-64. https://doi.org/10.4236/jgis.2016.81006

American Journal of Geographic Information System 2018, 7(4): 118-124
DOI: 10.5923/j.ajgis.20180704.03

Gis-Based Accuracy Assessment of Global Geopotential Models: A Case Study of Egypt

Ahmed El Shouny[1,2,*], Essam M. Al-Karagy[2], Hoda F. Mohamed[2], Gomaa M. Dawod[2]

[1]King AbdulAziz University, Department of Geomatics, Faculty of Environment Design, Jeddah, Saudi Arabia
[2]Survey Research Institute, National Water Research Center, Giza, Egypt

Abstract Geoid modelling is a fundamental procedure in geomatics and geosciences applications to estimate the orthometric heights from the ellipsoidal heights measured using **G**lobal **N**avigation **S**atellite **S**ystems (GNSS) observations. In case of no local geoid model is available for any area, a **G**lobal **G**eopotential **M**odel (GGM) is utilized for height conversion. However; the availability of too many GGMs, more than 160 models, makes the selection of the most acceptable one is a significant task. This paper aims to develop a straightforward scheme to acquire, manipulate, and investigate the accuracy of GGMs, within a **G**eographic **I**nformation **S**ystems (GIS) environment. Four GGMs, namely XGM2016, GECO, EIGEN-6C4, and EGM2008, have been utilized in Egypt. Accomplished results show that the standard deviations of the investigated GGMs' discrepancies, over Egypt, range from ± 10.90 mGal to ± 13.10 mGal for gravity anomalies, and from ± 0.23 m to ± 0.30 m for geoid heights. In order to pick up the optimum GGM, a dimensionless reliability index is computed for each GGM. Based on the investigated GGMs, the available datasets, and also the proposed criteria applied in analyzing results in this paper, we can conclude that the EGM2008 is still the most suitable GGM for representing the gravitational field over Egypt with an average reliability index of 5.10. The proposed efficient GIS-based process is practically beneficial for height conversion in several geodetic, environmental, surveying, and mapping applications in Egypt.

Keywords GGM, Geoid, Gravity, GNSS, GIS, Egypt

1. Introduction

Civil and surveying engineers deal with three fundamental surfaces of the Earth and; consequently, several types of heights. These surfaces include the terrain or physical surface, geoid or the true irregular equipotential surface of the Earth, and the ellipsoid or the most nearest regular mathematical surface to the geoid. The ellipsoidal height is measured from an ellipsoid, while the orthometric height is based on the geoid. The vertical separation between these both surfaces represents the geoid undulation or geoidal height. Hence, geoid modelling is needed for transforming the ellipsoidal heights, related to the ellipsoid surface, estimated from (GNSS) measurements into orthometric heights, related to the Mean Sea Level (MSL), which obtained using levelling works. This transformation is necessary because the important needs of this orthometric heights in topographic maps, and many other applications in civil engineering. The comparison of (GGM)s over a spatial region is crucial to choose the most suitable one to be used in geoid modelling [1]. In addition, the availability of more than 160 GGMs currently makes the assessment of their performance in representing the gravitational field over a selected area is essential, e.g., Japan [2], and Argentina [3]. In Egypt, geoid modelling and different (GGM)s evaluation have been tremendously investigated in the last couple of decades, e.g. [4] and [5].

Number of researches has utilized Geographic Information Systems (GIS) in geodetic applications in general, and in geoid modelling in particular. GIS-based raster analysis has been used to improve the GGM-derived geoidal heights through linear sharpening the original raster representation of the models [6]. [7] Investigated the possibility of developing a local geoid model by evaluating several GGMs within a GIS environment. However, this study used GIS just to compare the results obtained from an online service for point-by-point geoid calculations, which is not the case of the present study. Over a small spatial region where little number of known GNSS/levelling points are available, GIS could be used, first, to build a local geoid model, and then to interpolate geoidal heights at other unknown GNSS stations to estimate their corresponding orthometric heights [8] and [9].

The International Center for Global Earth Model (ICGEM) organization, recently, starts an online service to compute

* Corresponding author:
elshoney2003@yahoo.com (Ahmed El Shouny)
Published online at http://journal.sapub.org/ajgis
Copyright © 2018 The Author(s). Published by Scientific & Academic Publishing
This work is licensed under the Creative Commons Attribution International License (CC BY). http://creativecommons.org/licenses/by/4.0/

many geoidal properties and deliver them in a grid format [10]. Based on that precious service, the assessment of GGMs utilizing national geodetic data could be carried out, solely, by GIS. The main objective of this paper is to develop a simple scheme to acquire, manipulate, investigate the accuracy of GGMs over Egypt region, to determine the most appropriate model and enhance its precision, completely, within a GIS environment. This work can be considered as an extra GIS-based geodetic application for height conversion in Egypt.

2. Global Geopotential Models

GGMs have been developed since 1960s to express the gravitational potential of the Earth (V) into a series of spherical harmonics as: (for more details, refer for example to [11])

$$V = \frac{GM}{r}\left(\sum_{n=0}^{N\max}(\frac{a}{r})^n\sum_{m=0}^{n}\left[C_{nm}\cos m\lambda + S_{nm}\sin m\lambda\right]P_{nm}(\cos\vartheta)\right) \quad (1)$$

where: GM is the gravitational constant, r is the radial distance, a is the equatorial radius of the Earth, θ and λ are the latitude and longitude respectively, J_n are the zonal harmonics, those contain the S_{nm} and C_{nm} are the tesseral harmonics, P_{nm} are the associated Legendre coefficients n and m are the degree and order of the geopotential model, and N_{max} is the maximum degree of the model. The geoidal undulations or geoidal heights (N), representing the difference between the geoid and ellipsoid surfaces, can be evaluated through two methods based on available geodetic measurements. First, it can be computed through the well-known Stokes' formula, if gravity anomalies are utilized, N_{grav}, as:

$$N_{grav} = \frac{R}{4\pi\gamma_o}\iint_{\sigma}\Delta g S(\Psi)d\sigma \quad (2)$$

Where: R is the radius of the Earth, Δg is the gravity anomalies, and S (Ψ) is the Stokes' function, and dσ is an infinitesimal surface element on the unit sphere σ. In practice, the geoidal undulation, N, is divided into three components and computed as:

$$N_{grav} = N_{res} + N_{GGM} + N_H \quad (3)$$

Where, N_{res} is the geoidal undulation component related to residual gravity anomalies, N_{GGM} is the component related to GGM, and N_H is the component related to topography effect. Consequently, geoid modelling requires the utilization of a GGM to represent the global variations or long wavelengths of the Earth gravitational field, along with a Digital Elevation Model (DEM) to depict the topography of the local area and determine its effects on the developed geoid model.

The second manner of computing geoidal heights is the so-called GNSS/levelling or the geometric approach, where $N_{geometric}$ can be computed from both GNSS-based ellipsoidal heights relative the ellipsoid surface (h) and the orthometric heights related to MSL (H) as:

$$N_{geometric} = h - H \quad (4)$$

In this paper, four GGMs have been selected for evaluation, namely: Experimental Gravity Field Model (XGM2016), GOCE and EGM2008 combined model (GECO), European Improved Gravity model of the Earth by (EIGEN-6C4), and Earth Geopotential Model (EGM2008). Although the first one is a medium-resolution model, it has a great attention since it would be the basis for the upcoming Earth Geopotential Model 2020 (EGM2020), while the other three GGMs have been selected since they represent high-resolution models with degree and order equal 2190. A brief description of each model is follows:

- XGM2016: The experimental gravity model is a GGM up to 719 degree and order, supported by an improved terrestrial global data of 15'x15' gravity anomalies, along with satellite-based gravity data from the Gravity Recovery and Climate Experiment (GRACE) and the Gravity and Ocean Circulation Explorer (GOCE). XGM2016 utilized, in addition, new promising processing methodology [12].
- GECO: A global gravity model utilizes the GOCE satellite-based gravity data to improve the accuracy of the EGM2008 GGM in low and medium frequencies. GECO is developed, in 2015, up to degree and order 2190 [13]. GECO is the most-recent published high -resolution GGM until 2017.
- EIGEN-6C4: A model released in 2014, that utilizes satellite tracking data (from LAGEOS, GRACE, and GOCE missions) along with a global surface gravity anomaly grid and altimetry data. The model is up to 2190 degree, developed by both the Germany GFZ research center, and the French CNES research center [14].
- EGM2008: An integrated GGM developed by the US National Geospatial-Intelligence Agency (NGA) up to 2190 degree. It was developed in 2008 based on GRACE-based satellite tracking data, terrestrial gravity data, and altimetry data. It was a millstone in GGM development, since its preceding model did not exceed 360 maximum degree [15].

The evaluation of equation 2 over a spatial region requires a specific mostly-academic software package, e.g., GRAVSOFT and GRAFIM, prior to apply GIS for modelling and mapping obtained results. However, the handling and assessment of GGMs carried out in this study, is performed, totally, within a GIS environment. The performance of each GGM in representing the gravity field over Egypt is, first, investigated and then, the obtained GGM-based free-air gravity anomalies against the free-air gravity anomalies of the known terrestrial stations (Δg) are compared. At these stations, relative gravity have been measured and tied to the national absolute gravity network, to obtain absolute gravity values. So, the free-air gravity anomalies are computed as:

$$\Delta g = g + 0.3086H - \left[\gamma_a \frac{1 + p\sin^2 \vartheta}{\sqrt{1 - e^2 \sin \vartheta}} \right] \quad (5)$$

Where: g is the known absolute gravity, H is the orthometric height obtained from precise levelling, γ_a and γ_b are the equatorial and polar normal gravity values, e^2 is the second eccentricity of the used ellipsoid, and p = (b γ_b / a γ_a) - 1, where a and b are the WGS84 semi-major and semi-minor ellipsoidal axis respectively.

The second GIS-based comparison step judges the GGM-based geoidal heights against the known GNSS/levelling undulations at the utilized stations in Egypt. Differences in both steps are; consequently, statistically investigated to define the accuracy and reliability of the tested GGMs.

3. Processing and Analysis

The available terrestrial geodetic datasets include (as shown in Fig. 1): The first-order Egyptian national gravity networks of both 1997 and 1977 containing 247 measured gravity points (shown in red dots symbol); and 976 GNSS/levelling stations (shown in green dots symbol) all over Egypt, that were observed by the Survey Research Institute (SRI) in various projects over the last five years. It worth mentioning that the average accuracy of the Egyptian National Gravity Standardization Network of 1997 (ENGSN97) is ± 0.02 mGal; while the corresponding value of the National Gravity Standard Base Network of 1977 (NGSBN77) is ± 0.08 mGal. Although, there are other available second-order gravity measurements in Egypt, particularly in the western desert, their accuracy in both gravity and coordinates are questionable. The utilized GPS/levelling points have been surveyed using the first-order levelling, and the first-order GPS geodetic network standards, and their average accuracy could be estimated as ± (3 – 4) cm. Thus, the most-precise available national datasets have been utilized, herein, to investigate the reliability of the four tested GGMs as will be discussed in details in the next section.

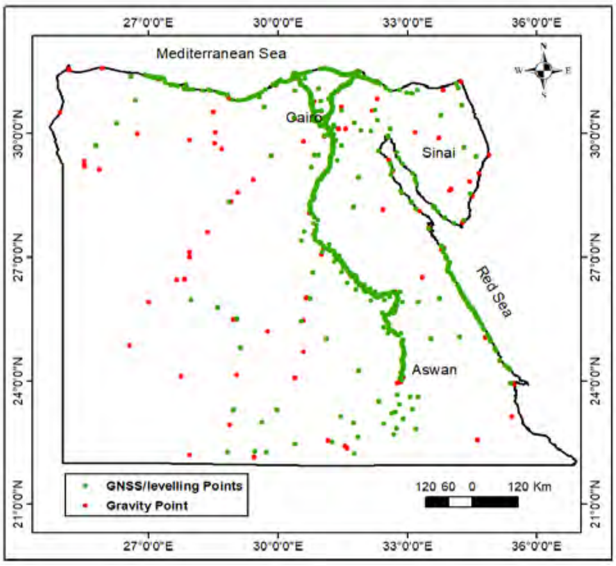

Figure 1. Available Terrestrial Data

As stated previously, the ICGEM organization starts an online service to compute many geoidal properties (for some GGM) and deliver them in a grid format [10]. For any GGM, a specified grid could be computed online and downloaded for a variety of geoidal characteristics such as geoid heights, height anomaly, gravity anomaly, and gravity disturbance. Each grid has a gdf format, which can be easily manipulated to be applicable for GIS. Therefore, two 5'x5' grids, for gravity anomaly and geoid heights, have been downloaded for each model of the other three tested GGMs. The interpolated gravity anomaly and geoid undulation values at each control point have been compared against their known values, and their differences are statistically investigated. The ArcGIS 10 software has been utilized, herein, for interpolation and mapping as an example of GIS packages. Figures 2 and 3 depict the gravity anomaly and geoidal undulations for those GGMs.

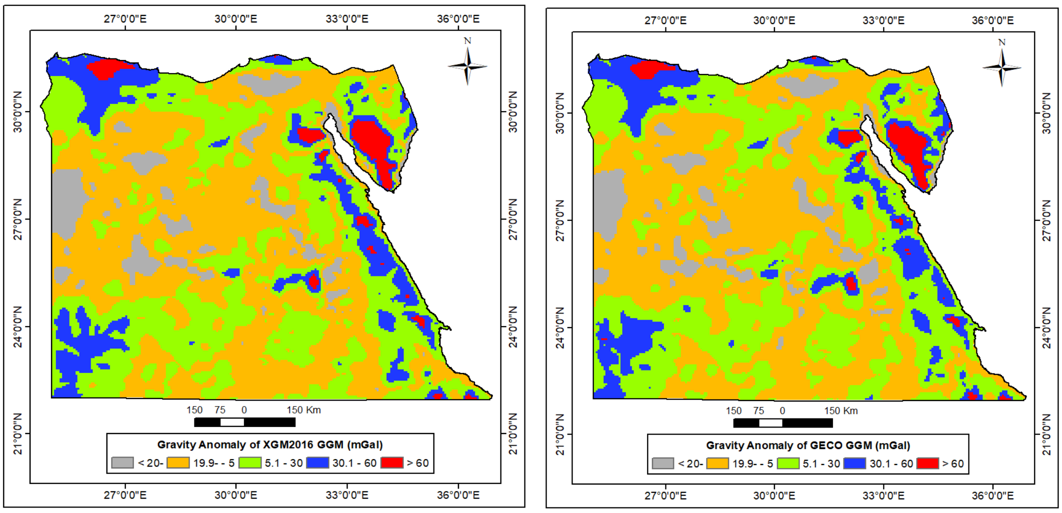

(a) (b)

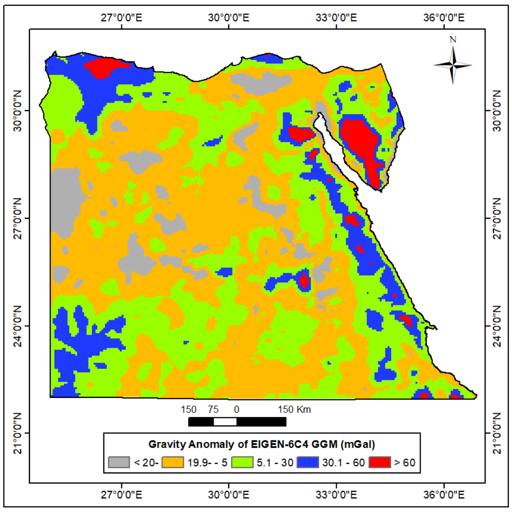

(c)

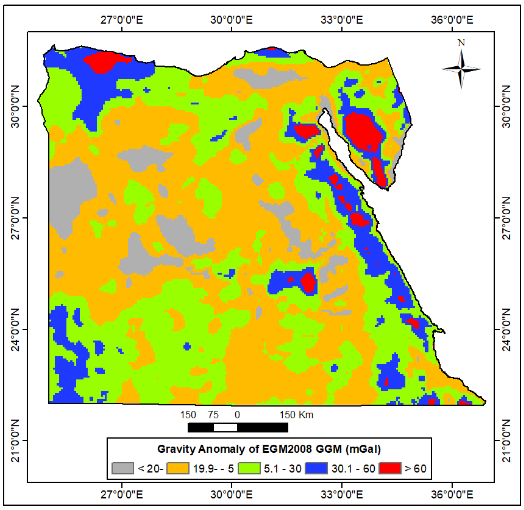

(d)

Figure 2. Gravity Anomaly of: (a) XGM2016, (b) GECO, (c) EIGEN-6C4, (d) EGM2008 Models

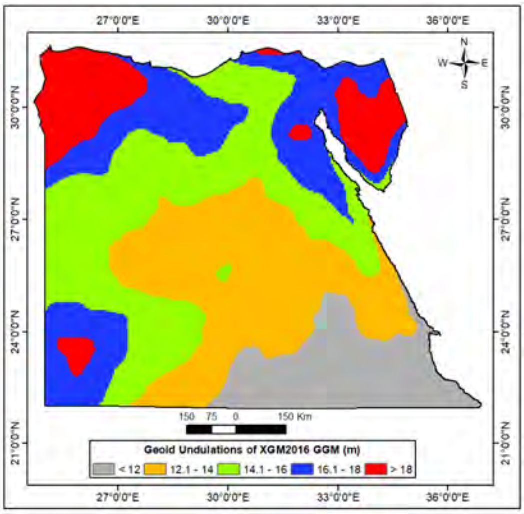

(a)

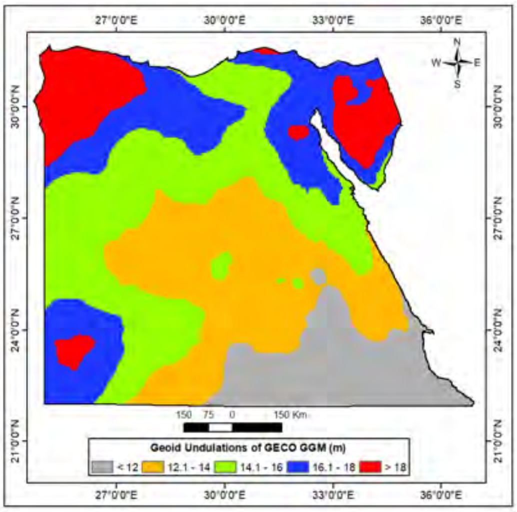

(b)

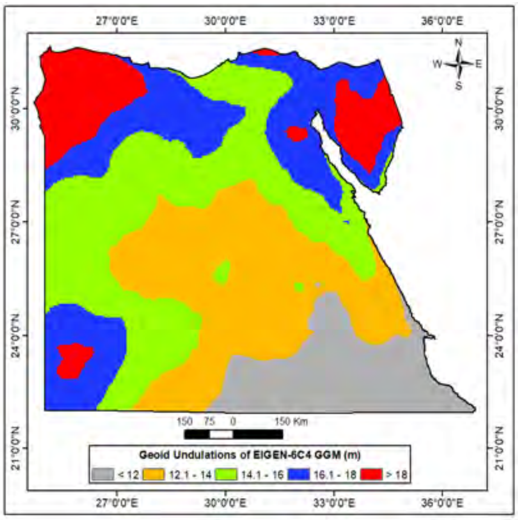

(c)

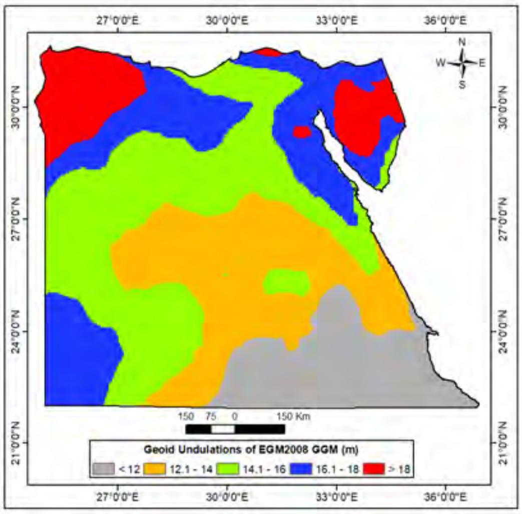

(d)

Figure 3. Geoid Undulations of: (a) XGM2016, (b) GECO, (c) EIGEN-6C4, (d) EGM2008 Models

In the next step, the two utilized control point datasets have been used to interpolate the GGM-based gravity anomalies and geoidal heights from each GGM corresponding raster. The Inverse Distance Weighted (IDW) interpolation method has been adopted, since the geoid variations over Egypt region are moderately depend inversely on distances. Then, the known gravity anomaly and geoid undulation, for each station, have been compared against the corresponding values obtained from each GGM. Table 1 presents the statistical properties of those differences for the utilized four GGMs, while Fig. 4 depicts the histograms of those differences.

It can be realized, from Table 1 and the histograms in Fig. 4 that the standard deviations of the investigated GGMs' discrepancies, over Egypt, range from ± 10.90 to ± 13.10 mGal for gravity anomalies, and from ± 0.23 to ± 0.30 m in geoid heights. It is interesting to notice, from Fig. 4, that the results of the XGM2016 model, even though its degree equal 790, are close to those of the other high-resolution GGMs. Moreover, table 4 indicates that the statistical measures vary from one model to another, for example, EIGEN-6C4 has the best standard deviation, while GECO has the least range of differences, and EGM2008 got the least average in gravity anomalies. The same remark is valid; also, for the GGMs-based geoid undulation differences. Therefore, judging the performances of GGMs should not be accomplished based on a single statistical measure. Hence, the concept of reliability index, as introduced by [16], is applied herein. A reliability index (RI) is computed, for each GGM, as a weighted mean of three individual indices define the relative value for the three statistical measures: the mean, range, and standard deviation.

Table 1. GGM Differences at Local Known Control Points

GGM	XGM2016	GECO	EIGEN-6C4	EGM2008
Minimum dΔg (mGal)	-45.85	-30.74	-34.79	-41.43
Maximum dΔg (mGal)	45.90	40.89	41.96	43.55
Range dΔg (mGal)	91.74	71.62	76.75	84.98
Mean dΔg (mGal)	-1.79	-1.82	1.25	-0.97
Standard Déviation dΔg (mGal)	± 13.10	± 11.01	± 10.90	± 11.32
Minimum dN (m)	-1.52	-1.52	-1.44	-0.90
Maximum dN (m)	0.44	0.44	0.46	0.09
Range dN (m)	1.96	1.96	1.91	0.99
Mean dN (m)	-0.57	-0.57	-0.60	-0.55
Standard Deviation dN (m)	± 0.30	± 0.30	± 0.30	± 0.23

For each statistical measure, the values of all GGMs have been sorted in a descending order, and descending ranks, on a scale of 10. So, unique dimensionless RI values are obtained for the mean, range, and standard deviation. Then, the overall RI is computed as the weighted mean of the individual RI values. The utilized weights are 4 for the standard deviation, and 3 for both the mean and range. Therefore, it can be realized that the mean RI is unitless in nature that describes the overall accuracy performance of each GGM. That procedure has been repeated twice to obtain final RI for both gravity anomalies and geoidal heights of each investigated GGM. Accomplished results are tabulated in Table 2, which reveals that the EGM2008 is the optimum GGM for representing the gravitational field over Egypt with an average reliability index of 5.10, the EIGEN-6C4 comes in the second place, and the GECO comes third while the XGM2016 is the most worst GGM of the four investigated GGMs. Once more, it can be seen that the XGM2016 medium-resolution GGM performance is approximately similar to the GECO and EIGEN-6C4 high-resolution models.

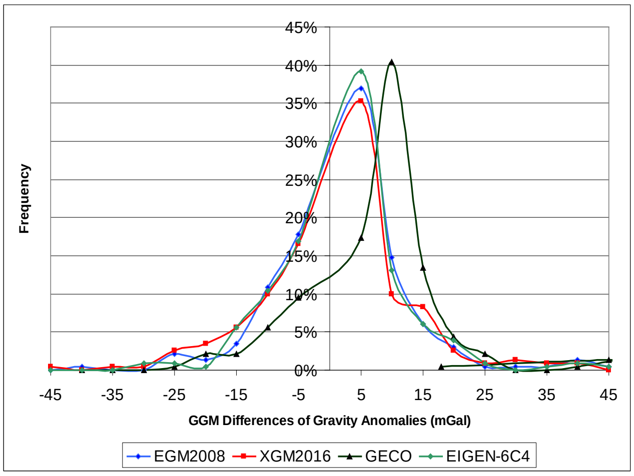

(a)

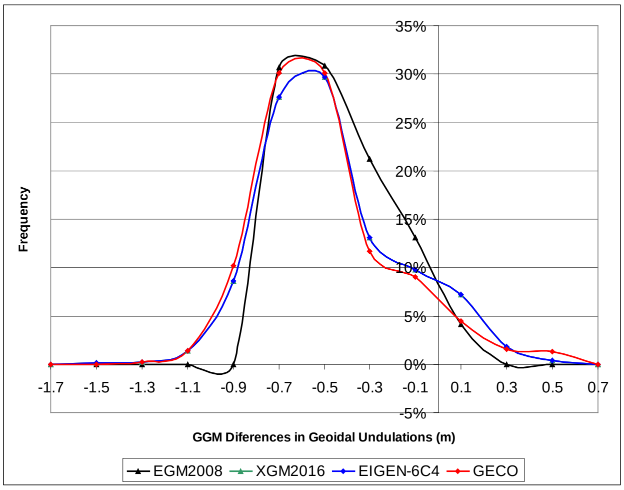

(b)

Figure 4. Histograms of GGMs differences for: (a) Gravity anomalies, (b) Geoidal Undulations

Table 2. Reliability Indices of GGM Differences (Unitless, on a scale of 10)

GGM	XGM2016	GECO	EIGEN-6C4	EGM2008
RI for dΔg	3.46	4.04	4.37	4.56
RI for dN	3.67	3.67	3.70	5.64
Mean RI	3.56	3.85	4.03	5.10

According to the obtained results represented, two important remarks should be highlighted here regarding the investigated GGMs and the available data. First notice is that the EGM2008 is the most suitable GGM, until now, to be applied in geoid modelling in Egypt. Second one: the XGM2016 is a promising model to represent the long wavelength of gravity, which indicates that the upcoming EGM2020 would be more precise in representing the Earth's gravitational field. Finally, the undulation errors of EGM2008 have been spatially modeled, using the IDW interpolation method, as a raster format (Fig. 5). Therefore, equation 4 will be modified into:

$$H = h - (N_{EGM\,2008} - E_{EGM\,2008}) \qquad (6)$$

Where, $N_{EGM2008}$ is the original geoid undulation of the EGM2008 model, and $E_{EGM2008}$ represents its error estimate as interpolated from the correction surface at any GNSS observed station.

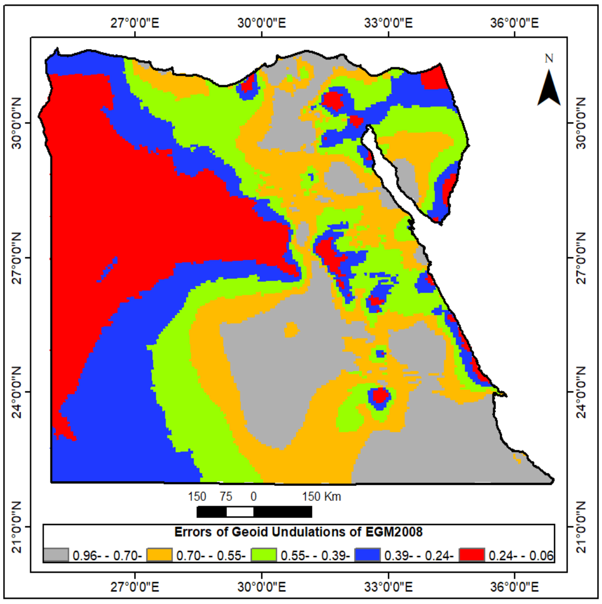

Figure 5. EGM2008's Geoidal Undulations Correction Surface

Along the current study area, it will be easy for GNSS users after observing the geodetic height of any point (h), to calculate its orthometric height (H) by estimating undulation value at this point using EGM2008 and also estimating undulation corresponding value from the EGM2008 correction surface, which should be open-access available. Consequently, within a specific level of precision applicable to small-scale mapping, such a practice significantly reduces the economic costs of field data collection stage as a result of dispensing levelling works anymore. Such a developed process is valuable for all GNSS-based surveying, mapping, data collection, and GIS activities in Egypt. Same procedures could be applied for heights transformation in any other country or regions.

4. Conclusions

GIS has been widely applied in numerous geodetic, surveying, and mapping activities. The creation of local geoid models over small areas and geoid interpolation have been, also, investigated using GIS. This paper presents a straightforward scheme to acquire, manipulate GGMs, and determine the most appropriate model and enhance its precision, entirely, within a GIS environment. Such a task, typically, was accomplished using specific mostly-academic geodetic software. GNSS and GIS users can considerably benefit from our proposed simple method in various geodetic activities. It is a matter of fact that an optimum GGM is required to convert the GNSS-based ellipsoidal heights into the MSL-based orthometric heights, or elevations, which is used in civil engineering different applications. The developed plan is mainly based on the ICGEM service, through downloading two grid files for each GGM, one for the gravity anomalies and the other for geoidal undulations. Using GIS, the precision and reliability of each GGM can be assessed over national geodetic databases, to determine the most suitable GGM to be used along any country or spatial region. The proposed method can be considered as a powerful GIS-based geodetic application for height conversion along Egypt region.

The current study has utilized four GGMs in Egypt along with precise local geodetic datasets. Based on the introduced reliability measure and the available datasets, it has been concluded that the EGM2008 is still the best possible GGM, out of the investigated models, for representing the gravitational field over Egypt with an average reliability index of 5.10 on a scale of 10. A GIS-based correction surface has been; also, developed to increase its accuracy in GNSS height conversion for several geodetic, environmental, surveying, and mapping applications. The proposed approach could be; similarly, applied in other countries as well.

REFERENCES

[1] Al-Krargy, E., Hosny, M. and Dawod, G. (2015) Investigating the precision of recent global geoid models and global digital elevation models for geoid modelling in Egypt, *Regional Conference on Surveying and Development*, Sharm El-Sheikh, Egypt, Oct. 3-6.

[2] Odera, P. and Fukuda, Y. (2017) Evaluation of GOCE-based global gravity field models over Japan after the full mission using free-air gravity anomalies and geoid undulations, *Earth, Planets and Space*, DOI: 10.1186/s40623-017-0716-1.

[3] Gomez, M., Perdomo, R., and Cogliano, D. (2017) Validation of recent geopotential models in Tierra Del Fuego, *Acta Geophysics*, No. 65: 931-943.

[4] Alnaggar, D. (1986) Determination of the geoid in Egypt using heterogeneous geodetic data, PhD dissertation, Faculty of Engineering, Cairo University, Egypt.

[5] Abd-Elmotaal, H. (2015) Egyptian geoid using best estimated response of the Earth's crust due to the topographic loads, Presented at the International Association of Geodesy Symposium, Switzerland, DOI: 10.1007/1345_2015_194.

[6] Hassouna, R. and Asal, F. (2016) Using GIS-based digital raster analysis for improving harmonic models-derived geoidal heights, *Applied Geomatics*, 8:151–162.

[7] Idrizi, B. (2013) Developing model for utilization of global earth gravimetrical models in Macedonian territory, Proceedings of the FIG Working Week 2013, Abuja, Nigeria, May 6–10.

[8] Liu, S., Li, J., and Wang, S. (2011) The GPS height conversion method based on moving-surface fitting, Proceedings of the International Conference on Computer Science and Network Technology, December 24-26, Harbin, China, pp. 2113-2116.

[9] Das, R., Samanta, S., Jana, S. and Rosa, R. (2017) Polynomial interpolation methods in development of local geoid model, *The Egyptian Journal of Remote Sensing and Space Sciences*, DOI: 10.1016/j.ejrs.2017.03.002.

[10] ICGEM (The International Center for Global Earth Model) (2018), http://icgem.gfz-potsdam.de/tom_longtime, Accessed 20 February 2018.

[11] Hofmann-Wellenhof, B. and Moritz, H. (2005) *Physical geodesy*, SpringerWien, New York.

[12] Pail, R. Fecher, T., Barnes, D., Factor, J., Holmes, S., Gruber, T., and Zingerle, P. (2017) Short note: the experimental geopotential model XGM2016, *Journal of Geodesy*, DOI: 10.1007/s00190-017-1070-6.

[13] Gilardoni, M., Reguzzoni, M., Sampietro, D. (2016) GECO: a global gravity model by locally combining GOCE data and EGM2008; *Studia Geophysica et Geodaetica*, Vol 60: 228-247.

[14] Förste, C., Bruinsma, S., Abrikosov, O., Lemoine, J., Marty, J., Charles, F., Frank, B., Barthelmes, F., Biancale, R. (2014) EIGEN-6C4: The latest combined global gravity field model including GOCE data up to degree and order 2190 of GFZ Potsdam and GRGS Toulouse, Presented in the 5th GOCE user workshop, Paris, France, Nov. 25-28, DOI: 10.5880/ICGEM.2015.1.

[15] Pavlis, N.K., Holmes, S.A., Kenyon, S.C., Factor, J.K. (2008) An Earth Gravitational Model to Degree 2160: EGM2008, Presented in the EGU general assembly, Vienna, Austria, April 13-18.

[16] Dawod, G. and Al-Ghamdi. K. (2017) Reliability of recent global digital elevation models for geomatics applications in Egypt and Saudi Arabia, *Journal of Geographic Information System*, V. 9(6): 685-698.

American Journal of Geographic Information System 2018, 7(4): 107-117
DOI: 10.5923/j.ajgis.20180704.02

Development and Accuracy Assessment of High-Resolution Digital Elevation Model Using GIS Approaches for the Nile Delta Region, Egypt

Mohammed El-Quilish[1,*], Mohamed El-Ashquer[1], Gomaa Dawod[2], Gamal El Fiky[1]

[1]Construction Engineering and Utilities Department, Faculty of Engineering, Zagazig University, Zagazig, Egypt
[2]Survey Research Institute, National Water Research Center, Giza, Egypt

Abstract A high accuracy Digital Elevation Model (DEM) for the Nile delta region, Egypt is needed for several environmental applications, particularly for investigating the hazardous impacts of sea level rise and land subsidence phenomena. Since there is no official published national DEM for Egypt, an original high accuracy local digital elevation model (LDEM) for that region has been created using nine Spatial Interpolation Methods (SIMs) within a Geographic Information Systems (GIS) environment. The interpolation process took place after digitizing over than 220 topographic maps of scale 1:25,000, where more than 810,000 elevation (spot heights) points have been extracted from these maps. Multiple parameters and criteria for each SIM were applied to reach the optimal settings to produce a LDEM for environmental applications. The developed LDEMs have been compared against eight free Global Digital Elevation Models (GDEMs) using about 200 known GPS/levelling Ground Control Points (GCPs), where a statistical assessment has been accomplished for both GDEMs and LDEMs residuals after applying a vertical and horizontal datum matching for all the used data sets, and an outlier detection procedure. Also, a Reliability Index (RI) has been calculated to determine the best DEM for the Nile Delta region. The accomplished results showed that EARTHEnv-DEM90 attained the highest RI of 5.47 as the optimum global DEM. For local DEM's interpolation methods, it is concluded that the Kriging-based local DEM attained highest RI of 9.27. Consequently, it has been concluded that the new developed high accuracy LDEM improves the overall accuracy and reliability of the best available GDEM by almost 41%, and, hence, it is appropriate for geospatial, environmental, and GIS studies in Egypt.

Keywords Digital Elevation Model (DEM), Spatial Interpolation Methods (SIMs), GPS/levelling, GIS

1. Introduction

A Digital Elevation Model (DEM) is a digital cartographic representation of ground surface topography or terrain's elevations with different accuracies for different field applications. It is also defined as a quantitative 3D representation of the Earth's surface providing basic information about the terrain relief and considered one of the most popular data models used for the purpose of terrain modeling. DEM has been applied to a wide range of GIS, surveying, civil engineering and military planning tasks and applications depending on its accuracy such as: geomatics, geodetic, geological, hydrological, environmental, meteorological studies, and Mapping applications. Even though there are several available free global DEMs, their accuracy and spatial resolutions vary significantly, and a national DEM is required in several countries for national spatial Infrastructure and other accurate geospatial applications (e.g. Verhulp, 2015, and Kokkonen et al., 2017).

For Egypt, it is a matter of fact that there is no official published precise LDEM, and several research studies have been carried out using global DEMs despite their poor accuracies. On the other hand, many scholars have developed LDEM in the last two decades. For example, Abd-Elmotaal (1999, 2004, 2009, 2011, 2013), and Abd-Elbaky et al. (2009) have created several detailed DEMs with 1" arc-sec spatial resolution for Egypt and the surrounding region using the ASTER GDEM and filled the gaps with 30″×30″ SRTM30+ after using the kriging interpolation technique to the same grid size. El-Sagheer (1995, and 2004) has developed a LDEM for EGYPT (called DTM-2003) through digitizing 1:250,000 and 1:100,000 hard copy topographic maps. Shaker (2015) has introduced an approach for contour-based DEM generation based on multiple polynomials interpolation from 1:100,000

* Corresponding author:
mayd_007@yahoo.com (Mohammed El-Quilish)
Published online at http://journal.sapub.org/ajgis
Copyright © 2018 The Author(s). Published by Scientific & Academic Publishing
This work is licensed under the Creative Commons Attribution International License (CC BY). http://creativecommons.org/licenses/by/4.0/

topographic contours for Sinai Peninsula, with a vertical accuracy of 2.38 m. (Rabah et al., 2017) have compared three GDEMs (namely SRTM 1, SRTM 3, and ASTER) over precise GPS/levelling control points. Their results showed that the SRTM 1 had the smallest differences and the most accurate one, that it produced mean height difference and standard deviations equal 2.89 and ±8.65 m respectively. Dawod and Al-Ghamdi (2017) have investigated the reliability of eight recent GDEMs (namely EarthEnv-D90, SRTM 1, SRTM 3, ASTER, GMTED2010, GLOBE, GTOPO30, and AW3D30) for geomatics and GIS applications in the Nile delta region, where 416 GPS/levelling control points. They have introduced the reliability Index (RI), which is a statistical measure for judging DEMs based on the weighted average mean concept, and they have applied for the study area. Their results showed that the EarthEnv-D90 and SRTM1 models attain high RI in the Nile delta region.

Several GDEM have been developed and released in the last two decades. Nevertheless, their spatial resolution, precision and accuracy vary significantly. In this research, eight existing GDEMs were freely downloaded from their respective websites and utilized in order to cover the study area namely (AW3D30, ASTER EARTHEnv-DEM90, GLOBE, GMTED2010, GTOPO30, SRTM1, and SRTM3). Table 1 summarizes the characteristics of these selected GDEMs.

Table 1. Characteristics of the utilized global DEM

GDEM	Full Name	Released Year	Spatial Resolution		download from
			arc second	m	
AW3D30	The Advanced Land Observing Satellite	2015	1”	~30	https://www.eorc.jaxa.jp/ALOS/en/aw3d30/
SRTM 1	Shuttle Radar Topography Mission	2015	1”	~30	https://earthexplorer.usgs.gov/
ASTER v.2	Advanced Space borne Thermal Emission and Reflection Radiometer	2011	1”	~30	https://asterweb.jpl.nasa.gov/gdem.asp
EARTHEnv -DEM90	-	2014	3”	~90	https://www.earthenv.org/DEM
SRTM 3	Shuttle Radar Topography Mission	2009	3”	~90	https://srtm.csi.cgiar.org/
GMTED2010	Global Multi-resolution Terrain Elevation Data 2010	2011	7.5”	~225	https://topotools.cr.usgs.gov/gmted_viewer/viewer.htm
GLOBE	Global Land One-km Base Elevation	2000	30”	~900	https://www.ngdc.noaa.gov/mgg/topo/globe.html
GTOPO30	Global 30 Arc-Second Elevation	1996	30”	~900	https://earthexplorer.usgs.gov/

On another hand, the suitability of various interpolation methods for creating DEMs comprises a major issue that has been studied in several papers. For example, Her (2008) has evaluated the potential and performance of seven interpolation techniques as a means of resolution refining for hydrological applications. The obtained elevation, slope, aspect, sink, and stream networks from the interpolated DEM were compared quantitatively with those derived from the original DEM. The results showed that the interpolation techniques were not significantly different in deriving elevation, total flow length, and delineating watersheds. However, all methods produced shallower slopes than the original DEM and had a smoothed surface with fewer sinks. Additionally, Luo, (2008) has compared seven spatial interpolation techniques to determine their suitability for estimating daily mean wind speed surfaces, from data recorded at nearly 190 locations across England and Wales. Cross – validation was used to evaluate the performance of each interpolation method by calculating the RMSE for each interpolation method. The results indicated that Kriging was most likely to produce the best estimation of continuous surface for wind speed in the study area. Moreover, Sun (2009) has compared three interpolation methods to determine their suitability for interpolating depth to groundwater in the Minqin oasis of northwest China. Attained results indicated that simple Kriging was the optimal method for interpolating depth to groundwater in the study area. Also, Eldrandaly (2011) has compared six GIS-based SIMs to determine their suitability for estimating mean monthly air temperature surfaces in Western Saudi Arabia. The interpolation techniques included four deterministic methods (IDW, Global Polynomial, Local Polynomial, and Radial Basis Function ‘Thin-Plate Spline’) and two geostatistical methods (Ordinary Kriging, and Universal Kriging). Quantitative assessment of the continuous surfaces showed that there was a large difference between the accuracy of the six interpolation methods and that the geostatistical methods were superior to the deterministic methods. Ikechukwu et al. (2017) examined the accuracy of SIMs in modeling landform (topography) in relation to their mathematical formulation. The performance of Kriging, IDW and Spline interpolation methods were evaluated theoretically, mathematically and experimentally in estimating unobserved elevation values and modeling landform. A comparative analysis based on the prediction mean error, prediction RMSE and cross validation outputs of

these SIMs were evaluated and the results showed that Spline provided a better and more accurate interpolation within the sample space than the IDW and Kriging methods. This research study has two main objectives: investigating the optimum spatial inteerpolation method to create LDEM for detailed environmntal applications; and comparing the accuracy of the developed LDEM versus the available GDEM using GPS/levelling accurate terrstrial geodetic datasets, within a GIS enviroment.

2. Study Area and Available Data

The study area covers most of the Nile delta region north of Egypt from Alexandria at the west (29.6°E) to Port Said at the east (32.3°E) and from the northern Mediterranean coasts at the north (31.6°N) to Cairo at the south (30.0°N), as shown in (Figure 1). It is bounded by the two branches of the Nile river “Damietta and Rosetta”, and extending from both sides to cover coastal areas, with an overall area of approximately 23,235 km^2. The length of the study area is approximately 180 km from north to south, and it covers about 300 km of coastline at the Mediterranean Sea (17.75% of the Egyptian Mediterranean coast). The shoreline is occupied by three major coastal lakes “Lake Burullus, Lake Idku, and Lake Mariut”. The Suez Canal runs to the east of the Delta, entering the coastal Lake Manzala in the northeast of the Delta. The topography of the region smoothly slopes northwards towards the Mediterranean coast, where the difference in elevation between its southern peak, at Cairo, and northern coastal fringes is approximately 18 meter (Embabi 2000).

The available ground control points comprise almost 200 First-Order Bench Marks (BM) with measured accurate GPS coordinates, laying mainly on the two branches of the Nile river and on the coasts of the Mediterranean sea (Figure 1). This dataset has been utilized in evaluating the performance of GDEMs, and to judge the anticipated accuracy of the new developed LDEMs. The accuracy of these points is within five centimetres in both horizontal and vertical coordinates ((Dawod and Al-Ghamdi, 2017).

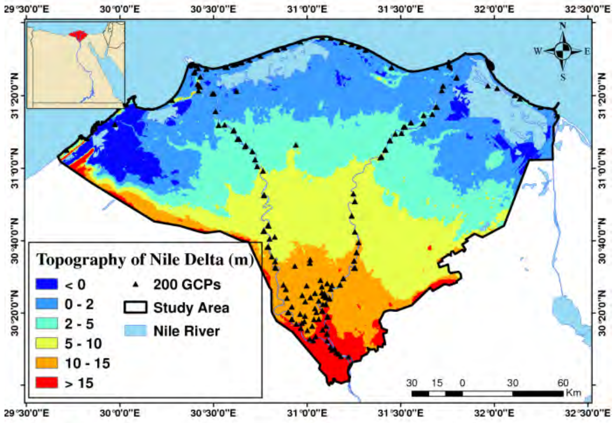

Figure 1. The study area and The Available Ground Control Points

3. Development of a Local DEM

3.1. Digitizing Process

The digitizing process was conducted by obtaining the available topographic maps for the study area as it is covered by 220 topographic maps scale 1:25,000 with contour interval of 50 cm. These maps were published by the survey of Egypt (1924-1951) and derived from ground surveys at the Nile Delta region. In addition, Topographic maps with scale of 1:50,000 and 1:100,000, with a contour interval of 1 m, have been also used to complete the missing zones of the study area due to damages at the 1:25,000 topographic maps. Then, georeferencing and projection process for the horizontal datum was conducted for each one of these maps using the built-in projection tool in ArcGIS from ETM red belt / GCS Egypt 1907 projection to WGS84. That step was just used in the comparison stage of all GDEM and LDEM, while the final LDEM was produced with respect to the local coordinates system. Furthermore, these maps were manually digitized by extracting all the available contour lines and elevation (spot heights) points. The obtained data were about 810,534 points (92,071 from spot height points and 718,463 from contour lines) with an average density of 35 elevation points/km² (Figure 2). Once the digitizing process was completed, LDEMs were created using nine different SIMs.

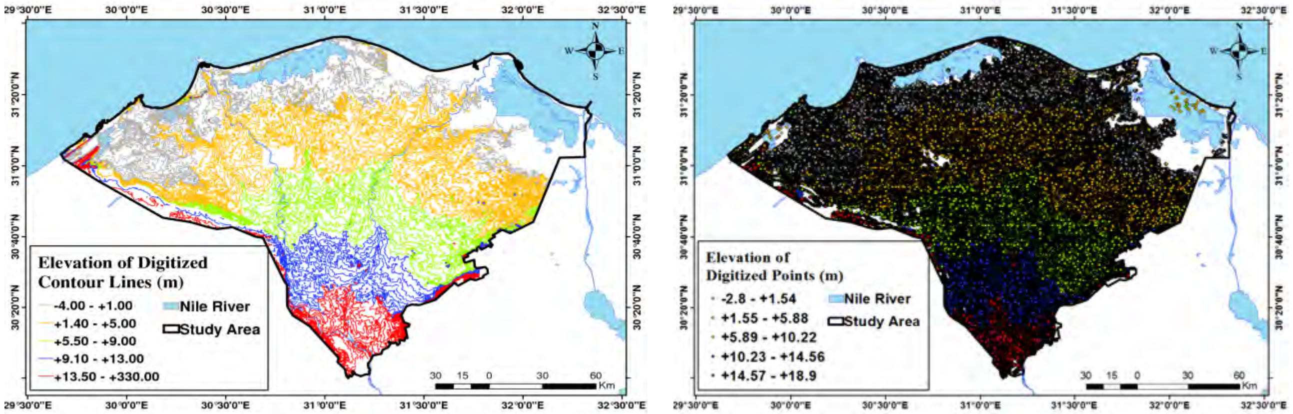

Figure 2. The digitized contour lines (left), elevation points (right) from the topographic maps of the Delta region

3.2. Spatial Interpolation Process and Creating LDEMs

Interpolation is the process of using points with known values or sample points to estimate values at other unknown points. It can be used to predict unknown values for any geographic point data, such as elevation, rainfall, chemical concentrations, noise levels, etc. (Mitas, 1999). It is important to mention that no single interpolation method is optimal in all conditions, or that a given interpolation method does better than the other without taking into consideration, the aim of the study, type and nature of the dataset, and phenomenon involved. So, the best interpolation method for a specific situation can only be obtained by comparing the different methods results (e.g., Pohjola, 2009, and Ikechukwu et al., 2017).

This research study has utilized nine SIMs, namely the Inverse Distance Weighted (IDW), Natural Neighbour Inverse Distance Weighted (NNIDW), Global Polynomial Interpolation (GPI), Spline with Barriers (SWB), Topo to Raster (TTR), Kriging, Radial Basis Function (RBF), Empirical Bayesian Kriging (EBK), and Local Polynomial Interpolation (LPI). Further more, multiple parameters and criteria have been tested for each SIM to reach the optimal settings to produce a DEM. This research study aims to compare the performance of such SIMs trying to achieve the optimum one to be utilized in creating a LDEM for environmental applications.

4. DEM Evaluation

4.1. Vertical Datum Matching

Geodetic datums represent positioning surfaces to which all geodetic measurements are refereed. The geodetic vertical datum conceptually enables a definition of the height of benchmarks in levelling network with respect to some adopted reference surface. For the orthometric height system, the geoid is adopted as the reference surface, which may be defined in a sense as the equipotential surface which best approximates the Mean Sea Level (MSL) over the whole earth.

Many elevation datasets were used in this paper, and each one of them has different datums (Table 2). Before conducting any evaluations on the GDEMs or the LDEMs a unification on the datums must be occurred to unify all the horizontal datums into The World Geodetic System 1984 (WGS84), and all the vertical datums into The Geodetic Vertical Datum in Egypt (VDE1906) which has been set as the MSL at Alexandria harbor, based on daily readings of high and low water level during the years 1898 to 1906 (Cole 1939).

As GCPs measured from the GPS uses and computes their heights relative to the WGS84, and its ellipsoidal height (h) were vertically referenced to the local geopotential geoid model (MSL). Hence, it is important for comparison of GCPs with other DEMs to consider a conversion for the ellipsoidal heights (h) into orthometric heights (H) using local geoid undulations ($N_{VDE1906}$). As geoid undulation (N) can be defined as the difference between the reference ellipsoidal height from GPS (h) and the orthometric height from levelling (H) as shown in (Figure 3) and derived in (equation 1).

Table 2. List of HZ and VL Datum for different elevation datasets used in this paper

Elevation Datasets	Horizontal Datum (Projection / Ellipsoid)	Height & Vertical Datum
GCPs	WGS84	Ellipsoidal Height (h) VDE 1906 (MSL)
Digitized points	ETM Red Belt/Helmert 1907	Orthometric Height (H) VDE 1906 (MSL)
Generated LDEMs	WGS84	Orthometric Height (H) VDE 1906 (MSL)
Acquired GDEMs	WGS84	Orthometric Height (H) EGM96

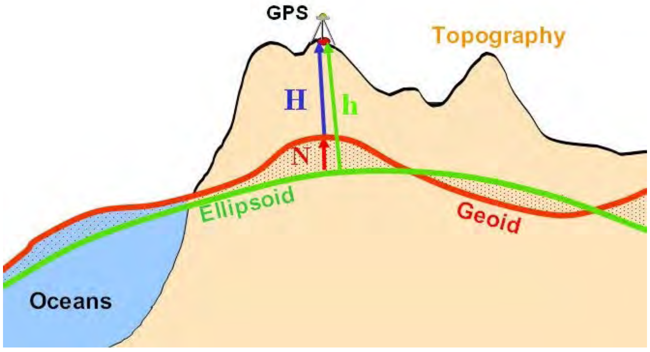

Figure 3. Orthometric, geoid, and ellipsoid heights

$$N = h_{Ellipsoidal} - H_{Orthometric} \quad (1)$$

As for the Elevation points (DPs) digitised from the topographic maps its vertical datum is VDE1906 which can be considered as the MSL. DPs coordinates were transformed into horizontal datum WGS84 using built-in projection tools in ArcGIS.

As LDEMs were generated from the DPs, they use and compute their heights relative to WGS84. And their orthometric heights (H) were referred to the local geoid model VDE1906, for that no conversion was required for these models.

In order to match the same vertical datum for GDEM, their heights were derived for all 200 GCPs through bilinear interpolation using GIS techniques from the surrounding grid points of the original spatial resolution of each GDEM. Such interpolated DEM orthometric heights (H_{EGM96}) that were vertically referenced to the global geopotential model Earth Gravitational Model 1996 (EGM96) were then transformed to ellipsoidal heights (h_{GDEM}) using geoid undulations from EGM96 (N_{EGM96}) as shown in (equation 2).

$$h_{GDEM} = H_{EGM\,96} + N_{EGM\,96} \quad (2)$$

Finally, a transformation on ellipsoidal heights (h_{GDEM}) to orthometric heights ($H_{EGY\text{-}HGM2016}$) using hybrid local geoid

model undulations for Egypt ($N_{EGY\text{-}HGM2016}$) was conducted as shown in (equation 3). Where Hybrid local geoid model for Egypt (EGY-HGM2016) involves different datasets in terms of gravity anomalies determined from the GOCE (gravity field and steady-state ocean circulation explorer) and EGM2008 combined with terrestrial gravity datasets. In addition, orthometric heights from GPS/levelling measurements had been considered during the modelling process to improve the determination of the hybrid gravimetric geoid over the Egyptian region (El-Ashquer et al., 2017).

$$H_{\text{EGY-HGM2016}} = h_{GSEM} - N_{\text{EGY-HGM2016}} \quad (3)$$

A statistical evaluation for the difference between H_{EGM96} and $H_{EGY\text{-}HGM2016}$ for all GDEMs is presented in Table 3. As a lot of significant difference exists between the EGM96 global geoid model and the hybrid local geoid model for Egypt as most geoid can only approximate the real shape of the earth.

Table 3. Statistical evaluation for the difference between H_{EGM96} and $H_{VDE1906}$ for all GDEMs

Max	Min	Mean	SD
0.15	-0.44	-0.12	0.11

All farther evaluations on the GDEMs conduct their statistical calculations on the new generated orthometric heights ($H_{EGY\text{-}HGM2016}$) which use hybrid local geoid model for Egypt.

4.2. DEMs Validation with GCPs

Nine LDEM have been developed, in this research study, based on the utilized SIMs, and their accuracies have been evaluated. The evaluation of the DEMs performance is based on the height difference, DEM errors, or the residuals (ΔH) between GCPs (H_m) and its corresponding DEM-based elevation (H_{DEM}) which were extracted from each GDEMs and LDEMs by deriving all 200 GCPs through bilinear interpolation at the point location using GIS techniques, as shown in Figure 4 and Figure 5. These differences help to identify large-scale systematic errors "such as offsets" and small-scale anomalies "such as voids" in the individual models.

$$\Delta H = H_m - H_{DEM} \quad (4)$$

After determining ΔH for each DEM, several statistical measures were calculated, and the utilized basic equations are just briefed herein. First an outlier detection and removing procedure was conducted on the raw residual data set (ΔH) using Z score statistical test, as outliers and gross errors in DEMs which considered as an erroneous observation that appears to depart significantly from the remaining observations of the sample corrupt statistical accuracy measures.

$$Z_i = \left(Y_i - \bar{Y}\right) / SD$$
$$\left|Z_i\right| > 3SD \quad \Rightarrow \text{ Outlier} \quad (5)$$

Where, (Y) is an observation, ($\bar{Y}$) denotes the sample mean, and (SD) is the sample standards deviation. If the absolute of the computed (Z_i) score, for each observation, is compared against the value of (3SD) and the score exceeds the given limits, it is considered as a possible outlier and should be removed.

Next, six statistical measures have been calculated and evaluated individually:

1. The correlation coefficient between observed elevations of the control points (X or H_m) and their respective elevation from a particular DEM (Y or H_{DEM}) is computed as:

$$\rho = S_{XY} / \sqrt{S_{XX} S_{YY}} \quad (6)$$

$$S_{XX} = \sum X^2 - \left(\sum X\right)^2 / n \quad (7)$$

$$S_{YY} = \sum Y^2 - \left(\sum Y\right)^2 / \text{n} \quad (8)$$

$$S_{XY} = \sum XY - \left(\sum Y\right)\left(\sum X\right) / n \quad (9)$$

Where (ρ) represents the correlation coefficient between (X) and (Y), (ΣX), (ΣY), and (ΣXY) are the summation of (X), (Y), and (XY) respectively, and (n) is the total number of available sample points.

2. The range of (ΔH) is evaluated as the difference between the maximum and minimum computed from the (ΔH) for each DEM.

$$Range = Max\left(\Delta \text{H}\right) - \text{Min}\left(\Delta \text{H}\right) \quad (10)$$

3. The standard deviation (SD) of (ΔH) is computed as:

$$SD = \sqrt{\sum \left(\Delta H\right)^2 / \left(n-1\right)} \quad (11)$$

Where (n) is the number of the utilized control points.

4. The skewness (Sk) is computed as:

$$Sk = \sqrt{n} \sum \left(Y - \bar{Y}\right)^3 / \left(\sum \left(Y - \bar{Y}\right)^2\right)^{3/2} \quad (12)$$

5. The kurtosis (Kr) is computed as:

$$Kr = n \sum \left(Y - \bar{Y}\right)^4 / \left(\sum \left(Y - \bar{Y}\right)^2\right)^2 \quad (13)$$

6. Root Mean Square Error (RMSE) is computed as:

$$RMSE = \sqrt{\sum \Delta H^2 / n} \quad (14)$$

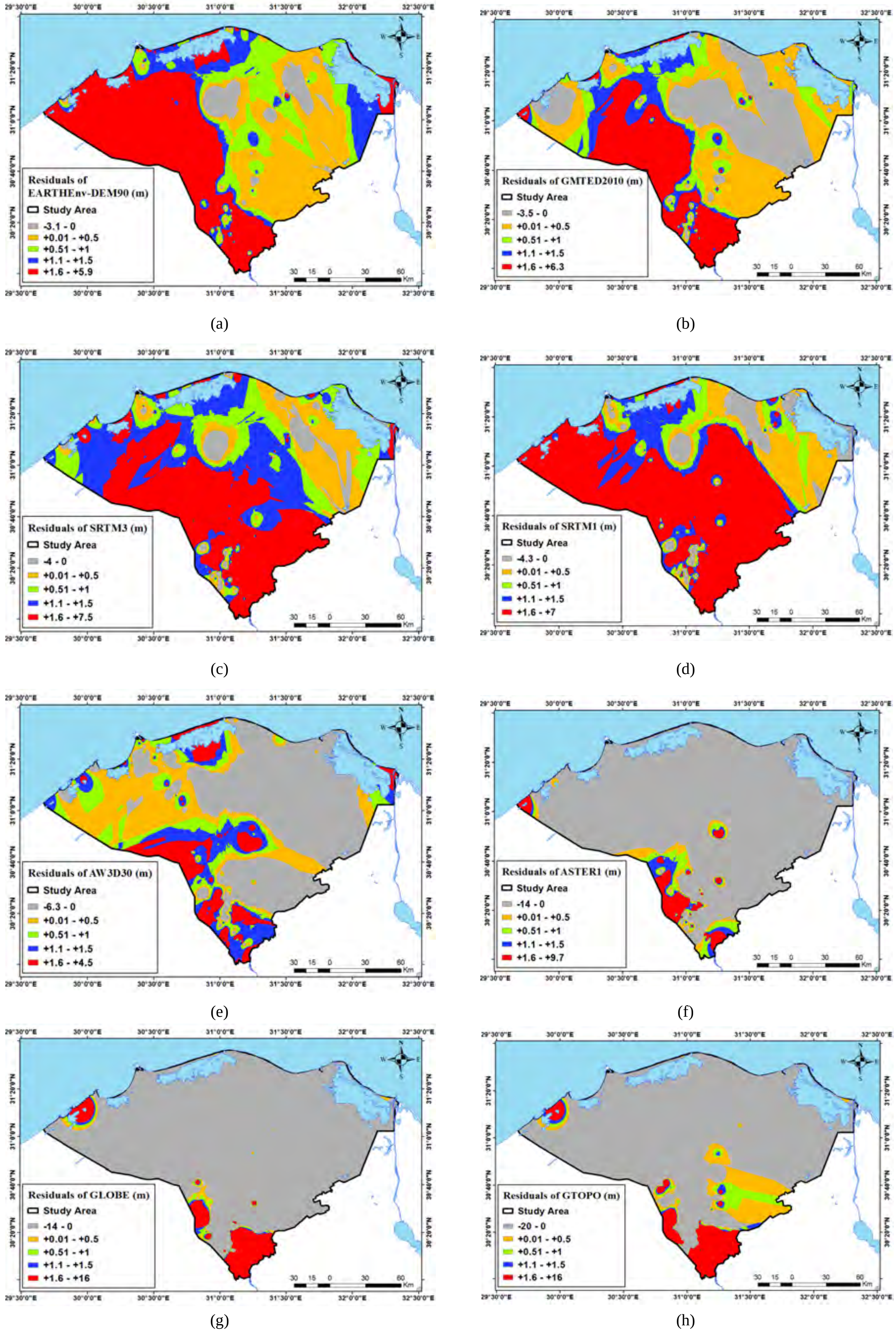

Figure 4. Residuals of global DEM in Nile delta study area (a) EARTHEnv3 DEM; (b) GMTED2010 DEM; (c) SRTM 3 DEM; (d) SRTM 1 DEM; (e) AW3D30 DEM; (f) ASTER DEM; (g) GLOBE DEM; (h) GTOP30 DEM

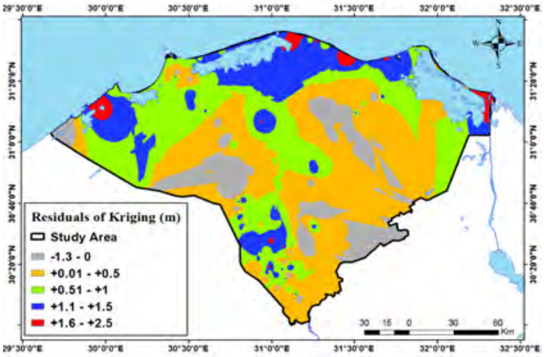
Residuals of Kriging (m)
Study Area
-1.3 - 0
+0.01 - +0.5
+0.51 - +1
+1.1 - +1.5
+1.6 - +2.5

(a)

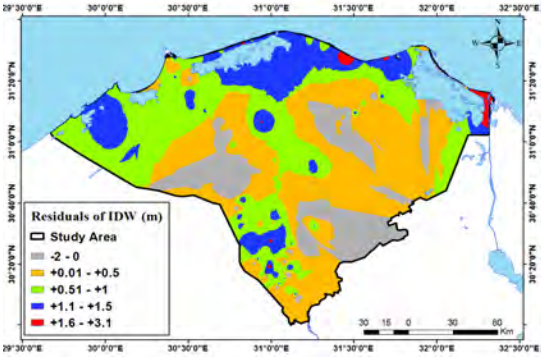
Residuals of IDW (m)
Study Area
-2 - 0
+0.01 - +0.5
+0.51 - +1
+1.1 - +1.5
+1.6 - +3.1

(b)

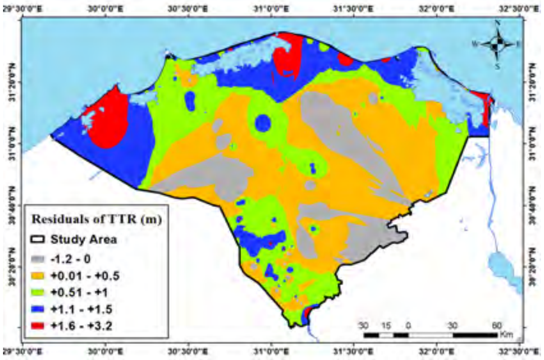
Residuals of TTR (m)
Study Area
-1.2 - 0
+0.01 - +0.5
+0.51 - +1
+1.1 - +1.5
+1.6 - +3.2

(c)

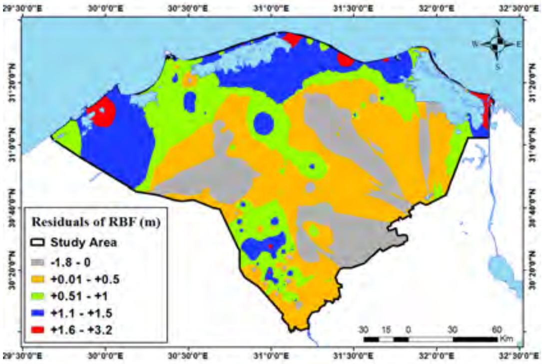
Residuals of RBF (m)
Study Area
-1.8 - 0
+0.01 - +0.5
+0.51 - +1
+1.1 - +1.5
+1.6 - +3.2

(d)

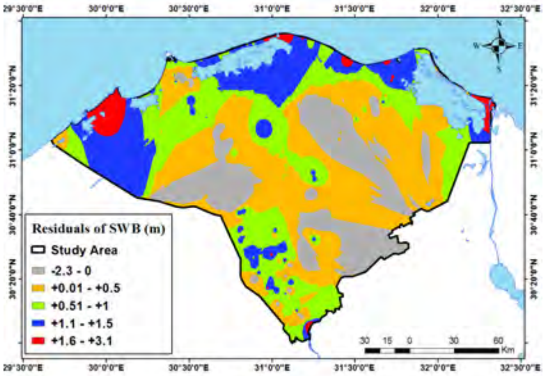
Residuals of SWB (m)
Study Area
-2.3 - 0
+0.01 - +0.5
+0.51 - +1
+1.1 - +1.5
+1.6 - +3.1

(e)

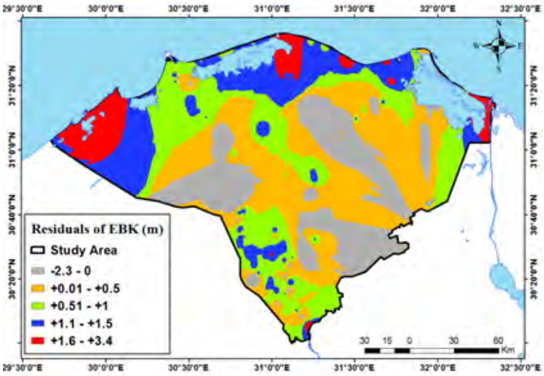
Residuals of EBK (m)
Study Area
-2.3 - 0
+0.01 - +0.5
+0.51 - +1
+1.1 - +1.5
+1.6 - +3.4

(f)

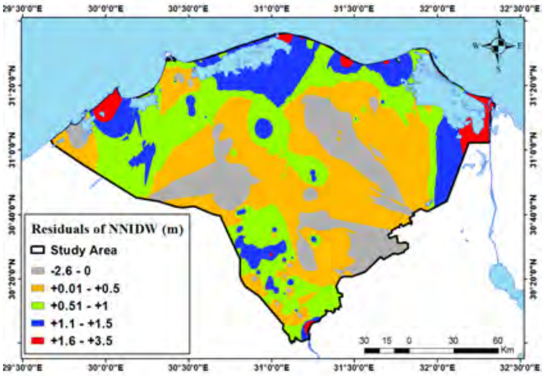
Residuals of NNIDW (m)
Study Area
-2.6 - 0
+0.01 - +0.5
+0.51 - +1
+1.1 - +1.5
+1.6 - +3.5

(g)

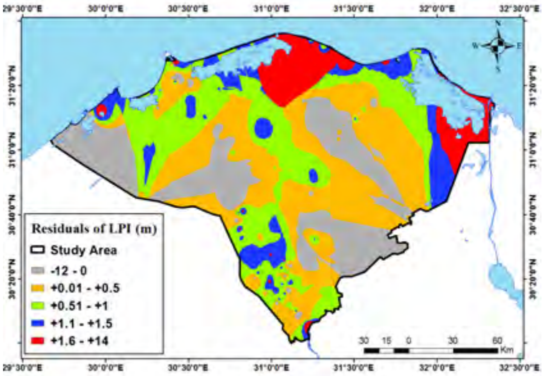
Residuals of LPI (m)
Study Area
-12 - 0
+0.01 - +0.5
+0.51 - +1
+1.1 - +1.5
+1.6 - +14

(h)

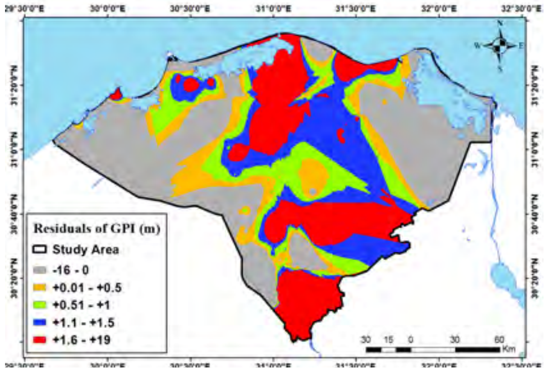

(i)

Figure 5. Residuals of local DEM in Nile delta study area. (a) Kriging DEM; (b) IDW DEM; (c) TTR DEM; (d) RBF DEM; (e) SWB DEM; (f) EBK DEM; (g) NNIDW DEM; (h) LPI DEM; (i) GPI DEM

In the first evaluation step, the statistical results for the utilized DEMs have been computed and presented in Table 4, and Table 5. It can be realized from this Table 4 that the EARTHEnv-DEM90 and SRTM3 have the biggest correlation to the observed values. Next, the outlier detection procedure has been applied using the Z-score approach and if the score exceeded the limits, it is considered as a possible outlier and removed. A comparison between these two tables emphasis the fact that removing outliers enhances the accuracy performance of geodetic datasets. After removing outliers, it can be seen that, the EarthEnv-DEM90 and SRTM3 models attain the smallest standard deviation ±1.60, and ±1.91 m, respectively. As for Table 5, it can be realized that most LDEMs have high correlation of 0.99 to the observed values. After applying the outlier detection procedure using the Z-score approach and removing all the possible outliers, it can be seen that, the LDEM interpolated from Kriging and IDW SIMs attain the smallest standard deviation ±0.82, and ±0.85 m, respectively. These accuracy measures for both the GDEMs and LDEMs confirm the known fact that GDEMs should not be the first option to be utilized in high-precision geomatics activities. Next, the height differences or DEMs' residuals (ΔH) have been computed, for all utilized models. From Table 4, and Table 5, it can be realized that the EarthEnv-DEM90 model has the lowest mean value of the GDEM residuals, while Kriging has it for LDEMs residuals. Additionally, the EarthEnv-DEM90 model has the smallest error range of the GDEMs as for LDEMs the DEM interpolated from Kriging SIM has the smallest error range. Consequently, it can be said that judgment of DEMs performance cannot be evaluated based on just one statistical quantity.

Next, for that the six statistical measures attained for each DEM were categorized in a certain manner and a specific rank was assigned for each statistical measure based on the frequency distribution of their values to assure a uniform distribution for all the models across its range (Table 6). For the correlation, range, skewness, RMSE, and standard deviation measures, the ranks vary from 1 to 15 based on the ascending order of those measures for each DEM.

Finally, a unique reliability index (RI) has been proposed and computed based on the ranks of the statistical measures for each DEM Where (ΣW) denotes the sum of the utilized weight, i.e. 15. It is based on the weighted mean approach, as it ranges from zero as the lowest reliability of a DEM, to value of 15 which represents the highest reliability (Dawod and Al-Ghamdi, 2017). The selected weights (W_j) are shown in Table 7. Since the SD and RMSE are the basic statistical measures of DEM's vertical accuracy, they are given the largest weights in computing the reliability index. The RI measure is computed as:

$$RI = \sum R_i W_j / \sum W \tag{15}$$

Where (ΣW) denotes the sum of the utilized weight, i.e. 15.

Table 4. Statistical measures of GDEM elevations in delta region (m)

DEM	Min	Max	Range	Mean	Correlation	SD After Removing Outliers	Kurtosis	Skewness	RMSE	RI
AW3D30	-6.31	4.55	10.86	0.28	0.93	2.18	2.87	-0.52	2.19	4.87
ASTER1 v.2	-14.39	9.69	24.08	-2.57	0.68	4.45	3.05	0.16	5.13	4.13
EARTHEnv-DEM90	-3.13	5.89	9.02	1.51	0.96	1.60	2.89	0.20	2.20	5.47
GLOBE	-14.33	15.70	30.03	-3.14	0.52	6.57	3.13	0.64	7.26	2.93
GMTED2010	-3.52	6.26	9.78	1.22	0.94	1.98	2.93	0.06	2.32	5.47
GTOPO30	-19.95	15.55	35.50	-2.36	0.45	6.94	3.13	0.47	7.32	2.87
SRTM 1	-4.27	7.04	11.32	1.37	0.93	2.24	2.99	-0.06	2.62	5.20
SRTM 3	-4.03	7.43	11.46	1.37	0.95	1.91	3.33	0.22	2.35	5.33

Table 5. Statistical measures of LDEM elevations in delta region

DEM	Min	Max	Range	Mean	Correlation	SD After Removing Outliers	Kurtosis	Skewness	RMSE	RI
IDW	-2.10	3.27	5.36	0.58	0.99	0.85	3.30	-0.23	1.02	9.07
NNIDW	-2.60	3.58	6.18	0.60	0.99	0.90	4.11	-0.14	1.08	6.53
GPI	-15.64	18.85	34.49	0.09	0.70	4.78	6.99	0.16	4.77	4.40
SWB	-2.27	3.06	5.34	0.57	0.99	0.89	3.16	-0.25	1.05	7.47
TTR	-1.17	3.16	4.33	0.65	0.99	0.85	2.82	-0.02	1.07	8.73
Kriging	-1.38	2.81	4.19	0.60	0.99	0.82	2.55	-0.25	1.02	9.27
RBF	-1.94	3.20	5.14	0.58	0.99	0.85	3.10	-0.26	1.03	8.73
EBK	-2.36	3.66	6.02	0.61	0.99	0.96	3.43	-0.04	1.14	6.73
LPI	-12.57	14.22	26.79	0.61	0.94	2.15	30.26	0.27	2.23	5.20

Table 6. Statistical Measures Ranks

Rank	Correlation	Range	Skewness	Standard Deviation	RMSE	Kurtosis
1	0.00 ≤ Ri < 0.40	50 ≤ Ri	2.00 ≤ |Ri|	9 ≤ Ri	24 ≤ Ri	Kr < 3 Ri = 3
2	0.40 ≤ Ri < 0.60	40 ≤ Ri < 50	1.60 ≤ |Ri| < 2.00	0.8 ≤ Ri < 9	10 ≤ Ri < 24	
3	0.60 ≤ Ri < 0.70	35 ≤ Ri < 40	1.10 ≤ |Ri| < 1.60	0.5 ≤ Ri < 0.8	7 ≤ Ri < 10	
4	0.70 ≤ Ri < 0.75	20 ≤ Ri < 35	0.80 ≤ |Ri| < 1.10	0.3 ≤ Ri < 0.5	6 ≤ Ri < 7	Kr = 3 Ri = 8
5	0.75 ≤ Ri < 0.80	10 ≤ Ri < 20	0.70 ≤ |Ri| < 0.80	0.2 ≤ Ri < 0.3	5 ≤ Ri < 6	
6	0.80 ≤ Ri < 0.94	6.5 ≤ Ri < 10	0.50 ≤ |Ri| < 0.70	0.1 ≤ Ri < 0.2	2 ≤ Ri < 5	
7	0.94 ≤ Ri < 0.95	5.5 ≤ Ri < 6.5	0.40 ≤ |Ri| < 0.50	0.06 ≤ Ri < 0.1	1.07 ≤ Ri < 2	
8	0.95 ≤ Ri < 0.98	5.0 ≤ Ri < 5.5	0.30 ≤ |Ri| < 0.40	0.05 ≤ Ri < 0.06	1.06 ≤ Ri < 1.07	Kr > 3 Ri = 5
9	0.98 ≤ Ri < 0.99	4.5 ≤ Ri < 5.0	0.20 ≤ |Ri| < 0.30	0.04 ≤ Ri < 0.05	1.05 ≤ Ri < 1.06	
10	0.99 ≤ Ri < 1.00	Ri < 4.5	|Ri| < 0.20	Ri < 0.04	Ri < 1.05	

Table 7. Statistical Weights

	SD	RMSE	Range	Correlation	Kurtosis	Skewness	Total Weight
Selected Weights (W_j)	5	4	2	2	1	1	15

Hence, it can be seen that, for GDEMs the EARTHEnv-DEM90 and GMTED2010 models attain highest RI as both have 5.47, and the older DEMs, namely GLOBE and GTOPO30, came in the last places with RI of 2.93, 2.87 respectively. As for LDEMs the LDEM interpolated from Kriging and IDW SIMs attain the highest RI of 9.27, 9.07 respectively.

4.3. GDEM versus LDEM Comparison

For the pixel-to-pixel comparison between GDEM and LDEM, as it is of course a compromise to compare two different sensors, characterized by different technologies and resolutions, it was important to make sure that all DEMs were under the same horizontal resolution of 90 m (3” arc-sec) to ensure that both datasets become spectrally consistent.

The comparison was made by subtracting the raster maps of the best GDEM “EARTHEnv-DEM90” from the raster maps of the best LDEM “Kriging” using raster math tool in ArcGIS and producing a new raster map that presents all the height differences between each cell of the DEMs to show how they fit to each other, to locate areas of larger discrepancies, and to detect large-scale systematic effects (Figure 6). The results of the comparison map showed that the height differences are higher in urban areas and lower at water surface areas than in areas where bare ground can be sensed from space. This is can be explained as the heights of all GDEMs are considered DSM which reflects the surface of the Earth (including vegetation and buildings) rather than its actual topography, on the other hand the heights of all LDEMs are considered DTM which reflects the surface of the actual topography only (Figure 6).

A statistical evaluation for the comparison between the best GDEM “EARTHEnv-DEM90” and the best LDEM “Kriging” is presented in Table 8.

Table 8. A statistical evaluation for the comparison between the best GDEM and the best LDEM

Max	Min	Mean	SD
29.2	-58.86	-0.02	1.95

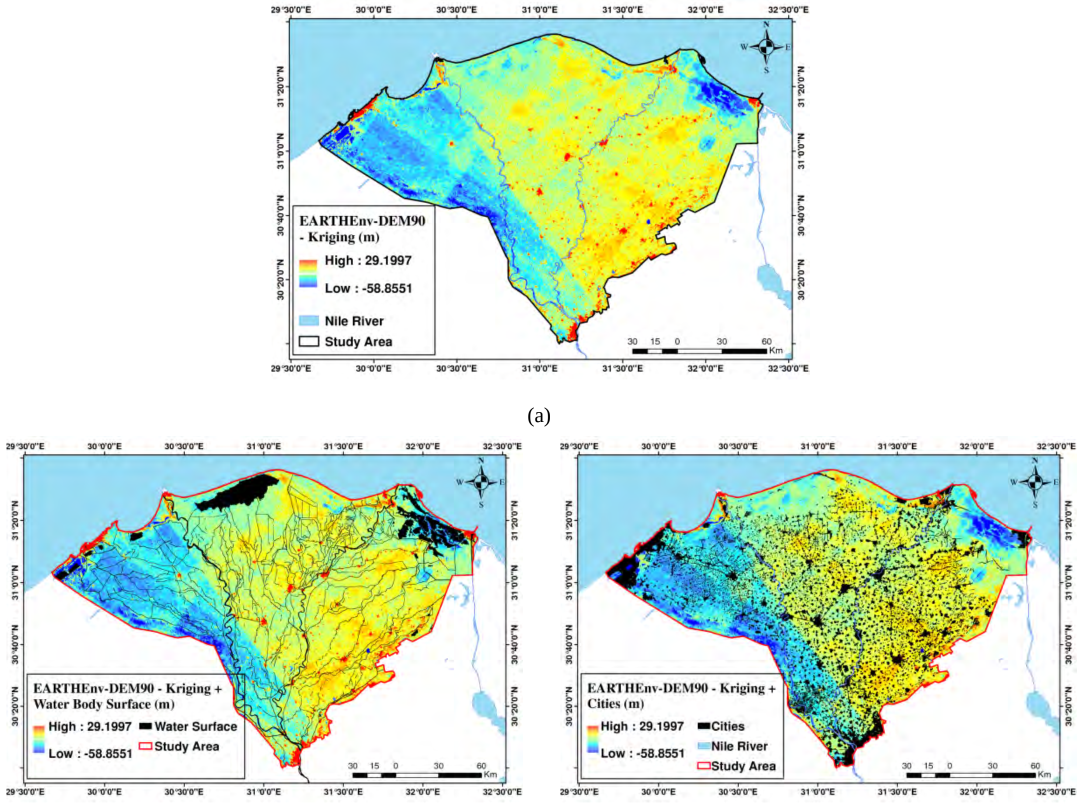

(a)

(b) (c)

Figure 6. a) the result of subtracting GDEM EARTHEnv-DEM90 from LDEM Kriging. b) Using water body surfaces to cover –ve results of subtraction. C) Using land use map to cover the +ve results of subtraction

5. Summary and Conclusions

Egypt, as many developing countries, has no officially published precise local DEM, and mainly depends on available global DEMs for several environmental and GIS applications despite their low accuracies. Consequently, a precise national DEM is required for monitoring environmental hazards, such as the sea level rise particularly in deltas and coastal regions. This research study has utilized GIS techniques and approaches to create an original high accuracy LDEM for the Nile delta region, Egypt by digitizing over 220 topographic maps then applying nine spatial interpolation methods (namely; IDW, NNIDW, GPI, SWB, TTR, Kriging, RBF, EBK, and LPI).

On the other hand, the study investigated the accuracies of eight recent GDEMs (namely; EarthEnv-D90, SRTM1, SRTM 3, ASTER, GMTED2010, GLOBE, GTOPO30, and AW3D30) which were downloaded from their respective websites and utilized with the study area. About 200 known GPS/levelling ground control points have been utilized to evaluate the performance and accuracy of both the GDEMs and the newly-developed LDEMs. The DEMs validation with ground control points was carried out based on the statistical assessment using six statistical measures including (range, standard deviation, root mean square error, correlation, kurtosis, and skewness). Prior to the actual evaluation process, DEMs datum matching was performed where vertical datum for all the used data sets were unified into the vertical datum of Egypt, and the horizontal datums into WGS84, also an outlier detection step has been applied which enhances the accuracy performance of geodetic datasets. It is concluded that judgment of DEMs performance cannot be evaluated based on just one statistical quantity. Therefore, an overall reliability index (RI) has been calculated to determine the best DEM from all the deduced LDEMs and the available GDEMs for the Nile Delta region.

The accomplished results showed that the EARTHEnv-DEM90 and GMTED2010 global models attain high RI of 5.47, and the older DEMs, namely GLOBE and GTOPO30, came in the last places as they have RI of 2.93, 2.87 respectively. Therefore, despite their low accuracies, GDEMs present a good candidate when accurate LDEMs are not available.

As for LDEMs, the models interpolated utilizing the Kriging and IDW SIMs attain the highest RI equal 9.27, 9.07 respectively. Accordingly, the IDW and Kriging could be the optimum interpolation methods for developing digital elevation models in the Nile delta region. Finally, it is found that the accuracy of the optimum developed LDEM has improved the overall accuracy of the best GDEM, in the study area, by almost 41%. So, a local precise DEM is extremely essential for geospatial, GIS, and environmental activities in Egypt and other developing countries.

Finally, a pixel to pixel comparison was held between the best downloaded GDEMs and the best generated LDEMs and the results showed that the height differences are higher in urban areas and lower at water surface areas than in areas where bare ground can be sensed from space. This is can be explained as the heights of all GDEMs are considered DSM which reflects the surface of the Earth rather than its actual topography, on the other hand the heights of all LDEMs are considered DTM which reflects the surface of the actual topography only.

REFERENCES

[1] Abd-Elmotaal, H. (1999). The EGHA99 Digital Height Models for Egypt. Proceedings of the 1st Minia International Conference for Advanced Trends in Engineering. Minia, Egypt: 1, 205–211.

[2] Abd-Elmotaal, H. (2004). The AFH04 Digital Height Models for Africa. The IAG International Symposium on Gravity, Geoid and Space Missions "GGSM2004". Porto, Portugal.

[3] Abd-Elmotaal, H. (2011). "The New Egyptian Height Models EGH10." NRIAG Journal of Geophysics (Special Issue 249–261).

[4] Abd-Elmotaal, H. A., M. Abd-Elbaky, and M. Ashry, (2009). "30 Meters Digital Height Model for Egypt." 1st International Conference for a Unique Map of the Arab World (November 2016): 0-8.

[5] Abd-Elmotaal, H. a. A., M. (2013). The 3 ″ Digital Height Model for Egypt - EGH13. 8th International Conference of Applied Geophysics. Cairo, Egypt, February 25.

[6] Cole, J. (1939). "Revision of first order levelling lower Egypt." Survey Department Paper No. 44, Egyptian Survey Authority, Giza, Egypt.

[7] Dawod, G. and K. Al-Ghamdi (2017). "Reliability of Recent Global Digital Elevation Models for Geomatics Applications in Egypt and Saudi Arabia." Journal of Geographic Information System 09(06): 685-698.

[8] El-Ashquer, M., B. Elsaka, and G. El-Fiky, (2017). "EGY-HGM2016: an improved hybrid local geoid model for Egypt based on the combination of GOCE-based geopotential model with gravimetric and GNSS/levelling measurements." Arabian Journal of Geosciences 10(11).

[9] El-Sagheer, A. (1995). Development of a Digital Terrain Model for Egypt and its Application for a Gravimetric Geoid Determination. Shoubra Faculty of Engineering, Zagazig University, Egypt, Shoubra Faculty of Engineering. Ph.D.

[10] El-Sagheer, A. (2004). Towards Updated Concrete Digital Terrain Model for Egypt: DTM-2003. Civil Engineering Research Magazine (CERM). Al-Azhar University: 26, 21, 158–179.

[11] Eldrandaly, K. A. (2011). "Comparison of Six GIS-Based Spatial Interpolation Methods for Estimating Air Temperature in Western Saudi Arabia." Journal of Environmental Informatics 18(1): 38-45.

[12] Embabi, N. (2000). "Sand dunes in Egypt, in Sedimentary Geology of Egypt: Applications and Economics, Part 1." The Sedimentological Society of Egypt: 45-87.

[13] Her, Y., Heatwole, C (2008). Assessment of interpolation methods for refining SRTM and DEM. ASABE Annual International Meeting. Rhode Island.

[14] Ikechukwu, M. N., E. Ebinne, U. Idorenyin, and N. I. Raphael (2017). "Accuracy Assessment and Comparative Analysis of IDW, Spline and Kriging in Spatial Interpolation of Landform (Topography): An Experimental Study." Journal of Geographic Information System 09(03): 354-371.

[15] Luo, W., M. Taylor, and S. Paker, (2008). "A comparison of spatial interoplation methods to estimate continous wind speed surfaces using irregularly distributed data from England and Wales." International Journal of Climatology: 28, 947-959.

[16] Kokkonen, A., Kylmäaho, J. and Ursin, H. (2017). "Arctic Spatial Data Infrastructure (Arctic SDI)." Presented in the FIG Working Week, May 29–June 2, Finland.

[17] Mitas, L., and Mitasova, H. (1999). Spatial interpolation. In: Longley. Wiley, New Work.

[18] Pohjola, J., Turunen, J. and Lipping, T. (2009). Creating High-Resolution Digital Elevation Model Using Thin Plate Spline Interpolation and Monte Carlo Simulation. 2009-56. Tampere University of Technology, Pori, Finland: pp60.

[19] Rabah, M., A. El-Hattab, and M. Abdallahet (2017). "Assessment of the most recent satellite based digital elevation models of Egypt." NRIAG Journal of Astronomy and Geophysics 6(2): 326-335.

[20] Shaker, A., Saad, Abdullah, Salah, Mahmoud., I. Salama, (2015). "Multiple polynomial-based generation of DEM from topographic contour data." Regional Conference on Surveying & Development (December).

[21] Sun, Y., S. Kang, F. Li, and L. Zhang, (2009). "Comparison of interpolation methods for depth to groundwater and its temporal and spatial variations in the Minqin oasis of northwest China." Environmental Modelling & Software: 24, 1163-1170.

[22] Verhulp, J. (2015). "Towards a national digital elevation model." Proceedings of the Geomatics Indaba Conference, August 11-13, Ekurhuleni, South Africa.

Arabian Journal of Geosciences (2019) 12:246
https://doi.org/10.1007/s12517-019-4418-9

ORIGINAL PAPER

Accuracy assessment of the PGM17 global geopotential model: a case study of Egypt and Northeast Africa

Gomaa M. Dawod[1] · Hoda F. Mohamed[1] · Essam M. Al-Krargy[1]

Received: 18 April 2018 / Accepted: 13 March 2019
© Saudi Society for Geosciences 2019

Abstract

Global geopotential models play a fundamental role in height transformation to convert the Global Navigation Satellite Systems (GNSS)-based ellipsoidal heights into orthometric heights in several geosciences applications. The U.S. National Geospatial-Intelligence Agency (NGA) is preparing to release the Earth Geopotential Model 2020 (EGM2020) in the near future. Prior to that official release, two primary geopotential models (PGM17 and PGM18) will be distributed to selective members for assessment in different regions worldwide. Within the activities of that working group, the new PGM17 geopotential model has been obtained and judged over a regional scale in northeast Africa, and over a national basis of Egypt. The assessment has been carried out using terrestrial gravity and GPS/leveling datasets within a GIS environment. The utilized dataset consists of 231 terrestrial gravity points in northeast Africa, 247 measured gravity points in Egypt, and 978 GNSS/leveling stations in Egypt. Three other GGMs have been included in the comparison stage, namely GECO, EIGEN-6C4, and EGM2008. For each model, grids of gravity anomalies and geoidal undulations have been computed and, then, compared against the corresponding values at known terrestrial data. Next, statistical measures of mean, range, and standard deviations of the discrepancies have been analyzed. For northeast Africa area, the accomplished results indicated that the PGM17 attains 100% improvements over the old EGM2008, while the GECO, and EIGEN-6C4 models resulted in improvements of 11%, and 1% respectively. Accordingly, it can be concluded that PGM17 represents the gravitational field over northeast Africa in a more enhanced manner. On a national scale, the GGMs assessment has been performed, over Egypt, in two steps: using gravity data, and using GNSS/leveling data. The findings emphasize that PGM17 noticeably enhance the performance of EGM2008, when compared against terrestrial gravity stations in Egypt, by almost 55%. Furthermore, the assessment over GPS/leveling stations concluded that the overall improvements of PGM17 are approximately 54%. Other GGMs did not produce a comparable improvement level in both case studies. Thus, it can be concluded that PGM17 is significantly precise than the other investigated GGMs in representing the gravitational field over Egypt in particular and northeast Africa in general.

Keywords PGM17 · GGM · Geoid · Gravity · GNSS · Egypt

Introduction

Global Navigations Satellite Systems (GNSS) are satellite-based revolutionizing technologies for precise position, velocity, and attitude determination on a global basis, used for a wide range of applications in geosciences. GNSS comprise satellites, ground control stations, and user equipment, and support and even enable many activities in modern societies. GNSS consist of the American Global Positioning System (GPS), the Russian counterpart GLObal Navigation Satellite System (GLONASS), the European Galileo system, and the Chinese BeDiou, or Compass, system. Both GPS and GLONASS have been declared fully operational, while Galileo and BeDiou are still under development. Presently, there are 31, 24, 14, and 15 operational satellites belong to GPS, GLONASS, Galileo, and BeDiou systems respectively (QZSS 2018). GNSS have been utilized in enormous geosciences activities in the last few decades including for example surveying and mapping, agriculture, aviation, road transport, location-based services, railroad management,

Editorial handling: Abdullah M. Al-Amri

✉ Gomaa M. Dawod
dawod_gomaa@yahoo.com

[1] Survey Research Institute, National Water Research Center, Giza, Egypt

Published online: 28 March 2019

maritime navigation and safety, aerial search and rescue, deformation and crustal deformation monitoring, Geographic Information Systems (GIS) spatial data collection, and tide gauge calibration for estimating precise estimates of sea level rise (e.g., Rabiu 2015). For example, Casula (2016) has utilized GNSS measurements to estimate the tectonic and geodynamics characteristics of the Galabria region, Italy. Similarly, Mohamed et al. (2016) estimated deformation parameters of the northern part of Egypt using GNSS datasets. In addition, Stal et al. (2016) have used tidal buoys equipped with GNSS for the analysis and prediction of tide in the Belgian North Sea. GNSS has been, also, utilized in establishing geodetic control networks and updating national geodetic datums for surveying and mapping (e.g., Fazilova 2017). Hydrographic surveys employed the kinematic GNSS technique to attain a significant real-time accuracy level for both horizontal and vertical positioning (e.g., Berber and Wright 2016). Furthermore, GNSS data analysis is proved to be a promising tool for monitoring the Earth's atmosphere and ionosphere layers (e.g., Ghoniem et al. 2017). Also, GNSS-based spatial data have been utilized in various environmental risk assessment activities (e.g., Kaya et al. 2018). Along with these global positioning techniques, some others provide regional satellite-based positioning capabilities, such as Indian Regional Navigation Satellite System (IRNSS), and the Japan's Quasi-Zenith Satellite System (QZSS) system.

Moreover, augmentation services exist in several parts of the world to increase the precision and reliability of satellite-based positioning systems. The basic idea behind such services is the utilization of GNSS measurements taken by reference stations, transferring them to a central computing center (s) to estimate GNSS errors, and then broadcast these corrections, through geostationary satellites or any other communication methods, to normal users over a specific spatial area. Examples of such augmentation services include the European Geostationary Navigation Overlay Services (EGNOS), the U.S. Wide Area Augmentation System (WAAS), and the Japanese Multi-functional Satellite Augmentation System (MSAS). Additionally, there are some commercial GNSS augmentation services such as Starfix and OmniStar. In addition, a number of surveying and mapping local authorities, in many cities worldwide, provide real-time GNSS corrections by means of a ground-based augmentation service through Continuously Operating Reference Stations (CORS) to increase the local GNSS accuracy.

In most geosciences applications, utilized heights are referenced to the Mean Sea Level (MSL) vertical datum. However, GNSS heights are relative to the surface of an ellipsoid, which necessitates a height transformation process. The vertical separation between MSL-based orthometric height and the ellipsoidal height is the geoidal undulation or geoid height (Fig. 1). Consequently, geoid modeling is an essential step in GNSS applications for geosciences activities, such as aerial surveys (e.g., Barzaghi et al. 2016), crustal and mantle density estimation (e.g., Li and Fang 2017), oceanographic surveys (e.g., Deng et al. 2013), surveying and mapping (e.g., Wu et al. 2015), and geological studies of oceans (e.g., Sreejith et al. 2013).

Global Geopotential Models (GGMs) play a significant role in case there are local geoid models available or published in certain areas or countries. Even if terrestrial geodetic datasets are accessible for geoid modeling, a specific GGM is required to represent the long wavelength of the Earth's gravitational field. Therefore, the comparison of GGMs over a country or a region is vital in order to choose the optimum one to be utilized in geoid modeling (e.g., Yakubu et al. 2017, and Al-Krargy et al. 2015). In addition, the availability of more than 160 GGMs currently makes the assessment of their performance in representing the gravitational field over a selected area is essential, e.g., Japan (Odera and Fukuda 2017), Argentina (Gomez et al. 2017), West Siberia and Kazakhstan (Karpik et al. 2016), Turkey (Yılmaz et al. 2017), Poland (Godah and Krynski 2013), and Africa (Abd-Elmtaal 2015).

In Egypt, the geoid modeling and GGM assessment have been extremely investigated in the last couple of decades. Since the development of the first pioneer national-scale geoid (Alnaggar 1986), several geoid researches have been carried out. For example, Dawod (1998) has developed a national geoid model based on the data of the Egyptian National Standardization Gravity Network of 1997 (ENGSN97) along with GPS/leveling data. Furthermore, Dawod et al. (2010) have investigated the accuracy of EGM2008 over the Nile delta area, Egypt. Next, Mahmoud (2012) has investigated the performance of 25 GGMs over Egypt using 236 terrestrial GPS/leveling stations. He concluded that the EGM2008 is the optimum GGM with a standard deviations of 0.42 m. In addition, Al-Karagy et al. (2014) have investigated the utilization of GPS/leveling in developing geoid models for small areas in Egypt. Moreover, Abd-Elmotaal (2015) has developed a gravimetric geoid model utilizing the best estimated response of the Earth's crust due to the topographic loads. Also, Abd-Allah (2015) has investigated the GOCE-based satellite-only GGMs in Egypt, and concluded that the accuracy of such models over Egypt is about 0.40 m for geoid undulations and 12.6 mGal for gravity anomalies. More recently, El-Ashquer (2016) have investigated the better fitting of GGMs to local gravity and GNSS/leveling databases towards the definition of a national geoid model. He developed a hybrid gravimetric quasigeoid model, called EGY-HGM2016, that has a mean standard deviation of 0.17 m. Similarly, Al-Krargy (2016) has developed a national geoid model for Egypt, called SRI-GEOID16–2, utilizing the least-square collocation technique based on the EGM2008 combined with precise local geodetic datasets. He concluded that the average accuracy of the developed model is 0.12 m. Ashry (2016) has compared between different techniques of combining gravity field wavelengths in the remove-

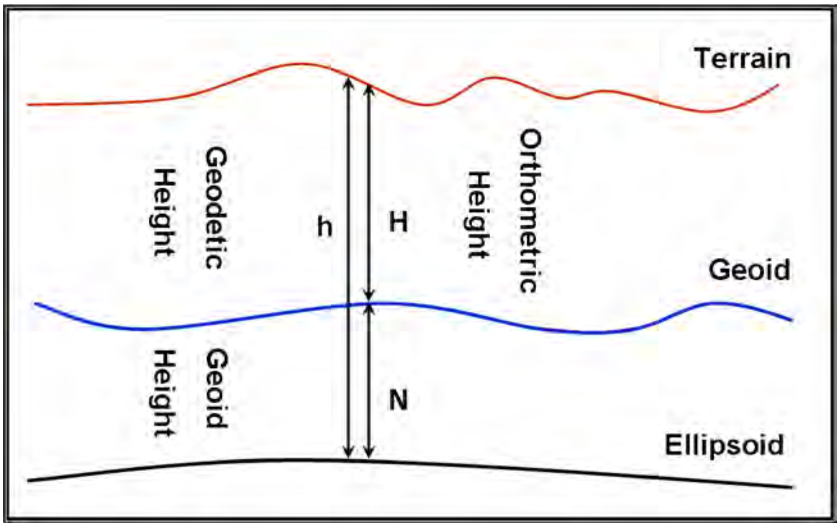

Fig. 1 Height systems

restore process for determining an optimum geoid for Egypt. Based on a survey of the available geodetic datasets and resources of all governmental agencies, Dawod and Hosny (2017) have designed a proposed strategy to develop a national precise geoid model for Egypt based on collecting available and new accurate heterogeneous data.

Typically, the global geopotential models come in text format including the original coefficients of the spherical harmonics representing the gravitational field of the Earth. Thus, a specific software package is needed to compute the geoidal characteristics, for example the gravity anomalies and the geoidal undulation, over a spatial area. Out of the available GGMs, only the Earth Gravitational Model 2008 (EGM2008) has been delivered in many formats, one of them is the raster format appropriate for the Geographic Information Systems (GIS) applications. It is a matter of reality that GIS has been extensively utilized in a wide range of geosciences applications, such as coastal management (Mahapatra et al. 2017), environmental flooding hazards (Huang et al. 2017), irrigation management (Srivastava and Singh 2016), solar energy harvesting (Dawod and Mandoer 2016), and seismic hazard assessment (Ahmed and Singh 2016). Additionally, GIS could be a precious tool for several geodetic and gravimetric applications (Hassouna and Asal 2016). Recently, the International Center for Global Earth Model (ICGEM) organization starts an online service to compute many geoidal properties and deliver them in a grid format. Therefore, the assessment of GGMs utilizing national geodetic data could be accomplished within a GIS environment.

The U.S. National Geospatial-Intelligence Agency (NGA) is preparing to release the Earth Geopotential Model 2020 (EGM2020) in the near future. The University of Texas at Austin and U.S. National Geodetic Survey (NGS) has initiated a scientific cooperation working group for the assessment of EGM2020, consisting of 20 experts from all over the world. Prior to that EGM2020 official release (as scheduled in December 2019), two primary geopotential models (PGM17 and PGM18) will be distributed (in December 2017 and 2018 respectively) and assessed by that working group. As the first author is a member of that group, the new PGM17 geopotential model has been acquired in the form of spherical harmonic coefficients. The main objective of this study is evaluating the accuracy performance of the new PGM17, along with other GGMs, over a regional scale in northeast Africa, and particularly on a national basis of Egypt.

Global geopotential models

Global geopotential models have been developed since 1960 in order to express the gravitational potential of the Earth (V) into a series of spherical harmonics as (for more details, refer for example to Hofmann-Wellenhof and Moritz 2005):

$$V = \frac{GM}{r}\left(\begin{array}{l} 1-\sum_{n=2}^{\infty}\left(\frac{a}{r}\right)^{n} J_n P_n(\cos\vartheta) + \sum_{n=2}^{\infty}\sum_{m=1}^{n}\left(\frac{a}{r}\right)^{n} \\ \left[C_{nm}\cos m\lambda + S_{nm} sin m\lambda\right] P_{nm}(\cos\vartheta) \end{array}\right) \quad (1)$$

Table 1 Characteristics of selected GGMs

GGM	Year	Degree	Utilized data
GECO	2015	2190	EGM2008, S(GOCE)
EIGEN-6C4	2014	2190	A, G, S (GOCE, GRACE, Lageos)
EGM2008	2008	2190	A, G, S(GRACE)
PGM17	2017	2190	Classified (at the time being)

A, altimetry data; G, geodetic data; S, satellite data (after ICGEM 2018)

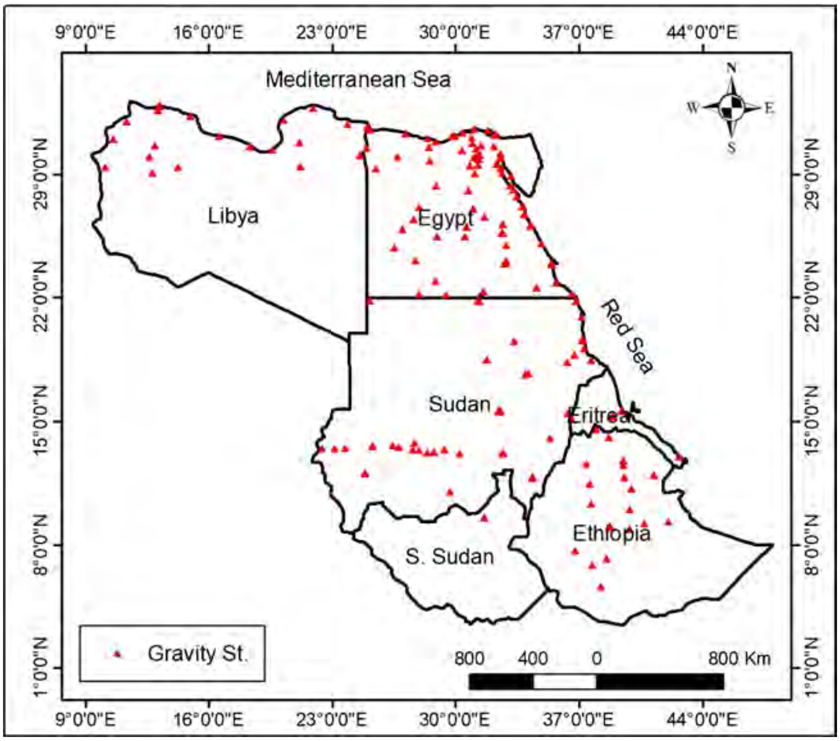

Fig. 2 Available terrestrial data in North-East Africa

where GM is the gravitational constant, r is the radial distance, a is the equatorial radius of the Earth, θ and λ are the latitude and longitude respectively, J_n are the zonal harmonics, those contain the S_{nm} and C_{nm} are the tesseral harmonics, P_{nm} are the associated Legendre coefficients, n and m are the degree and order of the geopotential model.

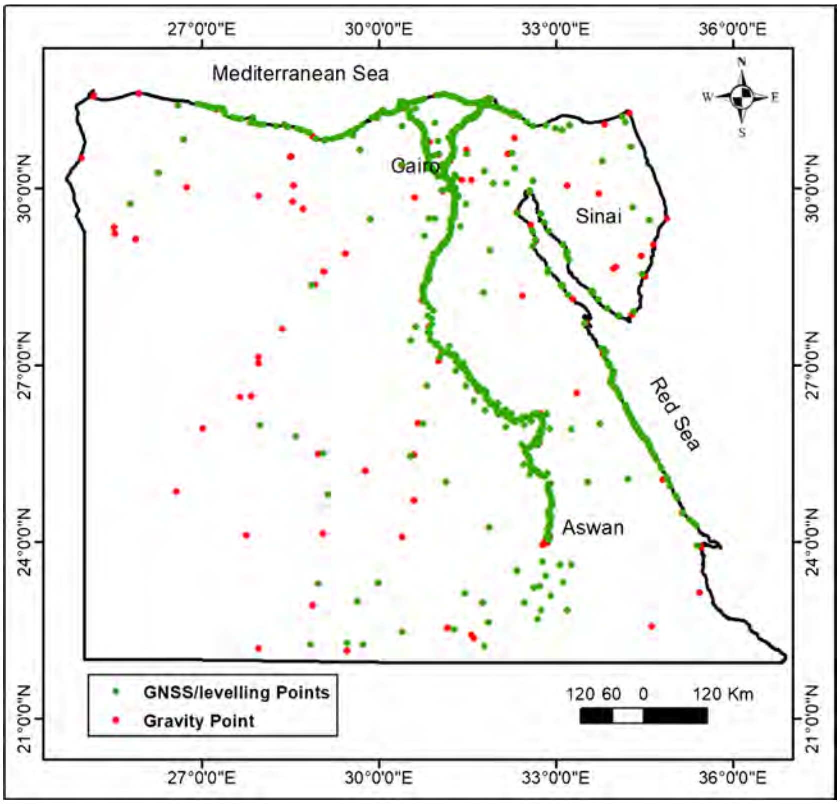

Fig. 3 Available terrestrial data in Egypt

The free-air gravity anomaly of a GGM ($\Delta g'$), in terms of spherical harmonic expansion, could be computed as (ibid):

$$\Delta g' = \gamma\left(\sum_{n=2}^{n}(n-1)\sum_{m=0}^{n}(\Delta C_{nm}\cos m\lambda + S_{nm}\sin m\lambda)P_{nm}\sin\vartheta\right) \quad (2)$$

where $\Delta C_{nm} = C_{nm} - C^0_{nm}$, and γ is the normal gravity.

The geoidal undulations or geoidal heights (N), representing the difference between the geoid and ellipsoid, can be evaluated through two methods based on the type of available geodetic measurements. First, it can be computed through the well-known Stokes formula, if gravity anomalies are utilized, as:

$$N = \frac{R}{4\pi\gamma_o}\iint_\sigma \Delta g S(\Psi) d\sigma \quad (3)$$

where R is the radius of the Earth, Δg is the gravity anomalies, and $S(\Psi)$ is the Stokes function, and $d\sigma$ is an infinitesimal surface element on the unit sphere σ. The previous Stokes formula needs to be applied over the whole Earth; however, in practice gravity, datasets of the whole Earth are not available. Thus, the gravimetric geoid modeling methods break up the gravity anomalies (Δg) into three components:

$$\Delta g = +\Delta g_{GGM} + \Delta g_F + \Delta g_h \quad (4)$$

where Δg_F represents the free-air gravity anomalies, Δg_h is the effect of topography, and Δg_{GGM} represents the gravity anomalies of a reference gravity field represented by a GGM. Therefore, the full geoid undulation (N) is decomposed into three components too:

$$N = N_{GGM} + N_{\Delta g} + N_h \quad (5)$$

where $N_{\Delta g}$ is the contribution of the reduced gravity anomalies computed by Stokes's integral, N_h is the contribution of the topography, and N_{GGM} is the contribution of the reference gravity field, computed as:

$$N_{GGM} = \left({}^{GM}/_{r\gamma}\right)\sum_{n=2}^{n\max}(a/r)^n - \sum_{m=0}^{n}\left((C_{nm}\cos m\lambda) + (S_{nm}\sin m\lambda)\right)P_{nm}\sin\vartheta\Big) \quad (6)$$

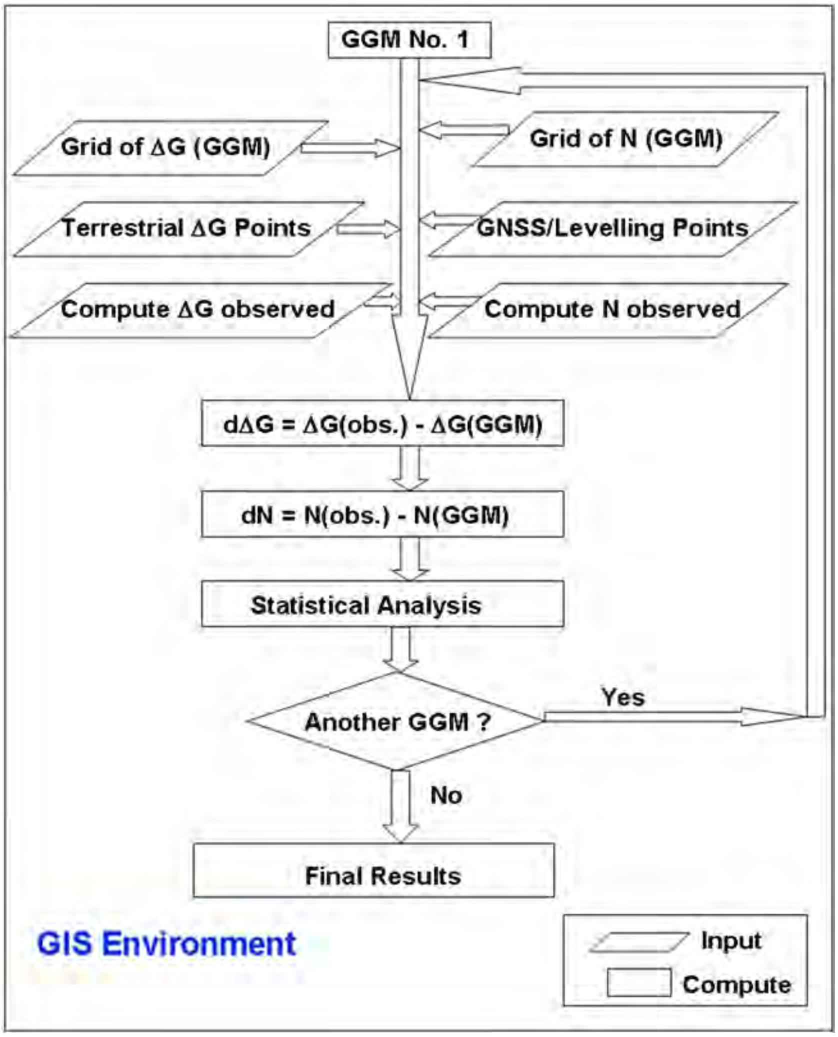

Fig. 4 Processing procedures

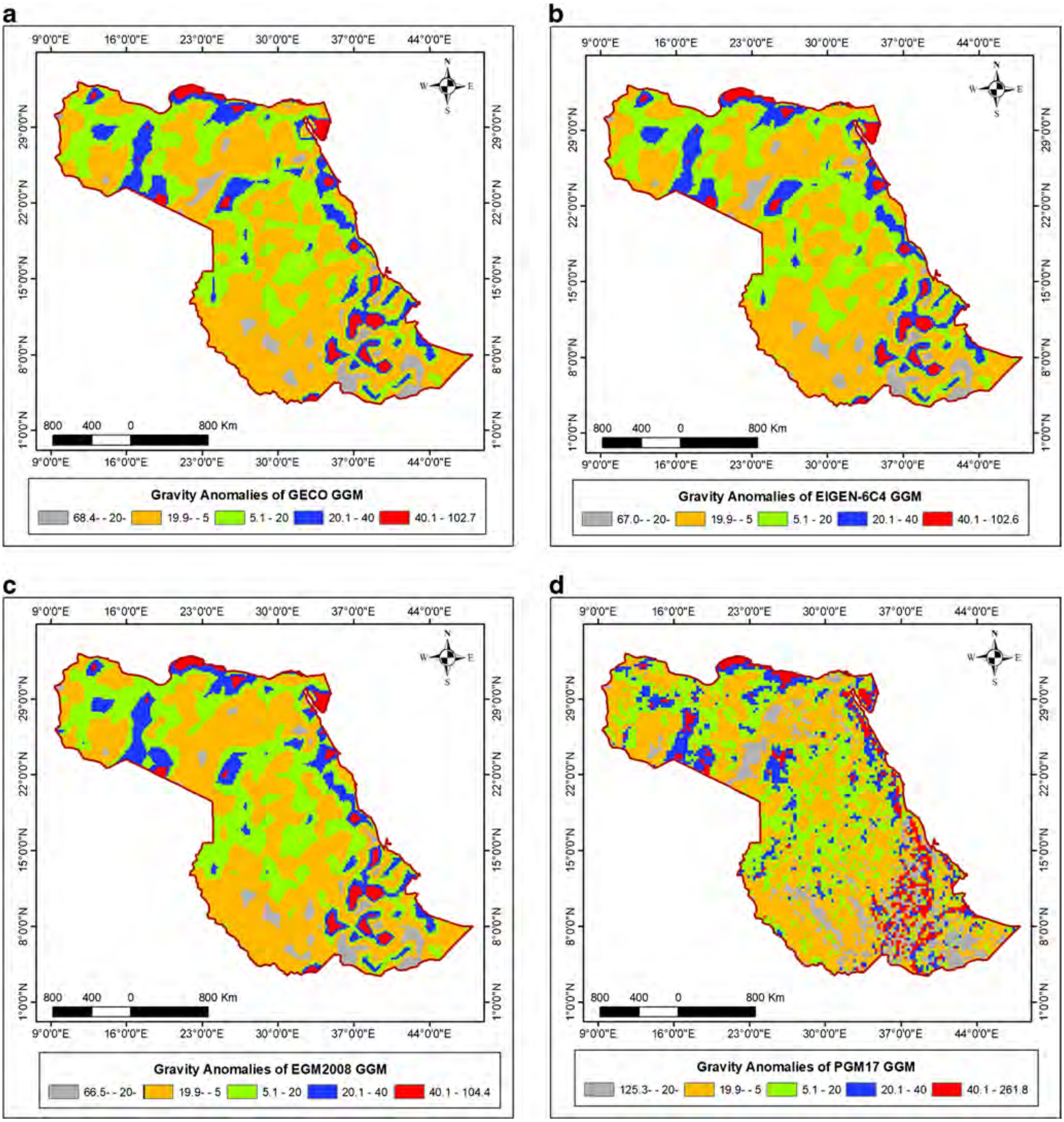

Fig. 5 Gravity anomaly over Northeast Africa of (**a**) GECO, (**b**) EIGEN-6C4, (**c**) EGM2008, (**d**) PGM17 models

Consequently, geoid modeling requires the utilization of a GGM to represent the global variations or long wavelengths of the Earth gravitational field, along with a digital elevation model (DEM) to depicts the topography of the local area and determine its effects on the developed geoid model.

The second manner of computing geoidal heights (N) is the so-called GNSS/leveling approach, where N can be computed from both GNSS-based ellipsoidal heights relative the ellipsoid surface (h) and the MSL-based orthometric heights (H) as:

$$N = h - H \tag{7}$$

In this evaluation study, other three GGM have been selected, namely GECO, EIGEN-6C4, and EGM2008 models.

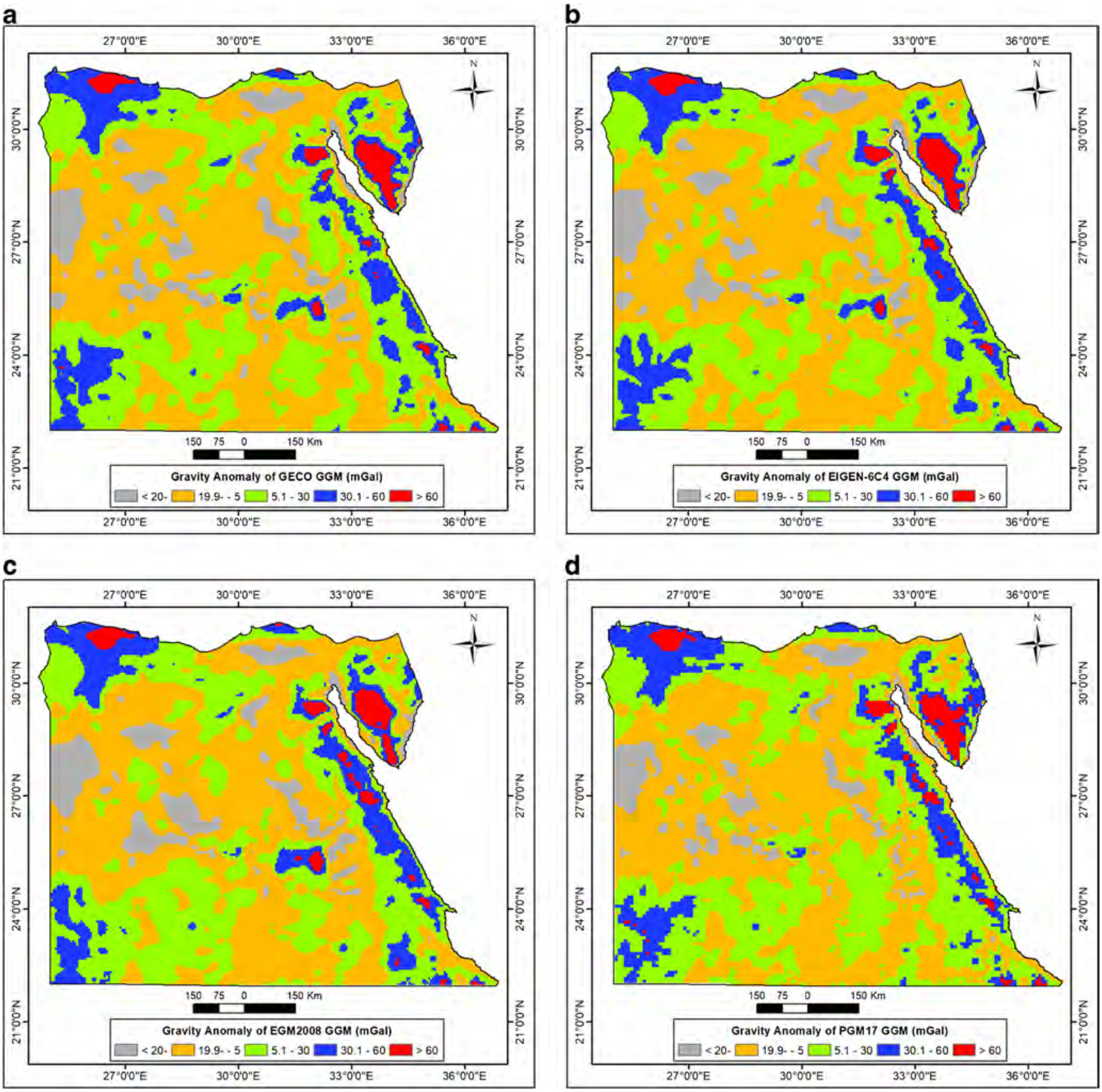

Fig. 6 Gravity anomaly over Egypt of (**a**) GECO, (**b**) EIGEN-6C4, (**c**) EGM2008, (**d**) PGM17 models

These models have been selected since they are the only (to date) high-resolution GGMs with degree of 2190. A brief description of each model is as follows (Table 1):

– PGM17: The primarily GGM under development by the U.S. National Geospatial Intelligence Agency. PGM17, up to 2190 degree, is a classified model so far, that was delivered particularly to the EGM2020 evaluation working group.
– GECO: A global gravity model utilizes the GOCE satellite-based gravity data to improve the accuracy of the EGM2008 GGM in low and medium frequencies. GECO is developed, in 2015, up to degree and order 2190 (Gilardoni et al. 2016). GECO is the most-recent published high-resolution GGM up until 2017.
– EIGEN-6C4: A model released in 2014, that utilizes satellite tracking data (from LAGEOS, GRACE, and GOCE missions) along with a global surface gravity anomaly grid and altimetry data. The model is up to 2190 degree, developed by both the Germany GFZ research center and the French CNES research center (Förste et al. 2014).

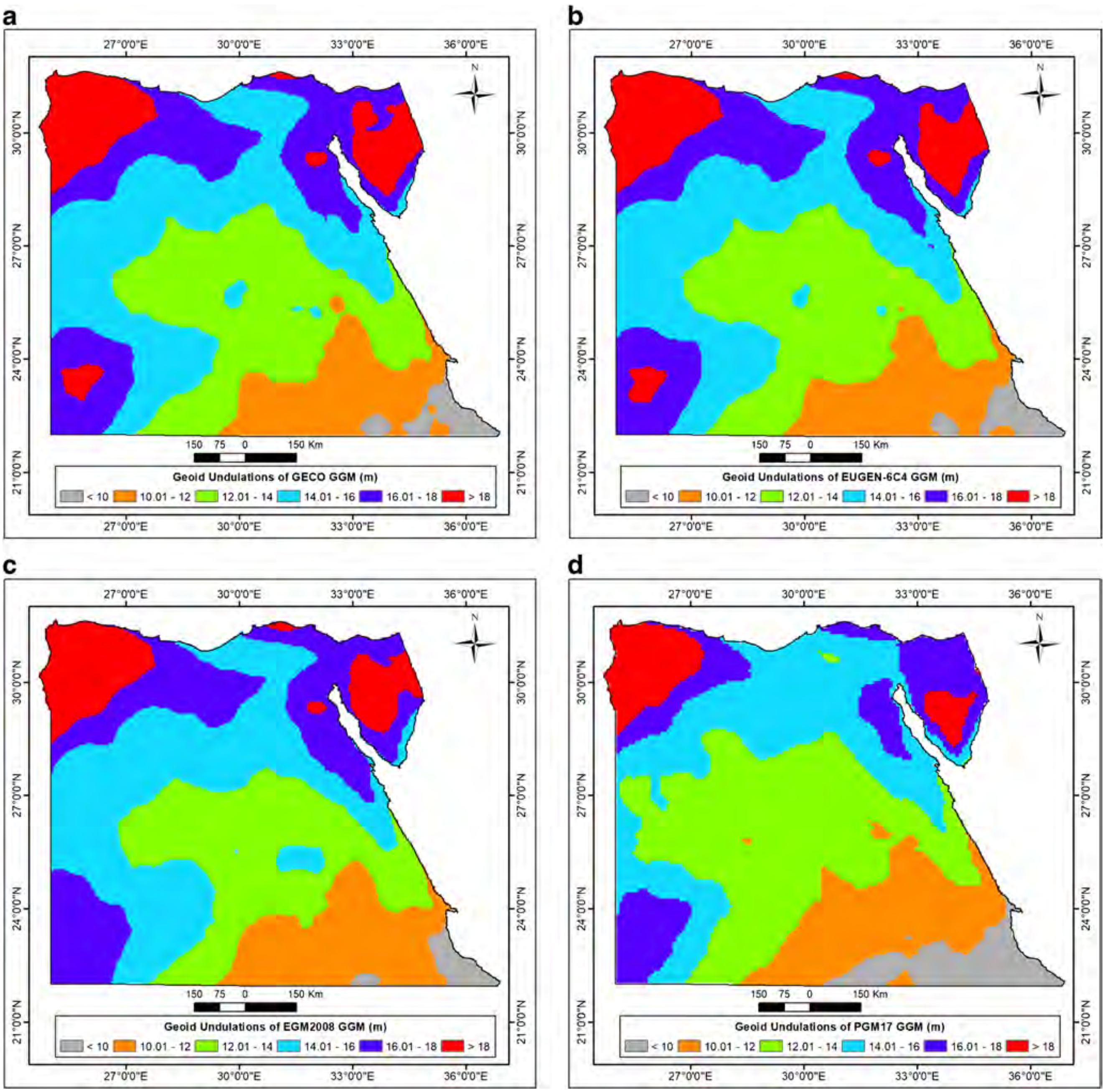

Fig. 7 Geoid undulations over Egypt of (**a**) GECO, (**b**) EIGEN-6C4, (**c**) EGM2008, (**d**) PGM17 models

Table 2 Statistical measures of GGMs over terrestrial gravity stations in Northeast Africa: before removing outliers (units of mGal)

	Minimum	Maximum	Range	Mean	St. dev.
EGM2008	− 260.7	393.3	654.0	− 4.4	± 56.9
GECO	− 258.4	391.5	649.9	− 4.2	± 56.6
EIGEN-6C4	− 260.4	393.3	653.0	− 4.1	± 56.9
PGM17	− 288.1	335.8	624.0	− 5.7	± 49.0

– EGM2008: An integrated GGM developed in 2008 by the U.S. NGA up to 2190 degree, based on GRACE-based satellite tracking data, terrestrial gravity data, and altimetry data. It was a millstone in GGM development, since its preceding model did not exceed 360 maximum degree (Pavlis et al. 2008).

The assessment of GGMs carried out in this study consists of two procedures performed within a GIS environment. First, the performance of each GGM in representing the gravity field over Egypt is investigated. The GGM-based gravity

Table 3 Statistical measures of GGMs over terrestrial gravity stations in Northeast Africa: After removing outliers (units of mGal)

	Minimum	Maximum	Range	Mean	Standard Deviation	
					Value	Improvements
EGM2008	− 88.1	114.7	202.7	− 2.8	± 29.9	NA
GECO	− 73.2	115.5	188.7	− 2.6	± 29.7	11%
EIGEN-6C4	− 80.5	116.5	197.0	− 2.6	± 30.0	1%
PGM17	− 42.0	42.6	84.6	− 2.0	± 14.8	100%

anomalies are obtained, and then compared against the gravity anomalies of the known terrestrial points. The second comparison step judges the GGM-based geoidal heights (Eq. 6) against the known GNN/leveling undulations (Eq. 7) at the utilized stations in Egypt. The differences in both steps are, then, statistically investigated in order to define the accuracy and reliability of the tested GGMs.

Available data and processing

The GGM evaluation has been made on two scales: a regional one in North-East Africa and a national basis in Egypt. For the first study case, gravity dataset has been downloaded from the International Gravimetric Bureau (BGI) covering Egypt, Sudan, South Sudan, Eretria, and Ethiopia (BGI 2018). Data of a total of 231 terrestrial gravity points have been obtained (Fig. 2). For Egypt, the available terrestrial geodetic datasets include (Fig. 3): the first-order Egyptian national gravity networks of both 1997 and 1977 containing 247 measured gravity points and 978 GNSS/leveling stations all over Egypt that were observed by the Survey Research Institute (SRI) in various projects over the last 5 years. It is worth mentioning that the average accuracy of the Egyptian National Gravity Standardization Network of 1997 (ENGSN97) is ± 0.02 mGal, while the corresponding value of the National Gravity Standard Base Network of 1977 (NGSBN77) is ± 0.08 mGal. Although there are other available second-order gravity measurements in Egypt, particularly in the western desert, their accuracy in both gravity and coordinates is questionable (e.g., Al-Krargy 2016 and Dawod 1998). On the other hand, the utilized GPS/leveling points have been surveyed using the first-order leveling and the first-order GPS geodetic network standards, and their average accuracy could be estimated as ± 3–4 cm. Thus, the most-precise available national datasets have been utilized, herein, to investigate the reliability of the four tested GGMs as will be discussed in details in the next section.

Table 4 Statistical measures of GGMs over terrestrial gravity stations in Egypt: before removing outliers (units of mGal)

	Minimum	Maximum	Range	Mean	St. dev.
EGM2008	− 140.6	114.2	254.8	− 2.3	22.5
GECO	− 133.2	110.9	253.4	− 3.3	21.4
EIGEN-6C4	− 133.7	110.9	244.6	− 2.6	21.0
PGM17	− 136.8	115.0	251.8	− 2.5	20.4

For PGM17, the Gravsoft package has been utilized to compute two grids (15′ × 15′ for Africa and 5′ × 5′ for Egypt) of gravity anomalies and geoidal undulations based on its harmonic coefficients. For the other GGMs, the ICGEM organization starts an online service to compute many geoidal properties (for some GGM) and deliver them in a grid format (ICGEM 2018). For any GGM, a specified grid could be computed online and downloaded for a variety of geoidal characteristics such as geoid heights, height anomaly, gravity anomaly, and gravity disturbance. Each grid has a gdf format, which can be easily manipulated in order to be applicable for GIS. Therefore, two grids, for gravity anomaly and geoid heights have been downloaded for each model of the other three tested GGMs. The interpolated gravity anomaly and geoid undulation values at each control point have been compared against its known values, and the differences are statistically investigated. Figure 4 depicts the flowchart of that processing methodology. The ArcGIS 10 software has been utilized, herein, for interpolation and mapping as an example of GIS packages. Figures 5, 6, and 7 depict the gravity anomaly and geoidal undulations for those GGMs in both case studies.

Results and discussions

Regional case study

The four selected GGM have been evaluated over the BGI gravity points in northeast Africa. First, the evaluation has carried out using all available 231 points, and then an outlier detection algorithm was applied to detect and remove erroneous stations. Additionally, points have low-accuracy gravity values have been, also, excluded. Thus, a number of 52 points, almost 23%, has been disqualified. The attained results are tabulated in Table 2 for all points and Table 3 for the remaining points after removing outliers. Results showed that, even before cleaning the BGI datasets, the PGM17 produces differences better than all other models. Removing outliers and

Table 5 Statistical measures of GGMs over terrestrial gravity stations in Egypt: after removing outliers (units of mGal)

	Minimum	Maximum	Range	Mean	Standard deviation	
					Value	Improvements
EGM2008	− 57.8	71.7	129.4	− 1.8	± 12.9	NA
GECO	− 49.6	49.5	99.1	− 2.8	± 11.6	10%
EIGEN-6C4	− 40.4	59.1	99.5	− 2.0	± 11.5	11%
PGM17	− 28.4	28.4	56.9	− 1.6	± 9.6	26%

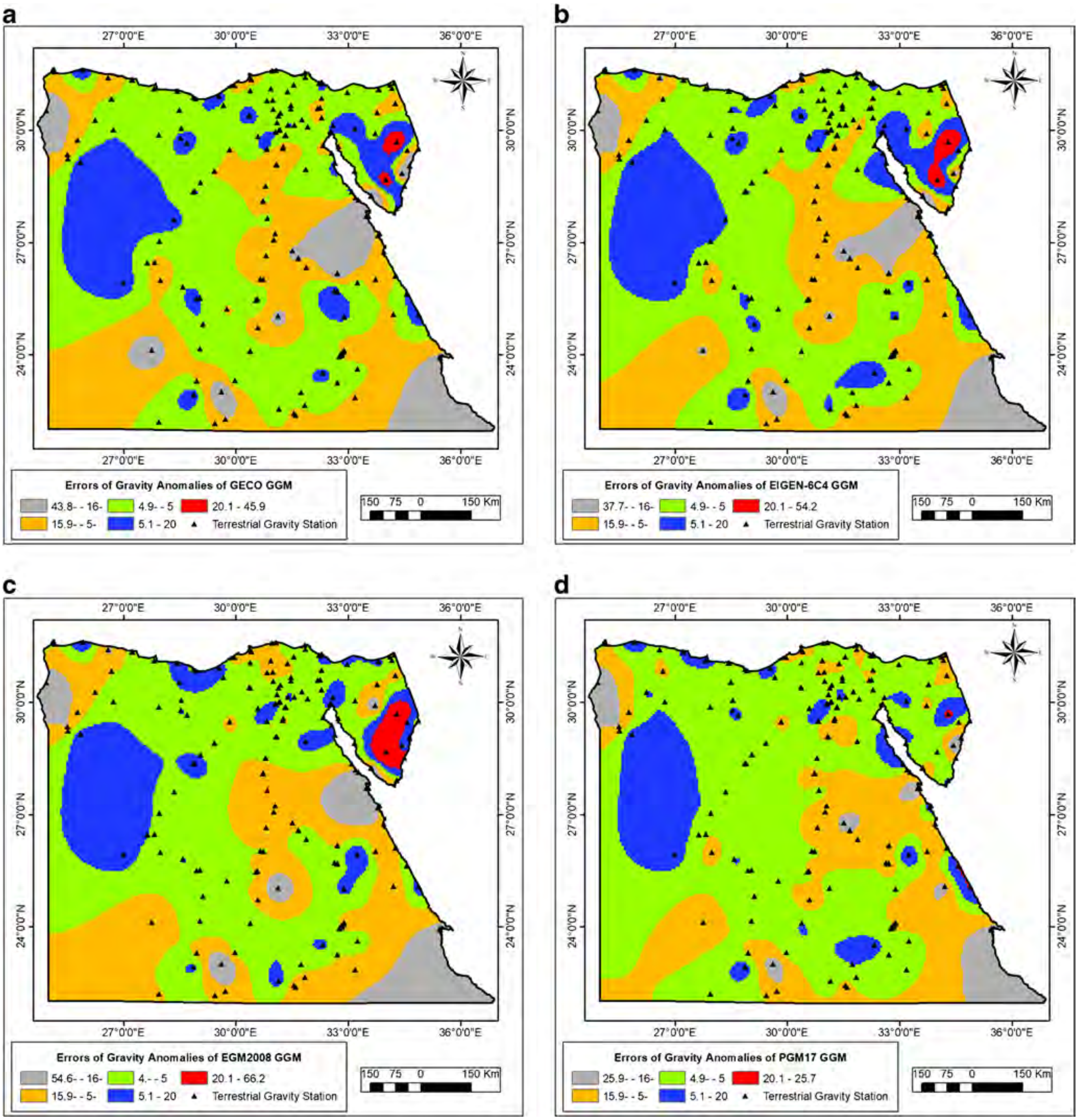

Fig. 8 Errors of gravity anomalies over Egypt of (**a**) GECO, (**b**) EIGEN-6C4, (**c**) EGM2008, (**d**) PGM17 models

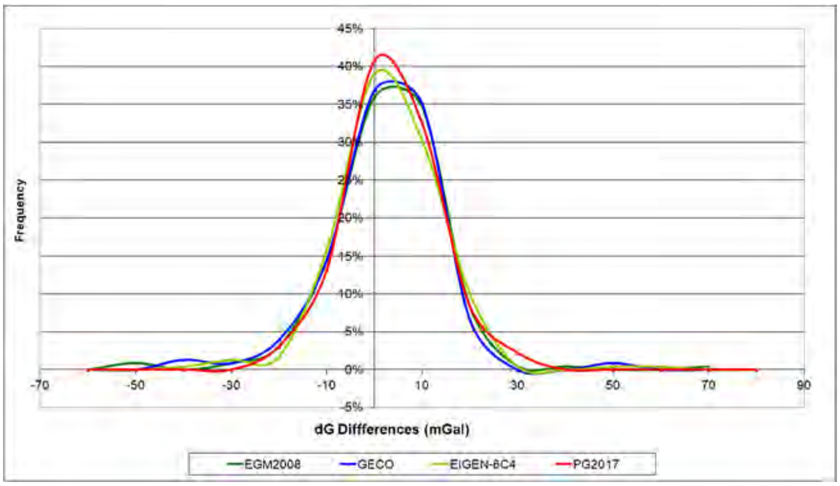

Fig. 9 Histogram of GGM differences of gravity anomaly in Egypt

suspected gravity points significantly enhances the findings for all GGMs as expected, and gives a general indication about the precision of the BGI holding datasets. The precision of the PGM17 has been improved from ± 49.0 mGal to ± 14.8 mGal. Table 3, also, shows that the range and the mean of differences of PGM17 are better than the other four models. Moreover, in terms of standard deviation, the PGM17 attain 100% improvements over the old EGM2008, while the GECO, and EIGEN-6C4 models resulted in improvements of 11%, and 1% respectively. As a result, it can be concluded that the PGM17 represents the gravitational field over northeast Africa in a better manner.

National Case Study

On a national basis over Egypt, the GGMs assessment has been performed in two steps: using gravity data, and using GNSS/leveling data. Once again, the evaluation was carried out using all available datasets, and using "good" data points after detecting and removing outliers. For terrestrial gravity stations, 19 out of 247 points (about 8%) have been flagged as excepted outliers. Tables 4 and 5 and Fig. 8 present the accomplished results. It can be seen, from Table 5, that the PGM17 produced a standard deviation of less than 10 mGal over the terrestrial gravity points in Egypt. Additionally, it can be realized that the PGM17 is better than the other four models not just in terms of standard deviation, but also in terms of the mean and range of differences. Furthermore, the GECO and EIGEN-6C4 GGMs produce almost 10% improvements over the old EGM2008, while that percentage is 26% for the PGM17 model. A similar conclusion could be drawn from Fig. 9 that depicts the histogram of gravity anomaly differences for the investigated four GGMs.

Rather than the standard deviation precision indicator, it can be seen from Table 5 that the PGM17 produced improvement of almost 128% in the range of discrepancies of gravity anomalies, while these improvements of GECO and EIGEN-6C4 are 31% and 30% respectively. Concerning the average differences of gravity anomalies, PGM17 improved EGM2008 by about 10%, while the other GGMs did not show any improvement. Such results emphasize that the new PGM17 noticeably enhance the performance of EGM2008, when compared against terrestrial gravity stations in Egypt, by almost 55%. Consequently, it can be concluded that PGM17 is better than the other investigated GGMs in representing the gravitational field over Egypt.

Second, the GGMs assessment has been performed using GNSS/leveling data. Similarly, the evaluation was carried out using all available datasets, and using "good" data points after detecting and removing outliers. For GNSS/leveling stations, 159 out of 967 points (about 16%) have been flagged as excepted outliers. A similar study concluded that this is an evident that there exist gross systematic errors in elevations of many bench marks in Egypt which should be investigated (Mahmoud 2012).

Tables 6 and 7 and Fig. 10 present the attained results. It can be seen, from Table 7, that the PGM17 produced a standard deviation of two decimeters in geoidal undulations over the available points in Egypt. Once again, it can be realized that the PGM17 is better than the other four models in terms of standard deviation of differences. Furthermore, the GECO, and EIGEN-6C4 GGMs produce 4%, and 17% improvements, respectively, over the old EGM2008, while that percentage is 20% for the PGM17

Table 6 Statistical measures of GGMs over GNSS/leveling stations in Egypt: before removing outliers (units of m)

	Minimum	Maximum	Range	Mean	St. dev.
EGM2008	− 1.19	0.09	1.28	− 0.64	0.28
GECO	− 1.69	0.44	2.14	− 0.64	0.31
EIGEN-6C4	− 1.70	0.46	2.16	− 0.66	0.31
PGM17	− 0.74	1.57	2.31	0.30	0.33

Table 7 Statistical measures of GGMs over GNSS/leveling stations in Egypt: after removing outliers (units of m)

	Minimum	Maximum	Range	Mean	Standard deviation	
					Value	Improvements
EGM2008	− 1.19	0.08	1.27	− 0.68	± 0.25	NA
GECO	− 1.69	0.19	1.88	− 0.70	± 0.24	4%
EIGEN-6C4	− 1.46	− 0.11	1.35	− 0.74	± 0.21	17%
PGM17	− 0.52	0.60	1.12	0.21	± 0.20	20%

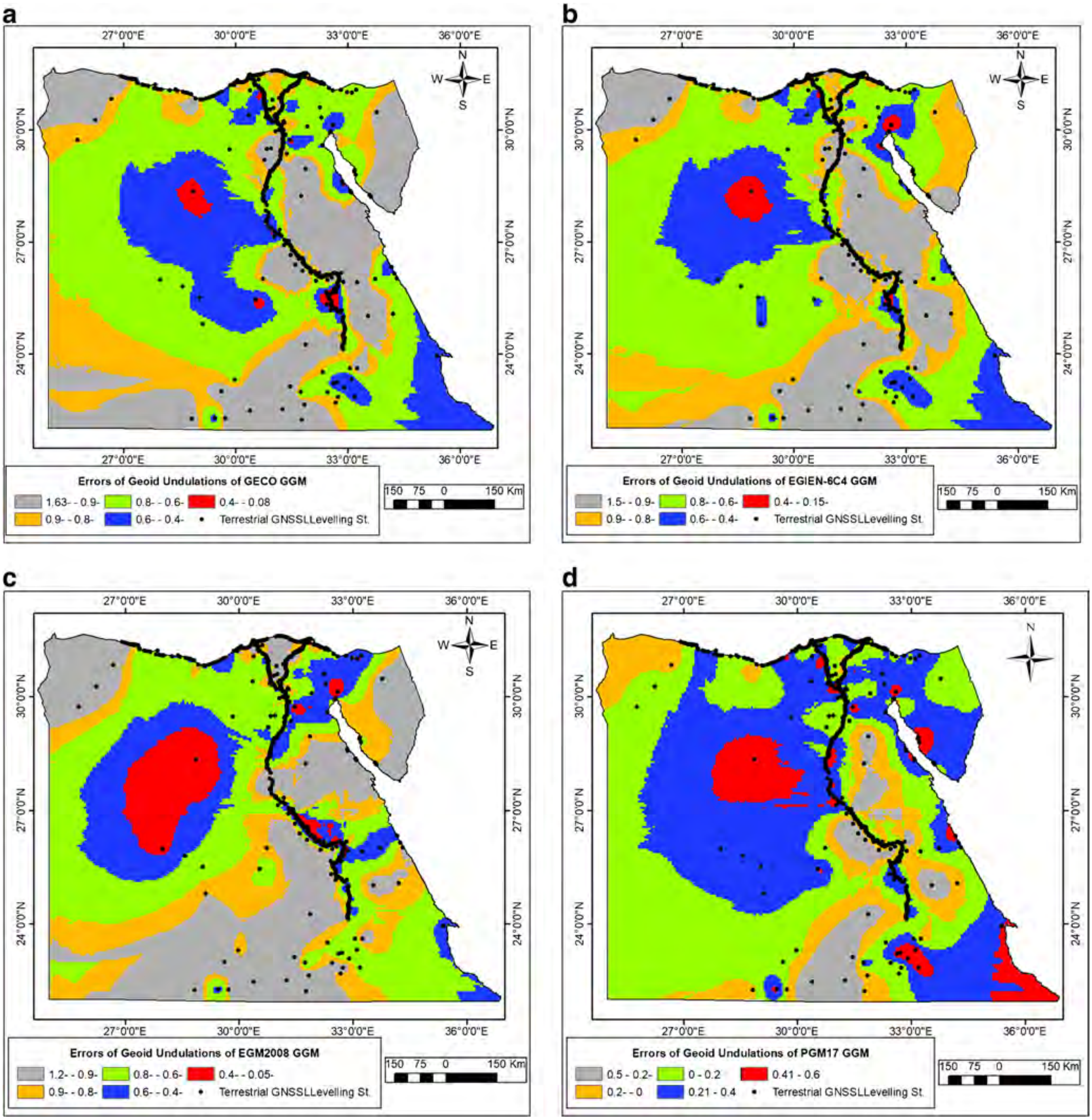

Fig. 10 Errors of geoid undulations over Egypt of: (**a**) GECO, (**b**) EIGEN-6C4, (**c**) EGM2008, (**d**) PGM17 models

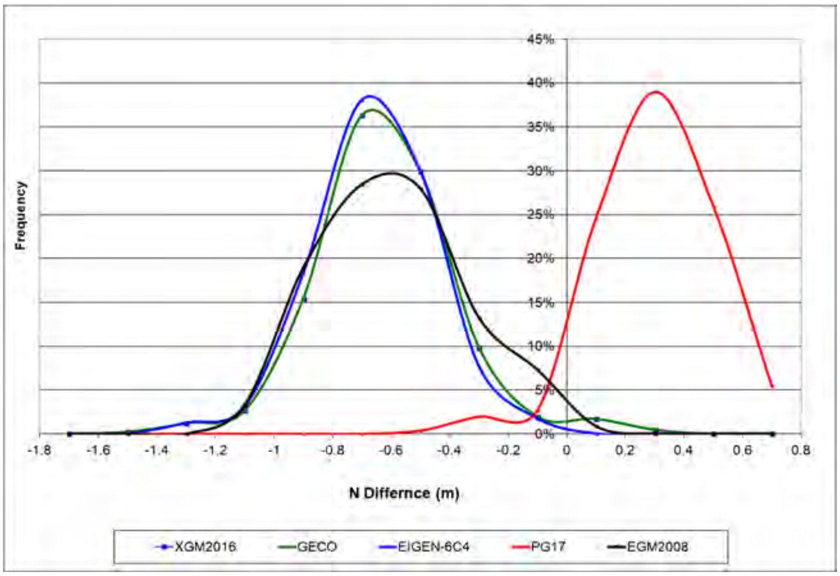

Fig. 11 Histogram of GGM differences of geoid undulations in Egypt

model. So, EIGEN-6C4 and PGM17 are almost comparable in terms of standard deviation, and not significantly far away from the other models. This slightly low precision of GGMs might be contributed to two facts: (a) most GGMs do not include terrestrial geodetic datasets of Egypt, and (b) the vertical geodetic datum (MSL) of Egypt has not been updated since its establishment in 1906.

Other than the standard deviation precision indicator, it can be seen from Table 7 that the PGM17 produced improvement of almost 131% in the average of differences of gravity anomalies, while the other GGMs did not show any improvement (Fig. 11). For the range of geoidal heights' differences, the PGM17 improved EGM2008 over Egypt by about 12%, while the other GGMs, again, did not show any improvement. Hence, it can be said that the overall improvements of PGM17 is approximately 54% over EGM2008 in Egypt. Once again, these results emphasis that the new PGM17 is considerably better than the other investigated GGMs when compared to terrestrial GPS/leveling in Egypt. Hence, it can be concluded that, for the time being, the PGM17 could be considered as the optimum global geopotential model to be utilized in national geoid modeling in Egypt.

Conclusions

Global geopotential models are needed in height transformation to convert the GNSS-based ellipsoidal heights into MSL-based orthometric heights in several geosciences applications. This study investigated the performance of the new PGM17 geopotential model over Egypt in particular and in Northeast Africa in general. The comparison has been performed, also, for GECO, EIGEN-6C4, and EGM2008 high-resolution models utilizing terrestrial gravity and GPS/leveling datasets within a GIS environment. Using BGI terrestrial gravity data in northeast Africa, the attained results indicated that the PGM17 attains 100% improvements over the old EGM2008, while the GECO, and EIGEN-6C4 models resulted in improvements of 11%, and 1% respectively. Thus, it can be concluded that the PGM17 represents the gravitational field over northeast Africa in a better manner.

On a national basis over Egypt, the GGMs assessment has been performed in two steps: using gravity data, and using GNSS/leveling data. It is realized that the GECO and EIGEN-6C4 GGMs produce almost 10% improvements, in terms of gravity anomaly, over the old EGM2008, while that percentage is 26% for the PGM17 model. Rather than the standard deviation precision indicator, it can be seen that the PGM17 produced improvement of almost 128% in the range of discrepancies of gravity anomalies, while these improvements of GECO and EIGEN-6C4 are 31% and 30% respectively. Concerning the average differences of gravity anomalies, PGM17 improved EGM2008 by about 10%, while the other GGMs did not show any improvement. Such results emphasize that the new PGM17 noticeably enhance the performance of EGM2008, when compared against terrestrial gravity stations in Egypt, by almost 55%.

Regarding the comparison over the available GNSS/leveling data, it is seen that the GECO and EIGEN-6C4 GGMs produce 4, and 17% improvements, respectively, over the old EGM2008, while that percentage is 20% for the PGM17 model. Additionally, it is shown that the PGM17 produced improvement of almost 131% in the average of differences of gravity anomalies, while the other GGMs did not show any improvement. For the range of geoidal heights' differences, the PGM17 improved EGM2008 over Egypt by about 12%, while the other GGMs, again, did not show any improvement. Hence, it can be said that the overall

improvements of PGM17 is approximately 54% over EGM2008 in Egypt. Such results emphasis that the new PGM17 is considerably better than the other investigated GGMs when compared to terrestrial gravity and GPS/leveling in Egypt. Thus, it can be concluded that, for the time being, the PGM17 could be considered as the optimum global geopotential model to be utilized in national geoid modeling in Egypt. Furthermore, the results of this case study and other studies of the evaluation working group should be taken into consideration by NGA within the undergoing activities for developing the upcoming EGM2020 model.

Acknowledgements The authors acknowledge the truthful cooperation of the U.S. National Geospatial-Intelligence Agency (NGA), the U.S National Geodetic Survey (NGS), and Dr. Srinivas Bettadpur, the head of Center of Space Research, University of Texas at Austin, and the chair of the EGM2020 Evaluation Working Group. Also, the authors express honest gratitude to the International Gravimetric Bureau (BGI) for providing the gravity datasets of Northeast Africa.

References

Abd-Allah A (2015) Assessment of GOCE models in Egypt, Master thesis, Faculty of engineering, Cairo University, Egypt

Abd-Elmotaal H (2015) Egyptian geoid using best estimated response of the Earth's crust due to the topographic loads. Presented at the International Association of Geodesy Symposium, Switzerland. https://doi.org/10.1007/1345_2015_194

Abd-Elmtaal H (2015) Validation of GOCE models in Africa. Newton's Bulletin No. 5, pp 149–162

Ahmed R, Singh R (2016) Seismic hazard assessment of Syria using seismicity, DEM, slope, active faults and GIS. Remote Sensing Applications: Society and Environment (RSASE). https://doi.org/10.1016/j.rsase.2017.04.003

Al-Karagy E, Doma M, Dawod G (2014) Towards an accurate discrimination of the local geoid model in Egypt using GPS/levelling data: A case study at Rosetta area. The International Journal of Innovative Science and Modern Engineering (IJISME) 2(11):10–15

Al-Krargy E (2016) Development of a national geoid for Egypt using recent surveying data, PhD dissertation, Faculty of Engineering, Minufiya university, Egypt

Al-Krargy E, Hosny M, Dawod G (2015) Investigating the precision of recent global geoid models and global digital elevation models for geoid modelling in Egypt, Regional Conference on Surveying and Development, Sharm El-Sheikh, Egypt, Oct. 3–6

Alnaggar D (1986) Determination of the geoid in Egypt using heterogeneous geodetic data, PhD dissertation, Faculty of Engineering, Cairo University, Egypt

Ashry M (2016) Towards optimal combination of gravity field wavelengths in geoid determination for Egypt, Master thesis, Faculty of engineering, Minia university, Egypt

Barzaghi R, Carrion D, Pepe M, Prezioso G (2016) Computing the deflection of the vertical for improving aerial surveys: a comparison between EGM2008 and ITALGEO05 estimates. Sensors 16. https://doi.org/10.3390/s16081168

Berber M, Wright W (2016) Online kinematic GNSS data processing for small hydrographic surveys. Ocean Eng 112:335–339

BGI (International Gravimetric Bureau) (2018) http://bgi.omp.obs-mip.fr/data-products/Gravity-Databases/Land-Gravity-data. Accessed Jan. 2018

Casula G (2016) Geodynamics of the Calabrian Arc area (Italy) inferred from a dense GNSS network observations. Geodesy and Geodynamics 7(1):76–86. https://doi.org/10.1016/j.geog.2016.01.001

Dawod G (1998) A national gravity standardization network for Egypt. PhD dissertation, Faculty of Engineering at Shoubra, Zagazig University, Egypt

Dawod G, Hosny M (2017) Toward a centimeter-geoid model for engineering surveying in Egypt: status and undergoing activities. J Sci Eng Res 4(10):312–319

Dawod G, Mandoer M (2016) Optimum sites for solar energy harvesting in Egypt based on multi-criteria GIS, the first Future University international conference on new energy and environmental engineering, April 11–14, Cairo, Egypt, pp 450–456

Dawod G, Mohamed H, Ismail S (2010) Evaluation and adaptation of the EGM2008 geopotential model along the northern Nile Valley, Egypt: case study, ASCE. J Surv Eng, V 136(1):36–40

Deng X, Hua X, You Y (2013) Transfer of height datum across seas using GPS leveling, gravimetric geoid and corrections based on a polynomial surface. Comput Geosci 51:135–142

El-Ashquer M (2016) An improved hybrid local geoid model for Egypt, PhD dissertation, Faculty of Engineering, Zagazig University, Egypt

Fazilova D (2017) The review and development of a modern GNSS network and datum in Uzbekistan. Geodesy and Geodynamics 8(2):187–192. https://doi.org/10.1016/j.geog.2017.02.006

Förste C, Bruinsma S, Abrikosov O, Lemoine J, Marty J, Charles F, Frank B, Barthelmes F, Biancale R (2014) EIGEN-6C4: the latest combined global gravity field model including GOCE data up to degree and order 2190 of GFZ Potsdam and GRGS Toulouse, presented in the 5th GOCE user workshop, Paris, France, Nov. 25-28. https://doi.org/10.5880/ICGEM.2015.1

Ghoniem I, Mousa A, El-Fiky G (2017) Distribution of the GNSS-LEO occultation events over Egypt. NRIAG J Astron Geophys 6:97–103. https://doi.org/10.1016/lj.nrjag.2017.03.005

Gilardoni M, Reguzzoni M, Sampietro D (2016) GECO: a global gravity model by locally combining GOCE data and EGM2008. Stud Geophys Geod 60:228–247

Godah W, Krynski J (2013) Evaluation of recent GOCE geopotential models over the area of Poland. Acta Geodyn Geomater 10(3): 379–386

Gomez M, Perdomo R, Cogliano D (2017) Validation of recent geopotential models in Tierra Del Fuego. Acta Geophys 65:931–943

Hassouna R, Asal F (2016) Using GIS-based digital raster analysis for improving harmonic modelsderived geoidal heights. Appl Geomat 8:151–162. https://doi.org/10.1007/s12518-016-0173-8

Hofmann-Wellenhof B, Moritz H (2005) Physical geodesy. SpringerWien, New York

Huang Q, Wangm J, Li M, Fei M, Dong J (2017) Modeling the influence of urbanization on urban pluvial flooding: a scenario-based case study in Shanghai, China. Nat Hazards 87:1035–1055

ICGEM (The International Center for Global Earth Model) (2018) http://icgem.gfz-potsdam.de/tom_longtime. Accessed Jun. 2018

Karpik A, Kanushin V, Ganagina I, Goldobin D, Kosarev N, Kosareva A (2016) Evaluation of recent Earth's global gravity field models with terrestrial gravity data. Contributions to Geophysics and Geodesy 46(1):1–11. https://doi.org/10.1515/congeo-2016-0001

Kaya E, Agca M, Adiguzel F, Cetin M (2018). Spatial data analysis with R programming for environment. Journal of Human and Ecological Risk Assessment. https://doi.org/10.1080/10807039.2018.1470896

Li H, Fang J (2017) Crustal and upper mantle density structure beneath the Qinghai-Tibet plateau and surrounding areas derived from EGM2008 geoid anomalies. ISPRS Int J Geo-Inf 6(4). https://doi.org/10.3390/ijgi6010004

Mahapatra M, Ratheesh R, Rajawat A (2017) Storm surge vulnerability assessment of Saurashtra coast, Gujarat, using GIS techniques. Nat Hazards 86:821–831

Mahmoud S (2012) Assessment of the gravitational global models in Egypt, Master thesis, Al-Azhar University, Cairo, Egypt

Mohamed A, Radwan A, Sharaf M, Hamimi Z, Hegazy E, Aly N, Gomaa M (2016) Evaluation of the deformation parameters of the northern part of Egypt using global navigation satellite system (GNSS). NRIAG J Astron Geophys 5:65–75

Odera P, Fukuda Y (2017) Evaluation of GOCE-based global gravity field models over Japan after the full mission using free-air gravity anomalies and geoid undulations. Earth Planets Space 69. https://doi.org/10.1186/s40623-017-0716-1

Pavlis NK, Holmes SA, Kenyon SC, Factor JK (2008) An earth gravitational model to degree 2160: EGM2008, presented in the EGU general assembly, Vienna, Austria, April 13-18

QZSS (2018) http://qzss.go.jp/en/technical/satellites/index.html. Accessed June 19, 2018

Rabiu B (2015) State of GNSS in Africa: applications, observational infrastructures, research implications and prospects, presented in the space weather workshop, April 13–17, Boulder, Colorado, USA

Sreejith K, Rajesh S, Majumdar T, Rao G, Radhakrishna M, Krishna K, Rajawat A (2013) High-resolution residual geoid and gravity anomaly data of the northern Indian Ocean - an input to geological understanding. J Asian Earth Sci 62:616–626

Srivastava P, Singh R (2016) GIS based integrated modelling framework for agricultural canal system simulation and management in Indo-Gangetic plains of India. Agric Water Manag 163:37–47

Stal C, Poppe H, Vandenbulcke A, Wulf A (2016) Study of post-processed GNSS measurements for tidal analysis in the Belgian North Sea. Ocean Eng 118:165–172

Wu Q, Kang J, Li S, Zhen J, Li H (2015) GNSS positioning by CORS and EGM2008 in Jilin province, China. Sensors 15:30419–30428. https://doi.org/10.3390/s151229806

Yakubu C, Ferreira V, Asante C (2017) Towards the selection of an optimal global geopotential model for the computation of the long-wavelength contribution: a case study of Ghana. Geosciences 7:113. https://doi.org/10.3390/geosciences7040113

Yılmaz M, Turgut B, Güllü M, Yılmaz I (2017) The evaluation of high-degree geopotential models for regional geoid determination in Turkey. AKÜ J Sci Eng (17):147–153. https://doi.org/10.5578/fmbd.50706

Available online www.jsaer.com

***Journal of Scientific and Engineering Research*, 2019, 6(6):55-64**

Research Article

ISSN: 2394-2630
CODEN(USA): JSERBR

Relative and Absolute Sea Level Rise based on Recent Heterogeneous Geospatial Data: A Case Study in the Nile Delta, Egypt

Gomaa M. Dawod*, Hoda F. Mohamed, and Ghada G. Haggag

Survey Research Institute, National Water Research Center,
308 Al-Ahram St., Giza, Egypt
* dawod_gomaa@yahoo.com, ORCID: 0000-0002-4426-8231

Abstract Sea level rise and vertical land movements (mainly land subsidence) comprise key elements in coastal engineering and environmental applications, particularly in river delta margins. This study aims to precisely estimate the recent relative sea level changes, vertical land movements, and absolute sea level rise along the coasts of the Nile delta, as a case study, based on modern heterogamous geospatial data. Tide gauge records at five locations along with Global Navigation Satellite Systems (GNSS) observations have been analyzed. The quality of the collected tide datasets is varying from a station to another. It has been found that the confidential relative sea level rise estimates in the Nile delta region, between 1990 and 2016, vary from 2.6 to 4.3 mm/year. In accordance with GNSS-based datasets, the vertical land movements rates at the tide gauge sites range between +0.09 and -4.3mm/year. So, it can be concluded that the absolute sea level rise differ between 5.0 mm/year at Alexandria to 6.9 mm/year at Port Said. Based on the available datasets; it might anticipated that by year 2050 the mean sea level will be raised about 17 and 23 cm, above the 2016-level, at Alexandria and Port Said respectively.

Keywords Sea Level, Land Subsidence, GNSS, Tide Gauges, Egypt

Introduction

Sea level rise is considered strongly related to the global warming phenomena and a major sign of climate changes worldwide. It might be attributed to some primary factors including: ocean thermal expansion; mountain glaciers and polar ice caps melt, and change in terrestrial storage. It is a matter of reality that sea level has been significantly raised in the 20th century on a global average as a measure of climate change. The observed global mean sea rise, from tide gauge records and satellite altimetry data, has been reported as 1.5, 2.0 and 3.2 mm/year for the period 1901-1990, 1971-2010, and 1993-2010 respectively [1]. Sea level changes have a strong regional pattern, with some geographic places show considerable differences of local and regional sea level change from the global rise rate [2]. Causes of such variations include, among other, variability of local surface winds, ocean currents, temperature, and salinity. Based on different scenarios, the anticipated global sea level in 2081-2100, will range from 0.40 to 0.63 m relative to the 1986-2005 level [1]. Few available analyses that go beyond 2100 indicate sea level rise to be less than 1 m above the pre-industrial level by 2300 [3].
Several hazardous impacts of sea level rise have been investigated worldwide, particularly in low-land deltas, which necessitates the development of risk assessment adaptation planning. The impact of sea level rise on urban flood probability has been studied and found significant [e.g. 4]. Additionally, Dessu et al. [5] concluded that sea level rise considerably affect freshwater management and water quality in the Florida coastal everglades. Accessibility of road networks in some regions within Europe could be degraded by sea level rise [e.g. 6]. The quality of groundwater will be altered significantly in coastal regions due to sea water intrusion [7 and 8]. Sea rise will cause shorelines retreat, dune replacement, and residential resilience in coastal areas [e.g.

9]. Geographic Information Systems (GIS) have been applied to create coastal vulnerability index and to develop digital spatial maps for coastal management [e.g. 10]. Regarding Egypt, sea level rise could reduce annual precipitation, increase drought risk, and affect both food security and local economy [e.g. 11].

Tide gauge datasets could not represent global or regional changes in the mass of water. Potential factors affecting the stability of the sea level records include: sea effects from coastal dynamics (such as erosion, sediment transport, air pressure changes, wind direction, storms, etc.), land effects (such as compaction, excavation, Earthquakes, groundwater extraction, etc.) and sea effects from sea level changes (such as temperature and salinity, long-term tectonics, glacial rebound, etc.). Accordingly; absolute sea level rise rate is determined as the sum of relative rise observed from tide gauge stations and the vertical land motion or subsidence rate. Geometrically, land subsidence can be defined as the downward displacement of land surface relative to a specific reference surface, such as the Mean Sea Level (MSL), the geoid, or a reference ellipsoid, or relative to a certain assumed stable point outside the prone subsidence area. Such natural hazard phenomena can be attributed to natural and/or human activities, such as tectonic activities (e.g. earthquake and faulting), volcanic activities, landslide, underground mining activities, excessive groundwater or oil/gas extraction, natural consolidation of alluvium soil, and load of huge constructions. Land subsidence can be monitored by several techniques including levelling, Global Navigation Satellite Systems (GNSS), and the Synthetic Aperture Radar (SAR). Several studies have utilized such techniques for land subsidence all over the world [e.g. 12 and 13]. For the Nile delta region, geological and soil investigations revealed that land subsidence could range from 3.7 to 8.4 mm/year [e.g. 14]. In addition, the subsidence spatial pattern is significantly varied across that region where the rate is higher in the eastern area than in the western part [e.g. 15].

Relative and absolute sea rise estimation have been investigated by several researchers worldwide. For example, Alothman et al. [16] reported that the absolute sea level rate in the Northwest Arabian gulf, between 1979 and 2007, equals 1.5 mm/year. In the East China sea, the relative sea rise rate, in the period 1959-2013, equal 3.4 mm/year [17]. In addition, Parker [18] found that the relative sea levels rose in China during the twentieth century and this part of the twenty-first century from − 1.2 to + 3.2 mm/year, on average + 1.4 mm/year. Moreover; the relative mean sea level rise in the Indian Ocean, between 1950 and 2009, amounts to 1.5 mm/yr [19]. In addition, analysis of several tide gauge records in New Zealand, between 2001 and 2013, revealed that the absolute sea level rise ranges from 1.31 to 2.14 mm/year [20]. The Mediterranean Sea presents an average sea level rise trend of 2.44 mm/year in the period 1993-2012, with considerable spatial variations [21].

Nationally; the sea level rise determination and the assessment of its impacts in Egypt have been investigated extensively in the last couple of decades. Mohamed [22] has analyzed tide gauge records at Alexandria from 1906 to 2003, and has estimated the absolute sea level rise as 2.3 mm/year. Additionally; Firhy et al. [23] found that the analysis of historical records obtained from tide gauges at Alexandria, Rosetta, Burullus, Damietta, and Port Said show a continuous relative rise in mean sea level fluctuating between 1.8 and 4.9 mm/year, where the smaller rate occurs at the Alexandria harbor, while the higher one at the Rosetta promontory. Moreover; Shaltout et al. [24] applied 1993-2013 altimetry dataset to estimate the relative sea level rise rate at the Egyptian Mediterranean coast, and found it to be 3.1 mm/year. Between 1926 and 2000, the absolute sea level rise has been estimated at Port Said as 2.3 mm/year [25]. Land subsidence over the Alexandria coastline, in the west of the Nile delta region, could be up to 2 mm/year and its average equals 0.4 mm/year [26]. Also, subsidence in the central delta ranged from 5 to 9 mm/year in the period 1993-2000 [27].

Impacts of sea level rise on urban areas within the Nile delta region, north of Egypt, has been investigated and found to be vulnerable to inundation under several future sea level rise [e.g. 28 and 29]. For instance, Refaat and Eldeberky [30] have concluded that about 7% of the Nile-delta area is at risk of inundation due to future sea level rise. Moreover; hazards of sea level rise in the Nile delta include decrease in water supply, land supply, food security, and local economy [11]. In addition; other studies have concluded that sea level rise would, also, affect groundwater heads and salinity in the Nile delta region [e.g. 31 and 32].

The current research aims at estimating both relative and absolute sea level rise in the Nile delta coastal region based on recent heterogeneous geospatial datasets. Such measures are extremely valuable for decision makers in coastal management development in the Nile delta region as a case study.

Study Area and Available Data

The overall coasts of Egypt extend approximately over more than 3500 km along both the Eastern Mediterranean and the Red Sea. The current study focuses only on the Nile delta sector, ranging from longitude 29.6° E to longitude 32.3° E, and from latitude 29.8° N to latitude 31.6° N (Fig. 1). With more than fifty million population, the Nile delta might be considered as one of the most densely populated regions worldwide. The topography of the study area (Fig.1) ranges from elevation -72 meter to 197 meter, with an average of 5.9 meter. As can be seen from that figure that the dominant elevation is less than 10 meter in the northern and middle parts of the delta. Moreover, it can be realized that the northern region of the delta area has an elevation less than almost 5 meter. Within this area, 5 tide gauge stations exist at Alexandria, Damietta, Burullus, Rosetta, and Port Said (Fig.1).

The available tide gauge dataset comprises data from different tide gauges along the Mediterranean coasts with variable time spans.. These tide gauges belong to different local organizations. For the Alexandria station, the historical gauge was established within the Alexandria civilian harbor at the end of the nineteenth century, aiming to define MSL to be adopted as the vertical geodetic datum of Egypt. Observations has been collected between 1898 and 1906, and the average has been set as the national MSL for the Bench Mark (BM) levelling network. Annual sea level data of this station is published by the Permanent Service of Mean Sea Level (PSMSL) international organization [33]. At the mid of 1990s, the Egyptian Navy Hydrographic Department (ENHD) established a new tide gauge at its headquarter in Alexandria, just few hundreds of meters from the historical one. For relating the new and the old gauges, a levelling was carried out and revealed that there was a datum shift of 18 cm between both scales. That implies that for combining datasets from both stations, such a shift should be considered. At the beginning of 2000s, the Survey Research Institute (SRI) of the National Water Research Center (NWRC) has cooperated with ENHD to update the instrument at this location, and start establishing new tide gauges at Port Said on the Mediterranean sea, Suez and Safaga on the Red sea. The other three tide gauges at Rosetta, Burullus, and Damietta belong to the Costal Research Institute (CoRI) of NWRC. Table 1 presents the characteristics of the collected tide gauge datasets at these five stations. It worth mentioning that the sea level measuring devices at these gauges are, recently, updated where pressure-type devices have been replaced by modern precise microwave ones as part of the activities of the undergoing project of adaptation to climate change in the Nile delta through integrated coastal zone management.

Table 1: Available Tide Datasets in the Nile Delta Coasts

Station	Period	Gaps	Data
Alexandria	1944 – 1989		Yearly
	1989 – 2008	2004 – 2007	Monthly
	2008 – 2016		Hourly
Damietta	1999 – 2016	2005 – 2011	Yearly
Burullus	1990 – 2016	2008 – 2012	Yearly
Rosetta	2004 – 2016	2010 – 2012	Yearly
Port Said	2008 – 2016		Hourly

For GNSS monitoring of subsidence in the Nile delta, 24-hours datasets at six stations, covering the period 2012-2015, have been utilized [34]. However; these stations did cover the Alexandria coast. Therefore; subsidence estimate is acquired for another GNSS station located at Alexandria belong to the Système d'Observation du Niveau des Eaux Littorales (SONEL) project, which is an international cooperation aims at providing high-quality continuous measurements of sea- and land levels at the coast from tide gauges (relative sea levels) and from modern geodetic techniques (vertical land motion and absolute sea levels) for studies on long-term sea level trends [35]. That GNSS station is located 3.1 km from the tide gauge. Even tough the number of these GNSS stations is relatively small, they have been utilized in this research since they constitute the only available GNSS data for the time being. The utilized seven GNSS stations are depicted in Fig. 1, and their estimated subsidence rates are shown in Table 2.

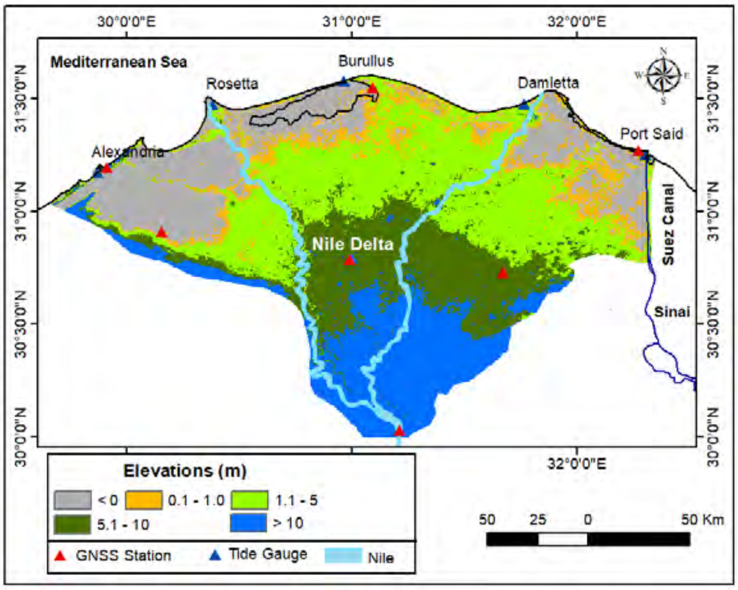

Figure 1: Topography of Study Area, Tide Gauges, and GNSS Stations

Table 2: Vertical Land Movements Rates at GNSS stations in the Nile Delta

Station	Period	Subsidence Rate (mm/year)	Reference
Cairo		+ 4.94	Mohamed et al. 2015
Port Said		- 4.72	
Abu Kebeer	2012-2015	+ 3.69	
Tanta		- 6.51	
Baltim		+ 0.71	
Abu El-Matameer		+ 0.55	
Alexandria	2002-2008	-0.85	SONEL 2019

The linear regression modelling describes the mathematical relationship in both relative and absolute sea level rise [e.g. 36]. Its basic equations could be in the form of:

$$MSL = aY + b \quad (1)$$

where, MSL is the annual mean sea level, a and b are coefficients to be determined, and y is the year.

To judge the attained regression trend, the coefficient of determination, R^2, is evaluated. It is a statistical measure about the quality of the regression model, representing the proportion of the variance in the dependant variable that is predictable from the independent variable. R^2 ranges from zero to one (or from 0 % to 100 %), computed as:

$$R = n(\sum xy) - (\sum x)(\sum y) \Big/ \sqrt{[n\sum x^2 - (\sum x)^2][n\sum y^2 - (\sum y)^2]} \quad (2)$$

where n is the number of known data points, x and y are the two dependant and independent variables to be modeled. Generally, the higher R^2, the better the linear regression model fits the data.

Results and Analysis

The first step was to analyze the sea level detailed characteristics at both Alexandria and Port Said stations that have available hourly observation records. That step was performed on the most-recent (2016) data. Fig. 2 (a and b) depicts the monthly variations of sea level at these stations. At Alexandria, the sea level varies from a minimum of 24.9 cm in February to a maximum of 31.5 cm in August, with a range of 6.6 cm. Similarly; for Port Said the sea level varies from a minimum of 42.1 cm in February to a maximum of 50.2 cm in August, with a range of 8.1 cm. Over August, the daily sea level variations have a range of almost 1 cm at both stations Fig. 3. Hourly discrepancies of sea level on August 27, that has the maximum daily average, at both Alexandria and

Port Said have been also investigated Fig. 4. It can be seen that both stations have a semi-diurnal tide pattern, with a daily tidal range of approximately 21 cm.

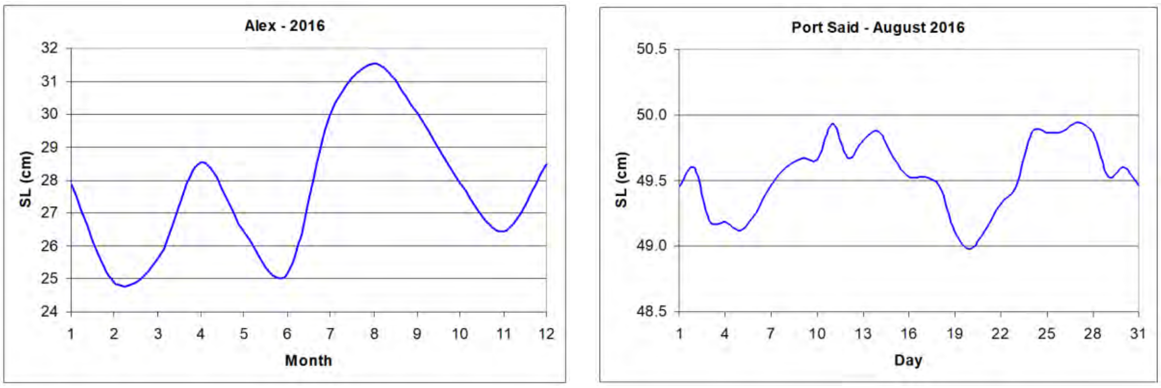

(a) Alexandria (b) Port Said

Figure 2: Monthly Sea Level Variations in 2016

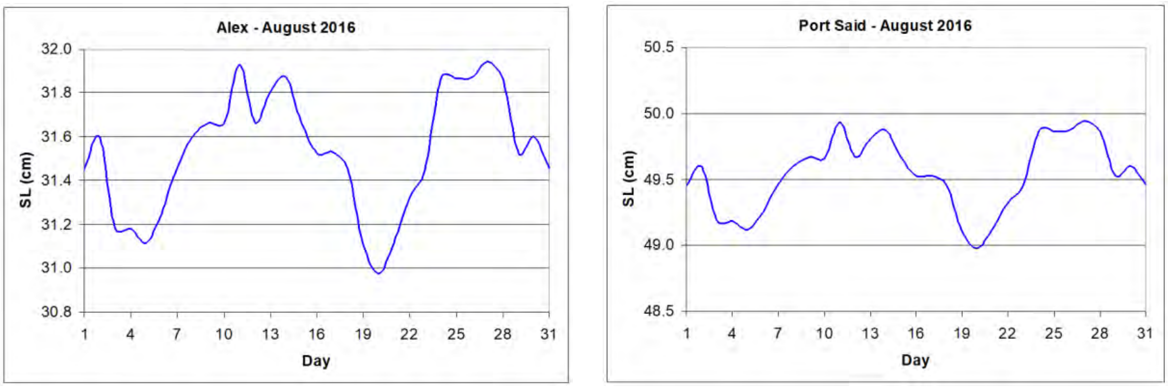

(a) Alexandria (b) Port Said

Figure 3: Daily Sea Level Variations in August, 2016

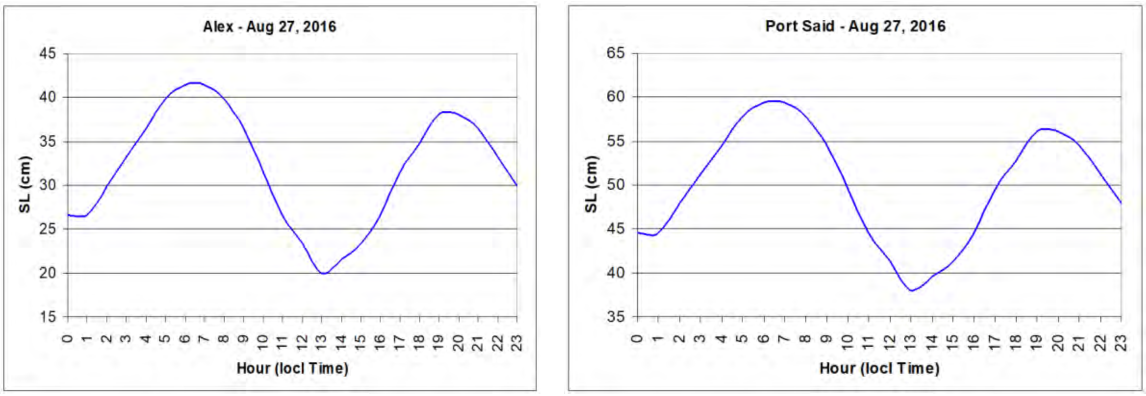

(a) Alexandria (b) Port Said

Figure 4: Hourly Sea Level Variations in August 27, 2016

Next, the annual averages of mean sea level have been inspected for modelling the relative sea level rise trend at the five locations for the period 1990-2016 Fig. 5. This figure might reveal that there is a datum shift between collected datasets at the five sites so it is recommended to perform a closed loop precise leveling along with GNSS circuit to define a unique vertical geodetic reference for all sea level measurements in the study area to tie each site to the closest BM since exist discrepancies in the national leveling network [e.g. 22].

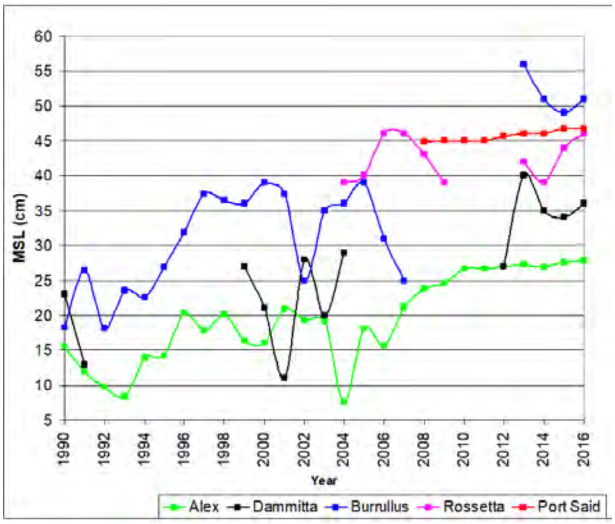

Figure 5: Annual Mean Sea Level Variations

Furthermore; the linear regression modelling has been performed to estimate the relative sea level rise at the five tide gauge sites. Table 3 presents the attained trend formulas along with their corresponding coefficients of determination. The analyses show that all Locations have positive sea rise with a significant quality of fitting, except for the Rosetta tide gauge. That small coefficient of determination suggests that sea level variations at Rosetta do not follow a linear trend. Therefore; the confidential relative sea level rise estimates in the Nile delta region are 4.3, 7.4, 10.3, and 2.6 mm/ year at Alexandria, Damietta, Burullus, and Port Said respectively. Fig. 6 depicts the spatial variations of sea level rise rates along the Nile delta coasts. It worth noting that the coefficient of determination of the regression are moderate for Damietta and Burullus, while its value are relatively higher for Alexandria and Port Said. It implies that the trend of sea rise at Alexandria and Port Said is better following a linear pattern with respect to time. On the other hand, the high sea level rise rates at Damietta and Burullus might be attributed to the specific spatial location of both sites close to the Nile river mouth and the Burullus Lake respectively.

Table 3: Relative Sea Level Rise in the Nile Delta

Station	Sea Rise Trend (cm)	R^2	Period
Alexandria	$MSL_1 = 0.4308\ y - 840.29$	0.76	2008 - 2016
Damietta	$MSL_2 = 0.7439\ y - 1464.3$	0.60	1999 - 2016
Burullus	$MSL_3 = 1.0348\ y - 2037.4$	0.63	1990 - 2016
Rosetta	$MSL_4 = 0.1336\ y - 226.09$	0.04	2004 - 2016
Port Said	$MSL_5 = 0.2569\ y - 471.27$	0.92	2008 - 2016

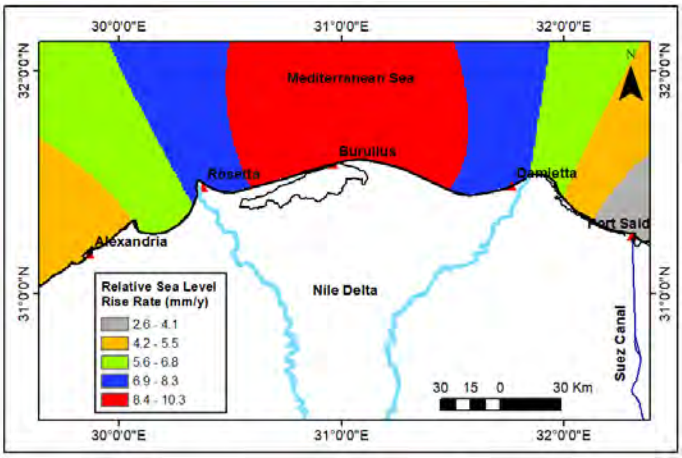

Figure 6: Sea Level Rise at Nile Delta Coasts

Moreover, the absolute sea level rise assessment starts first by estimating land subsidence in the study area. The subsidence rates at the collected GNSS stations have been utilized to develop a spatial subsidence model for the Nile delta (Fig. 7). The Arc GIS software has been applied to model such a phenomenon, and later to interpolate the subsidence rates at the tide gauges. It has been found that the vertical land movements in the Nile delta region vary from subsidence of -6.6 mm/year, at the northeast and central areas, to uplift of +4.9 mm/year, at the southeast part. Vertical land deformations are attributed to several factors such as soil compaction, tectonic movements, and groundwater extraction. Similar results have been reported by previous studies [e.g. 14, 15 and 27]. It has been found that the interpolated values of subsidence rates at the tide gauges equal -0.7, -1.8, -1.0, -4.3, and +0.09 mm/year at Alexandria, Damietta, Rosetta, Port Said, and Burullus respectively. Based on the estimated relative sea level rise and vertical land movements, the absolute sea level rise is determined (Table 4). It is concluded that the absolute sea level rise in the Nile delta region vary between 5.0 at Alexandria to 14.4 mm/year at Rosetta. However; the estimated value at Rosetta might not be trustable enough since its relative sea level rise trend has an insignificant quality measure. Also, the quality indicator of regression (R^2 in table 3) implies that the quality of relative sea level rise modelling at Alexandria and Port Said are better than those of at Damietta and Burullus. These two remarks suggest that estimates of both relative and absolute sea level rise at Alexandria and Port Said are of high confidence to be utilized in coastal management and environmental development policies. So, based on the quality of the collected datasets it can be concluded that the convinced absolute sea level rise, in the Nile delta area, could be considerably varying from 5.0 to 6.9 mm/year. Accordingly; it is anticipated that by year 2050 the mean sea level will be raised by about 17 and 23 cm, above the 2016-level, at Alexandria and Port Said respectively.

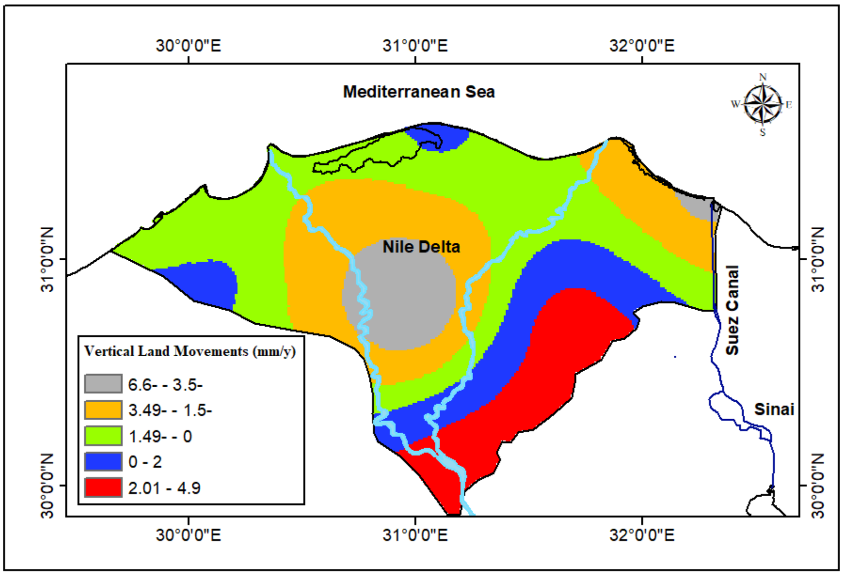

Figure 7: Vertical Land Movements in Nile Delta

Table 4: Relative and Absolute Sea Level Rise Rates in the Nile Delta

Station	Relative Rise (mm/year)	Absolute Rise (mm/year)
Alexandria	+ 4.3	+ 5.0
Damietta	+ 7.4	+ 9.2
Burullus	+ 10.3	+ 10.2
Rosetta	+ 13.4	+ 14.4
Port Said	+ 2.6	+ 6.9

Finally; the long-term analysis of relative sea level rise has been accomplished. Since only the Alexandria tide gauge has a long data series, this investigation has been performed in this location. The collected annual mean sea level, from different sources, cover 72 years from 1944 to 2016. To account for the 18.6-year cycle of lunar nodal tide, the available annual mean sea level dataset has been divided into several 20-year subgroups. The

linear regression modelling has been carried out on each sub-group, and on the entire 72-year dataset. Table 5 presents the attained findings, which indicates that there is a considerable increase of the sea rise rate over this time. Although the long-term relative sea rise rate equals 2.6 mm/year, the most recent rate is 4.3 mm/year. Thus; It is recommended that recent estimate of sea rise to be considered in future coastal development, plans rather than depending on the average rate over a long time span

Table 5: Long-Term Relative Sea Level Rise Rate at Alexandria

Relative Sea Rise Trend (cm)	R^2	Period
0.3199 y - 617.2	0.45	1944 - 1968
0.2213 y - 425.92	0.29	1968 - 1988
0.4194 y - 822.12	0.33	1988 - 2008
0.4308 y - 840.29	0.76	2008 - 2016
0.2570 y - 495.41	0.70	1944 - 2016

Conclusions

The Nile delta is one of the most vulnerable regions in the world to sea level rise. Precise estimates of both relative and absolute sea level rise are needed for a wide range of engineering and environmental activities. This study has utilized heterogeneous geospatial datasets with variable quality and time spans at five tide gauge stations along the delta coastlines. Corresponding vertical land movements have been interpolated from a GNSS-based vertical land movement spatial model.

The annual averages of mean sea level have been inspected for modelling the relative sea level rise trend at the five locations for the period 1990-2016. It is noted that there might be a datum shift between collected datasets at the five sites. So, it is recommended that a closed loop precise levelling along with GNSS circuit should be performed to define a unique vertical geodetic reference for all sea level measurements in the study area. Accomplished findings reveal that all investigated locations have positive relative sea rise with a significant quality of fitting, except for the Rosetta tide gauge. Therefore; the confidential relative sea level rise estimates in the Nile delta region are 4.3, 7.4, 10.3, and 2.6 mm/y at Alexandria, Damietta, Burullus, and Port Said respectively. The high values at Damietta and Burullus might be attributed to the specific spatial location of both sites close to the Nile river mouth and the Burullus lake. Even though the number of these GNSS stations is relatively small, they have been utilized in this research since they constitute the only available GNSS data for the time being. Thus; the vertical land movement rates have been estimated as -0.7, -1.8, -1.0, -4.3, and +0.09 mm/year at Alexandria, Damietta, Rosetta, Port Said, and Burullus respectively. Vertical land deformations in the Nile delta caused by several factors including soil compaction, tectonic movements, and groundwater extraction.

Based on the estimated relative sea level rise and vertical land movements, it is found that the absolute sea level rise in the Nile delta region vary between 5.0 at Alexandria to 14.4 mm/year at Rosetta. Accomplished results suggest that estimates of both relative and absolute sea level rise at Alexandria and Port Said are of high confidence to be utilized in coastal management and environmental development policies. So, based on the quality of the collected datasets it can be concluded that the convinced absolute sea level rise, in the Nile delta area, could be considerably varying from 5.0 to 6.9 mm/year. Accordingly; it is anticipated that by year 2050 the mean sea level will be raised by about 17 and 23 cm, above the 2016-level, at Alexandria and Port Said respectively.

For the long-term analysis of relative sea level rise at Alexandria, a dataset of annual mean sea level covering 72 years, from 1944 to 2016, has been inspected. It has been noticed that there is a considerable increase of the sea rise rate over this time period. Although the long-term relative sea rise rate equals 2.6 mm/year, the most recent rate is 4.3 mm/year. Accordingly; It is recommended that recent estimate of sea rise to be considered in future coastal development and environmental plans rather than depending on the average rate over a long time span. It is also recommended that detailed studies to be carried out to monitor and estimate both relative and absolute sea level rise in the Nile delta based on integrating different techniques and observations including tide gauge, satellite altimetry, GNSS, and radar satellite images.

Acknowledgment
The authors acknowledge the cooperation of the Costal Research Institute (CoRI), National Water Research Center (NWRC) for sharing some of their tide gauge datasets.

References

[1]. Church, J., Clark, P., Cazenave, A., Gregory, J, Jevrejeva, S., Levermann, A., Merrifield, M., Milne, G., Nerem, R., Nunn, P., Payne, A., Pfeffer, W., Stammer, D. and Unnikrishnan, A. (2013) Sea Level Change. In: *Climate Change* 2013: The Physical Science Basis. Contribution of Working Group I to the Fifth Assessment Report of the Intergovernmental Panel on Climate Change. Cambridge University Press, Cambridge, United Kingdom and New York, NY, USA.

[2]. Mohan, S. and Vethamony, P. (2017) Inter-annual and long-term sea level variability in the eastern Indian Ocean and South China Sea, *Climate Dynamics*, DOI: 10.1007/s00382-017-3800-0.

[3]. IPCC (Intergovernmental Panel on Climate Change) (2014) Climate Change 2014: Synthesis Report. Contribution of Working Groups I, II and III to the Fifth Assessment Report of the IPCC [Core Writing Team, R.K. Pachauri and L.A. Meyer (eds.)]. IPCC, Geneva, Switzerland, 151 pp.

[4]. Griffiths, J. Zhu, F., Chan, F., and Higgitt, D. (2018) Modelling the impact of sea-level rise on urban flood probability in SE China, *Geoscience Frontiers*, DOI: 10.1016/j.gsf.2018.02.012.

[5]. Dessu, S., Price, R., Troxler, T., and Kominoski, J. (2018) Effects of sea-level rise and freshwater management on long-term water levels and water quality in the Florida Coastal Everglades, *Environmental Management*, (211): 164-176.

[6]. Demirel, H., Kompil, M., and Nemry, F. (2015) A framework to analyze the vulnerability of European road networks due to Sea-Level Rise (SLR) and sea storm surges, *Transportation Research Part A*, DOI: 10.1016/j.tra.2015.05.002.

[7]. Hoover, D., Odigie, K., Swarzenski, P., and Barnard, P. (2015) Sea-level rise and coastal groundwater inundation and shoaling at select sites in California, USA, *Hydrology: Regional Studies*. DOI: 10.1016/j.ejrh.2015.12.055

[8]. Wassef, R., and Schüttrumpf, H. (2016) Impact of sea-level rise on groundwater salinity at the development area western delta, Egypt, *Groundwater for Sustainable Development*, (2-3): 85–103.

[9]. Grilli, A., Spaulding, M., Oakley, B. and Damon, C. (2017) Mapping the coastal risk for the next century, including sea level rise and changes in the coastline: application to Charlestown RI, USA, *Nat Hazards*, (88):389–414.

[10]. Ghoussein, Y., Mhawej, M., Jaffal, A., Fadel, A., El Hourany, R., and Faour, G. (2018) Vulnerability assessment of the South-Lebanese coast: A GIS-based approach, *Ocean and Coastal Management*, (158): 56–63.

[11]. Sušnik, J., Vamvakeridou-Lyroudia, L., Baumert, N., Kloos, J., Renaud, F., Jeunesse, I., Mabrouk, B., Savić, D., Kapelan, Z., Ludwig, R., Fischer, G., Roson, R., and Zografos, C. (2015) Interdisciplinary assessment of sea-level rise and climate change impacts on the lower Nile delta, Egypt, *Science of the Total Environment*, (503-504):279–288.

[12]. Atanasova, M. (2015) Study of deformation and movements on the Earth's crust of techogenic character based on repeated geodetic measurements, Presented at the FIG Working Week 2015, Sofia, Bulgaria, 17-21 May, 2015.

[13]. Kalkan, Y. (2014) Geodetic deformation monitoring of Ataturk dam in Turkey, *Arabian Journal of GeoSciences*, (7):397-405.

[14]. Stanley, J. (2017) Increased land subsidence and sea-level rise are submerging Egypt's Nile delta coastal margin, *GSA Today*, DOI: 10.1130/GSATG312A.1.

[15]. Fugate, J. (2014) Measurements of land subsidence rates on the North-western portion of the Nile delta using Radar interferometry techniques, MSC thesis, The University of Toledo, Ohio, USA.

[16]. Alothmana, A., Bosb, M., Fernandes, R., and Ayhan, M., (2014) Sea level rise in the north-western part of the Arabian Gulf, *Geodynamics* .DOI: 10.1016/j.jog.2014.09.002.

[17]. Cheng, Y., Ezer, T., and Hamlingto, B. (2016) Sea level acceleration in the China seas, *Water*. DOI:10.3390/w8070293
[18]. Parker, A. (2018) Relative sea level rise along the coast of China mid-twentieth to end twenty-first centuries, *Arabian Journal of Geosciences*. DOI: 10.1007/s12517-018-3620-5.
[19]. Palanisamy, H., Cazenave, A., Meyssignac, B., Soudarin, L., Wöppelmann, G., and Becker, M. (2014) Regional sea level variability, total relative sea level rise and its impacts on islands and coastal zones of Indian Ocean over the last sixty years, *Global and Planetary Change*, (116):54–67.
[20]. Denys, P., Beavan, J., Hannah, J., Palmer, N., Denham, M., Pearson, C., and Hreinsdottir, S. (2017) New Zealand's long term tide gauge record and the effect of seismically induced vertical land motion, Presented in the FIG Working Week 2017, Helsinki, Finland, May 29–June 2, 2017.
[21]. Bonaduce, A. , Pinardi, N. , Oddo, P. , Spada, G. , and Larnicol, G. (2016) Sea‐level variability in the Mediterranean Sea from altimetry and tide gauges, *Climate Dynamics*, (47):2851–2866.
[22]. Mohamed, H. Realization and redefinition of the Egyptian vertical datum based on recent heterogeneous observations, (2005) Ph.D. dissertation, Surveying engineering department, Faculty of engineering at Shoubra, Benha university, Egypt.
[23]. Frihy, O., Deabes, E., Shereet, S., and Abdalla, F. (2010) Alexandria-Nile Delta coast, Egypt: update and future projection of relative sea-level rise, *Environmental Earth Science*, (61):253–273.
[24]. Shaltout, M., Tonbol, K., and Omstedt, A. (2015) Sea-level change and projected future flooding along the Egyptian Mediterranean coast, *Oceanologia*, DOI: 10.1016/j.oceano.2015.06.004
[25]. Frihy, O. (2017) Evaluation of future land-use planning initiatives to shoreline stability of Egypt's northern Nile delta, *Arabian Journal of Geosciences*, DOI 10.1007/s12517-017-2893-4
[26]. Woppelmann, G., Le Cozannet, G., de Michele, M., Raucoules, D., Cazenave, A., Garcin, M., Hanson, S., Marcos, M., and Santamaria-Gomez, A. (2013) Is land subsidence increasing the exposure to sea level rise in Alexandria, Egypt, *Geophysical Research Letters*, (40):2953-2957.
[27]. Aly, M., Klein, A., Zebker, H., and Giardino, J. (2012) Land subsidence in the Nile delta of Egypt observed by persistent scatterer interferometry, *Remote Sensing Letters*, 3(7):621–630.
[28]. Abdrabo, M. and Hassaan, M. (2015) An integrated framework for urban resilience to climate change: Case study: Sea level rise impacts on the Nile Delta coastal, urban areas, *Urban Climate*. DOI: 10.1016/j.uclim.2015.09.005.
[29]. Dawod, M. and Mohamed, H., (2008) Estimation of sea level rise hazardous impacts in Egypt within a GIS environment, Proceedings of the third national GIS symposium in Saudi Arabia, Al-Khobar, April 7 - 9, 2008.
[30]. Refaat, M. and Eldeberky, Y. (2016) Assessment of coastal inundation due to sea-level rise along the Mediterranean coast of Egypt, *Marine Geodesy*. DOI: 10.1080/01490419.2016.1189471.
[31]. Abd-Elhamid, H., Javadi, A., Abdelaty, I., and Sherif, M. (2016) Simulation of seawater intrusion in the Nile delta aquifer under the conditions of climate change, *Hydrology Research*, DOI: 10.2166/nh.2016.157.
[32]. Noval., E., Fekry, A. and El-Didy, S. (2014) Adaptation to impact of sea level rise in the Nile delta coastal zone, Egypt, *American Science*, 9(10):17-29.
[33]. PSMSL (Permanent Service of Mean Sea Level) (2018) Available from: http://www.psmsl.org/, accessed June 2018.
[34]. Mohamed, H., Shaheen, B., Hosney, M., and Dawod, G. (2015) High-precision GPS monitoring of the land subsidence in the Nile Delta: Status and preliminary results, Regional Conference on Surveying and Development, Sharm El-Sheikh, Egypt, Oct. 3-6, 2015.
[35]. SONEL (Système d'Observation du Niveau des Eaux Littorales) (2018) Available from: http://www.sonel.org/, Accessed Jun 2018.
[36]. Nhan, N. (2016) Tidal regime deformation by sea level rise along the coast of the Mekong delta, *Estuarinem Coastal and Shelf Science*, (183):382-391.

Gomaa M. Dawod* and Tarek M. Abdel-Aziz

Utilization of geographically weighted regression for geoid modelling in Egypt

https://doi.org/10.1515/jag-2019-0009
Received March 4, 2019; accepted October 4, 2019

Abstract: Modelling the spatial variations of a specific Global Geopotential Model (GGM) over a spatial area is important to enhance its local performance in Global Navigation Satellite Systems (GNSS) surveying. This study aims to investigate the potential of utilizing some of Geographic Information Systems (GIS) geospatial analysis tools, particularly Geographically Weighted Regression (GWR), in geoid modelling for the first time in Egypt as a case study. Its main target is developing an optimum regression method to be applied in spatial modelling of the deviations of a specific GGM (e. g., PGM17). Using a precise local geodetic dataset of 803 GPS/levelling stations, PGM17 undulation differences have been modelled using different regression techniques to evaluate their precision and accuracy. Based on investigating 13 possible regression formulas of probable combinations of independent variables, results showed that the PGM17 discrepancies over Egypt depend mostly on the terrain heights and geoidal undulations. Over 80 checkpoints, the attained variations between the GWR model and known values varied from −0.574 m to 0.500 m, with a mean of 0.001 m and a standard deviation equals ±0.205 m. Based on available data, it has been found that GWR improved the PGM17 deviations by 9 % in terms of standard deviation and by 98 % in terms of the mean. Additionally, the study generates a reasonably innovative product for the local geodetic community by building an enhanced version of the PGM17. This surface will be a precious resource in GNSS surveying in Egypt for heights conversion, leading to considerable cost reduction in civil engineering works and mapping projects.

Keywords: Geospatial Analysis, Geoid, GGM, GNSS, GIS, GWR

***Corresponding author: Gomaa M. Dawod,** Survey Research Institute, National Water Research Center, Giza, Egypt, e-mail: dawod_gomaa@yahoo.com
Tarek M. Abdel-Aziz, Survey Research Institute, National Water Research Center, Giza, Egypt, e-mail: aziztm@hotmail.com

1 Introduction

Geoid modelling, over national or regional scales, requires a Global Geopotential Model (GGM) to depict the long wavelength of the Earth's gravitational field. Evaluating the accuracy performance of GGMs and picking up the optimal one has been investigated in many countries worldwide, e. g., [1]. Combining a GGM along with national geodetic datasets, particularly Global Positioning System (GPS)/Levelling data and gravity data, provides a fundamental technique for developing a national or regional geoid model such as in Egypt, e. g., [2], North America, e. g., [3], and New Zeeland, e. g., [4].

One of the most essential tasks of a geoid model is the transformation of ellipsoidal heights resulting from Global Navigation Satellite Systems (GNSS) surveys to the orthometric heights based on Mean Sea Level (MSL) commonly used in civil and surveying applications. In this regard, several techniques have been performed. For instance, Erol and Erol [5] have proposed the utilization of Artificial Neural Network (ANN) for precise height transformation. The polynomial interpolation approach provides a popular interpolation scheme not just in geoid applications, e. g., [6] and [7], but also in several geodetic transformation activities, e. g., [8]. Additionally, the Geographic Information Systems (GIS)-based interpolation processes, such as the Inverse Distance Weighted (IDW) and the Kriging methods, have been carried out in geoid investigations, e. g., [9]. Moreover, the least squares support vector machine approach has been proposed to be integrated with the traditional least-squares collocation method to enhance its predictability of geoid heights [10].

Basically in height conversion, a national GPS/levelling dataset is used to adopt a gravimetric geoid or a GGM to a national geometric datum for obtaining a height transformation model. The regression approach has been proposed as a simple mathematical model in various geodetic applications. For example, the U.S National Geospatial-Intelligence Agency (NGA) has proposed such regression formulas for datum transformation from World Geodetic System 1984 (WGS84) to a variety of local geodetic datums worldwide instead of the traditional transformation parameters approach [11]. Based on these regression equations, correction surfaces would be obtained over a specific spatial region, and the interpolation process would

Brought to you by | King Abdulaziz University
Authenticated
Download Date | 10/10/19 7:47 PM

be performed using a GIS or mapping package, e. g., [12]. Other researchers have investigated the utilization of other mathematical models, such as the exponential regression and ANN, in producing the correction surface for height transformation, e. g., [13]. However, any GIS package (the Arc GIS for example) contains many geospatial analysis tools that could be implemented in several geodetic applications. Some of these tools are the outlier detection, the ordinary least squares (OLS), the exploratory regression (ER), and the Geographically Weighted Regression (GWR).

In Egypt, the geoid modelling and GGM assessment have been extremely investigated in the last couple of decades. Since the development of the first pioneer national-scale geoid [14], several geoid researches have been carried out. For example, Dawod [15] has developed a national geoid model based on the data of the Egyptian National Standardization Gravity Network of 1997 (ENGSN97) along with GPS/levelling data. Furthermore, Dawod et al. [12] have investigated the accuracy of EGM2008 over the Nile delta area, Egypt. Also, Mahmoud [16] has investigated the performance of twenty-five GGMs over Egypt using 236 terrestrial GPS/Levelling stations. He concluded that the EGM2008 is the optimum GGM. Moreover, Abd-Allah [17] has investigated the GOCE-based satellite-only GGMs in Egypt and concluded that the accuracy of such models over Egypt is about 0.40 m for geoid undulations and 12.6 mGal for gravity anomalies. More recently, El-Ashquer et al. [18] have investigated the better fitting of GGMs to local gravity and GNSS/levelling databases towards the definition of a national geoid model. They developed a hybrid gravimetric quasigeoid model, called EGY-HGM2016, that has a mean standard deviation of 0.17 m. Similarly, Al-Karargy [19] has developed a national geoid model for Egypt, called SRI-GEOID16-2, utilizing the least-square collocation technique based on the EGM2008 combined with precise local geodetic datasets. He concluded that the average accuracy of the developed model is 0.12 m. Furthermore, Elshambaky [20] investigated the integration of soft computing techniques with the traditional least-square collocation approach to increase its geoidal height predictability by almost 10 % to 27 %.

On another sense, different methods of height transformation in Egypt has been investigated by several researchers. For example, Dawod et al. [12] utilized four mathematical regression models in developing a corrector surface fitting the EGM2008 GGM to local geodetic datasets to increase its accuracy performance. Additionally, Hassouna and Asal [21] proposed a GIS-based raster analysis filtering algorithm for enhancing the performance of GGM-based height grids by almost 8 %. Recently, Elshambaky [13] investigated the application of five mathematical models including neural network to develop a corrector surface to convert global geoid models to the regional geometric geoid. Such studies emphasized that there exist datum inconsistencies between global and local geodetic frameworks. For example, the vertical datum of Egypt has been defined in 1906, based on a single tide gauge station located at Alexandria harbour on the Mediterranean sea. Since then, it has not been updated although it is a fact that the sea level has been globally raised by a significant level in the 20th century. So, the geodetic community in Egypt tries to develop corrector surfaces based on several mathematical techniques in order to fit GGMs to the local vertical datum. In this regard, the current research aims to investigate the validity of utilizing GIS-based geospatial analysis tools, particularly the GWR, as an alternative method in geoid modelling probably for the first time in Egypt.

2 GIS-based geospatial analysis

Generally, regression contains a wide range of methods for modelling a relationship between a dependent variable (y) and a set of one or more independent variables (x). The traditional regression models may be stated as, e. g., [22]:

$$y_i = B_o + B_1 x_{1i} + B_2 x_{2i} + \cdots + B_m x_{mi} + \varepsilon_i \quad \text{for } i = 1, \ldots, n \tag{1}$$

where ϵ denotes the random error term, and $B_o, B_1, \ldots, B_n$ are the parameters to be estimated according to the OLS principle: $\sum_{i=1}^{n}(y_i - \hat{y}_i)^2$ is minimum, where $\hat{y}_i$ is the predicted or fitted value of y. In some cases, it is desirable to use different weights in a regression model to portray several levels of data uncertainty for the observations. Therefore, the process is called a weighted regression.

The capability of the regression model to reproduce the measured y values is measured by the goodness of fit (R^2), that ranges from 0 to 1 and measures the percentage of variations in y that is explained by the attained model. Adjusted-R^2 is another goodness indicator, that contains some adjustment for the number of variables in the model. The closer R^2 and adjusted-R^2 to 1, the better predictive performance of the model.

Exploratory regression is another GIS-based geospatial analysis procedure is used when there are many potential independent variables to be accounted for. This analysis can be considered as a data mining tool that will try all probable combinations of variables to judge which regression models will exceed the required criteria. So, it is similar to the stepwise regression approach or the sequential least-squares method.

Brought to you by | King Abdulaziz University
Authenticated
Download Date | 10/10/19 7:47 PM

In OLS process, the estimated parameters do not vary across the study area, and it is called a “global” regression model. In other words, the OLS calculation is based on the assumption that at each point of the study area the OLS model is representative and the variables’ relationship is constant. This is not usually valid when being applied to spatial data. If there is a spatial non-stationary effect, then the global estimate of spatial relationships will fake the real phenomena. Local regression techniques help to overcome such a problem by permitting the model parameters to differ across space. Thus, the basic idea underlying the GWR model is that the model’s coefficients can be estimated anywhere in the study area, and GWR is called a “local” regression model. The term “global regression” in GIS spatial analysis terminology means the OLS regression model since it gives a global or overall idea about the relationship between independent and dependent variables over the entire study area. on the other hand, GWR is called a “local regression” since it tries to understand/predict this relationship by fitting a regression equation to every feature in the dataset [23]. The typical GWR formula is:

$$y_i = B_{io} + \sum_{k=1}^{m} B_{i,k} x_{i,k} + \varepsilon_i \tag{2}$$

where y_i is the dependent variable at location i, $x_{i,k}$ is the k^{th} independent variable at location i, m is the number of independent variables, B_{io} is the intercept at location i, $B_{i,k}$ denotes the local regression coefficient for the k^{th} independent variable at location i, and ϵ_i is the random error at location i. This formula indicates that any coefficient is assumed to vary from point i to the next across the two-dimensional space. So, GWR allows estimating the parameters and, hence, the residuals at the spatial locations of observations or sample points. The solution of such a set of equations is usually carried out by a weighted least-squares approach.

Examining the results of GWR includes several statistical measures to be carefully inspected. For example, detecting spatial outliers and cluster constitutes another significant procedure in the analysis of standardized residuals. A spatial outlier is a feature with high value surrounding by features with low values, or a feature with low value neighboring with features of high values. The Anselin local Moran’s statistical test could be applied to produce a spatial representation of suspected outliers. Outliers should be removed (one by one) and the regression process is repeated. Moreover, the Variance Inflation Factor (*VIF*) should be examined since it measures redundancy among independent variables. Variables associated with *VIF* values larger than about 7.5 should be removed (one by one) from the regression model, e. g., [23].

The output of a GWR model contains the estimated parameter, their standard errors, and residuals at the sample points all over the study area along with various statistical indicators to judge the modelling. To figure out the accuracy of the model, a few observation points will not be used in modelling and will be kept as checkpoints. At these locations, the values of the estimated parameters can be spatially interpolated and the estimated dependent value could be computed. Comparing estimated and observed values at checkpoints give an estimation of the regression accuracy. It worth mentioning that GWR has been utilized in a wide range of physical and human applications including, for examples, satellite-derived bathymetry, e. g., [24], GPS meteorology, e. g., [25], modelling errors of Digital Elevation Model (DEM), e. g., [26], and analysis of unemployment, e. g., [27].

3 Study area and used data

The study area covers the entire Egyptian territories, and the utilized dataset comprises the most-precise available national geodetic data, and contains 803 GNSS/levelling stations observed by Survey Research Institute (SRI) in various projects over the last five years. They have been surveyed using first-order levelling, and first-order GPS geodetic network standards. Their average accuracy could be estimated as ±3–5 cm in terms of both ellipsoidal and orthometric heights [19]. Out of these stations, 80 points representing 10 % of the available known stations have been kept as checkpoints (Fig. 1). The selection of such stations has been based on their spatial location within the area of known points to avoid extrapolation in assessing the external accuracy of the utilized GWR method, e. g. [12] and [13]. Also, the gravity field of Egypt has been spatially modelled in a raster format based on 247 measured terrestrial gravity stations combining both the 1997 and 1977 national gravity networks (Fig. 2). Thus, the gravity value at all utilized and checkpoints have been interpolated.

The Preliminary Geopotential Model 2017 (PGM17) has been utilized in this study as a GGM (Fig. 3). PGM17 is a high-resolution model up to degree 2190, not published so far, developed by the NGA as a primary model in the development process of the Earth Geopotential Model 2020 (EGM2020). Dawod et al. [28] investigated the performance of 4 high-resolution GGMs, namely GECO, EIGEN-6C4, EGM2008, and PGM17, over Egypt and Northeast Africa. It has been realized that PGM17 produces differences of geoidal undulations, over the same dataset of GPS/levelling stations in Egypt, varying from −0.572 m to

Brought to you by | King Abdulaziz University
Authenticated
Download Date | 10/10/19 7:47 PM

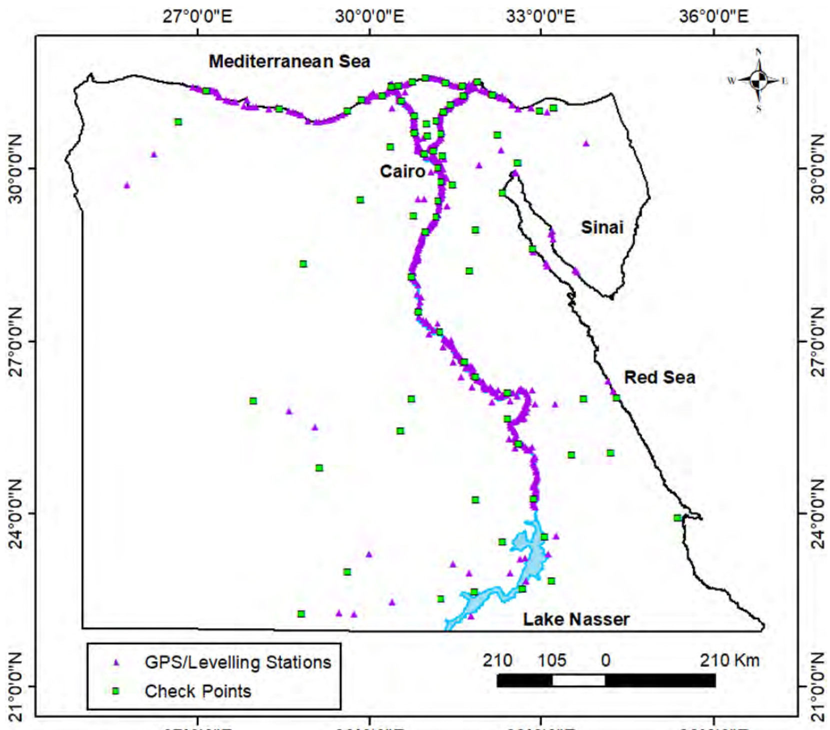

Figure 1: Available GPS/Levelling Points.

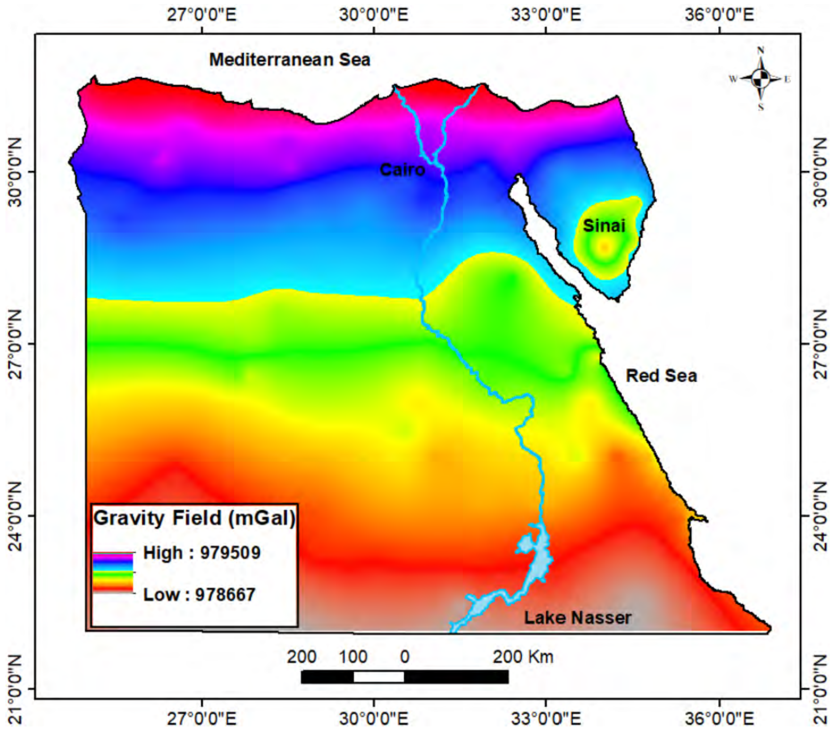

Figure 2: Gravity Field of Egypt.

Brought to you by | King Abdulaziz University
Authenticated
Download Date | 10/10/19 7:47 PM

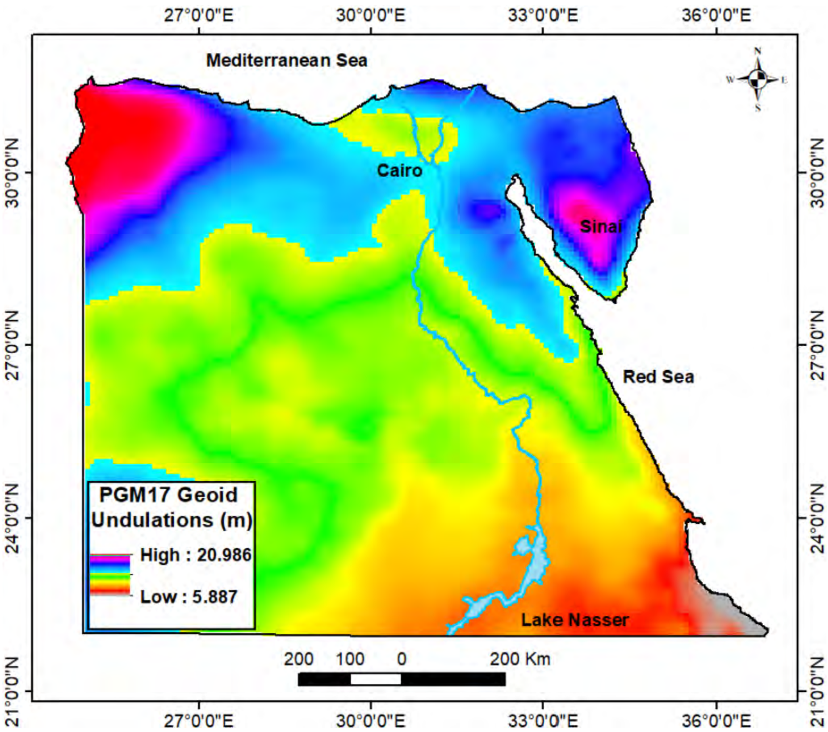

Figure 3: Geoidal Heights of PGM17 GGM.

0.584 m, with a mean of 0.211 m and a standard deviation of ±0.225 m. Also, it has been found that this GGM has enhanced the performance of the older EGM2008 model by about 100 % and 26 % in representing the gravity field over Northeast Africa and Egypt respectively. Moreover, It produces 20 % improvements in terms of standard deviation of GNSS/leveling known points in Egypt. Consequently, it has been concluded that the PGM17 model is significantly precise than other high-resolution GGMs in representing the gravitational field over Northeast Africa and Egypt.

Additionally, a Digital Elevation Model (DEM) is needed in creating an enhanced version of the PGM17 GGM in the final step. The main reason for utilizing a global DEM, herein, is that there is no published precise local DEM in Egypt. Geodetic and environmental studies, in general, utilize global DEMs even though their accuracy is not adequate enough. Dawod and Al-Ghamdi [29] have investigated eight global DEM models over Egypt and Saudi Arabia and concluded that the EarthEnvi-DEM90 model is the most reliable model for geomatics applications. Its height discrepancies over known checkpoints range from −7.6 m to 9.5 m, with a mean of 2.0 m and a standard deviation of ±1.9 m. Hence, EarthEnvi-90DEM (Fig. 4) is also employed herein to obtain height estimates over the entire Egyptian territories.

4 Processing and results

First, the traditional first-order regression has been carried out using the Microsoft Excel software, as usually done for creating a correction surface for GGM errors. Appling the traditional regression (Eq. 1), the residuals of the PGM17 GGM at the known GPS/Levelling stations (dN_{PGM17}) have been modelled as a function of latitude (φ) and longitude (λ). The attained regression equation, with $R^2 = 0.06$, is:

$$dN_{PGM17} = -0.2588364 + 0.007735\phi + 0.0075219\lambda \quad (3)$$

To estimate the accuracy of this regression formula, it has been applied on the available 80 checkpoints where the residuals are known. The remaining deviations range from −0.7104 m to 0.4203 m, with a mean of −0.0396 m and a standard deviation of 0.221 m.

Next, the OLS geospatial analysis tool has been applied, using the Arc GIS 10 package, to describe the PGM17 residuals (dN_{PGM17}) as a function of all possible candidate independent variables namely: latitude (φ), longitude (λ), height (H), PGM17 geoid undulation (N_{PGM17}), and gravity (G). The attained results are presented in Table 1.

From this table, it can be seen that the *VIF* coefficient is relatively high (more than 7.5) for the latitude PGM17 undulations and the gravity variables. This fact may indicate that there are dependency and multicollinearity between

Brought to you by | King Abdulaziz University
Authenticated
Download Date | 10/10/19 7:47 PM

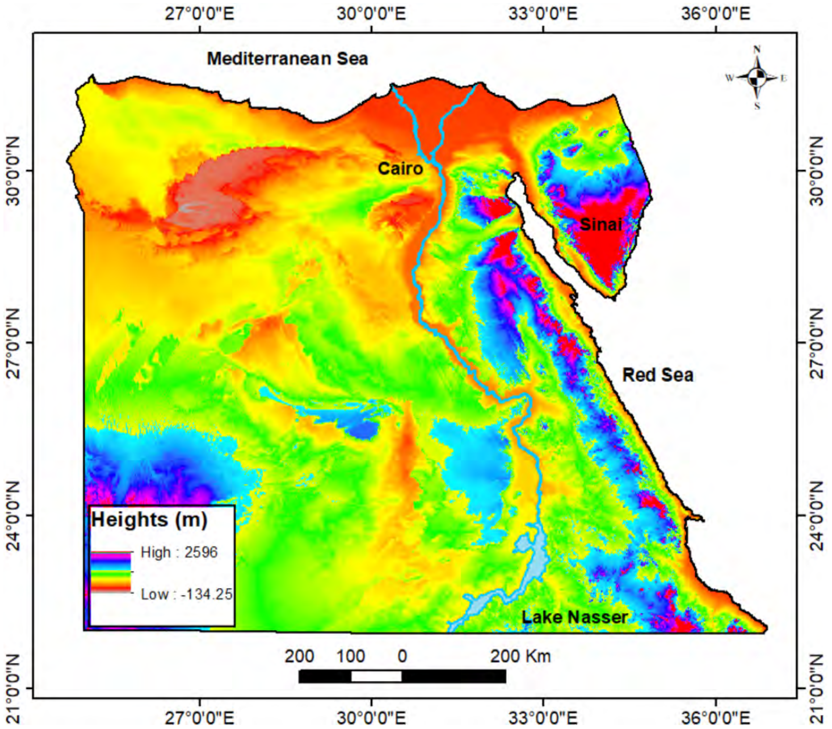

Figure 4: Topography of ErathEnv_DEM90.

Table 1: Results of OLS for 5 Possible Independent Variables Before Removing Spatial Outliers.

Variable	Coefficient	VIF
Intercept	1435.326612	NA
latitude (φ)	0.120404	97.11
Longitude (λ)	−0.003325	1.43
height (H)	−0.000971	2.44
PGM17 geoid undulation (N_{PGM17})	−0.013187	9.44
gravity (G)	−0.001469	120.81
R^2	0.082	
Adj-R^2	0.077	

Table 2: Results of OLS for 5 Possible Independent Variables After Removing Spatial Outliers.

Variable	Coefficient	VIF
Intercept	1597.7618	NA
latitude (φ)	0.136829	100.7
Longitude (λ)	−0.010906	1.44
height (H)	−0.000856	2.49
PGM17 geoid undulation (N_{PGM17})	−0.0102134	9.52
gravity (G)	−0.001635	127.8
R^2	0.074	
Adj-R^2	0.068	

them, and they do not improve the regression process. The small value of the R^2 coefficient of determination, in this study, might be expected since the utilized GPS/Levelling-based undulations contain considerable errors and uncertainties exist in the old national levelling network, e. g., [30]. More important in geosciences is the examination of external accuracy level and the performance improvements at checkpoints.

The detection of spatial outliers is considered a vital step in spatial regression. Therefore, the accomplished standardized residuals have been subjected to the Anselin local Moran's statistical test for outlier detection. 15 points have been flagged as spatial outliers (about 2 %), and they were removed one-by-one until a clean dataset had been developed. Next, another OLS has been carried out using that dataset (Table 2).

Subsequently, the ER process has been performed utilizing this fresh dataset to obtain an obvious idea about the significant group of independent variables to be utilized in the final regression. The ArcGIS package does not actually run all possible combinations of independent variables. It only gives some statistical measures about each possible combination, so that the user can judge them and choose the optimum one to be processed in the GWR stage [23]. Consequently, five groups of possible combinations of variables have been reported, along with their statistical

Brought to you by | King Abdulaziz University
Authenticated
Download Date | 10/10/19 7:47 PM

Table 3: Results of ER for 5 Possible Independent Variables.

No.	No. of Variables	Model's Variables	Adj-R^2	VIF
1		H	0.03	1
2	1	φ	0.00	1
3		G	0.00	1
4		H, N_{PGM17}	0.04	1.50
5	2	H, G	0.04	2.04
6		φ, G	0.03	96.6
7		φ, H, G	0.07	97.5
8	3	φ, H, N_{PGM17}	0.05	9.9
9		φ, N_{PGM17}, G	0.04	115.3
10		φ, H, N_{PGM17}, G	0.07	122.5
11	4	φ, λ, H, G	0.07	99.8
12		φ, λ, H, N_{PGM17}	0.05	10.8
13	5	φ, λ, H, N_{PGM17}, G	0.07	127.0

Table 4: Significance of ER Possible Independent Variables.

Variable	% Total Significance	% Negative	% Positive
H	100.00	100.00	0.00
φ	87.50	12.50	87.50
N_{PGM17}	75.00	93.75	6.25
G	75.00	62.50	37.50
λ	25.00	0.00	100.00

measures (Table 3). According to the criterion of *VIF*, only ER models from 1 to 5 could be accepted. Another interesting part of the ER output report describes the significance of the independent variables (Table 4). It can be noticed, from Table 4, that the longitude cannot be considered as a significant variable in the regression modelling. In addition, both variables of latitude and gravity present noticeable variations in their stability. These results suggest that those three variables might be omitted from the final GWR modelling.

The next analysis step tried to estimate the accuracy of several OLS models as global regression formulas. For each model, the attained regression equation was, then, applied to the checkpoints and compare its estimated values to the corresponding known ones. Tables 5a and 5b present the achieved findings. From these tables, it can be noticed that all OLS models result in similar standard deviation values, that means a comparable level of accuracy. However, equation 7 produced a smaller average of residuals at the checkpoints, which means that it is closer to the normal distribution. When comparing the precision of equation 7 with the traditional regression in equation 3, it can be seen that the standard deviation has been improved by almost 5 %. Therefore, the GWR process started with this OLS model as the optimal global regression of the PGM17 GGM variations over Egypt.

Table 5a: OLS Models for Possible Independent Variables.

No. of Variables	OLS Model	Eq.
5	$dN_{PGM17} = 1597.7618+0.136829\phi-0.010906\lambda-0.000856H-0.0102134N_{PGM17}-0.001635G$	4
4	$dN_{PGM17} = 1619.48391+0.137634\phi-0.000869H-0.011653N_{PGM17}-0.001657G$	5
3	$dN_{PGM17} = 0.198815+0.017751\phi-0.000669H-0.033997N_{PGM17}$	6
2	$dN_{PGM17} = 0.474172-0.000869H-0.016512N_{PGM17}$	7

Table 5b: Accuracy of OLS Possible Independent Variables at Checkpoints (m).

Eq.	Minimum	Maximum	Mean	Standard Deviation
4	−0.828	0.153	−0.346	±0.203
5	−0.972	0.006	−0.495	±0.202
6	−0.596	0.511	−0.006	±0.210
7	−0.583	0.529	−0.004	±0.211

The GWR analysis has been carried out for the PGM17 GGM deviations at the 803 GPS/Levelling stations as the dependent variables, and height and geoid undulations of PGM17 as independent variables (Eq. 2). Results indicate that the R2 coefficient equals 0.111, and the Adjusted-R2 equals 0.103. For each coefficient of the regression, its values are obtained at each utilized points in the output shapefile. Table 6 presents a summary of attained coefficients, while Figs. 5, 6, 7 depict the spatial variations of these coefficients over the study area. Applying these coefficients at checkpoints has indicated that the variations between the GWR model and known values range from −0.574 m to 0.500 m, with a mean of 0.001 m and a standard deviation equals ±0.205 m. These values represent the actual accuracy of the performed GWR analysis in geoid modelling, considering the available geodetic

Table 6: Summary of GWR Coefficients.

Parameter	Minimum	Maximum	Mean
Intercept	0.214741	0.900604	0.5537
H Coefficient	−0.001122	0.000097	−0.000649
N_{PGM17} Coefficient	−0.0045700	0.004862	−0.021583

Brought to you by | King Abdulaziz University
Authenticated
Download Date | 10/10/19 7:47 PM

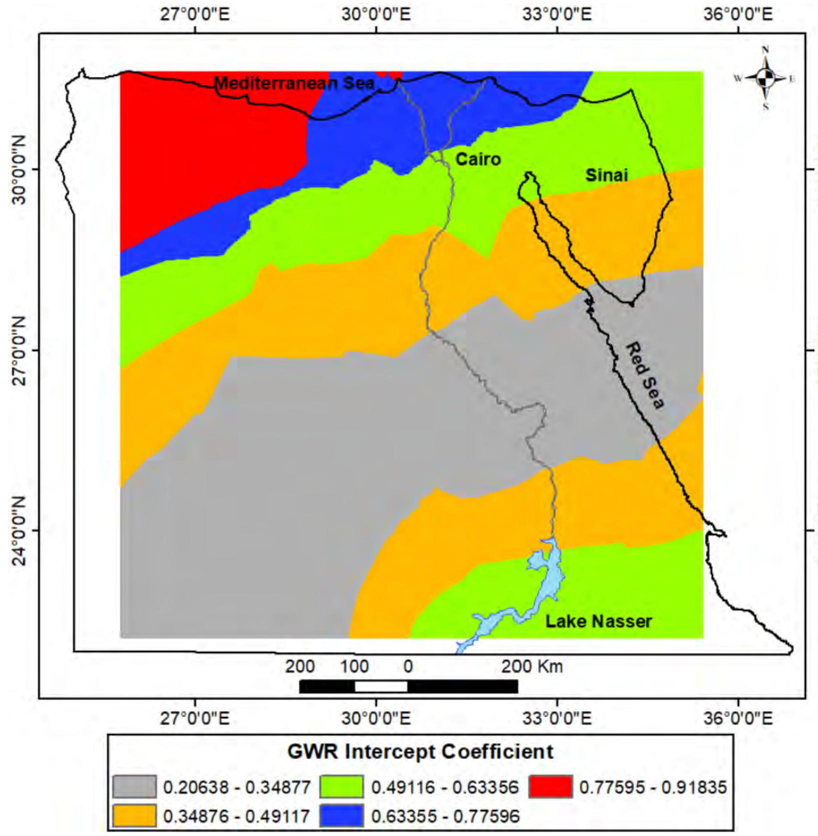

Figure 5: Surface of the Intercept Coefficient of GWR.

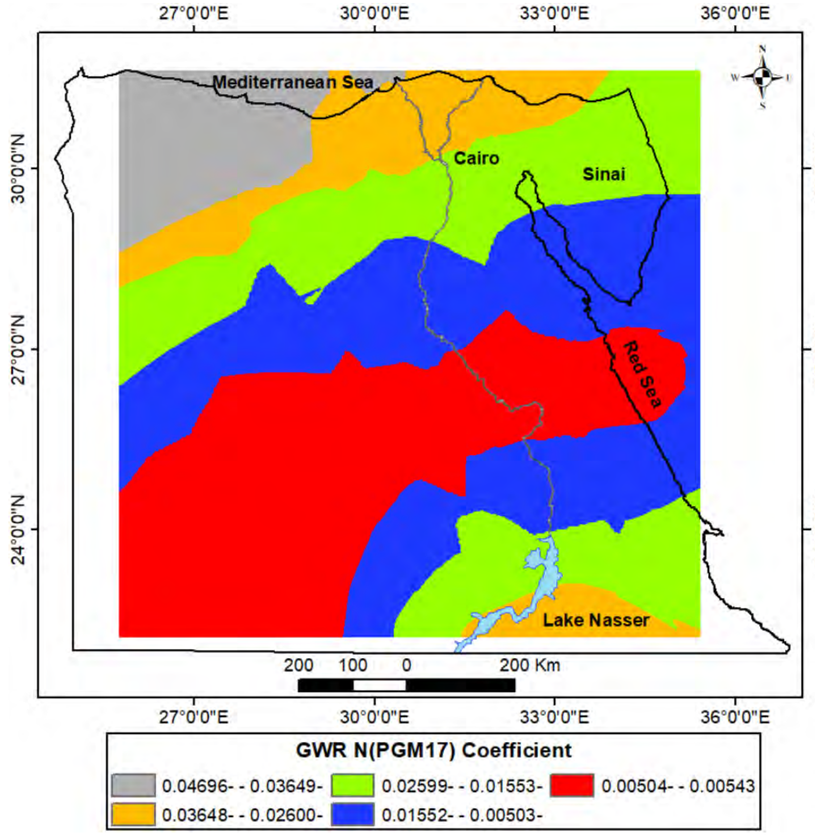

Figure 6: Surface of N_{PGM17} GWR Coefficient.

Brought to you by | King Abdulaziz University
Authenticated
Download Date | 10/10/19 7:47 PM

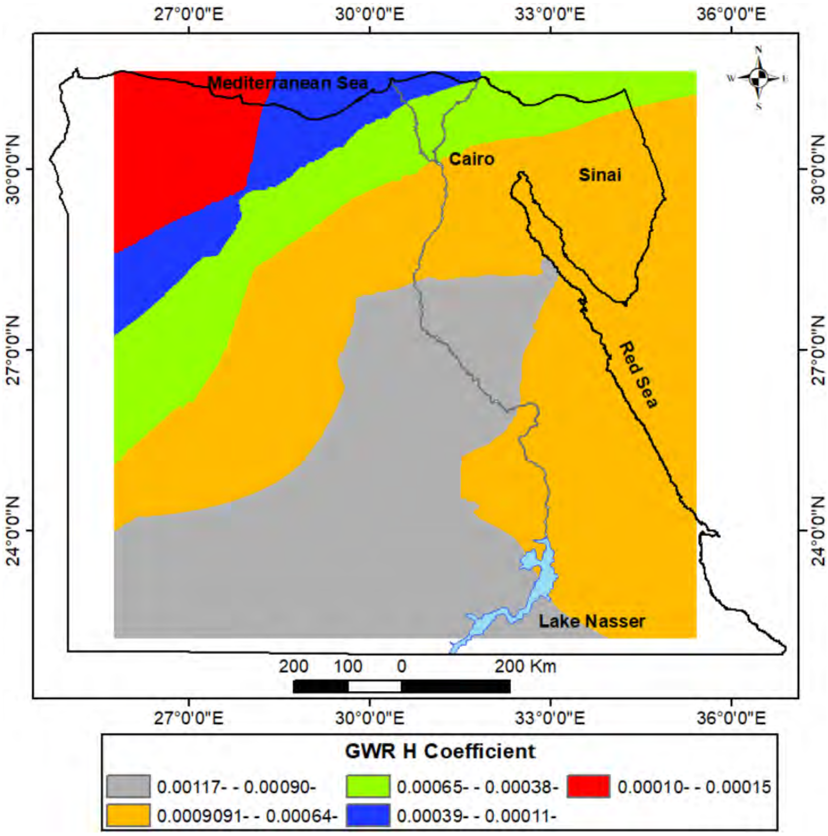

Figure 7: Surface of H GWR Coefficient.

datasets. It can be seen that the GWR is better than the global OLS using the same independent variables (Eq. 7) by almost 3 % and by almost 7 % over the traditional coordinate-based polynomial (Eq. 3). Furthermore, it can be concluded that the GWR process improved the PGM17 GGM deviations over Egypt, in terms of standard deviation, from ±0. 0.225 to ±0.205 m, i. e. by almost 9 %, and by approximately 98 % in terms of average deviations. Results of other mathematical models used in developing corrector surfaces, e. g. neural network, are approximately comparable, e. g., [13].

As a final product for the geodetic community in Egypt based on the performed GWR analysis, a correction surface has been developed along with an enhanced version of the PGM17 GGM model over Egypt. Since the optimum GWR modelling depends on both geoidal undulations of the PGGM17 GGM and the EarthEnvDEM90-based heights, two raster surfaces have been utilized herein. The first raster represents the geoidal heights of PGM17 (Fig. 3) and the second one is the ErathEnv_DEM90 global DEM (Fig. 4). A $5' \times 5'$ point shapefile has been created to cover the Egyptian territories, and height, PGM17 undulation, along with the three GWR variables have been interpolated at each point. Later, that shapefile has been converted to a 3D raster surface. Next, the raster of original geoid undulation of PGM17 has been summed to the GWR-based correction surface to come up with an enhanced version of the PGM17 GGM over Egypt (Fig. 8). This 3D surface plays a major role in GNSS surveying in Egypt to convert the ellipsoidal heights to the orthometric heights, replacing the traditional levelling, in a wide range of applications. This could be the optimum height transformation method until a national precise geoid model is developed. It is expected to result in considerable cost reduction, particularly in field data collection, in all civil engineering works and mapping projects. Furthermore, Fig. 9 depicts the improvements of PGM17-based geoidal undulations due to the GWR regression method (as the difference between Figs. 8 and 3). It can be recognized from Figs. 1 and 9 that the improvements almost vary from −0.09 to −0.05 m in areas with existing known stations, while larger values of more than a meter exist in void regions due to extrapolation, particularly in the eastern desert, western desert, and South Sinai peninsula. That emphasizes the demand of establishing homogenous GNSS/levelling networks across Egypt for better height transformation using GGMs.

Brought to you by | King Abdulaziz University
Authenticated
Download Date | 10/10/19 7:47 PM

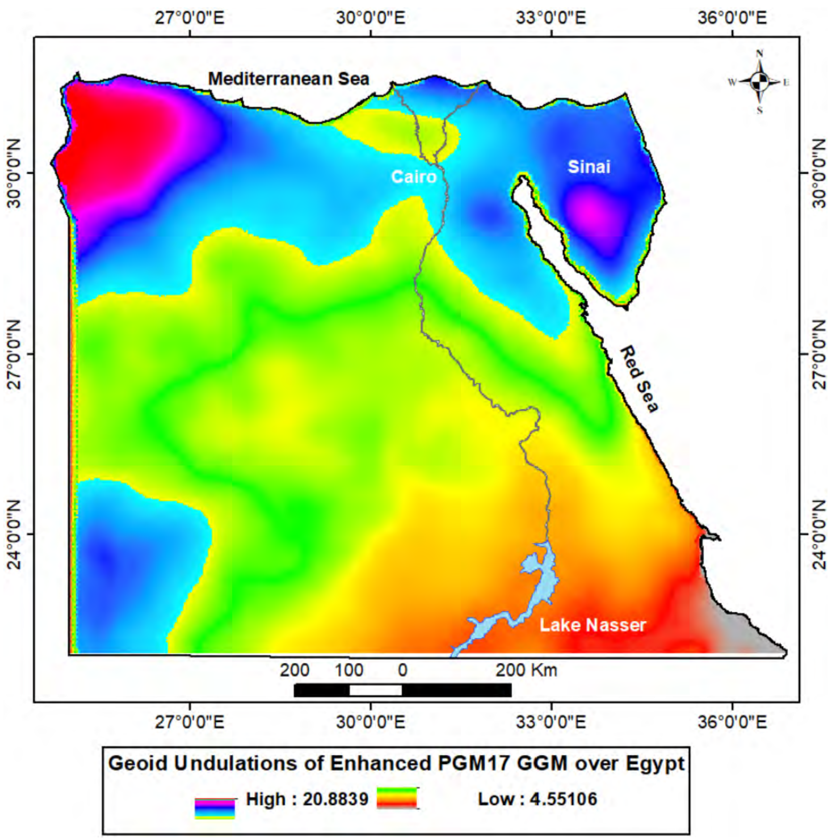

Figure 8: GWR-Based Enhanced PGM17 GGM.

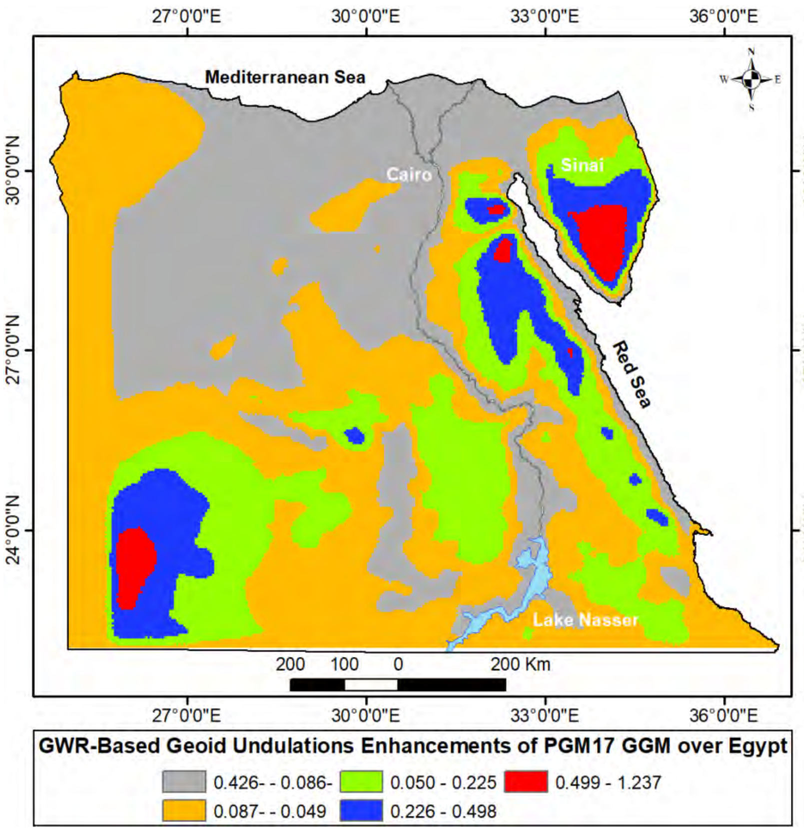

Figure 9: GWR-Based Enhancements of PGM17 GGM over Egypt.

Brought to you by | King Abdulaziz University
Authenticated
Download Date | 10/10/19 7:47 PM

5 Conclusion

Height conversion constitutes a chief demand for optimal utilization of global geopotential models in GNSS surveying and mapping activities, particularly in developing countries such as Egypt. While there are several mathematical techniques applied in geoid modelling and height transformation, GIS tools could play a key role in such a task. This study investigates the potential of applying some of these tools, particularly least-squares regression, exploratory regression, and geographically weighted regression, in height transformation probably for the first time at least in Egypt. It aims to come up with an optimum regression method to be applied in spatial modelling of the deviations of a specific global geopotential model (e. g., PGM17). Using a precise local geodetic dataset of 803 GPS/levelling stations, PGM17 undulation differences have been modelled using different regression techniques to get the optimal process in both precision and accuracy.

The current research investigates 13 possible regression formulas through all possible combinations of independent variables to attain corrector or transformation surfaces to align PGM17 to the local vertical geodetic datum in Egypt. In addition, the GWR approach proves to be superior to other investigated regression methods. From an accuracy perspective, GWR-based coefficients have been applied at checkpoints, and the variations between the model and true values range from −0.574 m to 0.500 m, with a mean of 0.001 m and a standard deviation equals ±0.205 m. Consequently, it can be seen that the GWR is better than the global OLS using the same independent variables by almost 3 %. More important, it was concluded that the GWR process has improved the PGM17 GGM deviations over Egypt by almost 9 % in terms of standard deviation and by almost 98 % in terms of the mean. Such a conclusion is derived from the reduction of the mean and standard deviations of PGM17's undulation discrepancies over Egypt from 0.211 m and ±0.225 m respectively to 0.004 m and ±0.202 m. Reported results of other mathematical models used in developing corrector surfaces, e. g. neural network, are approximately comparable. Finally, the study developed a reasonably novel product for the Egyptian local geodetic community by generating an enhanced version of PGM17. This spatial surface could be considered a valuable resource in GNSS surveying in Egypt to convert the ellipsoidal heights to the orthometric heights used in civil engineering projects and mapping activities.

References

[1] Gomez, M., Perdomo, R., and Cogliano, D. Validation of recent geopotential models in Tierra Del Fuego, Acta Geophysica., 65:931–943, DOI: 10.1007/s11600-017-0085-y, 2017.
[2] El-Ashquer, M., Elsaka, B., and El-Fiky, G., EGY-HGM2016: an improved hybrid local geoid model for Egypt based on the combination of GOCE-based geopotential model with gravimetric and GNSS/levelling measurements, Arabian Journal of Geosciences, 10:251, DOI: 10.1007/s12517-017-3042-9, 2017.
[3] Ahlgren, K., Wang, Y., Li, X., And Youngman, M., Towards a more consistent geoid model for North America, The FIG Congress 2018, Istanbul, Turkey, May 6–11, 2018.
[4] McCubbine, J., Amos, M., Tontini, F., Smith, E., Winefied, R., Stagpoole, V., and Featherstone, W., The New Zealand gravimetric quasigeoid model 2017 that incorporates nationwide airborne gravimetry, Journal of Geodesy, DOI: 10.1007/s00190-017-1103-1, 2017.
[5] Erol, B., and Erol, S., Learning-based computing techniques in geoid modelling for precise height transformation, Computers and Geosciences, 52:95–107, 2013.
[6] Tusat, E. and Mikailsoy, F., An investigation of the criteria used to select the polynomial models e mployed in local GNSS/leveling geoid determination studies, Arabian Journal of Geosciences, 11:801, DOI: 10.1007/s12517-018-4176-0, 2018.
[7] Das, R., Samanta, S., Jana, S., and Rosa, R., Polynomial interpolation methods in development of local geoid model, The Egyptian Journal of Remote Sensing and Space Sconces, DOI: 10.1016/j.ejrs.2017.03.002, 2017.
[8] Dawod, G., Mirza, M., and Al-Ghamdi, K., Simple precise coordinates transformations for geomatics applications in Makkah metropolitan area, Saudi Arabia, FIG Working Week 2010, Marrakech, Morocco, May 18–22, 2010.
[9] El Shouny, A., Al-Karagy, E., Mohamed, H., and Dawod, G., GIS-based accuracy assessment of global geopotential models: A case study of Egypt, American Journal of Geographic Information System, 7(4):118–124, DOI: 10.5923/j.ajgis.20180704.03, 2018.
[10] Elshambaky, H., Enhancing the predictability of least-squares collocation through the integration with least-squares-support vector machine, Journal of Applied Geodesy, DOI: 10.1515/jag-2018-0017, 2018.
[11] NGA (The U.S National Geospatial-Intelligence Agency), Department of Defense World Geodetic System 1984: Its definition and relationships with local geodetic system, A technical report No. NGA.STND.0036_1.0.0_WGS84, Virginia, USA, 2014.
[12] Dawod, G., Mohamed, H., and Ismail, S., Evaluation and Adaptation of the EGM2008 Geopotential Model along the Northern Nile Valley, Egypt: Case Study, Journal of Surveying Engineering, 136(1):36–40, DOI: 10.1061/_ASCE_SU.1943-5428.0000002, 2010.
[13] Elshambaky, H., Application of neural network technique to determine a corrector surface for global geopotential model using GPS/levelling measurements in Egypt, Journal of Applied Geodesy, DOI: 10.1515/jag-2017-0017, 2017.

Brought to you by | King Abdulaziz University
Authenticated
Download Date | 10/10/19 7:47 PM

[14] Alnaggar, D., Determination of the geoid in Egypt using heterogeneous geodetic data, PhD dissertation, Faculty of Engineering, Cairo University, Egypt, 1986.
[15] Dawod, G., A national gravity standardization network for Egypt, PhD dissertation, Faculty of Engineering at Shoubra, Zagazig University, Egypt, 1998.
[16] Mahmoud, S., Assessment of the gravitational global models in Egypt, Master thesis, Al-Azhar university, Cairo, Egypt, 2012.
[17] Abd-Allah, A., Assessment of GOCE models in Egypt, Master thesis, Faculty of engineering, Cairo university, Egypt, 2015.
[18] El-Ashquer, M., Elsaka, B., and El-Fiky, G., On the accuracy assessment of the latest releases of GOCE satellite-based geopotential models with EGM2008 and terrestrial GPS/levelling and gravity data over Egypt, International Journal of Geosciences, 7:1323–1344, 2017.
[19] Al-Krargy, E., Development of a national geoid for Egypt using recent surveying data, PhD dissertation, Faculty of Engineering, Minufiya university, Egypt, 2016.
[20] Elshambaky, H., Application of neural network technique to determine a corrector surface for global geopotential model using GPS/levelling measurements in Egypt, Journal of Applied Geodesy, DOI: 10.1515/jag-2017-0017, 2017.
[21] Hassouna, R. and Asal, F. Using GIS-based digital raster analysis for improving harmonic models-derived geoidal heights, Applied Geomatics, 8:151–162, DOI: 10.1007/s12518-016-0173-8, 2016.
[22] Charlton, M. and Fotheringham, S., Geographically weighted regression: white paper, National University of Ireland, Maynooth, Ireland, 2009.
[23] Arc GIS, Regression Analysis Basics, http://desktop.arcgis.com/en/arcmap/10.4/tools/spatial-statistics-toolbox/regression-analysis-basics.htm, Accessed Jan. 1, 2019.
[24] Vinayaraja, P., Raghavana, V. and Masumotob, S., Satellite-derived bathymetry using adaptive geographically weighted regression model, Journal of Marine Geodesy, 39(6):458–478, DOI: 10.1080/01490419.2016.1245227, 2016.
[25] Yao, Y., Zhang, B., Xu, C. and Yan, F., Improved one/multi-parameter models that consider seasonal and geographic variations for estimating weighted mean temperature in ground-based GPS meteorology, Journal of Geodesy, 88:273–282, DOI 10.1007/s00190-013-0684-6, 2014.
[26] Erdogan, S., Modelling the spatial distribution of DEM error with geographically weighted regression: An experimental study, Computers and Geosciences, 36:34–43, DOI: 10.1016/j.cageo.2009.06.005, 2010.
[27] Lewandowska-Gwarda, K., Geographically weighted regression in the analysis of unemployment in Poland, ISPRS International Journal of Geo-Information, 7(17), DOI: 10.3390/ijgi7010017, 2018.
[28] Dawod, G., Mohamed, H. and Al-Karagy, E., Accuracy assessment of the PGM17 global geopotential model: A case study of Egypt and Northeast Africa, Arabian Journal of Geosciences, 12(7), DOI: 10.1007/s12517-019-4418-9, 2019.
[29] Dawod, G. and Al-Ghamdi, K., Reliability of recent global digital elevation models for geomatics applications in Egypt and Saudi Arabia, Journal of Geographic Information System, 9(6):685–698, 2017.
[30] Saad, A., Towards the redefinition of the Egyptian vertical control network, PhD Dissertation, Shoubra Faculty of Engineering, Zagazig University, Cairo, Egypt, 1993.

Brought to you by | King Abdulaziz University
Authenticated
Download Date | 10/10/19 7:47 PM

Discover Sustainability

Research

DEMs and reliable sea level rise risk monitoring in Nile Delta, Egypt

Tarek Abdel-Aziz[1] · Gomaa Dawod[1] · Hala Ebaid[1]

Received: 17 September 2020 / Accepted: 19 November 2020
© The Author(s) 2020 OPEN

Abstract
This research aims to evaluate the accuracy and reliability of utilizing global Digital Elevation Models (DEMs) in risk monitoring of Sea Level Rise (SLR) in the Nile delta region, Egypt. Such a Geographic Information Systems (GIS)-based assessment process has been carried out using high-precision terrestrial surveys to develop a new local DEM (named SRI18) to precisely identify possible inundated areas by 2025. The presented DEM comparison approach has been performed based on spatial distribution rather than the traditional point-wise method. Based on novel proposed evaluation indicators, it has been found that the reliability of three investigated global models (namely: SRTM1, ASTER, and EarthEnvi-DEM90), in delineating sea level rise flooded areas, is less than 20%. Hence, it is concluded that the utilization of global DEMs may not be optimum in the planning and management of coastal areas in the Nile delta region. Such a methodology could be applied in other low-lying deltaic areas worldwide for investigating GDEMs reliability for SLR monitoring and assessment in coastal regions.

Keywords DEM · Sea level rise · Risk monitoring · GIS · Nile delta

1 Introduction

Natural hazards cause significant damages, kill thousands of people, and seriously affect the sustainability of natural and human resources worldwide. Successful thought, management, and reduction of risks from natural hazards is an interdisciplinary field of risk monitoring and analysis that relies upon collecting heterogeneous precise datasets. Geomatics technologies, particularly satellite-based positioning, remote sensing and Geographic Information Systems (GIS), play a crucial role in data gathering, visualization, and analysis of natural hazards risks. On a sense, sea level rise is considered as one of the most severe natural hazards threatening coastal zones all over the world in the last few decades.

It is a matter of fact that sea level has been recently rising as a vital sequence of global warming and climate changes phenomena. Sea Level Rise (SLR) might be attributed mostly to greenhouse effects and the melting of glaciers and polar ice sheets. SLR constitutes one of the most noteworthy challenges facing the world mainly in coastal zones and low-lying deltaic areas. Globally, the sea level has been considerably raised in the twentieth century with reported rates equal to 1.5 for 1901–1990, 2.0 for 1971–2010, and 3.2 mm/year for 1993–2010 [1]. Furthermore, the anticipated global sea level in 2081–2100 range from 0.40 to 0.63 m relative to the 1986–2005 level (ibid). Recent estimates of global SLR indicated that its rising rate is more than doubled throughout most of the twentieth century and it may reach 0.3 m above the 2000 levels by 2100 [2]. As a result, it is expected that 190 million capita could be subjected to coastal flooding worldwide by 2100 since they occupy global land below the projected high tide lines [3]. In this regard, it worth mentioning that several research studies have stated that Alexandria city in Egypt is considered one of twenty cities worldwide that are most exposed to hazardous natural risks particularly due to coastal

✉ Gomaa Dawod, dawod_gomaa@yahoo.com | [1]Survey Research Institute National Water Research Center, Giza, Egypt.

Published online: 14 December 2020

flooding by 2070 [4]. On another sense, the rise of sea level could impact coastal regions in several hazardous ways including the increase of the frequency and severity of coastal flooding, increasing the length and energy of waves, increasing the salinity of groundwater, and raising the groundwater surface elevation [5].

Nationally, sea level rise determination and the assessment of its impacts in Egypt have been investigated broadly in the last few decades. For example, Mohamed [6] analyzed tide gauge records at Alexandria from 1906 to 2003 and estimated the absolute sea level rise rate as 2.3 mm/year. Additionally, [7] applied altimetry dataset 1993–2013 to assess the relative sea level rise rate at the Egyptian Mediterranean coast, and found the rise rate is 3.1 mm/year. Between 1926 and 2000, the absolute sea level rise has been computed at Port Said as 2.3 mm/year [8]. Recently, [9] have figured out that the confidential relative sea level rise estimates in the Nile delta region, between 1990 and 2016, vary from 2.6 to 4.3 mm/year, while the absolute sea level rise rates differ between 5.0 mm/year at Alexandria to 6.9 mm/year at Port Said.

Several hazardous impacts of sea level rise have been investigated worldwide, particularly in low-land deltas, which necessitate the development of risk assessment adaptation planning (e.g. [10]). Examples of such hazardous impacts include the increase of urban flood probability e.g. [11], alteration of freshwater management and water quality (e.g. [12]), shorelines retreat, dune replacement, and residential resilience in coastal areas (e.g. [13]), and harmful changes of groundwater quality in coastal regions due to seawater intrusion (e.g. [14]). Geographic Information Systems (GIS) have been extensively applied, as cost-effective and efficient technical tools, in monitoring the sea level rise effects worldwide (e.g. [15]).

A Digital Elevation Model (DEM) is a three-dimensional digital representation of the Earth topography. Generally, DEM can be developed from a wide range of source datasets such as terrestrial field surveys, topographic contour maps, overlapped aerial photographs or satellite imageries, and airborne or satellite-based radar remote sensing measurements. Additionally, global DEMs (GDEMs) have been developed and released on a global basis in the last few decades. In Egypt, DEMs have been utilized in numerous researches and development projects such as: monitoring the subsidence of the Nile delta (e.g. [16]), monitoring land degradation (e.g. [17]), determination of hydro-morphological characteristics and assessment of flash flood potentially (e.g. [18]), and the potential sea level rise impacts on the Nile delta (e.g. [19]).

Delineation of SLR-induced inundated regions depends generally upon the accuracy of elevation information utilized in such an assessment. Accordingly, many research studies have been carried out to judge the accuracy and reliability of DEMs in geomatics and environmental applications in general and particularly in SLR impact assessment. For example, Dawod and Al-Ghamdi [20] have examined the accuracy of eight open-source global DEMs in Egypt and Saudi Arabia using terrestrial ground control points. The obtained results showed that the standard deviations of GDEMs range from ± 1.9 to ± 6.7 m over both regions. In addition, Global Positioning System (GPS)-based control points have been utilized to evaluate the accuracy of several global DEM models and have produced a comparable level of accuracy (e.g. [21]). In the same context, other research studies (e.g. [22, 23]) have figured out that the overall accuracy of GDEMs is in the order of a few meters. Similarly, it has been concluded that GDEMs are not the optimum source of elevations for flood risk assessment particularly for low-lying deltaic areas [24]. Hence, it could be concluded that GDEMs might be appropriate for planning and small-scale environmental studies but not optimum for coastal planning nor engineering projects. It worth mentioning that recent studies emphasized the utilization of local precise DEM for truthful monitoring and analyzing the potential impacts of SLR [25].

In Egypt, Ministry of Water Resources and Irrigation (WRI) has initiated a huge project for the adaptation to climate change in the Nile delta through integrated coastal zone management. An important requirement in this project was the development of a high-resolution high-accuracy DEM for the Nile delta coastal region for future coastal management activities. That part was assigned to the Survey Research Institute (SRI) of the National Water Research Center (NWRC). The developed local DEM was based on the utilization of GPS and terrestrial precise levelling datasets that cover the area from the shoreline to almost 1 km perpendicular to it. It has been concluded that such a 1.3 s spatial resolution DEM has a vertical accuracy of 5 cm approximately [26].

In the context of seal level rise hazard monitoring, several researches and even practical projects depend on the utilization of global DEMs in Egypt and other countries. It is a matter of reality that estimating the vertical accuracy of a local or global DEM is an essential aspect before its actual applications since the quality of a DEM affects the results of its application [27]. The current study investigates in details the accuracy and reliability of GDEMs for coastal environmental applications in general and for SLR monitoring in particular. Rather than the point-wise evaluation of GDEMs' vertical accuracy, this paper provides a novel approach of using several models with variable spatial resolution and

vertical accuracy for the accurate monitoring and assessment of sea level rise impacts in the Nile delta coastal areas. The expected findings would be crucial for decision makers not only in Egypt but also in other regions of low-lying deltas.

2 Study area and materials

The investigated coastal study area within the Nile delta coasts on the Mediterranean Sea sector extends from longitude 29.8°E to longitude 32.3°E, and from latitude 31.2°N to latitude 31.6°N (Fig. 1). With more than 50 million populations, the Nile delta might be considered as one of the most densely populated regions worldwide. In addition, it suffers from several environmental problems affecting the sustainable management of natural resources, such as saltwater intrusion, shoreline erosion, and land subsidence. The study area extends in the east–west direction over 273 km from Port Said at the east to Alexandria at the west, with approximately more than one kilometer perpendicular to the shoreline. The overall area of that region equals about 317 square kilometers. Types of land use over the study area have been extracted from TripleSat m spatial-resolution satellites imageries (Fig. 2). They have been verified by field campaigns utilizing GPS equipment [26]. Table 1 presents statistics about existing land uses, from which it can be noticed that the undeveloped areas cover almost 70% from the entire study area. Over this area, terrestrial field campaigns have been carried out to develop a new local high-precision high-resolution DEM. The observation strategy has combined Global Navigation Satellite Systems (GNSS) measurements with precise levelling. First, a geodetic control network has been established with 5-km spacing. Second, an MSL-based orthometric height for every control point has been determined through precise levelling routes to the nearest Bench Mark (BM). Third, a Post-Processing Kinematic (PPK) GNSS has been implemented in topographic surveying of the entire undeveloped areas. Therefore, about 184 thousands GNSS/Levelling points have been measured to create a local DEM and produce contour maps. The spatial resolution of the attained DEM estimated as 1.3 s [26].

Dawod et al. [9] have investigated relative and absolute sea level rise at the Nile delta area based on tide gauge records and GNSS-based datasets. That study concluded that the absolute sea level rise differs between 5.0 mm/year at Alexandria to 6.9 mm/year at Port Said, and the mean sea level will be raised about 17 and 23 cm at Alexandria and Port Said respectively by year 2025. Such results have been considered the basis in the current research to compare the performance of several DEMs in monitoring and assessing sea rise impacts.

Additionally, three Global DEM models (GDEMs) have been utilized in the current study, namely the Shuttle Radar Topography Mission (SRTM), EarthEnv-DEM90, and the Advanced Spaceborne Thermal Emission and Reflection Radiometer (ASTER). SRTM is a global DEM that has two versions: SRTM1 with a spatial resolution of 1 arc-second, i.e., approximately 30 m, and SRTM3 model with a 3 arc-second resolution (download from e.g. https://earthexplorer.usgs.gov/). The SRTM1 version is utilized herein. On the other hand, ASTER is 1 arc-second global DEM. The ASTER version 2 has been publically released in 2011 (download from e.g. https://asterweb.jpl.nasa.gov/gdem.asp). Additionally, the EarthEnv-DEM90 is a 3-arc-second global DEM derived from processing and merging SRTMv4 and ASTER v2 data products to provide continuous coverage of 91% of the globe (download from http://www.earthenv.org/DEM). These three GDEMs have been selected for several reasons; first, they produce a high-reliability index, exceeded 7 out of 10, in the Nile delta

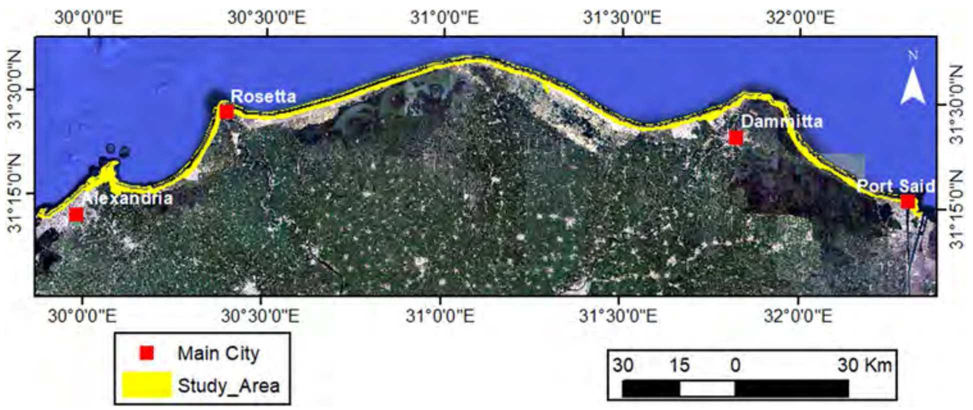

Fig. 1 Study area

Fig. 2 Land uses at main cities

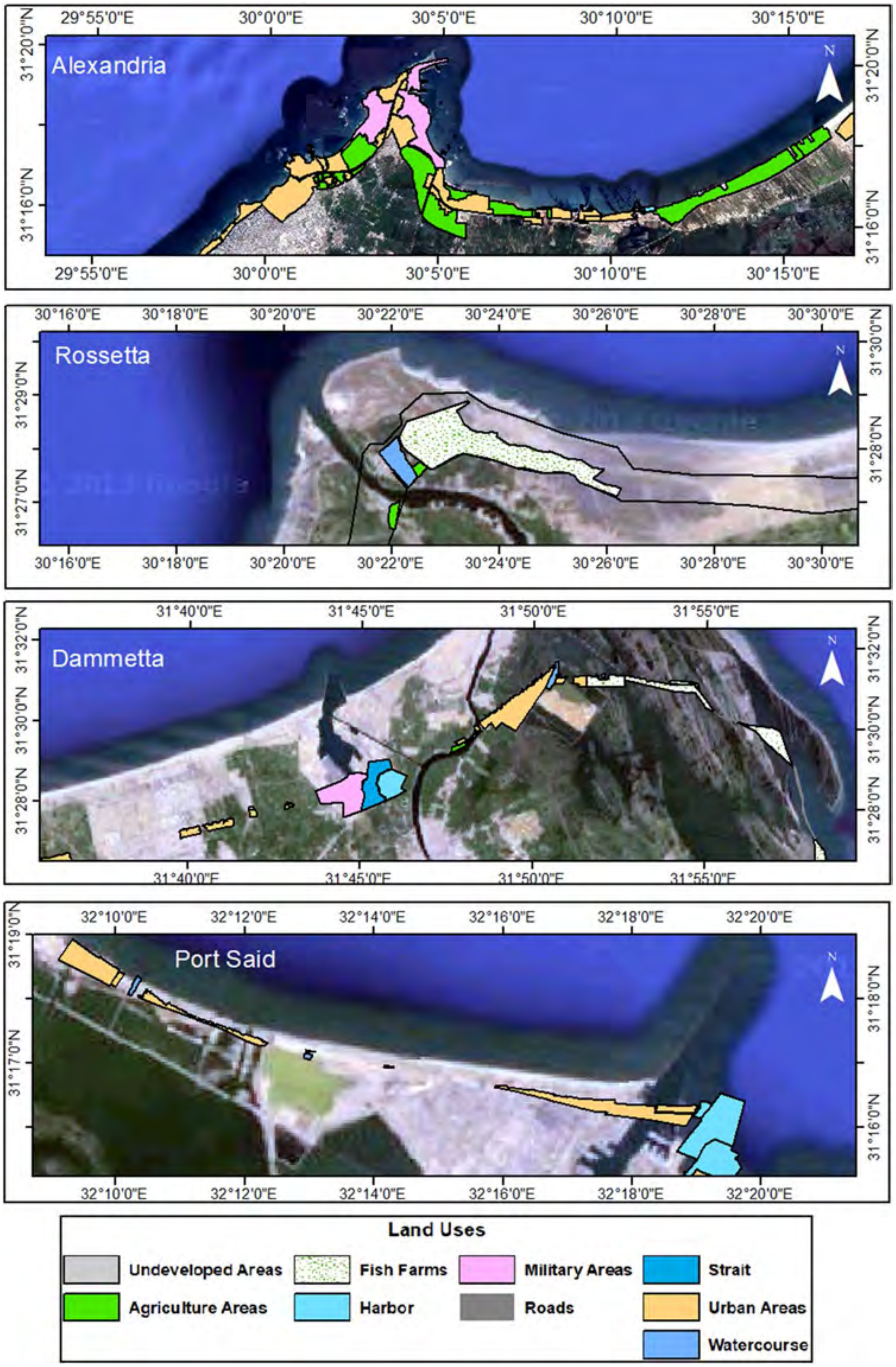

area as reported by [20]. Second, they represent different spatial resolutions (1 and 3 arc seconds) which would help assessing the sensitivity and precision of GDEMs to spatial variations in the process of SLR impact monitoring (e.g. [17]). Third, the SRTM1 and ASTER have been widely utilized in risk assessment due to sea level rise in Egypt [e.g. [28, 29]] and worldwide (e.g. [30, 31]). Lastly, they are open-source free-accessible topographic models with enhanced more-accurate versions periodically.

Table 1 Land uses in the study area

Type	Total area (km^2)	% of areas
Undeveloped areas	221.95	69.9%
Urban areas	33.736	10.6%
Fish farms	26.579	9.8%
Agriculture areas	17.957	6.6%
Military areas	8.759	3.2%
Harbor	4.620	1.7%
Strait	1.793	0.7%
Watercourse	1.580	0.6%
Roads	0.474	0.2%
Total	317.448	100%

3 Methodology and processing

The traditional method for evaluating GDEMs, presented in several research works, depends on the point-wise evaluation of a model over some known ground checkpoints and comparing the attained results through some statistical indicators (e.g. [20, 22, 23]). However, such a scheme might not be the optimum one dealing with SLR impact assessment that depends on spatial extents over a geographic area. Accordingly, the current research presents an innovative plan comprising several steps for manipulating and processing local and global DEMs over the study area within a GIS environment (Fig. 3). The central constituent of such a system is the utilization of GPS and terrestrial precise levelling datasets to depict accurately the topography of the coastal area with a few-centimeter level of precision. This high-precision level enables accurate estimation of SLR-based inundated regions and, subsequently, truthful estimation of GDEMs corresponding results and reliability. That methodology could be applied in other low-lying deltaic areas worldwide for investigating GDEMs reliability for SLR monitoring and assessment in coastal regions.

Starting with the observed 184 thousand GNSS/Levelling points, a local precise DEM, called SRI18-DEM, has been developed. Additionally, four contour maps, regarding the four utilized DEMs, have been generated using the 3D analyst tools. An overall statistical and spatial analysis of those models has been performed. On a pixel-by-pixel basis, the EarthEnv-90 model produces a smaller range of variations to SRI18 local model. Such variation differences amount to

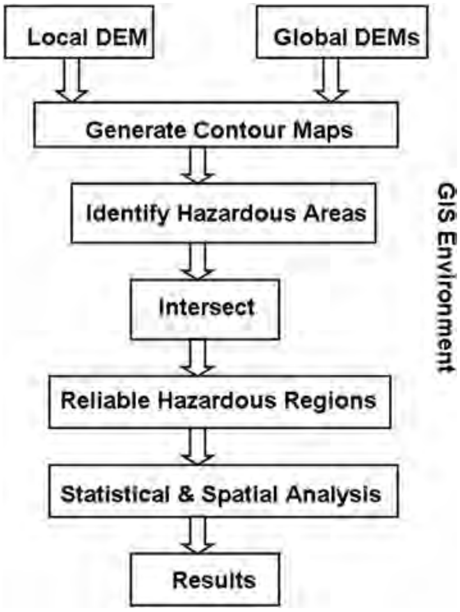

Fig. 3 Data processing steps

almost 50% of the corresponding differences of both SRTM 1 and ASTER GDEMs when compared to SRI18 model. This might be attributed to the fact that EarthEnv-DEM90 model has been derived from efficient new processing and merging SRTMv4 and ASTER v2 data products. These two results give an overall view of the performance of utilized global models. However, detailed investigations are still needed particularly regarding the hazardous effects of SLR.

Next, the recent estimate of SLR in the study area as reported by [9] has been adopted in the current research since they represent the most recent local SRL estimates in Egypt. Hence, an overall rise of 0.25 m is anticipated by the year 2025. The method utilized in this study is based on the determination of contour line corresponds to the anticipated SLR. Then, the areas surrounded by the zero contour (current sea level) and that contour would represent the expected inundated regions due to SRL rise by 2025. Consequently, the differences between contour lines zero and 0.25 m have been identified as hazardous areas. Subsequently, the total areas of these regions have been computed and analyzed for all cases. Table 3 presents the statistics concerning the utilized DEMs, which indicates some main findings. Such results only present quantitative measures regarding the precision of several DEM models with varying levels of accuracy and spatial resolution. A spatial perspective is still desired for accurate mapping of inundated regions due to SLR utilizing the ArcGIS 3D analysis and spatial analysis tools. Since the local DEM is accurate, the overlapped parts of the hazardous areas between the local model and a particular global model could be considered as a truth index for that model. A novel reliability index has been introduced, in this study, to differentiate between the performances of the utilized models. Statistical and spatial analyses have been performed to investigate the accomplished results as shown in the next section.

4 Results and discussions

Monitoring SLR-based inundated regions depends on the accuracy of elevation information utilized in such an assessment. While the classical method for evaluating GDEMs relies upon the point-wise evaluation of a model over some known ground checkpoints, the present study provides a new scheme for manipulating and processing local and global DEMs. The local SRTM18 DEM represents the basis of such evaluation due to its high accuracy in depicting the topography of the study area within few-centimeters accuracy level. The overall statistical measures of the investigated models and the deviations between them over the study area are presented in Table 2. It can be noticed, from this table, that the EarthEnv-90 GDEM produced smaller range, averages, and standard deviation values compared to the SRTM 1 model. Moreover, it can be noticed that the ASTER model produce the worst results over the study area. Similar results have been reported by other researchers (e.g. [20]). Figure 4 depicts the anticipated inundated regions, between levels 0 and 0.25, using the SRI18, EarthEnv-90, SRTM1, and ASTER models respectively. From SRI18 results, it has been found that the anticipated inundated regions vary in width between 30 and 250 m, with an average of 140 m approximately. These regions are spatially distributed almost over about 195 km of the shorelines that constitute about 70% of the study area coastlines. Such hazardous regions need to be considered for future development adaptation of sea level rise in the Nile delta.

A visual comparison between Fig. 4 clearly indicates the differences in delineating vulnerability areas obtained from the three digital elevation models. In addition, the total areas of these regions have been computed in all cases. Table 3 indicates some main findings. First, the total area of inundated regions due to sea level rise in the study area equals

Table 2 Statistics of DEMs over the study area (m)

DEM	Minimum	Maximum	Range	Mean	Standard deviation
Heights					
SRI18	− 2	17	19	1.35	1.49
EarthEnv-90	− 5	23	28	0.88	2.17
SRTM 1	− 24	59	83	1.36	3.69
ASTER	− 13	74	87	7.37	6.29
Differences					
SRI18-EarthEnv-90	− 15	15	30	0.34	2.05
SRI18-SRTM 1	− 43	17	60	0.33	3.43
SRI18-ASTER	− 62	12	74	− 6.26	5.66

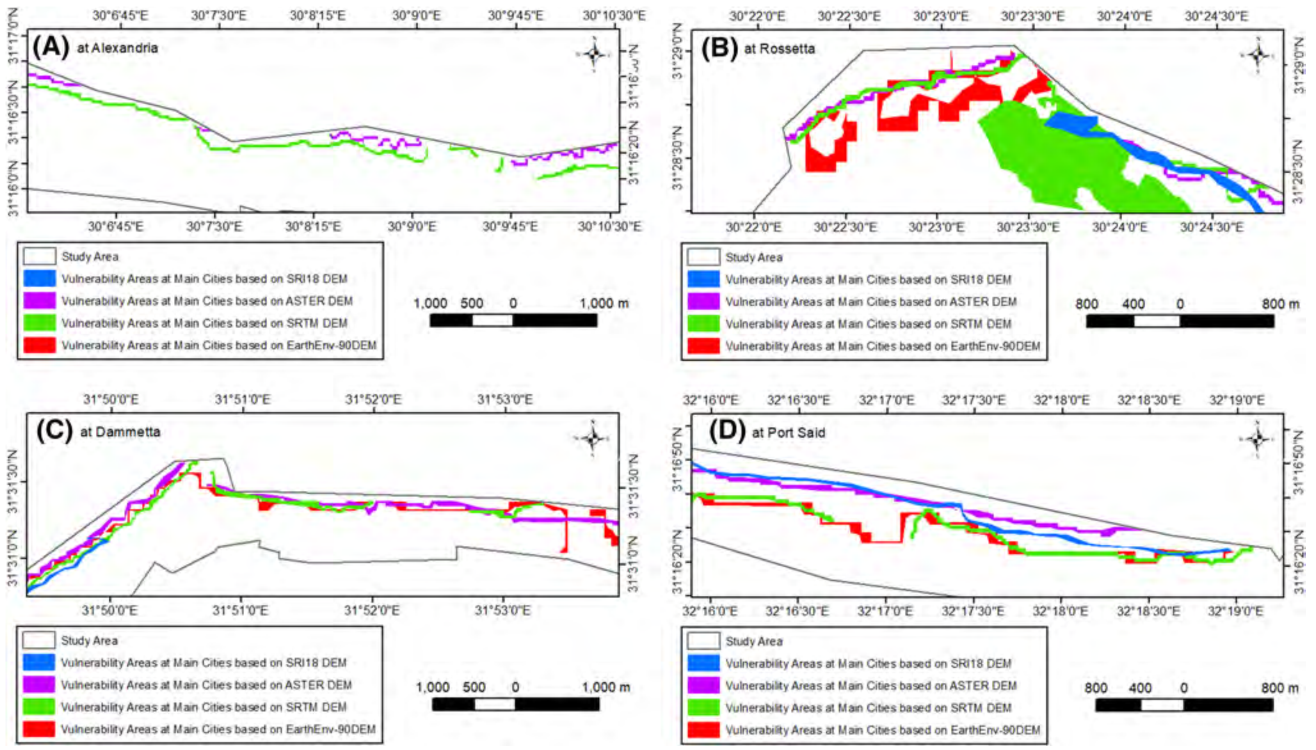

Fig. 4 Examples of vulnerability areas at main cities based on local and global DEMS

10.69 square kilometers that constitute just 4.8% of the undeveloped region. This represents a confident estimate when compared to results of previous researches that anticipated that the flooded areas could reach 49% of the Nile delta by the year 2100 under different scenarios of SLR (e.g. [18]). Compared to the local SRI18-DEM, the EarthEnv-90DEM model has exaggerated the anticipated inundated regions by approximately 111%. Second, the SRTM1, ASTER models produced about 79% and 74% of the regions given by the SRI18-DEM respectively. These two points highlight the significant discrepancies between local accurate DEM and global DEMs, particularly in development plans of coastal areas due to sea level rise.

Figure 5a–c represent examples of inundated regions over the study area based on several DEMs. The local SRI18 DEM has been chosen as the comparison bases since it represents the most accurate topography of the study area (just a few centimeters) for the first time in Egypt. This comparison demonstrates the reliability of each utilized GDEM in delineating the spatial distribution of its corresponding flooded regions compared to the truthful SRI18-DEM results. It can be noticed that the flooded areas resulting from global DEMs do not lie exactly on the corresponding locations from the local DEM. Therefore, it can be concluded that the total areas of inundated regions cannot be considered as an optimum measure of the global DEMs performances regarding the SLR impacts. Thus, the current study proposes the utilization of a novel index to represent the reliability of GDEMs in SLR monitoring and impact assessment. The proposed truth index, simply, equals the percentage of the intersected regions for each global model compared to the local accurate model. This approach has been applied for the three utilized GDEM, and the results are given in Table 4. It can be noticed, from this table, that the three GDEMs identify very small portions of the actual inundated regions resulted from the accurate local DEM. Therefore, the truth index for EarthEnv-90, SRTM1, and ASTER models equal 0.12, 0.09, and 0.10 respectively. The amplification percentage and the truth index (Tables 3 and 4) differ a little for each global DEM. So, a unique reliability index is introduced, herein as the result of dividing the amplification index by the corresponding truth index for each model. The values of that reliability index are shown in the last column of Table 4. From this table, it can be concluded that the investigated three GDEMs have a reliability index of 11%, 11%, and 13% for EarthEnv-90, SRTM1, and ASTER respectively. Hence, it can be said that the reliability of the three global models in delineating sea level rise flooded areas is less than 20%. The low-reliability of GDEMs could be attributed to several factors, including the date of their data collection, their spatial resolution, their accuracy in delineating shorelines, and the rapid undergoing shoreline retreat of

Fig. 5 Examples of inundated areas delineated from several DEMs

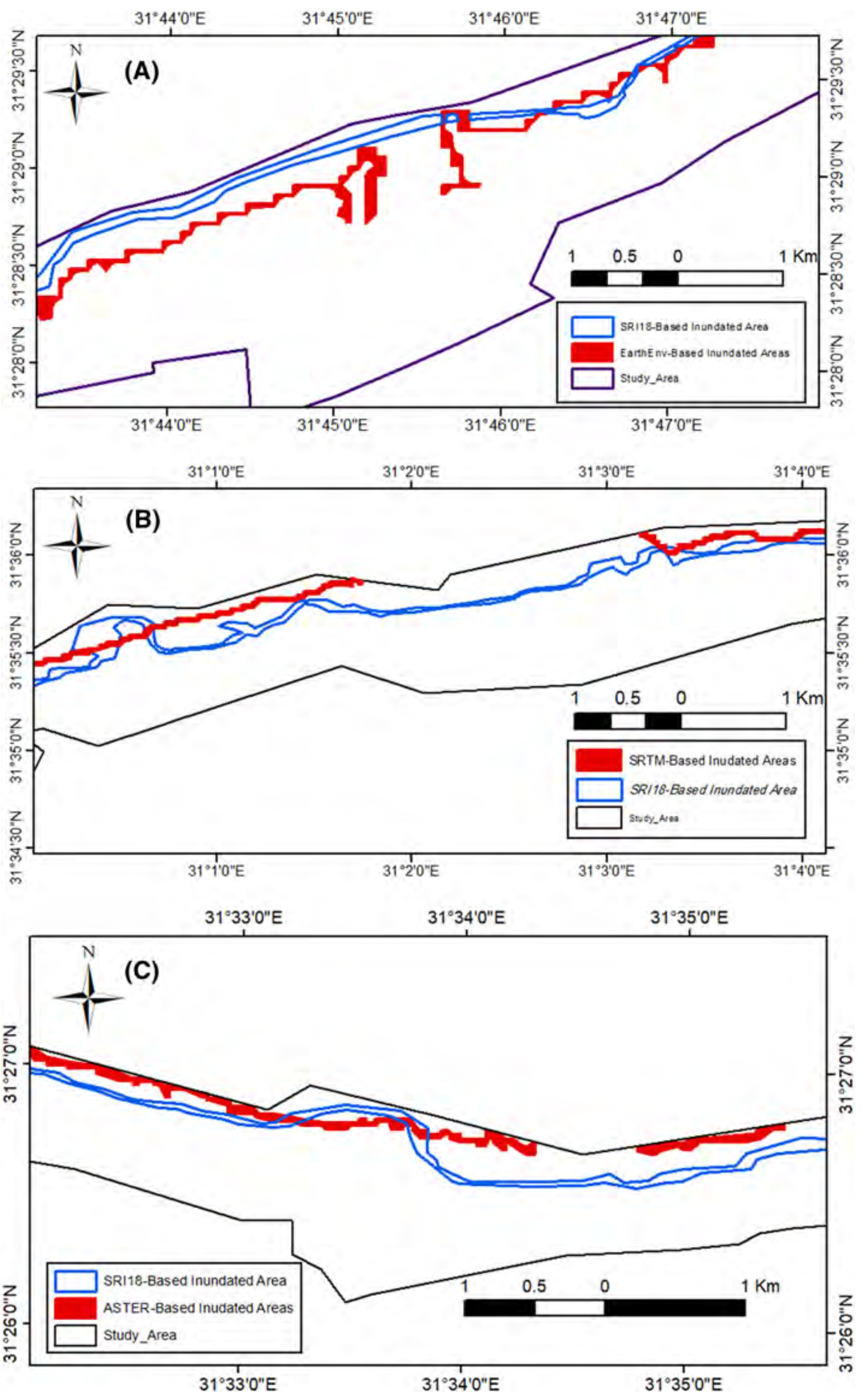

the Nile delta. Similarly, other researchers have stressed that a high-resolution high-accuracy DEM is crucial to attaining accurate results in environmental monitoring applications (e.g. [32]). It can be concluded that the accomplished findings herein are superior to those of previous studies in the Nile delta region due to the utilization of the local high-accuracy DEM for the first time in Egypt. It is a matter of reality that accurate topographic representation through a DEM model results in more accurate estimates of SLR impacts.

Table 3 Statistics of vulnerability areas due to SLR

DEM	Minimum area (km^2)	Maximum area (km^2)	Total area (km^2)	% of amplification
SRI-18	0.059	6.828	10.690	NA
EarthEnv-90	0.019	0.913	11.834	111%
SRTM 1	0.001	1.249	8.490	79%
ASTER	0.001	1.572	7.930	74%

Table 4 Intersection between local and global DEM

DEM	Sum of overlapped area (km^2)	Truth index	Reliability index
SRI-18	NA	NA	NA
EartEnv-90	1.484	12%	11
SRTM 1	1.128	9%	11
ASTER	1.233	10%	13

5 Conclusions

Coastal management and risk monitoring of sea level rise necessitate accurate datasets describing spatial variations of the coastal topography. The digital elevation model is an optimum digital representation of topography and it constitutes a major element in coastal development. Rather than the traditional method for evaluating DEMs that relies upon point-wise evaluation of a model over some known ground checkpoints, the current research presents a new plan embracing several steps for manipulating and processing local and global DEMs over the study area within a GIS environment. The current research investigates the accuracy and reliability of some global DEMs over the Nile delta coastal region, namely EarthEnvi-90, SRTM1, and ASTER. Such an evaluation has been carried out based on a local accurate DEM of the area generating from terrestrial GPS/levelling surveying of about 300 square kilometers. It worth mentioning that results of local DEM reveal that the anticipated inundated regions vary in width between 30 and 250 m, with an average of 140 m approximately. These regions are spatially distributed almost over about 195 km of the shorelines, which constitute about 70% of the study area coastlines. Such hazardous regions need to be considered for future development adaptation of sea level rise in the Nile delta.

Attained results highlighted that the flooded areas resulting from free global DEMs differ significantly from the corresponding areas resulting from local DEM, not just in total amount but also in spatial distribution. In addition according to the proposed indices for investigating the trustworthiness of DEMs, it has been concluded that the reliability of the three global models in delineating sea level rise flooded areas is less than 20%. Such findings play a major role for decision-makers to avoid the utilization of global DEM models in the accurate planning and integrated management of coastal areas in the Nile delta region. Based on available datasets, the accomplished results stress that a local accurate and up-to-date terrestrial DEM is a must for precise risk assessment of sea level rise in Egypt and other developing countries. The proposed methodology could be applied in other low-lying deltaic areas worldwide for investigating GDEMs reliability for SLR monitoring and analyzing in coastal regions.

Authors' contributions All authors have made substantial contributions and have agreed with the content of the manuscript.

Funding There is no funding for this research.

Conflict of interest No potential conflict of interest was reported by the authors.

Open Access This article is licensed under a Creative Commons Attribution 4.0 International License, which permits use, sharing, adaptation, distribution and reproduction in any medium or format, as long as you give appropriate credit to the original author(s) and the source, provide a link to the Creative Commons licence, and indicate if changes were made. The images or other third party material in this article

are included in the article's Creative Commons licence, unless indicated otherwise in a credit line to the material. If material is not included in the article's Creative Commons licence and your intended use is not permitted by statutory regulation or exceeds the permitted use, you will need to obtain permission directly from the copyright holder. To view a copy of this licence, visit http://creativecommons.org/licenses/by/4.0/.

References

1. Church J, Clark P, Cazenave A, Gregory J, Jevrejeva S, Levermann A, Merrifield M, Milne G, Nerem R, Nunn P, Payne A, Pfeffer W, Stammer D, Unnikrishnan A. Sea Level Change. In Climate Change 2013: The Physical Science Basis. Contribution of Working Group I to the Fifth Assessment Report of the Intergovernmental Panel on Climate Change (IPCC). Cambridge, UK: Cambridge University Press; 2013.
2. Lindsey, R. Climate change: Global sea level, 2020; https://www.climate.gov/news-features/understanding-climate/climate-change-global-sea-level, Accessed 25 Oct 2020.
3. Kulp S, Strauss B. New elevation data triple estimates of global vulnerability to sea-level rise and coastal flooding. Nat Commun. 2019. https://doi.org/10.1038/s41467-019-12808-z.
4. Siegel F. Adaptations of coastal cities to global warming, sea level rise, climate change and endemic hazards. Switzerland : Springer Briefs in Environmental Science; 2020. (**10.1007/978-3-030-22669-5_7**).
5. Raymond C, Conway-Cranos L, Morgan H, Faghin N, Spilsbury Pucci D, Krienitz J, Miller I, Grossman E, Mauger G. Sea level rise considerations for near-shore restoration projects in Puget Sound. A report prepared for the Washington Coastal Resilience Project. USA: University of Washington; 2018. https://cig.uw.edu/wp-content/uploads/sites/2/2018/11/Raymondetal_SLR_Restoration_2018_Compressed.pdf. Accessed Oct 2020.
6. Mohamed H. Realization and redefinition of the Egyptian vertical datum based on recent heterogeneous observations. Ph.D. diss. Egypt: Faculty of engineering at Shoubra, Benha university; 2005.
7. Shaltout M, Tonbol K, Omstedt A. Sea-level change and projected future flooding along the Egyptian Mediterranean coast. Oceanologia. 2015. https://doi.org/10.1016/j.oceano.2015.06.004.
8. Frihy O. Evaluation of future land-use planning initiatives to shoreline stability of Egypt's northern Nile delta. Arab J Geosci. 2017. https://doi.org/10.1007/s12517-017-2893-4.
9. Dawod G, Mohamed H, Haggag G. Relative and absolute sea level rise based on recent heterogeneous geospatial data: a case study in the Nile delta Egypt. Sci Eng Res. 2019;6:55–64.
10. Abutaleb K, Mohammed A, Ahmed M. Climate change impacts, vulnerabilities and adaptation measures for Egypt's Nile delta. Earth Syst Environ. 2018. https://doi.org/10.1007/s41748-018-0047-9.
11. Griffiths J, Zhu F, Chan F, Higgitt D. Modelling the impact of sea-level rise on urban flood probability in SE China. Geosci Front. 2018. https://doi.org/10.1016/j.gsf.2018.02.012.
12. Dessu S, Price R, Troxler T, Kominoski J. Effects of sea-level rise and freshwater management on long-term water levels and water quality in the Florida Coastal Everglades. Environ Manage . 2018;211:164–76.
13. Grilli A, Spaulding M, Oakley B, Damon C. Mapping the coastal risk for the next century, including sea level rise and changes in the coastline: application to Charlestown RI, USA. Nat Hazards. 2017;88:389–414.
14. Wassef R, Schüttrumpf H. Impact of sea-level rise on groundwater salinity at the development area western delta Egypt. Groundw Sustain Dev . 2016;2–3:85–103.
15. Ghoussein Y, Mhawej M, Jaffal A, Fadel A, El Hourany R, Faour G. Vulnerability assessment of the South-Lebanese coast: a GIS-based approach. Ocean Coast Manag. 2018;158:56–63.
16. El Bastawesy M, Cherif O, Sultan M. The geomorphological evidences of subsidence in the Nile Delta: analysis of high resolution topographic DEM and multi-temporal satellite images. Afr Earth Sci. 2017. https://doi.org/10.1016/j.jafrearsci.2016.10.013.
17. Kotb M, Ali R, El Semary M. Use of remote sensing and GIS for land degradation assessment of Qarun lake coastal area, El-Fayoum, Egypt, In: Water and Land Security in Dry lands. 2017. https://doi.org/10.1007/978-3-319-54021-4_22.
18. Wahid A, Madden M, Khalaf F, Fathy I. Geospatial analysis for the determination of hydro-morphological characteristics and assessment of flash flood potentiality in arid coastal plains: a case study in southwestern Sinai, Egypt. Earth Sci Res. 2016. https://doi.org/10.15446/esrj.v20n1.49624.
19. Hassan M, Adrabo M. Vulnerability of the Nile delta coastal areas to inundation by sea level rise. Environ Monit Assess. 2013;185:6607–16. https://doi.org/10.1007/s10661-012-3050-x.
20. Dawod G, Al-Ghamdi K. Reliability of recent global digital elevation models for geomatics applications in Egypt and Saudi Arabia. Geog Inform Syst. 2017;9:685–98.
21. Rawat K, Sing S, Singh M, Garg B. Comparative evaluation of vertical accuracy of elevated points with ground control points from ASTER DEM and SRTM DEM with respect to CARTOSAT-1 DEM. Remote Sens Appl Soc Environ. 2019;13:289–97.
22. Wang X, Holland D, Gudmundsoon H. Accurate coastal DEM generation by merging ASTER GDEM and IGESat GLAS data over Mertz glacier Antarctica. Remote Sens Environ. 2018;206:218–30.
23. Rabah M, El-Hattab A, Abdallah M. Assessment of the most recent satellite based digital elevation models of Egypt. NRIAG J Astron Geophys. 2017. https://doi.org/10.1016/j.nrjag.2017.10.006.
24. Sande B, Lansen J, Hoyng C. Sensitivity of coastal flood risk assessment to digital elevation models. Water. 2012;4:568–79.
25. Hassan A, Hassaan M. Potential impact of sea level rise on the geomorphology of Kuwait state coastline. Arab J Geosci. 2020;13:1139. https://doi.org/10.1007/s12517-020-06084-1.
26. Survey Research Institute. Final report of the research study of management plan of the costal areas over the Mediterranean sea from Port Said to Alexandria. Internal Report. Egypt: SRI; 2018.
27. Soliman A, Han L. Effects of vertical accuracy of digital elevation model (DEM) data on automatic lineaments extraction from shaded DEM. Adv Space Res. 2019;64:603–22.

28. Abou Samra R. The use of cartographic modelling to assess the impacts of costal flooding: a case study of Port Said governorate Egypt. Environ Monit Assess. 2017;189:435. https://doi.org/10.1007/s10661-017-6152-7.
29. Hasan E, Khan S, Hong Y. Investigation of potential sea level rise impact on the Nile delta, Egypt using digital elevation models. Environ Monit Assess. 2015. https://doi.org/10.1007/s10661-015-4868-9.
30. Ebaid H. Accuracy enhancement of SRTM and ASTER DEMs using weight estimation regression model. Int J Res Eng Tech. 2014;8:371–7.
31. Elkhrachy I. Vertical accuracy assessment for SRTM and ASTER digital elevation models: a case study of Najran city, Saudi Arabia. Ain Shams Eng J . 2017. https://doi.org/10.1016/j.asej.2017.01.007.
32. Pawluszek K. Landslide features identification and morphology investigation using high-resolution DEM derivatives. Nat Hazards. 2019;96:311–30. https://doi.org/10.1007/s11069-018-3543-1.

Publisher's Note Springer Nature remains neutral with regard to jurisdictional claims in published maps and institutional affiliations.

Proceedings of Engineering and Technology Innovation, vol. 18, 2021, pp. 15-24

Optimum Combinations of GGM and GDEM Models for Precise National Geoid Modelling

Essam Mohamed Al-Karargy*, Gomaa Mohamed Dawod

Department of physical geodesy, Survey Research Institute, National Water Research Center, Cairo, Egypt

Received 21 September 2020; received in revised form 17 December 2020; accepted 27 January 2021

DOI: https://doi.org/10.46604/peti.2021.6452

Abstract

This study aims to develop a Local Geoid Model (LGM) for Egypt to determine the optimal combinations of global models with Global Navigation Satellite Systems (GNSS/Levelling) data. A precise national geodetic dataset, four Global Geopotential Models (GGMs), and three global Digital Elevation Models (DEMs) have been utilized. Hence, twelve gravimetric LGMs have been developed using the Least-Square Collocation (LSC) method fitted to GNSS/Levelling data and judged over 100 checkpoints. Results revealed that improvements in local geoid accuracy are attributed mainly to GGMs models representing the long wavelength of the Earth's gravitational field. Regarding DEMs, the accuracy of LGMs does not significantly depend on the utilized DEM. Based on the available data, the attained optimum geoid of Egypt has been developed with a standard deviation, equals 0.129 m.

Keywords: GGM, DEM, GNSS, geoid, Egypt

1. Introduction

GNSS play a vital role in surveying geodetic activities worldwide. It produces geodetic or ellipsoidal heights reference to the surface of an ellipsoid, while most surveying and mapping activities depend on the orthometric heights referenced to the Mean Sea Level (MSL) datum. Hence, height conversion of GNSS heights to MSL heights necessitates a geoid model to define the vertical separation, geoid heights, between those two surfaces over a specific region. Geoid modelling, on a national scale, has been a crucial task for geodetic communities in several countries worldwide in the last few decades. For example, the U.S National Geodetic Survey (NGS) is currently developing a time-dependant geoid model for the entire USA to be completed by 2022 [1]. Similarly, an updated geoid model for the United Kingdom (UK) and Ireland has been developed to increase accuracy and homogeneity of height transformation across this region [2]. Additionally, The French Institut national de l'information géographique (IGN) is developing a new precise geoid model for France that could achieve a millimeter level of accuracy in height transformation [3]. More recently, the Geospatial Information Authority (GIA) of Japan is developing a new refined gravimetric geoid model on a 1x1.5 arc-second grid [4].

GGMs constitute a major factor in geoid modelling since they provide the long and medium wavelengths of the Earth's gravitational field. Since the mid-1960s, numerous GGMs have been developed and being applied in geoid modelling. Consequently, the evaluation of GGMs in a specific region has been extensively investigated by geodetic studies in the last few decades. For example, Fernádez et al. [5] and El-Ashquer et al. [6] have utilized free-air gravity anomalies and GNSS/Levelling datasets to study the selection of optimal GGM in Costa Rica and Kuwait respectively. Additionally, Gomez et al. [7] have utilized mean water level data in a lake in Argentina as a validation tool for GGM assessment. Since the Earth Geopotential Model 2008 (EGM2008) is the most well-known GGM worldwide, its precision performance has been

* Corresponding author. E-mail address: essamalkrargy@gmail.com
Tel.: +002-10-66361763; Fax: +002-02-33933536

investigated in several countries such as Egypt [8] and Sweden [9]. On the other hand, Global DEMs (GDEMs) have been utilized in geoid modelling for the evaluation of the terrain effects. So, the optimum DEM is also significant in such a task particularly in countries with no published precise DEM.

In Egypt, several geoid development tryouts have been carried out in the last few decades. Alnaggar [10] has developed the first pioneer national-scale geoid. Dawod [11] has developed a national geoid model based on the data of the Egyptian National Standardization Network of 1997 (ENGSN97) along with GPS/levelling data. Also, Abd-Elmotaal [12] has developed a gravimetric geoid model utilizing high-degree tailored reference geopotential model. Recently, Dawod and Abdel-Aziz [13] have studied the utilization of a Geographic Information Systems (GIS) technique in geoid modelling. The traditional manner of investigating the accuracy and reliability of GGMs and DEMs is the assumed point-wise comparison. In this approach, a specific GGM is evaluated over checkpoints with known geoidal undulations and the statistical indicators provide a measure for its reliability in geoid modelling [6]. Similarly, a particular DEM is judged over known stations with available orthometric heights.

A novel approach is proposed in the current study for deciding which GGM and DEM models are optimum for utilization in developing a national geoid model. Accordingly, this study aims at investigating the optimum combination of some selected GGMs and GDEMs models in developing a precise local geoid model of Egypt based on the available local heterogeneous geodetic datasets.

2. Methodology

The current study employs four GGMs models and three GDEMs models in developing twelve 5'x5' local geoid models for Egypt. GDEMs models have been utilized since there is no local precise DEM published for Egypt [14]. The utilized GGMs models include XGM2019e_2159, EGM2008, EIGEN-6C4, and GECO. These models have been selected since they are the only (to date) high-resolution GGMs with a degree of 2190. Concise descriptions of those models are presented in the following subsections:

2.1. Global geopotential models (GGMs)

(1) XGM2019e_2159: A recent GGM combines 15' terrestrial gravity anomalies datasets over land, 1' mean sea surface database over oceans, 5' GOCO06s GGM, and the EARTH2014 topographic model. It has been developed to degree 2190 (utilized herein) and later extended to degree 5400 [15].

(2) GECO: A global gravity model utilizes the GOCE satellite-based gravity data to improve the accuracy of the EGM2008 GGM in low and medium frequencies. GECO is developed, in 2015, up to degree and order 2190 [16]. GECO is the most-recent published high -resolution GGM up till 2017.

(3) EIGEN-6C4: A model released in 2014, that utilizes satellite tracking data (from the Laser Geodynamics Satellite: LAGEOS, the Gravity Recovery and Climate Experiment: GRACE, and the: Gravity-field and steady-state Ocean Circulation Explorer: GOCE missions) along with a global surface gravity anomaly grid and altimetry data. The model is up to 2190 degree, developed by both the Germany German Research Center for Geosciences (GFZ) and the French Centre National d'Études Spatiales (CNES) [17].

(4) EGM2008: An integrated GGM developed in 2008 by the U.S. National Geospatial-Intelligence Agency (NGA) up to 2190 degree, based on GRACE-based satellite tracking data, terrestrial gravity data, and altimetry data. It was a milestone in GGM development since its preceding model did not exceed 360 maximum degrees [18]. Table 1 shows the characteristics of those selected global GGMs.

Table 1 Characteristics of selected GGMs

GGM	Year	Degree	Utilized data	Average accuracy over 12035 GNSS/levelling stations (m)
XGM2019e_2159	2019	2190	A, G, S(GOCO06s), T	0.236
GECO	2015	2190	EGM2008, S(GOCE)	0.237
EIGEN-6C4	2014	2190	A, G, S (GOCE, GRACE, Lageos)	0.236
EGM2008	2008	2190	A, G, S(GRACE)	0.240
where: A = Altimetry data, G = Ground geodetic data, S = satellite data, T = Topographic Models (after [19])				

2.2. Global digital elevation models (GDEM)

On the other hand, the utilized GDEMs models, herein, include SRTM1, ASTER, and ACE2 models. Table 2 summarizes the characteristics of those selected global DEMs, including:

(1) SRTM: The Shuttle Radar Topography Mission (SRTM) is a global DEM, that has two versions: SRTM1 with a spatial resolution of 1 arc second, i.e., approximately 30 meters, and SRTM3 model with a 3 arc second resolution. SRTMGL1 v. 3 [20] has been utilized herein. (download from e.g. https://earthexplorer.usgs.gov/).

(2) ACE2: The Altimeter Corrected Elevations, Version 2 is a global digital elevation model created by synergistically merging the SRTM data set with Satellite Radar Altimetry within the region bounded by 60°N and 60°S. ACE2 was developed at resolutions of 3, 9 and 30 arc-seconds, and 5 arc-minutes [21]. The 3" ACE2, utilized herein (downloaded from https://sedac.ciesin.columbia.edu/data/set/dedc-ace-v2).

(3) ASTER: The Advanced Spaceborne Thermal Emission and Reflection Radiometer (ASTER) is a 1 arc-second global DEM [22]. The ASTER version 3 has been publically released in 2019 (download from e.g. https://asterweb.jpl.nasa.gov/gdem.asp). Table 2 shows the characteristics of those selected global DEMs.

Table 2 Characteristics of the utilized global DEMs

DEM	Released year	Spatial resolution	
		arc second	m
ASTER v.3	2019	1"	~ 30
ACE2	2019	3"	~ 90
SRTMGL1 v.3	2019	1"	~ 30

The topography of Egypt, as derived from ACE2 GDEM for example, is depicted in Fig. 1. It can be noticed that the Egyptian terrain heights range from -137 m to +2603 m with an average of 302 m. It can be realized that the mountainous areas are located only in the middle of Sinai peninsula, eastern deserts along the Red sea, and in Southwestern borders. The flat topography generally reduces the effects of terrain corrections in geoid modelling. For each combination, a 5'x5' gravimetric geoid is developed first, and then fitted to GNSS/levelling dataset.

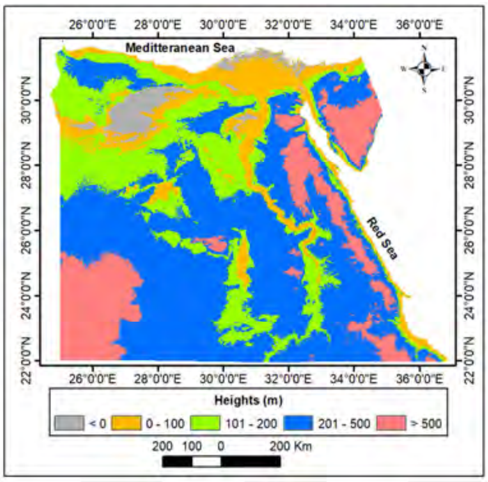

Fig. 1 Topography of Egypt

The least-square collocation is one of the most imperative tools for gravity field modelling due to its high capability of dealing with heterogeneous input features. The basic mathematical form of LSC, in a vector form, could be written as [23]:

$$x = Au + s + n \tag{1}$$

where x is the vector of measurements, n is the vector of the noise component in the measurements, s is the vector of signal components in the measurements to be predicted, and u is the vector of unknown parameters to be estimated.

Thus, LSC combines adjustment, filtering and prediction of the input Earth's gravity field parameters to estimate geoidal heights and other geodetic related values [ibid]. Solving that model requires constructing a covariance matrix that can be estimated based on the variances of the required noise and unknown parameters. The accuracy of LSC solution, as represented by the error covariance matrix, depends on the original covariance matrices or, in other words, on the accuracy of the input datasets.

The processing, in the current study, has been carried out using the LSC-based Gravsoft package [24]. With this software, the effects of a GGM and a DEM are first removed from the input datasets of the Earth's gravitational field to obtain a residual field, second computations of predicted quantities and error estimates are carried out, and finally re-adding the effects of both GGM and DEM to the attained residual parameters [23]. Additionally, an empirical covariance function is estimated based on the residual gravity anomaly data. The package decomposes the geoid undulations (N), in the remove-compute-restore processing strategy, into three components as [24]:

$$N = N_{GGM} + N_{\Delta g} + N_{TC} \tag{2}$$

where N_{GGM} provides the long to the medium wavelength of the gravitational field of the Earth as computed, $N_{\Delta g}$ represents the medium to short local wavelength deduced from local datasets, and N_{TC} represents the terrain corrections or the topography contribution as represented by a certain DEM. The three components of the geoidal undulation, in the last equation, are computed by the following equations [23]:

$$N_{GGM} = \left(\frac{GM}{r\gamma}\right) \sum_{n=2}^{\max-n} \left(\frac{a}{r}\right)^n \sum_{m=0}^{n} \left((\bar{C}_{nm} \cos m\lambda + \bar{S}_{nm} \sin m\lambda) P_{nm} \cos\varphi\right) \tag{3}$$

$$N_{\Delta g} = \frac{R}{4\pi\gamma} \int_{\sigma}\int_{o} S(\psi)(\Delta g - \Delta g_{GGM}) d\sigma \tag{4}$$

$$N_{TC} = G \iint_{\sigma} \int_{h_p}^{h} \frac{\rho(x,y,z)(h_p - z)}{r^3 (x_p - x, y_p - y, h_p - z)} dxdydz \tag{5}$$

where n is the degree of the GGM model, max-n is the maximum degree of the GGM model, m is the maximum order of the model, γ is the normal gravity of the reference ellipsoid, r is the geocentric radius of the computation point, G is the Newtonian gravitational constant, M is the mass of the Earth, R is the mean radius of the Earth, a is the semi-major axis, φ is the geocentric latitude, λ is the geocentric longitude, Δg is the gravimetric observations given as free-air gravity anomalies, Δg_{GGM} is the gravity anomalies computed by a specific GGM, $S(\Psi)$ is the Stokes' function,σ is a differential surface area on a unit sphere, $\sigma_\circ$ is the differential surface area on the computational cap, $\bar{C}_{nm}$ and $\bar{S}_{nm}$ are the fully normalized harmonic coefficients, $\rho_\circ$ is the surface atmosphere potential, $r_\circ$ is the sea-level radius of the Earth, $\rho(x,y,z)$ is the topographical density at running point, h_p and h are the computational and running point respectively, and P_{nm} is the fully normalized associated Legendre polynomial.

Next, all geoid combinations have been investigated using the ArcGIS 10 software, to interpolate the attained geoidal heights at the 100 checkpoints and compare them to their corresponding known values. To compare the performance of each attained LGM, three statistical measures have been used: standard deviation, average, and range of the discrepancies between the known and interpolated geoid undulations. Three descending ranks (*R1*, *R2*, *R3*) are given to each LGM over a scale of ten, where ten represents the minimum value of the statistical measure and one represents the maximum value. Weights of those ranks have been selected as 4, 3, and 3 respectively. Hence, a weighted mean rank (*R*) is computed for each LGM, using its corresponding three individual rank measures (*Ri*) and their assigned weights (*Wi*) to represent a unique indicator of its accuracy and to serve as a base of comparison between the twelve accomplished LGMs, as:

$$R = \frac{\sum R_i W_i}{\sum W_i} \tag{6}$$

Fig. 2 presents the overall steps utilized in the data processing of the proposed methodology.

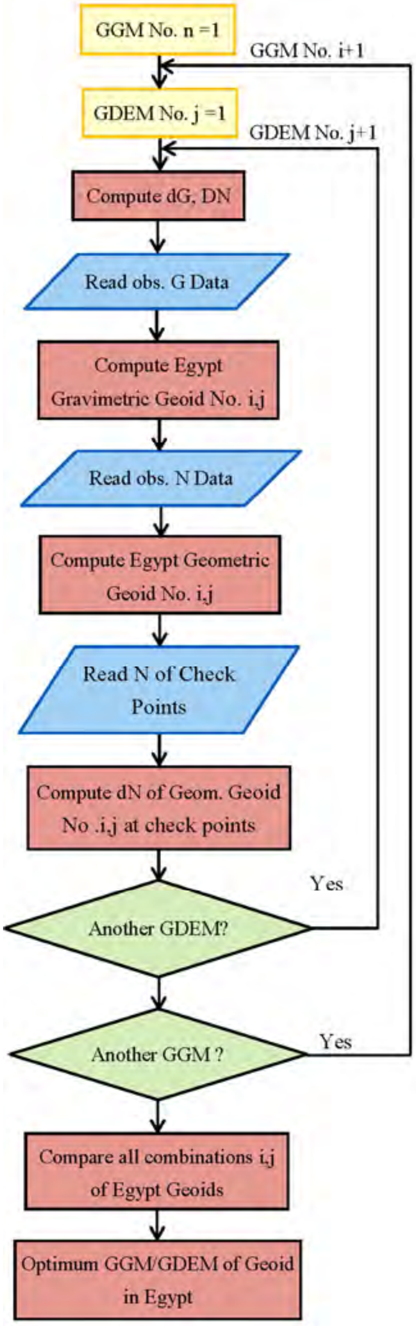

Fig. 2 Flow chart of data processing

3. Available Data

Regarding the available terrestrial data over Egypt, the study utilized two main types: terrestrial gravity data and GNSS/Levelling data (Fig. 3). The first-order Egyptian national gravity networks of both 1997 and 1977 contain 247 measured gravity points [11]; and 1100 GNSS/levelling stations all over Egypt, that were observed by the Survey Research Institute (SRI) in various projects over the last ten years [25]. It is worth mentioning that the average accuracy of the Egyptian National Gravity Standardization Network of 1997 (ENGSN97) is ±0.02 mGal, while the corresponding value of the National Gravity Standard Base Network of 1977 (NGSBN77) is ±0.08 mGal [11]. On the other hand, the utilized GNSS/levelling points have been surveyed using the first-order levelling and the first-order GNSS geodetic network standards, and their average accuracy could be estimated as ±3 - 4 cm [25]. Ten percent of the known GNSS/Levelling stations have been reserved as checkpoints to estimate the external accuracy of each developed LGM. It should be noticed that such local datasets may not adequate in number and they are not homogeneously distributed over Egypt. However, such data are the most-recent accurate geodetic measurements existing over the country [ibid].

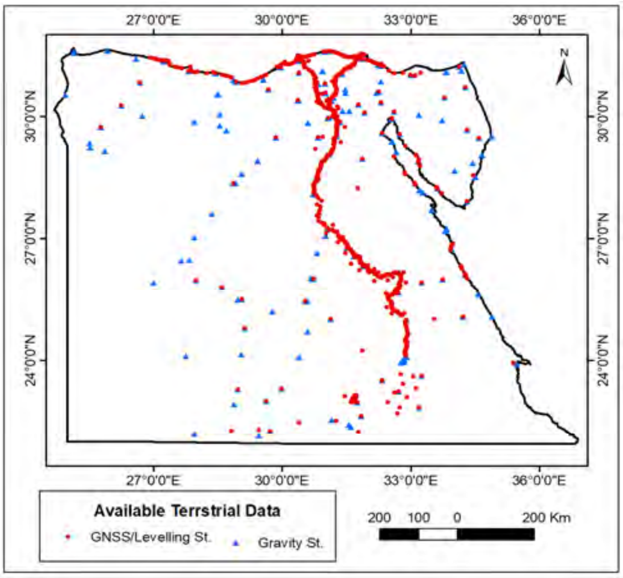

Fig. 3 Available terrestrial data in Egypt

4. Results and Discussion

Table 3 Overall accuracy of different GGMs and DEMS over checkpoints (m)

(A) Overall accuracy of LGMs based on different GGMs over checkpoints:		
GGM	Average Standard Deviation (m)	Improvements %
XGM2019e_2159	±0.137	17%
EGM2008	±0.140	
GECO	±0.159	
EIGEN-6C4	±0.157	
(B) Overall accuracy of LGMs based on different DEMs over checkpoints:		
DEM	Average Standard Deviation (m)	Improvements %
ACE2	±0.146	2%
ASTER v.3	±0.148	
SRTMGL1 v.3	±0.150	

The first investigation step has been carried out in the overall perspective to get the big picture about the contribution of GGMs and DEMs in geoid modelling for Egypt. Hence, the average standard deviation over checkpoints for each GGM-based LGM, averaging its performance using all DEMs, has been computed. Similarly, the mean standard deviation over check points for each DEM-based LGM, averaging its performance using all GGMs, has been also computed. Table 3 presents the accomplished findings that reveal two imperative remarks. First, local geoid accuracy levels range from ±0.137 m using the

XGM2019e_2159 model to ±0.159 m using the GECO GGM. It emphasizes that significant improvements of 17% approximately in local geoid accuracy are attributed to the utilization of GGMs models representing the long wavelength of the Earth gravitational field. Regarding the contribution of DEMs, it can be noticed from that table that the overall accuracy of LGMs does not significantly depend on the utilized DEM. That could be attributed to the almost flat topography of Egypt as depicted in Fig. 1, which reduces the effect of the topographic correction in the geoid modelling process.

Furthermore, the statistical characteristics of the developed twelve LGM of Egypt are tabulated in Tables 4-7. Several imperative remarks could be perceived from those tables. First, it can be recognized, from the first column in all tables, that the

Table 4 Chrematistics of XGM2019e_2159 GGM differences over checkpoints (m)

Measure/LGM No.	Utilized GDEM		
	ACE2	ASTER v.3	SRTMGL1 v.3
	1	2	3
Minimum	-0.276	-0.279	-0.275
Maximum	0.271	0.430	0.429
Range	0.547	0.710	0.704
Average	0.003	0.005	0.006
Standard Deviation	±0.129	±0.140	±0.141

Table 5 Chrematistics of GECO GGM differences over checkpoints (m)

Measure/LGM No.	Utilized GDEM		
	ACE2	ASTER v.3	SRTMGL1 v.3
	4	5	6
Minimum	-0.292	-0.301	-0.293
Maximum	0.649	0.607	0.663
Range	0.940	0.908	0.956
Average	0.016	0.015	0.017
Standard Deviation	±0.161	±0.156	±0.162

Table 6 Chrematistics of EIGEN-6C4 GGM differences over checkpoints (m)

Measure/LGM No.	Utilized GDEM		
	ACE2	ASTER v.3	SRTMGL1 v.3
	7	8	9
Minimum	-0.621	-0.633	-0.633
Maximum	0.369	0.375	0.376
Range	0.989	1.008	1.008
Average	0.010	0.010	0.010
Standard Deviation	±0.156	±0.157	±0.157

Table 7 Chrematistics of EGM2008 GGM differences over checkpoints (m)

Measure/LGM No.	Utilized GDEM		
	ACE2	ASTER v.3	SRTMGL1 v.3
	10	11	12
Minimum	-0.295	-0.317	-0.320
Maximum	0.322	0.327	0.328
Range	0.618	0.644	0.647
Average	0.019	0.018	0.019
Standard Deviation	±0.140	±0.140	±0.140

AEC2 GDEM generally produce the minimum range of variations over checkpoints. So, it might be concluded that AEC2 performs a little bit better than the other two GDEMs over Egypt, at least in geoid modelling applications. Moreover, it can be revealed that the standard deviation, as an accuracy indicator, ranges from ±0.129 m for LGM 1 to ±0.162 m for LGM 6. For the range of discrepancies over known checkpoints, the developed LGMs perform diversely and their variations range from a minimum of 0.547 m for LGM 1 to 1.008 m for LGM 8 and 9. However, all these levels of accuracy are not accurate enough for high-precision GNSS-based geodetic and mapping applications in Egypt. Consequently, this signifies the critical need for collecting more measured geodetic datasets in terms of number and homogenous distribution over the country.

To come up with the optimum LGM for Egypt, the twelve LGMs have been compared in terms of standard deviation, average, and ranges of their geoid undulations' variations over checkpoints. As mentioned earlier, a descending rank is assigned to each LGM, on a scale of ten, for each statistical measure. Subsequently, Eq. 2 is applied to compute the weighted mean rank for each model. The attained results are tabulated in Table 8. It can be realized that the overall rank of the LGMs, on a scale of ten, varies from 2.9 for LGM 6 to 10.0 for LGM 1. Consequently, based on the currently available local geodetic datasets, LGM 1 is the optimum model for Egypt. It has been developed based on the XGM2019e_2159 GGM and the ACE2 GDEM. Its geoid undulations (Fig. 4) range from 8.948 m to 21.088 m with a mean of 14.106 m. It is recommended to use this local geoid, for the time being, for GNSS-based surveying and mapping applications in Egypt.

Table 8 Ranks of developed LGMs for Egypt

LGM No.	R_1	R_2	R_3	R
1	10	10	10	10.0
2	9	9	1	7.2
3	8	8	2	6.8
4	3	5	5	4.0
5	7	6	4	6.1
6	1	4	6	2.9
7	6	7	3	5.7
8	4	7	3	4.7
9	4	7	3	4.7
10	9	2	8	6.7
11	9	3	7	6.8
12	9	2	9	6.9

where R_1, R_2, R_3 are the individual ranks for standard deviation, average, and range respectively. R is the weighted overall rank.

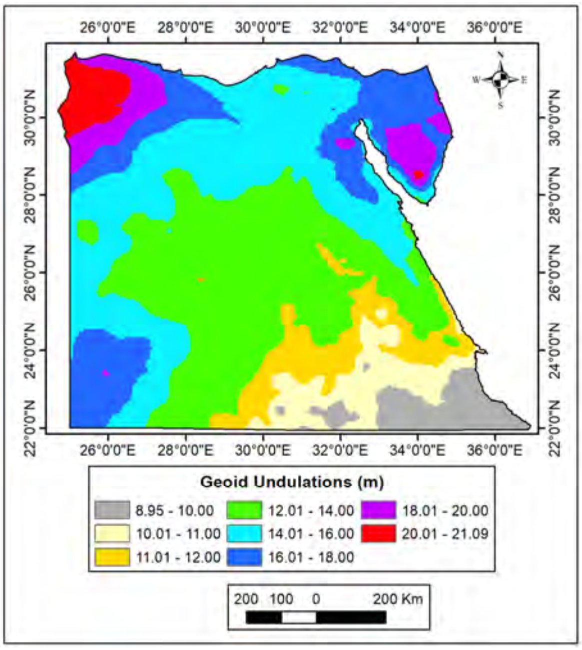

Fig. 4 Developed optimum local geoid of Egypt

5. Conclusions

Local geoid modelling involves a local geodetic dataset, an optimum GGM, and a GDEM. A precise geodetic dataset, comprising 247 terrestrial gravity points and 1000 GNSS/Levelling stations, has been utilized in the current research study using the Least-Square Collocation geoid modelling method. Rather than the classical point-wise method of investigating the accuracy of GGMs and DEMs, the current research proposed a new approach for deciding which GGM and DEM models are optimum for utilization in developing a national geoid model. Thus, four GGMs (namely XGM2019e_2159, EGM2008, EIGEN-6C4, and GECO) and three GDEMs (ASTER v.3, ACE2, and SRTMGL1 v.3) have been utilized and twelve 5'x5' gravimetric geoid models have been developed for Egypt. Such models have been, then, fitted to GNSS/Levelling stations and then judged over 100 checkpoints with known geoidal heights.

Accomplished findings revealed that the utilized GDEMs provide comparable results from a precision perspective, which could be due to the flat topography of Egypt. Thus, it can be concluded that the terrain effects in geoid modelling are quite small. Additionally, it has been found that the AEC2 model performs relatively better than the other two investigated GDEMs over Egypt. Furthermore, it has been found that the standard deviation of the twelve LGM ranges from ±0.129 m to ±0.162 m. On the other hand, the undulations discrepancies over known checkpoints vary from 0.547 m to 1.008 m. Concerning the general performance of all investigated GGMs, it has been concluded that the XGM2019e_2159 produces the best standard deviation (±0.129 m) while the GECO GGM produces the worst value ±0.162 m). Nevertheless, all these levels of accuracy cannot be as accurate as needed for high-precision GNSS-based geodetic and mapping applications in Egypt. As a result, there is a vital need for collecting extra local geodetic datasets in terms of number and homogenous distribution over the country. All specialized governmental, military and private organizations have to cooperate together to establish a recent integrated national dataset for geodetic and environmental applications.

Based on statistical ranking, it has been found that the LGM developed using the XGM2019e_2159 GGM and the ACE2 GDEM, could be considered as the optimum model for Egypt for the time being. Therefore, it is recommended to use this local geoid for GNSS-based surveying and mapping applications in Egypt.

Acknowledgement

The authors appreciated the revision of the manuscript and the valuable comments given by the late Prof. Dalal S. Alnaggar who passed away during the development of this research study. May God blesses her soul.

Conflicts of Interest

The authors declare no conflict of interest.

References

[1] K. M. Ahlgren, S. A. Holmes, X. Li, Y. M. WANG, and M. A. Youngman, “Geoid Modeling at NOAA’ s National Geodetic Survey as 2022 Approaches,” FIG Working Week, Helsinki, Finland, 2017.
[2] M. Greaves, P. Downie, and K. Fitzpatrick, “OSGM15 and OSTN15: Updated Transformations for UK and Ireland,” Geomatics World, No. 32/33, pp. 1-5, 2016.
[3] F. Duquenne and A. Coulomb, “The French Approach to Modernize Its Vertical Reference,” Finance Information Group Working Week, May 2015, pp. 17-21.
[4] K. Matsuo and Y. Kuroishi, “Refinement of a Gravimetric Geoid Model for Japan using GOCE and An Updated Regional Gravity Ffield Model,” Earth, Planets and Space, vol. 72, no. 1, pp. 1-18, March 2020.
[5] A. V. Fernádez, O. L. Castro, and J. G. León, “Geoid Heights in Costa Rica, Case of Study: Central Pacific Zone,” Revista Ingenieria, vol. 30, no. 1, pp. 1-20, November 2020.

[6] M. El-Ashquer, H. Al-Ajami, A. Zaki, and M. Rabah, "Study on the Selection of Optimal Global Geopotential Models for Geoid Determination in Kuwait," Survey Review, vol. 52, no. 373, pp. 373-382, May 2019.
[7] M. E. Gomez, R. Perdomo, and D. Del Cogliano, "Validation of Recent Geopotential Models in Tierra Del Fuego," Acta Geophysica, vol. 65, no. 5, pp. 931-943, September 2017.
[8] A. A. Saad and M. S. Elsayed, "Evaluation of GOCE Satellite Only Models Along the River Nile," Scientific and Academic Publishing, vol. 8, no. 3, pp. 131-140, 2019.
[9] M. Eshagh and S. Zoghi, "Local Error Calibration of EGM08 Geoid using GNSS/levelling Data," Journal of Applied Geophysics, vol. 130, pp. 209-217, July 2016.
[10] D. S. Alnaggar, "Determination of the Geoid in Egypt Using Heterogeneous Geodetic Data," PhD dissertation, Faculty of Engineering, Cairo University, 1986.
[11] G. M. Dawod, "A National Gravity Standardization Network for Egypt," PhD dissertation, Faculty of Engineering at Shoubra, Zagazig University, 1998.
[12] H. Abd-Elmotaal, "Gravimetric Geoid for Egypt Using High-Degree Tailored Reference Geopotential Model," National Research Institute of Astronomy and Geophysics Journal of Geophysics. Special issue, pp. 507-531, December 2008.
[13] G. Dawod, W. Resrach, and T. M. Abdelaziz, "Utilization of Geographically Weighted Regression for Geoid Modelling in Egypt," Journal of Applied Geodesy, vol. 14, no. 1, October, 2019.
[14] T. Abdel-Aziz, G. Dawod, and H. Ebaid, "DEMs and Reliable Sea Level Rise Risk Monitoring in Nile Delta, Egypt," Discover Sustainability, vol. 1, no. 1, pp. 1-11, December 2020.
[15] P. Zingerle, R. Pail, and T. Gruber, "High-Resolution Combined Global Gravity Field Modelling--Towards a Combined d/o 10800 Model," Geophysical Research Abstracts, vol. 21, January 2019.
[16] M. Gilardoni, M. Reguzzoni, and D. Sampietro, "GECO: A Global Gravity Model by Locally Combining GOCE Data and EGM2008," Studia Geophysica et Geodaetica, vol. 60, no. 2, pp. 228-247, March 2016.
[17] C. Förste, S. Bruinsma, O. Abrikosov, F. Flechtner, J. C. Marty, J. M. Lemoine, et al., "EIGEN-6C4-The Latest Combined Global Gravity Field Model Including GOCE Data up to Degree and Order 1949 of GFZ Potsdam and GRGS Toulouse," EGUGA, p. 3707, May 2014.
[18] N. K. Pavlis, S. A. Holmes, S. C. Kenyon, and J. K. Factor, "The Development and Evaluation of the Earth Gravitational Model 2008 (EGM2008)," Journal of Geophysics Research Solid Earth, vol. 117, no. B4, April 2012.
[19] "The International Center for Global Earth Model," http://icgem.gfz-potsdam.de/tom_longtime, October 12, 2020.
[20] "SRTMGL1 V003," The US Geological Survey, https://lpdaac.usgs.gov/products/srtmgl1v003/, 2020.
[21] R. Smith and P. Berry, "Altimeter Corrected Elevations, Version 2," https://sedac.ciesin.columbia.edu/data/set/dedc-ace-v2, 2019.
[22] "ASTER Digital Elevation Model V003," https://catalog.data.gov/dataset/aster-digital-elevation-model-v003, July 17, 2020.
[23] B. Hofmann-Wellenhof, "Moritz, H.(2005) Physical Geodesy", New York: Springer, 1967.
[24] R. Forsberg and C. C. Tscherning, GRAVSOFT: Geodetic Gravity Field Modelling Programs Manual, 2nd ed. Denmark: National Space Institute, 2008.
[25] E. M. Al. Krargy, "Development of a National Geoid for Egypt Using Recent Surveying Data," PhD dissertation, Faculty of Engineering, Minufiya university, Egypt, 2016.

Copyright© by the authors. Licensee TAETI, Taiwan. This article is an open access article distributed under the terms and conditions of the Creative Commons Attribution (CC BY-NC) license (https://creativecommons.org/licenses/by-nc/4.0/).

Journal of Geographic Information System, 2021, 13, 148-165
https://www.scirp.org/journal/jgis
ISSN Online: 2151-1969
ISSN Print: 2151-1950

The Validity of Open-Source Elevations for Different Topographic Map Scales and Geomatics Applications

Gomaa M. Dawod[1], Ibrahim E. Ascoura[2]

[1]Survey Research Institute, National Water Research Center, Giza, Egypt
[2]Umm Al-Qura University, Makkah, Saudi Arabia
Email: dawod_gomaa@yahoo.com, ieascoura@uqu.edu.sa

How to cite this paper: Dawod, G.M. and Ascoura, I.E. 2021) The Validity of Open-Source Elevations for Different Topographic Map Scales and Geomatics Applications. *Journal of Geographic Information System*, **13**, 148-165.
https://doi.org/10.4236/jgis.2021.132009

Received: February 20, 2021
Accepted: March 16, 2021
Published: March 19, 2021

Copyright © 2021 by author(s) and Scientific Research Publishing Inc.
This work is licensed under the Creative Commons Attribution International License (CC BY 4.0).
http://creativecommons.org/licenses/by/4.0/
Open Access

Abstract

This paper presents an analysis of four open-source Global Digital Elevation Models (GDEMs) and compares them on two topographic profiles (nearly flat, and hills regions) for mapping and geomatics applications. The chief intention is to investigate if GDEMs-based heights, contour intervals, slopes, and topographic profiles are valid for all map scales of topographic mapping, which constitutes a major issue in mapping activities. Two case studies, the Nile delta in Egypt and Makkah city in Saudi Arabia, have been utilized to represent flat and moderate-topography patterns. The investigated GDEMs include the most-recent released models: ASTER v.3, ACE 2, SRTMGL1 v.3, and NASADEM_HGT v.1 released in 2019 and 2020 with spatial resolutions of 1 and 3 arc seconds. Available accurate Ground Control Points (GCP) consist of 540 stations in the Nile delta and 175 stations in Makkah. Based on the available datasets in two study areas, it has been found that the accuracy of investigated GDEMs over known checkpoints ranges from ±2.5 and ±5.1 meters in the Nile delta region, while it varies between ±5.1 and ±8.0 meters in the Makkah area. That indicates that the utilization of GDEMs in topographic mapping differs significantly between flat and hilly spatial regions. Therefore, it is recommended to avoid using GDEMs for developing topographic maps of scale 1:25,000 or larger in flat regions and map scale 1:50,000 or larger in hilly regions. Additionally, the accomplished results showed that all GDEM-based slopes do not match with the actual slopes from known GCP over cross section's length up to 30 kilometers. Thus, it is concluded that GDEMs are not the appropriate heights' source for topographic mapping at medium and large map scales, and could not be utilized for topographic profiling in precise engineering and geomatics applications.

Keywords

Topographic Maps, GDEMs, Heights, Map Scales, Contour Interval

1. Introduction

Topographic maps represent a chief type of maps utilized in numerous geomatics applications, such as engineering projects, hydrological modelling, disaster risk assessment, geomorphological and hydrogeological analysis, and environmental applications. Contour lines represent a vital piece of information that appeared on printed and digital topographic maps. They represent the terrain topographic variations and enable estimating heights of required random points. Nowadays, the most frequent form of storage and analyzing height datasets is the Digital Elevation Model (DEM) digital format. It is known that heights used to generate contour lines could be obtained from a wide range of sources including terrestrial surveying, Global Navigation Satellite Systems (GNSS) data, aerial photos, satellite images, and GDEMs. On another hand, Geographic Information Systems (GIS) enables handling, processing, and analyzing DEMs to generate many forms of mapping terrain topography including generating contour lines for a wide range of applications. Some of such applications include the production of flood hazard maps [1], mapping of geological structural lineaments [2], analysis of fluvial landscape in mountainous regions [3], monitoring impacts of sea level rise [4], the production of topographic maps [5], and geoid modelling [6].

In many developing countries, precise national DEM models might be existed but unpublished for public usages. So, researchers usually utilize the available open-source free GDEMs. In the last few decades, many GDEM models, with variable coverages and spatial resolutions, have been produced and made freely accessible over websites. Examples of such GDEMs include the Shuttle Radar Topography Mission (SRTM), the Advanced Spaceborne Thermal Emission and Reflection Radiometer (ASTER), EarthEnv-DEM90, the Global Multi-resolution Terrain Elevation Data 2010 (GMTED2010, the Global Land One-km Base Elevation (GLOBE), the Global 30 arc-second (GTOPO30), and the Advanced Land Observing Satellite (ALOS)-based World 3D - 30 m (AW3D30).

The accuracy of open-source GDEMs constitutes a vital role in their utilization for mapping and environmental studies. Thus, many research studies have been focused on estimating the precision and accuracy of GDEMs. For example, Dawod and Al-Ghamdi [7] have examined the reliability of eight GDEM models for geomatics applications in both Egypt and Saudi Arabia. The results showed that their accuracy, in terms of standard deviation over checkpoints, ranges between ±1.9 and ±6.6 meters. Similar results have been reported in other regions such as the USA [8], India [9], and China [10].

Rather than the printed or digital topographic maps, several geomatics appli-

cations, particularly utilizing GIS, rely on a digital representation of the topography. Such activities need a definite level of height accuracy depending on its objectives and the spatial extent of the study area. Using GDEMs might not appropriate for high-accuracy geomatics applications. A typical example of such a situation is the impact assessment of Sea Level Rise (SLR) in small or moderate regions. It is known that the average anticipated SRL on a global basis in 2081-2100 is estimated to range between 0.40 and 0.63 meters relative to the 1986-2005 level [11]. Monitoring and estimating risk impacts of such small level rise necessitate a high-accuracy terrain representation. Abdel-Aziz *et al.* [12] have investigated the reliability of a few GDEMs in delineating inundated regions due to sea level rise over the Nile delta area. It has been found that the reliability of three investigated global models, when compared to a high-accuracy local DEM, is less than 20%. Similar results have reported by other researchers in other regions [13]. Another example is the utilization of low-accurate GDEMs in engineering applications. Zhang and Chu [14] emphasized that precise quantification of surface depression storage depend significantly on DEM-based topographic characteristics principally the vertical accuracy and spatial resolution. On the other hand, there exist some geomatics applications that could be performed utilizing the few-meters accuracy of GDEMs. Reconnaissance, project planning for medium or large spatial regions, hydrological modelling, surface runoff estimation, and geoid modelling could be examples of such activities.

The current research study aims to investigate the absolute accuracy and the validity of elevation data from different sources for contour generation at several topographic map scales. Additionally, it investigates two other relative topographic factors, namely slope and cross-sections, employed broadly in numerous geomatics applications. This comprises a vital concern in topographic mapping to investigate if GDEMs-based contours and topographic profiles could be utilized for all map scales and geomatics applications. As far as the authors' concern, it might be the first research study, at least in Egypt, to tackle such a significant subject.

2. Standards and Specifications of Topographic Maps

Standards and specifications have been developed worldwide for contour lines characteristics including the accuracy of collected data and the methods of representing such important lines. Contour intervals to be shown on a map vary with the required map scale. The term contour interval represents the vertical distance or the elevation difference between two successive contour lines. The scale of a map is the ratio between the length of a line on the map and its actual length on the ground. Traditionally, topographic maps are drawn on medium map scales such as 1:5000, 1:10,000, 1:25,000, and 1:50,000. Generally speaking, selecting the appropriate contour interval for a specific map depends on several factors including the map scale, the extent of the surveyed area, the nature of the topography, and the number and distribution of available height dataset, and the

purpose of the map itself [15]. A rule of thumb is that the appropriate contour interval on a map might be estimated as three times the Root Mean Square Error (RMSE) of the utilized input height data [16]. The vertical accuracy is represented by RMSE of the utilized height datasets as:

$$\text{RMSE} = \sqrt{\frac{\sum_{1}^{n}\left(P_i - O_i^2\right)}{n}} \tag{1}$$

where P_i and O_i are the predicted and observed height respectively of point i, and n is the total number of points.

Examples of standards and specifications of topographic maps, particularly for contour lines' characteristics, are summarized herein. The Australian map specifications state that the minimum elevation accuracy of datasets to generate contour lines are 5, 10, 25 meters for map scales 1:25,000, 1:100,000 and 1:250,000 respectively [17]. In Burundi, the contour intervals for 1:5,000 and 1:25,000 topographic maps equal 5 and 10 meters respectively and the vertical accuracy of these contour lines are less than 2.5 and 5.0 meters respectively [18]. Additionally, the suggested contour intervals in India for 1:5,000, 1:10,000 1:25,000, and 1:50,000 maps equal 1.25, 5.0, 8.0, and 15 meters respectively [19]. Also, the US Geological Survey (USGS) state that the vertical accuracy standard requires that the elevation of 90 percent of all utilized height points must be correct within half of the contour interval [20]. Additionally, the map specifications of the State of Qatar defined the appropriate contour intervals of 2 m, 5 m, and 10 m for map scales 1:5000, 1:10,000, and 1:200,000 respectively. Additionally, the RMS of heights used in topographic mapping is one-third of the required contour interval [21].

Nationally, the Egyptian Survey Authority (ESA) has published in the year 2020 the updated specifications of topographic maps [22]. For topographic maps' contour lines, the Egyptian standards state that the RMSE of utilized datasets to generate contour lines should be less than one-third of the contour interval. The utilized contour intervals for map scales 1:10,000, 1:25,000, 1:50,000, 1:100,000, and 1:250,000 are 2, 5, 10, 20, 50 meters respectively. If contour lines are not displayed on map scales 1:5,000 and 1:2,500, spot heights should be plotted on every 100 and 50 m horizontally with vertical accuracy levels equal 0.75 and 0.40 meter respectively. To conclude this issue, **Table 1** presents typical examples of contour interval and vertical accuracy used in producing topographic maps with several map scales worldwide.

The relief, slope, and cross-sections constitute important factors in characterizing the topography of a spatial region [23]. The relief, R, is the height difference between the maximum ($H_{\max}$) and minimum ($H_{\min}$) heights of the region. The slop between two points is their height difference divided by the horizontal distance between them. The slope could be evaluated in the units of degrees or as a percentage (Equation (3)):

$$R = H_{\max} - H_{\min} \tag{2}$$

Table 1. Typical standards of topographic maps.

Map Scale	Contour Interval (m)	Vertical Accuracy of Utilized Datasets (m)
1:5000	1.25	±0.4
1:10,00	2.0/5.0	±0.7/±1.7
1:25,000	5.0/8.0/10.0	±1.7/±2.6/±3.3
1:50,000	10.0	±3.3
1:100,000	10.0/20.0	±3.3/±6.7
1:250,000	25.0/50.0	±8.3/±16.7

$$S = \frac{\Delta H}{D} \times 100 \tag{3}$$

Additionally, a new factor called Slope Validity (*SV*) is proposed, herein, to compare the performance of GDEM-based estimated slopes when compared to precise slopes. It is computed as the percentage of the slope, between two points, from both GDEMs and known accurate heights at those checkpoints, as:

$$SV_{\text{GDEM}} = \frac{S_{\text{GDEM}}}{S_{\text{known}}} \times 100 \tag{4}$$

Concerning the terrain topography, it could be divided into classes according to several factors such as the slope. Table 2 presents an example of slope-based topography categories [24] [25].

3. Methodology and Available Data

The utilized GDEMs models, herein, include NASADEM_HGT v. 1, SRTMGL1 v. 3, ASTER v. 3, and ACE2 models. They constitute the most-recent global DEM models at the time of conducting this research. Table 3 summarizes the characteristics of those selected global DEMs, including:

1) SRTM: The Shuttle Radar Topography Mission (SRTM) is a global DEM, that has two versions: SRTM1 with a spatial resolution of 1 arc second, *i.e.*, approximately 30 meters, and SRTM3 model with a 3 arc second resolution. SRTMGL1 v. 3 [26] has been utilized herein. (download from e.g. https://earthexplorer.usgs.gov/).

2) ACE2: The Altimeter Corrected Elevations, Version 2 is a global digital elevation model created by synergistically merging the SRTM data set with Satellite Radar Altimetry within the region bounded by 60˚N and 60˚S. ACE2 was developed at resolutions of 3, 9 and 30 arc-seconds, and 5 arc-minutes [27]. The 3" ACE2, utilized herein (downloaded from https://sedac.ciesin.columbia.edu/data/set/dedc-ace-v2).

3) ASTER: The Advanced Spaceborne Thermal Emission and Reflection Radiometer (ASTER) is a 1 arc-second global DEM [28]. The ASTER version 3 has been publically released in 2019 (download from e.g. https://asterweb.jpl.nasa.gov/gdem.asp).

Table 2. Topography groups based on slope.

Topography Class	Slope Type	Slope %
Lowlands	Gentle	<3%
Plateaus	Moderate	3% - 8%
Upper terraces	Moderate	8% - 12%
Hills	High	12% - 40%
Mountains	Very High	>40%

Table 3. Characteristics of the utilized global DEMs.

DEM	Released Year	Spatial Resolution	
		Arcsecond	Meter
ASTER v.3	2019	1"	~30
ACE2	2019	3"	~90
SRTMGL1 v. 3	2019	1"	~30
NASADEM_HGT v. 1	2020	1"	~30

4) NASADEM_HGT v. 1: A GDEM developed by the US National Aeronautics and Space Administration (NASA) in collaboration with German and Italian agencies, and released in 2020. It is based on improved processing and merging of several data sources such as SRTM, ASTER, Ice, Cloud, and Land Elevation Satellite (ICESat) and other sources [29]. It can be downloaded from https://search.earthdata.nasa.gov/.

The main study area is the Nile delta region, Egypt. It extends from Damietta city on the east to Alexandria city along the Mediterranean sea and extends to the south to Cairo (Figure 1(a)). 540 GCPs with accurate heights, within ±0.05 meter, have been collected in the Nile delta. The four GDEMs have been downloaded, from their individual website, for this region. First, the topography pattern of the region has been investigated by utilizing the Arc GIS 10 software to convert GDEM-based heights into slope percentages. It has been found that the average slope of the Nile delta equals 3.1%, (Figure 1(b)) which indicates that its topography could be considered as a moderate or plateaus class (Table 2). Consequently, another study area has been added. It represents Makkah city in the Southwest region of the Kingdom of Saudi Arabia (KSA) about 70 km east of Jeddah city on the Red sea (Figure 2(a)). 175 GCPs with accurate heights, within ±0.05 meter, have been collected in Makkah. Similarly, the four GDEMs have been downloaded and the topography slopes have estimated (Figure 2(b)). It has been found that the average slope of the Makkah equals 17.4%, which indicates that its topography could be considered as a high or hills class.

Having downloading spatial grids of the four investigated GDEMs for both study areas (Figure 3 and Figure 4), their interpolated heights at the available GCPs have been compared to the known precise heights utilizing the Arc GIS 10 package. The accomplished results are presented and investigated in the next section.

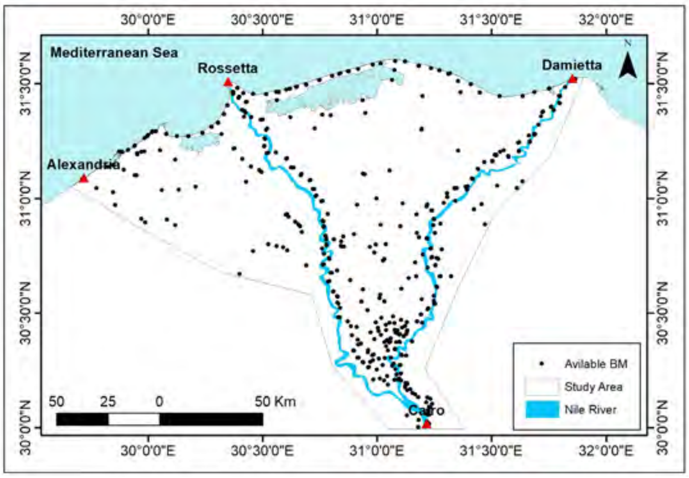

(a)

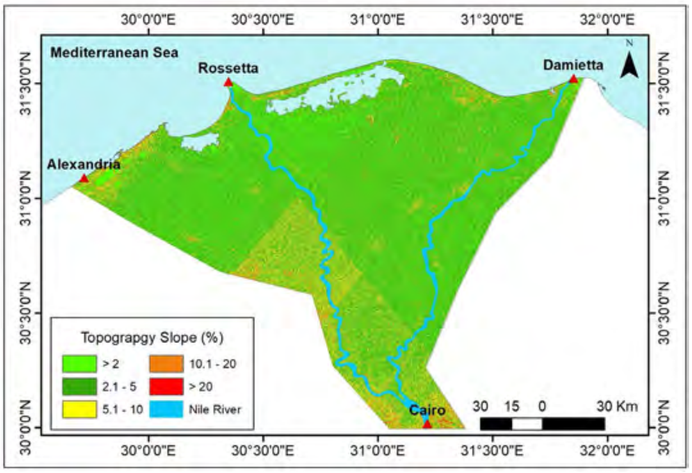

(b)

Figure 1. Nile delta study area. (a) Available data; (b) Topography.

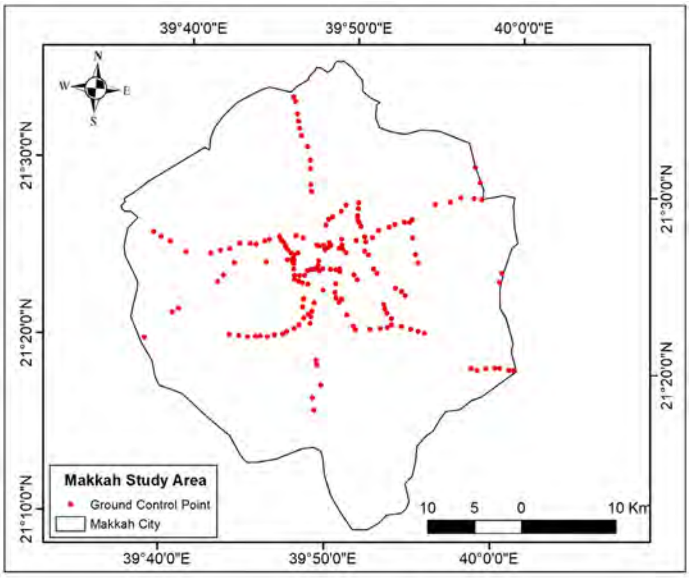

(a)

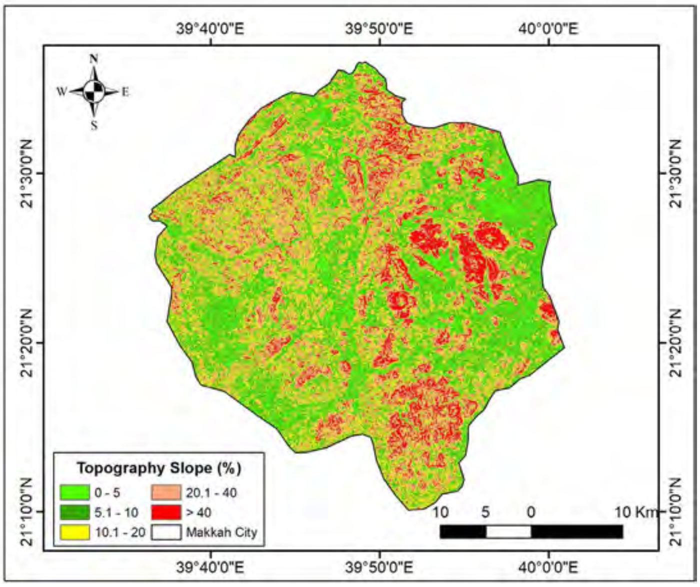

(b)

Figure 2. Makkah study area. (a) Available data; (b) Topography.

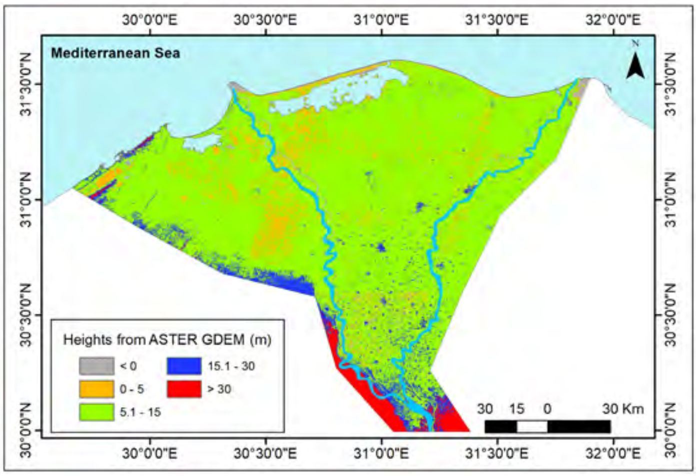

(a)

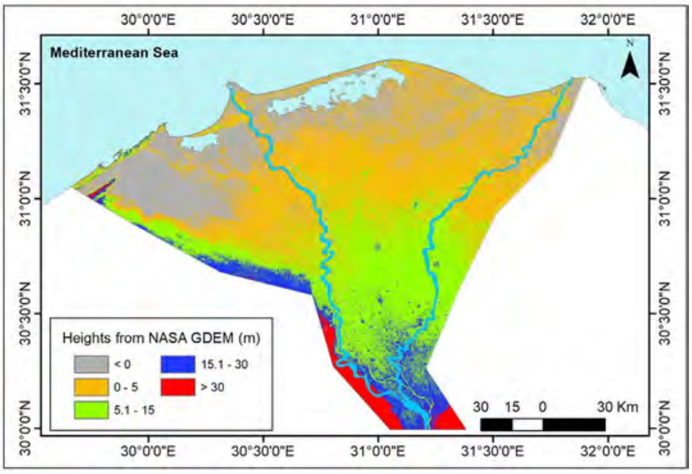

(b)

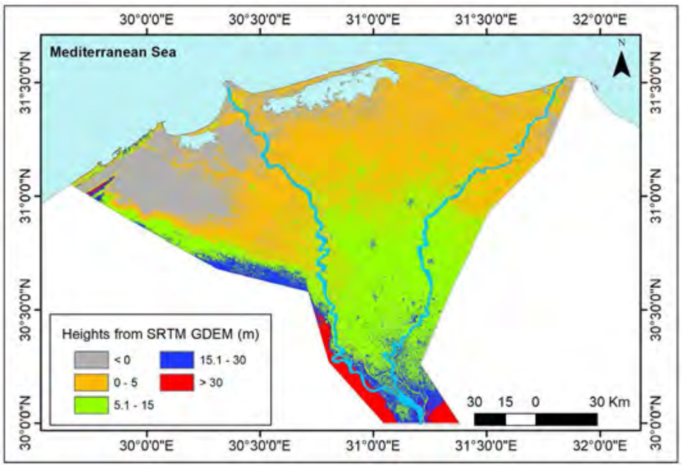

(c)

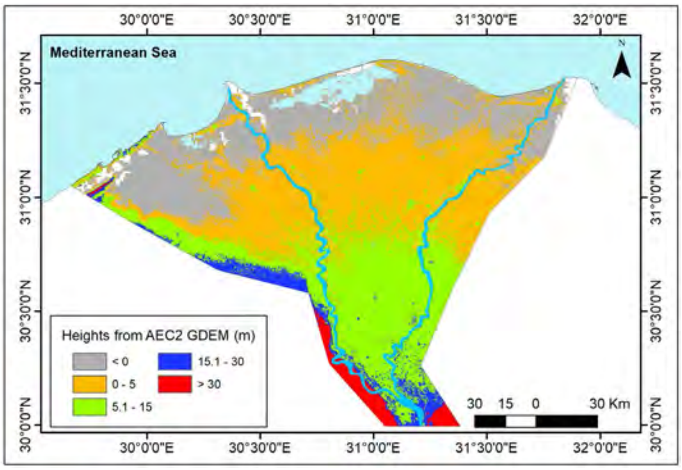

(d)

Figure 3. Topography of Nile delta from GDEMs. (a) ASTER GDEM; (b) NASADEM GDEM; (c) SRTM GDEM; (d) AEC2 GDEM.

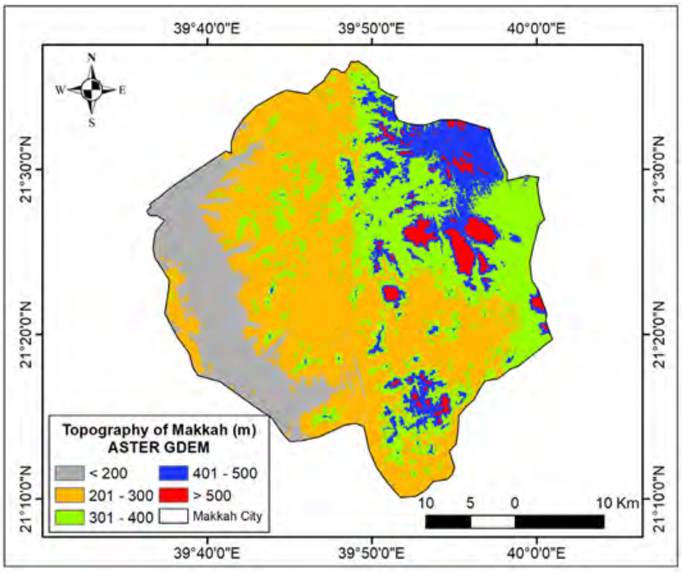

(a)

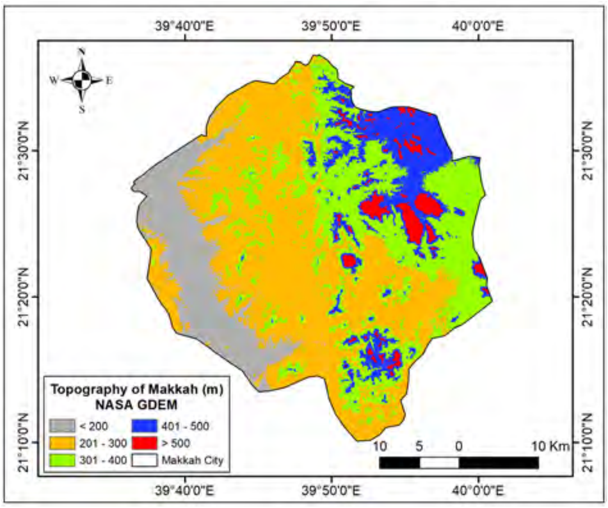

(b)

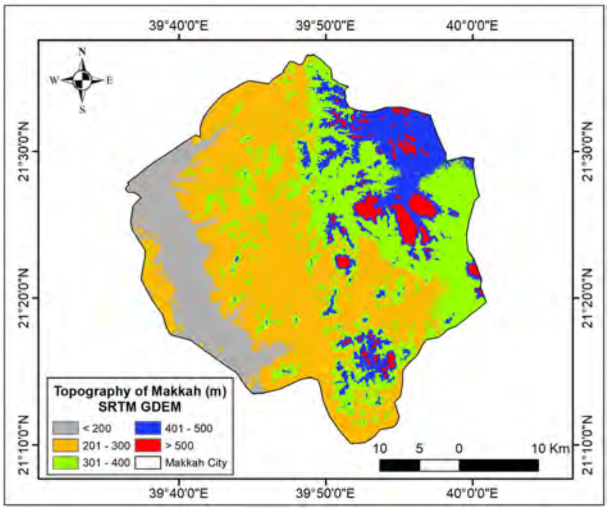

(c)

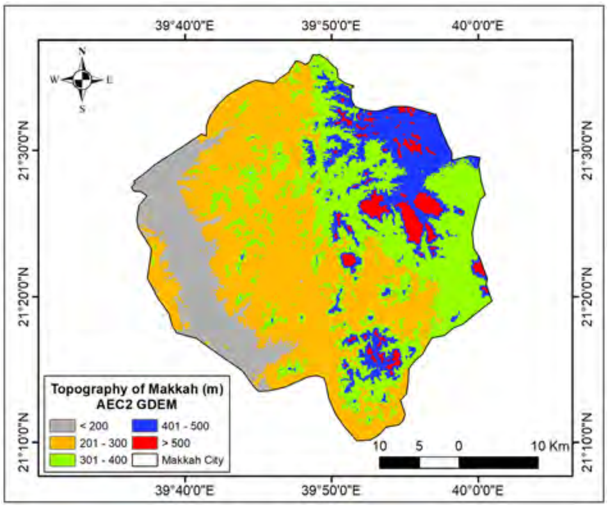

(d)

Figure 4. Topography of Makkah from GDEMs. (a) ASTER GDEM; (b) NASADEM GDEM; (c) SRTM GDEM; (d) AEC2 GDEM.

4. Results and Discussion

Table 4 presents the statistics of observed and GDEM-based heights in the Nile delta region. Generally, it can be noticed that the mean height and the relief (Equation (2)) of only the ASTER GDEM are not close to those of the observed heights, while the other three GDEMs produced relatively comparable estimates. Next, GDEMs' errors have been computed at the known heights of GCPs (Table 5). It can be noticed that the RMS (Equation (1)) of AEC2, STRMGL1, and NASADEM models equal ±2.5 meters approximately, while the ASTER model produces the highest RMS of ±5.1 meters. Concerning the average heights error, it can be seen that the NASADEM produce the smallest value of 1.8 meters compared to the other three models. The errors distribution has been plotted in Figure 5 for all GDEMs, which emphasizes the overall performance of the investigated GDEMs. It can be realized from that figure that the performance of the ASTER model is far from those of the other models.

Comparing the RMS values of the investigated GDEMs (Table 5) with the required vertical accuracy of utilized datasets (Table 1), it can be concluded (Table 6) that all GDEMs are not suitable for developing contour intervals less than 5 meters. That means that such models should not be utilized for topographic mapping of scale 1:25,000 or larger. For map scale 1:50,000 and 1:100,000 with contour intervals 8 or 10 meters, it can be seen that the ASTER model should be avoided while the other three models meet the required specifications. Additionally, it is clear that for map scales 1:250,000 or smaller, all investigated GDEMs could be utilized.

As mentioned previously, the Nile delta region represents a flat area in terms of topography. Hence, the same steps have been carried out to investigate the performance of GDEMs over Makkah city as a moderate-topography region. Table 7, Table 8 and Figure 6 present the accomplished findings based on the

Table 4. Statistics of height sources in Nile Delta Area.

Item	Minimum	Maximum	Relief	Mean	RMS
Observed Heights	−1.925	21.950	23.875	8.532	±5.814
ASTER v.3	−12.495	32.323	44.818	10.680	±5.565
ACE2	−6.659	27.153	33.812	6.244	±6.058
STRMGL1 v.3	−6.900	23.561	30.461	6.561	±6.139
NASADEM_HGT v.1	−5.900	23.922	29.822	6.776	±6.608

Table 5. Statistics of GDEM2 height errors in Nile Delta Area.

Item	Minimum	Maximum	Range	Mean	RMS
ASTER v.3	−19.901	18.895	38.796	-2.148	±5.108
ACE2	−11.518	9.248	20.766	2.288	±2.618
STRMGL1 v.3	−6.320	9.500	15.820	1.971	±2.584
NASADEM_HGT v.1	−5.438	9.243	14.681	1.756	±2.521

Table 6. Validity of GDEM2 for topographic mapping in Nile Delta Area.

Map Scale	Contour Interval (m)	Valid GDEMs
1:5000	1.25	NA
1:10,00	2.0/5.0	
1:25,000	5.0	
	8.0/10.0	ACE2, SRTMGL1 v.3, NASADEM_HGT v.1
1:50,000		
1:100,000	10.0	
	20.0	ASTER v.3, ACE2, SRTMGL1 v.3, NASADEM_HGT v.1
1:250,000	25.0	
	50.0	

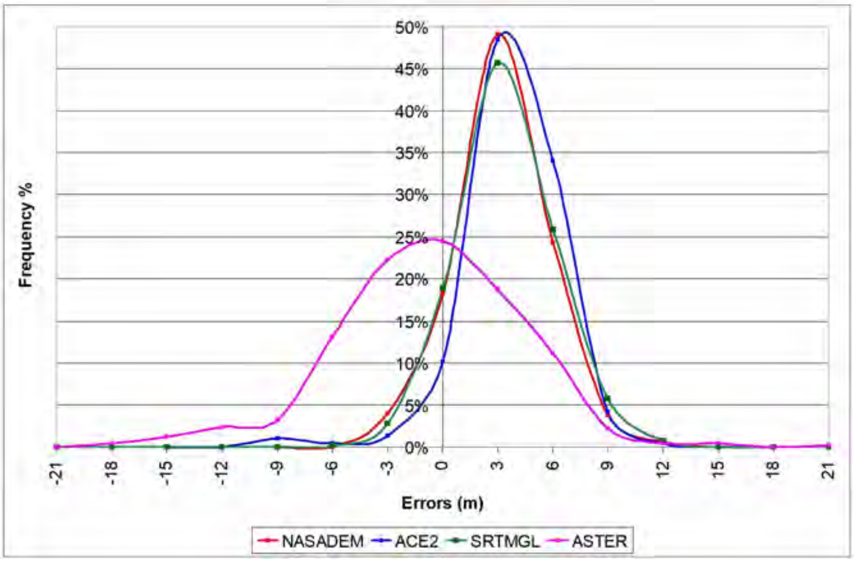

Figure 5. Histograms of height errors of GDEM2 in Nile delta area.

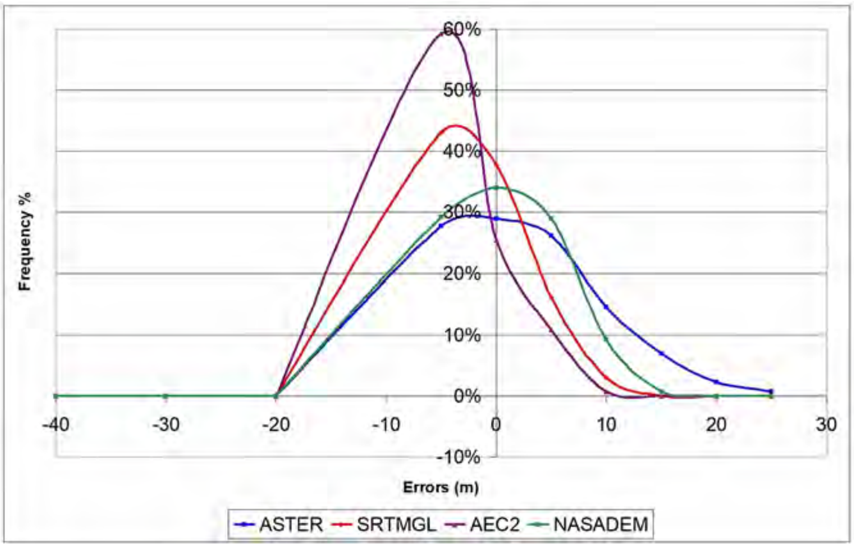

Figure 6. Histograms of height errors of GDEM2 in Makkah area.

Table 7. Statistics of height sources in Makkah Area.

Item	Minimum	Maximum	Relief	Mean	RMS
Observed Heights	147.135	423.187	274.823	272.146	±59.189
ASTER v.3	144.185	419.008	274.823	272.146	±59.189
ACE2	150.695	422.845	272.150	278.933	±60.068
STRMGL1 v.3	140.482	424.860	284.378	276.082	±59.541
NASADEM_HGT v.1	148.267	419.924	271.657	273.295	±59.005

Table 8. Statistics of GDEM2 height errors in Makkah Area.

Item	Minimum	Maximum	Range	Mean	RMS
ASTER v.3	−18.456	22.830	41.286	−0.334	±7.996
ACE2	−34.463	5.948	40.412	−7.121	±6.675
STRMGL1 v.3	−16.680	7.820	24.500	−4.270	±5.161
NASADEM_HGT v.1	−13.839	11.219	25.058	−1.483	±5.243

available datasets. It can be noticed from Table 7 that only the SRTMGL1 model produced relief estimates far from the observed precise one. For the mean height error, only the ACE2 model differs a little bit from the other three GDEMs. However, the results of height differences over known GCPs (Table 8) are more important to analyze the GDEMs precision. It can be realized that NASADEM and SRTMGL produced the smallest RMS values, while the ASTER model gives the largest one. Comparing error histograms over both study areas (Figure 5 and Figure 6), it can be noticed that the performance of the investigated GDEMs is more precise over the flat region in the Nile delta than that of the moderate-topography region in Makkah city. This conclusion is evident, too, when comparing the RMS values of GDEMs over both regions. In the Nile delta, the RMS ranges from ±2.5 and ±5.0 meters, while in Makkah RMS varies between ±5.2 and ±8.0 meters approximately. Hence, it can be concluded that the accuracy of the investigated GDEMs is almost one order worse in moderate topography regions than flat areas.

Again, a comparison has been performed between the RMS values of the investigated GDEMs in Makkah (Table 8) with the required vertical accuracy of utilized datasets (Table 1). It can be seen from Table 9 that all GDEMs are not suitable for developing contour intervals less than 5 meters. That means that such models are not suitable for topographic mapping of scale 1:50,000 or larger with contour intervals equal or less than 10 meters. For map scale 1:100,000 with contour intervals of 20 meters, it can be seen that the ASTER model should be avoided while the other three models meet the required specifications. From Figure 6, it can be seen that ASTER produced the least-precise frequency pattern of errors over checkpoints compared to other GDEMs. Additionally, it is clear that for map scales 1:250,000 or smaller with contour intervals more than 25 meters, all investigated GDEMs could be utilized. Furthermore, it can be concluded

Table 9. Validity of GDEM2 for topographic mapping in Makkah Area.

<table>
<tr><th>Map Scale</th><th>Contour Interval (m)</th><th>Valid GDEMs</th></tr>
<tr><td>1:5000</td><td>1.25</td><td rowspan="6">NA</td></tr>
<tr><td>1:10,00</td><td>2.0/5.0</td></tr>
<tr><td>1:25,000</td><td>5.0</td></tr>
<tr><td></td><td rowspan="2">8.0/10.0</td></tr>
<tr><td>1:50,000</td></tr>
<tr><td rowspan="2">1:100,000</td><td>10.0</td></tr>
<tr><td>20.0</td><td>ACE2, SRTMGL1 v.3, NASADEM_HGT v.1</td></tr>
<tr><td>1:250,000</td><td>25.0
50.0</td><td>ASTER v.3, ACE2, SRTMGL1 v.3, NASADEM_HGT v.1</td></tr>
</table>

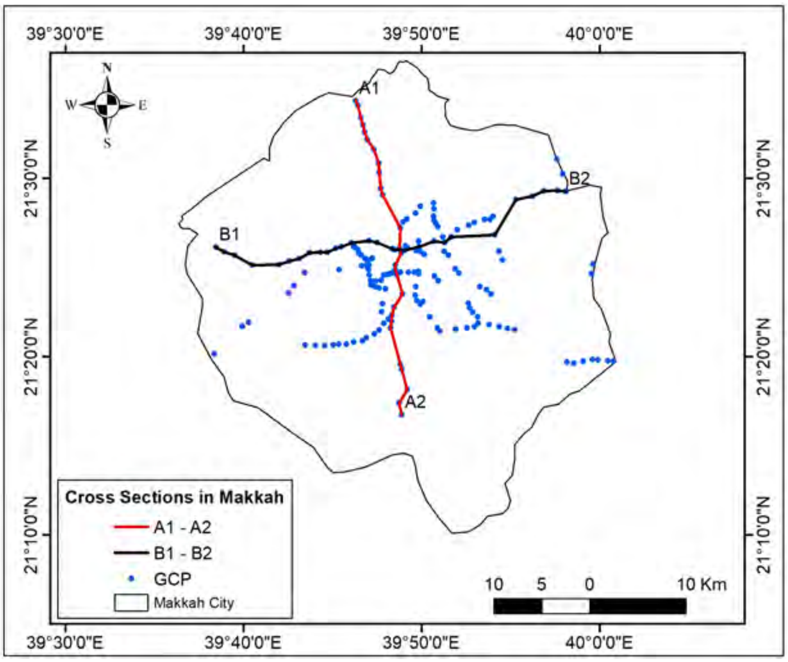

Figure 7. Cross sections in Makkah area.

from Table 6 and Table 9 that the utilization of GDEMs in topographic mapping differs significantly between flat and hilly spatial regions.

For analyzing estimated GDEM-based slopes (Equation (3)) and topographic profiles, two cross-sections have been constructed in Makkah city based on the available GCPs. The first one (B1-B2) runs from west to east passing by 28 GCP, while the other cross-section (A1-A2) runs from north to south along 27 GCP (Figure 7). The length of both cross-sections is approximately 35 kilometers. To investigate the validity of GDEM-based slope estimation along a cross-section, each one is divided by 5-kiolmeters intervals. Equation (4) has been applied to compute the slope validity factor (SV) at each interval for both sections. Figure 8 depicts the accomplished results, that reveals two important remarks. First, all GDEM-based slopes do not match with the actual slopes from known GCP over

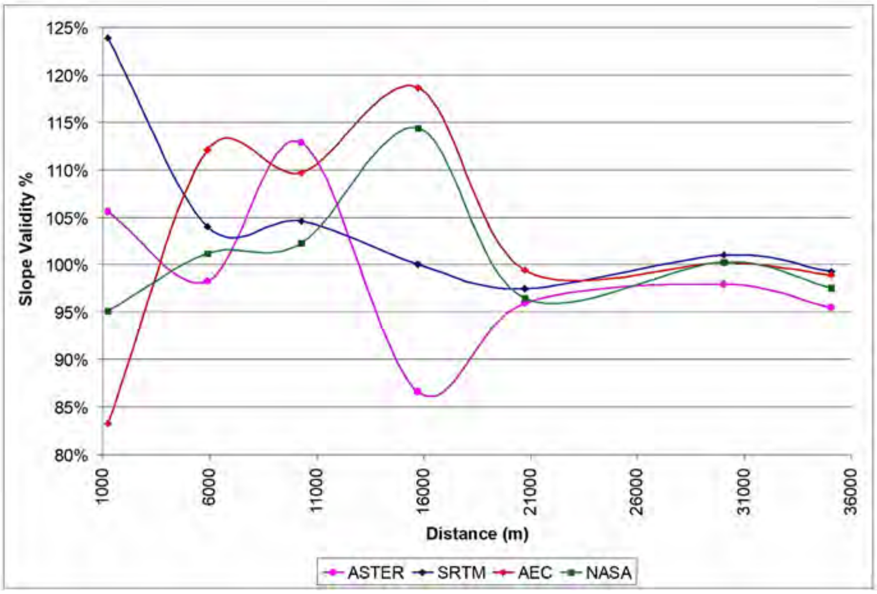

(a)

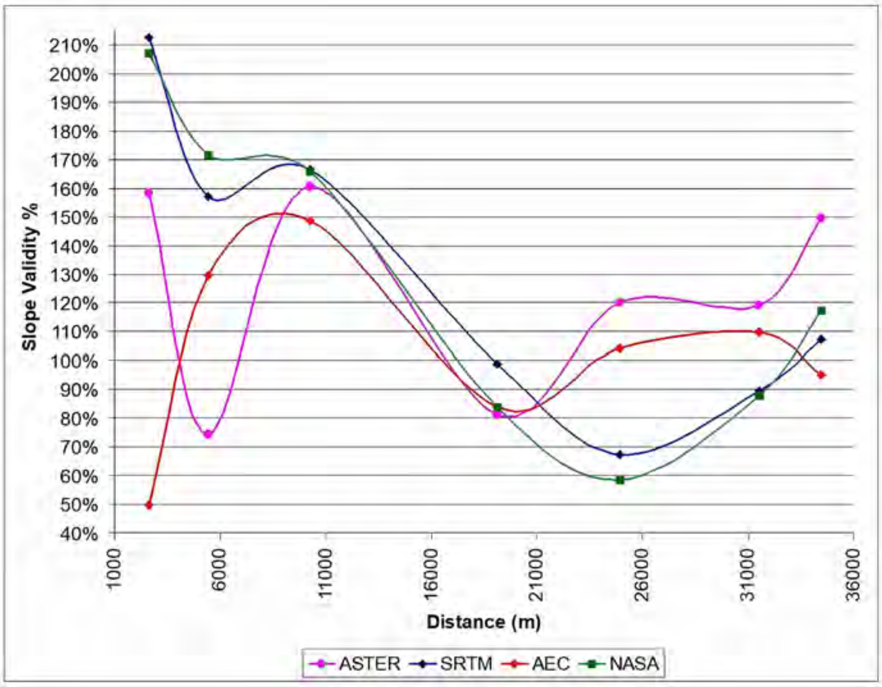

(b)

Figure 8. Slope validity over cross sections in Makkah area.

cross section's length up to 25 and 30 kilometers for both profiles respectively. Second, GDEM-based slopes for profiles more than 30-kilometers length close to the accurate slopes within a value of ±10% approximately. Hence, it can be concluded that GDEMs should not be utilized for developing topographic cross-sections less than 30 kilometers. Additionally, it can be said that GDEMs-based topographic profiles should not be utilized in engineering and geomatics applications that need precise heights and slopes information. Consequently, the attained

findings of the current study, based on the available datasets, showed that GDEMs are not the appropriate heights' source for topographic mapping at medium and large map scales, and could not be utilized for accurate topographic profiling in precise engineering and geomatics applications.

5. Conclusions

Open-source GDEMs have been utilized in the last couple of decades for topographic mapping and several geomatics activities. Specifications of topographic maps rely on the appropriate contour interval on each map scale and the accuracy of the utilized heights information. Examples of topographic mapping standards from several countries have been collected and investigated. The current study aims to examine the validity and reliability of GDEMs-based heights for topographic mapping at several map scales. Particularly, it investigates the performance of GDEMS for contour intervals, slope estimation, and generating topographic profiles needed for engineering and environmental applications in both Egypt and Saudi Arabia.

Two study areas have been utilized to investigate the performance of four GDEMs for topographic mapping at flat and moderate-topography patters. Based on the available datasets in the two study areas, several important findings have been attained. Using known checkpoints, it has been found that the accuracy of investigated GDEMs ranges from ±2.5 and ±5.1 meters in the Nile delta region, while it varies between ±5.1 and ±8.0 meters in the Makkah area. That indicates that the utilization of GDEMs in topographic mapping differs significantly between flat and hilly spatial regions. Based on the contour interval required on several topographic map scales, it has been found that GDEMs are not appropriate for generating contour interval less than 10 meters. Consequently, it is suggested not to use GDEMs for developing topographic maps of scale 1:25,000 or larger in flat regions and map scale 1:50,000 or larger in hilly regions.

In terms of slope estimation and developing a topographic profile, the obtained results revealed that all GDEM-based slopes do not fit the actual slopes from known GCP over cross-section lengths up to 30 kilometers. It has been also observed that GDEM-based slopes for profiles more than 30-kilometers length close to the accurate slopes within a value of ±10% approximately. As a result, it could be concluded that GDEMs are not the appropriate heights' source for topographic mapping at medium and large map scales, and could not be utilized for topographic profiling in precise engineering and geomatics applications.

Conflicts of Interest

The authors declare no conflict of interest regarding the publication of this paper.

References

[1] Ogania, J., Puno, G., Alivio, M. and Taylaran, J. (2019) Effect of Digital Elevation Model's Resolution in Producing Flood Hazard Maps. *Global Journal of Environ-*

mental Science and Management, **5**, 95-106.

[2] Seleem, T. (2013) Analysis and Tectonic Implication of DEM-Derived Structural Lineaments, Sinai Peninsula, Egypt. *International Journal of Geosciences*, **4**, 183-201. https://doi.org/10.4236/ijg.2013.41016

[3] Boulton, S.J. and Stokes, M. (2018) Which DEM Is Best for Analyzing Fluvial Landscape Development in Mountainous Terrains? *Geomorphology*, **310**, 168-187. https://doi.org/10.1016/j.geomorph.2018.03.002

[4] Hasan, E., Khan, S. and Hong, Y. (2015) Investigation of Potential Sea Level Rise Impact on the Nile Delta, Egypt Using Digital Elevation Models. *Environmental Monitoring and Assessment*, **187**, 649. https://doi.org/10.1007/s10661-015-4868-9

[5] Ouerghi, S., ELsheikh, R., Achour, H. and Bouazi, S. (2015) Evaluation and Validation of Recent Freely-Available ASTER-GDEM V.2, SRTM V.4.1 and the DEM Derived from Topographical Map over SW Grombalia (Test Area) in North East of Tunisia. *Journal of Geographic Information System*, **7**, 266-279. https://doi.org/10.4236/jgis.2015.73021

[6] Al-Karagy, E. and Dawod, G. (2021) Optimum Combinations of GGM and DEM Models for Precise National Geoid Development. *Proceedings of Engineering and Technology Innovation*.

[7] Dawod, G. and Al-Ghamdi, K. (2017) Reliability of Recent Global Digital Elevation Models for Geomatics Applications in Egypt and Saudi Arabia. *Journal of Geographic Information System*, **9**, 685-698. https://doi.org/10.4236/jgis.2017.96043

[8] Kulp, S. and Strauss (2016) Global DEM Errors Underpredict Coastal Vulnerability to Sea Level Rise and Flooding. *Frontiers in Earth Science*, **4**, 36. https://doi.org/10.3389/feart.2016.00036

[9] Patel, A., Katiyar, S. and Prasad, V. (2016) Performances Evaluation of Different Open Source DEM Using Differential Global Positioning System (DGPS). *The Egyptian Journal of Remote Sensing and Space Sciences*, **19**, 7-16. https://doi.org/10.1016/j.ejrs.2015.12.004

[10] Hu, Z., Peng, J., Hou, Y. and Shan, J. (2017) Evaluation of Recently Released Open Global Digital Elevation Models of Hubei, China. *Remote Sensing*, **9**, 262. https://doi.org/10.3390/rs9030262

[11] Church, J., Clark, P., Cazenave, A., Gregory, J, Jevrejeva, S., Levermann, A., Merrifield, M., Milne, G., Nerem, R., Nunn, P., Payne, A., Pfeffer, W., Stammer, D. and Unnikrishnan, A. (2013) Sea Level Change. In: *Climate Change* 2013: *The Physical Science Basis*. *Contribution of Working Group I to the Fifth Assessment Report of the Intergovernmental Panel on Climate Change* (*IPCC*), Cambridge University Press, Cambridge, 1137-1216.

[12] Abdel-Aziz, T., Dawod, G. and Ebaid, H. (2020) DEMs and Reliable Sea Level Rise Risk Monitoring in Nile Delta, Egypt. *Discover Sustainability*, **1**, Article No. 6. https://doi.org/10.1007/s43621-020-00006-7

[13] Sande, B., Lansen, J. and Hoyng, C. (2012) Sensitivity of Coastal Flood Risk Assessments to Digital Elevation Models. *Water*, **4**, 568-579. https://doi.org/10.3390/w4030568

[14] Zhang, J. and Chu, X. (2015) Impact of DEM Resolution on Puddle Characterization: Comparison of Different Surfaces and Methods. *Water*, **7**, 2293-2313. https://doi.org/10.3390/w7052293

[15] Survey of India (2009) Handbook of Topography. http://www.iism.nic.in/Documents/soichapter-xi.pdf

[16] ASPRS (American Society for Photogrammetry and Remote Sensing) (2015) ASPRS Positional Accuracy Standards for Digital Geospatial Data. Edition 1, Version 1. *Photogrammetric Engineering and Remote Sensing*, **81**, A1-A26. https://doi.org/10.14358/PERS.81.3.A1-A26

[17] Geoscience Australia (2021) National Topographic Database Structure and Specifications. http://www.ga.gov.au/mapspecs/topographic/v6/section1.html#MinimumPlanimetricElevationAccuracies

[18] JICA (Japan International Cooperation Agency) (2013) The Study on Establishing Digital Topographic Database for Bujumbura City, Burundi. A Technical Report. https://openjicareport.jica.go.jp/pdf/12121588_01.pdf

[19] NDMA (National Disaster Management Authority) (2016) National Technical Document Fir Establishing Cartographic Database in India: Generation of Large Scale (1:10,000 and 1:2,000 and Leaser) Maps for Disaster Management and Planning. A Technical Report. http://www.ndma.gov.in/sites/default/files/PDF/Technical%20Documents/national-technical-document-for-establishing-cartographic-base-in-india.pdf

[20] USGS (US Geological Survey) (1999) Map Accuracy Standards: Fact Sheet FS-171-99. A Technical Report. https://pubs.usgs.gov/fs/1999/0171/report.pdf

[21] Qatar GIS Center (2009) Qatar Survey Manual Version 1. A Technical Report, Qatar.

[22] ESA (Egyptian Survey Authority) (2020) Technical Specifications of Surveying and Mapping: Part 2: Topographic Maps. A Technical Report, Giza.

[23] Khal, M., Algouti, A., Algouti, A., Akdim, N., Stankevich, S. and Menenti, M. (2020) Evaluation of Open Digital Elevation Models: Estimation of Topographic Indices Relevant to Erosion Risk in the Wadi M'Goun Watershed, Morocco. *Geosciences*, **6**, 231-257. https://doi.org/10.3934/geosci.2020014

[24] Cahyaningsih, C., Crensonni, P., Suryadi, A., Kausarian, H., Choanji, T., Yuskar, Y. and Putra, D. (2019) Geomorphology and Structural Geology Characterization of Landslide Prone Area in Riau-West of Sumatra Highway. *IOP Conference Series Materials Science and Engineering*, **536**, Article ID: 012063. https://doi.org/10.1088/1757-899X/536/1/012063

[25] Mokarram, M. and Hojati, M. (2016) Comparison of Landform Classifications of Elevation, Slope, Relief and Curvature with Topographic Position Index in the South of Bojnoord. *Ecopersia*, **2**, 1343-1357. https://doi.org/10.18869/modares.ecopersia.4.2.1343

[26] USGS (US Geological Survey) (2021a) SRTMGL1 V003. https://lpdaac.usgs.gov/products/srtmgl1v003

[27] Smith, R. and Berry, P. (2019) Altimeter Corrected Elevations, Version 2. https://sedac.ciesin.columbia.edu/data/set/dedc-ace-v2

[28] US Open Data Catalouge (2021) ASTER Digital Elevation Model V003. https://catalog.data.gov/dataset/aster-digital-elevation-model-v003

[29] USGS (US Geological Survey) (2021b) NASADEM_HGT: Merged DEM Global 1 Arc Second v. 1. https://lpdaac.usgs.gov/products/nasadem_hgtv001

La Validité des Élévations Open-Source pour Différentes Échelles de Cartes Topographiques et Applications Géomatiques

Gomaa Mohammed Dawod*
Ibrahim Elsayed Ascoura**

RÉSUMÉ

Cet article présente une analyse de quatre modèles d'élévation numériques mondiaux (MNE) open source et les compare sur deux profils topographiques (régions presque plates et collines) pour des applications en cartographie et en géomatique. L'objectif principal est de vérifier si les hauteurs, les intervalles de courbes de niveaux, les pentes et les profils topographiques basés sur les MNE sont valides pour toutes les échelles de la cartographie topographique, ce qui constitue un problème majeur dans les activités de cartographie. Deux études de cas, le delta du Nil en Égypte et la ville de La Mecque en Arabie Saoudite, ont été utilisées pour représenter des sites à topographie plate et modérée. Les MNE mondiaux étudiés incluent les modèles les plus récents: ASTER v.3, ACE 2, SRTMGL1 v.3, et NASADEM_HGT v.1 publiés en 2019 et 2020 avec des résolutions spatiales de 1 et 3 secondes d'arc. Les points de contrôle au sol précis disponibles (Ground Control Points, *GCP*) comprennent 540 stations dans le delta du Nil et 175 stations à La Mecque. Sur la base des ensembles de données disponibles dans deux zones d'étude, il a été constaté que la précision des MNE étudiés sur les points de contrôle connus varie de ±2.5 à ±5.1 mètres dans la région du delta du Nil, alors qu'elle varie entre ±5.1 et ±8.0 mètres dans la zone de La Mecque. Cela indique que l'utilisation des MNE dans la cartographie topographique diffère considérablement entre les régions plates et les zones vallonnées. Par conséquent, il est recommandé d'éviter d'utiliser les MNE pour développer des cartes topographiques à l'échelle 1:25000 ou plus dans les régions plates et à l'échelle 1:50000 ou plus dans les régions vallonnées. De plus, les résultats obtenus ont montré que toutes les pentes basées sur les GDEM ne correspondent pas aux pentes réelles du GCP connu sur une longueur de section allant jusqu'à 30 kilomètres. Ainsi, il est conclu que les MNE ne sont pas une source appropriée de données altimétriques pour la cartographie topographique à moyenne et grande échelle, et ne devraient pas être utilisés pour le profilage topographique dans des applications d'ingénierie et de géomatique précises. **[Bul. Soc. Géog. d'Égypte, 2021, 94: 1-23]**

Mots-clés: Carte topographique, MNE, altitudes, échelles cartographiques, intervalle de courbes de niveaux.

---

* Professeur, Institut de Recherche d'Arpentage, Centre National de Recherche sur l'Eau, Gizeh, Égypte.

* Professeur Assistant, Département de Géographie, Faculté des Sociales Sciences, Université d'Umm Al Qura, KSA.

For Correspondence: e-mail: ieascoura@uqu.edu.sa

1. Introduction

Les cartes topographiques représentent un type principal de cartes utilisées dans de nombreuses applications géomatiques, telles que les projets d'ingénierie, la modélisation hydrologique, l'évaluation des risques de catastrophe, l'analyse géomorphologique et hydrogéologique et les applications environnementales. Les courbes de niveau représentent une information vitale apparaissant sur les cartes topographiques imprimées et numériques. Elles représentent les variations topographiques du terrain et permettent d'estimer les altitudes des points aléatoires requis. De nos jours, la forme la plus fréquente de stockage et d'analyse des ensembles de données altimétriques est le modèle numérique d'élévation (MNE). Il est bien connu que les hauteurs utilisées pour générer les courbes de niveau peuvent être obtenues à partir d'un large éventail de sources, notamment des levés terrestres, des données des systèmes mondiaux de navigation par satellite (Global Navigation Satellite Systems, *GNSS*), des photographies aériennes, des images satellite et des MNE. En outre, les systèmes d'information géographique (SIG) permettent la manipulation, le traitement et l'analyse des MNE pour générer de nombreux dérivés (outputs) pour la cartographie topographique du terrain, dont la génération de courbes de niveau pour une large gamme d'applications. Certaines de ces applications comprennent la production de cartes des risques d'inondation)Ogania et al., 2019), la cartographie des linéaments et structures géologiques)Seleem, 2013), l'analyse du paysage fluvial dans les régions montagneuses (Boulton et Stokes, 2018), le suivi des impacts de l'élévation du niveau de la mer (Hasan et al., 2015), la production de cartes topographiques (Ouerghi et al., 2015) et la modélisation du géoïde (Al-Karagy et Dawod, 2021).

Dans de nombreux pays en développement, des modèles MNE nationaux précis peuvent exister mais ne sont pas accessibles pour un usage public. Ainsi, les chercheurs utilisent généralement les MNE globaux gratuits open-source disponibles. Au cours des dernières décennies, de nombreux types de MNE, avec des couvertures et des résolutions spatiales variables, ont été produits et rendus librement accessibles sur des sites Web. Parmi ces MNE on peut citer: Shuttle Radar Topography Mission (SRTM), Advanced Spaceborne Thermal Emission and Reflection Radiometer (ASTER), EarthEnv-DEM90, Global Multi-resolution Terrain Elevation Data 2010 (GMTED2010), Global Land One-km Base Elevation (GLOBE), Global 30 secondes d'arc (GTOPO30) et Advanced Land Observing Satellite (ALOS)-based World 3D - 30 m (AW3D30).

La précision des MNE open source joue un rôle essentiel dans leur utilisation pour la cartographie et les études environnementales. Ainsi, de nombreuses études et recherches se sont concentrées sur l'estimation de la précision et de l'exactitude des MNE. Dawod et Al-Ghamdi (2017) ont

examiné la fiabilité de huit MNE globaux pour des applications géomatiques en Égypte et en Arabie Saoudite. Les résultats ont montré que leur précision, en termes d'écart type sur les points de contrôle, est comprise entre ±1.9 et ±6.6 mètres. Des résultats similaires ont été rapportés dans d'autres régions telles que les États-Unis (Kulp et Strauss, 2016), l'Inde (Patel et al., 2016) et la Chine (Hu et al., 2017).

Plutôt que les cartes topographiques imprimées ou numériques, plusieurs applications Géomatiques notamment, utilisant les SIG, reposent sur une représentation numérique de la topographie. De telles activités nécessitent un niveau de précision altimétrique en fonction de leurs objectifs et de l'étendue spatiale de la zone d'étude. L'utilisation de MNE peut ne pas convenir aux applications géomatiques de haute précision. L'impact de l'élévation du niveau de la mer (Sea Level Rise, *SLR*) dans des régions petites ou modérées en est un exemple typique. On sait que le SRL moyen anticipé sur une base globale en 2081-2100 est estimé entre 0.40 et 0.63 mètre par rapport au niveau 1986-2005 (Church et al., 2013). La surveillance et l'estimation des impacts des risques d'une si petite élévation du niveau de la mer nécessitent une représentation du terrain de haute précision. Abdel Aziz et al. (2020) ont étudié la fiabilité de quelques MNE dans la délimitation des régions inondées en cas d'élévation du niveau de la mer dans la région du delta du Nil. Il a été constaté que la fiabilité de trois modèles globaux étudiés, par rapport à un modèle numérique de terrain (MNT) local de haute précision, est inférieure à 20%. Des résultats similaires ont été rapportés par d'autres chercheurs dans d'autres régions (Sande et al., 2012). Un autre exemple est l'utilisation de MNE de faible précision dans les applications d'ingénierie. Zhang et Chu (2015) ont souligné que la quantification précise du stockage de la dépression de surface dépend de manière significative des caractéristiques topographiques basées sur le modèle numérique d'élévation MNT, principalement de la précision verticale et de la résolution spatiale. D'autre part, il existe certaines applications géomatiques qui pourraient être réalisées en utilisant la précision de quelques mètres des MNE. La reconnaissance, la planification de projets pour des régions spatiales moyennes ou grandes, la modélisation hydrologique, l'estimation du ruissellement de surface et la modélisation du géoïde pourraient être des exemples de telles activités.

L'objectif de cette recherche est d'étudier la précision absolue et la validité des données d'altitude provenant de différentes sources pour la génération de courbes de niveaux pour des cartes topographiques à différentes échelles. De plus, l'étude s'intéresse à deux autres facteurs topographiques, à savoir la pente et les sections transversales, largement utilisés dans de nombreuses applications géomatiques. Cela constitue une préoccupation vitale dans la cartographie topographique pour déterminer si les courbes de niveaux

et les profils topographiques basés sur les MNE open source pourraient être utilisés pour toutes les échelles de carte et les applications géomatiques. En ce qui concerne les auteurs, il pourrait s'agir de la première étude de recherche, du moins en Égypte, à aborder un sujet aussi important.

2. Normes et Spécifications des Cartes Topographiques

Des normes et des spécifications ont été développées dans le monde entier pour les caractéristiques des courbes de niveau, y compris la précision des données collectées et les méthodes de représentation de ces lignes importantes. Les intervalles des courbes de niveau à afficher sur une carte varient en fonction de l'échelle définie. Le terme intervalle des courbes de niveau ou équidistance représente la distance verticale ou la différence d'élévation entre deux courbes de niveau successives. L'échelle d'une carte est le rapport entre la longueur d'une ligne sur la carte et sa longueur réelle au sol. Traditionnellement, les cartes topographiques sont dessinées à des échelles cartographiques moyennes telles que 1:5000, 1:10000, 1:25000 et 1:50000. De manière générale, la sélection de l'intervalle des courbes de niveau approprié pour une carte spécifique dépend de plusieurs facteurs, notamment l'échelle de la carte, l'étendue de la zone étudiée, la nature de la topographie, le nombre et la distribution de l'ensemble de données de hauteur disponible, et le but de la carte lui-même (Survey of India, 2009). En règle générale, l'intervalle des courbes de niveau approprié sur une carte peut être estimé à trois fois l'erreur quadratique moyenne (Root Mean Square Error, *RMSE*) des données de hauteur d'entrée utilisées (ASPRS, American Society for Photogrammetry and Remote Sensing, 2015). La précision verticale est représentée par le RMSE des ensembles de données de hauteur utilisés selon l'équation:

$$RMSE = \sqrt{\frac{\sum_{1}^{n} (P_i - O_i)^2}{n}} \quad (1)$$

où P_i et O_i sont respectivement la hauteur prédite et observée du point i , et n le nombre total de points.

Des exemples de normes et de spécifications de cartes topographiques, en particulier pour les caractéristiques des courbes de niveau, sont résumés ici. Les spécifications de la carte australienne indiquent que la précision d'altitude minimale des ensembles de données pour générer des courbes de niveau est de 5, 10, 25 mètres pour les échelles de carte 1:25000, 1:100000 et 1:250000 respectivement (Geoscience Australia, 2021). Au Burundi, les intervalles des courbes de niveau pour les cartes topographiques 1:5000 et 1:25000 sont respectivement de 5 et 10 mètres et la précision verticale de ces

courbes de niveau sont respectivement inférieures à 2.5 et 5.0 mètres (JICA, Japan International Cooperation Agency, 2013). De plus, les intervalles des courbes de niveau suggérés en Inde pour les cartes 1:5000, 1:10000 1:25000 et 1:50000 sont respectivement de 1.25, 5.0, 8.0 et 15 mètres (NDMA, National Disaster Management Authority, 2016). En outre, l'Institut d'études géologiques des États-Unis (United States Geological Survey, *USGS*) déclare que la norme de précision verticale exige que l'élévation de 90 pour cent de tous les points de hauteur utilisés soit correcte dans la moitié de l'intervalle des courbes de niveau (USGS, US Geological Survey, 1999). De plus, les spécifications cartographiques de l'État du Qatar a défini les intervalles des courbes de niveau appropriés de 2 m, 5 m et 10 m pour les échelles cartographiques 1:5000, 1:10000 et 1:200000 respectivement. De plus, le RMSE des hauteurs utilisées dans la cartographie topographique est un tiers de l'intervalle des courbes de niveau requis (Qatar GIS Center, 2009).

Au niveau national, l'Egyptian Survey Authority (ESA) a publié en 2020 les spécifications mises à jour des cartes topographiques (ESA, Egyptian Survey Authority, 2020). Pour les courbes de niveau des cartes topographiques, les normes égyptiennes stipulent que le RMSE des ensembles de données utilisés pour générer les courbes de niveau doit être inférieur à un tiers de l'intervalle des courbes de niveau. Les intervalles des courbes de niveau utilisés pour les échelles de carte 1:10000, 1:25000, 1:50000, 1:100000 et 1:250000 sont respectivement de 2, 5, 10, 20, 50 mètres. Si les courbes de niveau ne sont pas affichées aux échelles de carte 1:5000 et 1:2500, les hauteurs ponctuelles doivent être tracées sur tous les 100 et 50 m horizontalement avec des niveaux de précision verticale équivalents respectivement à 0.75 et 0.40 mètre. Pour conclure ce point, le tableau (1) présente des exemples typiques d'intervalle des courbes de niveau et de précision verticale utilisés dans la production de cartes topographiques avec plusieurs échelles cartographiques dans le monde entier.

Le relief, la pente et les sections transversales constituent des facteurs importants pour caractériser la topographie d'une region (Khal et al., 2020). Le relief, R, est la différence de hauteur entre les hauteurs maximale (Hmax) et minimale (Hmin) de la région. La pente entre deux points est leur différence de hauteur divisée par la distance horizontale entre eux. La pente peut être évaluée en unités de degrés ou en pourcentage selon l'équation (3):

$$R = H_{max} - H_{min} \qquad (2)$$

Tableau 1. Normes types des cartes topographiques.

Echelle	Intervalle des courbes de niveau	Précision verticale (m)
1 : 5 000	1.25	±0.4
1 : 10 000	2.0/5.0	±0.7/±1.7
1 : 25 000	5.0/8.0/10.0	±1.7/±2.6/±3.3
1 : 50 000	10.0	±3.3
1 : 100 000	10.0/20.0	±3.3/±6.7
1 : 125 000	25.0/50.0	±8.3/±16.7

$$S = \frac{\Delta H}{D} x100 \qquad (3)$$

De plus, un nouveau facteur appelé (Slope Validity, *SV*) est proposé, ici, pour comparer les performances des pentes estimées basées sur des MNE par rapport aux pentes précises. Il est calculé comme le pourcentage de la pente, entre deux points, à partir des deux MNE et des hauteurs précises connues à ces points de contrôle, comme suit:

$$SV_{GDEM} = \frac{S_{GDEM}}{S_{known}} x100 \qquad (4)$$

Concernant la topographie du terrain, elle pourrait être divisée en classes selon plusieurs facteurs tels que la pente. Le **tableau (2)** présente un exemple d'unités topographiques basées sur les pentes (Cahyaningsih et al., 2016).

3. Méthodologie et Source de Données

Les modèles numériques d'élévation (MNE) utilisés, ici, incluent les données NASADEM_HGT v. 1, SRTMGL1 v. 3, ASTER v. 3 et ACE2. Ils constituent les MNT globaux les plus récents au moment de la réalisation de cette recherche. **Le tableau (3) résume** les caractéristiques de ces MNT sélectionnés, notamment:

1) **SRTM:** Shuttle Radar Topography Mission (SRTM) est un MNT global, qui a deux versions: SRTM 1 avec une résolution spatiale de 1 seconde d'arc, *i.e.*, soit environ 30 mètres, et le modèle SRTM 3 avec une résolution de 3 secondes d'arc. SRTMGL1 v. 3 (USGS, US Geological Survey, 2021a) a été utilisé ici. (Téléchargeable gratuitement depuis, le site; https://earthexplorer.usgs.gov/).

2) **ACE2:** The Altimeter Corrected Elevations (L'Altimètre Corrigé Elévations), Version 2 est un modèle d'élévation numérique global créé par fusion synergique de l'ensemble de données SRTM avec l'Altimétrie Radar Satellite dans la région délimitée par les coordonnées 60°N et 60°S. ACE2 a été développé à des résolutions de 3.9 et 30 secondes d'arc et 5 minutes d'arc (Smith et Berry, 2019). La résolution de 3 secondes d'arc a été utilisée les MNE sont disponibles en téléchargement à partir du site https://sedac.ciesin.columbia.edu/data/set/dedc-ace-v2).

3) **ASTER:** The Advanced Spaceborne Thermal Emission and Reflection Radiometer (Le radiomètre spatial avancé d'émission et de réflexion thermique (ASTER) est un MNT global de résolution d'une seconde d'arc (US Open Data Catalouge, 2021). La version 3 d'ASTER a été rendue publique en 2019 (téléchargeable depuis le site, https://asterweb.jpl.nasa.gov/gdem.asp).

4) **NASADEM_HGT v. 1:** Un MNE développé par la National Aeronautics and Space Administration (NASA) des États-Unis en collaboration avec des agences allemandes et italiennes, et publié en 2020. Il est basé sur un traitement amélioré et la fusion de plusieurs sources de données telles que SRTM, ASTER, Ice, Cloud, et Land Elevation Satellite (ICESat) et autres sources (USGS, US Geological Survey, 2021b). Il peut être téléchargé à partir de https://search.earthdata.nasa.gov/.

La principale zone d'étude est la région du delta du Nil, en Égypte. Elle s'étend de la ville de Damiette à l'est jusqu'à la ville d'Alexandrie le long de la mer Méditerranée et s'étend au sud jusqu'au Caire (Figure 1a). 540 GCP avec des hauteurs précises, à ±0.05 mètre, ont été collectés dans le delta du Nil. Les quatre MNE ont été téléchargés, à partir de leur site Web, pour cette région. Tout d'abord, le modèle topographique de la région a été étudié en utilisant le logiciel Arc GIS 10.4.1 pour convertir les hauteurs basées sur MNE en pourcentages de pente. Il a été constaté que la pente moyenne du delta du Nil est de 3.1% (Figure 1b) ce qui indique que sa topographie pourrait être considérée comme une classe modérée ou de plateaux (Tableau 2). Par conséquent, une autre zone d'étude a été ajoutée. Elle représente la ville de La Mecque dans la région sud-ouest du Royaume d'Arabie Saoudite (KSA) à environ 70 km à l'est de la ville de Djeddah sur la mer Rouge (Figure 2a). 175 GCP avec des hauteurs précises, de ±0.05 mètre, ont été collectés à La Mecque. De même, les quatre MNE ont été téléchargés et les pentes topographiques ont été estimées (Figure 2b). Il a été constaté que la

pente moyenne de la Mecque est de 17.4%, ce qui indique que sa topographie pourrait être considérée comme une classe élevée ou de collines.

Après avoir téléchargé les grilles spatiales des quatre MNE étudiés pour les deux zones d'étude (Figures 3 et 4), leurs hauteurs interpolées aux points de contrôle au sol (GCP) disponibles ont été comparées aux hauteurs précises connues en utilisant le Logiciel Arc GIS 10. Les résultats obtenus sont présentés et étudiés dans la section suivante.

Tableau 2. Classes topographiques basés sur la pente.

Classe topographique	Type de pente	Pente (%)
Basses-terres	Douce	<3%
Plateaux	Modérée	3% - 8%
Hautes terrasses	Modérée	8% - 12%
Collines	Forte	12% - 40%
Montagnes	Très forte	> 40 %

Tableau 3. Caractéristiques des MNT globaux utilisés.

MNE	Année	Résolution spatiale	
		Seconde d'arc	Mètre
ASTER v.3	2019	1"	~30
ACE2	2019	3"	~90
SRTMGL1 v. 3	2019	1"	~30
NASADEM_HGT v. 1	2020	1"	~30

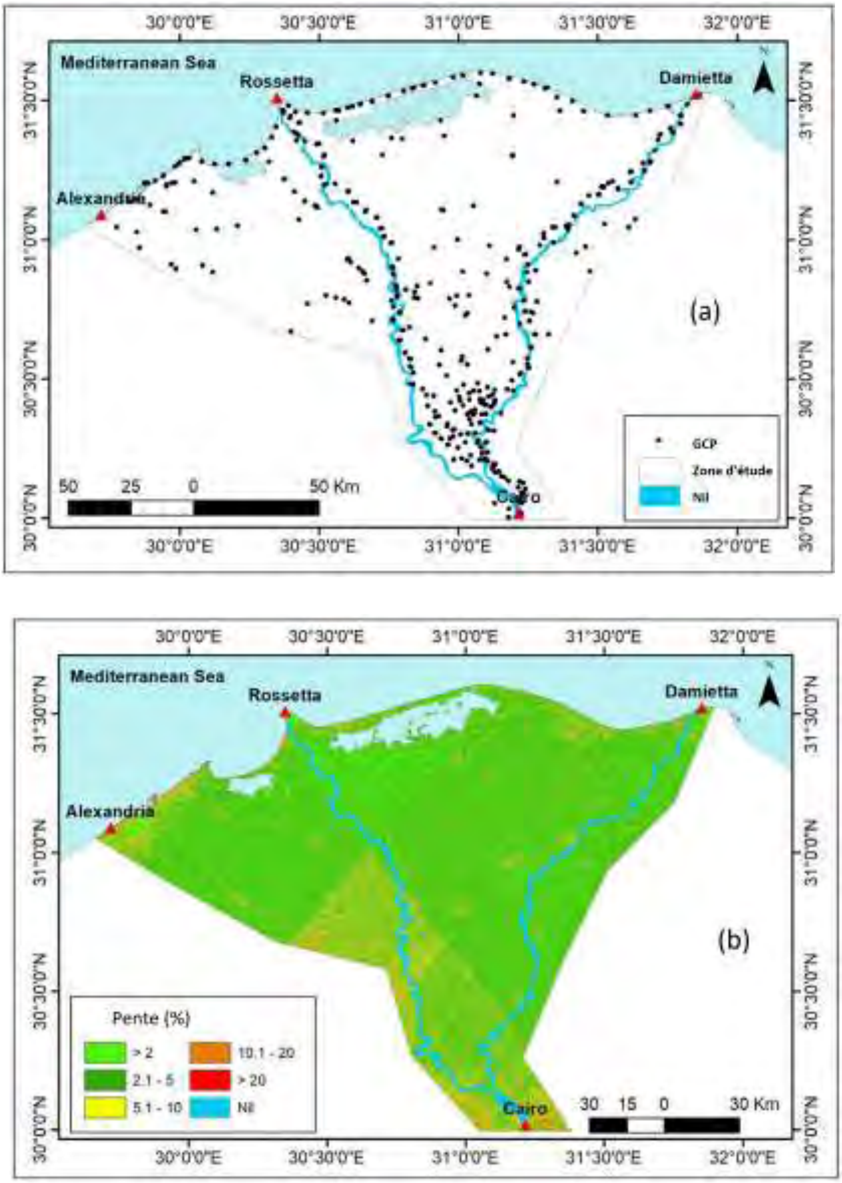

Figure 1. Zone d'étude du delta du Nil.
(a) Données disponibles; (b) Topographie.

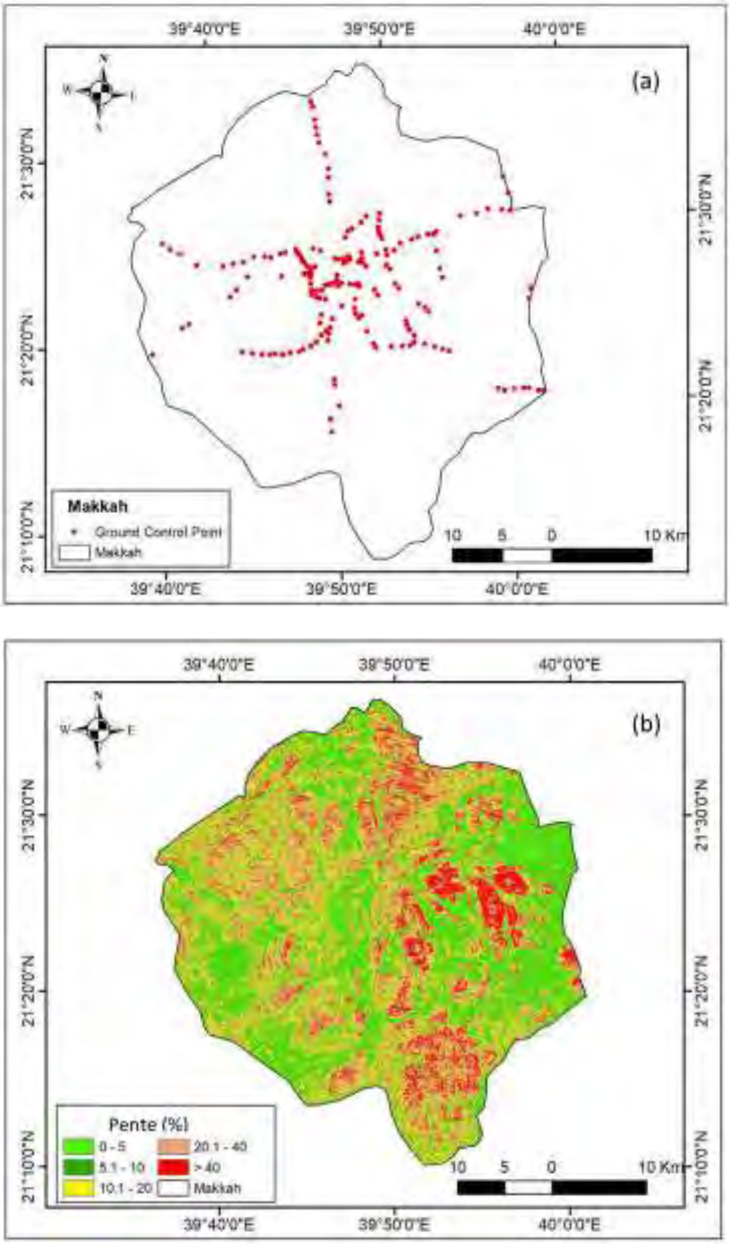

Figure 2. Zone d'étude de la Mecque.
(a) Données disponibles; (b) Topographie

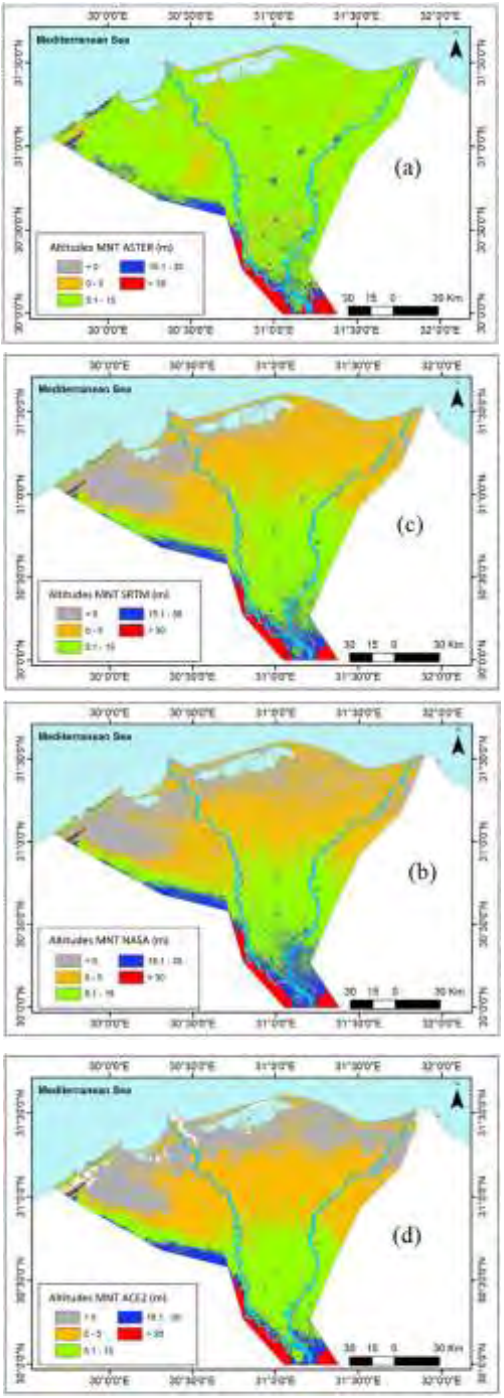

Figure 3. Topographie du delta du Nil à partir des MNE.
(a) ASTER; (b) NASADEM; (c) SRTM; (d) ACE2.

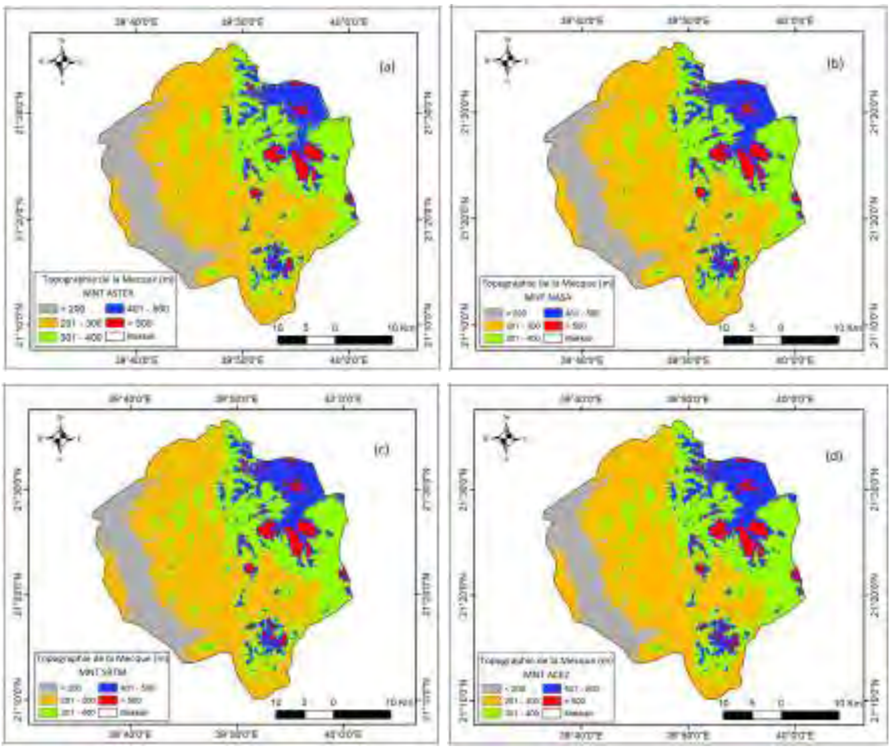

Figure 4. Topographie de La Mecque à partir des MNE.
(a) ASTER; (b) la NASA; (c) SRTM; (d) AEC2.

4. Résultats et Discussion

Le tableau (4) présente les statistiques des hauteurs observées et basées sur le MNE dans la région du delta du Nil. De manière générale, on peut remarquer que la hauteur moyenne et le relief (équation (2)) du seul MNE ASTER ne sont pas proches de ceux des hauteurs observées, tandis que les trois autres MNE ont produit des estimations relativement comparables. Ensuite, les erreurs des MNE ont été comparées aux hauteurs connues des GCP (Tableau 5). On peut remarquer que le RMSE (Équation (1)) des modèles AEC2, STRMGL1 et NASADEM est égal à ±2.5 mètres environ, tandis que le modèle ASTER produit le RMSE le plus élevé (±5.1 mètres). Concernant l'erreur de hauteur moyenne, on peut voir que le MNT NASA produit la plus petite valeur de 1.8 mètre par rapport aux trois autres modèles. La distribution des erreurs a été tracée sur la figure (5) pour tous les MNE, ce qui met l'accent sur les performances globales des MNE étudiés. On peut se rendre compte à partir de cette figure (5) que les performances du modèle ASTER sont loin de celles des autres modèles.

Tableau 5. Statistiques des erreurs d'altitude des MNE dans la zone du delta du Nil.

	Minimum	Maximum	Variation	Moyenne	RMSE
ASTER v.3	−19.901	18.895	38.796	-2.148	±5.108
ACE2	−11.518	9.248	20.766	2.288	±2.618
SRTM	−6.320	9.500	15.820	1.971	±2.584
NASA HGT	−5.438	9.243	14.681	1.756	±2.521

En comparant les valeurs RMSE des MNE étudiés (Tableau 5) avec la précision verticale requise des ensembles de données utilisés (Tableau 1), on peut conclure (Tableau 6) que tous les MNE ne sont pas adaptés pour développer des intervalles des courbes de niveau inférieurs à 5 mètres. Cela signifie que de tels modèles ne doivent pas être utilisés pour la cartographie topographique à l'échelle 1:25000 ou plus. Pour les cartes à l'échelle 1:50000 et 1:100000 avec des intervalles des courbes de niveau de 8 ou 10 mètres, on constate que le modèle ASTER doit être évité alors que les trois autres modèles répondent aux spécifications requises. De plus, il est clair que pour les échelles cartographiques de 1:250000 ou moins, tous les MNE étudiés pourraient être utilisés.

Tableau 6. Validité du MNE pour la cartographie topographique dans la zone du delta du Nil.

Echelle	Intervalles des courbes de niveau	MNE Valid
1 : 5000	1.25	NA
1 : 10000	2.0 / 5.0	
1 : 25000	5.0	
1 : 50000	8.0 / 10.0	ACE2, SRTMGL1 v.3, NASADEM_HGT v.1
1 : 100000	10.0	ASTER v.3, ACE2, SRTMGL1 v.3,
	20.0	
1 : 250000	25.0	NASADEM_HGT v.1
	50.0	

Comme mentionné précédemment, la région du delta du Nil représente une zone plate en termes de topographie. Par conséquent, les mêmes étapes ont été effectuées pour étudier les performances des MNE sur la ville de La

Mecque en tant que région à topographie modérée. Le tableau (7), le tableau (8) et la figure (6) présentent les résultats obtenus sur la base de l'ensemble des données disponibles. On peut remarquer à partir du tableau (7) que seul le modèle SRTMGL1 a produit des estimations de relief loin de la précision observée. Pour l'erreur de hauteur moyenne, seul le modèle ACE2 diffère un peu des trois autres MNE. Cependant, les résultats des différences de hauteur par rapport aux GCP connus (Tableau 8) sont plus importants pour analyser la précision des MNE. On peut se rendre compte que les MNT NASA et SRTMGL ont produit les plus petites valeurs RMSE, tandis que le modèle ASTER donne la plus grande. En comparant les histogrammes d'erreur sur les deux zones d'étude (Figures 5 et 6), on peut remarquer que la performance des MNE étudiés est plus précise sur la région plate du delta du Nil que celle à topographie vallonnée de la ville de La Mecque. Cette remarque est également valable lorsque l'on compare les valeurs RMSE des MNE dans les deux régions. Dans le delta du Nil, le RMSE varie de ±2.5 à ±5.0 mètres, tandis qu'à la Mecque le RMSE varie entre ±5.2 et ±8.0 mètres environ. Par conséquent, on peut conclure que la précision des MNE étudiés est plus faible dans les régions à topographie modérée que dans les zones plates.

Tableau 7. Statistiques des sources de hauteur dans la zone de la Mecque.

	Minimum	Maximum	Relief	Moyenne	RMSE
Hauteurs observées	147.135	423.187	274.823	272.146	±59.189
ASTER v.3	144.185	419.008	274.823	272.146	±59.189
ACE2	150.695	422.845	272.150	278.933	±60.068
SRTM	140.482	424.860	284.378	276.082	±59.541
NASA HGT	148.267	419.924	271.657	273.295	±59.005

Tableau 8. Statistiques des erreurs d'altitude des MNE dans la zone de la Mecque.

	Minimum	Maximum	Variation	Moyenne	RMSE
ASTER v.3	−18.456	22.830	41.286	−0.334	±7.996
ACE2	−34.463	5.948	40.412	−7.121	±6.675
SRTM	−16.680	7.820	24.500	−4.270	±5.161
NASA HGT	−13.839	11.219	25.058	−1.483	±5.243

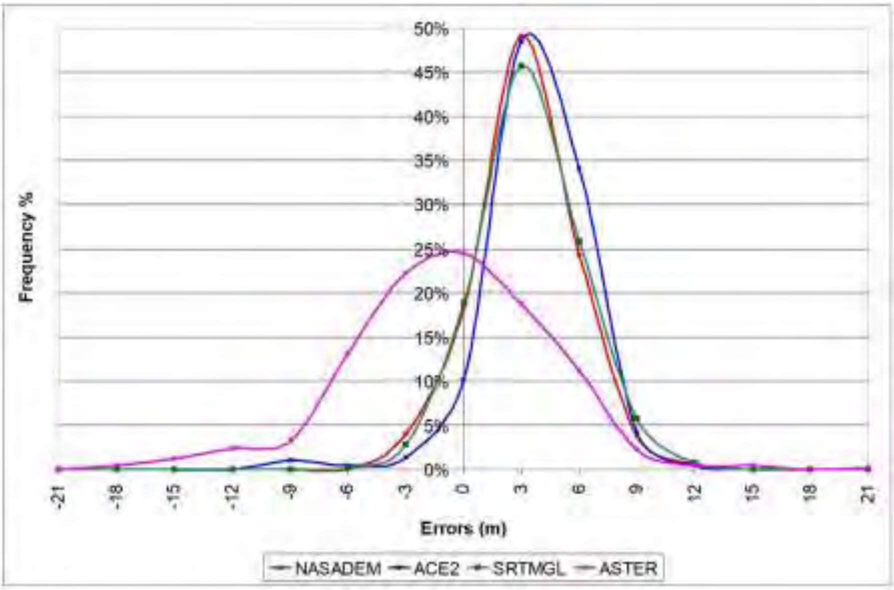

Figure 5. Histogrammes des erreurs de hauteur des MNE dans la région du Delta du Nil.

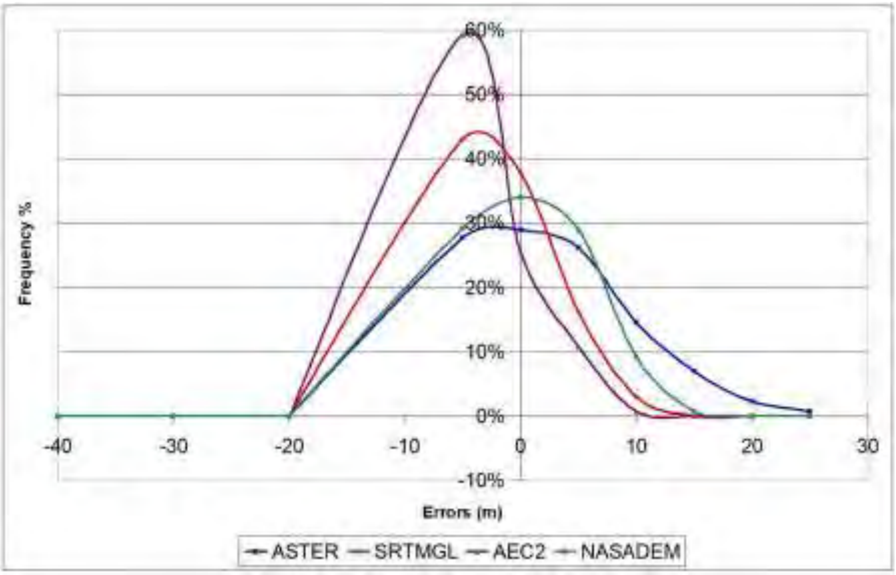

Figure 6. Histogrammes des erreurs de hauteur des MNE dans la région de La Mecque.

Une comparaison a été également effectuée entre les valeurs RMSE des MNE étudiés à La Mecque (Tableau 8) avec la précision verticale de l'ensembles des données utilisées (Tableau 1). On peut voir dans le tableau (9) que tous les MNE ne sont pas adaptés pour développer des intervalles des courbes de niveau inférieurs à 5 mètres. Cela signifie que ces modèles ne conviennent pas à la cartographie topographique à l'échelle 1:50000 ou plus avec des intervalles des courbes de niveau égaux ou inférieurs à 10 mètres. Pour une carte à l'échelle 1:100000 avec des intervalles des courbes de niveau de 20 mètres, on peut voir que le modèle ASTER doit être évité tandis que les trois autres modèles répondent aux spécifications requises. À partir de la figure (6), on peut voir qu'ASTER a produit le modèle de fréquence d'erreurs le moins précis sur les points de contrôle par rapport aux autres MNE. De plus, il est clair que pour les échelles cartographiques de 1:250000 ou moins avec des intervalles des courbes de niveau de plus de 25 mètres, tous les MNE étudiés pourraient être utilisés. De plus, on peut conclure d'après les tableaux (6) et (9) que l'utilisation des MNE dans la cartographie topographique diffère considérablement entre les régions plates et vallonnées.

Tableau 9. Validité du MNE pour la cartographie topographique dans la zone de la Mecque.

Echelle	**L'intervalle des courbes de niveau (m)**	**MNE valide**
1 : 5000	1.25	NA
1 : 10000	2.0 / 5.0	
1 : 25000	5.0	
1 : 50000	8.0 / 10.0	
1 : 100000	10.0	ACE2, SRTMGL1 v.3, NASADEM_HGT v.1
	20.0	
1 : 250000	25.0 50.0	ASTER v.3, ACE2, SRTMGL1 v.3, NASADEM_HGT v.1

Pour analyser les pentes estimées basées sur le MNE (équation (3)) et les profils topographiques, deux coupes transversales ont été réalisées dans la ville de La Mecque sur la base des GCP disponibles. La première (B1-B2) s'étend d'ouest en est en passant par 28 GCP, tandis que l'autre coupe transversale (A1-A2) s'étend du nord au sud le long de 27 GCP (Figure 7). La longueur des deux sections transversales est d'environ 35 kilomètres. Pour étudier la validité de l'estimation de pente basée sur le MNE le long d'une section transversale, chacun est divisé par des intervalles de 5 kilomètres. L'équation (4) a été appliquée pour calculer le facteur de validité de pente (SV) à chaque intervalle pour les deux sections. La figure 8

présente les résultats obtenus, ce qui révèle deux remarques importantes. Premièrement, toutes les pentes basées sur MNE ne correspondent pas aux pentes réelles du GCP connu sur la longueur de la section transversale jusqu'à 25 et 30 kilomètres pour les deux profils respectivement.

Deuxièmement, les pentes basées sur les MNE pour les profils de plus de 30 kilomètres de longueur sont proches des pentes précises dans une valeur de ±10% environ. Par conséquent, on peut conclure que les MNE ne devraient pas être utilisés pour développer des sections transversales topographiques inférieures à 30 kilomètres. De plus, on peut dire que les profils topographiques basés sur les MNE ne doivent pas être utilisés dans des applications d'ingénierie et de géomatique qui nécessitent des informations précises sur les hauteurs et les pentes. Par conséquent, les résultats obtenus de la présente étude, basés sur les ensembles de données disponibles, ont montré que les MNE ne sont pas des sources d'altitudes appropriées pour la cartographie topographique à des échelles cartographiques moyennes et grandes, et ne peuvent pas être utilisés pour un profilage topographique précis dans l'ingénierie et pour des applications géomatiques précises.

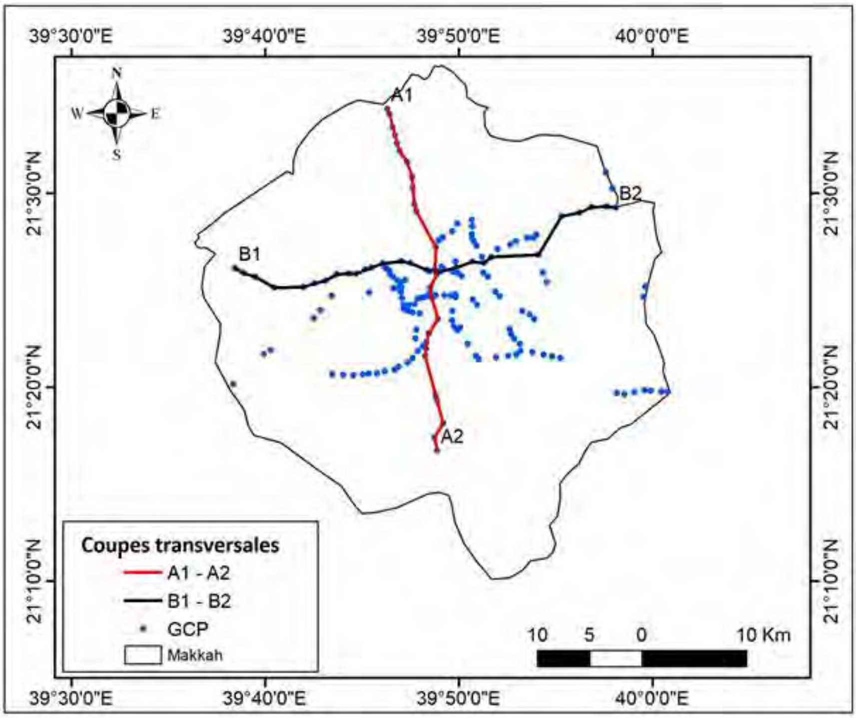

Figure 7. Coupes transversales dans la région de La Mecque.

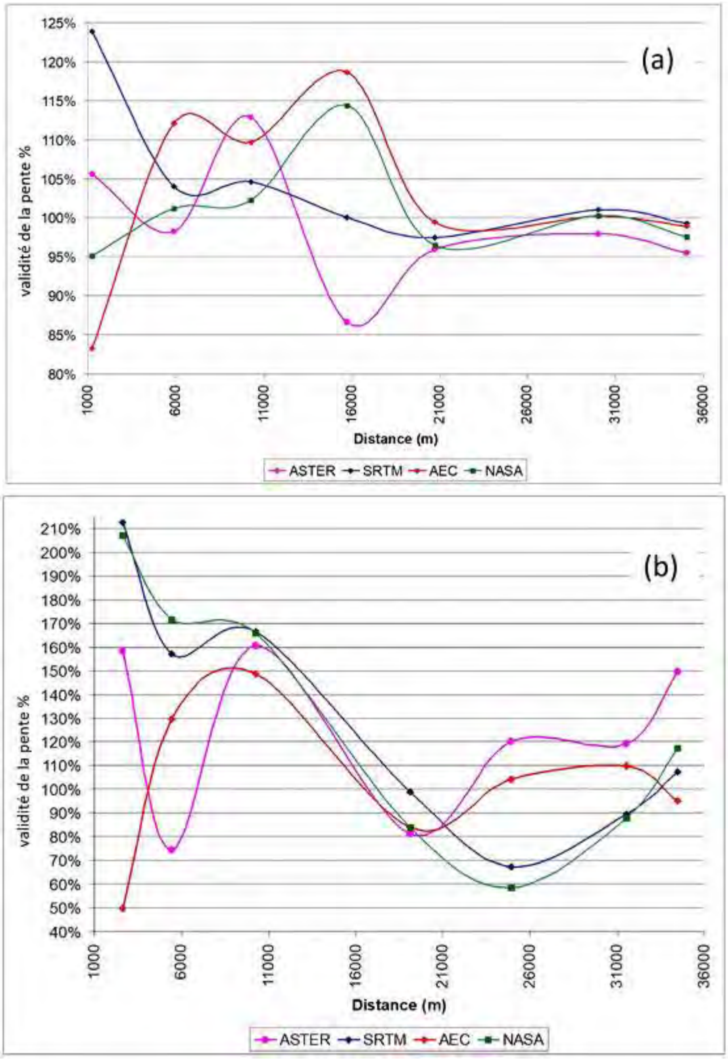

Figure 8. Validité de la pente sur des coupes transversales dans la région de La Mecque.

5. Conclusions

Les MNE open-source ont été utilisés au cours des deux dernières décennies pour la cartographie topographique et plusieurs activités géomatiques. Les spécifications des cartes topographiques reposent sur l'intervalle des courbes de niveau approprié pour chaque échelle de carte et sur la précision des informations sur les hauteurs utilisées. Des exemples de

normes de cartographie topographique de plusieurs pays ont été collectés et étudiés. La présente étude vise à examiner la validité et la fiabilité des altitudes basées sur les MNE pour la cartographie topographique à plusieurs échelles cartographiques. En particulier, elle étudie les performances des MNE pour les intervalles des courbes de niveau, l'estimation de la pente et la génération de profils topographiques nécessaires pour les applications d'ingénierie et environnementales en Égypte et en Arabie Saoudite.

Deux zones d'étude ont été utilisées pour étudier les performances de quatre MNE pour la cartographie topographique sur des régions topographie plate et vallonnée. Sur la base des ensembles de données disponibles dans les deux zones d'étude, plusieurs résultats importants ont été obtenus. En utilisant des points de contrôle connus, il a été constaté que la précision des MNE étudiés varie de ±2.5 à ±5.1 mètres dans la région du delta du Nil, alors qu'elle varie entre ±5.1 et ±8.0 mètres dans la région de La Mecque. Cela indique que l'utilisation des MNE dans la cartographie topographique diffère considérablement entre les régions plates et vallonnées. Sur la base de l'intervalle des courbes de niveau requis sur plusieurs échelles de cartes topographiques, il a été constaté que les MNE ne sont pas appropriés pour générer un intervalle des courbes de niveau inférieur à 10 mètres. Par conséquent, il est suggéré de ne pas utiliser les MNE pour réaliser des cartes topographiques à l'échelle 1:25000 ou plus dans les régions plates et à l'échelle 1:50000 ou plus dans les régions vallonnées.

En termes d'estimation de pente et de développement d'un profil topographique, les résultats obtenus ont révélé que toutes les pentes basées sur le MNE ne correspondent pas aux pentes réelles des GCP connus sur des longueurs de section transversale allant jusqu'à 30 kilomètres. Il a également été observé que les pentes basées sur le MNE pour les profils de plus de 30 kilomètres de longueur sont proches des pentes précises dans une valeur de ±10 % environ. En conséquence, on pourrait conclure que les MNE ne sont pas les sources d'altitudes appropriées pour la cartographie topographique à des échelles cartographiques moyennes et grandes, et ne pourraient pas être utilisés pour le profilage topographique dans des applications précises d'ingénierie et de géomatique.

Les conflits d'intérêts

Les auteurs ne déclarent aucun conflit d'intérêt concernant la publication de cet article.

Références

1. Abdel-Aziz, T., Dawod, G. & Ebaid, H., 2020, "DEMs and Reliable Sea Level Rise Risk Monitoring in Nile Delta, Egypt", *Discover Sustainability*, 1, Article no. 6.
https://doi.org/10.1007/s43621-020-00006-7

2. Al-Karagy, E. & Dawod, G. 2021, "Optimum Combinations of GGM and DEM Models for Precise National Geoid Development", *Proceedings of Engineering and Technology Innovation*, vol. 18, pp. 15-24

3. ASPRS (American Society for Photogrammetry and Remote Sensing), 2015, "ASPRS Positional Accuracy Standards for Digital Geospatial Data", Edition 1, Version 1. *Photogrammetric Engineering and Remote Sensing*, 81, A1-A26.
https://doi.org/10.14358/PERS.81.3.A1-A26

4. Boulton, S.J. & Stokes, M. 2018, "Which DEM Is Best for Analyzing Fluvial Land- scape Development in Mountainous Terrains?", *Geomorphology*, vol. 310, pp. 168-187.

5.Cahyaningsih, C., Crensonni, P., Suryadi, A., Kausarian, H., Choanji, T., Yuskar, Y. & Putra, D. 2019, "Geomorphology and Structural Geology Characterization of Landslide Prone Area in Riau-West of Sumatra Highway", *IOP Conference Series Materials Science and Engineering*, 536, Article ID: 012063;
https://doi.org/10.1088/1757-899X/536/1/012063

6. Church, J., Clark, P., Cazenave, A., Gregory, J, Jevrejeva, S., Levermann, A., Merri- field, M., Milne, G., Nerem, R., Nunn, P., Payne, A., Pfeffer, W., Stammer, D. & Unnikrishnan, A. 2013, "Sea Level Change", In: *Climate Change* 2013: *The Physical Science Basis. Contribution of Working Group I to the Fifth Assessment Report of the Intergovernmental Panel on Climate Change* (*IPCC*), Cambridge University Press, Cambridge, pp. 1137-1216.

7. Dawod, G. & Al-Ghamdi, K. 2017, "Reliability of Recent Global Digital Elevation Models for Geomatics Applications in Egypt and Saudi Arabia", *Journal of Geographic Information System*, vol. 9, no.6, pp. 685-698.
https://doi.org/10.4236/jgis.2017.96043

8. ESA (Egyptian Survey Authority), 2020, "Technical Specifications of Surveyingand Mapping": Part 2: Topographic Maps. A Technical Report, Giza.

9. Geoscience Australia, 2021, "National Topographic Database Structure and Specifi- cations",
http://www.ga.gov.au/mapspecs/topographic/v6/section1.html#MinimumPl animetr icElevationAccuracies

10. Hasan, E., Khan, S. & Hong, Y. 2015, "Investigation of Potential Sea Level Rise Impact on the Nile Delta, Egypt Using Digital Elevation Models", *Environmental Monitoring and Assessment*, 187, 649.
https://doi.org/10.1007/s10661-015-4868-9

11. Hu, Z., Peng, J., Hou, Y. & Shan, J. 2017, "Evaluation of Recently Released Open Global Digital Elevation Models of Hubei, China", *Remote Sensing*, 9, no.3, 262.
https://doi.org/10.3390/rs9030262

12. JICA (Japan International Cooperation Agency), 2013, “The Study on Establishing Digital Topographic Database for Bujumbura City, Burundi”, A Technical Report.
https://openjicareport.jica.go.jp/pdf/12121588_01.pdf
13. Khal, M., Algouti, A., Algouti, A., Akdim, N., Stankevich, S. & Menenti, M. 2020, “Evaluation of Open Digital Elevation Models: Estimation of Topographic Indices Relevant to Erosion Risk in the Wadi M’Goun Watershed, Morocco”, *Geosciences*, vol. 6, issue 2, pp. 231-257.
https://doi.org/10.3934/geosci.2020014
14.Kulp, S. & Strauss, 2016, “Global DEM Errors Underpredict Coastal Vulnerability to Sea Level Rise and Flooding”, *Frontiers in Earth Science*.
https://doi.org/10.3389/feart.2016.00036
15. Mokarram, M. & Hojati, M. 2016, “Comparison of Landform Classifications of Elevation, Slope, Relief and Curvature with Topographic Position Index in the South of Bojnoord”, *Ecopersia*, 2, 1343-1357.
https://doi.org/10.18869/modares.ecopersia.4.2.1343
16. NDMA (National Disaster Management Authority), 2016, “National Technical Document Fir Establishing Cartographic Database in India: Generation of Large Scale (1:10,000 and 1:2,000 and Leaser) Maps for Disaster Management and Planning”, A Technical Report. http://www.ndma.gov.in/sites/default/files/PDF/Technical%20Documents/national-technical-document-for-establishing-cartographic-base-in-india.pdf
17. Ogania, J., Puno, G., Alivio, M. & Taylaran, J. 2019, “Effect of Digital Elevation Model’s Resolution in Producing Flood Hazard Maps”, *Global Journal of Environmental Science and Management*, vol. 5, no. 1, pp. 95-106.
18. Ouerghi, S., ELsheikh, R., Achour, H. & Bouazi, S. 2015, “Evaluation and Validation of Recent Freely-Available ASTER-GDEM V.2, SRTM V.4.1 and the DEM Derived from Topographical Map over SW Grombalia (Test Area) in North East of Tunisia”, *Journal of Geographic Information System*, vol. 7, no. 3, pp. 266-279.
https://doi.org/10.4236/jgis.2015.73021
19. Patel, A., Katiyar, S. & Prasad, V. 2016, “Performances Evaluation of Different Open Source DEM Using Differential Global Positioning System (DGPS)”, *The Egyptian Journal of Remote Sensing and Space Sciences*, vol. 19, issue 1, pp. 7-16.
https://doi.org/10.1016/j.ejrs.2015.12.004
20. Qatar GIS Center, 2009, “Qatar Survey Manual”, Version 1. A Technical Report, Qatar.
21. Sande, B., Lansen, J. & Hoyng, C., 2012, “Sensitivity of Coastal Flood Risk Assessments to Digital Elevation Models”, *Water* 4, no. 3, pp. 568-579.
https://doi.org/10.3390/w4030568
22. Seleem, T. 2013, “Analysis and Tectonic Implication of DEM-Derived Structural Lineaments, Sinai Peninsula, Egypt”, *International Journal of Geosciences*, vol.4, no.1, pp.183-201.
https://doi.org/10.4236/ijg.2013.41016
23. Smith, R. and Berry, P., 2019, “Altimeter Corrected Elevations”, Version 2.
https://sedac.ciesin.columbia.edu/data/set/dedc-ace-v2
24. Survey of India, 2009, Handbook of Topography,
http://www.iism.nic.in/Documents/soichapter-xi.pdf

25. US Open Data Catalouge, 2021, "ASTER Digital Elevation Model", V003. https://catalog.data.gov/dataset/aster-digital-elevation-model-v003
26. USGS (US Geological Survey), 1999, "Map Accuracy Standards: Fact Sheet", FS-171-99. A Technical Report. https://pubs.usgs.gov/fs/1999/0171/report.pdf
27.USGS (US Geological Survey) (2021a) SRTMGL1 V003, https://lpdaac.usgs.gov/products/srtmgl1v003
28.USGS (US Geological Survey) (2021b). NASADEM_HGT: Merged DEM Global 1, Arc Second v. 1. https://lpdaac.usgs.gov/products/nasadem_hgtv001
29.Zhang, J. & Chu, X., 2015, "Impact of DEM Resolution on Puddle Characteriza- tion: Comparison of Different Surfaces and Methods", *Water* 7, no. 5, pp. 2293-2313. https://doi.org/10.3390/w7052293

صلاحية بيانات الارتفاعات للمصادر المفتوحة لمختلف مقاييس الخرائط الطبوغرافية وتطبيقات الجيوماتكس

الملخص العربى

تعرض هذه الورقة تحليلا لأربعة نماذج عالمية للارتفاعات الرقمية مفتوحة المصدر ومقارنتها بمظهرين طوبوغرافيين (مناطق شبه مسطحة ومناطق متضرسة) لرسم الخرائط الطبوغرافية وتطبيقات الجيوماتكس. والهدف الرئيس هو التحقق مما إذا كانت الارتفاعات والفواصل الكنتورية والانحدارات والملامح الطبوغرافية القائمة على نماذج الارتفاعات الرقمية مفتوحة المصدر صالحة لجميع مقاييس رسم الخرائط الطبوغرافية، حيث تمثل إشكالية غالبة في أنشطة رسم الخرائط. تم التطبيق على حالتين من الدراسة، دلتا النيل في مصر ومدينة مكة في المملكة العربية السعودية، حيث تمثل الحالة الأولى منطقة مسطحة التضاريس والثانية مثال للمناطق المتضرسة.

ونماذج الارتفاع الرقمية العالمية المستخدمة في هذه الدراسة تشمل أحدث النماذج:ASTER v.3 ، ACE 2، SRTMGL1 v.3 و NASADEM_HGT v.1 والذي تم اصدارة في العام ٢٠١٩م والعام ٢٠٢٠م بدقة مكانية تبلغ ١ و ٣ ثوان قوسية. تشمل نقاط التحكم الأرضية الدقيقة المتوفرة ٥٤٠ محطة في دلتا النيل و١٧٥ محطة في مكة. بناء على مجموعة البيانات المتوفرة في منطقتي الدراسة فقد وجد ان دقة نماذج الارتفاعات الرقمية العالمية المدروسة في نقاط التحكم السابقة الذكر تتراوح من ±٢.٥ إلى ±٥.١ متر في منطقة دلتا النيل، بينما تتراوح بين ±٥.١ و ±٨.٠ متر في منطقة مكة. وهذا يشير ان استخدام نماذج الارتفاعات الرقمية في رسم الخرائط الطوبوغرافية يختلف كثيرا بين المناطق المسطحة والمناطق الجبلية. لذلك، يوصى بتجنب استخدام نماذج الارتفاع الرقمية محل الدراسة لتطوير الخرائط الطبوغرافية ذات المقياس ١: ٢٥٠٠٠ أو أكثر في المناطق المسطحة والمقياس ١: ٥٠٠٠٠ أو أكثر في المناطق الجبلية. بالإضافة إلى ذلك، أظهرت نتائج الدراسة انه لا تتطابق المنحدرات المعتمدة على نماذج الارتفاعات الرقمية العالمية مفتوحة المصدر مع المنحدرات الفعلية لنقاط التحكم الارضية على طول مقطع يصل إلى ٣٠ كيلومترًا. وهكذا، يستنتج أن نماذج الارتفاعات محل الدراسة ليست مصدرًا مناسبًا لرسم الخرائط الطبوغرافية المتوسطة والكبيرة الحجم، ولا ينبغي استخدامها للتنميط الطبوغرافي في التطبيقات الهندسية والجيوماتية الدقيقة.

Assessing ITRF Conversion Models for Kinematic GNSS Topographic Mapping in Coastal Areas: A Case Study in Egypt

Gomaa M. Dawod and Hoda F. Mohamed, Egypt

ABSTRACT

Global Navigation Satellite Systems (GNSS) surveying has been extensively performed for a wide range of mapping activities. Precise Point Positioning (PPP) is considered a major approach for collecting and processing 3D GNSS data for static and kinematic applications. Processing PPP data results in 3D coordinates based on the most recent International Terrestrial Reference Frame (ITRF) while a national mapping system might be related to another frame. This study aims to investigate several simple ITRF transformation formulas (between ITRF 2014 and ITRF 1994), within the accuracy limits of kinematic surveying, particularly in coastal areas in Egypt. Twelve coordinate transformation methods, in 3D and 2D scenarios, have been analyzed using about two thousands GNSS points along the Red sea coastlines. Accuracy analysis has been performed for each model trying to figure out the optimal approach to be utilized in topographic mapping projects in Egypt. Results showed that almost all models produced comparable and four transformation models produce standard deviations less than 0.20 m while seven models produced a precision less than 0.10 m. Based on standards of medium-scale topographic maps, it can be concluded that those models might be considered as appropriate models for ITRF conversion in GNSS topographic surveys in Egypt.

Keywords: ITRF, GNSS, Coastal Regions, Topographic Maps, Egypt

Assessing ITRF Conversion Models for Kinematic GNSS Topographic Mapping in Coastal Areas: A Case Study in Egypt

Gomaa M. Dawod and Hoda F. Mohamed, Egypt

1. INTRODUCTION

Movement of the tectonic plates causes significant coordinates' changes over time. Such a natural phenomenon is noteworthy in the digital revolution and worldwide use of 3D digital spatial data. On another hand, precise and up-to-date topographic maps constitute a central aspect in integrated coastal planning and management. Kinematic Global Navigation Satellite Systems (GNSS) provide a cost-effective accurate tool for collecting 3D field spatial data needed for topographic mapping. Within GNSS methods, Precise Point Positioning (PPP) has been extensively utilized for positioning in the last couple of decades either in the static or kinematic modes just by using one GNSS receiver. PPP has been employed in several projects including shoreline monitoring (Marques et al., 2019), hydrographic surveys (Abdallah and Schweiger, 2015), deformation monitoring (Zheng et al., 2014)

Recently, online GNSS processing services have been used by several geomatics users worldwide as an easy and quick tool for processing raw GNSS data. Available services include, for examples, the Canadian Spatial Reference System (CSRS) Precise Point Positioning: CSRS-PPP (https://webapp.geod.nrcan.gc.ca/geod/tools-outils/ppp.php), the Australian Online GPS Positioning Service: AUSPOS (http://www.ga.gov.au/scientific-topics/positioning-navigation/geodesy/auspos), and the American Online Positioning User Services: OPUS (https://www.ngs.noaa.gov/OPUS/). Such positioning services generally apply correction models of the satellite orbits errors and the satellite clock errors, as determined by the International GNSS Service: IGS, to increase the accuracy of absolute positioning using a single GNSS receiver. Online GNSS processing services have been utilized extensively in the last decade in numerous surveying and geodetic applications worldwide (e.g. Isioye et al., 2019, Alkan et al., 2016, and Berber et al., 2014). Nationally, such processing services have been investigated and utilized in Egypt (e.g. El Shouny and Miky 2019, and Moamed et al., 2007).

ITRF is the realization of the International Terrestrial Reference System (ITRS) updated periodically since 1992 by the ITRF organization (Altamimi 2016). Transformation parameters between a recent ITRF and its preceding models are determined and published (ITRF 2020). The most recent model is the ITRF 2014. Several studies have investigated the coordinate transformation between different ITRF frames worldwide (e.g. Smith 2020). Nationally, Egypt has established the High-Accuracy Reference Network (HARN) in 1995 as the national GPS-based geodetic datum satisfying the 1: 10,000,000 accuracy standards (ESA 1997). HARN, depicted in Fig. 1, has been developed based on ITRF 1994 (epoch 1996.4992). Consequently, results attained from online GNSS processing services relative to the ITRF 2014 deviate significantly from the corresponding values tied to the HARN network. For instance, Dakhil (2015) has investigated updating the HARN network using PPP technique and found that the coordinates variations between ITRF2008 (epoch 2015) and the

ITRF 1994 (epoch 1996.4992) range from 0.34 to 0.37 m in the X coordinates, from -0.08 m to -0.11 m in the Y coordinates, and from -0.07 m to 0.08 m in the Z coordinates. Also, Ahmed and Hassan (2019) have utilized 8 common stations between the HARN network and the Continuously Operating Reference Station (CORS) network in Egypt and found that the average differences between the ITRF1994 and ITRF2008 equal 0.348 m, 0.342 m, and -0.200 m in the N, E, h directions respectively. Concerning such significant differences, Rabah, et al. (2015) have proposed the utilization of a semi-kinematic geodetic datum for Egypt instead of a fixed one to account for the tectonic movements.

Topographic mapping using online GNSS processing services result in 3D coordinates (X,Y,Z) usually based on the ITRF 2014. Such coordinated need to be converted to the local ITRF1994-based reference to be compatible with the Egyptian mapping datum. Additionally, the attained 3D coordinates might be projected to a 2D coordinate system for producing contour maps and Digital Elevation Model (DEM) for coastal management applications. As far as the authors' concern, there is no investigation has been carried out to define a simple relation between both ITRF frames over the HARN network in Egypt. Even though the transformation parameters are published between both frames, their accuracy might differ from one region to another because of the variations of tectonic movements. This paper investigates the reliability of some straightforward 2D and 3D coordinates conversion methods to facilitate kinematic GNSS surveying particularly for medium-scale topographic mapping in coastal areas.

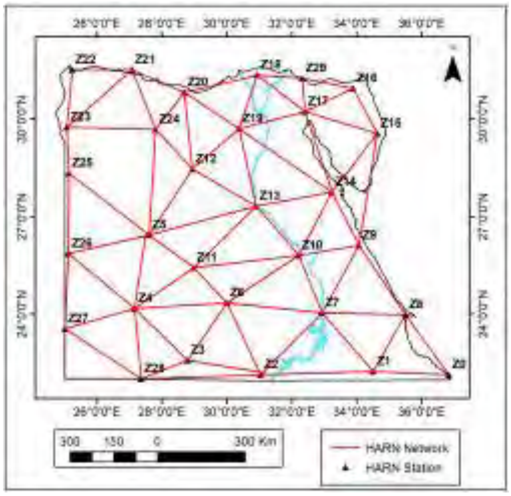

Fig. 1: The HARN Geodetic Network of Egypt

2. METHODOLOGY

Similarity or Helmert datum transformation process, in 2D or 3D coordinate systems, constitutes a normal task in geodetic and photogrammetric applications. 3D datum transformation models contain, among others, the Bursa- Wolf and the Molodensky-Badekas models. The basic mathematical model can be stated, in a matrix representation, as (e.g. Hofmann-Wellenhof et al, 2008):

$$X_T = c + sRX \qquad (1)$$

$$X_T = \begin{bmatrix} X_2 \\ Y_2 \\ Z_2 \end{bmatrix}, \quad X = \begin{bmatrix} X_1 \\ Y_1 \\ Z_1 \end{bmatrix}, \quad c = \begin{bmatrix} dX \\ dY \\ dZ \end{bmatrix}, \quad R = \begin{pmatrix} 1 & R_3 & -R_2 \\ -R_3 & 1 & R_1 \\ R_2 & -R_1 & 1 \end{pmatrix} \qquad (2)$$

where,
X_T and X are the coordinate vectors for both the transformed and the original 3D coordinate systems respectively, c is the shift vector, s is the scale factor expressed in part-per-million (ppm) units, and R is the 3D rotation matrix containing the three small rotations R_1, R_2, and R_3 about the X, Y, and Z-axis respectively.

For Bursa- Wolf model, the rotations are carried out at the origin of the transformed frame (Fig. 2a). However, Molodensky-Badekas model defines the rotations carried at a specific central point (X_0, Y_0, Z_0) (Fig. 2b). Consequently, the first model has seven unknown parameters and the second model has ten parameters. Assuming small values of the three rotation parameters, both models might be solved in four unknowns (three-shift parameters and a scale factor) and in other cases, three unknowns (shift parameters) could be enough for simplicity.

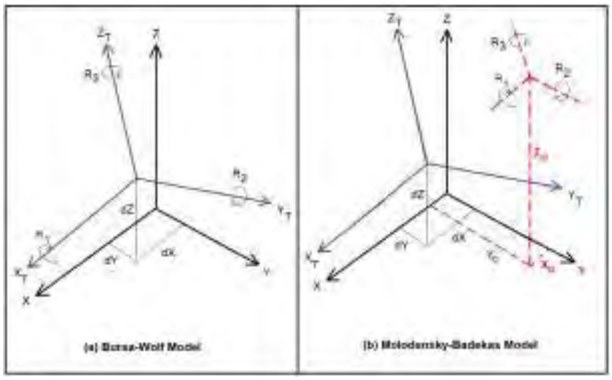

Fig. 2: 3D Datum Transformation Models

For the 2D transformation using a planner coordinates systems (UTM for example), the mathematical model could be written as (ibid):

$$X_T = \begin{bmatrix} E_2 \\ N_2 \end{bmatrix}, \quad X = \begin{bmatrix} E_1 \\ N_1 \end{bmatrix}, \quad c = \begin{bmatrix} dE \\ dN \end{bmatrix}, \quad R = \begin{pmatrix} \cos\alpha & -\sin\alpha \\ \sin\alpha & \cos\alpha \end{pmatrix} \qquad (3)$$

where: α is rotation angle between both 2D coordinate systems.

Equation 3 could be re-written explicitly as:

$$E_2 = dE + s\cos\alpha E_1 + s\sin\alpha N_1$$
$$Y_2 = dN + s\sin\alpha E_1 + s\cos\alpha N_1 \quad (4)$$

Equations 3 and 4 would be solved generally in four unknowns and might be solved in just two (shift) parameters for simplicity.

Other unconventional transformation models could integrate 3D and 2D coordinate systems in just one step. For example, the Leica Geomatics Office (LGO 8.4) software performs a direct transformation from X, Y, Z coordinates on the first reference to E, N planner coordinates on the second reference. For instance, it transforms X, Y, Z on ITRF 2014 (epoch 2019.9861) directly to E,N on ITEF 1994 (epoch 1996.4992). That step is called a one-step transformation model and solves for four unknowns: two coordinates of the rotation origin and two datum shift parameters. Additionally, LGO 8.4 performs another transformation process that combines a sequence of 3D Molodensky-Badekas transformation (X, Y, Z transformation between two datums) followed by a 2D transformation solved for the four aforementioned unknowns. Such a process is called the stepwise datum transformation that could be utilized to transforms X, Y, Z on ITRF 2014 (epoch 2019.9861) directly to E,N on ITEF 1994 (epoch 1996.4992). A third transformation process offered in LGO 8.4 is called a two-step transformation, which is similar to the stepwise transformation but using the Buras-Wolf 3D transformation model.

Since the spatial relation between two ITRF frames in a small area could be relatively systematic, the remove-average mathematical model might be applied too. That model is represented by the following two simple equations in 2D:

$$N_2 = N_1 - aver_{\Delta N}$$
$$E_2 = E_1 - aver_{\Delta E} \quad (5)$$

where $aver_{\Delta N}$ and $aver_{\Delta E}$ are the averages of N, E coordinates variations between the 2D planner coordinates for both systems respectively. Similarly, equation 5 could be written in 3D coordinates (X, Y, Z) too.

It worth mentioning that all the previous transformation models have been investigated herein, in terms of both precision and accuracy, for the sake of choosing an optimal simple datum transformation model that facilitates the GNSS-based topographic mapping for coastal management in Egypt.

3. AVAILABLE DATA

The dataset utilized in the current study has been extracted from the ongoing research project conducted by the Survey Research Institute (SRI) for GNSS mapping of coastlines of the Red Sea from Suez to the Egypt-Sudan borders. Data include 1850 points being surveyed, on

December 2019, by kinematic GNSS in four lines extending about 19 kilometers in length, with approximately a point every ten meters (Fig. 3).

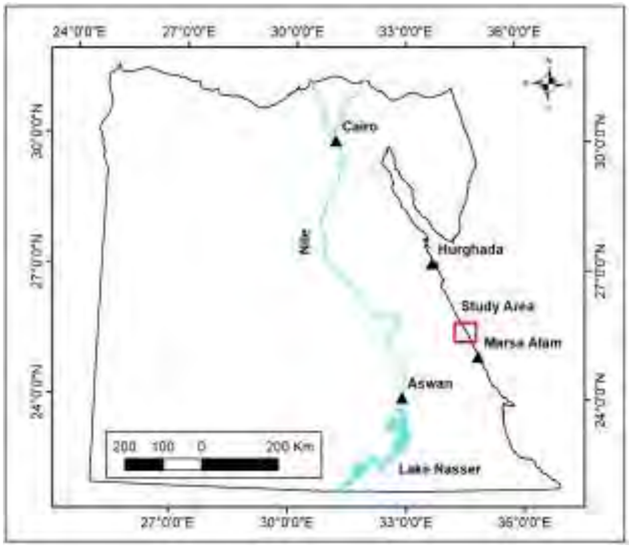

Fig. 3: The Study Area

4. RESULTS AND DISCUSSIONS

The utilized GNSS kinematic surveys have been tied, in a static session, to the HARN national GPS network and the Trimble Business Center (TBC) v. 4.1 software has been utilized for data processing. Consequently, the computed coordinates of the kinematic points are referenced to the ITRF 1994 (epoch 1996.4992) frame. On the other hand, the raw GNSS kinematic datasets have been uploaded to the CSRC-PPP website and their ITRF 2014 (epoch 2019.9861) coordinates have been obtained. The coordinates discrepancies between ITRF 2014 (epoch 2019.9861) and ITRF 1994 (epoch 1996.4992) have been computed and their statistical summary is presented in Table. 1. From this table, it can be recognized that the coordinates' variations between the two frames are in the order of half a meter in both 2D and 3D coordinates. Moreover, it can be seen that the range of horizontal coordinates variations vary from 0.08 to 0.15 m over the study area. That implies that the remove-average mathematical model (Eq. 5) could be utilized as a simple datum transformation model. Furthermore, it can be recognized that the resultant 2D vector of horizontal coordinates variations (on UTM), due to tectonic movements, equals 0.708 m in magnitude and its azimuth is N 51^{o} E. Such findings extremely necessitate datum transformation in GNSS mapping when utilizing the online GNSS processing survives.

Table 1: Coordinates Variations between ITRF 2014 (epoch 2019.9861) and ITRF 1994 (epoch 1996.4992) in Egypt (m)

Coordinates Variations (ITRF 2014 - ITRF 1994)	Minimum	Maximum	Average	Standard Deviation
dE (UTM)	0.455	0.611	0.553	± 0.016
dN (UTM)	0.402	0.483	0.442	± 0.012
dX	-1.043	-0.463	-0.740	± 0.130
dY	-0.47	0.367	0.415	± 0.096
dZ	0.014	0.462	0.238	± 0.086

Next, the aforementioned mathematical models have been applied to come up with transformation models between ITRF 2014 (epoch 2019.9861) and ITRF 1994 (epoch 1996.4992). So, the LGO 8.4 software has been used in determining similarity transformation equations in both 3D and 2D systems. Tables 2 and 3 presents the accomplished results.

Table 2: 3D Transformation Models between ITRF 2014 (epoch 2019.9861) and ITRF 1994 (epoch 1996.4992) in Egypt

<table>
<tr><th>Model No.</th><th>Model</th><th>No. of Parameters</th><th>Results</th></tr>
<tr><td>1</td><td rowspan="3">Bursa-Wolf</td><td>3</td><td>dX = 0.740 ± 0.003 m
dY = -0.170 ± 0.003 m
dZ = -0.238 ± 0.003 m</td></tr>
<tr><td>2</td><td>4</td><td>dX = 3.502 ± 1.467 m
dY = 1.733 ± 0.011 m
dZ = 1.362 ± 0.850 m
s = -0.582 ± 0.310 ppm</td></tr>
<tr><td>3</td><td>7</td><td>dX = -3.561 ± 8.458 m
dY = 95.957 ± 7.880 m
dZ = -98.511 ± 5.265 m
R_1= -3.016 ± 0.035 "
R_2 = 2.270 ± 0.245 "
R_3 = 2.355 ± 0.329 "
S = -0.583 ± 0.121 ppm</td></tr>
<tr><td>4</td><td rowspan="3">Molodensky-Badekas</td><td>6</td><td>X_o = 4736812.545 m
Y_o = 3264642.161 m
Z_o = 2744958.911 m
dX = 0.740 ± 0.003 m
dY = -0.170 ± 0.003 m
dZ = -0.238 ± 0.003 m</td></tr>
<tr><td>5</td><td>7</td><td>X_o, Y_o, Z_o, dX, dY, and dZ as above,
s = -0.583 ± 0.310 ppm</td></tr>
<tr><td>6</td><td>10</td><td>X_o, Y_o, Z_o, dX, dY, dZ, and s as above,
R_1= -3.016 ± 0.035 "
R_2 = 2.270 ± 0.245 "
R_3 = 2.355 ± 0.329 "</td></tr>
</table>

Table 3: 2D Transformation Models between ITRF 2014 (epoch 2019.9861) and ITRF 1994 (epoch 1996.4992) in Egypt

Model No.	Model	No. of Parameters	Results
7	Classical 2D (E,N to E,N)	4	X_o = 658074.948 m Y_o = 2838742.895 m dE = -0.553 ± 0.0003 m dN = -0.442 ± 0.0003 m
8		6	X_o, Y_o, dE, and dN as above, α = -0.092 ± 0.008 " s = -0.654 ± 0.039 ppm
9	Two Steps (X,Y,Z to E,N)	9	Bursa-Wolf 3D parameters: dX = 121.200 m, dY = -98.240 m, dZ = 10.800 m, R_3 = 0.544", s = -0.226 ppm Plus grid Transformation: dE = 10.854 ± 0.001 m. dN = 164.147 ± 0.001 m, X_o = 2838731.603 m, Y_0 = 657910.248 m
10	Stepwise (X,Y,Z to E,N)	12	Molodensky-Badekas 3D parameters: dX = 0.473 ± 0.0006 m, dY = -0.354 ± 0.0006 m, dZ = -0.393 ± 0.0006 m, X_o = 4736812.54 m, Y_0 = 3264642.161 m, Z_0 = 2744958.911m Plus grid Transformation: dE = 0.000 m. dN = 0.000 m, X_o = 658074.948 m, Y_0 = 2838742.895 m, α = -0.081 ± 0.016 ", s = -0.634 ± 0.079 ppm
11	Removing Average	2	$aver_{\Delta N}$ = 0.442 m $aver_{\Delta E}$ = 0.553 m

Precision analysis of the residuals, as expressed by their standard deviations, has been carried out for the utilized transformation models between ITRF 2014 (epoch 2019.9861) and ITRF 1994 (epoch 1996.4992) in Egypt. Table 4 presents the statistical characteristics of the attained results over the 1850 GNSS kinematic points. It can be noticed, from that table, that almost all models produce comparable results. Additionally, four transformation models (no. 3, 6, 10, and 11) produce standard deviations less than 0.20 m. Also, seven models (no. 3, 6, 7, 8, 9, 10, and 11) produce a precision less than 0.10 m. It is known that standards of medium-scale topographic maps and DEM development match a ten-centimeters tolerance in the horizontal coordinates. Then, it can be concluded that those models might be considered as appropriate models for ITRF conversion in GNSS topographic surveys in Egypt. From a precision point of view, either the Bursa-Wolf or the Molodensky-Badekas models with 7 and

10 parameters respectively (models no. 3 and 6) could be considered the optimum transformation model for 3D coordinates with a precision level less than 0.10 m. Also, the classical 2D transformation and removing average models are the best methods for planner coordinates transformation with a precision level of less than 0.05 m.

Table 4: Precision Analysis of Utilized Transformation Models (m)

Model No.	Minimum Residuals	Maximum Residuals	Average of Residuals	Overall Standard Deviation of Residuals
1	-0.302	0.277	0.0001	0.183
2	-0.302	0.278	0.0001	0.183
3	-0.151	0.188	0.0000	0.071
4	-0.302	0.277	0.0001	0.183
5	-0.302	0.278	-0.0001	0.183
6	-0.151	0.188	0.0000	0.071
7	-0.098	0.058	0.0000	0.020
8	-0.098	0.058	0.0000	0.019
9	-0.167	0.122	0.0000	0.074
10	-0.120	0.087	0.0000	0.047
11	-0.099	0.057	0.0000	0.020

5. CONCLUSIONS

Nowadays, the world witness a revolution in collecting, processing, and utilization of 3D spatial data. Precise 3D (and also 4D) coordinates play a major role in geomatics applications, particularly with the widespread of GNSS utilization. In this regard, the coordinates changes due to tectonic movements are noteworthy and should be considered in topographic mapping.

It is a matter of reality that 3D coordinates obtained from on-line GNSS processing services are based on the most recent ITRF while a national mapping system might be related to another frame. Hence, this study has investigated several simple ITRF transformation formulas (between ITRF 2014 and ITRF 1994), within the accuracy limits of kinematic surveying, particularly in coastal areas in Egypt. Twelve coordinate transformation methods have been analyzed using about two thousands GNSS points along the Red sea coastlines.

Accomplished results showed that almost all models produced comparable and four transformation models produce standard deviations less than 0.20 m while seven models produced a precision less than 0.10 m. Based on standards of medium-scale topographic maps, it can be concluded that those models might be considered as appropriate models for ITRF conversion in GNSS topographic surveys in Egypt. From a precision point of view, either the Bursa-Wolf or the Molodensky-Badekas models with 7 and 10 parameters respectively could be considered the optimum transformation model for 3D coordinates with a precision level less than 0.10 m. Also, the classical 2D transformation and removing average models are the best methods for planner coordinates transformation with a precision level of

less than 0.05 m. Since Egypt is entirely located within the Nubian tectonic plate, the attained ITRF transformation models are recommended to be utilized in all topographic mapping projects in the country.

6. REFERENCES:

Abdallah, A. and Schwieger, V. (2015) Kinematic Precise Point Positioning (PPP) solution for hydrographic applications, Presented at the FIG Working Week 2015, Sofia, Bulgaria, May 17-21.

Ahmed, K. and Hassan, K (2019) Transformation parameters between two ITRF-based networks for detection of land deformations in Egypt, Al-Azhar University Civil Engineering Research Magazine (CERM), V. 4, No. 2, pp. 305-317.

Alkan, R., Ilçi. V. and Ozulu, I., (2016) Web-based GNSS data processing services as an alternative to conventional processing technique, Presented at the FIG Working Week, May 2–6, New Zealand.

Altamimi Z (2016) The International Terrestrial Reference System and ETRS89: Part II: ITRS & ETRS89 relationship, Presented at the EUREF Toturial, San Sebastin, Spain, May 24.

Berber, M. , Ustun, A. and Yetkin, M. (2014) Rapid static GNSS data processing using online services, Journal of Geodetic Science, No. 4, pp. 123–129.

Dakhil, A. (2015) GPS measurements and its impact on geodetic datum maintenance, MSC Thesis, Faculty of Engineering, Mansoura University, Mansoura, Egypt.

El Shouny, A. and Miky, Y. (2019) Accuracy assessment of relative and precise point positioning online GPS processing services, Journal of Applied Geodesy, DOI: 10.1515/jag-2018-0046.

ESA (Egyptian Survey Authority) (1997) The new Egyptian datum of 1995: Results of the final adjustment of the new national geodetic network, Internal technical report, 129 pp.

Hofmann-Wellenhof, B., Lichtenegger, H., and Walse, E. (2008) GNSS: Global Navigation Satellite Systems, Springer-Verlag Wien, New York, USA.

Isioye, O., Moses, M. and Abdulmumin, L. (2019) Comparative Study of Some Online GNSS Post-Processing Services at Selected Permanent GNSS Sites in Nigeria, In: Sanli (Ed.): Accuracy of GNSS Methods, IntechOpen, London, U.K.

Marques, H., Gonçalves, R., Araujo, A., Pereira, P. and Queiroz, H. (2019) Shoreline monitoring by GNSS-PPP aiming to attendance the law 14.258/2010 from Pernambuco state, Brazil. Bulletin of Geodetic Sciences, V. 25, No. 2, DOI:10.1590/s1982-21702019000200012.

Mohamed, H., Dawod, G., and Ismail, S. (2007) Assessment of a cost-effective GPS data processing alternative in Egypt utilizing international on-line processing services, Journal of Al-Azhar University Engineering Sector (JAUES), V. 2, No. 12, pp. 364-375.

Rabah, M., Shaker, A. and Farhan, M. (2015) Towards a semi-kinematic datum for Egypt, Positioning, No. 6, pp. 49-60.

Smith, D. (2020) A GPS based estimate of the rotation of the Mariana plate in both ITRF2008 and ITRF2014, NOAA Technical report No. NOS NGS 74, August, 34 pp, National Geodetic Survey, Maryland, USA.

Zheng, Y., Zhang, R., and Gu, S. (2014) A new PPP algorithm for deformation monitoring with single-frequency receiver, Journal of Earth System Science, 123, 1919–1926, DOI:10.1007/s12040-014-0502-4.

CONTACTS:

Prof. Gomaa M. Dawod
Survey Research Institute, National Water Research Center,
308 Al-Ahram Street, Talbia
Giza 12111, Egypt
email: dawod_gomaa@yahoo.com

Dr. Hoda F. Mohamed
Survey Research Institute, National Water Research Center,
308 Al-Ahram Street, Talbia
Giza 12111, Egypt
email: hoda.faisal@yahoo.com

Quest Journals
Journal of Architecture and Civil Engineering
Volume 6 ~ Issue 8 (2021) pp: 24-38
www.questjournals.org

Research Paper

An Integrated Geomatics Approach for Projecting Sea Level Variations and Risks A Case Study in the Nile Delta, Egypt [1]

Gomaa M. Dawod*, Hala M. Ebaid, Ghada G. Haggag, and Essam M. Al-Karagy

Survey Research Institute, National Water Research Center, Giza, Egypt

ABSTRACT

Sustainable development of coastal areas depends fundamentally on the availability and comprehensive analysis of precise and up-to-date geospatial datasets. This study aims to develop an integrated geomatics approach for collecting and analyzing heterogeneous datasets within Geographic Information Systems (GIS) environment to predict potential risks of sea level variations over the Nile delta in 2025. Datasets include tide gauge (TG) records span 2008-2018, Global Navigations Satellite System (GNSS) observations to estimate land subsidence and consequently, absolute sea level rise, terrestrial high-accuracy Digital Elevation Model (DEM), and high-resolution satellite imageries were integrated to analyze and evaluate the impact of sea level rise on the coastal area of the Nile delta. Based on the available TG records over five sites, the statistical prediction has been carried out to forecast sea water variations in the next five years over the study area. Next, potentially inundated areas have been delineated for two cases: Mean Sea Level (MSL) and storm surges potential risks (High High water level (HHWL). The results indicate that the flooded area based on the MSL scenario represents only 5% of the total area of the entire study region, contrasting to earlier un-realistic estimates. Moreover, it has been found that the storm surge case produces potential risks 118% higher than those of MSL. Also, digital maps depicting all possible hazardous areas have been developed. Finally, it can be concluded that the presented integrated approach proves to be significantly effective in risk assessment over the Nile delta, helpful for decision makers to plan actions needed in coastal zone management, and it is reasonable to be applied in other similar regions worldwide.

KEYWORDS: *SLR, GNSS, GIS, Geomatics, Risk Assessment*

Received 10 August, 2021; Revised: 24 August, 2021; Accepted 26 August, 2021 © The author(s) 2021. Published with open access at www.questjournals.org

I. INTRODUCTION

Sea level rise is essentially attributed to global warming and climate changes factors including ocean thermal expansion, polar ice caps melt, and change in terrestrial storage (e.g. Khan 2019). It is a matter of fact that sea level has been significantly raised in the 20th century on a global average. The Intergovernmental Panel on Climate Change (IPCC) stated that SLR since the mid-19th century has been larger than the mean rate during the previous two millennia (IPCC 2014a). The observed global mean sea rise, from tide gauge records and satellite altimetry data, has been reported as 1.5, 2.0 and 3.2 mm/year for the period 1901-1990, 1971-2010, and 1993-2010 respectively (Church et al. 2013). According to various expected scenarios, the predictable global sea level in 2081-2100, might vary between 0.40 to 0.84 m relative to the 1986-2005 level (IPCC 2019). However, regional SLR rates could be several times larger or smaller than the global mean SLR for periods of several decades, due to fluctuations in ocean circulation, groundwater extraction, and land subsidence among other factors (ibid). Moreover, it has been observed that extreme sea levels (storm surges) have been increased since the last few decades. (ibid). It worth mentioning that due to projected SLR during the21st century, coastal systems and low-lying regions (such as the river deltas) would increasingly experience strong hazardous impacts (IPCC 2014b).

Hazardous impacts of sea level rise include, for example, shoreline retreat (e.g. Wang et al., 2019), economic impacts on coastal cities (Ruiz-Ramirez et al., 2019), coastal flooding and inundation (e.g. Fu and Peng, 2018), coastal erosion (e.g. Aucelli et al., 2018), decrease in water quality in coastal regions (e.g. Wassef and Schüttrumpf, 2016), decrease in areas and volumes of water bodies (e.g. Hossena and Negm, 2016), and

land degradation (e.g. El Baroudy and Moghanm, 2014). Sea Level Rise (SLR) could be estimated from a variety of techniques and datasets. Relative SLR (RSLR) is primarily measured at Tide Gauge (TG) sites, as well as from satellite altimetry data (e.g. Poitevin et al., 2019). Absolute SLR (ASLR) is a combination of RSLR and land subsidence estimated by levelling or Global Navigation Satellite Systems (GNSS) technique (e.g. Keogh and Törnqvist, 2019). Predicting sea level rise comprises an important task for geodetic and environmental communities

————————1 Under review

worldwide (e.g. Siddig et al., 2019). Several mathematical models have been implemented in such a task including ordinary regression (e.g. Dawod et al., 2019), harmonic analysis (e.g. Frota et al., 2016), Artificial Neural Network (ANN) (e.g. Temitope and Daniel, 2014), and moving average filter (e.g. Kaloop et al., 2016). Besides, Geographic Information Systems (GIS) have been widely employed as an integrated framework to investigate and delineate SLR risks (e.g. Neumann et al., 2010).

The Nile delta, Egypt has encountered significant SRL as one of the river deltas and low-lying regions worldwide. Additionally, land subsidence, water and natural gas extraction, and other critical natural aspects heighten vulnerability to coastal flooding and reduce freshwater supply to the delta. A recent study by the IPCC reports that an estimated 2660 km2 in the northern delta will be inundated by 2100 for GMSL of 0.44 m. Additionally, subsidence rates range from 0.4 mm/year in the west delta to 1.1 mm/year in the mid-delta and 3.4 mm/year in the east delta (IPCC 2019). The Egyptian government has committed 200 million USD to hard coastal protection at Alexandria and adopted integrated coastal zone management for the northern coast (ibid). In this regard, it worth mentioning that several research studies have stated that Alexandria city in Egypt is considered one of twenty cities worldwide that are most exposed to hazardous natural risks particularly due to coastal flooding by 2070 (Siegel, 2020).

SLR's analysis, prediction, and risk assessment have been extensively investigated in Egypt in the last couple of decades. For example, Dawod et al. (2019) have estimated both relative and absolute sea level rise in the Nile delta region using heterogeneous spatial datasets. GIS has been applied to analyze the sea level rise variations and vital impacts across the Nile delta coasts (Refaat and Eldeberky, 2016, and Mohamed, 2015). Additionally, El-Geziry and Said (2019) have investigated the sea level pattern and variations in El-Burulls new harbor on the Nile delta coastal region. Land subsidence and sea level rise across the Nile delta region have been investigated (e.g. Stanely, 2016). On the other hand, several research studies have been carried out to predict the potential impacts of sea level rise particularly on the Nile delta region (e.g. Hasan et al., 2015 and Hassan and Abdrabo, 2013). Additionally, AlbooHassan et al. (2015) have applied GIS and remote sensing to investigate the sea level rise impacts on coastal tourist services. Hereher (2015) developed a vulnerability index to sea level rise for the Egyptian costs.

Hazardous impacts of sea-water variations are not limited to the gradual SLR but more critically to the dangerous effects of sudden storm surges. A storm surge is an unusual increase of sea water caused by a storm, over and above the predicted astronomical tides. Such an unpredicted rise of the sea water level, due to climate changes, not only has inverse consequences on human life but also the environment, animals, and infrastructural facilities (Rajan and Saud, 2018). For example, on October 2019 the Nile delta and northern parts of Egypt have encountered an unusual type of storm that intimidates to bring forceful seas, tropical-storm strength winds, and probably up to 200 mm of rain to the region. Such rainfall could measure as much as 10 times the average monthly of October across this region, creating a risk of flooding (MODIS 2020). Storm surge is considered a major factor in defining coastal vulnerability over the Mediterranean coasts of Egypt (Torresan et al. 2020). Hence, the investigation of High High Water Level (HHWL) from TG time series would be beneficial in analyzing and defining the potential impacts of storm surges.

The current research study aims to utilize geomatics techniques, particularly TG data, GNSS data, a precise local DEM, GIS, and high-resolution satellite images, in an integrated approach for two objectives: First, to analyze and predict sea level variations (MSL and HHWL) along the Nile delta Mediterranean coasts, Second: to develop a risk assessment of their current and expected potential hazards by 2025.

II. STUDY AREA

The current research focuses primarily on the Nile delta coasts on the Mediterranean sea, ranging from longitude 29.6° E to longitude 32.3° E (Fig. 1). It is worth mentioning that with more than fifty million populations, the Nile delta region might be considered as one of the most densely populated regions worldwide. The topography of the study area (Fig.1) ranges from elevation -72 meter to 197 meters, with an average of 5.9 meters. The dominant elevation is less than 10 meters in the northern and middle parts of the delta. Additionally, it can be realized that the northern region of the delta area has an elevation of less than almost 5 meters. The actual study area extends in the east-west direction over 273 kilometers from Port Said at the east to Alexandria

at the west, with approximately more than one kilometer perpendicular to the shoreline. The overall area of that region equals about 317 square kilometers.

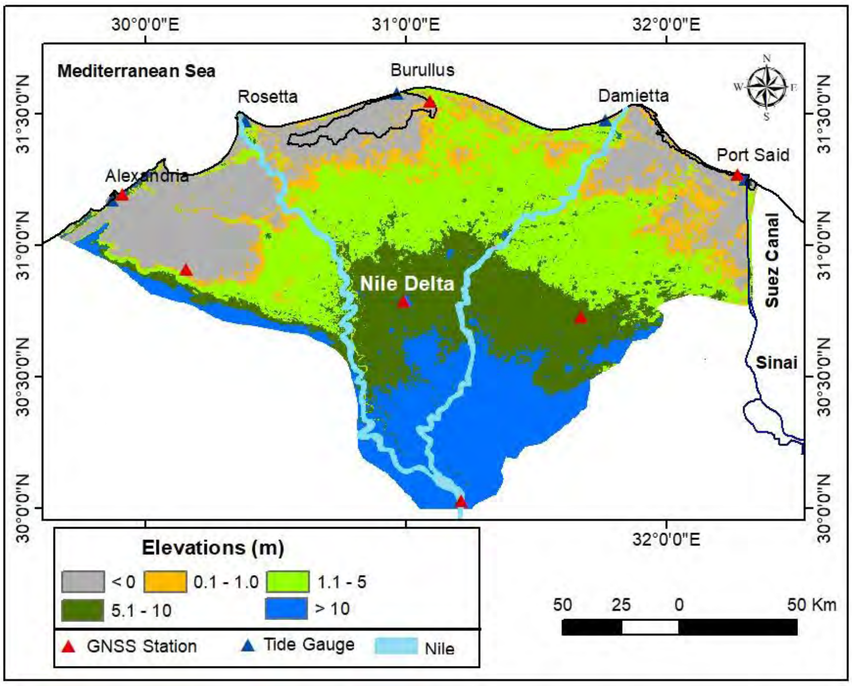

Fig. 1: Topography of the study area, Tide gauges, and GNSS stations

2.1 Data Sets

The available geospatial datasets comprise TG records for analyzing sea level variations, GNSS data to estimate land subsidence, a local high-accuracy DEM to represent the coastal topography, and highresolution satellite images to delineate the impacts of sea level rise. Those datasets are briefly demonstrated in the next subsections.

2.1.1 Tide Gauge data

Within the Nile delta study area, 5 tide gauge stations exist at Alexandria, Damietta, Burullus, Rosetta, and Port Said (Fig.1). The available tide gauge dataset comprises data from different tide gauge stations along the Mediterranean coasts with variable periods. These tide gauge stations belong to different local organizations, where the Alexandria and Port Said TG stations belong to the Survey Research Institute (SRI) of the National Water Research Center (NWRC), and the other three TG stations belong to the Coastal Research Institute (CoRI) of NWRC.

Table 1 describes the characteristics of the collected tide gauge datasets at these five stations. It should be noticed that the records of the last three TG, in this table, include the annual Mean Sea Level (MSL) and the annual High High Water Level (HHWL)that represents the maximum storm surge at each TG in each year. For the Alexandria and Port Said TG, both MSL and HHWL are estimated from the raw data using arithmetic and statistical functions in the Excel software.

Table 1: Tide Datasets characteristic for Delta coast

TG	Period	Gaps	Frequency
Alexandria	2008 – 2018	No	30 minutes
Port Said	2008 – 2017	No	30 minutes
Damietta	1990 – 2016	1992-1996 2004 – 2011	Yearly
Burullus	2003 – 2016	2010, 2012	Yearly
Rosetta	2004 – 2016	2010, 2012	Yearly

2.1.2 GNSS data

For GNSS monitoring of subsidence in the Nile delta, 24-hours datasets at six stations, covering the period 2012-2015, have been utilized (Mohamed et al., 2015). However; these stations did not cover the Alexandria coast. Therefore; subsidence estimate is acquired for another GNSS station located at Alexandria belong to the "Système d'Observation du Niveau des Eaux Littorales" (SONEL) project, which is international cooperation aims to afford continuous measurements of sea- and land levels at the coast from tide gauges (relative sea levels) and modern geospatial techniques (vertical land motion and absolute sea levels) for studies on long-term sea level trends (SONEL, 2019). That GNSS station is located 3.1 km from the tide gauge. Even though the number of these GNSS stations is relatively small, they have been utilized in this research since they constitute the only available GNSS data for the time being. The previous study revealed comparable results and subsidence rates in the Nile delta region. For example, investigating land subsidence in the Nile delta by satellite radar imageries over 20042010, Gebremichael et al. (2018) founded that there exit broad patterns of subsidence (average rate of −2.4 mm/year in the northern delta, almost-steady to small subsidence in the southern delta (average rate of 0.4 mm/year), separated by an uplift zone (average rate of 2.5 mm/year). Similarly, Rateb and Abotalib (2020) utilized Sentilel-1 satellite images over 2015-2019 for monitoring land subsidence in the Nile delta and found that three are three patterns of deformation: land subsides with rates ranging from −12 to −20 mm/year in major cities, subsidence rate ranges between −3 and −8 mm/year along the coastal margins and subsidence rate ranges from −20 to −16 mm/year and −6 to −12 mm/year in newly reclaimed lands on the west and east of the delta's region. The utilized seven GNSS stations are depicted in Figure 1, and their estimated subsidence rates are shown in Table 2. Figure 2 depicts the land vertical movement over the Nile delta region (Dawod et al. 2019).

Table 2 Vertical land movements rates at GNSS stations in the Nile Delta

Station	Period	Subsidence Rate (mm/year)	Reference
Cairo	2012-2015	+ 4.94	Mohamed et al. 2015
Port Said		- 4.72	
Abu Kebeer		+ 3.69	
Tanta		- 6.51	
Baltim		+ 0.71	
Abu El-Matameer		+ 0.55	
Alexandria	2002-2008	-0.85	SONEL 2019

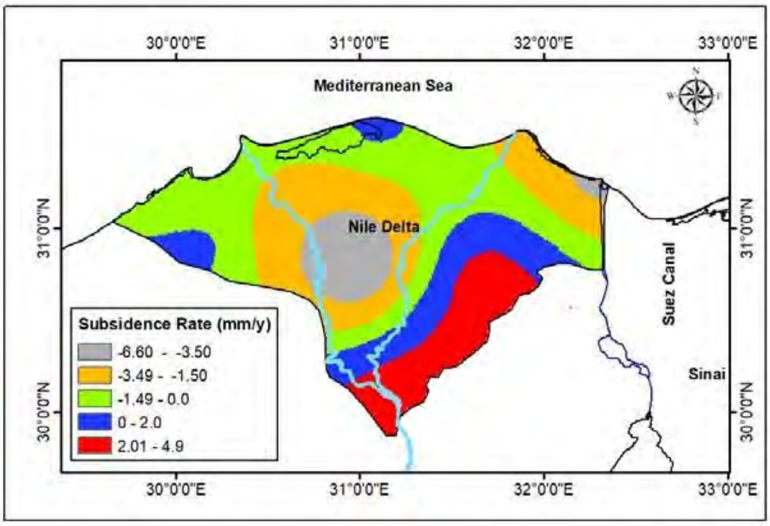

Fig. 2: Vertical land movements in Nile Delta
(ref. Dawod et al. 2019)

2.1.3 Local DEM

Over the study area, terrestrial field campaigns have been performed to develop a local high-precision high-resolution DEM. The utilized field strategy has integrated GNSS measurements with precise levelling. First, a geodetic control network has been established with 5-kilometers spacing. Then, an MSL-based orthometric height for every control point has been determined through precise levelling routes to the nearest Bench Mark (BM). Next, a Post-Processing Kinematic (PPK) GNSS has been implemented in topographic surveying of the entire undeveloped areas. So, about 184 thousand GNSS/Levelling points have been measured. The horizontal spatial resolution of the attained DEM estimated as 1.3 arc seconds, i.e. approximately 40 m, while its vertical accuracy is approximately 0.05 m (SRI 2018). The heights of that accurate DEM range from -2.035 m to 16.899 m with an average of 1.353 m.

2.1.4 Satellite imageries

TripleSat 1-meter spatial-resolution satellites imageries, dated 2016, have been utilized for land use mapping (Fig. 3). It worth mentioning that the available geospatial datasets applied in the current study have been collected, by SRI, during the period 2016-2018 (SRI 2018). It is a matter of fact that the coastal study area do not include large development projects and it is expected that the existing land uses do not change significantly over recent years. Table 3 showed statistics about the percentage of land uses covering, from which it can be noticed that the undeveloped areas cover almost 70% of the entire study area.

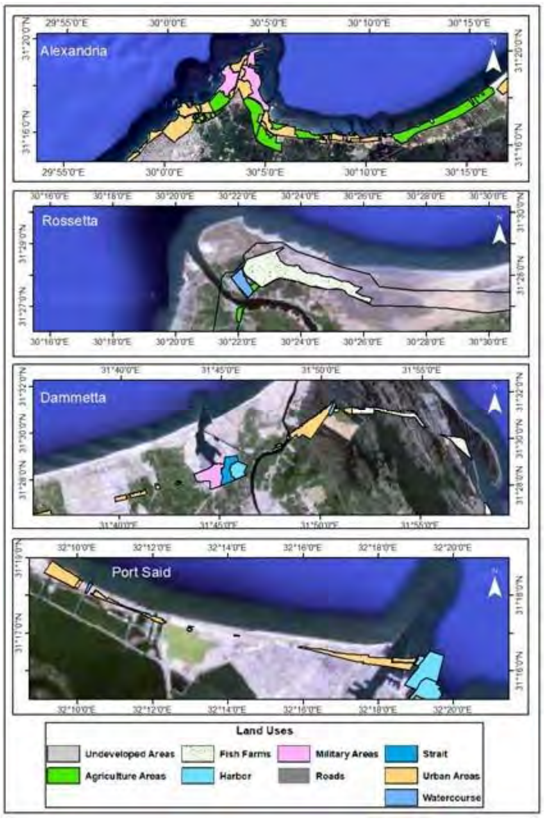

Fig. 3: Land uses at main cities

Table 3: Land uses for the study area

Type	Total Area (km^2)	% of Areas
Undeveloped Areas	221.95	69.9 %
Urban Areas	33.736	10.6 %
Fish Farms	26.579	9.8 %
Agriculture Areas	17.957	6.6 %
Military Areas	8.759	3.2 %

Harbor	4.620	1.7 %
Strait	1.793	0.7 %
Watercourse	1.580	0.6 %
Roads	0.474	0.2 %
Total	317.448	100 %

III. DATA PROCESSING

The approach of processing these integrated data aims to fulfill two objectives: analyzing and predicting sea level variations along the study area, and developing risk assessment of their projected potential hazards by 2025. Consequently, there exist two stages of data processing. First, regression modelling is carried out to analyze and model sea level variations at the utilized TG sites. Although there are several mathematical and statistical methods for modelling and predicting regional or global SLR from TG stations, the linear regression model is one of the most popular ones. It has been applied for such a task in several regions worldwide such as South Korea (Watson 2019), Saudi Arabia (Siddig et al. 2019), and Pacific islands (Martínez-Asensioa et al., 2019). The current research study does not concentrate on the comparison of mathematical SLR predicting methods, but rather on developing and applying an integrated geomatics approach for investigating SRL. The linear regression model, utilized herein, has the basic equations in the form of (e.g. Nhan, 2016).:

$MSL(Y) = ax + b$ changed (1)

where MSL is the annual mean sea level at a tide gauge, a and b are coefficients to be determined, and x is the year.

To judge the attained regression trend, the coefficient of determination, R^2, is evaluated. It is a statistical measure of the quality of the regression model, representing the proportion of the variance in the dependent variable that is predictable from the independent variable. R^2 ranges from zero to one (or from 0 % to 100 %), computed as:

$$R = \left[n(\sum xy) - (\sum x)(\sum y)\right] \Big/ \sqrt{[n\sum x^2 - (\sum x)^2][n\sum y^2 - (\sum y)^2]} \quad (2)$$

Where n is the number of known data points, x and y are the two dependent and independent variables to be modelled. Generally, the higher R^2, the better the linear regression model fits the data.

Additionally, studying the storm surges employs another regression analysis using HHWL records at each tide gauge station, as:

$HHWL(Y) = ax + b$ (3)

The second data processing stage has been performed based on the results of such regression equations (Eq. 1 and 3), for both MSL and HHWL to estimate their projected values for the year 2025. The ArcGIS tools are utilized to delineate and estimate potential inundated regions for these two scenarios (MSL and HHWL). Generally, many spatial interpolation methods exist that may be grouped into three categories: non-geostatistical, geostatistical, and combined techniques. Each method has its merits, disadvantages, and implicit parameters affecting its performance. The krigging geostatistical method, applied in the current study, performs better than non-geostatistical methods and often used in environmental applications (Li and Heap, 2008).

The 16 TripleSat high-resolution satellites images have been georeferenced and adjusted using 58 GNSS Ground Control Points (GCP) . The Erdas remote sensing software has been utilized in such procedure, where the rational polynomial function has been applied. Next, the extraction and classification of land use types have been obtained (SRI 2018). As stated earlier, it is realized that the study area of the current research does not include large current or near-future development planes since it is mainly used for coast guard activities. Therefore, it is expected that the land uses of 2016, as extracted from remote sensing satellite images, will not be altered considerably over the coming few years. Furthermore, such potential flooded areas are

overlaid on the land use map of the study area to assess the possible risks over the Nile delta region. A flowchart of the processing steps is depicted in Figure 4. That process starts by computing the relative SRL, at each station, from tide gauge MSL time series and adding them to the corresponding land subsidence rates to compute the absolute SRL at each TG. Next, the potential MSL in 2025 is computed based on the attained absolute SRL at those locations. Furthermore, a GIS environment has been developed in order to spatially delineate the potential flooded regions based on analyzing the DEM-based topography. Such hazardous regions are then, projected on the land use maps obtained from the processed satellite images. Digital maps and statistical indicators are developed to document the expected MSL risks by 2025. The same steps have been carried out for investigating the high high water level and its potential risks.

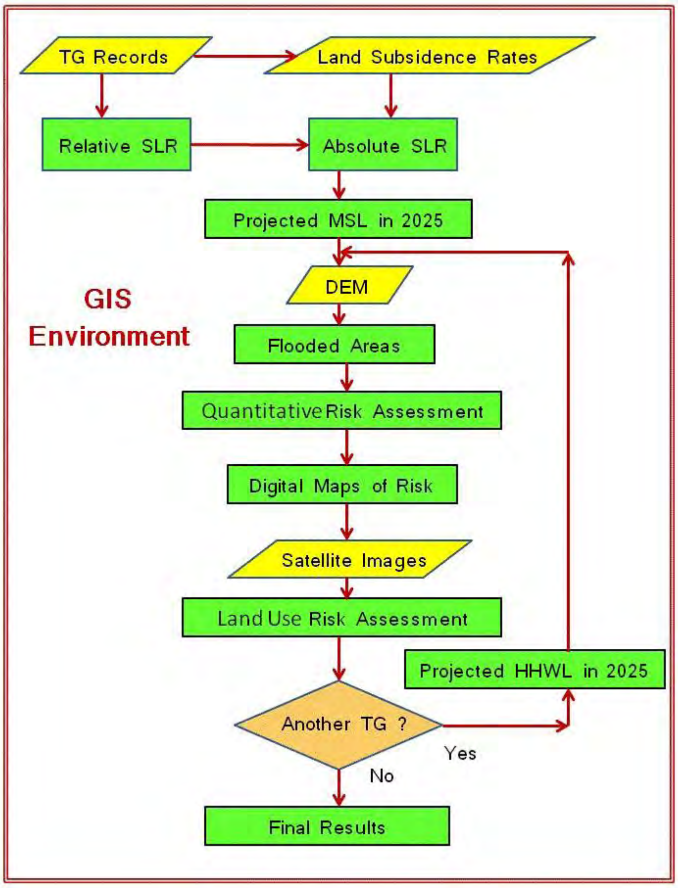

Fig. 4: Data processing flow chart

IV. RESULTS AND DISCUSSIONS

4.1 Results of Sea Level Variations

The results of analyzing the average annual seawater variations at the available five tide gauges are tabulated in Table 4 and were illustrated in Figures 5 and 6. It can be realized that the annual average of MSL range between 0.26 m at Damietta and 0.46 m at Pot Said. It is seen that four TG are close in MSL magnitude while that of Damietta is significantly different. This might be attributed to the long gap of the available dataset at this station. Also, it is noticed that the HHWL varies from 0.88 m at Alexandria to 1.10 m at Rosetta.

Table 4: Statistics of average annual sea water variations at five TG (m) stations

TG	MSL			HHWL
	Minimum	Maximum	Mean	
Alexandria	0.42	0.46	0.45	0.88
Port Said	0.45	0.47	0.46	0.90
Damietta	0.11	0.40	0.26	0.94

Burullus	0.25	0.63	0.41	1.15
Rosetta	0.39	0.46	0.42	1.10

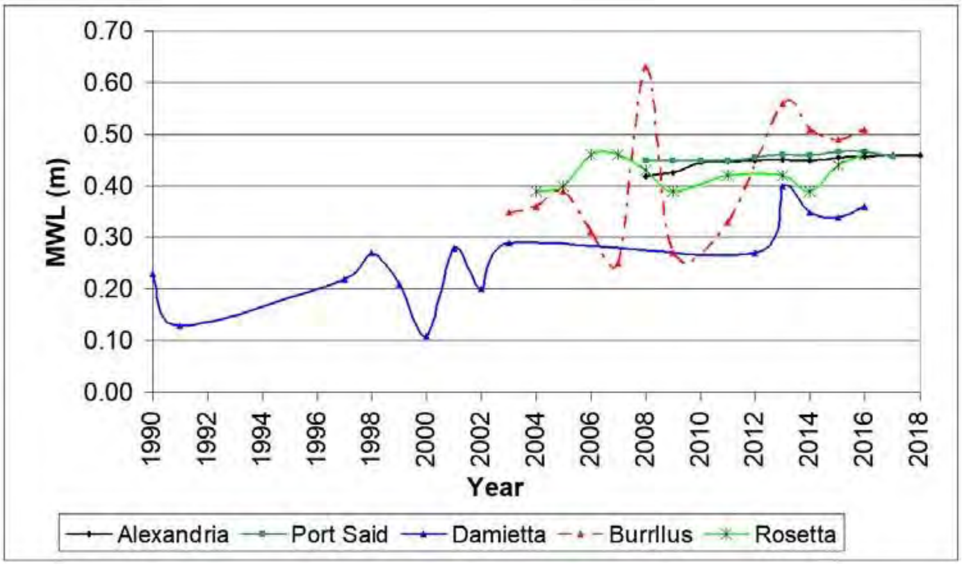

Fig. 5: Mean sea level variations at tide gauges

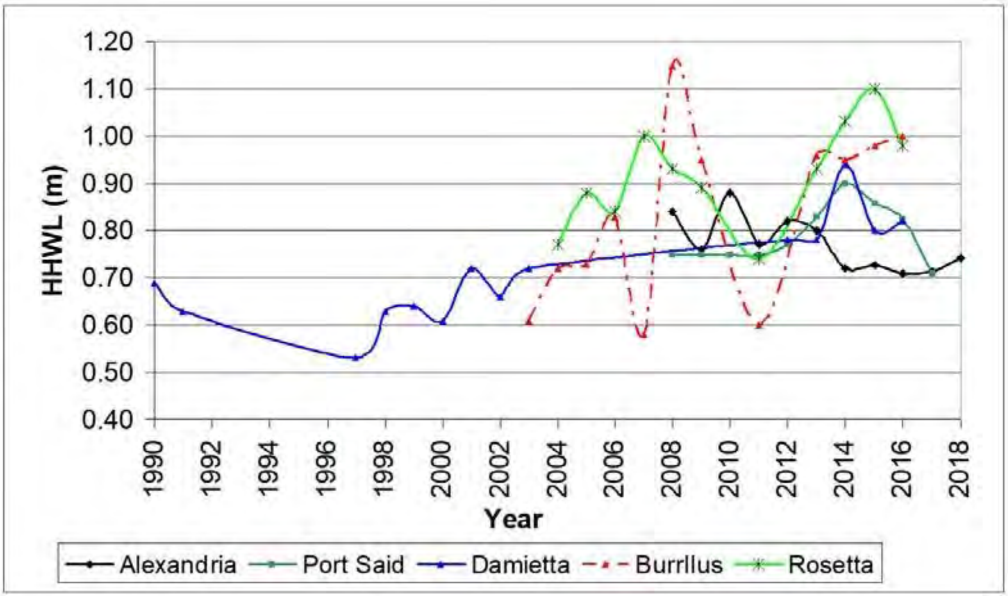

Fig. 6: High High water level variations at tide gauges

Since the available tide dataset contains half-hourly observations at both Alexandria and Port Said, a closer look at tide characteristics is accessible. Figures 7 and 8 depict the average monthly variations of sea water at both gauges over the period 2008-2017. The average monthly MSL at Alexandria ranges from 0.42 m in February to 0.49 m in August. The average HHWL ranges from 0.62 m in March and 0.75 m in August. For Port Said, the average monthly of MSL varies between 0.40 m on April and 0.53 m in August, while the average of HHWL ranges from 0.63 m in February and 0.77 m in September. However, the actual tide observations at these TG over the entire period (2008-2017) reveal that the maximum HHWL reached 0.88 m and 0.90 m at Alexandria and Port Said in August 2010 and March 2014 respectively (Table 5). This indicates that the storm surges could be as much as almost one meter at the Nile delta costs.

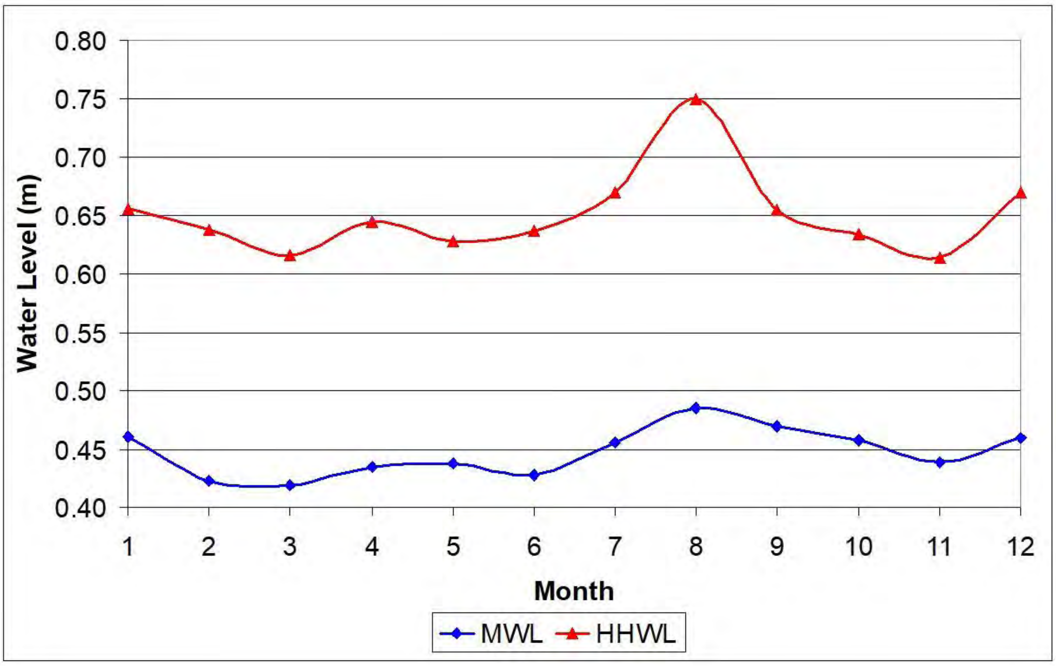

Fig. 7: Average monthly sea level variations at Alexandria TG

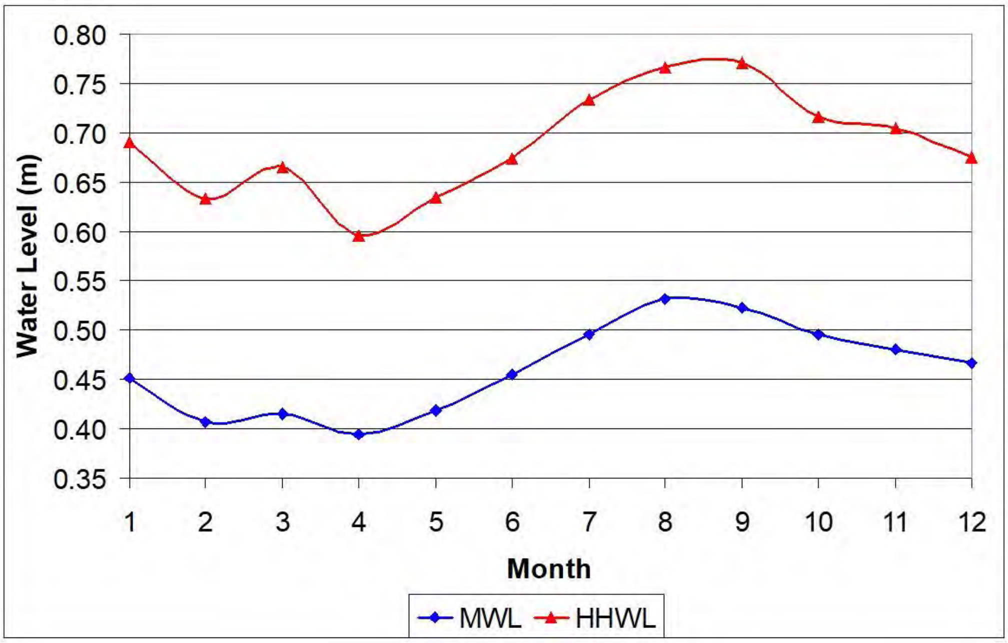

Fig. 8: Average monthly sea level variations at Port Said TG

Table 5: Statistics of actual observed HHWL variations at Alexandria and Port Said TG stations over 2008-2018 (m)

	Minimum HHWL		Maximum HHWL	
	Value (m)	Month	Value (m)	Month
Alexandria	0.46	4/2008	0.88	8/2010
Port Said	0.50	4/2010	0.90	3/2014

Furthermore, the regression analysis (Eq. 1, 3) has been carried out to model MSL and HHWL variations at each TG, along with their corresponding coefficient of determination (R^2) values (Eq. 2). Tables 6 and 7 illustrate the equations for both cases. The applied methodology, herein, depends on investigating the

attained values of R^2 (Tables 6 and 7) as a reasonable indicator for the fit of regression models. Consequently, models of "good" R^2 values are only considered for the prediction of MSL and HHWL potential risks. According to the available data, table 6 demonstrated that the R^2 values of both Burullus and Rosetta TG are very small, which indicates a weak linear regression at these sites based on their available data. Besides, the Damietta TG has a relatively higher trend of annual MSL relative rise (7.4 mm/year) although it lies between Alexandria and Port Said whose annual relative rise equal 3.5 and 1.9 mm/year respectively. Consequently, relative MSL rise rates are only trustable at Alexandria and Port Said TG. Those two rates (Eq. 4 and 5) are employed, next, in projecting sea rise and risk assessment procedures. On the other hand, Table 7 reveals that the regression models of HHWL are only significant for Alexandria and Damietta TG, with considerable R^2 values. That might indicates that, based on the available datasets, HHWL at the available TG sites does not, generally, follow a linear pattern. It worth mentioning that other regression models, such as second-order polynomial, logarithmic model, and exponential model, have been also investigated. However, the attained R^2 indicator of such mathematical models still under 0.40. So, only regression models (Eq. 9 and 11) will be utilized in the potential projection of sea rise and its risk assessment.

Table 6: Statistics of regression analysis of MSL at five TG

TG	Equation	R^2	Eq. No.
Alexandria	$MSL_1 = 0.0035Y - 6.6527$	0.75	4
Port Said	$MSL_2 = 0.0019Y - 3.4118$	0.69	5
Damietta	$MSL_3 = 0.0074Y - 14.643$	0.60	6
Burullus	$MSL_4 = 0.0014Y - 2.4566$	0.04	7
Rosetta	$MSL_5 = 0.0013Y - 2.2609$	0.04	8

Table 7: Statistics of regression analysis of HHWL at Five TG

TG	Equation	R^2	Eq. No.
Alexandria	$HHWL_1 = -0.0124Y + 25.787$	0.52	9
Port Said	$HHWL_2 = 0.0073Y - 13.811$	0.13	10
Damietta	$HHWL_3 = 0.0095Y - 18.419$	0.63	11
Burullus	$HHWL_4 = 0.0235Y - 46.371$	0.32	12
Rosetta	$HHWL_5 = 0.0154Y - 30.022$	0.36	13

Finally, equations 4, 5, 9, and 11 are utilized to predict relative MSL and HHWL estimates in 2025. The projection is limited, herein; to the next five years since the available datasets only cover almost ten years. Next, the land subsidence at each site has been interpolated from Fig. 2, to estimate the absolute sea water rise rates. It has been found the absolute MSL in 2025 equal 0.44 m and 0.46 m at Alexandria and Port Said respectively. Regarding HHWL, it has been found that the projected values at Alexandria and Damietta equal 0.68 m and 0.83 m respectively (Table 8). For other TG stations (with NA values in Table 8), their SLR potential risks in 2025 will be spatially interpolated by GIS.

Table 8: Statistics of projected MSL and HHWL in 2025 (m)

TG	Projected Land Subsidence	Projected MSL		Projected Absolute HHWL
		Relative	Absolute	
Alexandria	0.004	0.435	0.439	0.681
Port Said	0.026	0.436	0.462	NA
Damietta	0.011	NA		0.829

4-2. Results of Sea Level Rise Risk Assessment

Results of projected risk assessment by 2025 in the study area could be divided into two groups: expected constant hazards due to mean sea level rise, and irregular temporal risks due to the storm surge. Findings of both groups are presented in the next sections.

4-2-1. Results of MSL Rise Risk Assessment

Based on the available high-accuracy local DEM, contours zero and 0.45 m have been extracted using the ArcGIS 10 package to delineate potential MSL risks by 2025. It worth mentioning that the value 0.45 m has been used as the average of the projected absolute MSL at both Alexandria and Port Said (Table 8). Accordingly, the spatial area between those two contour lines has been delineated as the potential inundated region, by 2025, due to sea level rise on a mean basis. The area of such a flooded region equals 15.860 Km^2 that represents only 5% of the total area of the entire study region. This precise finding is crucial for decision makers since some previous estimates of sea level inundated regions have reached as much as few thousands of square kilometers (e.g. Hassaan and Abdrabo, 2013). That extremely exaggerated differences might be attributed to applying relatively high and unreliable estimates of sea level rise rate (from 0.64 to 2.45 meters by 2100) and the utilization of unaccurate mean for representing the Nile delta topography. It worth mentioning that a high-accuracy DEM has been utilized in the current study, probably for the first time in Egypt, to attain reliable sea rise risk assessment results.

Additionally, it has been noticed that the potential flooded regions do not follow a regular spatial pattern mainly due to the variations in topography. The width of such areas (i.e., the perpendicular direction to the shoreline) ranges from almost 35 meters to 330 meters. Next, the inundated areas have been projected on the land use GIS layer to assess MSL risk on land uses in the Nile delta region. Fortunately, it has been found that 99.9% of the flooded areas exist in undeveloped land use, while the remaining insignificant 0.1% belong to land use of watercourse. Digital maps depicting such hazardous areas have been developed for decision makers and coastal planners.

4-2-2. Results of HHWL Rise Risk Assessment

On the other hand, the accomplished findings of regression analysis showed that the HHWL variations at the utilized TG sites may not follow a linear regression model and its prediction may not be accurate enough. So, the current research investigated two different scenarios as follows. First, the study considered the linear regressions of HHWL at Alexandria and Damietta are "reasonably" good since their R^2 coefficient are larger than 0.5 (Table 7). So, their projected values in 2025 have been applied to monitor potential future risks. However, since the prediction of the attained regression output is not "very strong", the current research tries another alternative approach. In this regard, the study utilized the maximum recorded HHWL in the available datasets as the worst scenario that could be happened again in the next few years regardless of the expected possible climate changes for the time being. Results of both scenarios are presented, in the next sub-sections, to be considered by decision makers.

Based on the achieved regression model (Eq. 9 and 11), the projected HHWL values at Alexandria and Damietta equal 0.68 m and 0.83 m respectively (Table 8). So, a surface model has been developed by ArcGIS 10 to interpolate expected HHWL in 2025 over the entire study area. Next, the area has been divided into five sub-areas with varying intervals of projected HHWL (Fig. 9). For each sub-area, the potential flooded regions have been delineated. The sum of possible inundated regions due to storm surges (HHWL) is found to be 20.121 km^2 that represents only 8.23 % of the total study area. It can be realized that the hazards of that projected surge are almost 65% higher than those of the MSL. So, although storm surge is spatiotemporal irregular in nature, its hazardous effects exceed the permanent harmful influences of MSL rise. Moreover, it has been found that the possible flooded regions do not a regular spatial form due to the topography discrepancies. The width of such areas varies between 50 meters and 480 meters approximately. Similarly, the inundated areas have been projected on the land use GIS layer to assess HHWL risk on land uses. Table 9 tabulates the statistics of probable risks on land uses in the study area. Fortunately, it can be seen that 99.68% of the flooded areas exist in undeveloped land use type, while the remaining irrelevant 0.32% belong to other land uses.

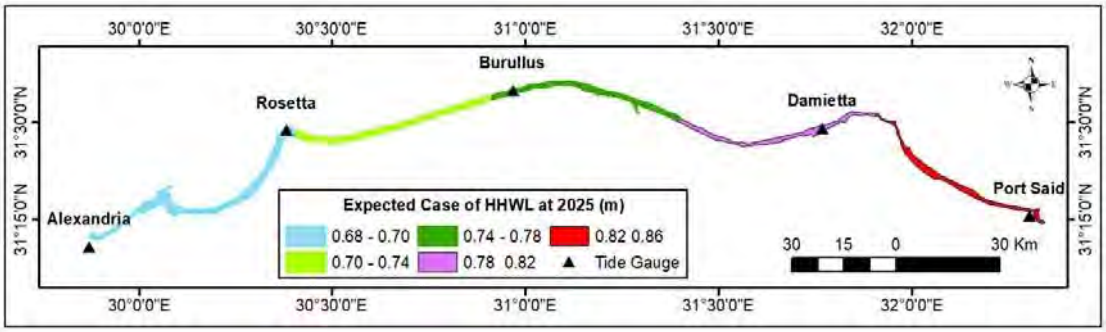

Fig. 9: Variations of expected HHWL in 2025

Second, the worst possible case depends on the potential HHWL of the maximum recorded values in the last decade (last column in Table 4) regardless of any expected possible climate changes for the time being. Another GIS-based interpolation and 3D surface generation have been carried out using those values (Fig. 10). Subsequently, possible inundated regions have been identified over the study area, and the affected land uses have been recognized. It has been found that this HHWL scenario results in flooded regions of a total area of 34.571 km^2, representing 10.89 % of the study area. That means that this worst scenario of possible storm surge is 32% higher than the mathematically-expected situation, and at the same time, it is 118% higher than the MSL risks. So, storm surges should be noticeably considered by the coastal planners in the Nile delta region. The variable width of such flooded areas ranges between 40 and 1200 meters. Risks of this scenario mainly affect undeveloped areas (by 99.66%), and to a minor extent influence, other land uses (Table 9).

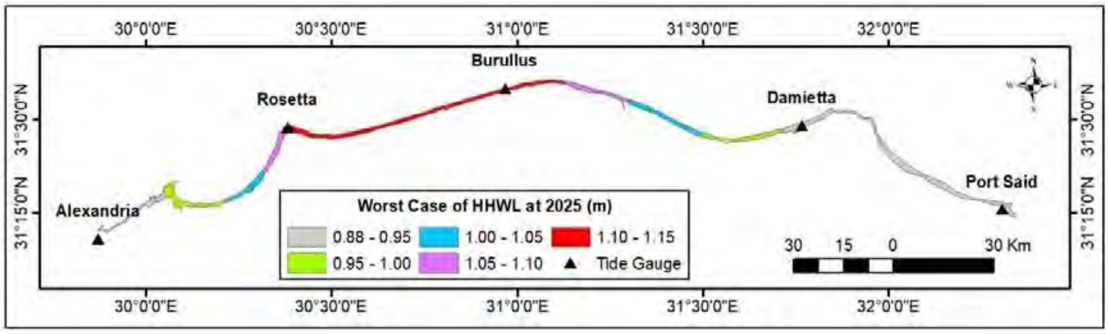

Fig. 10: Variations of worst HHWL in 2025

Table 9: Statistics of two scenarios of surge assessment in 2025

Flooded Land Use	Expected HHWL Scenario		Worst HHWL Scenario	
	Area (km^2)	%	Area (km^2)	%
Undeveloped Areas	26.037	99.68%	34.452	99.66%
Urban Areas	0.066	0.25%	0.029	0.08%
Fish Farms	-	-	0.041	0.12%
Agriculture Areas	0.005	0.02%	0.025	0.07%
Military Areas	-	-	-	-
Harbor	0.006	0.02%	0.0002	0.001%
Strait	0.005	0.02%	0.009	0.03%
Watercourse	0.002	0.01%	0.015	0.04%
Roads	-	-	-	-
Total Area (km^2)	26.121		34.571	
% of Study Area	8.23 %		10.89%	

The utilized precise geospatial datasets, in this study, led to precise estimates of SRL potential risks in the Nile delta region. The main two factors behind such a conclusion is the utilization of accurate national DEM and the determination of reliable estimates of SRL based on national TG stations. Previous studies usually rely on the utilization of global open-source DEM models, which have accuracy levels in the range of three meters in depicting the topography of the Nile delta (Dawod and Al-Ghamdi 2017). A recent study proves that the reliability of such global DEM models in delineating SRL risks is approximately 20% (Abdel-Aziz et al. 2020). Also, previous researches used an unsensible estimate of possible SLR that could reach 2.5 m by 2100 (e.g. Hassaan and Abdrabo 2013). As mentioned in the previous sections, the absolute SLR in the Nile delta is in the range of 0.68 and 0.83 m by the 2025 at Alexandria and Port Said respectively. Results of that study have indicated that approximately 22.5%, 42.2 %, and 49.2 % of the total area of coastal governorates of the Nile delta would be susceptible to inundation under different scenarios of SLR. Similarly, Refaat and Eldeberky (2016) have applied global DEM models (namely GTOPO30 and SRTM) and found that 1401 km^2 of the Nile delta would be subjected to inundation under SLR of 1.0 m by 2100. Also, Hasan et al. 2015) utilized ASTER and SRTM3 global DEM models and concluded that between 6% and 21% of the Nile delta coastal regions (about 500 km^2) would be inundated due to SRL impacts of 0.5 m and 1.0 m respectively by 2100. As a result, it can be concluded that although the global DEM models are free and open-source models for depicting the terrain topography, their utilization in SRL risk assessment could produce insignificant and impractical estimates due to their low vertical accuracy, particularly in low-lying deltaic regions. Hence, acquiring high-accuracy DEM is a vital aspect of SLR risk estimation for coastal management in Egypt and other countries.

V. CONCLUSIONS

Coastal planning and sustainable development rely, on a sense, on the availability of precise up-to-date geospatial information about current and predictable hazards of sea water variations, particularly in low-elevation regions such as river deltas. This research study presented an integrated GIS-based approach, for accomplishing such a fundamental task, comprising tide gauge data, GNSS data, local precise DEM, and high-resolution satellite images. That approach has been carried out, probably for the first time, in the Nile delta region, Egypt as a case study to project the potential sea rise risks in 2025.

The accomplished results indicate that the absolute MSL in 2025 equal 0.44 m and 0.46 m at Alexandria and Port Said respectively, while the projected HHWL at Alexandria and Damietta equal 0.68 m and 0.83 m respectively. On the other hand, findings of projected risk assessment by 2025 could be divided into two groups: expected constant hazards due to mean sea level rise and irregular temporal risks due to the storm surges. The area of such MSL-based flooded region represents only 5% of the total area of the entire study region. Fortunately, it has been found that 99.9% of that flooded areas exist in undeveloped land use, while the remaining insignificant 0.1% belong to land use of watercourse.

Regarding the HHWL-based potential risks, the current research investigated two different scenarios: risk assessment due to the best- attained regression model as the mathematically-expected scenario, and risk assessment due to the worst HHWL situation might happen shortly. For the first scenario, it has been concluded that the sum of possible inundated regions due to storm surges would represent only 8.23 % of the total study area. The GIS-based risk assessment showed that 99.68% of those flooded areas exist in undeveloped land use type. Results of the second HHWL scenario concluded that the inundated regions represent 10.89 % of the study area that means that this worst scenario of possible storm surge is 32% higher than the mathematically-expected situation. Risks of that worst scenario mainly affect undeveloped areas, and to minor extent influence, other land uses. Since HHWL-based potential risks found to be 118% higher than those of MSL, it can be concluded that storm surges should be noticeably considered by the coastal planner in the Nile delta region. It worth mentioning that the accomplished findings prove that the potential impacts of both SRL and surges are significant even though their estimates are significantly less than those of other studies in the literature review. Digital maps depicting all possible hazardous areas have been developed for decision makers and coastal planners. The presented integrated geomatics approach proves to be significantly effective in risk assessment over the Nile delta region, and readable to be applied in other similar regions worldwide.

Declarations:
The authors declare that no funds were allocated for this research
The authors declare that they have no conflict of interest

REFERENCES:

[1]. Abdel-Aziz T, Dawod G, and Ebaid H (2020) DEMs and reliable sea level rise risk monitoring in Nile Delta, Egypt, Discover Sustainability, V. 1, No. 1, https://doi.org/10.1007/s43621-020-00006-7.

[2]. Alboo-Hassan A, Zidan E, Metwally, Z and Elnaggar A (2015) Changes in coastal line and their impact on coastal tourist services in Damietta governorate, Egypt by Using Remote Sensing and GIS Techniques, Int. J. Eng. Res., 6(7):61-71.

[3]. Aucelli P, Paola G, Rizzo A, and Rosskopf C (2018) Present day and future scenarios of coastal erosion and flooding processes along the Italian Adriatic coast: the case of Molise region, Environ. Earth Sci., https://doi.org/10.1007/s12665-018-7535-y.
[4]. Church J, Clark P, Cazenave A, Gregory J, Jevrejeva S, Levermann A, Merrifield M, Milne G, Nerem R, Nunn P, Payne A, Pfeffer W, Stammer D and Unnikrishnan A, (2013) Sea Level Change. In: Climate Change 2013: The Physical Science Basis. Contribution of Working Group I to the Fifth Assessment Report of the Intergovernmental Panel on Climate Change [Stocker, T.F., D. Qin, G.-K. Plattner, M. Tignor, S.K. Allen, J. Boschung, A. Nauels, Y. Xia, V. Bex and P.M. Midgley (eds.)]. Cambridge University Press, Cambridge, United Kingdom and New York, NY, USA.
[5]. Dawod G and Al-Ghamdi K (2017) Reliability of recent global digital elevation models for geomatics applications in Egypt and Saudi Arabia, J. Geogr. Inf. Syst., 9(6):685-698.
[6]. Dawod G, Mohamed H and Haggag G (2019) Relative and absolute sea level rise based on recent heterogeneous geospatial data: A case study in the Nile delta, Egypt, J. sci. eng , 6(6):55-64.
[7]. El Baroudy A and Moghanm F (2014) Combined use of remote sensing and GIS for degradation risk assessment in some soils of the Northern Nile Delta, Egypt, Egypt. J. Remote. Sens. Space Sci., https://doi.org/10.1016/j.ejrs.2014.01.001
[8]. El-Geziry T and Said M (2019) Sea level variations in El-Burullus new harbour, Egypt, Arab. J. Geosci, 12:460, https://doi.org/10.1007/s12517-019-4620-9.
[9]. Frota F, Truccolo E and Schettini C (2016) Tidal and sub-tidal sea level variability at the northern shelf of the Brazilian Northeast Region, Anais da Academia Brasileira de Ciências (2016) 88(3): 1371-1386, https://doi.org/DOI: 10.1590/0001-3765201620150162.
[10]. Fu X and Peng Z (2018) Assessing the sea-level rise vulnerability in coastal communities: A case study in the Tampa Bay Region, US, Cities, https://doi.org/10.1016/j.cities.2018.10.007
[11]. Gebremichael E, Sultan M, Becker R, El Bastawesy M, Cherif O and Emil M (2018) Assessing land deformation and sea encroachment in the Nile delta: A radar interferometric and inundation modeling approach, J. Geophys. Res. Solid Earth, 123, 3208–3224. https://doi.org/10.1002/2017JB015084.
[12]. Hassaan M and Abdrabo M (2013) Vulnerability of the Nile Delta coastal areas to inundation by sea level rise, Environ. Monit. Assess., 185:6607–6616, https://doi.org/10.1007/s10661-012-3050x.
[13]. Hasan E, Khan S and Hong Y (2015) Investigation of potential sea level rise impact on the Nile Delta, Egypt using digital elevation models, Environ. Monit. Assess. 187:649, https://doi.org/10.1007/s10661-015-4868-9.
[14]. Hereher M (2015) Coastal vulnerability assessment for Egypt's Mediterranean coast, Geomatics, Nat. Hazards Risk, 6(4):342–355, https://doi.org/10.1080/19475705.2013.845115.
[15]. Hossena H and Negm A (2016) Change detection in the water bodies of Burullus Lake, Northern Nile Delta, Egypt, using RS/GIS, Procedia Eng., 154:951 – 958.
[16]. IPCC (2014a) Climate Change 2014: Synthesis Report. Contribution of Working Groups I, II and III to the Fifth Assessment Report of the Intergovernmental Panel on Climate Change [Core Writing Team, R.K. Pachauri and L.A. Meyer (eds.)]. IPCC, Geneva, Switzerland, 151 pp.
[17]. IPCC (2014b) Climate Change 2014: Impacts, Adaptation, and Vulnerability. Part A: Global and Sectoral Aspects. Contribution of Working Group II to the Fifth Assessment Report of the Intergovernmental Panel on Climate Change [Field, C.B., V.R. Barros, D.J. Dokken, K.J. Mach, M.D. Mastrandrea, T.E. Bilir, M. Chatterjee, K.L. Ebi, Y.O. Estrada, R.C. Genova, B. Girma, E.S. Kissel, A.N. Levy, S. MacCracken, P.R. Mastrandrea, and L.L. White (eds.)]. Cambridge University Press, Cambridge, United Kingdom and New York, NY, USA, 1132 pp.
[18]. IPCC (2019) IPCC Special Report on the Ocean and Cryosphere in a Changing Climate [H.-O. Pörtner, D.C. Roberts, V. Masson-Delmotte, P. Zhai, M. Tignor, E. Poloczanska, K. Mintenbeck, A. Alegría, M. Nicolai, A. Okem, J. Petzold, B. Rama, N.M. Weyer (eds.)]. In press
[19]. Kaloop M, Rabah M and Elnabwy M (2016) Sea Level Change Analysis and Models Identification based on Short Tidal Gauge Measurements in Alexandria, Egypt, Mar. Geodesy, https://doi.org/10.1080/01490419.2015.1134735.
[20]. Keogh M and Törnqvist T (2019) Measuring rates of present-day relative sea-level rise in lowelevation coastal zones: a critical evaluation, Ocean Sci., 15:61–73, https://doi.org/10.5194/os15-61-2019.
[21]. Khan A (2019) Why would sea-level rise for global warming and polar ice-melt?, Geosci. Front., 10:481-494, https://doi.org/10.1016/j.gsf.2018.01.008.
[22]. Li J and Heap D (2008) A review of spatial interpolation methods for environmental scientists, Report
[23]. 2008/23, Geoscience Australia, 137 pp., Australia
[24]. Martínez-Asensioa A, Wöppelmanna G, Ballua V, Beckera M, Testuta L, Magnanc A, and Duvata V (2019) Relative sea-level rise and the influence of vertical land motion at Tropical Pacific Islands, Glob Planet Change, 176:132-149.
[25]. Mohamed H (2015) Spatial analysis of sea level rise in Egypt's northern coast and its influence on the geodetic vertical datum, International Journal of Geomatics and Geosciences, 6(1):45-55.
[26]. Mohamed H, Shaheen B, Hosney M, and Dawod G (2015) High-precision GPS monitoring of the land subsidence in the Nile Delta: Status and preliminary results, Regional Conference on Surveying and Development, Sharm El-Sheikh, Egypt, Oct. 3-6, 2015.
[27]. MODIS (Moderate Resolution Imaging Spectroradiometer) (2020) October26, 2019 Rare storm over
[28]. Mediterranean sea, Available from: https://modis.gsfc.nasa.gov/gallery/individual.php?db_date=2019-10-26, Accessed 18 Dec, 2020.
[29]. Neumann J, Hudgens D, Herter J and Martinich J (2010) Assessing sea-level rise impacts: A GIS-based framework and application to coastal New Jersey, Coast Manage, 38(4):433-455.
[30]. Nhan N (2016) Tidal regime deformation by sea level rise along the coast of the Mekong delta, Estuar. Coast. Shelf Sci., (183):382-391.
[31]. Poitevin C, Wöppelmann G, Raucoules D, Cozannet G, Marcos M and Testut L (2019) Vertical land motion and relative sea level changes along the coastline of Brest (France) from combined space-borne geodetic methods, Remote Sens. Enviro., 222:275–285, https://doi.org/10.1016/j.rse.2018.12.035.
[32]. Rajan C and Saud J (2018) Storm surge and its effect - A review on disaster management in coastal area, J. Civ. Eng. Res., 4(5):204-210.
[33]. Rateb A and Abotalib A (2020) Inferencing the land subsidence in the Nile Delta using Sentinel-1 satellites and GPS between 2015 and 2019, Sci. Total Environ. 729:138868, https://doi.org/10.1016/j.scitotenv.2020.138868
[34]. Refaat M and Eldeberky Y (2016) Assessment of coastal inundation due to sea-level rise along the Mediterranean coast of Egypt, Mar. Geodesy, https://doi.org/10.1080/01490419.2016.1189471.
[35]. Ruiz-Ramirez J, Euan-Avila J and Rivera-Monroy V (2019) Vulnerability of coastal resort cities to mean sea level rise in the Mexican Caribbean, Coast Manage, https://doi.org/10.1080/08920753.2019.1525260.

[36]. Siegel F (2020) Adaptations of Coastal Cities to Global Warming, Sea Level Rise, Climate change and endemic hazards, Springer Briefs in Environ. Sci., Switzerland; https://doi.org/10.1007/978-3030-22669-5_7.
[37]. Siddig N, Al-Subhi A and Alsaafani M (2019) Tide and mean sea level trend in the west coast of the Arabian Gulf from tide gauges and multi-missions satellite altimeter, Oceanologia, 61:401— 411.
[38]. SONEL (Système d'Observation du Niveau des Eaux Littorales) (2019) Available from: http://www.sonel.org/, Accessed 22 Jun 2019.
[39]. Stanley J (2016) Increased land subsidence and sea level rise are submerging Egypt's Nile delta costal margin, GSA Today, V. 27, https://doi.org/10.1130/GSATG312A.1.
[40]. SRI (Survey Research Institute) (2018) The final report of the research study of management plan of the costal areas over the Mediterranean sea from Port Said to Alexandria, Internal Report, 199 pp., Egypt.
[41]. Temitope B and Daniel U (2014) Modelling and Prediction of Water Level for a Coastal Zone Using Artificial Neural Networks, Int. J. Comput. Eng. Sci., 4(6):26-41.
[42]. Torresan S, Furlan E, Critto A, Michetti M and Marcomini A (2020) Egypt's coastal vulnerability to sea-level rise and storm surge: Present and future conditions, Integr. Environ. Assess. Manag., 16(5):761–772.
[43]. Wang F, Lia J, Shia P, Shanga Z, Lia Y and Wang H (2019) The impact of sea-level rise on the coast of Tianjin-Hebei, China, China Geol., 1:26−39.
[44]. Wassef R and Schüttrumpf H (2016) Impact of sea-level rise on groundwater salinity at the development area western delta, Egypt, Groundw. Sustain. Dev., (2-3): 85–103.
[45]. Watson P (2019) Updated mean sea level analysis: South Korea, J Coast Res, 35(2):241-250.

ITRF-Based Tectonic Coordinates Changes using GNSS-CORS Networks: A Case Study of Egypt

Ashraf Abdallah, Tarek Agag, and Gomaa Dawod

ABSTRACT: Recently, the establishment of Continuously Operation Reference Stations (CORS) networks has been fundamental for Global Navigation Satellite Systems (GNSS)-based geomatics activities worldwide. The Egyptian Surveying Authority (ESA) established a CORS network in 2011 adjusted to the International Terrestrial Reference Frame (ITRF) ITRF2008 (epoch 2011.8096). CORS networks' coordinates must be updated regularly to remain consistent with the latest reference frame realization, so this study aims to update the ESA CORS network to the ITRF 2014 (epoch 2019.5833) reference frame, analyze the coordinates' changes, and determine the positional directions and velocities because of tectonic movements over 2011-2019. Results show that the 2D and 3D coordinate discrepancies during that time have averages of 0.237 m and 0.253 m, respectively. Furthermore, the average direction of horizontal movements is 55.4°, and the overall 2D and 3D regional velocities are 29.7 and 31.7 mm/year, respectively. Therefore, the tectonic movements in Egypt, over the last decade, should be considered in GNSS high-accuracy geomatics activities. In addition, the developed ITRF coordinates-conversion produced accuracy in the order of 1-2 cm. Therefore, we suggest this conversion model is appropriate for GNSS surveying applications in Egypt.

KEYWORDS: GNSS, ITRF, CORS, tectonic movements

Introduction

The first Continuously Operation Reference Station (CORS) system was introduced by the U.S National Oceanic and Atmospheric Administration's (NOAA) National Geodetic Survey (NGS) in 1994 (Snay and Soler 2008). The CORS is designed to provide the users with the geodetic latitude, longitude, height, orthometric height, geopotential, acceleration of gravity, and the vertical deflection of any point (Snay and Soler 2008). Globally, the International Global Navigation Satellite System (GNSS) Service (IGS) provides a worldwide collection of CORS network stations operated by many different organizations (IGS 2020). Applications of CORS stations include crustal motion monitoring and sea-level changes from stations near tide gauges. Further, CORS stations are used to estimate the tropospheric and ionospheric signal delays that significantly improve the accuracy of long-baseline solution or Precise Point Positioning (PPP) solution (IGS 2020).

Ashraf Abdallah, Faculty of Engineering, Aswan University, Aswan, Egypt. E-mail: <ashraf.abdallah@aswu.edu.eg>. **Tarek Agag**, Egyptian Surveying Authority, 1 Abdel-Salam Aref St., 12612, Giza, Egypt. E-mail: <tarekagag_2001@yahoo.com>. **Gomaa Dawod**, Survey Research Institute, National Water Research Center, 308 Al-Ahram St., Giza, 12111, Egypt. E-mail: <dawod_gomaa@yahoo.com>.

Plate tectonics move geodetic control points over, say, a decade over distances large enough to affect control surveys, so it is necessary to determine each station's associated direction and velocity. Such a natural phenomenon is noteworthy in the digital revolution and worldwide use of 3D digital spatial data. Hence, a geodetic frame must be updated periodically to account for the continuous motion of the Earth's tectonic plates. In this regard, each International Terrestrial Reference Frame (ITRF), as a realization of the International Terrestrial Reference System (ITRS), has been updated periodically since 1992 by the International Earth Rotation and Reference Systems Service (IERS) organization (Altamimi 2016; Altamimi et al. 2002, 2011, 2016). Transformation parameters between a recent ITRF and its preceding models are determined and published (ITRF 2020). However, such transformations only approximate the tectonic movements over a global scale. Fine-scale applications for regions or local regions requires more detail as provided by a regional deformation or a plate tectonic model (Hassan et al. 2017; Rabah et al. 2015). On the other hand, updating an ITRF in a country, through converting station coordinates, is a crucial procedure for high-accuracy surveying and geodetic applications (Abdallah 2015). Some such activities have been performed in Nigeria (Bawa et al. 2019), New Zealand (Crook et al. 2016), Nepal (Pearson 2016), Russia (Karpik and Lipatnikov 2016), and Egypt (Hussein 2019).

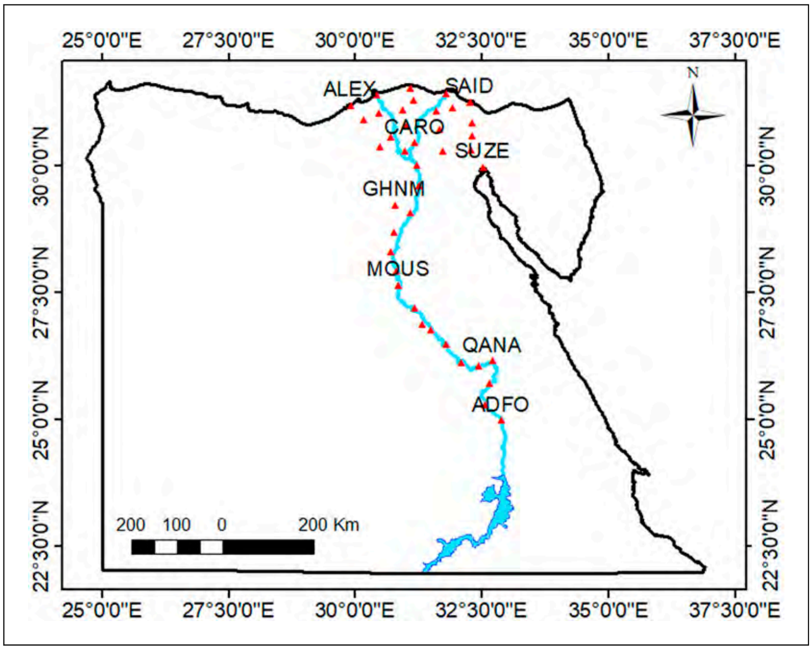

Figure 1. The layout of ESA CORS stations.

Generally, the high-precision geodetic networks need to periodically update their reference frame to the most recent one (Banko et al. 2020 and Yazid et al. 2019).

There are other frames called an International GNSS Reference Frame (IGSxx where xx denotes a specific year) developed by the IGS, as a special version of the ITRFxx, realized solely using GNSS stations. The main difference between an ITRF and an IGS realization is from the handling and calibration of both receivers' and satellites' antennas. This research utilized IGS stations without transformation between ITRFxx and IGSxx, so IGSxx frames are the result. In this regard, it should be mentioned that the global average difference between both types of frames is almost zero (Figurski and Nykiel 2017). In January 2012, ESA established the first permanent Egyptian CORS network. The 40-station network was adjusted relative to ITRF2008 epoch 2011.8096 (ESA 2012). Figure 1 shows the layout of the ESA stations, and Figure 2 shows the photographs of some stations. The CORS network has been tied to the ITRF2008 (epoch 2011.8096), whereas the older passive GNSS reference network, called the High-Accuracy Reference Network (HARN), established in 1995 has been referenced to the ITRF1994 (epoch 1996.4992). El-Tokhey et al. (2017) found that the mean coordinate differences between both networks over six common points in the Nile delta region are on the order of 0.36 m, −0.16 m, and 0.23 m in *X*, *Y*, and *Z*, respectively. Moreover, Baraka et al. (2015) investigated the discrepancies of 2D coordinates between these two networks and found the mean differences in North and East coordinates could be as much as 0.35 ± 0.07 m and 0.34 ± 0.06 m, respectively.

Such sizable differences prompted Rabah et al.

Figure 2. Photographs of some ESA CORS stations.

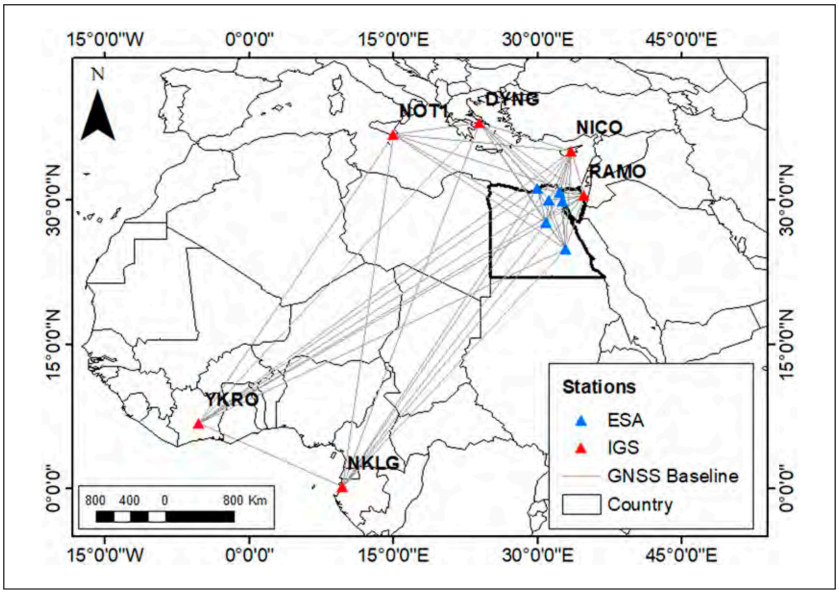

Figure 3. Utilized ESA CORS and IGS stations.

(2015) to propose a semikinematic geodetic datum for Egypt instead of a fixed one to account for tectonic movements. However, as far as the authors are aware, no investigation has been carried out to define the relation between the most recent ITRF 2014 and the older ITRF 2008 over the CORS network in Egypt. This study investigates updating the Egyptian CORS networks and examine the tectonic movements coordinates variations between ITRF 2014 and ITRF 2008 over Egypt.

Methodology

We used raw GNSS data (GPS and GLONASS) for 48-hour simultaneous observation sessions for 33 stations of the ESA CORS network observed in 2019. Our processing strategy consists of several steps that are the same as those used to establish the CORS network in Egypt (ESA 2012). SP3 files that include precise satellite orbits and satellite clock corrections were downloaded from the IGS website and used in GNSS data processing. Ionospheric delays, tropospheric delays, and ocean tide loading were considered and modeled (Trimble 2020), which is important to achieve high-precision GNSS results, particularly for static high-accuracy networks (Mohamed 2016).

First, six ESA CORS stations were tied to and processed with the IGS network using IGS stations YKRO, DYNG, NICO, NKLG, NOT1, and RAMO. Those ESA stations (ADFO, ALEX, CARO, MOUS, QANT, and SUZE) were selected to cover the marginal borders of the ESA CORS network (Figure 3). In this adjustment, the ITRF 2014 (epoch 2019.5833, i.e., the observations' day) coordinates were held fixed to obtain the corresponding coordinates of the six ESA CORS stations. Trimble Business Center (TBC) V 5.0 processed the raw datasets.

In the **second step**, the available ESA network was processed and adjusted with TBC V 5.0 relative to the six sets of step-one IGS coordinates. In this step, only 33 CORS stations, out of the original 40 stations, were used because they have raw GNSS data in 2019. Figure 4 provides a flowchart showing a general procedure of data processing and network adjustments in this study.

Next, the adjusted coordinates in ITRF 2014 (epoch 2019.5833) were compared with the original CORS coordinates in ITRF 2008 (epoch 2011.8096) to examine the variations because of tectonic movements in terms of magnitude, direction, and velocity. The 3D and 2D coordinates' changes over the CORS network were revealed by using both Cartesian (*XYZ*) and projected coordinates (Universal Transverse Mercator [UTM] Zone 36N). Similar studies have investigated the coordinate transformation between ITRF 2014 and ITRF 2008 in other parts of the world (Smith 2020).

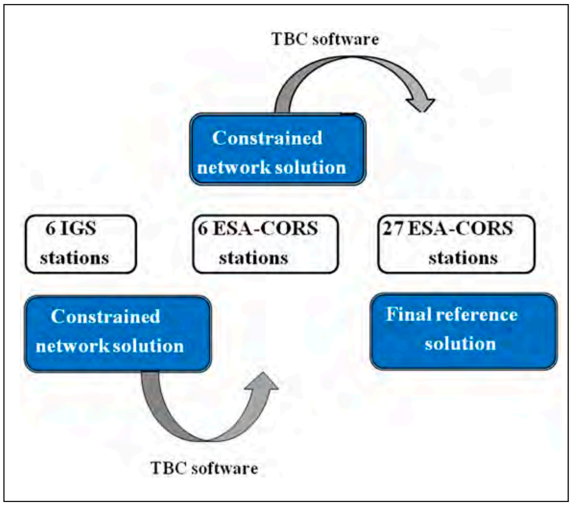

Figure 4. Flowchart of data processing and network adjustment.

Error	Minimum (m)	Maximum (m)	Mean (m)	Standard Deviation (m)
X coordinates	0.0000	0.0100	0.0033	±0.0021
Y coordinates	0.0000	0.0060	0.0020	±0.0014
Z coordinates	0.0000	0.0070	0.0021	±0.0017
3D coordinates	0.0000	0.0136	0.0045	±0.0030

Table 1. Statistics of ESA CORS adjustment results in ITRF 2014 (epoch 2019.5833).

CORS, continuously operation reference stations; ESA, Egyptian surveying authority; ITRF, International terrestrial reference frame.

We developed a simple transformation model that can be used to transform GNSS coordinates between both ITRF 2014 and ITRF 2008 in Egypt. This model depends only on the determination of both 2D and 3D datum shift parameters (Jaffar et al. 2019 and Smith 2020). The mathematical formulation is:

$$\begin{pmatrix} \Delta X \\ \Delta Y \\ \Delta Z \end{pmatrix} = \begin{pmatrix} X \\ Y \\ Z \end{pmatrix}_{ITRF2014} - \begin{pmatrix} X \\ Y \\ Z \end{pmatrix}_{ITEF2008}$$

Processing Data

Raw GNSS data were acquired for continuous 48-hour observation sessions for the ESA CORS network in 2019. Fifty-one baselines were processed to connect the ESA CORS to the IGS network (Figure 3). The lengths of such baselines range from 225,919 m to 4907,041,901 m. In the second processing step, 193 independent GNSS baselines were observed to adjust the ESA CORS network. The 3D vectors have lengths that vary between 21,699 m and 751,432 m. The primarily published coordinates of this network relative to ITRF 2008 (epoch 2011.8096) have been obtained from ESA for later comparisons.

The BERNESE and GAMIT/GLOBK scientific software for GNSS data processing are widely accepted standards for processing GNSS data for applications like this one. However, a recent study showed that new versions of commercial GNSS software (e.g., TBC) proved to achieve comparable accuracy results for national geodetic control networks (Sherif 2018). In this study, the TBC v.5.00 GNSS processing software was used to process and adjust the data. Also, the ArcGIS mapping and spatial analysis package has been applied particularly for converting the projected coordinates of discrete points to a spatial surface that represents the ITRF transformation model in the study area.

Analysis and Results

The adjusted Cartesian coordinates of the ESA CORS network were obtained in the ITRF 2014 (epoch 2019.5833) from the first two steps of the completed processing strategy. During the adjustment process, the outliers, or erroneous baselines, were detected based on the Tau statistical criteria implemented in the TBC package. Outlier baselines were examined carefully and disabled one-by-one from the adjustment process to ensure the maximum precision level of the final network. Table 1 and Figure 5 present the statistics of the final coordinates. The overall accuracy of the 3D coordinates ranges from 0.000 m to 0.0136 m with an average of 0.0045 m and the standard deviation is ±0.0030 m. Such an accuracy level agrees with the national specifications

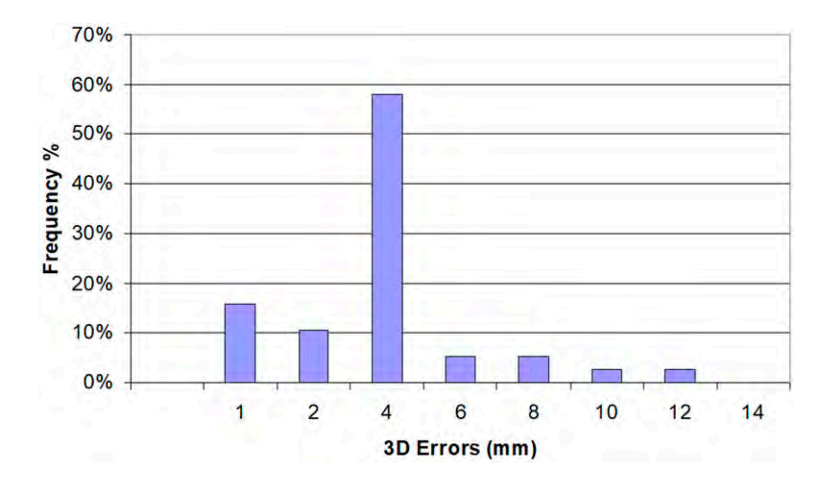

Figure 5. Frequency of 3D errors in ESA CORS in ITEF 2014 (epoch 2019.5833).

Differences	Minimum (m)	Maximum (m)	Mean (m)	Standard Deviation (m)
X coordinates	−0.299	−0.178	−0.222	±0.024
Y coordinates	0.062	0.117	0.091	±0.015
Z coordinates	0.044	0.117	0.077	±0.014
3D coordinates	0.229	0.313	0.253	±0.018

Table 2. Statistics of ESA CORS Cartesian coordinates differences between ITRF 2014 (epoch 2019.5833) and ITRF 2008 (epoch 2011.8096).

CORS, continuously operation reference stations; ESA, Egyptian surveying authority; ITRF, International terrestrial reference frame.

of high-precision GNSS networks (ESA 2020). Consequently, the ESA CORS network has an updated high-precision coordinates relative to the ITRF 2014 (epoch 2019.5833) frame.

Next, the ESA CORS coordinates on both ITRF 2014 (epoch 2019.5833) and ITRF 2008 (epoch 2011.8096) were compared. Table 2 and Figure 6A-D shows the computed Cartesian-coordinate discrepancies. The *X* coordinates' differences range from −0.299 m to −0.178 m with a mean of −0.222 m and a standard deviation of ±0.024 m. Additionally, the *Y* coordinates differences vary between 0.062 m and 0.117 m with an average of 0.091 m and a standard deviation of ±0.015 m, and the *Z* coordinates differences range from 0.044 m to 0.117 m with a mean of 0.077 m and a standard deviation of ±0.014 m. Moreover, the 3D coordinate discrepancies between both frames vary between 0.299 m and 0.313 m with a mean of 0.253 m and a standard deviation of ±0.018 m. Such estimates reveal that the tectonic movements in Egypt, over the last decade, are quite significant and needed to be considered in GNSS surveying and mapping activities.

The 2D projected coordinates (UTM 36N) in both ITRF 2014 (epoch 2019.5833) and ITRF 2008 (epoch 2011.8096) were computed. Table 3 and Figure 7A-D show the computed coordinate differences. These reveal that the differences of the Easting coordinates range from 0.1760 m to 0.2340 m with a mean of 0.1950 m and a standard

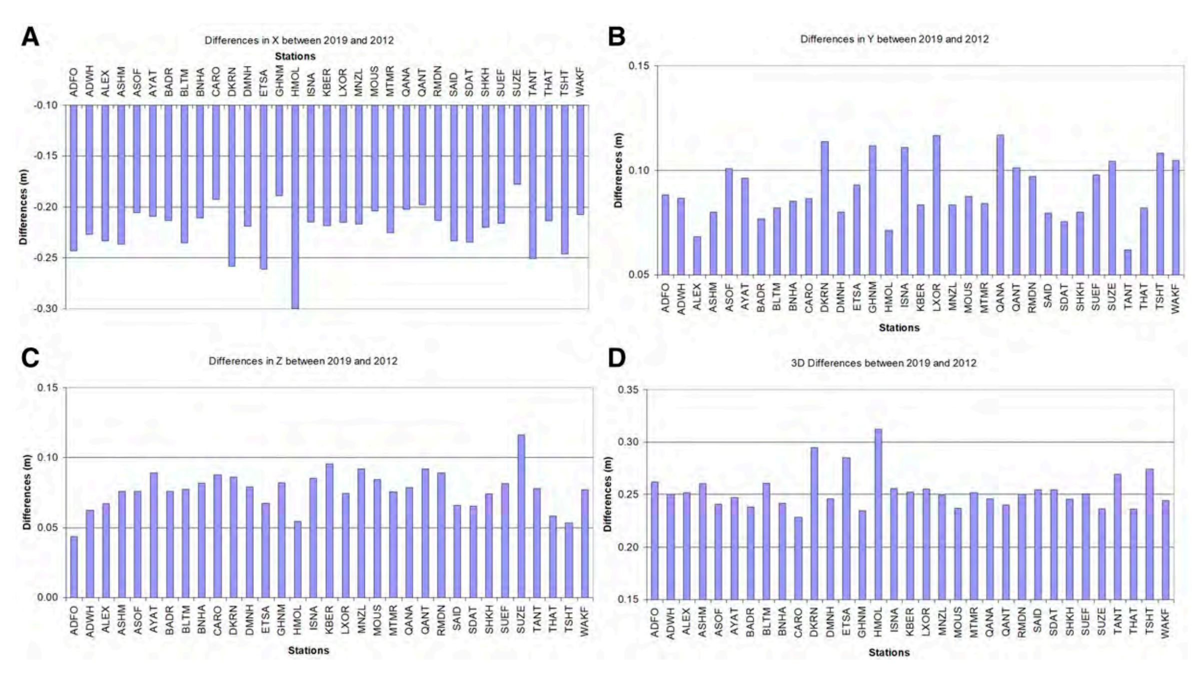

Figure 6. Cartesian differences between ITRF 2014 (epoch 2019.5833) and ITRF 2008 (epoch 2011.8096) (A) X differences (B) Y differences (C) Z differences (D) 3D differences.

Differences	Minimum (m)	Maximum (m)	Mean (m)	Standard Deviation (m)
East coordinates	0.1760	0.2340	0.1950	±0.0140
North coordinates	0.1050	0.1570	0.1340	±0.0130
2D coordinates	0.2150	0.2800	0.2370	±0.0130
Geodetic height coordinates	−0.1590	−0.0230	−0.0860	±0.0260

Table 3. Statistics of ESA CORS projected (UTM) coordinates differences between ITRF 2014 (epoch 2019.5833) and ITRF 2008 (epoch 2011.8096).

CORS, continuously operation reference stations; ESA, Egyptian surveying authority; ITRF, International terrestrial reference frame.

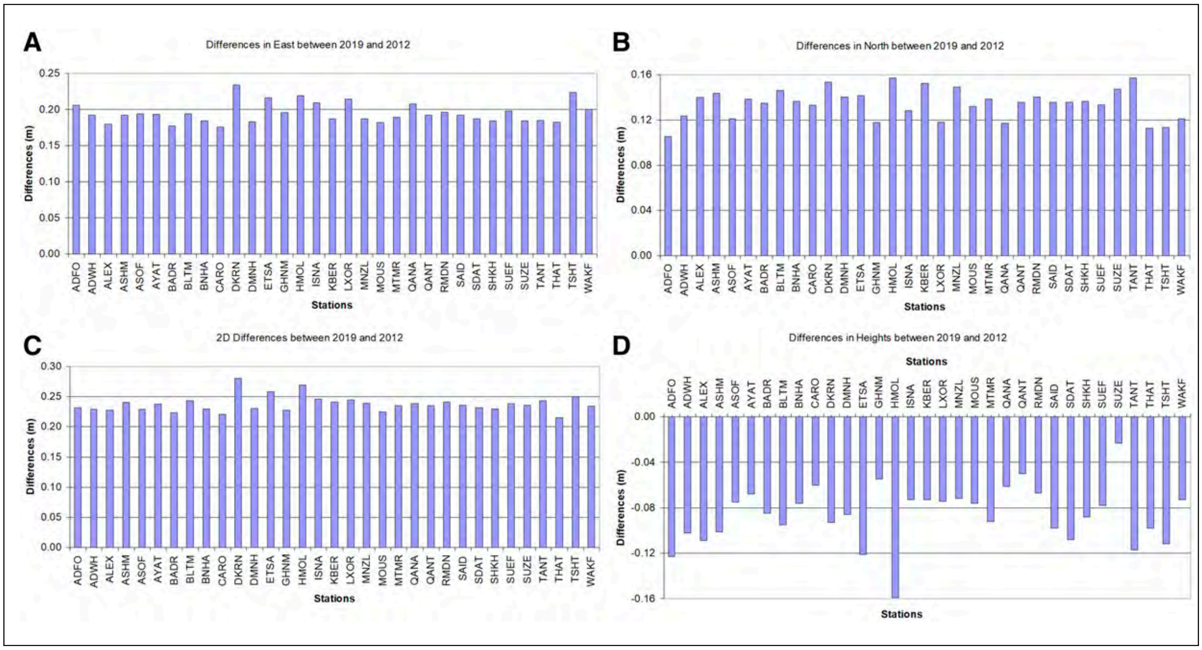

Figure 7. Projected differences between ITRF 2014 (epoch 2019.5833) and ITRF 2008 (epoch 2011.8096) (A) East differences (B) North differences (C) 2D Differences (D) Geodetic height differences.

deviation of ±0.0140 m, and the Northing coordinates variations range between 0.1050 m and 0.1570 m with a mean of 0.1340 m and a standard deviation of ±0.0130 m. Therefore, the 2D coordinate discrepancies between both frames vary between 0.2150 m and 0.2800 m, with an average of 0.2370 m and a standard deviation of ±0.0130 m. The geodetic height discrepancies

Differences	Minimum	Maximum	Mean	Standard Deviation
2D horizontal direction (deg)	49.6°	63.2°	55.4°	±3.4°
2D horizontal velocity (mm/year)	26.8	35.0	29.7	±1.6
1D vertical velocity (mm/year)	−19.9	−2.9	−10.8	±3.2
3D Velocity (mm/year)	28.6	39.1	31.7	±2.2

Table 4. Statistics of magnitude and directions of regional velocities over ESA CORS between ITRF 2014 (epoch 2019.5833) and ITRF 2008 (epoch 2011.8096).

CORS, continuously operation reference stations; SA, Egyptian surveying authority; ITRF, International terrestrial reference frame.

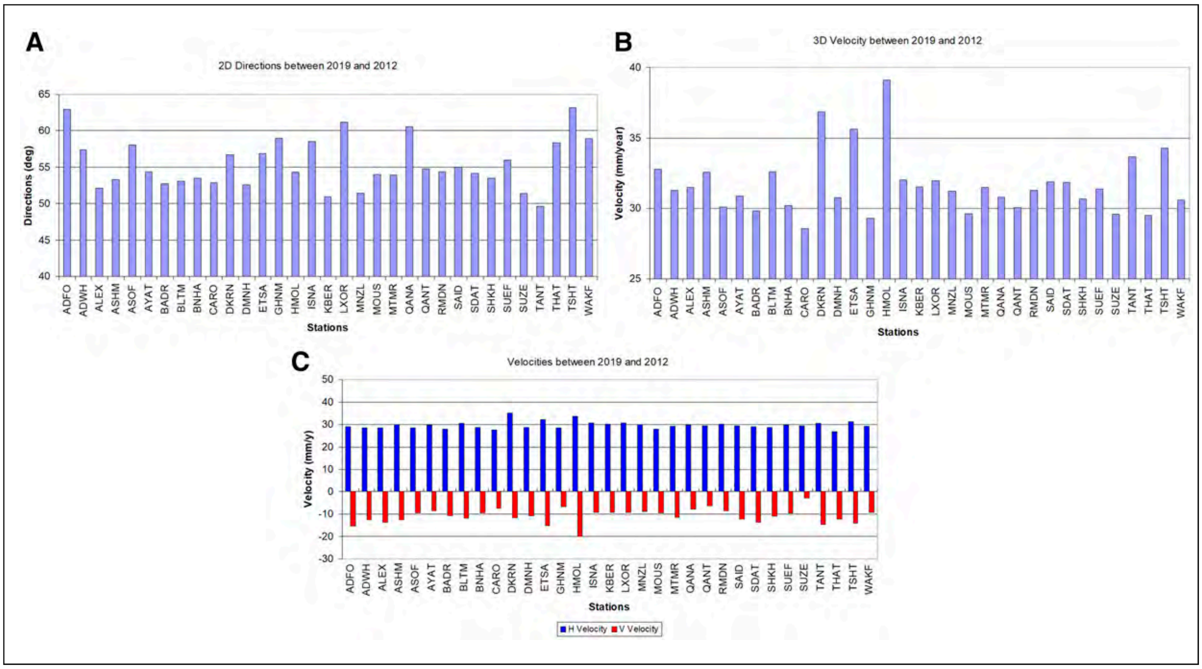

Figure 8. Velocity magnitude and direction between ITRF 2014 (epoch 2019.5833) and ITRF 2008 (epoch 2011.8096) (A) Horizontal velocity directions (B) 3D velocity magnitude (C) 2D and 1D velocity magnitude.

vary between −0.1590 m and −0.0230 m with a mean of −0.0860 m and a standard deviation of ±0.0260 m. As a result, it can be concluded that the GNSS-based mapping activities in Egypt should account for ITRF changes, particularly for large-scale maps.

The next step concerns the magnitude and directions of tectonic movements over Egypt over the period 2011-2019. From the attained GNSS coordinate variations, both directions and velocities of tectonic movements have been estimated. The attained results are tabulated in Table 4 and depicted in Figure 8A-C. The directions of horizontal movements range from 49.6° to 63.2° with an average of 55.4° (Figure 9). The overall 1D, 2D, and 3D regional velocities over the ESA CORS network equal −10.8 mm/year, 29.7 mm/year, and 31.7 mm/year, respectively. Such

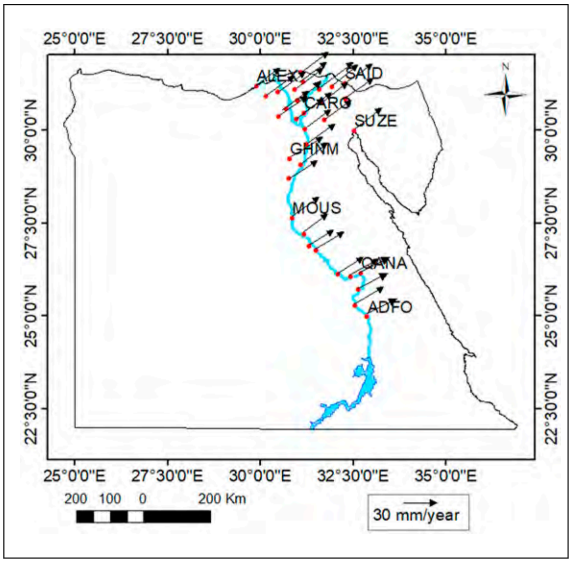

Figure 9. Directions of 2D regional horizontal movements between ITRF 2014 (epoch 2019.5833) and ITRF 2008 (epoch 2011.8096).

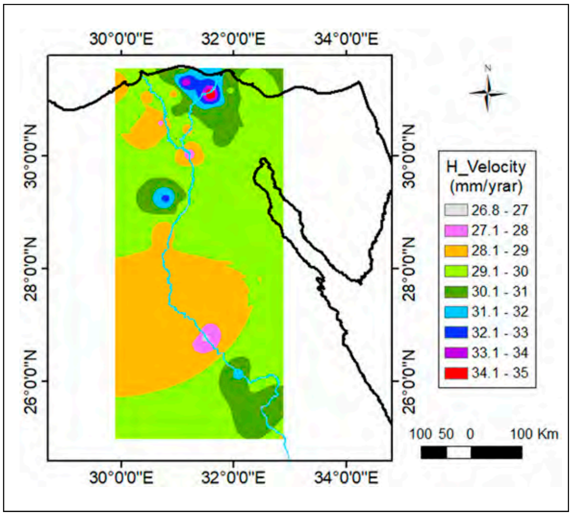

Figure 10. GIS-based 2D regional horizontal velocity transformation model between ITRF 2014 (epoch 2019.5833) and ITRF 2008 (epoch 2011.8096).

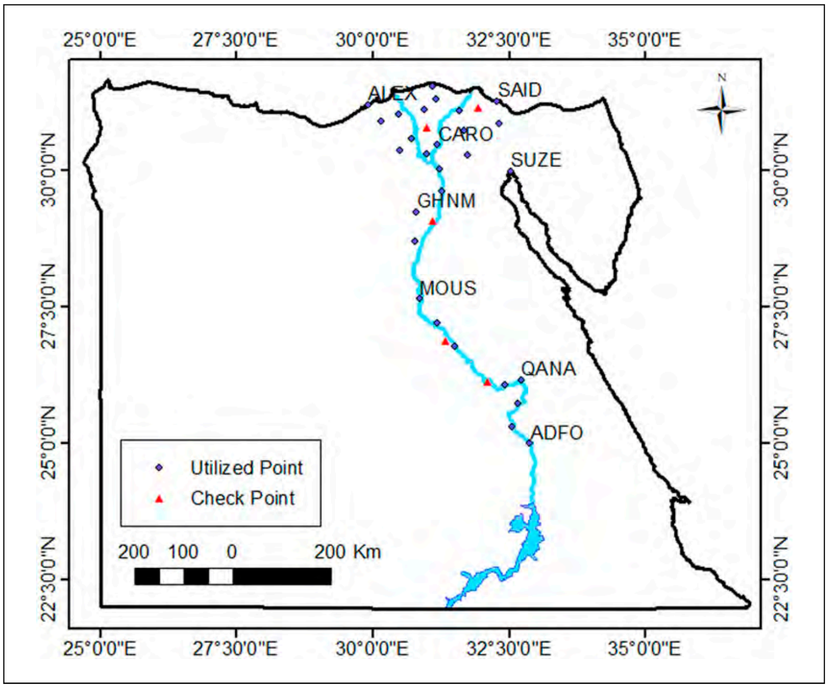

Figure 11. ESA CORS stations for datum shift modeling between ITRF 2014 (epoch 2019.5833) and ITRF 2008 (epoch 2011.8096).

results agree with the known trend of the Nubian tectonic plate (Altamimi et al. 2012; Rabah et al. 2016). The kriging method in the ArcGIS 10 software was used to spatially model the horizontal regional velocity over the Nile valley and delta (Figure 10). Higher velocities exist mainly in the north-eastern region, which can be attributed to the pressure accumulated between the Nile valley and the Gulf of Suez (Mohamed et al. 2016). Comparable results have been reported by other research studies for different regions within Egypt (Mohamed et al. 2016; Sakr et al. 2015; Hegazy 2014).

The final processing step focuses on the development of datum shift models to transform GNSS coordinates between the investigated ITRF frames. To investigate the expected accuracy of such models, only 28 stations are utilized while five stations are kept as checkpoints (Figure 11). Table 5 presents the attained results. The developed transformation models produce accuracy levels, over the checkpoints, in the order of 1-2 cm. Finally, it can be concluded that those conversion models are practically appropriate for GNSS surveying and mapping activities in Egypt.

Conclusions

Building and maintaining GNSS-based CORS stations worldwide in general, and particularly in Egypt, is considered a major concern in providing precise positioning and navigation services. Plate tectonic motions require that geodetic networks to update their frame to be the most recent ITRF. In 2012, the Egyptian Surveying Authority (ESA) finished creating the first permanent CORS network adjusted relative to ITRF 2008 (epoch 2011.8096). The current research aimed to update this national geodetic network and investigate the coordinate discrepancies at their stations. GNSS raw datasets have been acquired for the ESA CORS in 2019, tied to IGS global GNSS network, and adjusted with respect to ITRF 2014 (epoch 2019.5833) frame. The overall accuracy of the adjusted 3D coordinates has an average of 0.0045 m with a standard deviation of ±0.0030 m, which fulfils the national specifications of high-precision GNSS networks. Accordingly, such

Parameters	Using 28 Points		Over Five Check Points	
	Value	Standard Deviation	Average Difference	Standard Deviation
Δ *E*	0.1950	± 0.0140	0.0010	±0.0170
Δ *N*	0.1350	± 0.0130	−0.0060	±0.0150
Δ *X*	−0.2230	± 0.0240	0.0070	±0.0200
Δ *Y*	0.0900	± 0.0150	0.0060	±0.0150
Δ *Z*	0.0770	± 0.0140	0.0000	±0.0140

Table 5. Statistics of 2D and 3D datum shift transformations between ITRF 2014 (epoch 2019.5833) and ITRF 2008 (epoch (2011.8096).

ESA, Egyptian surveying authority; ITRF, International terrestrial reference frame.

updated coordinates should be utilized as the most-recent GNSS geodetic and geodynamic national frame in Egypt.

Additionally, the current research study investigates coordinates changes over the ESA CORS network over the period 2011-2019. The results show that the 3D coordinate discrepancies between both frames vary between 0.2990 m and 0.3130 m with a mean of 0.2530 m and a standard deviation of ±0.0180 m. Similarly, the 2D coordinate discrepancies between both frames vary between 0.2150 m and 0.2800 m, with an average of 0.2370 m and a standard deviation of ±0.0130 m. Such estimates reveal that the tectonic movements in Egypt, over the last decade, are quite significant and need to be considered in GNSS geomatics activities.

Concerning the magnitude and directions of tectonic movements over Egypt, the findings showed that the directions of horizontal movements range from 49.6° to 63.2° with an average of 55.4°. Additionally, it has been figured out that the overall 1D, 2D, and 3D regional velocities over the ESA CORS network equals −10.8, 29.7, and 31.7 mm/year, respectively. Furthermore, the study developed a datum shift model to transform GNSS coordinates between the investigated ITRF frames. Investigating the expected accuracy of such models over a few checkpoints revealed that the developed 2D and 3D transformation models produce accuracy levels in the order of 1-2 cm. Hence, it is concluded that this conversion model is practically appropriate for GNSS surveying and mapping activities particularly in the Nile delta and valley regions of Egypt.

ACKNOWLEDGMENTS

The authors acknowledge the Egyptian Surveying Authority (ESA) for providing the utilized 2019 GNSS datasets.

REFERENCES

Abdallah, A. 2015. The effect of convergence time on the static-PPP solution. In*: 2nd International workshop on "Integration of Point- and Area-wise Geodetic Monitoring for Structures and Natural Objects."* Institute of Engineering Geodesy (IIGS), Stuttgart, Germany. pp. 27-29.

Altamimi, Z. 2016. The international terrestrial reference system and ETRS89: Part II: ITRS & ETRS89 relationship. In: *Presented at the EUREF Toturial,* San Sebastin, Spain.

Altamimi, Z., L. Métivier, and X. Collilieux. 2012. ITRF2008 plate motion model. *Journal of Geophysical Research* 117(B7). DOI: 10.1029/2011JB008930.

Altamimi, Z., P. Rebischung, L. Métivier, and X. Collilieux. 2016. ITRF 2014: A new release of the International Terrestrial Reference Frame modeling nonlinear station motions. *Journal of Geophysical Research: Solid Earth* 121: 6109-31.

Altamimi, Z., P. Sillard, and C. Boucher. 2002. ITRF2000: A new release of the International Terrestrial Reference Frame for earth science applications. *Journal of Geophysical Research: Solid Earth* 107: ETG 2-1-ETG 2-19.

Altamimi, Z., X. Collilieux, and L. Métivier. 2011. ITRF2008: An improved solution of the international terrestrial reference frame. *Journal of Geodesy* 85: 457-73.

Banko, A., T. Banković, M. Pavasović, and A. Đapo. 2020. An all-in-one application for temporal coordinate transformation in geodesy and geoinformatics. *International Journal of Geo-Information* 9(5). DOI: 10.3390/ijgi9050323.

Baraka, M., A. El-Shazly, A. Hassan, K. Amin, T. Agag, and S. Abdelmoneim. 2015. Toward the determination of transformation parameters between active national geodetic control (CORS) and passive national geodetic control (HARN) in Egypt. In: *The Regional Conference on Surveying & Development.* Sharm El Sheikh, Egypt.

Bawa, S., L. Ojigi, J. Dodo, and K. Lawal. 2019. Realization of time-dependent geocentric datum transformation parameters for Nigeria. *SN Applied Sciences* 713. DOI: 10.1007/s42452-019-0711-1.

Crook, C., D. Hansen, and P. Gentle. 2016. Aligning the New Zealand national datum with the international terrestrial reference frame in the face of tectonic deformation. *FIG Working Week* 2016: 2-6. Christchurch, New Zealand.

El-Tokhey, M., T. Fath-Allah, Y. Mogahed, and M. Mamdouh. 2017. Consistency between CORS and NACN Egyptian networks in cairo and Nile Delta. *International Journal of Scientific and Engineering Research* 8(5): 625-30.

ESA (Egyptian Surveying Authority). 2012. *The processing report of the Egyptian virtual reference stations, Internal technical report.* Giza, Egypt: Egyptian Survey Authority.

ESA (Egyptian Surveying Authority). 2020. *An updated standards and specifications of surveying and mapping in Egypt: Volume 1: Standards of surveying works, Internal technical report.* Giza, Egypt: Egyptian Survey Authority.

Figurski, M., and G. Nykiel. 2017. Investigation of the impact of ITRF2014/IGS14 on the positions of the reference stations in Europe. *Acta Geodynamica et Geomaterialia* 14(43): 401-10.

Hassan, T., M. El-Tokhey, T, Fath-Allah, and E.A. Ragheb. 2017. Assessment of different approaches of dynamic/static datum transformation in Egypt

using different plate motion models. *International Journal of Engineering and Advanced Technology* 7(2): 152-9. (IJEAT).

Hegazy, E. 2014. Evaluation of the deformation parameters of the Northern part of Egypt using global navigation satellite systems (GNSS). In: *United Nations/ ICTP Workshop on the use of Global Navigation Satellite Systems for Scientific Applications*. Trieste, Italy.

Hussein, A. 2019. *Compute a unique transformation parameters set for updating the Egyptian HARN and NACN network to the most recent international terrestrial reference frame.* Master od science. Benha, Egypt: Faculty of Engineering, Benha University, Benha.

IGS. 2020. *IGS.* IGS (International GNSS Service) [online]. [http://www.igs.org/; accessed 26 June 2020].

ITRF. 2020. *ITRF.* ITRF (International Terrestrial Reference Frame). [http://itrf.ensg.ign.fr/; accessed 26 June 2020].

Jaffar, N., T. Musa, and W. Aris. 2019. Assessment of geocentric datum of Malaysia 2000 (GDM2000). *The International Archives of the Photogrammetry, Remote Sensing and Spatial Information Sciences* XLII-4(W16): 271-6.

Karpik, A., and L. Lipatnikov. 2016. Velocities validation in the new Russian reference frame GSC-2011. *FIG Working Week* 2016: 2-6. Christchurch, New Zealand.

Mohamed, A., A. Radwan, M. Sharf, Z. Hamimi, E. Hegazy, N. Abou Aly, and M. Gomaa. 2016. Evaluation of the deformation parameters of the northern part of Egypt using global navigation satellite system (GNSS). *NRIAG Journal of Astronomy and Geophysics* 5(1): 65-75.

Mohamed, H. 2016. Assessment of factors influencing static GNSS precise point positioning: A case study in Egypt. *International Journal of Applied Science and Engineering Research* 4(5): 692-701.

Pearson, C. 2016. Towards a modernized geodetic datum for Nepal: Options for developing an accurate terrestrial reference frame following the April 25, 2015 Mw7.8 Gorkha earthquake. *FIG Working Week* 2016: 2-6. Christchurch, New Zealand.

Rabah, M., A. Shaker, and M. Farhan. 2015. Towards a semi-kinematic datum for Egypt. *Positioning* 6: 49-60.

Rabah, M., M. Elmewafey, and M. Farahan. 2016. Datum maintenance of the main Egyptian geodetic control networks by utilizing Precise Point Positioning "PPP" technique. *NRIAG Journal of Astronomy and Geophysics* 5(1): 96-105.

Sakr, K., A. Radwan, M. Rashwan, and M. Gomaa. 2015. Estimation of crustal movements using the Global Positioning System (GPS) measurements along Nile Valley area, Egypt from 2007 to 2012. *NRIAG Journal of Astronomy and Geophysics* 4(1): 55-63.

Sherif, A. 2018. Assessment of precise point positioning for establishing geodetic continuously operating reference stations, *MSC thesis*, Mansoura University, Mansoura, Egypt.

Smith, D. 2020. A GPS based estimate of the rotation of the Mariana plate in both ITRF2008 and ITRF2014, *NOAA Technical report No. NOS NGS 74*, August, 34 pp., National Geodetic Survey, Maryland.

Snay, R., and T. Soler. 2008. Continuously operating reference station (CORS): History, applications, and future enhancements. *Journal of Surveying Engineering* 134(4): 95-104.

Trimble. 2020. *Trimble Bussines Center: Adjustng the network, Training manual*, Trimble Inc., [http://www.trimble.com/; accessed 5 June 2020].

Yazid, N., A. Din, N. Abdullah, and A. Omar. 2019. The international archives of the photogrammetry. *Remote Sensing and Spatial Information Sciences* XLII-4(W16): 685-90.

■

Quest Journals
Journal of Research in Environmental and Earth Sciences
Volume 8 ~ Issue 1 (2022) pp: 19-28
ISSN(Online) :2348-2532
www.questjournals.org

Research Paper

Accuracy Assessment of Horizontal and Vertical Datum Transformations in Small-Areas GNSS Surveys in Egypt

Gomaa M. Dawod, Essam M. Al-Krargy, Huda A. Amer
(Survey Research Institute, National Water Research Center, Giza, Egypt)
Corresponding Author: ***Gomaa M. Dawod***

ABSTRACT:
Global Navigation Satellite Systems (GNSS) surveys in small spatial areas might require simplified datum transformation and height conversion methods. The site calibration is one of several approaches that enable GNSS users to work with local coordinate systems and orthometric heights in real-time. This paper investigates the accuracy of such a method in different spatial scenarios utilizing geodetic datasets in southern Egypt. Based on the available data and attained results, it has been found that accuracy of quite a few centimeters could be achieved. Also, it has been noticed that this method performs better than the conventional geodetic datum transformation and geoid-based height conversion in small areas of less than fifteen square kilometers. Accordingly, it is concluded that site calibration is an efficient straightforward method to be utilized in GNSS surveys for engineering activities in small spatial regions in Egypt.
KEYWORDS: *GNSS, Datum Transformation, Height Conversion, Site Calibration.*

***R**eceived 04 Jan, 2022; **R**evised 13 Jan, 2022; **A**ccepted 15 Jan, 2022 © The author(s) 2022.*
P**ublished with open access at* ***www.questjournals.org

I. INTRODUCTION

With the widespread of GNSS in Egypt and worldwide, the issue of datum transformation becomes more significant. It is a matter of reality that GNSS-based coordinates are relative to the World Geodetic System of 1984 (WGS84) which, in many cases, is not the national datum of a country. Consequently, a datum conversion procedure is needed to employ GNSS data in surveying and mapping on a national scale. Geodetic datum transformation is the mathematical process of defining the 3D spatial relationship between two geodetic datums. Such a process has been carried out in several countries in the last couple of decades, such as Indonesia [1], Ethiopia [2] , Croatia [3], China [4], Saudi Arabia [5] and Russia [6].

The task of datum transformation has been frequently investigated in Egypt in the last few years. For example, [7] (2000) have investigated the utilization of the multiple regression approach as a precise alternative for the traditional similarity transformation between the WGS84 and Helmert 1906 national Egyptian datum. In addition, [8] (2007) have utilized the regression datum shift concept to mathematically define the relationship between WGS84 and the local datums. [9] (2007) proposed improving the datum transformation process by applying the remove-restore technique. Recently, [10] (2018) have proposed the utilization of the Artificial Neural Network (ANN) technique as a novel model for increasing the accuracy of datum transformation.

On another hand, GNSS-based heights are ellipsoidal heights related to WGS84 while surveying projects depend on the orthometric heights relative to the Mean Sea Level (MSL) datum as an approximation of the geoid. Similarly, a height conversion procedure is vital in GNSS civil engineering and surveying activities. The vertical difference between these two datums is the well-known geoidal undulation or geoidal height. Therefore, a geoid or geopotential model is required to perform such a height conversion process. Since the 1960s, many Global Geopotential Models (GGM) have been developed and distributed by the International Center for Global Earth Models (ICGEM). So far, there exist 177 GGM models with variable characteristics, that could be free downloaded [11]. Out of the available GGM models, the Earth Gravitational Model 2008 (EGM2008) constitute a well-known model that has been utilized in height conversions worldwide [12].

The development of a national geoid model for GNSS height transformation in Egypt has been a major task for the geodetic community in the last few decades. Since the development of the pioneer national-scale geoid model by [13], several geoid models have been produced. For instance, [14] have computed a hybrid geoid model based on heterogonous geodetic datasets, that produced a standard deviation of 0.17 meter. Lately,

[15] have investigated the optimum combination of GGMs and global digital elevation models and developed a national geoid with an estimated accuracy of 0.13 meter.

The aforementioned traditional datum transformations, for both horizontal and vertical scenarios, are usually devoted to national-scale activities or large-areas GNSS projects. On the other hand, such transformation parameters and geoid models may not be available for all GNSS surveyors in some countries. Thus, other unconventional approaches have been developed and integrated into GNSS processing software to facilitate datum transformations in small-regions surveying projects. This paper aims to investigate the reliability and accuracy of such simple coordinate-conversion models particularly for small-areas GNSS surveys in Egypt.

II. GEODETIC DATUM TRANSFORMATIONS

3D Similarity or Helmert datum transformations contain, among others, the Bursa-Wolf and the Molodensky-Badekas models. The essential mathematical model can be stated, in a matrix representation, as (e.g. [16]):

$$X_T = c + sRX \quad (1)$$

$$X_T = \begin{bmatrix} X_2 \\ Y_2 \\ Z_2 \end{bmatrix}, \quad X = \begin{bmatrix} X_1 \\ Y_1 \\ Z_1 \end{bmatrix}, \quad c = \begin{bmatrix} dX \\ dY \\ dZ \end{bmatrix}, \quad R = \begin{pmatrix} 1 & R_3 & -R_2 \\ -R_3 & 1 & R_1 \\ R_2 & -R_1 & 1 \end{pmatrix} \quad (2)$$

Where,

XT and X are the coordinate vectors for the transformed and the original 3D coordinate systems respectively, c is the shift vector, s is the scale factor expressed in part-per-million (ppm) units, and R is the 3D rotation matrix containing the three small rotations R1, R2, and R3 about the X, Y, and Z-axis respectively. The Molodensky-Badekas model executes the rotations at an arbitrary point whose coordinates (Xo, Yo, Zo) are to be estimated too in the solution of the transformation parameters.

That model has seven unknown parameters in its general form. However, assuming small values of the three rotation parameters, it might be solved in four unknowns (three-shift parameters and a scale factor) and in other cases; three unknowns (shift parameters) could be enough for simplicity. [7] Have computed a precise set of transformation parameters from WGS 84 to the Helmert 1906 datums using the Molodensky-Badekas modeland found that:

Table 1: Transformation Parameters between WGS84 and Helmert 1906 [7]

Parameter	Value	Standard Deviation	Unit
*d*X	125.457	±0.41	m
*d*Y	-113.943	±0.41	m
*d*Z	10.880	±0.41	m
R_1	-1.434	±0.23	second
R_2	-1.073	±0.42	second
R_3	5.088	±0.43	second
s	-5.4606	±1.08	ppm
X_o	4810523.5586	NA	m
Y_o	2925116.9363	NA	m
Z_o	2962668.8097	NA	m

It is a matter of fact that the traditional similarity datum transformation models assume that the relationship between two geodetic coordinate systems is uniform and can be modelled by a selected number of parameters. However, in reality, the actual parameterization is not as simple as implied in those models. For example, the old geodetic datum, which has been built up over years, does not have a uniform accuracy. Also, there exist distortions in the old datums as new precise data are fitted into these geodetic frames. Hence, the development of more precise relationships between geodetic datums should be considered [7]. The multiple regression technique depends on modelling the 3D differences in latitude, longitude, and heights ($\Delta\phi$, and $\Delta\lambda$, and Δh) between the geodetic coordinates of two systems by three polynomials of sufficient terms to represent the differences over the network, to a given degree of accuracy. This unconventional datum transformation technique has been used to describe the relationships between the WGS84 and 83 local geodetic datums all over the world where the basic formula could be stated as [17]:

$$\Delta \varphi = A_o + A_1 U + A_2 V + A_3 U^2 + A_4 UV + A_5 V^2 + ... + A_{99} U^9 V^9 \quad (3)$$

where,

Ao : is a constant,

A_o, A_1, ... A_{nn}: are coefficients to be determined,

$U = k (\phi - \phi_m)$: is the normalized geodetic latitude of the computation point,

$V = k (\lambda - \lambda_m)$: is the normalized geodetic longitude of the computation point,

k: is a scale factor and degree-to-radian conversion,

ϕ and λ: are local geodetic latitude and longitude (in degrees) of the computation point,

ϕ_m and λ_m : are mid-latitude and mid-longitude values (in degrees) of the local geodetic datum area.

Similar equations could be written for both $\Delta\lambda$ and Δh by replacing $\Delta\phi$ in the left side of the previous formal.

For instance, [7] have developed a multiple regression model for Egypt with a precision equals ±0.03 m, as:

$$\Delta\phi'' = -320.474 + 30.6751\, \phi_{84} + 3.0402\, \lambda_{84} - 1.7380\, \phi^2_{84} + 0.0436\, \phi^3_{84} - 0.0004\, \phi^4_{84} - 0.1056\, \lambda^2_{84} + 0.0012\, \lambda^3_{84} \quad (4)$$

$$\Delta\lambda'' = 4357.7294 - 734.6377\, \lambda_{84} + 49.4639\, \lambda^2_{84} - 0.1705\, \phi_{84} - 1.6600\, \lambda^3_{84} + 0.0278\, \lambda^4_{84} + 0.0037\, \phi^2_{84} - 0.0002\, \lambda^5_{84} \quad (5)$$

where,

$\Delta\phi$" and $\Delta\lambda$" are the differences, expressed in arc seconds, in both latitude and longitude respectively between the WGS 84 and Helmert 1906 geodetic datums, and ϕ84 and λ84 are geodetic coordinates relative to the WGS84 datum.

For GNSS surveys carried out in small areas, other simple datum transformation processes have been proposed. GNSS software manufactures have developed such models and integrated them into their processing prog rams. An example of such a method exist in the Leica Go Office (LGO) of Leica Geosystems and is called a none-step transformation [18]. It produces a set of transformation parameters that enable transforming the WGS84-based Cartesian coordinates (X,Y,Z) directly to a local datum projected coordinates (E,N). Another example of those processes is called site calibration developed by Trimble Co. [19]. It consists of a series of mathematical transformations to establish the relation between WGS84-based GNSS data and local control positions expressed as local projected grid coordinates along with MSL-based elevations. Those transformation procedures contain (ibid):

- A three-parameter datum transformation to convert the WGS-84 3D geodetic coordinates to 3D geodetic coordinates relative to the ellipsoid of the local map grid.
- A map projection to convert the local 2D ellipsoid coordinates into local 2D map grid projected coordinates.
- A geoid model to WGS-84 heights to obtain approximate elevations above the sea level.
- A horizontal least-squares adjustment of the transformed grid 2D coordinates to best fit local control data. This adjustment deals with any local variations in the projection system that cannot be accommodated in the overall datum transformation.
- A height least-squares adjustment converting the heights above the elevations derived from the geoid to the local MSL-based control elevations.

The site calibration, and other similar datum transformation processes, could be considered as unconventional solutions for coordinate conversion just in small areas. It can be concluded from the previous steps that the least-squares adjustment, for both horizontal and vertical coordinates, are utilized to best fit the GNSS-based coordinates to the local system. Such a fit would be valid only inside the project area and could not be applied outside such a small region. However, the merit of this solution is to give GNSS users to work in real-time with a local coordinate system since such a process could be performed during the field campaign.

III. METHODOLOGY AND AVAILABLE DATA

The collected GNSS database comprises 22 stations distributed over an area of 22 x 1 kilometers in southern Egypt. Those stations have known geodetic coordinates in both WGS84 and Helmert 1906 datums. In addition, their orthometric heights have been available too. Based on their spatial distributions, five different scenarios have been applied in the processing stage as presented in Table 2 and depicted in Figure 1.For each

case, the site calibration has been accomplished utilizing at least four points that lay on the area's boundaries. Next, the coordinates of checkpoints are computed utilizing the attained site calibration outputs. Similar steps will be performed for the vertical site calibration too. On another hand, the site calibration outputs are compared against the results of utilizing traditional geodetic transformation and regression-based transformation models (Equation 1-2 and 4-5). Similarly, the vertical site calibration results of each case are judged against the global EGM2008 and the SRI2021 recent national geoid models. Those data processing procedures are depicted in Figure 2.

Table 2: Cases of Data Processing

Case	Region (km)	Area (km2)	No. of Calibration Points	No. of Check Points
1	23 x 0.8	18.4	5	17
2	17 x 0.8	13.6	5	15
3	13 x 0.8	10.4	4	13
4	8 x 0.8	6.4	4	12
5	0.6 x 0.8	0.48	4	10

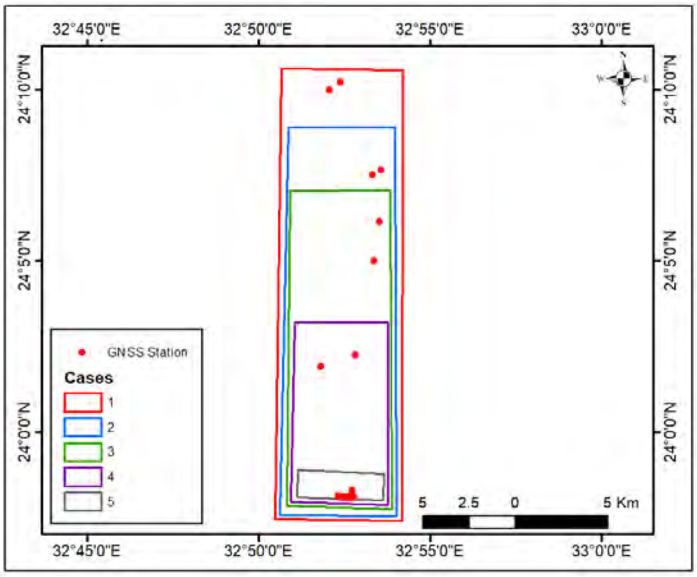

Figure 1: Data Processing Cases

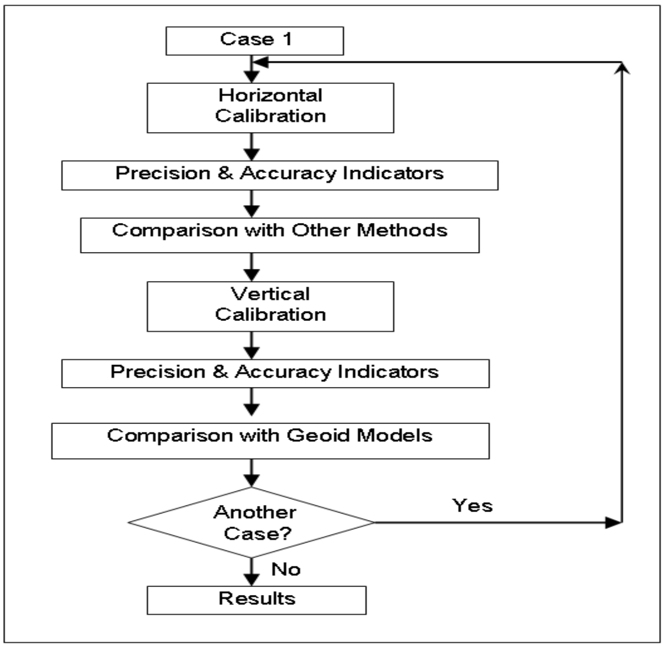

Figure 2: Processing Workflow

IV. RESULTS AND DISCUSSIONS

The accomplished results of site calibrations in terms of horizontal and vertical calibration are discussed in the next sub-sections. Additionally, the comparative results of site calibration with other transformation methods and geoid models are presented and analyzed.

4.1 Precision of Horizontal Transformations

The statistics of horizontal residuals of the site calibration process for the five different cases have been computed, tabulated in Table 3, and depicted in Figure 3. It can be noticed that the mean residuals vary between 0.020 m for case five and 0.045 m for case 1. The standard deviation of the horizontal residuals, as a precision indicator, ranges between ±0.005 m for the last case and ±0.021 m for the first one. Figure 3 shows that both average residual and standard deviation decrease with a small area of the project region as expected. That indicates that the smallest site calibration region, the better the precision of the anticipated output.

Table 3: Precision Statistics of Horizontal Calibration (m)

Case	1	2	3	4	5
Minimum Residual	0.023	0.023	0.001	0.002	0.026
Maximum Residuals	0.073	0.071	0.066	0.057	0.014
Average Residual	0.045	0.041	0.037	0.032	0.020
Standard Deviation	±0.021	±0.023	±0.030	±0.025	±0.005

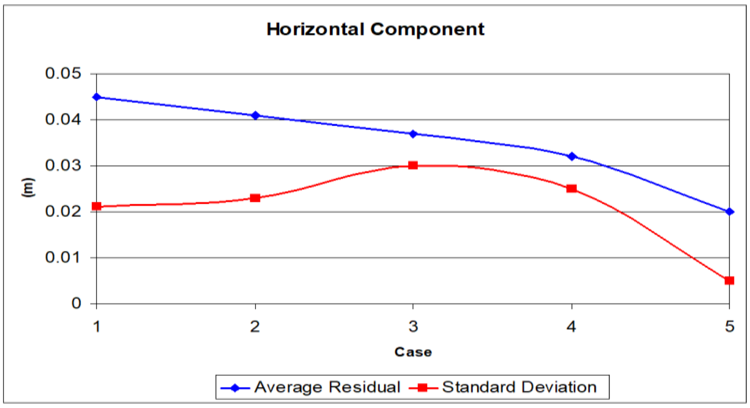

Figure 3: Precision Indicators in Horizontal Direction

4.2 Precision of Vertical Transformations

Similarly, the statistics of vertical residuals of site calibration for the five different cases have been obtained (Table 4 and Figure 4). It can be noticed that the mean residuals are almost zero for the five different cases. The standard deviation of the vertical residuals, as a precision indicator, ranges between ±0.001 m for the last case and ±0.021 m for the first one. Figure 4 shows that both average residual and standard deviation decrease with a small area of the project region as expected. That indicates that the smallest site calibration region, the better the precision of the anticipated output. However, the accuracy indicators are more reliable than the precision ones. The next sub-sections deal with estimating the accuracy indicators of the site calibration method.

Table 4: Precision Statistics of Vertical Calibration (m)

Case	1	2	3	4	5
Minimum Residual	-0.026	-0.011	-0.001	-0.001	-0.002
Maximum Residuals	0.027	0.012	0.001	0.001	0.001
Average Residual	0.000	0.000	0.000	0.000	0.000
Standard Deviation	±0.021	0.010	±0.001	±0.001	±0.001

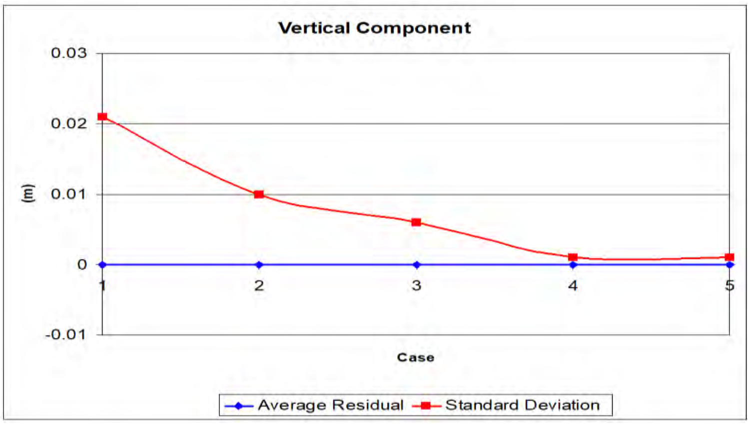

Figure 4: Precision Indicators in Vertical Direction

4.3 Accuracy of Horizontal Transformations

Over checkpoints, the coordinates resulted from the site calibration method have been compared against the corresponding known coordinates. The residuals and their standard deviations, in each case, provide a reliable accuracy indicator. For horizontal accuracy, Table 5 and Figure 5 and 6 present the accomplished findings. From this table, it can be noticed that the average residuals in the East direction range from - 0.183 m to 0.061 m and the standards deviations vary between ±0.348 m for case 1 and ±0.021 m for case 5. On the other hand, the average residuals in the North direction range from 0.153 m to 0.062 m and the standards deviations vary between ±0.236 m for case 1 and ±0.045 m for case 5. Thus, it can be concluded that accuracy of fewer than five centimeters could be attained in the smallest region (less than a square kilometer) as far as the available observations are considered.

Table 5: Accuracy Statistics of Horizontal Calibration (m)

Case	1	2	3	4	5
East Direction					
Minimum Residual	-0.773	-0.586	-0.113	-0.089	-0.001
Maximum Residuals	0.199	0.199	0.054	0.052	0.034
Average Residual	-0.183	-0.072	0.192	0.169	0.061
Standard Deviation	±0.348	±0.242	±0.110	±0.092	±0.021
North Direction					
Minimum Residual	-0.086	-0.079	-0.070	-0.063	-0.059
Maximum Residuals	0.739	0.753	0.032	0.027	0.008
Average Residual	0.153	0.149	0.147	0.117	0.062
Standard Deviation	±0.236	±0.243	±0.062	±0.055	±0.045

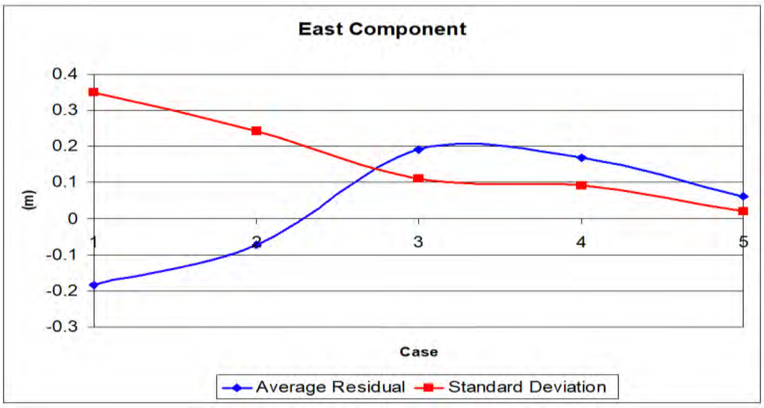

Figure 5: Accuracy Indicators in East Direction

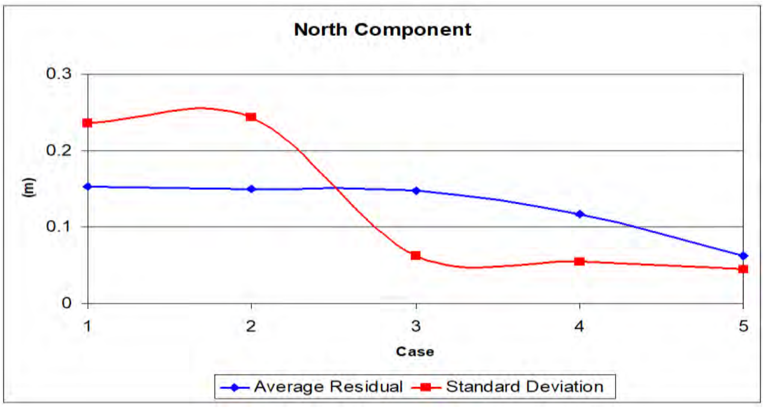

Figure 6: Accuracy Indicators in North Direction

4.4 Accuracy of Vertical Transformations

Similar to the horizontal coordinates, the heights obtained from the site calibration method have been compared to the corresponding known heights (Table 6 and Figure 7). So, it can be found that the average height residuals range from 0.150 m to 0.065 m, and the standards deviations vary between ±0.163 m for case 1 and ±0.019 m for case 5. In addition, the mean residual and standard deviation are decreasing as long as the area of the project region is decreasing. Consequently, it can be concluded that accuracy of fewer than five centimeters could be attained in cases 2 to 5 where the area of the study region varies from 14 to less than one square kilometer. More significant, it is noticed that accuracy of just two centimeters in height could be obtained from the site calibration method when the study area is less than a square kilometer.

Table 6: Accuracy Statistics of Vertical Calibration (m)

Case	1	2	3	4	5
Minimum Residual	-0.036	-0.070	-0.140	0.011	0.043
Maximum Residuals	0.417	0.092	0.128	0.104	0.104
Average Residual	0.150	0.042	0.061	0.054	0.065
Standard Deviation	±0.163	±0.043	±0.039	±0.032	±0.019

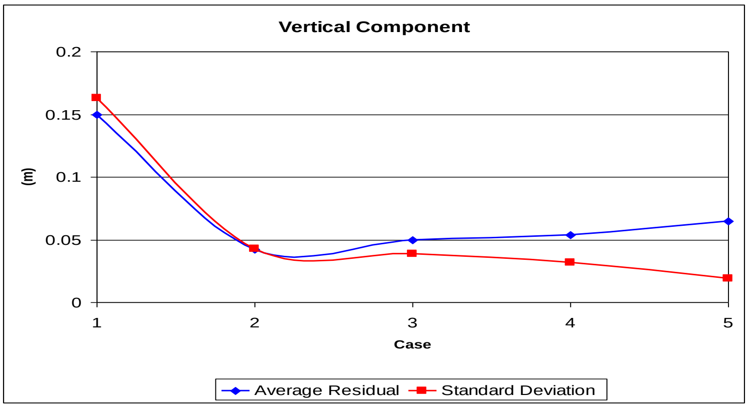

Figure 7: Accuracy Indicators of Vertical Component

Plotting the attained accuracy indicators of all cases against the area of the study region, Figure 8 concludes that the accuracy of the site calibration method is getting better as long as the project region is decreased. It is obvious, from this figure, that accuracy of almost ten centimeter could be expected for regions less than ten square kilometers. Five-centimeter accuracy, on the other hand, could be attained for study areas less than three square kilometers. Such findings conclude that the site calibration method should be utilized in GNSS surveying only for small-area projects.

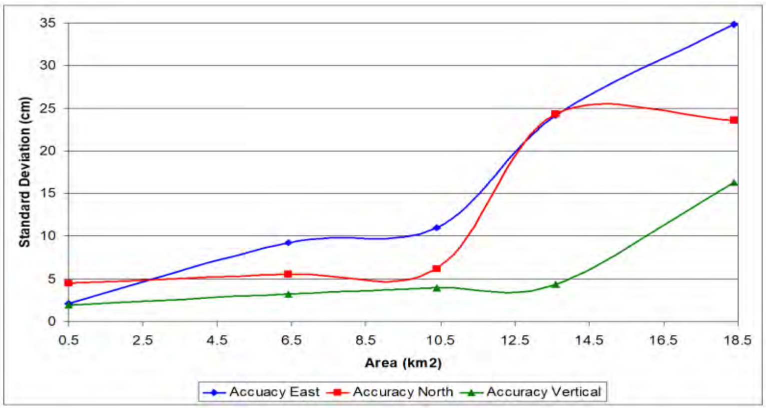

Figure 8: Accuracy Variations with Area

4.5 Comparisons to Other Methods

Having investigated the precision and accuracy of the site calibration method, the final analysis step is to compare its performance to traditional geodetic approaches in both horizontal and vertical components. First, the 3D conventional datum transformation using the Molodensky-Badekas model, with the parameters presented in Table 1, has been utilized over all available checkpoints. Next, the resultant geodetic coordinates have been projected on the Helmert 1906 local datum and, then, compared against their corresponding known 2D coordinates. Similarly, the multiple regression transformation (Equation 4-5) has been carried out. Table 7 and Figure 9 present the results of both datum transformation approaches over the entire study area. It can be realized that the first method produced an accuracy level, in East and North coordinates, varying between ±0.441 m and ±0.594 m while the second one produced accuracy standard deviations range from ±0.373 m and ±0.545 m. Comparing such findings with the corresponding results of the site calibration method (Table 5), it can be noticed that the results of site calibration in both projected coordinates are better than those of the traditional and multiple-regression methods in all investigated cases. This highlights the power of the site calibration for GNSS surveys in small areas. In another sense, both EGM2008 and SRI2021 geoid models have been used to interpolate geoidal undulations at known points, compute their geoid-based orthometric heights, and compare them to known heights. From Table 7 and Figure 9, it can be realized that the accuracy of both geoid models equals ±0.147 m and ±0.106 m respectively. Again, a comparison has been carried out between such results and the corresponding findings of the site calibration method (Table 6). Thus, it can be noticed that both geoid models perform better than the site calibration only in case 1 where the area of the project region equal 18.4 square kilometers. In all other study cases, the site calibration method is superior to the investigated global and local geoid models. Thus, it can be concluded that the site calibration method could be considered an optimum method for datum transformation and height conversion in small-areas GNSS surveys.

Table 7: Accuracy Statistics of Other Methods (m)

	Minimum Variations	Maximum Variations	Average Variations	Standard Deviation
3D Similarity Transformation: East	-1.155	-0.050	-0.677	±0.441
3D Similarity Transformation: North	-2.359	-1.185	-1.684	±0.594
Regression Transformation: East	2.217	3.241	2.659	±0.373
Regression Transformation: North	5.009	6.306	5.408	±0.545
EGM2008 Geoid	0.047	0.460	0.277	±0.147
SRI2021 Geoid	0.103	-0.258	-0.030	±0.106

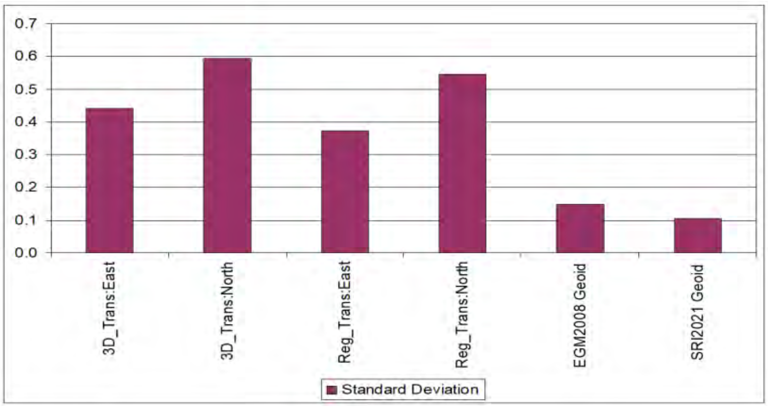

Figure 9: Accuracy Indicators of Other Methods

V. CONCLUSIONS

This paper investigates one of such untraditional datum and height conversions particularly for small-areas GNSS applications; the so-called site calibration. A geodetic dataset in southern Egypt, relative to both WGS83 and Helmert 1906 datums, has been utilized in several scenarios with variable lengths. It has been found that the precision of site calibration range from ±0.030 and ±0.005 in the horizontal direction and between ±0.021 and ±0.001 m in the vertical components. Over checkpoints, the accuracy of this method could be less than ±0.045m in both East and North coordinates, and ±0.019 m in heights particularly in areas less than a square kilometer.

A comparison has been carried out of those results to results of traditional geodetic datum transformation and multiple-regression approaches. It has been noticed that the site calibration method performs better than both approaches in all investigated scenarios. Another comparison has been performed between the heights resulted from site calibration and those obtained by utilizing global and national geoid models. For study regions less than fifteen square kilometers, the site calibration produces more accurate orthometric heights over checkpoints.

Based on the available data, it could be concluded that the site calibration method is optimum for converting WGS-84 geodetic coordinates to projected local coordinates and orthometric heights. Additionally, another merit of this method is to give GNSS users the capability to work in real-time with a local coordinate system since such a process could be performed during the field campaign.

REFERENCES

[1]. Syetiawan, A., Ramdani, D., Safii, A., Ardhitasari, Y., Gaol, Y., and Annuriah, I. (2019) Development of parameter transformation of Indonesian geospatial reference system 2013, Proceedings of the 1st International Conference on Geodesy, Geomatics, and Land Administration 2019 (GEODETA 2019), pp. 77-94.

[2]. Hassen, A. (2019) Determination of parameters for datum transformation between WGS 84 and ADINDAN-Ethiopia, MSC Thesis, Addis Ababa University, Addis Ababa, Ethiopia.Al-Karargy, E. and Dawod, G. (2021) Optimum combinations of GGM and DEM models for precise national geoid development, Proceedings of Engineering and Technology Innovation, V. 18, pp. 15-24.

[3]. Varga, M., Grgic, M. and Basic, T. (2015) Empirical comparison of the geodetic coordinate transformation models: A case study of Croatia, Survey Review, DOI: 10.1080/00396265.2015.1104092.

[4]. Zhen, J. Yang, G., Kang, J., Zhang, X. And Wang, H. (2016) The method of inter-transformation between horizontal and space coordinate, Proceedings of the International Conference on Civil, Structure, Environmental Engineering (I3CSEE 2016), pp. 68-72.

[5]. Dawod, G., Mirza, M. And Al-Ghamdi, K. (2011) Simple precise coordinates transformations for geomatics applications in Makkah metropolitan area, Saudi Arabia, Presented at the FIG Working Week 2010, May 18-22, Marrakech, Morocco.

[6]. Gienko, E., Mazurova, E., And Karpik, A. (2015) The estimation of geodetic datum transformation parameters, Presented at the FIG Working Week 2015, Sofia, Bulgaria, May 17-21.

[7]. Dawod, G. and Alnaggar, D. (2000) Optimum geodetic datum transformation techniques for GPS surveys in Egypt, Proceedings of Al-Azhar Engineering Sixth International Conference, Sept. 1-4, Cairo, Egypt, Volume 4, pp. 709-718.

[8]. Saad, A. And Elsayed, M. (2007) Simple model for improving the accuracy of the Egyptian geodetic triangulation network, Presented at the FIG Working Week 2007, May 13 -17, Hong Kong.

[9]. Shaker, A., Saad, A., El-Sayed, M., and Ali, A. (2007) Remove-restore Technique for improving the datum transformation process, Presented at the FIG Working Week 2007, May 13 -17, Hong Kong.

[10]. Elshambaky, H., Kaloop, M. and Hu, J. (2018) A novel three-direction datum transformation of geodetic coordinates for Egypt using artificial neural network approach, Arabian Journal of Geosciences (2018) 11:110, DOI: 10.1007/s12517-018-3441-6.

[11]. ICGEM (International Center for Global Earth Models) (2021) Global gravity field models, http://icgem.gfz-potsdam.de/tom_longtime, accessed May 20.

[12]. Peprah, M., Ziggah, Y. and Yakubu, I. (2017) Performance evaluation of the Earth Gravitational Model 2008 (EGM2008) – A case study, South African Journal of Geomatics, V. 6, No. 1, pp. 47-72.

[13]. Alnaggar, D. (1986) Determination of the geoid in Egypt using heterogeneous geodetic data, PhD dissertation, Faculty of Engineering, Cairo University, Cairo, Egypt.

[14]. El-Ashquer, M., Elsaka, B. and El-Fiky, G. (2017) EGY-HGM2016: an improved hybrid local geoid model for Egypt based on the combination of GOCE-based geopotential model with gravimetric and GNSS/levelling measurements, Arabian Journal of Geosciences, 10: 251, DOI: 10.1007/s12517-017-3042-9.
[15]. Al-Karargy, E. and Dawod, G. (2021) Optimum combinations of GGM and DEM models for precise national geoid development, Proceedings of Engineering and Technology Innovation, V. 18, pp. 15-24.
[16]. Hofmann-Wellenhof, B., Lichtenegger, H., and Walse, E. (2008) GNSS: Global Navigation Satellite Systems, Springer-Verlag Wien, New York, USA.
[17]. NGA (The US National Geospatial-Intelligence Agency) (2014) Department of defense world geodetic system 1984: Its definition and relationships with local geodetic systems, Technical report no. NGA.STND.0036_1.0.0_WGS84, Available at: http://gis-lab.info/docs/nima-tr8350.2-wgs84fin.pdf, Accessed May 24, 2021.
[18]. Leica Geosystems (2016) Leica Geo Office V. 8.4 user manual, Heerbrugg, Switzerland.
[19]. TBC (Trimble Business Center) (2019) TBC software V. 5.2 user guide, Trimble Navigation Limited, Ohio, USA.

Available online www.jsaer.com

***Journal of Scientific and Engineering Research*, 2022, 9(3):83-90**

Research Article

ISSN: 2394-2630
CODEN(USA): JSERBR

Gis-Based Estimation of Land Subsidence Impacts on Water Resources Infrastructures: A Case Study in the Nile Delta, Egypt

Gomaa M. Dawod*, Hoda F. Mohamed

Survey Research Institute, National Water Research Center, Giza, Egypt
* dawod_gomaa@yahoo.com, ORCID = 0000-0002-4426-8231

Abstract This paper aims to investigate and quantify the hazardous impact of the vertical land movements phenomenon on water resources infrastructures in Egypt probably for the first time. It depends on the results of the Global Navigation Satellite Systems (GNSS)-based estimation of that natural hazard over 2012-2019 previously carried out by the Surrey Research Institute (SRI). The geospatial analysis and interpolation of the land subsidence/uplift have been performed within a Geographic Information System (GIS) environment and a novel danger factor has been proposed. Based on available datasets and accomplished results, it has been found that the average factors over main canals and main drains equal 43% and 37% respectively. Furthermore, it has been found that danger factors on barrages range between 11% and 63% and those over pump stations range between 4% and 71%. The attained findings could be considered primarily due to the short time of the GNSS-based datasets used to quantify the vertical land movements in the Nile delta region. However, they should be considered by decision makers in the operation, maintenance, and development of water resources infrastructures in Egypt. It is recommended that other data collection techniques, such as the radar remote sensing imageries, should be utilized along with GNSS data for monitoring and quantifying the land vertical movement phenomenon more accurately. Also, it is highly recommended that the presented approach should be carried out over the overall water resources infrastructures in the entire territories of Egypt.

Keywords GIS, GNSS, Vertical Land Movements, Water Resources, Natural Hazards

1. Introduction

Natural hazards affect human, economic, and environmental activities worldwide. Such hazards include Sea Level Rise (SLR), land subsidence, landslides, storm surges, drought, flash floods, desertification, and seawater intrusion among many types of hazards. Geospatial techniques, particularly the Geographic Information Systems (GIS) and satellite-based Remote Sensing (RS), provide significant state-of-the-art approaches for monitoring, analysis, and risk assessment for natural and man-made hazards. For an instant, GIS has been utilized in delineating areas subject to severe droughts in Ethiopia [1]. Also, Abdelkarim et al. [2] (2020) have applied GIS to assess flood hazards in Saudi Arabia. In Kuwait, GIS has analysis has been carried out to assess coastal inundation due to future SRL [3] (Neelamani et al. 2021). Parallel research has been conducted in Alexandria, Egypt for coastal vulnerability assessment using GIS [4]. On another scene, GIS is used to evaluate economical vulnerability due to a natural hazard such as land subsidence [5].

Land subsidence constitutes one of the vital environmental hazards that causes physical, human, and economic risky impacts globally, mainly in low-land areas and coastal areas. Fundamentally, land subsidence could be attributed to both natural and human-induced reasons such as geology structures, soil characteristics, withdrawal of groundwater and natural gas and other factors. A number of geodetic approaches have been applied in monitoring land subsidence, particularly the Global Navigation Satellite Systems (GNSS) [6], the Differential

Synthetic Aperture Radar Interferometry (DInSAR) [7], satellite altimetry and tide gauges data [8], and levelling data [9]. A combination of several observing techniques would be more efficient in monitoring land subsidence. GIS-based analysis of topographic and geological could be utilized to model land subsidence over a specific spatial area [10]. It is to mention that the absolute SLR is the result of both relative SRL as measured at Tide Gauge (TG) stations and the land subsidence. In Egypt, the relative SLR at the Nile delta from two TG stations equals 3.5 and 1.9 mm/year at Alexandria and Port Said respectively [11]. Regarding the recent results of GNSS-based vertical land movements in the Nile delta, it is estimated that the absolute SRL rate at Alexandria and Port Said equal 6.0 and 7.6 mm/year respectively [12].

The evaluation of natural hazards' risks is a principal aspect in efficient decision making and the development of strategic policies and plans. This paper investigates the utilization of GIS in estimating the risky impacts of land subsidence in the Nile delta region. It aims to quantify the hazardous impact of that phenomenon on canals, drains, and water resources structures, within the study area, probably for the first time in Egypt.

2. Study Area and Available Data

The Nile delta (Fig. 1) extends from longitude 29.7° E to longitude 32.6° E, and from latitude 29.8° N to latitude 31.6° N, and its overall area equals approximately 35,000 square kilometers.

GNSS raw data of 23 stations of the Virtual Reference Stations (VRS) belonging to the Egyptian Survey Authority (ESA) over 2012-2019 have been utilized to estimate recent precise trends of the vertical land movements over the Nile delta [12]. The Arc GIS package has been applied to construct a 3D spatial surface of vertical land movements. It has been found that the land motion range from subsidence of -5.49 mm/year to uplift equals +4.66 mm/.year, with an average of +0.32 mm/year (ibid). That spatial model has been, in the current research, for further investigations particularly for estimating the impacts of vertical land movements on water resources infrastructures in the Nile delta region.

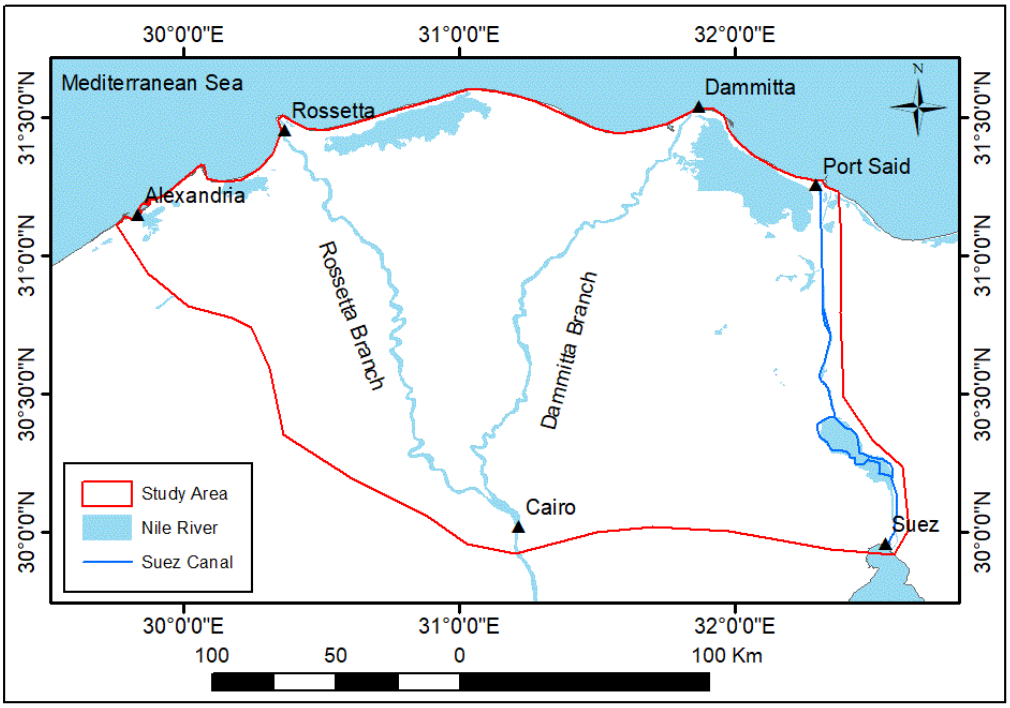

Figure 1: The Study Area

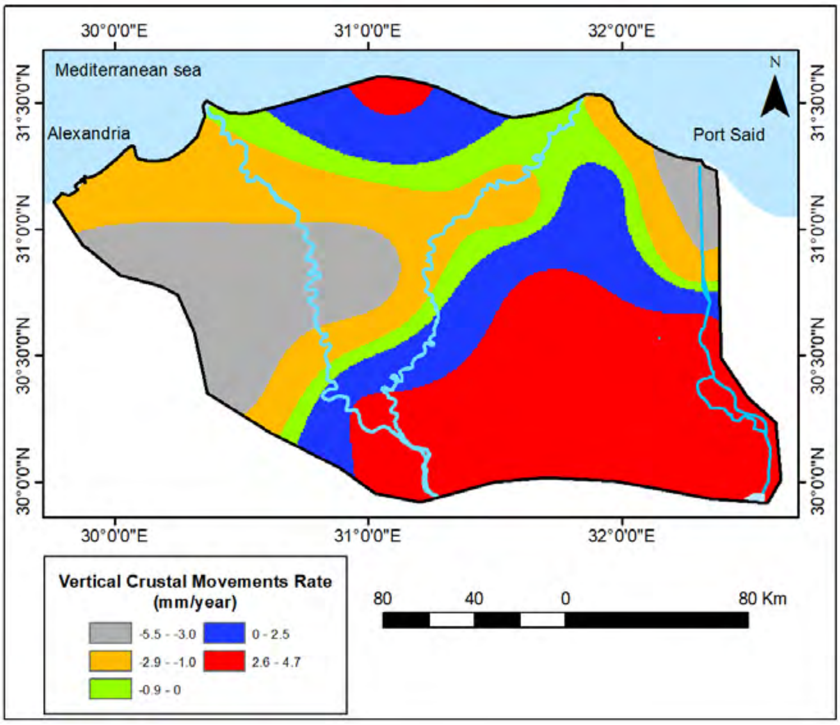

Figure 2: Vertical Land Movements in the Nile Delta over 2011-2019 (after SRI 2022)

3. Methodology

The processing strategy starts with developing an integrated geodatabase of water resources infrastructures in the study area. Several datasets have been collected from various sources and four layers have been assembled to represent the canals, drains, barrages, and water pumping stations (Fig. 3). Since the constructed geodatabase consists of thousands of features, the current study focuses only on canals and drains whose lengths are greater than 20 and 40 kilometers respectively. Next, the krigging interpolation method, within the Arc GIS 10 package, has been performed to interpolate the vertical land movement (Fig. 2) at each pump station, and barrage directly. However, because a specific canal or drain might pass by different categories on the vertical land movements, a novel indicator has been proposed, that consists of the following steps:

- Interpolate the minimum land movement trend (R_{min}) on a specific canal or drain,
- Interpolate the maximum land movement trend (R_{max}) on a specific canal or drain,
- Interpolate the average land movement trend (R_{mean}) on a specific canal or drain,
- Compute the Dangerous Factor (Dang1) for each canal or drain by dividing its average land movement rate by 5.5 (that is the maximum value of land movements, mm/year, in the study area) multiplied by 10 (to be on a scale of 10):

$$Dang1 = (R_{mean}/5.5) * 10 \quad (1)$$

- Since some canals and drains, as polyline features, would cross different categories of vertical land movements (subsidence and uplift as noticed from both R_{min} and R_{max} values), another Dangerous Factor (Dang2) is proposed to consider such a situation by adding a constant equals 5 to represent such a more risky case:

$$Dang2 = Dang1 + 5 \quad \text{(if there exist both +ve and –ve movements)}$$

$$Dang2 = Dang1 \quad \text{(if there exist even +ve or –ve movements)} \quad (2)$$

- Re-classify the attained dangerous factors, of both canals and drains, into percentages by dividing it by 15 (that equals the maximum dang2 factor) and multiplying it by 100 just to be easier for interpretation and comparisons:

$$Dang\% = \frac{Dang2 * 100}{15} \quad (3)$$

- For pumping stations and barrages as point features, re-classify the attained dangerous factors, as similar to Eq 1, but directly to percentages (Dang11) as:

$$Dang11 = (\frac{R_{mean}}{5.5}) * 100 \quad (4)$$

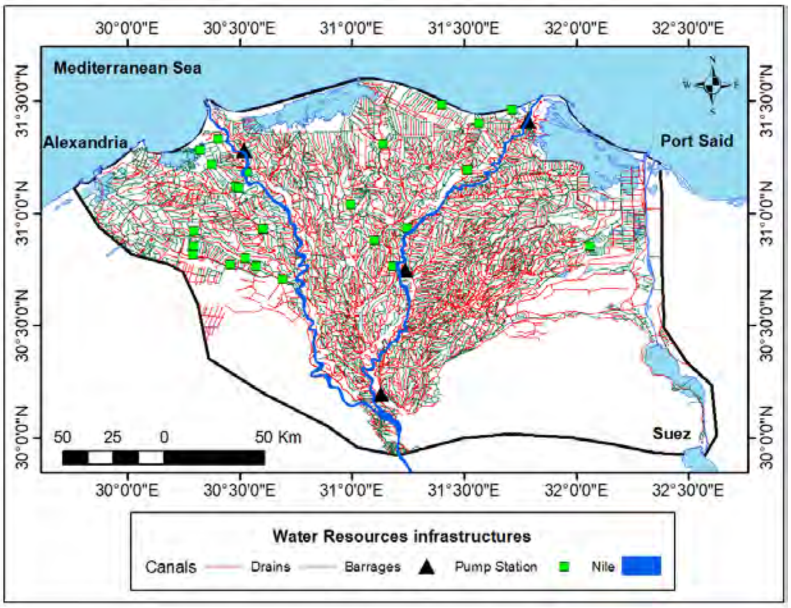

Figure 3: Water Resources Infrastructures in the Nile delta Area

4. Results and Discussions

The GIS-based developed geodatabase consists of 3270 canals with variable lengths between 0.04 km and 132.35 km, and 1997 drains whose lengths range between 0.01 km and 105.76 km, 27 pumping stations, and 4 barrages. The danger factor (Eq. 3) has been computed for the 16 main canals (Table 1). It has been noticed that this factor range between 26% for Meet Tazeed canal and 61 % for El-Bagoryia canal, with an overall average equals 43%. Fig. 4 depicts the categories of danger factors on main canals where it has been divided into three groups: low danger (26%-34%), medium danger (35%-47%), and high danger (48%-61%). Comparing Fig. 2 and 3, it can be realized that the high-danger main canals exist primarily in the middle and the east of the Nile delta where maximum vertical land movements occurred.

Table 1: Land movements' Danger Factors on Main Canals

No	Canal Name	Canal Length (km)	Danger Factor %	No	Canal Name	Canal Length (km)	Danger Factor %
1	El-Neanayia	91.2	52%	9	El-Ryaah El-Tawofekey	66.1	53%
2	Meet Yazeed	63.3	26%	10	El Hager	87.2	42%
3	El Mahmoudyia	75.5	31%	11	El Nobaryia	119.2	42%
4	Bahr Shebeen	113.2	51%	12	El-Esmaliyai	132.4	47%
5	El-Bagoryia	91.6	61%	13	Suez	91.2	49%
6	Bahr Tiyara	69.3	43%	14	Port Said	74.8	53%
7	El-Rayah El Nasrey	84.3	34%	15	Bahr Mowis	68.3	30%
8	El Rayah El Beheri	95.1	39%	16	El-Salam	89.1	42%

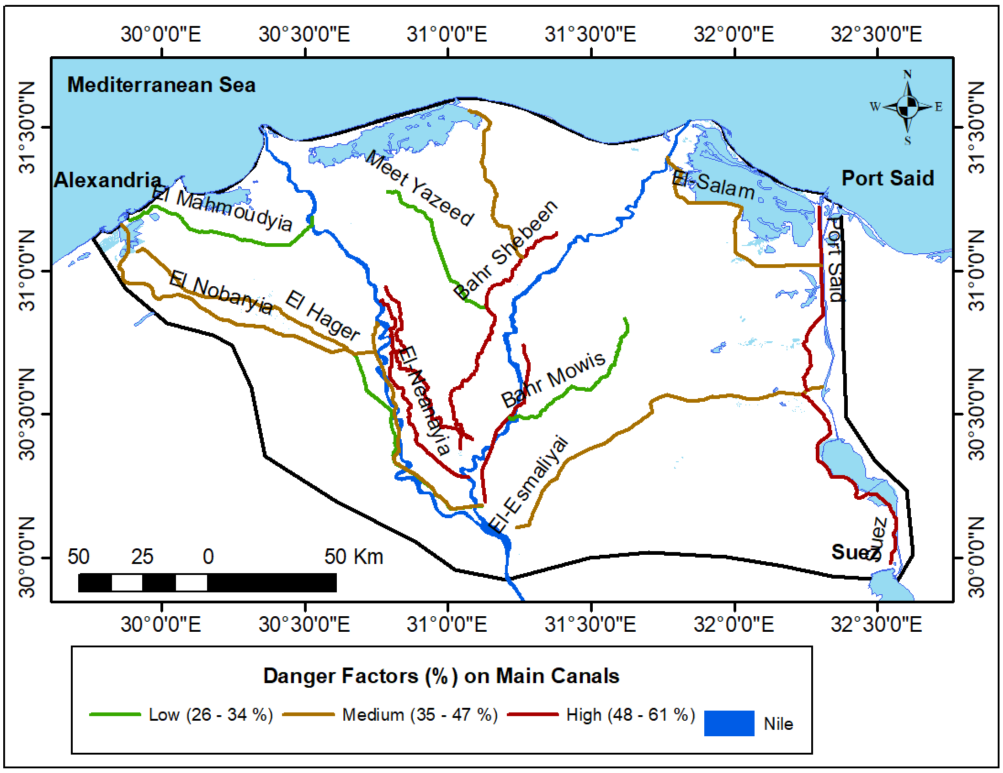

Figure 4: Land movements' Danger Factors on Main Canals

Similarly, the danger factor has been computed for the 13 main drains (Table 2). It has been noticed that this factor range between 16% for Nemra 1 High drain and 49 % for Al Mhsma drain, with a mean of 37%. Fig. 5 depicts the categories of danger factors on main drains where it has been grouped into three categories: low danger (16%-19%), medium danger (20%-40%), and high danger (41%-49%). Comparing Fig. 2 and 5, it can be realized that the high-danger main canals exist, as expected, principally in the east and the middle of the study area where maximum vertical land movements occurred.

Table 2: Land movements' Danger Factors on Main Drains

No	Drain Name	Drain Length (km)	Danger Factor %	No	Drain Name	Drain Length (km)	Danger Factor %
1	Shobrakheit Wamtdada	45.7	40%	8	West Al-Nubaria	59.0	38%
2	Al Qrnein	43.6	47%	9	Al Amoum	40.0	34%
3	Al Aarein	42.9	42%	10	Al Gharbiya Main	69.0	40%
4	Belbis	65.9	44%	11	Bahr Sft Southern	75.5	19%
5	Bahr Hadous	57.5	38%	12	Al Mhsma	40.0	49%
6	Al Qalioubiya Main	73.5	33%	13	Bahr Al Bqr	105.8	46%
7	Nemra 1 High	45.2	16%				

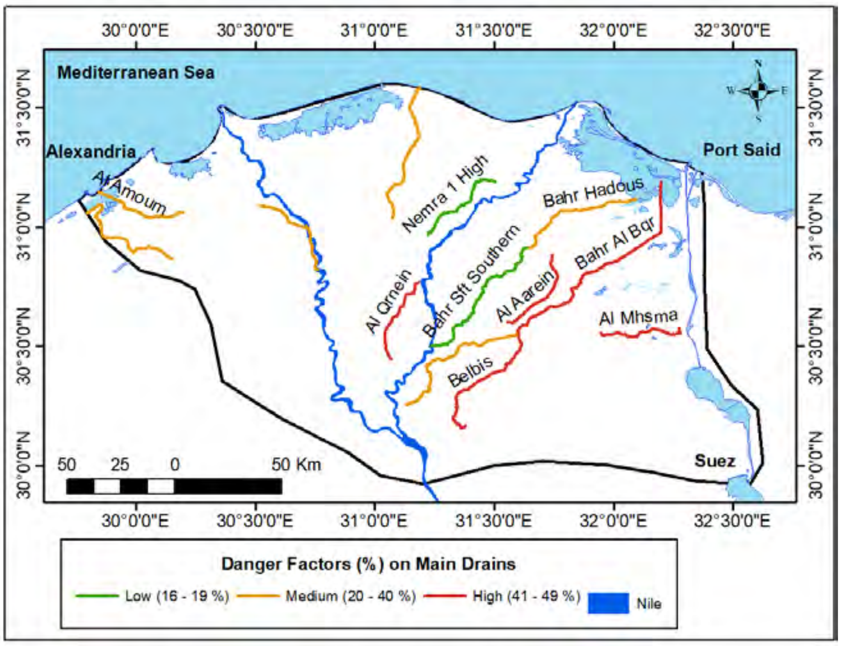

Figure 5: Land movements' Danger Factors on Main Drains

Next, Eq. 4 has been applied to estimate the danger factors of barrages and pumping stations. Danger factors on barrages, within the study area. Have been found to be 11%, 20%, 26%, and 63% for Farskoor dam, Zifta, Edfina, and Delta barrages respectively. From Fig. 2, it is noticed that the delta barrage exists in the region with maximum uplift, thus its danger factor is the highest one.

Next, the danger factors have been estimated at the 27 pump stations within the study area (Fig. 6). The accomplished danger factors range between 4% and 71%, with a mean of 42%. Fig. 7 depicts the frequency histogram of the danger factors on pump stations, where it is noticed that 11% of the stations have danger factors less than 10%, 7% stations of have factors between 10-20%, 33% of stations got factors between 20-40%, 15% of stations have danger ranging from 40% to 60%, and 33% of stations got high danger factors between 60%-71 %.

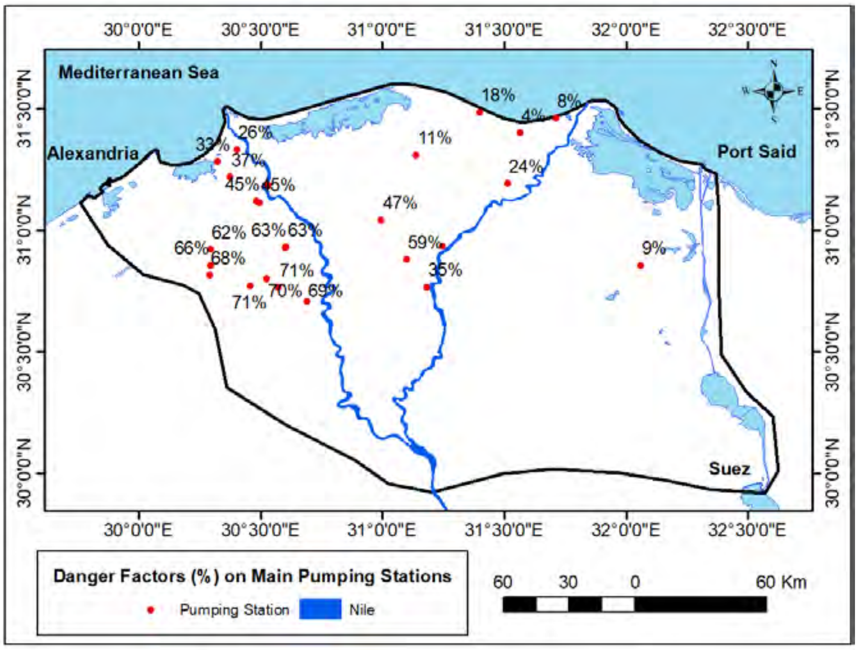

Figure 6: Land movements' Danger Factors on Main Pumping Stations

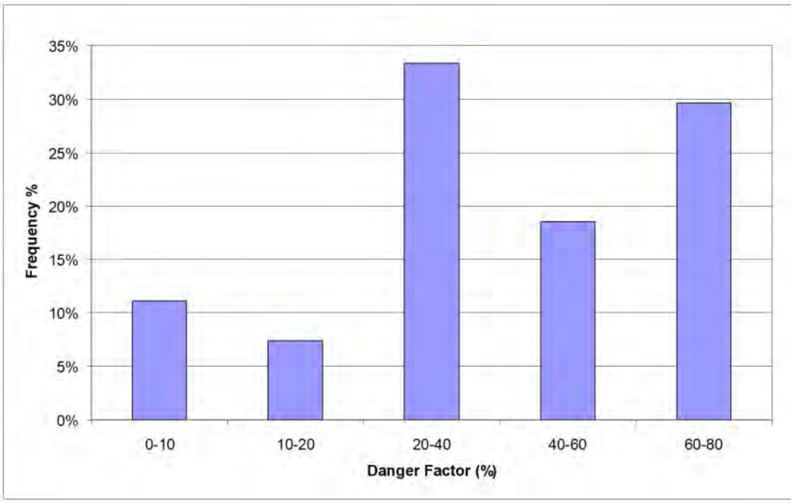

Figure 7: Frequencies of Land movements' Danger Factors on Main Pumping Stations

5. Conclusions

Estimating the risks of natural hazards represents a significant feature in decision making and the development of strategic plans. The current study examines the utilization of GIS in estimating the risky impacts of land subsidence, in the Nile delta region, particularly on canals, drains, and water resources structures possibly for the first time in Egypt as far as the authors' concern. The study depends basically on the GNSS-based vertical land movements determination, over 2012-2019, carried out by SRI in 2022. The GIS has been applied to construct a 3D spatial surface of vertical land movements and interpolates its dangerous effects on water resources infrastructures through a few proposed novel indicators.

Based on available datasets and accomplished results, it has been found that the danger factors over main canals range between 26% and 61 %, with an overall average equals 43%. In the same way, it has been concluded that the danger factors over main drains range between 16% and 49 %, with a mean of 37%. Moreover, it has been realized that the high-danger main canals and drains occurred, as expected, mostly in the east and the middle of the study area where maximum vertical land movements exist. Furthermore, it has been found that danger factors on barrages range between 11% and 63%. Also, it is noticed that the delta barrage exists in the region with maximum uplift, thus its danger factor is the highest one. Finally, the accomplished danger factors over pump stations range between 4% and 71%, with a mean of 42%. The attained findings could be considered primarily due to the short time span of the GNSS-based datasets used to quantify the vertical land movements in the Nile delta region. However, they should be considered by decision makers in the operation, maintenance, and development of water resources infrastructures in Egypt.

6. Recommendations

Few recommendations could be drawn, based on the achieved outcomes, for future works such as:

1- The vertical land movements natural phenomenon significantly affect water resources infrastructures, and thus it is recommended to monitor such hazard continuously.
2- GNSS data should be collected over a longer time in order to estimate more reliable estimates of vertical land movements.
3- Other data collection techniques, such as the radar remote sensing imageries, should be utilized along with GNSS data for monitoring and quantifying the land vertical movement phenomenon more accurately.
4- The approach presented in the current study should be carried out over the overall water resources infrastructures in the entire territories of Egypt.
5- Multi-disciplines research studies should be carried out to understand the nature of the vertical land movements phenomenon, its causes, and its physical, human, and environmental risks in Egypt.

References

[1]. Hirko, A., Mergia, G., Nigussie, A. and Dandesa, D. (2021). Meteorological drought assessment using GeoCLIM: Case study east and west Hararghe, Oromia, Ethiopia, *International Journal of Research in Environmental Science*, 7(1):-37, http://dx.doi.org/10.20431/2454-9444.0701004

[2]. Abdelkarim, A., Al-Alola, S., Alogayell, H., Mohamed, S., Alkadi, I. and Ismail, I. (2020). Integration of GIS-based multicriteria decision analysis and analytic hierarchy process to assess flood hazard on the Al-Shamal train pathway in Al-Qurayyat region, Kingdom of Saudi Arabia, *Water*, 12, 1702, http://dx.doi.org/10.3390/w12061702

[3]. Neelamani, S. , Al-Houti, D., Al-Ragum, A., Al-Salem, K. and Al-Saleh, A., (2021). Assessment of coastal inundation cost due to future sea level rise: A case study for Kuwait, *Marine Georesources & Geotechnology*, https://doi.org/10.1080/1064119X.2021.1909195

[4]. Mohamed, S. (2020). Coastal vulnerability assessment using GIS-Based multicriteria analysis of Alexandria-northwestern Nile Delta, Egypt, *Journal of African Earth Sciences*, https://doi.org/10.1016/j.jafrearsci.2020.103751

[5]. Hu, B., Zhou, J., Xu, S., Chen, Z., Wang, J., Wang, D., Wang, L., Guo, J. and Meng, W. (2013). Assessment of hazards and economic losses induced by land subsidence in Tianjin Binhai new area from 2011 to 2020 based on scenario analysis, *Natural Hazards*, https://doi.org/10.1007/s11069-012-0530-9

[6]. Mohamed, H. (2015). Assessment of factors influencing static GNSS precise point positioning: A case study in Egypt, *International Journal of Applied Sciences and Engineering Research*, 4(5): 692-701.

[7]. Bhattarai, R., Alifu, H., Maitiniyazi, A. and Kondoh, A. (2017). Detection of land subsidence in Kathmandu valley, Nepal, using DInSAR technique, *Land*, 6,39, https://doi.org/10.3390/land6020039

[8]. Letetrel, C. Karpytchev, M., Bouin, M-N., Marcos, M., SantamarÍa-Gómez, A., and Wöppelmann, G. (2015). Estimation of vertical land movement rates along the coasts of the Gulf of Mexico over the past decades, *Continental Shelf Research*, (111):42–51

[9]. Ali, M., Chu, H. and Burbey, T. (2020). Mapping and predicting subsidence from spatio-temporal regression models of groundwater-drawdown and subsidence observations, *Hydrogeology Journal*, 28L2865-2867, https://doi.org/10.1007/s10040-020-02211-0

[10]. Cao. J., Ma, F., Guo, J., Lu, R. and Liu, G. (2019). Assessment of mining-related seabed subsidence using GIS spatial regression methods: a case study of the Sanshandao gold mine (Laizhou, Shandong Province, China), *Environmental Earth Sciences*, 78:26 https://doi.org/10.1007/s12665-018-8022-1

[11]. Dawod, G., Ebaid, H., Haggag, G. and Al-Krargy, E. (2021). An integrated geomatics approach for projecting sea level variations and risks: A case study in the Nile Delta, Egypt, *Journal of Architecture and Civil Engineering*, 6(8):4-38.

[12]. SRI (Survey Research Institute) (2022). *Assessing and modelling of land subsidence in the Nile delta area and its effect on water structures, canals and drains*, Internal Technical Report, Giza, Egypt.

American Journal of Geographic Information System 2022, 11(1): 1-8
DOI: 10.5923/j.ajgis.20221101.01

Enhancing Vertical Accuracy of Global Digital Elevation Models for Coastal and Environmental Applications: A Case Study in Egypt

Gomaa M. Dawod[1,*], Ahmed M. Amin[2]

[1]Geodesy Department, Survey Research Institute, National Water Research Center, Giza, Egypt
[2]GIS Department, Survey Research Institute, National Water Research Center, Giza, Egypt

Abstract A major source of Digital Elevation Models (DEM) is the open-source Global DEM (GDEM) developed and distributed free-of-charge and, thus, became accepted in a wide range of coastal end environmental applications worldwide. The vertical accuracy of such GDEMs should be investigated to determine their applicability for utilization in specific activities. Moreover, increasing the vertical accuracy of GDEMs should be carried out by the integration of local terrestrial geodetic datasets over a spatial region. The current study investigates the accuracy of three GDEM models over the Egyptian costs along the Mediterranean sea and tries to enhance such accuracy by adding terrestrial data through the utilization of two methods of spatial modelling within a Geographic Information Systems (GIS) environment. Based on the available datasets and attained results, it has been found that the regression modelling method results in enhancing the vertical accuracy of the investigated GDEMs by 15% and 4% while the krigging geostatistical method produced 24% and 16% improvements. Furthermore, it has been concluded that adding terrestrial local datasets to a global DEM could considerably increase its overall vertical accuracy. However, the number of added terrestrial points should be appropriate to the desired level of vertical accuracy and the area of study. Moreover, it has been concluded that the achieved vertical accuracy of the enhanced models, herein, could be suitable for small-scale mapping and overall management of coastal regions, but it might not be appropriate for accurate environmental studies such as Sea Level Rise (SLR) monitoring and risk assessment which requires a more accurate DEM.

Keywords DEM, Global DEM, Vertical Accuracy, Coastal Management, GIS, Egypt

1. Introduction

A Digital Elevation Model (DEM) is a 3D digital illustration of the Earth's topography. It can be developed in several ways based on the utilized input data. A DEM could be constructed by scanning and digitizing contour maps, by using terrestrial surveys of traditional spirit levelling or by Global Navigation Satellite Systems (GNSS) data. Also, a DEM could be generated from stereoscopic aerial photographs, stereoscopic satellite imageries, and Light Detection and Ranging (LiDAR) measurements. Recently, a DEM can be generated from data obtained by drones equipped with GNSS or LiDAR sensors. Another valuable source of DEM is the open-source Global Digital Elevation Models (GDEM) developed and provided free-of-charge organizations. That source became accepted in a wide range of applications worldwide due to its easy availability.

* Corresponding author:
dawod_gomaa@yahoo.com (Gomaa M. Dawod)
Received: Mar. 15, 2022; Accepted: Apr. 8, 2022; Published: Apr. 15, 2022
Published online at http://journal.sapub.org/ajgis

GDEMs have been utilized in several types of civil and environmental applications such as designing water reservoirs [1], geoids modelling [2], topographic mapping [3], climate change assessment [4], coastal protection [5], flash flood assessment [6], and land subsidence monitoring [7]. The most-critical question dealing with GDEMs concerns their level of vertical accuracy. To judge such an accuracy level, several approaches have been proposed. Examples of such evaluation ways is the assessment utilizing a high-resolution high-accuracy local DEM [8], the utilization of Differential Global Positioning System (DGPS) terrestrial measurements [9], and the comparison with LiDAR-based elevation datasets [10].

GDEMs accuracy level has been investigated in several spatial regions worldwide. For an instant, Dawod and Al-Khamdi [11] have investigated the accuracy of ten GDEMs in both Egypt and the Kingdom of Saudi Arabia (KSA) representing different topography patterns. They reported that such GDEM models produce standard deviations of height differences vary between ± 2.0 m and ± 6.7 m in flat regions, and from ± 4.7 m to ± 18.6 m in mountainous areas. Additionally, Rabah et al. [12] have

investigated several GDEMs in Egypt and stated that the overall estimated accuracy range between ± 2.9 m and ± 8.7 m. In India, such accuracy levels range between ± 12.6 and ± 17.8 m [13]. Similarly, Ouerghi et al [14] concluded that the accuracy of some GDEMs in Tunisia vary from ± 7.6 m to ± 10.5 m. In addition, it has been concluded that GDEMs vertical accuracy in China depends on terrain complexity and equal 5 m approximately for plains, 10 m approximately for hills, and 20 m approximately for mountains [15].

Some approaches have been suggested to enhance the vertical accuracy of GDEMs. Rabah et al. [12] stated that some GDEMs utilized a particular Global Geopotential Model (GGM) to convert the originally measured ellipsoidal heights to Mean Sea Level (MSL)-based orthometric heights as the final published product of a GDEM, which is more applicable in civil and environmental applications worldwide. They suggest that replacing those geoidal undulation values with another more-precise GGM would increase the accuracy of a GDEM. Another proposed method considered the utilization of the krigging regression statistical tool to spatially model the GDEM errors [16]. Other researchers suggest filling the gap of a fine-resolution DEM by interpolating their corresponding values from a coarse-resolution one [17,18].

This paper aims to fulfill the following objectives:

- Investigating the vertical accuracy of different resolution GDEMs over the 1000-kilometrs Egyptian coasts along the Mediterranean sea using accurate GNSS/Levelling datasets,
- Studying different mathematical and statistical models for incorporating new data into GDEMs,
- Performing GDEMs enhancement process within a GIS environment in an effortlessly and sensibly manner,
- Analyzing the expected accuracy improvement of different GDEMs by adding a specific number of terrestrial data points,
- Exploring the applicability of enhanced GDEMs for mapping, engineering and environmental applications.

2. Methodology

Two mathematical and statistical techniques have been utilized, herein, to incorporate GNSS/Levelling datasets to the investigated GDEMS, mainly the first-order regression and the ordinary Kriging approaches. Due to their applicability and versatility, both models have been utilized extensively in various geomatics applications. For instance, the first-order regression has been applied to model and predict sea level changes [19]. Also, the Kriging interpolation has been utilized in geoid modelling and refinement [20].

Three GDEM models with variable horizontal resolutions have been investigated herein. The first one is the Shuttle Radar Topography Mission (SRTM 1) model with a resolution of 1 arcsecond or approximately 30 m. SRTMGL1 v. 3 [21] has been utilized herein. (download from e.g. *https://earthexplorer.usgs.gov/*). The second model is the ALOS PALSAR model representing Phased Array type L-band Synthetic Aperture Radar (PALSAR) measurements obtained from the Advanced Land Observing Satellite (ALOS). Its spatial resolution is 12.5 m and could be downloaded from *https://search.asf.alaska.edu/*. ALOS PLASAR (simply PALSAR herein) has been developed by integrating the SRTMGL1 model with the US National Elevation Data (NED) and other datasets and was re-sampled to the 12-m resolution. The datum of the final PLASER is the World Geodetic System 1984 (WGS-84) ellipsoid with the utilization of the Earth Geopotential Model 1996 (EGM96) to convert MSL-based heights to the corresponding ellipsoidal heights [22]. The third GDEM is the Altimeter Corrected Elevations, Version 2 (ACE2 developed by synergistically merging the SRTM data set with Satellite Radar Altimetry within the region bounded by 60°N and 60°S. ACE2 was developed at resolutions of 3, 9 and 30 arc-seconds, and 5 arc-minutes [23]. The 3" ACE2, utilized herein (downloaded from *https://sedac.ciesin.columbia.edu/data/set/dedc-ace-v2*). Although ACE2 is a 90-m resolution model, it produced reasonable accuracy over 1100 GNSS/Levelling checkpoints over Egypt [2].

Table 1. Characteristics of the investigated GDEMs

GDEM	Horizontal Resolution (m)	Height Type	Description
SRTMGL 1	30	Orthometric	A new processing of the SRTM 1 dataset
ALOS PALSAR	12.5	Ellipsoidal	A resample combination of SRTMGL 1 and the US NED and other sources
ACE2	90	Orthometric	A Combination of SRTM and satellite radar altimetry

The first step in the processing strategy concerns the unification of the vertical datums of utilized datasets. The orthometric heights of the collected GNSS/Levelling terrestrial points and heights interpolated from SRTMGL1 GDEM are referenced to the MSL while the PALSAR model produces WGS84-based ellipsoidal heights. Hence, a geoid model is required to unify the vertical datum of all datasets to be MSL-based orthometric heights. This study utilized the Survey Research Institute 2021 geoid model as the most recent most precise local geoid for Egypt (ibid). Thus [24]:

$$H_{PALSAR} = h_{PALSAR} - N_{SRI2021} \quad (1)$$

Next, the SRTMGL GDEM has been enhanced based on the concept provided by Rabah et al. [12]. Instead of utilizing the EGM96 GGM in height conversion originally carried out in developing the SRTMGL, the SRI2021 will be used to develop a Modified Egyptian SRTM (MESTTM) as [12]:

$$H_{MESRTM} = H_{SRTMGL} - N_{EGM96} + N_{SRI2021} \quad (2)$$

Next, the four investigated DEMs, namely PALSAR, SRTMGL, ACE2, and MESRTM, have been judged over the available GNNS/Levelling control points. The average and standard deviation of height difference, or DEM errors, for each model, are estimated as:

$$\Delta H_{i,j} = H_{i,j} - H_{DEM} \quad (3)$$

$$\bar{H}_i = \sum Hi \Big/ n \quad (4)$$

$$s_i = \sqrt{\sum (H_{i,j} - \bar{H}_i \Big/ n-1} \quad (5)$$

where,

$H_{i,j}$ is the known orthometric height of a control point no. j,

H_{DEM} is the corresponding orthometric height estimated from a specific DEM,

$\Delta H_{i,j}$ is the ith DEM error in estimating orthometric height for point j,

i range from 1 to 4 investigated models,

$\bar{H}_i$ represents the average height error for the ith DEM,

s_i represents the standard deviation of height error for the ith DEM,

The model producing the best vertical accuracy, in terms of the standard deviation of height differences, will be obtained. Then, its height errors over the control points will be spatially modeled by two approaches. First, the regression analysis statistical toll will be applied to model modelling differences (ΔH) as a function of Easting (Ei) and Northing (Ni) UTM coordinates:

$$\Delta H_{i,j} = a_o + a_1 E_i + a_2 N_i \quad (6)$$

The second modelling approach of DEM errors concerns the utilization of the GIS-based kriging geostatistical analysis. It takes into account the spatial distribution of the sample points to explain the variations in the 3D surface. The general form of the kriging interpolator is [25,26]:

$$\hat{Z}(S_o) = \sum_{i=1}^{n} \lambda_i Z(s_i) \quad (7)$$

where,

$Z(s_i)$ is the measured quantity at the ith location,

λ_i represents an unknown weight for point i,

s_o is the prediction location, and

n equals the measurements number.

Within the ordinary kriging technique, there are many statistical models, or variograms, to model the spatial correlation of datasets. Types of variograms include spherical, circular, exponential, Gaussian and linear.

The results of both modelling steps will be judged over checkpoints to compare their accuracies. Finally, the precise enhanced GDEM will be selected to be applicable for coastal and environmental applications over the study area. The overall processing strategy is depicted in Fig. 1.

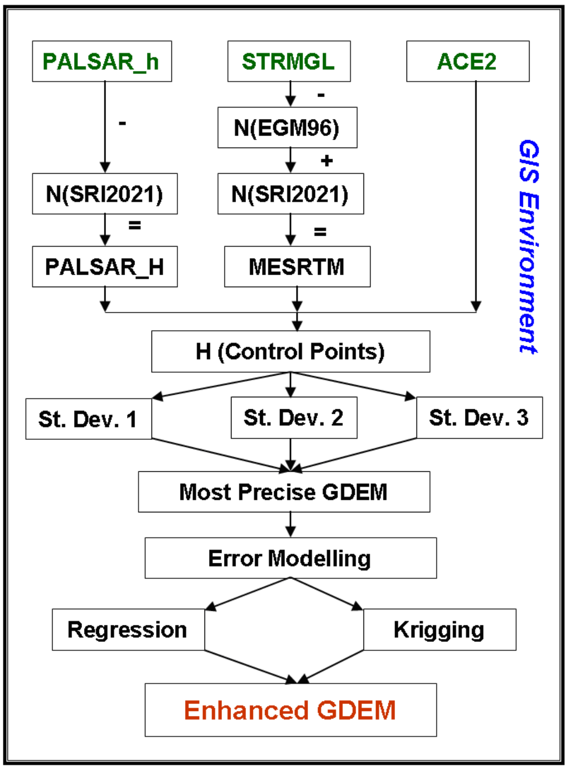

Figure 1. Processing Steps

3. Study Area and Available Data

The study area occupies the Egyptian coasts over the Mediterranean sea from Sallum city at the east to Raffah city at the west (from 25.10 E to 34.20 E) with a variable width equals approximately 25 kilometers (from 30.70 N to 31.60 N). Its overall area equals almost 25,000 square kilometers (Fig. 2). A number of 199 precise-levelling Bench Marks (BM) have been established by the Survey Research Institute (SRI) of the National Water Research Center (NWRC) in the last few years as a part of the Spatial Data Infrastructure (SDI) for coastal and environmental applications. Such BM exist mainly (64%) in the Nile delta region between Alexandria and Port Said cities while there exist 19 BM in the Sinai peninsula and 53 BM in the west coast region. It is worth mentioning that the overall accuracy of both vertical and horizontal coordinates of such a precise geodetic network is less than five centimeters [24]. Twenty-five points (almost 13%) have been reserved as checkpoints to judge the enhanced models' quality. It is worth mentioning that despite the minimal amount of available GNSS/Levelling data points, these datasets comprise the most-accurate geodetic data within the study area.

The three investigated GDEMs, namely, SRTMGL 1, PALSAR, and ACE2, have been downloaded from their

particular websites. The Arc GIS 10 software package has been utilized to clip the terrain of the study area from each GDEM model (Fig. 3). The overall heights over the study area range between -72 - 267 m, -54 - 258 m, and -54 - 286 m for the three GDEM models respectively. It can be seen from Fig. 3a that there exist a few gaps in the coverage of the PLASDAR model over the study area particularly at the middle of the Delta and at the far west of the Egyptian boundaries. So, even there exist few BM at such gaps, the study did not include them to have consistency in evaluation the three investigated GDEM models over identical checkpoints.

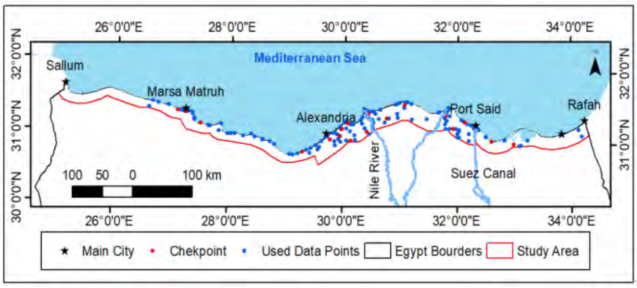

Figure 2. The Study Area and **Available** Data

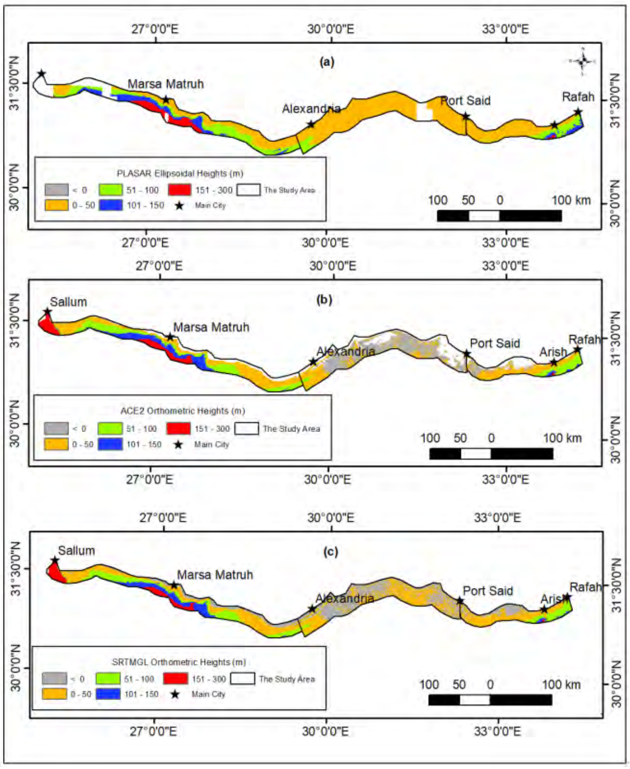

(a) PLASAR, (b) ACE2, and (c) SRTMGL1

Figure 3. The Utilized GDEM Models

4. Results and Discussion

The first step in the data processing stage has been performed to evaluate the vertical accuracy of the original three GDEMs over the available terrestrial precise network. The Arc GIS analysis tools have been carried out to interpolate the GDME-based height at each checkpoint from each GDEM and compare it to the corresponding known height to compute the mean error and standard deviation, using Equations 3 to 5, for all the three GDEMs. Table 2 presents the accomplished findings. It can be realized that, over the known 199 BM, the PALSAR model produced the worst vertical accuracy, in terms of the standard deviation of height differences, while the other two models produced the same level of accuracy. In addition, it can be noticed that the vertical accuracy of the GDEMs, over the Egyptian coasts, equals approximately ± 3 m as other researchers have pointed out in other countries.

Table 2. Statistics of GDEMs-Based Heights Differences at Known Points (m)

	PALSAR	SRTMGL	ACE2
Minimum Height Difference	-24.4	-7.3	-7.7
Maximum Height Difference	4.4	9.1	8.7
Mean Height Difference	-15.21	1.57	1.55
Standard Deviation of Differences	± 3.43	± 2.85	± 2.85

Next, the study obtained two geoid models, namely the global EGM96 model and the local SRI2021 model. The first is used to unify height datums particularly for the PALSAR model (Eq. 1) and the second is used to enhance the performance of the SRTMGL 1 model (Eq. 2). Table 3 presents the statistics of geoidal undulations of both models over the study area. Both models produced almost identical accuracy in height conversion.

Table 3. Statistics of GGMs Geoid Undulations over the Study Area (m)

	EGM96	SRI2021
Minimum Undulation	14.8	14.4
Maximum Undulation	21.2	20.6
Mean Undulation	17.1	16.5
Standard Deviation of Undulation	± 1.4	± 1.4

Thus, equations 1 and 2 have been applied to construct two modified GDEM models: (1) the PLASAR-Ortho producing orthometric heights instead of the original ellipsoidal heights and (2) the Modified Egyptian SRTM (MESRTM) model. The terrain heights over the study area vary between -72 m and 238 m for the MESRTM model and range from -50 m to 266 m for the PLASAR-Ortho model (Fig. 4).

Similarly, the performance of two modified GGMs has been investigated over the terrestrial control points. Table 4 presents the statistics of the accomplished results. Hence, it can be noticed that the vertical accuracy levels equal ± 2.98 m, ± 2.81 m, and ± 2.85 m for the PLASAR-Orth, MESRTM, and ACE2 models respectively.

Comparing Tables 2 and 4, several important notes could be concluded. As expected, it can be concluded that the PALSAR-Orth model is better than the original PLASAR one after converting its height type from ellipsoidal to

orthometric types used already in measuring the heights of checkpoints over the study area. Second, the performance of MESRTM model is fairly better than the original SRTMGL 1 model after replacing the height conversion model from the global EGM96 model to the SRI2021 geoid model. That means that such a procedure produced an improvement of almost 1 % over the checkpoints in the study area. Third, it could be realized that the PLASR models (both ellipsoidal and orthometric) produced worse accuracy than the other two investigated GDEMs although its horizontal resolution is small. That might be contributed to its description provided in the last column of Table 1. Accordingly, the remaining procssing steps have been carried out using only MESRTM and ACE2 models.

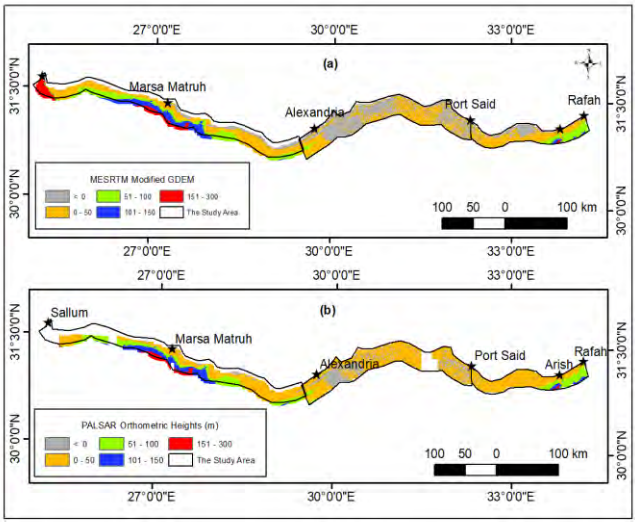

(a) PLASAR Orthometric and (b) MESRTM

Figure 4. The Modified GDEM Models

Table 4. Statistics of Modified GDEMs-Based Heights Differences Known Points (m)

	PALSAR_Ortho	MESRTM	ACE2
Minimum Height Difference	-7.6	-6.7	-7.7
Maximum Height Difference	11.6	10.9	8.7
Mean Height Difference	1.58	2.80	1.55
Standard Deviation of Differences	± 2.98	± 2.81	± 2.85

As noted in the methodology section of this research study, two statistical tools have been applied to model the GDEMs-based errors over the study area. Basically, such tools are based on the regression and krigging approaches. Before performing the regression, 174 available BM have been used in error modelling while the remaining 25 BM (almost 13% of the total number of the accessible dataset) have been kept as checkpoints to evaluate the accomplished results.

First, the linear regression (Eq. 6) has been estimated twice for the two GDEMs models. The attained regression equations are:

$$Error_{MESRTM} = 63.4 - 3.46*10^{-6} E_i - 1.73*10^{-5} N_i \quad (8)$$

$$Error_{ACE2} = -71.3 + 4.55*10^{-6} E_i + 2.07*10^{-5} N_i \quad (9)$$

Then, these two equations have been spatially applied, within the Arc GIS environment, to construct two correction surfaces: CorrMESRTM and CorrACE2. Next, two enhanced GDEM models, namely EnhMESRTM and EnhACE2, have been obtained by adding the original models to the corresponding correction surface:

$$Enh_{MESRTM} = MESRTM + Corr_{MESRTM} \quad (10)$$

$$Enh_{ACE2} = ACE2 + Corr_{ACE2} \quad (11)$$

The GDEMs' corrections (Fig. 5), over the entire study area, range between 1.35 m and 4.19 m for the enhanced MESRTM model and from -0.33 m and 3.28 m for the enhanced ACE2 model.

Likewise, the performance of the two enhanced GGMs has been investigated over the 25 terrestrial control points. Table 5 presents the statistics of the accomplished results. Hence, it can be noticed that the vertical accuracy levels equal ± 2.39 m and ± 2.74 m for the enhanced MESRTM and the enhanced ACE2 models respectively.

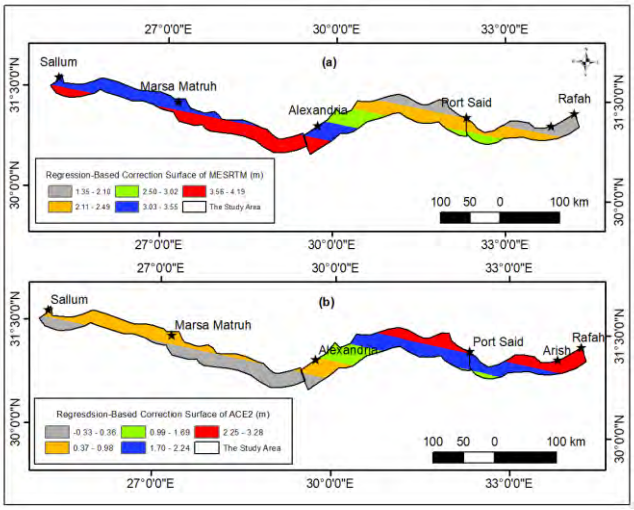

(a) MESRTM and (b) ACE2

Figure 5. The Regression-Based Correction Surfaces of the Enhanced GDEM Models

Table 5. Statistics of Height Differences of Regression-Based Enhanced GDEMs at Known Points

	EnhMESRTM	EnhACE2
Minimum Height Difference	-4.72	-2.81
Maximum Height Difference	4.81	6.77
Mean Height Difference	-0.19	1.77
Standard Deviation of Differences	± 2.39	± 2.74

Comparing Tables 4 and 5, it could be concluded that the regression modelling of height errors has decreased the overall vertical accuracy of the MESRTM model from ± 2.81 m to ± 2.39 m (almost 15% improvements). Similarly, such a modelling approach has decreased the overall vertical

accuracy of the ACE2 model from ± 2.85 m to ± 2.74 m (almost 4% improvements only).

The second modelling approach is the kriging statistical tool (Eq. 7) has been applied to model spatially the errors of the GDEMs over the study area. Correspondingly, other two correction surfaces have been obtained for the MESRTM and ACE2 models. The corrections, over the entire study area, range between -0.337 m and 5.215 m for the MESRTM model and from -2.227 m and 4.703 m for the ACE2 model. Later, each correction surface has been added to the corresponding original GDEM to obtain the kriging-based enhanced version, over the study area, explicitly the Enh_2_MESRTM and the Enh_2_ACE2 models (Fig. 6).

Finally, the vertical accuracy of those two models has been judged over the 25 checkpoints. The accomplished results are tabulated in Table 6, which shows that the overall accuracy of the MESRTM model has been decreased from ± 2.81 m to ± 2.15 m and that of the ACE2 model has been decreased from ± 2.85 m to ± 2.40 m. Thus, it can be concluded that the kriging-based enhanced versions of the two GDEMs have improvements equal 24% and 16% for the MESRTM and ACE2 models respectively.

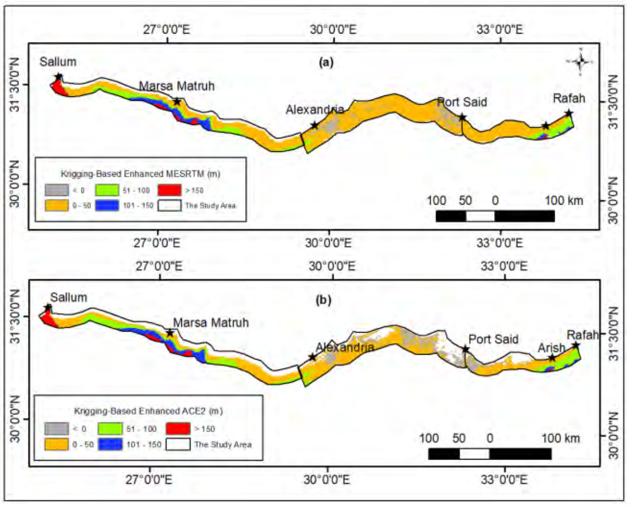

(a) Enh_2_MESRTM and (b) Enh_2_ACE2

Figure 6. The Krigging-Based Enhanced GDEM Models

Table 6. Statistics of Height Differences of Krigging-Based Enhanced GDEM at Known Points

	Enh_2_MESRTM	Enh_2_ACE2
Minimum Height Difference	-6.282	-3.959
Maximum Height Difference	3.246	4.552
Mean Height Difference	-0.429	0.888
Standard Deviation of Differences	± 2.15	± 2.40

Comparing the results of both modelling approaches, it has been found that the regression method produced improvements of 15% and 4% for the investigated MESRTM and ACE2 models respectively. On the other hand, the attained improvements equal 24% and 16% for the same GDEMs. That concludes that the krigging geostatistical modelling is better than the regression method since it takes the spatial correlation between the data points.

Regarding the utilization of different variogram types within the kriging process, five variograms have been utilized in the development of kriging-based enhanced GDEMs, namely the spherical, circular, exponential, Gaussian, and linear variograms. The accomplished results were very close within the centimeter-level in terms of both mean and standard deviation. However, such insignificant findings could be due to the study area's small size and the limited number of datasets available. As a result, the role of variogram types in enhancing GDEMs should be studied more thoroughly over wider spatial regions and with more data points.

The current study not only evaluates the performance of GDEMs as various previous researches but extends its objectives to enhance such global models by incorporating more terrestrial local datasets. It is a matter of reality that, in many developing countries, there are no accessible precise DEMs and the utilization of low-accuracy GDEMs is the affordable cost-effective alternative. Thus, enhancing the performance of GDEMs is valuable for environmental and mapping activities. The current research addresses this need by presenting a straightforward GIS-based solution. However, because of the limited number of attainable terrestrial data points, such a technique should be thoroughly examined in other larger areas with a sufficient number of data points.

5. Conclusions

Global Digital Elevation Models provide open-source free-of-charge accessible data to represent the topography of a spatial area. Such models have been developed and distributed worldwide and have been extensively applied in several coastal management and environmental applications. It is a matter of reality that each activity requires a certain level of vertical accuracy to meet its requirements and specifications. The current research investigates the vertical accuracy of different resolution GDEMs (namely PALSAR, SRTMGL 1, and ACE2) over the 1000-kilometrs Egyptian coasts along the Mediterranean sea using accurate GNSS/Levelling datasets. The vertical datum of those models has been first unified and a local geoid model has been utilized for height conversion. In addition, the study tries to enhance such accuracy levels by adding terrestrial precise datasets and utilizing both the regression and the krigging statistical methods to spatially model the GDEM-based height errors.

Based on the available datasets, few conclusions have been drawn. Being judged over terrestrial precise BM, the vertical accuracy of the original GDEMs be ± 3.43 m for the PALSAR model and ± 2.85 m for both SRTMGL 1 and ACE2 models. Converting the PLASAR vertical datum from the WGS84 one to the MSL datum reduce its vertical accuracy to 2.98 m over the available ground points.

Replacing the utilized geoid model used in height transformation of the SRTMGL 1 model, from the global EGM96 geoid to the local SRI2021 one, enhance its accuracy a little bit. Applying the regression modelling method results in enhancing the vertical accuracy of MESRTM and ACE2 by 15% and 4% respectively. On the other hand, the kriging geostatistical method produced 24% and 16% improvements for the MESRTM and the ACE2 respectively. Accordingly. It is concluded that the kriging geostatistical modelling is better than the regression method since it takes the spatial correlation between the data points.

According to the accomplished findings, few significant concluding remarks could be summarized. First, the presented approach of adding terrestrial local BM datasets to a global DEM could considerably increase its overall vertical accuracy. Second, the number of added terrestrial points should be appropriate to the desired level of vertical accuracy and the area of study. For instance, 200 BM have been added in the current research study to decrease the overall accuracy of a particular GDEM from ± 2.85 m to ± 2.15 m over the current study area. Thus, it might be concluded that enhancing the accuracy of GDEMs to a sum-meter level may require collecting a huge number of BM, which is obviously expensive. Third, the achieved vertical accuracy of the enhanced models, herein, could be suitable for small-scale mapping, hydrological investigations, and overall management of coastal regions. However, it might not be appropriate for accurate environmental studies such as Sea Level Rise (SLR) monitoring and risk assessment which requires accurate DEM for representing the topography of a particular area.

Declaration of Interest Statement

No potential interest was reported by the authors.
No funding was allocated for this research.

REFERENCES

[1] Khasanov, K. and Ahmedov, A. (2021). Comparison of digital elevation models for the designing water reservoirs: a case study of Pskom water reservoir, *E3S Web of Conferences*, 264, 03058, doi:10.1051/e3sconf/202126403058.

[2] Al-Krargy, E. and Dawod, G. (2021). Optimum combinations of GGM and DEM models for precise national geoid development, *Proceedings of Engineering and Technology Innovation*, V. 18, pp. 15-24, doi:10.46604/peti.2021.6452.

[3] Dawod, G. and Ascoura, I. (2021). The Validity of open-source elevations for different topographic map scales and geomatics applications, Journal of Geographic Information System, V. 13, No. 2, pp. 148-165.

[4] Khalil, H. and Hassaan, M. (2017). Developing a reliable digital elevation model for climate change applications, case study: the Nile delta, *Alexandria Research Center for Adaptation to Climate Change (ARCA) working paper No. 6*, Alexandria University, Alexandria, Egypt.

[5] Sumanathna, A., Madurapperuma, B., Hangawatta, T., Pathirage, I., and Fernando, G. (2018). Developing coastal Digital Elevation Model (DEM) to indicate tsunami flooding topography in Arugam bay, Sri Lanka, *Proceedings of the Institute of Professional Studies and Skills Development (IPSSD) Grand Day Online Conference*, pp. 1-14.

[6] Wahid, A., Madden, M., Khalaf, F., and Fathy, I. (2016). Geospatial analysis for the determination of hydro-morphological characteristics and assessment of flash flood potentiality in arid coastal plains: A case in southwestern Sinai, *Egypt, Earth Sciences Research Journal*, 20(1), E1-E9, https:// doi.org/10.15446/esrj.v20n1.49624.

[7] Gaber, A., Darwish, N., and Koch, M. (2017). Minimizing the residual topography effect on interferograms to improve DInSAR results: Estimating land subsidence in Port-Said city, Egypt, *Remote Sensing*, 9, 752, doi:10.3390/rs9070752.

[8] Abdel-Aziz, T., Dawod, G., and Ebaid, H., (2020). DEMs and reliable sea level rise risk monitoring in Nile Delta, Egypt, Discover Sustainability, V. 1, No. 1, doi:10.1007/s43621-020-00006-7.

[9] Patel, A., Katiyar, S. and Prasad, V. (2016). Performance evaluation of different open source DEM by Differential Global Positioning System (DGPS), *The Egyptian Journal of Remote Sensing and Space Sciences*, No. 19, pp. 7-16.

[10] Kulp, S. and Strauss, B. (2016). Global DEM Errors under predict coastal vulnerability to sea level rise and flooding, *Frontiers in Earth Science*, 4:36. doi:10.3389/feart.2016.00036.

[11] Dawod, G. and Al-Ghamdi. K. (2017). Reliability of recent global digital elevation models for geomatics applications in Egypt and Saudi Arabia, *Journal of Geographic Information System*, V. 9, No. 6, pp. 685-698.

[12] Rabah, M., El-Hattab, A. and Abdallah, M. (2017). Assessment of the most recent satellite based digital elevation models of Egypt, *NRIAG Journal of Astronomy and Geophysics*, doi:10.1016/j.nrjag.2017.10.006.

[13] Mukherjee, S., Joshi, P., Mukherjee, S., and Ghosh, A. (2013). Evaluation of vertical accuracy of open source Digital Elevation Model (DEM), *International Journal of Applied Earth Observation and Geoinformation*, No. 21, pp. 205-217.

[14] Ouerghi, S., Abdalla ELsheikh, R. Achour, H. and Bouazi, S. (2015). Evaluation and Validation of Recent Freely-Available ASTER-GDEM V.2, SRTM V.4.1 and the DEM Derived from Topographical Map over SW Grombalia (Test Area) in North East of Tunisia, *Journal of Geographic Information System*, No. 7, pp. 266-27.

[15] Leon, J., Heuvelink, G., and Phinn, S. (2014). Incorporating DEM uncertainty in coastal inundation mapping, *PLoS ONE*, V. 9, No. 9: e108727, doi:10.1371/journal. pone.0108727.

[16] Hu, Z., Peng. J., Hou, Y. and Shan, J. (2017). Evaluation of Recently Released Open Global Digital Elevation Models of Hubei, China, *Remote Sensing*, 9, 262; doi: 10.3390/rs9030262.

[17] Wang, X., Holland, D., and Gudmundsson, H. (2018). Accurate coastal DEM generation by merging ASTER GDEM and ICESat/GLAS data over Mertz Glacier, Antarctica, *Remote Sensing of Environment*, No. 206, pp.

218-230.

[18] *Abd-Elmotaal, H., Abd-Elbaky, M. and Ashry, M. (2013). 30 Meters Digital Height Model for Egypt,* Presented at the VIII Hotine-Marussi Symposium, *June 17-22, Rome, Italy*.

[19] Jamali, A., Mustapha, A., and Mostafa, S. (2021) Prediction of sea level oscillations: Comparison of regression-based approach, *Engineering Letters*, V. 29, No. 3, pp. 1-6.

[20] Orejuela, I., Gonzalez, C., Guerra, X., Mora, E., and Toulkeridis, T. (2021) Geoid undulation modeling through the Cokriging method - A case study of Guayaquil, Ecuador, *Geodesy and Geodynamics*, No. 12, pp. 356-367.

[21] USGS (The US Geological Survey), (2022). *SRTMGL1 V003*, Available at: https://lpdaac.usgs.gov/products/srtmgl1v003/, Accessed 6 Jan, 2022.

[22] ASF (Alaska Satellite Facility) (2022). *ALOS PLASAR – Radiometric Terrain Correction*, https://asf.alaska.edu/data-sets/derived-data-sets/alos-palsar-rtc/alos-palsar-radiometric-terrain-correction/, Accessed 6 Jan, 2022.

[23] Smith, R. and Berry, P. (2019). *Altimeter Corrected Elevations, Version 2 (ACE2)*, A Technical Report, 22p, Columbia University, New York, USA.

[24] SRI (Survey Research Institute) (2018). *Establishing accurate geodetic networks along the Egyptian coastlines*, Internal Technical Report, No. 1.

[25] Brimicombe, A. (2010). GIS, *environmental modeling and engineering*, Second Edition, CRC Press, New York, USA, 361 pp.

[26] ESRI (Environmental Systems Research Institute) (2021). *How krigging works*, https://desktop.arcgis.com/en/arcmap/10.3/tools/3d-analyst-toolbox/how-kriging-works.htm, Accessed 12 Dec, 2021.

Copyright © 2022 The Author(s). Published by Scientific & Academic Publishing
This work is licensed under the Creative Commons Attribution International License (CC BY). http://creativecommons.org/licenses/by/4.0/

International Journal of Engineering Inventions
e-ISSN: 2278-7461, p-ISSN: 2319-6491
Volume 11, Issue 2 [Mar.-Apr. 2022] PP: 25-32

GIS-Based Geoid Refinement by GNSS/Levelling Data: A Case Study of Egypt

Gomaa M. Dawod and Hoda F. Mohamed
Geodesy Dept., Survey Research Institute, National Water Research Center, Giza, EGYPT
Corresponding Author: Gomaa M. Dawod

ABSTRACT: *As an alternative to the extensive process of entirely re-developing a geoid model when new geodetic datasets are available, this paper proposes a simple, efficient, and fast approach for geoid refinement within a Geographic Information Systems (GIS) environment. It investigates several mathematical approaches for incorporating Global Navigation Satellite Systems (GNSS)/Levelling datasets. Such methods include 2-parametres, 4-parameters, and 7-parameters regression, Inverse Weighted Distance (IDW) method, and the krigging geostatistical method. Based on the available data, the recent SRI 2021 national geoid model has been refined using the five approaches with 220 new GNSS/Levelling data points. Based on available data and attained results, it has been realized that all investigated methods generate roughly the same accuracy level, and an improvement of almost 10% has been achieved. Such a small level of enhancement might be accredited to the non-homogeneous spatial distribution of the utilized datasets over the country. The final developed geoid model, named SRI 2022, has overall accuracy equals ± 0.14 m. It is recommended that in order to achieve a 1-5 centimeter accuracy of a geoid model in Egypt, updating/establishing of both GNSS and Levelling networks, with a good homogenous spatial distribution, is a must.*

Date of Submission: 11-04-2022 Date of Acceptance: 28-04-2022

I. INTRODUCTION

Geoid modelling comprises an essential duty for geodesists worldwide, particularly with the rapid growth of utilizing the Global Navigation Satellite Systems (GNSS) technology. A geoid model plays the most significant role in converting the GNSS-based ellipsoidal heights to orthometric heights or elevations related to the Mean Sea Level (MSL) datum usually utilized in surveying, mapping, and civil engineering. Several national or regional geoid models have been investigated recently in quite a few countries such as Indonesia [1], Chile and Spain [2], and Vietnam [3]. Furthermore, other geoid models have been developed on a local basis within a country, such as the west desert in Egypt [4], and Jeddah city in Saudi Arabia [5]. The accuracy of geoid models differs significantly from one region to another based on the precision, number, and spatial distribution of the utilized datasets. A level of 1-cm has been achieved for a geoid model in Colorado state in the United States of America [6] and even 5-mm accuracy has been reported in Estonia [7]. On a national basis, many geoid models have been developed in Egypt even nationally such as Saadon et al. [8] or locally such as Elshewy et al. [9].

Refinement of a geoid model, a global or a national one, is a procedure that took place after its original creation by incorporating more new geodetic datasets. Such a process has been investigated by several researchers in the last decade. For example, Al-Kherayef et al. [10] have examined the addition of new observed GNSS/Levelling datasets to the Saudi geoid named KSA-Geoid17. Also, Pasuya et al. [11] have analyzed the refinement of the gravimetric geoid of Malaysia by incorporating terrestrial, marine, and airborne gravity datasets. Similarly, Wang et al. [12] proposed the enlargement of the Chinese geoid model by adding satellite altimetry levelling datasets. The mathematical and statistical methods of such geoid refinement comprise an essential research topic where several approaches have been proposed. Such models include, among others, the moving least squares approach [13], polynomial regression and Artificial Neural Network (ANN) approach [14], the 4-paratmeter removal [15], finite elements based bivariate [16], and minimum curvature surface [17].

Traditionally as far as new GNSS/Levelling datasets are available, a new geoid national model is developed using one of the geoid modelling packages such as the GravSoft scientific program. Instead, this paper proposes a simple and fast approach for refinement of an existing geoid model. Thus, based on one of the most-recent geoid models of Egypt, the current research examined the incorporation of more GNSS/Levelling datasets to improve its accuracy on a national scale. Such refinement procedure is carried out within a Geographic Information Systems (GIS) environment where several mathematical and statistical methods are applied and compared.

II. METHODOLOGY

Several mathematical and statistical models have been proposed for interpolating scatter data points and constructing a 3D spatial surface in various geodetic tasks. Of then, the regression method is expensively utilized in different mathematical forms. The simple linear equation formula [18] for geoidal errors (ΔN) in terms of latitude ϕ and longitude λ is given by :

$$\Delta N1 = a_o + a_1 \cos\phi + a_2 \cos\lambda + \varepsilon \quad (1)$$

The 4-parameters and 7-parameters regression models used in several geodetic applications [15] could be written as:

$$\Delta N2 = a_o + a_1 \cos\phi\cos\lambda + a_2 \cos\phi\sin\lambda + a_3 \sin\phi + \varepsilon \quad (2)$$

$$\Delta N3 = a_o + a_1 \cos\phi\cos\lambda + a_2 \cos\phi\sin\lambda + a_3 \sin\phi + a_4 (\cos\phi\sin\phi\cos\lambda)/W + a_5 (\cos\phi\sin\phi\sin\lambda)/W + a_6 (\sin^2\phi)/W + \varepsilon \quad (3)$$

where,

a_o, a_1, a_2, a_3, a_4, a_5, and a_6 are the unknowns to be estimated,

$$W = \sqrt{1 - e^2 \sin^2\phi} \quad (4)$$

e2 is the second eccentricity of the WGS84 ellipsoid, and ε represents the residuals or errors of the regression process.

Each observation point gives one observation equation (of 1 or 3) and the least-squares adjustment method will be applied to solve all equations simultaneously to produce unique estimates of the unknowns. Within a GIS environment, there exist quite a few models for converting scatter data points into a grid or a 3D surface. Such methods include for example the kriging, spline, trend, natural neighbor, and the Inverse Distance Weighted (IDW) technique. The IDW is a mathematical deterministic method that computes the value of an unknown point by averaging the values of neighboring known points. However, IDW takes into account the distances to each known point so that the weights are inversely proportional to distances. The basic formula of the IDW method is [19]:

$$\Delta N4_{i,j} = \sum_{k=1}^{n} \Delta N_k , d_k^{-r} \Big/ \sum_{k=1}^{n} d_k^{-r} \quad (5)$$

where

$\Delta N4i,j$ is the geoidal error of the unknown points,

ΔNk is the geoidal error of the known points,

dk represents the distance between a known and an unknown point, and

r is a power weighting function, usually in practice equals 2.

Moreover, the kriging is a geostatistical analysis that takes into account the spatial distribution of the sample points to explain the variations in the 3D surface. The general form of the kriging interpolator is (ibid):

$$\hat{Z}(S_o) = \sum_{i=1}^{n} \lambda_i Z(s_i) \quad (6)$$

where,

Z(si) is the measured quantity at the ith location,

λi represents an unknown weight for point i,

so is the prediction location, and

n equals the number of measurements.

Accordingly, each equation (Eq. 1 to 6) will be utilized in a GIS environment to model spatially the geoidal errors and construct a 3D corrector surfaces. Each corrector surface will be added to the original geoid model to attain a modified or enhanced version:

$$Enh_geoid_i = SRI\ 2021 + Corrector_i \quad (7)$$

Finally, the accuracy of all enhanced geoid models will be externally evaluated, in terms of standard deviations, over the known checkpoints. The overall processing steps are depicted in Fig. 1.

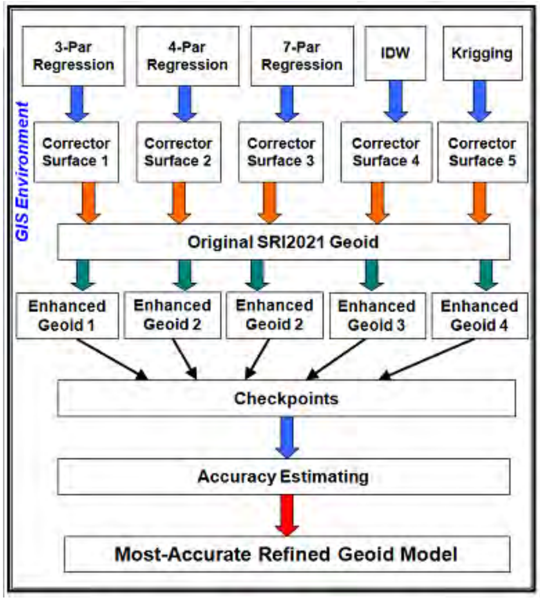

Fig. 1: Workflow of the Processing Strategy

III. AVAILABLE DATA

The basic piece of information utilized in this research is the SRI2021 geoid model developed by Al-Krargy and Dawod [20]. This research has investigated the utilization of several Global Geopotential Models (GGMs) and Global Digital Elevation Models (GDEMs) to find out their optimum combination in geoid modelling of Egypt. Additionally, it utilized 247 terrestrial gravity stations to develop a gravimetric geoid then fit it to 1100 GNSS/Leveling points. The resulting optimum national geoid model, SRI2021, has an accuracy level of ± 0.151 m when judged over 100 GNSS/Levelling checkpoints (Fig. 2). In addition, a total of 245 GNSS/Levelling points have been collected from the projects carried out by the Survey Research Institute (SRI) in the last few years. Mostly, they cover the shorelines of the Red Sea, Suez Gulf, and Aqaba Gulf. Herein, those available points have been divided into two groups: 223 stations used in the processing stage, and 22 stations kept as checkpoints to judge the attained results (Fig. 3).

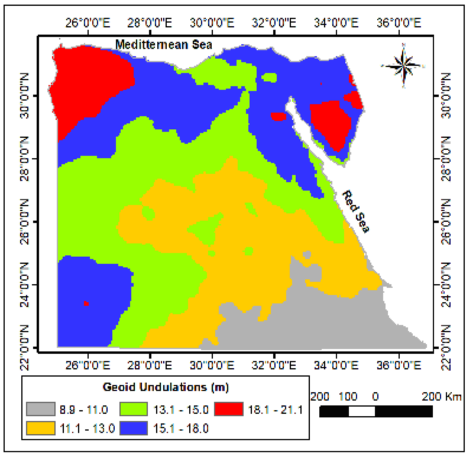

Fig. 2: The SRI2021 Geoid Model of Egypt
(after Al-Krargy and Dawod 2021)

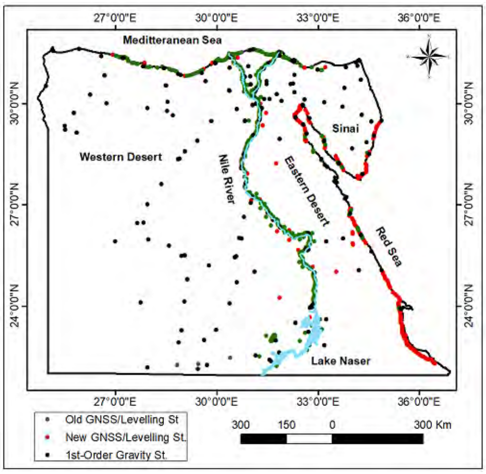

Fig 3: Available GNSS/Levelling Stations

IV. PROCESSING AND RESULTS

The first step has been performed using the known geoid undulations, N, at the utilized 223 GNSS/Levelling stations and comparing them to the corresponding values of the SRI2021 geoid to compute their residuals ΔN. Next, the different investigated regression equations (Eq. 1, 2, and 3) have been solved. The attained regression models are:

$$\Delta N1 = -2.3288 + 1.0852 \cos\phi + 2.0604 \cos\lambda \quad (8)$$

$$\Delta N2 = -8.8548 + 7.8536 \cos\phi\cos\lambda + 3.5186 \cos\phi\sin\lambda + 3.6557 \sin\phi \quad (9)$$

$$\Delta N3 = -430.7820 + 326.7796 \cos\phi\cos\lambda + 232.1219 \cos\phi\sin\lambda + 8267.1712 \sin\phi - 501.4360 (\cos\phi\sin\phi\cos\lambda)/W - 374.0123 (\cos\phi\sin\phi\sin\lambda)/W - 232.8917 (\sin^2\phi)/W \quad (10)$$

With the coefficient of determination, R2, equals 0.029 , 0.033, and 0.147 respectively.

Next, a rectangular 2-km x 2-km grid has been created covering the entire territory of Egypt. Using the Arc GIS 10.8 package, the results of Eq. 8, 9, and 10 have been estimated at each corner of that grid. The attained surfaces represent the three correction surfaces for these regression models. Next, the IDW and Krigging tools have been applied to model the geoidal errors of SRI2021 using the IDW and Krigging methods (Eq. 5 and 6). Accordingly, five correction surfaces have been developed for the five investigated refinement models (Fig. 4). The statistics of those correction models are presented in Table 1. Even though Fig. 4 shows considerable differences in the spatial distribution of geoid errors for the utilized models, Table 1 proves that there are no statistical variations in the overall performance of all models over Egypt. Thus, it can be said that the smaller values of standard deviations characterize the precision of the investigated models not their accuracy of geoid enhancement.

Table 1: Statistics of Correction Surfaces (m)

Model	Correction Surfaces			
	Minimum	Maximum	Average	Standard Deviation
2-Parametrs Regression	0.303	0.545	0.426	± 0.054
4-Parametrs Regression	0.303	0.544	0.426	± 0.055
7-Parametrs Regression	0.301	0.545	0.425	± 0.055
IDW	0.302	0.545	0.426	± 0.055
Krigging	0.302	0.544	0.425	± 0.054

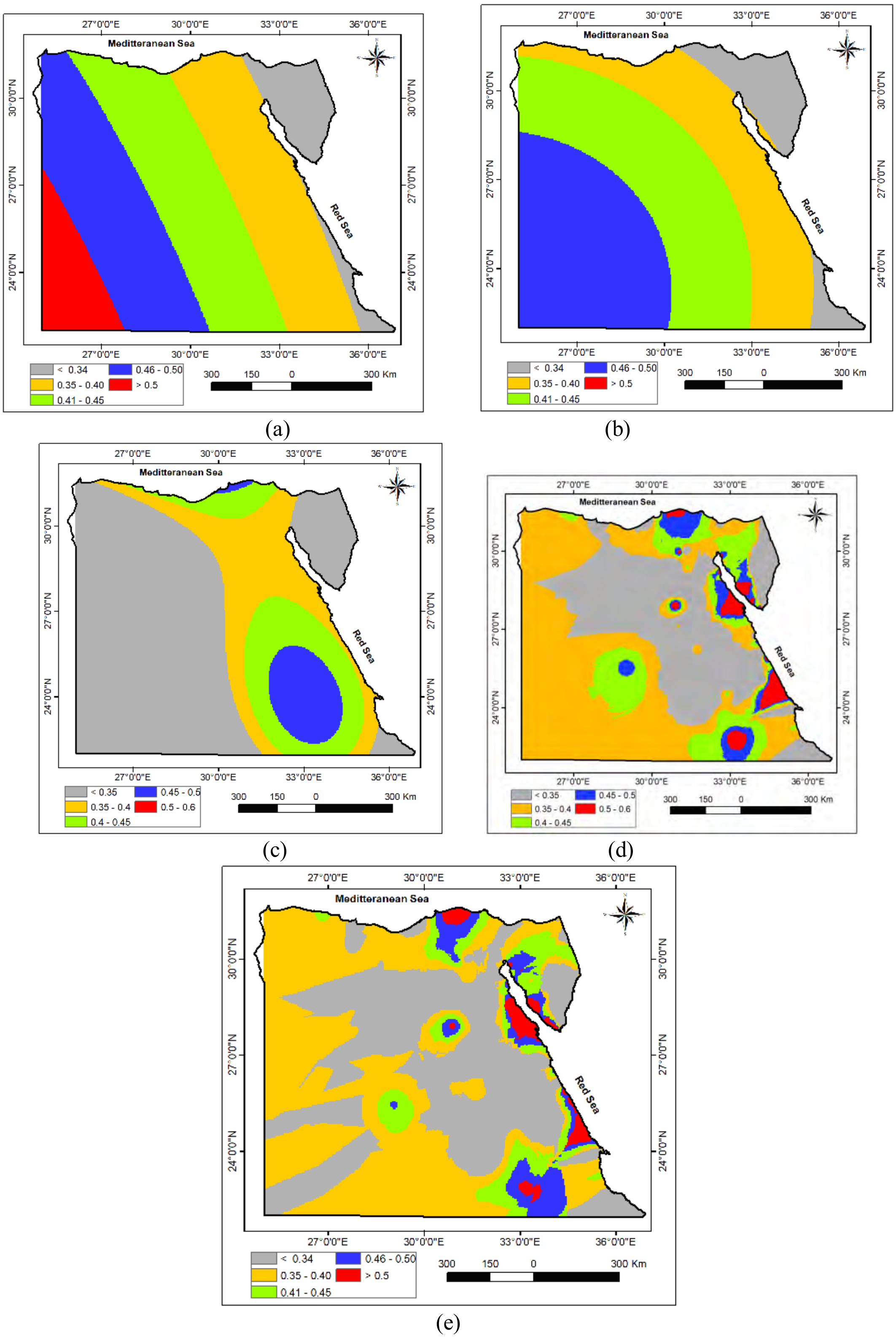

(a) 2-parametr regression, (b) 4-parametr regression, (c) 7-parametr regression,
(d) IDW, and (e) Krigging

Fig. 4: The Attained Correction Surfaces

Next, Equation 7 has been applied to develop five new geoid models by adding each corrector surface to the original SRI 2021 geoid. In order to judge the accuracy of such geoid models, they have been compared over the known 22 checkpoints. Table 2 presents the accomplished findings. First, it can be realized from this table that all investigated methods produce almost the same accuracy level. Second, a comparison between the

new refinement geoid models and the original SRI 2021 one reveals that an improvement of almost 10% has been achieved. Third, the 4-praemetr regression approach relatively provide the best improvement level. This model is called SRI 2022 geoid whose external overall accuracy equals ± 0.136 m and produced 9.3% improvements. This level of accuracy is generally compatible with those of other recent geoid modelling in Egypt (e.g. Saadon et al. 2021). Finally, based on the achieved findings, it can be concluded that the proposed GIS-based approach of geoid refinement is straightforward, efficient, and rapid. It should be carried out as long as new GNSS/Levelling datasets are available.

Table 2: Statistics of Undulations of Different Geoid Models Over Checkpoints (m)

Geoid Model	Geoid Undulation				
	Minimum	Maximum	Average	Standard Deviation	Improvement %
SRI 2021 Geoid	7.158	16.799	12.753	± 3.049	NA
Geoid of 2-Parametrs Regression	7.046	16.866	12.768	± 2.768	9.2 %
Geoid of 4-Parametrs Regression	7.066	16.860	12.766	± 2.766	9.3 %
Geoid of 7-Parametrs Regression	6.934	16.316	12.518	± 2.773	9.1 %
Geoid of IDW	6.966	16.240	12.517	± 2.774	9.0 %
Geoid of Krigging	6.966	16.234	12.515	± 2.779	8.9 %

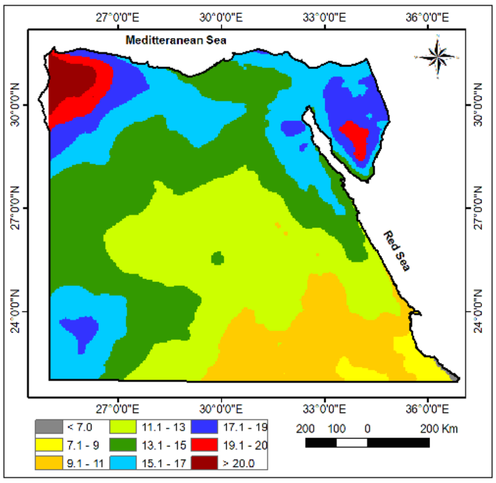

Fig. 5: The SRI 2022 Egyptian Geoid

Furthermore, the attained findings reveal that adding almost two hundred of GNSS/Levelling points enhance the accuracy of the existing national geoid of Egypt by only 10% approximately. This might be attributed to the spatial distribution of the utilized datasets which is not homogenous over the country (Fig. 3). Such a situation exists in all trials to develop an accurate Egyptian geoid. Fig. 6 depicts the distribution of the most available geodetic datasets accessed by researchers and academia in the geodetic community. That figure clearly shows that significant spatial gaps are presented in the Eastern desert, the Western desert, and the Sinai peninsula. As far the authors' concern, there exist other datasets owned by other authorities such as the geological survey authority (terrestrial gravity data) and the nuclear energy authority (airborne gravity data). It is highly recommended that all datasets should be collected, analyzed, and utilized in developing a precise national geoid of Egypt.

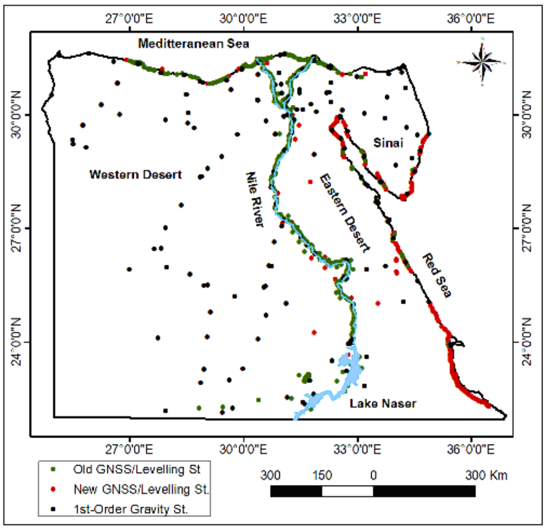

Fig. 6: The Currently Available Geodetic Datasets for Geoid Modelling

V. CONCLUSIONS

The current research proposes a simple and fast approach for the refinement of an existing national or regional geoid model. Based on one of the most-recent geoid models of Egypt, the current research examined the incorporation of more GNSS/Levelling datasets to improve its accuracy on a national scale. Several mathematical and statistical methods have been investigated and judged. Such models include 2-parameters, 4-parameters, 7-parametres regression models, the inverse weighted distance, and the krigging approach. All those models have been applied, along with two hundred GNSS/Levelling stations, within a GIS environment for efficient and simple refinement of the geoid in Egypt.

The accomplished results indicated that all investigated methods generate roughly the same accuracy level. Additionally, an improvement of almost 10% has been achieved based on the available datasets. Such a small level of enhancement might be accredited to the non-homogenous spatial distribution of the utilized datasets over the country. The final developed geoid model, SRI 2022, has an overall accuracy equals ± 0.136 m. Based on the achieved findings, it can be concluded that the anticipated GIS-based technique of geoid refinement should be carried out as long as new GNSS/Levelling datasets are available.

Few recommendations could be drawn based on the results of the current study, as:

1. All available geodetic datasets should be collected from all local organizations, analyzed, and utilized in developing a precise national geoid of Egypt.
2. Achieving a few-centimeter accuracy of a geoid model in Egypt requires the updating/establishment of both GNSS and Levelling networks with a good homogenous distribution over the country.
3. A Geodetic Data Infrastructures (GDI) should be developed and is accessible to professionals as a component of the undergoing Spatial Data Infrastructures (SDP) huge project

REFERENCES

[1] Ramdani, D , Hartanto, A., Oktaviani, N , and Hariyono, M., Verification of the Jakarta geoid model from the gravity data of 2.5 km resolution with gravimetric geoid, IOP Conf. Series: Earth and Environmental Science 873 (2021) 012045, https://doi.org/10.1088/1755-1315/873/1/012045, 2021.

[2] Mosquera, J., Silva, M. Isla, F. and Prado, C., Assessment of hybrid geoids in Chile and Spain, combining GGM and GNSS/Leveling observations, Geodesy and Geodynamics, No. 12, 2021, 65-92.

[3] Vu, D., Bruinsma, S. and Bonvalot, S., A high-resolution gravimetric quasigeoid model for Vietnam, Wart, Planets and Space, 71:65, https://doi.org/10.1186/s40623-019-1045-3, 2019.

[4] Elwan, M., Helaly, A., Zharan, K., Issawy, E. and Abd El-Gawad, A., Local geoid model of the Western Desert in Egypt using terrestrial gravity data and global geopotential models, Arabian Journal of Geosciences, 14:1436 https://doi.org/10.1007/s12517-021-07817-6, 2021.

[5] Borghi, A., Barzaghi, R., Al-Bayari, O. and Al Madani, S., Centimeter precision geoid model for Jeddah region (Saudi Arabia), Remote Sensing, 12,2066, https://dpi.org/10.3390/rs12122066, 2020.

[6] Grigoriadis, V., Vergos, G., Barzaghi, R., Carrion, D. and Koc, O., Collocation and FFT-based geoid estimation within the Colorado 1 cm geoid experiment, Journal of Geodesy, 95:52 https://doi.org/10.1007/s00190-021-01507-7, 2021.

[7] Ellmann, A., Mardla, S. and Oja, T., The 5 mm geoid model for Estonia computed by the least squares modified Stokes's formula, Survey Review, https://doi.org/10.1080/00396265.2019.1583848, 2019.

[8] Saadon, A., El-Ashquer, M., Elsaka, B. and El-Fiky, G., Determination of local gravimetric geoid model over Egypt using LSC and FFT estimation techniques based on different satellite- and ground-based datasets, Survey Review, https://doi.org/10.1080/00396265.2021.1932148, 2021.

[9] Elshewy, M. Elsheshtawy, A. and Chistiakova, E., Developing a local geoid model in Egypt using artificial neural networks: A case study on the Red Sea coast, Geodesy and Aerophoto surveying. Vol.65. No.6., 2021, 615-624, https://doi.org/10.30533/0536-101X-2021-65-6-615-624

[10] Al-Kherayef, O. Golubinka, I., Al-Shahrani, S. and Grebenitcharsky, R., An improved hybrid geoid model over Kingdom of Saudi Arabia utilizing new GNSS ellipsoidal heights on benchmarks of KSA national vertical network, Presented at the FIG working week 2020, Amsterdam, the Netherlands, May 10–14, 2020.

[11] Pasuya, M., Din, A., Yusoff, M., Abbak, R., and Hamden, M., Refinement of gravimetric geoid model by incorporating terrestrial, marine, and airborne gravity using KTH method, Arabian Journal of Geosciences, 14: 2003, https://doi.org/10.1007/s12517-021-08247-0, 2021.

[12] Wang, Z., Chao, N. and Chao, D., Using satellite altimetry leveling to assess the marine geoid, Geodesy and Geodynamics, No. 11, 2020, 106-111.

[13] Kiani, M., Local geoid height approximation and interpolation using moving least squares approach. Geodesy and Geodynamics, No. 11, 2020, 120-126.

[14] Ahmed, H., Mohamed, E. and Shaheen, B., Evaluating two numerical methods for developing a local geoid model and a local digital elevation model for the Red Sea coast, Egypt, Journal of King Saud University – Engineering Sciences, https://doi.org/10.1016/j.jksues.2021.04.004, 2021.

[15] Wu, Q., Wang, H., Wang, B., Chen, S. and Li, H., Performance comparison of geoid refinement between XGM2016 and EGM2008 based on the KTH and RCR methods, Remote Sensing, 12,324, https://doi.org/10.3390/rs12020324, 2020.

[16] Erol, S. and Erol, B., A comparative assessment of different interpolation algorithms for prediction of GNSS/levelling geoid surface using scattered control data, Measurement, https://doi.org/10.1016/j.measurement.2020.108623, 2020.

[17] Rabah, M. and Kaloop, M., The use of minimum curvature surface technique in geoid computation processing of Egypt, Arabian Journal of Geosciences, 6:1263-1272, https://doi.org/ 10.1007/s12517-011-0418-0, 2013.

[18] Shaker, A., Saad, A., Salah, M. and Salama, I., Multiple polynomial-based generation of DEM from topographic contour data, Presented at the Regional Conference on Surveying & Development Sharm El-Sheikh, Egypt, 3-6 October, 2015.

[19] Brimicombe, A., GIS, environmental modeling and engineering, Second Edition, CRC Press, New York, USA, 361 pp, 2010.

[20] Al-Krargy, E. and Dawod, G., Optimum combinations of GGM and DEM models for precise national geoid development, Proceedings of Engineering and Technology Innovation, V. 18, 2021, 15-24, DOI: https://doi.org/10.46604/peti.2021.6452

American Journal of Engineering Research (AJER)
e-ISSN: 2320-0847 p-ISSN : 2320-0936
Volume-11, Issue-05, pp-10-18
www.ajer.org
Research Paper Open Access

Accuracy and Applicability of GNSS PPP for GNSS Surveys: A Case Study in the Nile Delta, Egypt

Gomaa M. Dawod*, Ahmed M. Amin and Hoda F. Mohamed
Survey Research Institute, National Water Research Center, Giza, Egypt

ABSTRACT : *The Due to its technical and economical merits, the Precise Point Positioning (PPP) approach of Global Navigation Satellite Systems (GNSS) has been utilized for a wide range of surveying and geodetic applications in recent years. However, its accuracy and applicability are significantly limited by the occupation time. This paper investigates the relationship between accuracy and static occupation time of PPP in Egypt as a case study. Based on the available GPS+GLONASS datasets, accomplished results showed that precision of few centimeters in both latitude and longitude could be obtained by occupation of more than half an hour. In addition, a sub-centimeter accuracy requires occupation of two hours at least. From an accuracy point of view, two-centimeters accuracy is attained with four hours of static occupation. It can be concluded that civil engineering applications require occupations varying from 1 to 4 hours according to the required accuracy. Furthermore, an occupation of half an hour or less should be assigned only for reconnaissance and small-scale mapping activities. The current study's conclusions should be taken into account in surveying, mapping, and civil engineering applications in Egypt.*

KEYWORDS *GNSS, PPP, Occupation Time, Accuracy, Applicability, Egypt.*

Date of Submission: 18-04-2022 Date of acceptance: 03-05-2022

I. INTRODUCTION

PPP has become a powerful widely-used positioning technique utilizing satellite-based GNSS for a wide range of applications. With the PPP technique, GNSS satellites' observations collected by a single receiver, without the need of a nearby base or reference station, are used to determine its 3D coordinates. In nowadays, PPP is regarded as a dominant solution where precise positioning and navigation are required in remote locations, where reference station infrastructure is not available. From an economic perspective, PPP is a cost-effective method since it works with a single GNSS receiver in the static or kinematic mode.

The most important feature of the GNSS PPP technique is its utilization of precise satellite orbits and satellite clock corrections from either commercial or public service. Traditionally, PPP was applied as a relative GNSS processing technique where one/or more station from the International GNSS Services (IGS) network are downloaded along with the precise orbits and clocks. The baseline between such a station and the observed one was, then, being post-processed to compute the precise coordinates of the occupied station. In the last few years, absolute PPP was introduced by collecting and utilizing precise satellites orbits and clocks to estimate the coordinates of the occupied station directly without ting to the IGS network. Such processing could be post-processing or real-time. The occupation time or GNSS session plays a critical role in the anticipated accuracy of the PPP solution. For example, Abdallah and Schwieger [1] found that a centimeter accuracy of 3D coordinates could be obtained after 4 hours of static occupation. Similarly, Harima et al. [2] found that ten centimeter horizontal accuracy could be achieved when the static occupation time equals half an hour. Moreover, a two-centimeter level of accuracy has been reported in Egypt based on two-hour static occupation [3].

PPP has been utilized for several geodetic and environmental applications. For example, Bahadur and Nohutcu [4] showed that PPP could provide a positioning solution appropriate for establishing geodetic control points in Turkey. Vazquez-Ontiveros et al [5] have utilized PPP for monitoring structural health of bridges. The utilization of PPP processing of smartphones has been recently investigated particularly in urban environments [6]. Also, Rabah et al. [7] have proposed the utilization of PPP for establishing a Continuously Operating Reference Station (CORS) network in Kuwait. Recently, PPP is proposed to be utilized with smartphones where it could reach sub-meter errors in static mode of a few minutes occupation time [8].

This paper aims to investigate the accuracy and applicability of GNSS PPP (particularly GPS+GLONASS) in GNSS surveys in Egypt as a case study. Three scenarios have been investigated, namely short occupation (1 to 60 minutes), medium occupation (1 to 6 hours), and long occupation (6 to 24 hours). Accomplished results in both 3D and 2D cases have been analyzed.

II. METHEDOLOGY

The basic mathematical models of the PPP approach for both pseudorange and carrier phase are [9]:

$$L_i^k - \rho_i^k - c(\Delta t_i - \Delta t^k) - \alpha_i^k T_i + I_i^k - \lambda B_i^k - \varepsilon = 0 \quad (1)$$

$$P_i^k - \rho_i^k - c(\Delta t_i - \Delta t^k) - \alpha_i^k T_i + I_i^k - c(b^k + b_i) - \varepsilon = 0 \quad (2)$$

where,

L_i^k, P_i^k : undifferenced carrier phase and code observations (meters),
ρ_i^k : geometric distance between satellite and receiver,
B_i^k : carrier phase bias,
N_i^k, δN_i^k : integer carrier phase ambiguity and non-zero initial fractional phase,
Δt_i, Δt^k : receiver and satellite clock offset,
T_i : troposheric total zenith delay,
α_i^k : troposheric mapping function,
I_i^k : slant ionospheric delay,
b_i, b^k, d_i, d^k : receiver and satellite code and phase hardware delays,
λ : corresponding carrier wavelength,
c : speed of light, and
ε : random error or residual.

PPP technique provides accuracy in the range of centimeter-to-decimeter level depending on the occupation time of static GNSS surveys [10]. Many online GNSS processing services are applying the absolute PPP technique for fast processing and precise output. Such services include the free post-processing Canadian Spatial Reference System PPP (CSR-PPP) [11] and the non-free real-time Trimble RTX. For example, Trimble RTX could provide 2 centimeters horizontal accuracy and 5 centimeters vertical accuracy having collected static GNSS observations for at least 15 minutes [12]. Other online processing services, such as the Australian AUSPOS and the American OPUS, still utilized the relative PPP approach.

III. Study Area and Available Data

The study area is located in the north of Egypt covering Port Said, Alexandria and Cairo cities (Fig. 1). It is bounded by latitudes 29.9° N and 31.6° N and longitudes 29.7° E and 32.3° E. The utilized dataset comprises three GNSS stations, just as a case study, belong to the CORS network established and operated by the Egyptian Survey Authority (ESA). Those stations are located in Port Said. Alexandria, and Cairo cities. A 24-hours raw GNSS dataset in the Receiver Independent Exchange Format (RINEX) has been obtained for each station. The data has been observed, with a 30-second interval, on January 23rd, 2019 and include data from only GPS and GLONASS systems as the installed receivers only track those satellites signals. The processing has been carried out using the Trimble TBC v. 5.2. It uses precise satellite orbit, clock and bias corrections derived from a global GNSS network to compute accurate user positions worldwide.

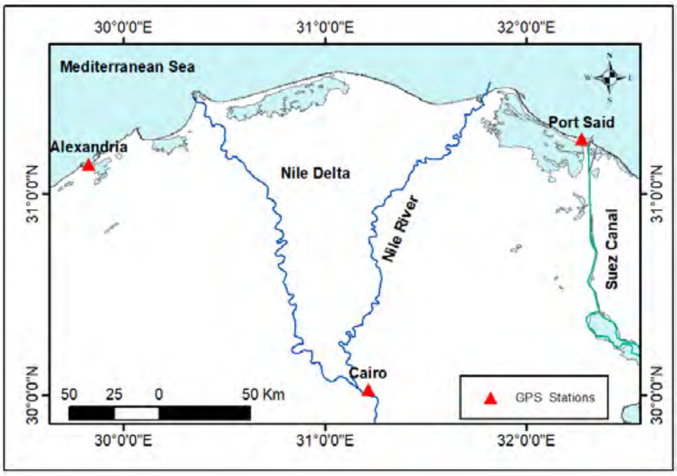

Fig. 1: The Study Area

IV. PROCESSING AND RESULTS

To investigate the applicability of the PPP approach, each observation file has been cut into several small files each represents a special scenario of occupation session. Those scenarios could be divided into three main cases: short occupation (1, 2, 5, 15, 30, and 60 minutes), medium occupation (1, 2, 3, 4, 5, and 6 hours), and long occupation (12, 18, and 24 hours). All raw RINEX files have been processed by the Trmibal TBS v. 5.2 (that utilizes equations 1 and 2) and the attained results have been analyzed in the three major scenarios. Both geodetic and Universal Transfers Mercator (UTM) zone 35 coordinates have been investigated relative to the World Geodetic System 1984 (WGS84) datum. Based on the date of collected data, the International Terrestrial Reference Frame (ITRF) of 2014 epoch 2019.1 has been the datum of the output. Statistical indicators for precision and accuracy have been determined. Based on the results of each station, the average indicators of each scenario have been computed, and presented herein, instead of dealing with three different GNSS stations.

The first scenario presents short GNSS occupation sessions ranging from one minute to sixty minutes. The precision of each case is expressed by the standard deviation indicator. Table 1 and Figure 2 present the average precision of each occupation time. It can be noticed that the standard deviations of occupations of lengths 1-5 minutes are greater than one meter. The occupation of 15 minutes produces precision of less than a meter, while precision of few centimeters could be obtained from sessions of lengths equal to or greater than half an hour.

Table 1: Precision of GPS+GLONASS Short Occupation Times

Occupation (minutes)	Standard Deviation of the Average (m)		
	Latitude	Longitude	Height
1	±2.452	±3.271	±5.098
2	±1.527	±2.479	±3.250
5	±0.784	±0.837	±1.468
15	±0.172	±0.365	±0.535
30	±0.019	±0.017	±0.063
60	±0.011	±0.011	±0.036

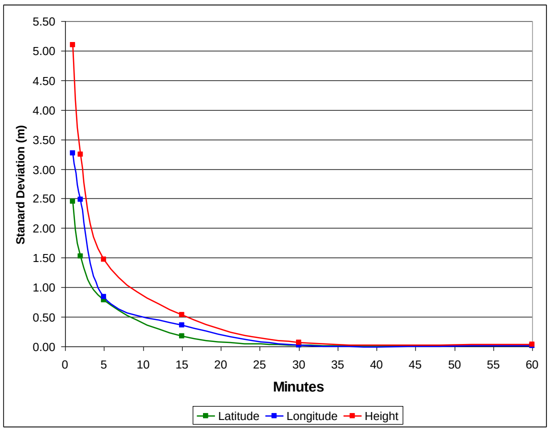

Fig. 2: Precision of GPS+GLONASS Short Occupation Times

The second investigated scenario represent medium occupation sessions varying between 1 and 6 hours. Similarly, Table 2 and Figure 3 present the average precision of each occupation time in such a case. It can be seen that the precision of occupation of 2 hours is less than a centimeter for both latitude and longitude, but the height's precision is still greater than 2 centimeters. In addition, it can be realized that longer occupation times significantly enhance the precision of the height more than the precision of both latitude and longitude. For instance, the precision of height at the 6-hour scenario is almost 157% and 71% better than those of the 1-hour and 2-hours cases respectively.

Table 2: Precision of GPS+GLONASS Medium Occupation Times

Occupation (hours)	Standard Deviation of the Average (m)		
	Latitude	Longitude	Height
1	±0.011	±0.011	±0.036
2	±0.007	±0.008	±0.024
3	±0.005	±0.006	±0.019
4	±0.004	±0.005	±0.017
5	±0.004	±0.004	±0.015
6	±0.003	±0.004	±0.014

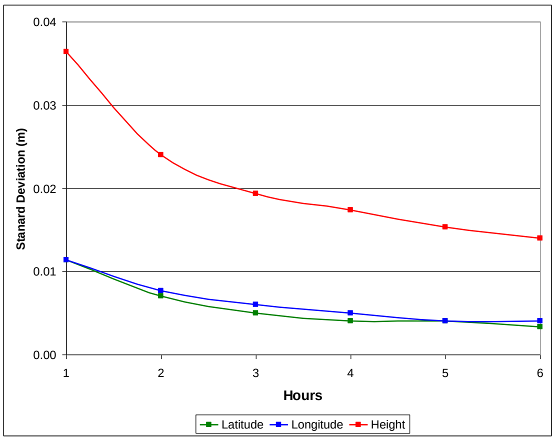

Fig. 3: Precision of Medium GPS+GLONASS Occupation Times

Table 3 and Figure 4 demonstrate the attained results of the third case for long occupation sessions varying between 12 and 24 hours. It can be noticed that the precision of occupation of 18 and 24 hours produce precision of two millimeters in both latitude and longitude and eight millimeters for the height. Also, it can be seen that the 24-hour session produces precision similar to the 24-hour one. Based on available data, it might say that 18 hours of GNSS occupation is optimum to achieve few-millimeters precision for precise geodetic GNSS activities.

Table 3: Precision of GPS+GLONASS Long Occupation Times

Occupation (hours)	Standard Deviation of the Average (m)		
	Latitude	Longitude	Height
12	±0.003	±0.003	±0.010
18	±0.002	±0.002	±0.008
24	±0.002	±0.002	±0.008

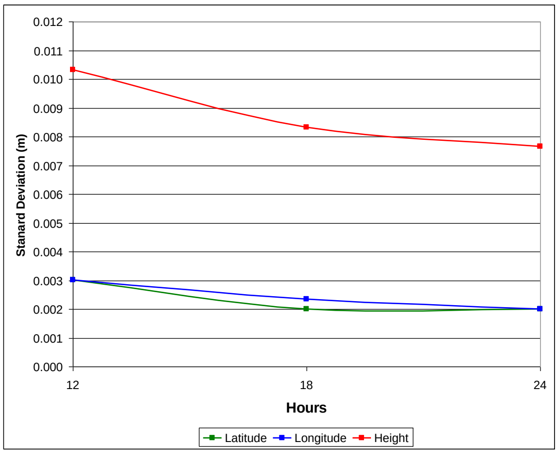

Fig. 4: Precision of GPS+GLONASS Long Occupation Times

Next, the study tries to investigate the accuracy of the GNSS PPP rater than its precision. In this regard, it is known that estimating the accuracy of measurements requires the knowledge of true values. The study considers the 24-hour coordinates of each GNSS station as a possible candidate for the true coordinates. Consequently, comparing the 24-hours coordinates to the results of each scenario might be considered as an accuracy estimation.

Table 4, and Figures 5, 6, and 7 present the attained results in terms of accuracy indicators. Several significant remarks could be drawn. First, it can be realized that the accuracy of occupation times less than 15 minutes are in the order of few decimeters, which is not appropriate for GNSS surveying applications. Next, it can be seen that the accuracy of few centimeters could be obtained when the occupation time is more than a quarter an hour. Starting from 1-hour of occupation, an accuracy of 2-centimeters becomes feasible. The level few-millimeters accuracy could be achieved in latitude and longitude when the occupation time is more than three hours. Additionally, the longer the occupation time the more increase of height accuracy. On the other hand, the errors in height estimation have been decreased by more than two orders of magnitude at the 18-hours occupation compared to the 4-hours results. Generally, it can be concluded that surveying-grade GNSS activities, with accuracy of 5 centimeters, require an occupation time of more than 15 minutes. However, 24-hours occupations still needed for accurate geodetic GNSS applications such as the establishment of control points and monitoring crustal deformation. Similar results have been reported by Abou Galala et al. [13].

Table 4: Accuracy of GPS+GLONASS Short, Medium, and Long Occupation Times

Occupation (minutes)	Average Absolute Errors (m)		
	Latitude	Longitude	Height
1	-0.119	0.462	0.362
2	-0.051	0.347	0.502
5	-0.091	0.240	0.303
15	0.045	-0.041	-0.050
30	0.030	0.000	0.006
60	0.021	0.001	0.005
Occupation (hours)	Average Absolute Errors (m)		
	Latitude	Longitude	Height
1	0.021	0.001	0.005
2	0.015	0.000	0.004
3	0.015	0.000	0.002
4	0.015	-0.001	0.000
5	0.013	-0.001	0.001
6	0.011	-0.001	0.001
Occupation (hours)	Average Absolute Errors (m)		
	Latitude	Longitude	Height
12	0.006	-0.002	0.002
18	0.004	-0.001	0.001

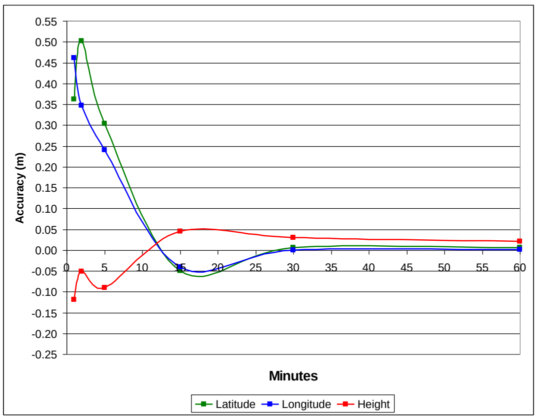

Fig. 5: Accuracy of GPS+GLONASS Short Occupation Times

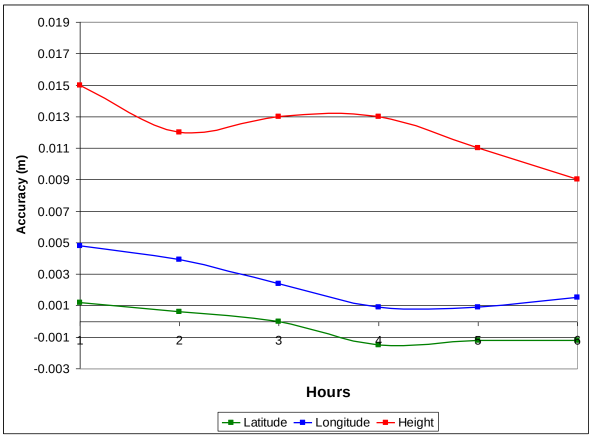

Fig. 6: Accuracy of GPS+GLONASS Medium Occupation Times

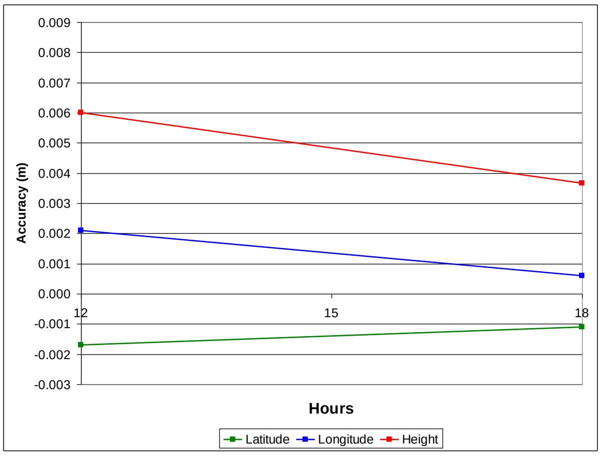

Fig. 7: Accuracy of GPS+GLONASS Long Occupation Times

The second analysis step concerns the estimation of projected coordinates' accuracy, particularly the UTM coordinates, for mapping applications at each scenario of GNSS occupation time. Table 5 and Figures 8, 9, and 10 present the accomplished findings. It can be seen that the sub-decimeter level of accuracy is achieved after a 15-minute occupation, while the sub-centimeter level is attained with 30-minutes or more of occupation time. Also, the millimeter level of accuracy is obtained with an occupation time of 3 hours and more.

Table 5: Accuracy of GPS+GLONASS Short, Medium, and Long Occupation Times for the UTM Coordinates

Occupation (minutes)	Average Absolute Errors (m)	
	North	East
1	0.478	0.321
2	0.358	0.445
5	0.248	0.266
15	-0.042	-0.044
30	0.000	0.004
60	0.000	0.004
Occupation (hours)	Average Absolute Errors (m)	
	North	East
1	0.000	0.004
2	0.001	0.003
3	0.000	0.001
4	-0.001	0.000
5	-0.001	0.000
6	-0.001	0.001

Occupation (hours)	Average Absolute Errors (m)	
	North	East
12	-0.001	0.001
18	0.000	0.000

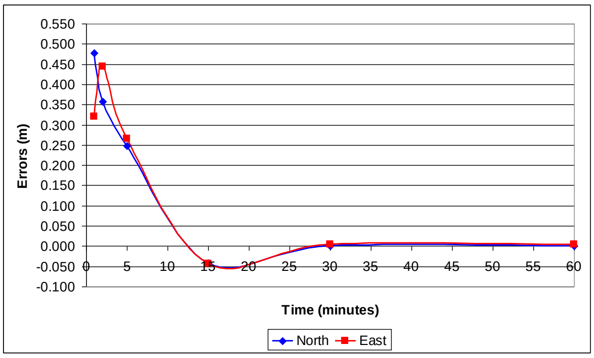

Fig. 8: Accuracy of GPS+GLONASS Short Occupation Times for the UTM Coordinates

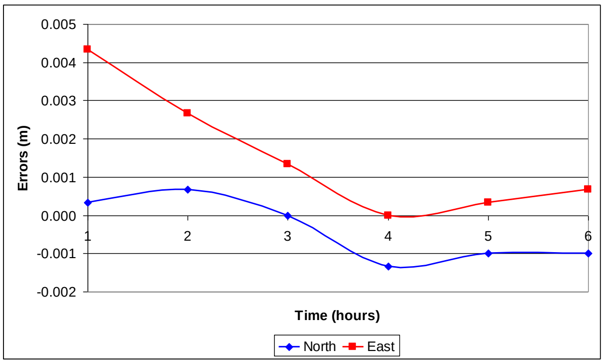

Fig. 9: Accuracy of GPS+GLONASS Medium Occupation Times for the UTM Coordinates

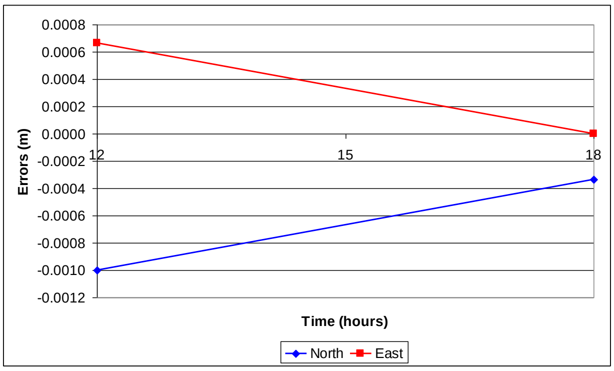

Fig. 10: Accuracy of GPS+GLONASS Long Occupation Times for the UTM Coordinates

The 3D estimates of both precision and accuracy have been computed and presented in Table 6. From this table, few final remarks could conclude the findings of the current research study. From a precision point of view, it is a must to have a GNSS occupation time of more than 15 minutes to achieve the sub-meter level. Thus, occupation times of few minutes should be avoided in GNSS surveying and mapping activities. For surveying applications require sub-decimeter precision, occupation of 15 minutes or more. If the required precision is less than five centimeters, the time of occupation should be at least one hour. A one-centimeter precision could be achieved when the occupation time is at least 12 hours. Similar results have been reported by Abou-Galala et al. [14].

Table 6: 3D Accuracy and Precision of GPS+GLONASS Short, Medium, and Long Occupation Times

Occupation (minutes)	3D Accuracy (m)	3D Precision (m)
1	0.599	±6.535
2	0.612	±4.364
5	0.397	±1.863
15	0.078	±0.670
30	0.030	±0.068
60	0.021	±0.040
Occupation (hours)	3D Accuracy (m)	3D Precision (m)
1	0.021	±0.040
2	0.016	±0.026
3	0.015	±0.021
4	0.015	±0.018
5	0.013	±0.016
6	0.011	±0.015
Occupation (hours)	3D Accuracy (m)	3D Precision (m)
12	0.007	±0.011
18	0.004	±0.009
24	NA	±0.008

According to the Egyptian surveying standards [15], it can be concluded that first-order geodetic networks require occupation of at least 4 hours. In addition second and third-order networks need static occupation of at least 1 and 0.5 hours respectively. Deformation and crustal monitoring geodetic applications require the highest precision and accuracy. Thus, a 24-hour occupation is appropriate for such high-precision activities. For civil engineering works, it is obvious that the precision of static GNSS occupation of less than half an hour could only be suitable for reconnaissance and small-scale mapping. Other engineering activities would require occupation ranging from 1 to 4 hours based on the required precision limits for each project.

V. CONCLUSIONS

The accuracy of the GNSS PPP technique depends on several factors, but the occupation time is the most critical one. Based on 24-hour GNSS datasets at Alexandria, Port Said, and Cairo, the accuracy and applicability of PPP (mainly GPS+GLONASS) in Egypt have been investigated. The analysis has been carried out for short, medium, and long occupation times.

Regarding the precision of 3D geodetic coordinates, attained results showed that the standard deviations of occupations of lengths 1-5 minutes are greater than one meter, while precision of few centimeters could be obtained from sessions of lengths equal to or greater than half an hour. For medium occupation, it has been noticed that the precision of occupation of 2 hours is less than a centimeter for both latitude and longitude, but the height's precision is still greater than 2 centimeters. Furthermore, it has been realized that longer occupation times significantly enhance the precision of the height more than the precision of both latitude and longitude. Based on available data, it might say that 18 hours of GNSS occupation is optimum to achieve few-millimeters precision for precise geodetic GNSS activities. From an accuracy perspective, it is noticed that at least 1-hour of occupation produce accuracy of 2-centimeters, while the level few-millimeters accuracy could be achieved in latitude and longitude when the occupation time is more than three hours.

It has been concluded that first-order geodetic network requires occupation of at least 4 hours, and second and third-order networks need static occupation of at least 1 and 0.5 hours respectively. Moreover, a 24-hour occupation would be appropriate for high-precision activities. For civil engineering works, it is clear that the precision of static GNSS occupation of less than half an hour could only be suitable for reconnaissance and small-scale mapping. Other engineering activities would require occupation ranging from 1 to 4 hours based on the required precision limits for each project. The concluded remarks of the current study should be considered in surveying, mapping, and civil engineering applications in Egypt.

REFERENCES

[1]. Abdallah, A. and Schwieger, V.: The effect of convergence time on the static- PPP solution, Presented at the 2nd International workshop on "Integration of Point- and Area-wise Geodetic Monitoring for Structures and Natural Objects", March 23-24, Stuttgart, Germany (2015).

[2]. Harima, K., Choy. S., Rizos, C. , and Satoshi, K.: Performance of real-time precise point positioning in New Zealand, Presented at the FIG Working Week 2016, May 2–6, New Zealand (2016).
[3]. El Manaily, E., Abd Rabbou, M., El-Shazly, A. and Baraka, M.: Evaluation of quad-constellation GNSS precise point positioning in Egypt, Artificial Satellites, Vol. 52, No. 1, pp. 9-18 (2017).
[4]. Bahadur, B. and Nohutcu, M.: Multi-GNSS PPP: An alternative positioning technique for establishing ground control points, International Journal of Environment and Geoinformatics, 7(1): 88-92. https://doi.org/10.30897/ijegeo.710304 (2020)
[5]. Vazquez-Ontiveros, J., Vazquez-Becerra, G., Quintana, J., Carrion, F., Guzman-Acevedo, M. and Gaxiola-Camacho, R. Implementation of PPP-GNSS measurement technology in the probabilistic SHM of bridge structures, Measurements, https://doi.org/10.1016/j.measurement.2020.108677 (2020)
[6]. Shinghal, G. and Bisnath, S.: Conditioning and PPP processing of smartphone GNSS measurements in realistic environments, Satellite Navigation, 2:10, https://doi.org/10.1186/s43020-021-00042-2 (2021)
[7]. Rabah, M. Zedan, Z. Ghanem, E., Awad, A. and Sherif, S.: Study the feasibility of using PPP for establishing CORS network, Arabian Journal of GeoSciences, 9: 613, DOI: 10.1007/s12517-016-2647-8 (2016).
[8]. Wang, L., Li, Z., Wang, N. and Wang, Z.: Real-time GNSS precise point positioning for low-cost smart devices, GPS Solutions, 25:69, DOI: 10.1007/s10291-021-01106-1 (2021).
[9]. Hofmann-Wellenhof, B., Lichtenegger, H. and Wasle, E.: GNSS: Global Navigation Satellite Systems. GPS, GLONASS, Galileo and more, Springer Wien, New York, USA (2008).
[10]. Choy, S. and Harima, K.: Satellite delivery of high-accuracy GNSS precise point positioning service: an overview for Australia, Journal of Spatial Science, DOI: 10.1080/14498596.2018.1427155 (2018).
[11]. CSR-PPP (Canadian Spatial Reference System Precise Point Positioning): https://webapp.geod.nrcan.gc.ca/geod/tools-outils/ppp.php, Accessed Jun 4 (.2021).
[12]. Trimble Navigation: Center Point RTX, https://positioningservices.trimble.com/services/rtx/centerpoint-rtx/, Accessed Jun 1 (. 2021).
[13]. Abou Galala, M., Rabah, M. and Zidan, Z.: Assessment of the accuracy and convergence period of precise point positioning, Mansoura Enginnerring Joyrnal, 41(2): C1-C5 (2016).
[14]. Abou-Galala, M., Rabah, M., Kaloop, M., and Zidan, Z.: Assessment of the accuracy and convergence period of precise point positioning, Alexandria Engineering Journal, No. 57, pp. 1721-1726 (2018).
[15]. ESA (Egyptian Surveying Authority): Technical specifications for surveying and mapping works, Part 1: Surveying specifications, A technical report, ESA, Giza, Egypt (2020).

Gomaa M. Dawod, et. al. "Accuracy and Applicability of GNSS PPP for GNSS Surveys: A Case Study in the Nile Delta, Egypt."*American Journal of Engineering Research (AJER),* vol. 11(05), 2022, pp. 10-18.

Available online www.jsaer.com

Journal of Scientific and Engineering Research, 2022, 9(4):7-16

Research Article

ISSN: 2394-2630
CODEN(USA): JSERBR

Recent GNSS-Based Estimates of Vertical Land Movements in the Nile Delta, Egypt Over 2012-2019

Hoda F. Mohamed, Gomaa M. Dawod*

Survey Research Institute, National Water Research Center, Giza, Egypt
* dawod_gomaa@yahoo.com, ORCID = 0000-0002-4426-8231

Abstract This paper aims to determine reliable and up-to-date estimates of the vertical land movements in the Nile delta region based on high-precision datasets of Global Navigation Satellite Systems (GNSS) observations covering the period 2012-2019. Repeated data, every 6 months, of 23 GNSS stations have been collected, processed, and analyzed using the Precise Point Positioning (PPP) GNSS technique. Geographic Information Systems (GIS) tools have been applied to model the 3D spatial variations of crustal deformation across the Nile delta. Based on the available data and the accomplished results, it is concluded that the vertical land movements within the study area range from subsidence equals -5.5 mm/year to uplift equals 4.2 mm/year, with an overall average of -0.08 mm/year. Additionally, it has been found that Port Said, Kafr El-Zaiat, and Tanta cities suffer from high land subsidence rates while Cairo, Belbis, Fakous and Burrllus cities are subjected to high trend of uplift. Regarding the Sea Level Rise (SLR) in the Nile delta, it is estimated that taking land subsidence into account, the absolute SRL at Alexandria and Port Said equal 6.0 mm/year and 7.6 mm/year respectively. Such findings should be highly considered in the development plans of those cities, particularly for huge infrastructures. Furthermore, the current research recommends the continuation of GNSS-based monitoring of such phenomena over a longer time.

Keywords GNSS, Sea Level Rise, Land Subsidence, PPP, GIS, Nile Delta

Introduction

Monitoring vertical land movements, subsidence or uplift, comprise an essential geodetic theme to explain the geodynamics of the planet Earth over a specific spatial extent. Land subsidence, among other environmental hazards, causes several physical and human dangerous impacts to the public worldwide, particularly in low-land areas and coastal regions. Basically, land subsidence could be identified as the down displacement of the land surface relative to a definite reference surface, such as Mean Sea Level (MSL) or an ellipsoid. This phenomenon could be attributed to both natural and human-induced reasons such as geology structures, soil characteristics, groundwater withdrawal and other factors [1]. In the last few decades, the geodetic community has paid attention to precisely monitoring such phenomena. Several techniques and datasets have been utilized in monitoring land subsidence, particularly the Global Navigation Satellite Systems (GNSS) [2], the Interferometric Synthetic Aperture Radar (InSAR) [3], satellite altimetry and tide gauges data [4], and levelling data [5]. A combination of several observing techniques would be more efficient in monitoring land subsidence. Many research studies have been conducted in several countries for the monitoring and risk assessment of land subsidence, e.g. in Indonesia [6], Turkey [7], and the Czech Republic [8].

The Nile delta, as other rivers' deltas, is typically subjected to land subsidence. Additionally, it is subjected to several other environmental and human challenges such as coastal erosion, land-use changes, water quality determination, sea level rise, soil degradation, groundwater pollution, and shoreline retreat [9]. Ground

subsidence and sea level rise are the most environmental hazards that affect the Nile delta region. Generally, the rate of land subsidence over the entire Nile delta region varies from 2 to 9 mm/year [10]. AbouAly et al [11] have utilized GNSS datasets over 2013-2015 over the Nile delta and Northern part of Egypt and found that land subsidence in the delta range between mm/year 2.5 and 10 mm/year. Rateb and Abotalib [12] have utilized Sentinel-1 radar satellite and GNSS data between 2015 and 2019 to investigate land subsidence in the Nile delta region. They reported subsidence rates of 12-20 mm/year in major cities, such as Zagazig and Tanta in the middle of the delta region, and subsidence rates of 3-8 mm/year along the coasts of the delta. Similarly, Saleh and Becker [13] have estimated land subsidence in major cities in the delta as 6.4, 4.0, 4.8, 10.0, 10.3, and 4.9 mm/year for Cairo, Tanta, Mahala, Mansoura, Damietta, and Port Said respectively. On the other hand, the effects of land subsidence include aquifer salinization, infrastructure damage, increased vulnerability to flooding and storm surges, and permanent inundation of low-lying land [14].

Traditionally, the GNSS consist of both the American Global Positioning System (GPS) and its Russian counterpart (GLONASS). Currently, satellites belonging to both the European Galileo system and the Chinese BeDiou system have been visible for tracking worldwide. Therefore, the expression "quad-GNSS" becomes noticeable in geodetic high-precision applications. The Precise Point Positioning (PPP) is the most accurate GNSS processing method nowadays. It provides the accuracy level needed for high-precision crustal deformation and land subsidence monitoring [15]. Due to its accuracy, Rabah et al. [16] have proposed to utilize the PPP method for datum maintenance and updating of the national geodetic networks of Egypt. Recently, the PPP technique has been applied to estimate the tectonic coordinates changes in Egypt [17].

This paper investigates the utilization of GNSS PPP observations in monitoring the land subsidence in the Nile delta region. It aims to determine reliable and up-to-date estimates of land subsidence in the Nile delta region based on high-precision datasets of GNSS observations covering the period 2012-2019.

Study Area and Available Data

The Nile delta, as the study area, extends from longitude 29.7° E to longitude 32.6° E, and from latitude 29.8° N to latitude 31.6° N (Fig. 1). That region extends more than 300 kilometers along the Mediterranean costs from Port Said on the east to Alexandria on the west, and extends almost 200 kilometers perpendicular south to the coastline to Cairo. Thus, its overall area equals approximately 35,000 square kilometers. With more than fifty million people, that delta could be considered as one of the most densely populated areas worldwide. The topography of the study area (Figure 2) ranges from elevation -29 meters to 870 meters, with an average of 31.9 meters. It can be seen from that figure that the dominant elevation is less than 10 meters in the northern and middle parts of the delta. Moreover, it can be realized that the northern region of the delta area has an elevation of less than almost 5 meters. That reality necessitates performing vulnerability analysis studies regarding the sea rise global phenomena and its hazardous impacts on the Nile delta region. However, researchers emphasize the fact that land subsidence in the Nile Delta might be more environmentally hazardous than the sea level rise phenomena [18].

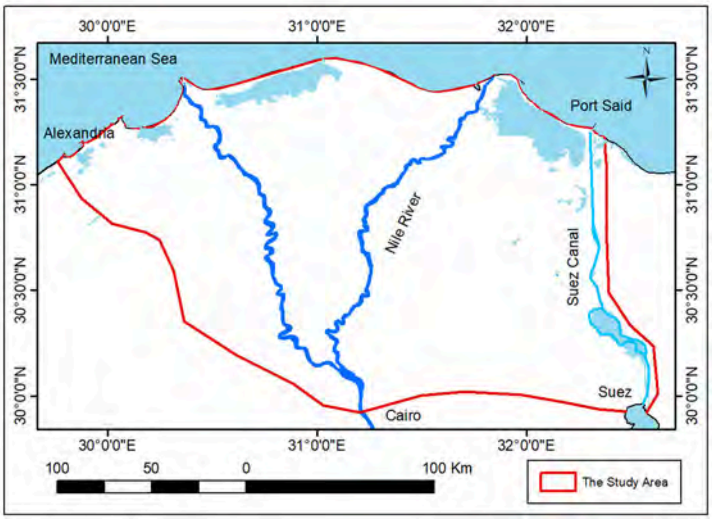

Figure 1: The Study Area

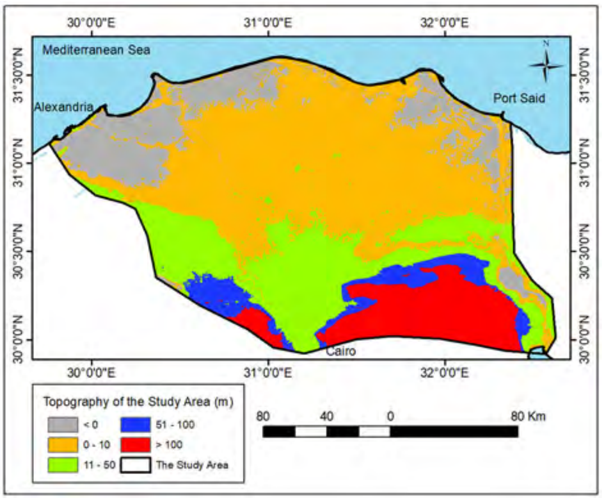

Figure 2: Topography of the Study Area

The utilized dataset (Fig. 3) compresses GNSS raw data of 23 stations of the Virtual Reference Stations (VRS) belonging to the Egyptian Survey Authority (ESA). Forty Continuously Operating Reference Systems (CORS) have been established by ESA in 2010 covering the Nile delta and valley (Fig. 4). Each station is equipped with a dual-frequency GNSS receiver fixed on the top of an ESA building, and every station sends its raw data in real-time to the central ESA office in Cairo. The collected dataset of each utilized session consists of a 24-hour continuous GNSS data in the RINEX (Receiver-INdependent EXchange) format covering the period 2012-2019 with two sessions per year (Table 1). The Trimble Business Center (TBC) v. 5.1 package has been utilized for PPP GNSS data processing [19].

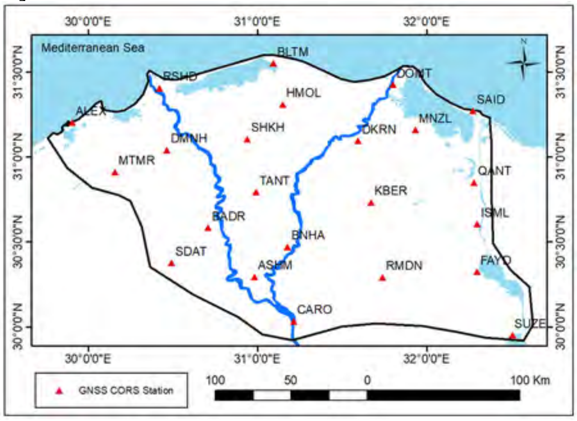

Figure 3: The Utilized GNSS VRS Stations

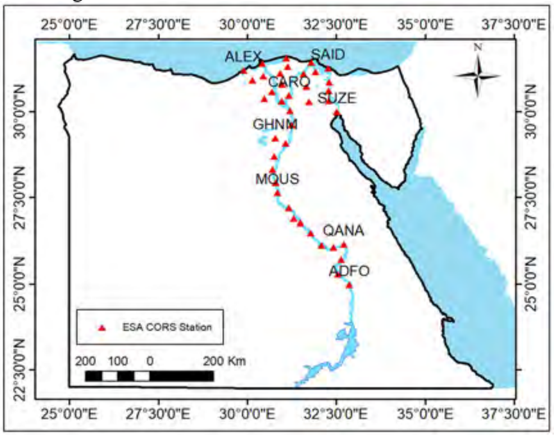

Figure 4: The GNSS VRS Stations in Egypt

Table 1: The Utilized GNSS Raw Data

St. No.	1	2	3	4	5	6	7	8	9	10	11	12	13	14	15	16	17	18	19	20	21	22	23
Year/St.	ALEX	ASHM	BADR	BLTM	BNHA	CARO	DKRN	DMNH	DOMT	FAYD	HMOL	ISML	KBER	MNZL	MTMR	QANT	RMDN	RSHD	SAID	SDAT	SHKH	SUEZ	TANT
2/2012	■	■	■	■	■	■	■	■	■	■	■	■	■	■	■	■	■	■	■	■	■	■	■
1/2013															■								■
7/2013				■									■										■
1/2014				■											■								
7/2014						■							■						■				
1/2015						■							■						■				
7/2015		■	■		■	■			■								■	■					
1/2016	■	■	■			■			■				■			■	■						
7/2016		■	■			■				■			■				■			■			
1/2017	■	■	■		■	■	■	■	■	■		■	■	■	■	■	■	■	■		■		■
7/2017		■	■	■	■	■		■	■		■	■	■	■	■		■		■			■	■
1/2018	■		■	■		■		■	■			■	■	■	■	■	■	■	■				■
7/2018			■	■		■		■				■		■	■		■	■	■	■		■	■
1/2019	■	■	■	■	■	■		■	■		■	■		■	■	■	■		■	■	■	■	■

Methodology

The fundamental idea of the PPP GNSS processing technique comprises the estimation of precise satellites orbits and satellite clock errors based on observations from a high quality global fiducial network, and then the utilization of such information to solve the station parameters of any other sites. The PPP position determination is based on the processing of the following ionosphere-free combination of the un-differenced code and phase observations [20]:

$$P_{Li} = \rho + d_{orb} + c(dT - dt) + d_{ion(L_i)} + d_{trop} + d^{r}_{hd(P_{Li})} - d^{s}_{hd(P_{Li})} + d_{multi(P_{Li})} + d_{noise(P_{Li})} \quad (1)$$

$$\phi_{Li} = \rho + d_{orb} + c(dT - dt) + d_{ion(L_i)} + d_{trop} - \lambda_{Li} N_{Li} + d^{r}_{hd(P_{Li})} - d^{s}_{hd(P_{Li})} + d_{multi(P_{Li})} + d_{noise(P_{Li})} \quad (2)$$

where,

P_{Li} and φ_{Li} represent the pseudorange and carrier phase measurements (in meters) on the frequency L_i respectively,

ρ refers to the geometric distance between the satellite and the receiver,

d_{orb} is satellite orbit error (in meters),

c equals the speed of light in vacuum (in meter/second),

dT and dt denote the clock error of the satellite and the receiver respectively (in seconds),

$d_{ion(Li)}$ is the first-order ionospheric effect on the frequency Li (in meters),

d_{trop} is the troposheric delay (in meters),

$d^{s}_{hd(PLI)}$ and $d^{r}_{hd(PLI)}$ are satellite and receiver hardware delays (in meters) for the Li pseudorange respectively,

$d^{s}_{hd(\varphi LI)}$ and $d^{r}_{hd(\varphi LI)}$ are satellite and receiver hardware delays (in meters) for the Li carrier-phase respectively,

$d_{multi(PLI)}$ and $d_{multi(\varphi LI)}$ represent the multipath errors of the pseudorange and carrier-phase respectively on the frequency L_i (in meters),

$d_{noise(PLI)}$ and $d_{noise(\varphi LI)}$ denote the noise errors of the pseudorange and carrier-phase respectively on the frequency L_i (in meters),

N_{LI} is the ambiguity term on the frequency L_i in cycles, and

λ_{LI} is the wavelength of the frequency L_i (in meters).
The pseudorange and carrier-phase ionospheric-free linear combinations are formed as:

$$P_{if} = \frac{f_1^2 P_1 - f_2^2 P_2}{f_1^2 - f_2^2} \quad (3)$$
$$= \rho + d_{orb} + c(dT - dt) + d^r_{hd(P_{Li})} - d^s_{hd(P_{Li})} + d_{multi(P_{Li})} + d_{noise(P_{Li})}$$

$$\phi_{if} = \frac{f_1^2 \phi_1 - f_2^2 \phi_2}{f_1^2 - f_2^2} \quad (4)$$
$$= \rho + d_{orb} + c(dT - dt) - \lambda_{if} N_{if} + d^r_{hd(\phi_{Li})} - d^s_{hd(\phi_{Li})} + d_{multi(\phi_{Li})} + d_{noise(\phi_{Li})}$$

where,
N_{if} denotes the ionospheric-free ambiguity term (in cycles), and
λ_{if} represents the ionospheric-free wavelength (in meter).
The above formulas show that the unknown parameters to be estimated in PPP include position coordinates, phase ambiguity terms, receiver clock offset, and the troposheric effect. Precise satellite orbits and clock products with the centimeter-level accuracy needed for PPP are now widely available from several global scientific societies. One of such respective organizations is the International GNSS Service (IGS).
It is a matter of reality that the PPP results are, in general, superior to the traditional GNSS data processing. For example, Mohamed [21] has concluded that the accuracy improvements due to using dual-GNSS datasets, i.e. GPS+GLONASS, equal 32%, 35%, and 24% in the X, Y, Z coordinates respectively in Egypt. Generally, applying PPP with observations from quad-GNSS constellation enhances the positional accuracy significantly for multi-frequency or even single-frequency measurements [22].
The processing steps start with importing raw data for the first station, downloading the corresponding precise and clock files from the IGS website, and computing the final coordinates for that station in the first available time epoch. Next, another epoch is similarly processed for that specific station. Having processed all data for this station, their ellipsoidal heights are compared to estimate the vertical movement trend over time. Next, statistical analysis is performed to judge the quality of the accomplished regression results. Iteratively, another station is processed in the same manner until all stations are done. Finally, the Arc GIS software is utilized to develop a 3D surface for the vertical land movements across the study area. Such a processing strategy is depicted in Fig. 5.

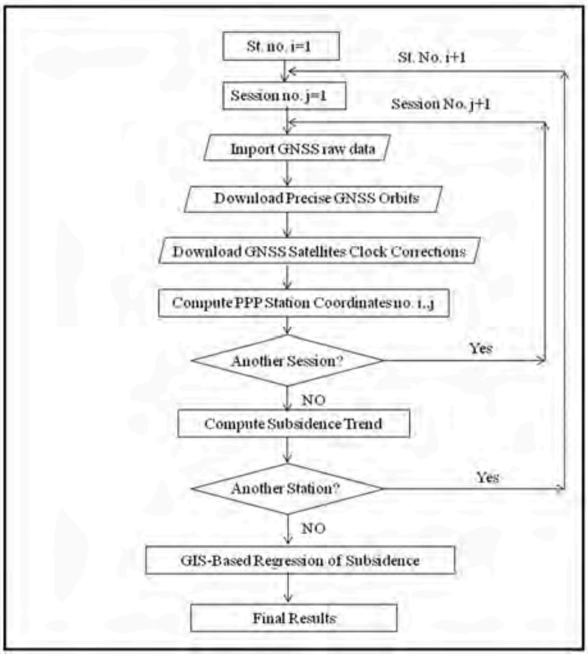

Figure 5: Data Processing Strategy

Moreover, to judge the goodness of the attained linear regression height model at each GNSS station, the coefficient of determination statistical measure, R^2, is applied. It shows the proportion of the variation in the dependant variable that is estimated from the independent variable and it ranges from zero to +1. The higher this value the better the regression model. The coefficient of determination could be estimated as:

$$R^2 = \frac{\sum(\hat{y} - \bar{y})^2}{\sum(y - \bar{y})^2} \tag{5}$$

where,

$\hat{y}$ and $\bar{y}$ represent the estimated and average values of the dependant variable respectively.

Processing and Results

Raw GNSS datasets for all available stations have been processed utilizing the PPP approach for each session with respect to the International Terrestrial Reference Frame 2014 (ITRF2014) epoch 2019. Over the utilized GNSS stations, the accomplished findings show that the standard deviation of the X coordinates ranges from 0.011 m to 0.014 m, while it varies from 0.014 m to 0.018 m for the Y coordinates. Similarly, it has been noticed that the standard deviation of the Z coordinates ranges from 0.006 m to 0.009 m. For the geodetic heights, the standard deviation varies between 0.009 m and 0.0011 m. Consequently, it can be concluded that the average precision of the obtained coordinates is at the centimeter level

Furthermore, the variations of height at each station, over the period 2012-2019, have been investigated and a linear regression model has been performed. The coefficient of determination, R^2, in Equation 5 has been computed for the accomplished linear regression model at each station. Table 2 presents the attained findings and reveals important remarks. First, there are 7 stations where R^2 is less than 0.20 which concludes that the linear regression model does not reflect the height variations at those stations. Second, there are four stations with only available 3 observations (GNSS raw data) which shows that the degree of freedom, in the regression modelling, just equals one. Thus, the reliability of the attained regression equations, at these stations, could not be considered trustable. Accordingly, such 11 stations have been neglected and the results of the remaining 12 stations are further investigated (Fig. 6). Table 3 tabulated the reliable results of the regression analysis (R^2 is greater than 0.40) and the attained vertical movements trends in the study area. Thus, it is concluded that the vertical land movements at the twelve reliable GNSS stations within the study area range from subsidence equals -5.5 mm/year to uplift equals 4.2 mm/year, with an overall average of -0.08 mm/year.

Table 2: Statistics of the Attained Regression Models

No	Station	R^2	No. of Observations	No	Station	R^2	No. of Observations
1	ALEX	0.46	9	13	KBER	0.60	6
2	ASHM	0.85	6	14	MNZL	0.51	4
3	BADR	0.004	10	15	MTMR	0.08	5
4	BLTM	0.85	6	16	QANT	0.39	4
5	BNHA	0.01	4	17	RMDN	0.87	5
6	CARO	0.14	7	18	RSHD	0.71	3
7	DKRN	0.88	4	19	SAID	0.55	8
8	DMNH	0.01	7	20	SDAT	0.44	5
9	DOMT	0.88	5	21	SHKH	0.07	3
10	FAYD	0.87	3	22	SUEZ	0.08	4
11	HMOL	0.69	3	23	TANT	0.50	5
12	ISML	0.53	7				

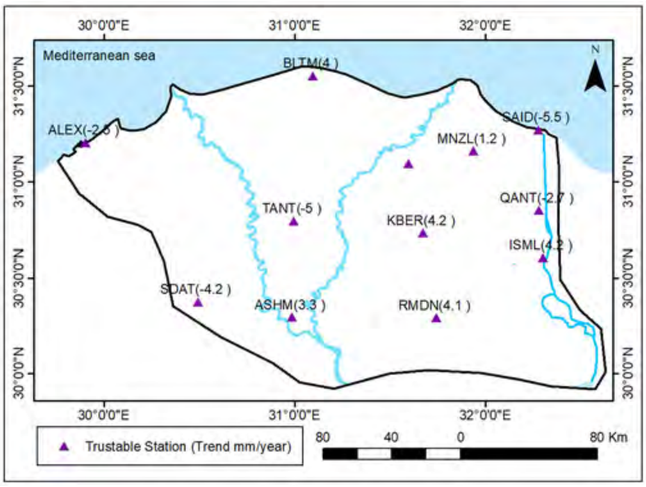

Figure 6: Trustable GNSS Stations and Trends

Table 3: Results of the Attained Vertical Land Movements

No	Station	Regression	Vertical Land Movement Rate (mm/year)
1	ALEX	H = -0.0025 year + 71.935	-2.5
2	ASHM	H = 0.0033 year + 33.144	+3.3
3	BLTM	H = 0.004 year + 22.283	+4.0
4	DKRN	H = -0.0021 year + 42.467	-2.1
5	ISML	H = 0.0042 year + 34.808	+4.2
6	KBER	H = -0.0012 year + 35.579	-1.2
7	MNZL	H = 0.0012 year + 34.593	+1.2
8	QANT	H = -0.0027 year + 39.622	-2.7
9	RMDN	H = 0.0041 year + 141.28	+4.1
10	SAID	H = -0.0055 year + 40.979	-5.7
11	SDAT	H = -0.0042 year + 80.095	-4.2
12	TANT	H = -0.005 year + 51.013	-5.0

Next, the Arc GIS 10 software has been utilized to construct a spatial 3D model of vertical land movements over the Nile delta region (Figure 7). From such a model, it can be concluded that the land motion range from -5.49 mm/year to +4.66 mm/.year, with an average of +0.32 mm/year. That spatial model could be applied to interpolate the vertical land movement annual rate at any location within the study area. Hence, it is quite important in engineering projects in general and particularly for water resources management applications. The attained findings are generally compatible with those of other studies such as Rateb et al. [12] (2020), Saleh et al. [13] (2019), and AbouAly et al. [11] (2021a).

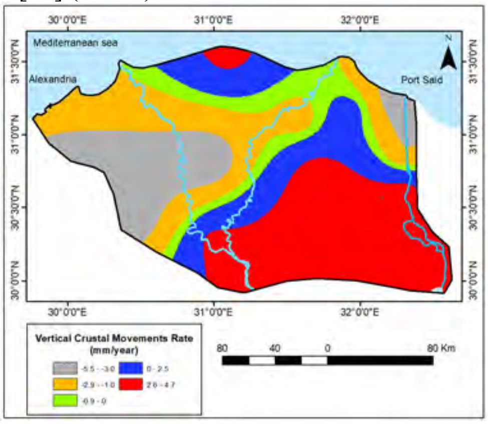

Figure 7: Vertical Land Movements in the Nile Delta over 2012-2019

Next, the main cities in the Nile delta region have been plotted on the attained 3D surface of vertical land movements (Fig. 8). It can be noticed that Port Said, Kafr El-Zaiat, and Tanta cities suffer from high land

subsidence rates ranging between 4.0 and 5.5 mm/year. On the other hand, Cairo, Belbis, Fakous and Burrllus cities subjected to a high trend of uplift within 3.1-4.7 mm/year. Such findings should be highly considered in the development plans of those cities, particularly for huge infrastructures.

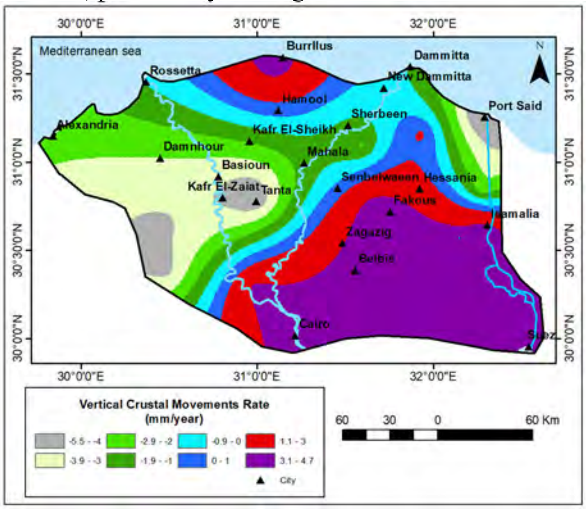

Figure 8: Vertical Land Movements in the Nile Delta at Main Cities

Finally, the effect of vertical land movements on Sea Level Rise (SLR) has been investigated too. It is worth mentioning that SLR observed at Tide Gauge (TG) is relative and the absolute SLR has to account for land subsidence at TG locations. Recent estimates of relative SLR at the Nile delta from two TG stations reveal that its annual rates equal 3.5 and 1.9 mm/year at Alexandria and Port Said respectively [23]. Regarding the accomplished results of vertical land movements in the Nile delta, it can be estimated that the absolute SRL rate at Alexandria and Port Said equal 6.0 and 7.6 mm/year respectively. Such imperative findings should be considered in any existing and upcoming development plans of the Nile Delta region.

Conclusions

Vertical land movements have major risky impacts from economic, environmental, and social perspectives. GNSS technologies have been commonly applied as a fundamental technical tool for monitoring horizontal and vertical land movements. In Egypt, several studies have been carried out for observing land subsidence as a hazardous phenomenon, particularly in the Nile delta region. The current research utilizes 24-hour GNSS datasets for 23 stations to observe vertical land motion over the period 2012-2019.

The variations of height, at each station, have been investigated and a linear regression model has been performed. Based on the available datasets, the coefficient of determination of the regression is found to be less than 0.20 over 7 stations which conclude that the linear regression model does not reflect the height variations at those stations. In addition, it has been realized that four stations have only 3 available observations (GNSS raw data) which means that the degree of freedom, in the regression modelling, just equals one. Accordingly, the reliability of the attained regression equations, at these stations, could not be considered confidential and those 11 stations have been neglected. Thus, the accomplished findings showed that the vertical land movements within the study area range from subsidence equals -5.5 mm/year to uplift equals 4.2 mm/year, with an overall average of -0.08 mm/year. Such land subsidence rates are very close to the results of other studies in the Nile delta region utilizing other techniques and datasets.

Recommendations

Few recommendations could be drawn, based on the achieved outcomes, for future works such as:

1. It is recommended that the accomplished results should be taken into account by decision makers in any existing and upcoming development plans of the Nile Delta resources management, particularly for water resources huge structures design such as barrages, weirs, and even canals or drains.
2. It is a matter of reality that vertical land motion is quite a vital phenomenon to be continuously monitored and analyzed particularly in low-land river deltas.
3. The current research recommends the continuation of GNSS-based monitoring of such phenomena over a longer time.

4. Furthermore, it is highly recommended to carry out comprehensive investigations for the natural, human, and geological factors affecting the land subsidence in the Nile delta area.

References

[1]. Othman, A. and Aboutalib, A. (2019). Land subsidence triggered by groundwater withdraw under hyper-arid conditions: case study from central Saudi Arabia, *Environmental Earth Sciences*, 78:243, https://doi.org/10.10007/s12665-019-8254-8.

[2]. Mohamed, H. (2015a). Assessment of factors influencing static GNSS precise point positioning: A case study in Egypt, *International Journal of Applied Sciences and Engineering Research*, 4(5):692-701.

[3]. Bozzano, F., Esposito, C., Franchi, S., Mazzanti, P., Perissin, D., Rocca, A., and Romano, E., (2015). Understanding the subsidence process of a quaternary plain by combining geological and hydrogeological modelling with satellite InSAR data: The Acque Albule Plain case study, *Remote Sensing of Environment*, (168):219–238.

[4]. Letetrel, C. Karpytchev, M., Bouin, M-N., Marcos, M., SantamarÍa-Gómez, A., and Wöppelmann, G. (2015). Estimation of vertical land movement rates along the coasts of the Gulf of Mexico over the past decades, *Continental Shelf Research*, (111):42–51.

[5]. Psimoulis, P., Ghilardi, M., Fouache, E., and Stiros, S. (2007). Subsidence and evolution of the Thessaloniki plain, Greece, based on historical leveling and GPS data, *Engineering Geology*, (90):55–70.

[6]. Yuwono, B., Awaluddin, M., Kun, F. and Lutfi, E. (2017). Evaluation of base station CORS UDIP and CSEM for monitoring ground deformation Sayung Demak Indonesia, The 5th Geoinformation Science Symposium 2017, https://doi.org/10.1088/1755-1315/98/1/012047.

[7]. Caló, F., Notti, D., Galve, J., Abdikan, S., Görüm, T., Pepe, A, and Sanli, F. (2017). DInSAR-Based detection of land subsidence and correlation with groundwater depletion in Konya plain, Turkey, *Journal of Remote Sensing*, (9), https://doi.org/10.3390/rs9010083.

[8]. Lamich, D., Marschalko, M., Yilmaz, I., Bednarova, P., Niemiec, D., Kubecka, K., and Mikulenka, V. (2015). Subsidence measurements in roads and implementation in land use plan optimization in areas affected by deep coal mining, *Journal of Environ Earth Science*, 75(69), https://doi.otg/10.1007/s12665-015-4933-2.

[9]. Frihy, O. (2017). Evaluation of future land-use planning initiatives to shoreline stability of Egypt's northern Nile delta, *Arabian Journal Geosciences*, https://doi.otg/10.1007/s12517-017-2893-4.

[10]. Stanley, J. and Clemente, P. (2017). Increased land subsidence and sea-level rise are submerging Egypt's Nile delta coastal margin, *The Geographical Society of America: GSA Today*, 27(5): 4-11.

[11]. AbouAly, N., Hussien, M., Rabah. M., Zidan, Z., and Saleh, M. (2021a). Land deformation monitoring by GNSS in the Nile delta and the measurements analysis, *Arabian Journal of Geosciences*, 14:150, https://doi.otg/10.1007/s12517-021-06497-6.

[12]. Rateb, A. and Abotalib, A. (2020). Inferencing the land subsidence in the Nile delta using Sentinel-A satellites and GPS between 2015 and 2019, *Science of the Total Environment*, https://doi.otg/10.1016/j.scitotenv.2020.138868.

[13]. Saleh, M. and Becker, M. (2019). New estimation of Nile delta subsidence rates from InSAR and GPS analysis, *Environmental Earth Science*, 78:6, https://doi.otg/10.1007/s12665-018-800-6.

[14]. Higgins, S. (2015). Review: Advances in delta-subsidence research using satellite methods, *Hydrogeological Journal*, https://doi.org/10.1007/s10040-015-1330-6.

[15]. AbouAly, N., Elhussien, M., Rabah. M., and Zidan, Z. (2021b). Assessment of NRCAN PPP on;ine service in determination of crustal velocity: case study northern Egypt GNSS network, *Arabian Journal of Geosciences*, 14:188, https://doi.otg/10.1007/s12517-021-06530-8.

[16]. Rabah, M., Elmewafey, M. and Farahan, M. (2016). Datum maintenance of the main Egyptian geodetic control networks by utilizing Precise Point Positioning (PPP) technique, *NRIAG Journal of Astronomy and Geophysics*, (5):96-105.

[17]. Abdallah, A., Agag, T. and Dawod, G. (2021). ITRF-based tectonic coordinates changes using GNSS-CORS network: A case study of Egypt, *Surveying and Land Information Science*, 80(2):69-78.

[18]. Zaid, S., Mamoun, M., and Al-Mobark, N. (2014). Vulnerability assessment of the impact of sea level rise and land subsidence on north Nile Delta region, *World Applied Sciences Journal*, 32(3):325-342.

[19]. SRI (Survey Research Institute) (2022). *Assessing and modelling of land subsidence in the Nile delta area and its effect on water structures, canals and drains*, Internal Technical Report, Giza, Egypt.

[20]. Hofmann-Wellenhof, B., Lichtenegger, H. and Wasle, E. (2007). *GNSS: Global Navigation Satellite Systems GPS, GLONASS, Galileo, and more*, Springer, New York, USA.

[21]. Mohamed, H., Shaheen, B., Hosney, M., and Dawod, G. (2015b). High-precision GPS monitoring of the land subsidence in the Nile Delta: Status and preliminary results, *Regional Conference on Surveying and Development*, Sharm El-Sheikh, Egypt, Oct. 3-6.

[22]. Abd Rabbou, M., El-Shazly, A., and Ahmed, K. (2017). Comparative analysis of multi-constellation GNSS single-frequency precise point positioning, *Survey Review*, https://doi.otg/10.1080/00396265.2017.1296628.

[23]. Dawod, G., Ebaid, H., Haggag, G. and Al-Krargy, E. (2021). An integrated geomatics approach for projecting sea level variations and risks: A case study in the Nile Delta, Egypt, *Journal of Architecture and Civil Engineering*, 6(8):24-38.

JES, Vol. 50, No. 4, July 2022 DOI: 10.21608/JESAUN.2022.114295.1105 Part A: Civil Engineering

Journal of Engineering Sciences
Faculty of Engineering
Assiut University
مجلة العلوم الهندسية
كلية الهندسة
جامعة أسيوط
journal homepage: http://jesaun.journals.ekb.eg

Mean Sea Level and Tides Variations at Alexandria, Egypt over 1906-2020

Received 02 January 2022; Revised 11 May 2022; Accepted 11 May 2022

Gomaa M. Dawod[1]
Hoda F. Mohamed[2]
Ghada G. Haggag[3]

Keywords
Tides - Tide Gauge - Mean Sea Level - Sea Level Rise - Vertical Datum – Egypt.

Abstract

Sea Level Rise (SLR) is a vital outcome of the environmental global warming phenomenon. This paper aims to investigate the basic properties of tides in Alexandria, Egypt and to analyze SLR in Egypt over a long period to examine the differences in Egypt's vertical geodetic datum. The annual relative SLR at Alexandria between 1906 and 2020 was found to be 2.6 mm/year. Moreover, the relative SLR has been 3.1 mm/y for the last two decades, 2001-2020. It could be considered the most appropriate value to be taken into consideration in Egypt's coastal management activities. Carrying out additional investigations is suggested to investigate possible major variations of MSL in Egypt at other TG sites over both the Mediterranean and Red seas. Based on available data and accomplished results, it is recommended to regard Egypt's MSL datum as a semi-kinematic rather than a fixed one.

1. Introduction

Tides, as a natural phenomenon, are the rise and fall of the ocean and sea surface height caused mainly by the gravity of both the Sun and Moon. The tidal phenomenon differs significantly over space and time. Thus, tidal analysis is one of the main aspects of navigation, harbor activities, and coastal management. A Tide Gauge (TG) station has been traditionally set up to measure and record the tidal variations in a country. Tide patterns have been recently investigated in several TG locations in Egypt such as Mersa Matruh [1] and Alexandria eastern harbor [2,3]. In addition, Ibrahim and El-Gindy [4] have analyzed the tides and storm surges in the eastern Mediterranean Sea from 1923 to 2019. The average of sea heights over a long time series at a TG is conventionally used to define Mean Sea Level (MSL) as a national vertical geodetic datum in a country. Based on such a definition of a specific MSL, the vertical geodetic network is established through many Benches Mark (BM) stations over a spatial region. In Egypt, the first historical TG has been established in Alexandria harbor more than a century ago. The mean value of all observations over 1898-1906 was taken as the MSL datum of Egypt. A central question has been raised in the last few

1 dawod_gomaa@yahoo.com, Professor, Survey Research Institute, National Water Research Center, Egypt
2 dr.ghadahaggag@gmail.com, Researcher, Survey Research Institute, National Water Research Center, Egypt
3 hoda.faisal@yahoo.com, Researcher, Survey Research Institute, National Water Research Center, Egypt

https://doi.org/10.21608/JESAUN.2022.114295.1105
This is an open access article under the CC BY-NC-ND license (http://creativecommons.org/licenses/by-nc-nd/4.0/).

decades about the stability of a specific MSL datum over time and its need for continuous updating [5,6].

Sea Level Rise (SLR) is essentially attributed to global warming and climate change factors including ocean thermal expansion, polar ice caps melt and change in terrestrial storage [7]. The Intergovernmental Panel on Climate Change (IPCC) stated that SLR since the mid-19th century has been larger than the mean rate during the previous two millennia [8]. Global SLR will be raised between 0.43 m and 0.84 m by 2100 (ibid). The observed global mean sea rise, from tide gauge records and satellite altimetry data, has been reported as 1.5, 2.0 and 3.2 mm/year for the period 1901-1990, 1971-2010, and 1993-2010 respectively [9]. SLR could be estimated from a variety of techniques and datasets. Relative SLR is primarily measured at TG sites, as well as from satellite altimetry data [10,11]. In another scene, absolute RLR accounts for both relative SLR and vertical movements at the TG sites [12,6]. Dangerous impacts of SLR include, for example, shoreline retreat [13], coastal flooding and inundation [14], coastal erosion [15], and a decrease in water quality in coastal regions [16].

SLR analysis, prediction, and risk assessment have been extensively investigated in Egypt in the last couple of decades. For example, Dawod et al. [17] have estimated both relative and absolute sea level rise in the Nile Delta region using heterogeneous spatial datasets. Their results indicated that absolute sea level rise, over Delta, differed between 5.0 mm/year at Alexandria to 6.9 mm/year at Port Said. Utilizing satellite altimetry data from 1993 to 2013, Shaltout et al. [18] estimated the relative SLR in the Egyptian Mediterranean coast to equal 3.1 mm/year. Additionally, El-Geziry and Said [19] have investigated the sea level pattern and variations in El-Burulls new harbor in the Nile Delta coastal region. Land subsidence and sea level rise across the Nile Delta region have been investigated [20]. That study found that absolute SLR across the Nile Delta varies between 6.7 and 11.4 mm/year. On the other hand, several research studies have been carried out to predict the potential impacts of sea level rise particularly on the Nile Delta region [21]. Additionally, here her [22] developed a vulnerability index to sea level rise for the Egyptian costs. He showed that more than one-third of the 1000-km long coasts are severely vulnerable to SLR. The current study aims to fulfill four objectives. First, to investigate the basic properties of tides at Alexandria in 2020 based on recent 30-minutes tide records. Second, to unify TG datasets come from different sources and construct an integrated dataset at Alexandria, Egypt extends over almost a century. Third, to apply several regression methods and statistical indicators to mathematically define the SLR trend over Egypt. Fourth and finally, to investigate SLR in Egypt over the entire period and on several twenty-year phases to describe the variations of Egypt's MSL vertical datum.

2. Tide and Mean Sea Level

2.1. Title

Tides are the response of the ocean and seas to the gravitational attraction of the Earth, Moon and Sun. That attraction normally produces a semi-diurnal pattern (two cycles per day) as the main component of tides. However, diurnal, and mixed regimes of tides exist in some parts of the world. There are several types of devices utilized to measure and record the variations of sea heights at a specific site or a Tide Gauge (TG). Mainly such instruments (Fig.1) could be divided into floating, pressure, acoustic, and microwave or radar devices [23]. In the float gauge, a pen and chart are used to record graphically the variations of sea height over mostly a day. The pressure gauges constitute instruments that measure subsurface pressure instead of sea level directly. Knowledge of seawater density and gravitational acceleration is required to make the conversion from pressure to sea level. Acoustic tide gauges depend on measuring the travel time of acoustic pulses reflected vertically from the sea surface and then converting it to sea height. Radar or microwave instruments use the

same concept of acoustic type but use a microwave instead of acoustic waves. Each type of tide gauge has its own merits regarding the accuracy, accessibility, field requirements, and costs (ibid).

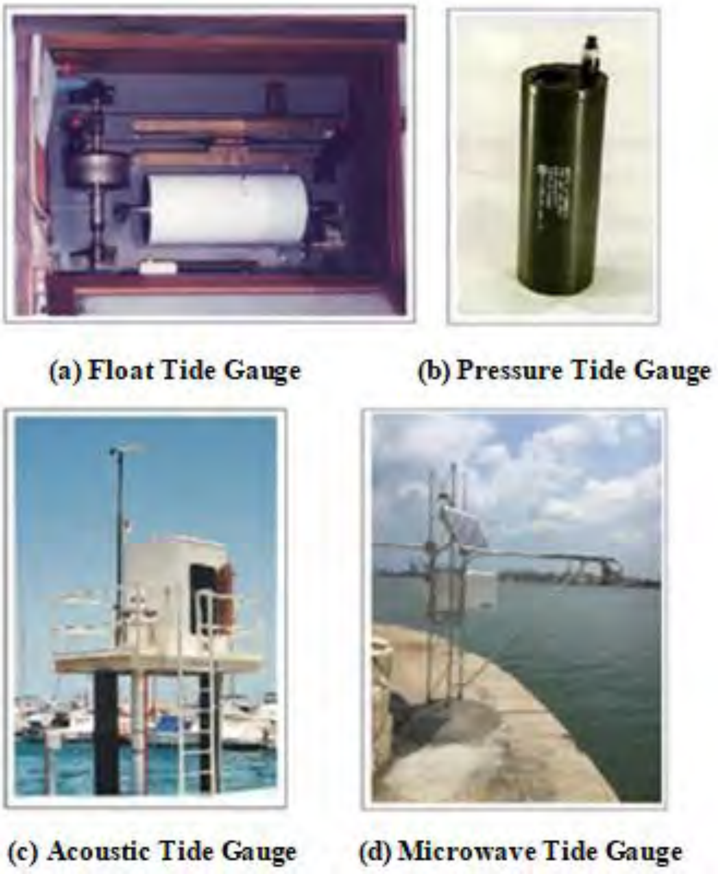

Fig. 1: Examples of the Different Types of Tide Gauges

2-2. Mean Sea Level

Sea level measurements from a TG are usually averaged over a year to estimate its mean annual values. Sea level Rise (SLR) could be investigated by collecting a time-series dataset of such observations at the TG location. Such a series is used to fit the dependent variable (Y), the Mean Sea Level (MSL), as predicted by the independent variable (X) or annual mean sea levels. There is a wide range of regression mathematical formulas applied in such a task to estimate the unknown parameters: a, b, c, and d shown in the following set of equations. A coefficient of determinations, R2, is then computed to represent the goodness of the regression process. Recently, more-complicated models, such as machine learning and neural network, have been utilized in SLR research [24]. The current study, herein, presents a few basic regression models in a general way and the interested readers could refer to any mathematical textbook for more details [25].

(a) Linear regression:

$$Y = aX + b \tag{1}$$

(b) Quadratic polynomial regression:

$$Y = aX^2 + bX + c \tag{2}$$

(c) Cubic polynomial regression:

$$Y = aX^3 + bX^2 + cX + d \tag{3}$$

(d) Logarithmic regression:

$$Y = a + b\ln(X) \tag{4}$$

(e) Hyperbolic regression:

$$Y = a + \frac{b}{X} \tag{5}$$

Additionally, the coefficient of determination, R2, is estimated as:

$$R^2 = 1 - \frac{\sum_i (Y_i - Y_{comp})^2}{\sum_i (Y_i - Y_{mean})^2} \tag{6}$$

where, Y_{comp} is the computed or fitted value of the ith observation, and Y_{mean} is the average of observations.

3. Study Area and Datasets

The city of Alexandria, founded in 331 BC by Alexander the Great, is located on the Mediterranean Sea at longitude 29.87o E and latitude 31.17o N approximately. With a population of more than five million, it is the third-largest city in Egypt and the largest city in the Mediterranean. The first tide gauge, called Port TG herein, has been established in the western harbor of Alexandria (Fig. 2). The device used in that TG was a floating type and the daily high and low water levels were recorded. The mean value of all observations over 1898-1906 was taken as the MSL datum of Egypt. That datum has been defined as 33.8 cm above the zero of the fixed tide staff. It is worth mentioning that the entire precise levelling networks of Egypt have been established based on that MSL datum [6].

In the early 1990s, the Egyptian Navy Hydrographic Department (ENHD) of the Egyptian Naval Force constructed a new tide gauge, Navy TG herein, approximately 800 m west of the historical Port TG (Fig. 2). Also, a floating device has been utilized at that site to record water levels on an hourly basis. It was thought that both TG is on the same ground level, which implicitly meant that the MSL is located also at 33.8 cm above the bottom of the fixed staff. Later, a precise levelling has been carried out to connect both TG sites and the results revealed that the Navy TG is 18 cm higher than the historical Port TG. An agreement has been signed between ENHD and the Survey Research Institute (SRI) of the National Water Research Center (NWRC) in the year 2000 to start scientific cooperation around sea level variations and environmental monitoring. Thus, the device of the Navy TG has been replaced by a modern pressure type and a metrological weather station and a fixed Global Positioning System (GPS) receiver have been installed too [6]. Hence, digital sea level observations of the Navy TG have been recorded since 2001 up till now. Recently, a microwave type TG has been installed in that TG as a precise backup system [26].

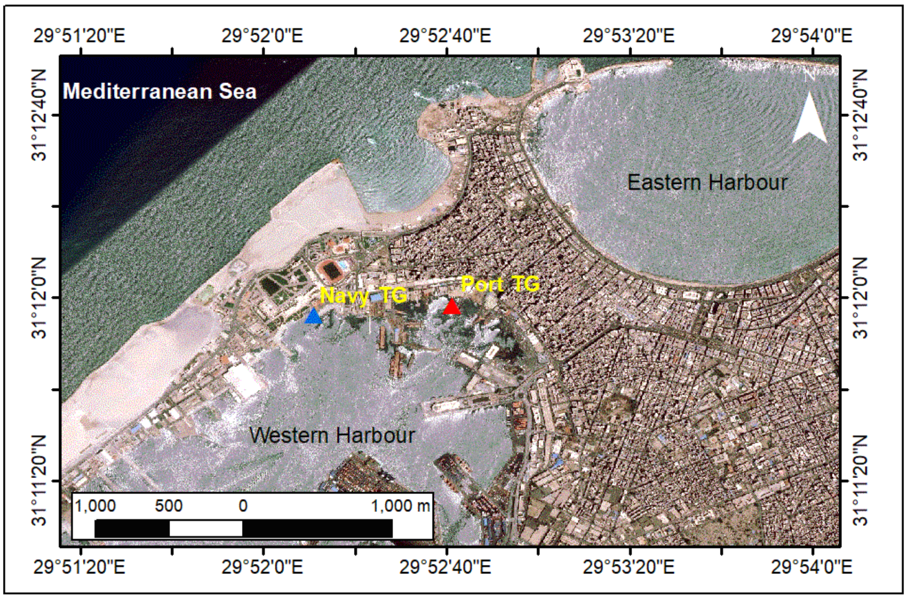

Fig. 2: Tide Gauges at Alexandria City

The datasets utilized in this study consist of four different groups (Table 1). First, the monthly and annual MSL related to the historical Port TG from 1944 to 1992 has been obtained from the Permanent Service of Mean Sea Level (PSMSL) website [27]. It is worth mentioning that this dataset is referenced to the Revised Local Reference (RLR) and a constant of 7.019 m should be subtracted to reference it to the local MSL datum of Egypt [28]. The second group of data contains the hourly sea heights of the Navy TG from 1993 to 2000. As previously stated, a sum of both constants (33.8 and 18 cm) has been subtracted from the original measurements to relate them to the Egyptian MSL datum [6]. The third data source is the Navy TG dataset from 2001 to 2018 as recorded by the pressure-type device every half hour. Lastly, the fourth dataset comes also from the microwave device installed in 2019 at the Navy TG. For both the third and fourth data groups, only 18 cm are subtracted to relate them to the national datum. Consequently, this research has integrated a unique database of sea level heights at Alexandria from 1944 to 2020 referenced to the national MSL vertical datum of Egypt of 1906 for the first time.

Table 1: Utilized Tide Data Sources at Alexandria

Tide Gauge	Data Source	Period	Frequency	Gaps
Port TG	PSMSL	1944-1993	Monthly	1948, 1949
Navy TG	ENHD	1993-2000	Hourly	NA
	SRI	2001-2020	30 minutes	

4. Results and Discussion

4-1. Alexandria's Tide Characteristics

The 30-minutes tide dataset of 2020 has been investigated to illustrate the basic properties of tides at Alexandria city. First, Figure 3 depicts typical hourly tides variations at Alexandria on the 1st of January 2020 (just a typical day in the most-recent available datasets). Tides, on that day, vary between 0.177 m and 0.380 m, with a range equal to 0.203 m and an average value of 0.279 m. It follows the semi-diurnal pattern with two maximum values occurring at midnight and 1.5 PM and two minimum values at almost 7.5 AM and 7.5 PM of local time. Similar results have been reported

by El-Geziry and Dabbous [3]. Next, the minimum and maximum values of daily tides over the entire 2020 have been defined. It has been found the maximum tide occurred on August 20 and the minimum tide occurred on February 29 (Fig. 4 and 5). It has been found that a minimum tide equals 0.042 m while the recorded maximum tide equals 0.542. Next, Fig. 6 depicts the monthly annual tide variations of 2020. It reached its highest value from July to August, and the minimum values took place in February and March.

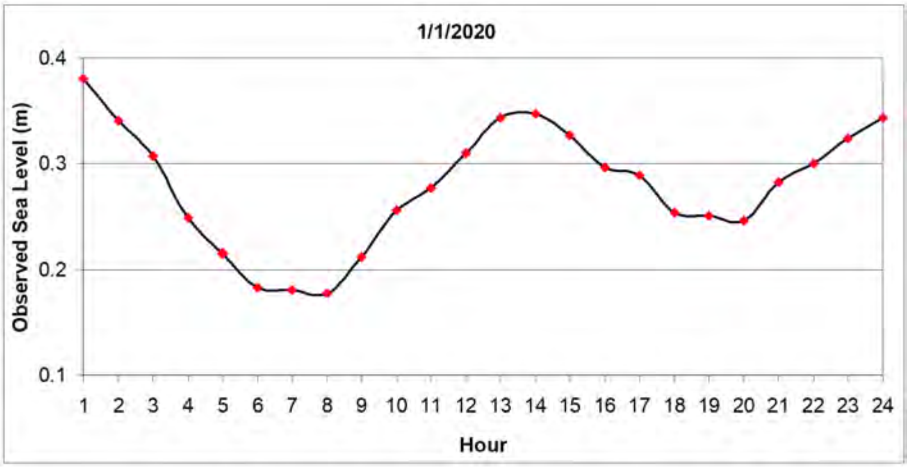

Fig. 3: Typical Hourly Tides of Alexandria on January 1st, 2020

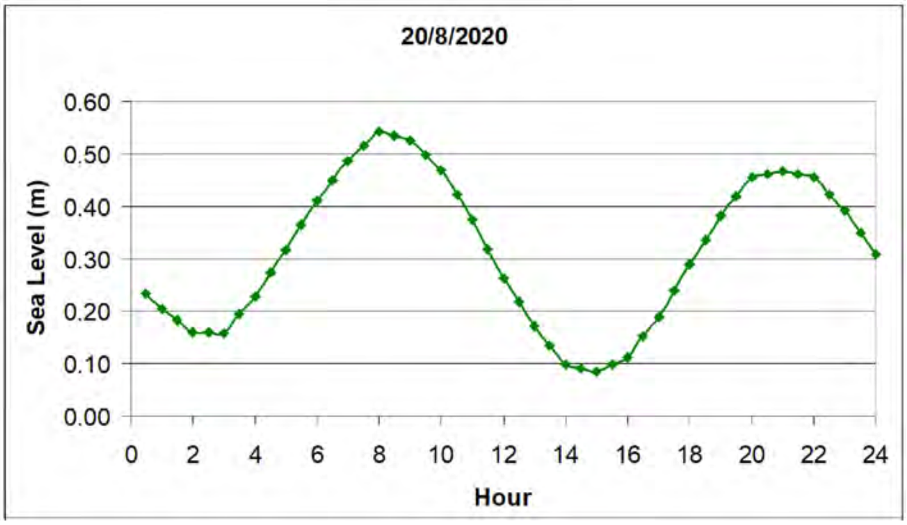

Fig. 4: Maximum Tides of Alexandria in 2020

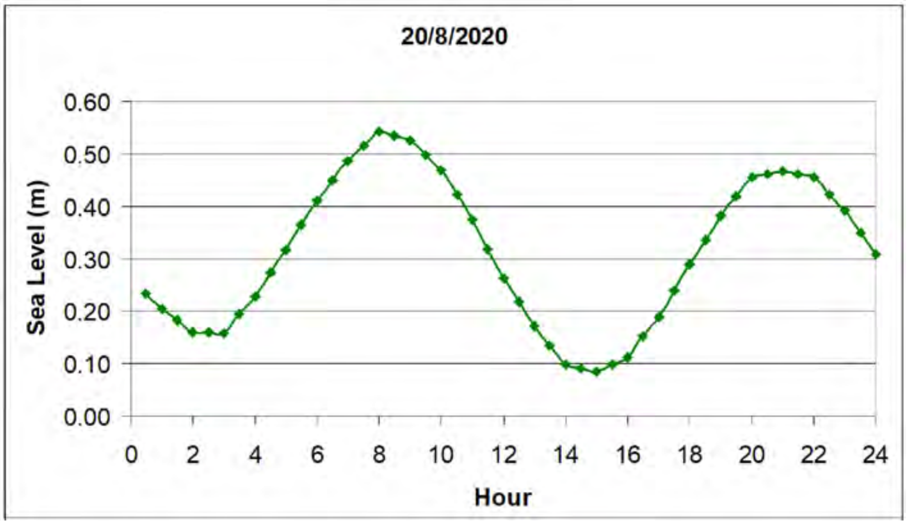

Fig. 5: Minimum Tides of Alexandria in 2020

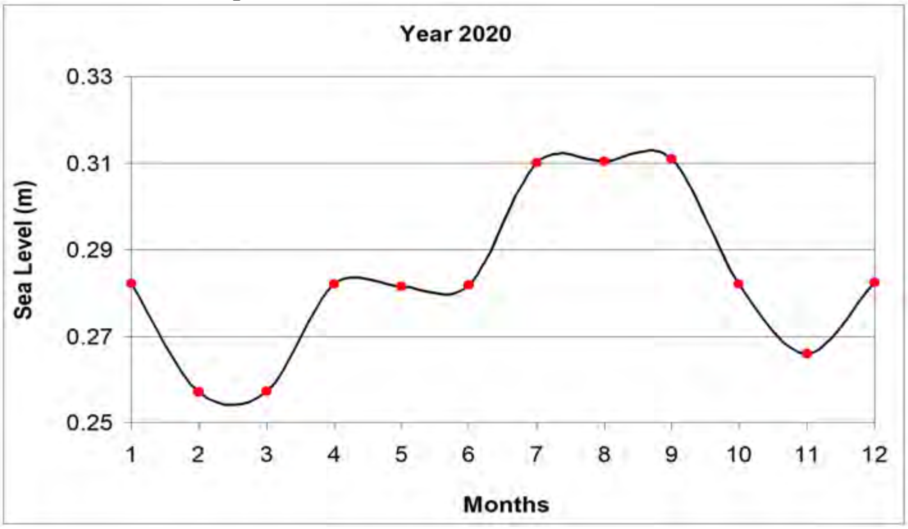

Fig. 6: Monthly Tides of Alexandria in 2020

4.2. Egypt's Mean Sea Level Variations

The unique integrated tide database of Alexandria has been utilized in investigating the relative SLR and MSL variations over 1944-2020 (relative to 1906 MSL datum) for the first time in Egypt. Keeping in mind that few data gaps exist, that database contains annual MSL for 76 years. Fig. 7 portrays the general trend of MSL variations over that specific period, which clearly show a rising MSL. Statistical fitting approaches have been performed to describe that trend mathematically. Linear, quadratic, and cubic polynomial, logarithmic, and hyperbolic formulas (Eq. 1 to 5) have been fitted to the known data and the R2 indicator (Eq. 6) has been computed for each case (Table 2). This table showed that although the quadratic and cubic polynomial model produced a slightly better fit, the linear trend is most utilized in SLR studies for its simplicity in defining and forecasting the SLR [29]. Thus, it can be concluded that the annual linear SLR at Alexandria over 1906-2020 equals 2.6 mm/year. That figure highlights the general trend of relative SLR over more than a decade in Egypt. However, it might not the most appropriate to demonstrate recent SLR magnitude in the country.

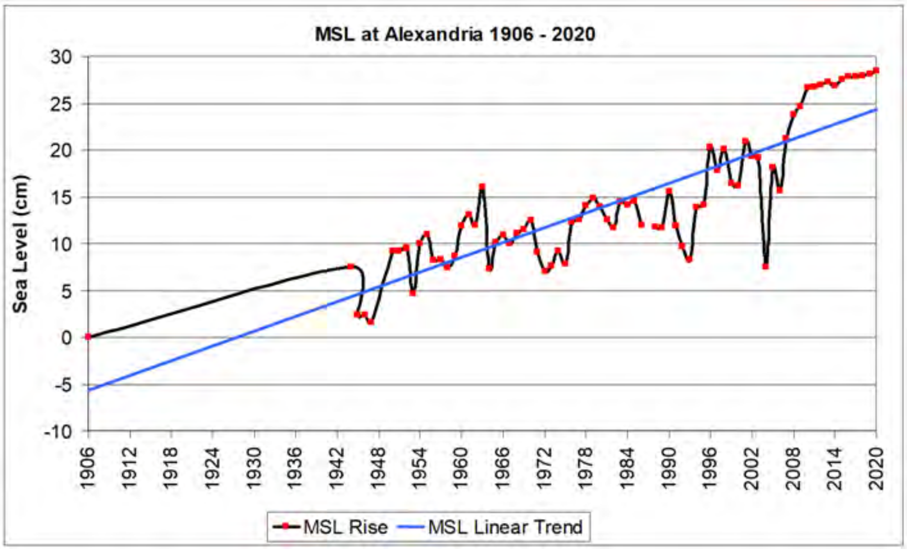

Fig. 7: MSL Variations at Alexandria over 1946-2020 relative to 1906 Datum

Table 2: Statistics of 1906-2020 MSL Fitting Methods

Type	Equation	R2
Linear	MSL = 0.2625 Year - 505.96	0.76
Quadratic Polynomial	MSL = 0.0023 Year2 - 9.0315 Year + 8683	0.82
Cubic Polynomial	MSL = 0.0000 Year3 - 0.0484 Year2 + 96.4235 Year - 41660.3323	0.85
Logarithmic	MSL = 517.88 Ln (Year) - 3917.4	0.76
Hyperbolic	MSL = 529.8565 - (1021780.9758/Year)	0.76

The previous relative SLR figure, 2.6 mm/y, highlights the general trend of SLR over more than a decade in Egypt (referenced to the 1906 Egyptian datum). However, it might not the most appropriate to demonstrate recent SLR magnitude in the country. Hence, the available dataset has been divided into 20-years intervals to consider the 18.6-year lunar-node cycle. That modal cycle is important in investigating SLR precisely [30]. Figures 8-11 and Table 3 demonstrate the attained findings. From these figures and table, several significant remarks could be obtained. First, the linear SLR trend is weak for the first three timespans: 1944-1960, 1961-1980, and 1981-2000 since the R2 values equal just 0.40, 0.01, and 0.20. It might be attributed to the nature and quality of corresponding datasets from PSMSL source (refer to Table 1). Second, the SLR over 1961-1980 is almost steady with no noteworthy rise. Third, the SLR magnitudes of 3.9, 0.04, and 2.0 mm/year corresponding to such periods are not trustable. Fourth, for the last couple of decades, 2001-2020, the attained results prove that the SLR at Alexandria is of high confidence since the R2 reaches 0.77. Fifth and based on that analysis, the relative SLR of 3.1 mm/y over 2001-2020 could be considered the most appropriate value to be taken into consideration in Egypt's coastal management activities. This figure should be regarded as an alarming finding reflecting that the SLR in the last couple of decades is significantly higher than the long-term rise over the entire twentieth century at Alexandria.

Table 3: Statistics of 1906-2020 MSL Fitting Methods

Period	Linear Equation	R2	SLR (mm/y)
1944-1960	MSL = 0.3889 Year - 751.82	0.40	3.9
1961-1980	MSL = 0.0336 Year - 55.03	0.01	0.04
1981-2000	MSL = 0.2024 Year - 389.45	0.20	2.0
2001-2020	MSL = 0.3122 Year – 5.91	0.77	3.1

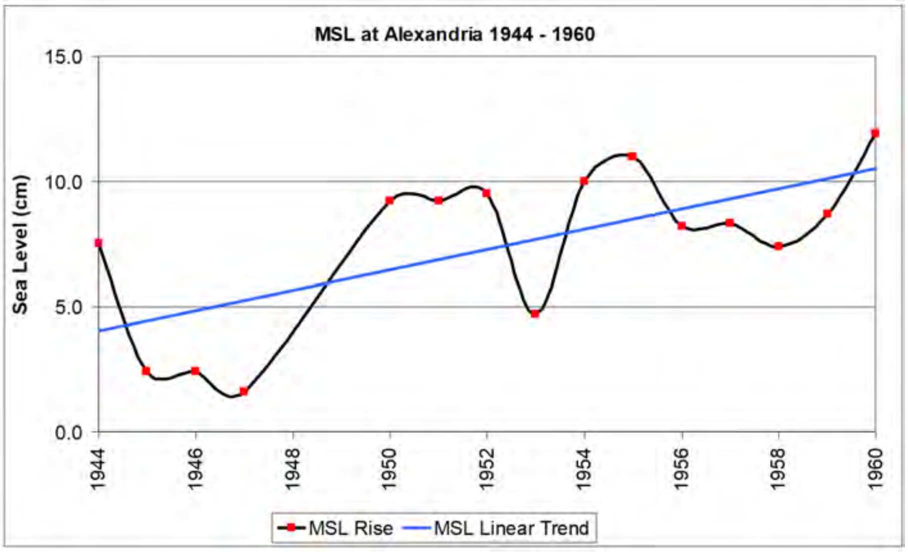

Fig. 8: MSL Variations at Alexandria over 1944-1960

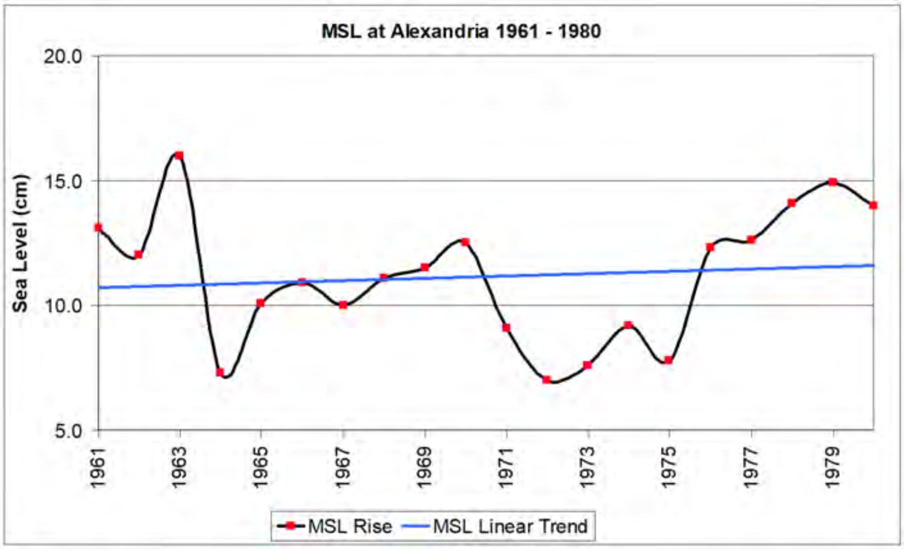

Fig. 9: MSL Variations at Alexandria over 1961-1980

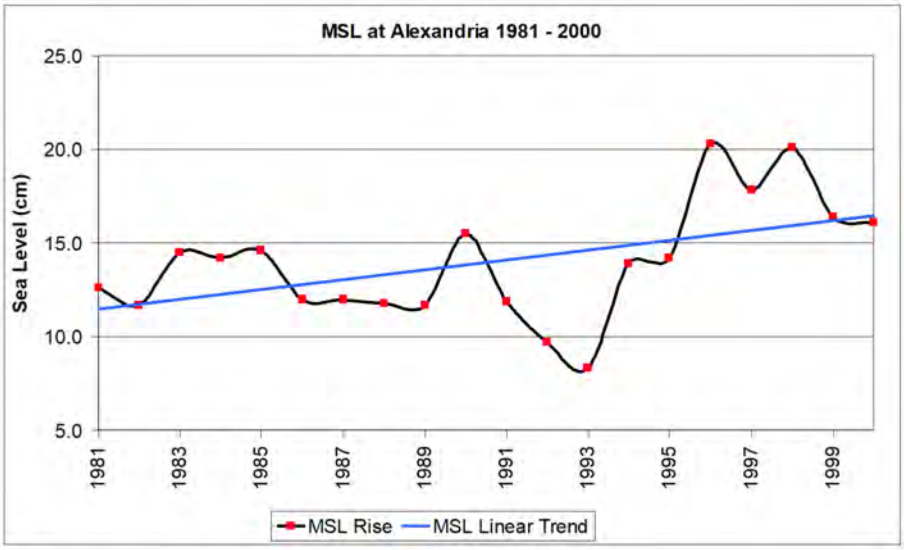

Fig. 10: MSL Variations at Alexandria over 1981-2000

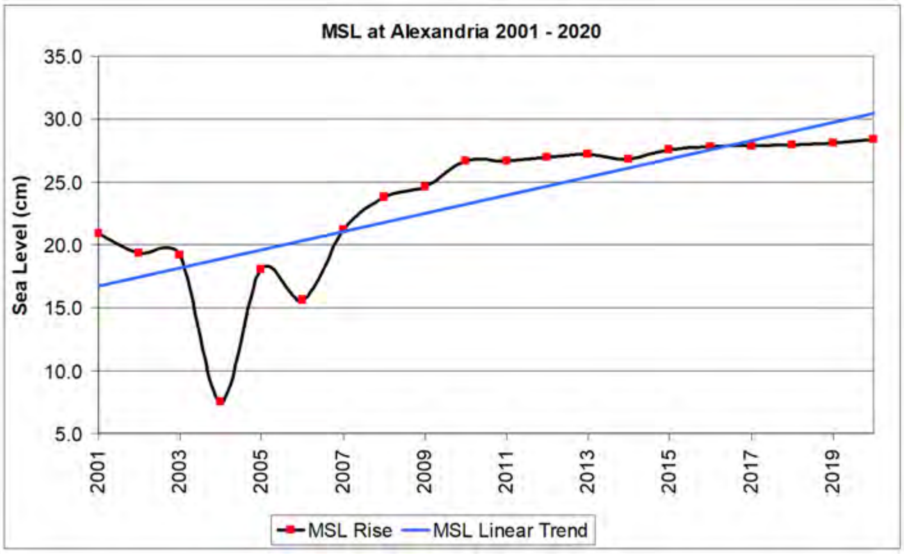

Fig. 11: MSL Variations at Alexandria over 2001-2020

Finally, the values of Egypt's MSL or vertical datum has been investigated over 20-years intervals. Table 4 and Figure 12 present the accomplished findings. Based on the available data, the value of the national vertical datum as defined at Alexandria in 1906 is varying considerably. Its value has been increasing to 7.4, 11.2, 13.4, and 23.8 cm over the 1944-1960, 1961-1980, 1982-2000, and 2001-2020 periods respectively. Additionally, it can be noticed that the MSL has been increased over 1961-1980 by 51% relative to the 1944-1960 mean value. Similarly, it increased by 20% and 78% over the periods 1981-2000 and 2001-2020 relative to each preceding 20-year time span. Thus, it is a matter of fact that the SLR is getting faster in Egypt in the last few decades.

Regarding the accessible datasets and attainable results, the current study implies that Egypt's MSL datum should not be considered as a fixed datum over time. Like the semi-kinematic horizontal geodetic datum of Egypt proposed by Rabah et al. [31], the results of the current research emphasize that the vertical datum should be regarded as semi-kinematic too. Simply, it means that its definition should be updated a suitable span, 20 years for instance. For the time being, it should be considered that the most recent Egypt's national MSL datum is 23.8 cm higher than the traditional 1906-defined one. That fact should be applied in environmental and geomatics activities and studies to get more reliable results. However, it is recommended to perform additional

investigations about other possible major variations of MSL in Egypt at other TG sites over both the Mediterranean and Red Seas. Such a task could be performed utilizing datasets of SRI's tide gauges recently established at Port Said, Suez, and Safaga cities.

Table 4: Average MSL Variations at Alexandria

Period	Average MSL (cm)	Increase Percent
1906 (original)	0.0	NA
1944-1960	7.4	
1961-1980	11.2	51%
1981-2000	13.4	20%
2001-2020	23.8	78%

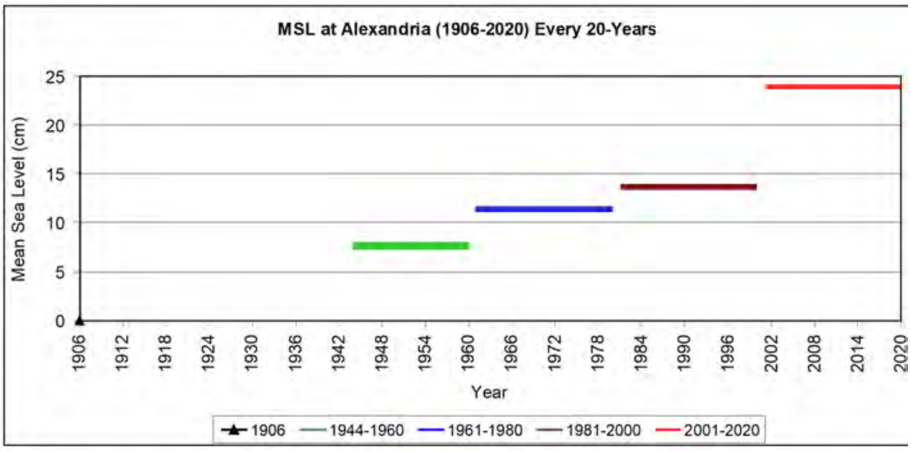

Fig. 12: MSL Variations at Alexandria over 1906-2020 every 20 Years

In addition, the accomplished results showed that elevations of the tide gauges and benchmarks in Egypt need to be corrected as the national vertical datum is changed since its old definition in 1906. The current study suggests that such a task could be performed by establishing and applying 4D databases of tide gauges, particularly over the Nile River, for efficient water resources management. It is a matter of reality that the absolute SLR combines the influences of both relative SLR, from TG, and the vertical land movement. Mohamed and Dawod [32] have utilized geodetic datasets from 2011 to 2019 and have estimated the land subsidence rate at Alexandria as 3.3 mm/year which concluded that the recent estimate of the absolute SLR equals 6.0 mm/year. Such a rate should be considered in environmental investigations and development activities over Alexandria.

5. Discussion/Conclusion

The tidal analysis is a chief feature in navigation and coastal management. On the other hand, it is a matter of reality that the sea level has been significantly raised in the 20th century on a global average. The current research has utilized data from different sources to construct a unique database of sea levels at Alexandria from 1944 to 2020, referenced to the national MSL 1906 vertical datum of Egypt, for the first time in the country. Regarding relative sea level rise, it can be concluded that the annual linear SLR at Alexandria from 1906 to 2020 equals 2.6 mm/year. Furthermore, the available dataset has been divided into 20-years intervals to consider the 18.6-year lunar-node

cycle. Attained findings reveal some significant remarks. First, the linear SLR trend is poor for the periods 1944-1960, 1961-1980, and 1981-2000 since the determination coefficients are less than half. Second, the SLR over 1961-1980 is almost steady with no noteworthy rise. Additionally, in the last couple of decades, 2001-2020, the relative SLR equals 3.1 mm/y. Thus, it could be considered the most appropriate value to be taken into consideration in Egypt's coastal management activities. The values of Egypt's MSL or vertical datum have been investigated over 20-years intervals and showed that the value of the national vertical datum as defined at Alexandria in 1906 is varying considerably. Consequently, the SLR is getting faster in Egypt in the last few decades. The current study showed that Egypt's MSL datum should not be considered a fixed datum over time. Based on accessible data and achieved findings, it is recommended that that datum should be regarded as semi-kinematic, which means that its definition should be updated a suitable time, 20 years for instance.

References

[1] Ibrahim O., Study of the Sea Level variability and Storm Surges at Mersa Matruh, Egypt. *Arab J Geosci* 14, 1678. DOI:10.1007/s12517-021-07907-5, 2021.

[2] El-Geziry, T., Sea-level, tides and residuals in Alexandria Eastern Harbour. Egypt. *Egyptian Journal of Aquatic Research*, 47(1), 29–35. DOI:10. 1016/j. ejar. 2020. 10. 003, 2021.

[3] El-Geziry, T. M., and Dabbous, A., Behavior of surges in Alexandria Eastern Harbor, Egypt. *Egyptian Journal of Aquatic Research*, 0–7. DOI:10. 1016/j. ejar. 2021. 02. 001, 2021.

[4] Ibrahim O and El-Gindy A., Comprehensive Analysis of Monthly Mean Sea Level in the Eastern Mediterranean as a Tool for Prediction and Risk Assessment of Future Expected Sea Level Rise, *Arabian Journal of Geosciences* 15(1): 3. DOI:10.1007/s12517-021-08845-y, 2021.

[5] Khedr, A., Abdelrahman, S., and Tonbol, K., Sea level characteristics referenced to specific geodetic datum in Alexandria, Egypt, *International Journal of Marine and Environmental Sciences*, vol. 12, no. 2, pp. 78-86, 2018.

[6] Mohamed, H., *Realization and redefinition of the Egyptian vertical datum based on heterogonous observations*, PhD Dissertation, Faculty of Engineering at Shoubra, Zagazig University, Egypt, 2005.

[7] Khan, A., Why would sea-level rise for global warming and polar ice-melt?, *Geosci. Front.*, 10:481-494, DOI: 10.1016/j.gsf.2018.01.008, 2019.

[8] IPCC (The Intergovernmental Panel on Climate Change), *Sea level rise and implications for low-lying islands, coasts and communities*, IPCC special report on the ocean and cryosphere in a changing climate [H.-O. Pörtner, D.C. Roberts, V. Masson-Delmotte, P. Zhai, M. Tignor, E. Poloczanska, K. Mintenbeck, A. Alegría, M. Nicolai, A. Okem, J. Petzold, B. Rama, N.M. Weyer (eds.)], 2019.

[9] Church, J., Clark, P., Cazenave. A., Gregory, J., Jevrejeva, S., Levermann, A,. Merrifield, M., Milne, G., Nerem, R., Nunn, P., Payne, A., Pfeffer, W., Stammer, D. and Unnikrishnan, A. *Sea Level Change*. In: Climate Change (2013): The Physical Science Basis. Contribution of Working Group I to the Fifth Assessment Report of the Intergovernmental Panel on Climate Change [Stocker, T.F., D. Qin, G.-K. Plattner, M. Tignor, S.K. Allen, J. Boschung, A. Nauels, Y. Xia, V. Bex and P.M. Midgley (eds.)]. Cambridge University Press, Cambridge, United Kingdom and New York, NY, USA, 2013.

[10] Poitevin, C., Wöppelmann, G., Raucoules, D., Cozannet, G., Marcos, M. and Testut, L., Vertical land motion and relative sea level changes along the coastline of Brest (France) from combined space-borne geodetic methods, *Remote Sensing of Environment*., 222:275–285, DOI: 10.1016/j.rse.2018.12.035, 2019.

[11] Mohamed B, Skiliris N., Steric and atmospheric contributions to interannual sea level variability in the eastern mediterranean sea over 1993–2019, *Oceanologia*, DOI:10.1016/j.oceano.2021.09.001, 2021.

[12] Mohamed B, Mohamed A, Alam El-Din K, Nagy H, Elsherbiny A., Sea level changes and vertical land motion from altimetry and tide gauges in the Southern Levantine Basin. *J. Geodyn.* 128, 1–10. DOI:10.1016/J.JOG.2019.05.007, 2019.

[13] Wang, F., Lia, J., Shia, P., Shanga, Z., Lia, Y. and Wang, H., The impact of sea-level rise on the coast of Tianjin-Hebei, China, *China Geology,* no. 1, pp 26−39, 2019.

[14] Fu, X. and Peng, Z., Assessing the sea-level rise vulnerability in coastal communities: A case study in the Tampa Bay Region, US, *Cities*, DOI: 10.1016/j.cities.2018.10.007, 2018.
[15] Aucelli, P., Paola, G., Rizzo, A. and Rosskopf, C., Present day and future scenarios of coastal erosion and flooding processes along the Italian Adriatic coast: the case of Molise region, *Environ. Earth Sci.*, DOI: 10.1007/s12665-018-7535-y, 2018.
[16] Wassef, R. and Schüttrumpf, H., Impact of sea-level rise on groundwater salinity at the development area western Delta, Egypt, *Groundw. Sustain. Dev.*, no. 2-3, pp. 85–103, 2016.
[17] Dawod, G, Mohamed, H. and Haggag, G., Relative and absolute sea level rise based on recent heterogeneous geospatial data: A case study in the Nile Delta, Egypt, *J. sci. eng* , vol. 6, no. 6, pp. 55-64, 2019.
[18] Shaltout, M., Tonbol, K. and Omstedt, A., Sea-level change and projected future flooding along the Egyptian Mediterranean coast, *Oceanologia*, no. 57, pp. 293-307, 2015.
[19] El-Geziry, T. and Said, M., Sea level variations in El-Burullus new harbour, Egypt, *Arab. J. Geosci*, 12:460, DOI: 10.1007/s12517-019-4620-9, 2019.
[20] Stanley, J., Increased land subsidence and sea level rise are submerging Egypt's Nile Delta costal margin, *GSA Today*, V. 27, DOI: 10.1130/GSATG312A.1, 2016.
[21] Abou-Mahmoud, M., Assessing coastal susceptibility to sea-level rise in Alexandria, Egypt, *Egyptian Journal of Aquatic Research*, DOI: 10.1016/j.ejar.2021.04.002, 2021.
[22] Hereher, M., Coastal vulnerability assessment for Egypt’s Mediterranean coast, *Geomatics, Nat. Hazards Risk*, 6(4):342–355, DOI: 10.1080/19475705.2013.845115, 2013.
[23] IOC (Intergovernmental Oceanographic Commission), *Manual on sea level: Measurements and interpretation*, Volume IV: An update to 2006, Technical Report No. 31, 78 pp, France, 2006.
[24] Hieronymus, M. Hieronymus, J. and Hieronymus, F., On the application of machine learning techniques to regression problems in sea level studies, *Journal of Atmospheric and Oceanic Technology*, vol. 36, pp. 1889-1902, 2019.
[25] Shumway, R. and Stoffer, D., *Time series analysis and applications*, Forth edition, Springer, New York, 2016.
[26] SRI (Survey Research Institute), *Observing the variations and effects of sea level on the Egyptian coasts over 2008-2018*, A technical Report, SRI, Giza, Egypt, 2019.
[27] PSMSL (Permanent Service of Mean Sea Level), *Annual Sea Level Data of Alexandria TG*, https://www.psmsl.org/data/obtaining/rlr.annual.data/503.rlrdata, accessed October 5, 2021.
[28] PSMSL (Permanent Service of Mean Sea Level), *Revised local reference of Alexandria tide gauge*, https://www.psmsl.org/data/obtaining/rlr.diagrams/503.php, accessed October 5, 2021.
[29] Jean, K., *Models describing the sea level rise in Key West, Florida*, MSC Thesis, 42 pp, Florida International University, Thesis No. 2274, Florida, USA, 2015.
[30] Baart, F., van Gelder, P., Ronde, J., Koningsveld, M. and Woutwers, B., The effect of the 18.6-year lunar nodal cycle on regional sea-level rise estimation, *Journal of Coastal Research*, vol. 28, no. 2, pp. 511-516, 2012.
[31] Rabah, M., Shaker, A. and Farhan, M., Towards a semi-kinematic datum for Egypt. *Positioning*, no. 6, pp. 49-60, 2015.
[32] Mohamed, H. and Dawod, G., Recent GNSS-based estimates of vertical land movements in the Nile Delta, Egypt over 2012-2019, *Journal of Scientific and Engineering Research*, vol. 9, no. 4, pp. 7-16, 2022

الملخص العربي

Available online www.jsaer.com

***Journal of Scientific and Engineering Research*, 2022, 9(5):85-100**

Research Article

ISSN: 2394-2630
CODEN(USA): JSERBR

Variations of Sea Levels and Atmospheric Parameters along the Egyptian Coasts Over 2008-2020

Gomaa M. Dawod*, Ahmed M. Amin, Ghada G. Haggag

Survey Research Institute, National Water Research Center, Giza, Egypt
* dawod_gomaa@yahoo.com, ORCID = 0000-0002-4426-8231

Abstract Recently, the climate changes and global warming phenomena have resulted in a significant Sea Level Rise (SRL) worldwide. The objectives of the current study include defining the recent Mean Sea Level (MSL) datum of Egypt, estimating SRL trends, and investigating the correlation between sea level and meteorological elements, principally air temperature and atmospheric pressure, and to give general indications about sea level and atmospheric elements' variations at four locations over the Egyptian coasts along both the Mediterranean and Red seas. It utilizes the most-recent heterogeneous hourly datasets from 2008 to 2020. Even though it is a relatively medium period, the achieved findings are significant for coastal management and risk assessment of environmental hazards. The attained results, as previous researches, reveal sea level is increasing as going east over the Mediterranean Sea and it decreases as going south over the Red Sea. In addition, it has been shown that sea level has a strong positive correlation with air temperature and a strong negative correlation at Alexandria, Port Said, and Suez sites. Concerning the spatiotemporal variations of sea level in Egypt, it has been noticed that the relative rising rate of the Mediterranean Sea range from 1.8 mm/year at Port Said to 3.1 mm/year at Alexandria. Regarding the Red Sea, the relative SRL varies between 2.7 mm/year at Suez and 4.3 mm/year at Safaga. Generally, the accomplished findings necessitate developing a national plan for dealing with the SLR phenomenon and its consequence hazardous environmental impacts. From a geodetic and surveying perspective, such reality should be significantly considered in the realization of a recent Egyptian vertical datum for mapping and surveying applications.

Keywords Environmental Changes, Global Warming, Sea Level Rise, Metrological Elements, Egyptian Costs

1. Introduction

Nowadays, it becomes a fact that the Earth suffered a global warming phenomenon, in the last couple of centuries, with serious environmental and economic hazards. One such crucial hazard is the accelerating Sea Level Rise (SRL) worldwide that causes sea flooding, particularly for low-elevation lands and coasts. According to the Intergovernmental Panel on Climate Change (IPCC), three chief remarks should be considered: (1) the global SRL has increased from 1.4 mm/year over the period 1901-1990 to 2.1 mm/year over 1970-2015 to 3.2 mm/year over 1993-2015 to 3.6 mm/year over 2006-2015, (2) under some specific scenarios, the global SRL could likely reach 0.84 m (0.61-1.10 m) by 2100 over the 1986-2005 level, and (3) if global warming is fast accelerating and the global air temperature is kept rising over the next three centuries, a global SRL could be over few meters by 2300 [1]. On another hand, it has been found that atmospheric pressure affects the sea level changes on a global basis over a long time [2-3]. Moreover, warm air temperature could contribute significantly to the generation of severe sea level changes and storm surges in coastal regions [4-5].

Global variations of sea levels are attributed to several factors such as thermal expansion, glaciers melting, and land water storage changes [6] (Oppenheimer et al. 2019). Moreover, Local or regional SLR are mostly due to

land subsidence, ocean dynamics, and climate changes (ibid). Global Sea Level Rise (GSLR) is a mean estimate of SLR worldwide, which varies from one specific region to another. Thus, many studies have been carried out to estimate SLR over different spatial areas. For example, Parker and Ollier [7] have reported that SLR in India, computed from datasets of 11 TG over 51 years, equals 1.06 mm/year. Similarly, the SLR in the north-western part of the Arabian Gulf was found to be 2.2 mm/year [8]. In Poland, the SLR over the period 1951-2017 was estimated as 2.99 mm/year [9].

Projecting SLR over future time comprises a vital research activity for estimating the vulnerability of such significant environmental hazards. An example of such projection reported by Mengel et al. [10] where sea level in 2100 could rise by 0.28-0.56 m, 0.37-0.77 m, and 0.57-1.31 m for different greenhouse gas concentration scenarios. Other studies have projected the SLR in the 21st century on a regional scale. For example, Edwards [11] has reported that in the United Kingdom there are three scenarios of sea level rise from 1990 to 2100 based on the expected rise in global temperature: (a) the low-to-medium case of possible SLR of 0.30 m, (b) the high scenario of possible 0.60 m of SLR, and (c) the extreme situation of SLR of 2.5 m. Similarly, Dawod et al. [12] have projected sea level at four TG stations along the Delta coastlines and estimated the risks of SLR and storm surges by 2025.

In Egypt, evaluating SLR has become a major concern not only to the government but also to the research community in the last few decades. For example, Dawod [13] (2001) has utilized datasets at Alexandria over 1944-1999 and at Port Said over 1926-1987 to estimate a long-term SRL over the Nile delta along the Mediterranean sea. He found that SRL equals 1.7 mm/year and 2.4 mm/year at Alexandria and Port Said respectively. Moreover, Dawod et al. [14] have utilized hourly tide datasets and Global Navigation Satellite Systems (GNSS) covering 2008-2016 to estimate relative SRL, land subsidence rates, and absolute SRL at both Alexandria and Port said. It has been found that the relative SRL in the Nile delta region varies from 2.6 mm/year to 4.3 mm/year, and the vertical land movements rates at the tide gauge sites range between +0.09 mm/year and -4.3mm/year, and hence the absolute SRL differ between 5.0 mm/year at Alexandria to 6.9 mm/year at Port Said. Recently, Radwan et al. [15] have utilized different datasets with variable time resolution (over the period 2009-2015) at Alexandria, Damietta, and Port Said along the Mediterranean sea to investigate the variations of sea level in the Nile delta region. They estimated the Mean Sea Level (MSL) relative to the 1906-based national datum equal 0.172 m, 0.601 m, and 0.513 m at Alexandria, Damietta, and Port Said respectively. Using a three-year tide dataset (covering 2012-2014), El-Geziry et al. [16] have inspected the general pattern of sea level in Safaga and Qussier harbors on the Egyptian Red sea costs, and they found that the MSL at those two sites equal 0.56 m and 0.50 m respectively.

The metrological elements that influence sea level variations comprise a wide range of factors as utilized in many research studies worldwide. For example, Zubier and Eyouni [17] have analyzed the relation between sea levels and air temperature, atmospheric pressure, wind speed and wind near Jeddah harbor, Saudi Arabia. Other researchers [18] have focused on the relationship between wind and air pressure on the variability of sea levels. Other studies have analyzed the influence of both air temperature and precipitation on sea level variations [19]. Moreover, Han et al. [20] have studied the impacts of only atmospheric pressure on sea levels in the Asian marginal seas. In Iraq and Egypt, Both Latfa [21] and El-Geziry et al. [22] have investigated sea level variations with air temperature, atmospheric pressure, and wind speed.

The relationship between sea level and metrological factors has been investigated extensively in the last few years in Egypt. Mohamed [23] and Dawod et al. [24] have investigated the inter-relationship between the MSL and meteorological variations at Alexandria. Based on the monthly tide and metrological records from 1985 to 2003, it has been concluded that the most-critical metrological elements are the air temperature that has a 60% positive correlation impact on the recorded tide, and the air pressure which has a negative correlation of 40%. Thus, the current research highlights the correlation between sea level and only air temperature and atmospheric pressure. Furthermore, Sharaf El Din [25] has investigated the relationship between sea level changes and metrological factors over three tide gauges in Egypt along both Mediterranean and Red seas over 1956-1966. Freshly, Ibrahim [26] has investigated the variability of sea level at Mersa Matruh along the Mediterranean sea and their relationship to pressure, air temperature, and wind speed. She concluded that air temperature and wind speed significantly affect the observed sea level at this site.

This paper aims to fulfill three objectives: (1) defining the recent MSL datum, (2) estimating SRL trends, and (3) investigating the correlation between sea level and meteorological factors, and (4) to give general indications about sea level and atmospheric elements' variations at four sites over the Egyptian coasts along both the Mediterranean and Red seas using most-recent heterogeneous datasets over the period 2008-2020.

2. Methodology

There are several approaches for analyzing the trend of sea level variations and their relationship to metrological elements, with a wide range of variability in mathematical formulation, flexibilities, and characteristics [27]. Some of such techniques are harmonic analysis [28], machine learning [29], and Artificial Neural Network: ANN [17]. However, the regression statistical analysis has been extensively utilized in modelling and predicting sea level variability worldwide. For example, Jamali et al. [30] have utilized regression to predict monthly variations of sea level in Malaysia. Moreover, Kumar [31] has investigated the variations of sea levels in the western South Pacific islands using the multiple regression approach with a selection of some oceanic and atmospheric parameters as input. Also, the regression approach has been applied to statistically reconstruct sea levels in the Baltic sea from tide gauge datasets [32].

Simply, the correlation coefficient quantifies the correlation between two or more variables. It is a unitless value that varies between +1, expresses strong positive agreement, and -1, describing a strange negative agreement, where 0 means no correlation between the investigated variables. The sample correlation coefficient, r_{xy}, between two variables x and y can be estimated as:

$$r_{xy} = \frac{\sum_{i=1}^{n}(x_i - \bar{x})(y_i - \bar{y})}{\sqrt{\sum_{i=1}^{n}(x_i - \bar{x})^2}\sqrt{\sum_{i=1}^{n}(y_i - \bar{y})^2}} \quad (1)$$

where,

n is the sample size,

x_i, y_i are the individual i^{th} sample point, and

$\bar{x}$ and $\bar{y}$ are the sample mean for both variables x and y.

Moreover, linear regression modelling has been performed to model the temporal variations of sea level and metrological elements over the period 2008-2020. A linear regression model can be estimated as:

$$Y = a + bX \quad (2)$$

where,

Y is a set of observed values of the dependent variable,

X is a set of predicted values of the independent variable, and

a and b are two unknowns to be estimated as:

$$a = \frac{(\sum y)(\sum x^2) - (\sum x)(\sum xy)}{n(\sum x^2) - (\sum x)^2} \quad (3)$$

$$b = \frac{n(\sum xy) - (\sum x)(\sum y)}{n(\sum x^2) - (\sum x)^2} \quad (4)$$

To judge the goodness of the attained linear regression model, a statistical measure called the coefficient of determination, R^2, is applied. Simply, it represents the proportion of the variation in the dependent variable that is estimated from the independent variable. Thus, its value ranges from zero to +1 and the higher this value the better the regression model. The coefficient of determination could be estimated as:

$$R^2 = \frac{\sum(\hat{y} - \bar{y})^2}{\sum(y - \bar{y})^2} \qquad (5)$$

where,

$\hat{y}$ *and* $\bar{y}$ represent the estimated and average values of the dependent variable respectively.

3. Study Area and Available Data

The study has utilized two integrated datasets: sea level data and metrological data, particularly air temperature and atmospheric pressure. Such datasets have been collected over along Egypt's Mediterranean coasts between Alexandria (31.13^0N, 29.88^0E) and Port Said (31.20^0N, 32.31^0E) and the Red sea cost from Suez (29.91^0N, 32.59^0E) to Safaga (26.71^0N, 33.95^0E) as depicted in Fig. 1.

The four Tide Gauges (TG) have been installed and operated by the Survey Research Institute (SRI) of the National Water Research Center (NWRC) under the umbrella of the Ministry of Water Resources and Irrigation. At Alexandria and Port Said, the installed (TG) are microwave devices (Fig. 2) while pressure devices are installed at Suez and Safaga sites. The collected Sea Level (SL) datasets comprise bi-hourly measurements from 2008 to 2020 for three TG, while the fourth one, namely Suez, has data since 2016. No gaps exist for the three sites, but Port Said TG did not have SL data in 2018 (Table 1). It is worth mentioning that the utilized TG data at all locations have an accuracy level of less than one centimeter. Moreover, the normality of the utilized datasets has been analyzed and proved and, thus, parametric modelling techniques, such as the regression analysis, could be carried out. Also, it should be stated that SL data at Alexandria are relative to the vertical national Egyptian datum as defined in 1906, while the other three TG have data tied to the nearest benchmark, where a datum shift of 0.18 m exists between those two vertical frames. It is worth mentioning that there are no hourly 30-years TG datasets available in Egypt to extremely analyze climate changes and global warming. Thus, the current available dataset have been utilized to give general indications about sea level and atmospheric elements' variations in Egypt.

Figure 1: The Study Area

Figure 2: A Utilized Tide Gauge

Normally, the investigation of long-term variations of sea level and metrological elements require long-span datasets of at least 30 years. However, the importance of that environmental issue and the lack of long-term data, in many situations, force several researchers to utilize data covering only fewer years. For example, Latfa [21] has analyzed the influence of atmospheric forces on sea-surface fluctuations in Iraq using hourly datasets covering the entire year of 2017. Also, El-Geziry et al. [22] have utilized datasets of two years (2012-2013) to investigate the variability of sea-level in Safaga harbor, Egypt in relation to metrological conditions and tidal characteristics. Also, Tur et al. [29] have utilized sea level and metrological datasets over 2014-2015 in investigating sea level prediction in Antalya harbor, Turkey.

The second dataset contains hourly metrological data at the four investigated sites over the period 2008-2020 with no gaps. Such dataset has been collected from several online sources, particularly the Automated Surface Observing System (ASOS) and the Automated Weather Observing System (AWOS) projects [33].

Table 1: Available Datasets

(a) Sea Level Data

Site	Data Span	Gaps
Alexandria	2008-2020	None
Port Said	2008-2020	2018
Suez	2016-2020	None
Safaga	2008-2020	None

(B) Metrological Data

Site	Data Span	Gaps
Alexandria Port Said Suez Safaga	2008-2020	None

4. Results and Discussions

The accomplished results have been presented and analyzed in the next four sub-sections.

4.1 Daily Variations

The hourly datasets of sea levels, air temperature, and atmospheric pressures at the utilized four TG have been investigated. The first of January 2020 (as the most-recent dataset) has been selected as a typical day for inspecting the daily patterns of sea level and metrological factors. Starting by studying the variations over the Mediterranean sea at both Alexandria and Port Said, Table 2 summarize the daily variations. It can be noticed that the sea level at Alexandria varies between 0.177 m and 0.380 m with an average equals 0.279 m. While at Port Said, it ranges from 0.288 m to 0.510 m with a mean of 0.403 m. Regarding air temperature at Alexandria, it changes daily from 13.0 ^{o}C to 16.2 ^{o}C with a mean equals 14.3 ^{o}C. At Port Said, the air temperature varies between 12.0 ^{o}C and 17.9 ^{o}C with an average of 14.9 ^{o}C. The atmospheric pressure at Alexandria ranges from 1014.0 hpa to 1019.0 hpa with an average of 1016.2 hpa. At Port Said, it varies between 1017.2 hpa and 1020.8 hpa with a mean of 1019.0 hpa. Fig. 3 and 4 depict the daily variations of such factors at Alexandria and Port Said respectively. It can be noticed that the sea level daily patterns at both sites are semi-diurnal (two maximum and two minimum values) in nature. As expected, the daily patterns of air temperature are diurnal at both sites. However, the atmospheric pressure does not possess a daily pattern.

Table 2: Variations Over the Mediterranean Sea on January 1st, 2020

Item	Minimum	Maximum	Mean
(A) At Alexandria			
Sea Level (m)	0.177	0.380	0.279
Air Temperature (^{o}C)	13.0	16.2	14.3
Atmospherics Pressure (hpa)	1014.0	1019.0	1016.2
(B) At Port Said			
Sea Level (m)	0.288	0.510	0.403
Air Temperature (^{o}C)	12.0	17.9	14.9
Atmospherics Pressure (hpa)	1017.2	1020.8	1019.0

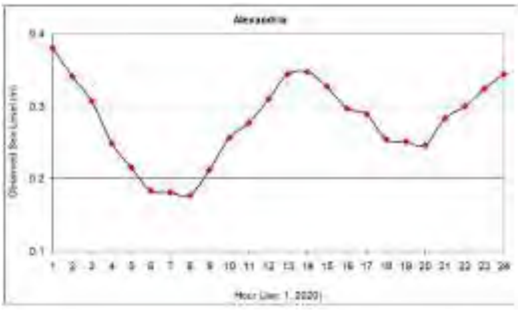

(a)

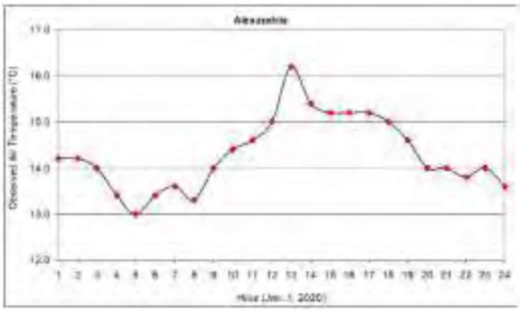

(b)

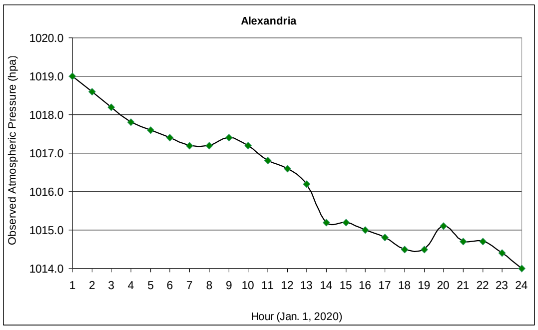

(c)

(a) Sea Level, (b) Air temperature, (c) Atmospheric Pressure

Figure 3: Variations Over Alexandria on January 1st, 2020

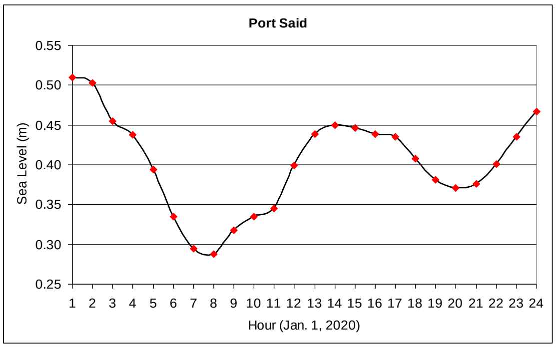

(a)

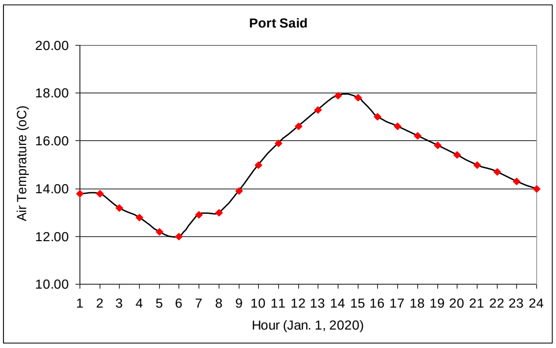

(b)

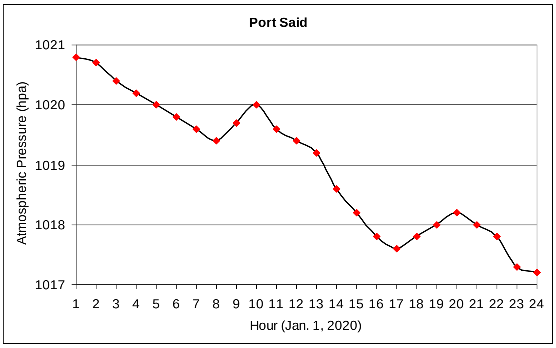

(c)

(a) Sea Level, (b) Air temperature, (c) Atmospheric Pressure

Figure 4: Variations Over Port Said on January 1st, 2020

Next, the variations over the Red sea at both Suez and Safaga have been inspected. Table 3 summarize the accomplished daily variations. It can be recognized that the sea level at Suez varies between 0.536 m and 1.597 m with an average equals 1.044 m. While at Safaga, it ranges from 0.361 m to 1.048 m with a mean of 0.733 m. On the other hand, the air temperature at Suez changes daily between 12.8 ºC and 18.4 ºC with a mean equal 15.2

ºC. At Safaga, the air temperature varies from 13.7 ºC to 21.4 ºC with an average of 17.6 ºC. The atmospheric pressure at Suez ranges from 1017.7 hpa to 1021.3 hpa with an average of 1019.6 hpa. At Safaga, it varies between 1014.3 hpa and 1017.8 hpa with a mean of 1016.1 hpa. Fig. 5 and 6 depict the daily variations of such factors at Suez and Safaga respectively. It can be noticed that the sea level daily patterns at both sites are also semi-diurnal in nature. Additionally, the daily patterns of both air temperature and atmospheric pressure are generally diurnal at both sites.

Table 3: Variations Over the Red Sea on January 1st, 2020

Item	Minimum	Maximum	Mean
(A) At Suez			
Sea Level (m)	0.536	1.597	1.044
Air Temperature (ºC)	12.8	18.4	15.2
Atmospherics Pressure (hpa)	1017.7	1021.3	1019.6
(B) At Safaga			
Sea Level (m)	0.361	1.048	0.733
Air Temperature (ºC)	13.7	21.4	17.6
Atmospherics Pressure (hpa)	1014.3	1017.8	1016.1

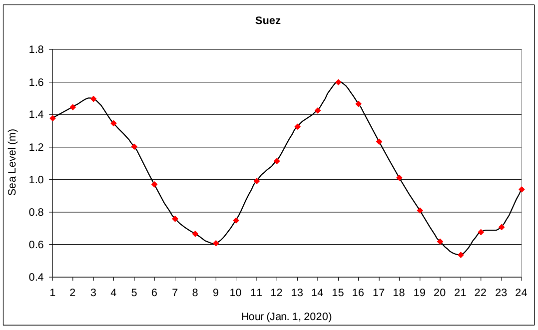

(a)

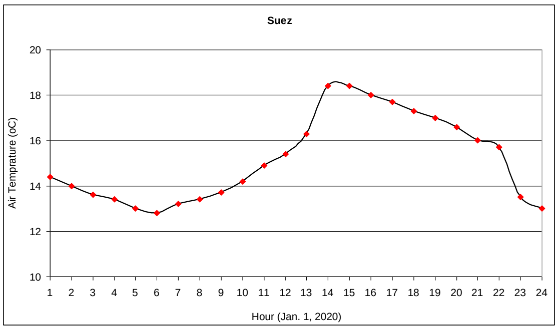

(b)

(c)

(a) Sea Level, (b) Air temperature, (c) Atmospheric Pressure

Figure 5: Variations Over Suez on January 1st, 2020

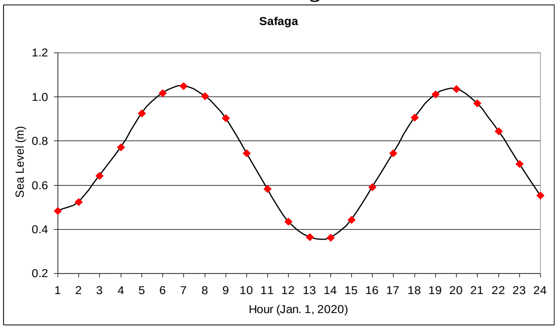

(a)

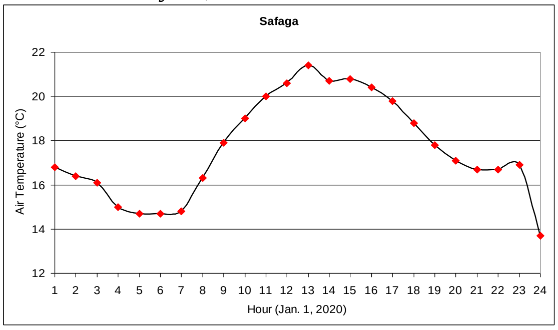

(b)

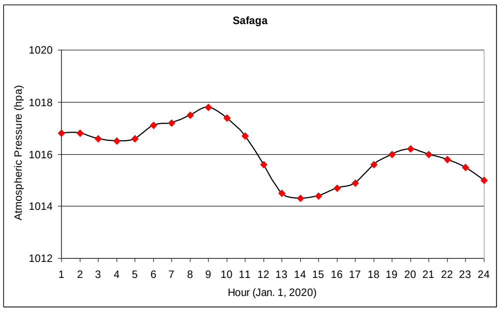

(c)

(a) Sea Level, (b) Air temperature, (c) Atmospheric Pressure

Figure 6: Variations Over Safaga on January 1st, 2020

4.2 Monthly Variations

The hourly data have been averaged to produce the daily values which have been averaged again to obtain the monthly means of sea level, air temperature, and atmospheric pressure at the four investigated locations in 2020. Tables 4, 5, and 6 presented the attained results. Regarding sea level, it can be noticed that it reached the minimum values in February for both Alexandria and Port Said and attained its maximum values in August-September. Over the Red sea, the minimum sea level occurred in January and June for Suez and Safaga respectively and attained the maximum in August and October. Similar results have been reported for other sites on the Mediterranean coasts of Egypt [34]. Furthermore, the air temperature almost follows the same patterns at the investigated sites, while the atmospheric pressure has a slightly different scheme.

A significant remark could be concluded from those tables, particularly concerning the spatial variations of sea level and metrological factors over both the Mediterranean and Red seas. First, from Table 4 and Fig. 7 it can be noticed that the mean annual value of sea level at Alexandria and Port said equal 0.284 m and 0.344 m respectively. That means that the sea level is increasing as going east over the Mediterranean sea. The mean sea level in 2020 at Suez equals 1.161 m. Thus, the sea level of the Red sea is higher than that of the Mediterranean sea at Port Said. Also, it is realized that the annual mean sea level at Suez and Safaga equals 1.161 m and 0.533 m respectively. Similar results have been reported by other studies [16, 32]. El-Geziry and Said [34] have reported the existence of spatial variations of sea level along the Egyptian Mediterranean coast where the mean sea level increase from the west (at Marsa Matruh) to the east (at Port Said) with a difference of 0.35 m.

In addition, comparing the sea level at Suez and Safaga reveals that the Red sea is decreasing as going south. Such an observation has been recognized by other researchers too. For example, regarding the MSL at both Safaga (1.4 m) and Qusseir (0.67 m) on the Red sea, as reported by El-Geziry et al. [16], it can be noticed that it decreases as going south. Also, Shirman and Nelzer [35] have reported the difference in sea level magnitudes and trends between the Mediterranean and Red seas using tide gauge records over 1958-2008. Moreover, comparing the MSL at Safaga on the Red Sea [28] and that of Alexandria on the Mediterranean sea [32] concluded that variations of sea levels between both seas. Also, comparable results have been reported by Alam El-Din and Abdelrahman [36]. Similarly, it can be concluded that the air temperature is increasing as going south while the atmospheric pressure is decreasing.

Table 4: Sea Level Monthly Variations in 2020 (m)

Site	Minimum	Maximum	Mean
Alexandria	0.257 (February)	0.311 (September)	0.284
Port Said	0.217 (February)	0.486 (August)	0.344
Suez	1.050 (January)	1.355 (August)	1.161
Safaga	0.496 (June)	0.563 (October)	0.533

Table 5: Air Temperature Monthly Variations in 2020 (°C)

Site	Minimum	Maximum	Mean
Alexandria	15.8 (February)	28.2 (August)	22.3
Port Said	14.2 (January)	28.7 (September)	22.1
Suez	15.3 (January)	31.2 (August)	24.1
Safaga	17.4 (January)	32.6 (August)	26.0

Table 6: Atmospheric Pressure Monthly Variations in 2020 (hpa)

Site	Minimum	Maximum	Mean
Alexandria	1007.4 (July)	1018.0 (December)	1013.0
Port Said	1008.2 (July)	1021.6 (January)	1014.9
Suez	1005.4 (January)	1020.9 (August)	1012.9
Safaga	1003.3 (July)	1020.0 (January)	1011.3

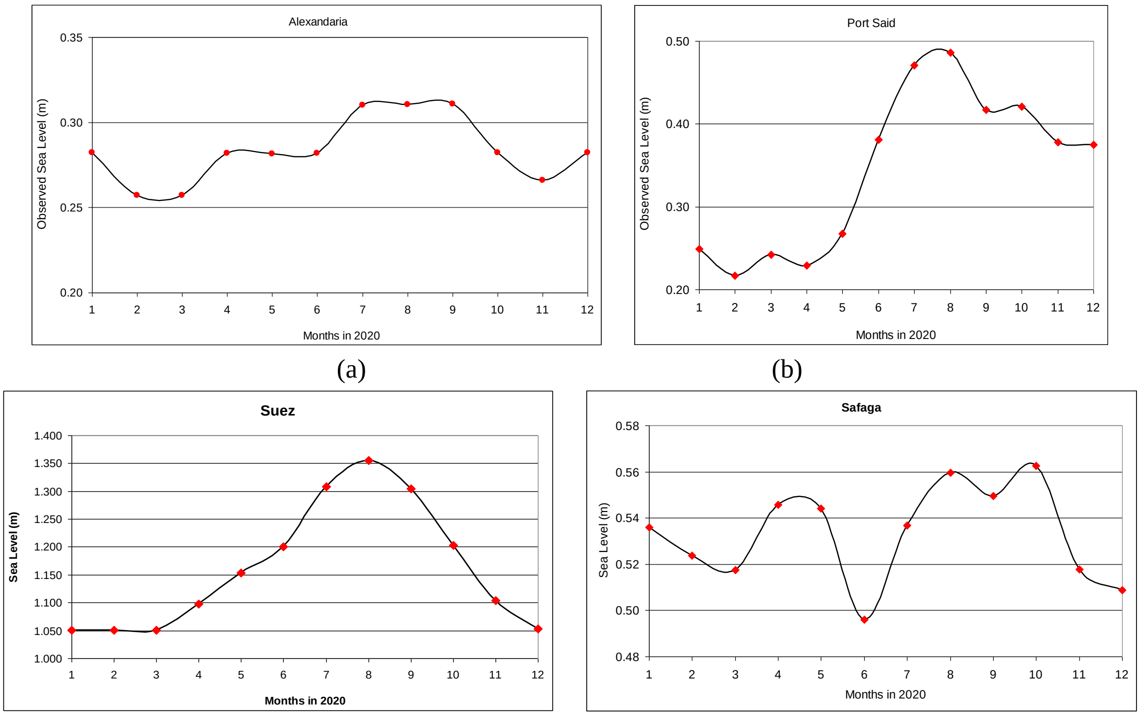

(a) (b)

(c) (d)

(a) Alexandria, (b) Port Said, (c) Suez, (d) Safaga

Figure 7: Sea Level Monthly Variations in 2020

4.3 Annual Variations

Furthermore, the monthly datasets of sea levels, air temperature, and atmospheric pressure have been investigated to reveal the correlation between sea levels and metrological elements. The accomplished findings are tabulated in Table 7. It can be concluded that sea levels have a strong positive correlation with air temperature and a strong negative correlation at Alexandria, Port Said, and Suez sites. At those sites, comparable correlation estimates have been reported by Dawood [37]. However, the estimated correlation at Safaga is moderate, which might need further deep investigation. In this regard, El-Geziry et al. [28] have concluded that the astronomical tides have a higher influence (1.5 times) on the observed sea levels at Safaga than the metrological circumstances.

Table 7: Correlation Between Sea Level and Atmospheric Elements in 2020

Site	Correlation to Air Temperature	Correlation to Atmospheric Pressure
Alexandria	0.80	-0.63
Port Said	0.85	-0.68
Suez	0.94	-0.87
Safaga	0.39	-0.31

4.4 Long-Term Variations

It is worth mentioning that the utilized hourly datasets, particularly sea level, might be considered the most-recent high-frequency data over a long period span in the 21st century from 2008 to 2020 in Egypt. Table 8 and Fig. 8 presented the spatiotemporal variations of sea level in Egypt. From that table, it can be noticed that the Mean Sea Level (MSL) over 2008-2020 equals 0.270 m, 0.459 m, 1.158 m, and 0.517 m at Alexandria, Port Said, Suez, and Safaga respectively. This is a critical fact that the global warming phenomena have significantly raised MSL in Egypt in the last years over the MSL national Egyptian vertical datum at Alexandria defined in 1906. Additionally, this fact necessitates developing a national plan for dealing with the SLR phenomenon and its consequence hazardous environmental impacts. From a geodetic and surveying perspective, such reality should be taken into consideration in the realization of a recent Egyptian vertical datum for mapping and surveying applications.

Table 8: Long-Term Sea Level Annual Variations Over 2008-2020 (m)

Site	Minimum	Maximum	Mean
Alexandria	0.238	0.284	0.270
Port Said	0.449	0.470	0.459
Suez	1.149	1.161	1.158
Safaga	0.480	0.533	0.517

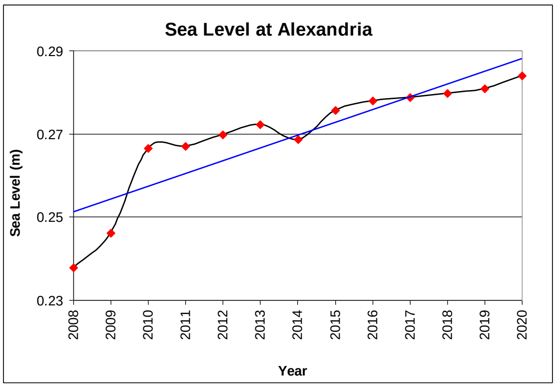

(a)

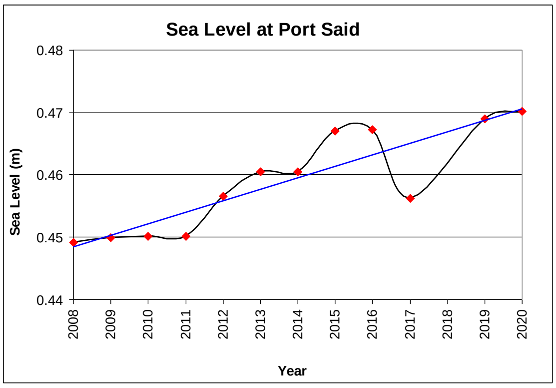

(b)

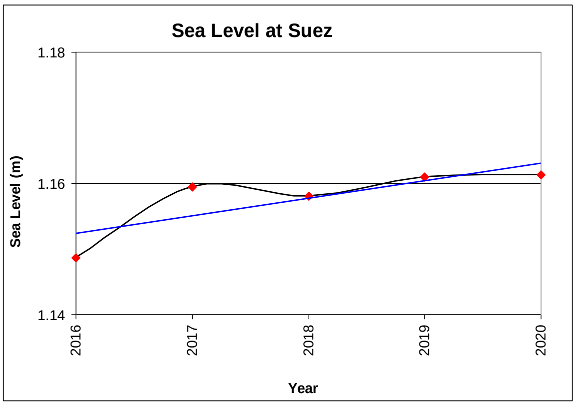

(c)

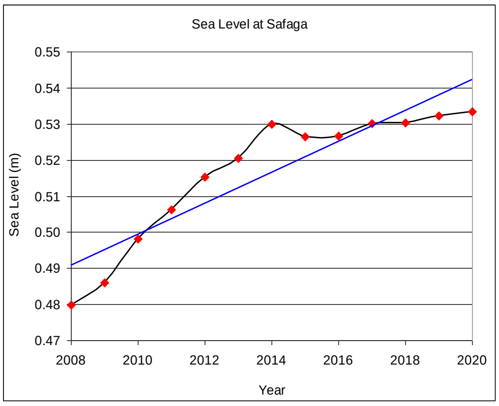

(d)

(a) Alexandria, (b) Port Said, (c) Suez, (d) Safaga

Figure 8: Long-Term Sea Level Variations over 2008-2020

Table 9 and Fig. 9 describe the annual variations of air temperature over the period 2008-2020 at the four investigated locations in Egypt. A common trend of increasing temperature, except at Port Said, could be noticed from this figure. Additionally, Table 10 and Fig. 10 describe the annual variations of atmospheric pressure over 2008-2020 at the examined sites. A common trend of decreasing pressure at Alexandria and Suez and increasing schemes at Port Said and Safaga could be realized from this figure. The utilization of a medium span of metrological data, herein, just gives overall indications about the metrological variations. In this context, it should

be mentioned that long-term metrological datasets, of at least 30-year, might be necessary to precisely investigate the climate changes over Egypt.

Table 9: Long-Term Air Temperature Annual Variations Over 2008-2020 (ºC)

Site	Minimum	Maximum	Mean
Alexandria	21.5	22.4	21.9
Port Said	21.8	22.9	22.1
Suez	23.5	25.1	24.2
Safaga	25.4	27.0	26.1

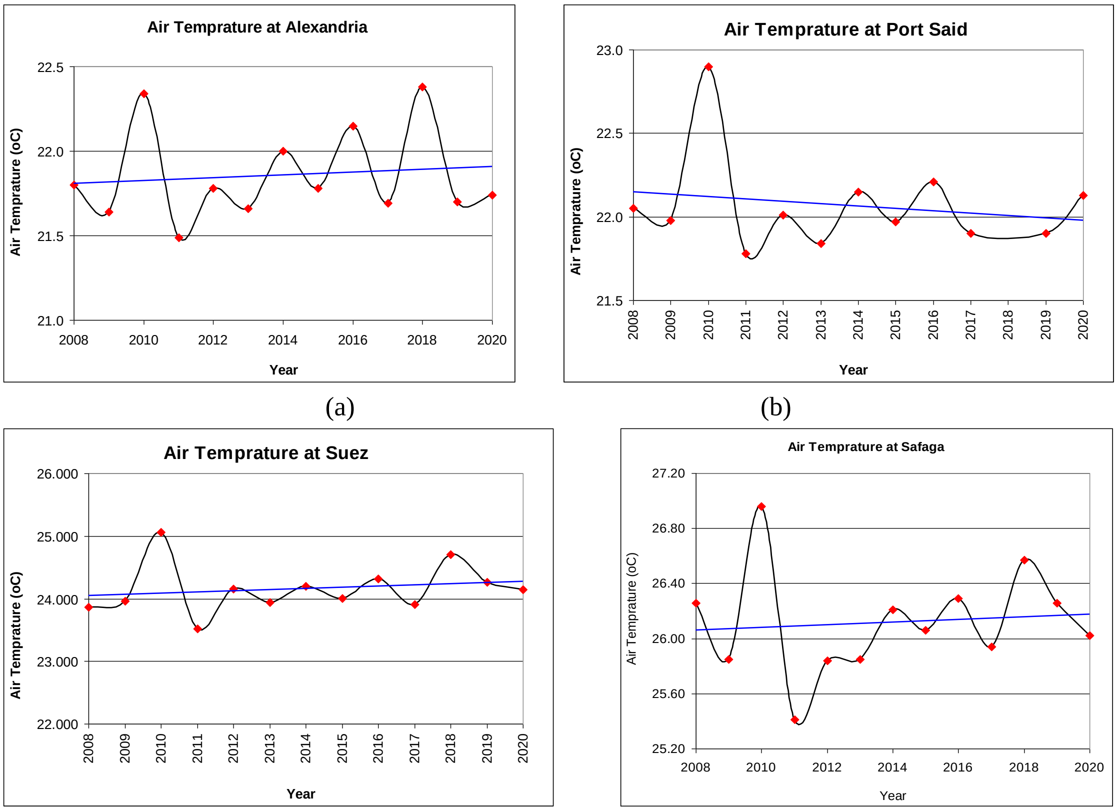

(a) (b)

(c) (d)

(a) Alexandria, (b) Port Said, (c) Suez, (d) Safaga

Figure 9: Long-Term Variations of Air Temperature over 2008-2020

Table 10: Long-Term Atmospheric Pressure Annual Variations Over 2008-2020 (hpa)

Site	Minimum	Maximum	Mean
Alexandria	1012.0	1014.2	1013.3
Port Said	1014.1	1015.9	1014.9
Suez	1012.8	1014.7	1013.8
Safaga	1010.5	1012.3	1011.4

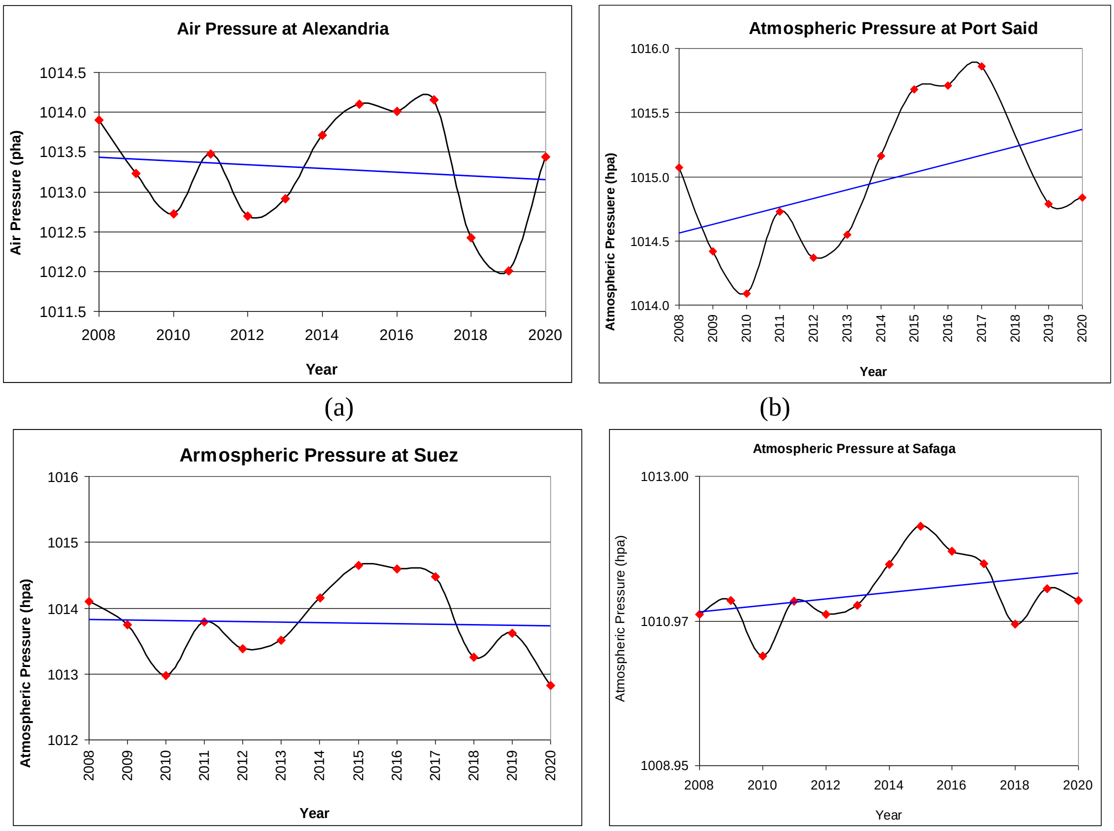

(a) (b)

(c) (d)

(a) Alexandria, (b) Port Said, (c) Suez, (d) Safaga

Figure 10: Long-Term Variations of Atmospheric Pressure over 2008-2020

Modelling the relative SLR is the next processing step where a linear regression model has been applied for the 2008-2020 collected data over the four tide gauges in Egypt. Table 11 presents the accomplished findings. First, it can be noticed the coefficient of determination (R^2) is generally high which concludes that the linear regression produces reliable results. Second, the computed annual rates of relative SRL indicated that sea level is rising over the Egyptian coasts, with variable rates, as a consequence of the global warming phenomena. The rising rate of the Mediterranean sea range from 1.8 mm/year at Port Said to 3.1 mm/year at Alexandria. Regarding the Red sea, the relative SRL varies between 2.7 mm/year at Suez and 4.3 mm/year at Safaga.

Concerning air temperature regression analysis (Table 12), it shows a rising trend at Alexandria, Suez, and Safaga but a decreasing rate at Port Said. Although the R^2 values are very weak, the overall trend is positive at the three sites. In addition, Table 13 presents the results of regression modelling of the atmospheric pressure. It can be noticed that the annual rate is positive at both Port Said and Safaga while it is negative at Alexandria and Suez. Alike, lower R^2 values for regression of both air temperature and atmospheric pressure have been reported for Alexandria over 2007-2018 [38]. These two findings might be attributed to the short time of the utilized metrological data that could not describe such a global phenomenon.

Table 11: Regression of Sea Level Variations Over 2008-2020

Site	Equation	Annual Rate (mm/year)	R^2
Alexandria	SL = 0.0031 Y – 5.9054	+ 3.1	0.77
Port Said	SL = 0.0018 Y – 3.2482	+ 1.8	0.78
Suez	SL = 0.0027 Y – 4.2734	+ 2.7	0.67
Safaga	SL = 0.0043 Y – 8.1382	+ 4.3	0.83

Table 12: Regression of Air Temperature Variations Over 2008-2020

Site	Equation	Annual Rate (ºC/year)	R^2
Alexandria	T = 0.0086 Y + 4.5948	+ 0.0086	0.01
Port Said	T = -0.143 Y + 50.887	- 0.0143	0.04
Suez	T = 0.0187 Y – 13.466	+ 0.0187	0.04
Safaga	T = 0.0096 Y + 6.7515	+ 0.0096	0.01

Table 13: Regression of Atmospheric Pressure Variations Over 2008-2020

Site	Equation	Annual Rate (hpa/year)	R^2
Alexandria	P = -0.0231 Y + 1059.9	- 0.0231	0.02
Port Said	P = 0.0672 Y + 879.61	+0.0672	0.21
Suez	P = -0.0086 Y + 1031	- 0.0086	0.01
Safaga	P = 0.0453 Y + 920.07	+ 0.0453	0.14

5. Conclusions

The global warming phenomenon has caused a significant rise of sea level worldwide in the last century. Since the rate of SLR changes spatially and over time, this paper focuses on giving general signals about sea level and atmospheric elements' variations at four locations in Egypt along with both the Mediterranean and the Red seas over the period 2008-2020. Correlation and relationships between SL and metrological elements, mainly air temperature and atmospheric pressure, have been, also, investigated. It is worth mentioning that, to the best of the authors' knowledge, no previous research have been published using such precise hourly datasets of sea levels and metrological elements covering almost thirteen years at four different sites on the Egyptian coasts. The accomplished findings reveal several important remarks. First, it has been noticed that the sea level daily patterns at the four investigated sites are semi-diurnal in nature. As expected, the daily patterns of air temperature is diurnal and the atmospheric pressure does not possess a daily pattern. Second, it has been concluded that the mean annual value of SL at Alexandria and Port said equal 0.284 m and 0.344 m respectively, which means, similar to results of previous studies, that sea level is increasing as going east over the Mediterranean sea. On the other hand, the mean SL at Suez equals 1.161 m, which indicates that the sea level of the Red sea is higher than that of the Mediterranean sea at Port Said, as other researchers have reported. In addition, it has been realized that the annual mean sea level at Suez and Safaga equals 1.161 m and 0.533 m respectively, which concluded that it decreases as going south. Third, it has been concluded that sea level has a strong positive correlation with air temperature and a strong negative correlation at Alexandria, Port Said, and Suez sites. However, that correlation at Safaga is moderate, which might need further deep investigation.

Although the utilized datasets cover a relatively medium period, the accomplished findings are considered important for coastal management and risk assessment of environmental hazards. Concerning the spatiotemporal variations of sea level in Egypt, it has been noticed that the MSL over 2008-2020 equals 0.270 m, 0.459 m, 1.158 m, and 0.517 m at Alexandria, Port Said, Suez, and Safaga respectively over the Alexandria defined national vertical datum in 1906. Such rises could be attributed to the global warming phenomena in the last years. The rising rate of the Mediterranean sea range from 1.8 mm/year at Port Said to 3.1 mm/year at Alexandria. Regarding the Red sea, the relative SRL varies between 2.7 mm/year at Suez and 4.3 mm/year at Safaga. Concerning air temperature regression analysis, it shows a rising trend at Alexandria, Suez, and Safaga but a decreasing rate at Port Said. Although the estimated values of the coefficient of determination are very weak, as formerly documented by other studies, the overall trend is positive at the three sites. Regarding the pressure trend over the period 2008-2020, it has been noticed that the annual rate is positive at both Port Said and Safaga while it is negative at Alexandria and Suez. Such findings might be attributed to the short time span of the utilized metrological data that could not describe such a global phenomenon.

Overall, the attained findings impose developing a national plan for dealing with the SLR phenomenon and its consequence hazardous environmental impacts. From a geodetic and surveying perspective, such reality should

be significantly considered in the realization of a recent Egyptian vertical datum for mapping and surveying applications.

References

[1]. Oppenheimer, M., Glavovic, B., Hinkel, J. , van de Wal, R., Magnan, A., Abd-Elgawad, A., Cai, R., Cifuentes-Jara, M., DeConto, R., Ghosh, T., Hay, J., Isla, F., Marzeion, B., B., Meyssignac, B. and Sebesvari, Z. (2019) *Sea Level Rise and Implications for Low-Lying Islands, Coasts and Communities*. In: IPCC Special Report on the Ocean and Cryosphere in a Changing Climate [H.-O. Pörtner, D.C. Roberts, V. Masson-Delmotte, P. Zhai, M. Tignor, E. Poloczanska, K. Mintenbeck, A. Alegría, M. Nicolai, A. Okem, J. Petzold, B. Rama, N.M. Weyer (eds.)]. In press.

[2]. Piecuch, C. G., P. R. Thompson, and K. A. Donohue (2016), Air pressure effects on sea level changes during the twentieth century, *Journal of Geophysical Research: Oceans*, (121):7917–7930, https://doi.org/10.1002/ 2016JC012131.

[3]. Oddo, P., Bonaduce, A., Pinardi, N. and Guarnieri, A. (2014) Sensitivity of the Mediterranean sea level to atmospheric pressure and free surface elevation numerical formulation in NEMO, *Geoscientific Model Development*, (7):3001–3015, https://doi.prg/10.5194/gmd-7-3001-2014.

[4]. El-Geziry, T. Dabbous, A. and Abdallah, A. (2020) General pattern of sea level in Safaga and Qussier harbors on the Egyptian Red sea coast, *Arabian Journal of Geosciences*, 13:436, https://doi.org./10.1007/s12517-020-05447-y

[5]. Huang, J., Liu, H. and Yin, K. (2018) Effects of meteorological factors on the temporal distribution of red tides in Tolo harbour, Hong Kong, *Marine Pollution Bulletin*, (126): 419-427, https://doi.prg/10.1016/j.marpolbul.2017.11.035.

[6]. Oppenheimer, M., B.C. Glavovic , J. Hinkel, R. van de Wal, A.K. Magnan, A. Abd-Elgawad, R. Cai, M. Cifuentes-Jara, R.M. DeConto, T. Ghosh, J. Hay, F. Isla, B. Marzeion, B. Meyssignac, and Z. Sebesvari, 2019: *Sea Level Rise and Implications for Low-Lying Islands, Coasts and Communities*. In: IPCC Special Report on the Ocean and Cryosphere in a Changing Climate [H.-O. Pörtner, D.C. Roberts, V. Masson-Delmotte, P. Zhai, M. Tignor, E. Poloczanska, K. Mintenbeck, A. Alegría, M. Nicolai, A. Okem, J. Petzold, B. Rama, N.M. Weyer (eds.)]. In press.

[7]. Parker, A. and Ollier, C. (2015) Sea level rise for India since the start of tide gauge records, *Arabian Journal of Geosciences*, (8):6483-6495.

[8]. Alothman, A., Bos, M., Ferenandes, R., and Ayhan, M. (2014) Sea level rise in the north-western part of the Arabian Gulf. *Journal of Geodynamics*, http://dx.doi.org/10.1016/j.jog.2014.09.002

[9]. Lyszkowicz, A. and Bernatowicz, A. (2018) Geocentric sea level changes at tide gauge station in Wladyslawowo, Presented at the *FIG Working Congress*, Istanbul, Turkey, May 6-11.

[10]. Mengel, M., Levermann, A., Frieler, K., Robinson, A. and Marzeion, B. (2016) Future sea level rise constrained by observations long-term commitment, *PNAS*, 113(10):2597-2602, https://doi.org/10.1073/pnas.1500515113

[11]. Edwards, T. (2017) *Current and future impacts of sea level rise on the UK*, A report to the UK government office for science, https://assets.publishing.service.gov.uk/government/uploads/system/uploads/attachment_data/file/663885/Future_of_the_sea_-_sea_level_rise.pdf, accessed January 2022.

[12]. Dawod, G., Ebaid, H., Haggag, G. and Al-Krargy, E. (2021) An integrated geomatics approach for projecting sea level variations and risks: A case study in the Nile Delta, Egypt, *Journal of Architecture and Civil Engineering*, 6(8):24-38.

[13]. Dawod, G. (2001) The magnitude and significance of long-term sea level rise in Egypt from a geodetic perspective, Proceedings of the *Eleventh International Conference on Environmental Protection*, Alexandria University, Alexandria, May 8-10, 2001, pp. 207-215.

[14]. Dawod, G., Mohamed, H. and Haggag, G. (2019) Relative and absolute sea level rise based on recent heterogeneous geospatial data: A case study in the Nile delta, Egypt, *Journal of Scientific and Engineering Research*, 6(6):55-64.

[15]. Radwan, A., Magdy, M., Rabah, M., Saber, A. and Zaki, A. (2021) Sea level analysis using tide gauge observations at the northern delta coast, Egypt, *NRIAG Journal of Astronomy and Geophysics*, 10:1, 361-371, https://doi.prg/10.1080/20909977.2021.1940742.

[16]. El-Geziry, T., Dabbous, A. and Abdallah, A. (2020) General pattern of sea level in Safaga and Qusseir harbours on the Egyptian Red Sea coast, *Arabian Journal of Geosciences*, 13: 436, https://doi.prg/10.1007/s12517-020-05447-y.

[17]. Zubiera, K. and Eyouni, L. (2020) Investigating the role of atmospheric variables on sea level variations in the eastern central Red Sea using an artificial neural network approach, *Oceanlogia*, (62):267-290, https://doi.org/10.1016/j.oceano.2020.02.002

[18]. Gao, Z., Zhang, Q., Wang, H., Zou, T., Liu, K. and Wu, S. (2016) The impacts of wind and air pressure on fluctuations of the mean Bohai sea level, *Journal of Coastal Research*, (74):13-21.

[19]. Hunicke, B. and Zorita, E. (2006) Influence of temperature and precipitation on decadal Baltic sea level variations in the 20th century, Tellus A: Dynamic Meteorology and *Oceanography*, (58A):141-153.

[20]. Han, M., Cho, Y., Kang, H., Nam, S., Byun, D., Jeong, K. and Lee, E. (2020) Impacts of atmospheric pressure on the annual maximum of monthly sea-levels in the northeast Asian Marginal seas, *Journal of Marine Science and Engineering*, 8, 425, https://doi.org/10.3390/jmse8060425

[21]. Latfa, A. (2021) Influence of atmospheric forces on sea-surface fluctuations in Iraq marine water, northwest of Arabian Gulf, *Arabian Journal of Geosciences*, 14:1639, https://doi.org/10.1007/s12517-021-07874-x

[22]. El-Geziry, T., Dabbous, A., Abdallah, A., and Eid, F. (2021) Temporal variability of sea-level in Safaga harbor, Egypt in relation with metrological conditions and tidal characteristics, *Arabian Journal of Geosciences*, 14:1206, https://doi.org/10.1007/s12517-021-07561-z

[23]. Mohamed, H. (2005) *Realization and redefinition of the Egyptian vertical datum based on recent heterogeneous observations*, PhD dissertation, Department of Surveying Engineering, Shoubra faculty of Engineering, Zagazig University, Egypt.

[24]. Dawod, G., Meligy, M. and Mohamed, H. (2005) Assessment and modelling of sea level rise and metrological changes in Egypt, Proceedings of *Ain Shams first International Conference on Environmental Engineering*, Cairo, Egypt, April 11-12, pp. 573-582.

[25]. Sharaf el Din, S. H. (2015). Variation of sea level on the Egyptian Mediterranean and Red sea coasts, *The International Hydrographic Review*, 52(1):63-73.

[26]. Ibrahim, O. (2021) Study of the sea level variability and storm surges at Mersa Matruh, Egypt, *Arabian Journal of Geosciences*, 14: 1678, https://doi.prg/10.1007/s12517-021-07907-5.

[27]. Visser, H., Dangendorf, S. and Petersen, A. (2015), A review of trend models applied to sea level data with reference to the ‘‘accelerationdeceleration debate’’, *Journal of Geophysical Research: Oceans*, 120, 3873–3895, https://doi.org/10.1002/2015JC010716

[28]. El-Geziry, T. and Dabbous, A. (2021) Behavior of surges in Alexandria eastern harbor, Egypt, *Egyptian Journal of Aquatic Research*, (47):171-178, https://doi.prg/10.1016/j.ejar.2021.02.001.

[29]. Tur, R., Tas, E., Haghighi, A. and Mehr, A. (2021) Sea level prediction using machine learning, *Water*, 13, 3566. https://doi.org/10.3390/w13243566

[30]. Jamali, A., Mustapha, A., and Mostafa, S. (2021) Prediction of sea level oscillations: comparison of regression-based approach, *Engineering Letters*, 29(3):23-29.

[31]. Kumar, V. (2020) *Statistical downscaling of island sea levels in the southwest Pacific: a multiple linear regression approach*, PhD Dissertation, Université Paul Sabatier, Toulouse, France.

[32]. Madsen, K., Høyer, J., Suursaar, Ü., She, J. and Knudsen, P. (2019) Sea level trends and variability of the Baltic sea from 2D statistical reconstruction and altimetry, *Frontiers in Earth Science*, 7:243, https://doi.org/10.3389/feart.2019.00243

[33]. NOAA (U.S National Oceanic and Atmospheric Administration) (2021) https://www.ncei.noaa.gov/products/land-based-station/automated-surface-weather-observing-systems, Accessed 12 November, 2021.

[34]. El-Geziry, T. and Said, M. (2019) Sea level variations in El-Burullus new harbor, Egypt, Arabian Journal of Geosciences, 12:460, https://doi.org/10.1007/s12517-019-4620-9

[35]. Shirman, B. and Melzer, Y. (2009) Long term monitoring of the Mediterranean and Red sea levels in Israel, Presented at the *FIG Working Week 2009 Conference*, Eilat, Israel, May 3-8.

[36]. Alam El-Din, K. and Abdelrahman, S (2010) Is the rate of sea level rise accelerating along the Egyptian coasts?, Presented at the *International Conference on Coastal Zone Management of River Deltas and Low Land Coastlines*, Alexandria, Egypt, March 6-10.

[37]. Dawood, A. (2017) The effect of sea level rise on Egyptian economy, *Journal of Environmental Science and Engineering*, (6):188-199, https://doi.org/10.17265/2162-5298/2017.04.003

[38]. Mahfouz, B., Osman, A., Saber, S. and Kanhalaf-Allah, H. (2020) Assessment of weather and climate variability over western harbor of Alexandria, Egypt, *Egyptian Journal of Aquatic Biology and Fisheries*, 24(5):323-339.

Arabian Journal for Science and Engineering
https://doi.org/10.1007/s13369-022-07013-y

RESEARCH ARTICLE-EARTH SCIENCES

Development of an Inundation Model for the Northern Coastal Zone of the Nile Delta Region, Egypt Using High-Resolution DEM

Mohammed El-Quilish[1] · Mohamed El-Ashquer[1] · Gomaa Dawod[2] · Gamal El Fiky[1]

Received: 22 September 2021 / Accepted: 1 March 2022
© The Author(s) 2022

Abstract

Egypt is facing several hazardous environmental phenomena, particularly Sea Level Rise (SLR) and land subsidence. It has been considered to be one of the countries most likely to be affected by SLR because of the low elevation of the Nile Delta region's northern coastal zone, like all world Deltas. For that, a GIS inundation model has been generated using an original high accuracy local digital elevation model for the Nile Delta region, Egypt (LDEM) and the SLR data measured by the tide-gauges. This model has been used to determine the vulnerable low laying areas to inundation from future SLR in 2050 and to determine land-use types and percentages that are most likely to be affected in the northern Mediterranean coast of Nile Delta region. Finally, a total Hazard Index Map (HIM) has been produced from combining SLR HIM, and the subsidence HIM for the study area which will present the full danger of the two phenomena on the coastal region. The results have shown that the inundated area calculated from the SLR in 2050 model is about 50 km^2. From the land-use maps, the areas flooded by the sea represent almost 38.40 km^2, 3.80 km^2, 5.20 km^2, and 2.60 km^2 for the urban, agricultural lands, fishing farms, and bare areas, respectively. The authorities and decision makers should pay more attention to the hazardous effects due to the impacts of subsidence and SLR in the Nile Delta region, especially the northern coastal zone. More protection construction such as seawalls and breakwaters should be built at the northern coastal zone of the Nile Delta region vulnerable to inundation of SLR, to prevent the occurrence of the predicted inundation scenarios that could be occurred to this region in the future.

Keywords Sea level rise (SLR) · Hazard Index map (HIM) · Geographic information system (GIS) · Nile delta · Egypt

1 Introduction

SLR relative to the land surface changes has happened repeatedly throughout Earth's history for natural reasons. Relative sea level changes develop due to a complex and dynamic interaction between local, regional and global factors. These factors are: global rise or fall of the eustatic sea-level (world sea-level) surface due to the changes in the volume of mid-ocean ridges, and ocean thermal expansion caused from global warming or climatic change due to the increasing concentrations of greenhouse gases in the atmosphere, regional or seasonal oceanographic processes (winds, storm surges, waves, tsunamis and cyclones), vertical movements of the land (neotectonic effects, Isostatic compaction, oil or groundwater extraction). Ocean thermal expansion has been expected to be the dominating factor behind SLR since it causes sea water to expand when heated, and leads to the melting of glaciers such as Greenland and Antarctica which adds to the rise [1, 2].

The impacts of SLR will not be globally uniform due to the local variations and regional factors in vertical crustal movements (subsidence), topography, wave climatology, long shore currents, and storm frequencies [3]. Low gradient coastal landforms are the most susceptible to inundation including low-lying river Deltas, estuaries, beaches and coastal wetlands, oceanic islands, and coral reefs. Because of the low elevation of the Nile Delta region's northern coastal zone, like all world Deltas, Egypt has been considered to be one of the countries most likely to be affected by SLR [4, 5], and is consequently vulnerable to the direct and indirect impacts of SLR. Possible implications of SLR include:

✉ Mohammed El-Quilish
mayd_007@yahoo.com

1 Construction Engineering and Utilities Department, Faculty of Engineering, Zagazig University, Zagazig, Egypt

2 Survey Research Institute, National Water Research Center, Giza, Egypt

Published online: 02 July 2022

- Acceleration of shoreline changes due to erosion and accretion
- Increased flooding due to increased storm surge, high tides, windstorms, and wave damage
- Direct inundation of wetlands and estuaries
- Saltwater intrusion and contamination (salinization) of soil, coastal lagoons, Nile River, and groundwater aquifer
- Damage to urban centers and threats to socioeconomic activities which are considered a major Gross Domestic Product (GDP) contributor of Egypt such as: agriculture lands, fisheries productivity, tourism, industrial activities, commercial centers, trading and transportation centers distributed across a wide range of harbors, human settlements and infrastructure

Researchers are working hard to define the nature of climate change, the rates at which change can take place, and the effects that change may have in the future on SLR to predict its rates. According to the Intergovernmental Panel on Climate Change (IPCC) scenarios, models of global climate have predicted that by the end of the twenty-first century, a global SLR of between 0.18 and 0.59 mm/year will occur [6]. Several tide gauges have been established in Egypt to monitor the variations of sea level [e.g., 7]. In other studies, the vulnerability of the northern coast of Egypt, in general, and the Nile Delta in particular, to inundation by SLR has been repeatedly considered [e.g., 8]. Frihy [1] have integrated the main factors that affect the Egypt's Nile Delta—Alexandria region (erosion and accretion patterns, topography, subsidence rates and relative SLR) to determine the degree of vulnerability to coastal erosion assuming a mean SLR ranging between 1.6 and 2.3 mm/year. They have also conducted a degree of vulnerability analysis to better locate which sectors for their study area need to be evaluated and adapted to possible SLR. Their Results have revealed that not all of The Nile Delta's coastal zone have been vulnerable to accelerated SLR at the same level and that the Nile Delta-Alexandria coast can be categorized into vulnerable (30%), invulnerable (55%) and coastal stretches artificially protected (15%). Frihy and El-Sayed [9] have established, analyzed, and ranked risk areas to suggest adaptation measures to mitigate the SLR's impact along the Egyptian Mediterranean coast based on analysis of vulnerability in society and biophysics. Hassaan and Abdrabo [10] have identified land use areas susceptible to flooding by SLR based on the latest SLR scenarios, using GIS techniques by the year 2100. Their results have indicated that, under various SLR scenarios, approximately 37.96% of the total area of the Nile Delta Coastal Governorates would be vulnerable to flooding. They also found 15.56% of the Nile Delta's total area would be vulnerable to flooding due only to land subsidence, even in the absence of any rise in sea level.

Haggag et al. [11] have developed a GIS inundation model taking in consideration sea or lakes connectivity, with DEM as the main input for understanding the impacts on existing coastal systems, infrastructures and properties and suggest some long-term adaptation measures. The SLR's impact has been assessed by mapping the inundated areas with an SLR 0.5, 1.0, 1.5, 2.0 and 2.5 m, respectively. Hassaan [12] has assessed and analyzed the risks of inundation and its implications of the expected SLR up to the year 2100 in the Governorate of Kafr El Sheik, Egypt, using GIS approaches. Solyman et al. [13] have presented an integrated web map solution methodology for accessing the effect of SLR scenarios on the northern coast of EGYPT. They have included important factors in the designing and implementing of the Egyptian SLR as a web GIS application such as functional module, graphic user interface, downloading time, system performance and the technology related. Hasan et al. [14] have performed a future impact assessment of SLR on Egypt's Nile Delta region by assessing the elevations of the SRTM and the ASTER-GDEMV2 DEMes. Ali and El-Magd [15] have processed Satellite images to identify impact of human interventions and coastal processes along the coast of the Nile Delta, Egypt over the 25 years (from 1990 to 2014) using GIS techniques. Elevation in general is considered to be the most critical factor in evaluating the potential impact of SLR on coastal areas of the Nile Delta region because this area is located in a relatively stable tectonic region [16], with a low land subsidence rates that ranges between approximately 6 mm/year to 8 mm/year [17]. Similarly, this region rarely experiences any catastrophically or disastrous large storm surge waves that are generated by frequent Tsunami earthquake events [18]. During the winter season, the average storm surge height is only 0.6 m [19].

Nevertheless, it can be concluded that the quite diverse estimates of the vulnerable areas to inundation in the Nile Delta coastal area could be due to the wide range of SLR hypothetical scenarios. It can be also concluded that despite their diverse estimates, previous studies agreed that the Nile Delta coastal zone would be highly vulnerable to inundation due to the expected SLR, and that inundation caused by SLR can be identified as a significant natural hazard affecting densely populated and built-up areas. It is also very important to mention that, The DEMs used to assess coastal vulnerability to flooding in previous studies have different horizontal and vertical resolutions. However, the quality of DEM used in environmental assessments can have a significant impact on the detection of topographical features and the magnitude of hydrological processes, since DEM is usually used to derive the information about slope, slope aspects, drainage identification, watershed delineation, flow accumulation, and flow direction. In regards to SLR vulnerability assessment, the estimates discussed in previous studies on Nile Delta inundation due to SLR did not pay much attention to improve the

accuracy of the topographical data which is the determinant factor in the accuracy of the inundation results. Thus, most of the available inundation studies are based on the Global DEM (GDEM) dataset.

Due to the insufficient vertical accuracy of the free GDEM available data sources, incorporating such inadequate elevations in SLR analysis will add more uncertainties to the estimation and assessment of the future impact of SLR on the Nile Delta region. For this reason, a coastal study has been performed on the northern Mediterranean coast of Nile Delta region using the SLR data measured by the tide-gauges installed at Alexandria, and Port Said, and the elevation data provided from the high accuracy LDEM generated by El-Quilish et al. [20] and shown at (Fig. 6).

2 Study Area

The studied area investigated in this study covers most of the Nile Delta region north of Egypt, where its boundaries extend from Alexandria in the west to Port Said in the east at longitudinal lines extend, respectively, from 29.6°E to 32.3°E, and from Cairo in the south to the northern Mediterranean coasts in the north at latitude circles extend, respectively, from 30.0°N to 31.6°N, as shown at (Fig. 1). It is bounded by the two branches of the Nile River of Damietta and Rosetta, and extends from both sides to cover coastal areas, with an overall area of about 23,235 km^2. The length of the study area is approximately 180 km from north to south, and it covers about 300 km of coastline at the Mediterranean Sea (18% of the Egyptian Mediterranean coast). Three major coastal lakes "Burullus, Idku, and Mariut" occupy the shoreline. The Suez Canal runs east of the Delta, into its northeast coastal Lake Manzala. The region's topography smoothly slopes north toward the Mediterranean coast, where the elevation difference between Cairo's southern peak and the northern coastal fringes is about 18 m (Fig. 2).

3 Data Acquisition

Several types of geospatial data have been acquired, manipulated, and analyzed in the current study. The following sub-sections present characteristics of each data type. The georeferencing of all the used data has been adjusted to World Geodetic System 1984 (WGS84) as horizontal datum and EGM96 as vertical datum.

3.1 Sea Level Rise

The absolute SLR is the product of the general worldwide (eustatic) rise in sea level in addition to any local land-level changes with respect to a geodetic datum and any regional or seasonal oceanographic processes. It is measured mainly by tide-gauges installed at a specific site. The relative continuation of SLR can be noticed in the year to year average measurements of tide gauge records. The SLR rates used in this study have been estimated from tide gauges installed at Alexandria, and Port Said (from 2012 to 2017) [21] (Fig. 3). Those absolute rates combine relative rise from tide gauge

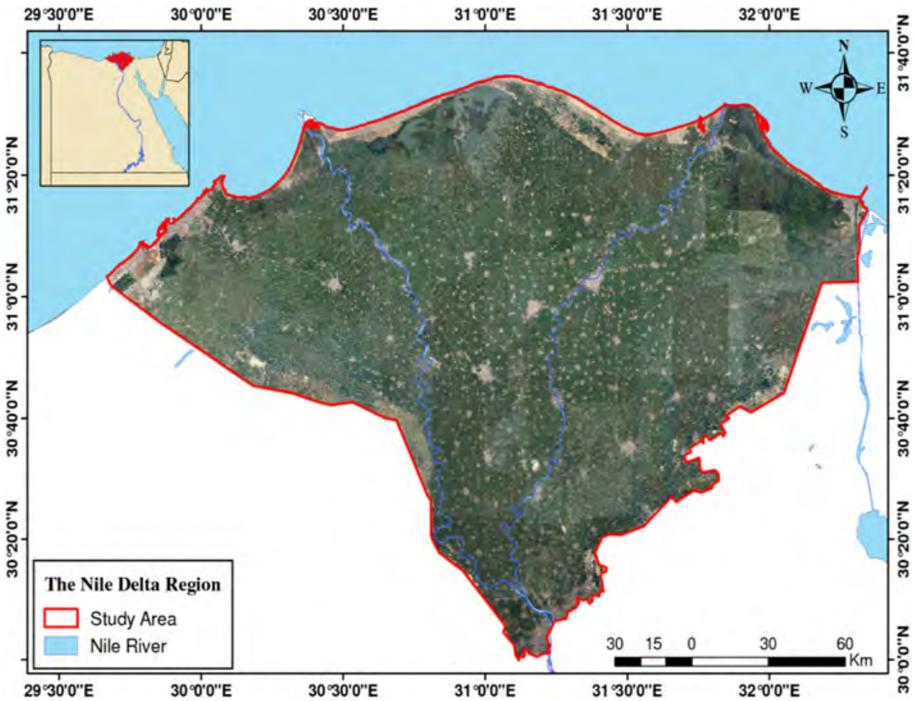

Fig. 1 The study area of the Nile Delta region (WGS84)

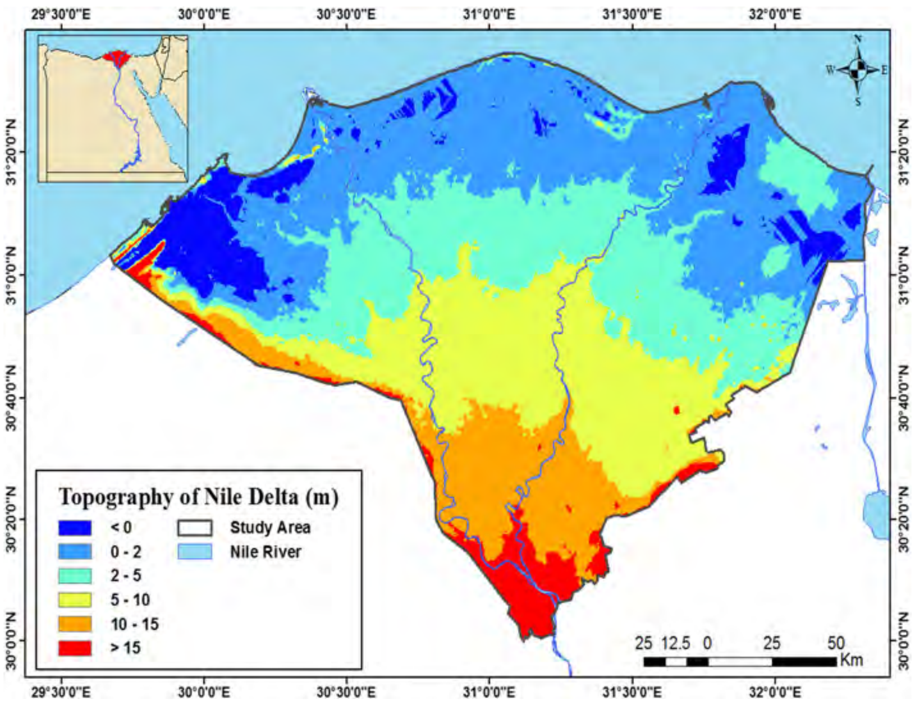

Fig. 2 The Topography of the Nile Delta region (WGS84) [25]

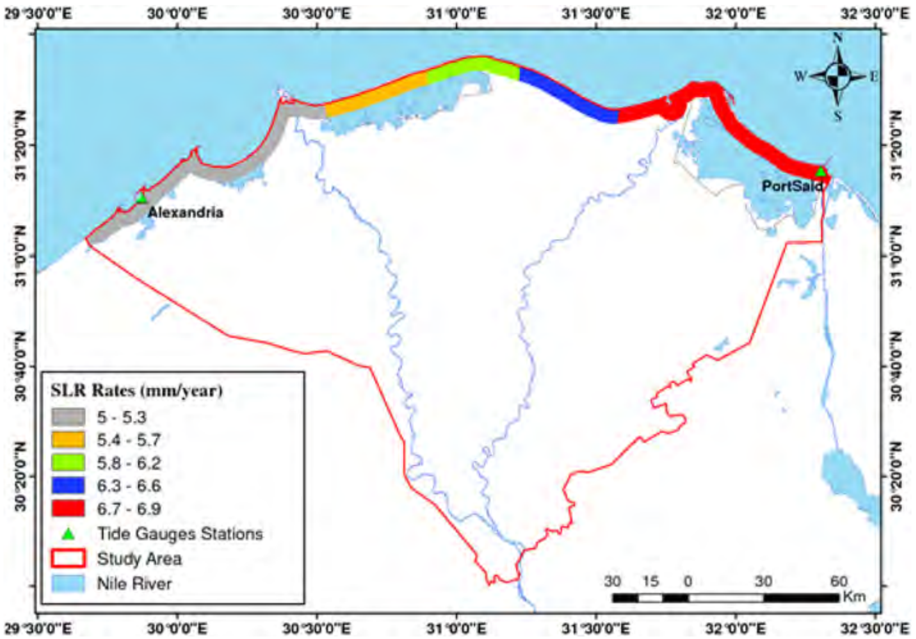

Fig. 3 SLR absolute rates at the coastal zone of the Delta in mm/year (WGS84) (Modified after Dawod [21])

records plus land subsidence rates from GPS data. Measurements indicate that sea level has been continuously rising at a rate of 5.0 and 6.9 mm/year (Table 1), respectively, with an average rate of 6.0 mm/year.

An interpolation process has been performed for the SLR rates points using GIS approaches to produce a SLR raster surface for the coastal zone of the Nile Delta region (Fig. 3). The produced raster of the expected SLR up to 2050 has been calculated by multiplying annual SLR rates by the number of years up to the year 2050. As a result of this step, a new raster surface has been generated representing the SLR for Nile Delta's northern coastal zone in 2050 in meters (Fig. 4).

Table 1 Absolute sea level rise rates 2012–2017

Station	ϕ	λ	Sea level rise rates (mm/year)
Port said	31.26	32.30	6.90
Alexandria	31.18	29.87	5.00

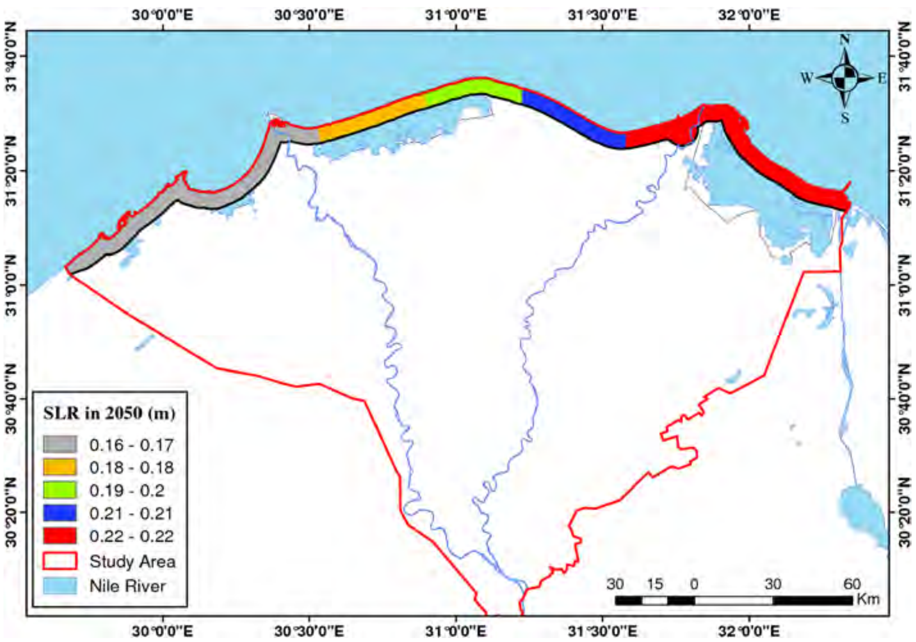

Fig. 4 SLR in 2050 at the coastal zone of the Delta in meters (WGS84)

3.2 Subsidence Rates

Although many geodetic monitoring methods and approaches are used to detect land subsidence and deformation such as tide gauge data analysis, radar remote sensing imageries, and repeated levelling data, GPS proves to be the most accurate and precise approach that can attain the millimeter level of accuracy. In the light of that the subsidence rates used in this study has been based on the work of Mohamed et al. [22], since they have developed a high-precision GPS geodetic techniques for seven stations to monitor land subsidence and horizontal deformation in the Nile Delta area covering the period from 2012 to 2015. The vertical land movement rates at these seven locations range from + 4.9 to − 6.5 mm/year as shown at Table 2, with subsidence exist in Port Said and Tanta, while the remaining four stations show uplifting. Furthermore, a spatial model for the vertical movements in the Nile Delta region (Fig. 5) has been developed using the IDW interpolation method within the GIS. From Fig. 5, it can be concluded that the average vertical movement, over the study area, equals − 0.68 mm/year with SD of ± 2.20. Additionally, it can be realized that the middle region of the Delta suffers from land subsidence, particularly at its eastern fringes, while the north-western and the south-eastern regions show an uplift.

3.3 Local Digital Elevation Model

Since there is no published official precise DEM for Egypt, the LDEM for the Nile Delta region, Egypt developed by [20] has been used to investigate the hazardous effects of SLR phenomena. The LDEM was developed by digitizing over 220 topographic maps and applying nine different spatial interpolation methods (namely; IDW, NNIDW, GPI, SWB, TTR, Kriging, RBF, EBK, and LPI), then comparing their accuracies against eight recent global DEMs (namely; EarthEnv-D90, SRTM1, SRTM 3, ASTER, GMTED2010, GLOBE, GTOPO30, and AW3D30), then using about 200 known GPS/levelling ground control points to evaluate the performance and accuracy of both the global DEMs and the newly developed LDEMs. Their results has shown that that the Kriging-based local DEM is the best and most accurate DEM for this region due to its nearly flat topography and it improved the overall accuracy and reliability of the best available global DEM "EARTHEnv-DEM90" by almost 42%, hence, it is appropriate for geospatial, environmental, and GIS studies in the Nile Delta region, Egypt (Fig. 6).

Table 2 Vertical land movements rates 2012–2015

Station	ϕ	λ	Vertical movement rate (mm/year)
Port said	31.27	32.28	− 4.72
Cairo	30.03	31.22	+ 4.94
Baltim	31.55	31.09	+ 0.71
Abu kebeer	30.73	31.67	+ 3.69
Tanta	30.79	30.99	− 6.51
Abu El_matameer	30.91	30.16	+ 0.55
Matroh	31.20	29.91	− 0.85

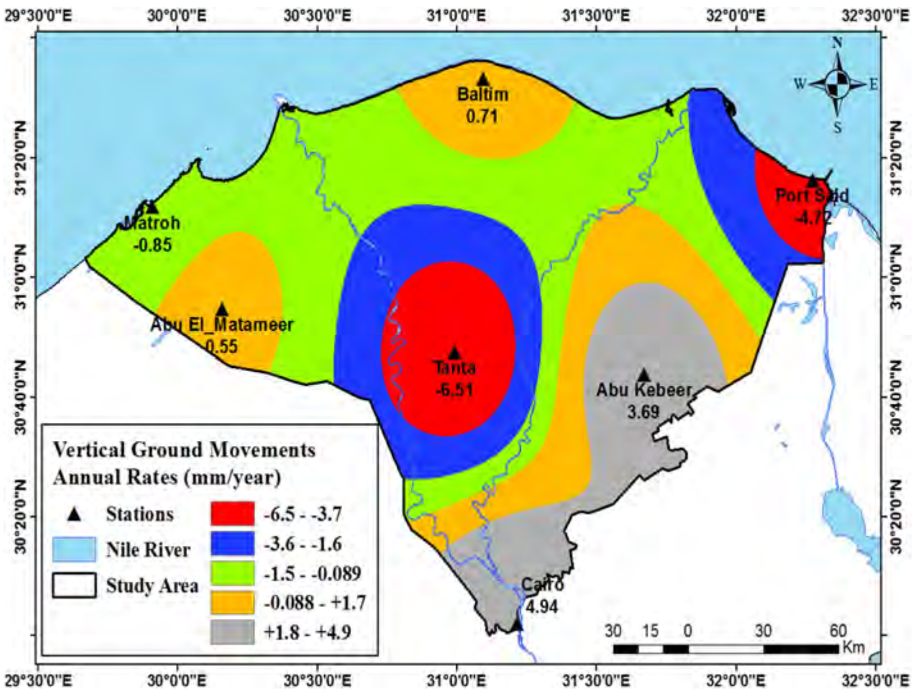

Fig. 5 Vertical Ground Movements Annual Rates in mm/year (WGS84) (Modified after Mohamed et al. [22])

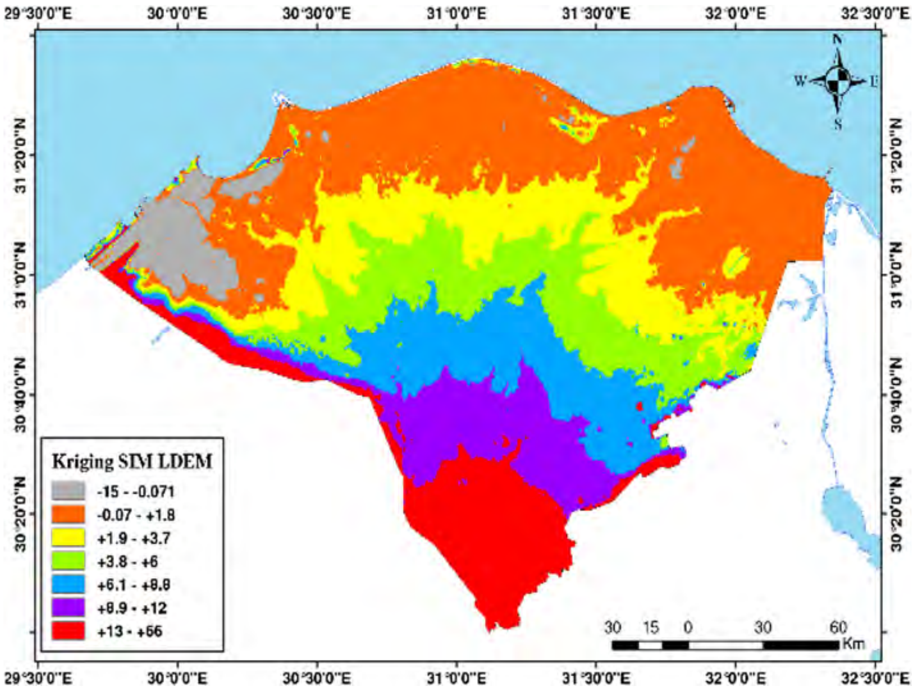

Fig. 6 Best LDEM by Kriging spatial interpolation method (WGS84) El-Quilish et al. [20]

3.4 Urban Land Use Areas

A new 2019 Google satellite map for the Nile Delta region has been used to extract the urban land use and settlement areas using GIS "Image Classification" tool which performs a classification on a series of input raster bands. Figure 7 shows that total urban area amounts 2,759.71 km^2, which represent 11.88% of the total study area.

3.5 Land Use Map

The Land use map for the Nile Delta region has been extracted from a raster map for the global land cover produced in 2013 by the National Mapping Organizations (GLCNMO) [23, 24]. The map covers the whole globe in grids of 500 m (15 s) intervals, and classifies the land cover status of the entire globe into 20 categories. The classification is based on the

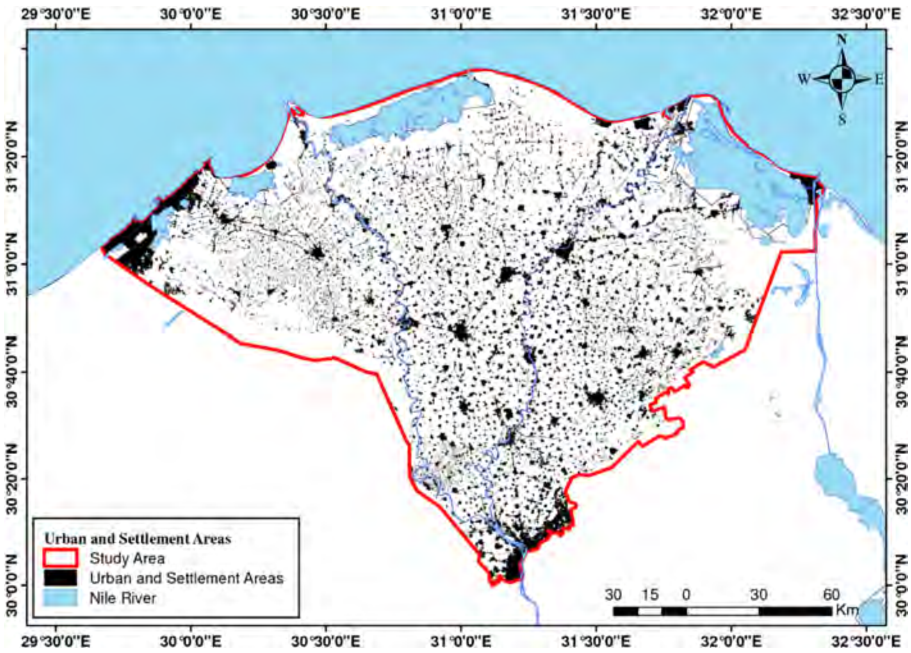

Fig. 7 Urban land use areas (2019)

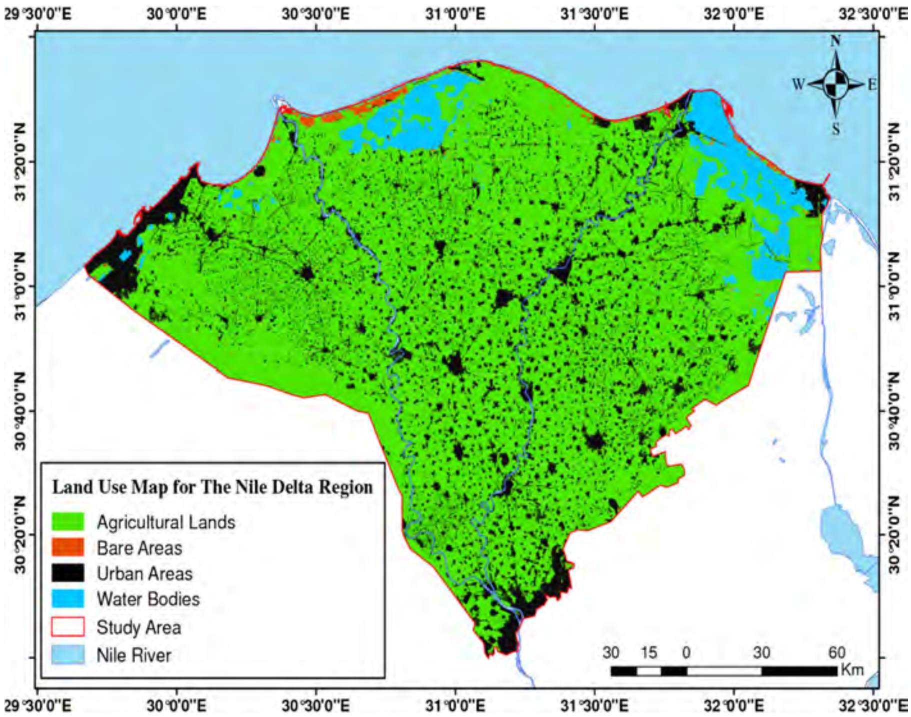

Fig. 8 Land use map for the Nile Delta region (2014)

FAO—developed land cover classification system. The map has been reclassified into 4 major categories: agricultural lands, urban areas, water surfaces, and Bare areas consolidated from sand, gravel or/and rock (Fig. 8). The urban land use map shown at (Fig. 7) has been combined with the global land use map to update the urban areas in the map.

3.6 Protection Against SLR

In the last few years, the Egyptian government has constructed few engineering projects to protect the coastal zones of the Delta form the dangerous effects of SLR to protect the beaches of Alexandria, Port Saied and Al-Arish, Damietta, Kafr E-Shikh, and El-Malaha area east of Port Saied. These protection constructions probably have been a major factor

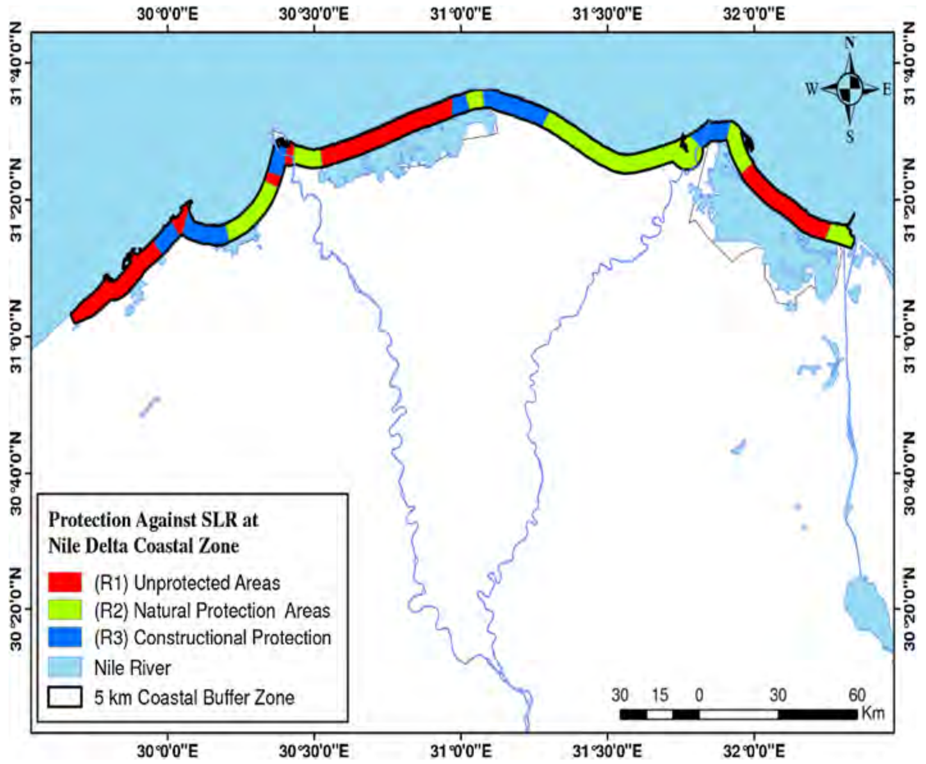

Fig. 9 Protection against SLR (Modified after Frihy et al. [9], and El-Hattab [5])

that assisted in the occurrence of phenomena such as accretion and erosion which had the main responsibility in the general shape of the beach front shoreline of the Delta to take a series of crescent shapes [15].

In this study, the protection areas along the Nile Delta coastal zone has been digitized from the works of Frihy et al. [9], and El-Hattab [5]. These areas have been classified into three main groups: natural protection areas, which are natural high-elevated morphologic features such as sand dunes, constructional protection areas such as seawalls and breakwaters, and finally unprotected areas (Fig. 9).

3.7 Data Management and Manipulation

The process and sequence of data management and manipulation conducted to all the previous set of data is presented in Table 3.

The available utilized geospatial datasets presented and discussed previously will help in developing a GIS model that will increase our understanding particularly for the SLR phenomenon, and eventually assist decision-making process.

4 Hazard Evaluation against SLR and Land Subsidence

This research study aims to generate an inundation model to determine the vulnerable low laying areas to flooding from future SLR in 2050, and to determine land use types and percentages that are most likely to be affected by overlying the inundation map upon the land use coverage. Then after identifying the inundated areas, a total HIM for the study area expected in 2050 is generated. The total HIM is combined from the produced coastal inundation hazard map, and the produced subsidence hazard map for all the Nile Delta region. The generated total HIM will present the full danger of the two phenomena on the coastal region along with presenting

Table 3 Data management and manipulation

No	Data	GIS preparation sequence
1	Sea level rise	Define attributes–Interpolation–Clip to study area–Raster calculator
2	Subsidence rates	Define attributes–Interpolation–Clip to study area
3	LDEM	Clip to study area
4	Urban land use Areas	Georeferencing–Image classification–Raster to Polygon–Clip to study area
5	Land use map	Georeferencing–Image classification–Raster to Polygon–Clip to study area
6	Protection against SLR	Georeferencing–Digitizing–Clip to study area–Define attributes

the effects of the subsidence only on the rest of the Delta. On the one hand, such an evaluation can help formulate effective adaptation options for specific localized SLR impacts. furthermore, such an analysis can significantly contribute to the development of an integrated approach to discuss and address the impacts of SLR and subsidence, helping Egyptian authorities and decision makers to face these challenges and to take proactive action to protect future generations from such serious threats.

The whole processing of hazard evaluation against SLR and land subsidence has been summarized at (Fig. 10).

4.1 Development and Processing of the Inundation Model

Despite the uncertainty associated with the proposed climate change scenarios and expected SLR in previous studies, the impacts of SLR need to be assessed and analyzed according to the precautionary approach. For this reason, a coastal study has been performed on the northern Mediterranean coast of Nile Delta region using the local topography represented by the high accuracy LDEM generated and evaluated by [20] shown a (Fig. 6), and the SLR data measured by the tide-gauges installed at Alexandria, and Port Said shown at (Table 1).

An inundation modeling approach has been used to determine the vulnerability of future SLR based on GIS techniques by using a deterministic line to separate the flooded areas from the dry ones. The areas susceptible to inundation have been identified by first converting the LDEM raster map into a contour map, with a fine contour step of 10 cm. Then, using the 2050 SLR value ranging from 0.16 to 0.22 m, the contour lines produced in the northern coastal zone have been classified, using GIS classification tool, into lines equal to or less than the SLR value and others greater than the SLR values (Fig. 11). Then, a digitizing process has been carried out to detect the contour line that separates the drowning areas from the dry ones. The barrier line that stops the sea advancement to the rest of the Delta regions is always surrounded by low level lines in front of it and some times behind it. The areas surrounded between the front lines that extend to the coast and the barrier line are considered to be the true flooded area.

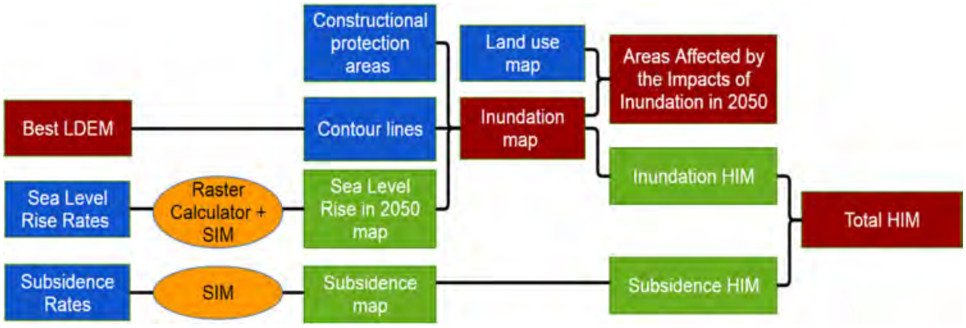

Fig. 10 The processing of hazard evaluation against SLR and land subsidence

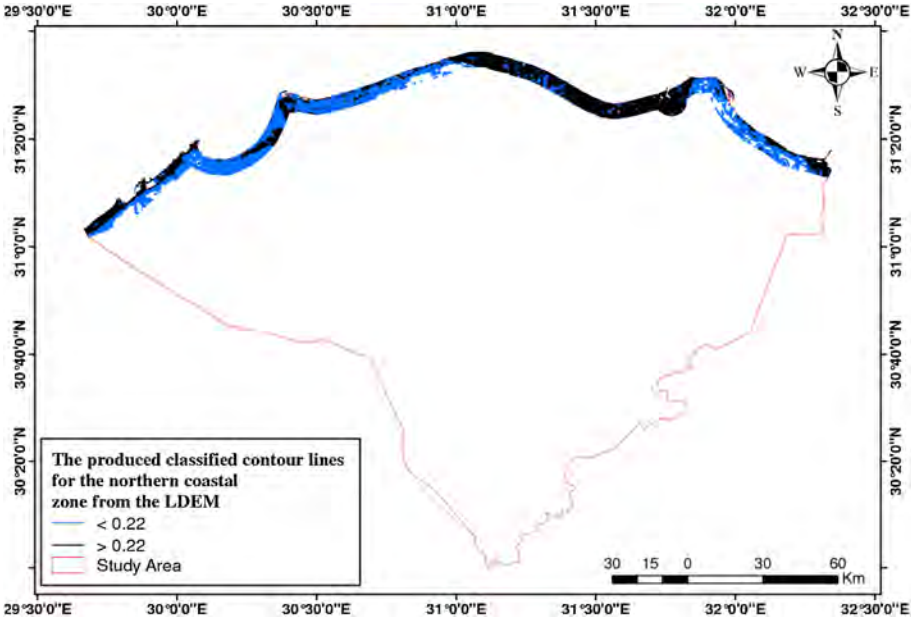

Fig. 11 The produced classified contour lines for the northern coastal zone from the LDEM (WGS84)

Fig. 12 A sample for the barrier line (red) separating low-lying areas (blue) near the coasts from high ones (black) or far away low-lying areas (WGS84)

As for the other areas behind the barrier line, they confuse the automated GIS techniques and make them incapable to detect the right inundated areas, because the barrier line is lost amid the low-lying lines surrounding it (Fig. 12), for that GIS techniques always approximate them together into one huge inundated area, which can be seen in previous studies as their results always exaggerate the actual occurred inundation. An accurate DEM is required to be used to detect the barrier line amid all the low-lying lines. Furthermore, the areas protected by constructions such as seawalls and breakwaters, shown at (Fig. 9), have been overlaid upon the inundation map to remove them, and to produce an inundation map that represents the areas currently exposed to the impacts of SLR in 2050. The final inundation map due to SLR in 2050 is shown at (Fig. 13). According to the available data the inundated area calculated from the SLR in 2050 model is about 50 km^2 representing 0.25% of the total study area.

Table 4 Areas affected by the impacts of inundation in 2050

No	Type of land	Area (km^2)
1	Agriculture land	3.8
2	Bare area (gravel, rock)	2.6
3	Fishing farms	5.2
4	Urban area	38.4
Total	50	

Finally, the inundation map projected for SLR in 2050 is overlaid upon the land use coverage to determine land use types that are most likely to be affected by the impacts of inundation. This has been intended to identify those land uses and other assets that would be vulnerable to inundation. The areas affected by the impacts of inundation in 2050 are shown at (Table 4). The urban areas flooded by the sea represent the major affected type of lands covering almost 38.40 km^2, as for the other flooded areas including agricultural lands, fishing farms, and bare areas, consolidated with sand, gravel, and/or rock, cover almost 3.80 km^2, 5.20 km^2, and 2.60 km^2, respectively.

The inundated and protected areas due to the SLR in 2050 for each one of the northern Nile Delta governorates are presented in (Fig. 14).

4.2 Total Hazard Index Map

The first part of the total HIM map is produced from the inundation map for the northern coastal zone of the study area in

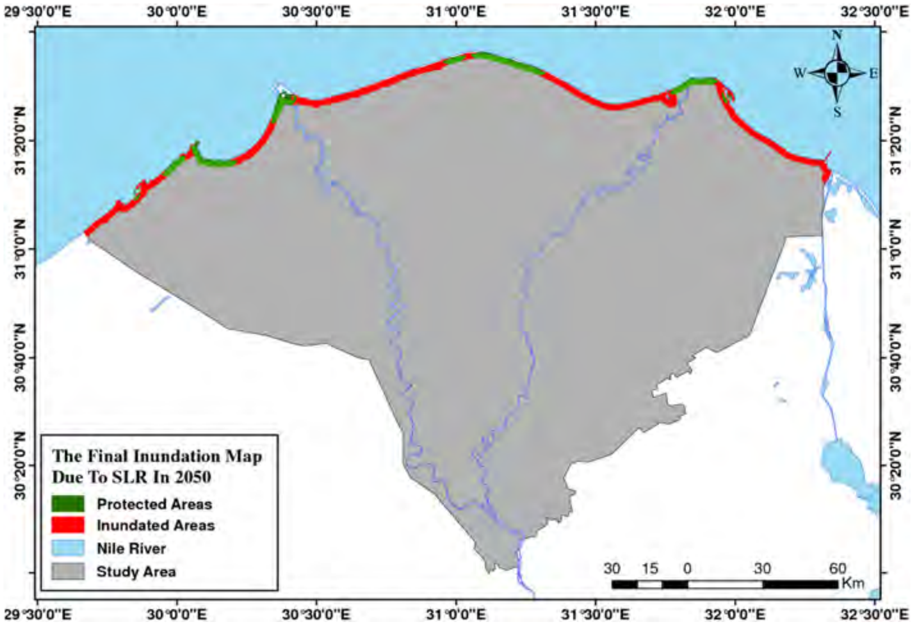

Fig. 13 The final inundation map due to SLR in 2050 (WGS84)

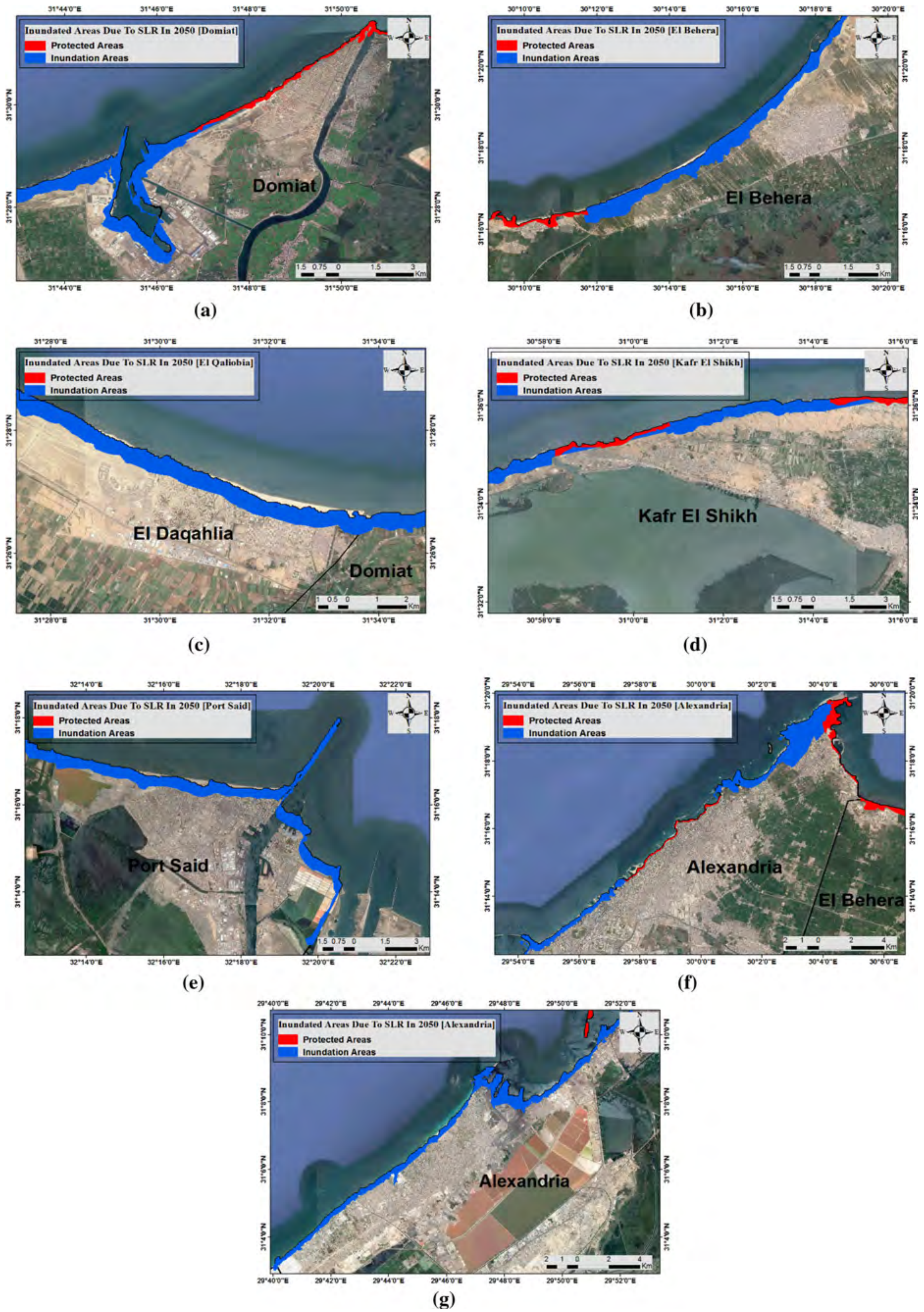

Fig. 14 Inundated Areas Due To SLR In 2050 in **a** Domiat; **b** El Behera; **c** El Qaliobia; **d** Kafr El Shikh; **e** Port Said; **f** Alexandria-North; **g** Alexandria-South

2050, shown at (Fig. 13) by using the using the "Reclassify" tool in ArcGIS to identify risk rank equal to 10 (high risk) for the inundated areas, and risk rank equal to zero (no risk) for the protected areas. The SLR HIM is shown at (Fig. 15).

The second part of the HIM is produced from the subsidence map shown at (Fig. 5) by using the "Reclassify" tool in ArcGIS. In the risk rank for the subsidence rates presented in (Table 5) the subsidence areas are ranked from 1 (low risk) to 10 (high risk) and ranked uplift areas from 1 low risk) to 5 (moderate risk), since the effect of subsidence is considered more dangerous than uplift. The result map is shown at (Fig. 16).

Finally, and due to the considerable risks provided mainly by SLR and the subsidence to the Nile Delta region, a total HIM is produced for the whole Nile Delta region (Fig. 17). The map is a result from combining the SLR HIM map produced for the northern coast of the study area (Fig. 15), and the subsidence HIM (Fig. 16).

5 Conclusions

In this research study a GIS coastal study has been performed on the northern Mediterranean coast of Nile Delta region using the high accuracy LDEM and the SLR data measured by the tide-gauges to generate an inundation model to determine the vulnerable low laying areas to flooding from future SLR in 2050, and to determine land use types and percentages that are most likely to be affected in 2050. A total hazard index map has been developed to depict the hazards of both land subsidence and sea level rise over the Nile delta.

The inundation caused by SLR can be identified as a significant natural hazard affecting densely populated and built-up areas. According to the available data the inundated areas calculated from the SLR in 2050 GIS model are about 50 km^2 representing 0.25% of the total study area. On the one hand, such an evaluation can help formulate effective adaptation options for specific localized SLR impacts, furthermore, such an analysis can significantly contribute to the development of an integrated approach to address the impacts of SLR helping Egyptian authorities and decision makers to

Table 5 Subsidence risk ranking

Subsidence rates range (mm/year)	Rank
(− 6.47, − 5.85)	10
(− 5.85, − 5.2)	9
(− 5.20, − 4.55)	8
(− 4.55, − 3.9)	7
(− 3.90, − 3.25)	6
(− 3.25, − 2.6)	5
(− 2.60, − 1.95)	4
(− 1.95, − 1.3)	3
(− 1.30, − 0.65)	2
(− 0.65, 0)	1
(0, 1)	1
(1, 2)	2
(2, 3)	3
(3, 4)	4
(4, 5)	5

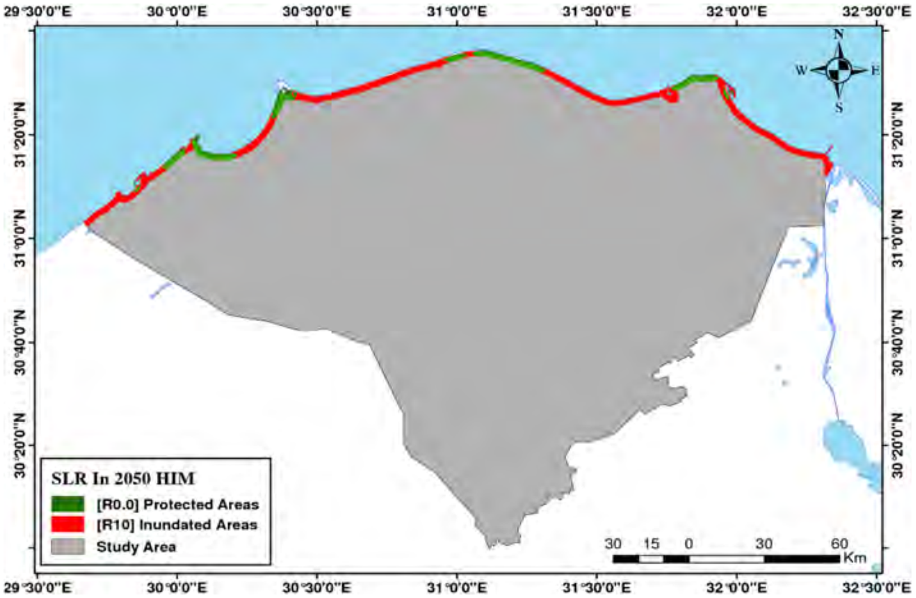

Fig. 15 SLR in 2050 HIM (WGS84)

Fig. 16 Subsidence HIM (WGS84)

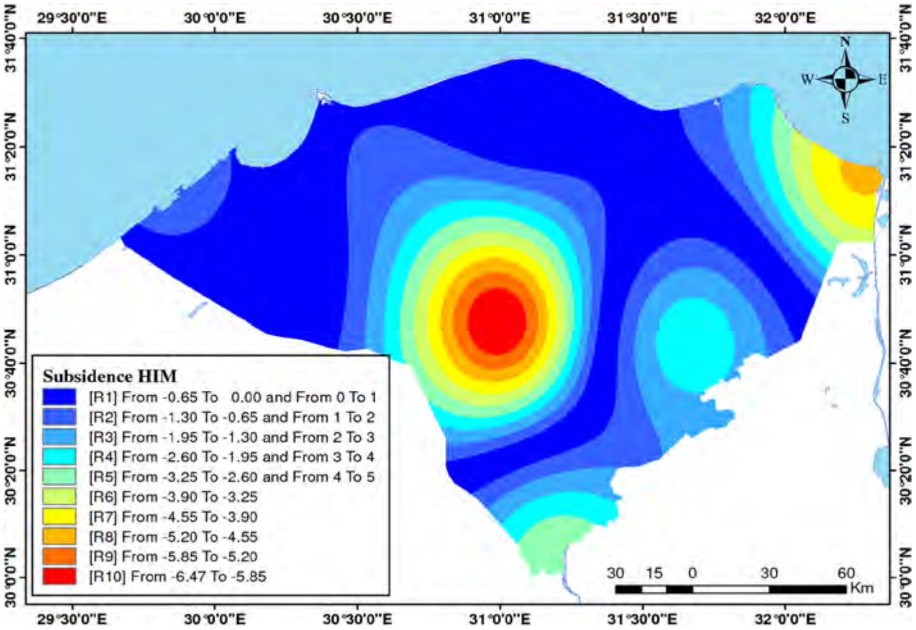

Fig. 17 Total HIM (WGS84)

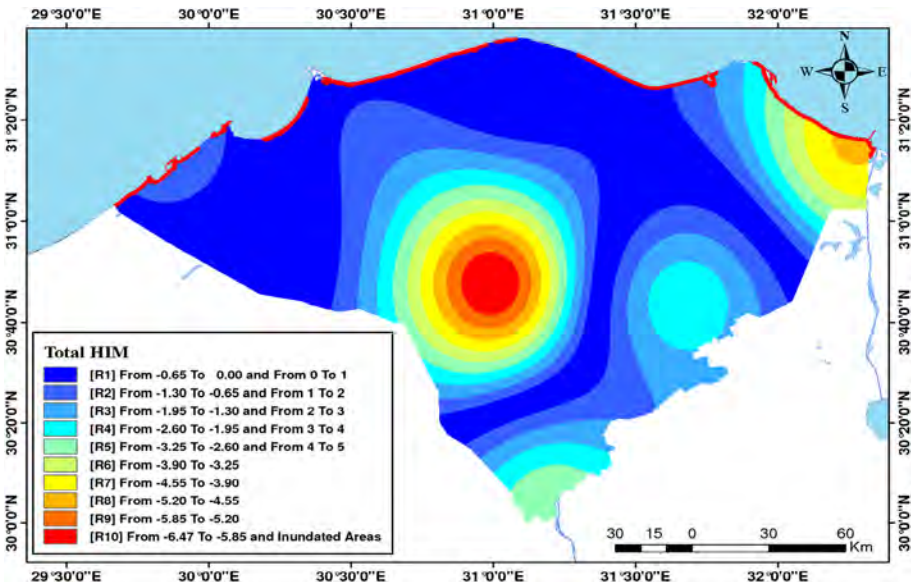

face these challenges and taking proactive action to protect future generations from such serious threats.

The use of automated GIS techniques should not be used to determine the barrier line that separate the flooded areas from the dry ones, as the barrier line is lost amid the low-lying lines surrounding it, for that GIS techniques always approximate them together into one huge inundated area, which can be seen in previous studies as their results always exaggerate the actual occurred inundation.

Total HIM presents the full danger of the SLR and subsidence phenomenon on the coastal region along with presenting the effects of the subsidence only on the rest of the Delta.

Finally, it is recommended that an integrated GIS database of all tide gauge measurements in Egypt should be developed, and the sea level rise should be spatially analyzed in more details to prevent the occurrence of hazardous scenarios that could be occurred in 2050. Also, the authorities and decision makers should pay more attention to the hazardous effects due to the impacts of subsidence and SLR in the Nile Delta region, especially the northern coastal zone, as it is vulnerable to the effects of both the previously mentioned phenomenon. For that more protection construction such as seawalls and breakwaters should be built at the northern coastal zone of the Nile Delta region vulnerable to inundation of SLR, to

prevent the occurrence of the predicted inundation scenarios that could be occurred to this region in 2050.

Funding Open access funding provided by The Science, Technology & Innovation Funding Authority (STDF) in cooperation with The Egyptian Knowledge Bank (EKB).

Open Access This article is licensed under a Creative Commons Attribution 4.0 International License, which permits use, sharing, adaptation, distribution and reproduction in any medium or format, as long as you give appropriate credit to the original author(s) and the source, provide a link to the Creative Commons licence, and indicate if changes were made. The images or other third party material in this article are included in the article's Creative Commons licence, unless indicated otherwise in a credit line to the material. If material is not included in the article's Creative Commons licence and your intended use is not permitted by statutory regulation or exceeds the permitted use, you will need to obtain permission directly from the copyright holder. To view a copy of this licence, visit http://creativecommons.org/licenses/by/4.0/.

References

1. Frihy, O.E.: The nile delta-Alexandria coast: vulnerability to sea-level rise, consequences and adaptation. Mitigat Adaptat Strat Global Change **8**(2), 115–138 (2003). https://doi.org/10.1023/A:1026015824714
2. Marshak, S.; Jack, R.: "Essentials of geology. WW Norton & Company, New York (2013)
3. Gornitz, V.: Global coastal hazards from future sea level rise. Palaeogeogr. Palaeoclimatol. Palaeoecol. **89**(4), 379–398 (1991)
4. Dawod, G.; Mohamed, H.: Estimation of sea level rise hazardous impacts in Egypt within a GIS environment. Proceedings of the Third National GIS Symposium in Saudi Arabia (on CD), Al-Khobar City, Saudi Arabia April 7 - 9 (2008)
5. El-Hattab, M.M.: Improving coastal vulnerability index of the Nile Delta coastal zone, Egypt. J Earth Sci Climat Change **6**(8), 293 (2015). https://doi.org/10.4172/2157-7617.1000293
6. IPCC (2007). "Climate change 2007: the physical science basis: summary for policymakers." Geneva: IPCC, DOI: https://doi.org/10.1260/095830507781076194
7. Dawod, G.M.: The Establishment of the first modern sea level monitoring system in Egypt. Proceedings of the twelfth international conference on environmental protection, Alexandria university, Alexandria, May 14–16, pp. 12–23 (2002)
8. Dawod, G.: The magnitude and significance of long-term sea level rise in Egypt from a geodetic perspective. Proceedings of the twelfth international conference on environmental protection, Alexandria university, Alexandria, May 8–10, pp. 207–215 (2001).
9. Frihy, O.E.; El-Sayed, M.K.: Vulnerability risk assessment and adaptation to climate change induced sea level rise along the Mediterranean coast of Egypt. Mitigat Adaptat Strateg Global Change **18**(8), 1215–1237 (2013). https://doi.org/10.1007/s11027-012-9418-y
10. Hassaan, M.A.; Abdrabo, M.A.: Vulnerability of the Nile Delta coastal areas to inundation by sea level rise. Environ Monitor Assess **185**(8), 6607–6616 (2013). https://doi.org/10.1007/s10661-012-3050-x
11. Haggag, M.; El-Shazly, A.; Rakha, K.: Impact of sea level rise on the Nile Delta, Egypt. Eng. Appl. Sci **60**(3), 211–230 (2013)
12. Hassaan, M.A.: GIS-based risk assessment for the Nile Delta coastal zone under different sea level rise scenarios case study: Kafr EL Sheikh Governorate, Egypt. J. Coast. Conserv. **17**(4), 743–754 (2013). https://doi.org/10.1007/s11852-013-0273-0
13. Solyman, A.A.; El-Hattab, M.M.; Rifai, R.I.; Fakhar, W.M.T.: An integrated web mapping solution to assess the effect of SLR on the Northern Coast of EGYPT: EGSLR thematic cartography for the Society, p. 23–31. Springer, Berlin (2014)
14. Hasan, E.; Khan, S.I.; Hong, Y.: Investigation of potential sea level rise impact on the Nile Delta, Egypt using digital elevation models. Environ Monitor Assess **187**(10), 649 (2015). https://doi.org/10.1007/s10661-015-4868-9
15. Ali, E.M.; El-Magd, I.A.: Impact of human interventions and coastal processes along the Nile Delta coast, Egypt during the past twenty-five years. Egypt. J. Aquat. Res. **42**(1), 1–10 (2016). https://doi.org/10.1016/j.ejar.2016.01.002
16. Meshref, W.: Tectonic framework. The Geolgy of Egypt **8**, 113–155 (1990)
17. Stanley, J.-D.; Clemente, P.L.: Increased land subsidence and sea-level rise are submerging Egypt's Nile Delta coastal margin. GSA Today **27**(5), 4–11 (2017). https://doi.org/10.1130/GSATG312A.1
18. Yalciner, A.C.; Zaytsev, A.; Aytore, B.; Insel, I.; Heidarzadeh, M.; Kian, R.; Imamura, F.: A possible submarine landslide and associated tsunami at the northwest Nile delta, Mediterranean sea. Oceanogr **27**(2), 68–75 (2014). https://doi.org/10.5670/oceanog.2014.41
19. Radwan, A.A.; El-Geziry, T.M.: Some statistical characteristics of surges at alexandria, Egypt. J King Abdulaziz University: Marine Sci **179**(1791), 1–17 (2013)
20. El-Quilish, M.; El-Ashquer, M.; Dawod, G.; El Fiky, G.: Development and accuracy assessment of high-resolution digital elevation model using GIS approaches for the Nile Delta Region, Egypt. Am J Geograp Inform Sys **7**(4), 107–117 (2018). https://doi.org/10.5923/j.ajgis.20180704.02
21. Dawod, G.; Mohamed, H.; Haggag, G.: "Relative and absolute sea level rise based on recent heterogeneous geospatial data: a case study in the Nile delta Egypt. J Scient Eng Res **6**(6July), 55–64 (2019)
22. Mohamed, H.F.; Bahaa, A.S.; Magdy, M.H.; Gomaa, M.D.: "High-Precision GPS Monitoring of the Land Subsidence in the Nile Delta: Status and Preliminary Results". Regional conference on surveying & Development. Sharm El-Sheikh, Egypt, 3–6 October (2015)
23. Tateishi, R.; Hoan, N.T.; Kobayashi, T.; Alsaaideh, B.; Tana, G.; Phong, D.X.: Production of global land cover data-GLCNMO2008. J. Geogr. **6**(3), 99 (2014). https://doi.org/10.5539/jgg.v6n3p99
24. Tateishi, R.; Uriyangqai, B.; Al-Bilbisi, H.; Ghar, M.A.; Tsend-Ayush, J.; Kobayashi, T.; Kasimu, A.; Hoan, N.T.; Shalaby, A.; Alsaaideh, B.: Production of global land cover data–GLCNMO. Int J Digital Earth **4**(1), 22–49 (2011). https://doi.org/10.1080/17538941003777521
25. Embabi, N.S.: "Sand dunes in Egypt, in sedimentary geology of Egypt: applications and economics, Part 1." The sedimentological society of Egypt: 45–87 (2000)

Chapter 1
Print ISBN: 978-81-19039-26-5, eBook ISBN: 978-81-19039-22-7

The Validity of Open-Source Elevations for Different Topographic Map Scales and Geomatics Applications in Egypt and Saudi Arabia

Gomaa M. Dawod [a*] and Ibrahim E. Ascoura [b]

DOI: 10.9734/bpi/npgees/v2/17786D

ABSTRACT

The representation of the Earth' topography in a 3D digital format is a vital constituent in a wide range of geographic, geomatics, environmental, and engineering activities. However, the accuracy of such representations could define its applicability and validity for a specific utilization. This chapter presents an analysis of four open-source Global Digital Elevation Models (GDEMs) and compares them on two topographic profiles (nearly flat, and hills regions) for mapping and geomatics applications in two countries. The main goal is to determine whether GDEMs-based heights, contour intervals, slopes, and topographic profiles are accurate for all topographic map scales, which is a significant problem in mapping operations. For the purpose of illustrating flat and moderate-topography patterns, two case studies—the Nile delta in Egypt and Makkah city in Saudi Arabia—have been used. The investigated GDEMs include the most-recent released models: ASTER v.3, ACE 2, SRTMGL1 v. 3, and NASADEM_HGT v.1 released in 2019 and 2020 with spatial resolutions of 1 and 3 arc seconds. There are 540 accurate Ground Control Points (GCP) available in the Nile delta and 175 in Makkah.

It has been determined based on the available datasets in two study locations that the accuracy of investigated GDEMs over known checkpoints range from ±2.5 and ±5.1 meters in the Nile delta region, while it varies between ±5.1 and ±8.0 meters in the Makkah area. This suggests that the use of GDEMs in topographic mapping varies greatly between spatial areas that are flat and those that are hilly. Therefore, it is advised against utilizing GDEMs to create topographic maps at scales of 1: 25,000 or greater in flat areas and 1: 50,000 or greater in hilly areas. Additionally, the achieved results demonstrated that throughout cross sections up to 30 kilometers in length, no GDEM-based slope matches the real slopes from known GCP. This leads to the conclusion that GDEMs are not the appropriate heights' source for topographic mapping at

[a] *Survey Research Institute, National Water Research Center, Giza, Egypt.*
[b] *Umm Al-Qura Univerity, Makkah, Saudi Arabia.*
**Corresponding author: E-mail: dawod_gomaa@yahoo.com;*

medium and large map scales, and could not be utilized for topographic profiling in precise engineering and geomatics applications. Such findings should be vitally taken into account in mapping and engineering applications not just in Egypt and Saudi Arabia but worldwide as well.

Keywords: Topographic maps; GDEMs; heights; map scales; contour interval.

1. INTRODUCTION

A Digital Elevation Model (DEM) is a Three-Dimensional (3D) representation of the Earth' topography. DEMs could be developed from a wide range of datasets including terrestrial levelling, remote-sensing imageries, and Global DEMs (GDEMs). Local DEMs and GDEMs have been utilized in a wide range of geomatics, environmental, and Engineering applications. Examples of such applications include airport site suitability [1], mapping folds at cave sites [2], morphometric analysis [3], and hydrologic activities [4]. The accuracy of a DEM, local or global, is a key element in assessing its accuracy and applicability.

Topographic maps represent a chief type of maps utilized in numerous geomatics applications such as engineering projects, hydrological modelling, disaster risk assessment, geomorphological and hydrogeological analysis, and environmental applications. Contour lines represent a vital piece of information that appeared on printed and digital topographic maps. They represent the terrain topographic variations and enable estimating heights of required random points. Nowadays, the most frequent form of storage and analyzing height datasets is the Digital Elevation Model (DEM) digital format. It is known that heights used to generate contour lines could be obtained from a wide range of sources including terrestrial surveying, Global Navigation Satellite Systems (GNSS) data, aerial photos, satellite images, and GDEMs. On another hand, Geographic Information Systems (GIS) enables handling, processing, and analyzing DEMs to generate many forms of mapping terrain topography including generating contour lines for a wide range of applications. Some of such applications include the production of flood hazard maps [5], mapping of geological structural lineaments [6], analysis of fluvial landscape in mountainous regions [7], monitoring impacts of sea level rise [8], the production of topographic maps [9], and geoid modelling [10].

In many developing countries, precise national DEM models might be existed but unpublished for public usages. So, researchers usually utilize the available open-source free GDEMs. In the last few decades, many GDEM models, with variable coverages and spatial resolutions, have been produced and made freely accessible over websites. Examples of such GDEMs include the Shuttle Radar Topography Mission (SRTM), the Advanced Spaceborne Thermal Emission and Reflection Radiometer (ASTER), EarthEnv-DEM90, the Global Multi-resolution Terrain Elevation Data 2010 (GMTED2010, the Global Land One-km Base Elevation (GLOBE), the Global 30 arc-second (GTOPO30), and the Advanced Land Observing Satellite (ALOS)-based World 3D - 30m (AW3D30).

The accuracy of open-source GDEMs constitutes a vital role in their utilization for mapping and environmental studies [11]. Thus, many research studies have been focused on estimating the precision and accuracy of GDEMs. For example, Dawod and Al-Ghamdi [12] have examined the reliability of eight GDEM models for geomatics applications in both Egypt and Saudi Arabia. The results showed that their accuracy, in terms of standard deviation over checkpoints, ranges between ±1.9 and ±6.6 meters. Similar results have been reported in other regions such as the USA [13], India [14], Saudi Arabia [15], and China [16].

Rather than the printed or digital topographic maps, several geomatics applications, particularly utilizing GIS, rely on a digital representation of the topography. Such activities need a definite level of height accuracy depending on its objectives and the spatial extent of the study area. Using GDEMs might not appropriate for high-accuracy geomatics applications. A typical example of such a situation is the impact assessment of Sea Level Rise (SLR) in small or moderate regions. It is known that the average anticipated SRL on a global basis in 2081-2100 is estimated to range between 0.40 and 0.63 meters relative to the 1986-2005 level [17]. Monitoring and estimating risk impacts of such small level rise necessitate a high-accuracy terrain representation. Abdel-Aziz et al. [18] have investigated the reliability of a few GDEMs in delineating inundated regions due to sea level rise over the Nile delta area. It has been found that the reliability of three investigated global models, when compared to a high-accuracy local DEM, is less than 20%. Similar results have reported by other researchers in other regions [19]. Another example is the utilization of low-accurate GDEMs in engineering applications. Zhang and Chu [20] emphasized that precise quantification of surface depression storage depend significantly on DEM-based topographic characteristics principally the vertical accuracy and spatial resolution. On the other hand, there exist some geomatics applications that could be performed utilizing the few-meters accuracy of GDEMs. Reconnaissance, project planning for medium or large spatial regions, hydrological modelling, surface runoff estimation, and geoid modelling could be examples of such activities.

Assessing a DEM or GDEM has been investigated mainly from an accuracy point of view. Mostly, a DEM is compared to a set of terrestrial points with known precise elevations and the standard deviations of height discrepancies used as a measure of DEM accuracy level. However, the validity of utilizing DEMs or GDEMs in topographic mapping and engineering applications has not been investigated extensively. Few researches have been performed concerning such an important point. For example, Dawod and Ascoura [21] have investigated the validity of GDEMs foe topographic mapping in Egypt and Saudi Arabia. Similarly, Bhardwaj [22] has examined the utilization of GDEMs in topographic mapping in India.

The current research study aims to investigate the absolute accuracy and the validity of elevation data from different sources for contour generation at several topographic map scales. Additionally, it investigates two other relative topographic factors, namely slope and cross-sections, employed broadly in

numerous geomatics applications. This comprises a vital concern in topographic mapping to investigate if GDEMs-based contours and topographic profiles could be utilized for all map scales and geomatics applications. As far as the authors' concern, it might be the first research study, at least in Egypt, to tackle such a significant subject.

2. STANDARDS AND SPECIFICATIONS OF TOPOGRAPHIC MAPS

Standards and specifications have been developed worldwide for contour lines characteristics including the accuracy of collected data and the methods of representing such important lines. Contour intervals to be shown on a map vary with the required map scale. The term contour interval represents the vertical distance or the elevation difference between two successive contour lines. The scale of a map is the ratio between the length of a line on the map and its actual length on the ground. Traditionally, topographic maps are drawn on medium map scales such as 1: 5,000, 1: 10,000, 1: 25,000, and 1: 50,000. Generally speaking, selecting the appropriate contour interval for a specific map depends on several factors including the map scale, the extent of the surveyed area, the nature of the topography, and the number and distribution of available height dataset, and the purpose of the map itself [23]. A rule of thumb is that the appropriate contour interval on a map might be estimated as three times the Root Mean Square Error (RMSE) of the utilized input height data [24]. The vertical accuracy is represented by RMSE of the utilized height datasets as:

$$RMSE = \sqrt{\frac{\sum_{1}^{n}(P_i - O_i)^2}{n}} \tag{1}$$

where P_i and O_i are the predicted and observed height respectively of point i, and n is the total number of points.

Examples of standards and specifications of topographic maps, particularly for contour lines' characteristics, are summarized herein. The Australian map specifications state that the minimum elevation accuracy of datasets to generate contour lines are 5, 10, 25 meters for map scales 1: 25,000, 1: 100,000 and 1 : 250,000 respectively [25]. In Burundi, the contour intervals for 1: 5,000 and 1: 25,000 topographic maps equal 5 and 10 meters respectively and the vertical accuracy of these contour lines are less than 2.5 and 5.0 meters respectively [26]. Additionally, the suggested contour intervals in India for 1: 5,000, 1 :10,000 1 : 25,000 , and 1 : 50,000 maps equal 1.25, 5.0, 8.0, and 15 meters respectively [27]. Also, the US Geological Survey (USGS) state that the vertical accuracy standard requires that the elevation of 90 percent of all utilized height points must be correct within half of the contour interval [28]. Additionally, the map specifications of the State of Qatar defined the appropriate contour intervals of 2 m, 5 m, and 10 m for map scales 1: 5,000, 1: 10,000, and 1: 200,000

respectively. Additionally, the RMS of heights used in topographic mapping is one-third of the required contour interval [29].

Nationally, the Egyptian Survey Authority (ESA) has published in the year 2020 the updated specifications of topographic maps [30]. For topographic maps' contour lines, the Egyptian standards state that the RMSE of utilized datasets to generate contour lines should be less than one-third of the contour interval. The utilized contour intervals for map scales 1: 10,000, 1: 25,000, 1: 50,000, 1: 100,000, and 1 : 250,000 are 2, 5, 10, 20, 50 meters respectively. If contour lines are not displayed on map scales 1 : 5,000 and 1 : 2,500, spot heights should be plotted on every 100 and 50 m horizontally with vertical accuracy levels equal 0.75 and 0.40 meter respectively. To conclude this issue, Table 1 presents typical examples of contour interval and vertical accuracy used in producing topographic maps with several map scales worldwide.

Table 1. Typical standards of topographic maps

Map Scale	Contour Interval (m)	Vertical Accuracy of Utilized Datasets (m)
1 : 5,000	1.25	±0.4
1 : 10,00	2.0 / 5.0	±0.7 / ±1.7
1 : 25,000	5.0/ 8.0 / 10.0	±1.7 / ±2.6 / ±3.3
1 : 50,000	10.0	±3.3
1 : 100,000	10.0 / 20.0	±3.3 / ±6.7
1 : 250,000	25.0 / 50.0	±8.3 / ±16.7

The relief, slope, and cross-sections constitute important factors in characterizing the topography of a spatial region [31]. The relief, R, is the height difference between the maximum (H_{max}) and minimum (H_{min}) heights of the region. The slop between two points is their height difference divided by the horizontal distance between them. The slope could be evaluated in the units of degrees or as a percentage (Eq. 3):

$$R = H_{\max} - H_{\min} \tag{2}$$

$$S = \frac{\Delta H}{D} x100 \tag{3}$$

Additionally, a new factor called Slope Validity (SV) is proposed, herein, to compare the performance of GDEM-based estimated slopes when compared to precise slopes. It is computed as the percentage of the slope, between two points, from both GDEMs and known accurate heights at those checkpoints, as:

$$SV_{GDEM} = \frac{S_{GDEM}}{S_{known}} x100 \tag{4}$$

Concerning the terrain topography, it could be divided into classes according to several factors such as the slope. Table 2 presents an example of slope-based topography categories [32,33].

Table 2. Topography groups based on slope

Topography Class	Slope Type	Slope %
Lowlands	Gentle	< 3 %
Plateaus	Moderate	3 - 8 %
Upper terraces	Moderate	8 - 12 %
Hills	High	12 - 40 %
Mountains	Very High	> 40 %

3. METHODOLOGY AND AVAILABLE DATA

The utilized GDEMs models, herein, include NASADEM_HGT v. 1, SRTMGL1 v. 3, ASTER v. 3, and ACE2 models. They constitute the most-recent global DEM models at the time of conducting this research. Table 3 summarizes the characteristics of those selected global DEMs, including:

(1) SRTM: The Shuttle Radar Topography Mission (SRTM) is a global DEM, that has two versions: SRTM1 with a spatial resolution of 1 arc second, i.e., approximately 30 meters, and SRTM3 model with a 3 arc second resolution. SRTMGL1 v. 3 [34] has been utilized herein. (download from e.g. https://earthexplorer.usgs.gov/).
(2) ACE2: The Altimeter Corrected Elevations, Version 2 is a global digital elevation model created by synergistically merging the SRTM data set with Satellite Radar Altimetry within the region bounded by 60°N and 60°S. ACE2 was developed at resolutions of 3, 9 and 30 arc-seconds, and 5 arc-minutes [35]. The 3" ACE2, utilized herein (downloaded from https://sedac.ciesin.columbia.edu/data/set/dedc-ace-v2).
(3) ASTER: The Advanced Spaceborne Thermal Emission and Reflection Radiometer (ASTER) is a 1 arc-second global DEM [36]. The ASTER version 3 has been publically released in 2019 (download from e.g. https://asterweb.jpl.nasa.gov/gdem.asp).
(4) NASADEM_HGT v. 1: A GDEM developed by the US National Aeronautics and Space Administration (NASA) in collaboration with German and Italian agencies, and released in 2020. It is based on improved processing and merging of several data sources such as SRTM, ASTER, Ice, Cloud, and Land Elevation Satellite (ICESat) and other sources [37]. It can be downloaded from https://search.earthdata.nasa.gov/.

The main study area is the Nile delta region, Egypt. It extends from Damietta city on the east to Alexandria city along the Mediterranean sea and extends to the south to Cairo (Fig. 1a). 540 GCPs with accurate heights, within ±0.05 meter, have been collected in the Nile delta. The four GDEMs have been downloaded, from their individual website, for this region. First, the topography pattern of the region has been investigated by utilizing the Arc GIS 10 software to convert GDEM-based heights into slope percentages. It has been found that the average

slope of the Nile delta equals 3.1%, (Fig. 1b) which indicates that its topography could be considered as a moderate or plateaus class (Table 2). Consequently, another study area has been added. It represents Makkah city in the Southwest region of the Kingdom of Saudi Arabia (KSA) about 70 km east of Jeddah city on the Red sea (Fig. 2a). 175 GCPs with accurate heights, within ±0.05 meter, have been collected in Makkah. Similarly, the four GDEMs have been downloaded and the topography slopes have estimated (Fig. 2b). It has been found that the average slope of the Makkah equals 17.4%, which indicates that its topography could be considered as a high or hills class.

Table 3. Characteristics of the utilized global DEMs

DEM	Released Year	Spatial Resolution	
		Arcsecond	Meter
ASTER v.3	2019	1"	~ 30
ACE2	2019	3"	~ 90
SRTMGL1 v. 3	2019	1"	~ 30
NASADEM_HGT v. 1	2020	1"	~ 30

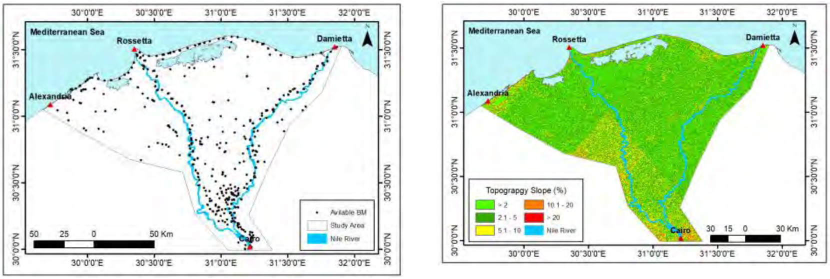

(a) Available Data (b) Topography

Fig. 1. Nile delta study area

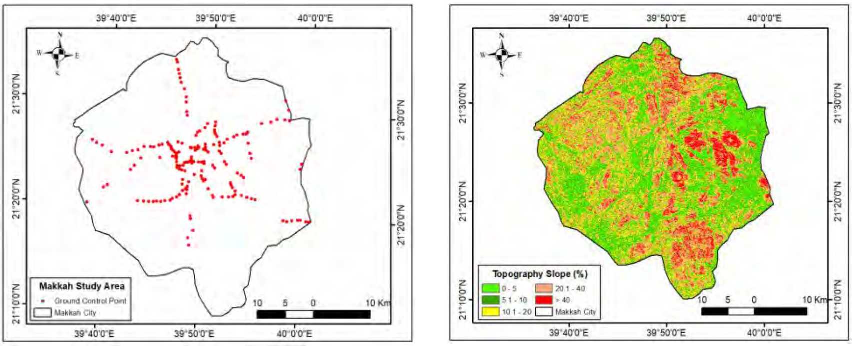

(a) Available Data (b) Topography

Fig. 2. Makkah study area

Having downloading spatial grids of the four investigated GDEMs for both study areas (Figs. 3 and 4), their interpolated heights at the available GCPs have been compared to the known precise heights utilizing the Arc GIS 10 package. The accomplished results are presented and investigated in the next section.

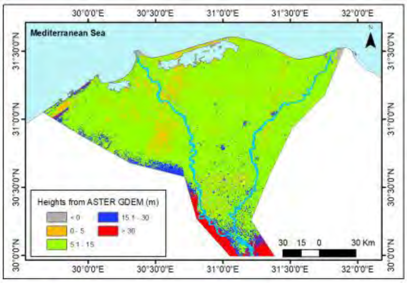

(a) ASTER GDEM

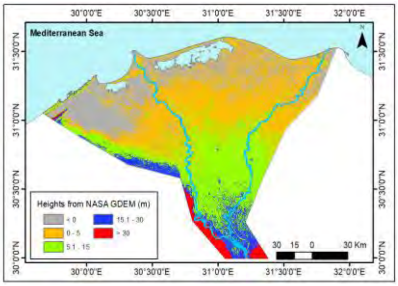

(b) NASADEM GDEM

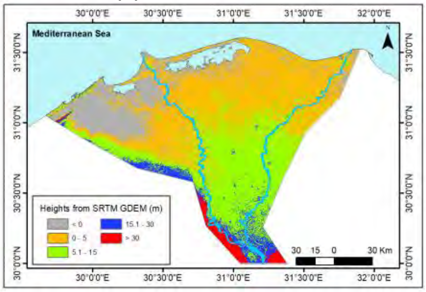

(c) SRTM GDEM

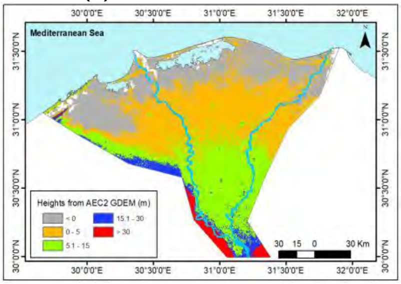

(d) AEC2 GDEM

Fig. 3. Topography of nile delta from GDEMs

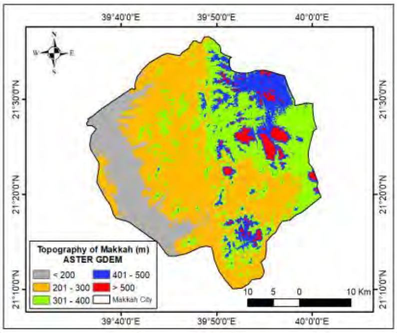

(a) ASTER GDEM

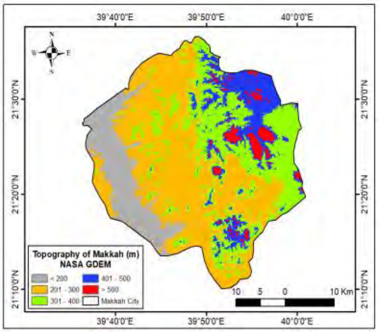

(b) NASADEM GDEM

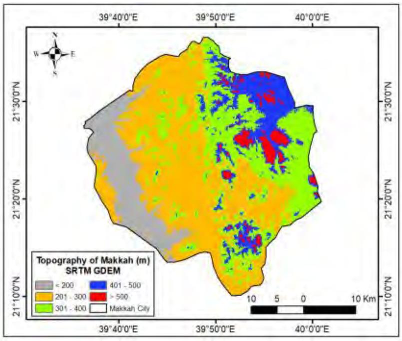

(c) SRTM GDEM

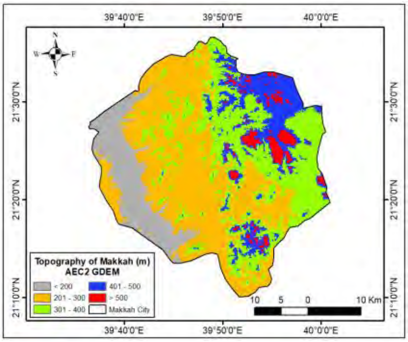

(d) AEC2 GDEM

Fig. 4. Topography of Makkah from GDEMs

4. RESULTS AND DISCUSSION

Table 4 presents the statistics of observed and GDEM-based heights in the Nile delta region. Generally, it can be noticed that the mean height and the relief (Eq. 2) of only the ASTER GDEM are not close to those of the observed heights, while the other three GDEMs produced relatively comparable estimates. Next, GDEMs' errors have been computed at the known heights of GCPs (Table 5). It can be noticed that the RMS (Eq. 1) of AEC2, STRMGL1, and NASADEM models equal ±2.5 meters approximately, while the ASTER model produces the highest RMS of ±5.1 meters. Concerning the average heights error, it can be seen that the NASADEM produce the smallest value of 1.8 meters compared to the other three models. The errors distribution have been plotted in Fig. 5 for all GDEMs, which emphasizes the overall performance of the investigated GDEMs. It can be realized from that figure that the performance of the ASTER model is far from those of the other models.

Table 4. Statistics of height sources in nile delta area

Item	Minimum	Maximum	Relief	Mean	RMS
Observed Heights	-1.925	21.950	23.875	8.532	±5.814
ASTER v.3	-12.495	32.323	44.818	10.680	±5.565
ACE2	-6.659	27.153	33.812	6.244	±6.058
STRMGL1 v.3	-6.900	23.561	30.461	6.561	±6.139
NASADEM_HGT v.1	-5.900	23.922	29.822	6.776	±6.608

Table 5. Statistics of GDEM2 height errors in nile delta area

Item	Minimum	Maximum	Range	Mean	RMS
ASTER v.3	-19.901	18.895	38.796	-2.148	±5.108
ACE2	-11.518	9.248	20.766	2.288	±2.618
STRMGL1 v.3	-6.320	9.500	15.820	1.971	±2.584
NASADEM_HGT v.1	-5.438	9.243	14.681	1.756	±2.521

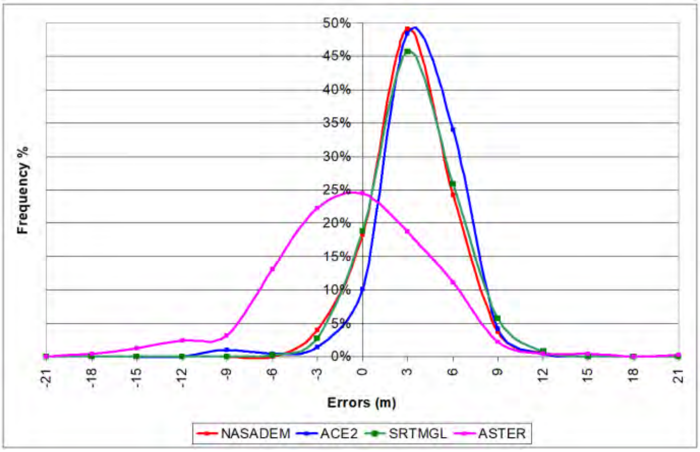

Fig. 5. Histograms of height errors of GDEM2 in nile Delta Area

Comparing the RMS values of the investigated GDEMs (Table 5) with the required vertical accuracy of utilized datasets (Table 1), it can be concluded (Table 6) that all GDEMs are not suitable for developing contour intervals less than 5 meters. That means that such models should not be utilized for topographic mapping of scale 1: 25,000 or larger. For map scale 1: 50,000 and 1: 100,000 with contour intervals 8 or 10 meters, it can be seen that the ASTER model should be avoided while the other three models meet the required specifications. Additionally, it is clear that for map scales 1 : 250,000 or smaller, all investigated GDEMs could be utilized.

Table 6. Validity of GDEM2 for topographic mapping in nile Delta area

Map Scale	Contour Interval (m)	Valid GDEMs
1 : 5,000	1.25	
1 : 10,00	2.0 / 5.0	NA
1 : 25,000	5.0	
		ACE2, SRTMGL1 v.3, NASADEM_HGT v.1
1 : 50,000	8.0 / 10.0	
1 : 100,000	10.0	
	20.0	
1 : 250,000	25.0	ASTER v.3, ACE2, SRTMGL1 v.3,
	50.0	NASADEM_HGT v.1

As mentioned previously, the Nile delta region represents a flat area in terms of topography. Hence, the same steps have been carried out to investigate the performance of GDEMs over Makkah city as a moderate-topography region. Tables 7, 8 and Fig. 6 present the accomplished findings based on the available datasets. It can be noticed from Table 7 that only the SRTMGL1 model produced relief estimates far from the observed precise one. For the mean height error,

only the ACE2 model differs a little bit from the other three GDEMs. However, the results of height differences over known GCPs (Table 8) is more important to analyze the GDEMs precision. It can be realized that NASADEM and SRTMGL produced the smallest RMS values, while the ASTER model gives the largest one. Comparing error histograms over both study areas (Figs. 5 and 6), it can be noticed that the performance of the investigated GDEMs is more precise over the flat region in the Nile delta than that of the moderate-topography region in Makkah city. This conclusion is evident, too, when comparing the RMS values of GDEMs over both regions. In the Nile delta, the RMS ranges from ±2.5 and ±5.0 meters, while in Makkah RMS varies between ±5.2 and ±8.0 meters approximately. Hence, it can be concluded that the accuracy of the investigated GDEMs is almost one order worse in moderate topography regions than flat areas.

Table 7. Statistics of height sources in Makkah area

Item	Minimum	Maximum	Relief	Mean	RMS
Observed Heights	147.135	423.187	274.823	272.146	±59.189
ASTER v.3	144.185	419.008	274.823	272.146	±59.189
ACE2	150.695	422.845	272.150	278.933	±60.068
STRMGL1 v.3	140.482	424.860	284.378	276.082	±59.541
NASADEM_HGT v.1	148.267	419.924	271.657	273.295	±59.005

Table 8. Statistics of GDEM2 height errors in Makkah area

Item	Minimum	Maximum	Range	Mean	RMS
ASTER v.3	-18.456	22.830	41.286	-0.334	±7.996
ACE2	-34.463	5.948	40.412	-7.121	±6.675
STRMGL1 v.3	-16.680	7.820	24.500	-4.270	±5.161
NASADEM_HGT v.1	-13.839	11.219	25.058	-1.483	±5.243

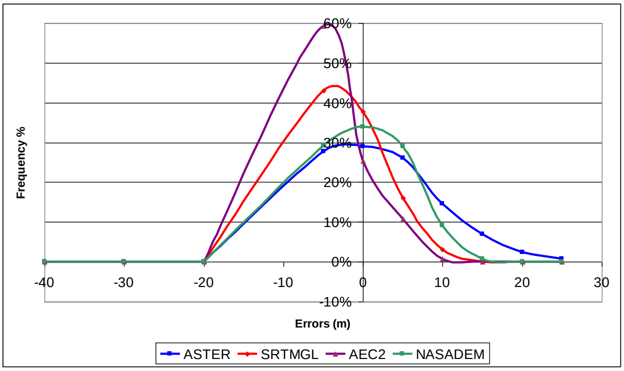

Fig. 6. Histograms of height errors of GDEM2 in Makkah area

Again, a comparison has been performed between the RMS values of the investigated GDEMs in Makkah (Table 8) with the required vertical accuracy of utilized datasets (Table 1). It can be seen from Table 9 that all GDEMs are not suitable for developing contour intervals less than 5 meters. That means that such models are not suitable for topographic mapping of scale 1 : 50,000 or larger with contour intervals equal or less than 10 meters. For map scale 1 : 100,000 with contour intervals of 20 meters, it can be seen that the ASTER model should be avoided while the other three models meet the required specifications. From Fig. 6, it can be seen that ASTER produced the least-precise frequency pattern of errors over checkpoints compared to other GDEMs. Additionally, it is clear that for map scales 1 : 250,000 or smaller with contour intervals more than 25 meters, all investigated GDEMs could be utilized. Furthermore, it can be concluded from Tables 6 and 9 that the utilization of GDEMs in topographic mapping differs significantly between flat and hilly spatial regions.

Table 9. Validity of GDEM2 for topographic mapping in Makkah area

Map Scale	Contour Interval (m)	Valid GDEMs
1 : 5,000	1.25	
1 : 10,00	2.0 / 5.0	
1 : 25,000	5.0	NA
	8.0 / 10.0	
1 : 50,000		
1 : 100,000	10.0	
	20.0	ACE2, SRTMGL1 v.3,
		NASADEM_HGT v.1
1 : 250,000	25.0	ASTER v.3, ACE2, SRTMGL1 v.3,
	50.0	NASADEM_HGT v.1

For analyzing estimated GDEM-based slopes (Eq. 3) and topographic profiles, two cross-sections have been constructed in Makkah city based on the available GCPs. The first one (B1-B2) runs from west to east passing by 28 GCP, while the other cross-section (A1-A2) runs from north to south along 27 GCP (Fig. 7). The length of both cross-sections is approximately 35 kilometers. To investigate the validity of GDEM-based slope estimation along a cross-section, each one is divided by 5-kiolmeters intervals. Equation (4) has been applied to compute the slope validity factor (SV) at each interval for both sections. Fig. 8 depicts the accomplished results, that reveals two important remarks. First, all GDEM-based slopes do not match with the actual slopes from known GCP over cross section's length up to 25 and 30 kilometers for both profiles respectively. Second, GDEM-based slopes for profiles more than 30-kilometers length close to the accurate slopes within a value of ±10% approximately. Hence, it can be concluded that GDEMs should not be utilized for developing topographic cross-sections less than 30 kilometers. Additionally, it can be said that GDEMs-based topographic profiles should not be utilized in engineering and geomatics applications that need precise heights and slopes information. Consequently, the attained findings of the current study, based on the available datasets, showed that GDEMs are

not the appropriate heights' source for topographic mapping at medium and large map scales, and could not be utilized for accurate topographic profiling in precise engineering and geomatics applications.

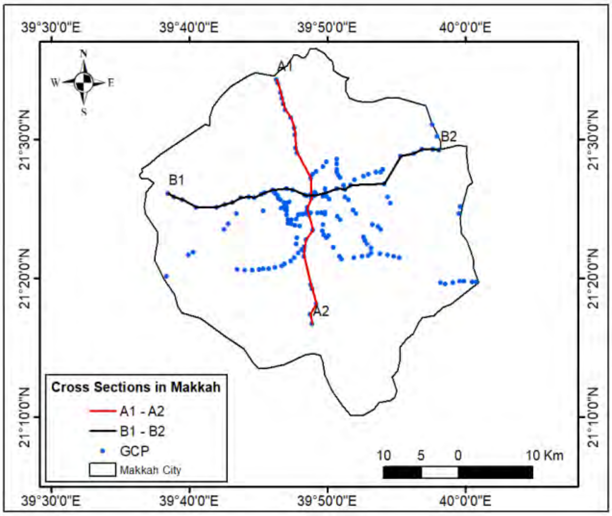

Fig. 7. Cross Sections in Makkah Area

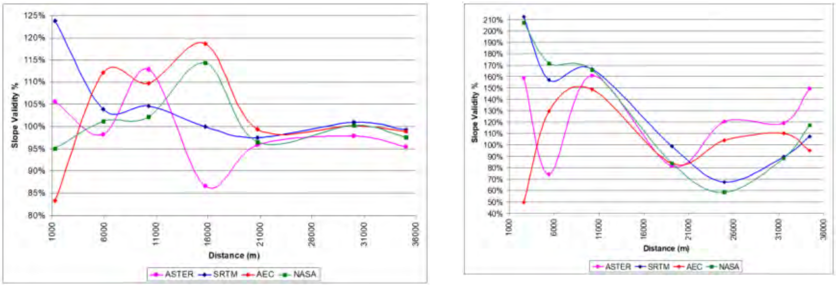

(a) Cross Section B1-B2

(b) Cross Section A1-A2

Fig. 8. Slope validity over cross sections in Makkah Area

5. CONCLUSIONS

Open-source GDEMs have been utilized in the last couple of decades for topographic mapping and several geomatics activities. Specifications of topographic maps rely on the appropriate contour interval on each map scale and the accuracy of the utilized heights information. Examples of topographic mapping standards from several countries have been collected and investigated.

The current study aims to examine the validity and reliability of GDEMs-based heights for topographic mapping at several map scales. Particularly, it investigates the performance of GDEMS for contour intervals, slope estimation, and generating topographic profiles needed for engineering and environmental applications in both Egypt and Saudi Arabia.

Two study areas have been utilized to investigate the performance of four GDEMs for topographic mapping at flat and moderate-topography patters. Based on the available datasets in the two study areas, several important findings have been attained. Using known checkpoints, it has been found that the accuracy of investigated GDEMs range from ±2.5 and ±5.1 meters in the Nile delta region, while it varies between ±5.1 and ±8.0 meters in the Makkah area. That indicates that the utilization of GDEMs in topographic mapping differs significantly between flat and hilly spatial regions. Based on the contour interval required on several topographic map scales, it has been found that GDEMs are not appropriate for generating contour interval less than 10 meters. Consequently, it is suggested not to use GDEMs for developing topographic maps of scale 1 : 25,000 or larger in flat regions and map scale 1 : 50,000 or larger in hilly regions.

In terms of slope estimation and developing a topographic profile, the obtained results revealed that all GDEM-based slopes do not fit the actual slopes from known GCP over cross-section lengths up to 30 kilometers. it has been also observed that GDEM-based slopes for profiles more than 30-kilometers length close to the accurate slopes within a value of ±10% approximately. As a result, it could be concluded that GDEMs are not the appropriate heights' source for topographic mapping at medium and large map scales, and could not be utilized for topographic profiling in precise engineering and geomatics applications. Such results should be seriously considered in mapping and engineering applications not just in Egypt and Saudi Arabia but worldwide too.

COMPETING INTERESTS

Authors have declared that no competing interests exist.

REFERENCES

1. Fawaz E, Mohamed M, Mohamed M. Airport site suitability and development based on multi[1]Criteria in Egypt. Eng Res J. 2022;176:C14-35.
   DOI: 10.21608/erj.2022.273112
2. Abolins M, Ogden A. Application of the global SRTM and AW3D30 digital elevation models to mapping folds at cave sites. Int J Speleol. 2021;50(1):75-89.
   DOI: 10.5038/1827-806X.50.1.2338
3. Bilous LF, Shyshchenco P, Samoilenko V, Havrylenko O. Spatial morphometric analysis of digital elevation model in landscape research.

Presented at the Geoinf 2020 Conference, May 11-14. Kyiv, Ukraine; 2020.
DOI: 10.3997/2214-4609.2020geo124

4. Zaidi SM, Akbari A, Gisen JI, Kazmi JH, Gul A, Fhong NZ. Utilization of satellite-based digital elevation model (DEM) for hydrologic applications: a review. J Geol Soc India. 2018;92(3):329-36.
DOI: 10.1007/s12594-018-1016-5
5. Ogania J, Puno G, Alivio M, Taylaran J. Effect of digital elevation model's resolution in producing flood hazard maps. Glob J Environ Sci Manag. 2019;5(1):95-106.
6. Seleem TA. Analysis and tectonic implication of DEM-derived structural lineaments, Sinai Peninsula, Egypt. Int J Geosci. 2013;04(1):183-201.
DOI: 10.4236/ijg.2013.41016
7. Boulton SJ, Stokes M. Which DEM is best for analyzing fluvial landscape development in mountainous terrains? Geomorphology. 2018;310:168-87.
DOI: 10.1016/j.geomorph.2018.03.002
8. Hasan E, Khan SI, Hong Y. Investigation of potential sea level rise impact on the Nile Delta, Egypt using digital elevation models. Environ Monit Assess. 2015;187(10):649.
DOI: 10.1007/s10661-015-4868-9, PMID 26410824.
9. Ouerghi S, ELsheikh R, Achour H, Bouazi S. Eval validation recent freely-available aster-GDEM. Vol. 2, SRTM. V4.1 and the DEM derived from topographical map over SW Grombalia (test area) in north east of Tunisia. Journal of Geographic Information System. 2015;7:266-79.
10. Al-Karagy E, Dawod G. Optimum combinations of GGM and DEM models for precise national geoid development. Proceedings of Engineering and Technology Innovation; 2021.
DOI: 10.46604/peti.2021.6452
11. Schumann G, Bates P. The need for a high-accuracy, open-access global DEM. Front Earth Sci. 2018;6:1-5.
12. Dawod G, Al-Ghamdi K. Reliability of recent global digital elevation models for geomatics applications in Egypt and Saudi Arabia. J Geogr Inf Syst. 2017;09(6):685-98.
DOI: 10.4236/jgis.2017.96043
13. Kulp S, Strauss BH. Global DEM errors underpredict coastal vulnerability to sea level rise and flooding. Front Earth Sci. 2016;4:36.
DOI: 10.3389/feart.2016.00036
14. Patel A, Katiyar SK, Prasad V. Performances evaluation of different open source DEM using Differential Global Positioning System (DGPS). Egypt J Remote Sens Space Sci. 2016;19(1):7-16.
DOI: 10.1016/j.ejrs.2015.12.004
15. Abdel-Wahab A. Accuracy assessment of ASTER and SRTM. Data w.r.t Lidar Data for Jeddah City- KSA. International Journal of Innovative Technology and Exploring Engineering. 2019;9(2):593-605.
16. Hu Z, Peng J, Hou Y, Shan J. Evaluation of recently released open global digital elevation models of Hubei, China. Remote Sens. 2017;9(3):262.
DOI: 10.3390/rs9030262

17. Church J, Clark P, Cazenave A, Gregory J, Jevrejeva S, Levermann A, et al. Sea level change. Clim Change. The Physical Science Basis. Contribution of Working Group I to the Fifth Assessment Report of the Intergovernmental Panel on Climate Change (IPCC); 2013.
18. Abdel-Aziz T, Dawod G, Ebaid H. DEMs and reliable sea level rise risk monitoring in Nile Delta, Egypt. Discov Sustain. 2020;1(1).
DOI: 10.1007/s43621-020-00006-7
19. van de Sande B, Lansen J, Hoyng C. Sensitivity of coastal flood risk assessments to digital elevation models. Water. 2012;4(3):568-79.
DOI: 10.3390/w4030568
20. Zhang J, Chu X. Impact of DEM sesolution on puddle characterization: Comparison of different surfaces and methods. Water. 2015;7(12):2293-313.
DOI: 10.3390/w7052293
21. Dawod GM, Ascoura IE. The validity of open-source elevations for different topographic map scales and geomatics applications. J Geogr Inf Syst. 2021;13(2):148-65.
DOI: 10.4236/jgis.2021.132009
22. Bhardwaj A. Quality Assessment of merged NASADEM products for varied topographies in India using ground control points from GNSS. Presented at the MOL2NET International Conference Series on Multidisciplinary Sciences, Jan 30. Miami; 2020.
23. Survey of India; Handbook of topography; 2009.
[cited Feb 8 2021].
Available:http://www.iism.nic.in/Documents/soichapter-xi.pdf
24. ASPRS (American Society for Photogrammetry and Remote Sensing). 1st ed, 1st version, Photogrammetric Engineering and Remote Sensing. ASPRS Positional accuracy standards for digital geospatial data. 2015;81(3):A1-A26.
25. Geoscience Australia; National Topographic Database Structure and Specifications; 2021.
[cited Feb 8 2021].
Available:http://www.ga.gov.au/mapspecs/topographic/v6/section1.html#MinimumPlanimetricElevationAccuracies.
26. JICA (Japan International Cooperation Agency). The study on establishing digital topographic database for Bujumbura city, Burundi, A technical Report; 2013.
[cited Feb 8 2021].
Available:https://openjicareport.jica.go.jp/pdf/12121588_01.pdf
27. NDMA (National Disaster Management Authority). National technical document fir establishing cartographic database in India: generation of large scale (1:10,000 and 1:2,000 and leaser) maps for disaster management and planning, A technical report; 2016.
[cited Feb 11 2021].
Available:http://www.ndma.gov.in/sites/default/files/PDF/Technical%20Documents/national-technical-document-for-establishing-cartographic-base-in-india.pdf

28. USGS (US Geological Survey). Map accuracy standards: fact Sheet FS-171-99, A technical report; 1999.
[cited Feb 8 2021].
Available from: https://pubs.usgs.gov/fs/1999/0171/report.pdf
29. Qatar GIS Center. Qatar survey manual version 1, A technical report, Qatar; 2009.
30. ESA (Egyptian Survey Authority). Technical specifications of surveying and mapping: Part 2: Topographic maps, A technical report, Giza, Egypt; 2020.
31. Khal M, Algouti A, Algouti A, Akdim N, A. Stankevich S, Menenti M. Evaluation of open digital elevation models: Estimation of topographic indices relevant to erosion risk in the Wadi M'Goun watershed, Morocco. Geosciences. 2020;6(2):231-57.
DOI: 10.3934/geosci.2020014
32. Cahyaningsih C, Crensonni PF, Suryadi A, lKausarian H, Choanji T, Yuskar Y, et al. Geomorphology and structural geology characterization of landslide prone area in Riau-West of Sumatra Highway. IOP Conf Ser.: Mater Sci Eng. Presented in the International Conference on Science and Innovated Engineering (I-COSINE) IOP conference Series. 2019;536(1).
DOI: 10.1088/1757-899X/536/1/012063
33. Mokarram M, Hojati M. Comparison of landform classifications of elevation, slope, relief and curvature with topographic position index in the south of Bojnoord. Ecopersia. 2016;4(2):1343-57.
DOI: 10.18869/modares.ecopersia.4.2.1343
34. USGS (US Geological Survey). SRTMGL1 V003; 2021a.
[cited Feb 7 2021].
Available:https://lpdaac.usgs.gov/products/srtmgl1v003/
35. Smith R, Berry P. Altimeter corrected elevations. Version 2; 2019.
[cited Feb 9 2021].
Available:https://sedac.ciesin.columbia.edu/data/set/dedc-ace-v2
36. Open Data Catalouge US. ASTER digital elevation model V003; 2021.
[cited Feb 12 2021].
Available:https://catalog.data.gov/dataset/aster-digital-elevation-model-v003
37. USGS (US Geological Survey). NASADEM_HGT: merged DEM global 1 arc second. 2021b;1.
[cited Feb 3 2021].
Available:https://lpdaac.usgs.gov/products/nasadem_hgtv001/

Biography of author(s)

Dr. Gomaa M. Dawod
Survey Research Institute, National Water Research Center, Giza, Egypt.

Research and Academic Experience:

- Solid experience in surveying and mapping disciplines including design, field campaigns, data processing, and analysis for a wide range of applications such as: establishment of geodetic control networks, cadastral and topographic mapping, hydrographic surveying, Geographic Information System (GIS); and crustal movements monitoring studies.
- Participating in numerous surveying and mapping projects on national and regional levels.
- Supervising many academic thesis in Egypt and Saudi Arabia
- Refereed many manuscripts in international journals.

Research Area: His research area includes in Geodetic Networks , Surveying and Mapping , Geographic Information Systems , Environmental Studies.

Number of Published papers: He has published 81 papers in national and international journal of repute. He also Published twenty-four scientific books in Arabic

Special Award:

- Member, Who is Who encyclopaedia, Edition 11, Science and Engineering 2011-2012.
- Prizes of the best scientific research paper in Surveying Engineering, Egypt, 2004, 2005, 2006, 2007, and 2010.
- Prize of the best scientific research paper in Nile protection and development, Egypt, 2008.

Any other remarkable point(s):

- Developing more than two-hundred training videos on YouTube

Dr. Ibrahim E. Ascoura
Umm Al-Qura Univerity, Makkah, Saudi Arabia.

Research and Academic Experience: He has 18 years teaching expereinces in several universities, participant in the preparation of many strategic urban plans for cities in Saudi Arabia and Egypt.

Research Area: His research area includes Urban Geography and Planning.

Number of Published papers: He has published 9 papers in national and international journal of repute.

© Copyright (2023): Author(s). The licensee is the publisher (B P International).

DISCLAIMER
This chapter is an extended version of the article published by the same author(s) in the following journal.
Journal of Geographic Information System, 13: 148-165, 2021.

Peer-Review History: During review of this manuscript, double blind peer-review policy has been followed. Author(s) of this manuscript received review comments from a minimum of two peer-reviewers. Author(s) submitted revised manuscript as per the comments of the peer-reviewers. As per the comments of the peer-reviewers and depending on the quality of the revised manuscript, the Book editor approved the revised manuscript for final publication.

International Research Journal of Earth Sciences ISSN 2321 – 2527
Vol. **11(1),** 1-7, February **(2023)** *Int. Res. J. Earth Sci.*

Case Study

The Role of Spatial Geodetic Data Infrastructures (GDI): A Case Study in the Nile Delta, Egypt

Gomaa M. Dawod*, Essam M. Al-Krargy and Ghada G. Haggag
Survey Research Institute, National Water Research Center, Giza, Egypt
dawod_gomaa@yahoo.com

Available online at: www.isca.in
Received th June 2020, revised th September 2020, accepted th December 2020

Abstract

Engineering activities and development plans rely chiefly on the availability of precise spatial data, which in turn depends on the accessibility of an accurate Geodetic Data Infrastructure (GDI) as reference frames for all geospatial measurements. A GDI is considered a key component in the undergoing National Spatial Data Infrastructure (NSDI) for Egypt. The current study proposes a structure of a GDI in Egypt that has multi-discipline utilizations and aims to develop an integrated database combining several types of geodetic datasets within a Geographic Information Systems (GIS) environment. The study develops such a GDI for the Nile delta region, as a case study, containing the available heterogeneous geodetic datasets. The problems and advantages of such a GDI are thoroughly investigated herein. Accordingly, some recommendations are presented, too, for constructing an integrated GDI over a national scale in Egypt.

Keywords: GDI, NSDI, GIS, Geodetic data, Nile Delta.

Introduction

In the last few decades, it has been a matter of reality that geospatial data play a critical role in the economic growth and sustainable development of countries. A Spatial Data Infrastructure (SDI) could be defined as a collection of geospatial data/metadata, technologies, standards, human resources, and policies that aims to acquire, process, and manage in an efficient manner. Spatial data includes, but not limited to, geodetic, topographic and cadastral information along with aerial photos, satellite imageries, and statistics. SDI has been proposed, in the nineties, as a tool for facilitating spatial data sharing among different users on a national, regional, or international basis[1]. A National SDI (NSDI) could be defined as technologies, policies, criteria, standards and technicians used to promote multiple-sources geospatial data sharing among local governments, the private sector, non-profit organizations, and academic units of a country[2]. Accordingly, SDI in general and NSDI in particular, composed of five factors[3]: organizations, human resources, information, access network, and financial resources. The implementation of SDI has numerous merits for decision-makers and development planners. For example, SDI provides unique datasets originating from multi-users that could be applied for multi-usages. Also, it creates unified policies for spatial data sharing and data access. It defines specific technical rules to be performed to check data quality and to integrate different data sources with different accuracies. In addition, SDI establishes institutional arrangements and user/provider relationships. Economically speaking, SDI reduces the costs and time of data collection in a region[4]. NSDI has been developed in several countries in the last few years, such as Pakistan[5], Tanzania[6], Europe[7], and Finland[8]. The development of an NSDI for Egypt has been investigated since two decades ago. For example, Hussein[9] has proposed a prototype SDI depending on the spatial and non-spatial data acquired by the Egyptian Survey Authority (ESA) and recommended that all other governmental and private organizations should cooperate in sharing their data/metadata in that unique national SDI. Ali[10] has designed the spatial database model of an SDI system on a multi-governorates basis in south Egypt. Since 2014, the Ministry of Planning has initiated a national project for building an NSDI in Egypt based on the cooperation of ministries, authorities, and academic units[11]. That NSDI depends upon conducting recent aerial photography of entire Egypt with a suitable spatial resolution permits the required accuracy of establishing a Geographic Information Systems (GIS) and a digital base map of a scale 1: 2,500. At the core of a NSDI, the geodetic datasets play a critical role in unifying multiple data sources, coordinate systems, and geodetic datums.

In addition, a Geodetic Data Infrastructure (GDI) produces several outputs essential for geodetic and environmental activities. Previous studies have highlighted the significance of constructing a GIS-based database comprising several types of geodetic data over a country[12]. This paper proposes the development of a GDI system within the undergoing ESDI project. The Nile delta region has been utilized as a case study where all available geodetic datasets have been collected, stored, and analyzed in terms of adequacy, spatial distribution, accuracy, and need for updating.

SDI and GDI

A GDI is a major component of an NSDI system. It describes the characteristics of the geodetic framework to which all other spatial datasets are linked together. GDI is represented the fundamental core of the entire SDI structure[13]. A national GDI provides the basic required reference information for spatial data infrastructure in a country[14]. In addition, geodetic datasets within an SDI could be utilized in analyzing geodetic variations over time and inspecting their utilization in natural hazards. For instance, keeping records of sea levels at tide gauges allowing the investigation of Sea Level Rise (SLR) and its hazardous impacts particularly on coastal regions. Similarly, the crustal deformations could be estimated from 4D observations at Global Navigation Satellite Systems (GNSS) stations. An updated national geoid model, also, could be periodically estimated as long as the required geodetic datasets are updated. Accordingly, the current study proposes a structure of a GDI in Egypt that has multi-disciplines usage. Such a structure (Figure-1) aims to develop an integrated database combining several types of geodetic datasets. Its basic structure contains spatial data/metadata where the spatial data include both raster and vector formats. For each layer of geodetic data, basic metadata is mandatory. Such elements describe the geodetic characteristics of the datasets including source, date of measurements, accuracy, spatial coverage, and geodetic datums[15]. Vector datasets include, but are not limited to, Bench Marks (BM) of known orthometric heights, GNSS stations that could be divided into 3D and 4D data, gravity data (absolute and relative), and Tide Gauge (TG) records. On the other hand, raster datasets comprise the Digital Elevation Model (DEM), map of gravity anomalies, geoid maps, crustal deformation maps, and other relevant geodetic data. The proposed GDI will be based on the World Geodetic System 1984 (WGS84) ellipsoid and the Modified Transverse Mercator (MTM) map projection. It is known that the undergoing NSDI project is already utilized those criteria rather than the traditional Helmert 1906 and the Egyptian Transverse Mercator (ETM) datum and projection.

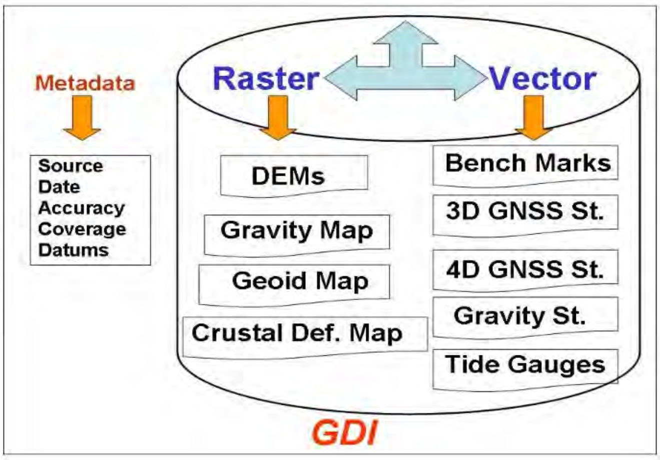

Figure-1: Proposed GDI Structure.

The study area: The study area, in the current research, covers the Nile delta region and its surrounding in northern Egypt (Figure-2). It lies between longitudes 29.7o E and 32.4o E and latitudes 29.9o N and 31.6o N. The Nile delta is considered one of the most densely populated regions worldwide, and also one of the low-lying deltas subject to the impacts of SRL phenomena. Since it contains almost half of the Egyptian population, several development activities and, hence, geodetic datasets are available within that region. The main concern, from a data perspective, is that several governmental authorities have acquired geodetic datasets that need to be collected, inspected, and combined in a unique GDI.

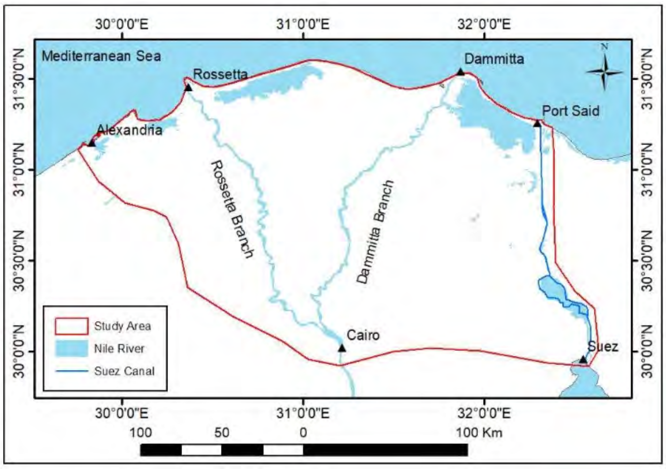

Figure-2: The Study Area.

The topography of the study area (Figure-3) is relatively flat where the heights above Mean Sea Level (MSL) decrease as going north. Al-Karagy and Dawod[16] have investigated the accuracy of several Global Digital Elevation Models (GDEMs) and found that the AEC2 DEM is the optimum one based to represent the Egyptian topography. From this model, it has been found that MSL-based heights of the study area range from -59 m to 872 m with an average of 35 m.

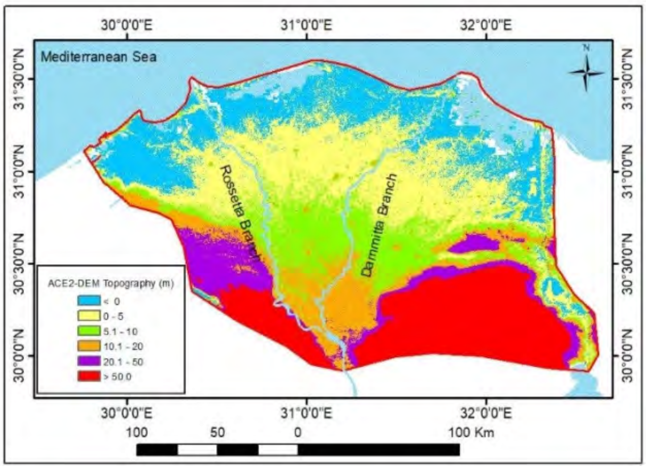

Figure-3: Topography of the Study Area.

Available Datasets

Regarding the available 3D and 4D GNSS stations within the study area, it has been found that there exist 3 stations belong to the High Accuracy Reference Network (HARN) established by the Egyptian Survey Authority (ESA) in 1995. Out of the 112 National Agricultural Cadastral Network (NACN) established by ESA, there exist 27 GNSS stations within the study area. Both HARN and NACN networks can be considered as 3D GNSS networks in Egypt. Both networks have been tied to the International Terrestrial Reference Farm (ITRF) of 1994 epoch 1996. On the other hand, ESA has established, in 2010, a Continuously Operation Reference Station (CORS) network as a 4D geodetic reference frame in Egypt. This network has been tied to ITRF of 2008 epoch 2011. Within the study area, it has been found that 23 CORS stations exist. Figure-4 depicts the distribution of GNSS stations in the study area. It is a matter of fact that such first-order geodetic stations are quite significant in executing surveying and mapping projects. Thus, GNSS stations present a major component in the GDI in Egypt.

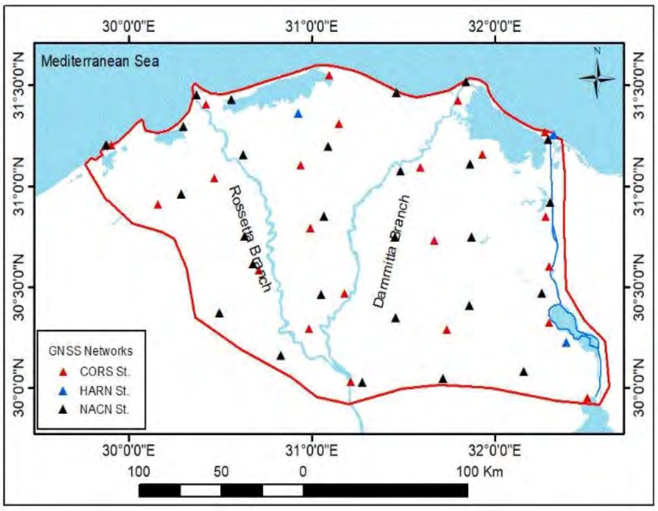

Figure-4: GNSS Networks at the Study Area.

Another constituent of a GDI is the GNSS/Levelling stations where both WGS84-based ellipsoidal and MSL-based orthometric heights are known at each point. From such points, a geometric geoid could be developed which is vital in the utilization of GNSS applications. Heterogeneous datasets from several organizations have been compiled into a unique dataset as a part of the proposed GDI. It has been found that 332 GNSS/ Levelling stations exist within the study area as depicted in Figure-5.

A geoid map plays a chief role in surveying and mapping activities in Egypt. It facilitates the conversion of GNSS heights to MSL levels needed for civil engineering projects. Geoid modelling has been a traditional task for the geodetic community in Egypt in the last few decades. The first pioneer Egyptian geoid model has been developed by Alnaggar[17]. The most recent geoid for Egypt has been performed by Al-Karargy and Dawod[16]. From that model, it has been found the geoidal heights or geoidal undulations over the study area vary between 13.99 m and 17.78 m with a mean of 15.39 m (Figure-6).

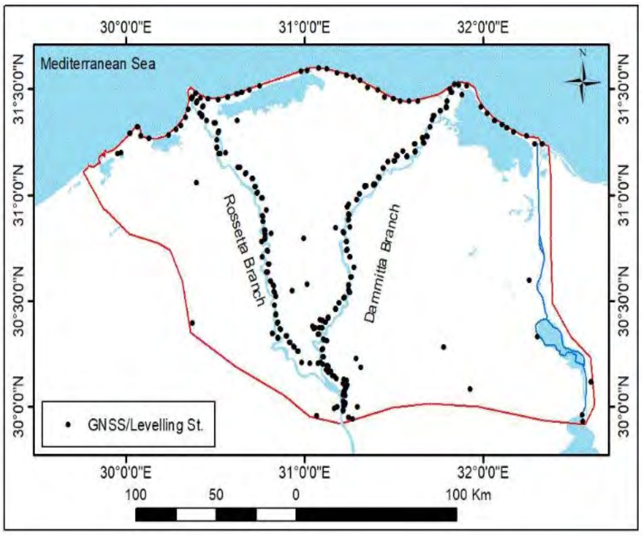

Figure-5: Available GNSS/Levelling Points.

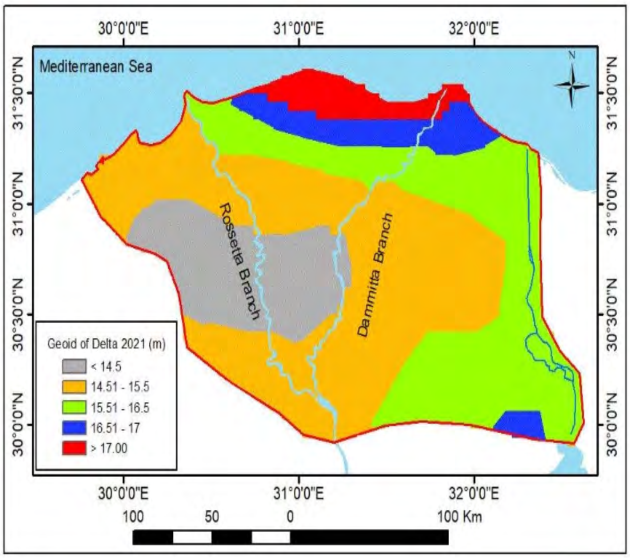

Figure-6: Geoid 2021 of the Study Area.

Gravity data is another main geodetic data to be incorporated in the proposed GDI in Egypt. The recent gravity network in Egypt has been established by SRI in 1997, called the Egyptian National Gravity Standardization Networks 1997 or simply ENGSN-97[18]. It consists of 5 absolute gravity stations and 145 relative gravity stations. Within the study area, it has been found that 28 ENGSN-97 points exist. Additionally, it has been realized that the gravity field in this region range from 979,267.5 mGal to 979,504.8 mGal with an average of 979,369.4 mGal (Figure-7).

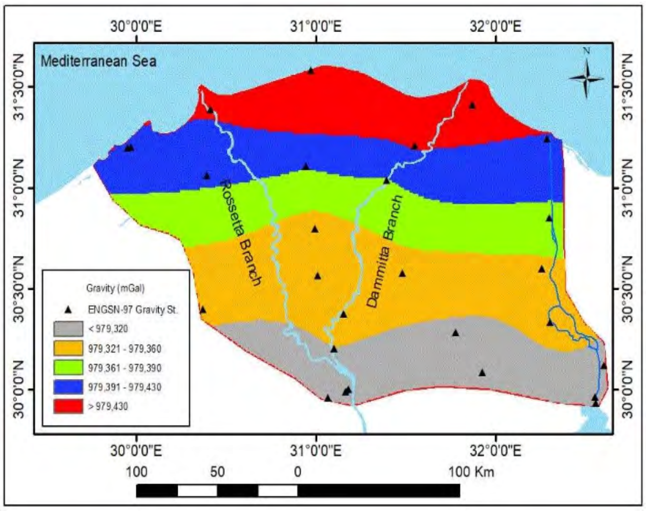

Figure-7: Gravity Variations at the Study Area.

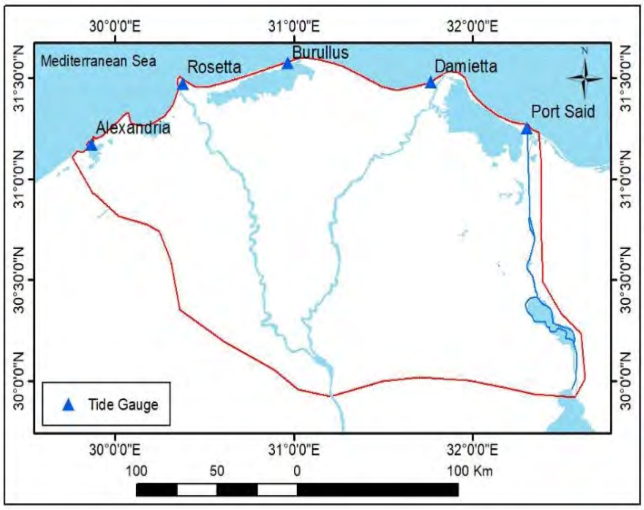

Figure-9: Tide Gauges at the Study Area.

Bench Marks (BM) with known MSL heights constitute an important component in the proposed GDI and all civil engineering activities in Egypt. In the last few years, SRI has established a unique BM network particularly for water resources management projects. Figure-8 presents the distribution of the collected 593 BM stations within the study area. Such network consists of 247 BM along the Nile river, 231 BM on main drains, 58 BM over the coastlines, and 57 BM along main irrigation canals.

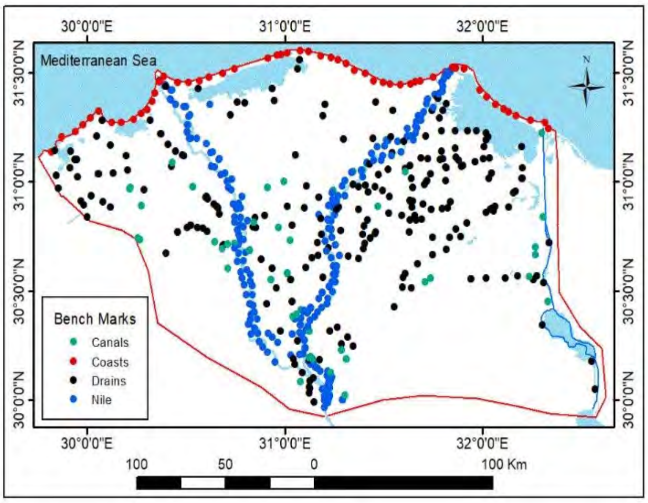

Figure-8: Bench Marks at the Study Area.

Tide Gauges (TG) are the geodetic stations where sea levels are continuously observed. Such geodetic stations are extremely noteworthy in monitoring Sea Level Rise (SRL) and studying its risks, particularly over coastal regions. Within the study area, five TG stations exist (Figure-9). Two of them, namely Alexandria and Port Said, belong to SRI while the other three belong to the Costal Research Institute of the National Water Research Center (NWRC).

Land subsidence is a natural phenomenon occurred mainly in low-land deltas worldwide. It is a hazardous phenomenon affecting huge infrastructures such as dams, reservoirs, and infrastructures. It should be frequently monitored by GNSS, levelling, or remote sensing satellite images. Mohamed et al.[19] have utilized seven GNSS CORS stations to estimate land subsidence over the Nile delta region in 2012-2015. Their results indicated that the land subsidence rate ranges from -4.8 mm/year to +6.5 mm/year with an average of 1.41 mm/year (Figure-10).

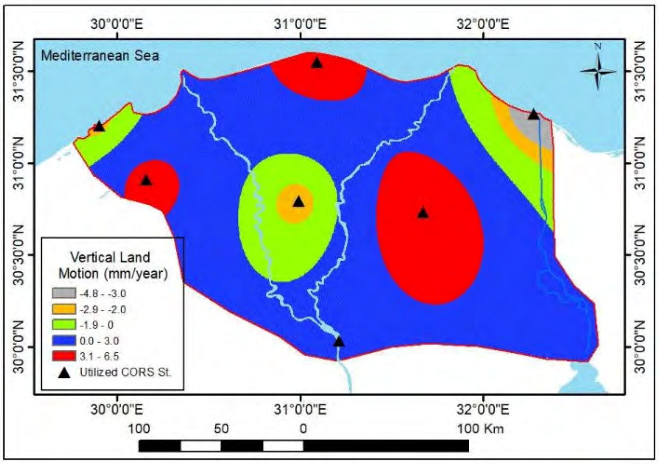

Figure-10: Land Subsidence at the Study Area.

Analysis and Discussion

Having the proposed GDI constructed with the SDI of Egypt, several benefits could be accomplished. Specialized SDI users could analyze the components of the GDI and utilize it in several applications. However, the GDI components should be updated regularly in terms of accuracy and spatial coverage. For instance, Figure-4 shows that the spatial distribution of GNSS networks over the study area is relatively homogeneous. But,

both HARN and NACN GNSS networks have been established a few decades ago. Due to urban expansion, many of such stations have been damaged and, therefore, need to be re-constructed and re-observed. On the other hand, Figure-5 reveals that the spatial distribution of available GNSS/Levelling stations in the study area is not uniform. Such a fact jeopardizes the development of a national geoid model to be applied in GNSS-based surveying and civil engineering projects. More GNSS/Levelling stations are required to get ride of such a dilemma. A similar situation exists for the distribution of available gravity networks in Egypt as depicted in Figure-7. Although the number of available BM is relatively good, their distribution (Figure-8) lacks a uniform pattern. It is a matter of reality that all surveying and geomatics applications depend on the availability and accuracy of BM network. On another sense, specialized SDI users could investigate the GDI components (spatial and attribute datasets) to reveal significant pieces of information. The TG stations at both Alexandria and Port Said, owned and operated by SRI, have sea levels observed over a long period[20]. Having their annual averages as attribute data within the proposed GDI, relative Sea Level Rise (SRL) trends could be obtained (Figure-11). Adding the subsidence rate at each TG (Figure-10) to such relative SRL values, absolute SRL could be estimated. Such piece of information is extremely noteworthy in monitoring the impacts of climate changes on Egypt, particularly over the coasts of the Nile delta region.

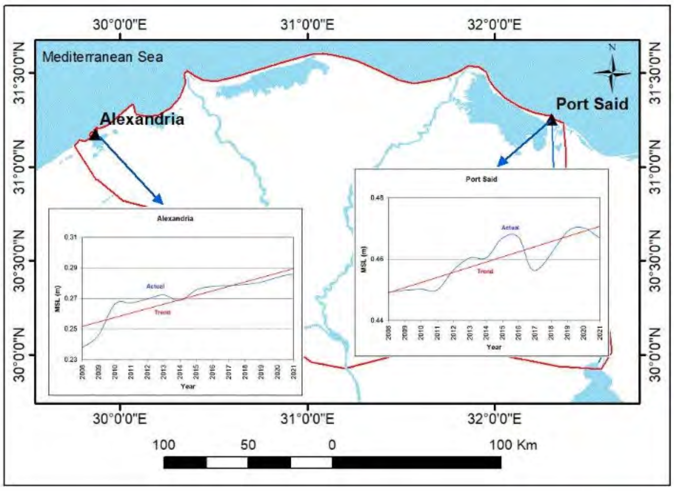

Figure-11: Mean Sea Level Trend at the Study Area.

Concerning the status and the key difficulties facing the development of a precise and comprehensive GDI in Egypt, several factors should be considered. First, the loss of many terrestrial geodetic control points due to urban expansion in the last few decades. Second, the accuracy variations of such geodetic networks since they have been observed over a long time using equipment and techniques vary significantly in precision. Third, there is a great demand to update national geodetic datums. For instance, the vertical datum of Egypt is the MSL of Alexandria in 1906. It is a matter of fact that such a datum need to be re-defined due to the SRL over the twentieth century[21]. Additionally, the GNSS-based horizontal geodetic datums vary between ITRF1994 for the HARN network and IREF2008 for the CORS network. Lastly, the need for honest cooperation between all governmental, civil, military, and private sectors to collect all available geodetic datasets to build an up-to-date precise GDI over a national scale.

Conclusion

GDI is considered a major constituent of a national SDI for a country. GDI offers optimal utilization of natural and human resources and facilitates efficient planning of development activities in Egypt. As a major component of the presently undergoing development of an NSDI in Egypt, an GDI is proposed in this research study. The available geodetic datasets, as far as the authors concern, have been collected in a GIS environment as a proposed GDI structure in the Nile delta region. Other components of such GDI could be suggested and incorporated too, such as aerial photographs, satellites imageries, topographic maps, and light detection and ranging (LIDAR) datasets. Furthermore, such a proposal should be enlarged to construct a GDI over a national scale in Egypt.

Based on the previous analysis and conclusions, some recommendations could be drawn. i. The collection of all available geodetic datasets in a unique GIS framework is urgently needed. ii. The update of both vertical and horizontal geodetic datums of Egypt should be carried out as soon as possible. iii. A national plan for densification of geodetic control networks, of all types, should be initiated and all governmental and private organizations should be participated in its activities to complete it in a short time. iv. Having developed a national updated GDI, it should be available and accessible to specialized governmental and academic users for analysis and utilization. v. A continuous update of a GDI is needed utilizing state-of-the-art technologies and equipment to accomplish, regularly, accurate definitions of geodetic data and datums in Egypt.

References

1. Mwungu, C. M. (2017). Spatial data infrastructure in Africa: A technical and institutional analysis (Doctoral dissertation, University of Nairobi)..

2. FGDC (US Federal Geographic Data Committee) (2020) National spatial data infrastructure strategic plan 2021-2024, A technical report, 17 pp, FGDC, Virginia, USA.

3. Merodio Gómez, P., Pérez García, M., García Seco, G., Ramírez Santiago, A., & Tapia Johnson, C. (2019). The Americas' spatial data infrastructure. ISPRS International Journal of Geo-Information, 8(10), 432.

4. Idrizi, B. (2018). General Conditions of Spatial Data Infrastructure. International Journal on Natural and Engineering Sciences. V. 12, No. 1, pp. 57-62.

5. Ali, A., & Imran, M. (2021). National Spatial Data Infrastructure vs. Cadastre System for Economic Development: Evidence from Pakistan. Land, 10(2), 188.

6. Lubida, A. (2019). Investigating Spatial Data Infrastructure Planning in Tanzania using System Modelling and Social Concepts. Lund University.

7. Crompvoets, J., Vancauwenberghe, G., Ho, S., Masser, I., & De Vries, W. T. (2018). Governance of national spatial data infrastructures in Europe. International Journal of Spatial Data Infrastructures Research, 13, 253-285.

8. Kokkonen, K., Kylmäaho, J. & Ursin, H. Arctic Spatial Data Infrastructure (ASDI) https://www.fig.net/resources/proceedings/fig_proceedings/fig2017/ppt/ts04e/TS04E_kokkonen_kylmaeaho_et_al_8732_ppt.pdf, Accessed 14 December, 2021.

9. Hussein, S. The role of ESA in building the Egyptian Spatial Data Infrastructure (ESDI) towards the Electronic https://www.fig.net/resources/proceedings/fig_proceedings/cairo/papers/ts_02/ts02_04_hussein.pdf, Accessed 12 December, 2021.

10. Ali, A. H. (2015). Developing Spatial Data Infrastructure in Egypt. International Journal of Emerging Engineering Research and Technology, V. 3, No. 10, pp. 19-36.

11. CAPMAS (Central Agency for Public Mobilization and Statistics), Country report of Egypt: The activities of the integration of statistical and geospatial information, https://ggim.un.org/country-reports/documents/Egypt-2016-country-report.pdf, Accessed 13 December, 2021.

12. Jasim, O., Hassoon, K., & Hussein, M. (2018). Preparing a comprehensive geodatabase for Iraq geodetic networks systems. In MATEC Web of Conferences (Vol. 162, p. 03030). EDP Sciences.

13. UN (United Nations) (2013) Spatial Data Infrastructure (SDI) manual for the Americans, UN report No. E/CONF.103/14, Rio de Janerio, Brazil.

14. Doskocz, A. (2016). The current state of the creation and modernization of national geodetic and cartographic resources in Poland. Open Geosciences, 8(1), 579-592.

15. FGDC (US Federal Geographic Data Committee) Geographic information framework data content standard. https://www.fgdc.gov/standards/projects/framework-data-standard/GI_FrameworkDataStandard_Part4_GeodeticControl.pdf, Accessed 11 December, 2021.

16. Al-Karargy, E. M., & Dawod, G. M. (2021). Optimum Combinations of GGM and GDEM Models for Precise National Geoid Modelling. Proceedings of Engineering and Technology Innovation, 18, 15.

17. Alnaggar, D. (1986). Determination of the geoid in Egypt using heterogeneous geodetic data (Doctoral dissertation, PhD dissertation, Faculty of Engineering, Cairo University, Egypt.

18. Dawod, G. (1998). A national gravity standardization network for Egypt (Doctoral dissertation, PhD dissertation, Faculty of Engineering at Shoubra, Zagazig University, Egypt.(

19. Mohamed, H., Shaheen, B., Hosney, M., & Dawod, G. (2015, October). High-Precision GPS Monitoring of the Land Subsidence in the Nile Delta: Status and Preliminary Results. In Regional Conference on Surveying and Development (3-6).

20. SRI (Survey Research Institute) (2019) Observing the variations and effects of sea level on the Egyptian coasts over 2008-2018, An internal technical Report, SRI, Giza, Egypt

21. Mohamed, H. (2005). Realization and redefinition of the Egyptian vertical datum based on recent heterogeneous observations (Doctoral dissertation, PhD dissertation, Faculty of Engineering Shoubra, Zagazig University, Egypt).

Geophysica (2023), 58 (1), 33–45

Recent High-Order Global Geopotential Models for Geoid Modelling in Egypt

Gomaa Dawod[1,*] *and Essam Al-Krargy*[1]

[1]Survey Research Institute, National Water Research Center, Giza, Egypt
[*]Corresponding mail address: gomaa_dawod@nwrc.gov.eg

(Submitted: 2023-03-07; Accepted: 2023-07-05)

Abstract

An optimum Global Geopotential Model (GGM) is required either to represent the long wavelength of the Earth's gravitational field in gravimetric geoid modelling or to act as a stand-alone national geoid in some developing countries. Thus, the current research aims to investigate the performance of seven recent high-order GGMs over Egypt utilizing the most recent precise Global Navigation Satellite Systems(GNSS)/Levelling datasets. Attained results showed that the investigated GGMs perform differently over Egypt with an accuracy level varying between $\pm 0.249\,\mathrm{m}$ *for the SGG-UGM-1 model and* $\pm 0.300\,\mathrm{m}$ *for the GECO model. Removing outliers in the terrestrial dataset reveal significant improvements, in terms of standard deviations. Consequently, the performance of the investigated GGMs has been modified where the EIGEN-6C4 model became the best model with a standard deviation equals* $\pm 0.172\,\mathrm{m}$. *Furthermore, a 3D spatial correction surface has been constructed and has been added to the original EIGEN-6C4 model to get an enhanced version of the global EIGEN-6C4. Over checkpoints, the average error of the enhanced model equals* $-0.018\,\mathrm{m}$ *with a standard deviation equal* $\pm 0.011\,\mathrm{m}$. *That means that incorporating terrestrial geodetic data into the global EIGEN-6C4 model has increased its accuracy in Egypt by almost 36 %. Accordingly, such developed enhanced GGM represent the optimum stand-alone geoid model in Egypt. Nevertheless, such accuracy levels of GGMs do not fulfill the requirements of high-accuracy surveying and civil engineering applications. That concludes that a precise national geoid model is still crucial. It is recommended that all available geodetic datasets should be collected from all governmental and private organizations to construct a national geodetic database that would be implemented in modelling an Egyptian local geoid.*

Keywords: Global Geopotential Models (GGMs); geoid modelling; GNSS/levelling; gravity field; corrector surface

1 Introduction

A geoid model is required in a wide range of geodetic, mapping, civil engineering, and environmental applications as a height conversion tool to transform the Global Navigation Satellite Systems (GNSS)-based ellipsoidal heights to the Mean Sea Level (MSL)-based orthometric heights. A geoid model can be developed from large enough and well-distributed gravity and/or GNSS/Levelling datasets over a particular spatial region. Geoid modelling is still an essential task for geodesists worldwide in different countries and continents such as Indonesia (*Lestari et al.*, 2022), Iraq (*Jassim and Yousef*, 2021), Thailand (*Phinyo et al.*, 2021), Africa (*Abd-Elmotaal et al.*, 2020), Saudi Arabia (*Borghi et al.*, 2020), India (*Singh and Srivastava*, 2018), and Egypt (*Dawod and Mohamed*, 2022).

Published by the Geophysical Society of Finland, Helsinki

Global Geopotential Models (GGM) have been developed during the last few decades to describe the long wavelength of the Earth's gravitational field. GGM can also be utilized as a local geoid model in a regional scale acknowledging their precision limits and their validation in different geodetic and geophysical activities. Analysis of the properties of the available GGMs for selecting the optimum model in a region or a country is necessary as their accuracies are varying spatially. Such an analysis has been performed recently in several countries. For example, *Tocho et al.* (2022) investigated the accuracy of five high-resolution GGMs over GNSS/Levelling points in Argentina. Similarly, *Isik et al.* (2022) analyzed the performance of GGMs for gravimetric geoid modelling in Turkey. Also, high-order GGMs were evaluated over Sudan based on GNSS/Levelling datasets (*Osman et al.*, 2021). *Liang et al.* (2022) proposed a new method for improving GGMs using GNSS/Levelling data and applying this approach in China.

GGM analysis has been done extensively in Egypt, in the last couple of decades, either nationally or regionally. For an instant, *Hamdy and Elshewy* (2022) tested the GGMs performance in Northern Egypt over GNSS/Levelling stations. In addition, *Elsaka and El-Ashquer* (2022) combined GGMs-based gravity anomalies and terrestrial gravity observations to determine a local geoid model in the Western desert of Egypt. *Elwan et al.* (2021) developed a local geoid model also for the western desert of Egypt combining terrestrial gravity and GGMs. Also, GGMs were investigated for geoscience and archaeology activities in Egypt (*Klokočníka et al.*, 2020). In addition, (*Dawod et al.*, 2019) examined the accuracy of a particular GGM over Egypt and Northeast Africa using gravity and GNSS/Levelling datasets.

An optimum GGM is required either as a tool to derive geoid undulation or to be utilized in gravimetric geoid modelling over an area. The current study aims to assess the local accuracy of some recent high-resolution GGMs using local geodetic datasets to determine the most accurate one which has geoid undulations best fit the observed GNSS/Levelling values over the Egyptian territories.

2 *Available data*

Since 1966, the International Center for Global Earth Model (ICGEM) has collected and published GGMs with variable data characteristics and maximum orders or maximum degree of spherical harmonics (*ICGEM*, 2023). Out of the available 178 GGMs, seven models were selected for this study. All of them are high order with order ranges between 1949 and 2190 released between 2011 and 2020. Table 1 summarized the characteristics of the selected models. The ICGEM organization evaluates the accuracy of each GGM, i.e., the Root Mean Square (RMS) about the mean of GNSS/levelling minus gravity field model derived geoid heights, over 24 014 GNSS/Levelling points in several countries and publishes the RMS of those discrepancies (Table 2.1). It can be noticed that the accuracy (indicated by the RMS) of the selected GGMs ranges between ± 0.173 m and ± 0.187 m.

Egypt lies in the Northeast region of Africa from 24.7°E to 37°E and from 22°N to 31.6°N (Fig. 2.1). Its topography is nearly smooth, MSL heights vary between -137 m in the Katarra depression and in some northern lakes to 2600 m in mountainous regions in

Table 2.1: Characteristics of the Utilized High-Order GGMs (after *ICGEM*, 2023).

No	GGM	Year	Degree	Data*	Accuracy: RMS (m)	Reference
1	SGG-UGM-2	2020	2190	A, EGM2008, S(GOCE), S(Grace)	± 0.177	*Liang et al.*, 2020
2	XGM2019e_2159	2019	2190	A, G, S(GOCO6s), T	± 0.173	*Zingerle et al.*, 2020
3	GECO	2015	2190	EGM2008, S(GOCE)	± 0.176	*Gilardoni et al.*, 2016
4	EIGEN-6C4	2014	2190	A, G, S(GOCE), S(Grace), S(Lageos)	± 0.178	*Förste et al.*, 2014
5	EGM2008	2008	2190	A, G, S(Grace)	± 0.187	*Pavlis et al.*, 2012
6	SGG-UGM-1	2018	2159	EGM2008, S(GOCE)	± 0.176	*Liang et al.*, 2018
7	EIGEN-6C3stat	2014	1949	A, G, S(GOCE), S(Grace), S(Lageos)	± 0.179	*Förste et al.*, 2012

* where A denotes altimetry, S is for satellite gravity missions (e.g., GRACE, GOCE, LAGEOS), G for ground data (e.g., terrestrial, shiborne and airborne measurements) and T is for topography.

the Sinai, Red Sea coasts, and in southwest regions. The average MSL height of Egypt is 302 m.

In total 736 national GNSS/Levelling points were utilized to investigate the accuracy of the selected GGMs over Egypt (*SRI*, 2022). These points were measured by the Survey Research Institute (SRI) of the National Water Research Center (NWRC) in several national projects over the last few years. Their accuracies, in terms of both ellipsoidal and orthometric heights, have been estimated to be less than ±0.05 m (ibid). Thus, they might be considered the most accurate geodetic datasets in Egypt. Figure 2.1 depicts the spatial distribution of the available geodetic dataset.

3 Methodology

Overall, the processing methodology of the current research (Fig. 3.1) comprises few steps: estimating the GGMs-based geoid undulations, comparing them to the corresponding values over the known GNSS/Levelling checkpoints, to determine the best GGM that describes the Earth's gravitational field over Egypt accurately.

Global geopotential models express the gravitational potential of the Earth (V) into a series of spherical harmonics as (*Hofmann-Wellenhof and Moritz*, 2005)

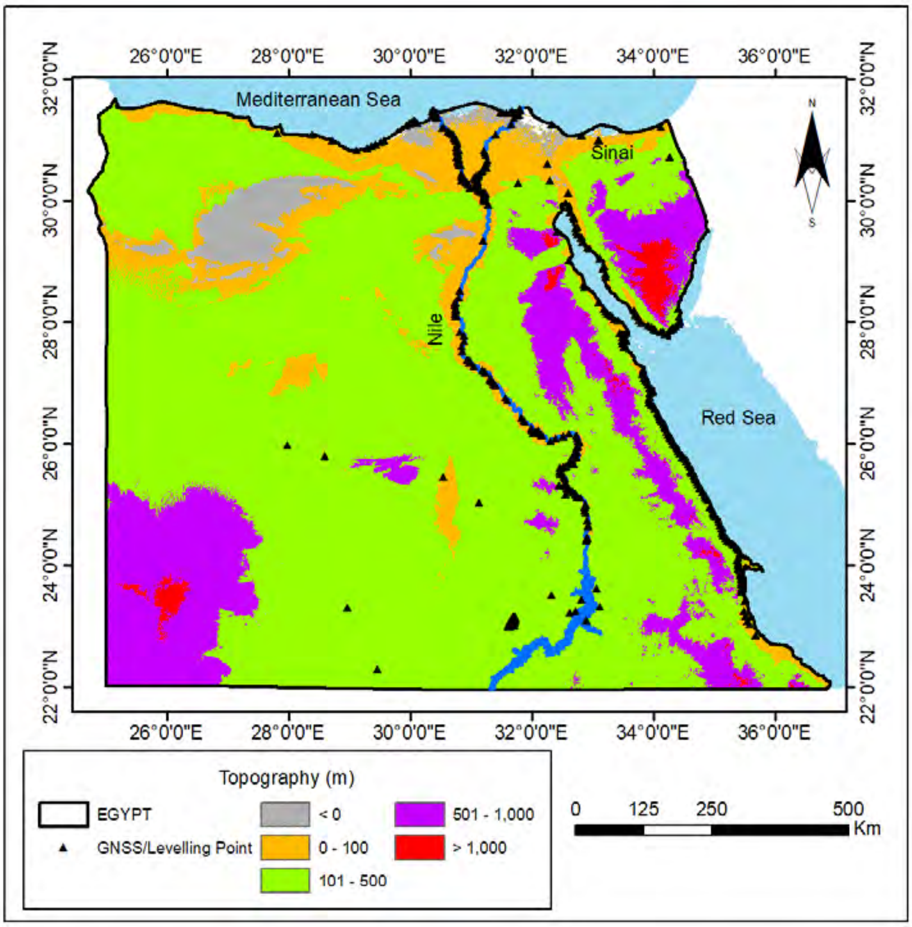

Fig. 2.1: The Study Area and Available Data.

$$V = \frac{GM}{r}\left(1 - \sum_{n=2}^{\infty}\left(\frac{a}{r}\right)^{n} J_{n} P_{n}(\cos\vartheta) + \sum_{n=2}^{\infty}\sum_{m=1}^{n}\left(\frac{a}{r}\right)^{n}[C_{nm}\cos m\lambda + S_{nm}\sin m\lambda]\,P_{nm}(\cos\vartheta)\right), \tag{3.1}$$

where GM is the gravitational constant, r is the radial distance, a is the equatorial radius of the Earth, θ and λ are the geodetic latitude and longitude respectively, J_n are the zonal harmonics, those contain the S_{nm} and C_{nm} are the tesseral harmonics, P_{nm} are the associated Legendre coefficients, n and m are the degree and order of the geopotential model.

Then, the geoid undulations of each investigated GGM, N_{GGM}, could be evaluated as (*Dawod et al.*, 2019):

$$N_{GGM} = \frac{GM}{r\gamma}\sum_{n=2}^{n_{max}}\left(\frac{a}{r}\right)^{n} - \sum_{m=0}^{n}[(C_{nm}\cos m\lambda) + (S_{nm}\sin m\lambda)]\,P_{nm}(\sin\vartheta)\,, \tag{3.2}$$

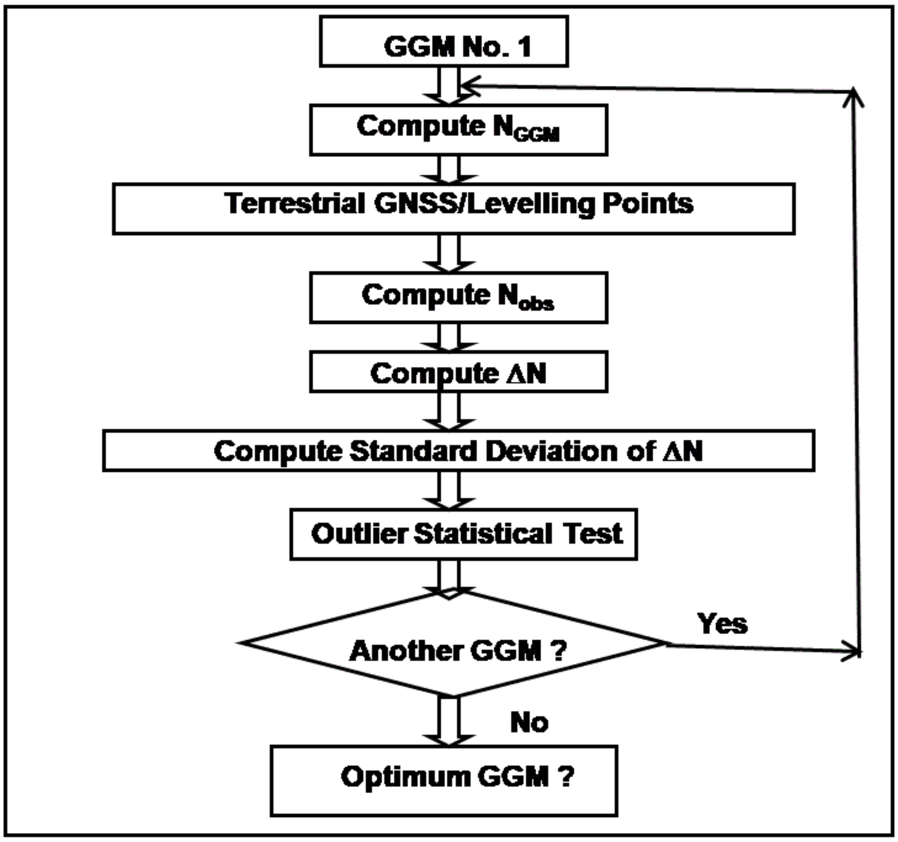

Fig. 3.1: The processing flow.

where $n_{\max}$ is the maximum degree of the GGM, and γ is the normal gravity.

On the other hand, the observed geoid undulations, N_{obs}, is the difference between GNSS ellipsoidal heights, h, and the MSL orthometric heights, H, at each observed terrestrial station:

$$N_{\text{obs}} = h - H \tag{3.3}$$

Thus, the GGM's errors, ΔN, can be defined at each observed point as

$$\Delta N = N_{\text{GGM}} - N_{\text{obs}} \ . \tag{3.4}$$

The standard deviation of the GGM discrepancies, $\sigma_{\Delta N}$, can be estimated as

$$\sigma_{\Delta N} = \sqrt{\sum_{\text{i}=1}^{\text{P}} (\Delta N_i - \Delta N_{\text{mean}})^2} \ , \tag{3.5}$$

where P denotes the total number of available GNSS/Levelling points, and ΔN_{mean} is the average of GGM's errors [Eq. (3.4)] at all stations.

Furthermore, an outlier detection statistical test was used to detect and remove erro-

neous levelling measurements. The utilized criteria for an outlier in the observation is

$$\frac{[\Delta N_{\mathrm{i}}]}{\sigma_{\Delta N}} > 3 \; . \tag{3.6}$$

4 Processing and results

The harmonic coefficients of the each selected GGM were downloaded from the ICGEM website (*ICGEM*, 2023). The Gravsoft package (*Forsberg and Tscherning*, 2008) was used for generating a grid presenting geoid undulation in Egypt for each selected GGM. The grid values are initiated with label of latitude (φ) and longitude (λ) and spacing. The grid label defines the exact latitude and longitude of the grid points, irrespectively whether the grids point values or average values over grid cells. The gridding procedure could be also applied using the UTM projected coordinates (ibid). Table 4.1 summarizes the characteristics of the attained results. Together with spatial analysis it can be concluded that there are no significant differences between the selected GGMs in Egypt. Geoid undulation and spatial distribution of the selected GGMs are almost identical expect some minor differences in the Sinai Peninsula and the western desert.

Table 4.1: Statistics of the GGM-Based Geoid Undulations in Egypt

No.	GGM	Minimum (m)	Maximum (m)	Average (m)
1	`SGG-UGM-2`	5.1	23.6	14.8
2	`XGM2019e_2159`	5.1	23.6	14.8
3	`GECO`	5.0	23.6	14.8
4	`EIGEN-6C4`	5.1	23.6	14.8
5	`EGM2008`	5.2	23.7	14.8
6	`SGG-UGM-1`	5.1	23.6	14.8
7	`EIGEN-6C3stat`	5.1	23.6	14.8

Next, each selected GGM was compared with the SRI 2021 national gridded geoid model developed by *Al-Karargy and Dawod* (2021). This model has an accuracy of ± 0.13 m (ibid) and it was developed using 247 first-order terrestrial gravity observations and fitted to 900 GNSS/Levelling stations. It can be considered as the most recent and accurate national geoid model of Egypt, and thus the comparison of the selected GGMs with this model is useful in determining the optimum GGM. The differences between the geoid undulations are shown in Table 4.2.

Furthermore, a comparison between the GNSS/Levelling points and the GGMs was done. The GGMs perform roughly similarly with a minimum standard deviation of ± 0.249 m for the `SGG-UGM-1` model and a maximum ± 0.300 m for the `GECO` model (Table 4.3). However, such levels of accuracy are greater than the ones presented in Table 2.1 for the GGMs. That might indicate that the terrestrial dataset may include some erroneous measurements or outliers. Thus, the statistical test [Eq. (3.6)] was performed and as a result, almost 10 % of the available points were removed from the dataset. After removing outliers significant improvements, in terms of standard deviations, were

Table 4.2: Differences between the GGMs and the SRL2021 Local Geoid Model (SDs = Standard Deviations).

No.	GGM	Minimum (m)	Maximum (m)	Average (m)	SDs (m)
1	SGG-UGM-2	−1.7	2.6	0.8	± 0.37
2	XGM2019e_2159	−0.5	3.2	0.8	± 0.33
3	GECO	−1.7	2.2	0.7	± 0.36
4	EIGEN-6C4	−1.9	2.4	0.7	± 0.36
5	EGM2008	−2.9	2.7	0.7	± 0.51
6	SGG-UGM-1	−1.7	2.2	0.7	± 0.36
7	EIGEN-6C3stat	−1.9	2.4	0.7	± 0.36

obtained (Table 4.4). Fig. 4.2 depicts the histogram distribution of GGMs errors over the entire spatial study area. It shows that some GGMs depict closely the normal distribution curve while others do not. From this figure and table, it can be recognized that the EIGEN-6C4 model became the best model with a standard deviation of ±0.172 m and the SGG-UGM-1 model the worst one with a standard deviation of ±0.194 m.

Table 4.3: Discrepancies of the GGM-Based Geoid Undulations over GNSS/Levelling Stations Before Removing Outliers (SDs = Standard Deviations).

No.	GGM	Minimum (m)	Maximum (m)	Average (m)	SDs (m)
1	SGG-UGM-2	−0.712	0.703	−0.371	± 0.286
2	XGM2019e_2159	−0.700	0.703	−0.347	± 0.287
3	GECO	−0.719	0.717	−0.332	± 0.300
4	EIGEN-6C4	−0.710	0.688	−0.342	± 0.275
5	EGM2008	−0.666	0.638	−0.298	± 0.252
6	SGG-UGM-1	−0.660	0.649	−0.362	± 0.249
7	EIGEN-6C3stat	−0.709	0.707	−0.340	± 0.284

Table 4.4: Discrepancies of the GGM-Based Geoid Undulations over GNSS/Levelling Stations After Removing Outliers (Min = Minimum, Max = Maximum, Avg = Average).

No.	GGM	Min (m)	Max (m)	Avg (m)	Standard Deviations (m)	
					Value	Improvements
1	SGG-UGM-2	−0.499	0.478	−0.258	± 0.190	51%
2	XGM2019e_2159	−0.500	0.506	−0.250	± 0.205	40%
3	GECO	−0.501	0.494	−0.223	± 0.190	58%
4	EIGEN-6C4	−0.504	0.484	−0.216	± 0.172	60%
5	EGM2008	−0.493	0.505	−0.208	± 0.191	32%
6	SGG-UGM-1	−0.501	0.498	−0.250	± 0.194	28%
7	EIGEN-6C3stat	−0.499	0.496	−0.216	± 0.179	59%

The discrepancies of the EIGEN-6C4 model over the 666 GNSS/Levelling stations (remain after outlier detection over the available 736 points) were spatially modeled to construct a spatial correction surface over Egypt. Furthermore, 66 points were reserved for the final quality check. The obtained correction surface was added to the original

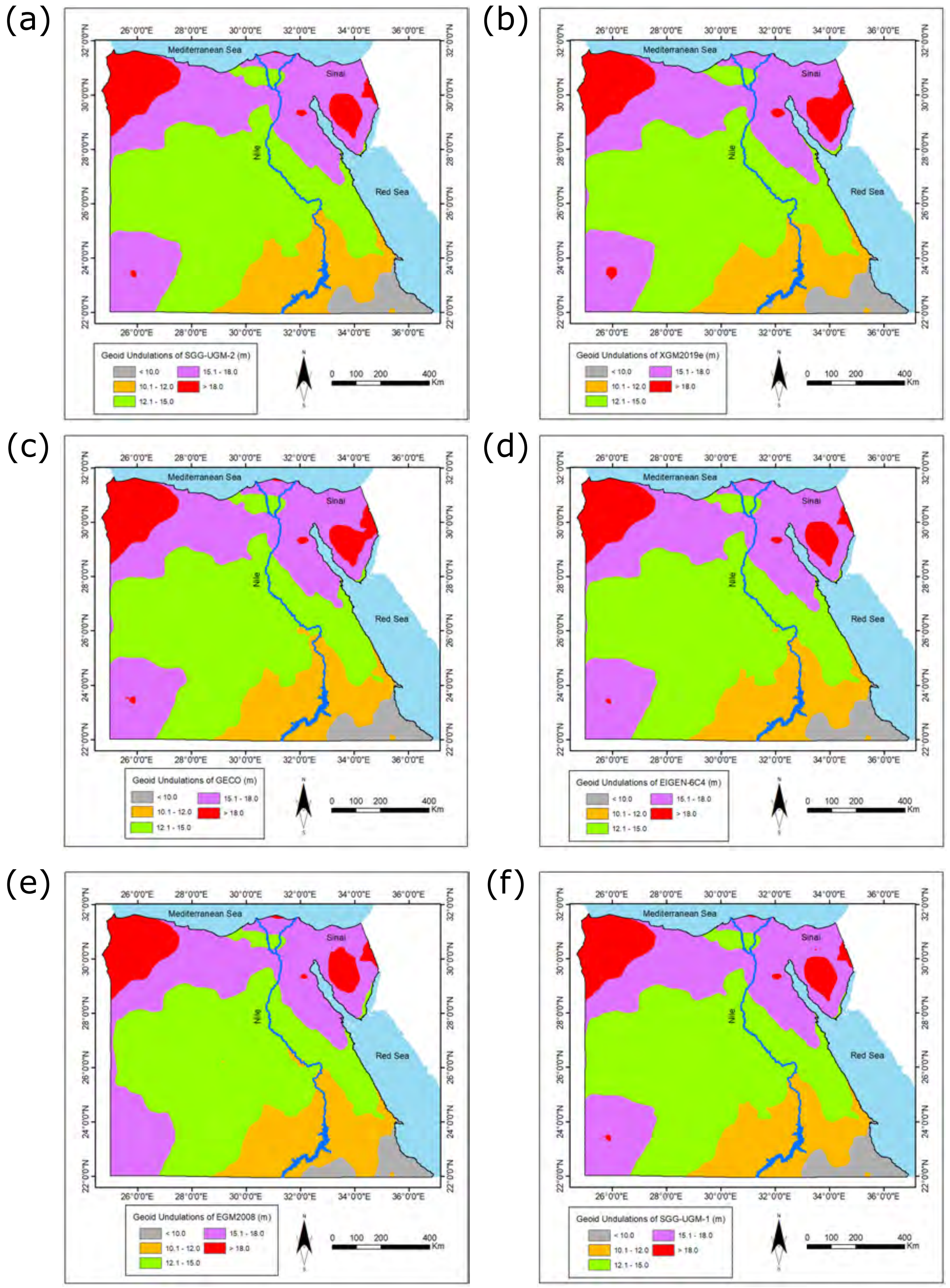

Fig. 4.1: GGM-Based Geoid Undulations over Egypt, (a) SGG-UGM-2, (b) XGM2019e_2159, (c) GECO, (d) EIGEN-6C4, (e) EGM2008, (f) SGG-UGM-1, (g) EIGEN-6C3stat (see next page).

EIGEN-6C4 model and an updated version of the global model was generated (Fig. 4.3). Over the 66 checkpoints, the errors of the updated model vary between −0.180 m and

(g)

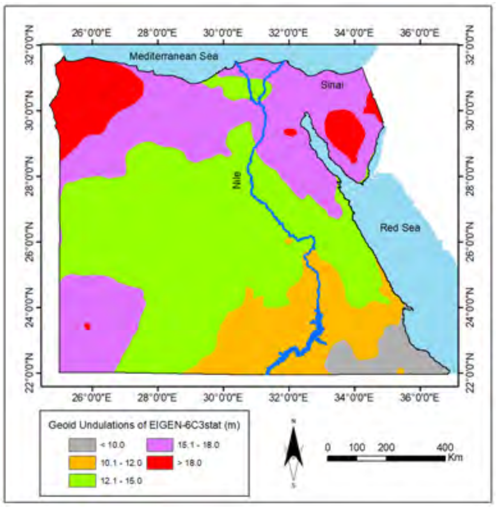

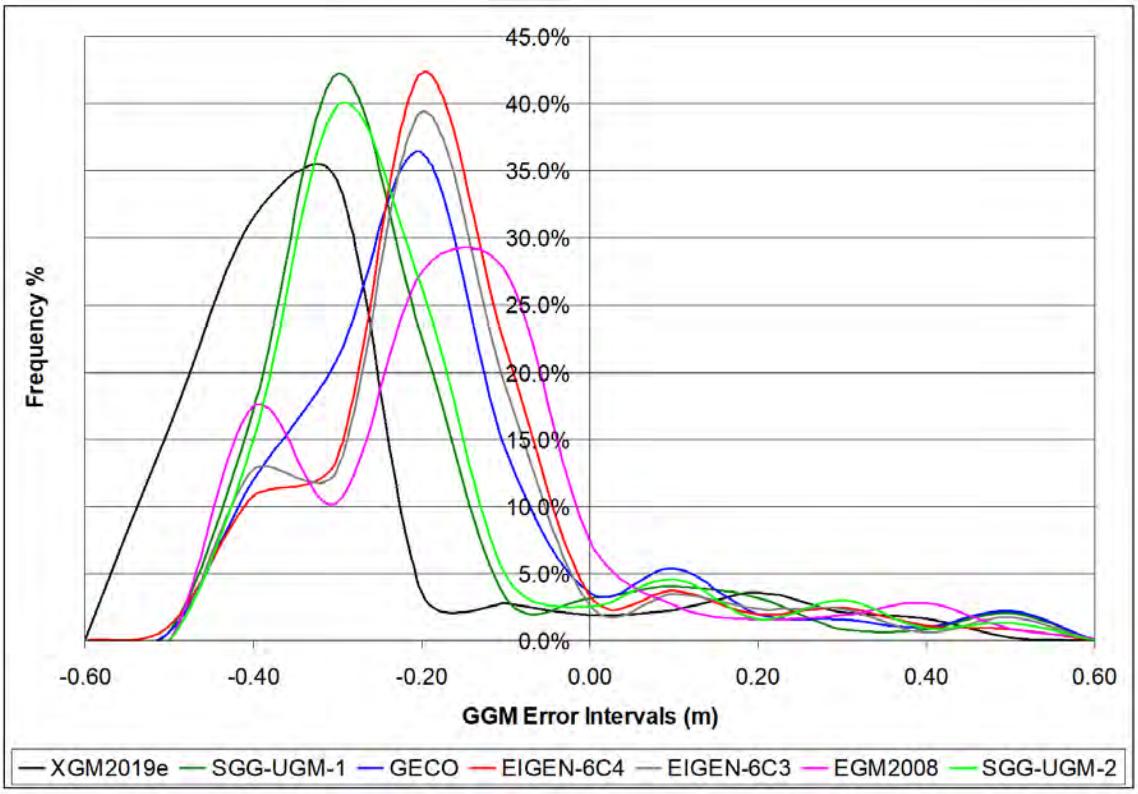

Fig. 4.2: Histograms of GGM Errors.

0.143 m with a mean of −0.018 m and a standard deviation equals ±0.011 m. Incorporating terrestrial geodetic data into the global `EIGEN-6C4` model has increased its accuracy in Egypt by almost 36 % as the overall standard deviation has been decreased from ±0.172 m to ±0.110 m. Even though some previous studies (e.g., *Hamdy and Elshewy*, 2022) estimated smaller errors of other GGMs over certain small spatial regions within Egypt, the attained findings in the current research might be superior since the processing has been performed over the entire Egyptian territories. Thus, the accomplished updated GGM (Fig. 4.3) provides the optimum stand-alone geoid model in Egypt.

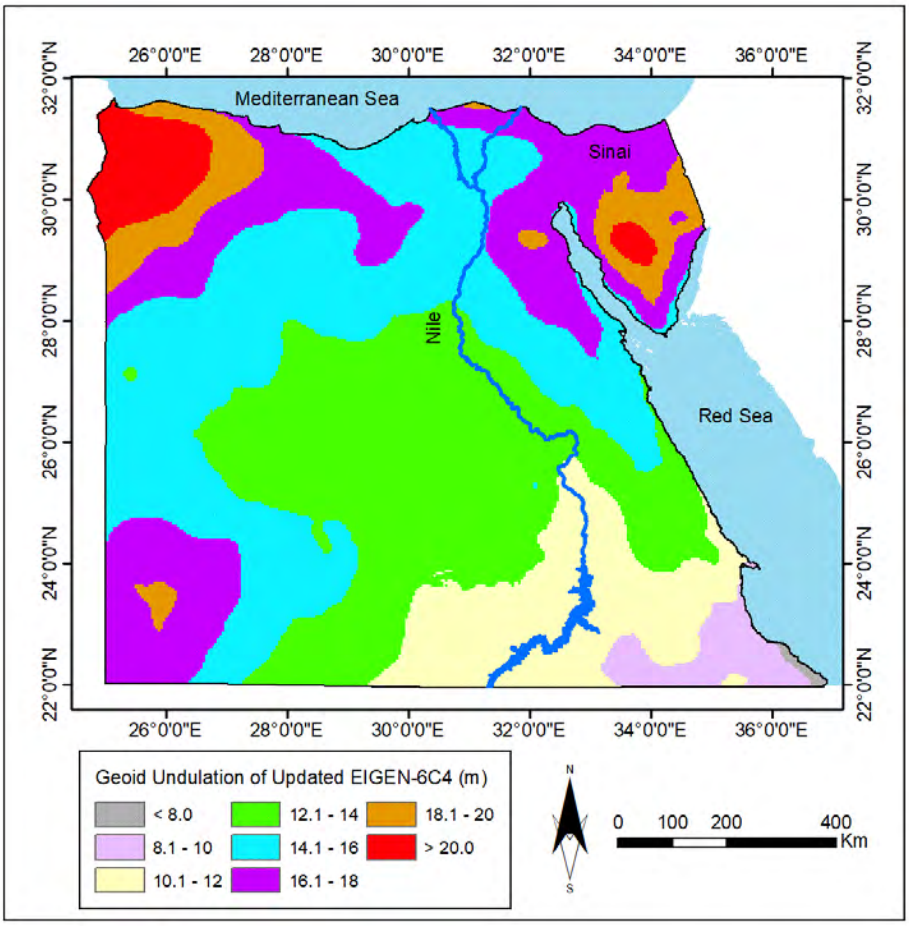

Fig. 4.3: Updated EIGEN-6C4 GGM Geoid Undulations in Egypt.

5 *Discussion and conclusions*

An optimum Global Geopotential Model (GGM) is necessary either to represent the long wavelength of the Earth's gravitational field in gravimetric geoid modelling or to act as a stand-alone national geoid in some developing countries. In several developing countries, there are no published accurate geoid models to be utilized as a height conversion tool in GNSS surveying and mapping projects. Thus, selecting the optimum GGM and updating it with local geodetic datasets in a country could be a cost-effective alternative. The current research aims to investigate the performance of seven recent high-order GGMs in Egypt. The investigated models consist of `SGG-UGM-2`, `XGM2019e_2159`, `GECO`, `EIGEN-6C4`, `EGM2008`, `SGG-UGM-1`, and `EIGEN-6C3stat` models. The assessment has been performed utilizing the most recent precise Global Navigation Satellite Systems(GNSS)/Levelling datasets in Egypt.

Over the available GNSS/Levelling stations, the investigated GGMs perform roughly comparable with a standard deviation varies between ±0.249 m and ±0.300 m. Since those levels of accuracy are different from the published worldwide ones, it might indicate that the terrestrial dataset may include some erroneous measurements or outliers. Performing a statistical test for outlier detection resulted in removing almost 10 % of the

available stations After outliers are flagged and removed, a 3D spatial correction surface over the Egyptian territories has been constructed and it has been added to the original `EIGEN-6C4` model to get an updated version of the global `EIGEN-6C4`. The comparison over checkpoints revealed that the errors of the updated model have a mean of -0.018 m and a standard deviation equals ± 0.011 m. That concludes that incorporating terrestrial geodetic data into the global `EIGEN-6C4` model has increased its accuracy in Egypt by almost 36 % as the overall standard deviation has been decreased from ± 0.172 m to ± 0.110 m.

It should be noticed that some previous studies reported small errors of GGMs over small particular regions within Egypt, the current research has the advantage of performing the GGMs analysis over the entire country to select the most accurate model from a national perspective. Thus, such an accomplished updated GGM represents the optimum stand-alone geoid model in Egypt.

However, such accuracy levels of GGMs do not meet the requirements of high-accuracy surveying and civil engineering applications. That concludes that a precise national geoid model is still a must. It is recommended that all available geodetic datasets should be collected from all governmental and private organizations to construct a national geodetic database that will be implemented in modelling an Egyptian local geoid.

References

Abd-Elmotaal, H. A., N. Kühtreiber, K. Seitz and B. Heck, 2020. “A Precise Geoid Model for Africa: AFRgeo2019”. In: *Beyond 100: The Next Century in Geodesy*. Ed. by J. T. Freymueller and L. Sánchez. Cham: Springer International Publishing, 77–87. ISBN: 978-3-031-09857-4.

Borghi, A., R. Barzaghi, O. Al-Bayari and S. Al Madani, 2020. Centimeter precision geoid model for Jeddah region, Saudi Arabia. *Remote Sensing*, **12**, 2066. DOI: 10.3390/rs12122066.

Dawod, G. and H. Mohamed, 2022. GIS-based geoid refinement by GNSS/levelling data: A case study of Egypt. *International Journal of Engineering Inventions*, **11** (2), 25–32.

Dawod, G., H. Mohamed and E. Al-Krargy, 2019. Accuracy assessment of the PGM17 global geopotential model: a case study of Egypt and Northeast Africa. *Arabian Journal of Geosciences*, **12**, 246. DOI: 10.1007/s12517-019-4418-9.

Elsaka, B. and M. El-Ashquer, 2022. Determination of local quasi-geoid models using FFT estimation technique based on combined gravity anomalies from CHAMP, GRACE, GOCE, future satellite missions and in-situ gravity observations in western desert of Egypt. *IOSR Journal of Applied Geology and Geophysics*, **10** (1), 15–24.

Elwan, M., A. Helaly, K. Zharan, E. Issawy and A. Abd El-Gawad, 2021. Local geoid model of the western desert in Egypt using terrestrial gravity data and global geopotential models. *Arabian Journal of Geosciences*, **14**, 1436. DOI: 10.1007/s12517-021-07817-6.

Forsberg, R. and C. Tscherning, 2008. *Gravsoft geodetic gravity field modelling programs*. National Space Institute, Denmark.

Förste, C., S.L. Bruinsma, F. Flechtner, J.C. Marty, J.M. Lemoine, C. Dahle, O. Abrikosov, K. Neumayer, R. Biancale, F. Barthelmes and G. Balmino, 2012. "A preliminary update of the Direct approach GOCE Processing and a new release of EIGEN-6C". Presented at AGU Fall Meeting, San Francisco, USA.

Förste, C., L. Sean, O. Abrikosov, J. Lemoine, J. Marty, F. Flechtner, G. Balmino, F. Barthelmes and R. Biancale, 2014. *EIGEN-6C4 The latest combined global gravity field model including GOCE data up to degree and order 2190 of GFZ Potsdam and GRGS Toulouse*. DOI: 10.5880/ICGEM.2015.1.

Gilardoni, M., M. Reguzzoni and D. Sampietro, 2016. GECO: a global gravity model by locally combining GOCE data and EGM2008. *Studia Geophysica et Geodaetica*, **60**, 228–247. DOI: 10.1007/s11200-015-1114-4.

Hamdy, A. and M. Elshewy, 2022. Assessing the accuracy of the geoid heights calculated by interpolation and extrapolation from global geoid models in northern Egypt. *Journal of Al-Azhar University Engineering Sector*, **17** (63), 502–511.

Hofmann-Wellenhof, B. and H. Moritz, 2005. *Physical geodesy*. New York: SpringerWien.

ICGEM, 2023. *International Center for Global Earth Model*. Accessed Jan 10. URL: http://icgem.gfz-potsdam.de/home.

Isik, M., M. Çevikalp, B. Erol and S. Erol, 2022. Improvement of GOCE-based global geopotential models for gravimetric geoid modeling in Turkey. *Geosciences* (12). DOI: 10.3390/geosciences12120432.

Jassim, M. and M. Yousef, 2021. Local geoid model generation using the geometrical approach. *Journal of Civil Engineering and Architecture* (15), 437–445. DOI: 10.17265/1934-7359/2021.08.005.

Al-Karargy, E and G. Dawod, 2021. "Optimum combinations of GGM and GDEM models for precise national geoid modelling". In: *Proceedings of Engineering and Technology Innovation*. Vol. 18, 15–24.

Klokočníka, J., V. Cílekb, J. Kosteleckýc and A. Bezděk, 2020. Gravity aspects from recent Earth gravity model EIGEN 6C4 for geoscience and archaeology in Sahara, Egypt. *Journal of African Earth Sciences*, **168**. DOI: 10.1016/j.jafrearsci.2020.103867.

Lestari, R., B. Bramanto, K. Prijatna, A. Pahlevi, W. Putra, R. Muntaha and F. Ladivanov, 2022. Local geoid modeling in the central part of java, Indonesia, using Q1 terrestrial-based gravity observations. *Geodesy and Geodynamics*. DOI: 10.1016/j.geog.2022.11.007.

Liang, W., J. Li, X Xu, S. Zhang and Y. Zhao, 2020. A High-Resolution Earth's Gravity Field Model SGG-UGM-2 from GOCE, GRACE, Satellite Altimetry, and EGM2008. *Engineering*, 860–878. DOI: 10.1016/j.eng.2020.05.008.

Liang, W., R. Pail, X. Xu and J. Li, 2022. A new method of improving global geopotential models regionally using GNSS/levelling data. *Geophysical Journal International*, **221**, 542–549. DOI: 10.1093/gji/ggaa047.

Liang, W., X. Xu, J. Li and G. Zhu, 2018. The determination of an ultra high gravity field model SGG-UGM-1 by combining EGM2008 gravity anomaly and GOCE observation

data. *Acta Geodaeticaet Cartographica Sinica*, **47** (4), 425–434. DOI: 10.11947/j.AGCS.2018.20170269.

Osman, A., M. Anjasmara1, A. Ruby and Z. Udama, 2021. "Assessment of high-degree reference models and Recent Goce/Grace Global Geopotential Models over Sudan based on the GPS/Leveling data". In: *IOP Conf. Series: Earth and Environmental Science*. Vol. 936. DOI: 10.1088/1755-1315/936/1/012035.

Pavlis, N.K, S.A Holmes, S.C Kenyon and J.K. Factor, 2012. The development and evaluation of the Earth Gravitational Model 2008 (EGM2008). *Journal of Geophysical Research: Solid Earth*, **117**, B04406. DOI: 10.1029/2011JB008916.

Phinyo, K., P. Dumrongchai, C. Srimanee and B. Witchayangkoon, 2021. Methodology of Local Geoid Improvement Using Least-Squares Collocation with Parameters and an Optimal Covariance Function. *International Transaction Journal of Engineering, Management, & Applied Sciences & Technologies*, **12** (5). DOI: 10.14456/ITJEMAST.2021.105.

Singh, D. and R. Srivastava, May 6–11, 2018. "Development of geoid model – a case study on western India". In: *Proceedings of the FIG Congress*. Istanbul, Turkey.

SRI, 2022. A geodatabase of GNSS/Levelling data over Egypt. Tech. rep. 2. Giza, Egypt: Survey Research Institute.

Tocho, C., E. Antokoletz, A. Gómez, H. Guagni and D. Piñon, 2022. Analysis of high-resolution global gravity field models for the estimation of International Height Reference System (IHRS) coordinates in Argentina. *Journal of Geodetic Science*, (12), 131–140.

Zingerle, P., R. Pail, T. Gruber and X. Oikonomidou, 2020. The combined global gravity field model XGM2019e. *Journal of Geodesy*, **94**, 66. DOI: 10.1007/s00190-020-01398-0.

Available online www.jsaer.com

***Journal of Scientific and Engineering Research*, 2023, 10(11):63-71**

Research Article

ISSN: 2394-2630
CODEN(USA): JSERBR

Monitoring Vertical Land Movements in the Nile Delta, Egypt by GNSS Datasets Over 2012-2023

Gomaa M. Dawod*, Hoda F. Mohamed, Ahmed M. Amin

Survey Research Institute, National Water Research Center, Giza, Egypt
*Email: dawod_gomaa@yahoo.com

Abstract Vertical land movement is a natural and human hazard that should be precisely monitored. Global Navigation Satellite Navigation (GNSS), terrestrial levelling, and radar remote sensing provide various technical alternatives to monitor land subsidence. The current research has utilized 23 GNSS stations cover the period 2012-2023 to estimate precise rates of vertical land movements in the Nile delta region, Egypt. The Precise Point Positioning (PPP) approach of GNSS data processing has been utilized. An average accuracy of two millimeters has been accomplished using 24-hours continuous GNSS dataset at each station. The accomplished 3D findings demonstrate that the land vertical movements over the entire Nile delta region vary between -7.2 mm/year and +2.6 mm/year with an average equals -1.4 mm/year. Hence, it is recommended to take into account the influences of such hazardous phenomenon on the huge infrastructures and development plans in the Nile delta region that contains almost half of the population of Egypt.

Keywords GNSS, Land Subsidence, Uplift, PPP, Natural Hazards.

1. Introduction

The Nile delta region in Egypt, as a low-elevation coastal region, suffers from several environmental natural hazards affecting the population and the economy. Some of these global climate-change based hazards include, among others, Sea Level Rise (SLR), land subsidence, sea-water intrusion [1], soil degradation [2], SLR inundation [3], and coastline retreat [4]. The vertical land movements comprise a vital hazard depends on natural and human causes. Vertical land movements, particularly land subsidence, defined as the settlement of the land surface resulted from human-induced and natural-driven processes. Land subsidence could be attributed to natural compaction of unconsolidated deposits, groundwater extraction for examples. A recent study highlighted that nineteen percent of the global population face a high probability of subsidence [5]. On another scene, land subsidence could be dangerous and reach as high as 44 mm/year in some regions worldwide [6].

Several approaches have been carried out to monitor subsidence particularly in the Nile delta region. Gebremichael et al. [7] have utilized radar interferometric approach over 2004 to 2010 to monitor land subsidence over the entire Nile delta of Egypt. Their results showed that land subsidence could be as -9.7 mm/year over the north central and northeastern delta where uplift of 2.5 mm/year occurred that separates the highly subsiding northern block from the stable or slightly uplifting southern delta block. Moreover, Becker and Sultan [8] utilized radar remote sensing images over 1992-1999 and showed that land subsidence could be as much as -8 mm/year over the Nile delta region. Land subsidence could be also estimated from tide gauges and satellite altimetry measurements [9]. Traditionally, land subsidence have been monitored by precise levelling [10]. More recently, the Global Navigation Satellite Systems (GNSS) have been utilized to precisely estimate land subsidence [11]. AbouAly et al. [12] have utilized 8 GNSS stations through 2013-2015 to estimate land subsidence over the Nile delta. Their results showed that the highest subsidence rate is found at Mansoura and

Port Said city where it ranges between 2.5 mm/year to 10 mm/year. The Precise Point Positioning (PPP) is considered one of the most precise GNSS data processing alternative to ensure high precision in land subsidence and crustal deformation [13].

The current research employed the PPP approach for processing GNSS datasets over 2012-2023 to estimate recent rates of vertical land movements in the Nile delta.

2. Study Area and Available Data

The study area in the current research not only limited by the classical definition of the Nile delta as bounded by the two branches of the Nile River. It is extended in the west direction to include the Alexandria city and in the east direction to include the Suez Canal too. Accordingly, it extends from longitude 29.8^0 E to 32.4^0 E and from latitude 29.9^0 N to 31.6^0 N covers 34785.6 km^2 as depicted in Fig. 1.

23 GNSS stations have been acquired from the Egyptian Survey Authority (ESA) over the study area (Fig. 1). A set of several observation files for each station covering continuous 24-hour session have been collected annually from 2012 to 2023. Few observation files have been missing at some stations due to communication problems between the stations and the GNSS data center at ESA headquarter. The collected GNSS datasets are tabulated in Appendix 1.

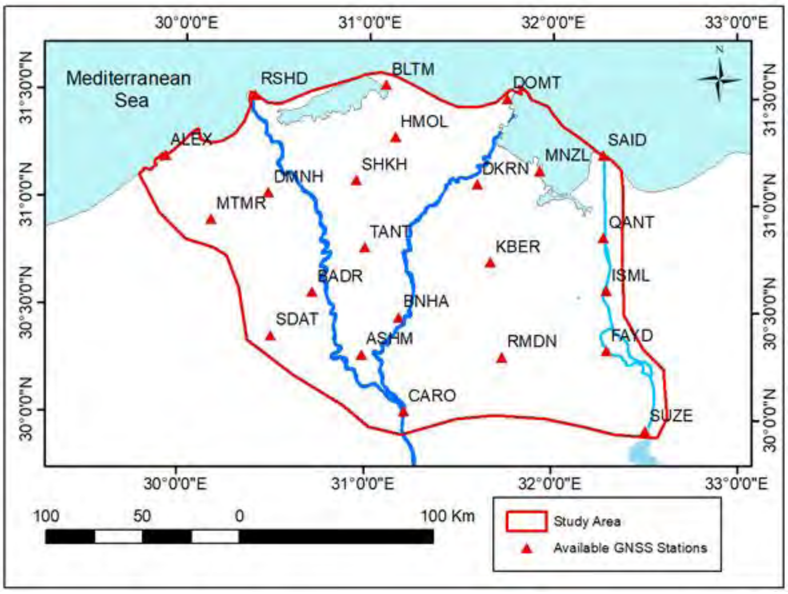

Figure 1: Study Area and Available GNSS Stations

3. Methodology

First, the PPP approach of the GNSS data processing has been carried out several times at each stations for all available observation sessions. PPP modeling relates the ionosphere-free combinations of dual-frequency GPS pseudorange (P_i, i = 1, 2) and carrier phase observations (ϕ_i) to the unknown parameters according to the following simplified observation equations [14]:

$$l_P = \rho(X_s, X_r) + c(dT - dt) + T_r + \varepsilon_P \quad (1)$$

$$l_\phi = \rho(X_s, X_r) + c(dT - dt) + T_r + N\lambda + \varepsilon_\phi \quad (2)$$

where,

l_P is the ionospheric-free combination of P_1 and P_2 pseudoranges,

l_ϕ is the ionospheric-free combination of ϕ_1 and ϕ_2 carrier phases,

N is the non-integer ambiguity,

X_s is the satellite Cartesian coordinates at transmission time,

X_r is the GPS Cartesian coordinates at reception time,

dT is the GPS receiver clock offset from the GPS time,

dt denotes the satellite clock offset from the GPS time,

T_r is the signal path delay to the neutral-atmospheric (mainly troposphere),

λ is the wavelength, and

ε denotes the noises.

The Trimble Business Center (TBC) version 5.2 software has been utilized to perform the PPP computations. The satellite precise orbits and clock corrections have been downloaded from the International GNSS Service (IGS) website: https://igs.org/. Consequently, a time series of ellipsoidal elevations has been obtained, relative to International Terrestrial Reference Frame 2014 (ITF2014) for each station over its corresponding available time span.

Next, a first-order regression is fitted for the elevations of each station to model its vertical movements in the form of:

$$h = a_0 + a_1 Year \qquad (3)$$

where, a_0 and a_1 are unknowns to be determined and Year represents the observation time in years. The unknown a_1 represents the annual vertical movement at such a station.

The coefficient of determination, R^2, is computed to describe the goodness of the regression as:

$$R^2 = 1 - \frac{\sum (h_i - h_p)^2}{\sum (h_i - h_m)^2} \qquad (4)$$

where,

h_i is the i^{th} observed elevation of the current station,

h_p is the i^{th} predicted elevation observation of the current station,

h_m is the i^{th} mean elevation observation of the current station,

Statistically speaking, R^2 represents the goodness of fit of a regression model. It ranges from 0 to 1, and as it goes to 1 indicates the strength of the model. If its value is less than 0.5, the attained regression model might not be trustable.

Collecting all trustable regression trends of vertical land movements at available GNSS stations, the Arc GIS 10.8 software is utilized to build a 3D model of land movement phenomena over the study area. The processing steps are depicted in Fig. 2.

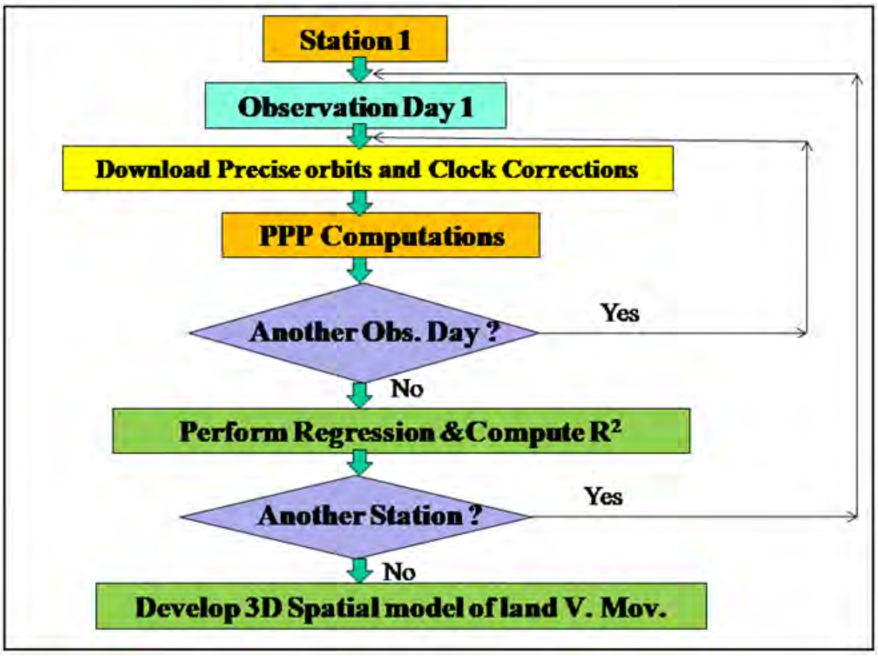

Figure 2: Flowchart of the Processing Steps

4. Processing and Results

Investigating the results of PPP GNSS processing showed that the attained elevation typical accuracy range from ±0.002 to ±0.006 m with an average equals ±0.003 m (Fig. 3). Such an accuracy level was expected since

the utilized GNSS sessions comprise 24-hour continuous datasets. Next, the findings of the regression modelling indicate that 15 out of the utilized GNSS stations have a good-fit regression models with R^2 values greater than 0.5. Fig. 4 depicts a typical example of such a situation at Port Said station. Such stations along with their statistics are depicted in Fig. 5 and tabulated in Table 1. The remaining stations, with weak R^2 values, might be an indication that the vertical land movements phenomenon do no posses a linear regression model over 2012-2023 and more GNSS data are required. From Table 1, it can be realized that the vertical land movements in the Nile delta region consists generally from subsidence ranges between -0.0005 m at MTMR station and -0.005 m at both SAID and TANT stations. Few GNSS stations showed uplift varying between +0.001 at Suez and +0.002 m at BADR [15]. It worth mentioning that the accomplished findings generally agree with results of similar research studies at the Nile delta region.

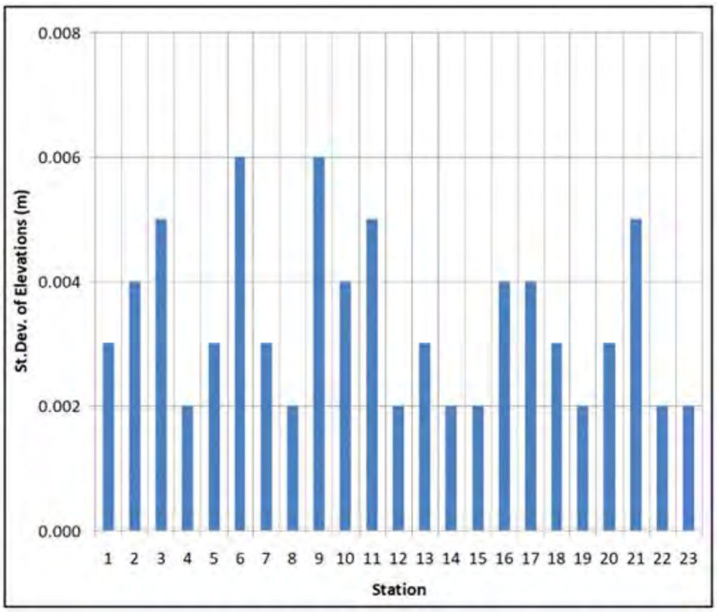

Figure 3: Typical Accuracy of Accomplished GNSS Elevations

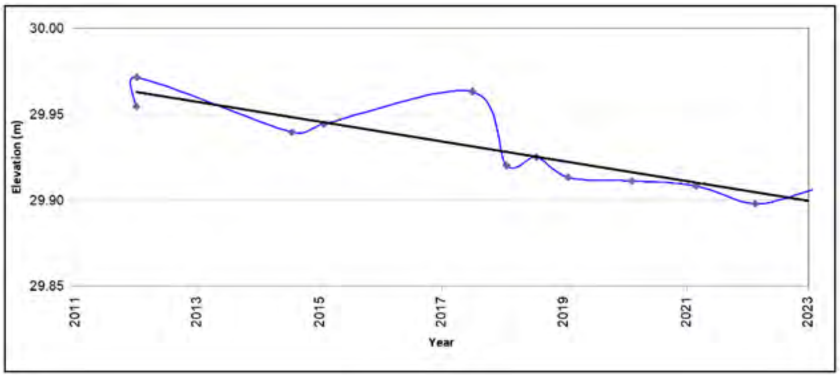

Figure 4: A Typical Example of Linear Regression at Port Said GNSS Station

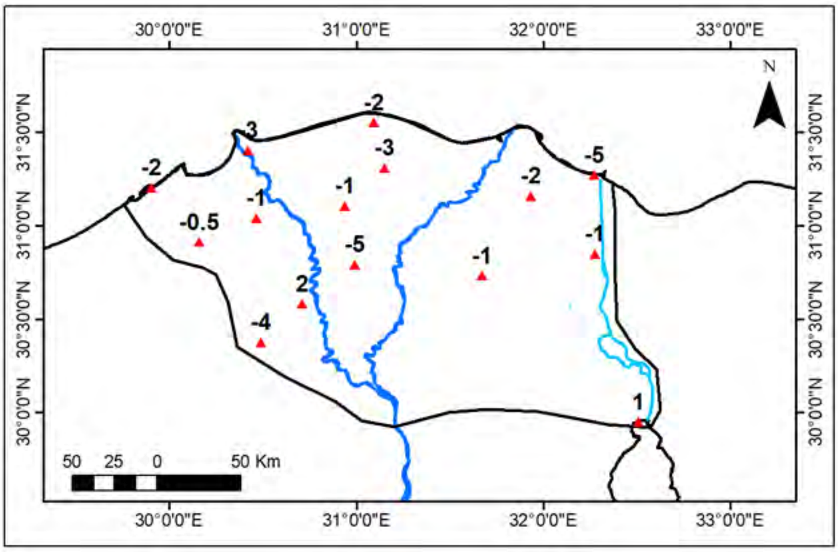

Figure 5: Rates of Vertical Land Movements at GNSS Stations

Table 1: Statistics of Linear Regression at GNSS Stations

Station	Regression	Annual Trend (mm/year)	R2
BLTM	h = -0.002 year + 36.11	-2	0.93
SKKH	h = -0.001 year + 34.09	-1	0.82
BADR	h = 0.002 year + 43.98	+2	0.81
MNZL	h = -0.002 year + 41.57	-2	0.78
DMNH	h = -0.001 year + 45.25	-1	0.77
SAID	h = -0.005 year + 41.51	-5	0.77
RSHD	h = -0.003 year + 44.83	-3	0.73
TANT	h = -0.005 year + 51.38	-5	0.71
ALEX	h = -0.002 year + 72.09	-2	0.71
KBER	h = -0.001 year + 35.57	-1	0.68
HMOL	h = -0.003 year + 50.14	-3	0.67
SUEZ	h = 0.001 year + 44.31	+1	0.55
SDAT	h = -0.004 year + 81.42	-4	0.54
MTMR	h = -0.0005 year + 34.1616	-0.5	0.54
QANT	h = -0.001 year + 36.33	-1	0.53

Finally, the GIS-based analysis tools have been performed to convert the vertical land movements rates at discrete GNSS points to a 3D spatial model (Fig. 6). Accordingly, the land vertical movements over the entire Nile delta region found to range from -7.2 mm/year and 2.6 mm/year with an average equals -1.4 mm/year. Fig. 6 shows also that the higher subsidence occurred at the most northeast of the study area at Port Said city and the central west area around Tanta city. Additionally, the uplift occurs in the eastern area around Suez city and around Badr city too. Furthermore, the vertical land movement phenomenon has been investigated over the governorates (administration units) in the study area. Fig. 7 and Table 2 present the accomplished findings. Thus, it can be recognized that Gharbiya, Daqahlia, and Port Said governorates have the higher rates of annual land subsidence. Thus, it is recommended to pay attention to the effects of land subsidence mainly in the operation and management planes of huge infrastructures in such regions.

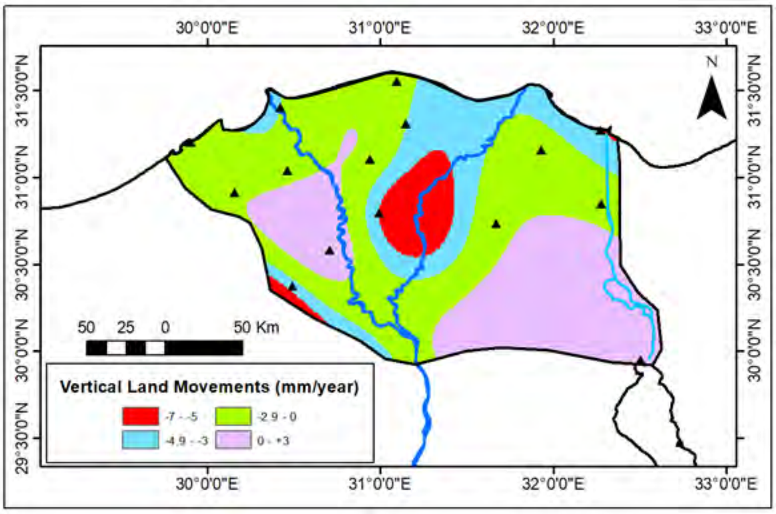

Figure 6: 3D Model of Vertical Land Movements in The Nile Delta Region

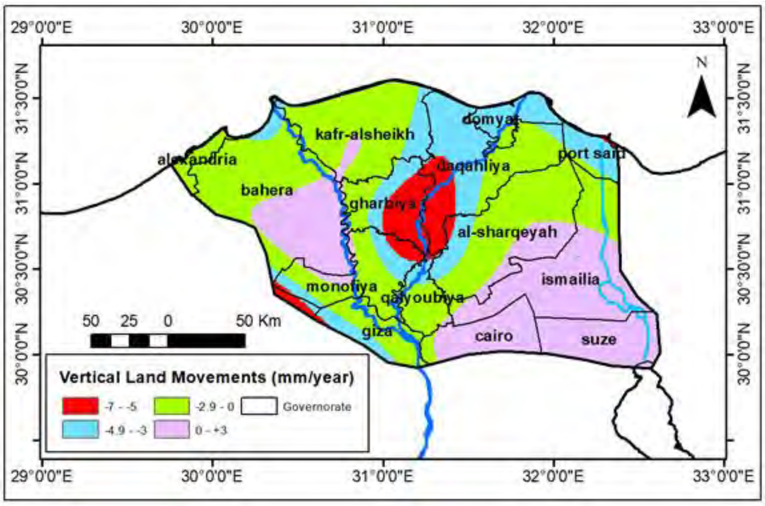

Figure 7: Vertical Land Movements in The Nile Delta Governorates

Table 2: Statistics of Vertical Land Movements in The Nile Delta Governorates (mm/year)

Governorate	Min	Max	Mean
Gharbiya	-5.98	0.97	-4.32
Daqahlia	-7.15	-1.39	-3.92
Port Said	-5.21	-2.55	-3.69
Damietta	-4.25	-2.39	-3.42
Menofia	-7.16	1.06	-2.47
Giza	-5.88	-0.62	-2.43
Qalioubiya	-5.68	0.31	-1.984
Alexandria	-2.9	-1.39	-1.94
Kafr El-Sheikh	-4.93	0.17	-1.49
Sharqiya	-5.99	0.77	-1.21
Beherra	-5.41	2.55	-0.4
Ismalia	-2.95	1.66	0.48
Suez	0.13	2.11	1.29
Cairo	-0.96	2.38	1.4

5. Conclusions

The PPP approach of GNSS comprise an effective and cost-effective technical method for monitoring vertical land movements over a region. Based on GNSS datasets at 23 stations over the 2012-2023 period, the current study aims to precisely monitor the vertical land movement phenomena in the Nile delta region, Egypt. It has been found that 15 stations showed trustable land movement trends while the remaining stations do not, which implicitly recommend that more GNSS data are required over longer period of times.

Land subsidence is an ongoing natural and human phenomenon in the Nile delta region. Based on the results of 23 GNSS, it has been shown that several locations in the study area have experienced land subsidence, with an average rate of about -1.4 mm/year and can go up to about -5 mm/year in certain locations. Moreover, some regions in that area showed relatively minor uplift of almost 2 mm/year.

Causes of land subsidence, such as groundwater extraction and urban development, need to be investigated in details. Effects of land subsidence to the absolute estimation of sea level rise should be studied too. Additionally, it has been recognized that Gharbiya, Daqahlia, and Port Said governorates have the higher rates of annual land subsidence. Thus, it is recommended to take into consideration such effects in the operation and management plans of huge infrastructures in such regions.

Conflicts of interest statement: The authors declare that there is no conflicts of interest.

Funding information: Mo fund was allocated to the current research study.

References

[1]. Abdelfattah, M., Abu-Bakrm H., Aretouyap, Z., Sheta, M., Hassan, T., Geriesh, M., Shaheen, S., Alogayell, H., EL-Bana, E., and Gaber, A. (2023) Mapping the impacts of the anthropogenic activities and seawater intrusion on the shallow coastal aquiver of Port Said, Egypt, Frontiers in Earth Science, 11:1204742. https://doi.org/10.3389/feart.2023.1204742

[2]. Abowaly, M., Ali, R., Moghanm, F., Gharib, M., Moustapha, M., Elbagory, M., Omara, A., and Elmahdy, S., (2022) Assessment of soil degradation and hazards of some heavy metals, using Remote Sensing and GIS techniques in the Northern part of the Nile Delta, Egypt, Agriculture, https://doi.org/10.3390/agriculture13010076

[3]. El-Quilish, M., El-Ashquer, M., Dawod, G. and El Fiky, G. (2023) Development of an Inundation Model for the Northern Coastal Zone of the Nile Delta Region, Egypt Using High-Resolution DEM, Arabian Journal for Science and Engineering, 48:601–614, https://doi.org/10.1007/s13369-022-07013-y

[4]. El-Asmar, H. and Al-Olayan, H. (2013) Environmental Impact Assessment and Change Detection of the Coastal Desert along the Central Nile Delta Coast, Egypt, International Journal of Remote Sensing Applications, V. 3, No. 3, pp. 159-170.

[5]. Herrera-Garcia, G., Ezquerro, P., Tomás, R., Béjar-Pizarro, M., López-Vinielles, J., Rossi, M., Mateos, R., Carreón-Freyre, D., Lambert, J., Teatini, P., Cabral-Cano, E., Erkens, G., Galloway, D., Hung, W., Kakar, N., Sneed, M., Tosi, L., Wang, H., and Ye, S. (2021) Mapping the global threat of land subsidence, Insights, https://doi.org/ 10.1126/science.abb8549.

[6]. Karlsrud, K., Tunbridge, L., Khanh, N. and Dinh, N. (2020) Preliminary results of land subsidence monitoring in the Ca Mau Province, Proc. IAHS, No. 382, pp. 111–115.

[7]. Gebremichael, W., Sultan, M., Becker, R., El Bastawesy, M., Cherif, O. and Emil, M. (2018) Assessing Land Deformation and Sea Encroachment in the Nile Delta: A Radar Interferometric and Inundation Modeling Approach, Journal of Geophysical Research: Solid Earth, 123, 3208–3224, https:/doi.org/10.1002/%202017JB015084

[8]. Becker, R. and Sultan, M. (2009) Land subsidence in the Nile Delta: inferences from radar interferometry, The Holocene, V. 19, No. 6, pp. 949–954.

[9]. Braitenberg, C., Mariani, P., Tunini, L., Grillo, B. and Nagy, I. (2010) Vertical crustal motions from differential tide gauge observations and satellite altimetry in southern Italy, Journal of Geodynamics, https://doi.org/10.1016/j.jog.2010.09.003

[10]. Fisher, B. and Minkel, D. (2009) Evaluation of Survey Control Stations Height Stability in Subsidence Zone, Available from: https://content.civicplus.com/api/assets/12cd72e5-aba7-45e8-974b-5fa181530efb, Accessed Sept. 12, 2023 .

[11]. Facio, Y. and Berber, M. (2019) Subsidence is determined in the heart of the Central Valley using Post Processed Static and Precise Point Positioning techniques, Applied Geodesy, https://doi.org/10.1515/jag-2019-0043.

[12]. AbouAly, N., Hussien, M., Rabah, M., Zidan, Z. and Saleh, M. (2021a) Land deformation monitoring by GNSS in the Nile Delta and the measurements analysis, Arabian Journal of Geosciences,14:150, https://doi.org/10.1007/s12517-021-06497-6

[13]. AbouAly, N., Hussien, M., Rabah, M., and Zidan, Z. (2021b) Assessment of NRCAN PPP online service in determination of crustal velocity: case study Northern Egypt GNSS Network, Arabian Journal of Geosciences, 14:188, https://doi.org/10.1007/s12517-021-06530-8.

[14]. Ayhan, M. and Almuslmani, B. (2021) Positional accuracy and convergence time assessment of GPS precise point positioning in static mode, Arabian Journal of Geosciences, 14: 1263, https://doi.org/10.1007/s12517-021-07428-1.

[15]. SRI (Survey Research Institute) (2023) Assessing and modelling of land subsidence in the Nile delta area over 2012 – 2023, A technical report in Arabic, Giza, Egypt.

Appendix 1: Available GNSS Stations

St. No.	1	2	3	4	5	6	7	8	9	10	11	12	13	14	15	16	17	18	19	20	21	22	23
Year/St.	ALEX	ASHM	BADR	BLTM	BNHA	CARO	DKRN	DMNH	DOMT	FAYD	HMOL	ISML	KBER	MNZL	MTMR	QANT	RMDN	RSHD	SAID	SDAT	SHKH	SUEZ	TANT
Feb-12	■	■	■	■	■	■	■	■	■	■	■	■	■	■	■	■	■	■	■	■	■	■	■
Jan-13															■								■
Jul-13				■									■										■
Jan-14				■											■								
Jul-14						■							■						■				
Jan-15						■							■						■				
Jul-15		■	■		■	■			■								■	■					
Jan-16	■	■	■			■			■				■			■	■						

Jul-16																							
Jan-17																							
Jul-17																							
Jan-18																							
Jul 18																							
Jan-19																							
Jan-20																							
Jan-21																							
Jan-22																							
Jan-23																							

DE GRUYTER J. Appl. Geodesy 2025; aop

Gomaa Dawod* and Ghada Haggag

Factors affecting the fitting of a global geopotential model to local geodetic datasets over local areas in Egypt using multiple linear regression approach

https://doi.org/10.1515/jag-2024-0102
Received November 24, 2024; accepted December 20, 2024; published online January 8, 2025

Abstract: The increasing accuracy of the recently released Global Geopotential Models (GGMs) make them a reasonable geoid models, particularly in developing countries. Incorporating local geodetic datasets into a GGM could enhance its performance significantly. However, such integration requires appropriate mathematical modelling. The current research investigates the factors influencing the fitting of a GGM to heterogeneous geodetic data over local areas. The Multiple Linear Regression (MLR) approach is performed with variable independent factors to model the GGM discrepancies over two study areas in Egypt. Observed Global Navigation Satellite Systems (GNSS)/levelling and measured terrestrial gravity anomalies are investigated, among other independent variables, in the regression modelling. Based on the available data and attained findings, it has been demonstrated that MLR approach could produce a good fitting of a specific GGM's geoid undulations, namely the XGM2019e_2159 model, locally with a coefficient of determination of more than 0.99. The regression equation has decreased the standard deviation of the investigated GGM-based undulations from ±0.130 m to ±0.046 m. Accordingly, the accuracy of a particular GGM has been enhanced considerably with improvements achieved 99 % and 64 % over the investigated two case study regions in Egypt.

Keywords: GGM; GNSS/Levelling; MLR; gravity; geoid; fitting

***Corresponding author: Gomaa Dawod**, Survey Research Institute, National Water Research Center, 308 Al-Ahram St., Talbia 11211, Giza, Egypt, E-mail: dawod_gomaa@yahoo.com. https://orcid.org/0000-0002-4426-8231
Ghada Haggag, Survey Research Institute, National Water Research Center, 308 Al-Ahram St., Talbia 11211, Giza, Egypt

1 Introduction

The data collection field campaigns, like levelling, in the geodetic applications are generally time-consuming and economically expensive. Thus, observed quantities at some sample discrete stations have to be utilized to estimate such amounts at other un-surveyed locations. In this regard, interpolation techniques constitute a main duty for geodesists. Several methods have been investigated such as Artificial Neural Network [1], multi-quadratic surface modelling [2], geographically weighted regression [3], plane fitting [4], the Geographic Information Systems (GIS)-based correction surface [5], minimum curvature technique [6], and least-squares approach [7]. The classical multiple linear regression has been applied in various geodetic applications such as datum transformation [8], the creation of a digital elevation model [9], and height transformation [10].

In developing countries where there is no published precise geoid model, Global Geopotential Models (GGMs) provide an appropriate alternative. It is worth to mention that recent high-order GGM models reach an accuracy level of less than a couple of decimeters when compared to GNSS/Levelling stations worldwide [11]. Incorporating local geodetic datasets in such global models could enhance their performance significantly. Such a task has been performed in several countries such as Ecuador [5], Japan [12], Egypt [6], and Malaysia [13]. Furthermore, the XGM2019e_2159 Global Geopotential Model (GGM) has been utilized, herein, since it is one of the most recently released high-order GGMs in the last decade. That GGM is utilized as a candidate global models to investigate the regression approach.

The Multiple Linear Regression (MLR) represents a powerful method that has been performed in various geodetic applications. For example, it has been utilized to model the shifts in latitude and longitude from one geodetic datum to another [14]. Also, MLR has been carried out for the development of a Digital Elevation Model (DEM) from topographic contour data [9]. In addition, such an approach has been utilized in fitting a gravimetric geoid to GNSS/Levelling datasets [15].

The current research study investigates the utilization of the MLR approach with variable independent factors to model the spatial variations of a particular GGM's errors over two case studies in Egypt using heterogeneous local geodetic datasets. The novelty of the current research is the usage of the MLR approach to investigate the factors that affect the fitting a GGM over a local region and the development of an optimal fitting mathematical model to get benefits of GGMs in developing countries.

2 Study area and available data

Two study areas have been utilized in the current research. The first one, the Nile Delta, extends about 300 km along the Mediterranean Sea from Alexandria (29.76° E) to Port Said (32.39° E) and extends almost 180 km south to Cairo (31.22° N), with a total area equals 31,511 square kilometers (Figure 1). The second region, the Nile Valley, extends about 800 km from Cairo to Aswan in the south, have a width varies between 150 and 250 km with an overall area equals 135,825 square kilometers. The Nile Delta region includes 161 observed GNSS/Levelling stations, 30 GNSS/Levelling stations reserved as checkpoints, and 25 observed terrestrial gravity points. Similarly, the Nile Valley region includes 264 observed GNSS/Levelling stations, 26 GNSS/Levelling checkpoints, and 27 observed terrestrial gravity points. It is worth mentioning that those stations have been observed by the Survey Research Institute (SRI) using precise static GNSS surveys and first-order levelling approaches to establish geodetic control points in Egypt mainly for water resources management applications. In addition, the gravity stations have been observed by SRI as a part of the Egyptian National Gravity Standardization Network (ENGSN 97) which consists of 5 absolute gravity stations and 145 relative gravity stations.

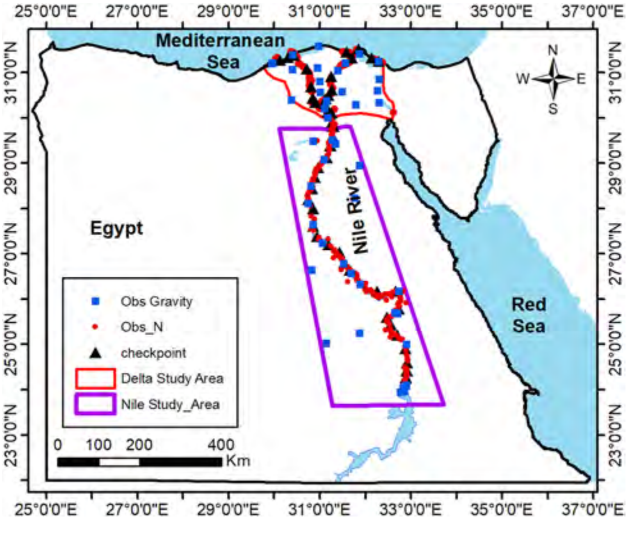

Figure 1: The two study areas.

Since there is no published precise national DEM for Egypt, the NASA DEM has been utilized, the NASADEM [16] has been selected as an appropriate global DEM candidate since it is the most recent released model and it presents the most accurate global model performance over Egypt [17]. NASADEM has been utilized, herein, to convert heights to slopes in order to be added as a variable in a MLR equation. It is worth mentioning that both utilized orthometric and geodetic heights are already observed. Thus, the dependence of that GDEM on WGS84/EGM2008 might affect the estimated slope but would not affect the MLR results considerably. Regarding the NASADEM, it was derived from original telemetry data from the Shuttle Radar Topography Mission (SRTM). In addition to Terra Advanced Spaceborne Thermal and Reflection Radiometer (ASTER) Global Digital Elevation Model (GDEM) Version 2 data, NASADEM also relied on Ice, Cloud, and Land Elevation Satellite (ICESat) Geoscience Laser Altimeter System (GLAS) ground control points of its LiDAR shots to improve surface elevation measurements that led to improved geo-location accuracy. Other reprocessing improvements include the conversion to geoid reference and the use of GDEMs and Advanced Land Observing Satellite Panchromatic Remote-sensing instrument for Stereo Mapping (PRISM) AW3D30 DEM, and interpolation for void filling [16].

The spatial and geodetic characteristics of both study areas have been investigated as depicted in Figures 2 and 3. It has been recognized that the orthometric heights of the Nile Delta region varies between −72.3 m and 522.2 m with an average of 23.5 m, while the Nile Valley area has orthometric heights ranging between −103.2 m and 879.4 m with a mean equals 292.7 m (Table 1). The Arc GIS spatial analysis tools have been carried out to estimate the terrain slopes over both study areas based on that DEM. It has been found that the slopes in the first study area vary between 0 and 54.5° with an average of 2.0°. Additionally, the slopes in the Nile Valley area range between 0 and 75.5° with an average of 3.4°.

Furthermore, the XGM2019e_2159 Global Geopotential Model (GGM) has been utilized herein. It is one of the most recently released high-order GGMs in the last decade [18]. Out of several GGM models, the XGM2019e_2159 proves to be the most accurate one over Egypt [19] and Kuwait too [20]. Its geoid undulations and free-air gravity anomalies have been downloaded from the International Center for Global Earth Model [11].

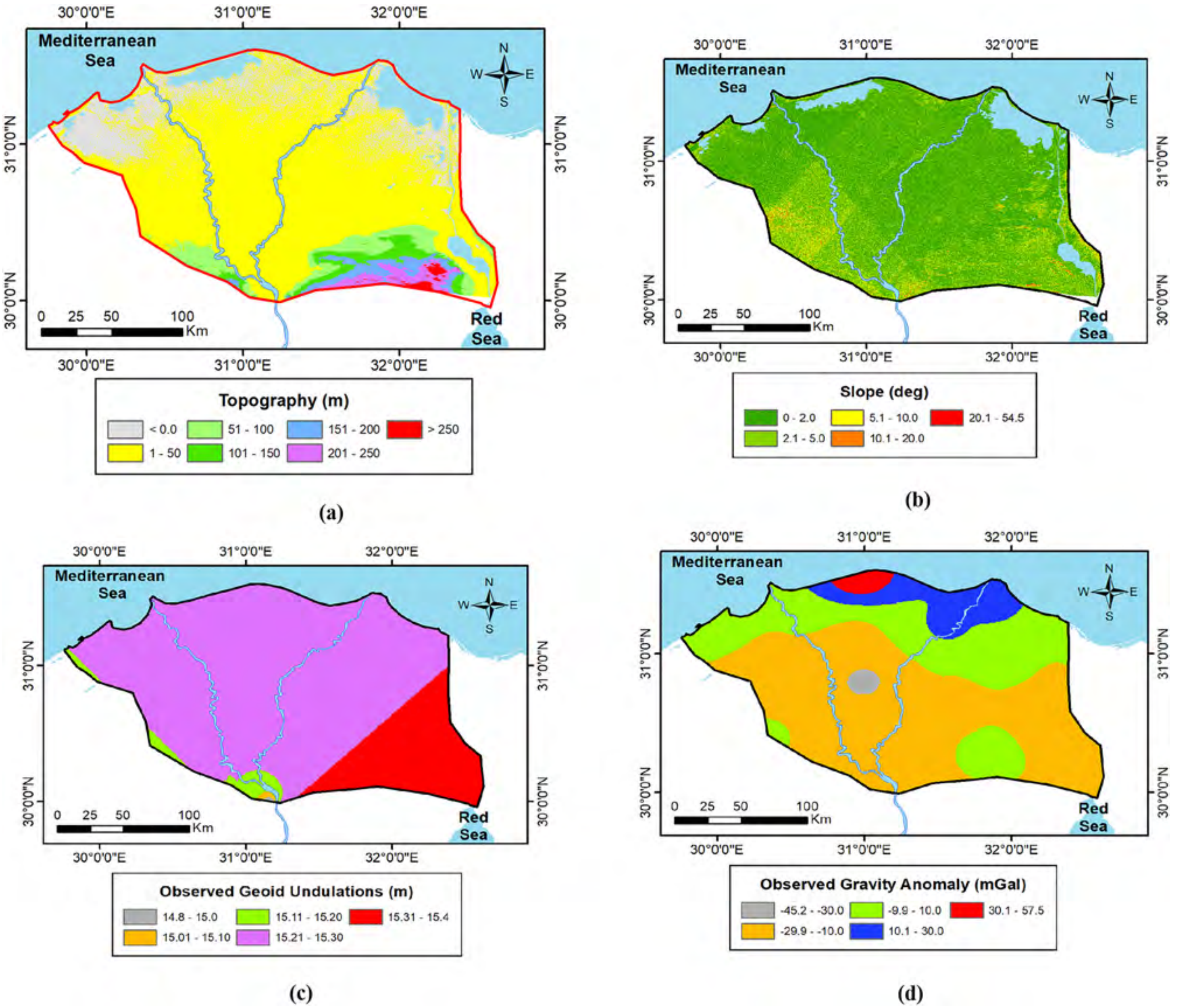

Figure 2: Characteristics of Nile Delta Study Area.

3 Methodology

Based on the observed ellipsoidal (h) and orthometric (H) heights at available stations in both study areas, the observed geoid undulation, Nobs, are computed as:

$$N_{obs} = h - H \tag{1}$$

Afterward, the undulation discrepancies of the investigated GGM model, ΔN, is estimated as the difference between the observed and the GGM-based, N_{GGM}, interpolated undulation at every station:

$$\Delta N = N_{obs} - N_{GGM} \tag{2}$$

Subsequently, the investigated Multiple Linear Regression (MLR) equations consist of nine different mathematical models with variable independent factors as:

$$\Delta N = f(\phi, \lambda) + \varepsilon \tag{3}$$

$$\Delta N = f(\phi, \lambda, N_{GGM}) + \varepsilon \tag{4}$$

$$\Delta N = f(\phi, \lambda, h) + \varepsilon \tag{5}$$

$$\Delta N = f(\phi, \lambda, h, H) + \varepsilon \tag{6}$$

$$\Delta N = f(\phi, \lambda, h, H, N_{GGM}) + \varepsilon \tag{7}$$

$$\Delta N = f(\phi, \lambda, h, H, S) + \varepsilon \tag{8}$$

$$\Delta N = f(\phi, \lambda, h, H, , S, N_{GGM}) + \varepsilon \tag{9}$$

$$\Delta N = f(\phi, \lambda, h, H, S, N_{GGM}, GGM\Delta g_{FA}) + \varepsilon \tag{10}$$

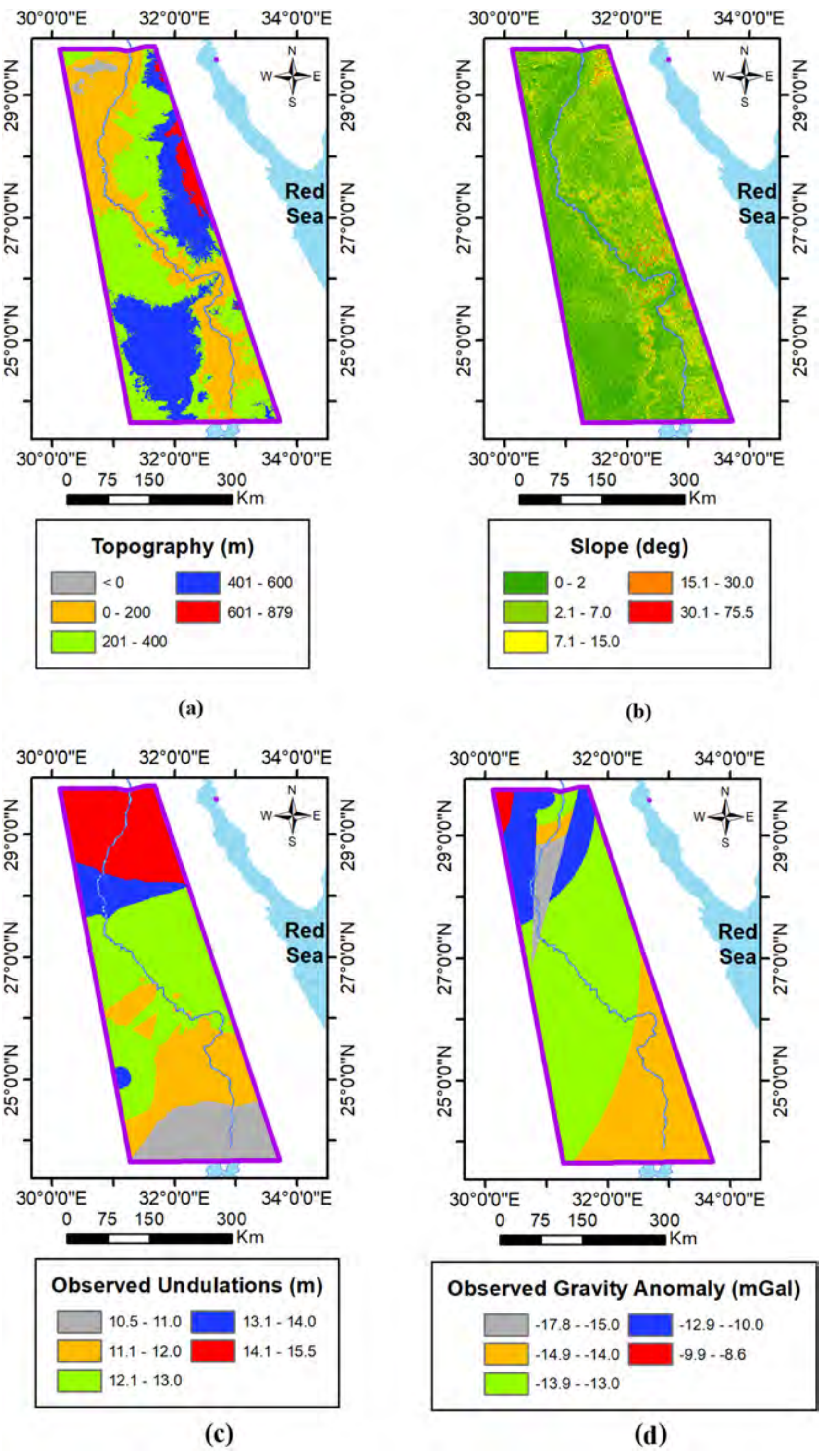

Figure 3: Performance of GGM-Based over Nile Delta Study Area.

Table 1: Statistics of geodetic characteristics of both study areas.

	Minimum	Maximum	Average
Nile Delta Study Area			
Topography (m)	−72.3	522.2	23.5
Slope (deg)	0	54.5	2.0
Observed geoid undulations (m)	14.139	17.466	15.462
Observed gravity anomaly (mGal)	−84.481	54.980	−8.650
Nile Valley Study Area			
Topography (m)	−103.2	879.4	292.7
Slope (deg)	0	75.5	3.4
Observed geoid undulations (m)	10.571	15.522	12.895
Observed gravity anomaly (mGal)	−61.066	30.754	−16.523

Table 2: Statistics of geodetic characteristics of both study areas.

	Minimum	Maximum	Average
Nile Delta Study Area			
Observed geoid undulations (m)	14.804	15.357	15.256
GGM-based geoid undulations (m)	14.740	18.637	16.128
Observed gravity anomalies (mGal)	−36.026	54.965	−8.350
GGM-based gravity anomalies (mGal)	−45.206	57.457	−7.046
Nile Valley Study Area			
Observed geoid undulations (m)	10.577	15.481	12.524
GGM-based geoid undulations (m)	11.249	18.317	13.745
Observed gravity anomalies (mGal)	−17.852	−8.566	−13.682
GGM-based gravity anomalies (mGal)	−42.937	68.309	1.033

$$\Delta N = f(\phi, \lambda, h, H, S, N_{GGM}, obs\Delta g_{FA}, GGM_\Delta g_{FA}) + \varepsilon \tag{11}$$

where,

N_{obs} is the observed geoidal undulation,

N_{GGM} is the GGM-based geoidal undulation,

ϕ, λ are the geodetic latitude and longitude coordinates,

h is the WGS1984-based observed ellipsoidal height,

H is the MSL-based observed orthometric height,

S denotes the slope of the terrain,

$\text{obs}\Delta g_{\text{FA}}$ is the observed free-air gravity anomaly.

$\text{GGM_}\Delta g_{\text{FA}}$ is the GGM-based free-air gravity anomaly. And

ε is the random error.

Having the regression is accomplished, the coefficient of determination, R^2, is estimated. It is a statistical measure about the goodness of the regression model. Its value varies between 0 and 1. As it approaches 1, the attained regression is strong, and as its value is close to 0 the regression is weak. It is computed as:

$$R^2 = 1 - \frac{\sum\left(\Delta N_i - \Delta \underset{\hat{i}}{\hat{N}}\right)^2}{\sum\left(\Delta N_i - \Delta N^-\right)^2} \tag{12}$$

where,

ΔN_i is the observed quantity,

ΔN^- is the mean of the observed quantities, and

$\Delta N^\wedge$ is the predicted quantity.

4 Processing and results

Investigating the performance of the utilized GGM over both local regions has been performed as the first step. Table 2 and Figures 4 and 5 present the accomplished findings. It can be recognized that the GGM-based geoid undulations present smooth patterns since such global models only provide the long and medium wavelengths of the Earth's gravitational field. For instance, the mean GGM-based undulation equals 16.128 m and 13.745 m in the Nile Delta and the Nile Valley regions respectively. On the other hand, the observed geoid undulations in these two regions equal 15.256 m and 12.524 m. A similar remark could be seen too in the differences between the observed and the GGM-based free-air gravity anomalies. Accordingly, there exist considerable undulation discrepancies, over both the investigated study areas, which are needed to be mathematically modeled.

Equations (3)–(11) of MLR have been performed to model the geoid undulation errors of the GGM model. Tables 3 and 4 present those equations with their coefficient of determination R^2 in both study areas. Therefore, it can be commonly noticed that all equations result in more confidence levels (greater R^2) than the traditional regression in only geodetic coordinates (Eq. (3)). Thus, it can be, in general, concluded that the MLR approach yields precise spatial modelling of geoidal undulation discrepancies.

Furthermore, it can seen from Tables 3 and 4 that Eqs. (7), (9)–(11) produce large R^2 values which indicates a strong regression model with high-quality goodness of fitting. Similar results have been reported by [21]. Those equations constitute 5, 6, 7, and 8 independent variables respectively to model the geoid undulation errors of the GGM. The remaining equations contain redundant variables which explains why no attained improvements in the regression fitting. Thus, it can be concluded that the more geodetic variables the better MLR goodness.

Judging the MLR equations over checkpoints composes a more important analysis step in the current investigation. Tables 5 and 6 present the attained results in both

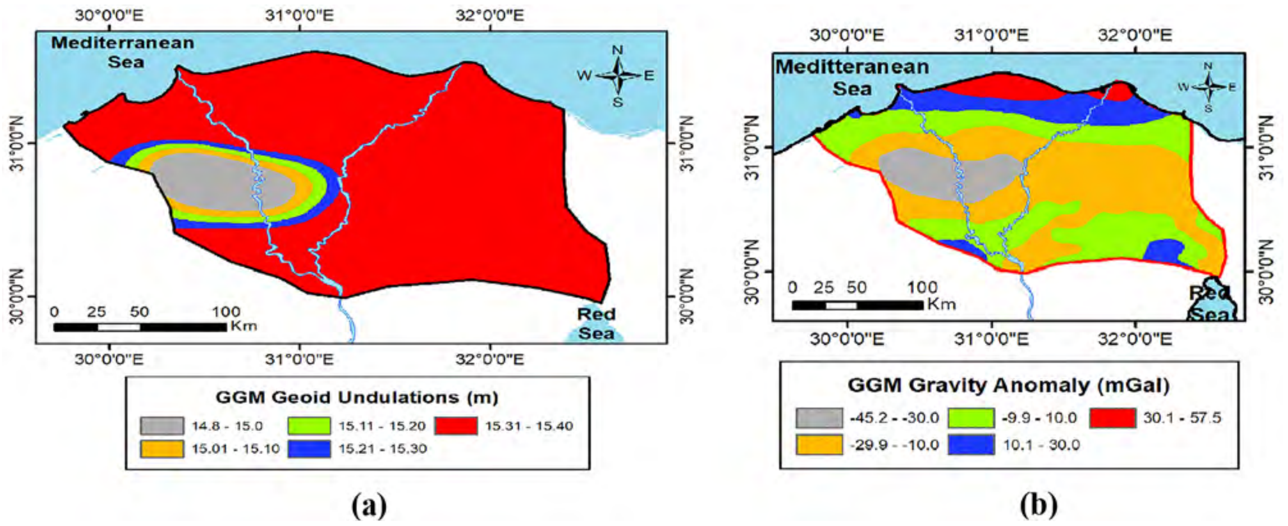

Figure 4: Performance of GGM-Based over Nile Delta Study Area. (a) Geoid undulations. (b) Gravity anomaly.

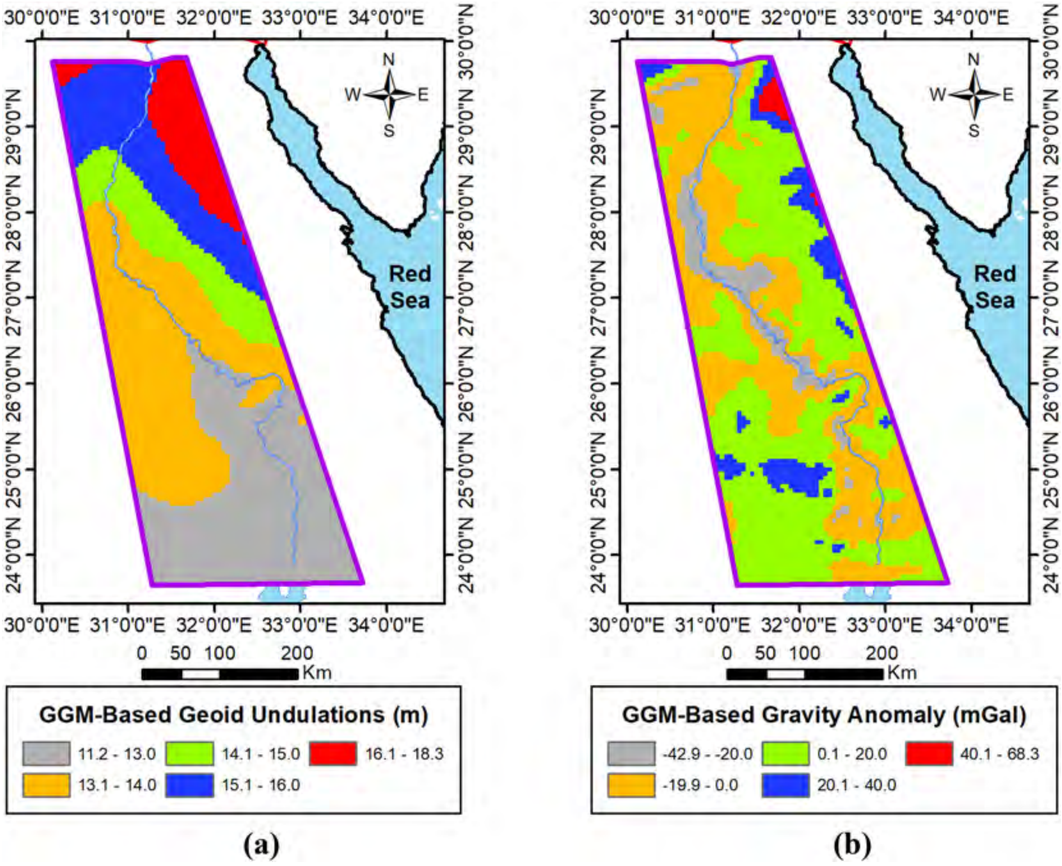

Figure 5: Performance of GGM-Based over Nile Valley Study Area. (a) Geoid undulations. (b) Gravity anomaly.

case study regions. From Table 5, it can be recognized that Eqs. (7), (9)–(11) decrease the GGM-based standard deviation over checkpoints from ±0.134 m to a tenth of a millimeter with an improvement percentage higher than 99.9 in the Nile Delta region. For the Nile Valley area, Eq. (5) is the most accurate MLR model that decreases the standard deviation of the GGM-based undulations from ±0.130 m to ±0.046 m with 64 % improvement. It is worth mentioning

Table 3: Regression equations over checkpoints in the Nile Delta Study.

Eq.	Regression equation	R^2
(3)	$\Delta N = 2.6741783 - 0.0271074\ \phi - 0.0803839\ \lambda$	0.066
(4)	$\Delta N = -0.5931948 + 0.0541170\ \phi - 0.0219059\ \lambda - 0.0653159\ N_{XGM}$	0.098
(5)	$\Delta N = 1.0987955 + 0.0371610\ \phi - 0.0973412\ \lambda + 0.0049070\ h$	0.114
(6)	$\Delta N = 3.4846326 - 0.0273302\ \phi - 0.1324816\ \lambda + 0.0501645\ h - 0.0459169\ H$	0.128
(7)	$\Delta N = 0.0000679 - 0.0000049\ \phi + 0.0000021\ \lambda + 1.0000255\ h - 1.0000257\ H - 1.0000234\ N_{XGM}$	0.999
(8)	$\Delta N = 2.6545019 - 0.0010180\ \phi - 0.1320461\ \lambda + 0.0486701\ h - 0.0443242\ H + 0.0067842\ S$	0.140
(9)	$\Delta N = 0.0002361 - 0.0000105\ \phi + 0.0000024\ \lambda + 1.0000285\ h - 1.0000287\ H - 0.0000015\ S - 1.0000262\ N_{XGM}$	0.999
(10)	$\Delta N = 0.0001592 - 0.0000086\ \phi + 0.0000059\ \lambda + 1.0000320\ h - 1.0000322\ H - 0.0000015\ S - 1.0000350\ N_{XGM} + 0.0000020\ \Delta g_{XGM}$	0.999
(11)	$\Delta N = 0.00003093 - 0.0000113\ \phi + 0.0000049\ \lambda + 1.0000324\ h - 1.0000326\ H - 0.0000015\ S - 1.0000373\ N_{XGM} + 0.0000017\ \Delta g_{XGM} + 0.0000026\ \Delta g_{obs}$	0.999

Table 4: Regression equations over checkpoints in the Nile Valley Study.

Eq.	Regression equation	R^2
(3)	$\Delta N = 2.354801964 - 0.010911916\ \phi - 0.086058036\ \lambda$	0.110
(4)	$\Delta N = -0.9998409 + 0.1006532\ \phi - 0.288434\ \lambda - 0.1086912\ N_{XGM}$	0.132
(5)	$\Delta N = 1.0987955 + 0.0371610\ \phi - 0.0973412\ \lambda + 0.0049070\ h$	0.138
(6)	$\Delta N = 16.67440213 - 0.490287257\ \phi - 0.299405357\ \lambda + 0.428835535\ h - 0.431090734\ H$	0.358
(7)	$\Delta N = 0.6224423 - 0.0167917\ \phi - 0.0104367\ \lambda + 1.0024046\ h - 1.0025129\ H - 0.9898915\ N_{XGM}$	0.9991
(8)	$\Delta N = 16.8134486 - 0.4940501\ \phi - 0.3005561\ \lambda + 0.4309029\ h - 0.4332356\ H - 0.0051733\ S$	0.366
(9)	$\Delta N = 0.6170971 - 0.0166392\ \phi - 0.0103611\ \lambda + 1.0024884\ h - 1.0025950\ H + 0.0000788\ S - 0.9900905\ N_{XGM}$	0.9992
(10)	$\Delta N = 0.6795683 - 0.00192158\ \phi - 0.0112538\ \lambda + 1.0029346\ h - 1.0030482\ H + 0.0000843\ S - 0.9879789\ N_{XGM} - 0.0000779\ \Delta g_{XGM}$	0.9992
(11)	$\Delta N = 0.4052989 - 0.0122362\ \phi - 0.0069847\ \lambda + 1.0026643\ h - 1.0027337\ H + 0.0000417\ S - 0.9931661\ N_{XGM} - 0.0000797\ \Delta g_{XGM} - 0.0015559\ \Delta g_{obs}$	0.9993

Table 5: Performance of regression over checkpoints in the Nile Delta.

Model	Minimum	Maximum	Average	Standard deviation	Improvement
Original GGM	−0.973	−0.522	−0.746	±0.134	NA
3	−0.768	−0.595	−0.666	±0.049	10.7 %
4	−0.284	0.150	−0.081	±0.131	2.6 %
5	−0.253	0.132	−0.076	±0.116	13.3 %
6	−0.235	0.112	−0.072	±0.109	19.1 %
7	−0.000002	0.000009	0.000005	±0.000003	99.997 %
8	−0.232	0.133	−0.070	±0.110	17.9 %
9	−0.000007	0.000017	0.000004	±0.000005	99.996 %
10	−0.000057	0.000076	0.000006	±0.000036	99.973 %
11	0.000191	0.000396	0.000303	±0.000060	99.955 %

that Eq. (7) has fewer parameters or independent variables than the other equations. Thus, it might be considered as the optimum MLR mathematical form to model the GGM discrepancies.

That dissimilarity in the accomplished findings might be attributed to the difference in overall areas, number, and spatial distribution of the available utilized GNSS/Levelling stations in both study areas. Additionally, Figure 1 shows that the Nile Valley case study extends longitudinally more than the Nile Delta case study, which may explain the low improvement of the MLR results in that region.

A similar conclusion has been demonstrated by [21] concerning the factors that could influence the fitting results.

Table 6: Performance of regression over checkpoints in the Nile Valley.

Model	Minimum	Maximum	Average	Standard deviation	Improvement
Original GGM	−0.795	−0.269	−0.599	±0.130	NA
3	−0.746	−0.599	−0.675	±0.059	55 %
4	0.384	0.720	0.513	±0.111	15 %
5	−0.713	−0.583	−0.648	±0.046	64 %
6	−0.795	−0.548	−0.661	±0.070	46 %
7	−0.795	−0.412	−0.617	±0.107	18 %
8	−0.786	−0.542	−0.665	±0.071	45 %
9	−0.795	−0.411	−0.617	±0.107	18 %
10	−0.373	−0.076	−0.162	±0.114	13 %
11	−0.755	−0.415	−0.608	±0.100	23 %

5 Conclusions

The interpolation techniques are usually necessary for geodetic applications to estimate some specific quantities at un-measured locations based on some sample or observed stations. On the other hand, recent high-order global geopotential models produce reasonable accuracy that could be enhanced significantly by incorporating local geodetic datasets over local regions. In this regard, an efficient interpolation technique is in high demand. The current research investigates the utilization of a multiple linear regression approach to model the spatial variation of a GGM model, namely the XGM2019e_2159, over local regions.

The current study has been carried out in two local regions within Egypt; namely the Nile Delta and the Nile Valley. The overall area of such case studies equals 31,511 square kilometers and 135,825 square kilometers respectively. The Nile Delta region includes 161 observed GNSS/Levelling stations, 30 GNSS /Levelling stations reserved as checkpoints, and 25 observed terrestrial gravity points. Likewise, the Nile Valley region includes 264 observed GNSS /Levelling stations, 26 GNSS /Levelling checkpoints, and 27 observed terrestrial gravity points. The investigated MLR equations consist of different mathematical models with variable independent factors including geodetic coordinates, geodetic height, orthometric height, terrain slope, GGM-based geoid undulations, and free-air gravity anomalies.

Based on the available data, the accomplished results have revealed that the MLR approach yields precise spatial modelling of geoidal undulation discrepancies. Additionally, it has been seen that some regression equations produce large coefficients of determination which points out a high-quality goodness of fitting. Such equations constitute 8 independent variables to model the geoid undulation errors of the GGM. Additionally, some of the investigated MLR equations contain redundant variables which clarifies why no attained improvements in the regression fitting. Thus, it can be concluded that the more geodetic independent variables the better MLR goodness.

Assessing the MLR equations over checkpoints has shown that some regression models decrease the GGM-based standard deviation over checkpoints from ±0.134 m to a tenth of a millimeter with an improvement percentage higher than 99.9 in the Nile Delta region. Concerning the Nile Valley area, a regression equation has decreased the standard deviation of the GGM-based undulations from ±0.130 m to ±0.046 m with a 64 % improvement. That variation in the accomplished findings might be attributed to the difference in overall areas, number, and spatial distribution of the available utilized GNSS/Levelling stations in both study areas. Also, the Nile Valley case study extends longitudinally more than the Nile Delta case study, which might clarify the low improvement of the MLR results in that region. In addition, It has been concluded that Eq. (7) contains fewer independent variables than the other equations. Consequently, it might be considered the optimum MLR mathematical form to model the GGM discrepancies. Finally, the attained findings have demonstrated that multiple linear regression is a proper simple mathematical approach to model the errors of a GGM over local regions.

Research ethics: Not applicable.
Informed consent: Not applicable.
Author contributions: Gomaa Dawod has, reviewed the first manuscript, review the findings, finalize the conclusions, and prepare the final version. Ghada Haggag has prepared the first draft, collect the required datasets and participate in preparing the final version.
Use of Large Language Models, AI and Machine Learning Tools: None declared.
Conflict of interest: The authors state no conflict of interest.
Research funding: The authors declare that no funds were allocated to the current study.

Data availability: The data belongs to the Survey Research Institute and might be available by sending an email to: sri.nwrc_eg@yahoo.com.

References

1. Ahmed H, Mohamed E, Bahaa S. Evaluating two numerical methods for developing a local geoid and a local digital elevation model for the Red Sea coast, Egypt. J King Saud Univ, Eng Sci 2023;35:384–92.
2. Soycan M, Soycan A. Surface modelling of GPS-levelling geoid determination. Int Serv Geoid's Newton Bull 2003;41–51.
3. Dawod G, Abdel-Aziz T. Utilization of geographically weighted regression for geoid modelling in Egypt. Appl Geodesy 2019;14:1–12.
4. Pahlevi A, Syafarianty A, Susilo S, Lumban-Gaol Y, Putra W, Triarahmadhana B, et al. Geoid undulation model as vertical reference in Indonesia. Sci Data 2024;11:822.
5. Orejuela I, Gonzalez C, Guerra X, Mora E, Toulkeridis T. Geoid undulation modelling through the Cokriging method: a case study of Gauyaquil, Ecuador. Geodesy Geodyn 2021;12:356–67.
6. Rabah M, Kaloop M. The use of minimum curvature surface technique in geoid computation processing of Egypt. Arabian J Geosci 2011;6:1263–72.
7. Guo D, Chen X, Xue Z, He H, Xing L, Ma X, et al. High-accuracy quasi-geoid determination using Molodensky series solutions and integrated gravity/GNSS/Levelling data. Rem Sens 2023;15: 5414.
8. Dawod G, Alnaggar D. Optimum geodetic datum transformation techniques for GPS surveys in Egypt. In: Proceedings of Al-Azhar sixth international conference, September 1-4. Cairo, Egypt; 2000, vol 4:709–18 pp.
9. Shaker A, Abdullah A, Mahmoud S, Ibrahim S. Multiple polynomial-based regression of DEM from topographic contour data. In: Proceedings of the regional conference on surveying and development. Egypt: Sharm El-Sheikh; 2015.
10. Soycan A, Yilmaz Y, Soycan M. Evaluation of several geoid models for GNSS height transformation in Turkey. Sigma J Eng Nat Sci 2023:130–44.
11. ICGEM (the International Center for Global Earth Model); 2024. http://icgem.gfz-potsdam.de/home [Accessed 20 Nov 2024].
12. Matsuo K, Kuroishi Y. Refinement of a gravimetric geoid model for Japan using GOCE and an updated regional gravity field model. Earth Planets Space 2020;72:33.
13. Nyoka C, Din A, Pa'suya M, Omar A. A combined regional geopotential model using optimized global gravity field solutions. In: The 8th international conference on geomatics and geospatial technology; 2022.
14. Ruffhead A. Introduction to multiple regression equations in datum transformations and their reversibility. Surv Rev 2016;50:82–90.
15. Abd-Elmotaal H, Makhloof A. Two alternative techniques for fitting the gravimetric geoid for Egypt. Contrib Geophys Geodesy 2023;53/4:377–98.
16. USGS (US Geological Survey). NASADEM_HGT: merged DEM global 1 arc second v. 1; 2021. Available from: https://lpdaac.usgs.gov/products/nasadem_hgtv001.
17. Dawod G, Ascoura I. The validity of open-source elevations for different topographic map scales and geomatics applications in Egypt and Saudi Arabia. In: Turkman M, editor. Novel perspectives of geography, environment and earth sciences; 2023, vol 2:1–19 pp.
18. Zingerle P, Pail R, Gruber T, Oikonomidou X. The combined global gravity field model XGM2019e. J Geodesy 2020;94:66.
19. Al-Krargy E, Dawod G. Optimum combinations of GGM and DEM models for precise national geoid development. Proc Eng Technol Innov 2021;18:15–24.
20. Al-Ajami H, Zaki A, Rabah M, El-Ashquer M. A high-resolution gravimetric geoid model for Kuwait using the least-squares collocation. Front Earth Sci 2022;9:753269. https://doi.org/10.3389/feart2021.753269.
21. Jalal S, Musa T, Din A, Aris W, Shen W, Pa'suya M. Influencing factors on the accuracy of local geoid model. Geodesy Geodyn 2019;10:439–45.

Gomaa M. Dawod* and Essam M. Al-Krargy

Recent estimates of crustal deformation and land subsidence in the Nile Delta, Egypt using GNSS-PPP datasets over 2012–2024

https://doi.org/10.1515/jag-2025-0026
Received February 18, 2025; accepted March 29, 2025;
published online April 23, 2025

Abstract: The Precise Point Positioning (PPP) technique has been utilized to process the Global Navigation Satellite Systems (GNSS) annual datasets at 24 stations in the Nile Delta region, Egypt from 2012 to 2024. The present study aims to present recent estimates of horizontal crustal deformation, vertical land movements, and the analysis of the International Terrestrial Reference Frame (ITRF) coordinate conversion between the two utilized ITRF frames in Egypt, namely ITRF2020 (epoch 2024) and ITRF2008 (epoch 2012). Based on the accomplished findings, it has been found that the land subsidence in the Nile Delta region ranges between −3.9 mm/year and 2.3 mm/year with an average of −1.5 ± 1.9 mm/year. Regarding the horizontal crustal movements, it is recognized that such crustal deformations vary between 25.8 mm/year to 27.6 mm/year with an average equals 27.0 ± 1.0 mm/year. In addition, the average direction of that deformation equals 38.6° ± 2.1°. Such results agree normally with those of other studies concerning the regional movements of the Nubia tectonic plate. The attained simple mathematical model describing the relationship between ITRF2024 and ITRF2008 frames shows that the average Cartesian displacement vector equals −0.312 m ± 0.026 m, 0.153 m ± 0.010 m, and 0.152 m ± 0.020 m in the X, Y, and Z directions respectively. Additionally, the velocities are −24 ± 2 mm/year, 12 ± 1 mm/year, and 12 ± 2 mm/year respectively.

Keywords: PPP; GNSS; ITRF; crustal deformation; land subsidence

***Corresponding author: Gomaa M. Dawod**, Survey Research Institute, National Water Research Center, 308 Al-Ahram St., Talbia, Giza 11211, Egypt, E-mail: dawod_gomaa@yahoo.com.
https://orcid.org/0000-0002-4426-8231
Essam M. Al-Krargy, Survey Research Institute, National Water Research Center, 308 Al-Ahram St., Talbia, Giza 11211, Egypt

1 Introduction

The Nile Delta is considered one of the most extensive oases worldwide that was created by the longest river. In addition, this region is one of the most highly populated areas in Egypt and worldwide. Accordingly, it has been subjected to geoscientific studies, particularly regarding its crustal deformation and land subsidence characteristics [1]. It is worth mentioning that most of the world's major river deltas are sinking relative to local sea level. The influences of such land subsidence include aquifer salinization, infrastructure damage, increased vulnerability to flooding and storm surges, and permanent inundation of low-lying land. Thus, determining delta subsidence is a vital topic of ongoing research [2].

Vertical land movements in the Nile Delta have been notably investigated in the last couple of decades. Analysis of GNSS datasets between 2013 and 2015 showed that the land subsidence in this region varies between 2 mm/year in the western part to 10 mm/year in the eastern part [3]. Similarly, Rateb and Abotalib [4] have utilized both Sentinel-1 satellite images and GPS data between 2015 and 2019 and have concluded that the subsidence rates range from −12 to −20 mm/year in major cities, from −3 to −8 mm/year along the coastal margins, and from −20 to −16 mm/year in newly reclaimed lands on the west and east of the Nile Delta. Another research utilized GNSS data over 2013–2015 and has reported that the annual vertical velocity range from west to east with an average rate of 4.9 ± 0.95 mm/year where the maximum subsidence is located at Damietta Branch and Lake Manzala [5]. It is worth mentioning that increasing groundwater abstraction increases land subsidence in the Nile Delta region which might cause various damages to different properties [6]. Recently, utilizing GNSS data over 2012–2023 has reported that the land vertical movements over the entire Nile delta region vary between −7.2 mm/year and +2.6 mm/year with an average equals −1.4 mm/year [7].

Several studies have demonstrated that there is a direct relationship between groundwater extraction and land subsidence. For example, a subsidence value of 200 cm has been resulted in an area where groundwater reduction reaches

36 m in Iran. In addition, the deformation rate decreased gradually as the pore water pressure decreased stage by stage in China [8]. The results by Rahnama and Moafi [9] and Rajabi and Ghorbani [10] show that discharging of groundwater is the main factor of the land subsidence in Rafsanjan zone, Iran.

From another perspective, Seismic characteristics could affect the crustal deformation in Egypt and worldwide. A comparison between seismic and geodetic crustal moment-rates showed that the seismic coupling coefficient is low in the Nile Delta region that has intermediate seismic activities while it reaches more than 60 % in the Gulf of Aqba region that has high seismic activities [11]. Crustal contraction occurs on northern Nile Delta and offshore with E–W and N–S orientations, respectively [12].

Due to the worldwide natural phenomena of plate tectonics, the monitoring of crustal deformation has become a vital task for the geodetic communities in several countries such as Ukraine [13], Europe [14], Turkey [15], and Egypt [16]. Conversely, crustal deformation and horizontal coordinate changes have been widely investigated too in the Nile Delta region. Several data sources have been utilized in such investigations including GNSS, Radar remote sensing imageries, and terrestrial gravity. For example, Mohamed et al. [17] utilized GNSS from 2009 to 2019 and reported that the average absolute velocity ranges between 14 and 22 mm/year with an accuracy of 3 mm/year. Additionally, Mahrous et al. [18] have estimated the average horizontal movement in the Nile Delta between 2013 and 2020 to be 2.5 mm/year while the vertical velocities range between −0.11 mm/year at Helwan to −9.1 mm/year at Mansoura. Moreover, Abdallah [5] has found that the annual horizontal velocity in the Nile Delta region, over 2013–2015, is about 23.6 ± 0.3 mm/year in the east direction and 18.5 ± 0.3 mm/year in the north direction. Also, Aly [19] has applied ERS-1 and ERS-2 radar datasets to monitor the Nile Delta land subsidence and has reported that the rate of subsidence in greater Cairo, Mansoura, and Mahala cities are 7, 9, and 5 mm/year respectively. Furthermore, utilizing GNSS and seismological data over 2013–2020 has concluded that the average crustal horizontal deformation in the Nile Delta region is 0.56 mm/year and −4.6 mm/year for the average vertical subsidence [20].

The International Terrestrial Reference Frame (ITRF) constitutes a 4D unique reference system for geodetic and geodynamic applications. The ITRF is updated frequently to consider the tectonic plate motions worldwide. Since 1994, there exist several versions of the ITRF frame and the most recent one is the ITRF2020 [21]. The ITRF is applied in precise geodetic and Earth science activities, particularly in monitoring crustal deformation [22]. In Egypt, there exist two utilized ITRF realizations, namely the ITRF1996 and the ITRF2008. In 1995, the Egyptian Survey Authority (ESA) has established the GPS High-Accuracy Reference Network (HARN) which has been adjusted using the ITRF1994 (epoch 1996.4992). Moreover, in 2012, ESA established the Continuously Operation Reference Stations (CORS) network. That 40-station network was adjusted relative to ITRF2008 epoch 2011.8096 [23]. A new adjustment of the CORS network relative to the ITRF2014 (epoch 2019.5833) has concluded that the 2D and 3D coordinate discrepancies during that time have averages of 0.237 m and 0.253 m, respectively. Additionally, the average direction of horizontal movements is 55.4°, and the overall 2D and 3D regional velocities are 29.7 and 31.7 mm/year, respectively. Another recent research has concluded that the average discrepancies between the ITRF 2014 (epoch 2019) and ITRF 1994 (epoch 1996) in the east of Egypt equal −0.74 m, 0.42 m, and 0.24 m in the X, Y, and Z coordinates respectively [24]. Table 1 presents a comparison between the main accomplished results of the previous studies.

The current research study aims to present the recent results of applying GNSS Precise Point Positioning (PPP) datasets over 2012–2024 in horizontal displacements, land subsidence, and ITRF conversion in the Nile Delta region, north of Egypt.

2 Study area and available data

2.1 Spatial extents

The study area is extended in the west direction to include the Alexandria city (29.7° E) and in the east direction to include the Suez Canal too (32.7° E). Also, it extends from latitude 29.9° N to 31.6° N and covers 34,148.8 km^2 as depicted in Figure 1. The available dataset consists of 23 GNSS CORS stations have been acquired from the Egyptian Survey Authority (ESA) over the study area (Figure 1). Most of the CORS stations have Trimble R10 geodetic receivers [23]. A set of several observation files for each station covering continuous 24-h session have been collected annually from 2012 to 2024. A few observation files have been missing at some stations due to communication problems between the stations and the GNSS data center at the ESA headquarter.

2.2 Geological and hydrogeological settings

The geological units of the aquifer scheme are the top unit of Holocene clay (aquitard), quaternary and late tertiary

Table 1: A comparative summary of previous studies.

Study reference	Data type	Spatial extents	Data span	Main findings
[7]	GNSS	Nile Delta	2012–2023	Vertical land movements vary between −7.2 mm/year and +2.6 mm/year with an average equals −1.4 mm/year.
[6]	Seismic and groundwater data	Middle Nile Delta	Not specified	Decreasing groundwater recharge by 94.4 %, 88.8 %, and 83.2 % led to −30, −60, and −90 mm land subsidence, respectively, while increasing abstraction by 146 %, 193 %, and 233 % led to land subsidence by −190, −380, and −560 mm, respectively.
[18]	GNSS	Nile Delta	2013–2020	The local horizontal movement rate is averaged by 2.5 mm per year, which represents a low rate. The vertical velocities showed a significant subsidence ranging from-0.11 mm per year to −9.1 mm per year.
[20]	GNSS and seismological data	Nile Delta	2013–2020	Crustal movements and deformation parameters show; VN average values: 0.56 mm/year, VE average values: 0.62 mm/year for local velocities and average values −4.60 mm/year for vertical subsidence.
[12]	GNSS and seismological data	Entire Egypt	Not stated	On the Nile Delta, the maximum horizontal stress pattern shows scattered orientations. Crustal contraction occurs on northern Nile Delta and offshore with E–W and N–S orientations, respectively.
[11]	GNSS and seismological data	Entire Egypt	Not stated	Based on the computed seismic-geodetic moment-rate ratio (seismic coupling coefficient SCC) for the studied sources, three main categories were differentiated according to their seismic behavior in and around Egypt. The first region/category comprises a large sector of the delimited sources: the Red Sea, the Gulf of Aqaba, the Nile Delta, and the Nile Valley. They are characterized by low SCC values. The second region, characterized by moderate SCC values comprises the southern Gulf of Aqaba, northeastern Sinai and the Eastern Mediterranean coast, the Gulf of Suez, and the Cairo–Suez district. Finally, the third region that has higher SCC values extends along the GoA–DST. These values highlight a fully seismic deformation behavior in this region.
[3]	GNSS	Nile Delta	2013–2015	The northern part of Egypt can be divided into three major parts; the western part shows subsidence rate of 2 mm/year downward; Nile Delta of 2.5–10 mm/year downward from west to east and the eastern part shows an uplift.
[24]	GNSS topographic Data	Red Sea Coasts	2019	Investigating several simple ITRF transformation formulas (between ITRF 2014 and ITRF 1994), for kinematic surveying, showed that almost all models produced comparable results.
[23]	GNSS	Entire Egypt	2012 and 2019	The directions of horizontal movements range from 49.6 to 63.2 with an average of 55.4. Additionally, it has been figured out that the overall 1D, 2D, and 3D regional velocities over the ESA CORS network equals 210.8, 29.7, and 31.7 mm/year, respectively.
[4]	Sentinel-1 remote sensing and GPS	Nile Delta	2015–2019	There are three patterns of land subsidence: In major cities the subsidence ranges between −12 and −20 mm/year due to urban-induced loading, in coastal margins the subsidence varies between −3 and −8 mm/year due to natural sediment dewatering and compaction, and in newly reclaimed areas the subsidence ranges between −20 and −6 mm/year due to groundwater overexploitation.

Table 1: (continued).

Study reference	Data type	Spatial extents	Data span	Main findings
[17]	GNSS and seismological data	North Nile Delta	2009–2019	The average absolute velocity ranges between 14 and 22 mm/year with an accuracy of 3 mm/year, and the residual velocity is estimated at 0.51–4.98 mm/year with an accuracy of 2.5 mm/year.
[5]	GNSS	Nile Delta	2013–2015	The estimated annual horizontal velocity of the selected stations in northern Egypt and Nile Delta region is about 23.6 $\pm$ 0.3 mm/year in the east direction, while 18.5 $\pm$ 0.3 mm/year in the north direction. The annual vertical velocity shows that, all station suffer from subsidence rate increase from west to east with average rate of -4.9 ± 0.95 mm/year. While the Saini region shows uplift about 0.04 ± 1.11 mm/year.
[19]	Radar remote sensing imageries	1993–2000	Nile Delta	The measured rates of subsidence in greater Cairo, Mansoura, and Mahala are 7, 9, and 5 mm/year, respectively.

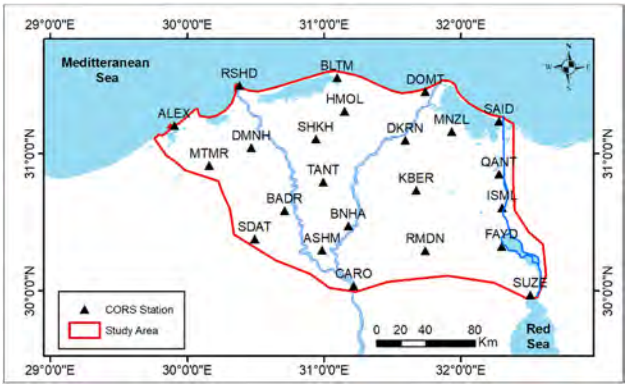

Figure 1: Study area and available GNSS stations.

gravels and sands (aquifer), and base unit. The clay cap thickness in the southern part of the Nile Delta ranges from 5 to 25 m, however it reaches 50 m in the northern part, 3–4 m above Mean Sea Level (MSL) in the middle, and 5 m above MSL in the south, northern part. The Quaternary aquifer's thickness ranges from 200 m near Cairo in the south to around 1,000 m towards the Mediterranean Sea in the north. The chief aquifer of the Nile Delta area is the Quaternary aquifer. The top layer of the quaternary aquifer is a clay layer, so it is considered a semi-confined aquifer. The level of groundwater in the area increases from north to south. It varies from 1 to 2 m above MSL in the north, 3–4 m above MSL in the middle, and 5 m above MSL in the south [6].

2.3 Tectonic settings

Most recent sedimentary land mass occupying the Study area is described by a thick sedimentary layer. In the Pleistocene Nile deposits, it was forming a thick alluvium layer, and a faulty hinge line orientated WNW to ESW designated at Kafr El Sheikh Latitude city separates the Nile delta into two zones. The faulty flexure that divides the south delta zone from the north delta plain basin is known as this hinge line. Previous studies have recognized the structural trends as following;

- The Tethyan trend, an east-west trend that may be associated with the early Mesozoic and probably earlier continental margin rifting of the southern Mediterranean. The Oligo-Miocene Hinge Zone, Mit Ghamr Fault, the northern and southern flexures of the Nile Delta onshore flexures are the most well-known instances of this trend.
- A northeast-southwest trend known as the Rosetta trend Age of the Late Cretaceous. The faults are supposed to have started in Alexandrina, which is found in the Mediterranean Sea's north-east corner. These faults have both vertical and horizontal motion, as well as strike slip displacement.
- During the Miocene, the northwest-southeast trend was active, Temsah or Bardawil Line in the eastern offshore Nile Delta. Structural of the Eastern Mediterranean is the consequence of a complex interplay between three primary fault trends (Figure 2).

The faults that characterize the Messiniansalt basin include the NW-SE (Temsah) fault trend, the NE-SW (Rosetta) fault trend, and the E-W faults. These trends appear to be old hereditary basement faults that reactivate periodically throughout the history of the region, and they are parallel to the Mediterranean plate borders [18].

The Nile Delta is situated in the northern section of the active rift, which is thought to be linked to Red Sea tectonics.

Figure 2: Structural trends in the study area (after Mahrous et al. [18]).

The majority of crustal deformation is predicted to occur in northern Africa active mountain belts, which have high seismicity and topography, due to the African plate northward convergence. According to seismicity maps, focal mechanisms, and stress field maps, Egypt can be classified into eight seismic zones. The delta itself has low seismic activity. It is affected by the most active zones in Egypt and adjacent areas such as seismic zones of the Eastern Mediterranean, Red Sea Northern side also the active part of the Gulf of Aqaba and Suez as well as recently Dahshour area (ibid).

3 Methodology

The PPP approach of the GNSS data processing has been carried out several times at each stations for all available observation sessions. PPP modeling relates the ionosphere-free combinations of dual-frequency GNSS pseudorange (P_i, $i = 1, 2$) and carrier phase observations (ϕ_i) to the unknown parameters according to the following simplified observation equations [25]:

$$l_P = \rho(X_s, X_r) + c(\mathrm{d}T - \mathrm{d}t) + T_r + \varepsilon_P \tag{1}$$

$$l_\phi = \rho(X_s, X_r) + c(\mathrm{d}T - \mathrm{d}t) + T_r + N\lambda + \varepsilon_\phi \tag{2}$$

where,

l_P is the ionospheric-free combination of P_1 and P_2 pseudoranges,

l_ϕ is the ionospheric-free combination of ϕ_1 and ϕ_2 carrier phases,

N is the non-integer ambiguity,

X_s is the satellite Cartesian coordinates at transmission time,

X_r is the GNSS Cartesian coordinates at reception time,

$\mathrm{d}T$ is the GNSS receiver clock offset from the GPS time,

$\mathrm{d}t$ denotes the satellite clock offset from the GPS time,

T_r is the signal path delay to the neutral-atmospheric (mainly troposphere),

λ is the wavelength, and

ε denotes the noises.

For the vertical land movement assessment, a first-order regression is built-in for the elevations of each station to model its vertical movements as:

$$h = a_0 + a_1 \mathrm{Year} \tag{3}$$

where, a_0 and a_1 are unknowns to be determined and Year represents the observation time in years. The unknown a_1 represents the annual vertical movement at such a station.

To describe the goodness of the regression, the coefficient of determination, R^2, is estimated as:

$$R^2 = 1 - \frac{\sum (h_i - h_p)^2}{\sum (h_i - h_m)^2} \tag{4}$$

where,

h_i is the ith observed elevation of the current station,

h_p is the ith predicted elevation observation of the current station,

h_m is the ith mean elevation observation of the current station.

Statistically speaking, R^2 varies from 0 to 1, the closer to 1 indicates the strength of the model. If its value is less than 0.5, the attained regression model might not be confident. The coefficient of determination, R^2, presents an indicator about the goodness of the attained regression model. Thus, if R^2 is less than 0.5, it means that the regression model fits only 50 % of the observed data and consequently the regression model is week. Chicco et al. [26] have demonstrates that the coefficient of determination (R-squared) is more informative and truthful than symmetric mean absolute percentage error (SMAPE) and other statistical indicators.

Similar to the methodology followed by Mohamed et al. [27] and Dakhil [28]; the horizontal components of the coordinates displacement at each GNSS station would be computed from the difference of adjusted coordinates of the stations from the last epoch relative to the first epoch. Most of these displacement vectors can be attributed mainly to the movement within the study area in those measurements. Thus, the Universal Transverse Mercator (UTM) projected coordinates (E and N) have been computed from the GNSS geodetic coordinates and the total horizontal movements between 2010 and 2023 (HM) and its direction (HD) are estimated using the displacement components ΔE and ΔN:

$$\Delta E = E_{2023} - E_{2010} \tag{5}$$

$$\Delta N = N_{2023} - N_{2010} \quad (6)$$

$$HM = \sqrt{\Delta E^2 + \Delta N^2} \quad (7)$$

$$HD = \tan^{-1}\frac{\Delta N}{\Delta E} \quad (8)$$

Accordingly, the annual average horizontal velocity (AHV) is estimated as:

$$\mathrm{AHV} = \mathrm{HM}/(2023 - 2010) \quad (9)$$

For the ITRF conversion between ITRF 2020 and ITRF 2008, the simple mathematical model proposed by Abdallah et al. [23] is applied as:

$$\begin{pmatrix} \Delta X \\ \Delta Y \\ \Delta Z \end{pmatrix} = \begin{pmatrix} X \\ Y \\ Z \end{pmatrix}_{\mathrm{ITRF2020}} - \begin{pmatrix} X \\ Y \\ Z \end{pmatrix}_{\mathrm{ITRF2008}} \quad (10)$$

The Trimble Business Center (TBC) version 5.2 software has been used, herein, to carry out the PPP computations. Such processing is based on treating the error sources of satellite orbits and clock, receiver clock, phase wind-up effects, antenna phase center, and troposheric and ionospheric delays [29]. That software/technique has been utilized in Egypt for the evaluation of the country's national GPS datum [30] and for the construction of new GPS geodetic station [31]. It has produced a millimeter-level of accuracy. The basic processing modelling step could be modeled by [32]:

$$\lambda\phi^s_v(ti) = \overset{-s}{\rho}_v(ti) - c, \overset{-s}{\tau}(ti) + \overset{\approx s}{\alpha}(t_i) - \overset{\approx s}{I}(t_i) - \overset{\approx s}{\beta}(t_i) \quad (11)$$

$$\rho^{-s}_v(t_i) = \overset{-s}{\rho}_v(t_i) - c, \overset{-s}{\tau}(t_i) + \overset{\approx s}{\alpha}(t_i) + \overset{\approx s}{I}(t_i) - \overset{\approx s}{\gamma}(t_i) \quad (12)$$

where,

ϕ^s_v is the reconstructed carrier phase observation at approximate rover location v,

$\overset{-s}{\rho}_v$ is the reconstructed pseudorange observation at approximate rover location v,

$\overset{-s}{\rho}_v$ is the geometric range from location v to satellites computed from the estimated precise orbit,

$\overset{-s}{\tau}$ is the estimated precise satellite clock error,

$\overset{\approx s}{\alpha}$ is the non-dispersive atmospheric delay at location v estimated (interpolated) from regional network,

$\overset{\approx s}{I}$ is the dispersive atmospheric delay at location v estimated (interpolated) from regional network,

$\overset{\approx s}{\beta}$ is the satellite carrier phase bias estimated from regional network, and

$\overset{\approx s}{\gamma}$ is the satellite clock bias estimated from global network.

Table 2: Statistics of vertical land movements over 2012–2024.

Station	Regression	Vertical trend (mm/year)	R^2
Baltim	$Y = -0.0026x + 35.698$	−2.6	0.92
DKRN	$Y = -0.002x + 42.46$	−2.1	0.88
SHKH	$Y = -0.0015x + 33.541$	−1.5	0.71
BADR	$Y = 0.0023x + 43.26$	2.3	0.88
MNZL	$Y = -0.002x + 41.073$	−2.0	0.73
RSHD	$Y = -0.0021x + 41.126$	−2.1	0.83
FAYD	$Y = 0.0028x + 37.682$	2.8	0.85
TANTA	$Y = -0.0037x + 48.283$	−3.7	0.91
ALEX	$Y = -0.002x + 72.09$	−2.0	0.71
KBER	$Y = -0.001x + 35.57$	−1.0	0.68
HMOL	$Y = -0.003x + 50.14$	−3.0	0.67
SUEZ	$Y = 0.0016x + 43.881$	1.6	0.63
SDAT	$Y = -0.0048x + 81.257$	−3.9	0.92
MTMR	$Y = -0.0005x + 34.1616$	−0.5	0.54
ASHM	$y = -0.0039x + 47.514$	−3.9	0.53
	Minimum	−3.9	
	Maximum	2.3	
	Average	−1.5	
	Standard deviation	±1.9	

4 Processing and results

The TBC v. 5.2 package has been used, herein, to carry out the PPP computations. The satellite's precise orbits and clock corrections have been downloaded from the International GNSS Service (IGS) website: https://igs.org/. Consequently, a time series of Cartesian coordinates and ellipsoidal elevations has been obtained for each station over its corresponding available time span. Since the accuracy of the PPP-based coordinates has been estimated in the millimeter level, the attained horizontal and vertical displacement estimations

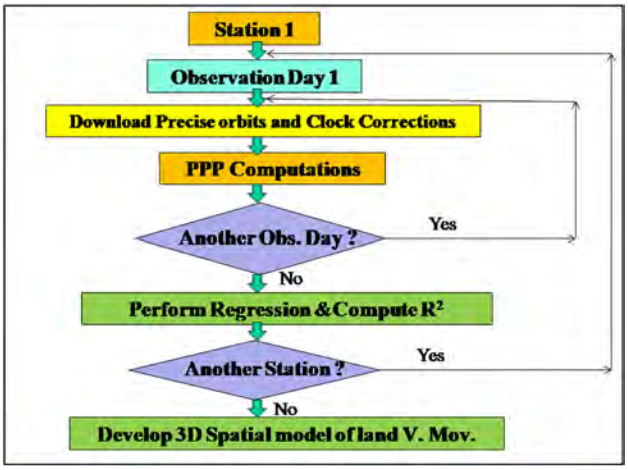

Figure 3: Flowchart of the processing steps.

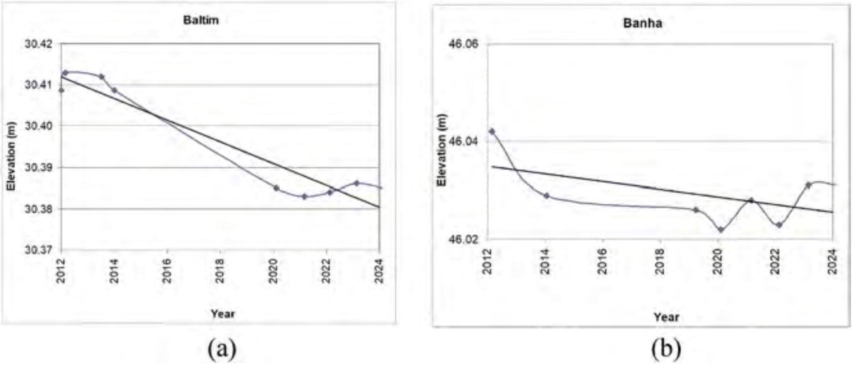

Figure 4: Typical examples of regression goodness. (a) High R^2 at Baltim station. (b) Low R^2 at ? Benha station.

could be in almost the same accuracy. Similar results have been reported by Rabaha et al. [33].

4.1 Results of vertical land movements

Applying Eqs. (3) and (4), regression models of R^2 greater than 0.5 have been obtained at only 15 GNSS stations (Table 2). Figure 3 depicts the processing flow chart. The remaining 9 stations yield regression with R^2 less than the required confidence value. Figure 4 presents typical examples of both cases. Thus, it can be recognized that the land subsidence in the Nile Delta region ranges between −3.9 mm/year at both SADT and ASHM stations and 2.3 mm/year at BADR station with an average of −1.5 ± 1.9 mm/year. The Arc GIS software has been utilized to convert such discrete GNSS stations into a 3D spatial surface representing the vertical land movements over the study area (Figure 5). For simplicity, the vertical land movements have been divided into three subsidence groups while the forth category is the uplift. Such categories are based on the following vertical land movement rates: high subsidence ranges between −3.8 and −3.0 mm/year, medium subsidence ranges between −3.1 and −2.0 mm/year, low subsidence ranges between −2.1 and −1.0 mm/year, and uplift ranges between 0 and +2.3 mm/year. Thus, it can seen that a moderate rate of land subsidence almost exists all over the area, particularly in the central region, smaller subsidence rates exist around Sadat, Tanta, and Ashmon cities, and uplift arises around Badr and Suez cities. It is worth mentioning that the land subsidence phenomena depend on several natural and human factors mainly on the groundwater extraction and soil characteristics.

Next to investigate the spatial variation of the vertical land movements over individual governorates in the study area, Arc GIS spatial analysis tools have been performed. The accomplished statistics of such step are tabulated in Table 3 and depicted in Figure 6. Thus, it can be noticed that the maximum average annual vertical velocity exists in both the Giza and Kalyoubia governorates in the southern region of the study area. A possible reason behind those large

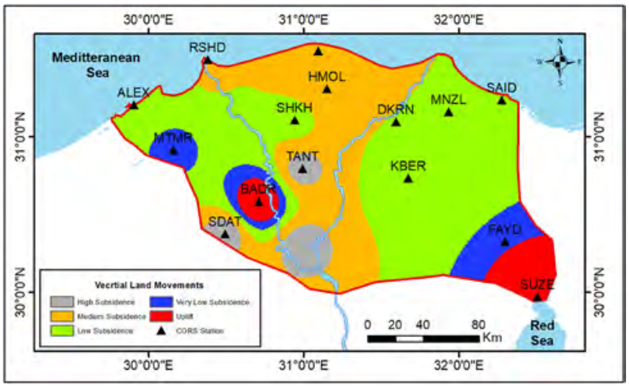

Figure 5: The vertical land movements over 2012–2024.

Table 3: Statistics of vertical land movements over individual governorates (mm/year).

Governorate	Min	Max	Mean
Suez	−1.31	1.60	0.34
Sharkia	−2.62	−1.00	−1.64
Port Said	−1.88	−1.68	−1.79
Menoufia	−3.90	1.79	−2.21
Kalyoubia	−3.78	−1.96	−2.84
Kafr Elshikh	−3.00	−1.50	−2.19
Ismailia	−1.83	0.45	−1.19
Giza	−3.65	−2.25	−2.95
Gharbia	−3.70	0.84	−2.47
Damietta	−2.36	−1.97	−2.09
Dakahlia	−2.72	−1.46	−2.15
Cairo	−2.73	−1.13	−1.86
Behera	−3.89	2.30	−1.22
Alex	−2.00	−1.43	−1.84

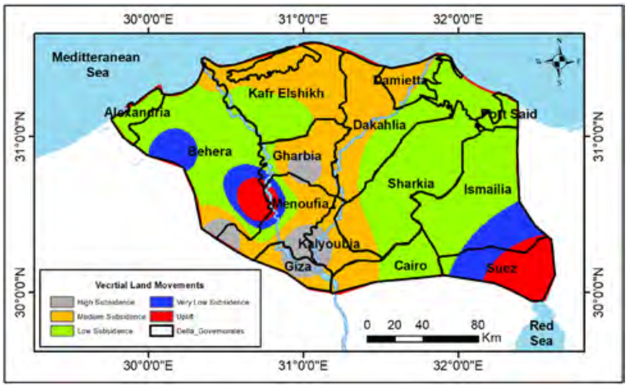

Figure 6: The vertical land movements over governorates.

annual velocities could be the rapid and huge urbanization pattern in such arid regions [34]. Accordingly, such a remark should be considered in the development strategy of those two specific regions partially for the establishment of huge infrastructures. These results agree in general of those of Mahrous et al. [18] who has reported vertical land movement trends range from +0.42 mm/year and −9.16 mm/year over the Nile Delta in the period 2013–2020.

4.2 Results of horizontal land movements

According to the attained accurate coordinates of the utilized ORS stations in the Nile Delta area in 2024, only 14 stations have been compared to their initial UTM coordinates and the crustal motions have been estimated (Eqs. (5)–(8)). The horizontal components at each station (Eqs. (5) and (6)) were computed from the difference of adjusted coordinates of the stations. The horizontal displacement vectors were calculated from the coordinate changes. Table 4 and Figure 7 present the accomplished findings. It can be concluded that the horizontal crustal deformation in the study area varies between 25.8 mm/year at the HMOL station to 27.6 mm/year at the FAYD station with an average equals 27.0 mm/year and a standard deviation of ±1.0 mm/year. Additionally, the direction of that deformation ranges from 35.4° to 421.6° with a mean equals 38.6° ± 2.1°. The uncertainty in coordinates changes and velocities could be estimated from the accuracy of the coordinates themselves according to the laws of error propagation. Since the XYZ coordinates are very accurate (mm level), the velocity would be in the same accuracy level.

The attained results agree with those of previous studies concerning the regional movements of the Nubia tectonic plate in the Nile Delta region and in Nigeria (e.g. [18, 22]). It worth to mention that Mahrous et al. [18] has reported the local horizontal movement rate of 2.5 mm/year and a regional movement rate varies between 17.05 and 23.65 mm/year which is consistent with the attained results herein. Additionally, the accomplished results agree generally with those of Abdallah [5] although he used less GNSS stations (only 8 points) over lower time span (2013–2015) in the Nile Delta region. For ease, the horizontal land movements have been divided into three groups as: high ranges between 25.8 and 26.8 mm/year, medium ranges between

Table 4: Statistics of horizontal crustal movements over 2012–2024.

Station	ΔN (m)	ΔE (m)	Rate ΔN (mm/year)	Rate ΔE (mm/year)	HM (mm/year)	HD (deg)
ASHM	0.218	0.280	16.8	21.5	27.3	37.9
BADR	0.216	0.263	16.6	20.2	26.2	39.4
BLTM	0.236	0.294	18.2	22.6	29.0	38.8
BNHA	0.217	0.274	16.7	21.1	26.9	38.4
CARO	0.228	0.257	17.5	19.8	26.4	41.6
DMNH	0.212	0.273	16.3	21.0	26.6	37.8
FAYD	0.229	0.276	17.6	21.2	27.6	39.7
HMOL	0.194	0.273	14.9	21.0	25.8	35.4
ISML	0.222	0.277	17.1	21.3	27.3	38.7
KBER	0.229	0.272	17.6	20.9	27.4	40.1
SAID	0.205	0.279	15.8	21.5	26.6	36.3
SDAT	0.210	0.273	16.2	21.0	26.5	37.6
SHKH	0.216	0.277	16.6	21.3	27.0	37.9
SUZE	0.233	0.270	17.9	20.8	27.4	40.8
	Minimum		14.9	19.8	25.8	35.4
	Maximum		17.9	21.5	27.6	41.6
	Average		16.8	21.1	27.0	38.6
	Standard deviation		±1.1	±0.8	±1.0	±2.1

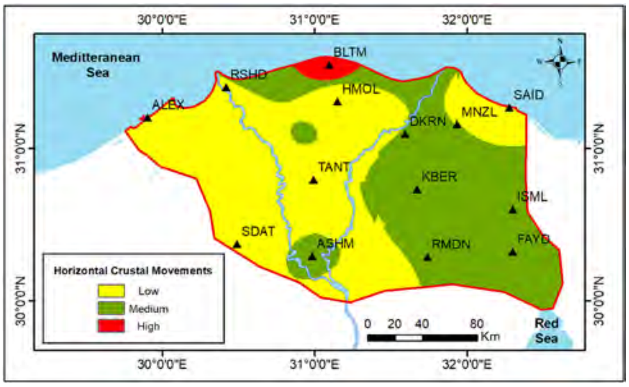

Figure 7: The horizontal crustal movements over 2012–2024.

26.9 and 27.7 mm/year, and low ranges between 27.8 and 28.9 mm/year.

4.3 Results of ITRF conversion

To investigate the coordinates changes between two ITRF frames in The Nile Delta region, the Cartesian XYZ values are compared together (Eq. (10)). The accomplished vector magnitude and velocities at the utilized 14 GNSS stations are (Table 5). The ITRF2020 is the most-recent ITRF model while the ITRF 2008 constitutes the reference of the Egypt's GNSS datum defined by the Continuously Operating Reference Network (CORS).

$$\begin{pmatrix} X \\ Y \\ Z \end{pmatrix}_{\text{ITRF2020}} - \begin{pmatrix} X \\ Y \\ Z \end{pmatrix}_{\text{ITRF2008}} = \begin{pmatrix} -0.312 \\ 0.153 \\ 0.152 \end{pmatrix}$$

It can be recognized that the ΔX varies between -0.395 m and -0.284 m with an average of -0.312 m $\pm$ 0.026 m. Additionally, ΔY ranges between 0.138 m and 0.166 m with an average of 0.153 m $\pm$ 0.010 m. Also, ΔZ ranges between 0.108 m and 0.190 m with a mean equals 0.152 m $\pm$ 0.020 m. The average annual rate of changes, velocities, has been found to be -24 ± 2 mm/year, 12 ± 1 mm/year, and 12 ± 2 mm/year in the X, Y, Z directions respectively.

Table 5: Statistics of coordinate changes between ITRF2020_Epoch 2024.1 and ITF2008_Epoch 2012.1.

Station	Magnitude (m)			Velocities (mm/year)		
	ΔX	ΔY	ΔZ	V_X	V_Y	V_Z
ASHM	−0.324	0.153	0.145	−25	12	11
BADR	−0.297	0.146	0.154	−23	11	12
BLTM	−0.326	0.157	0.157	−25	12	12
BNHA	−0.303	0.158	0.157	−23	12	12
CARO	−0.294	0.138	0.159	−23	11	12
DMNH	−0.298	0.160	0.148	−23	12	11
FAYD	−0.304	0.165	0.173	−23	13	13
HMOL	−0.395	0.142	0.108	−30	11	8
ISML	−0.305	0.162	0.162	−23	12	12
KBER	−0.299	0.154	0.165	−23	12	13
MNZL	−0.302	0.142	0.161	−23	11	12
QANT	−0.296	0.166	0.167	−23	13	13
SAID	−0.331	0.140	0.118	−25	11	9
SDAT	−0.335	0.143	0.126	−26	11	10
SHKH	−0.305	0.159	0.150	−23	12	12
SUZE	−0.284	0.166	0.190	−22	13	15
Minimum	−0.395	0.138	0.108	−30	11	8
Maximum	−0.284	0.166	0.190	−22	13	15
Average	−0.312	0.153	0.152	−24	12	12
Standard **deviation**	±0.026	±0.010	±0.021	±2	±1	±2

5 Conclusions

Regular monitoring and accurate measurement of subsidence and coastline retreat in the Nile Delta is becoming gradually more imperative for better understanding of these two phenomena and to offer decision-makers with constructive information for the purpose of sustainable development.

The PPP technique has been utilized to process the annual GNSS datasets at 24 stations in the Nile Delta region, Egypt from 2012 to 2024. The objectives of the current research study include the determination of recent horizontal crustal deformation rates, present vertical land movements, and the analysis of ITRF coordinate conversion between the two utilized ITRF frames in Egypt.

The attained results have concluded that the land subsidence in the Nile Delta region ranges between −3.9 mm/year and 2.3 mm/year with an average of -1.5 ± 1.9 mm/year. Additionally, the spatial surface representing the vertical land movements over the study area has demonstrated that a moderate rate of land subsidence is roughly present all over the area chiefly in the central region, smaller subsidence rates occur around the Sadat, Tanta, and Ashmon cities, and uplift arises around the Badr and Suez cities. Moreover, it is noticed that the maximum average annual vertical velocity exists in both the Giza and Kalyoubia governorates in the southern region of the study area. Therefore, such a comment should be taken into account in the development policies of those two specific regions partially for the establishment of huge infrastructures.

Regarding the horizontal crustal movements, it is recognized that such crustal deformation in the study area varies between 25.8 mm/year to 27.6 mm/year with an

average equals 27.0 mm/year and a standard deviation of ±1.0 mm/year. As well, the direction of that deformation ranges from 35.4° to 421.6° with a mean equals 38.6° ± 2.1°. Such findings are compatible with those of previous studies concerning the regional movements of the Nubia tectonic plate.

Furthermore, the attained simple mathematical model describing the relationship between ITRF2020 (epoch 2024) and ITRF2008 (epoch 2012) frames shows that the ΔX varies between −0.395 m and −0.284 m with an average of −0.312 m ± 0.026 m. Additionally, ΔY ranges between 0.138 m and 0.166 m with an average of 0.153 m ± 0.010 m. Also, ΔZ ranges between 0.108 m and 0.190 m with a mean equals 0.152 m ± 0.020 m. The average annual rate of changes, velocities, is −24 ± 2 mm/year, 12 ± 1 mm/year, and 12 ± 2 mm/year in the X, Y, Z directions respectively.

Research ethics: Not applicable.
Informed consent: Not applicable.
Author contributions: Gomaa Dawod has reviewed the first manuscript, review the findings, finalize the conclusions, and prepare the final version. Essam Al-Krargy has prepared the first draft, collect the required datasets and participate in preparing the final version.
Use of Large Language Models, AI and Machine Learning Tools: The authors declare that AI has not been utilized in any part of the current manuscript.
Conflict of interest: The authors declare that no conflict of interest exists.
Research funding: The authors declare that no funds were allocated to the current study.
Data availability: Not applicable.

References

1. Saleh S. 3D crustal structure and its tectonic implication for the Nile Delta and greater Cairo regions, Egypt, from geophysical data. Acta Geod Geophys Hung 2012;47:402–29.
2. Higgins S. Review: advances in delta-subsidence research using satellite methods. J Hydrol 2015;24:587–600.
3. AbouAly N, Hussien M, Rabah M, Zidan Z, Saleh M. Land deformation monitoring by GNSS in the Nile Delta and the measurements analysis. Arabian J Geosci 2021;14:150.
4. Rateb A, Abotalib A. Inferencing the land subsidence in the Nile Delta using sentinel-1 satellites and GPS between 2015 and 2019. Sci Total Environ 2020;729:138868.
5. Abdallah M. Study of the subsidence of Nile Delta using GNSS techniques [MSC thesis]. Faulty of Engineering, Mansoura University; 2018.
6. Abd-Elhamid H, Abd-Elkader B, Wahed O, Zelenkove M, Abd-Elaty I. Assessment of hanging the abstraction and recharge rates on the land subsidence in the Nile Delta, Egypt. Water 2022;14:1096.
7. Dawod G, Mohamed H, Amin A. Monitoring vertical land movements in the Nile Delta, Egypt by GNSS datasets over 2012–2023. J Sci Eng Res 2023;10:63–71.
8. Cao Y, Wei Y, Fan W, Peng M, Bao L. Experimental study of land subsidence in response to groundwater withdrawal and recharge in Changping District of Beijing. PLoS One 2020;15:e0232828.
9. Rahnama M, Moafi H. Investigation of land subsidence due to groundwater withdraw in Rafsanjan plain using GIS software. Arabian J Geosci 2009;2:241–6.
10. Rajabi A, Ghorbani E. Land subsidence due to groundwater withdrawal in Arak plain, Markazi province, Iran. Arabian J Geosci 2016;9:738.
11. Sawires R, Peláez JA, Sparacino F, Radwan AM, Rashwan M, Palano M. Seismic and geodetic crustal moment rates comparison: new insights on the seismic hazard of Egypt. Appl Sci 2021;11: 7836.
12. Rashwan M, Sawires R, Radwan A, Sparacino F, Peláez J, Palano M. Crustal strain and stress fields in Egypt from geodetic and seismological data. Remote Sens 2021;13:1398.
13. Ishchenko M. Determination of crustal strain in the northern region of Ukraine based on the analysis of GNSS observations. Kinemat Phys Celest Bodies 2017;33:302–8.
14. Maciuk K, Szombara S. Annual crustal deformation based on GNSS observations between 1996 and 2016. Arabian J Geosci 2018; 11:667.
15. Mosad R, El-kutb A, El-Hattab A, Rabah M, El-Koshy A. Detection of seismic movements using GNSS data. Port Said Eng Res J 2020;24:77–85.
16. Saleh M, Masson F, Mohamed A, Boy J, Abou-Aly N, Rayan A. Recent ground deformation around lake Nasser using GPS and InSAR, Aswan, Egypt. Tectonophysics 2018:319–21. https://doi.org/10.1016/j.teco.07.005.
17. Mohamed A, AbuBakr M, Awad M, Sakr K, Etman M. Utilisation of GNSS and seismiity for monitoring crustal deformation of the northern part of the Nile Delta, Egypt. NRIAG J Astron Geophys 2020;10:1–9.
18. Mahrous M, Radwan A, Abd El-Hafez T, Mahmoud S, Gomaa M, Zayed M. Estimation of crustal movements along the Nile Delta, Egypt using GNSS measurements. Egypt J Aquat Res 2022;48:367–73.
19. Aly M. Radar interferometry for monitoring land subsidence and coastal change in the Nile Delta, Egypt [Ph.D. dissertation]. USA: Texas A&M university; 2006. Available from: https://core.ac.uk/download/pdf/147132625.pdf [Accessed 20 Mar 2025].
20. Mahrous M, Radwan A, Abd El-Hafez T, Mahmoud S, Gomaa M, Zayed M. The current state of deformation parameters in the Nile delta, Egypt using GNSS and seismological data. Iraqi Geol J 2022;55. https://doi.org/10.46717/igj.55.2A.2Ms-2022-07-18.
21. Altamimi Z, Rebischung P, Collilieux X, Metivier L, Chanard K. ITRF 2020: an augmented reference frame refining the modelling of non-linear station motions. J Geod 2023;97:47.

22. Bawa S, Ojigi L, Dodo J, Lawal K. A methodology for estimating accurate velocity field of NigNET based on new ITRF realization. Contrib Geophys Geodes 2022;52:57−76.
23. Abdallah A, Agag T, Dawod G. ITRF-based tectonic coordinates changes using GNSS-CORS networks: a case study of Egypt. Survey Land Inf Sci 2021;80:69−78.
24. Dawod G, Mohamed H. Assessing ITRF conversion models for kinematic GNSS topographic mapping in coastal areas: a case study in Egypt, the FIG e-working week; 2021. Available from: https://fig.net/resources/proceedings/fig_proceedings/fig2021/papers/ts05.1/TS05.1_dawod_mohamed_11042_abs.pdf [Accessed 20 Mar 2025].
25. Ayhan M, Almuslmani B. Positional accuracy and convergence time assessment of GPS precise point positioning in static mode. Arabian J Geosci 2021;14:1263.
26. Chicco D, Warrens M, Jurman G. The coefficient of determination R-squared is more informative than SMAPE, MAE, MAPE, MSE and RMSE in regression analysis evaluation. PeerJ Comput Sci 2021;7:e623.
27. Mohamed A, Mahmoud S, Teleab A, Othman A, Hamed D. Recent crustal deformation and seismicity studies at Abu-Dabbab area, Red Sea, Egypt. Arabian J Geosci 2013;6:1283−93.
28. Dakhil A. GPS measurements and its impact on geodetic datum maintenance [MS thesis]. Egypt: Faulty of Engineering, Mansoura University; 2015. Available from: https://www.researchgate.net/publication/281526273_GPS_Measurements_and_Its_Impact_on_Geodetic_Datum_Maintenance [Accessed 20 Mar 2025].
29. Leandro R, Landau H, Nitschke M, Glocker M, Seeger S, Chen X, et al. RTX positioning: the next generation of cm-accurate real-time GNSS positioning. A technical report. Germany: Trimble Terrasat GmbH; 2011. Available from: https://www.researchgate.net/profile/Markus-Nitschke/publication/290278269_RTX_positioning_The_next_generation_of_cm-accurate_real-time_GNSS_positioning/links/56cf160f08aeb52500c964eb/RTX-positioning-The-next-generation-of-cm-accurate-real-time-GNSS-positioning.pdf [Accessed 20 Mar 2025].
30. Rabah M, Elmewafey M, Farahan M, Awad A, Jaafar. Evaluating the Egyptian HARN network by GNSS precise point positioning (PPP). Int J Sci Eng Res 2015;6:858−66.
31. El-Tokhey M, Mogahed Y, Mamdouh M, Hassan T. Establishment of new continuous operating reference station (CORS) at Faculty of Engineering, Ain Shams University. Int J Eng Adv Technol 2018;7:7−13.
32. Chen X, Allison T, Cao W, Ferguson K, Grünig S, Gomez V, et al. Trimble RTX, an innovative new approach for network RTK. In: Proceedings of the 24th international technical meeting of the satellite division of the institute of navigation (ION GNSS 2011), September 20−23, 2011. Oregon; 2011:2214−19 pp. Available from: https://www.3dgeosolutions.hu/wp-content/uploads/2017/02/Trimble-RTX_a_halozati_RTK_uj_megkozelitese.pdf [Accessed 20 Mar 2025].
33. Rabaha M, Elmewafey M, Farahan M. Datum maintenance of the main Egyptian geodetic control networks by utilizing precise point positioning (PPP) technique. NRIAG J Astron Geophys 2016;5:96−105.
34. Nabil A, El-Ashquer M, Saleh M, Mousa A, El-Fiky G. Crustal deformation in East of Cairo, Egypt, induced by rapid urbanization, as seen from remote sensing and GNSS data. J Appl Geodesy 2024. https://doi.org/10.1515/jag-2024-0094.

البحوث المنشورة بواسطة

أ.د. جمعة محمد داود

الإصدار الأول (٨٧ بحث بين ١٩٩٢ – ٢٠٢٥)